Morton A. Meyers

Dynamic Radiology of the Abdomen



Normal and Pathologic Anatomy

FIFTH EDITION



Springer

Dynamic Radiology of the Abdomen

FIFTH EDITION

Springer
New York
Berlin
Heidelberg
Barcelona
Hong Kong
London
Milan
Paris
Singapore
Tokyo

Morton A. Meyers

With Contributions by Stephen R. Baker, Alfred S. Berne, Chusilp Charnsangavej, Kyunghee C. Cho, Michiel A.M. Feldberg, Bruce Javors, Hiromu Mori, Michael Oliphant, Catherine Roy, Maarten S. van Leeuwen, Ronald Wachsberg

Dynamic Radiology of the Abdomen

Normal and Pathologic Anatomy

FIFTH EDITION

With 1133 Figures in 1796 Parts, 18 in Color

Springer

eBook ISBN: 0-387-21804-1
Print ISBN: 0-387-98845-9

©2005 Springer Science + Business Media, Inc.

Print ©2000, 1994, 1988, 1982, 1976 Springer–Verlag New York, Inc.
New York

All rights reserved

No part of this eBook may be reproduced or transmitted in any form or by any means, electronic, mechanical, recording, or otherwise, without written consent from the Publisher

Created in the United States of America

Visit Springer's eBookstore at: http://ebooks.springerlink.com
and the Springer Global Website Online at: http://www.springeronline.com

To my wife,
Bea,
and my children,
Richard and Amy



There are some things which cannot be learned quickly, and time, which is all we have, must be paid heavily for their acquiring. They are the very simplest things; and, because it takes a man's life to know them, the little new that each man gets from life is very costly and the only heritage he has to leave.

Ernest Hemingway
Death in the Afternoon

The greatest thing a human soul ever does in this world is to see something. . . . To see clearly is poetry, prophecy, and religion, all in one.

John Ruskin
Modern Painters

Preface to the Fifth Edition

The preface to the first edition of *Dynamic Radiology of the Abdomen: Normal and Pathologic Anatomy* stated that this book introduces a systematic application of anatomic and dynamic principles to the practical understanding and diagnosis of intraabdominal diseases. The clinical insights and rational system of diagnostic analysis stimulated by an appreciation of the dynamic intraabdominal relationships outlined in previous editions have been universally adopted. Literally thousands of scientific articles in the literature have attested to their basic precepts. Formulations and analytic approaches introduced in the first edition are now widely applied in clinical medicine so that many of the terminologies, definitions, and concepts of pathogenesis have solidly entered the public domain. These insights lead to the uncovering of clinically deceptive diseases, the evaluation of the effects of disease, the anticipation of complications, and the determination of the appropriate diagnostic and therapeutic approaches. Spanish, Italian, Japanese, and Portuguese editions have encouraged more widespread application of the principles which in turn has led to further contributions to our understanding of the features of spread and localization of intraabdominal diseases. These principles have been applied to the full range of imaging modalities—from plain films and conventional contrast studies to CT, US, MRI and endoscopic, laparoscopic, and intraoperative ultrasonography—leading to this fifth edition in 24 years.

In the pursuit of comprehending the pattern, all methods of investigation have been used, including (a) anatomic cross–sectioning of cadavers frozen to maintain relationships; (b) cadaver injections and dissections performed to determine preferential planes of spread along ligaments, mesenteries and extraperitoneal fascial compartments; (c) selected clinical cases with the fullest range of imaging studies including plain films, tomograms, and conventional contrast studies; presacral retroperitoneal pneumography and peritoneography; sinography which occasionally provided serendipitous display of normal and pathologic anatomy akin to an *in vivo* model; and computed tomography, ultrasonography, nuclear medicine studies, magnetic resonance imaging, and endoscopic ultrasonography; (d) peritoneoscopy; and (e) surgical operations, surgical pathology and autopsies.

The basic aims in writing this book have not changed from the first edition and it is produced in the same spirit as its predecessors. The quest of science has always sought the identification of a pattern of circumstances. With this recognition, there follows insight and understanding into the nature and dynamics of events and thereby their predictability, management, and consequences. This book establishes that the spread and localization of diseases throughout the abdomen and pelvis are not random, irrational occurences but rather are governed by laws of structural and dynamic factors.

To satisfy these aims, special attention has been given to keeping the book current with clinical and technological advances that have so dramatically altered the practice of abdominal imaging in the past several years. Six completely new chapters have been added and virtually all others have been extensively updated and enlarged. This edition is expanded by more than 180 pages and more than 520 new illustrations.

Many of the new chapters are by international authorities who have pioneered advances in the crucial appreciation and precise recognition of a wide spectrum of intraabdominal diseases. An introductory chapter on general considerations underscores the book's continuing thematic approach based upon anatomic relation-

ships, dynamic factors, and visual perception of the image. This is followed by a chapter on clinical embryology, emphasizing an understanding of disease entities which often are only first clinically apparent in the adult. The manifestations of intraperitoneal air, often subtle on plain films but nevertheless highly significant, are precisely described and illustrated. A new chapter is devoted to oncoradiology and the TNM staging of gastrointestinal cancers, delineating the normal anatomic mural components by sectional imaging and the extent of intramural and regional neoplastic spread. Other chapters deal with the discrete identification of the pathways of lymph node metastases in cancers of the gastrointestinal and hepatobiliary tracts and the pathways of regional spread in pancreatic cancer.

Developments in understanding the intraperitoneal spread of infections include the normal and pathologic anatomy of the lesser sac. Features of the significance of the gastropancreatic plica, the superior and lower recesses of the lesser sac, and the imaging features of the dimensions and relationships of the foramen of Winslow are detailed. The clinical significance of the spread of infection via the perihepatic ligaments is greatly expanded.

Concepts of the pathways of dissemination of malignancies have been highly expanded and richly illustrated with the full range of imaging modalities. Normal and pathologic anatomy are made graphic by spiral CT with planar reconstructions, MR, endoscopic ultrasonog–raphy and laparoscopic ultrasonography. The position and nomenclature of lymph node stations in gastric carcinoma as classified by the Japanese Research Society for Gastric Cancer have been updated and correlation is made with the TNM staging system. Further advances in the understanding of the intraperitoneal spread of malignancies include features of seeded perihepatic and subdiaphragmatic metastases, subcapsular liver metastases, spread to anterior mediastinal lymph nodes, implantation on the falciform ligament and within the interhepatic fissures, hepatic invasion by advanced gastric cancer, Sister Mary Joseph's nodule, Krukenberg tumors of the ovaries, the pathogenesis and differential diagnosis of the omental cake and of peritoneal thickening and enhancement in peritoneal carcinomatosis; instrumental, operative and needle track seeding; hematogeous metastases to the small bowel from metastatic melanoma, breast carcinoma and bronchogenic carcinoma. Developments and advances in imaging the spread and localization of intraperitoneal malignancies are discussed and illustrated. The unifying perspective of the subperitoneal space of the abdomen and pelvis, establishing the discrete planes of subserous connective tissue and lymphatics, is extended to the thoraco-abdominal continuum; this holistic concept provides an explanation for what has long been thought of as illogical circumstances.

Numerous major developments have also refined our precise evaluation of the extraperitoneal fascia and spaces. A new section defines the compartmentalization of the anterior pararenal space, in keeping with progressive application of embryologic/anatomic circumstances to clinical imaging. The section on the extraperitoneal paravesical pelvic spaces and their continuities with the abdominal spaces has been refined and expanded. Fundamental anatomic characteristics of the fascia and spaces are documented and their clinical relevance richly illustrated. These include the potential midline communication of the perirenal spaces, the inferior apex of the cone of renal fascia, the retromesenteric plane, the attachment of the adrenal gland to the renal fascia superiorly, and the identification of the two lamellae of the posterior renal fascia. Further enlarged are the discussions and illustrations of the lumbar triangle pathway and its relationship to Grey Turner's sign in pancreatitis and retrorenal hemorrhage; and of extension along the perihepatic ligaments and its relationship to Cullen's sign. Occasional instances of splenic trauma leading to clinically masked extraperitoneal bleeding are explained. Staging of renal cell carcinoma is significantly updated, with comparison of Robson's classification and the TNM system and the value of magnetic resonance imaging. Perirenal diseases beyond abscesses and hemorrhage have been expanded to include perirenal metastases, lymphoma, extramedullary hematopoiesis and retroperitoneal fibrosis. The anatomy of the iliopsoas compartment is clarified and the features of psoas abscess are illustrated. Controversies regarding rupture of abdominal aortic aneurysms with extension of hemorrhage to the extraperitoneal spaces are resolved.

Other additions include discussions of renocolic fistulas; the precise anatomy and importance of the ligament of Treitz; characteristic localizing features of scleroderma, carcinoid and Crohn disease of the small bowel; and the CT features and differential diagnosis of internal paraduodenal hernias.

While diagnostic criteria are emphasized throughout the book, there is also discussion of foreseeable complications and appropriate management of many disease processes.

As in previous editions, great care has been taken with the layout to give prominence to selected illustrations and, most importantly, to position the figures as closely as possible to their citation in the text so that the reader's time and effort are not wasted referring to pages some distance apart.

The color atlas details anatomic features of clinical significance.

The references have been considerably expanded and continue to include both classic articles and recent citations. They are not restricted to the English language and, when pertinent, refer to the original descriptions. A lengthy index with cross-references provides immediate access to the detailed material presented.

Many persons have contributed importantly to the fifth edition and I thank them sincerely. I wish to express my particular appreciation to Angel Arenas, M.D., Hospital Universitario "12 de Octubre," Madrid, Spain; Yong Ho Auh, M.D., Asan Medical Center, Seoul, Korea; Emil Balthazar, M.D., New York University School of Medicine, New York City; James Brink, M.D., Yale University Medical School, New Haven, Connecticut; Gary G. Ghahremani, M.D., Evanston Hospital—Northwestern University, Evanston, Illinois; Jay P. Heiken, M.D., Mallinckrodt Institute of Radiology, St. Louis, Missouri; Dean T. Maglinte, M.D., Methodist Hospital, Indianapolis, Indiana; Hiromu Mori, M.D., Oita Medical University, Oita, Japan; Michael Oliphant, M.D., Crouse Hospital, State University of New York, Syracuse, New York; Richard C. Semelka, M.D., University of North Carolina Hospitals, Chapel Hill, North Carolina; Ann Singer, M.D., Cleveland Clinic Foundation, Cleveland, Ohio, and Francis Weill, M.D., University of Besançon School of Medicine, Besançon, France for their contributions. Additionally, I wish to express my gratitude to the contributing authors who have added luster to this edition.

I am distinctly grateful to Michiel A. M. Feldberg, M.D., Ph.D., University Hospital, Utrecht, Netherlands, for his selfless cooperation and the stimulating pleasure of sharing intellectual enthusiasms.

I have submitted this fifth manuscript to Springer-Verlag, confident that their skills have produced another edition of high technical quality.

Morton A. Meyers, M.D.
Stony Brook, New York
January, 2000

Foreword to First Edition

Few books present so fresh an approach and so clear an exposition as does *Dynamic Radiology of the Abdomen: Normal and Pathologic Anatomy.*

This well-documented, clearly written, and beautifully illustrated book details the answers not only to "what is it?" but also "how?" and "why?" Such fundamental information regarding the pathogenesis of disease within the abdomen reinforces and simplifies accurate radiologic analysis. The characteristic radiologic features of intraabdominal diseases are shown to be easily identified, expanding the practical application of the term "pattern recognition." It certainly is of practical value in daily clinical experience and will be of considerable help for further advances.

The traditional *dissectional* method of learning anatomy disturbs the intimate relationships of structures. The *sectional* anatomy presented in this book is the framework for understanding the findings in conventional radiology—in plain films and routine contrast studies—as well as in ultrasonography and computed tomography of the abdomen.

This is not just a review of others' experiences, but a crystallization of the author's contributions over the past several years. Dr. Meyers' concept of dynamic circulation within the peritoneal cavity is a breakthrough in our understanding of the spread of intraabdominal disease, particularly abscesses and malignancies. Peritoneography, the opacification of the largest lumen in the body, offers a potential yield of vast diagnostic information. The precise definition of the three extraperitoneal spaces represents a charting of previously unexplored territory. Awareness of the renointestinal and duodenocolic relationships, the spread of pancreatitis along mesenteric planes, and the pathways of extrapelvic spread of disease again underscores the practical importance of anatomic features. The approach to the mesenteric and antimesenteric borders of the small bowel and to the haustral pattern of the colon adds a new dimension to the interpretation of abdominal radiology.

This book confirms Dr. Meyers' reputation as one of the authorities in normal and pathologic radiologic anatomy of the abdomen.

1976

Richard H. Marshak, M.D.
Clinical Professor of Radiology
Mount Sinai School of Medicine
New York, New York

Foreword to First Edition

Dr. Morton A. Meyers indeed has developed a dynamic text relating to radiologic aspects of abdominal disease. But this statement, with its emphasis on radiology, is misleading. This book is an important reading source for surgeons. Dr. Meyers' observations have not been confined to those arising from a purely radiologic study of the abdomen. The inclusion of observations based on injection studies both in the cadaver and *in vivo* has given this work a noteworthy comprehensiveness.

The insights provided by both the atlas of full-page color anatomic cross sections of the abdomen and pelvis and the excellent anatomic-radiologic correlations found in the text make the book indispensable. The atlas establishes the basis for intimate anatomic relationships which are then applied to the practical areas of clinical diagnosis and treatment of intraabdominal pathology. Presentations of these diagnostic and therapeutic considerations are enhanced by illustrated discussions relative to the new techniques of ultrasonography and computed tomography.

Dr. Meyers' presentation of this timely information is valuable, but what makes this book invaluable is the vast personal experience he is able to bring to it. This is not "just another" book purporting to give us something *new* in this important field. I believe the special approach given to this subject by Dr. Meyers is truly innovative. The radiologist and surgeon looking for the latest techniques in angiography for the diagnosis and treatment of massive bleeding form the gastrointestinal tract will not find it here. What they will find is major help in the understanding of, and indeed, therapeutic approach to a number of common intraabdominal problems, including infection and malignancy.

1976

Lloyd M. Nyhus, M.D., F.A.C.S
Warren H. Cole Professor
and Chairman, Department of Surgery
The Abraham Lincoln School of Medicine
University of Illinois at the Medical Center
Chicago, Illinois

Contents

Preface to the Fifth Edition vii
Foreword to the First Edition by R.H. Marshak xi
Foreword to the First Edition by L.M. Nyhus xiii
Contributors xxi
Color Insert ..... facing p. 539

1 General Considerations: Dynamics of Image Analysis 1
Normal Anatomic Relationships and Dynamic Principles of Pathways of Spread and Localization of Disease 1
Visual Factors: Perception of the Image 4
References 7

2 Clinical Embryology of the Abdomen: Normal and Pathologic Anatomy 9
Bruce R. Javors, M.D., Hiromu Mori, M.D., Morton A. Meyers, M.D., and Ronald H. Wachsberg, M.D.
Early Development of the Embryo, ... 9
Diaphragm 9
Gastrointestinal Tract 10
Duodenal Web and Bowel Duplication 10
Embryologic Rotation and Fixation of Gut 13
Volvulus 16
Meckel's Diverticulum 19
Hepatobiliary System 21
Hepatic Lobar Agenesis 21
Ectopic and Accessory Gallbladders 23
Choledochal Cyst 23
Hepatic Duct Diverticulum 25
Portal Venous System 25
Portohepatic Venous Shunt 27
Preduodenal Portal Vein 27
Ductus Venosus 31
Aneurysmal Dilation of the Portal Vein 31
Agenesis of the Portal Vein 32
Pancreas 32
Annular Pancreas 33
Pancreas Divisum 33
Agenesis of the Dorsal Pancreas 34
Pancreatic Arteriovenous Malformation 36
Pancreatic Cysts 36
Spleen 43
Accessory Spleen 43
Wandering Spleen 43
Polysplenia Syndrome 44

Internal Hernias *44*
Urogenital System *45*
Urinary Tract 45
Genital System 50
References *51*

3 Intraperitoneal Spread of Infections 57
Anatomic Considerations *57*
The Posterior Peritoneal Attachments 57
Detailed Anatomy of the Right Upper Quadrant 59
Radiologic Features *79*
The Spread and Localization of Intraperitoneal Abscesses 79
The Sectional and Isotopic Imaging Modalities *118*
Management *124*
References *128*

4 Intraperitoneal Spread of Malignancies 131
Direct Invasion from Noncontiguous Primary Tumors *132*
Invasion Along Mesenteric Reflections 132
Invasion by Lymphatic Permeation 166
Direct Invasion from Contiguous Primary Tumors *182*
Intraperitoneal Seeding *192*
Anatomic Features 192
Pathways of Ascitic Flow 193
Seeded Sites 193
Developments and Advances in Imaging 233
Embolic Metastases *238*
Metastatic Melanoma 239
Breast Metastases 243
Bronchogenic Carcinoma 245
Renal Carcinoma 245
References *255*

5 Staging of Gastrointestinal Cancers 265
Importance of Staging *265*
Carcinoma of the Esophagus 265
Carcinoma of the Stomach 266
Colorectal Carcinoma 269
Delineation of Normal Mural Components by Sectional Imaging *270*
T Staging *272*
T1 Stage 272
T2 Stage 275
T3 Stage 275
T4 Stage 275
Lymph Node Metastases *283*
References *284*

6 Pathways of Lymph Node Metastases in Cancer of the Gastrointestinal and Hepatobiliary Tracts 287
Chusilp Charnsangavej, M.D.
The Supramesocolic Compartment 287
Anatomic Consideration 287
Peritoneal Ligaments of the Liver 288
Peritoneal Ligaments of the Stomach 288
Lymphatic Drainage of the Liver and Pathways of Lymph Node Metastasis 289
Lymphatic Drainage of the Stomach and Pathways of Lymph Node Metastasis 292
The Inframesocolic Compartment 297
Anatomic Consideration 297
Lymphatic Drainage of the Colon and Pathways of Lymph Node Metastasis 300
References 307

7 Manifestations of Intraperitoneal Air 309
Kyunghee C. Cho, M.D., and Stephen R. Baker, M.D.
Detection of Intraperitoneal Air 309
Supine Abdominal Films 309
Supine Film Signs of Pneumoperitoneum 310
Depiction of Ligaments Protruding into the Peritoneal Cavity 310
Visualization of the Peritoneal Surface of Intraabdominal Organs 316
Detection of Free Air Confined in Specific Peritoneal Recesses 319
Recognition of Free Air Superimposed on the Liver 326
References 330

8 The Extraperitoneal Spaces: Normal and Pathologic Anatomy 333
Anatomic Considerations 334
The Three Extraperitoneal Compartments and Perirenal Fasciae 334
The Psoas Muscle 353
The Hepatic and Splenic Angles 355
Anterior Pararenal Space 356
Roentgen Anatomy of Distribution and Localization of Collections 356
Sources of Effusions 357
Compartmentalization of the Anterior Pararenal Space 396
Maarten S. van Leeuwen, M.D., and Michiel A.M. Feldberg, M.D.
Anatomic Considerations 396
Normal Imaging Features 402
Abnormal Imaging Features 402
Perirenal Space 409
Roentgen Anatomy of Distribution and Localization of Collections 409
Posterior Pararenal Space 451
Roentgen Anatomy of Distribution and Localization of Collections 451
Clinical Sources of Effusions 451
Diffuse Extraperitoneal Gas 463
Rectal Perforation 466
Sigmoid Perforation 466

Extraperitoneal Gas of Supradiaphragmatic Origin 467
Differential Diagnosis of Small Amounts of Supradiaphragmatic Gas 471
Psoas Abscess and Hematoma *473*
The Extraperitoneal Paravesical Pelvic Spaces *477*
Catherine Roy, M.D.
Anatomic Considerations 477
Abnormal Imaging Features 480
References *484*

9 The Renointestinal Relationships: Normal and Pathologic Anatomy 493
Anatomic Considerations *493*
The Right Kidney 493
The Left Kidney 494
Radiologic Observations *496*
Characteristic Mass Displacements 496
Ptosis and Rotation 504
Invasive Renal Cell Carcinoma 505
Perinephritis and Renointestinal Fistulas 505
Renal Agenesis and Ectopia 512
Direct Intestinal Effects Unique to Renal Ectopia 532
References *536*

10 The Duodenocolic Relationships: Normal and Pathologic Anatomy 539
Anatomic and Normal Radiologic Features *539*
Abnormal Radiologic Features *544*
Defect of Mesocolon with Internal Herniation into Lesser Sac 544
Masses Within the Mesocolic Leaves 544
Effect upon the Descending Duodenum by Carcinoma of the Hepatic Flexure 546
Duodenocolic Fistulas 546
Effect of Gallbladder Disease on the Duodenocolic Relationships 549
Duodenocolic Displacements from Right Renal Masses 560
Effect on Colon of Mass Arising in Descending Duodenum 560
Inframesocolic Extension of Neoplasm of Third Duodenum 560
Acute Pancreatitis 561
Duodenojejunal Junction: Relation to Colon 561
References *563*

11 Intestinal Effects of Pancreatitis: Spread Along Mesenteric Planes 565
Anatomic Considerations *565*
Effects of Pancreatitis on the Colon: Spread Along the Transverse Mesocolon *569*
Hepatic Flexure 569
Transverse Colon and Splenic Flexure 569
Effects of Pancreatitis on the Duodenum, Small Bowel, and Cecum: Spread Along Small Bowel Mesentery *584*
Duodenum 584
Small Bowel and Cecum 584
References *593*

12 Pathways of Regional Spread in Pancreatic Cancer 595
Chusilp Charnsangavej, M.D.
Anatomy of the Pancreas 595
Vascular Anatomy 596
Lymphatic Anatomy 597
Pancreatic Nerve Plexus 598
Imaging Studies 598
CT Anatomy of the Pancreatic Head 598
Pathways of Regional Spread in Pancreatic Cancer 599
Local Organ Invasion 599
Vascular Involvement 601
Nodal Metastasis 603
Perineural Invasion 605
Conclusion 605
References 605

13 The Subperitoneal Space: Normal and Pathologic Anatomy 607
Michael Oliphant, M.D., Alfred S. Berne, M.D., and Morton A. Meyers, M.D.
Embryologic Considerations 607
Anatomic Considerations 611
Ventral Mesentery Derivatives 612
Dorsal Mesentery Derivatives 612
Lateral Continuity 614
Continuity with the Female Organs 614
Abnormal Imaging Features 615
References 634

14 The Small Bowel: Normal and Pathologic Anatomy 635
Anatomic Considerations 635
Normal Radiologic Observations 636
Axis of the Root of the Small Bowel Mesentery 636
Undulating Changeable Nature of Coils of Bowel Loops 636
Identification of Mesenteric and Antimesenteric Borders of Small Bowel Loops 640
Abnormal Radiologic Features 644
Diverticulosis of the Small Intestine 644
Meckel's Diverticulum 646
Scleroderma 646
Intestinal Duplication 650
Seeded Metastases 651
Hematogenous Metastases 651
Carcinoid Tumors 652
Regional Enteritis 654
Lymphoma 657
Intramural and Mesenteric Bleeding 657
References 663

15 The Colon: Normal and Pathologic Anatomy 665
Anatomic Considerations 667
Classification of Organization of Haustral Rows 669
Normal Radiologic Observations 670
Abnormal Radiologic Features 675
Lesions Within the Gastrocolic Ligament 675
Lesions Within the Transverse Mesocolon 681
Distinction Between Intraperitoneal and Extraperitoneal Processes 683
Diverticulosis and Diverticulitis 692
Summary 704
References 708

16 Internal Abdominal Hernias 711
Paraduodenal Hernias 712
Anatomic Considerations 712
Clinical Features 713
Radiologic and Arteriographic Features 713
Internal Hernias Through the Foramen of Winslow 731
Pericecal Hernias 737
Intersigmoid Hernias 738
Transmesenteric and Transmesocolic Hernias 739
Hernias Through the Falciform Ligament 744
Retroanastomotic Hernias 744
References 746

17 Pathways of Extrapelvic Spread of Disease 749
Anatomic Considerations 751
Radiologic Findings 752
References 761

Index 763

Contributors

Stephen R. Baker, M.D.
Professor and Chairman
Department of Radiology
University Hospital C320
UMD New Jersey Medical School
150 Bergen Street
Newark, NJ
USA

Alfred S. Berne, M.D.
Professor of Radiology
SUNY Health Science Center
750 East Adams Street
Syracuse, NY
USA

Chusilp Charnsangavej, M.D.
Professor of Radiology
Department of Diagnostic Radiology
The University of Texas M.D. Anderson Cancer Center
1515 Holcombe Boulevard
Houston, TX
USA

Kyunghee C. Cho, M.D.
Professor of Radiology
Department of Radiology
University Hospital C320
UMD New Jersey Medical School
150 Bergen Street
Newark, NJ
USA

Michiel A.M. Feldberg, M.D., Ph.D.
Professor of Radiology
Department of Radiology
University Hospital Utrecht
Heidelberglaan 100
Utrecht 3584 CX
Netherlands

Bruce Javors, M.D.
Chief of G. I. Radiology
Vice-Chairman
Department of Radiology
St. Vincents Hospital and Medical Center
New York, NY
USA

Hiromu Mori, M.D.
Professor and Chairman
Department of Radiology
Oita Medical University
Hasama-Machi
Oita 879-55
Japan

Michael Oliphant, M.D.
Chief of Radiology and Medical Director
Department of Medical Imaging
Crouse Hospital
736 Irving Avenue
Syracuse, NY
USA
and
Clinical Professor of Radiology
SUNY Health Science Center
Syracuse, NY
USA

Catherine Roy, M.D.
Professor of Radiology
Chef de Service
Service de Radiologie B
Les Hopitaux Universitaires de Strasbourg—BP426
F-67091 Strasbourg Cedex
France

Maarten S. van Leeuwen, M.D., Ph.D.
Department of Radiology
University Hospital Utrecht
Heidelberglaan 100
Utrecht 3584 CX
Netherlands

Ronald Wachsberg, M.D.
Associate Professor of Radiology
Department of Radiology
University Hospital C320
UMD New Jersey Medical School
150 Bergen Street
Newark, NJ
USA

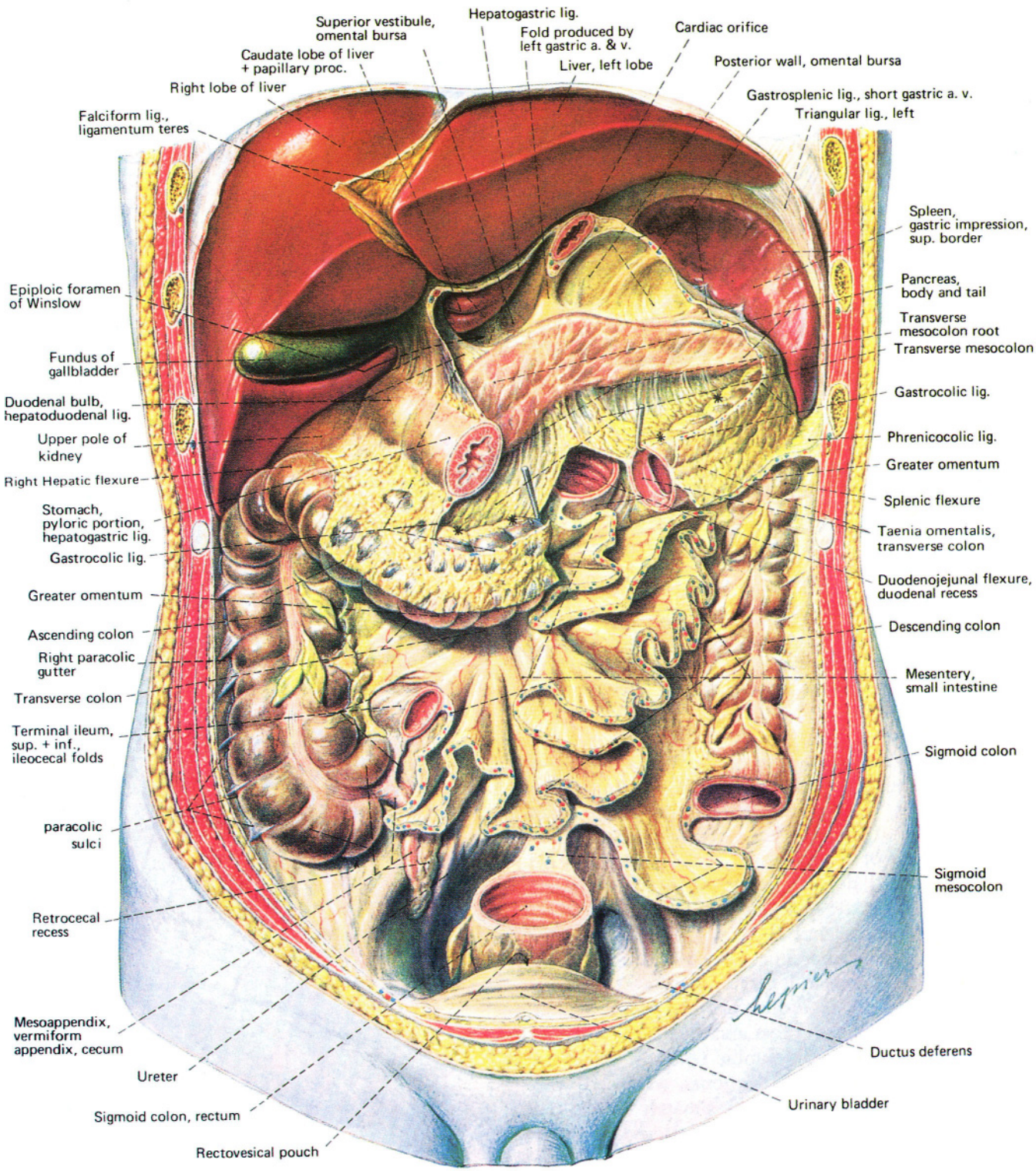


Fig. 1–2. Abdominal viscera.

The stomach has been removed from the cardia to the pylorus, revealing the lesser sac (omental bursa) and structures on the posterior wall.

(From Sobotta, Courtesy of Urban & Schwarzenberg.)

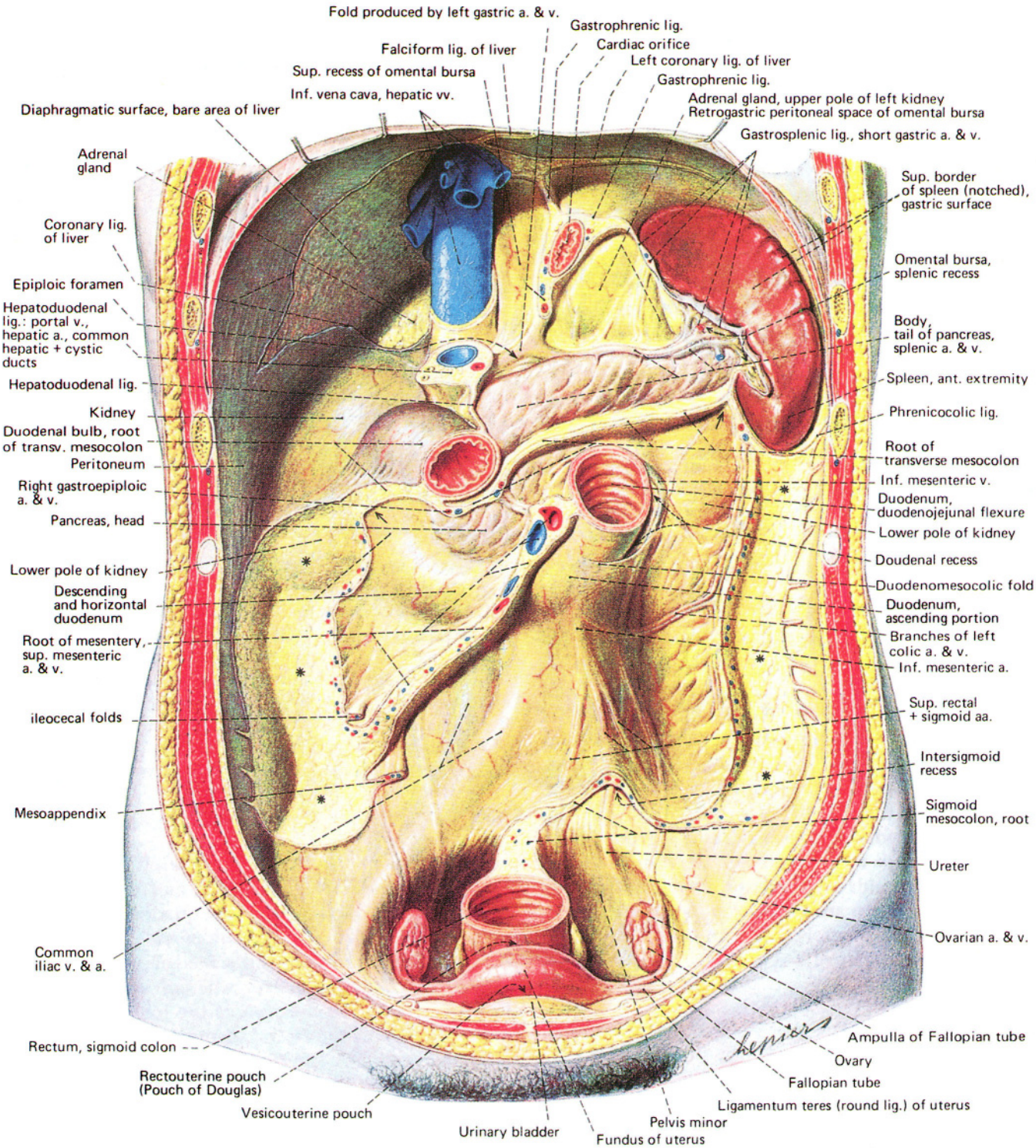


Fig. 1–3. Retroperitoneum of an adult female.
(From Sobotta, Courtesy of Urban and Schwarzenberg.)

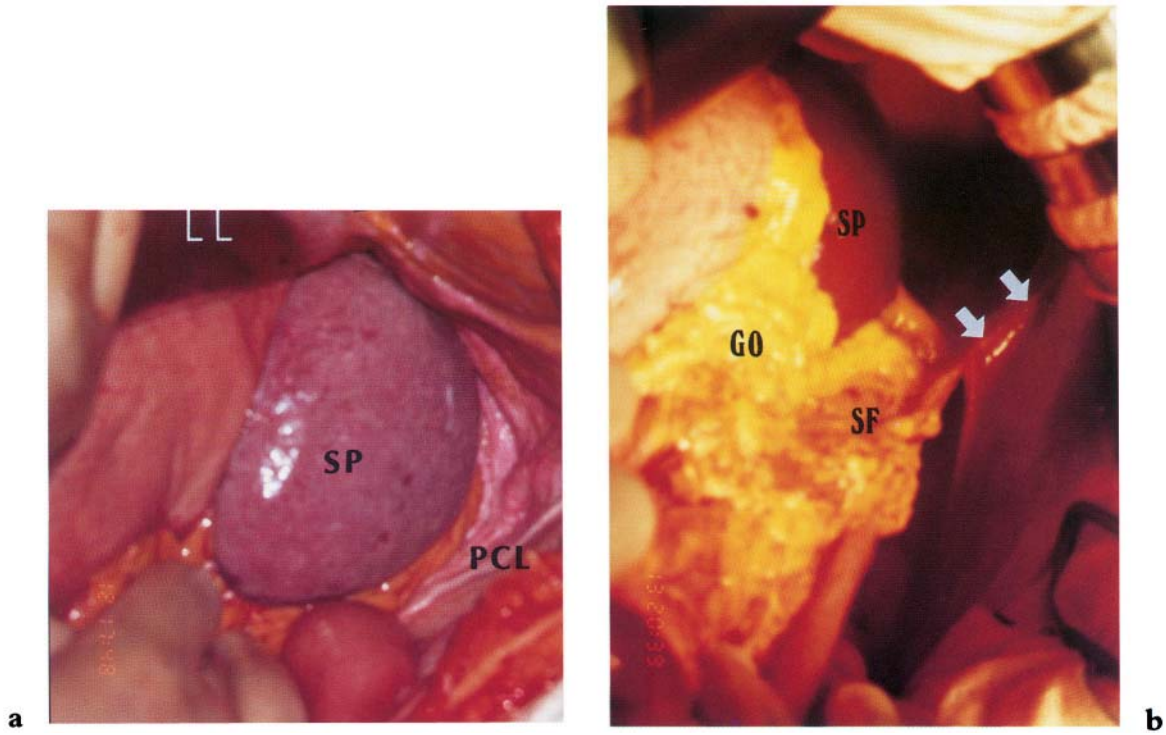


Fig. 3–16. The phrenicocolic ligament as seen at surgery in two different cases.
(a) The phrenicocolic ligament *(PCL)* is the elevated peritoneal fold inferolateral to the spleen *(SP)*. *LL* = left lobe of liver.
(b) After retracting the stomach and greater omentum *(GO)*, the phrenicocolic ligament is apparent as an elevated ridge *(arrows)* extending from the anatomic splenic flexure of the colon *(SF)* posteriorly to the diaphragm. The ligament is seen inferolateral to the spleen *(SP)*.
(Courtesy of Yong Ho Auh, M.D., Asan Medical Center, Seoul, Korea)

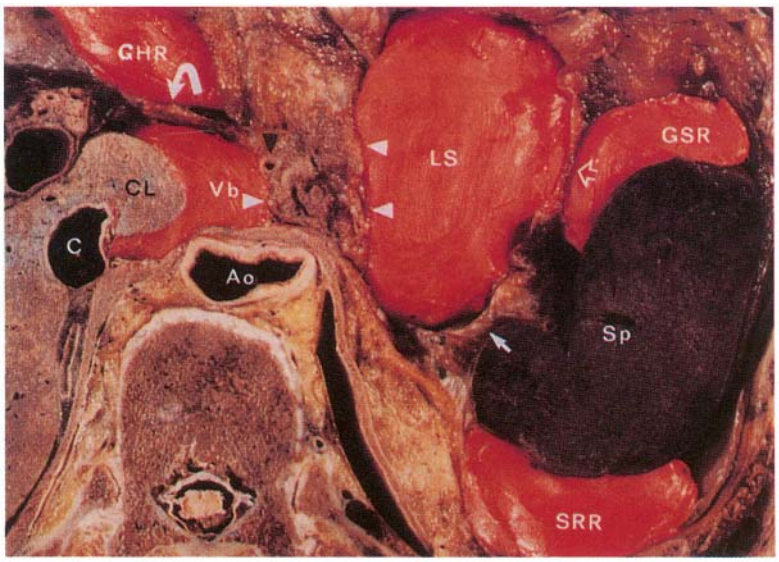
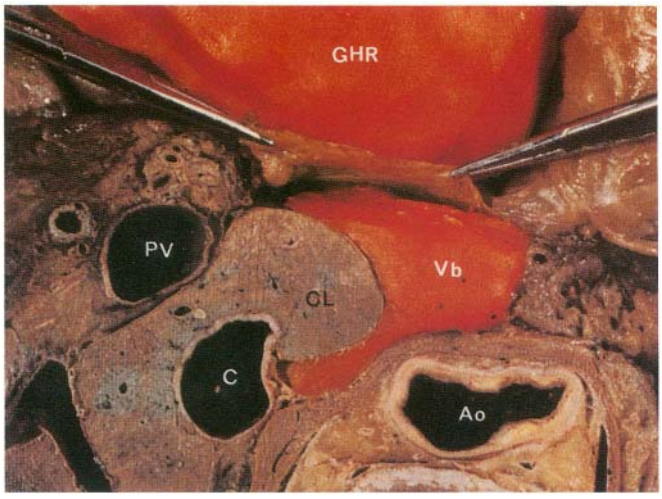
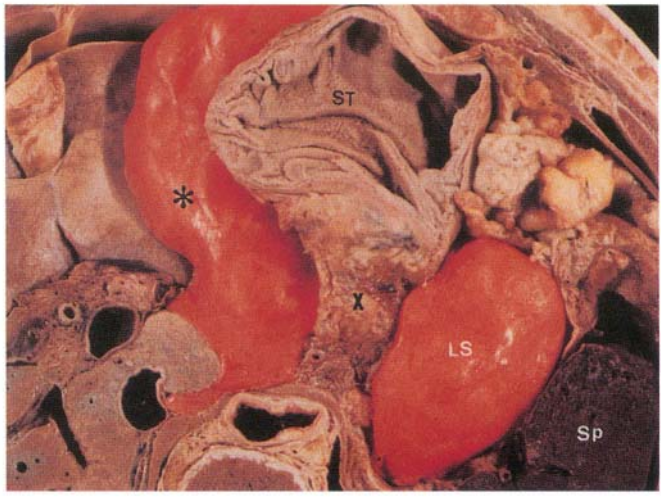


Fig. 3–31. Anatomy of the lesser sac and the gastropancreatic plica.
(a) Anatomic specimen with spaces injected. The gastropancreatic plica *(white arrowheads)*, within which courses the left gastric artery *(black arrowhead)*, is a structure of some dimension. It separates the vestibule *(Vb)* in relationship to the caudate lobe *(CL)* from the larger lateral recess of the lesser sac *(LS)*. The latter is separated by the gastrosplenic ligament *(open arrow)* from the gastrosplenic recess *(GSR)* and by the splenorenal ligament *(white arrow)* from the splenorenal recess *(SRR)*. The vestibule is separated by the gastrohepatic ligament *(curved arrow)* from the gastrohepatic recess *(GHR)*. *Ao* = aorta; *C* = inferior vena cava; *Sp* = spleen.
(Reproduced from Kumpan.[27])

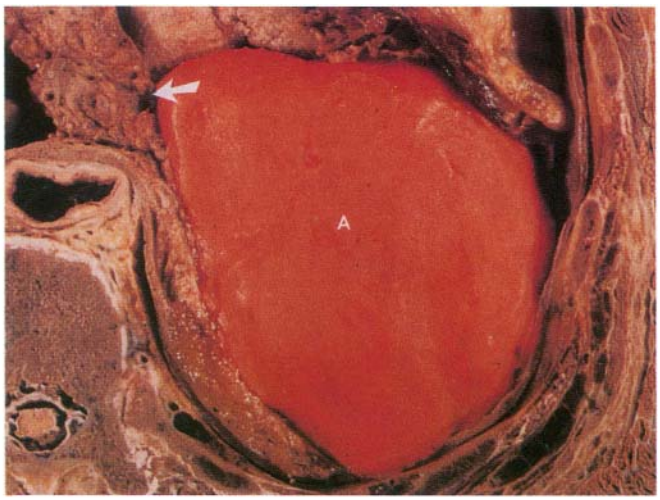


a



b

Fig. 3–110. Abscess localization in postoperative neocompartment following transection of gastrohepatic ligament.
(a) Axial anatomic section with injection to simulate abscess formation within the vestibule *(Vb)* of the lesser sac clearly separated by an intact gastrohepatic ligament (between the clamps) from abscess within the gastrohepatic recess *(GHR)* of the greater peritoneal cavity. *CL* = caudate lobe; *Ao* = aorta; *C* = inferior vena cava; *PV* = portal vein.
(b) After resection of the gastrohepatic ligament, a neocompartment *(asterisk)* is formed by communication of the gastrohepatic recess and vestibule. *X* = gastropancreatic plica; *ST* = stomach; *LS* = lesser sac; *Sp* = spleen.
(Reproduced from Kumpan[27])



b

Fig. 3–112. Abscess localization in postoperative neocompartment.
Following splenectomy with resection of the gastrosplenic and splenorenal ligaments, communication is established between the left subphrenic (perisplenic) space and the lesser sac.
(b) Axial anatomic section with injection after removal of spleen to simulate abscess *(A)*. *Arrow* = gastropancreatic plica.
(Reproduced from Kumpan[27])

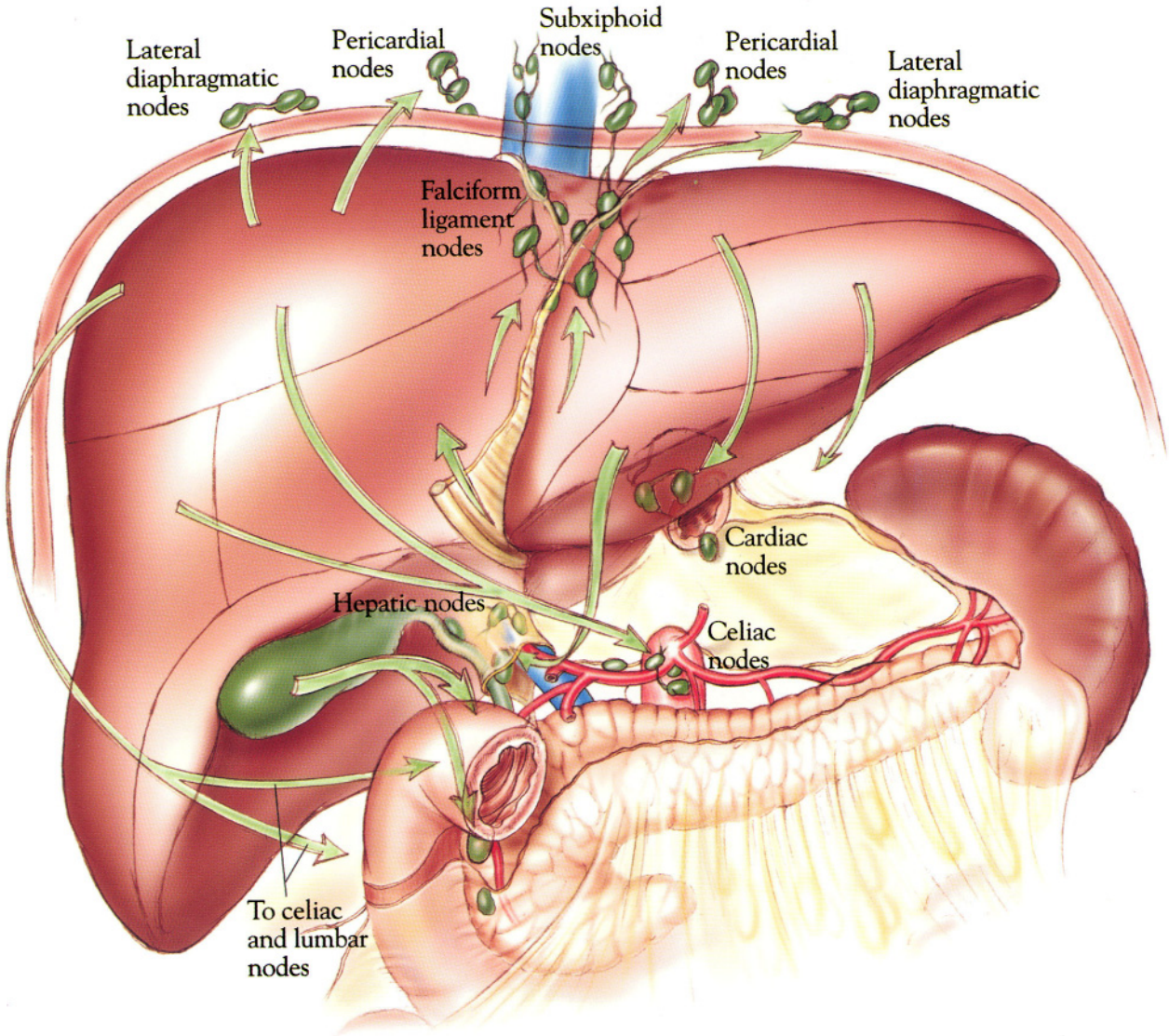


Fig. 6–1. Superficial pathways of lymphatic drainage of the liver.
Note that the anterior diaphragmatic nodes consist of two groups: the lateral anterior diaphragmatic group and the medial group, which includes the pericardiac nodes and the subxiphoid nodes behind the xiphoid cartilage. The nodes in the falciform ligament drain into the anterior abdominal wall along the superficial epigastric and deep epigastric lymph nodes. The epigastric and the subxiphoid nodes drain into the internal mammary nodes.

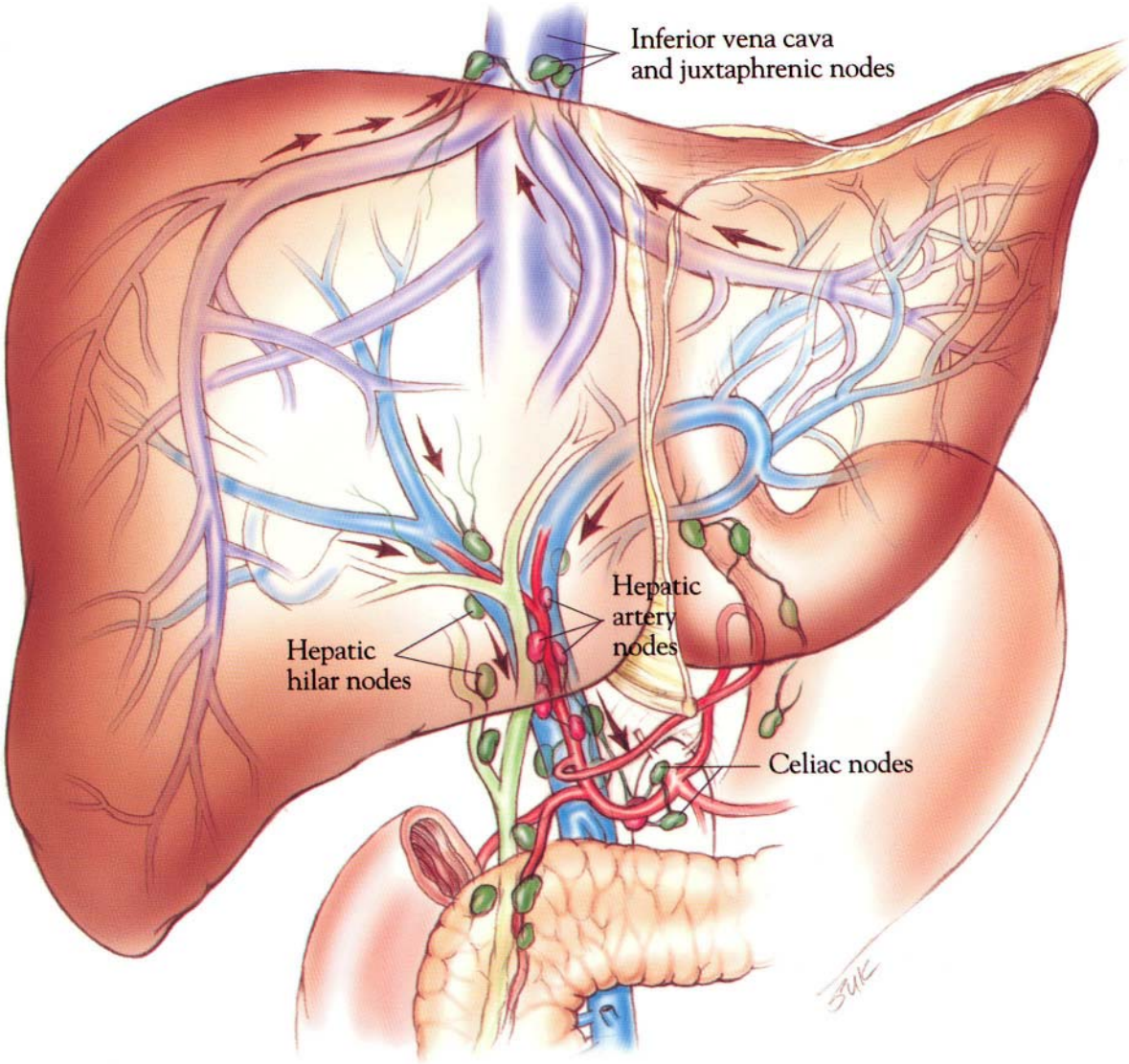


Fig. 6–2. Deep pathways of lymphatic drainage of the liver.
The deep pathways follow the hepatic veins to the inferior vena cava nodes and the juxtaphrenic nodes that follow along the phrenic nerve. These nodal groups are considered as the middle diaphragmatic nodes. The pathways that follow the portal vein drain to the hepatic hilar nodes and the nodes in the hepatoduodenal ligament. They drain into the celiac node and the cisterna chyli.

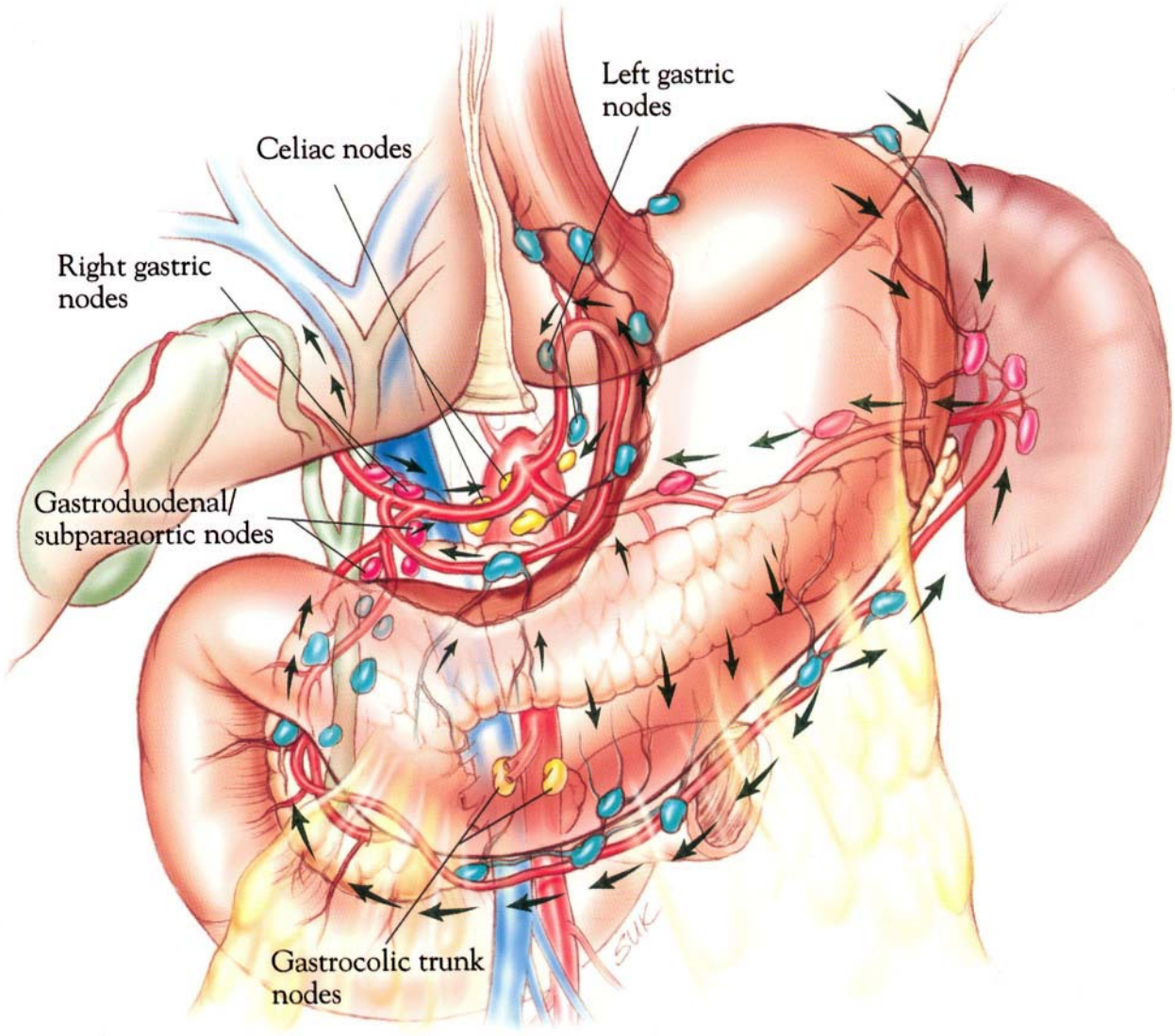


Fig. 6–7. Pathways of lymphatic drainage of the stomach.

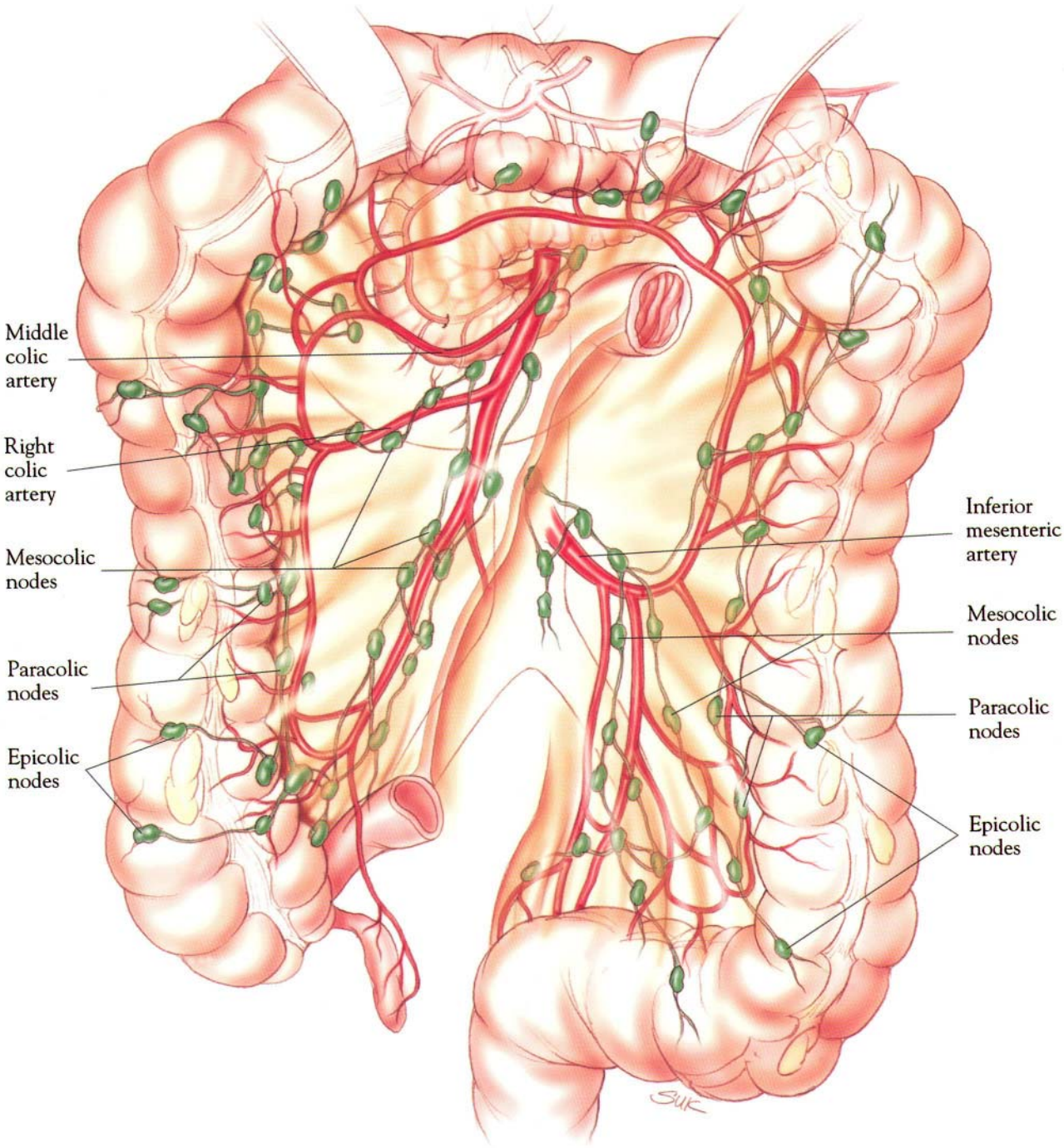
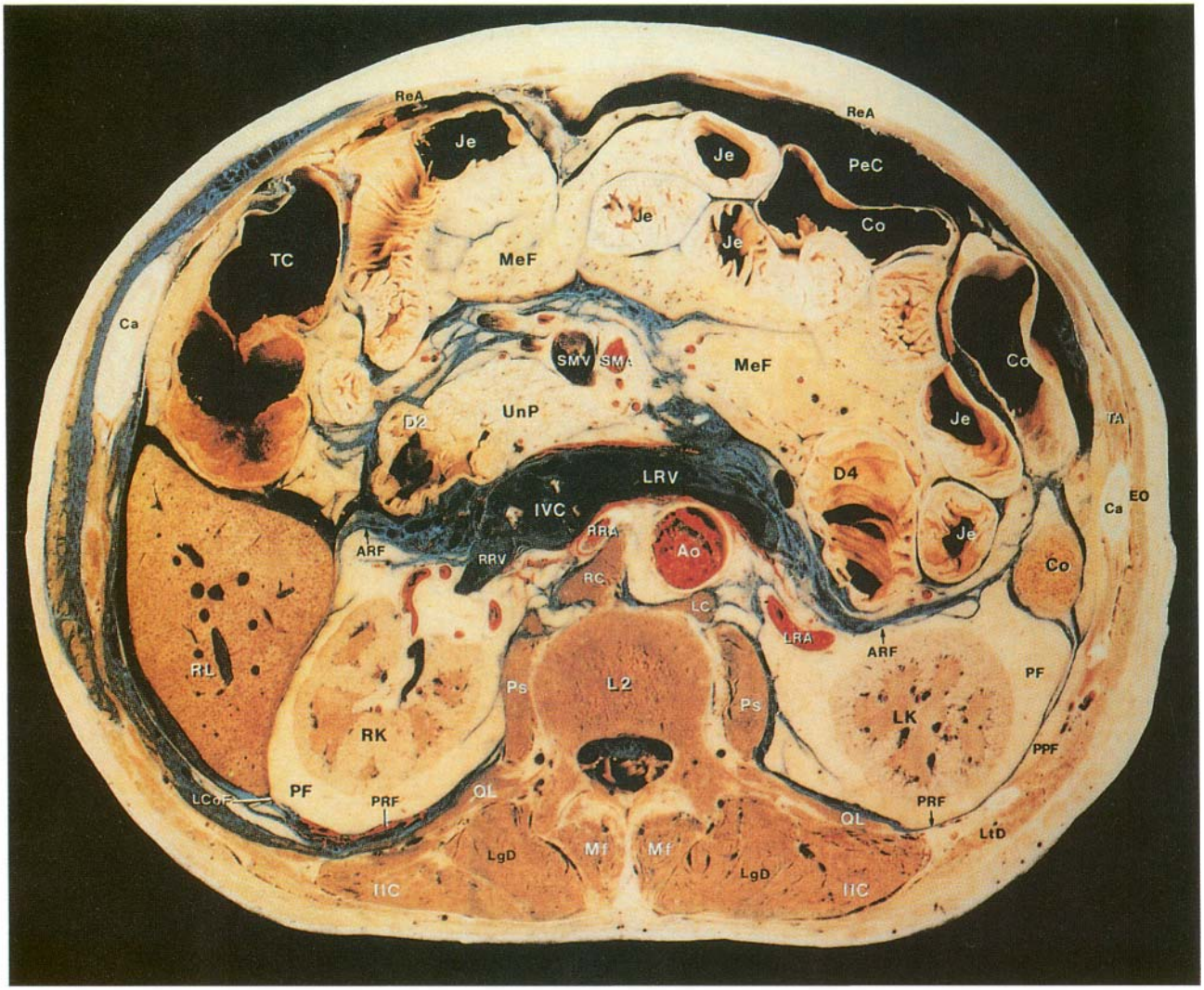


Fig. 6–13. Pathways of lymphatic drainage of the colon.



a

Fig. 8–17. Transverse anatomic cross-sections.

Connective tissues of spaces as well as mesenteries and fasciae are stained by dye permeation.

(a) Level of uncinate process of pancreas and renal arteries.

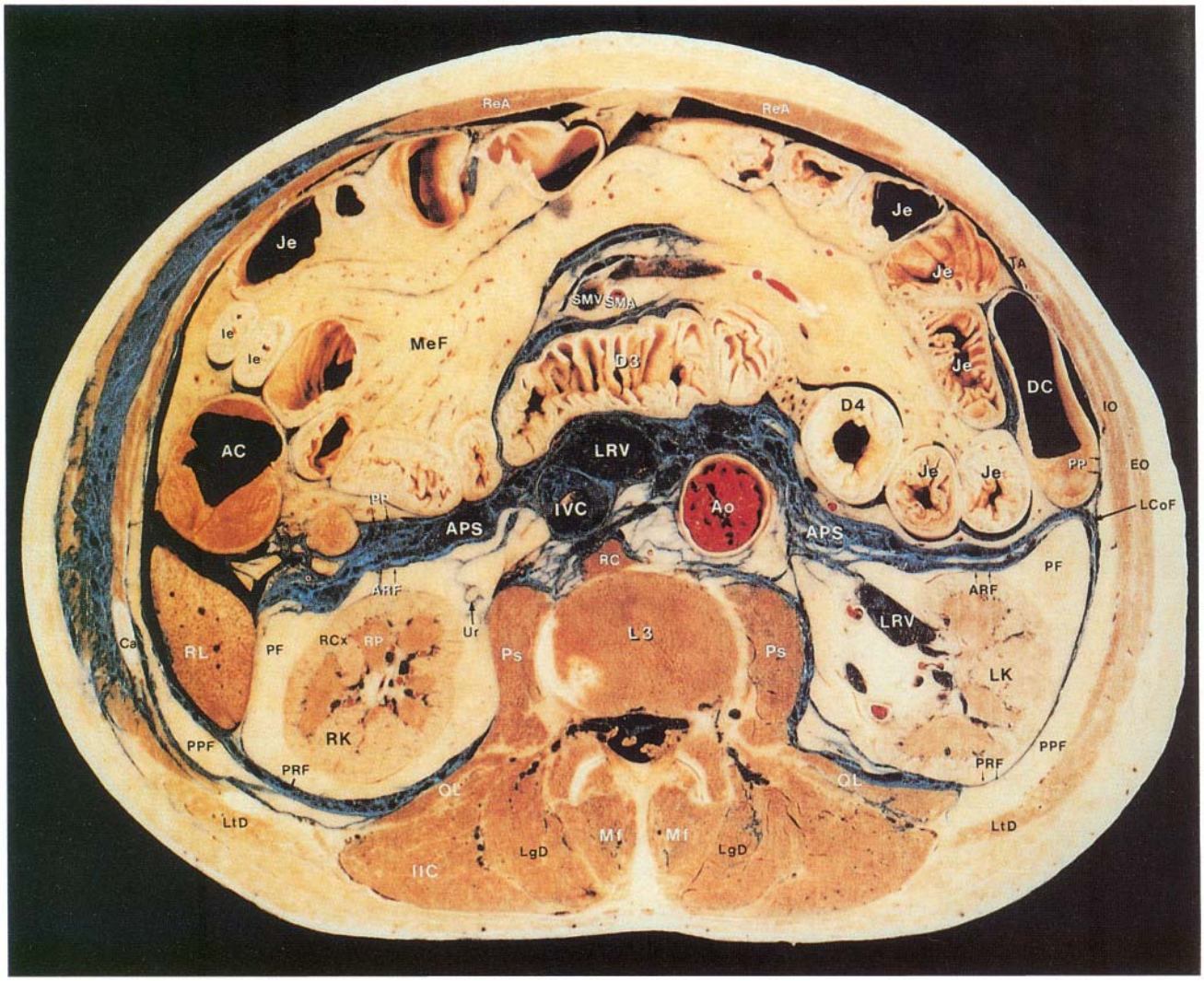
(b) Level of third portion of duodenum and the infrarenal abdominal aorta.

These stained sections demonstrate particularly relevant features:

1. Anatomically, the anterior pararenal space is potentially continuous across the midline.
2. The perirenal spaces at these levels share no bilateral continuity; there is midline termination of the anterior renal fascia.
3. The anterior pararenal space ventrally is anatomically continuous with the roots of the small bowel mesentery and similarly of the transverse mesocolon. Lesions of the perirenal contents, including the kidneys and adrenals, are provided anatomic continuity along their major vessels to the aorta and inferior vena cava and thereby to the small bowel mesentery and transverse mesocolon. Extraperitoneal and intraperitoneal structures constitute the continuum designated as the subperitoneal space. This is fully discussed in Chapter 13.
4. Rupture of an abdominal aortic aneurysm can be anticipated as likely occurring into the perirenal space or dissecting into the posterior pararenal space or psoas muscle on the left. Anatomic considerations include the point of rupture both on the circumference of the aorta and on the cephalocaudal level. Other factors include the acuity, force, and volume of the rupture and preexisting adhesions.

(Reprinted with permission from Han M-C, Kim C-W: Sectional Human Anatomy, 2nd ed. Ilchokak, Seoul, Korea, 1989.)

Continued on following page



b

AC = Ascending colon
APS = Anterior pararenal space
ARF = Anterior renal fascia
Ao = Aorta
Ca = Cartilage
Co = Colon
D2 = Second portion of duodenum
D3 = Third portion of duodenum
D4 = Fourth portion of duodenum
DC = Descending colon
EO = External oblique muscle
IO = Internal oblique muscle
IVC = Inferior vena cava
IE = Ileum
IlC = Iliocostalis muscle
Je = Jejunum
L1-2 = L1-2 intervertebral disc
L2 = L2 vertebral body
L3 = L3 vertebral body
LC = Left diaphragmatic crus
LCoF = Lateroconal fascia
LK = Left kidney
LRA = Left renal artery
LRV = Left renal vein
LgD = Longissimus dorsi muscle
LtD = Latissimus dorsi muscle
MeF = Mesenteric fat
Mf = Multifidus muscle
PF = Perirenal fat
PP = Parietal peritoneum
PPE = Posterior pararenal fat
PRE = Posterior renal fascia
PeC = Peritoneal cavity
Ps = Psoas muscle
OL = Quadratus lumborum muscle
RC = Right diaphragmatic crus
RCx = Renal cortex
RK = Right kidney
RL = *Right* lobe of liver
RP = Renal pelvis
RRA = Right renal artery
RRV = Right renal vein
ReA = Rectus abdominis muscle
Ri = Rib
SMA = Superior mesenteric vein
TA = Transversus abdominis muscle
TC = Transverse colon
UnP = Uncinate process of pancreas, head
Ur = Ureter

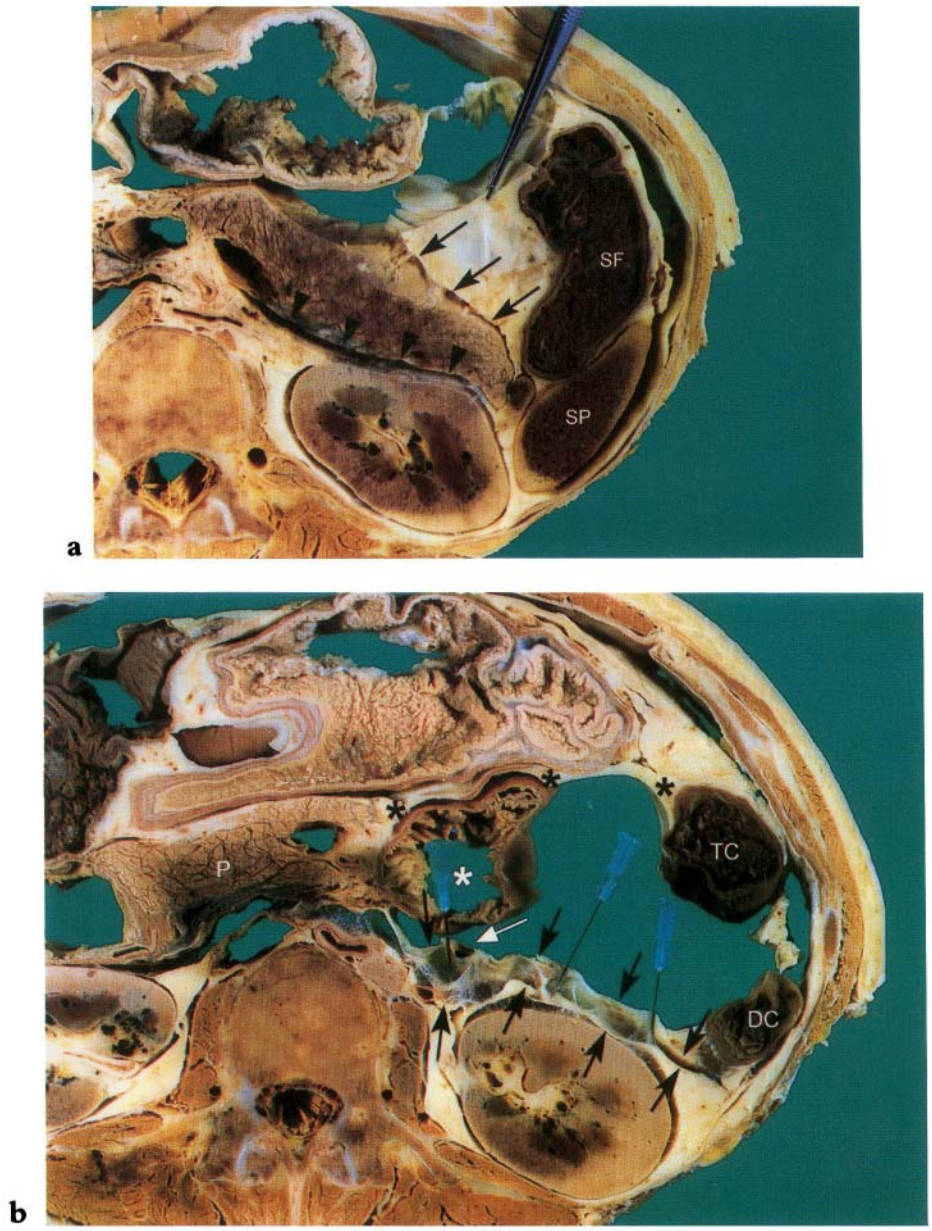


Fig. 8–108. Anatomic sections of fusion fasciae.
(a) Section at the level of the pancreatic tail, with slight anterior traction on the left colonic fat. The mesenteric fat medial to the splenic flexure *(SF)* of the colon portrays the continuity between transverse mesocolon mediocranially and left colonic compartment laterocaudally. Note the loose areolar tissue *(arrows)* between this mesenteric fat and the pancreatic tail, representing the fusion fascia posterior to the transverse mesocolon medially and the cranial extension of the left retromesenteric plane, also called left fascia of Toldt, laterally. A space, also bridged by loose areolar tissue *(arrowheads),* appears between the pancreatic tail and perirenal space, representing the fusion fascia between the left pancreaticoduodenal compartment and primitive retroperitoneum. *SP* = spleen.
(b) Section at the level of pancreatic head *(P)* and neck, with traction on the left colonic compartment. The left colonic compartment is demarcated from the primitive retroperitoneum by loose areolar tissue representing the left retromesenteric plane *(black arrows).* Anteriorly, the transverse mesocolon *(black asterisks)* attaches to the pancreatic neck, posterior to the stomach, and anterior to the duodenojejunal junction *(white asterisk)* in the left paraduodenal fossa. *White arrow* = inferior mesenteric vein; *DC* = descending colon; *TC* = transverse colon.

Continued on following page

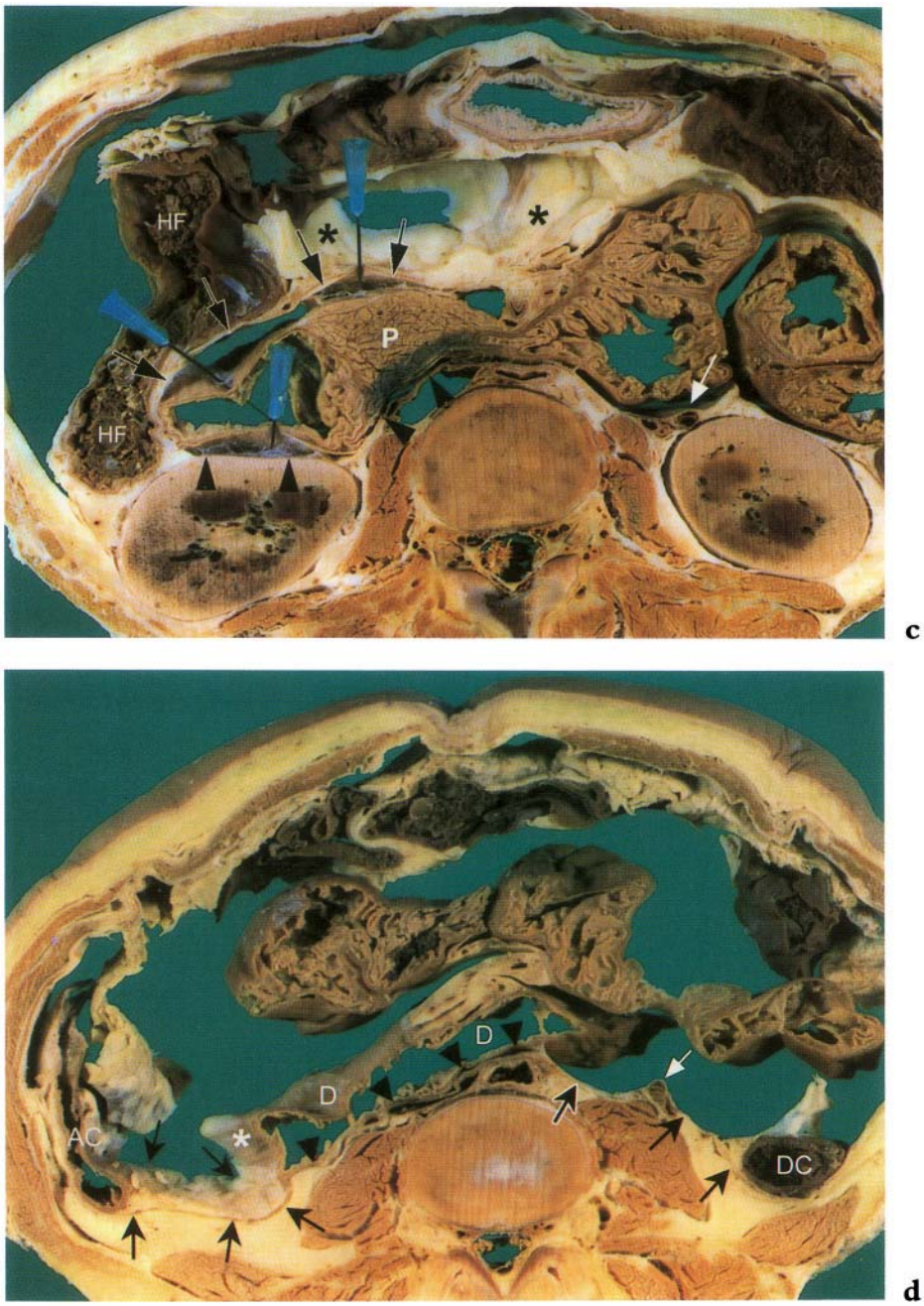


Fig. 8–108. (Continued) (c) Section at the level of the pancreatic head *(P).* The right pancreaticoduodenal compartment is demarcated posteriorly by the loose areolar tissue of the retropancreaticoduodenal fusion fascia *(arrowheads),* also called fascia of Treitz, and anteriorly by the loose areolar tissue of the cranial extension of the right retromesenteric plane, also called right fascia of Toldt *(arrows).* Note the continuity of the transverse mesocolon *(asterisks)* with the right colonic compartment, located anterior to the right perirenal space. *White arrow* = inferior mesenteric vein; *HF* = hepatic flexure.
(d) Section below the level of the pancreatic head, demonstrating the slender right and left colonic compartments at this level *(black arrows).* Note how the right colonic compartment covers the right side of the pancreaticoduodenal compartment *(white asterisk),* while the medial extension of the left colonic compartment *(black-and-white arrow)* lies posterior to the left extension of the horizontal part of the duodenum *(D).* The retropancreaticoduodenal fusion fascia is located posterior to the duodenum and anterior to the primitive retroperitoneum, aorta, and inferior caval vein. *AC* = ascending colon; *DC* = descending colon.

General Considerations: Dynamics of Image Analysis

1

Normal Anatomic Relationships and Dynamic Principles of Pathways of Spread and Localization of Disease

A basic knowledge of normal anatomic relationships and variants is essential to understanding the effects of pathologic processes. Fundamental considerations include constant anatomic landmarks, variations in positions of structures, relationships maintained and bounded by peritoneal and fascial attachments, distribution of intraperitoneal and extraperitoneal fat providing the contrasting interfaces of organ and viscus contours, and governance of the spread and localization of many diseases by specific anatomic characteristics and general physical laws.

Since abdominal symptoms are commonly nonspecific, there are many clinical instances in which the site of primary disease is not clear originally. Radiologic investigation is often initiated by a study focusing attention on another organ or body system. Abnormal findings peripheral to the anticipated area of interest may therefore be of considerable importance in directing attention immediately to the true primary site of disease. A primary site of disease in the abdomen or pelvis may spread along specific pathways, governed by anatomic and physical factors, to a remote site. In many instances, this discrete locus of dissemination may be anticipated and therefore diagnosed at its earliest stage. Conversely, it is not rare that a patient may first present with disease remote from a clinically occult primary site. An integrated understanding of the pathways of spread and localization then reveals the true nature of the condition.



Fig. 1–1. W.E. Hill's "My Wife and My Mother-in-Law."
Both images are present in the drawing. The viewer first sees either an old woman or a young lady. The old woman's prominent nose in profile is the young woman's chin. This drawing illustrates that perception is determined by the relationships.

Figure 1–1 illustrates that the image one first sees is determined by the relationship established between individual features. In a similar manner, clinical and radio-

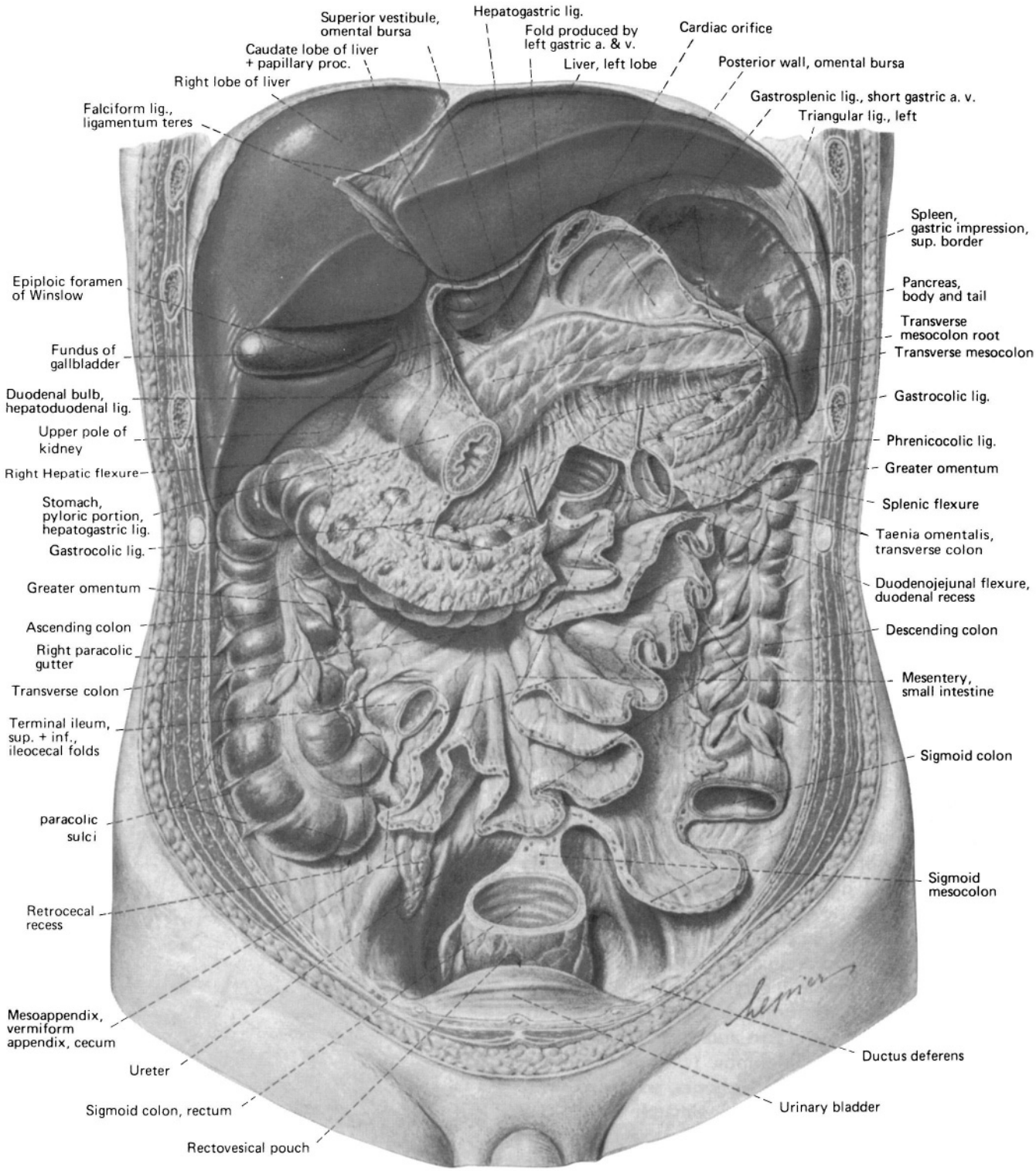


Fig. 1–2. Abdominal viscera.
The stomach has been removed from the cardia to the pylorus, revealing the lesser sac (omental bursa) and structures on the posterior wall. **(This figure also appears in the color insert.)**
(From Sobotta, Courtesy of Urban & Schwarzenberg.)

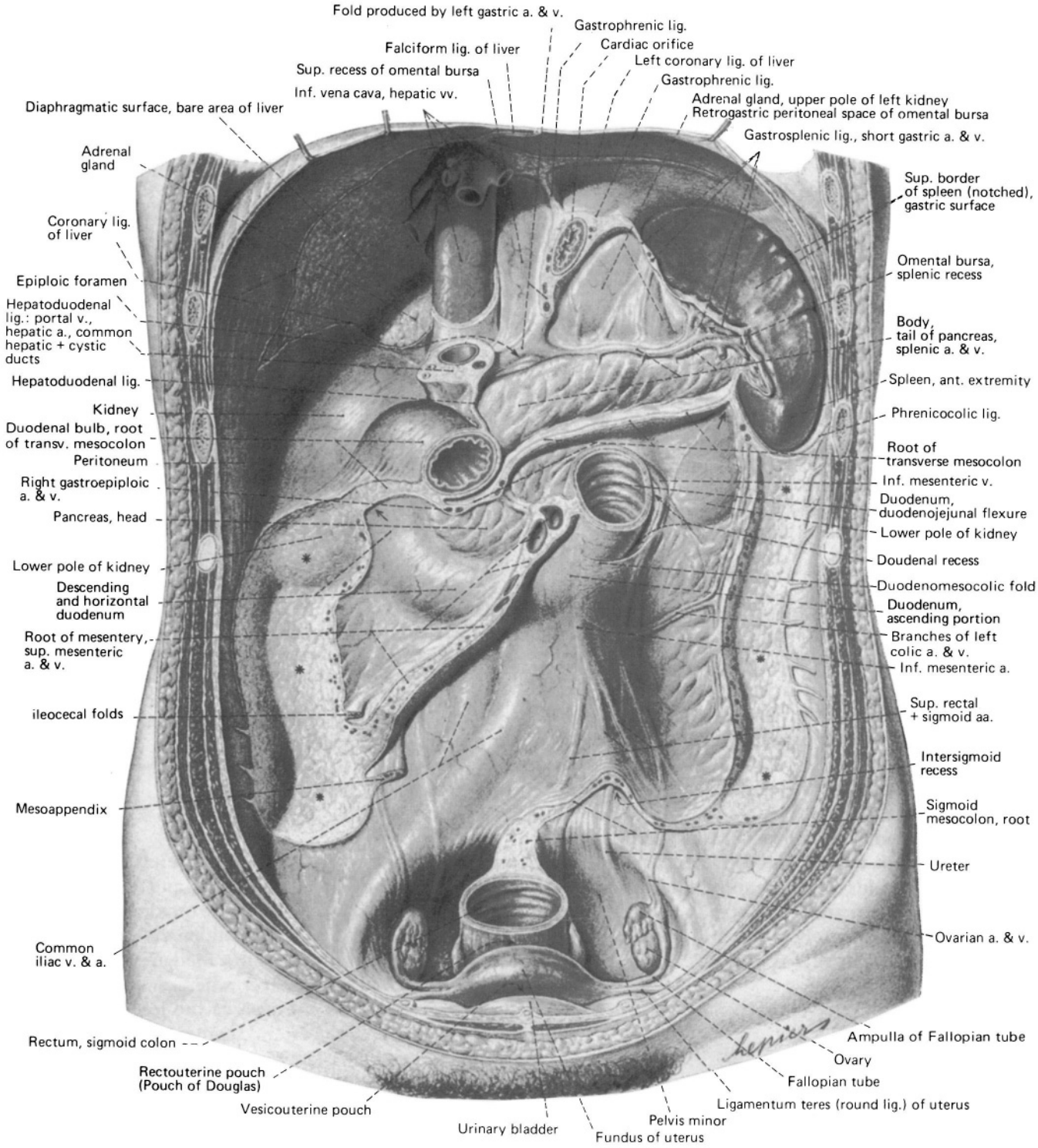


Fig. 1–3. Retroperitoneum of an adult female. (This figure also appears in the color insert.)
(From Sobotta, Courtesy of Urban and Schwarzenberg.)

logic diagnosis is based on the extraction of a set of features characteristic of a particular process. Deviation from the normal, however, must be recognized before a lesion can be suspected.

Figures 1–2, 1–3, and 1–4 illustrate a detailed overview of the complex anatomic relationships within the abdomen and pelvis. Critical intimate relationships, crossroads, planes of diminished resistance, and channels of flow as influenced by gravity and subatmospheric pressures provide the key for accurate diagnosis and therapy involving the spread and localization of intra-abdominal disease.

Visual Factors: Perception of the Image

Visual search is the first step in reading a radiograph. At the luminance available for reading an abdominal x-ray, photopic vision is employed. This allows for the greatest visual acuity when the image is focused on the fovea centralis. However, this is a relatively small area owing to the fact that the cones, which are responsible for visual acuity, are concentrated at the fovea, especially at its center, and this accounts for the rapid decline in acuity just a few degrees from the fovea centralis. Of necessity, then, peripheral vision is used as the initial step in reading a radiograph. Use of peripheral vision allows for a considerably larger, although not as acute, field of vision in which to select possible abnormal areas from numerous areas of suboptimal quality images projected on the retina. There is a direct relationship between visual field size and the time required to locate a target.[1] After an object of possible interest is located, the eye then moves to a position that focuses the fovea centralis on this point. In this position, detailed information can be obtained.

After an area of interest is identified, the eye moves to another area of interest.[2,3] Each movement, known as

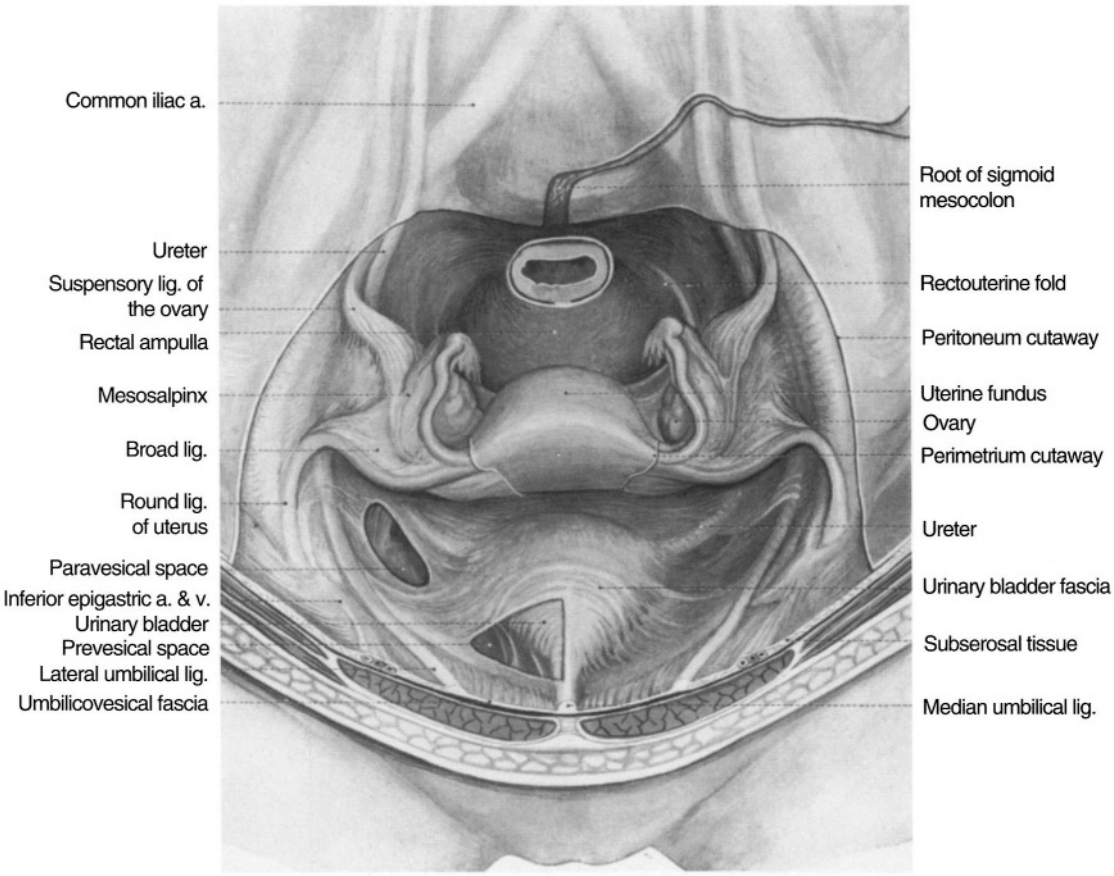
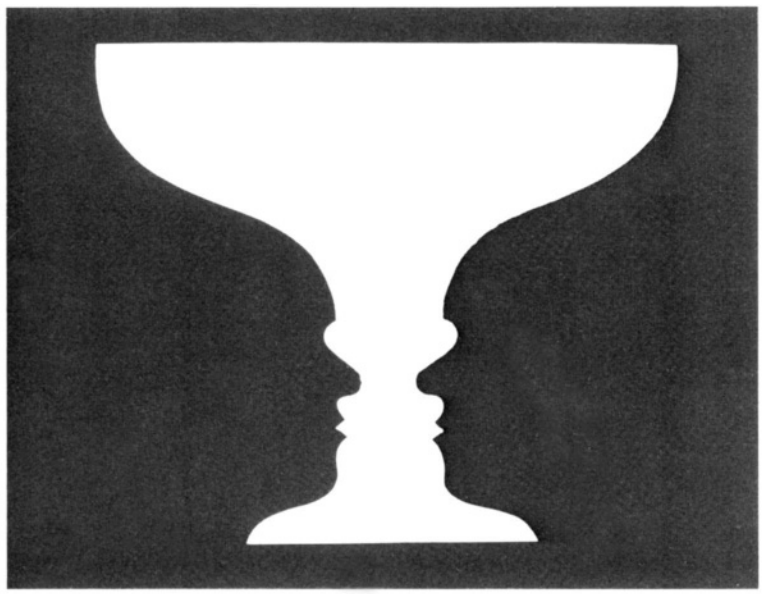
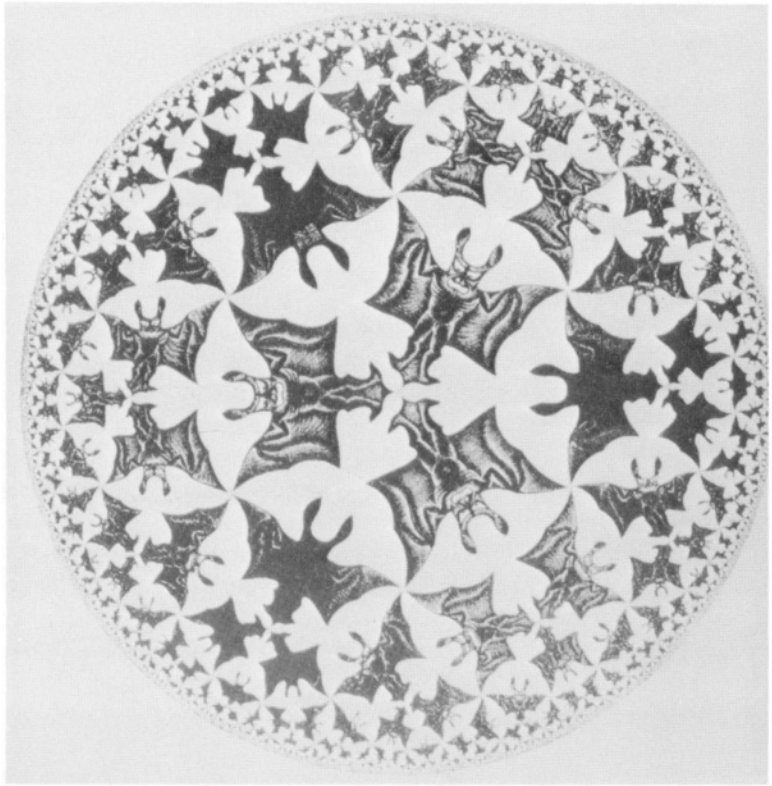


Fig. 1–4. Pelvic contents and relationships of an adult female.



a



b

Fig. 1–5. Examples of multistability and figure-ground reversal.
(a) The white area can be viewed as a goblet or the black area as the silhouettes of two profiles. Both images, however, cannot be perceived simultaneously.
(b) The black images can be seen as devils or the white outlines as angels. (Reproduced from M. Escher.)

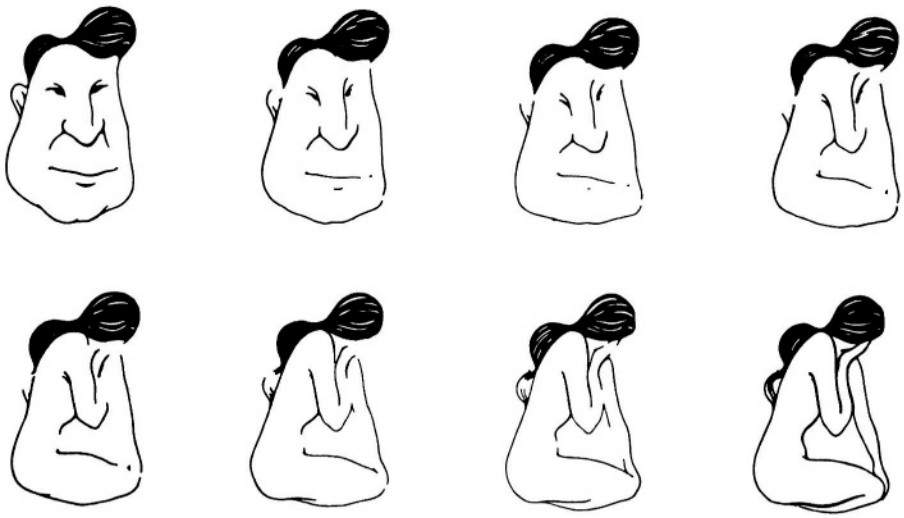


Fig. 1–6. A drawing of a man's face subtly changes to the outline of a young female.
The transition point is dependent not only on subjective variations but on the sequence followed.

a saccade, allows for the fovea centralis to fix on a new point of interest. Typically there are two to three saccadic movements per second. The actual visual fixations occupy 90% of viewing time and the saccadic movements 10%. The normal human eye, using photopic vision, can resolve a visual angle of only 2.0°. Translated to reading a 14 × 17 in. film of the abdomen, this means that at 30 in. detailed vision is equal to a circle of 1 in. in diameter, or that 300 separate eye fixations are necessary to cover the entire film.[4]

Visual fixations tend to cluster around angles and sharp curves.[2,3] In addition, if a contour is unpredictable or unusual, that is, it changes direction irregularly and rapidly, visual fixation also will cluster at these points. Wide individual variations in regard to search patterns by radiologists are influenced by prior knowledge.[4,5]

In addition to topographic changes, other factors such as contrast, size, and shape are important. A target of relatively high contrast will be rapidly detected by peripheral vision. Also, a single high-contrast target that occupies an empty field is detected easily and almost immediately fixated.[6] Similar items of the same shape and size take a prolonged time to detect if the contrast is low.[7] Size and luminance also have been shown to affect eye fixation.[8]

It can be concluded that the brain has chosen certain informative details in order to remember or recognize an object. This internal perception within the brain can then take place either by the serial recognition or by the one-step holistic process. Recent evidence, especially in regard to visual perception, tends to support the step-by-step theory. Visual perception and internal perception are not mechanical recordings of elements, but working together are the means for grasping significant structural patterns.[9] Examples of this are dramatically illustrated by figure-ground reversal or multistability in perception[10] (Fig. 1–5). How one image superimposed upon another or projected within another is appreciated visually is determined by which is seen as the figure and which is perceived as the background. The factors that influence the perception of shape in the basic figure-ground relationship of any picture have been extensively studied,[11–14] and are directly applicable to analysis of images of the abdomen and pelvis. These laws of visual organization involve area, closedness, symmetry, and continuity. The smaller a closed region, the more an area has closed contours; the more symmetrical a closed region, the more it tends to be seen as a figure. It is often these features that permit the identification of an abnormality discriminated from the background of normalcy.[15]

The point of basic interest in multistable images that spontaneously alternate, as in Figure 1–5, is that one line can have two shapes. A simple curved line is convex on one side but concave on the other. The perceptual representation of a contour is specific to which side is regarded as primary. This achieves added significance when one regards the internal representation or memory of an object as a step-by-step process.

It must also be appreciated, however, that expecta-

tions that the reader brings to a film may be misleading. This has been demonstrated by psychologists by a series of drawings with subtle progressive differences until the last panel depicts an illustration radically different from the first (Fig. 1–6). The recognizable point of transition where the image shifts in the viewer's perception is different, depending whether the viewer traces the series from left to right or backward. This illustrates that preconditioning—in other words, the concepts of expectation, prior knowledge, and experience—determine in large measure visual perceptions. "Perception depends on learning. It is not that (the radiologist) will see only what he expects to see, but that he will also see what contradicts his expectations."[16] The influence of prior knowledge aids the radiologist not only to fixate on important areas of an image, but to search or scan other areas to confirm or refute his or her memory expectation. Distinction is made between perceptual errors, in which image features are not appreciated, and cognitive or reasoning errors, in which the image features, though appreciated, lead to wrong conclusions.[17] In wide experiences, perceptual error and underreading (false-negative errors) occur many times more frequently than cognitive error or overreading (false-positive errors).[17,18]

The limitations to computational theories of perception that integrate work in neurophysiology, psychology, and artificial intelligence[19,20] testify to the astonishing complexity and sophistication of human vision.

References

1. Johnston D: Search performance as a function of peripheral acuity. Hum Factors 1965; 7:527–535.
2. Noton D, Stark L: Scan paths in eye movements during pattern reception. Science 1971; 171:308–311.
3. Noton D, Stark L: Eye movements and visual perception. Sci Am 1971; 224:34.
4. Llewellyn TE, Landown EL: Visual search patterns in radiologists in training. Radiology 1963; 81:288–292.
5. Kundel HL, Wright DJ: The influence of prior knowledge on visual search strategies during viewing of chest radiographs. Radiology 1969; 93:315–320.
6. Lusted LB: Applications of signal detectability theory. *In* Symposium on Perception of the Roentgen Image. Radiol Clin North Am 1969; 7:435–445.
7. Thomas EL: Search behavior. Radiol Clin North Am 1969; 7:403–417.
8. Steinman RM: Effect of target size, luminance, and color on monocular fixation. J Opt Soc Am 1965; 55:1158–1165.
9. Arnheim R: Art and Visual Perception. A Psychology of the Creative Eye. University of California Press, Berkeley, 1971.
10. Attneave F: Multistability in perception. Sci Am 1971; 225:62.
11. Cornsweet TN: Visual Perception. Academic Press, New York, 1970.
12. Dodwell PC: Visual Pattern Recognition. Holt, Rhinehart & Winston, New York, 1970.
13. Koffka K: Principles of Gestalt Psychology. Harcourt, Brace, New York, 1935.
14. Wertheimer M: Principles of perceptual organization. *In* Readings in Perception. Edited by D Beardslee, M Wertheimer. Van Nostrand, Princeton, NJ, 1958, pp 115–135.
15. Meyers MA, Oliphant M: Pitfalls and pickups in plain-film diagnosis of the abdomen. Curr Probl Radiol 1974; 4(2):1–37.
16. Hebb DO, Favreau O: The mechanism of perception. *In* Symposium on Perception of the Roentgen Image. Radiol Clin North Am 1969; 7:393–401.
17. Kundel HL: Perception errors in chest radiography. Semin Respir Med 1989; 10:203–210.
18. Renfrew DL, Franken EA Jr, Berbaum KS, et al: Error in radiology: Classification and lessons in 182 cases presented at a problem case conference. Radiology 1992; 183:145–150.
19. Marr D: Vision: A Computational Investigation into the Human Representation and Processing of Visual Information. WH Freeman, San Francisco, 1982.
20. Hoffman DD: Visual Intelligence: How We Create What We See. WW Norton, New York, 1998.

Clinical Embryology of the Abdomen: Normal and Pathologic Anatomy

2

Bruce R. Javors, M.D.
Hiromu Mori, M.D.
Morton A. Meyers, M.D.
Ronald H. Wachsberg, M.D.

An understanding of the rudiments of embryologic development is essential not only to a fuller appreciation of the anatomic structures and their dynamic relationships in the abdomen and pelvis but also to the critical awareness of congenitally based disorders that may be initially manifested into adulthood. These disorders may be clinically encountered in a wide spectrum involving the digestive and urogenital tracts, including the peritoneal cavity and its mural structures. Clinical presentations range from an asymptomatic condition in which the findings might even be misinterpreted or vague nonspecific symptoms to episodic distress or an acute fulminating crisis. Imaging plays a critical role in their diagnosis.

The final positions and relationships of the abdominal organs and structures can be traced in large part to the branching, growth, and rotation of an originally straight tubular gastrointestinal tract as well as to three generations of renal primordia. Although their development may be conceived as individual events, many of these organs develop and even regress simultaneously.

Early Development of the Embryo

After fertilization, the zygote undergoes a rapid transformation into a ball of cells and then into a trilaminar disc with three distinct layers: endoderm, mesoderm, and ectoderm. The endoderm becomes the lining of the gastrointestinal tract, as well as the liver and pancreatic glandular tissue. The ectoderm gives rise to the epidermis and nervous system. Most other tissue is derived from the mesoderm.

The mesodermal middle layer of this disc develops a lateral cleft in connection with the yolk sac[1] (Fig. 2–1). Eventually, the lateral margins move ventrally and medially to encompass the yolk sac (Fig. 2–2). This incorporates the intraembryonic coelom to form a tube within a tube. The outer tube is the body cavity while the inner tube is the primitive gastrointestinal tract. The inner tube maintains a posterior attachment to the body cavity via a dorsal mesentery. Most of its ventral attachment involutes, except at the level of the distal foregut.[2]

Diaphragm

The fourth to sixth weeks of development mark the division of the coelom into the definitive pericardial, pleural, and peritoneal spaces. The pleuropericardial membranes, mesenchyme derived from the septum transversum, the dorsal mesentery of the esophagus, and myoblasts from the abdominal wall all contribute to the formation of the diaphragm (Fig. 2–3).

Failure of the diaphragmatic components to properly unite may leave an opening, especially on the left, for abdominal contents to pass into the thorax (foramen of

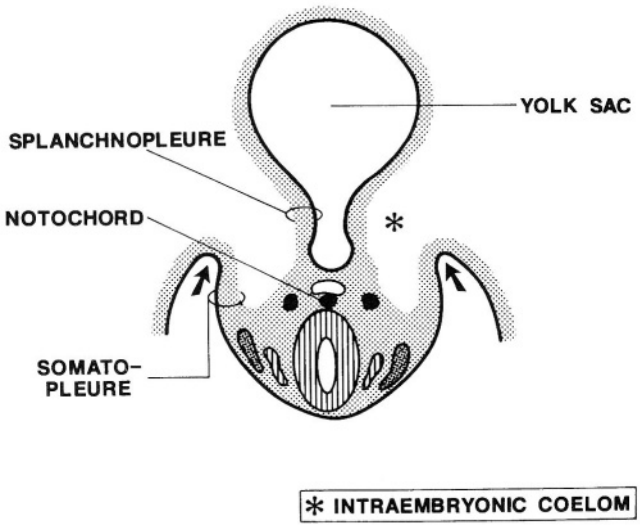


Fig. 2–1. Cross-sectional schematic through the midportion of the embryo early in the fourth week shows infolding of the ectoderm and mesoderm (somatopleure) as it begins to encase the intraembryonic coelom. This will eventually encompass the body cavity. The splanchnopleure's (endoderm and mesoderm) contribution to the formation of the midgut is evident as well.
(From Javors BR, Sloves JH.[4])

Bochdalek hernia)[2,3] (Fig. 2–4). A retrosternal weakness (more frequently on the right) at the defect through which the superior epigastric vessels pass may allow herniation of omentum and, less likely, colon through the resultant foramen of Morgagni.[4]

Gastrointestinal Tract

The primitive gastrointestinal tract starts out as a relatively straight tube. In the distal foregut, it maintains both its ventral and dorsal mesenteries. The ventral mesentery that lies between the distal foregut (stomach and duodenum) and the liver forms the gastrohepatic and, more distally, the hepatoduodenal ligaments.[5] That portion of the ventral mesentery that lies between the developing liver and the anterior abdominal wall persists as the falciform ligament, with the obliterated umbilical vein (ligamentum teres) lying in its free edge. However, during the second month of development, the distal foregut undergoes asymmetric growth with the dorsal aspect growing much more rapidly. Along with this dorsal bulge, the distal foregut rotates clockwise (as seen from the front) about its anteroposterior axis and as clockwise (as seen from below) about its longitudinal axis. Therefore, the dorsal bulge presents to the left and is convex inferolateral, forming the greater curvature of the stomach. The original ventral concavity of the developing stomach is carried to the right, forming the definitive lesser curvature (Fig. 2–5).

The change from the foregut to the midgut is marked by a change in arterial supply, from the celiac to the superior mesenteric arteries, respectively. This occurs at the level of the duodenal papilla. As the stomach rotates to the left, the duodenum, which had buckled ventrally (completing an S-shaped configuration with the dorsal gastric bulge), is carried to the right into its definitive position. Its dorsal mesentery is eventually resorbed, resulting in its "retroperitoneal" location, although its anterior surface is still covered by peritoneum. Failure of the mesentery to be completely absorbed results in an elongated and redundant appearance of the proximal duodenum (Fig. 2–6).

Duodenal Web and Bowel Duplication

The gastrointestinal tract starts as a hollow tube. Proliferation of the lining endothelium results in obliteration of the lumen. With time, vacuoles form within this cel-

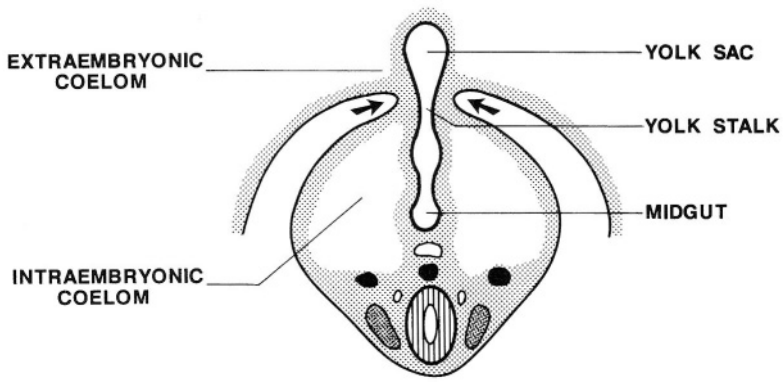


Fig. 2–2. Cross-section at the end of the fourth week of embryonic development. The envelopment of the intraembryonic coelom is almost complete. The yolk sac has otherwise separated into a more definitive yolk stalk and midgut as well.
(From Javors BR, Sloves JH.[4])

lular plug; they coalesce and a normal diameter lumen is reestablished. Failure of complete resorption may lead to either atresia or stenosis. Stenosis may range from a conical narrowing to a weblike constriction (Fig. 2–7). An alternative hypothesis for atresia and stenosis of the intestinal tract is intrauterine ischemia.[6,7] Very rarely, especially in the duodenum, ongoing peristalsis may propel intestinal contents against a web, stretching it out until it resembles a wind sock, forming an intraluminal diverticulum[8] (Fig. 2–8). In addition, incomplete merging of the vacuoles may result in intestinal duplication.[9–11] This is almost invariably seen along the mesenteric border, sharing the blood supply of the normal intestinal lumen. In the stomach, a duplication lies along the greater curvature (site of the initial dorsal mesentery, later the greater omentum)[12,13] (Fig. 2–9), and in the colon along the medial wall of the ascending and descending colon and the superior wall of the transverse colon[11,14] (Fig. 2–10).

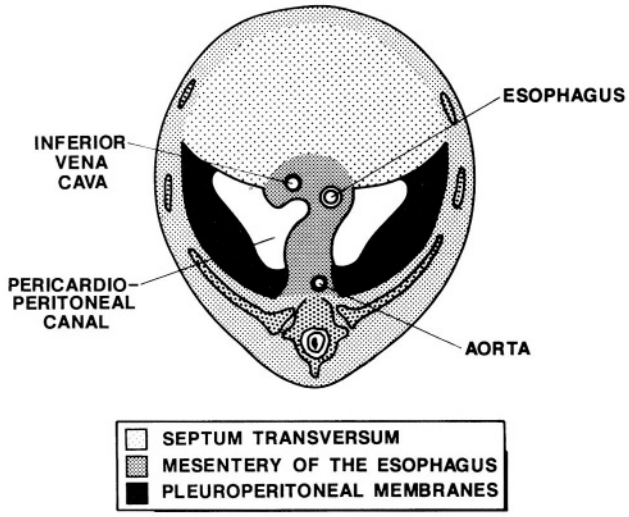


Fig. 2–3. Diagram of a five-week embryo.
The relative contributions of the septum transversum, esophageal mesentery, and pleuroperitoneal membranes will change with further development.
(From Javors BR, Sloves JH.[4])

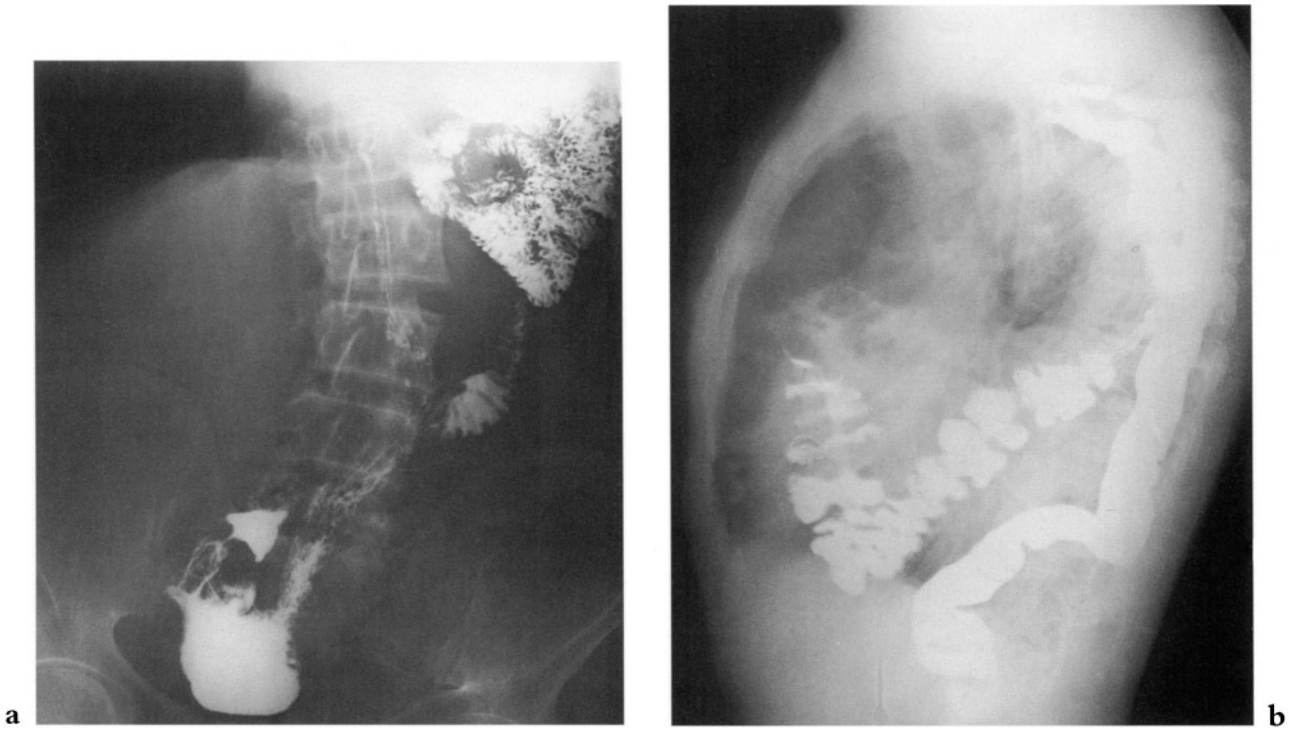


Fig. 2–4. Foramen of Bochdalek hernia.
(a) Upper gastrointestinal series shows a normal subdiaphragmatic position of the stomach. The jejunum enters the thoracic cavity through a diaphragmatic opening (foramen of Bochdalek) that is situated on the left and is more lateral than the position of a conventional hiatal or foramen of Morgagni hernia.
(b) Lateral chest radiograph reveals the barium-filled colon reaching almost to the apex of the chest. The colon is seen to enter the chest through a diaphragmatic opening that is far posterior.
(From Javors BR.[3])

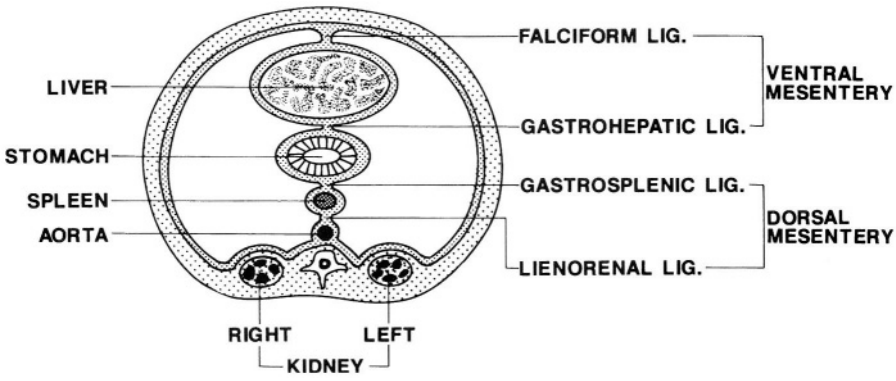


Fig. 2–5. Cross-section through a five-week embryo at the level of the liver shows the paired superior peritoneum (right and left) separated by both the ventral and dorsal mesenteries. Even at this stage of development, the origins of many of the suspensory ligaments of the adult are clearly demonstrated. (From Javors BR, Sloves JH.[4])

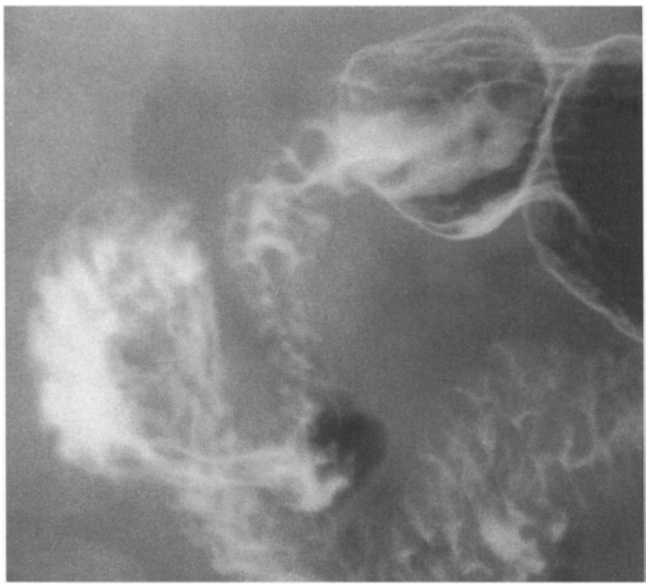


Fig. 2–6. "Hammock" duodenum.
Left lateral film from an upper GI series shows an elongated, redundant postbulbar segment of duodenum proximal to the descending portion. This represents a persistent duodenal mesentery.

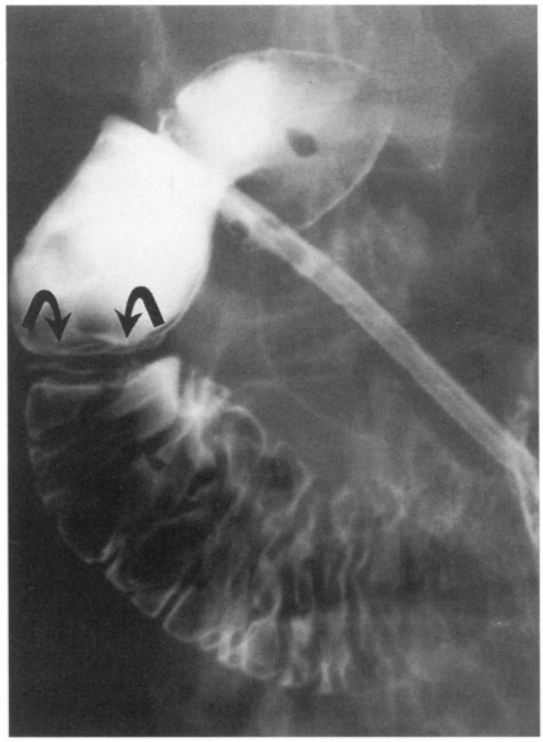


Fig. 2–7. Duodenal web.
Left posterior oblique film from a double-contrast enteroclysis demonstrates a very thin annular constriction in the descending duodenum *(curved arrows)* from a duodenal web.

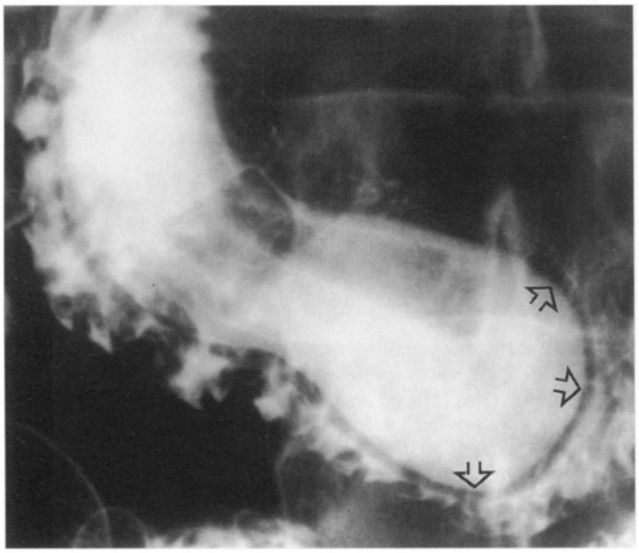
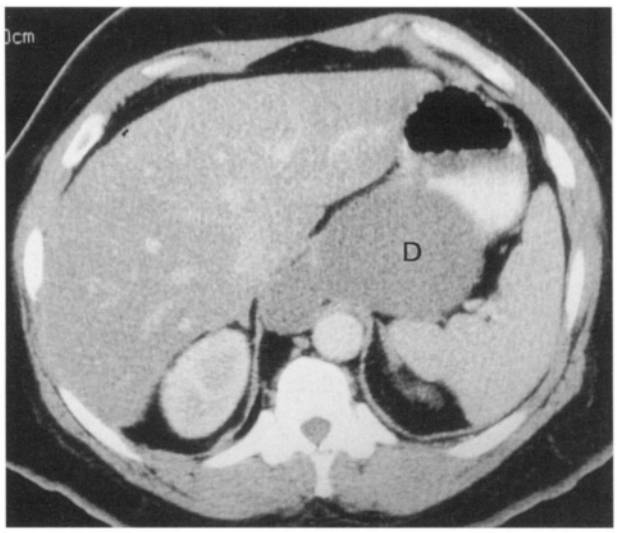


Fig. 2–8. Intraluminal diverticulum.
Spot film from a single-contrast upper GI series reveals a saclike structure filled with debris and barium separated from the remainder of the duodenal lumen by a thin wall *(arrows).* Although termed an intraluminal diverticulum, this is actually a "ballooned out" duodenal web.
(Courtesy of N. Spier, M.D.)

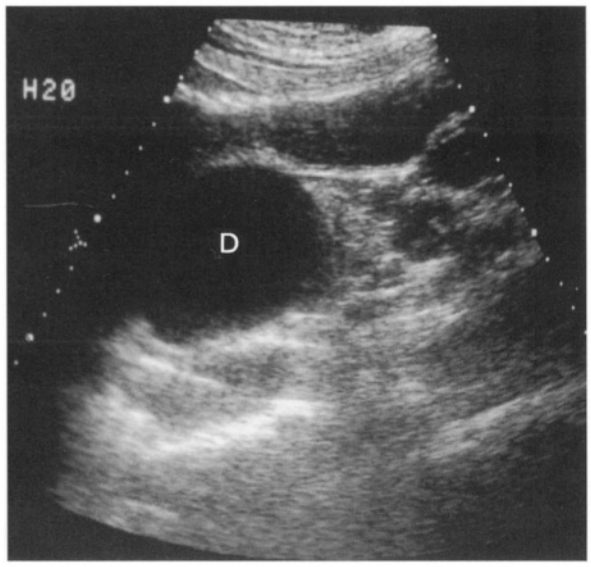
Embryologic Rotation and Fixation of Gut

The suspending dorsal mesentery of the distal foregut and midgut elongates considerably as the stomach and duodenum go through their complex rotation. This leads to the development of the lesser peritoneal sac and the greater omentum. As the dorsal bulge of the stomach becomes more marked, it carries the mesentery along with it to the left side of the abdomen. As this rotation takes place, the peritoneal space that originally lay to the right of the mesentery extends posterior to the stomach into the left hemiabdomen[15] (Fig. 2–11). This eventually becomes the lesser sac. The elongated mesentery also doubles back on itself to form an apron that hangs down from the greater curvature covering the peritoneal cavity (Fig. 2–12). Eventually, the potential space within the omentum is obliterated. If the fusion is incomplete, an omental cyst may form. The differentiation of omental, enteric, mesenteric, and neurenteric cysts and/or dissecting pancreatic pseudocysts depends on their lining cell elements and wall constituents.[16] The suspending dorsal mesentery of the transverse colon fuses with the greater omentum, forming the definitive transverse mesocolon[5,9] (Fig. 2–12).

Relatively early in its development, the intestinal tract markedly elongates, reaching a length too great to be contained within the abdominal cavity. It therefore her-



a



b

Fig. 2–9. Gastric duplication cyst.
(a) Contrast-enhanced CT reveals a bilobate low-density mass (*D*) along the greater curvature of the stomach.
(b) Sagittal sonogram confirms the cystic nature of this gastric duplication cyst.

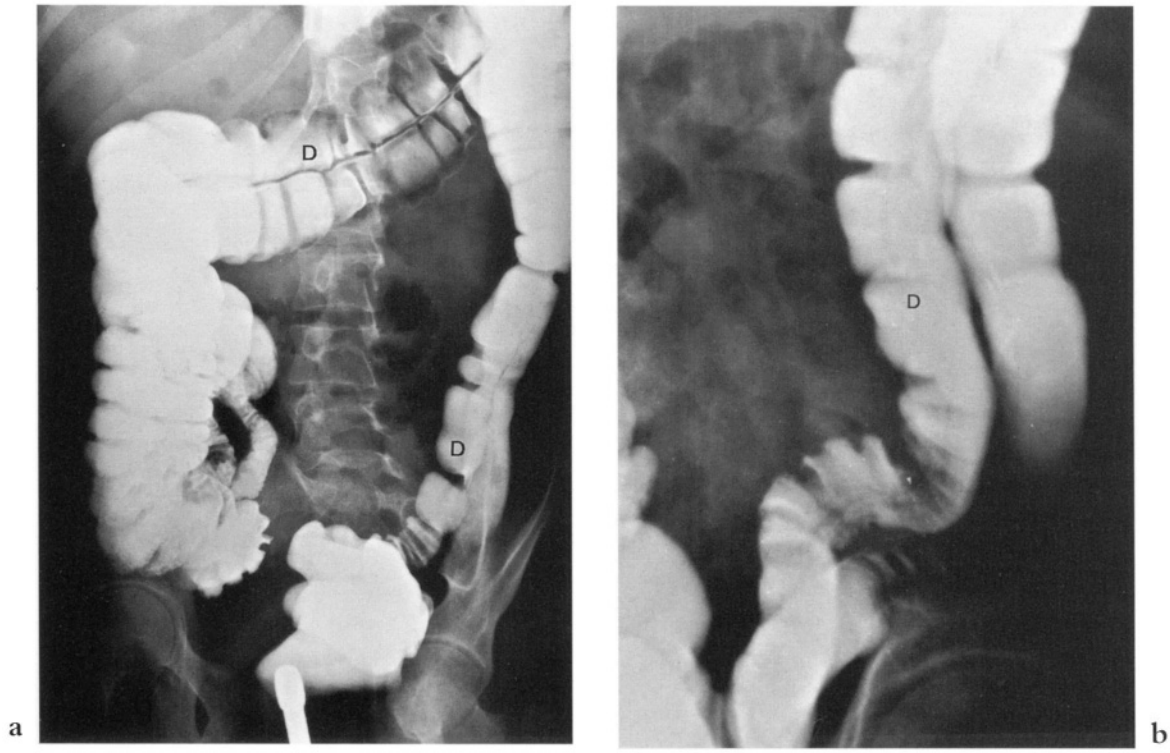


Fig. 2–10. Duplication of the colon.
(a) Barium enema study demonstrates a communicating colonic duplication (*D*) within the mesentery of the transverse colon and descending colon.
(b) Spot film clearly shows the features of the opacified duplication along the medial wall of the descending colon.

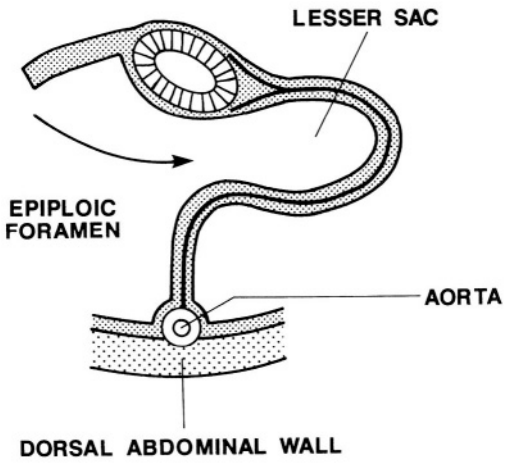


Fig. 2–11. Diagram of the upper abdomen (as seen from below) during gastric rotation.
The suspending dorsal mesentery (mesogastrium) has elongated and is carried to the left of midline. This allows the right hemiperitoneum to extend posterior to the stomach, starting the formation of the lesser sac.

niates into the yolk sac. The superior mesenteric artery acts as the axis of this physiologic herniation. At the apex of this loop is the omphalomesenteric (vitelline) duct. This midgut elongation is predominantly composed of that segment that lies proximal to the duct, the prearterial limb. In order to accommodate this increase in length, the small bowel is thrown into a serpentine pattern, an appearance it maintains into adulthood. The more distal segment, distal to the omphalomesenteric duct, is labeled postarterial and becomes the distal ileum, appendix, and large bowel proximal to the splenic flexure. The cecum starts as a small bud just distal to the apex of the loop and plays an important role in the reduction of the physiologic herniation (Fig. 2–13).

The herniated loop of midgut undergoes a 270° counterclockwise rotation (as seen from the front). The prearterial limb, which starts out superiorly, is carried first to the right and then inferiorly. Conversely, the distal postarterial limb is carried first to the left and then superiorly. Thus, the two limbs find themselves located 180° opposite to their original locations.

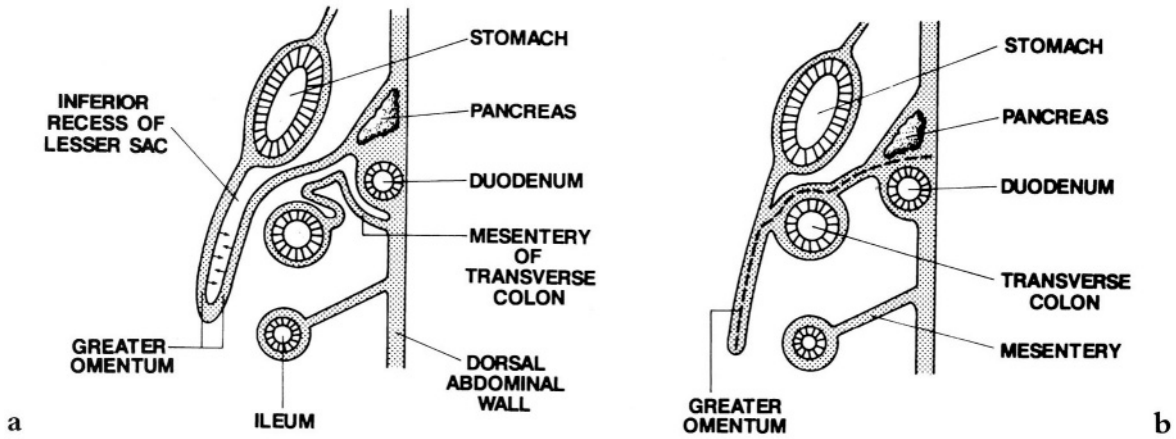


Fig. 2–12. Greater omentum and transverse mesocolon.
(a) Longitudinal schematic drawing showing the fusion of the two leaves of the greater omentum with obliteration of the inferior recess of the lesser sac.
(b) Fusion of the greater omentum with the transverse colon and its dorsal mesentery gives rise to the definitive gastrocolic ligament and transverse mesocolon.
(From Javors BR, Sloves JH.[4])

Eventually, the body cavity enlarges sufficiently to allow the herniated bowel to return (Fig. 2–14). As it does so, the final 90° rotation is completed. The developing cecal bud hinders the return of the postarterial midgut, and therefore the prearterial limb returns to the abdomen first.[9,17–19] As the final part of the rotation occurs, the prearterial limb is carried into the left upper quadrant, crossing beneath the superior mesenteric arterial axis. Therefore, the transverse duodenum is carried inferior to the superior mesenteric artery.

The postarterial midgut and hindgut are now forced to the periphery of the abdomen. The right colon, which develops from the distal limb of midgut, is carried in front of the superior mesenteric artery into the right upper quadrant (Fig. 2–15). It is further growth of the right colon, rather than any additional rotation, that carries it into the right lower quadrant.[9] The suspending dorsal mesentery of the ascending and descending colons is eventually resorbed and united with the posterior abdominal wall. This results in the so-called retroperitonealization of those structures. In actuality, they maintain a peritoneal surface along their anterior aspect, similar to that of the duodenum.

The appendix develops from the cecal bud. It originates as a triangular projection with a wide orifice that is in line with the longitudinal axis of the right colon. The ileocecal valve impedes the growth of the colonic wall at its entry site, and the opposite wall continues to grow, effectively moving the appendix to the same side of the cecum as the valve.[20] In addition, further increase

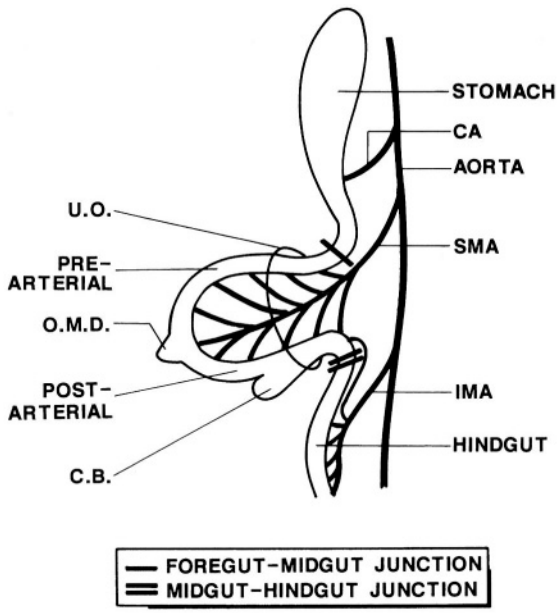


Fig. 2–13. Longitudinal view of the intestinal tract at 6 weeks of development.
The superior mesenteric artery *(SMA)* acts as the axis for midgut rotation. The omphalomesenteric duct (*OMD*) divides the midgut into pre- and postarterial limbs. Also seen is the physiologic herniation of the midgut through the umbilical orifice *(UO)*. Heavy lines mark the foregut-midgut (/) and the midgut-hindgut (//) junctions. The celiac axis *(CA)* is the major artery of the foregut; the inferior mesenteric artery *(IMA)* supplies the hindgut. *CB* = cecal bud.
(From Javors BR, Sloves JH.[4])

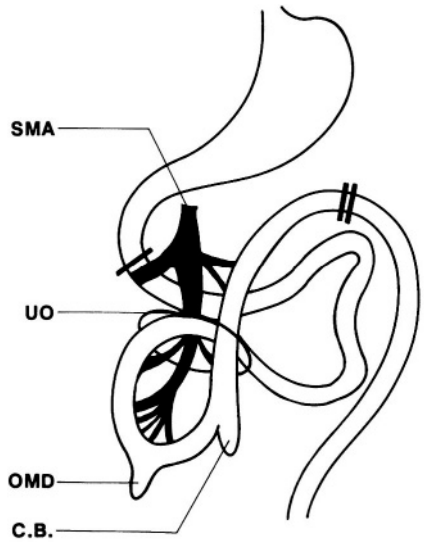


Fig. 2–14. Frontal view of a 10-week fetus.
The elongated redundant prearterial limb has reentered the abdomen and crossed to the left of and behind the SMA. This displaces the hindgut to the left. Heavy lines mark the foregut–midgut (/) and the midgut–hindgut (//) junctions. *CB* = cecal bud; *OMD* = omphalomesenteric duct; *UP* = umbilical orifice.
(From Javors BR, Sloves JH.[4])

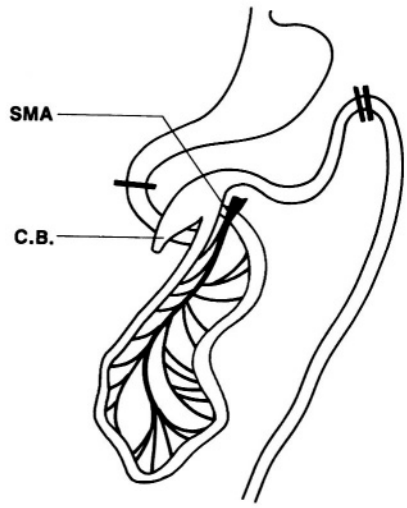


Fig. 2–15. Reduction of the physiologic herniation.
This is complete one week after the configuration shown in Figure 2–14. The postarterial limb has partially completed its 180° rotation. The cecum now lies in the upper abdomen on its way to the right side. *CB* = cecal bud.
(From Javors BR, Sloves JH.[4])

in the transverse diameter of the cecum, without further growth of the appendiceal lumen, brings about the more familiar vermiform (wormlike) appearance of the appendix.

This complex series of twists and turns and subsequent mesenteric resorption leaves the gastrointestinal tract prone to many and often complex errors of rotation and fixation.[9,10,21,22]

Volvulus

Gastric volvulus is a rare condition encountered in the adult as well as the pediatric age group. The majority of cases are of the mesenteroaxial type rather than the organoaxial type.[23] Anomalies associated with acute gastric volvulus include diaphragmatic defects, intestinal malrotation, and wandering spleen.[24] Most cases of gastric volvulus seem to be secondary to deficient fixation. Absence of the gastrophrenic ligament and the gastrosplenic ligament as well as an absence of the spleen may lead to gastric volvulus in asplenic patients.[25] Elongation or absence of the splenorenal ligament even with preservation of the gastrosplenic ligament may lead to mesenteroaxial gastric volvulus (Fig. 2–16). Gastric volvulus can be recurrent, intermittent, or resolve spontaneously or by placement of a nasogastric tube.

Cecal volvulus is a rare cause of cecal distention and accounts for 11% of all intestinal volvulus.[26] It develops in association with an abnormal fixation of the cecum to the posterior parietal peritoneum; a freely mobile cecum is a prerequisite for it. An abnormally distended cecum is demonstrated in the midabdomen on radiographs, sometimes recognizable as the coffee bean sign. Contrast enema is usually diagnostic, but a whirl sign, which is composed of the twisted portion of the cecum and mesentery, may be shown on CT (Fig. 2–17).[27]

Nonrotation, often called malrotation, is the most commonly encountered major anomaly of rotation. In actuality, it is incomplete rotation that stops after the first 90°.[9,10,22] At this point, the prearterial limb lies in the right hemiabdomen, and the postarterial lies in the left. In addition, the order of the returning loops of midgut is reversed, with the distal limb leading the proximal. This results in the jejunum lying in the right upper abdomen, whereas the colon lies to the left of midline (Fig. 2–18). The duodenal sweep is not formed, and there may be an unusual redundancy to the duodenum on the right side of the spine. The duodenal–jejunal junction then usually lies medial to the left pedicle of the spine.[28]

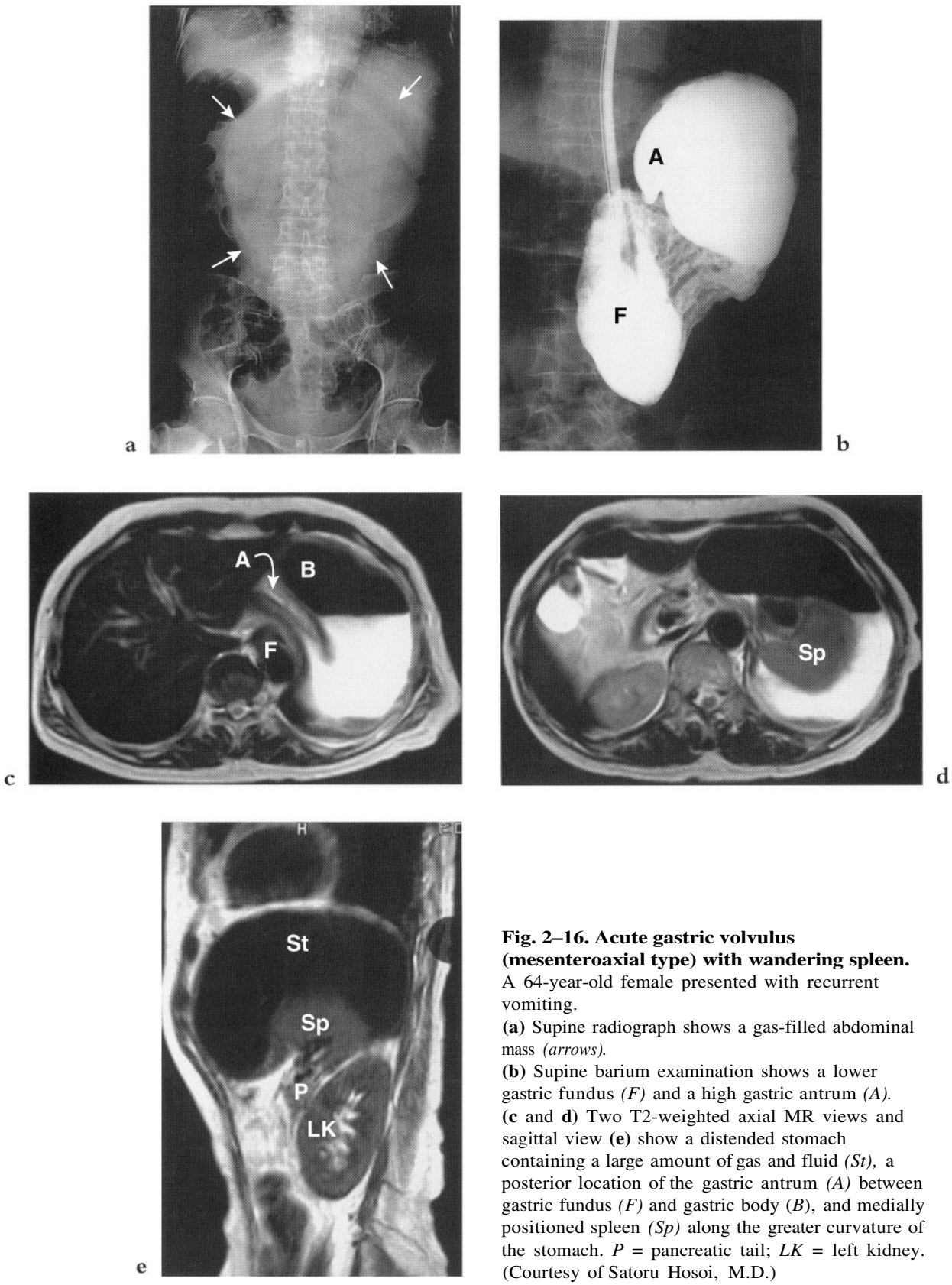


Fig. 2–16. Acute gastric volvulus (mesenteroaxial type) with wandering spleen.
A 64-year-old female presented with recurrent vomiting.
(a) Supine radiograph shows a gas-filled abdominal mass *(arrows).*
(b) Supine barium examination shows a lower gastric fundus *(F)* and a high gastric antrum *(A).*
(c and **d)** Two T2-weighted axial MR views and sagittal view **(e)** show a distended stomach containing a large amount of gas and fluid *(St),* a posterior location of the gastric antrum *(A)* between gastric fundus *(F)* and gastric body (*B*), and medially positioned spleen *(Sp)* along the greater curvature of the stomach. *P* = pancreatic tail; *LK* = left kidney. (Courtesy of Satoru Hosoi, M.D.)

Most of the bowel shares a common mesentery that is prone to volvulus, particularly with a short mesenteric root. Patients with malrotation in whom the cecum is found in either upper quadrant are the most prone to develop a volvulus. Midgut volvulus is usually considered a surgical emergency, generally occurring in infants during the first weeks of life. It has been recently recognized that midgut volvulus may occur in adults, and its clinical presentations may be vague and chronic or recurrent.[28,29] On CT, the whirled appearance representing intestinal loops and mesenteric fat with branches of mesenteric vessels, thrombosed or patent, wrapping around the superior mesenteric artery, which may be thrombosed, calcified, or patent, can be diagnostic. Dilated collateral veins and/or congested or edematous mesentery may be present distally (Fig. 2–19). Because the proximal limb returns to the abdomen first, an abnormally rotated proximal limb does not always result in an abnormally positioned distal limb. However, an abnormally positioned distal limb is almost invariably associated with an abnormal proximal one.[4] Faulty resorption of the suspending dorsal mesentery of the colon

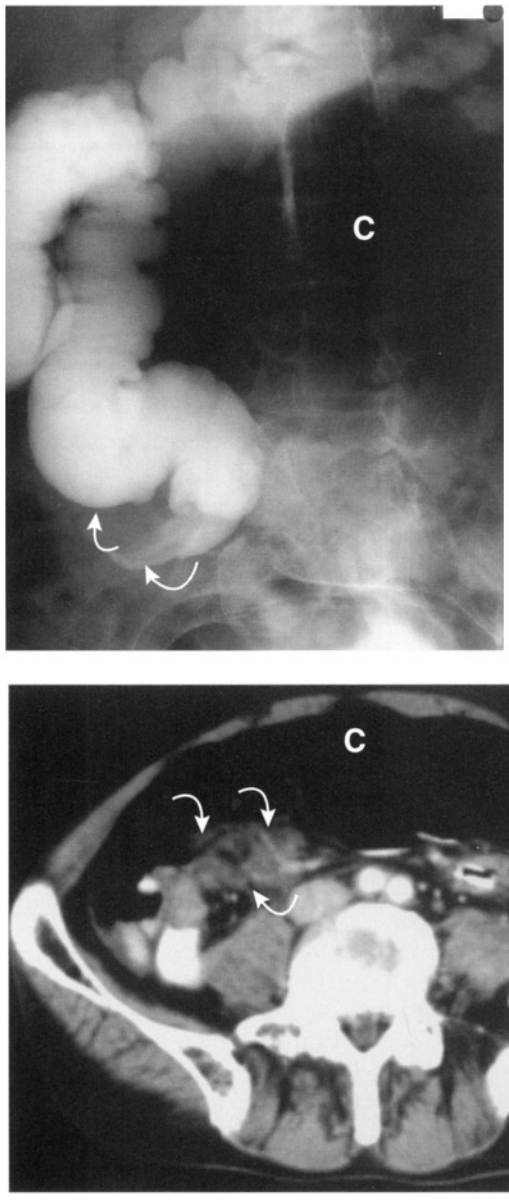


Fig. 2–17. Cecal volvulus.
A 65-year-old male presented with abdominal pain and vomiting.
(a) Contrast enema shows a twisting *(curved arrows)* of the abnormally located cecum (*C*) that is markedly distended.
(b) Postcontrast CT shows a distended air-filled cecum (*C*) and twisted portion of cecum and mesentery *(curved arrows).*
Emergency surgery revealed a cecal volvulus with an elongated, nonattached ascending colon and cecum.
(Courtesy of Yoshiki Senba, M.D.)



Fig. 2–18. Midgut nonrotation.
Upper GI series with small bowel follow-through demonstrates the jejunum in the right upper quadrant and the cecum and ascending colon in the midline. These are the classic findings of midgut nonrotation.

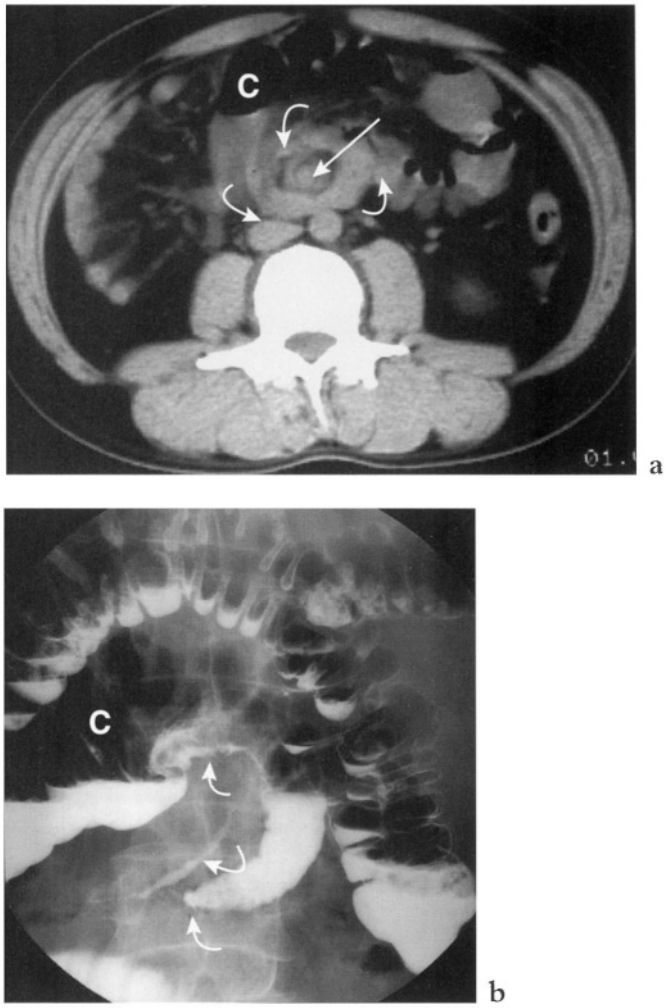


Fig. 2–19. Chronic recurrent midgut volvulus.
A 29-year-old male presented with recurrent episodic abdominal pain.
(a) Precontrast CT shows small bowel loops and mesenteric vessels *(curved arrows)* wrapping around the superior mesenteric artery *(straight arrow).* High and medially positioned cecum (*C*) and small bowel loops occupying the right side of the abdomen are noted. An increased attenuation of mesenteric fat indicates congestion or edema.
(b) Barium enema examination shows a high and medial position of the cecum (*C*) and volvulated ileal loops *(arrows).*

may result in excessive mobility of the bowel (Fig. 2–20) and may predispose it to volvulus[30] (Fig. 2–21).

Meckel's Diverticulum

Failure of the omphalomesenteric duct to completely involute may lead to a persistent outpouching along the antimesenteric border of the distal ileum, a Meckel's diverticulum (Fig. 2–22). Meckel's diverticulum occurs in approximately 2% of the general population, and it is the most common congenital abnormality of the gastrointestinal tract. Stasis of intestinal contents within the diverticulum predisposes to the development of enteroliths (Fig. 2–23). Obstruction is the predominant symptom (39%). Hemorrhage, perforation, diverticulitis, and intussusception are the other symptoms (12–14% each).[10,31,32] Hemorrhage and perforation are usually associated with the presence of ectopic gastric mucosa (Fig. 2–24), while perforation due to ingested foreign body has rarely been reported.[33]



Fig. 2–20. Persistent descending mesocolon.
A double-contrast barium enema reveals a short descending colon with a long, redundant transverse colon. This represents incomplete fusion of the descending colon mesentery, with its remnant allowing excessive mobility. In addition, the cecum is pointed superiorly in the right upper quadrant, which represents premature arrest of the postarterial rotation. Therefore, this patient has a not uncommon combination of incomplete rotation and malfixation.
(From Javors BR, Sloves JH.[4])

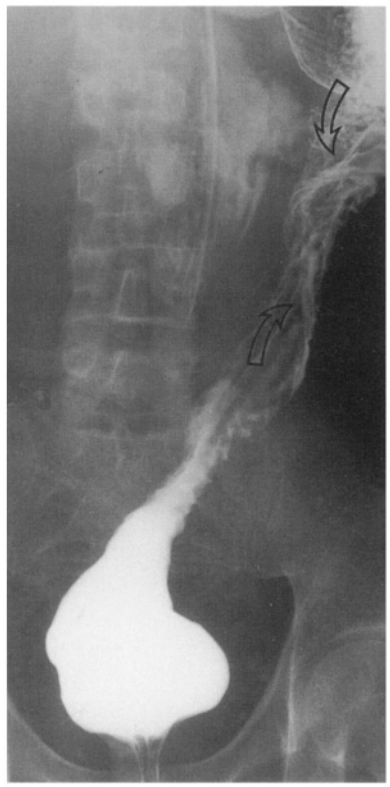


Fig. 2–21. Volvulus of the splenic flexure of the colon.
In a patient with a markedly dilated splenic flexure, this postevacuation film from a barium enema reveals the classic criss-crossing mucosal fold pattern *(arrows)* of a volvulus. In this patient, there was an elongated left colon on a persistent mesentery, a lack of proper resorption.

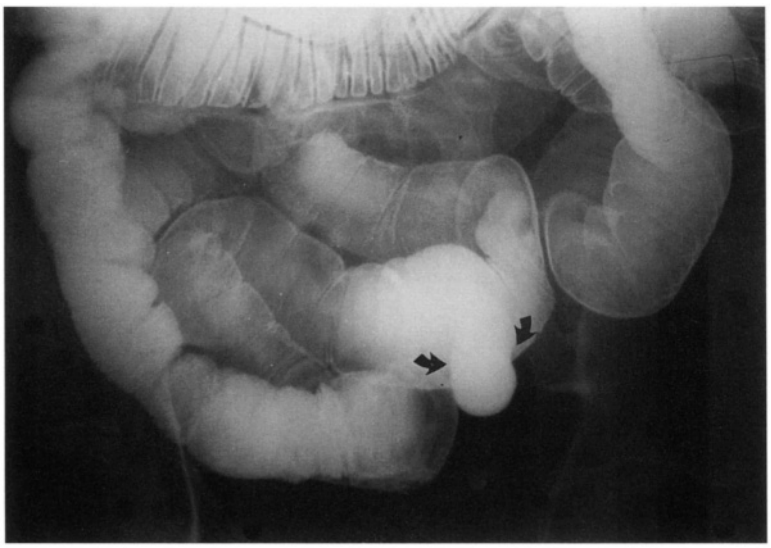


Fig. 2–22. Meckel's diverticulum.
Enteroclysis study reveals a barium-filled Meckel's diverticulum *(arrows)* arising from the antimesenteric border of the distal ileum.

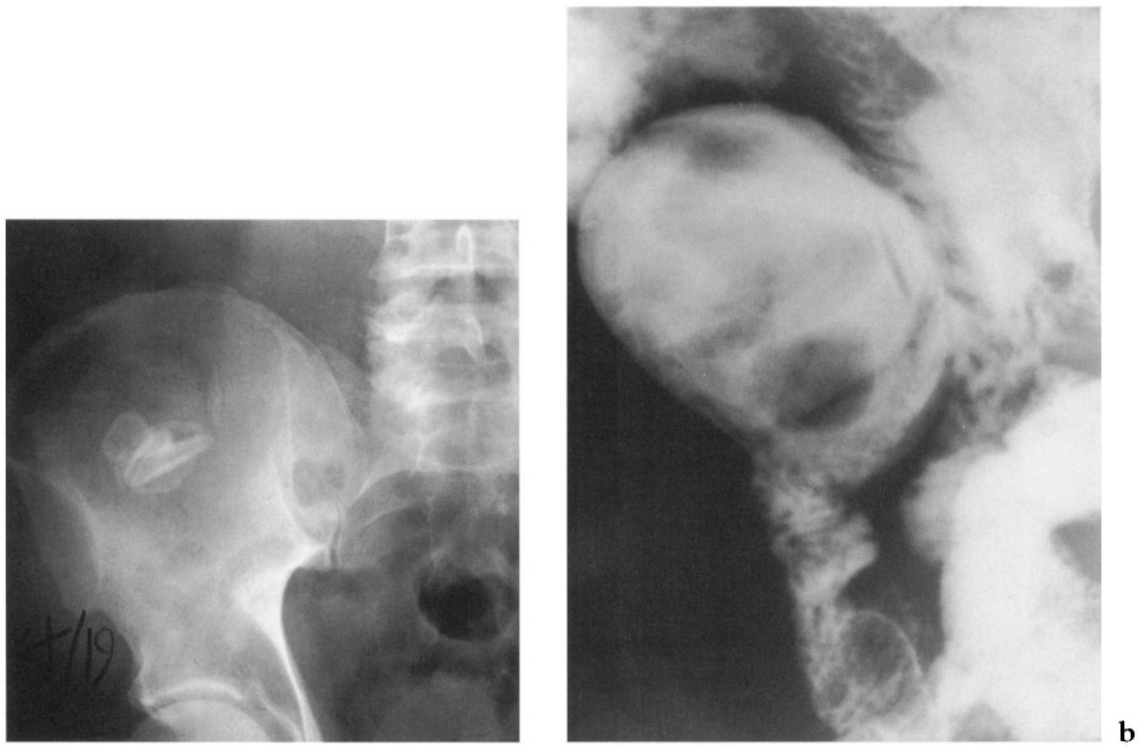


Fig. 2–23. Meckel's diverticulum with enteroliths.
(a) Coned-down view of the right lower quadrant shows multiple faceted calcifications.
(b) Spot film of the same area from a small bowel study demonstrates these enteroliths to lie within a large Meckel's diverticulum.

Hepatobiliary System

The hepatobiliary structures develop from a diverticulum that originates on the ventral aspect of the distal foregut, extends into the septum transversum, and divides. The larger, more cranially located pars hepatica gives rise to the liver and intrahepatic ducts, whereas the caudal pars cystica develops into the gallbladder and cystic duct. The pedicle of the hepatic diverticulum narrows and recanalizes to form the extrahepatic bile duct. The common bile duct is carried 90° clockwise (as viewed from below) along with the duodenum. It rotates an additional 180° to ultimately lie adjacent to the pancreatic duct of Wirsung (from the ventral anlage) in the concavity of the duodenal sweep. The reticuloendothelial elements of the liver arise from the mesoderm of the septum transversum. As it enlarges, most of the liver becomes peritonealized, but the posterior aspect retains contiguity with the diaphragm in the region known as the bare area.[34] During this complex process, islands of liver cords may lose their connection to the liver proper, resulting in ectopic foci of liver tissue[35] (Fig. 2–25). These are usually found in the gallbladder, pancreas, and lesser omentum, which share a relatively common embryologic origin, but they may also occur in other structures such as the adrenal gland.

Hepatic Lobar Agenesis

After birth, possibly because of abrupt termination of the oxygenated umbilical venous inflow, the left lobe shrinks considerably so that the fetal lateral segment often comes to be located closer to the midline than the fetal medial segment. However, by convention, the fetal nomenclature for these segments is maintained after birth. The ligamenta teres and venosus lie within fissures that separate the left medial and lateral segments and the caudate lobe. Location of the liver can be abnormal, with one or more segments hypoplastic or absent[36–38] (Fig. 2–26). Occasionally, the right rather than the left

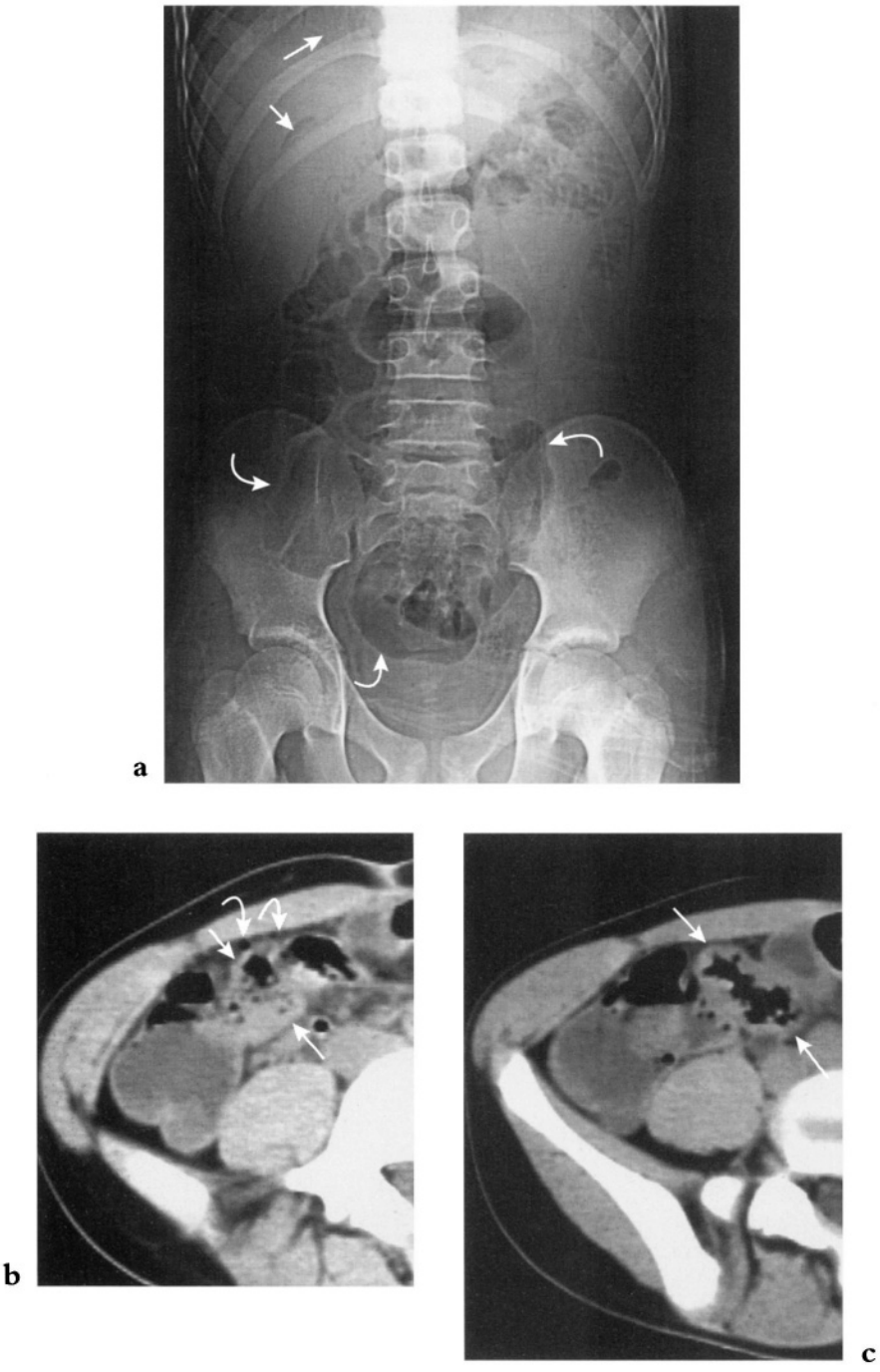


Fig. 2–24. Perforation of Meckel's diverticulum in a 12-year-old male who presented with abdominal pain and vomiting.
(a) Abdominal radiograph shows an air-filled dilatation of small bowel loops *(curved arrows)* and gas bubbles in the peritoneal cavity *(arrows).*
(b and **c)** CT shows a part of ileum with thickening of its wall *(straight arrows)* with surrounding intraperitoneal gas bubbles *(curved arrows).*
Emergency surgery revealed a perforation of an inflamed Meckel's diverticulum containing ectopic gastric mucosa.

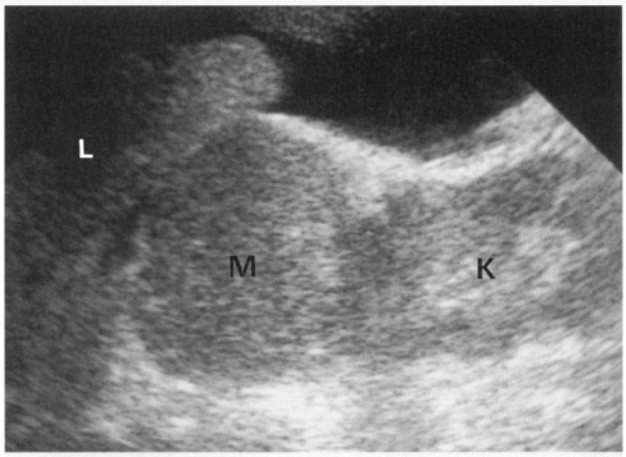


Fig. 2–25. Ectopic liver tissue with malignancy.
Longitudinal sonogram in a patient with cirrhosis shows a large soft tissue mass (*M*) between the liver (*L*) and right kidney (*K*). At autopsy, the mass proved to be hepatocellular carcinoma that was entirely separate from the liver, having likely developed within ectopic liver tissue.



Fig. 2–26. Agenesis of right hepatic lobe.
Postcontrast CT scan shows nearly complete agenesis of the right hepatic lobe, of which only a rudimentary portion (*r*) is present lateral to the gallbladder (*g*). The hypertrophied left lobe accounts for the vast majority of liver tissue. Note the fissure of the ligamentum teres *(arrow)* between the lateral (*L*) and medial (*M*) segments of the left hepatic lobe, which is diffusely infiltrated with fat.

umbilical vein persists, in which case the ligamentum teres fissure may be located to the right of the gallbladder.[39] Variations of the usual branching of the hepatic vasculature are common and of great significance for liver surgeons.[40] Although the hepatic and portal veins are the anatomic basis for delineating the segmental anatomy of the liver,[41,42] recent work has questioned the accuracy of imaging studies in correctly localizing focal lesions.[43]

Ectopic and Accessory Gallbladders

A communication between the bile ducts of the right lobe and the gallbladder exists during fetal development. When it persists into adulthood, this cystohepatic duct of Luschka (Fig. 2–27) may be severed during a cholecystectomy, resulting in a bile leak.[44,45] Other anomalies that may involve the gallbladder include a "wandering gallbladder" in which an elongated suspending mesentery allows marked mobility of the gallbladder[46–48] (Fig. 2–28). When the more caudal of the biliary buds from the foregut does not fully separate from the cranial, the gallbladder may actually develop within the liver parenchyma[46,49–51] (Fig. 2–29). Duplication and triplication of the gallbladder, with or without a separate cystic duct, may also occur due to abnormal branching of the foregut buds[52–54] (Figs, 2–30 and 2–31). Faulty recanalization of the biliary bud may also lead to agenesis of the gallbladder associated with other congenital anomalies.[46,50,55,56]

Choledochal Cyst

Cystic disease of the liver may encompass many findings, including intra- and extrahepatic (renal and pancreatic) cysts and hepatic fibrosis. Choledochal cysts are a separate entity, although they may also exhibit a wide range of radiographic findings. Proposals regarding their cause include intrauterine bile duct obstruction, atypical junction of the pancreatic and common bile ducts (Fig. 2–32), an anomalous course of the primitive common bile duct through the duodenal wall, a malformed common bile duct, viral infections, and faulty recanalization of the primitive choleductus.[55–59]

Five different types of choledochal cysts have been described.[60] Aneurysmal dilatation of the distal common bile duct, with or without proximal extension, is the most common[60–62] (Fig. 2–32). Stasis within the dilated biliary tree may lead to the development of cholangio-

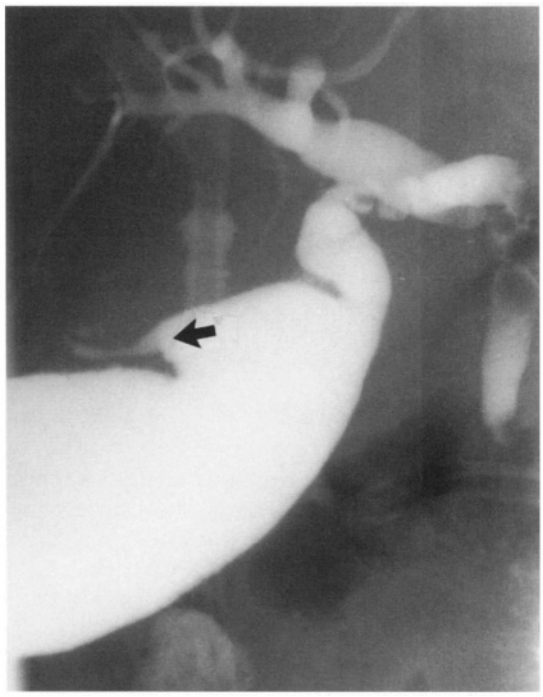


Fig. 2–27. Cystohepatic duct of Luschka.
Tube cholecystostomy study shows a short, tubular structure (the cholecystohepatic duct of Luschka) *(arrow)* arising from the superior aspect of the gallbladder and extending towards the liver parenchyma. No deformity of the gallbladder is seen to suggest a localized perforation. No extravasation is noted to infer filling of an arterial, venous, or lymphatic vessel. Multiple air bubbles were inadvertently introduced into the biliary tree during the performance of the examination.
(From Javors BR, et al.[45])

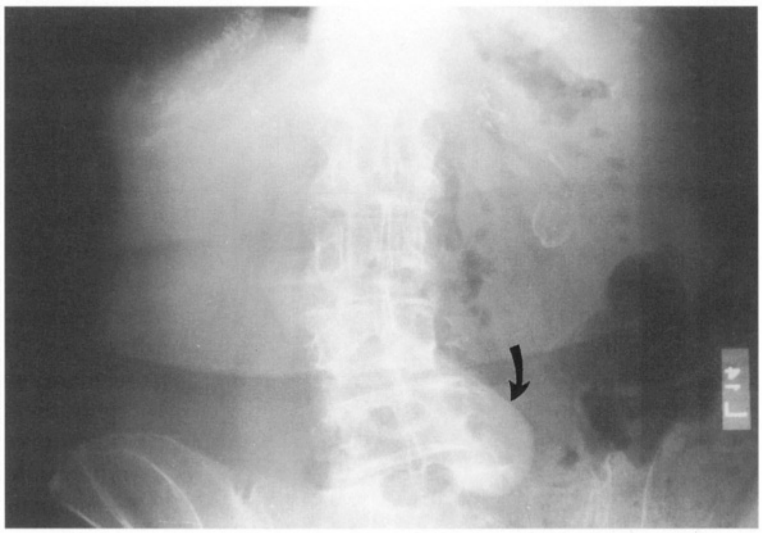


Fig. 2–28. Wandering gallbladder.
Prone radiograph as a part of an oral cholecystogram reveals the opacified gallbladder *(curved arrow)* to lie in the left upper pelvis. This excessive mobility represents a "wandering gallbladder."

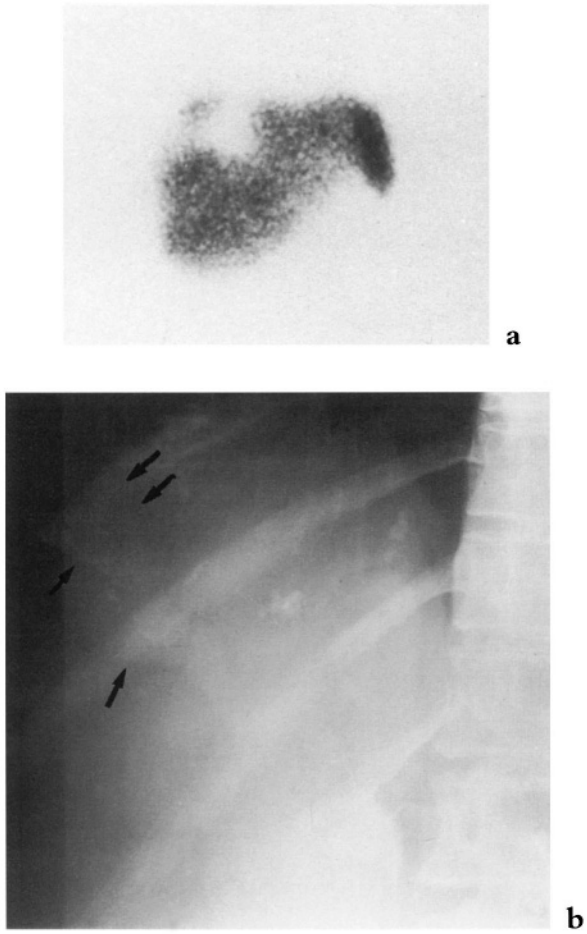


Fig. 2–29. Intrahepatic gallbladder.
(a) Radionuclide sulfur colloid liver-spleen scan shows a photon deficient area high in the right lobe of the liver.
(b) Film of the right upper quadrant from an intravenous cholangiogram confirms an intrahepatic gallbladder *(arrows)* as the cause.
(From Javors BR.[3])

carcinoma. A choledochocele (Figs. 2–33 and 2–34), similar in appearance to a simple ureterocele, multifocal segmental dilatation, and Caroli's disease are other less common types of choledochal cysts. Caroli's disease is characterized by segmental dilatation of the intrahepatic ducts. Recurrent bouts of cholangitis secondary to stasis within the ducts are a common complication of Caroli's disease. Rarest of choledochal cysts is a distal common bile duct diverticulum.

Hepatic Duct Diverticulum

In the development of the biliary system, while the extrahepatic bile ducts develop from the embryonic hepatic diverticulum, the intrahepatic bile ducts originate within the liver from the ductal plate. Diverticula of the hepatic duct are extremely rare, but cholestasis occurring within the diverticula may result in recurrent gallstone formation, biliary tract obstruction, and sepsis[63,64] (Fig. 2–35).

Portal Venous System

Of the three major venous systems traversing the upper fetal abdomen (i.e., the cardinal, vitelline, and umbilical systems), the latter two are integral to the development of the hepatic vasculature. The right vitelline and left umbilical veins persist, whereas their respective contralateral counterparts are short-lived. The right vitelline vein forms a plexus surrounding the duodenum and extending to the septum transversum, where it interacts with the developing liver cords to form the hepatic sinusoids (Fig. 2–36). The hepatic sinusoids become the

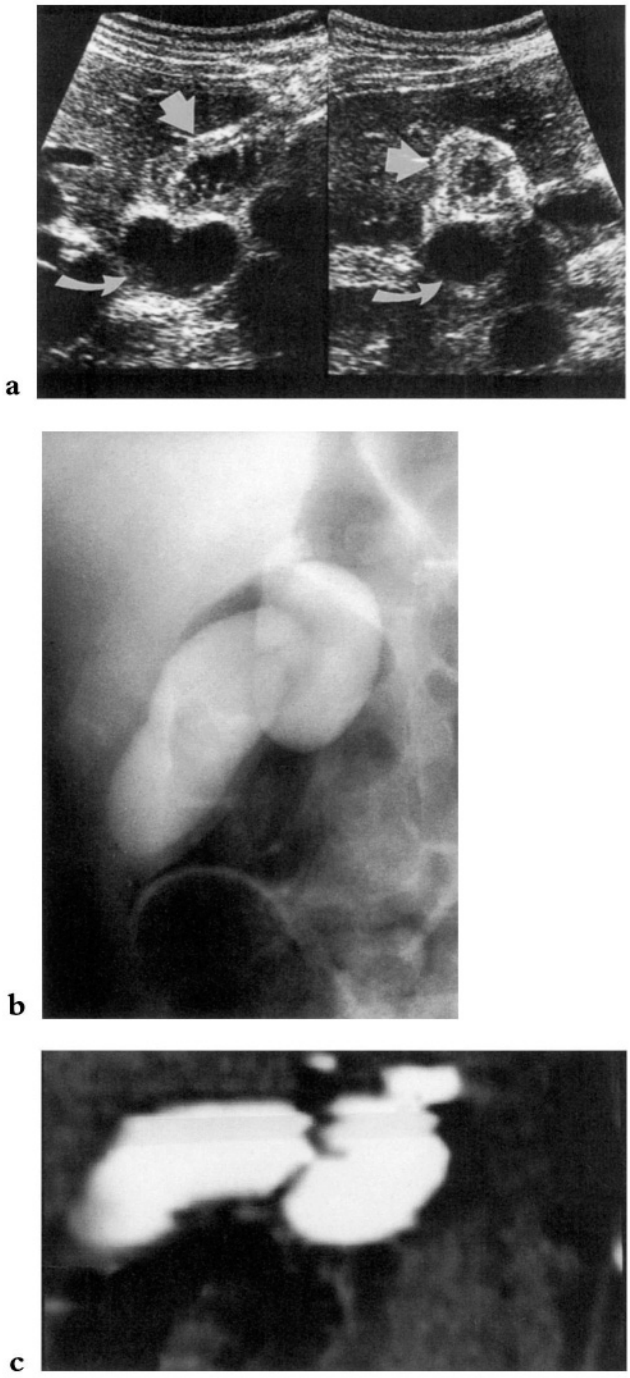


Fig. 2–30. Duplication of the gallbladder in a 66-year-old man, proved at surgery.
(a) Sagittal *(left)* and transverse *(right)* ultrasound images show the gallbladders lying side by side. One has cholesterol crystals and sludge in the lumen with a thickened wall *(thick arrows).* The other gallbladder appears to be normal *(curved arrows).*
(b) Oral cholecystogram (OCG) opacifies both gallbladders.
(c) Reformatted CT in coronal plane after OCG shows both gallbladders.
(Reproduced from Özgen et al.[54])

intrahepatic portal vein branches and the hepatic veins. Meanwhile, a single oblique channel among the hepatic sinusoids becomes dominant (the ductus venosus) and drains directly into the inferior vena cava (IVC). The right umbilical vein disappears during the second month, whereas the left umbilical vein persists and anastomoses with the ductus venosus.

The ductus venosus (Fig. 2–37) develops to provide a direct communication between the placental and systemic venous circulations, with a variable proportion of

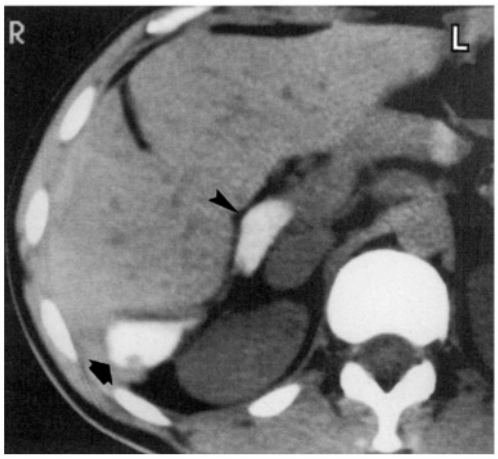


Fig. 2–31. Duplicated gallbladder with cholelithiasis after cholecystectomy in a 45-year-old man.
CT after OCG shows the ectopically located gallbladder with a stone in it *(arrow).* A widened common bile duct is present *(arrowhead).* The patient had a repeat cholecystectomy.
(Reproduced from Özgen et al.[54])

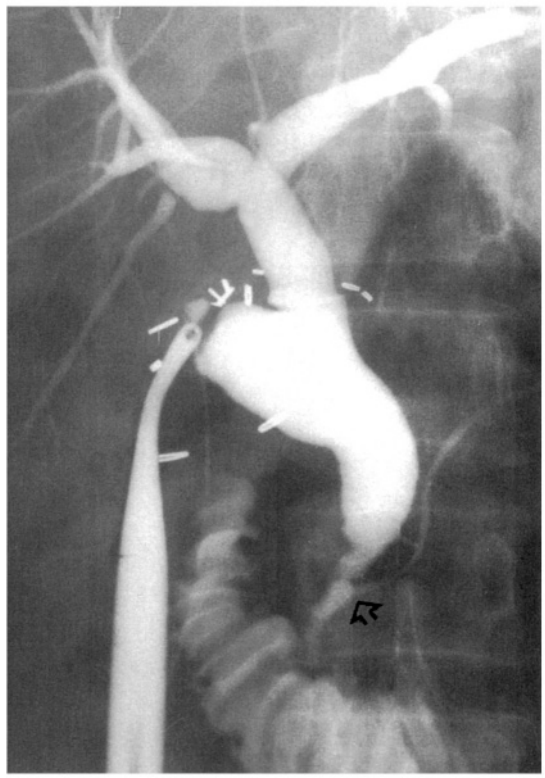


Fig. 2–32. Choledochal cyst.
Intraoperative cholangiogram demonstrates fusiform dilatation of the common bile duct, a form of choledochal cyst. Note the high junction of the pancreatic duct and the distal common bile duct *(open arrow),* commonly cited as a cause of choledochal cyst formation.
(From Javors BR.[3])

umbilical venous blood continuing to traverse the sinusoids via the left portal vein. The ductus venosus is obliterated soon after birth, and its remnant is called the ligamentum venosus. The umbilical vein also atrophies and is henceforth known as the ligamentum teres. A narrow umbilical vein lumen often remains patent into adulthood (Fig. 2–38). The plexus investing the duodenum coalesces to form the superior mesenteric and portal veins. The cephalic portion of the vitelline vein gives rise to the hepatic veins and upper inferior vena cava.[34,37]

Persistence of the primitive hepatic sinusoids, subhepatic ventral intervitelline anastomotic vein, ductus venosus, and anastomosis between the right subcardinal vein and right vitelline vein lead to intrahepatic portal–systemic venous shunts, preduodenal portal vein, patent ductus venosus, and fistula between the portal vein and IVC, respectively.[65,66] Associated anomalies of foregut, midgut, and hindgut as well as those of the vascular system may accompany these malformations. Incomplete obliteration of the anastomoses leads to a formation of a diverticula-like protrusion of the vein, namely "aneurysm" of the portal vein or of any vein. Excessive obliteration of these anastomoses may produce agenesis or hypogenesis of the portal vein and branches.

Portohepatic Venous Shunt

Although intrahepatic portal–systemic (hepatic) venous shunt had been thought to be a rare disease, recent advances in ultrasound, CT, and MRI have made it possible to depict this condition in an increasing number of patients[67–69] (Figs. 2–39 and 2–40). A high degree of shunt may produce hepatic encephalopathy due to hyperammonemia. Single or multiple shunts may be present, and there may be other anomalies such as membranous obstruction of the IVC.[70] It has recently been reported that hepatic adenoma, hepatocellular carcinoma, or nodular hyperplasia may develop in the ischemic liver in the presence of portosystemic shunts.[71,72]

Preduodenal Portal Vein

Preduodenal portal vein consists of the persistence of a preduodenal vitelline communicating vein (a caudal in-

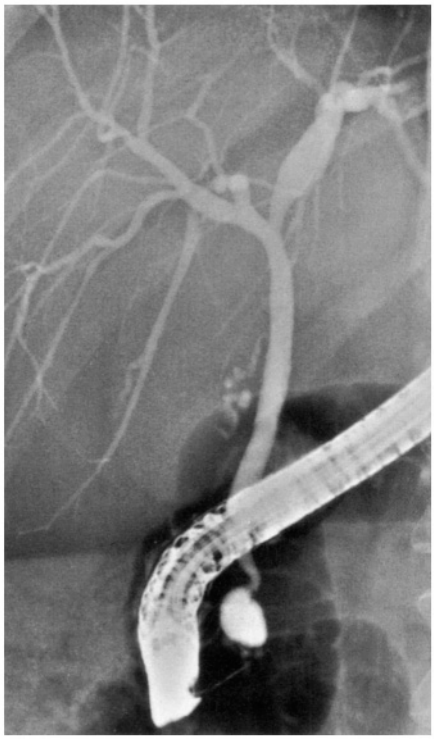


Fig. 2–33. Choledochocele.
ERCP shows that the common bile duct terminates in a localized saccule pouting into the descending duodenum. Note fusiform dilatation of the left hepatic duct.

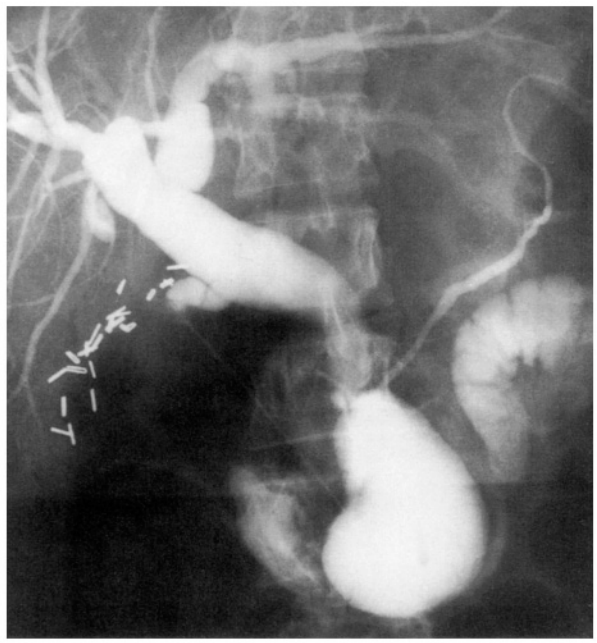
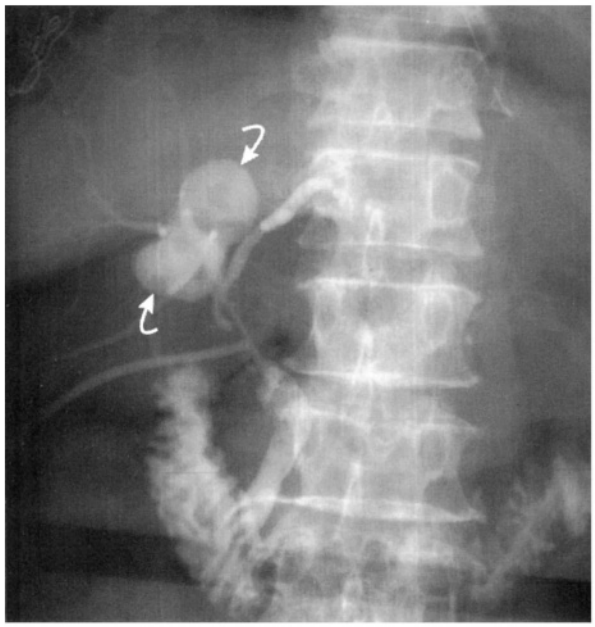
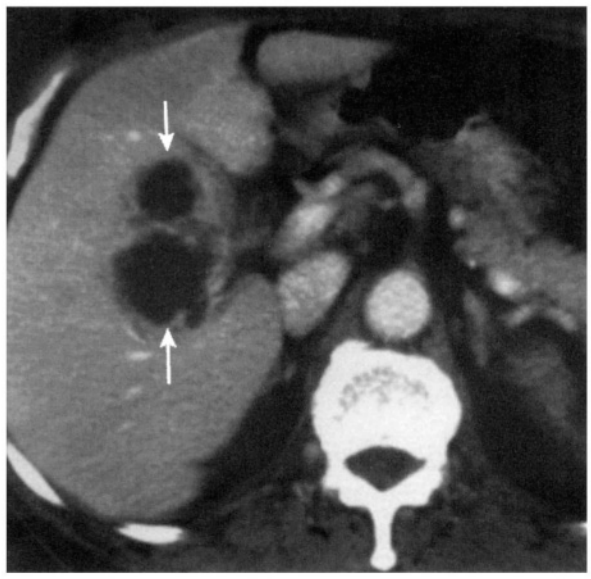


Fig. 2–34. Choledochocele.
Intraoperative cholangiogram demonstrates a large saccular collection of contrast bulging into the transverse duodenum.



a



b

Fig. 2–35. Recurrent gallstones formation within a diverticulum of the right hepatic duct and cholangitis in a 71-year-old male.
(a) A cholangiogram taken during cholecystectomy reveals a diverticulum originating from the right hepatic duct *(curved arrows).* Filling defects represent gallstones within it.
(b) After removal of gallstones within the diverticulum, the patient had recurrent episodes of cholangitis. CT shows thickening of the diverticulum with septation *(arrows)* with recurrent gallstones *(not shown).*
(Courtesy of Kimihiro Nakashima, M.D.)

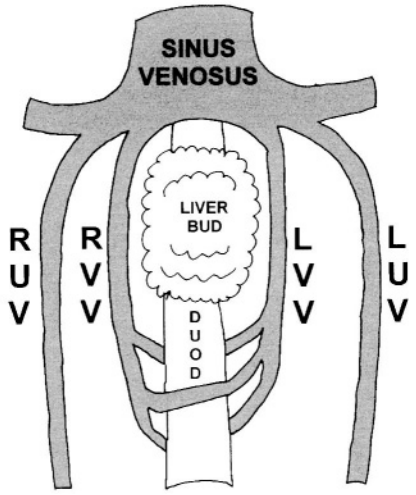


Fig. 2–36. Schematic diagram of a 4-week old embryo as seen from the front shows the paired right (*RVV*) and left (*LVV*) vitelline veins forming a plexus about the duodenum (*DUOD*). More laterally, the right (*RUV*) and left (*LUV*) umbilical veins can be seen coursing toward the sinus venosus. The developing liver bud can be seen projecting from the duodenum (distal foregut).

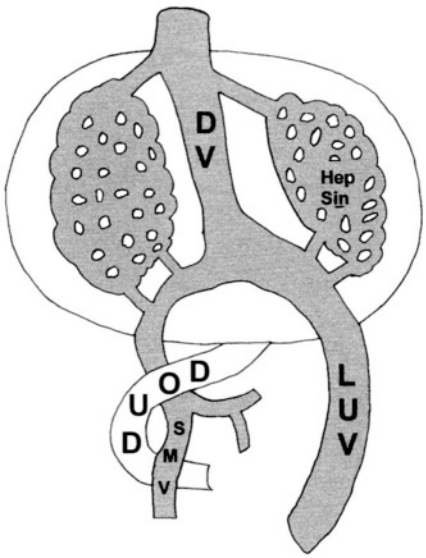


Fig. 2–37. Schematic diagram of a 3-month fetus as seen from the front shows the development of the ductus venosus (*DV*) from the left portal vein. The persistent connection between the left portal vein and the hepatic sinusoids *(Hep Sin)* is also evident. The plexus of veins around the duodenum (*DUOD*) has given rise to the splenic and superior mesenteric veins (*SMV*) draining into the portal vein derived from the right vitelline vein. The latter also has given rise to the hepatic veins.

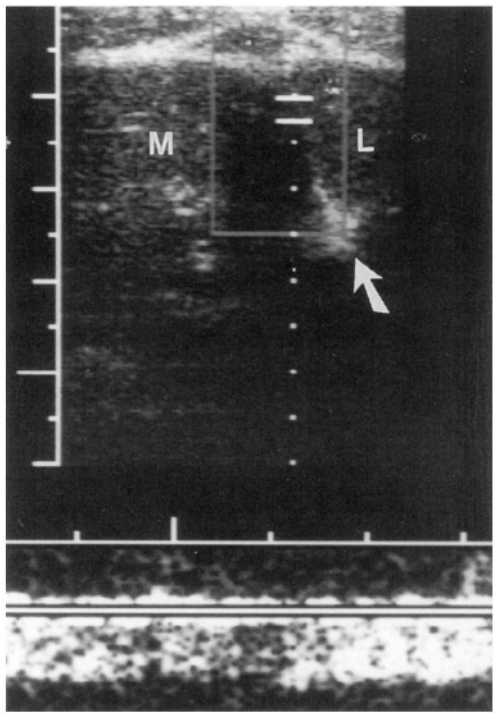


Fig. 2–38. Umbilical vein within ligamentum teres. Transverse duplex Doppler sonogram in a normal adult shows the ligamentum teres fissure *(arrow)* separating the lateral (*L*) and medial (*M*) segments of the left hepatic lobe. Note hepatopedal flow (below the Doppler baseline) in a persistently patent umbilical vein.

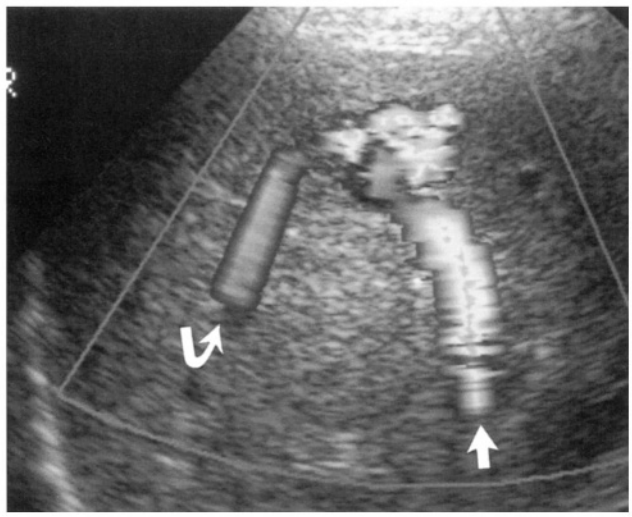
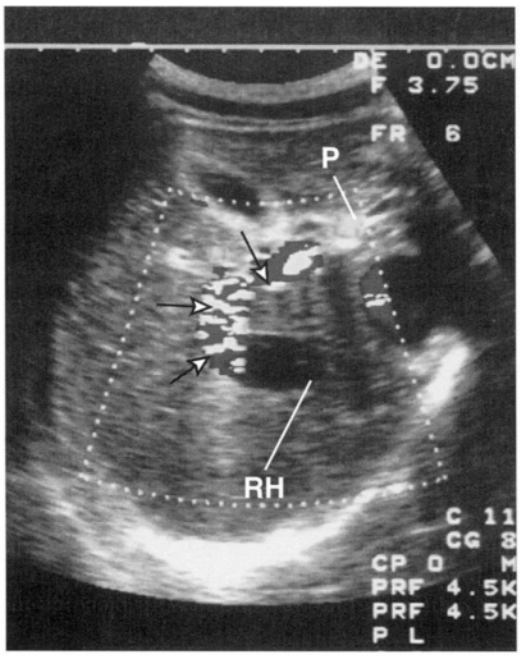
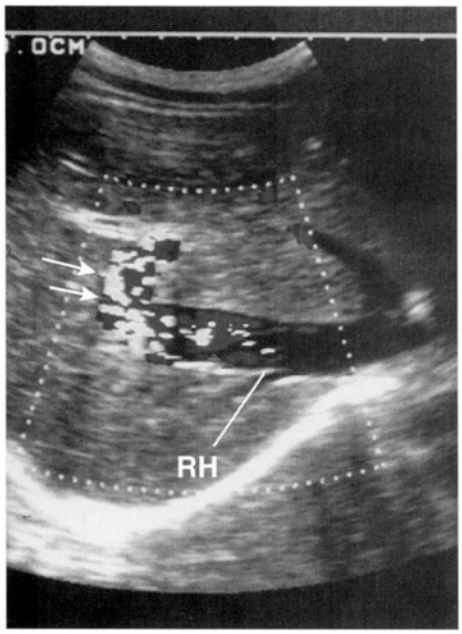


Fig. 2–39. Portohepatic venous shunt. Longitudinal color Doppler sonogram (depicted in gray scale) of the liver shows the portal *(straight arrow)* and hepatic *(curved arrow)* venous limbs of a congenital portohepatic venous shunt.





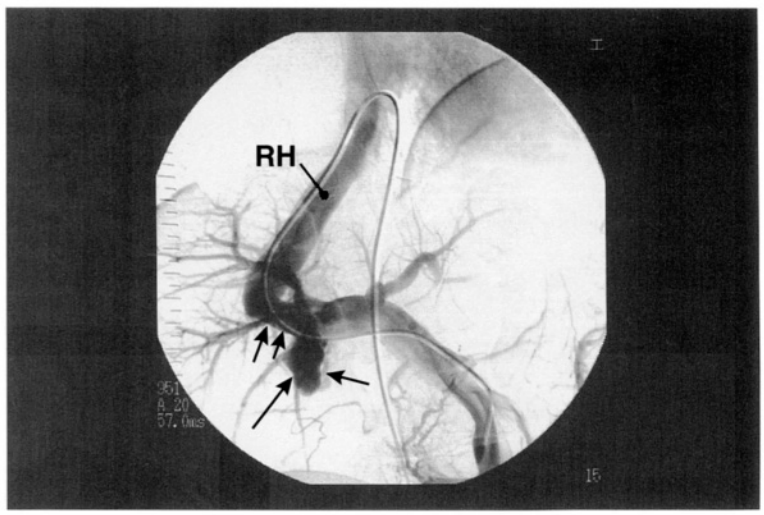


Fig. 2–40. Intrahepatic portal–hepatic venous shunt.
A 32-year–old woman was admitted because of altered mental status with vague physical symptoms for a few years.
(a and **b)** A large shunt *(arrows)* between the posterior branch of the right portal vein (*P*) and an enlarged right hepatic vein (*RH*) was discovered and confirmed by ultrasound (color Doppler ultrasonography, transverse scans, depicted in gray scale).
(c) Angiography with the catheter tip placed in the portal vein demonstrates a large shunt *(arrows)* between the right portal vein and enlarged right hepatic vein (*RH*).

tervitelline anastomosis.[73] Most patients with preduodenal portal vein have been reported to present with duodenal stenosis or intestinal obstruction in childhood. Other associated anomalies include polysplenia, annular pancreas, biliary atresia, duplicated or interrupted inferior vena cava, intestinal malrotation, and pancreatic abnormalities.[74] For asymptomatic patients, the correct imaging diagnosis of a preduodenal portal vein before abdominal surgery or laparoscopic procedures may prevent accidental injury to this vessel (Fig. 2–41).

Ductus Venosus

The ductus venosus *in utero* carries blood from the umbilical vein (Fig. 2–42) via the left portal vein into the IVC. It has been reported that the ductus is patent in 100% of neonates 1–2 days after birth and is still patent in 68% of neonates 6–7 days after birth.[75] Beyond this age of life, patent ductus venosus causes pulmonary hypertension, hypoxemia, cardiac failure, hepatic dysfunction, and hyperammonemia.[76] Ultrasound, CT, and/or angiography are used for diagnosis[77] (Fig. 2–43).

Aneurysmal Dilatation of the Portal Vein

The rare condition of aneurysmal dilatation of the portal vein has been found incidentally by ultrasound or CT or in patients having abdominal pain, gastrointestinal bleeding, portal vein thrombosis, or obstructive jaundice[78–80] (Fig. 2–44). An incomplete obliteration of the caudal–ventral intervitelline anastomotic vein or the intermediate–dorsal, intervitelline anastomotic vein



Fig. 2–41. Preduodenal portal vein.
An asymptomatic 45-year-old man presented with a minimal hepatic dysfunction.
(a and **b)** Enhanced CT shows a portal vein (*PV*) straddling the duodenum (*D*) and pancreas (*P*) and running adjacent to the gallbladder (*G*). The point of confluence with the splenic vein and superior mesenteric vein was far more caudal than usual. Associated anomalies were the interruption of the inferior vena cava with hemizygos continuation *(arrows),* midgut malrotation, and agenesis of the caudate lobe of the liver.

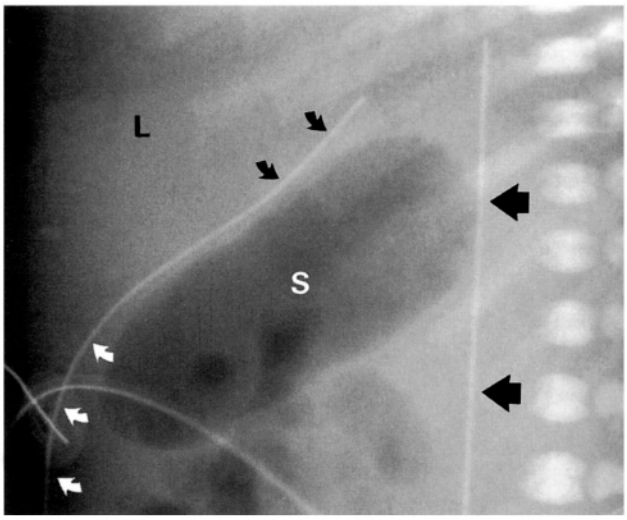


Fig. 2–42. Ductus venosus.
Lateral abdominal radiograph of a neonate shows an umbilical venous catheter traversing the patent umbilical vein *(white curved arrows)* and ductus venosus (*curved black arrows*). An umbilical artery catheter ending in the proximal abdominal aorta (*large straight arrows*) is seen more posteriorly.

may cause a diverticulum-like protrusion that may subsequently enlarge to give rise to the aneurysmal dilatation.

Agenesis of the Portal Vein

Hypoplasia or agenesis of the portal vein may be secondary to excessive obliteration of the primitive hepatic or vitelline sinusoids to the venae advehentes, which later become intrahepatic branches of the portal vein or to perinatal thrombosis of the portal vein. Associated nodular hyperplasia, hepatic adenoma, or hepatocellular carcinoma in the ischemic liver due to poor portal venous supply may be clinically important[81–83] (Fig. 2–45).

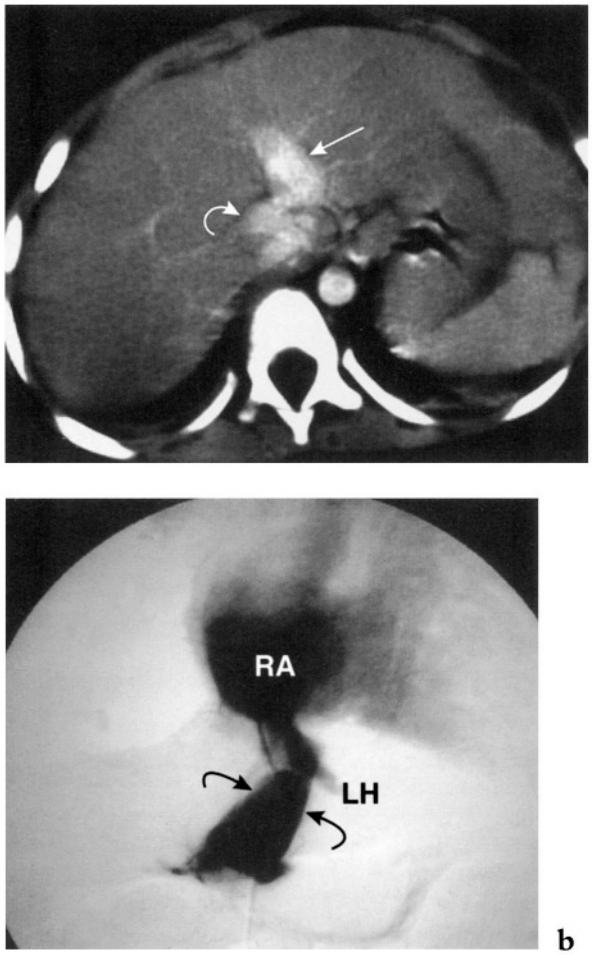


Fig. 2–43. Patent ductus venosus in a 3-year-old female with cardiac failure.
(a) Enhanced CT shows a moderately dilated left portal vein *(arrow)* and a large vessel *(curved arrow)* connecting the left portal vein and IVC.
(b) Angiography with a catheter placed at the left portal vein inserted via the IVC confirms the patent ductus venosus *(curved arrows)* ending at the confluence of the left hepatic vein *(LH)* and IVC. *RA* = right atrium.

Pancreas

Ventral and dorsal buds from the distal foregut contribute to the formation of the pancreas (Fig. 2–46). The uncinate process and inferior portion of the pancreatic head are derived from the slightly more caudal ventral bud, which is originally bifid in shape.[84–87] The body, tail, and superior portion of the head develop from the dorsal bud, which grows into the mesenchyme of the mesoduodenum (dorsal mesentery of the duodenum). The pancreatic buds follow the duodenum in the latter's 90° rotation. The anteriorly located ventral bud undergoes an additional 180° rotation that brings it rightward, posteriorly, and finally leftward to lie in the concavity of the duodenal "C-loop." The fusion of the two primordia occurs at the end of the sixth week, and their ducts anastomose. The dorsal pancreatic bud has a greater propensity for fatty infiltration than the ventral bud, which allows distinction between the pancreatic embryological anlagen on imaging studies in some in-

dividuals (Fig. 2–47). As the mesoduodenum is resorbed, the pancreas assumes its retroperitoneal location, with the exception of a small portion of the tail that lies near the hilum of the spleen that thus remains intraperitoneal in position.[84] Variations in the lateral contour of the normal head of the pancreas are common. CT scans of more than 30% of patients without pancreatic diseases have shown discrete lobulations of the pancreas greater than 1 cm lateral to the gastroduodenal or anterior superior pancreaticoduodenal artery.[88] These lobulations may mimic pancreatic masses on CT (Fig. 2–48).

Annular Pancreas

Annular pancreas is the second most common congenital anomaly of the pancreas and occurs when the two pancreatic anlagen fuse too early. On cholangiography, CT, ultrasound, and MRI, this condition may be diagnosed when pancreatic tissue is noted surrounding the descending duodenum[89–92] (Figs. 2–49 and 2–50). It may even be clearly indicated on plain films (Fig. 2–51). This condition may cause symptomatic duodenal stenosis in the neonate. A less symptomatic or asymptomatic clinical presentation can be encountered in older children and adults. This anomaly is often associated with duodenal atresia, pancreas divisum, or esophageal atresia.

Pancreas Divisum

Pancreas divisum is the most common congenital anomaly of the pancreas, occurring in approximately 5–10% of the population. Failure of the dorsal and ventral pancreatic primordia to fuse may result in separate draining of the ducts of Wirsung and Santorini (Figs. 2–52 and 2–53). Perhaps 25% of these develop pancreatitis secondary to stenosis or obstruction of one or both ducts,

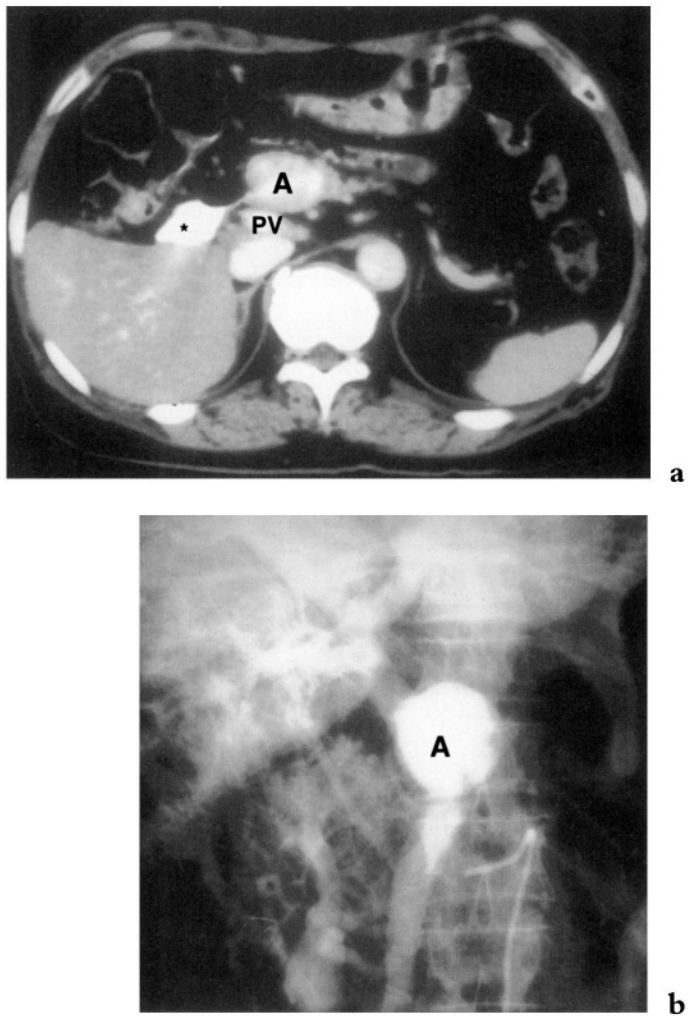


Fig. 2–44. Aneurysmal dilatation of the portal vein.
A 62-year-old woman presented with abdominal pain.
(a) Enhanced CT shows an aneurysmal dilatation *(A)* originating from and protruding anteriorly to the main portal vein (*PV*). *Asterisk* = contrast medium in colon.
(b) Transarterial portography reveals an aneurysmal dilatation of the portal vein *(A)* with a diameter of 30 mm.

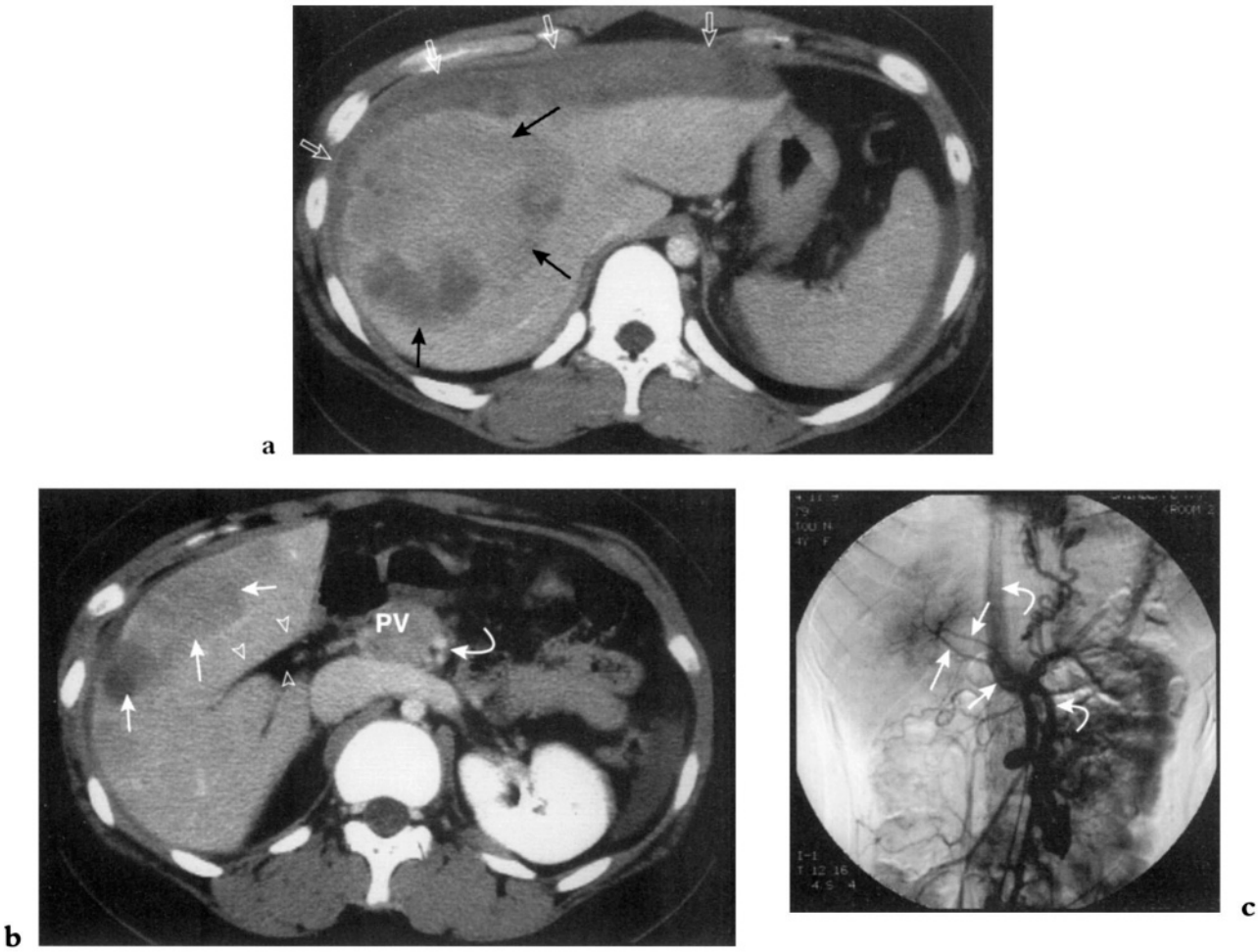


Fig. 2–45. Hepatocellular carcinoma (ruptured) associated with agenesis of the portal vein.
A 12-year-old female presented with shock and intraperitoneal bloody ascites.
(a and **b)** Enhanced CT shows a large hepatic tumor *(arrows)* with subcapsular hematoma and bloody ascites *(open arrows).* A small superior mesenteric vein *(curved arrow)* empties into the porta hepatis without opacification of the portal vein (*PV*) and intrahepatic branches (*arrowheads*). An enlarged left renal vein and IVC are noted.
(c) Transarterial portography reveals hypogenesis of the portal vein *(arrows)* and collateral circulation of mesenteric blood flow to the IVC via mesenteric–gonadal venous anastomosis *(curved arrows).*
Autopsy proved ruptured hepatocellular carcinoma.

and recently, endoscopic therapy has been developed for symptomatic patients.[93–95] The pancreatitis is usually limited to the dorsal anlage due to the small orifice of the duct of Santorini.[96–97] MR cholangiopancreatography may be useful for demonstrating pancreas divisum and anomalous pancreaticobiliary duct union.[98]

Agenesis of the Dorsal Pancreas

Agenesis of the entire pancreas is incompatible with life.[99] Hypoplasia or aplasia of the uncinal process has been reported in patients with intestinal nonrotation.[100] Agenesis of the dorsal pancreas has been found more frequently, occasionally reported as part of the polysplenia syndrome.[101] Patients with this anomaly often present with abdominal pain and symptoms of diabetes mellitus. Ultrasound or CT is usually diagnostic in revealing a round hypertrophied head of the pancreas without evidence of the body and tail of the pancreas[102] (Fig. 2–54). The finding that there is no evidence of pancreatic duct in the region of the body and tail of the pancreas ventral to the splenic vein is important to differentiate it from pancreatic atrophy secondary to a proximally located pancreatic carcinoma.

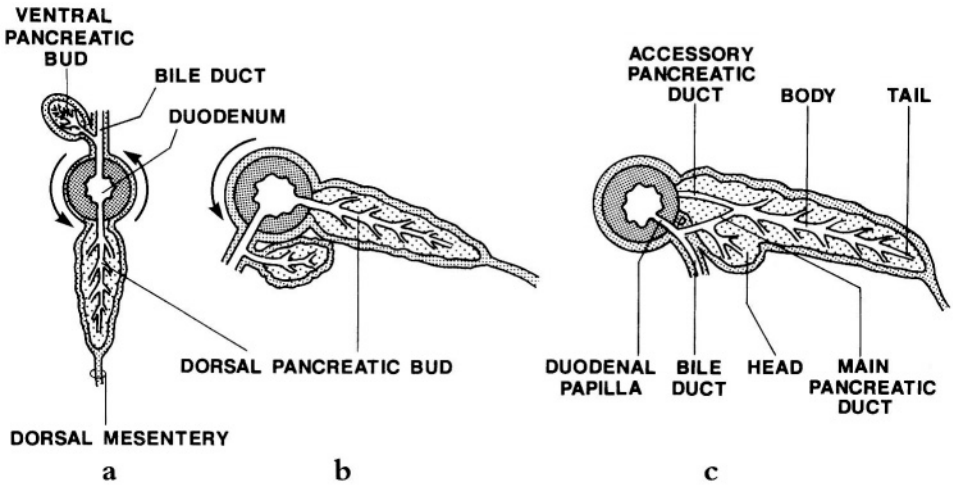


Fig. 2–46. Formation of the pancreas.
(a) Starting in the fourth week, the ventral pancreatic anlage rotates 180° (first to the right, and then posteriorly) as the duodenum rotates 90° as well. This results in a total rotation of 270°, with the original ventral anlage coming to the left of the duodenum. This rotation also carries the distal common bile duct posterior to the duodenum.
(b) The dorsal anlage is carried along by the duodenal rotation so that it too lies to the left of the duodenum.
(c) By the seventh to eighth week, the ducts of the two pancreatic buds fuse, with the ventral pancreas contributing the distal portion of the main pancreatic duct. Most of the proximal main duct arises from the dorsal anlage.
(From Javors BR, Sloves JH.[4])

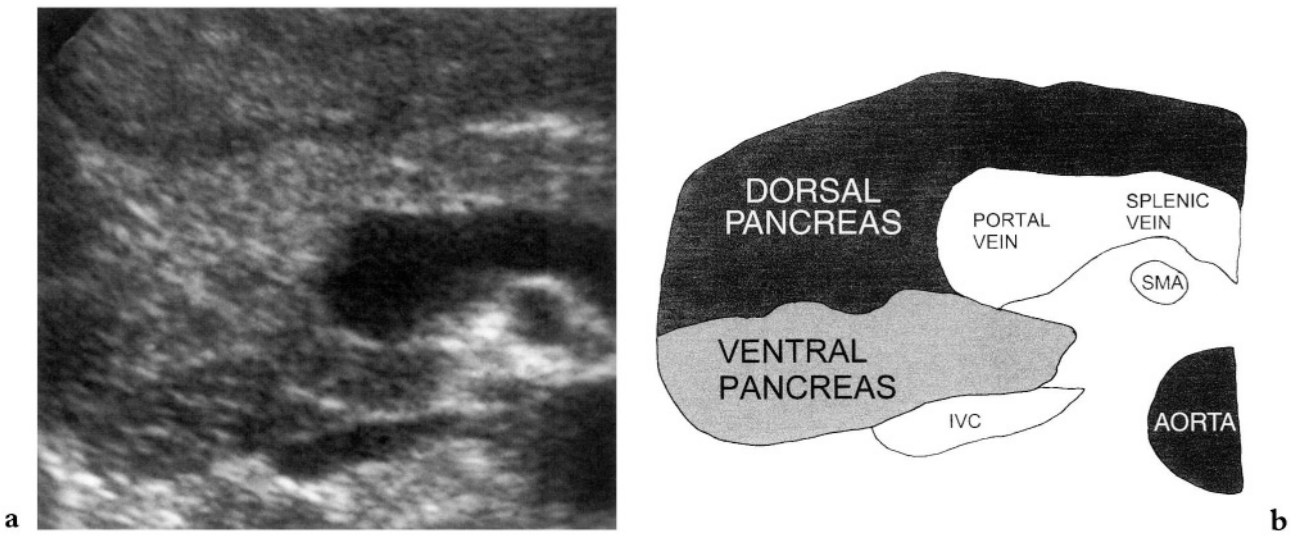


Fig. 2–47. Distinction between the pancreatic anlagen.
(a) Transverse sonogram of the midabdomen shows differential fatty infiltration of the pancreas. Note that the posteroinferior pancreatic head and uncinate process, representing the embryologic ventral pancreas, are less echogenic than the remainder of the gland, which develops from the dorsal pancreatic bud.
(b) Schematic diagram shows the relative positions of the ventral and dorsal anlagen of the pancreas in relation to the major blood vessels of that region.

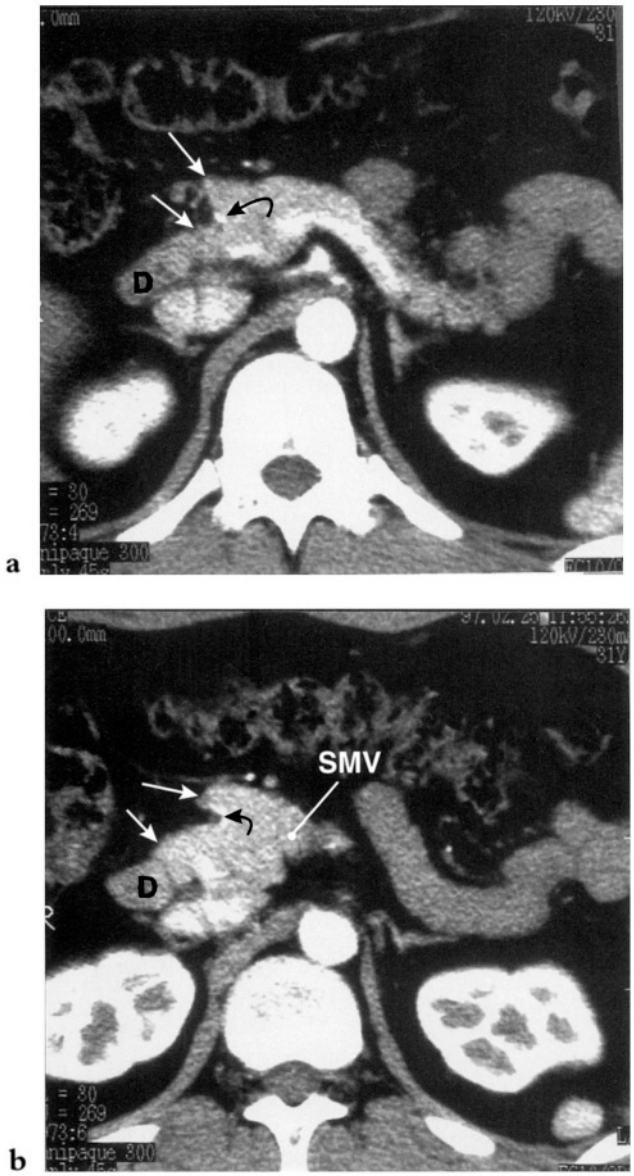


Fig. 2–48. Prominent lateral contour of the head of the pancreas (normal variant).
(a and **b)** Enhanced CT scans in a 35-year-old man show prominent lateral contours anteriorly and posteriorly *(arrows)* lateral to the gastroduodenal artery (*curved arrows*). *D* = duodenum; *SMV* = superior mesenteric vein.

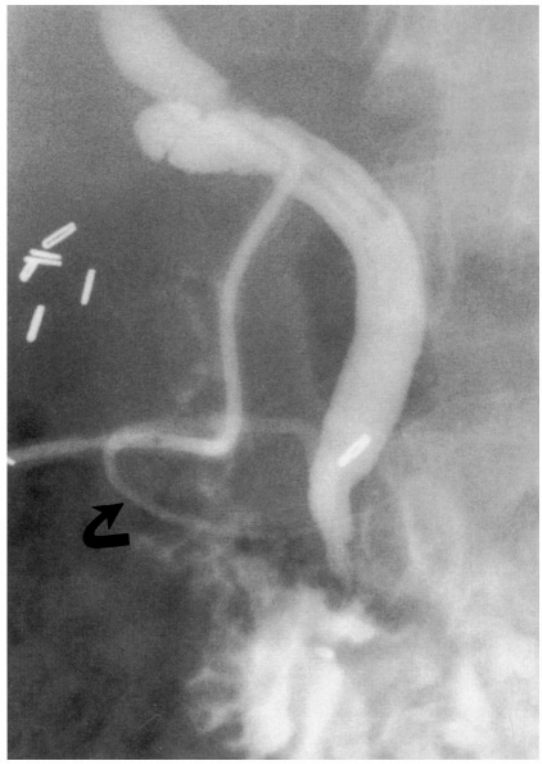


Fig. 2–49. Annular pancreas.
T-tube cholangiogram shows reflux into a circumduodenal pancreatic duct *(curved arrow),* confirming the presence of an annular pancreas.
(From Javors BR, Sloves JH.[4])

Pancreatic Arteriovenous Malformation

More than 30 cases of pancreatic arteriovenous malformation (AVM) have been reported in the literature.[103–105] The etiology of this condition is not clear. Most had been regarded as congenital, whereas the others were presumed to be secondary to pancreatitis or liver cirrhosis. Clinical manifestations of pancreatic AVM include abdominal pain, recurrent gastrointestinal tract bleeding, portal hypertension, and duodenal ulcer. Angiography or the artery-dominant phase of dynamic CT is diagnostic (Fig. 2–55). MR imaging and color Doppler ultrasonography may also be useful.

Pancreatic Cysts

Congenital pancreatic cysts may be single or multiple. Multiple true pancreatic cysts are more common than single ones and have been found in autosomal dominant polycystic kidney disease, von Hippel-Lindau disease (an autosomal dominant trait), and cystic fibrosis.[106,107] Pancreatic cysts or macrocystic adenomas are seen in more than one-half of patients with von Hippel-Lindau disease. Demonstration of pancreatic cysts on CT, MRI, or ultrasound associated with evidence of retinal angiomatosis, cerebellar hemangioblastoma, and cysts of various organs and with family history is diagnostic (Fig. 2–56).

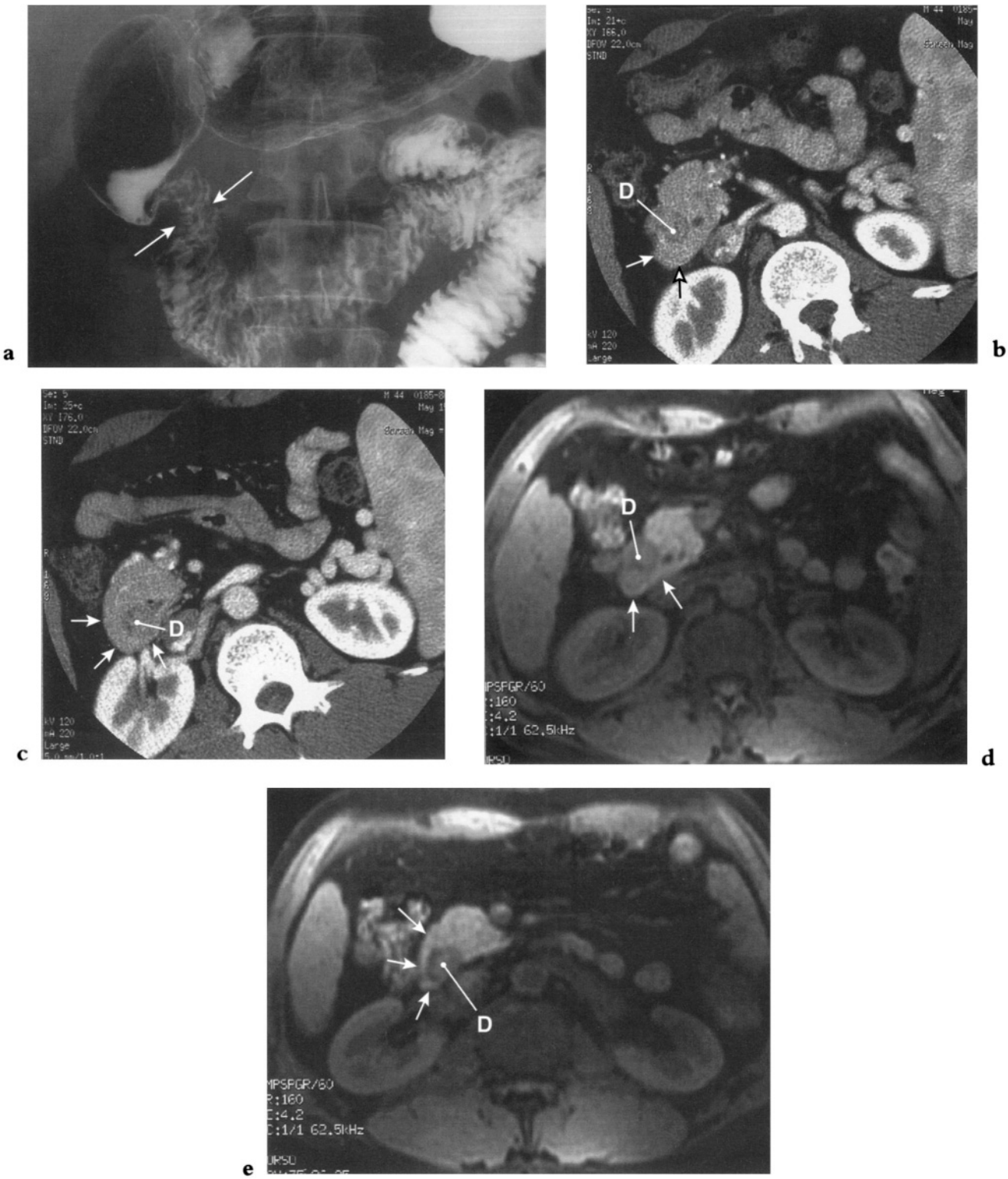


Fig. 2–50. Annular pancreas.
A 44-year-old man presented with abdominal pain.
(a) Upper GI series shows a localized stenosis of the descending duodenum *(arrows).*
(b and **c)** Enhanced CT scans and MR images **(d** and **e)** show pancreatic tissue *(arrows)* encircles the descending duodenum (*D*).



Fig. 2–51. Annular pancreas.
Coned-down view from a supine radiograph of the abdomen shows an air-filled duodenal sweep. A short constriction is noted in the proximal descending portion *(arrows)* secondary to the presence of an annular pancreas. (From Jadvar H, Mindelzun RE.[90])

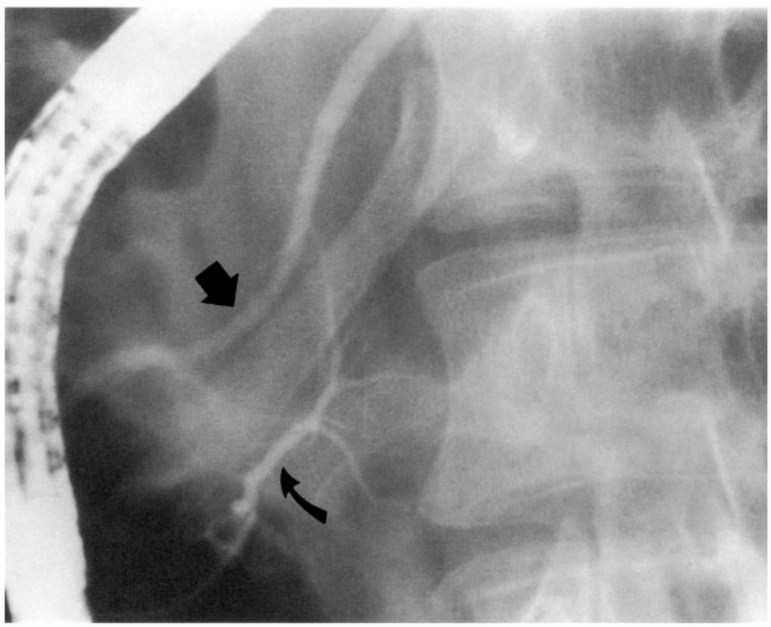


Fig. 2–52. Pancreas divisum.
Cannulation of the major papilla during an ERCP opacifies the small ductal system *(curved arrow)* of the ventral pancreatic bud. Previous cannulation of the minor papilla had opacified the much larger and noncommunicating accessory duct *(straight arrow)* arising from the dorsal pancreatic anlage in this patient with a pancreas divisum.
(From Javors BR.[3])

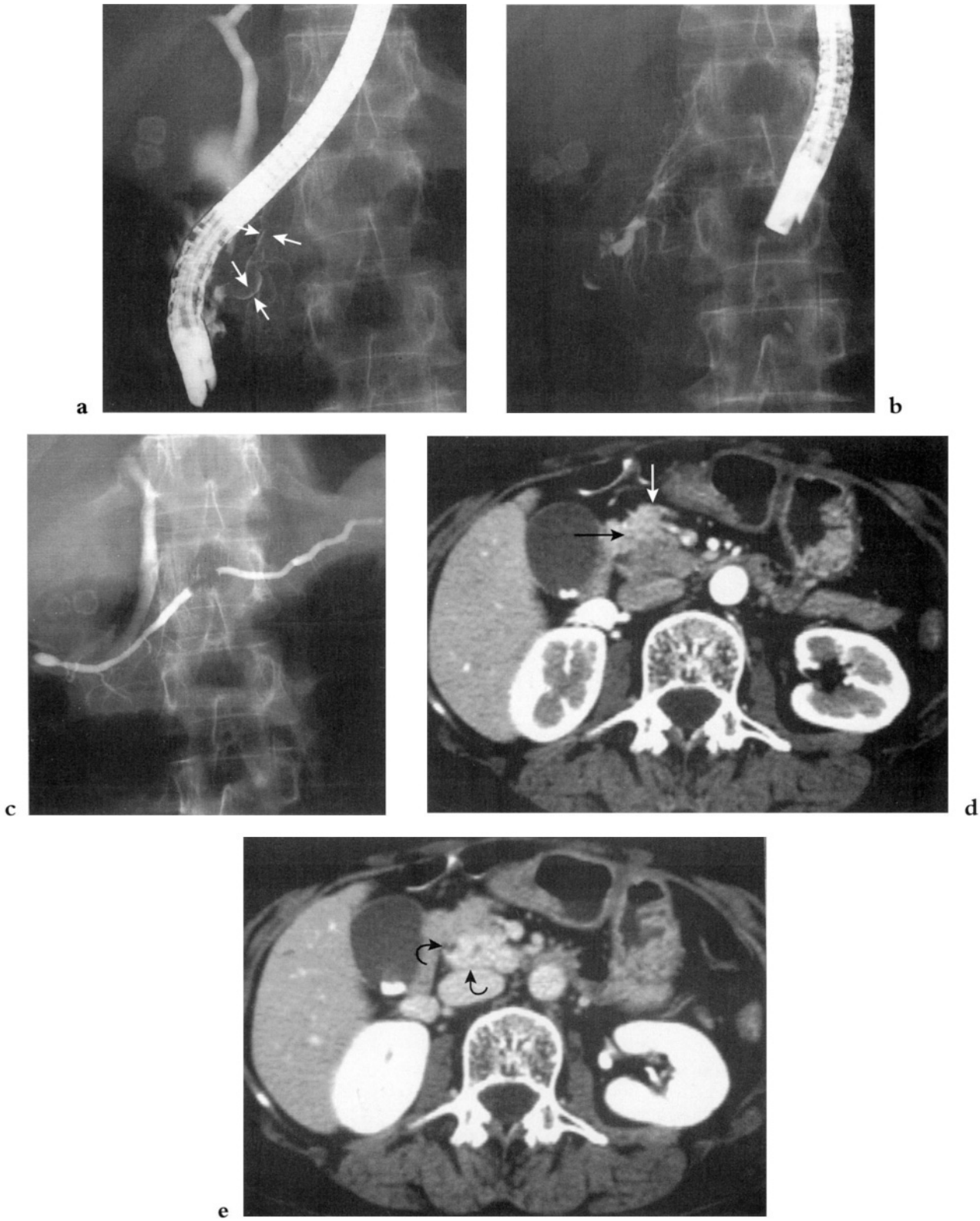


Fig. 2–53. Pancreas divisum with focal pancreatitis of ventral anlage presenting with bleeding in the pancreatic duct.
A 55-year-old woman with history of recurrent tarry stool for several years presented with acute GI tract bleeding.
(a) Endoscopic retrograde injection of contrast medium into the major papilla shows filling defects within the dilated branches of the ventral ducts representing blood clots *(arrows).*
(b and **c)** ERCP performed 2 weeks later confirms pancreas divisum.
Multiphase dynamic CT scans **(d)** taken at 30 sec and **(e)** at 180 sec after the start of infusion of intravenous contrast medium show early enhancement of dorsal anlage *(straight arrows)* and late enhancement of ventral anlage *(curved arrows).* Partial pancreatectomy revealed chronic pancreatitis with moderate fibrosis of the ventral anlage.

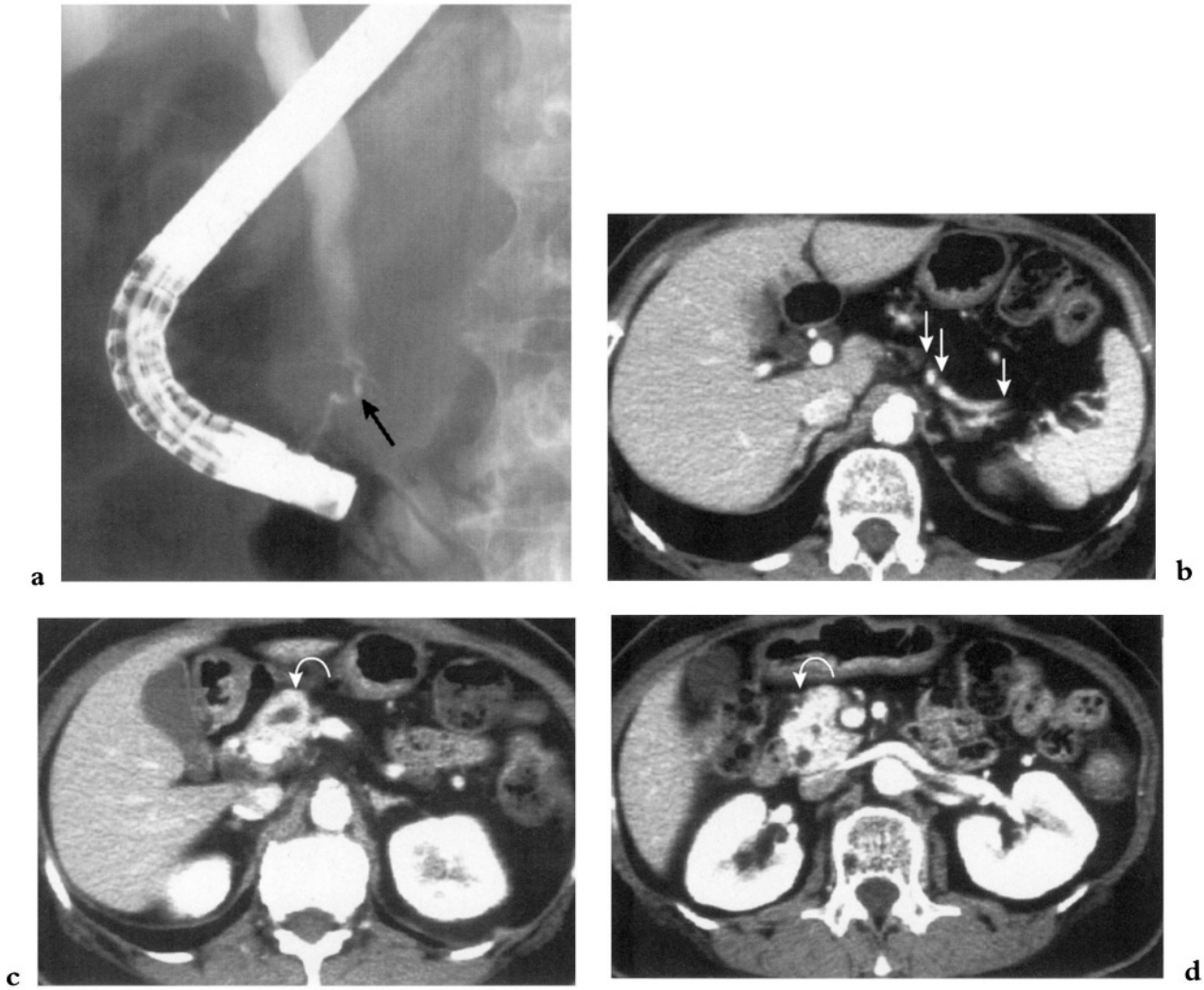


Fig. 2–54. Agenesis of the dorsal pancreas.
A 66-year-old woman presented with abdominal pain and mild diabetes mellitus.
(a) ERCP shows a short, tortuous pancreatic duct *(arrow).*
(b to **d)** Enhanced CT scans show a round-shaped head of the pancreas *(curved arrows)* without evidence of the body and tail of the pancreas ventral to the splenic vein *(straight arrows).* There is minimal dilatation of the pancreatic duct in the head and neck of the pancreas but no evidence of pancreatic duct in the region of the body and tail.

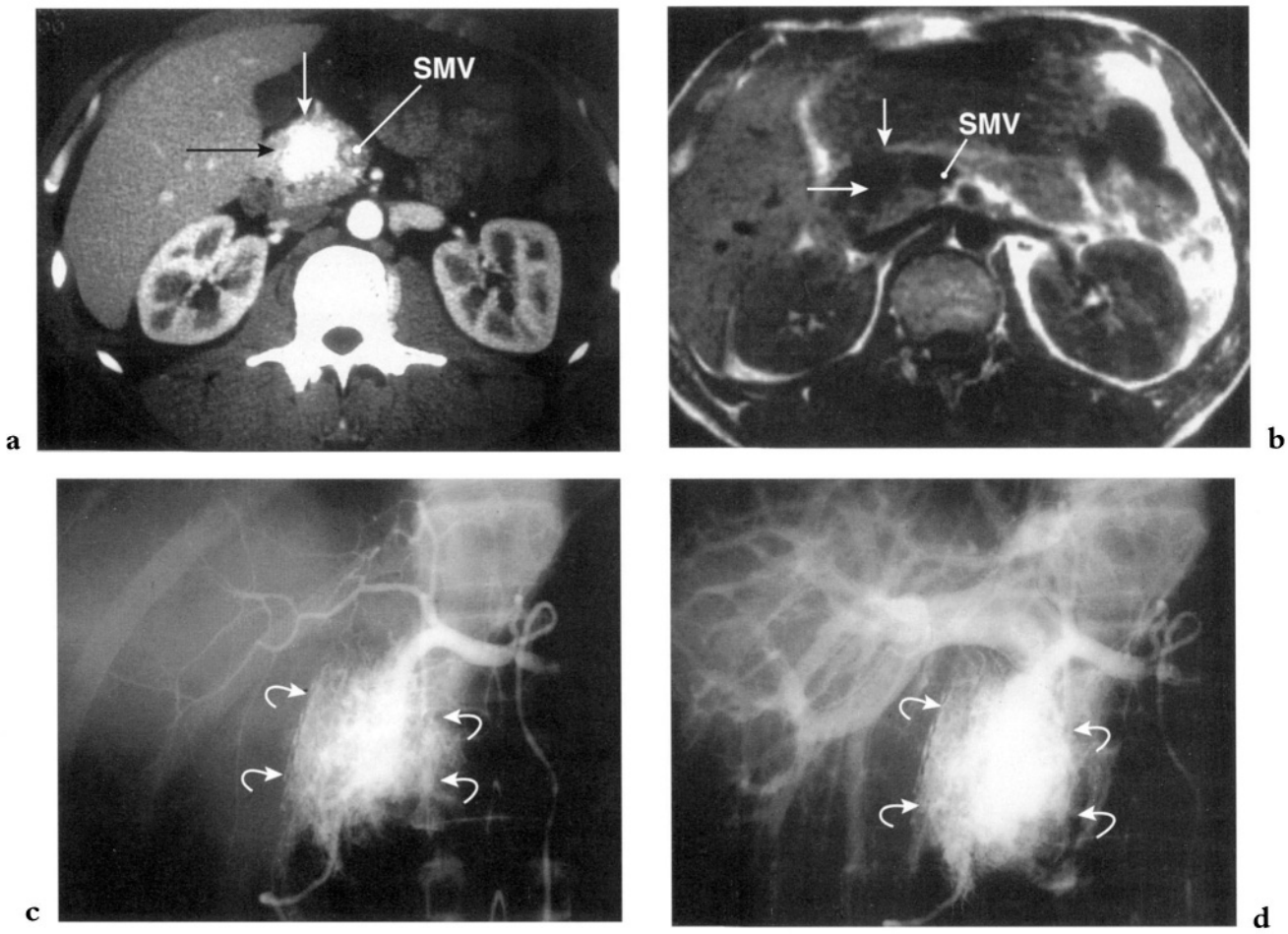


Fig. 2–55. Arteriovenous malformation in the region of the head of the pancreas.
A 34-year-old man presented with recurrent duodenal ulcer.
(a) CT scan at artery-dominant phase shows an intense enhancement of the region of the head of the pancreas *(arrows). SMV* = superior mesenteric vein.
(b) T1-weighted MRI demonstrates an area of signal void in the head of the pancreas *(arrows).*
(c and **d)** Angiography reveals arteriovenous malformation *(curved arrows)* in the head of the pancreas fed by pancreatic and duodenal arteries and draining to pancreaticoduodenal veins and the superior mesenteric vein.

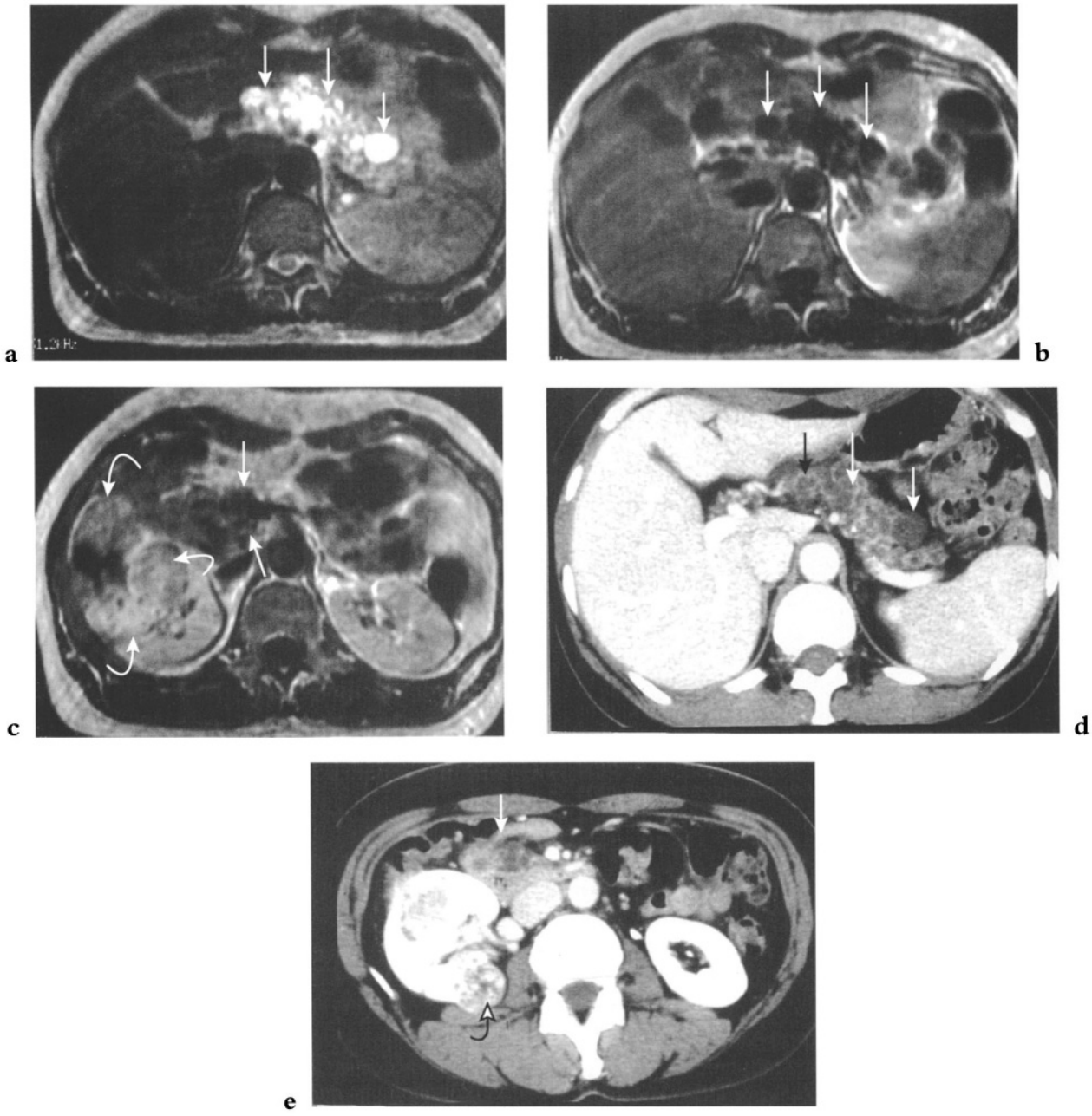


Fig. 2–56. Pancreatic cysts and renal carcinomas in von Hippel-Lindau disease.
A 48-year-old woman had a family history of von Hippel-Lindau disease.
(a to **c)** T2-weighted and postcontrast T1-weighted MR images show multiple cysts of the pancreas *(arrows)* and a mass of the right kidney *(curved arrows).*
(d and **e)** CT scans demonstrate pancreatic cysts *(arrows)* and another mass of the right kidney *(curved arrow).* Right nephrectomy revealed multiple renal cell carcinomas of the right kidney.

Spleen

A condensation of multiple mesenchymal clusters gives rise to the spleen within the elongated dorsal mesentery of the stomach. The more anterior portion of the mesogastrium connects the spleen to the stomach, becoming the gastrosplenic ligament. That portion of the mesentery between the spleen and the posterior abdominal wall becomes the lienorenal (splenorenal) ligament (Fig. 2–5). As the dorsal bulge of the stomach rotates, the elongated mesogastrium carries the developing spleen to the left. This dorsal mesentery then partially fuses with the posterior abdominal wall over the left kidney, forming the definitive lienorenal ligament (Fig. 2–57). If the various cell clusters do not fully unite, excessive splenic lobulation or an accessory spleen may result.[108,109]

Accessory Spleen

Accessory spleen, reported in 10–31% of cases in autopsy series,[110] are usually located in the splenic hilum or along the splenic vessels or associated ligaments (Fig. 2–58). Most remain small nodules, but following a splenectomy, residual splenic tissue can undergo compensatory enlargement[111] (Fig. 2–59). This identification can be easily verified with isotopic studies. Rarely, the accessory tissue may even be intrapancreatic in location.[112] An overlooked accessory spleen may result in therapeutic failure of splenectomy in patients with hematologic disorders[113] (Fig. 2–60).

Wandering Spleen

The suspending ligaments of the spleen may be absent or may elongate due to congenital or acquired causes, leading to a migration of the spleen from its normal location in the left upper quadrant on an elongated pedicle containing splenic vessels. This is called a "wandering spleen" (Fig. 2–61) and renders that organ susceptible to torsion and possible infarction. It occurs most frequently in women of childbearing age. The clinical diagnosis of this entity can be very difficult.[114–116] Patients may have an asymptomatic mass, a mass with sub-

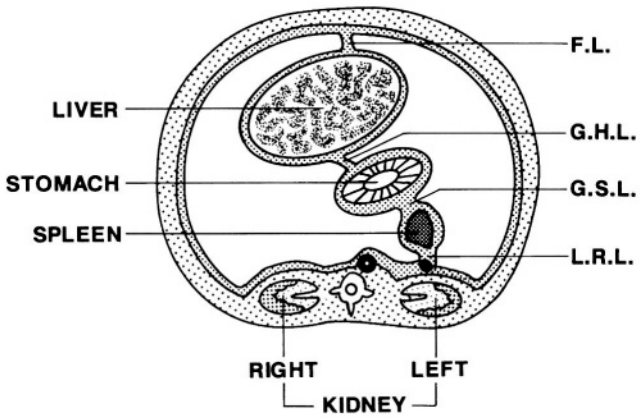


Fig. 2–57. Schematic cross-sectional diagram through the upper abdomen reveals continued rotation of the elongated mesogastrium containing the splenic bud. This rotation brings the dorsal mesentery to lie along the posterior abdominal wall. Eventual involution and fusion of the mesentery leaves the lienorenal ligament (*L.R.L.*) as its remnant. The gastrosplenic ligament (*G.S.L.*) forms one of the borders of the lesser sac. The gastrohepatic ligament (*G.H.L.*) persists as the lesser omentum. The falciform ligament (*F.L.*) continues to separate the right side of the peritoneum from the left, anteriorly and superiorly in the subphrenic space.
(From Javors BR, Sloves JH.[4])

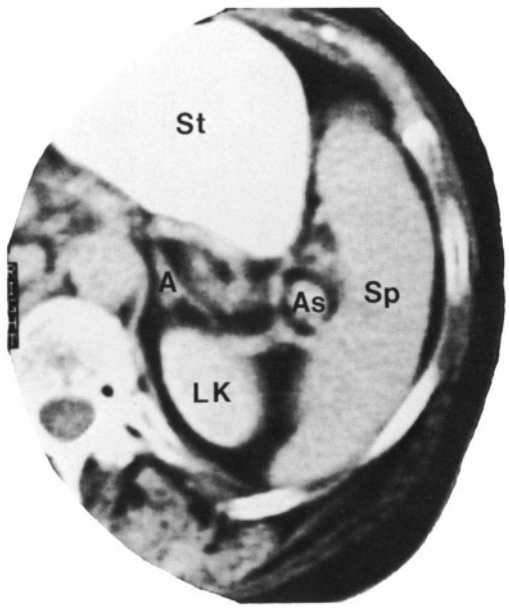


Fig. 2–58. Accessory spleen.
Contrast-enhanced CT scan demonstrates nodule of accessory spleen *(As)* in the hilus of the spleen (*Sp*) within the branching of the splenic artery. *LK* = left kidney; *A* = adrenal gland; *St* = stomach.

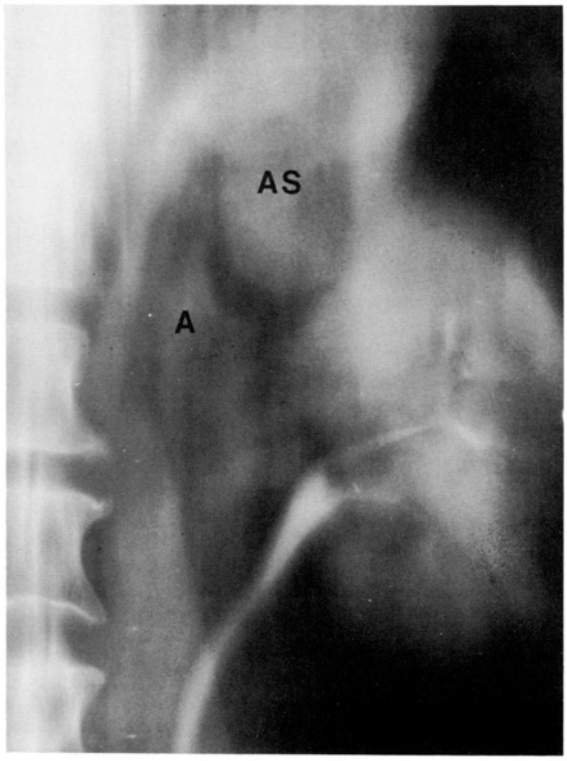


Fig. 2–59. Hypertrophied residual accessory spleen. Nephrotomogram in a postsplenectomy patient shows lateral deviation of the left kidney and demonstrates the soft-tissue mass of an accessory spleen (*AS*), presumably hypertrophied. The accessory spleen was further verified by arteriography and a splenic scan. The normal left adrenal gland (*A*) is also identified.

acute abdominal or gastrointestinal symptoms, or acute abdominal findings. When there is uncertainty whether the mass truly represents an ectopically located spleen, radionuclide imaging with technetium-99m (^{99m}Tc) sulfur colloid can resolve the dilemma. Most commonly, the pedicle becomes constricted because of torsion, and venous occlusion causes splenic congestion and progressive enlargement. Complete occlusion may result in hemorrhagic infarction, subcapsular hemorrhage, gangrene, or functional asplenism. Barium enema studies may demonstrate medial and anterior displacement of the splenic flexure or a bandlike colonic impression caused by the pressure from the splenic pedicle. The classic radiographic findings of torsion include an ectopic location and on CT, a whirled appearance along its medial aspect[117,118] (Fig. 2–62). Torsion of a wandering accessory spleen has also been reported.[119]

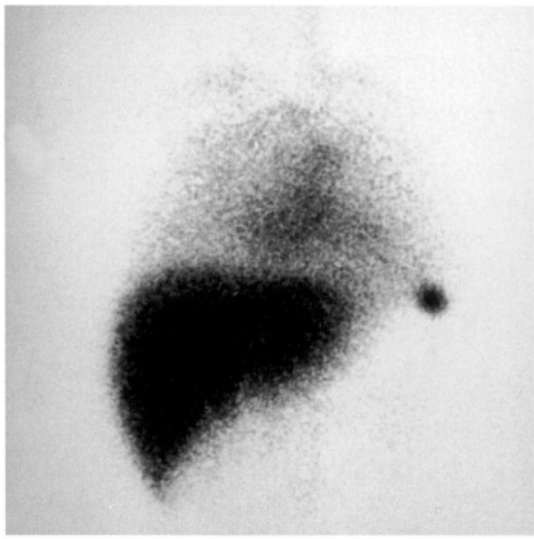


Fig. 2–60. Overlooked accessory spleen, postsplenectomy, in a patient with bleeding disorder. Heat-damaged red blood cell radionuclide scan shows a small focus of activity in the anterior left upper quadrant consistent with an accessory spleen. The patient had idiopathic thrombocytopenic purpura, and a previous splenectomy had failed to correct the low platelet count. The presence of an accessory spleen was confirmed at laparotomy. (Courtesy of Sam Wang, M.D.)

Polysplenia Syndrome

Polysplenia syndrome is a congenital disorder that is a type of situs ambiguous characterized by left isomerism (bilateral left sidedness). In addition to multiple spleens, there are often cardiac anomalies, interruption of the IVC with azygos continuation, bilateral hyparterial bronchi, and abdominal heterotaxia.[120,121] Most patients die by the age of 5 years because of the severe cardiac anomalies. However, the syndrome may be first seen in adulthood, particularly when there is no accompanying congenital heart defect[120–122] (Figs. 2–63 and 2–64).

Internal Hernias

An internal hernia is a protrusion of a viscus through a normal or abnormal aperture within the peritoneal cavity. Most internal hernias are the consequence of congenital anomalies of intestinal rotation and peritoneal attachment. Whereas they may occur in the pediatric age group, the majority are clinically encountered in



Fig. 2–61. Wandering spleen.
(a) CT through the upper abdomen reveals a stomach with oral contrast delineating its posterior wall *(arrows).*
(b) CT through the pelvis of the same patient shows a multilobate mass in the left lower quadrant. The absence of the spleen in the left upper quadrant and visualization of normally located kidneys *(not shown)* help confirm the diagnosis of a wandering spleen.
(Courtesy of Kyunghee C. Cho, M.D.)

adults. Internal abdominal hernias are discussed in detail in Chapter 16.

Urogenital System

Urinary Tract

The embryologic development of the kidneys encompasses three phases. These are the pronephros, mesonephros, and metanephros. They go through overlapping cycles of growth and regression, resulting in the formation of the definitive kidneys and urogenital system from the latter two stages.

At the end of the third week, paired collections of primitive tubules form and empty into paired excretory ducts that lead to the cloaca.[123] This pronephros never functions in humans and involutes by the early fifth week.[124]

While the pronephros is already involuting, a pair of structures forms just caudal to the pronephros. The tubules of this mesonephros actually function. They reach their full maturation by the end of the seventh week. Development, maturation, and involution all proceed in a craniocaudal progression, with considerable overlapping.[124]

The intermediate mesoderm from which the mesonephros originates is divided by a longitudinal cleft, and a medially placed mesonephric duct is formed. A few days later, this duct communicates with the cloaca. Arteries that originate from the iliac arteries and the distal aorta supply the mesonephros itself. Drainage of the tubules is via the mesonephric duct (previously called the Wolffian duct). The latter partially involutes while play-

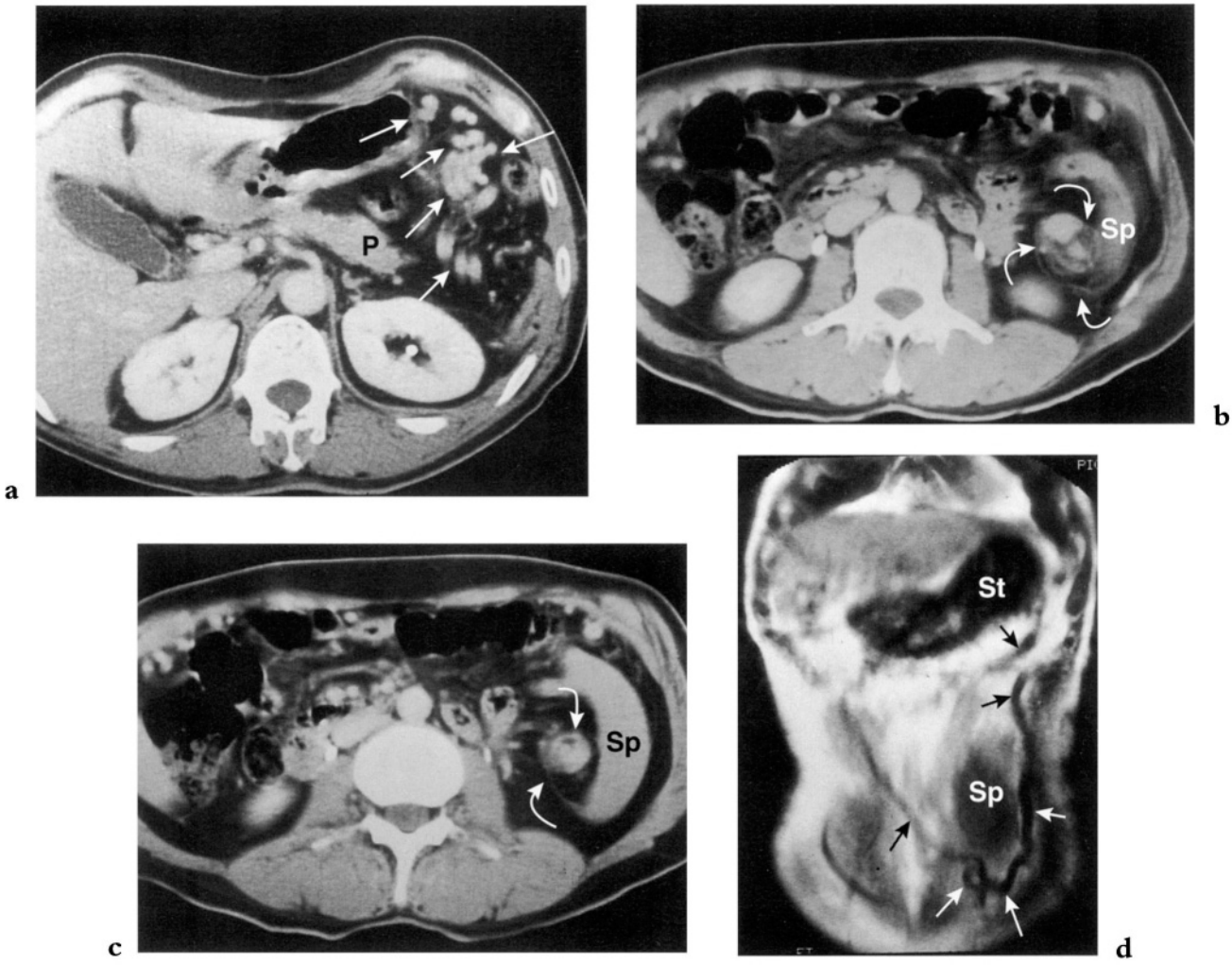


Fig. 2–62. Wandering spleen with torsion of vascular pedicle.
A 56-year-old man with chronic volvulus of an ectopic spleen.
(a) CT of the upper abdomen shows no evidence of the spleen in the left upper quadrant. There are prominent collateral veins *(arrows)* secondary to occlusion of the splenic vein. *P* = pancreas.
(b and **c)** The spleen *(Sp)* is located in the left lower abdomen. The vascular pedicle of the splenic hilum shows a whirled appearance *(curved arrows).*
(d) MRI (T1-weighted coronal view) displays the spleen *(Sp)* in the left lower quadrant and numerous serpentine collateral veins *(arrows). St* = stomach.



Fig. 2–63. Polysplenia syndrome in a 44-year-old man with abdominal pain.
(a) CT of the upper abdomen demonstrates a left-sided liver with absence of the hepatic segment of the IVC, a dilated hemiazygos vein *(arrow)* adjacent to the descending aorta, a right-sided heart (*C*), and two splenules on the right, lateral to a right-sided stomach (*S*).
(b) CT 4 cm lower shows a deep fissure divides the relatively normal-sized spleen.
(Reproduced from Gayer et al.[122])

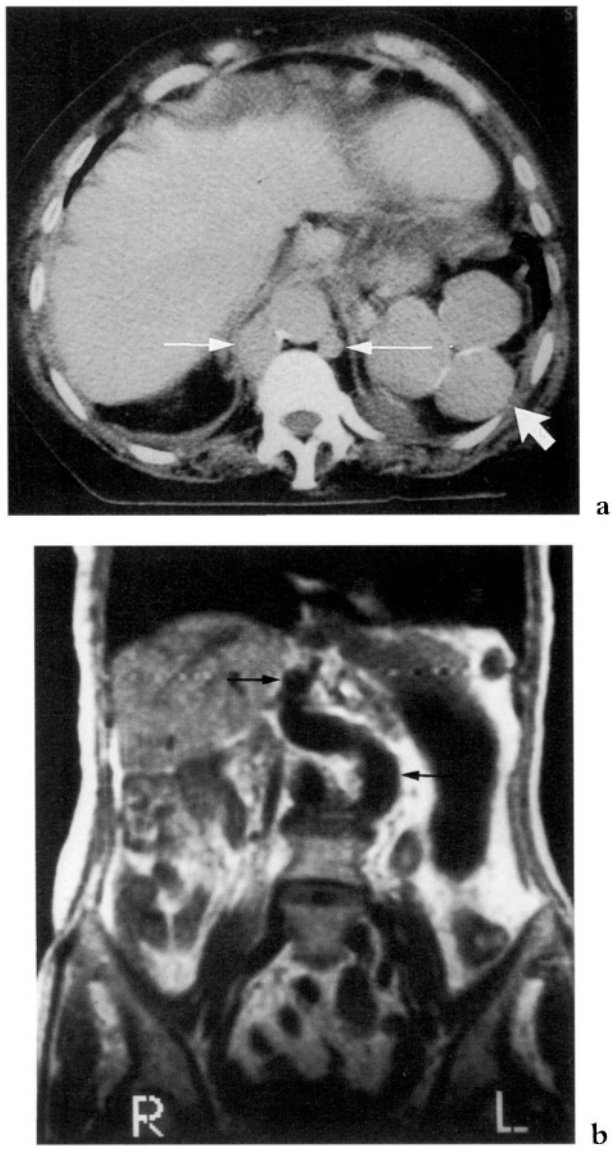


Fig. 2–64. Polysplenia syndrome in a 70-year-old woman.
(a) CT of the upper abdomen shows three rounded splenules in the left upper quadrant *(thick arrow)* and dilated azygos and hemiazygos veins in the retrocrural area *(thin arrows).*
(b) Coronal T1-weighted MR image demonstrates the anomalous course of the interrupted IVC with its azygos continuation *(arrows).*
(Reproduced from Gayer et al.[122])

ing a major role in the development of the genital system in the male.

As the mesonephros and its duct regress, the metanephros starts to develop, culminating in the development of the definitive kidney and ureter. This process starts with the formation of a small bud from the mesonephric duct, just proximal to its emptying into the cloaca (Fig. 2–65). As this bud elongates, it develops a bulbous end (ampulla) and a slender neck. The ampullary end eventually becomes the renal pelvis, and the slender neck becomes the ureter proper.[124] Specialized cells at the ampullary end interact with the surrounding mesoderm (metanephric blastema) to form the nephrons and connective tissue of the kidney.[123]

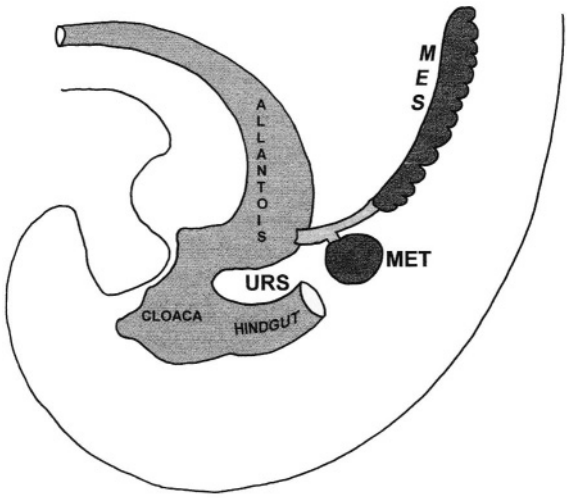


Fig. 2–65. Sagittal schematic of a 5-week embryo shows the allantois and hindgut emptying into the cloaca. The developing urorectal septum *(URS)* has started to partition the cloaca into separate GI and urinary compartments. The mesonephros (*MES*) and its duct are seen dorsally and superiorly. A short diverticulum from the mesonephric duct (developing ureter) is capped by the metanephric blastema *(MET).*

The ureteric bud undergoes simultaneous lengthening and division. The developing metanephros grows into the space vacated by the regressing mesonephros.[124] The branching of the ureteric bud continues through many generations, leading to the development of the renal pelvis, calyces, papillae, cribriform plates, and even the collecting tubules. This branching also leads to the lobular contours of the fetal kidney that may persist into adulthood. The fetal kidney also undergoes a gradual fusion of calyces, but not papillae, that continues into the postpartum period, resulting in compound calyces.[123]

The development of the metanephros is accompanied by a change in its position and orientation. When the ureteral bud first contacts the metanephric blastema, it is at the level of the lower lumbar spine or upper sacrum. Originally, the paired metanephros almost touch each other in the midline. During the rapid growth of the caudal end of the fetus, they grow into the space occupied by the involuting mesonephros. Straightening of the fetal spinal curvature adds to the apparent migration of the kidney.[125] By the end of the third month, the kidney is located at the level of the second or third lumbar vertebra, and at birth, it has ascended to the T12-L1 level. Rotation of the kidney along its longitudinal axis accompanies this ascent. The original renal pelvis lies along the anterior aspect of the developing kidney, eventually reaching an anteromedial location by the ninth week. Rarely, the kidney overrotates, leading the blood vessels to wrap around its posterior surface.

The blood supply to the developing kidney also undergoes change as it migrates cephalad. Lateral sacral branches from the distal aorta supply the metanephros. As the kidney migrates superiorly, lateral stem (end) arteries from more rostral levels of the aorta progressively supply it until the definitive renal arteries develop. Persistence of the more caudal arteries results in multiple and/or aberrant renal arteries.

Renal Agenesis

Agenesis of the kidney may result from failure of the ureteral bud to form, failure of the bud to encounter and induce the metanephric blastema, or absence of the blastema itself. When agenesis occurs, it is associated with abnormalities of the ipsilateral genital structures, including seminal vesicle cysts.[126] A hemitrigone may be formed in the urinary bladder (Fig. 2–66). Agenesis of the kidney is discussed and illustrated in Chapter 9.

Crossed Fused Renal Ectopia, Horseshoe Kidney, and Blind-Ending Bifid Ureter

If there is asymmetric inhibition of ureteral bud growth prior to the separation of the metanephric blastemae, a crossed fused ectopia will occur[127] (Fig. 2–67). If the inhibition is symmetric, then a horseshoe kidney results (Fig. 2–68). The two portions of the kidney may be united at their lower pole by either a band of fibrous tissue or, more commonly, functioning parenchyma.[124] The renal pelves are still directed anteriorly, and the ureter must pass over and anterior to the resultant mass effect. This accounts for the common ureteropelvic (UPJ) obstruction. A crossing renal vessel may exacerbate this as well.[124] The fused lower poles of a horseshoe kidney may also press on the underlying IVC, causing obstruction of that vessel and resultant bilateral leg edema.[128] If inhibition occurs after the separation, either uni- or bilateral ectopia will occur.[127] Early division of the ureteral bud that does not contact a metanephric blastema gives rise to a blind-ending bifid ureter. Although clearly demonstrated on excretory urography (Fig. 2–69) or a retrograde pyelogram, a blind-ending bifid ureter may be very difficult to diagnose on cross-sectional imaging.[129] Early division that does contact the blastema leads to a partially or completely duplicated ureter and collecting system.[127]

Urinary Bladder

The bladder and portions of both the male and female genital tract are partially derived from the distal hindgut.



Fig. 2–66. Bladder hemitrigone associated with renal agenesis.
Supine film from an intravenous urogram reveals a large solitary kidney on the right. The distal ureter is noted to cross the midline *(arrows)* emptying onto a hemitrigone in this patient with left renal agenesis.
(Courtesy of Marc Z. Simmons, M.D.)



Fig. 2–67. Crossed-fused renal ectopia.
Left retrograde ureterogram shows a cross-fused ectopia. The left kidney lies inferior and medial to the previously opacified right kidney (*curved arrow*). The distal right ureter *(straight arrow)* can be seen in its normal location.
(Courtesy of Marc Z. Simmons, M.D.)

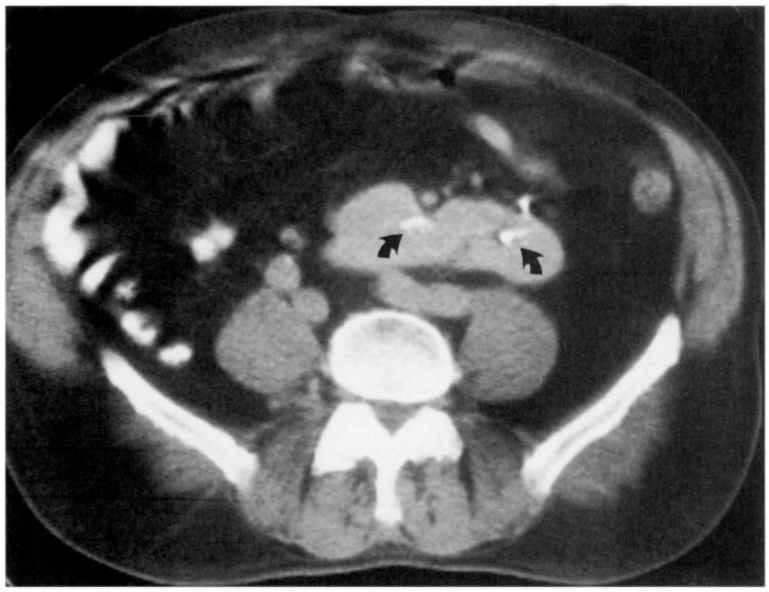


Fig. 2–68. Horseshoe kidney.
Contrast-enhanced CT of the pelvis demonstrates a horseshoe kidney. Both renal pelves can be seen along the anterior border (*curved arrows*). The two kidneys are connected by functioning renal parenchyma.
(Courtesy of Marc Z. Simmons, M.D.)



Fig. 2–69. Blind-ending ureteral bud.
Supine view of the pelvis from an intravenous urogram shows a short, blind-ending segment of ureter that lies just medial to the normal ureter draining the right kidney. No collecting system or functioning renal parenchyma is visualized.

The cloaca is the endoderm-lined terminal hindgut. This cavity is in continuity with the allantois (a yolk sac diverticulum).[9] Urorectal folds grow in from the side wall, forming a septum that separates the ventral urogenital sinus from the more dorsal rectum (Figs. 2–65 and 2–70).

The allantois and a portion of the cloaca unite to eventually form the definitive bladder. The allantois that connects the dome of the bladder to the umbilicus eventually becomes atretic and is called the urachus. The obliterated fibrous connection can be seen in adults as the medial umbilical fold. Similar to the omphalomesenteric duct from the gastrointestinal tract, draining umbilical sinuses or a diverticulum-like outpouching of the bladder may be seen.[124] A urachal sinus is the most common anomaly, with a urachal cyst next in frequency. A patent urachus is much less commonly encountered.[130] The urachus may become the site of dysplasia, leading to the development of carcinoma. The distal mesonephric ducts and the metanephric diverticulum are separately incorporated into the urogenital sinus. The mesonephric ducts become the vas deferens, seminal vesicles, and ejaculatory ducts in the male and minimally contribute to the urethra, while the metanephric ducts become the ureters.[124]

Genital System

The chromosomal and genetic sex of an embryo is determined at the time of fertilization. Early development is the same for both sexes and is called the indifferent stage. Mesodermal epithelium that lines the posterior abdominal wall, the underlying mesenchyme, and primordial germ cells (from the yolk sac) all contribute to the gonadal formation.

Some of the mesodermal epithelium medial to the mesonephros thickens along with growth of the underlying mesenchyme. This produces a bulge called the gonadal ridge. Epithelial cells grow into the mesenchyme, becoming, respectively, the cortex and medulla of the indifferent gonad. In males, the cortex regresses, and the medulla forms the testis. The converse occurs in females, with the cortex forming the ovary and the medulla regressing.

The primordial germ cells originate from the endoderm of the yolk stalk, migrating along the suspending dorsal mesentery of the hindgut to reach the subperitoneum[131] (Fig. 2–71). There they are incorporated into the primary sex cords. Various hormonal influences determine the ultimate differentiation into testes or ovaries. In females, gonadal development is delayed compared with males.

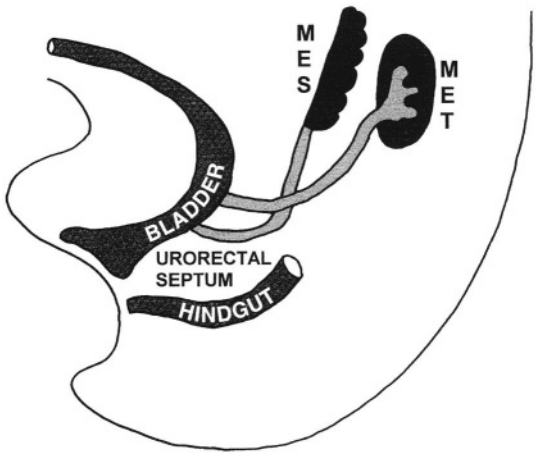


Fig. 2–70. Sagittal schematic of 7-week embryo
demonstrates the growth of the ureteric bud and development of the kidney proper from the metanephros *(MET).* The degenerating mesonephros (*MES*) and its duct are still evident. The urorectal septum has completed the compartmentalization of the cloaca into the bladder and the hindgut (rectum).

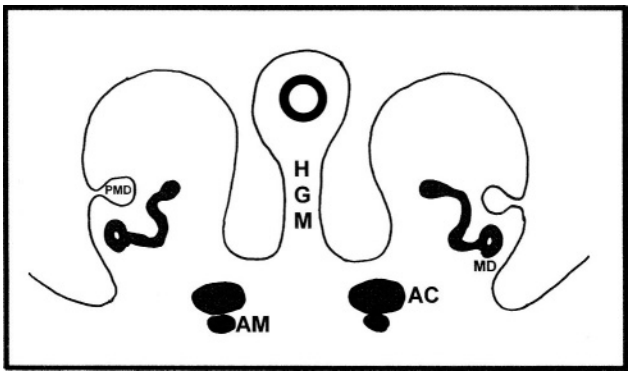


Fig. 2–71. Schematic of an axial section through the pelvis of a six-week embryo shows the infolding of the lateral margin of the gonadal ridge as it starts to form the paramesonephric duct (*PMD*). The mesonephric duct (*MD*) and associated tubule can be seen in the urogenital ridge. The hindgut mesentery (*HGM*) is the pathway for the migrating primordial germ cells. The developing adrenal cortex *(AC)* and medulla *(AM)* can be seen in the retroperitoneum.

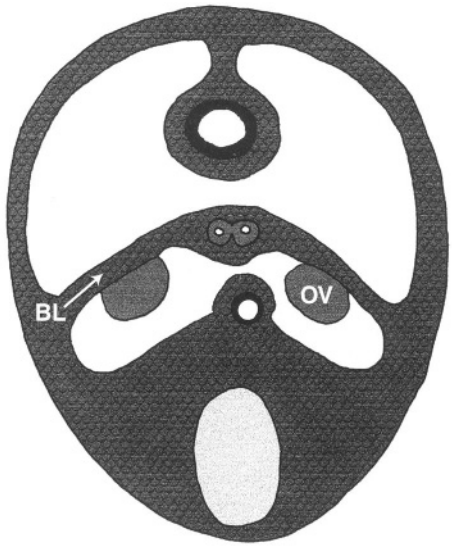


Fig. 2–72. Schematic of an axial section through the pelvis of an 8-week female embryo shows the fusing paramesonephric ducts in the midline supported by the broad ligament (*BL*) that attach to the lateral pelvic wall. The developing ovary (*OV*) can be seen along the ligament's posterior aspect. The developing bladder is noted anteriorly.

The mesonephric ducts, which play such an important role in the development of the definitive ureter and kidney, continue to be important in the formation of the male genital tract. Under the trophic influence of androgens, the proximal end becomes part of the epididymis and the vas deferens.[131] A distal outpouching becomes the seminal vesicle. Even more distally, the mesonephric duct becomes the ejaculatory duct as it joins the urethra.

An infolding occurs along the lateral aspect of the gonadal ridge, giving rise to the paramesonephric duct (Fig. 2–71). This structure is open cranially into the developing greater peritoneal cavity, and inferiorly it is incorporated into the uterovaginal primordium. It eventually becomes the Fallopian tube proximally and, with fusion of its opposite-sided partner distally, forms the uterus and upper vagina[131] (Fig. 2–72). Various anomalies of the uterus and/or the vagina may result from incomplete fusion of these ducts. The anomalies range from an arcuate uterus through uterus bicornis (separate uterine horns empty via separate cervices into one vagina) to uterus didelphys (two uterine tubes, horns, and cervices open into a duplicated vagina). They respectively represent the sequelae from minimal to complete lack of fusion of the muellerian ducts.[132]

As the paramesonephric ducts fuse in the midline caudally, its stalk of mesoderm overlying and connecting it to the genital ridge (containing the degenerating mesonephros) is elongated and carried laterally. This connecting stalk then becomes the suspending mesentery of the uterus, the broad ligament[131] (Fig. 2–72). It connects the fused paramesonephric ducts to the pelvis side wall. The mesonephric duct becomes a solid cord, the round ligament, connecting the ovary to the labia majora via the inguinal canal.

References

1. Moore KL: The Developing Human, 4th ed. WB Saunders, Philadelphia, 1988, pp 50–59.
2. Moore KL: The Developing Human, 4th ed. WB Saunders, Philadelphia, 1988, pp 159–169.
3. Javors BR: Pertinent embryology of the gastrointestinal tract: A brief review. Radiologist 1995, 2:51–63.
4. Javors BR, Sloves JH: Applied embryology of the gastrointestinal tract. *In* Textbook of Gastrointestinal Radiology. Edited by RM Gore, MS Levine, I Laufer. WB Saunders, Philadelphia, 1994, pp 1362–1378.

5. Balfe DM, Peterson RR, van Dyke JA: Normal abdominal and pelvic anatomy. *In* Computed Body Tomography with MRI Correlation, 2nd ed. Edited by JKT Lee, SS Sagel, RJ Stanley. Raven, New York, 1989, pp 415–475.
6. Earlam RJ: A study of the aetiology of congenital stenosis of the gut. Ann R Coll Surg Engl 1972; 51:126–130.
7. de Sa DJ: Congenital stenosis and atresia of the jejunum and ileum. J Clin Pathol 1972; 25:1063–1070.
8. Op den Orth JO: Duodenum (stomach and duodenum). *In* Alimentary Tract Roentgenology, 3rd ed. Edited by AA Margulis, HJ Burhenne. Mosby, St. Louis, 1983, pp 800–831.
9. Moore KL: The Developing Human, 4th ed. WB Saunders, Philadelphia, 1988, pp 217–245.
10. Maglinte DDT, Bisset III GS: Congenital and Developmental Anomalies of the Small Bowel in Adolescents and Adults. *In* Clinical Imaging of the Small Intestine, 2nd Edition. Edited by H Herlinger, DDT Maglinte, BA Birnbaum. Springer-Verlag, New York, 1999, pp 227–258.
11. Kottra JJ, Dodds WJ: Duplication of the large bowel. AJR 1971; 113:310–315.
12. Seaman WB: Nonneoplastic lesions (stomach and duodenum). *In* Alimentary Tract Roentgenology, 3rd ed. Edited by AA Margulis, HJ Burhenne. Mosby, St. Louis, 1983, pp 529–603.
13. Koehler RE, Memel DS, Stanley RJ: Gastrointestinal Tract. *In* Computed Body Tomography with MRI Correlation, 3rd edition. Edited by JKT Lee, SS Sagel, RJ Stanley, JP Heiken. Lippincott-Raven, Philadelphia, 1998, pp 637–700.
14. Beyer D, Friedmann G, Müller J: Duplication of the colon: Report of two cases and review of the literature. Gastrointest Radiol 1981; 6:151–156.
15. Dodds WJ, Foley WD, Lawson TL, et al: Anatomy and imaging of the lesser peritoneal sac. AJR 1985; 144:567–575.
16. Ros PR, Olmsted WWJ, Moser RP Jr, et al: Mesenteric and omental cysts: Histologic classification with imaging correlation. Radiology 1987; 164:327–332.
17. Snyder WH Jr, Chaffin L: Intermediate stage in return of the intestines from the umbilical cord. Anat Rec 1952; 113:451–457.
18. Snyder WH Jr, Chaffin L: Embryology and pathology of intestinal tract: Presentation of 40 cases of malrotation. Ann Surg 1954; 140:368–379.
19. Maglinte DDT, Herlinger H: Embryology of the small intestine. *In* Clinical Radiology of the Small Intestine. Edited by H Herlinger, D Maglinte. WB Saunders, Philadelphia, 1989, pp 3–6.
20. Balthazar EJ, Gade M: The normal and abnormal development of the appendix. Radiology 1976; 121:599–604.
21. Balthazar EJ: Congenital positional anomalies of the colon: Radiographic diagnosis and clinical implications. II. Abnormalities of fixation. Gastrointest Radiol 1977; 2:49–56.
22. Balthazar EJ: Congenital positional anomalies of the colon: Radiographic diagnosis and clinical implications. I. Abnormalities of rotation. Gastrointest Radiol 1977; 2:41–47.
23. Miller DL, Pasquale MD, Seneca RP, et al: Gastric volvulus in the pediatric population. Arch Surg 1991; 126:1146–1149.
24. Ue A, Kao SC, Sanders KD, et al: Gastric volvulus and wandering spleen. Am J Gastroenterol 1988; 93:1146–1148.
25. Aoyama K, Tateishi K: Gastric volvulus in three children with asplenic syndrome. J Pediatr Surg 1986; 21:307–310.
26. Ismail A: Recurrent colonic volvulus in children. J Pediatr Surg 1997; 32:1739–1742.
27. Frank AJ, Goffner LB, Fruauff AA, et al: Cecal volvulus: The CT whirl sign. Abdom Imaging 1993; 18:288–289.
28. Bodard E, Monheim P, Machiels F, et al: CT of midgut malrotation presenting in an adult. J Comput Assist Tomogr 1994; 18:501–502.
29. Mori H, Hayashi K, Futagawa S, et al: Vascular compromise in chronic volvulus with midgut malrotation. Pediatr Radiol 1987; 17:277–281.
30. Lantieri R, Teplick SK, Labelle MJ: Splenic flexure volvulus: Two case reports and review. AJR 1979; 132:463–464.
31. Ponka JL: Intussusception due to invaginated Meckel's diverticulum. Presentation of two cases and an analysis of fifty-two cases collected from the literature. Am J Surg 1956; 92:545–557.
32. Bemelman WA, Hugenholtz E, Heij HA, et al: Meckel's diverticulum in Amsterdam: Experience in 136 patients. World J Surg 1995; 19:734–736.
33. Halverson JM, Butterman MK, Legier JF, et al: Perforation of a Meckel's diverticulum caused by ingestion of a coin. South Med J 1994; 87:823–824.
34. Sadler TW, editor: Langman's Medical Embryology, 5th ed. Williams & Wilkins, Baltimore, 1985, pp 203–205, 230–232.
35. Hamdani SD, Baron RL: Ectopic liver simulating a mass in the gallbladder wall: Imaging findings. AJR 1994; 162:647–648.
36. Radin DR, Colletti PM, Ralls PW, et al: Agenesis of the right lobe of the liver. Radiology 1987; 164:639–642.

37. Brookes M, Zeitman A: Clinical Embryology: A Color Atlas and Text. CRC Press, Boca Raton, FL, 1998, pp 136–139.
38. Chou CK, Mak CW, Lin MB, et al: CT of agenesis and atrophy of the right hepatic lobe. Abdom Imaging 1998; 23:603–607.
39. Maetani Y, Itoh K, Kojima N, et al: Portal vein anomaly associated with deviation of the ligamentum teres to the right and malposition of the gallbladder. Radiology 1998; 207:723–728.
40. Soyer P, Bluemke DA, Choti MA, et al: Variations in the intrahepatic portions of the hepatic and portal veins: Findings on helical CT scans during arterial portography. AJR 1995; 164:103–108.
41. Couinaud C: Le foie: études anatomiques et chirugicales. Masson, Paris; 1957, pp 9–12.
42. Bismuth H: Surgical anatomy and anatomical surgery of the liver. World J Surg 1982; 6:3–9.
43. Fasel JHD, Selle D, Evertsz CJG, et al: Segmental anatomy of the liver: Poor correlation with CT. Radiology 1998; 206:151–156.
44. Hayes NA, Goldenberg IS, Bishop CC: The developmental basis for bile duct anomalies. Surg Gynecol Obstet 1958; 107:447–456.
45. Javors BR, Simmons MZ, Wachsberg RH: Cholangiographic demonstration of the cholecystohepatic duct of Luschka. Abdom Imaging 1998; 23:620–621.
46. Giovannelli AS, Friedman A: Liver: Embryology, anatomy, histology and variations. *In* Radiology of the Liver, Biliary Tract, Pancreas and Spleen. Edited by A Friedman. Williams & Wilkins, Baltimore, 1987, pp 3–36.
47. Pontes JF, Pinotti WH: Anomalies of the gallbladder and biliary system. *In* Gastroenterology, 3rd ed. Edited by HL Bockus. WB Saunders, Philadelphia, 1976, pp 651–665.
48. Naganuma S, Ishida H, Konno K, et al: Sonographic findings of anomalous position of the gallbladder. Abdom Imaging 1998, 23:67–72.
49. Berk RN: Oral cholecystography. *In* Radiology of the Gallbladder and Bile Ducts: Diagnosis and Intervention. Edited by RN Berk, JT Ferrucci Jr, GR Leopold. WB Saunders, Philadelphia, 1983, pp 121–142.
50. Singleton E: Pediatric diseases of the gallbladder and bile ducts: Diagnosis and intervention. *In* Radiology of the Gallbladder and Bile Ducts: Diagnosis and Intervention. Edited by RN Berk, JT Ferrucci Jr, GR Leopold. WB Saunders, Philadelphia, 1983, pp 513–546.
51. Wysong CB, Gorten RJ: Intrahepatic gallbladder. South Med J 1980; 73:825–826.
52. Boyden EA: The accessory gallbladder–an embryological and comparative study of aberrant biliary vesicles occurring in man and the domestic mammals. Am J Anat 1926; 38:177–231.
53. Diaz M, Fowler W, Hnatow J: Congenital gallbladder duplication: Preoperative diagnosis by ultrasonography. Gastrointest Radiol 1991; 16:198–200.
54. Özgen A, Akata D, Arat A, et al: Gallbladder duplication: Imaging findings and differential considerations. Abdom Imaging 1999; 24:285–288.
55. Netter FH: Digestive system: Part III. Liver, biliary tract and pancreas. *In* The Ciba Collection of Medical Illustrations, vol 3. Ciba Pharmaceutical Products, Summit, NJ, 1957; pp 2–3.
56. Hatfield PM, Wise RE: Anatomic variation in the gallbladder and bile ducts. Semin Roentgenol 1976; 11:157–164.
57. Babbitt DP, Starshak RJ, Clemett A: Choledochal cyst: A concept of etiology. AJR 1973; 119:57–62.
58. Ghahremani GG, Lu CT, Woodlief RM, et al: Choledochal cyst in adults. A clinical and radiologic study in ten cases. Gastrointest Radiol 1977; 1:305–313.
59. Imri H, Honda H, Jimi M: Value of MR cholangiopancreatography in evaluating choledochal cysts. AJR 1998; 171:1381–1385.
60. Todani T, Watanabe Y, Narusue M, et al: Congenital bile duct cysts. Am J Surg 1977; 134:263–268.
61. Lindberg C-G, Hammarström L-E, Holmin T; et al: Cholangiographic appearance of bile-duct cysts. Abdom Imaging 1998; 23:611–615.
62. Govil S,Justus A, Korah I, et al: Choledochal cysts: Evaluation with MR cholangiography. Abdom Imaging 1998; 23:616–619.
63. Ikematsu Y, Eto T, Tomioka T, et al: Biliary diverticulum with pancreaticobiliary maljunction. Hepatogastroenterology 1994; 41:70–72.
64. Flowers MB, Ho KJ: A rare common hepatic duct diverticulum causing fatal biliary obstruction and sepsis. Arch Pathol Lab Med 1998; 122:197–198.
65. Larsen WJ: Human Embryology, 2nd ed. Churchill Livingstone, New York, 1997, pp 202–211.
66. Williams PL: Embryology and development—Development of the veins. *In* Gray's Anatomy, 39th ed. Edited by H Gray, LH Bannister, MM Berry, PL William. Churchill Livingstone, New York, 1995, 320–326.
67. Raskin NH, Price JB, Fishman RA: Portosystemic encephalopathy due to congenital intrahepatic shunts. N Engl J Med 1964; 270:225–229.
68. Mori H, Hayashi K, Fukuda T, et al: Intrahepatic portosystemic venous shunt: Occurrence in pa-

tients with and without liver cirrhosis. AJR 1987; 149:711–714.
69. Park JH, Cha SH, Han JK, et al: Intrahepatic portosystemic venous shunt. AJR 1990; 155:527–528.
70. Mori H, Hayashi K, Amamoto Y, et al: Membranous obstruction of the inferior vena cava associated with intrahepatic portosystemic shunt. Cardiovasc Intervent Radiol 1986; 9:209–213.
71. Joyce AD, Howard ER: Rare congenital anomaly of the portal vein. Br J Surg 1988; 75:1038–1039.
72. Kawakatsu M, Vilgrain V, Belghiti J, et al: Association of multiple liver cell adenomas with spontaneous intrahepatic portosystemic shunt. Abdom Imaging 1994; 19:438–440.
73. Gray SW, Skandalakis JF: Embryology for Surgeons: The Embryological Basis for the Treatment of Congenital Defects. WB Saunders, Philadelphia, 1972; pp 177–178.
74. Sener RN, Alper H: Polysplenia syndrome: A case associated with transhepatic portal vein, short pancreas, and left inferior vena cava with hemiazygos continuation. Abdom Imaging 1994; 19:64–66.
75. Loberant N, Barak M, Gaitini D, et al: Closure of the ductus venosus in neonates: Findings on real-time gray-scale, color-flow doppler, and duplex doppler sonography. AJR 1992; 159:1083–1085.
76. Yanai S, Minami T, Sonada K, et al: Patent ductus venosus associated with a hyperintense globus pallidum on T1-weighted magnetic resonance imaging and pulmonary hypertension. Eur J Pediatr 1995; 154:526–529.
77. Farrant P, Meire HB, Karani J: Ultrasound diagnosis of portocaval anastomosis in infants—a report of eight cases. Br J Radiol 1996; 69:389–393.
78. Schild H, Schweden F, Braun B, et al: Aneurysm of the superior mesenteric vein. Radiology 1982; 145:641–642.
79. Thompson PB, Oldham KT, Bedi DG, et al: Aneurysmal malformation of the extrahepatic portal vein. Am J Gastroenterol 1986; 81:695–697.
80. Lee H-C, Yang Y-C, Shih S-L, et al: Aneurysmal dilatation of the portal vein. J Pediatr Gatroenterol Nutr 1989; 8:387–389.
81. Wanless IR, Mawdsley C, Adams R: On the pathogenesis of focal nodular hyperplasia of the liver. Hepatology 1985; 5:1194–1200.
82. Shimamatsu K, Wanless IR: Role of ischemia in causing apoptosis, atrophy, and nodular hyperplasia in human liver. Hepatology 1997; 26:343–350.
83. Howard ER, Davenport M: Congenital extrahepatic portocaval shunts—the Abernethy malformation. J Pediatr Surg 1997; 32:494–497.
84. Friedman AC, Birns MT: Embryology, anatomy, histology and physiology (pancreas). *In* Radiology of the Liver, Biliary Tract, Pancreas and Spleen. Edited by Friedman A. Williams & Wilkins, Baltimore, 1987, pp 619–642.
85. Ravitch MM: The pancreas in infants and children. Surg Clin North Am 1975; 55:377–385.
86. Moore KL, Persaud TVN, editors: The Developing Human: Clinically Oriented Embryology, 6th ed. WB Saunders, Philadelphia, 1998, pp 280–283.
87. Skandalakis LJ, Rower JS, Gray SW, et al: Surgical embryology and anatomy of the pancreas. Surg Clin North Am 1993, pp 73:661–697.
88. Ross BA, Jeffrey RB Jr, Mindelzun RE: Normal variations in the lateral contour of the head and neck of the pancreas mimicking neoplasm: Evaluation with dual-phase helical CT. AJR 1996; 166:799–801.
89. Glazer G, Margulis A: Annular pancreas: Etiology and diagnosis using ERCP. Radiology 1979; 133:303–306.
90. Jadvar H, Mindelzun RE: Annular pancreas in adults: Imaging features in seven patients. Abdom Imaging 1999; 24:174–177.
91. Reinhart RD, Brown JJ, Foglia RP, et al: MR imaging of annular pancreas. Abdom Imaging 1994; 19:301–303.
92. Lecesne R, Stein L, Reinhold C, et al: MR cholangiopancreatography of annular pancreas. J Comput Assist Tomogr 1998, 22:85–86.
93. Lehman GA, Sherman S: Diagnosis and therapy of pancreas divisum. Gastrointest Endosc Clin N Am 1998; 8:55–77.
94. Yedlin ST, Dubois RS, Philippart AI: Pancreas divisum: A cause of pancreatitis in childhood. J Pediatr Surg 1984; 19:793–794.
95. Wagner CW: Pancreas divisum and pancreatitis in children. Am Surg 1988; 54:22–25.
96. Sanada Y, Yoshizawa Y, Chiba M, et al: Ventral pancreatitis in a patient with pancreas divisum. J Pediatr Surg 1995; 30:655–667.
97. Lehman GA, Sherman S: Diagnosis and therapy of pancreas divisum. Gastrointest Endosc Clin N Am 1998; 8:55–77.
98. Bret PM, Reinhold C, Taourel P, et al: Pancreas divisum: Evaluation with MR cholangiopancreatography. Radiology 1996; 199:99–103.
99. Wilding R, Schnedl WJ, Reisinger EC, et al: Agenesis of the dorsal pancreas in a woman with diabetes mellitus and in both of her sons. Gastroenterology 1993; 104:1182–1186.
100. Inoue Y, Nakamura H: Aplasia or hypoplasia of the pancreatic uncinate process: Comparison in patients with and patients without intestinal nonrotation. Radiology 1997; 205:531–533.

101. Herman TE, Siegel MJ: Polysplenia syndrome with congenital short pancreas. AJR 1991; 156:799–800.
102. Macari M, Giovanniello G, Blair L, et al: Diagnosis of agenesis of the dorsal pancreas with MR pancreatography. AJR 1998; 170:144–146.
103. Chuang VP, Pulmano CM, Walter JF, et al: Angiography of pancreatic artero-venous malformation. Br J Radiol 1977; 129:1015–1018.
104. Mizutani N, Masuda Y, Naito N, et al: Pancreatic arteriovenous malformation in a patient with gastrointestinal hemorrhage. Am J Gastroenterol 1981; 176:141–144.
105. Koito K, Namieno T, Nakagawa T, et al: Diagnosis of arteriovenous malformation of the pancreas by color doppler sonography. Abdom Imaging 1998; 23:84–86.
106. Horton WA, Wong V, Eldridge R: von Hippel-Lindau disease: Clinical and pathological manifestations in nine families with 50 affected members. Arch Intern Med 1976; 136:769–777.
107. Hough DM, Stephens DH, Johnson CD, et al: Pancreatic lesions in von Hippel-Lindau disease: Prevalence, clinical significance, and CT findings. AJR 1994; 162:1091–1094.
108. Dachman AH: Anomalies and congenital disorders (spleen). *In* Radiology of the Liver, Biliary Tract, Pancreas and Spleen. Edited by A Friedman. Williams & Wilkins, Baltimore, 1987, pp 913–930.
109. Blaustein A: The Spleen. McGraw Hill, New York, 1963, p 45.
110. Curtis GM, Moritz D: The surgical significance of the accessory spleen. Ann Surg 1946; 123:276–298.
111. Beahrs JR, Stephens DH: Enlarged accessory spleens: CT appearance in postsplenectomy patients. AJR 1980; 135:483–486.
112. Churei H, Inoue H, Nakajo M: Intrapancreatic accessory spleen: case report. Abdom Imaging 1998; 23:191–193.
113. Ambiz P, Munoz R, Quintanar E, et al: Accessory spleen compromising response to splenectomy for idiopathic thrombocytopenia purpura. Radiology 1985; 155:793–796.
114. Desai DC, Hebra A, Davidoff AM, et al: Wandering spleen: A challenging diagnosis. South Med J 1997; 90:439–443.
115. Buehner M, Baker MS: The wandering spleen. Surg Gynecol Obstet 1992; 175:373–387.
116. Allen KB, Gay BB Jr, Skandalakis JE: Wandering spleen: Anatomic and radiologic considerations. South Med J 1992; 85:976–984.
117. Hon TY, Chan CC, Loke T, et al: Torsion of the wandering spleen. Australas Radiol 1998; 42:258–261.
118. Fujiwara T, Takehara Y, Isoda H, et al: Torsion of the wandering spleen: CT and angiographic appearance. J Comput Assist Tomogr 1995; 19:84–86.
119. Vails C, Mones L, Guma A, et al: Torsion of a wandering accessory spleen: CT findings. Abdom Imaging 1998; 23:194–195.
120. Winer-Muram HT, Tonkin ILD: The spectrum of heterotaxic syndromes. Radiol Clin North Am 1989; 27:1147–1170.
121. Peoples WM, Moller HJ, Edwards JE: Polysplenia: A review of 146 cases. Pediatr Cardiol 1983; 4:129–137.
122. Gayer G, Apter S, Jonas T, et al: Polysplenia syndrome detected in adulthood: Report of eight cases and review of the literature. Abdom Imaging 1999; 24:178–184.
123. Davidson AJ: Radiologic anatomy of the kidney and ureter. *In* Radiology of the Kidney and Urinary Tract. Edited by AJ Davidson. WB Saunders, Philadelphia, 1994, pp 53–96.
124. Elkin M: Radiology of the Urinary System. Little Brown. Boston, 1980, pp 62–147.
125. Friedland GW, de Vries P: Renal ectopia and fusion: Embryologic basis. Urology 1975; 5:698–706.
126. van den Ouden D, Blom JH, Bangma C, et al: Diagnosis and management of seminal vesicle cysts associated with ipsilateral renal agenesis: A pooled analysis of 52 cases. Eur Urol 1998; 33:433–440.
127. Friedland GW: Congenital anomalies of the urinary tract. *In* Uroradiology: An Integrated Approach. Edited by GW Friedland, R Filly, ML Goris, et al. Churchill Livingstone, New York, 1983, pp 1349–1519.
128. Gittes GK, Snyder CL, Murphy JP, et al: Inferior vena caval obstruction from a horseshoe kidney: Report of a case with operative decompression. J Pediatr Surg 1998; 33:764–765.
129. Rubenstein DJ, Brenner RJ: Misleading features of blind-ending bifid ureter on computerized tomography examination. J Urol 1985; 134:342–343.
130. Cilento BG Jr, Bauer SB, Retik AB, et al: Urachal anomalies: defining the best diagnostic modality. Urology 1998; 52(1):120–122.
131. Moore KL: The Developing Human. 4th ed. Philadelphia: Saunders, 1988:246–285.
132. Brookes M, Zietman A: Clinical Embryology: A color atlas and text. Boca Raton: CRC Press 1998; 240–243.

Intraperitoneal Spread of Infections

3

A remarkable change in the epidemiology of subphrenic and subhepatic abscesses has occurred over the past several decades. In the past, the most common causes included perforations of anterior gastric or duodenal ulcers and rupture of a gangrenous appendix. Today, 60–71% of such abscesses are postoperative and are particularly frequent following gastric and biliary tract operations and colonic surgery.[1–3] Many of the cases of postoperative abscesses are secondary to anastomotic leaks.[4] More prompt diagnosis currently in conditions such as peptic ulcer and appendicitis, leading to earlier surgical intervention, results in an increasing proportion of postoperative abscesses. The bacterial flora generally consist of multiple strains of aerobic and anaerobic organisms. The aerobes include particularly *Escherichia coli, Streptococcus, Klebsiella,* and *Proteus;* the anaerobes, *Bacteroides* and cocci.[2]

Paralleling this epidemiologic change has been a change in the clinical presentation. The fulminating course described classically is no longer generally seen, and today abscesses most often present in an insidious fashion, typically consisting of mild abdominal pain, malaise, and a slight fever. Later, the patient may develop a mass, referred pain to the shoulder, and subcostal or flank pain. The clinical spectrum is illustrated by this analogy:

> It can rapidly build up a crater of sepsis giving the patient an acute illness with a clear cut diagnosis … on the other hand, it may linger apparently quiescent, causing only a slight fever, only to erupt unexpectedly some weeks or months later. Finally, it may be like Vesuvius, apparently extinct, apart from occasional rumbles, making its presence felt only by causing ill health.[5]

Early radiologic identification and localization of an intraabdominal abscess are of extreme importance, since morbidity and mortality increase with delay in treatment. Diagnosis can be most prompt and accurate when there is an understanding of the intraperitoneal routes of spread of contaminated material.

Anatomic Considerations

The Posterior Peritoneal Attachments

Figure 3–1 shows the roots of the mesenteric attachments of the intraperitoneal segments of bowel, and Figure 3–2 illustrates the reflections of the peritoneum from the posterior abdominal wall deep to the bowel, liver, and spleen. The *transverse mesocolon* constitutes the major barrier dividing the abdominal cavity into supramesocolic and inframesocolic compartments. The obliquely oriented *root of the small bowel mesentery* further divides the inframesocolic compartment into two spaces of unequal size: (a) the smaller *right infracolic space* bounded inferiorly by the junction of the mesentery with the attachment of the ascending colon, and (b) the larger *left infracolic space,* which is open anatomically toward the pelvis.

The *pelvis* constitutes about one-third of the volume of the peritoneal cavity and is its most dependent part in either the supine or erect position. It is anatomically continuous with both paracolic gutters the peritoneal

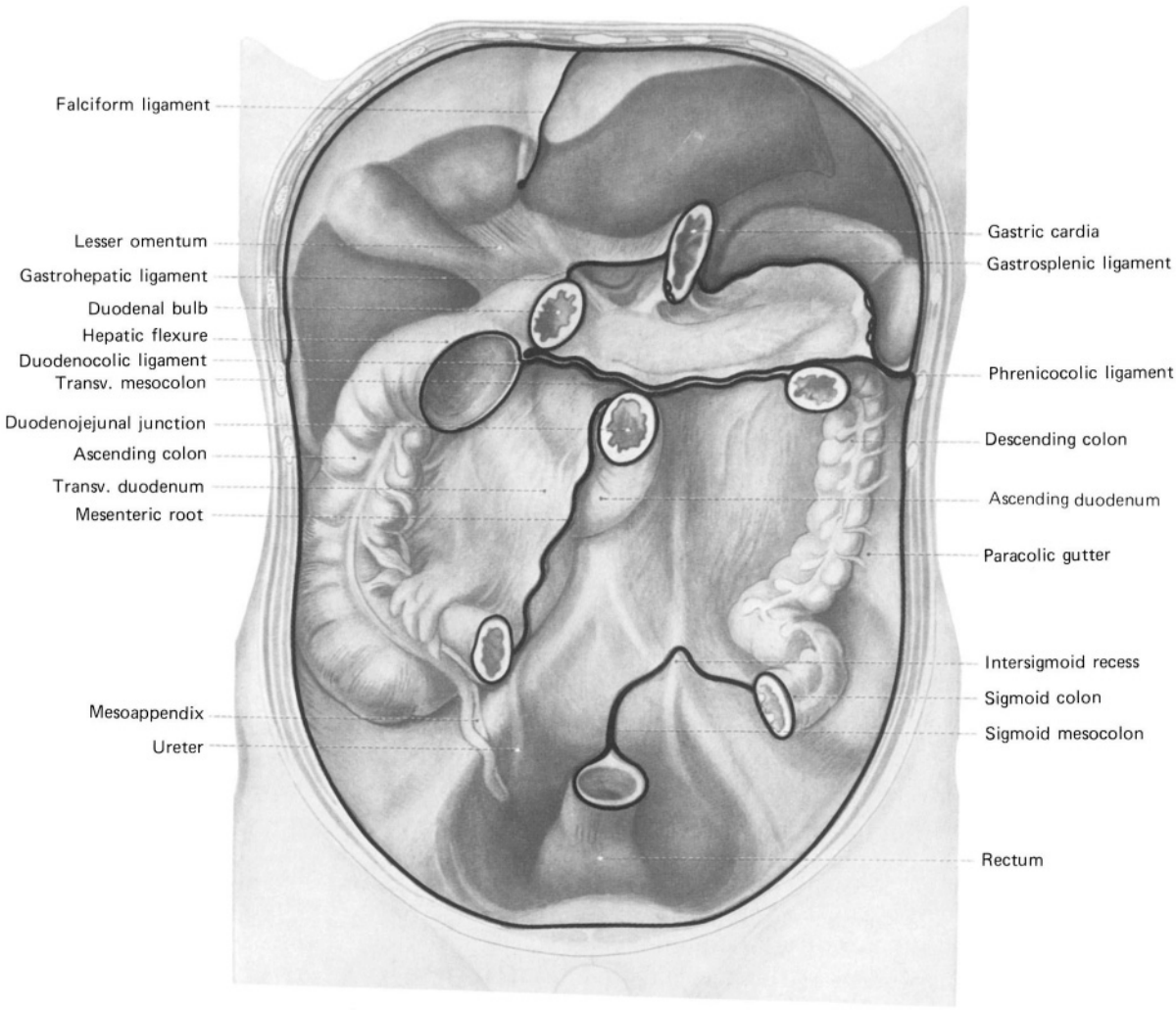


Fig. 3–1. The peritoneal investment of the extraperitoneal segments of the alimentary tract.
The mesenteric portions of the gut have been removed, including the stomach, small bowel, transverse colon, and sigmoid colon.

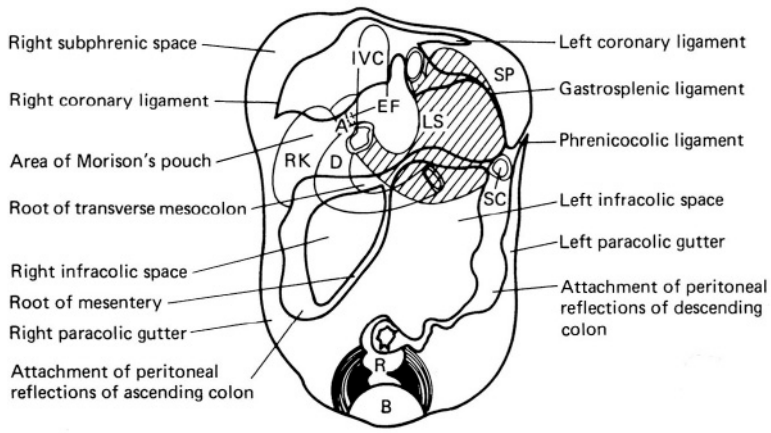


Fig. 3–2. Posterior peritoneal reflections and recesses.
SP = spleen; *LS* = lesser sac; *IVC* = inferior vena cava; *EF* = epiploic foramen of Winslow; *RK* = right kidney; *D* = duodenum; *A* = adrenal gland; *SC* = splenic flexure of colon; *R* = rectum; *B* = urinary bladder. The removed stomach is indicated.
(Modified from Meyers.[6])

recesses lateral to the ascending and descending colon. The *right paracolic gutter* is wide and deep and is continuous superiorly with the right subhepatic space and its posterosuperior extension deep to the liver, which is surgically known as *Morison's pouch*[7] (Fig. 3–3). The *right subhepatic space* is anatomically continuous with the *right subphrenic space* around the lateral edge of the *right coronary ligament* of the liver. In contrast, the *left paracolic gutter* is narrow and shallow and is interrupted from continuity with the *left subphrenic space* (perisplenic or left perihepatic space) by the *phrenicocolic ligament,* which extends from the splenic flexure of the colon to the left diaphragm.

Detailed Anatomy of the Right Upper Quadrant

Since Barnard's original classification[8] in 1908, a great deal of confusion in the definition and true anatomic location of right upper quadrant abscesses has arisen. All pus accumulations in the supramesocolic compartment tended to be termed "subphrenic abscesses," but this is misleading because only some of the abscesses lie immediately below the diaphragm. In 1938, Ochsner and DeBakey[9] cited the right posterior subphrenic space as the most frequent site of infection. This recess is now recognized as actually subhepatic in position. In 1955, Harley[10] helped to clarify the topography:

> My view is that the subphrenic region extends from the diaphragm to the transverse colon and mesocolon. It is divided into the suprahepatic and infrahepatic compartments by the liver. The suprahepatic compartment is divided into right and left portions by the falciform ligament and the infrahepatic compartment is similarly divided by the ligamentum teres and ligamentum venosum.

The key to the problem lies in the locations of the ligamentous attachments of the liver. A generation of surgeons schooled on "keyhole" incisions had believed that the right lobe of the liver is suspended superiorly from the diaphragm by the right coronary ligament. Although pointed out by Mitchell[11] in 1940, it was not until 1966 that Boyd clearly defined the coronary ligament as actually suspending the right lobe of the liver from the parietes *posteriorly*[12,13] (Figs. 3–4 and 3–5). In

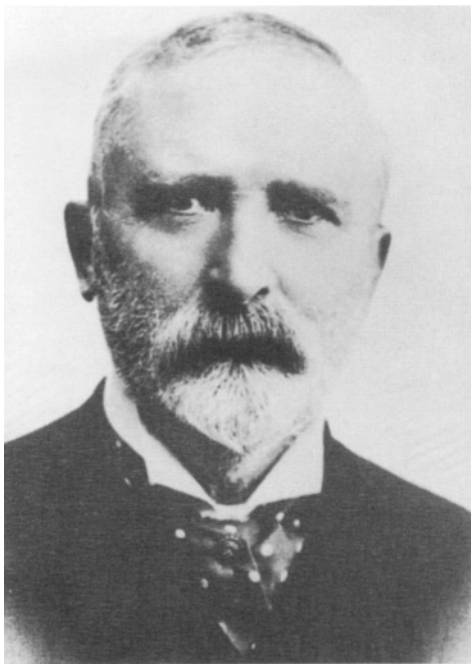


Fig. 3–3. Rutherford Morison (1853–1939).
Morison, an English surgeon, is best known for the pouch that he described in *The Anatomy of the Right Hypochondrium Relating Especially to Operations for Gallstones* in 1894. He emphasized that "bile leaks drain into this area but the external drain must extend to the very depths of the pouch."
(Courtesy of Wellcome Institute of the History of Medicine, London.)

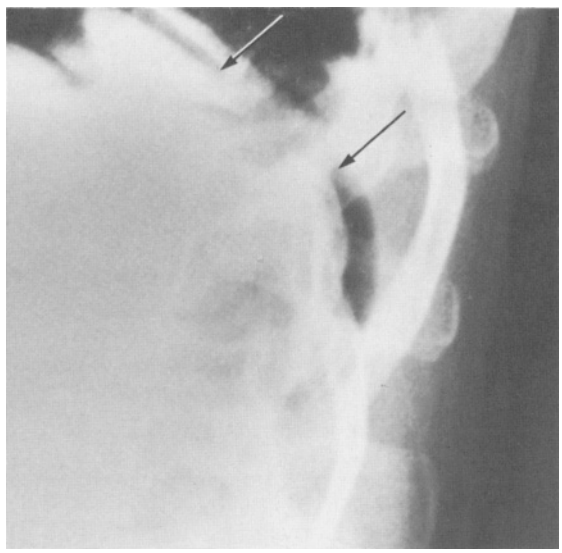


Fig. 3–4. Reflections of the right coronary ligament *(arrows)* suspending the right lobe of the liver are outlined by free peritoneal air in the lateral view.
The inferior leaf is at the level of the 12th rib. The nonperitonealized bare area of the posterior surface of the right lobe lies between the reflections of the ligament.

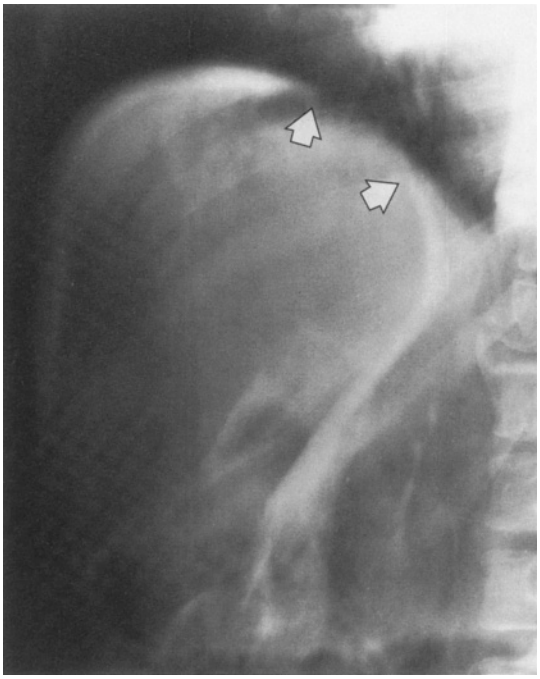


Fig. 3–5. The reflections of the right superior and inferior coronary ligaments *(arrows)* are outlined by in vivo contrast peritoneography.
Between them is the nonperitonealized bare area of the right lobe of the liver. The right subhepatic and subphrenic spaces are distinguished.

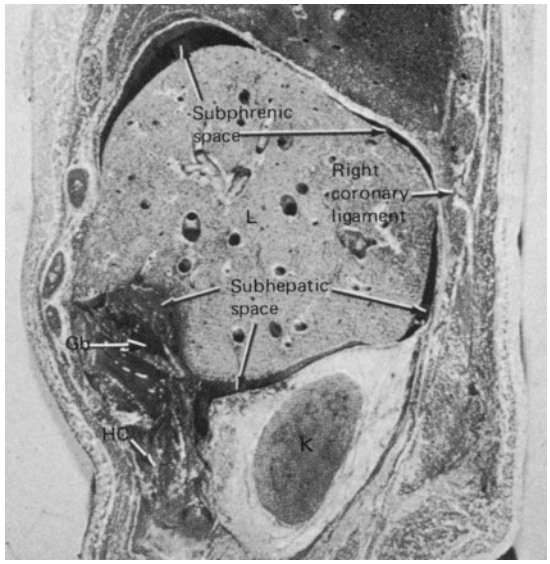


Fig. 3–6. Right parasagittal anatomic section.
The right coronary ligament suspends the liver from the diaphragm posteriorly and divides the peritoneal cavity around the right lobe into a subphrenic space and a subhepatic space. *Gb* = gallbladder; *HC* = hepatic flexure of the colon; *K* = right kidney.

this way, the peritoneal recess around the right lobe of the liver is grossly compartmentalized into a subphrenic space and a subhepatic space (Fig. 3–6).

The Right Subhepatic Space

Underlying the visceral surface of the right lobe of the liver, the right subhepatic space is composed of two compartments (Figs. 3–7 and 3–8).

1. The *anterior subhepatic space* is limited inferiorly by the beginning of the transverse colon and mesocolon.
2. The *posterior subhepatic space* lies in close relationship to the posterior parietal peritoneum overlying the right kidney. It projects upward in the form of a recess between the renal impression of the liver in front and the upper pole of the right kidney behind. The posterosuperior extension of the right subhepatic space to its margination above by the right coronary ligament is known anatomically as the *hepatorenal fossa* and clinically as *Morison's pouch.*

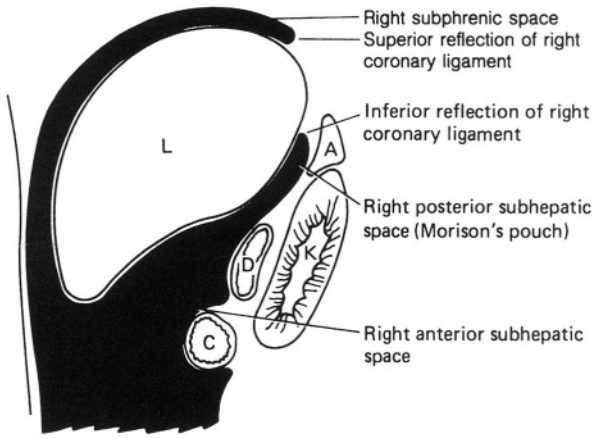


Fig. 3–7. Right parasagittal diagram.
The right subhepatic space is composed of anterior and posterior (Morison's pouch) compartments and is anatomically continuous with the right subphrenic space. The reflections of the coronary ligament mark the site of the nonperitonealized "bare area" of the liver (*L*). *K* = right kidney; *A* = adrenal gland; *D* = descending duodenum; *C* = transverse colon.

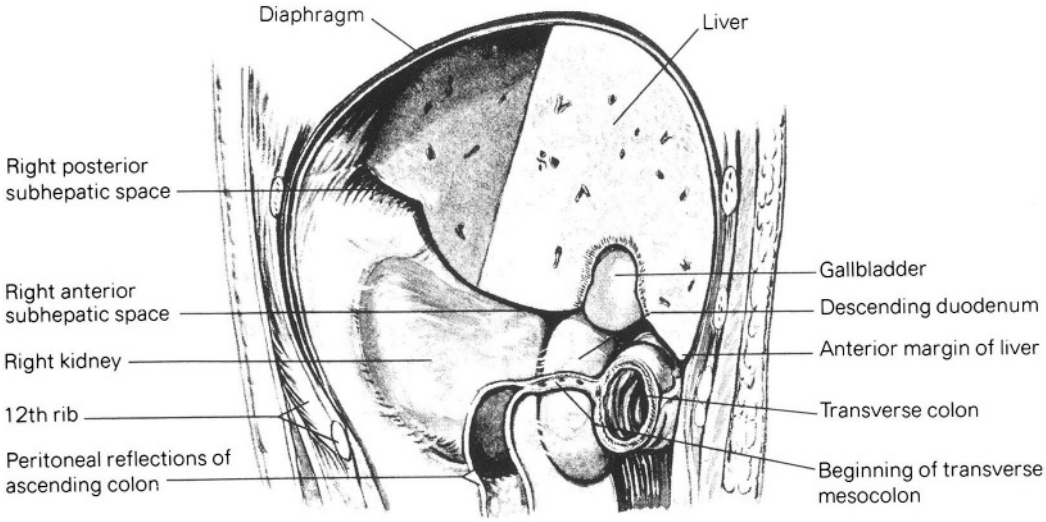


Fig. 3–8. Right parasagittal anatomic drawing, viewed from the right.
The relationships of the right anterior and posterior subhepatic spaces are shown.

Morison's pouch is of great significance in the spread and localization of intraperitoneal infections since it is the lowest part of the right paravertebral groove when the body is in the supine position. Figures 3-9 through 3–11 illustrate its important anatomic relationships. Inferiorly, it is bounded by the hepatic flexure of the colon and the peritoneal reflections at the beginning of the transverse mesocolon and medially by the second portion of the duodenum as it descends anterior to the hilus of the kidney. Laterally, it communicates deep to the liver around the margin of the right coronary ligament with the subphrenic space above and the right paracolic gutter in the flank.

Although these two compartments communicate freely anatomically, they are frequently separated by the development of pyogenic membranes (Fig. 3–12).

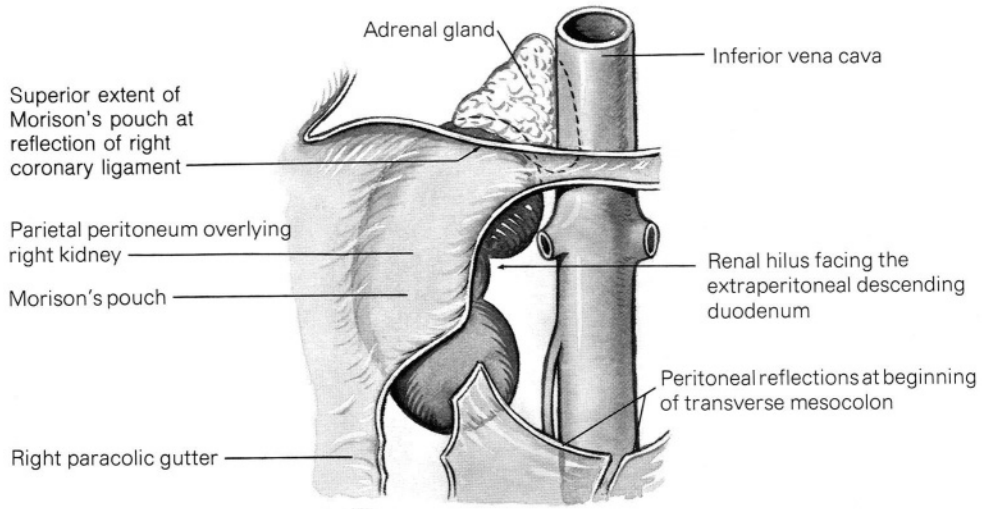


Fig. 3–9. Frontal view of the anatomic relationships of Morison 's pouch facing the deep visceral surface of the right lobe of the liver.

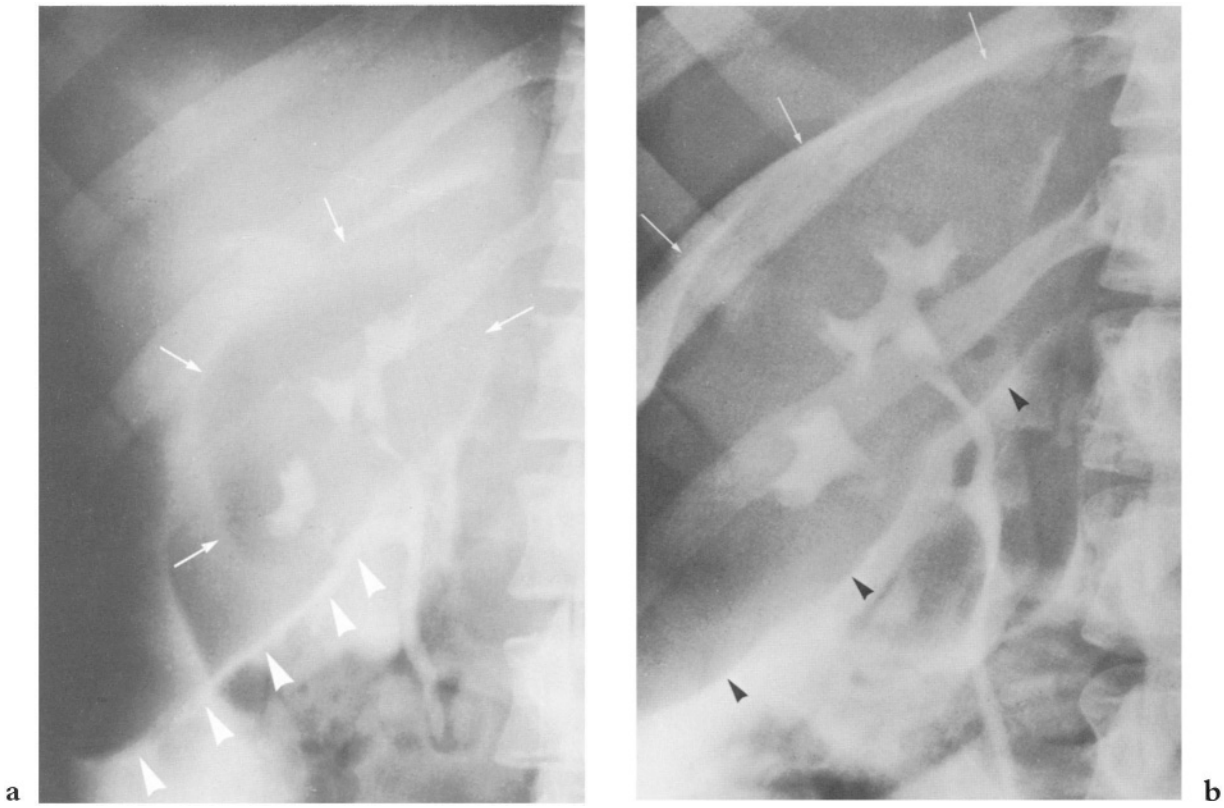


Fig. 3–10. Visceral surface of right lobe of liver.
(a) Supine peritoneography. Positive-contrast medium parallels the posteroinferior edge of the liver *(arrowheads).* Gas within Morison's pouch outlines the contours of the renal fossa on the posterior surface of the liver *(arrows).* **(b)** Prone peritoneography. The inferior reflection of the coronary ligament, immediately below the bare area of the liver marking the superior extent of Morison's pouch, is outlined *(upper arrows).* Note that here it corresponds to the level of the 11th posterior rib. Positive-contrast medium also pools along the notched anteroinferior border of the liver (*arrowheads*).
(Reproduced from Meyers.[14])



Fig. 3–11. Fluid-filled Morison 's pouch.
Ascites occupies the hepatorenal fossa *(asterisks).*

The Right Subphrenic Space

The right subphrenic space is a large continuous compartment extending over the diaphragmatic surface of the right lobe of the liver to its margination posteriorly and inferiorly by the right coronary ligament. No true anatomic separation into anterior and posterior subphrenic spaces actually occurs, but such compartmentalization of abscesses frequently takes place by the formation of pyogenic membranes (Fig. 3-12).

The falciform ligament separates the right and left subphrenic spaces. Mitchell[11] has stressed that the region below and on either side of the free margin of the falciform ligament resembles a delta in which the two subphrenic and the right subhepatic spaces communicate.

The Left Subphrenic Space

The suspending coronary ligament of the left lobe of the liver, unlike the right, is attached superiorly, almost in the center of the abdomen and more anteriorly than the right coronary and triangular ligaments.[11,15–17] It is quite small and usually insignificant for the margination of abscess cavities. The anatomic spaces surrounding the left lobe of the liver are thus freely communicating (Fig. 3–13). Generally, therefore, the whole left side should be considered as one potential abscess area.[12,13,15] The mesenteric attachments of the left upper quadrant, i.e., the splenorenal ligament, the gastrosplenic ligament, and the lesser omentum, aided by the development of inflammatory adhesions, may serve to compartmentalize abscess to the immediate subphrenic (between the diaphragm and the gastric fundus), subhepatic (between the visceral surface of the liver and the stomach), or perisplenic areas (Fig. 3–14).

A structure of particular significance in the left upper quadrant of the abdomen is the phrenicocolic ligament.[18] (Figs. 3–14b through 3–20). This is a strong falciform peritoneal fold that extends from the anatomic splenic flexure of the colon to the diaphragm at the level of the 11th rib. Older literature refers to it also as the "sustentaculum lienis," since it is in immediate inferior relationship to and serves the purpose of supporting the spleen at its tip.[20] Its importance in limiting the spread of infection is based on the anatomic fact that it separates partially the perisplenic space from the left paracolic gutter.

The Lesser Sac

During fetal life, the development of the dorsal mesogastrium and the rotation of the stomach cut off a bay of peritoneum, the lesser sac (omental bursa), from the rest of the peritoneal cavity. The narrow inlet is known as the epiploic foramen (foramen of Winslow).[21]

The foramen of Winslow is limited above by the caudate lobe of the liver, behind by the vena cava, and anteriorly by the hepatoduodenal ligament and its contents (portal vein, hepatic artery, and bile ducts). It has a tri-

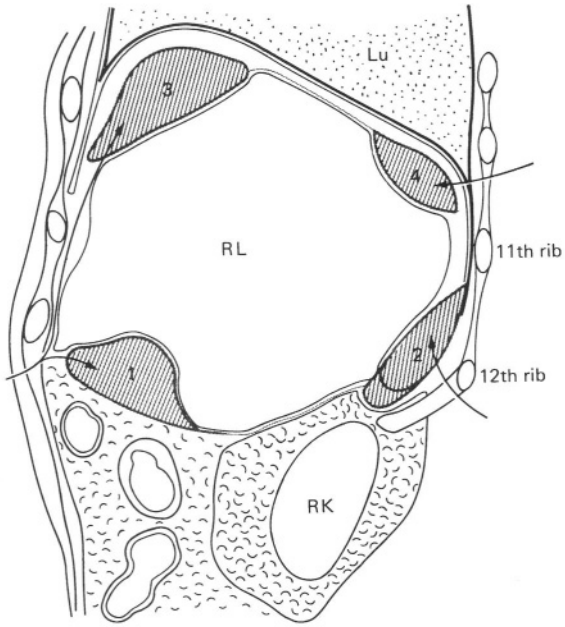


Fig. 3–12. The four sites of localized abscesses around the right lobe of the liver.
(See Fig. 3–6) (*1*) Anterior subhepatic, (*2*) posterior subhepatic, *(3)* anterior subphrenic, *(4)* posterior subphrenic. The surgical approaches to the spaces are indicated. *Lu* = lung; *RL* = right lobe of liver; *RK* = right kidney.
(After Boyd.[12])



Fig. 3–13. Sagittal section through the left lobe of the liver.
The smaller left lobe *(LL)* of the liver lies anterior to the stomach *(S),* including both its upper fundic and distal body portions. *Ao* = aorta.

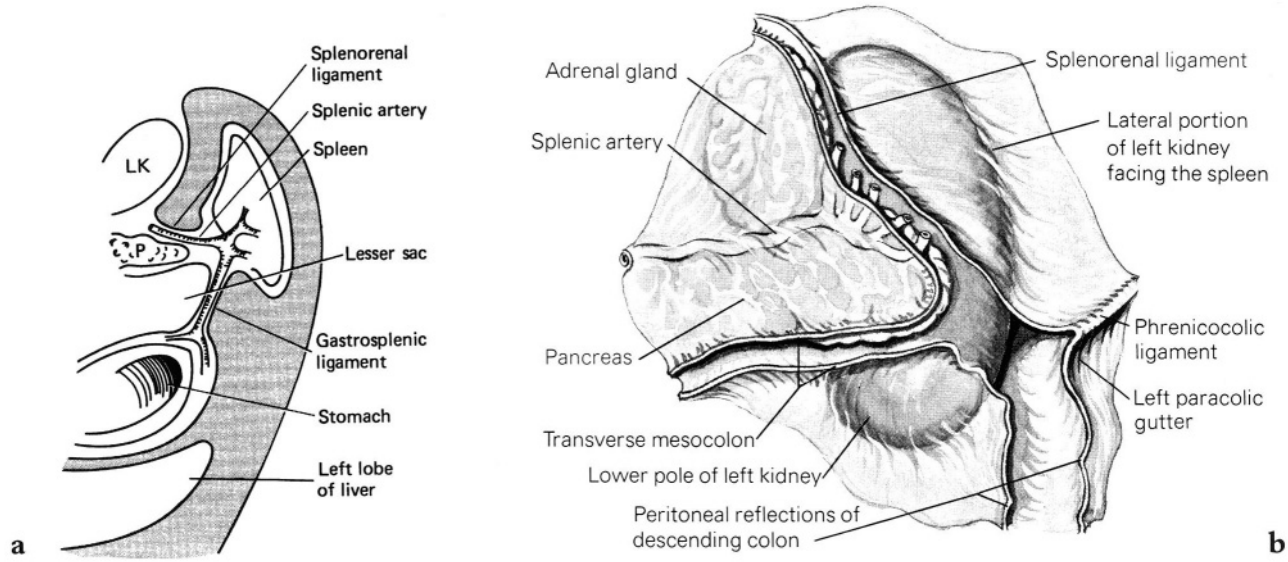


Fig. 3–14. Peritoneal attachments and recesses of the left upper quadrant.
(a) Diagram of horizontal section. The intraperitoneal spaces around the left lobe of the liver and the spleen are freely continuous *(gray area).* The perisplenic space is bounded by the splenorenal and gastrosplenic ligaments. *LK* = left kidney; *P* = tail of pancreas.
(b) Frontal drawing (spleen removed). The phrenicocolic ligament partially bridges the junction between the perisplenic space and the left paracolic gutter. The lesser sac resides above the transverse mesocolon and medial to the splenorenal ligament.

angular form with the apex cephalad[22] (Fig. 3–21) and varies in size, but generally will admit one (an approximately 4.5 cm circumference) or most commonly two fingers (9 cm circumference).[24] In normal circumstances, it is a potential opening, with mesothelial surfaces gliding over each other.

The lesser sac (Figs. 3–14a, 3–22 to 3–24) lies behind the lesser omentum, the stomach and duodenal bulb, and the gastrocolic ligament. It is bounded inferiorly by the transverse colon and the mesocolon (Fig. 3–25), although a well-defined inferior recess persists in a few individuals between the anterior and posterior reflections of the greater omentum (Figs. 3–26 and 3–27). The lesser sac is defined posteriorly chiefly by most of the pancreas; to the right, the caudate lobe of the liver projects into the upper recess of the sac (Figs. 3–28 to 3–30).[25,26]

A prominent oblique fold of peritoneum, the gastropancreatic plica, is raised from the posterior abdominal wall by the left gastric artery. The plica is a fatty triangular structure measuring 2–3 cm in cross section at its base and is inclined toward the posterior wall of the stomach[27] (Fig. 3–31). This fold often divides the lesser sac into two compartments:

1. A smaller medial compartment to the right composed of the vestibule to the lesser sac, where the anatomic landmark is the caudate lobe of the liver (Figs. 3–23 and 3–30), and a superior recess dorsal to the medial segment of the left hepatic lobe.
2. A larger lateral compartment to the left inferiorly (Fig. 3–23).

text continues on page 71

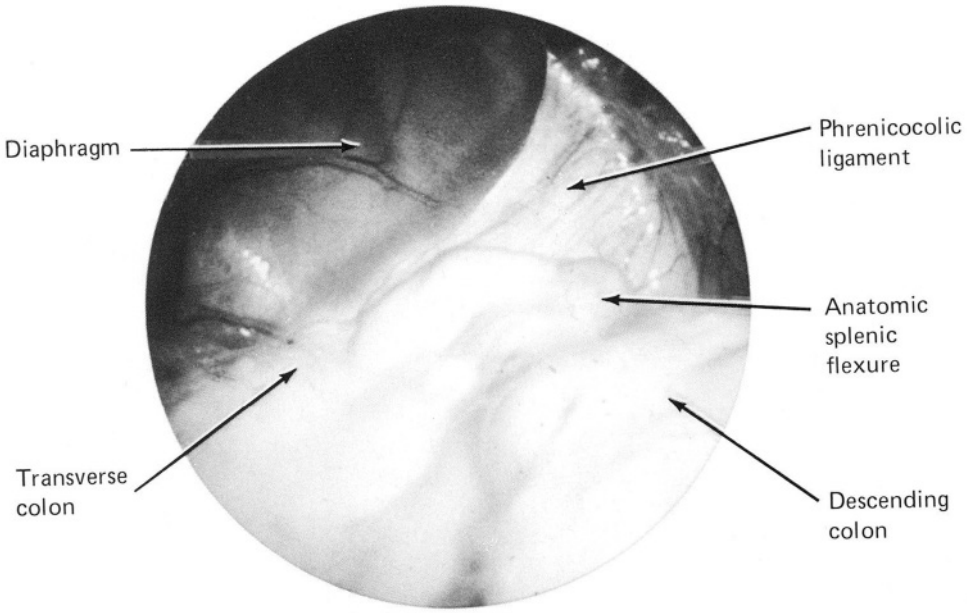


Fig. 3–15. The phrenicocolic ligament as seen *in vivo* by peritoneoscopy.

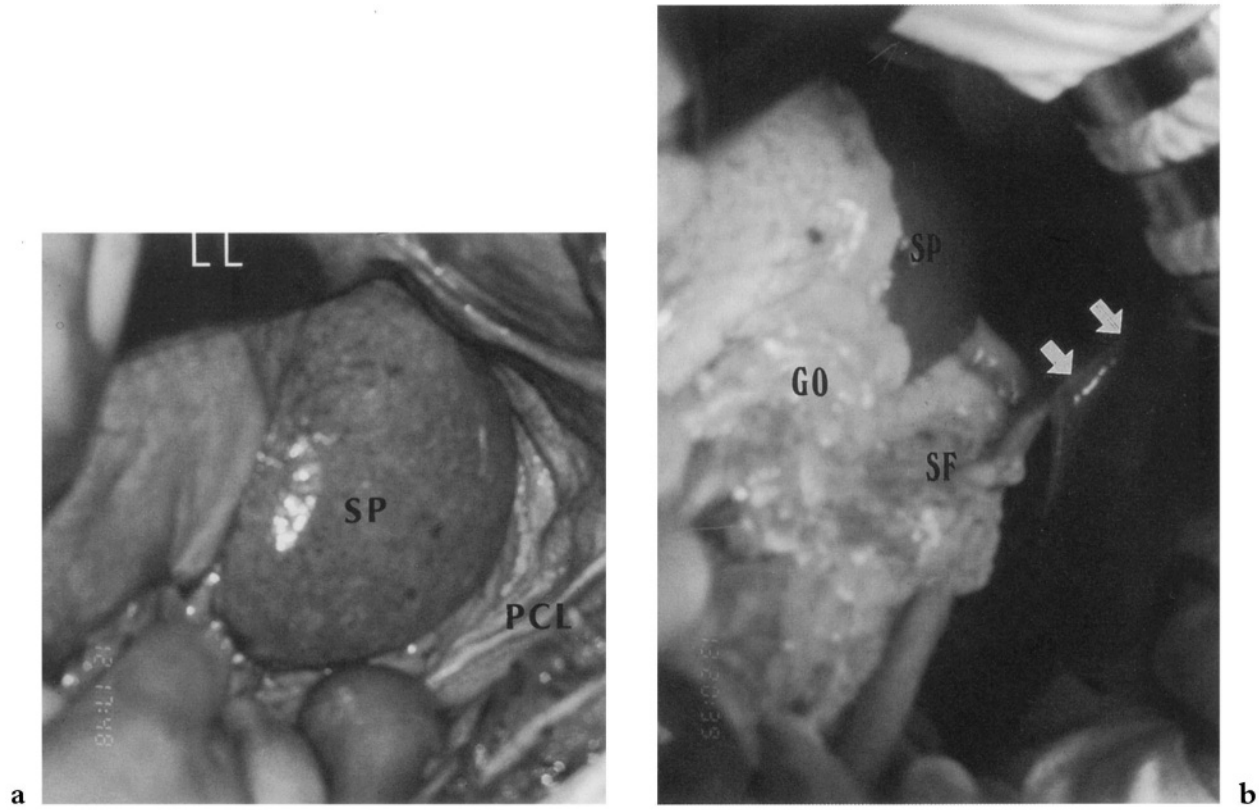


Fig. 3–16. The phrenicocolic ligament as seen at surgery in two different cases.
(a) The phrenicocolic ligament *(PCL)* is the elevated peritoneal fold inferolateral to the spleen (*SP*). *LL* = left lobe of liver. **(b)** After retracting the stomach and greater omentum (*GO*), the phrenicocolic ligament is apparent as an elevated ridge *(arrows)* extending from the anatomic splenic flexure of the colon (*SF*) posteriorly to the diaphragm. The ligament is seen inferolateral to the spleen (*SP*).
(Courtesy of Yong Ho Auh, M.D., Asan Medical Center, Seoul, Korea) **(These figures also appear in the color insert.)**

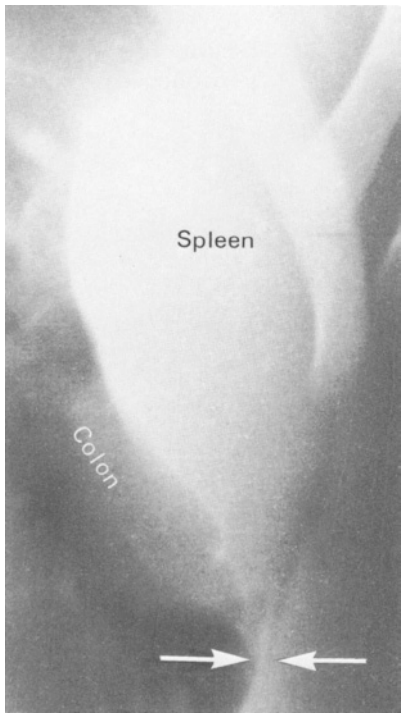


Fig. 3–17. The phrenicocolic ligament *(arrows).*
On this plain film, this ligament is seen as a striplike density subtending the splenic angle at the level of the anatomic splenic flexure of the colon.
(Reproduced from Meyers.[18])

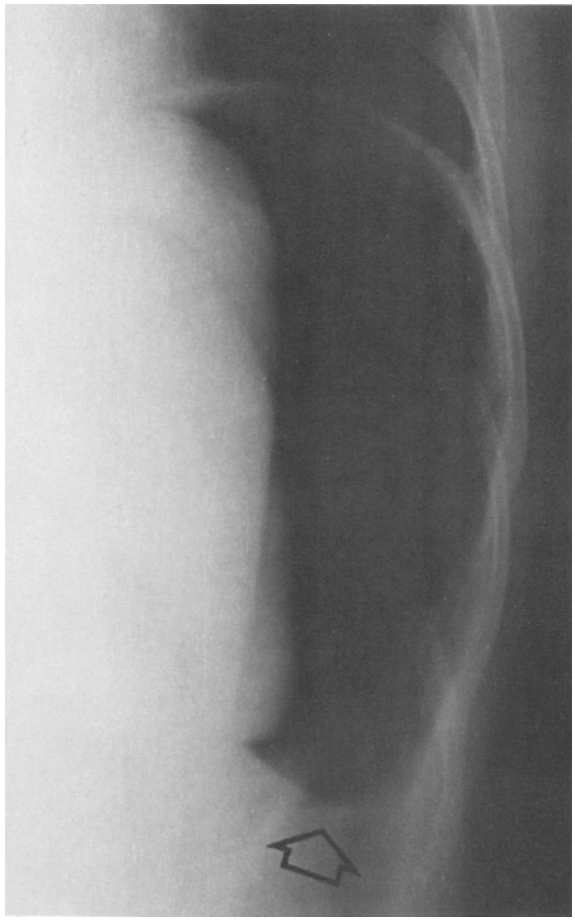


Fig. 3–18. The phrenicocolic ligament is seen *(arrow)* partially subtending the left subphrenic (perisplenic) space in a case of free intraperitoneal air. Decubitus projection. The liver and spleen have fallen to the right.
(Reproduced from Meyers.[18])

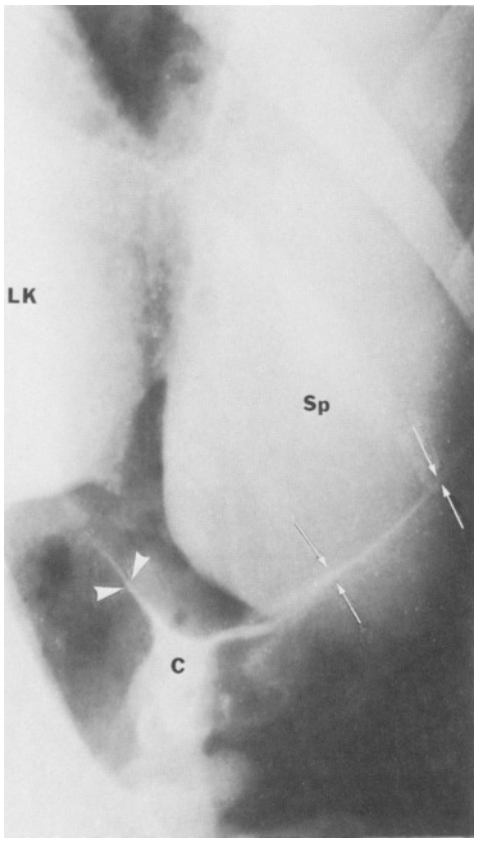


Fig. 3–19. Prone peritoneography outlines the phrenicocolic ligament *(arrows).*
This structure supports the spleen *(Sp)* as it extends from the splenic flexure of the colon (*C*) to the left diaphragm and is in continuity with the gastrosplenic ligament *(arrowheads)* seen on end. The close relationship of the posterior margin of the spleen to the left kidney *(LK)* is shown.
(Reproduced from Meyers.[14])

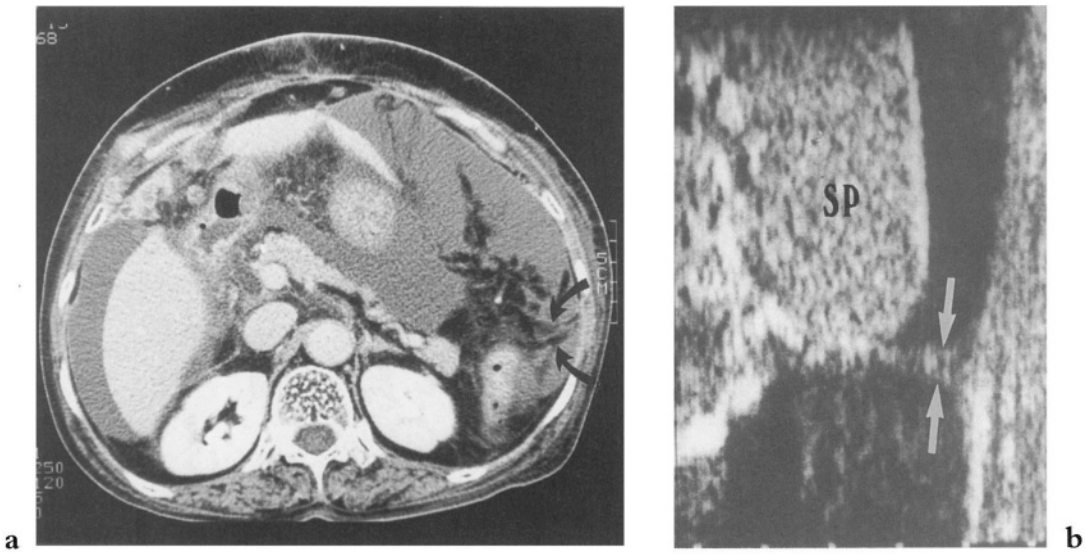


Fig. 3–20. The phrenicocolic ligament.
(a) CT demonstrates the phrenicocolic ligament *(curved arrows)* as a triangular fat-containing structure extending from the splenic flexure of the colon to the diaphragm at the level of the 10th or 11th rib.
(b) Coronal sonogram of the left flank shows a bandlike echogenic structure *(arrows)* extending from the colon to the abdominal wall, just inferior to the tip of the spleen *(SP).* Left paracolic ascites is separated from the perisplenic ascites by the phrenicocolic ligament.
(Courtesy of Yong Ho Auh, M.D., Asan Medical Center, Seoul, Korea)

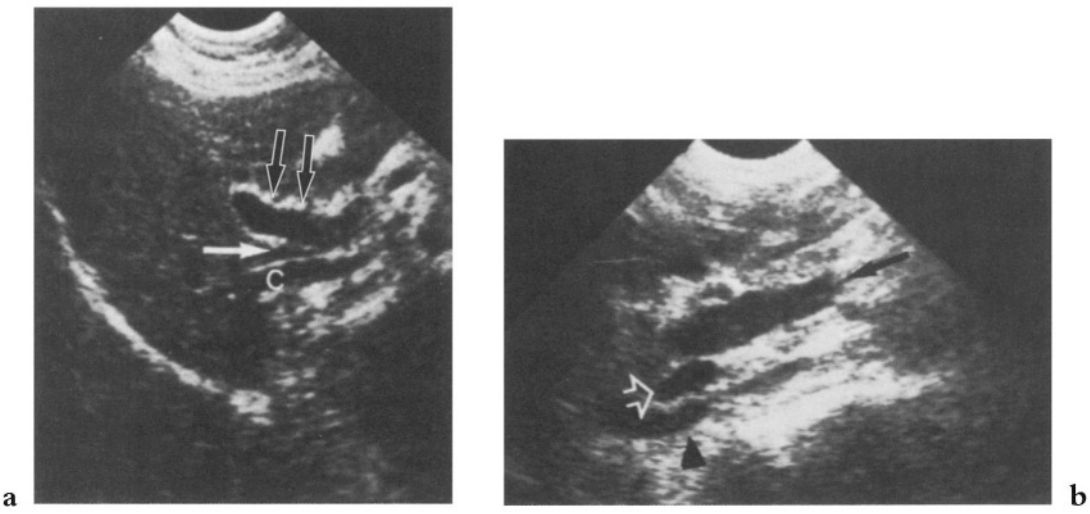


Fig. 3–21. The foramen of Winslow.
(a) Sagittal ultrasonography. The foramen of Winslow is indicated by the triangular zone *(white arrow)* between the portal vein *(double arrows)* and the inferior vena cava (C).
(Reproduced from Weill.[22])
(b) Sagittal ultrasonography. In a patient with ascites, a small amount of fluid enters the foramen *(open arrow)* between the portal vein *(arrow)* and the vena cava (*arrowheads*).
(Reproduced from Weill and Manco-Johnson.[23])

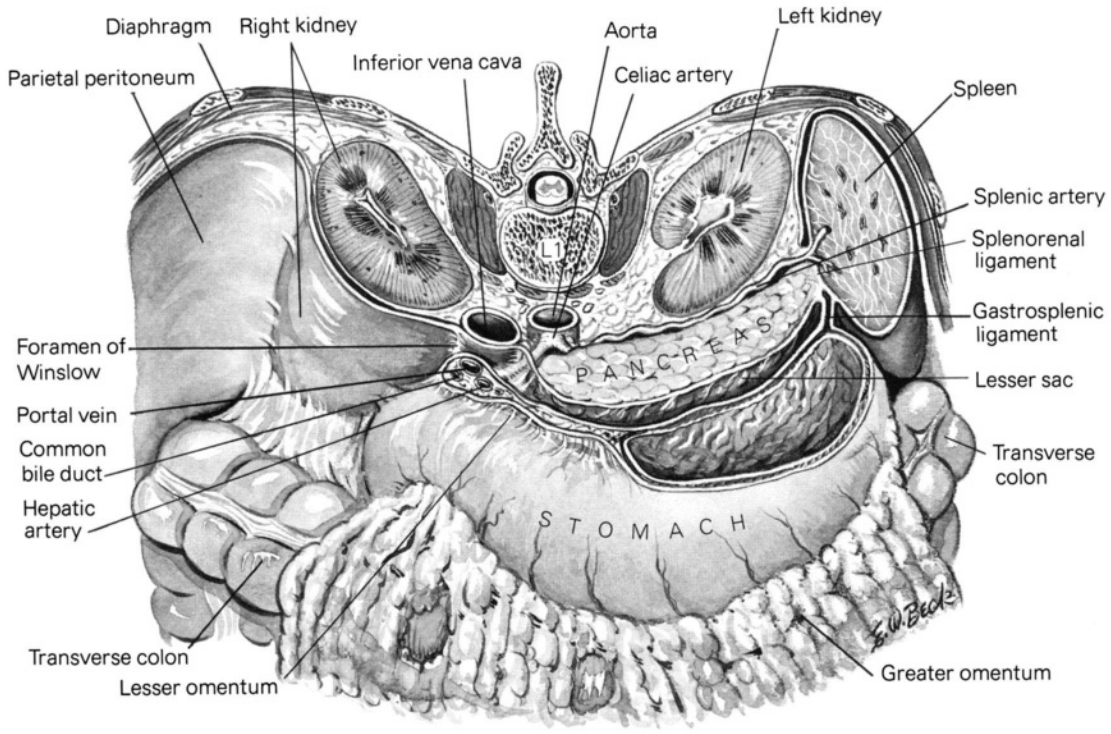


Fig. 3–22. The lesser sac and its relationships.
The foramen of Winslow is generally only large enough to admit the introduction of one to two fingers, but *in vivo* it represents merely a potential communication between the greater and lesser peritoneal cavities.

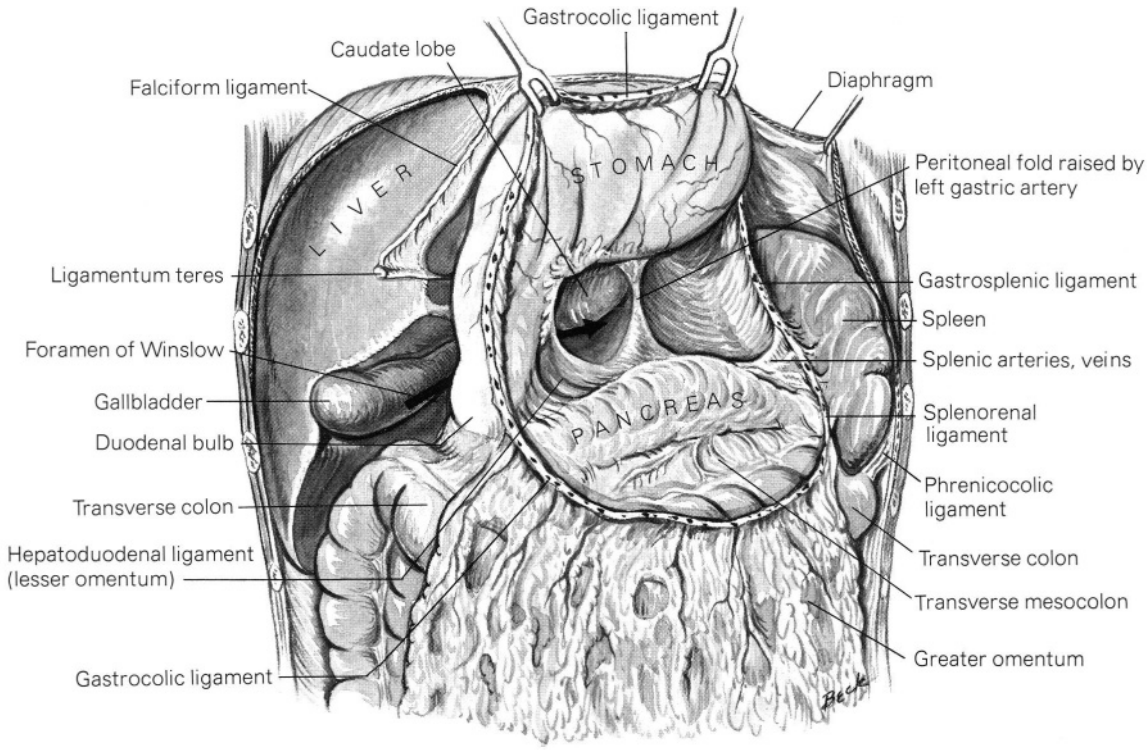


Fig. 3–23. The lesser sac and its relationships, shown with the stomach upraised.
Foramen of Winslow (see *arrow*).

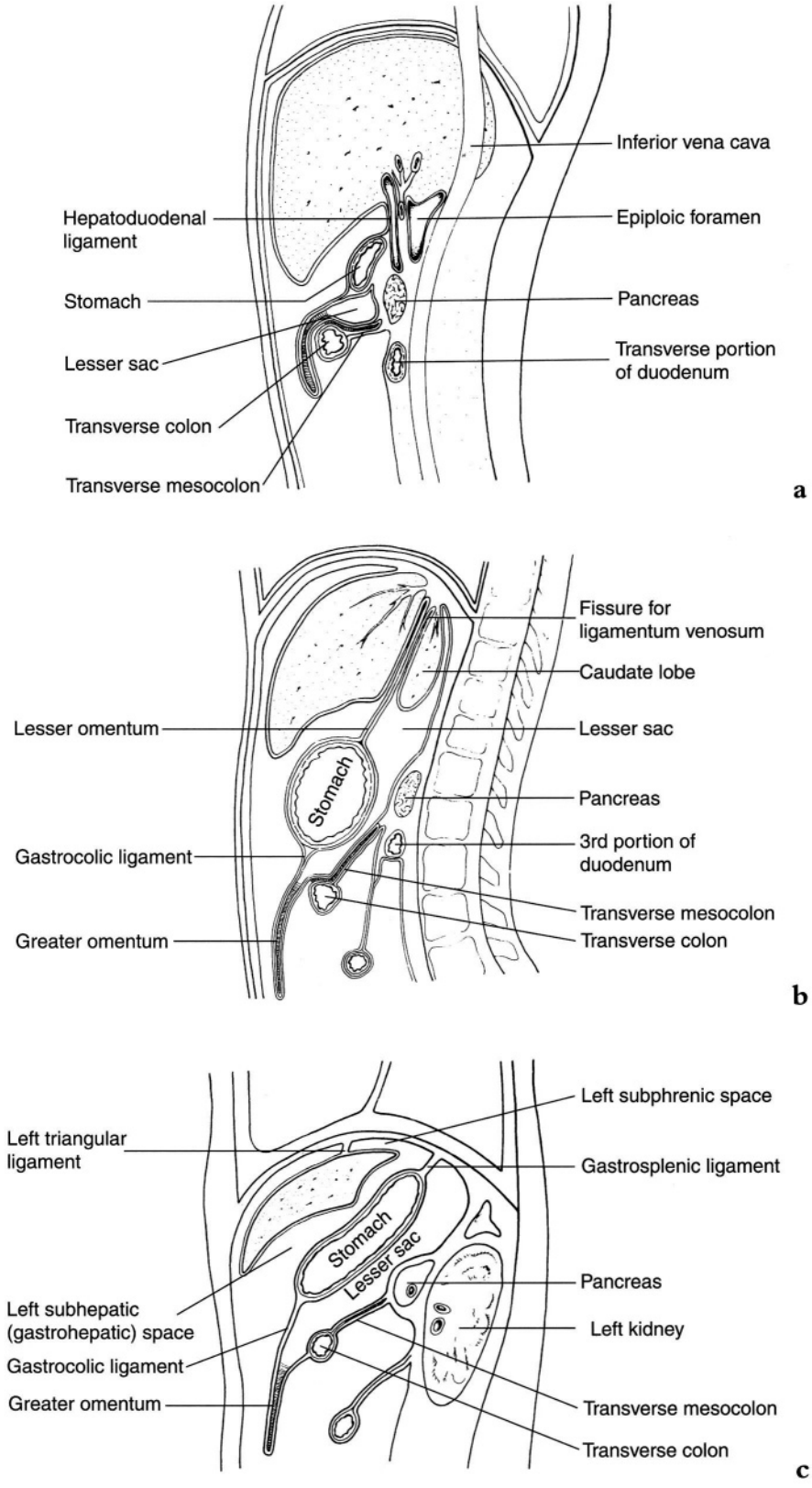


Fig. 3–24. Lesser sac anatomy illustrated by sagittal sections of the upper abdomen through the inferior vena cava (a), midline (b), and left kidney (c).
(a) The epiploic foramen is well demonstrated between the inferior vena cava and hepatoduodenal ligament. A small portion of the lesser sac is seen anterior to the pancreas. In this section, the greater omentum and transverse mesocolon are relatively short. Note fusion of the inner two layers of the greater omental peritoneum and adhesion of the posterior layer of the greater omentum with the anterior layer of the transverse mesocolon.
(b) The lesser omentum extends from the stomach to the fissure for the ligamentum venosum. The posterior peritoneal layer of the lesser omentum reflects back to the caudate lobe. In this section, the greater omentum and the transverse mesocolon are elongated. The anterior boundaries of the lesser sac are the lesser omentum, stomach, and gastrocolic ligament. The posterior ones are posterior parietal peritoneum and the transverse mesocolon with greater omentum. The inferior one is fused greater omentum.
(c) The lesser sac is bounded by the stomach and the gastrocolic ligament anteriorly, the gastrosplenic ligament superiorly, and transverse mesocolon posteriorly. The lesser sac is separated from the posterior left subphrenic space and left subhepatic space (gastrohepatic space) by the stomach and gastrosplenic ligament.
(Courtesy of Yong Ho Auh, M.D., Asan Medical Center, Seoul, Korea)

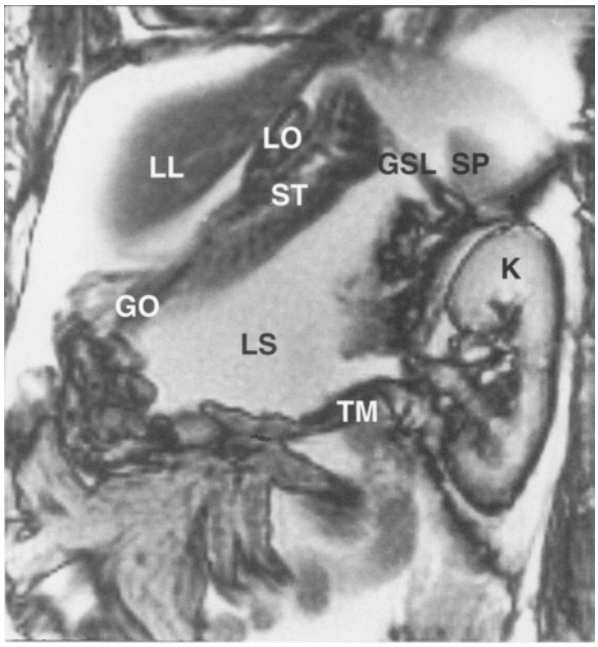


Fig. 3–25. The lesser sac *(LS)* seen on sagittal MRI at level of the left kidney (*K*). T2-weighted MRI in presence of ascites shows boundaries of the lesser sac. *LL* = left lobe of liver; *LO* = lesser omentum; *ST* = stomach; *SP* = spleen; *GSL* = gastrosplenic ligament; *GO* = greater omentum; *TM* = transverse mesocolon. (Courtesy of Yong Ho Auh, M.D., Asan Medical Center, Seoul, Korea)

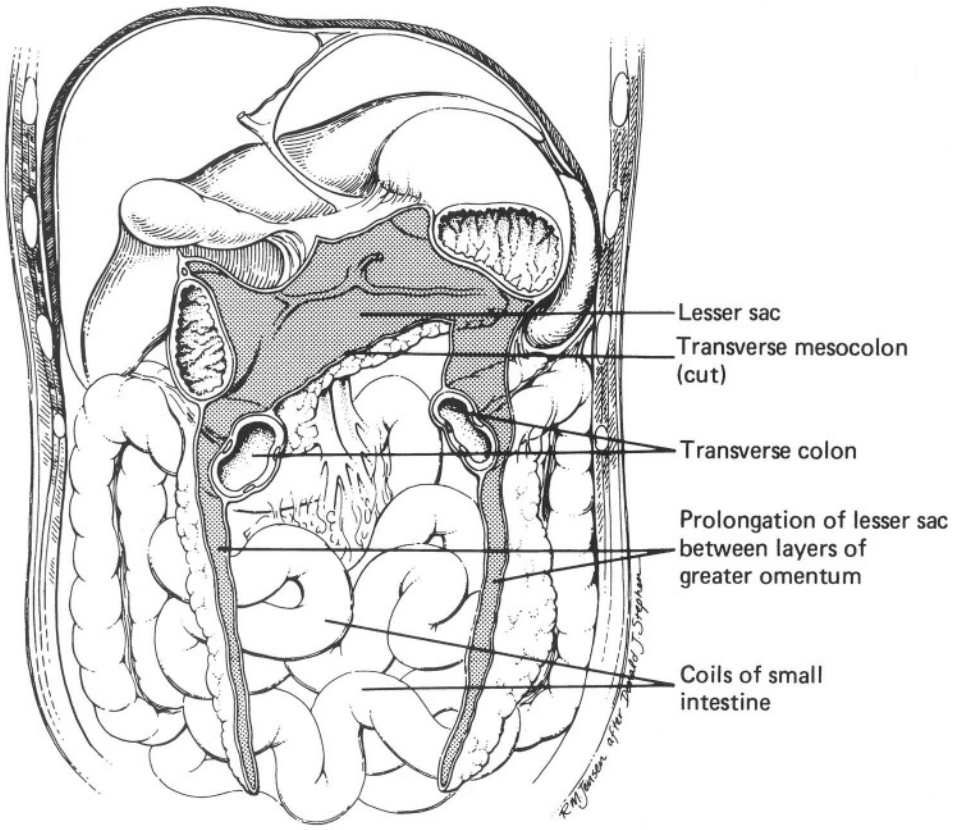


Fig. 3–26. Extent of lesser sac within greater omentum. Lesser omentum and stomach cut and section removed from greater omentum and transverse colon. Drawing shows potential inferior extension of lesser sac between the layers of the greater omentum.

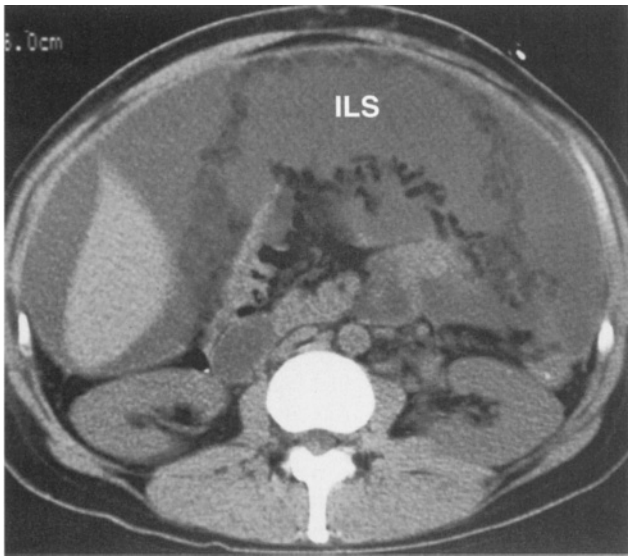


Fig. 3–27. Ascites between the leaves of the greater omentum.
In a patient with metastatic adenocarcinoma, ascitic fluid has dissected into the inferior recess of the lesser sac *(ILS)* between the unfused anterior and posterior leaves of the omentum. These are each evident by virtue of their fat-laden nature. Marked ascites is also present in the greater peritoneal cavity.
(Courtesy of Robert Mindelzun, M.D., Stanford University, Palo Alto, CA.)

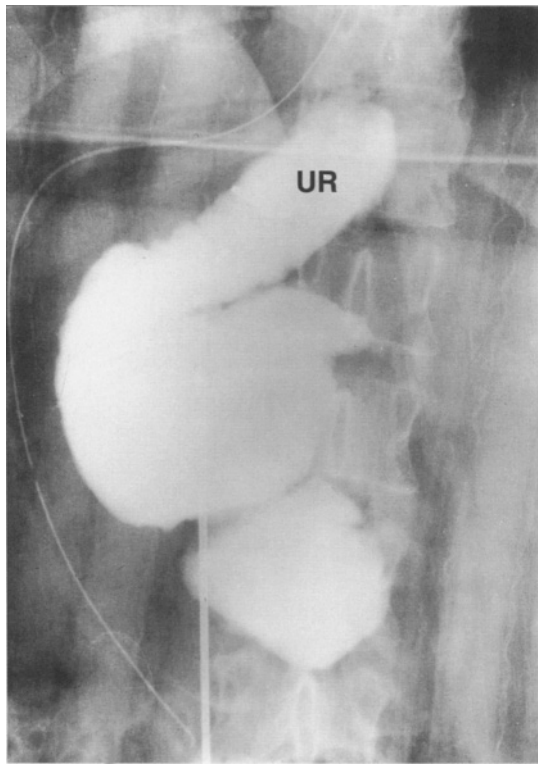


Fig. 3–28. Opacification of the lesser sac *in vivo*.
Following percutaneous puncture before a drainage procedure and contrast injection, the anatomic extent of the vestibule and the upper recess *(UR)* of the lesser sac is clearly depicted.
(Courtesy of Jacques Pringot, M.D., Brussels, Belgium.)

The base of the fold can be identified indirectly by virtue of its typical location and associated vessels (Fig. 3–31) and directly in the presence of fluid collections on both sides (Figs. 3–32 through 3–34). The fold should not be confused with a minor delicate membrane, termed the gastropancreatic ligament, between the posterior gastric wall and the pancreas, which often remains unnoticed and is not visualized by computed tomography.[27,28]

On the left, the lesser sac is bounded by the splenic attachments—the gastrosplenic ligament in front and the splenorenal ligament behind (Figs. 3–14a, 3–31a, 3–35, and 3–36). On the right side, the space extends just to the right of the midline, where it communicates, at least potentially, behind the free edge of the lesser omentum with the right subhepatic space via like foramen of Winslow (Figs. 3–23, 3–37, 3–38).

The ultrasonographic features of the lesser sac have been described,[23,30,31] but it is computed tomography that clearly demonstrates the anatomic characteristics *in vivo*[32–34] (Figs. 3–31 to 3–33, 3–35, 3–36, 3–39, 3–40). Lesser sac collections can be easily distinguished from loculated fluid collections in perihepatic spaces and hepatic fissures[19] (Figs. 3–41 and 3–42). Details are also identifiable by MR imaging (Fig. 3–43).[35]

text continues on page 79

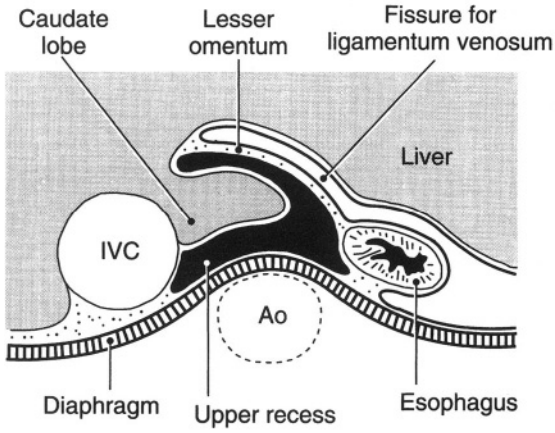


Fig. 3–29. Boundaries of superior recess of the lesser sac. The borders of this cul-de-sac include the diaphragm posteriorly, the caudate lobe of the liver anteriorly, the intraabdominal segment of the esophagus to the left, and the inferior vena cava *(IVC)* to the right. *Ao* = aorta.
(After Sauerland EK, Grant's Dissector, 10th ed. Williams & Wilkins, Baltimore, 1991.)

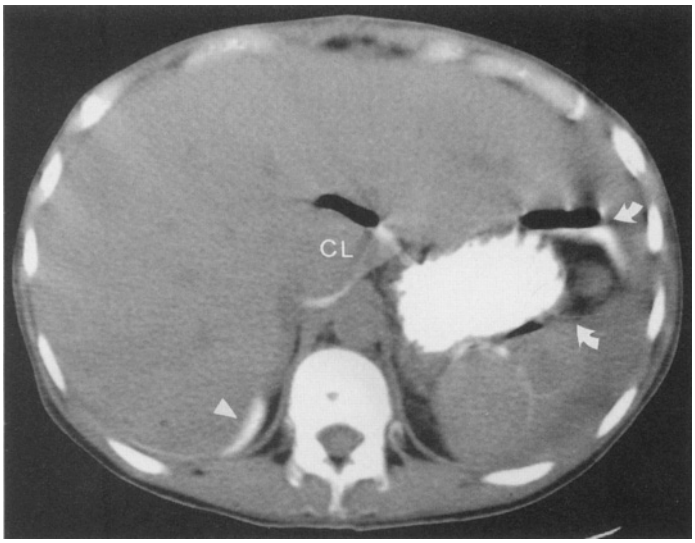
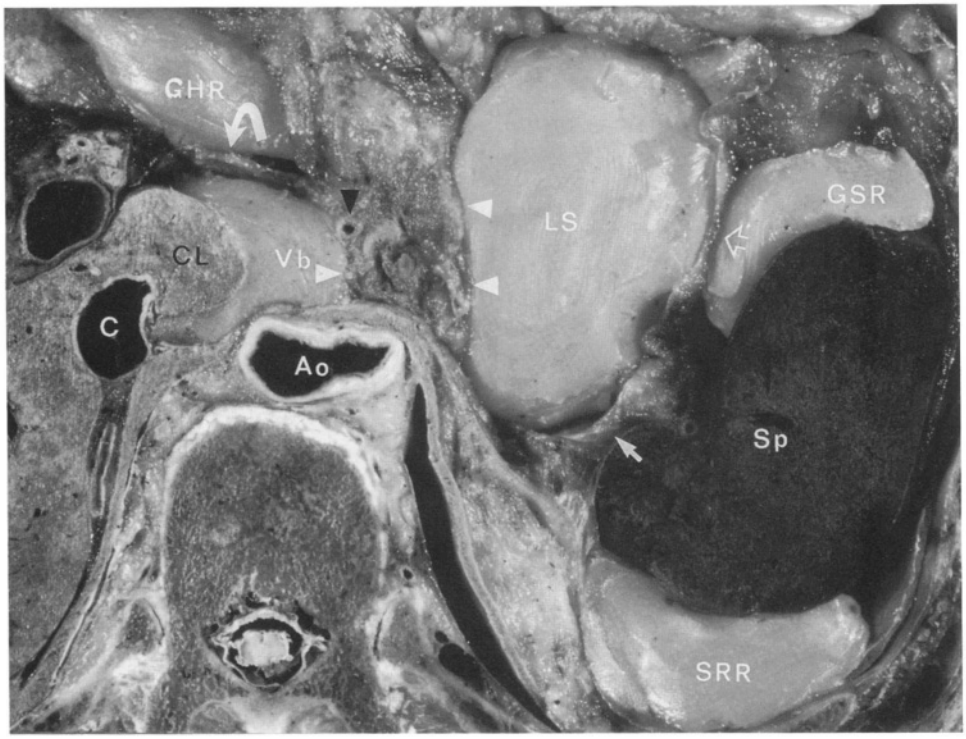
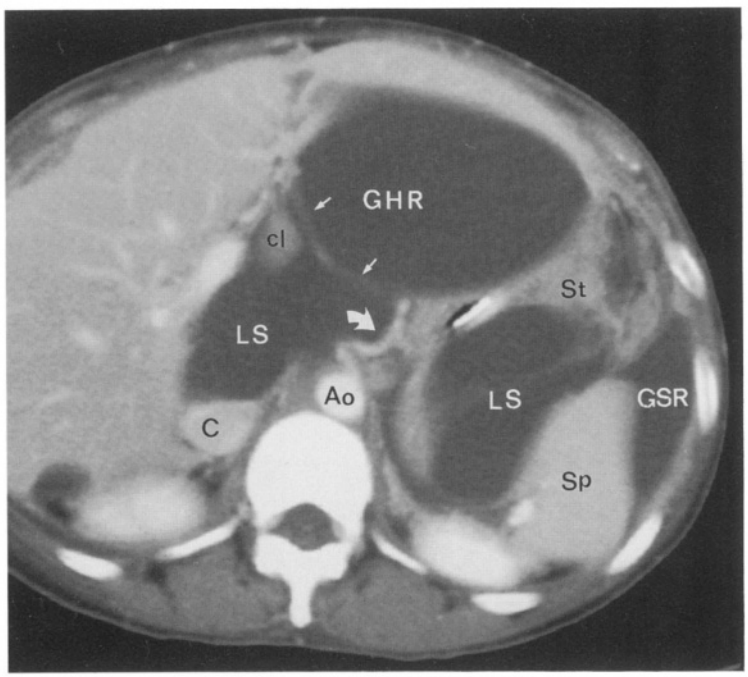


Fig. 3–30. The caudate lobe of the liver (*CL*) projects into the upper recess of the lesser sac.
It is discretely outlined by air and contrast medium from a perforated gastric ulcer studied by an upper GI series. Contrast also outlines the lateral border of the lesser sac (*arrows*). A small amount has escaped through the foramen of Winslow into the subhepatic space *(arrowhead).*



a



b

Fig. 3–31. Anatomy of the lesser sac and the gastropancreatic plica.
(a) Anatomic specimen with spaces injected. The gastropancreatic plica *(white arrowheads),* within which courses the left gastric artery *(black arrowhead),* is a structure of some dimension. It separates the vestibule (*Vb*) in relationship to the caudate lobe (*CL*) from the larger lateral recess of the lesser sac (*LS*). The latter is separated by the gastrosplenic ligament *(open arrow)* from the gastrosplenic recess *(GSR)* and by the splenorenal ligament *(white arrow)* from the splenorenal recess *(SRR).* The vestibule is separated by the gastrohepatic ligament *(curved arrow)* from the gastrohepatic recess (*GHR*). *Ao* = aorta; *C* = inferior vena cava; *Sp* = spleen. (Reproduced from Kumpan.[27]) **(This figure also appears in the color insert.)**
(b) In a case of ascites, CT demonstrates the gastropancreatic plica through which the left gastric artery courses *(curved arrow)* separates the fluid collections within the two recesses of the lesser sac (*LS*). This is bounded anteriorly by the gastrohepatic ligament *(small arrows)* from fluid in the gastrohepatic recess *(GHR)* and laterally and posteriorly by the gastrosplenic and splenorenal ligaments from fluid in the gastrosplenic *(GSR)* and splenorenal recesses, respectively. *Ao* = aorta; *C* = inferior vena cava; *cl* = papillary process of caudate lobe; *St* = stomach; *Sp* = spleen.

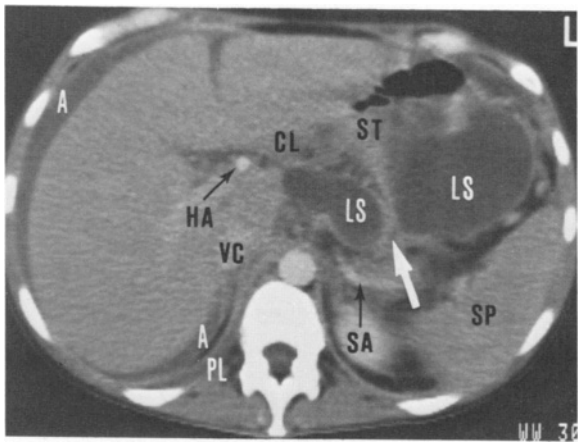


Fig. 3–32. CT anatomy of the lesser sac.
Identification of landmarks enhanced by intraperitoneal fluid. The lesser sac (*LS*) is divided into two compartments by a peritoneal fold *(white arrow)* enclosing the left gastric artery as it passes from the posterior abdominal wall to reach the lesser curvature of the stomach *(ST).* Differentiation between ascites fluid (*A*) and intrapleural fluid (*PL*) is clear. *CL* = caudate lobe of liver; *HA* = hepatic artery; *SA* = splenic artery; *SP* = spleen; *VC* = vena cava.
(Reprinted by permission from Feldberg MAM; Computed Tomography of the Retroperitoneum. Martinus Nijhoff, Boston, 1983.)

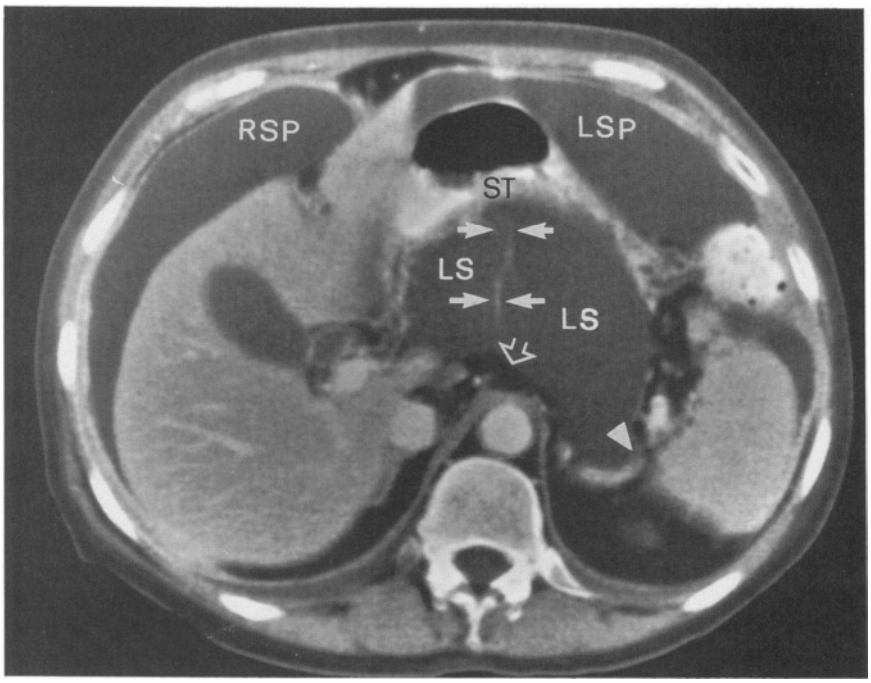


Fig. 3–33. CT anatomy of the lesser sac.
The lesser sac (*LS*), distended with ascites, is traversed by the stretched peritoneal fold *(arrows)* in which the left gastric artery courses to reach the lesser curvature of the stomach (*ST*).
Based on this anatomic feature, the potential clinical loculation of fluid to one or the other compartment can be anticipated. The extraperitoneal fat near the base of origin within the gastropancreatic plica is identifiable (*open arrow*).
On the left, note the posterior extent of the lesser sac bounded by the splenorenal ligament within which distal splenic vessels course (*arrowhead*).
Ascites within the right (*RSP*) and left (*LSP*) subphrenic spaces is separated by the falciform ligament.

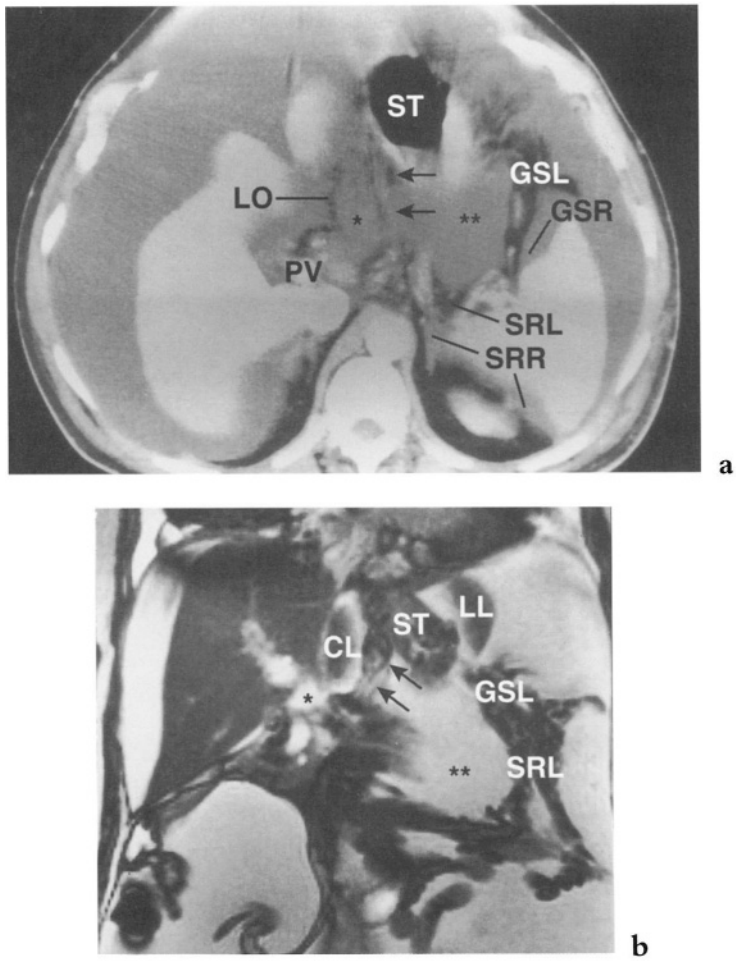


Fig. 3–34. The gastropancreatic fold seen on axial CT (a) and coronal MRI (b). The gastropancreatic fold *(arrows)* is seen as a fat-containing pleat in the lesser sac. It divides the lesser sac into the small superior (medial) *(one asterisk)* and large inferior (lateral) *(two asterisks)* recess. In MRI, the caudate lobe occupies the superior recess of lesser sac. *LO* = lesser omentum; *GSL* = gastrosplenic ligament; *SRL* = splenorenal ligament; GSR = gastrosplenic recess; *SRR* = splenorenal recess; *ST* = stomach; *CL* = caudate lobe; *PV* = portal vein; *LL* = left lobe of liver. (Courtesy of Yong Ho Auh, M.D., Asan Medical Center, Seoul, Korea)

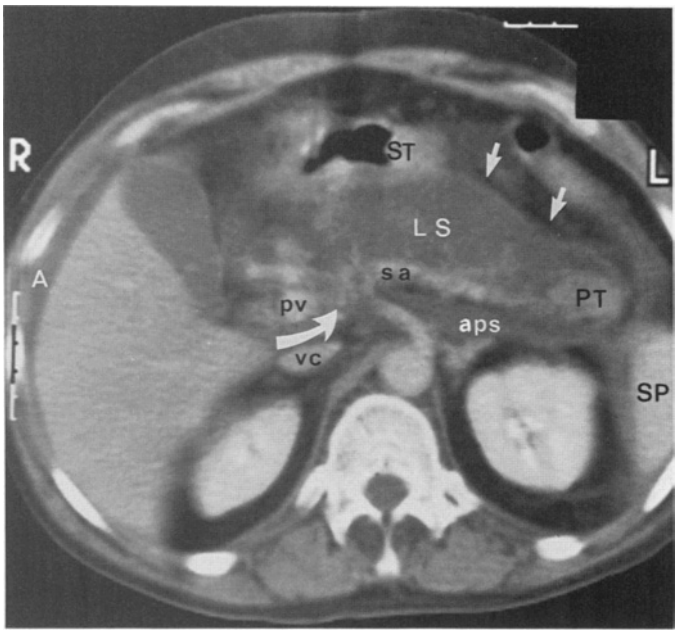


Fig. 3–35. CT anatomy of the lesser sac.
Fluid in the lesser sac (*LS*) behind the stomach (*ST*) is bounded anteriorly by the gastrocolic ligament *(white arrows)* and communicates via the epiploic foramen (*curved arrow*) between the inferior vena cava *(vc)* and portal vein *(pv)* with ascitic fluid *(A)* in the greater peritoneal cavity. Deep to the splenic artery (*sa*) and pancreatic tail (*PT*) there is associated fluid within the anterior pararenal space (*aps*) extending to the angle of the spleen (*SP*).

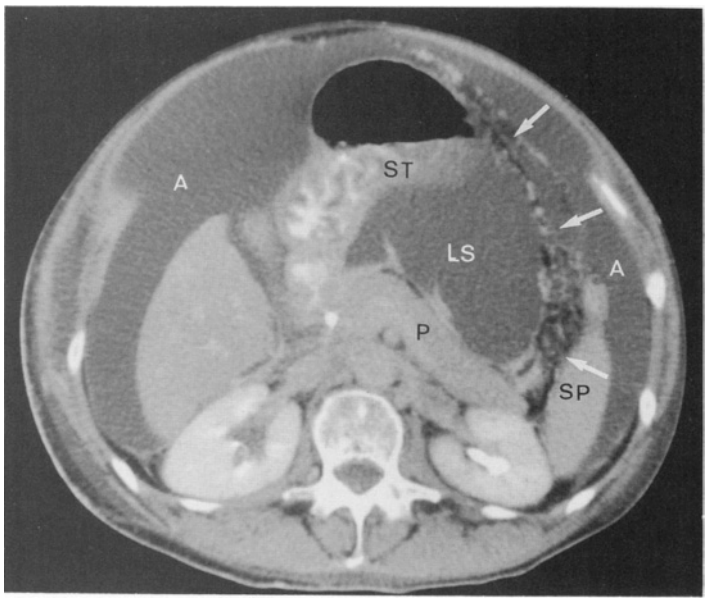


Fig. 3–36. CT anatomy of the lesser sac.
Ascites is present in the greater peritoneal cavity *(A)* and in the lesser sac *(LS)* between the pancreas (*P*) and stomach (*ST*), where it is distinctly demarcated laterally by the gastrosplenic ligament (*arrows*). *SP* = spleen.

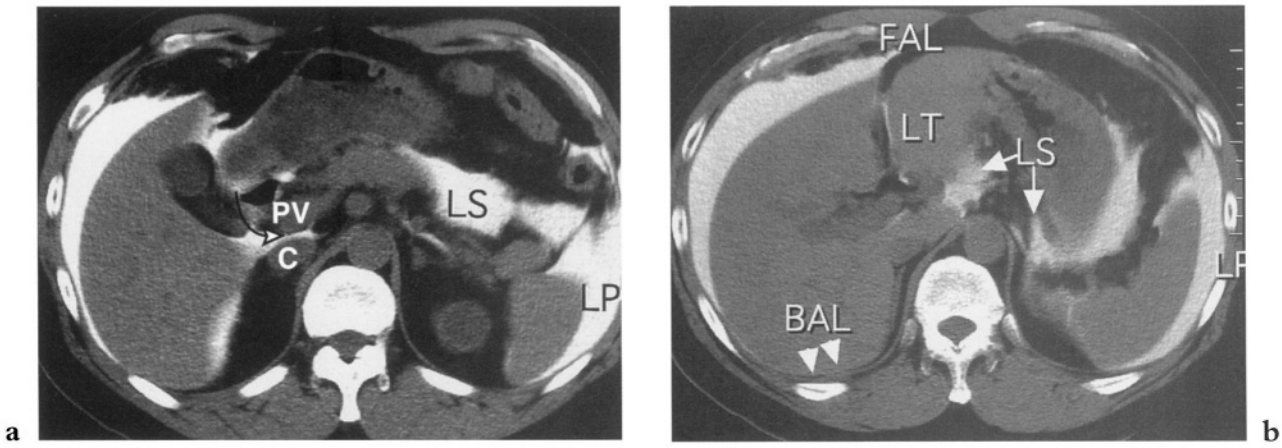
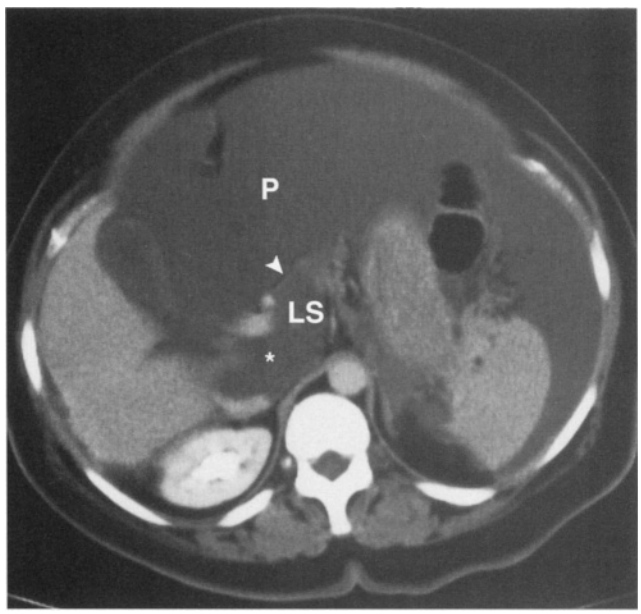


Fig. 3–37. CT anatomy of the foramen of Winslow entrance into the lesser sac.
(a and **b)** CT scans of the abdomen following intraperitoneal injection of contrast show communication of the greater peritoneal cavity with the lesser sac (*LS*) via the epiploic foramen of Winslow *(curved arrow),* between the inferior vena cava (*C*) and portal vein *(PV).*
Perihepatic contrast is limited anteriorly by the falciform ligament *(FAL),* where some tracks along the ligamentum teres *(LT),* and posteriorly at the level of the bare area of the liver *(BAL). LP* = left perisplenic space.
(Courtesy of Hiromu Mori, M.D., Oita Medical University, Oka, Japan.)

Fig. 3–38. CT anatomy of the foramen of Winslow entrance into the lesser sac.
Contrast-enhanced CT shows that ascites in the greater peritoneal cavity (*P*) gains entrance through a widened foramen of Winslow *(asterisk)* in the portacaval space to the lesser sac (*LS*). Visualization of the hepatoduodenal ligament *(arrowhead)* is achieved by virtue of fluid on both sides.
(Reproduced from DeMeo et al.[29])



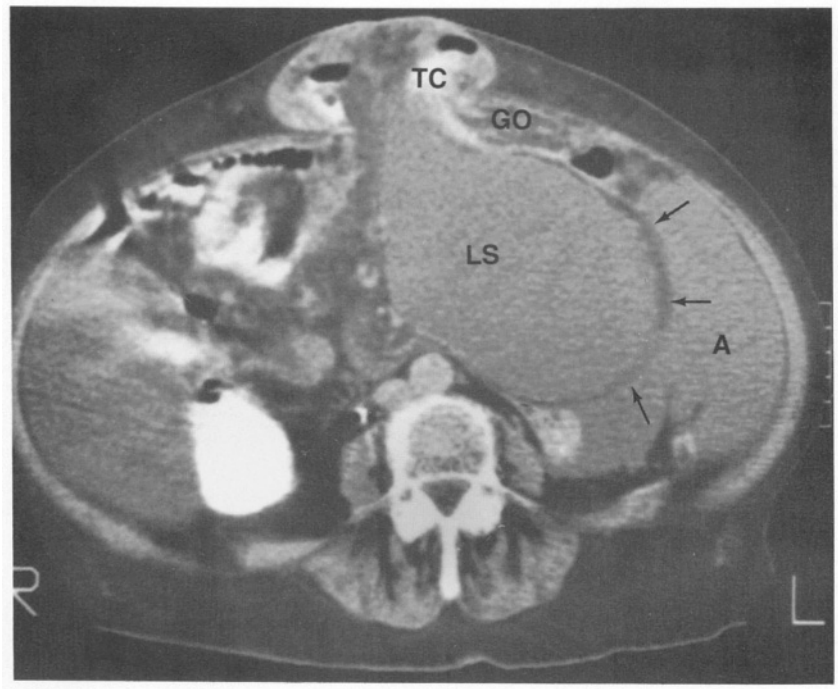


Fig. 3–39. Fluid in the herniated lesser sac.
Umbilical herniation containing fluid in the lesser sac *(LS),* the middle portion of the transverse colon *(TC)* and a segment of the distal transverse mesocolon, as well as the greater omentum (*GO*) in a patient with gastric carcinoma. The gastrosplenic ligament *(arrows)* is bowed toward the ascites in the general peritoneal cavity *(A).*
(Courtesy of César Pedrosa, M.D., Hospital Universitario San Carlos, Madrid, Spain.)

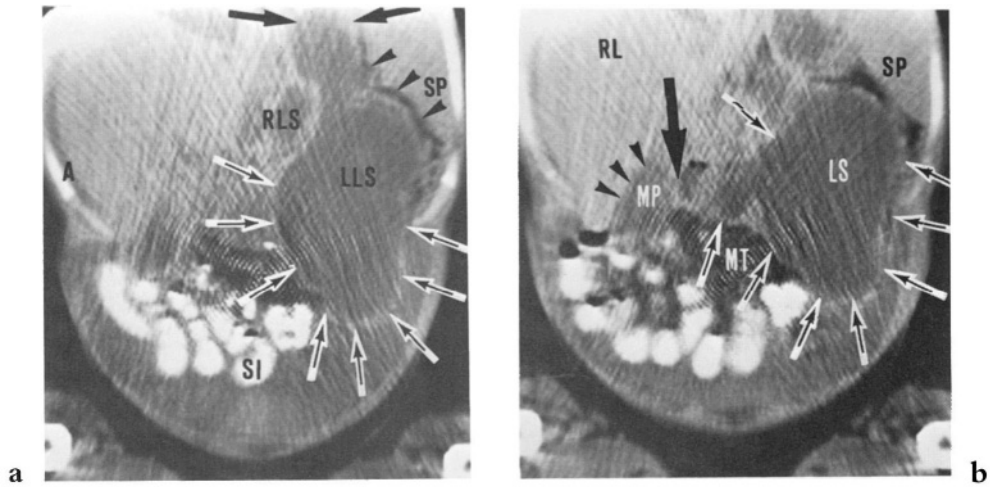


Fig. 3–40. CT anatomy of the lesser sac. Fluid in lesser sac.
(a) Direct coronal image demonstrates extent of right *(RLS)* and left *(LLS)* compartments of the lesser sac. *LSS* is larger and its inferior recess *(black* and *white arrows)* may extend between anterior and posterior leaves of greater omentum. Superiorly the left part of the lesser sac extends to a level below the apex of the diaphragm *(black arrows).* The greater omentum *(arrowheads)* is compressed between the lesser sac and the spleen *(SP). A* = ascites around liver; *SI* = opacified small intestine.
(b) The lesser sac (*LS*) communicates with Morison's pouch *(MP)* through the epiploic foramen of Winslow *(black arrow). MT* = mesentery of small intestine.
(Reprinted by permission from Feldberg MAM: Computed Tomography of the Retroperitoneum. Martinus Nijhoff, Boston, 1983.)

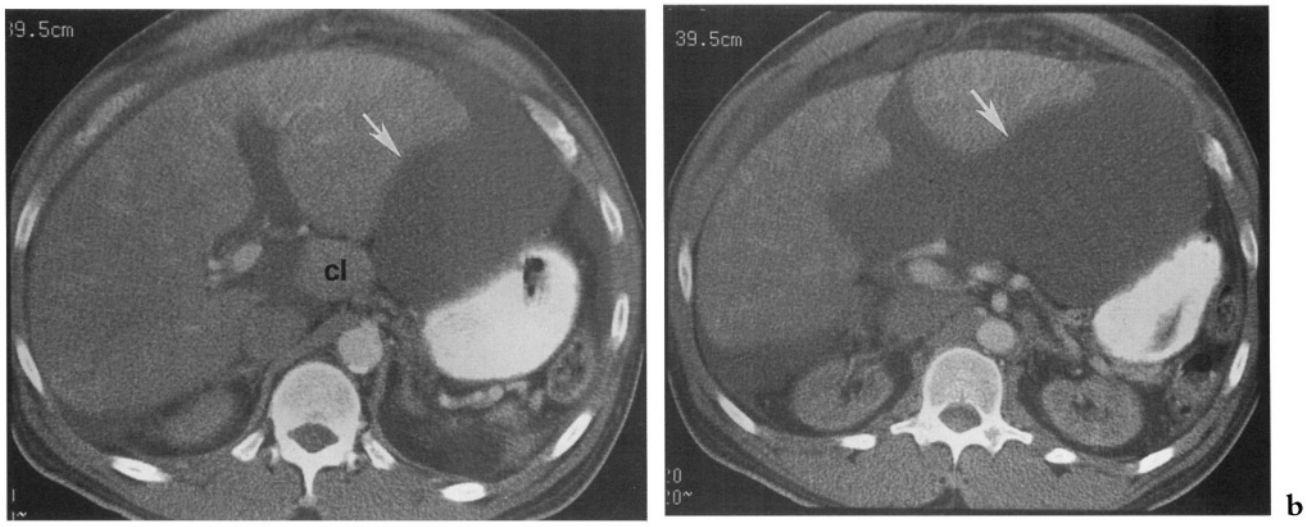


Fig. 3–41. Ascitic fluid in gastrohepatic recess simulating fluid in lesser sac.
(a and **b)** Contrast-enhanced CT in a patient with alcoholic liver disease reveals a large fluid collection *(arrows).* This is localized in the gastrohepatic recess since the fluid follows the lateral surface of the left lobe lateral segment posteriorly into the fissure for the ligamentum venosum and extends to the left and right portal veins. Fluid does not engulf the caudate lobe *(cl)* to indicate that this is fluid within the lesser sac.
(Courtesy of James Brink, M.D., Yale University School of Medicine, New Haven, CT.)

Radiologic Features

The Spread and Localization of Intraperitoneal Abscesses

I have documented that the spread of infection within the peritoneal cavity is governed by (a) the site, nature and rapidity of outflow of the escaping visceral contents; (b) mesenteric partitions and peritoneal recesses; (c) gravity; *(1)* intraperitoneal pressure gradients; and (2) the position of the body.[6,14,18,36]

The dynamic pathways of flow of intraperitoneal fluid *in vivo* have been established in a series of adult patients by peritoneography.[6,14] The peritoneal reflections and recesses provide watersheds and drainage basins for the spread and localization of infection (Table 3–1).

Intraabdominal abscesses may be radiologically manifested by demonstrating (a) a soft-tissue mass, (b) a collection or pattern of extraluminal gas, (c) viscus displacement, (d) loss of normally visualized structures, (e) fixation of a normally mobile organ, or (f) opacification of a communicating sinus or fistulous tract. Secondary signs include scoliosis, elevation or splinting of a diaphragm, localized or generalized ileus, and pulmonary basilar changes. These pathways and localizing features are evident not only by conventional radiologic techniques, but they have also been confirmed by ultrasonography,[37,38] isotopic studies[39] and computed tomography.[40,41] Knowledge of the preferential pathways of spread and subsequent compartmentalization permits the early diagnosis of abscess formation often remote from its site of origin.[6,36]

Pelvic Abscesses

Fluid introduced into the inframesocolic compartment almost immediately seeks the pelvic cavity, first filling out the central pouch of Douglas (cul-de-sac)[42] and then

Table 3-1. Radiologic–Anatomic Classification of Intraperitoneal Abscesses[a]

Supramesocolic	Inframesocolic
Right subphrenic	Pelvic
Anterior	Paracolic
Posterior	Right
Right subhepatic	Left
Anterior	Infracolic
Posterior (Morison's pouch)	Right
Left subphrenic	Left
Lesser sac	

[a]*Modified from Meyers MA, Whalen JP.*[36]

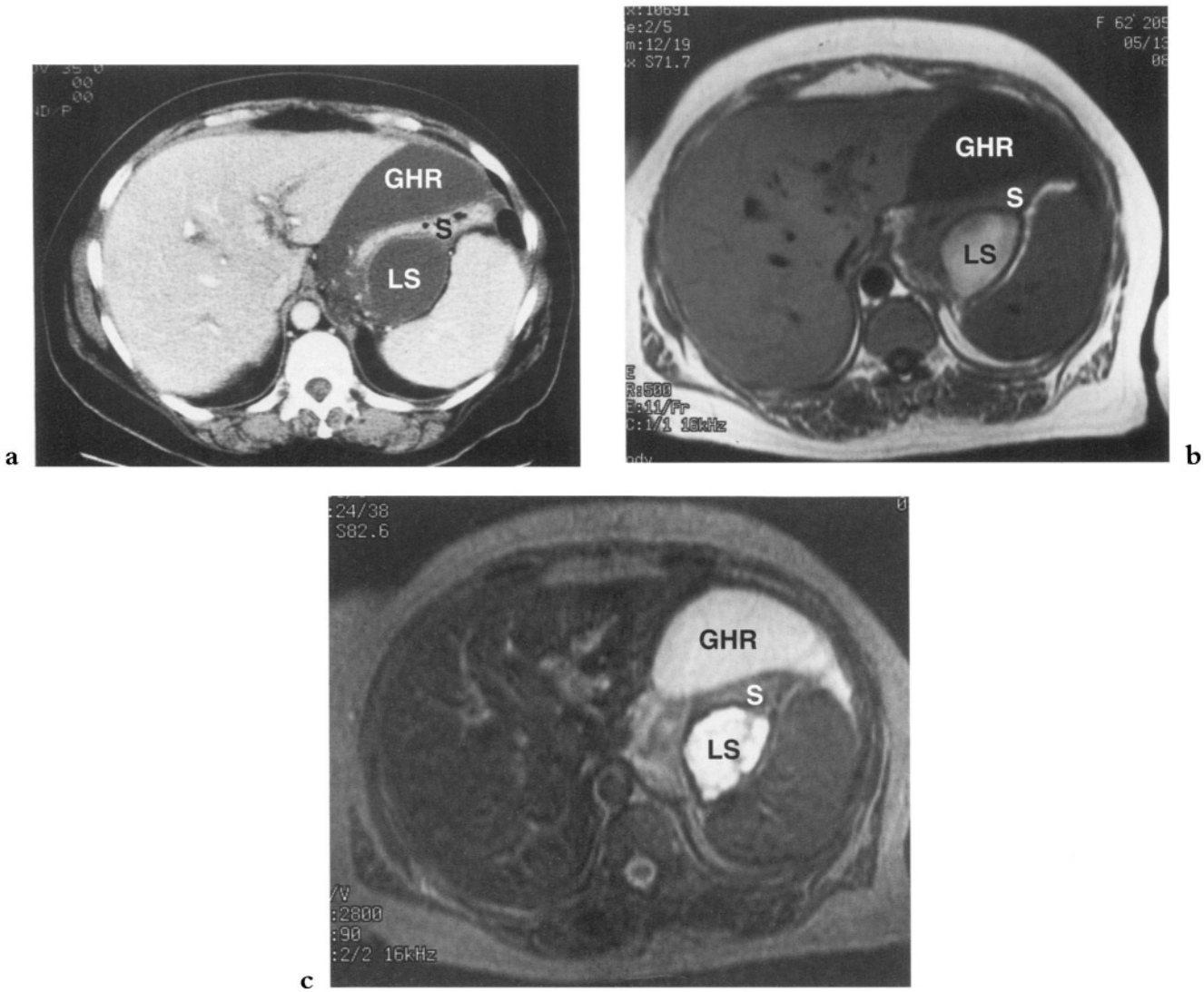


Fig. 3–42. Distinction between fluid collections in the lesser sac and gastrohepatic recess in a patient with metastatic ovarian carcinoma.
(a) CT demonstrates two fluid collections compressing the midbody of the stomach (*S*). One within the gastrohepatic recess *(GHR)* is seen anteriorly, while a lesser sac collection (*LS*), confined laterally by the gastrosplenic ligament, is seen posteriorly.
(b) T1-weighted and **(c)** T2-weighted MR images show that the lesser sac collection exhibits high signal intensity on both, compatible with a resolving hematoma in the extracellular methemoglobin phase. A thin hypointense rim around the collection is attributed to hemosiderin within macrophages. The gastrohepatic collection is nonhemorrhagic ascites, with signal similar to cerebrospinal fluid.

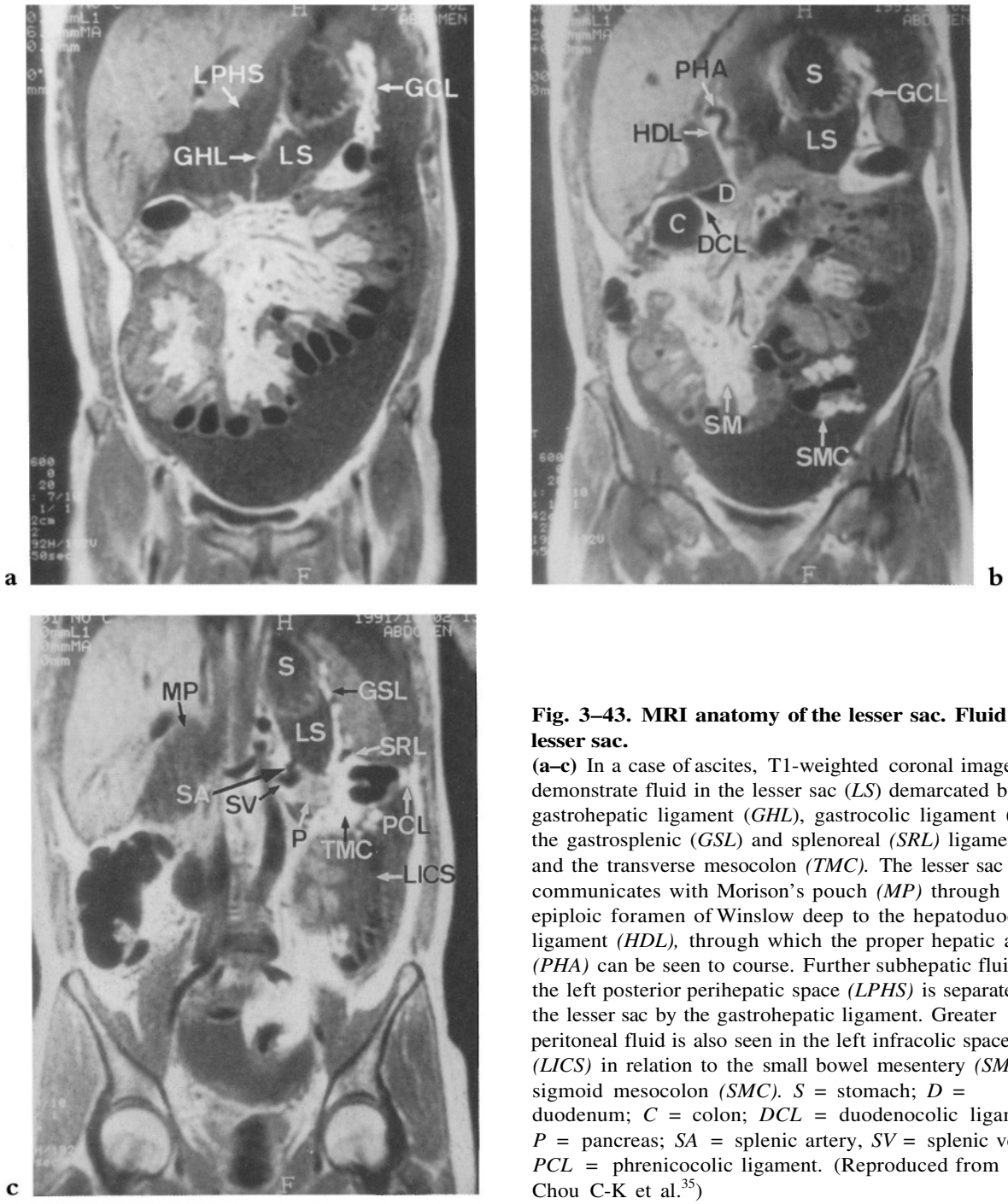
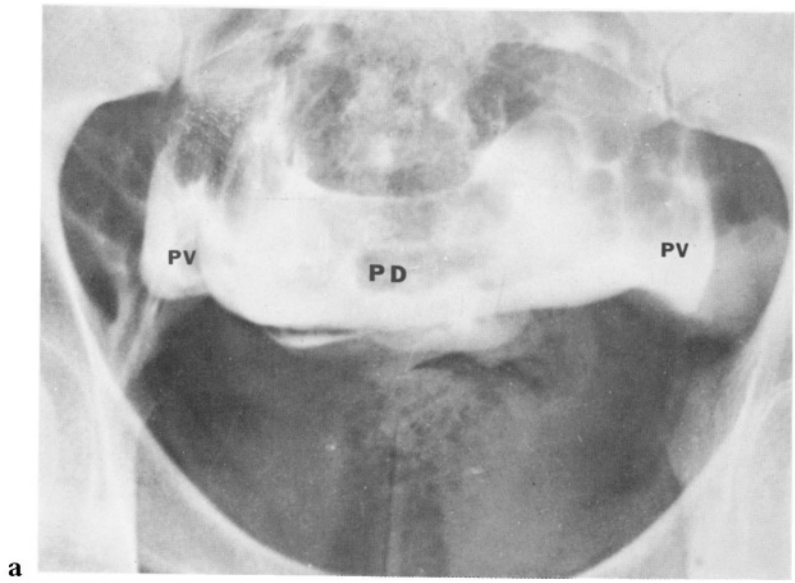


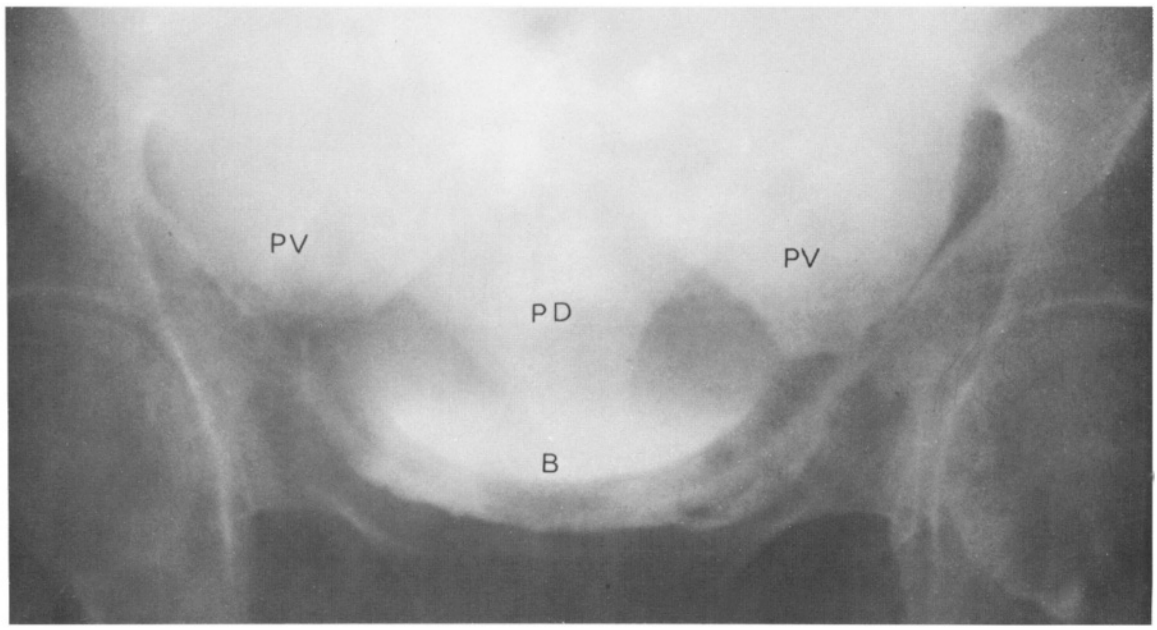
Fig. 3–43. MRI anatomy of the lesser sac. Fluid in the lesser sac.
(a–c) In a case of ascites, T1-weighted coronal images demonstrate fluid in the lesser sac (*LS*) demarcated by the gastrohepatic ligament (*GHL*), gastrocolic ligament (*GCL*), the gastrosplenic (*GSL*) and splenoreal *(SRL)* ligaments, and the transverse mesocolon *(TMC).* The lesser sac communicates with Morison's pouch *(MP)* through the epiploic foramen of Winslow deep to the hepatoduodenal ligament *(HDL),* through which the proper hepatic artery *(PHA)* can be seen to course. Further subhepatic fluid in the left posterior perihepatic space *(LPHS)* is separated from the lesser sac by the gastrohepatic ligament. Greater peritoneal fluid is also seen in the left infracolic space *(LICS)* in relation to the small bowel mesentery *(SM)* and sigmoid mesocolon *(SMC). S* = stomach; *D* = duodenum; *C* = colon; *DCL* = duodenocolic ligament; *P* = pancreas; *SA* = splenic artery, *SV* = splenic vein; *PCL* = phrenicocolic ligament. (Reproduced from Chou C-K et al.[35])

the lateral paravesical fossae (Figs. 3–44 and 3–45). A small amount in the left infracolic space readily pursues this course, but on the right, it is first arrested at the confluence of the small bowel mesentery with the colon before it overflows into the dependent recesses of the pelvis. This pathway is a function primarily of gravity and explains why the pelvis is the most common site of any residual abscess formation following generalized peritonitis (Figs. 3–46 and 3–47).

Fluid within the pouch of Douglas may be identified easily on supine plain film as a soft-tissue density superior to the urinary bladder (Fig. 3–48), at times with symmetric circular extensions representing further fluid collections within the paravesical fossae.[44] In cases of



a



b

Fig. 3–44. Fluid accumulation in pelvic recesses.
(a) A small amount of contrast medium introduced into the peritoneal cavity immediately gravitates to the pelvis, filling out the central pouch of Douglas (*PD*) and then the lateral paravesical fossae *(PV).*
(b) In another patient, erect view shows a larger amount of intraperitoneal contrast medium distending the midline pouch of Douglas (*PD*) and the lateral paravesical fossae *(PV).* The urinary bladder *(B)* is opacified.

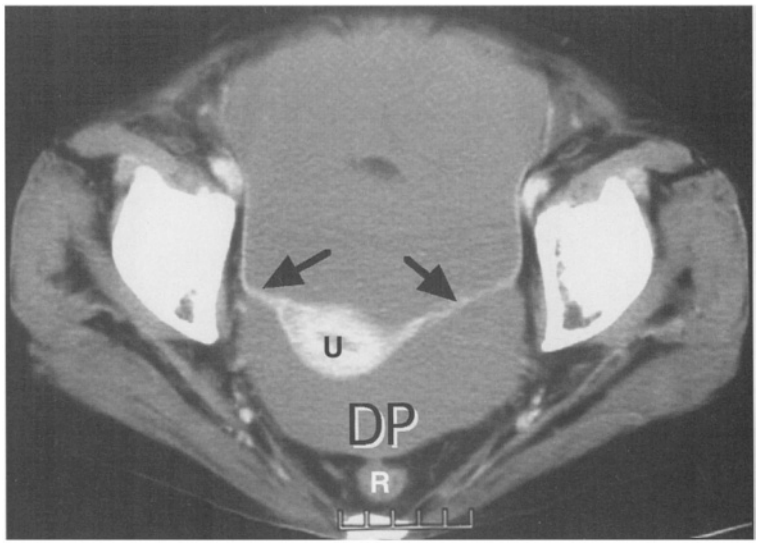


Fig. 3–45. Intraperitoneal fluid in the pelvic recesses.
CT shows massive ascites accumulating in the pelvic spaces. Fluid is present in the pouch of Douglas (*DP*), between the rectum (*R*) posteriorly and the uterus *(U)* and broad ligaments *(arrows)* anteriorly.

abdominal trauma, it may be the earliest and most reliable sign of the laceration or rupture of an organ. If doubt exists, a prone film permits the fluid to escape and the radiographic density is lost. Mass displacements by an abscess are seen most easily by extrinsic distortion of the dome of the urinary bladder, by compression on the rectosigmoid junction, or by displacement of the sigmoid colon, usually posteriorly and superiorly (Figs. 3–49 through 3–51). Lateral displacement of sigmoid loops may occur if the abscess extends beyond the midline. A huge abscess may arise out of the pelvis, displacing the intestine superiorly and to the side.

Fluid collections in additional pelvic fossae may be identifiable by CT and ultrasonography.[45]

Right Subhepatic and Subphrenic Abscesses

From the pelvis, fluid ascends both paracolic gutters. Passage up the shallower left one is slow and weak, and cephalad extension is limited by the phrenicocolic ligament.[6,38] The major flow from the pelvis is up the right paracolic gutter[6] (Fig. 3–52). It then progresses deep to the inferior edge of the liver into the right subhepatic space, particularly draining into its posterior extension (Morison's pouch) (Figs. 3–53 through 3–55). The right paracolic gutter consistently provides an avenue of spread for exudates. Abscess formation may coalesce in the anterior subhepatic space (Fig. 3–56), but this is unusual. Fluid preferentially seeks first the most dependent recess of Morison's pouch. This is formed by the triangular groove between the lateral aspect of the descending duodenum and the underlying right kidney, just above the beginning of the transverse mesocolon (Fig. 3–57). Thereafter, fluid occupies the entire pouch (Figs. 3–57 through 3–59). This drainage pathway from the pelvis is so constant that if the right paracolic groove can be referred to as a "gutter," then the "sewer" into

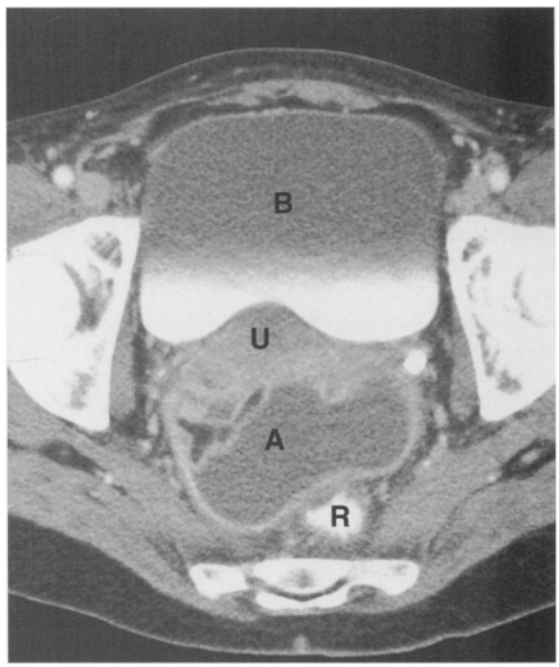


Fig. 3–46. Pouch of Douglas abscess.
CT demonstrates an abscess with an enhancing wall *(A),* secondary to appendicitis, that has localized in the cul-de-sac between the rectum *(R)* and the uterus *(U). B* = urinary bladder.

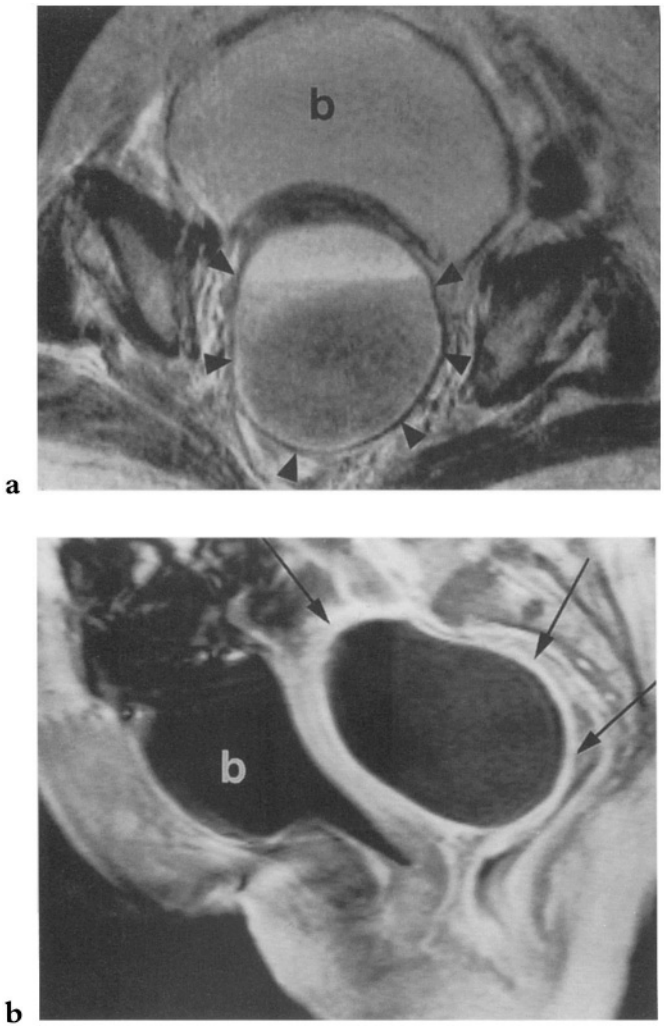


Fig. 3–47. Pouch of Douglas abscess.
(a) T2-weighted fat-suppressed spin-echo MR image reveals a complex fluid collection *(arrowheads)* behind the urinary bladder *(b).* Low-signal intensity debris is layered in the dependent portion of the abscess.
(b) Sagittal gadolinium-enhanced T1-weighted fat-suppressed SGE MR image shows substantial enhancement of the wall of the abscess *(arrows).*
(Reproduced from Semelka et al.[43])

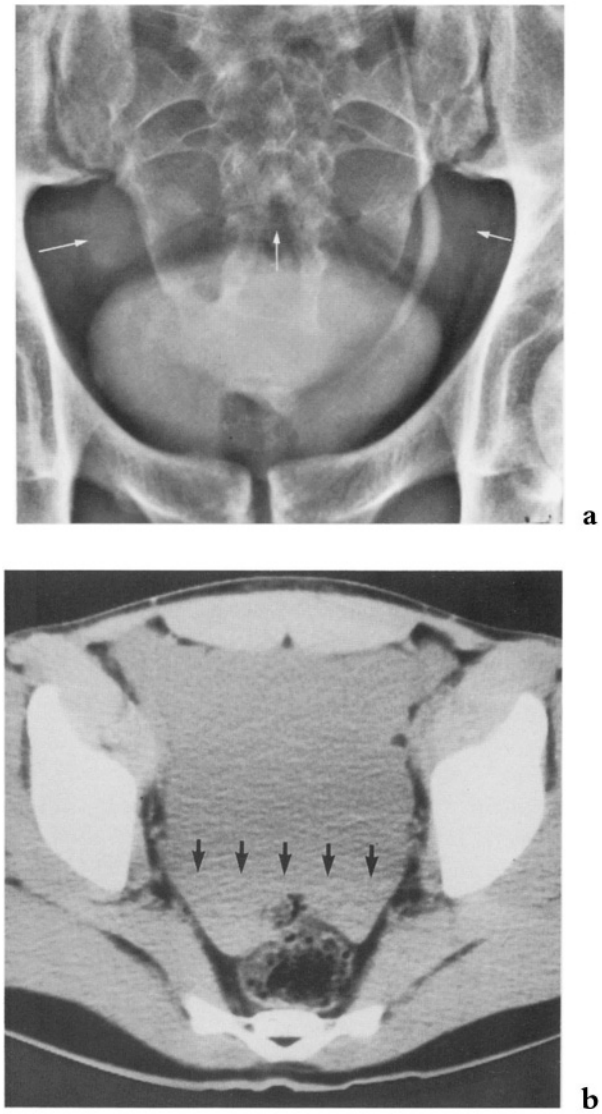


Fig. 3–48. Intraperitoneal blood gravitating to the pelvic recesses.
(a) This can be identified as a soft-tissue density *(arrows)* superior to the urinary bladder in this intravenous urogram.
(b) In another patient with a large amount of blood in the pelvis, CT correlation can be made. Note the hematocrit effect *(arrows)* with the high attenuation acute hemorrhage becoming dependent in the pararectal fossae.

which it preferentially drains its contaminated material is clearly Morison's pouch.

Intraperitoneal fluid lateral to the liver may be radiographically noted by identifying the lateral margin of the liver that becomes medially displaced (Hellmer's sign[47]) (Figs. 3–60 and 3–61). The appreciable difference in density is secondary to the attenuation coefficients between ascitic fluid and the hepatic parenchyma.[44,48] Blood, however, does not possess any difference in attenuation from the liver to be seen in this manner.

It is important to recognize that only after Morison's pouch is contaminated does the infected material reach the right subphrenic space (Figs. 3–62 through 3–67).

The fluid extends around the inferior edge of the liver or laterally from Morison's pouch along the inferior reflection of the right coronary ligament and then

text continues on page 89

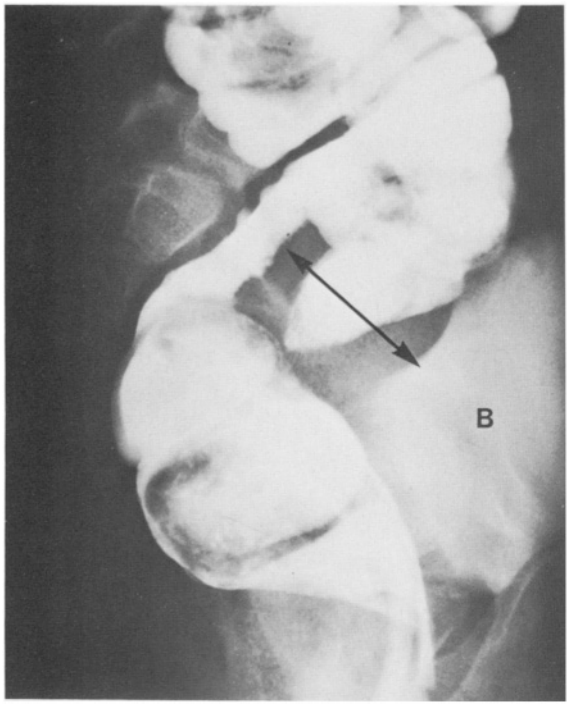


Fig. 3–49. Pelvic abscess in a child postappendectomy.
A large soft-tissue mass compresses and separates the rectosigmoid junction and the urinary bladder *(B).* A redundant sigmoid loop seen in this lateral view projects in this area but is truly off the midline.

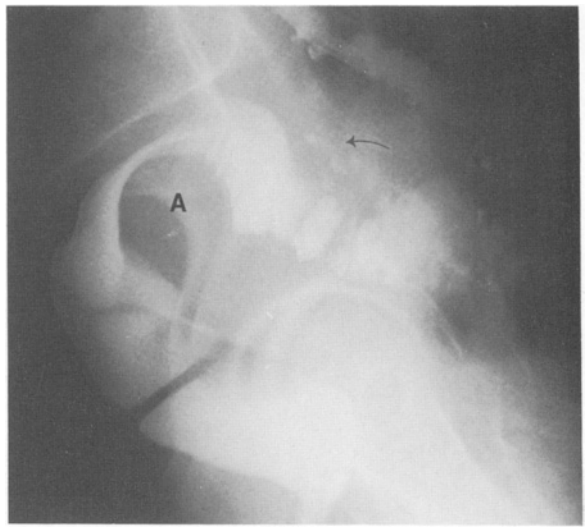


Fig. 3–50. Pelvic abscess secondary to sigmoid diverticulitis.
Following perforation of a diverticulum of the sigmoid colon *(arrow)* in the left lower quadrant, drainage into the pelvis results in an abscess *(A)* in the pouch of Douglas, shown by its characteristic compression on the rectosigmoid junction.

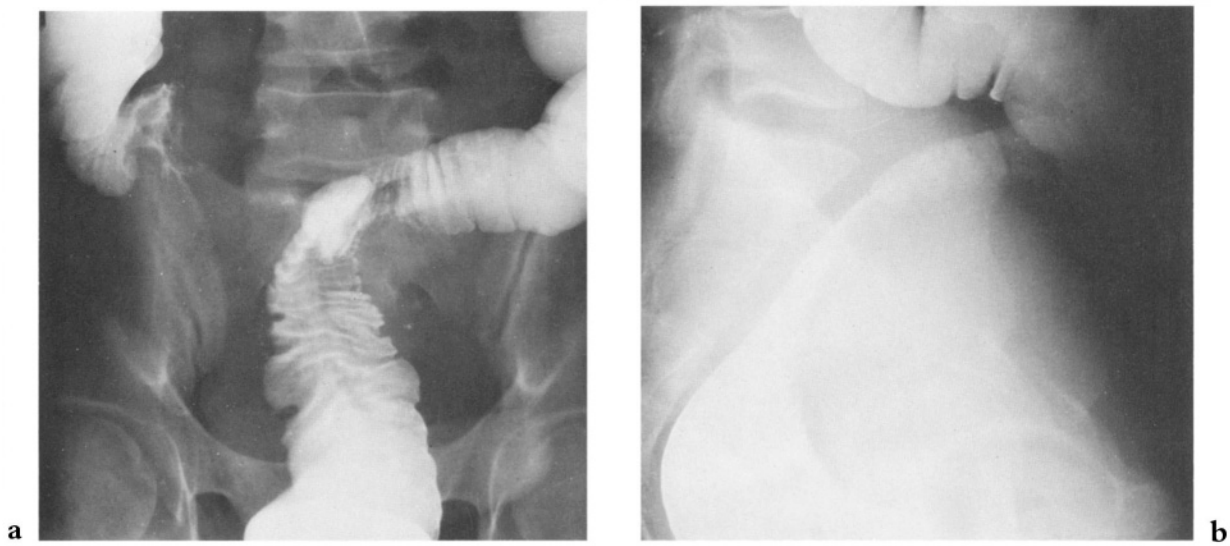


Fig. 3–51. Large pelvic abscess drains from an appendiceal abscess that also deforms the caput of the cecum. Gravitational flow is clearly indicated in the frontal **(a)** and lateral **(b)** views, with the large pelvic abscess displacing the rectum posteriorly against the sacral hollow.
(Reproduced from Meyers.[6])

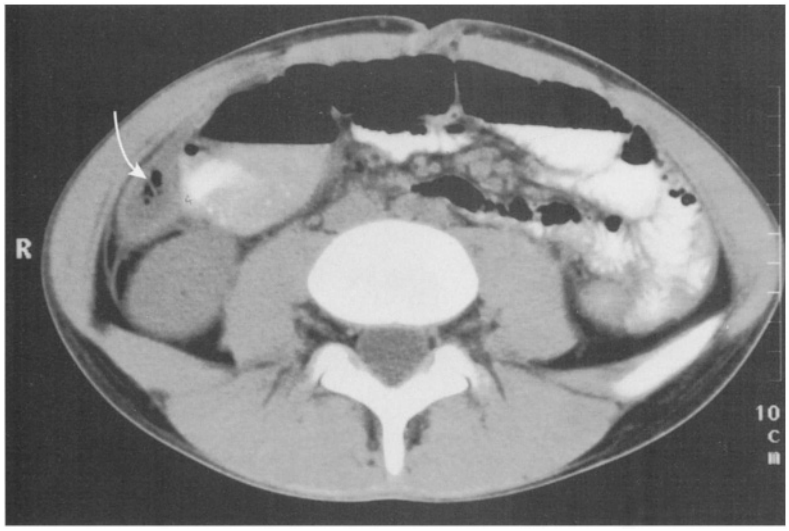


Fig. 3–52. Abscess in the right paracolic gutter. Unenhanced CT shows a gas-containing abscess *(arrow)* encapsulated within the right paracolic gutter.

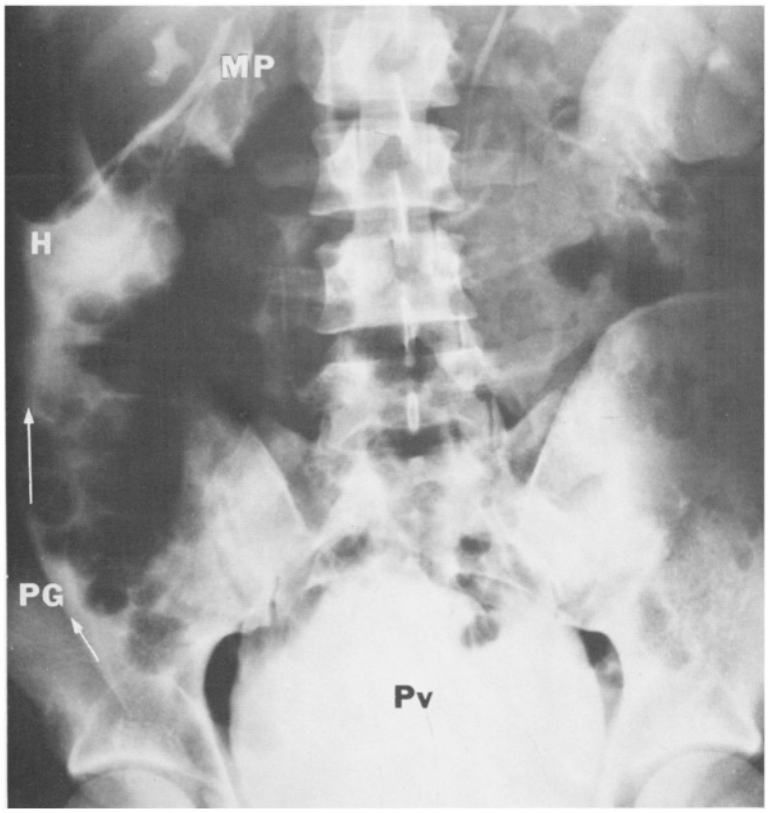


Fig. 3–53. Preferential spread up right paracolic gutter. Peritoneography in a patient demonstrates that contrast material, after first filling the pelvis *(Pv),* then extends directly up the right paracolic gutter (*PG*). It then outlines the hepatic angle *(H)* and progresses preferentially into Morison's pouch *(MP).* (Reproduced from Meyers.[6])

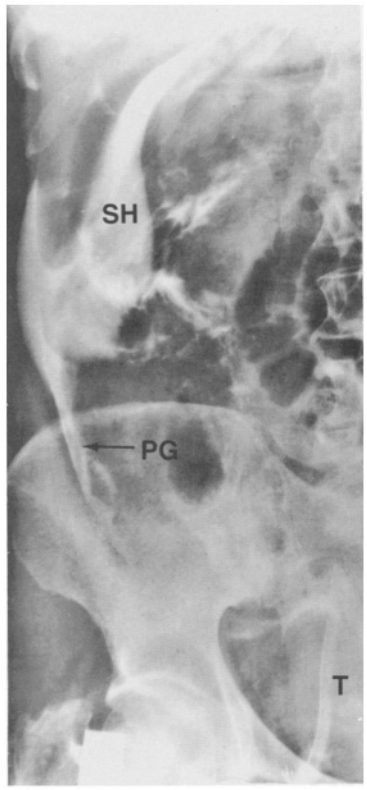


Fig. 3–54. Contrast medium injected through a misplaced cystotomy tube (*T*) whose tip is outside the urinary bladder. The fluid proceeds up the right paracolic gutter (*PG*) to the subhepatic spaces (*SH*).



Fig. 3–55. Leak from anastomotic site following an ileotransverse colostomy. Lateral radiograph shows that extravasation seeks the right subhepatic space *(arrows).*

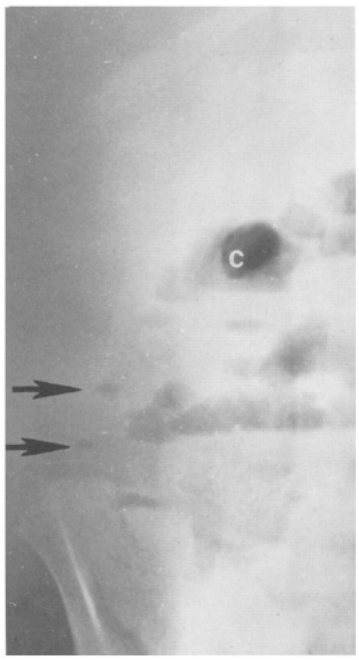


Fig. 3–56. Right paracolic and anterior subhepatic abscesses, postappendectomy.
Exudate containing a few gas bubbles *(arrows)* extends up the right paracolic gutter to a subhepatic abscess. This depresses the proximal transverse colon (*C*) and, by lifting the edge of the liver from its bed of extraperitoneal fat, results in loss of visualization of the hepatic angle. (Reproduced from Meyers.[6])

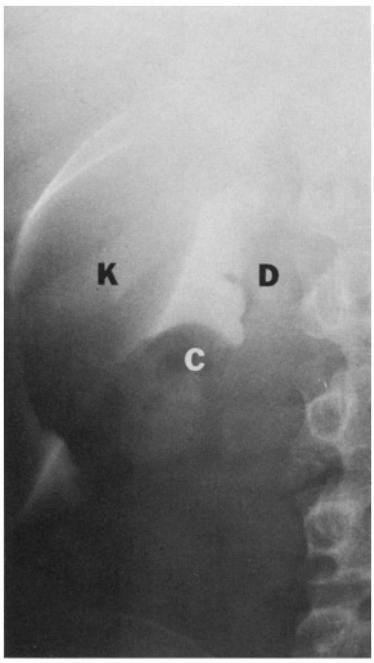


Fig. 3–57. The triangular dependent recess of Morison's pouch is opacified by a small amount of contrast medium. This is bounded posteriorly by the kidney (K), medially by the descending duodenum (D), and inferiorly by the proximal transverse colon (C). The outline particularly of gaseous collections at this site has been referred to as the *Doge's cap sign,* since its configuration typically has the shape of a peaked cap reminiscent of "Il corno," the renaissance headgear worn by the Doge of Venice.[46] (Reproduced from Meyers.[6])



Fig. 3–58. Abscess of Morison's pouch. Injection into the localized abscess cavity through a drainage tube identifies its size and position. Note the relationship of the abscess to the 10th and 11th posterior ribs. Residual barium outlines the hepatic flexure of the colon, which serves as the inferior boundary of the abscess. The development of pyogenic membranes may prevent spread to other compartments. (Reproduced from Meyers.[6])

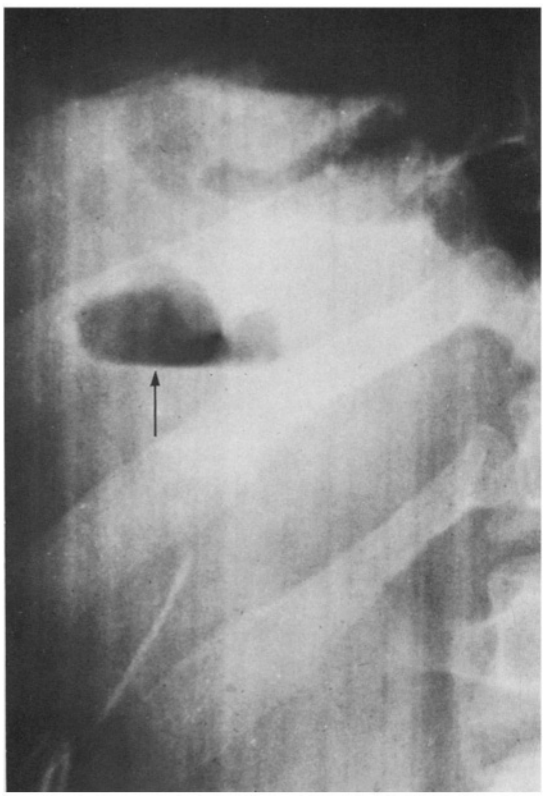


Fig. 3–59. Abscess of Morison's pouch. Erect view identifies a conspicuous air-fluid level *(arrow)* characteristically in relation to the upper pole of the right kidney at the level of the 11th rib.

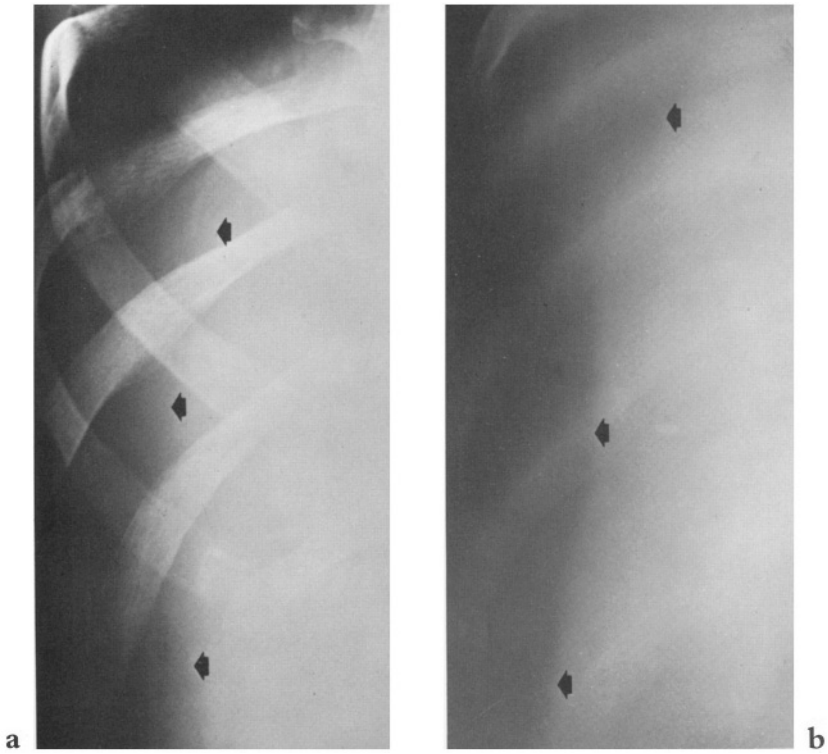


Fig. 3–60. Fluid lateral to the liver.
(a) Plain film visualization of the lateral margin of the right lobe *(arrows)* is highlighted by the differences in density between the intraperitoneal fluid and the displaced liver.
(b) These changes are confirmed by tomography following the effect of total body opacification.

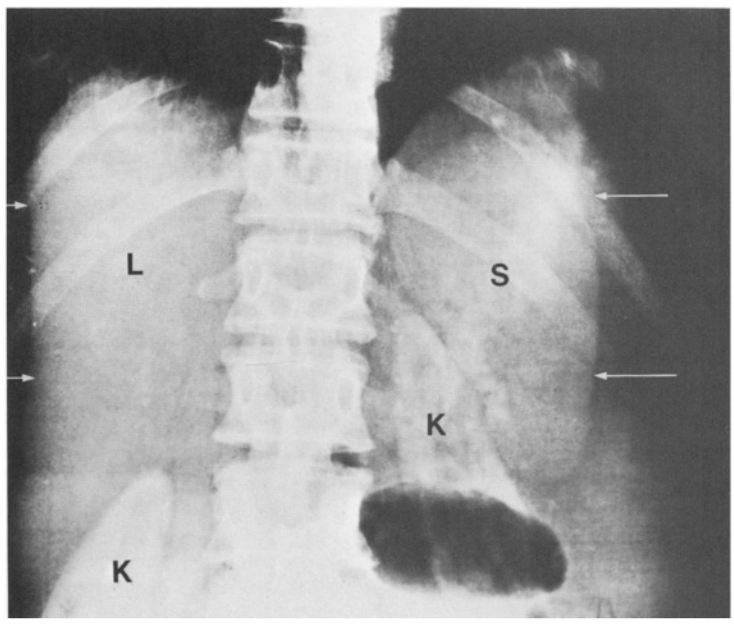


Fig. 3–61. Fluid lateral to the liver and spleen.
The enhancement of visualization of the liver (*L*) and spleen (*S*) during intravenous infusion of contrast medium clearly demonstrates their medial displacement in a case of ascites. *Arrows* point out their lateral borders. These changes help to explain the occasional plain film observation of Hellmer's sign. *K* = kidneys.

ascends in the flank to the space above the dome of the liver. Pyogenic membranes may compartmentalize an abscess solely to Morison's pouch (Figs. 3–58 and 3–59). Characteristically, this presents as a discrete air–fluid level posteriorly at the level of the 10th to 12th ribs. Whether further spread occurs is probably related to many factors, including particularly the rapidity with which the infection develops and the virulence of the infecting organisms. Fluid collections in the right posterior subphrenic space cannot extend medial to the cor-

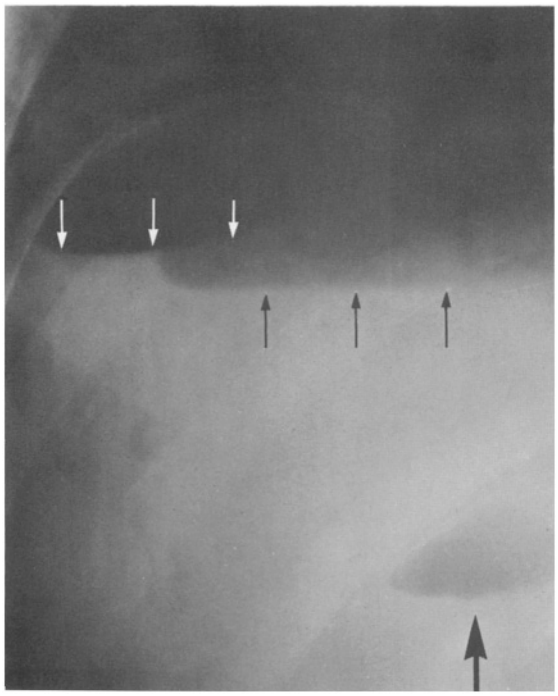


Fig. 3–62. Right subhepatic and subphrenic abscesses.
Upright film demonstrates an abscess within Morison's pouch *(single arrow)* and two air–fluid levels beneath the diaphragm *(arrows),* representing collections in the right subphrenic spaces over the dome of the liver.

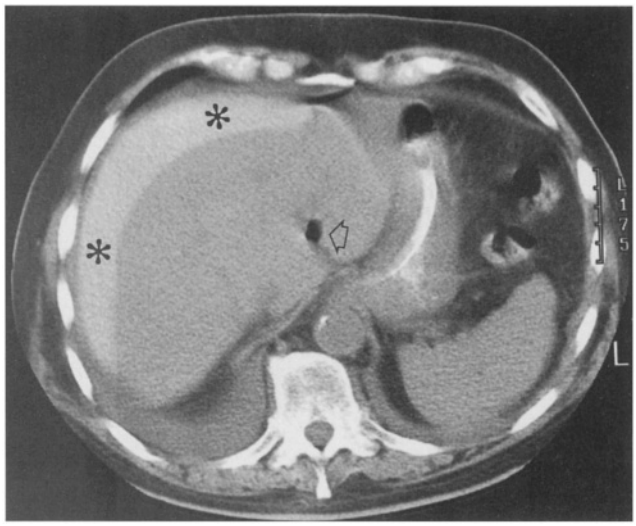


Fig. 3–63. Right perihepatic fluid following a perforated duodenal ulcer.
Following the introduction of water-soluble contrast medium in a nasogastric tube, CT demonstrates a gas bubble in the region of the porta hepatis *(arrow)* and high-density contrast material in the right perihepatic space *(asterisks).*

onary ligamentous attachments (Fig. 3–64). This is a useful landmark, then, in the distinction from other processes.[49,50] Direct passage from the right subphrenic space across the midline to the left subphrenic space is prevented by the falciform ligament.

These dynamics of flow explain the incidence and location of intraperitoneal abscesses reported empirically in large clinical series. The frequency of subphrenic and subhepatic abscesses is two to three times greater on the right than on the left,[49] and the most common site is

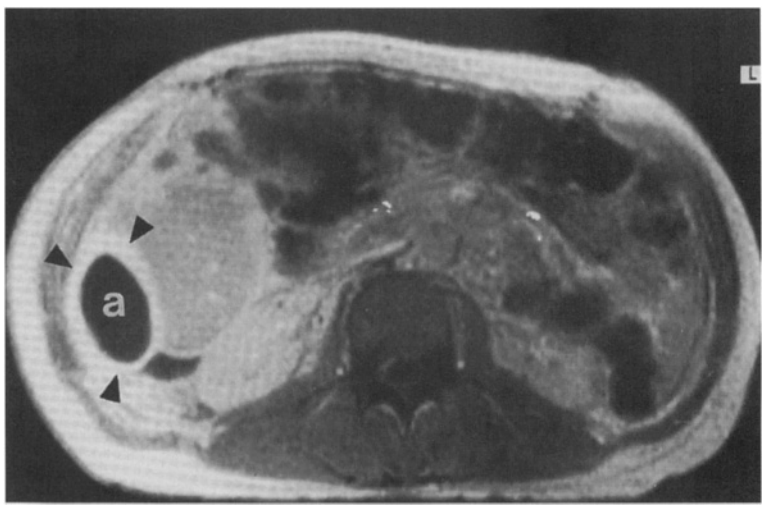


Fig. 3–64. Right subphrenic abscess.
Gadolinium-enhanced T1-weighted SGE MR image demonstrates a right perihepatic abscess *(a)* with a characteristic thick enhancing inflammatory capsule *(arrowheads).*
(Reproduced from Semelka et al.[43])

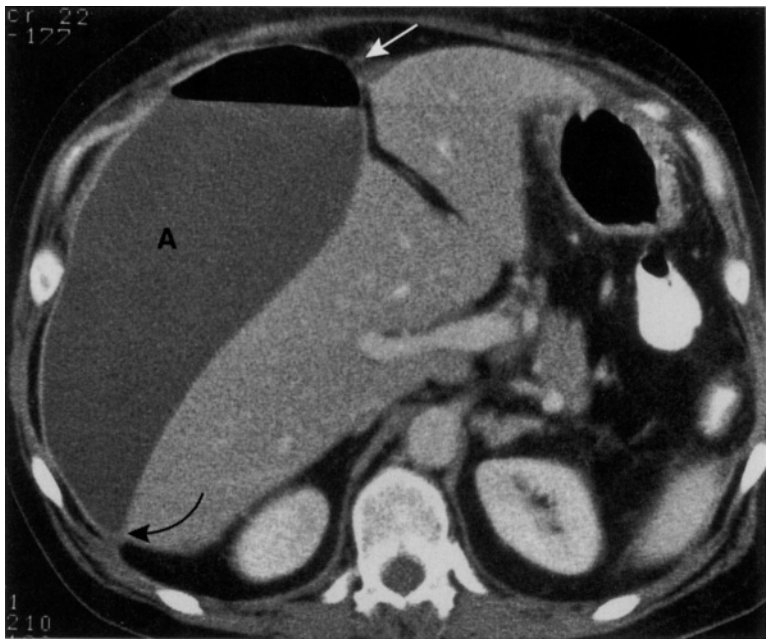


Fig. 3–65. Right subphrenic abscess, following perforation of a duodenal ulcer.
CT demonstrates a large gas-containing abscess *(A)* compressing the right lobe of the liver. It is demarcated by the attachments of the falciform ligament anteriorly *(arrow)* and the superior coronary ligament posteriorly *(curved arrow).*

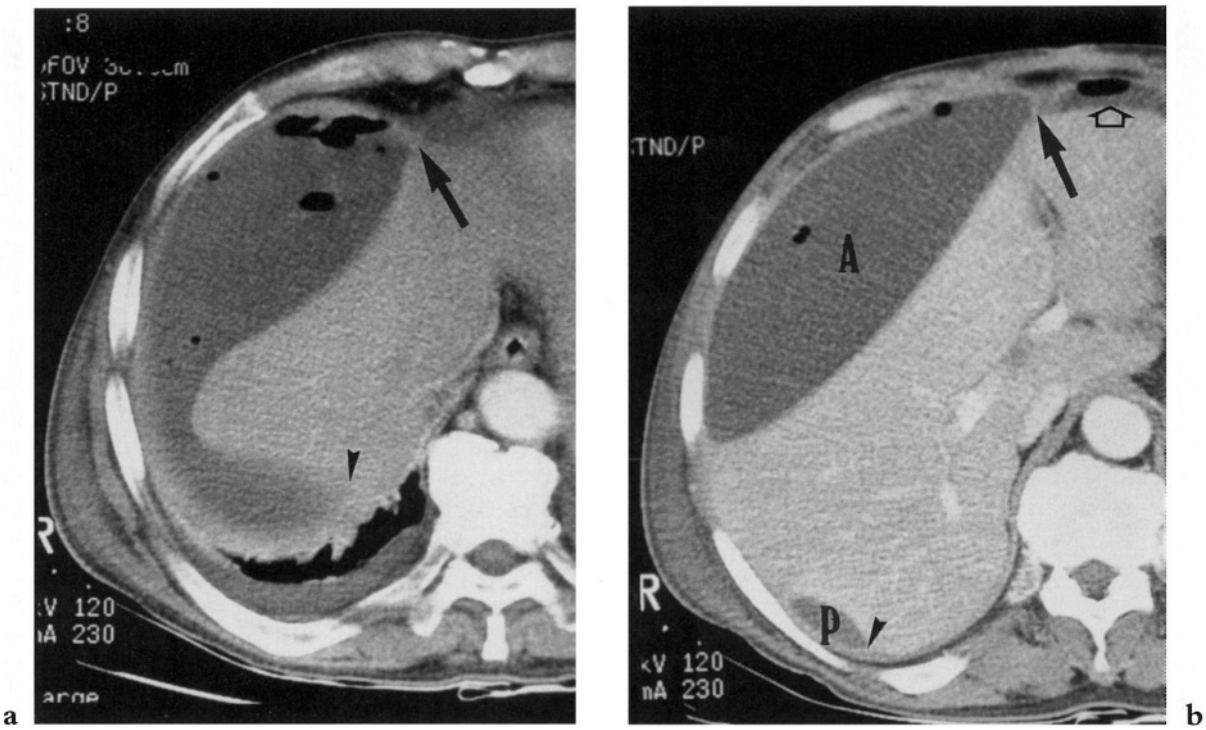


Fig. 3–66. Right subphrenic abscess
(a and **b)** CT at two different levels demonstrates a large subphrenic abscess with gas bubbles. Anteriorly, it is marginated by the falciform ligament *(arrow)* and posteriorly by the right coronary ligament at the bare area of the liver *(arrowhead).* **(b)** The right subphrenic abscess is divided into a large anterior one *(A)* and a small posterior one *(P).* A small left subphrenic abscess is seen to the left of the falciform ligament *(open arrow).*

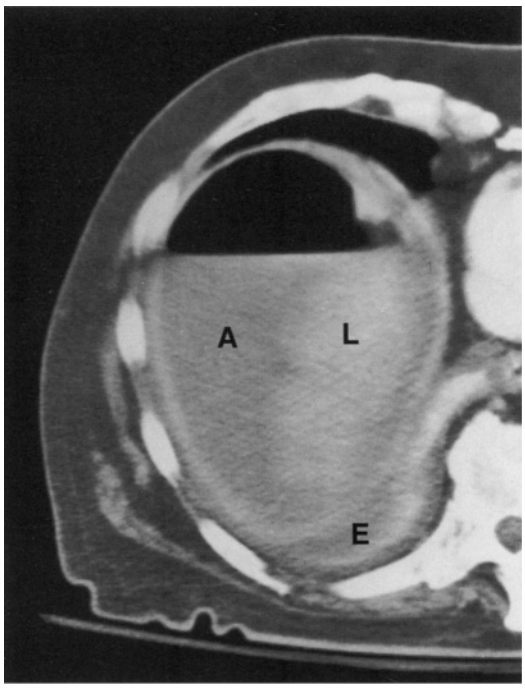


Fig. 3–67. Right subphrenic abscess.
CT demonstrates a large gas-containing abscess *(A)* in the right subphrenic space over the dome of the liver (*L*) with a thick enhancing rim. A small pleural effusion *(E)* extends into the medial costophrenic angle.
(Courtesy of Gary Ghahremani, M.D., Evanston Hospital, Evanston, IL.)

Morison's pouch.[9] Abscesses localized solely to the right anterior subhepatic space are relatively uncommon. Abscesses of Morison's pouch and the right subphrenic space often coexist. Clinical evidence of abscesses limited to the right subphrenic space, however, is not uncommon, but it can be assumed that some contamination of the right posterior subhepatic space had already occurred, perhaps manifested only by some residual inflammatory adhesions.

Hydrostatic Considerations. In addition to the anatomic pathways and action of gravity, variations in intraperitoneal pressure also determine the distribution of peritoneal fluid. Egress from the pelvis upward is not a function simply of overflow. Fluid surmounts the sacral promontory and flank muscles to extend upward, whether the patient is horizontal or erect. Autio[51] first documented the intraperitoneal extension of radiographic contrast medium into the upper abdominal recesses even in the erect position. Ten milliliters of oily contrast medium were introduced into the ileocecal, paracecal, and paraduodenal regions of 38 patients in connection with appendectomy or cholecystectomy. Although the oil derivative tended to fragment, it had an advantage in that it persisted in the peritoneal cavity for at least 3 days before being absorbed. It was therefore possible to see that its distribution on the first day, when the patient was supine, was the same as that on later days, when the patient was erect for lengthy periods of time, and achieved its final disposition within 3 hours of insertion. The contrast medium moved both down into the pelvis and up into the subphrenic space via the two-way avenue of the right paracolic gutter.

The hydrostatic pressure of the contents of the abdominal cavity together with the flexibility of a portion of the abdominal wall determine, for the most part, the pressure within the abdominal cavity. Overholt[52] demonstrated in animals that the hydrostatic pressure in the subdiaphragmatic region is lower than that elsewhere in the abdomen and that the pressure varies with respiration. The intraperitoneal pressure in the upper abdomen is subatmospheric and decreases further during inspiration. This negative subdiaphragmatic pressure and its relation to breathing are maintained in the horizontal or erect position. This is explained by the outward movement of the ribs during inspiration, which enlarges the space in the upper abdomen more than it is decreased by the descent of the diaphragm. Salkin[53] subsequently confirmed these observations in humans, noting in a series of 50 cases that most showed an intraperitoneal pressure of from 0 to – 30 mm H_2O and that pressure is less in the epigastrium than in the hypogastrium. Drye[54] recorded that in the supine position intraperitoneal pressure averages 8 cm H_2O and in the upright position pressure in the lower abdomen is almost three times as great as in the supine position. These pressure differences with positional and respiratory variations have been confirmed by others. Hydrostatic pressure differences between the lower and upper abdomen are capable then, even in the upright position, of conveying infected material.

Fluid introduced into the right supramesocolic area follows similar pathways.[6] Preferential flow is directly into Morison's pouch, with progression to the right subphrenic space and, via the right paracolic gutter, to the pelvis. In 1940, Mitchell,[11] using sequential injections of barium emulsions in infant cadavers, concluded that exudates do not progress directly from beneath the liver to the subphrenic area but first follow a circuitous route over and ventral to the proximal transverse colon to contaminate the right infracolic space. Although many

of his basic observations have been subsequently confirmed, he incorrectly concluded that the right paracolic gutter is not the major path of communication by which infection spreads to and from the upper and lower peritoneal compartments. It was not until the development of peritoneography that the effects of intraabdominal pressure gradients and body movements *in vivo* on the flow of fluid were accurately observed radiologically.[6,14]

Lesser Sac Abscesses

Anatomically, Morison's pouch communicates with the lesser sac via the epiploic foramen. Noninfected intraperitoneal fluid originating within the greater peritoneal cavity may thus readily gain entrance to the lesser sac (Figs. 3–68 through 3–71). However, this slitlike connection is easily sealed off by adhesions, so the lesser sac is not usually contaminated in generalized peritonitis unless the primary infection arises in the walls of the lesser sac itself. Abscesses here are therefore encountered most often following perforated posterior ulcers of the stomach or duodenal bulb and pancreatitis (Figs. 3–72 through 3–79).

Lesser sac abscesses typically distend the space and displace the stomach anteriorly and the transverse colon inferiorly. I have noted that adhesions developing along the peritoneal fold raised by the left gastric artery often clearly partition an abscess to one of its two major compartments (Figs. 3–73, 3–75 through 3–82). This has since been confirmed by others.[27] Infection may occasionally follow acute rupture of the gallbladder, presumably since the bile is discharged into the lesser sac before the foramen can be sealed off (Fig. 3–83).

Fluid collections within the lesser sac may occasionally extend into its lower recess between the leaves of the greater omentum (Figs. 3–84 and 3–85).

Perforation of the posterior wall of the intraabdominal esophagus extends directly into the lesser sac.[55]

Left Subphrenic Abscesses

Abscesses in the left subphrenic space may result from perforated anterior ulcers of the stomach or duodenal bulb, but they are seen particularly as complications of gastric or colonic surgery and of splenectomy.

The most consistent aspect of flow of fluid arising in the left upper quadrant is that it is preferentially directed upward to the subphrenic area, where an abscess typically coalesces[56] (Figs. 3–86 through 3–88). This is a function of the negative intraabdominal pressure beneath the diaphragm related to respiration.

Figure 3–89 details the pathway from a perforation of the anterior wall of the stomach extending deep to the left lobe of the liver to abscess development in the immediate left subphrenic area. Coalescence of an abscess between the stomach and the left lobe of the liver is unusual. A similar direct cephalad extension is shown in an instance of colonic perforation in Figure 3–90.

Anastomotic leaks are being increasingly recognized as a source of postoperative left subphrenic abscesses. These may be small and loculated (Fig. 3–91) or extensive (Figs. 3–92 and 3–93).

When the volume of infected material in the left subphrenic space is considerable, one of two routes becomes available:

1. Spread may occur across the midline, beneath the free edge of the falciform ligament, to the right subhepatic, right subphrenic, and then the right paracolic recesses. Figure 3–94 shows the pathways of infection across three quadrants of the abdomen, arising from a perforated ulcer of the stomach.
2. More often, the infected material simply overflows the strut of the phrenicocolic ligament. Ordinarily, inferior extension from the left subphrenic space tends to be arrested by this strong peritoneal reflection. However, large amounts simply proceed over it to the left paracolic gutter and then the pelvis (Figs. 3–95 through 3–97). From this site, contamination may rise up the paracolic gutter to the subhepatic and subphrenic spaces on the right.

Infection arising in the pelvis may extend upward to some degree within the shallow left paracolic gutter (Fig. 3–98), where the relatively slow flow may permit the development of adhesions and thereby coalesce into an abscess (Figs. 3–99 and 3–100). Medial displacement of the descending colon may result, and discrete gas shadows may be seen in the area of the infected fluid. Bulging of the posterolateral abdominal wall may be evident. The properitoneal fat line, radiologically referred to as the "flank stripe," is generally maintained. Loss of clear visualization of this implies extension of the infection across the peritoneal surface into the abdominal wall. Livingston's description[57] that "fluid may well upward out of the pelvis . . . to pass into the left paracolic groove, to extend farther upward into the perisplenic space" is generally not true. I have noted that an intact phrenicocolic ligament usually prevents spread to the left subphrenic area. This explains the repeatedly noted infrequency of left upper quadrant abscesses following generalized peritonitis. However, if the

text continues on page 103

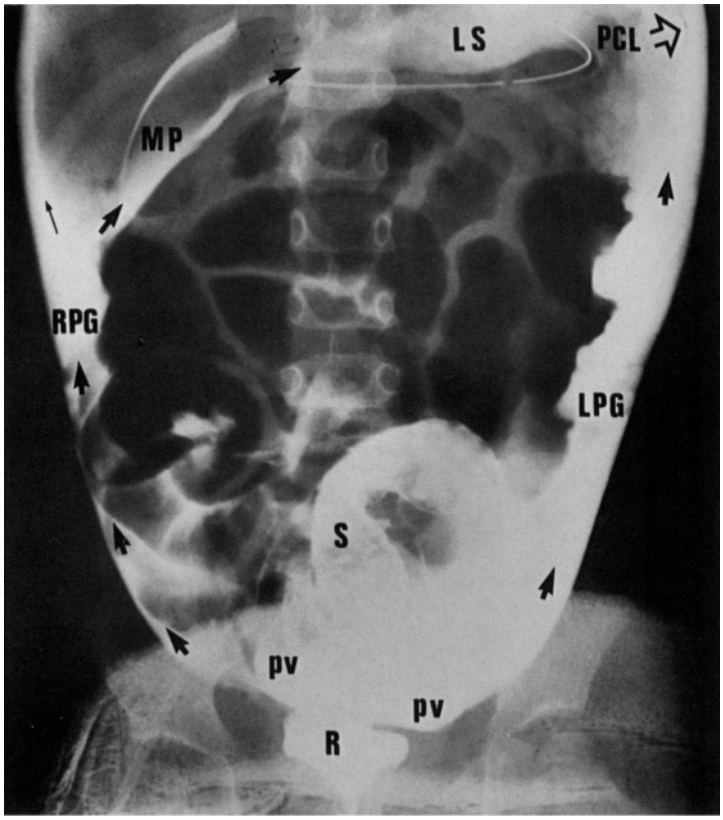


Fig. 3–68. Extension of intraperitoneal fluid into the lesser sac.
Contrast enema performed in a child following perforation of the rectosigmoid junction (*R* = rectum; *S* = sigmoid colon). Extravasation opacifies the paravesical fossae *(pv)* and the right paracolic gutter *(RPG).* Flow continues to Morison's pouch *(MP),* through the epiploic foramen to the lesser sac *(LS).* Extension up the left paracolic gutter *(LPG)* is impeded at the phrenicocolic ligament *(PCL).* (Courtesy of William Thompson, M.D., University of Minnesota School of Medicine, Minneapolis, MN.)

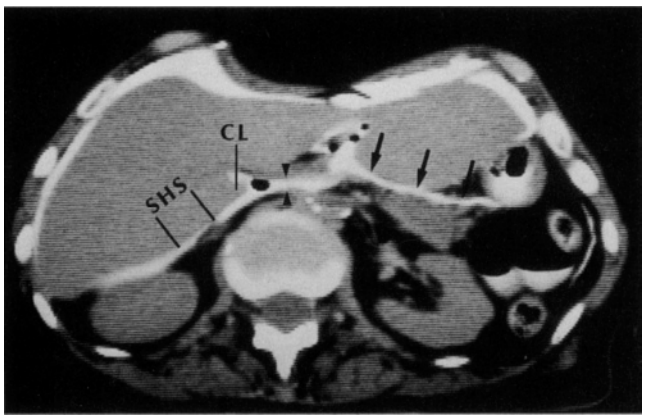


Fig. 3–69. Medial extension of posterior right subhepatic space into the lesser sac.
Postmortem CT following intraperitoneal injection of diluted contrast medium shows opaque fluid in the lesser and greater sacs. The right subhepatic space *(SHS)* extends continuously into the lesser sac *(arrows)* via the epiploic foramen *(arrowheads). CL* = caudate lobe
(Courtesy of Yong Ho Auh, M.D., Asan Medical Center, Seoul, Korea

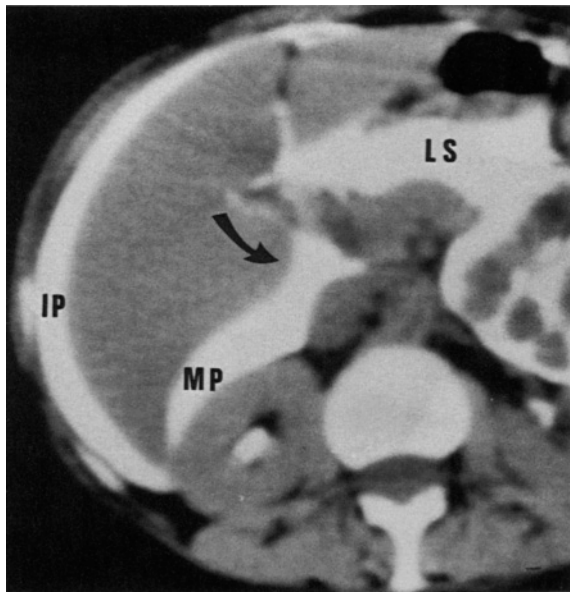


Fig. 3–70. Extension of intraperitoneal fluid into the lesser sac.
Following intraperitoneal *(IP)* injection of water-soluble contrast medium in vivo, CT demonstrates direct communication of fluid from Morison's pouch (*MP*) through the epiploic foramen *(arrow)* to the lesser sac (*LS*).



Fig. 3–71. Lesser sac abscess secondary to leak from ileoascending colostomy.
Acute postoperative leakage from the anastomotic site has led directly to a large gas-producing infected collection within the lesser sac. Ready access from the adjacent site of leak was achieved before adhesions sealed off the foramen of Winslow. (Courtesy of Gary Ghahremani, M.D., Evanston Hospital, Evanston, IL.)

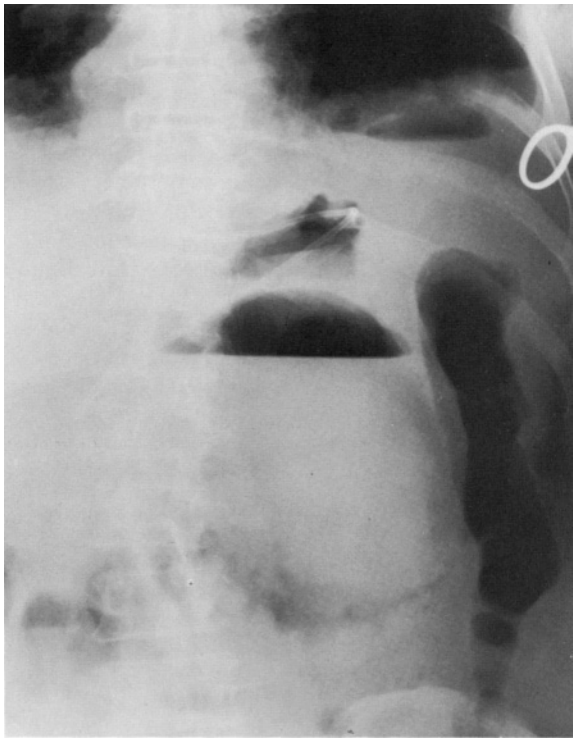


Fig. 3–72. Lesser sac abscess following perforation of a posterior gastric ulcer.
Erect plain film shows a large gas-containing abscess within the lesser sac displacing the transverse colon downward. (A smaller component extends beneath the left diaphragm.)

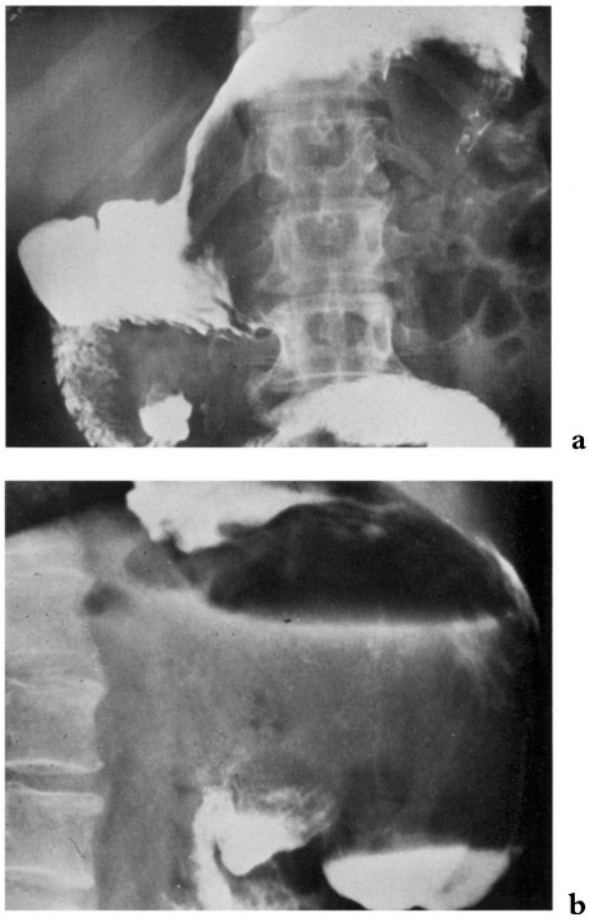


Fig. 3–73. Lesser sac abscess, following perforation of a posterior gastric ulcer.
Frontal **(a)** and erect lateral **(b)** views demonstrate a large gas-containing abscess behind the stomach. The collection is compartmentalized within the lateral compartment of the omental bursa by adhesions along the peritoneal fold of the left gastric artery.

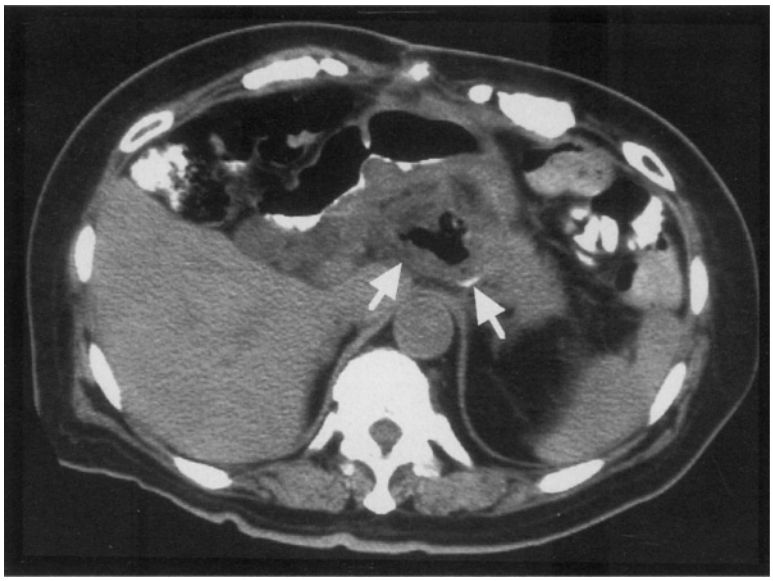


Fig. 3–74. Lesser sac abscess following gastric surgery.
CT demonstrates a gas-containing abscess *(arrows)* in the lesser sac, displacing the stomach and thickening its posterior wall. (Courtesy of Hiromu Mori, M.D., Oita Medical University, Oita, Japan.)



Fig. 3–75. Lesser sac abscess following surgery for a perforated gastric ulcer.
CT demonstrates communication of oral contrast medium to retrogastric abscess collection in the lateral compartment of the lesser sac. The abscess is bounded laterally by the gastrosplenic ligament.

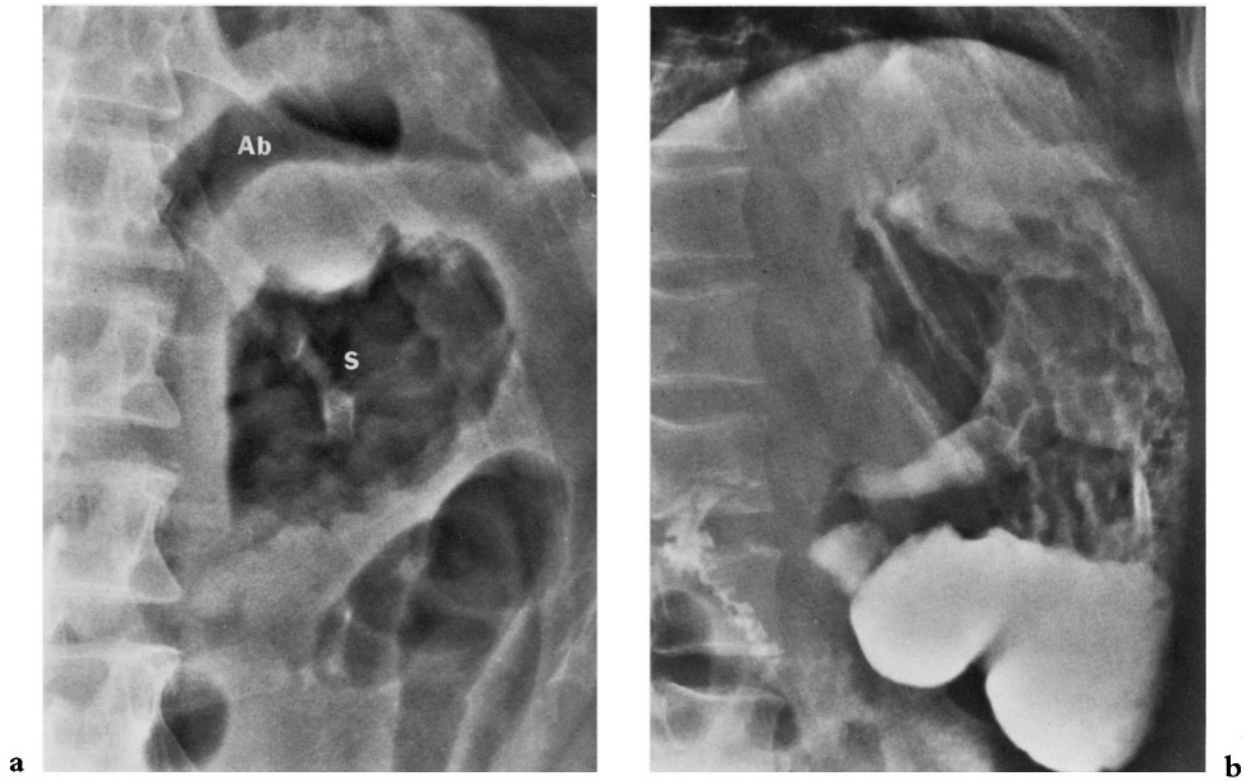


Fig. 3–76. Lesser sac abscess secondary to duodenal ulcer.
(a) Right lateral decubitus plain film. There is a loculated gas-containing abscess *(Ab)* compressing the top of the fundus of the stomach (*S*). On a frontal projection, this might suggest a subphrenic collection within the greater peritoneal cavity. There are associated changes at the base of the left lung.
(b) Upper GI series. Lateral view shows extravasation into the lesser sac behind the stomach from a posterior ulcer of the duodenal bulb.

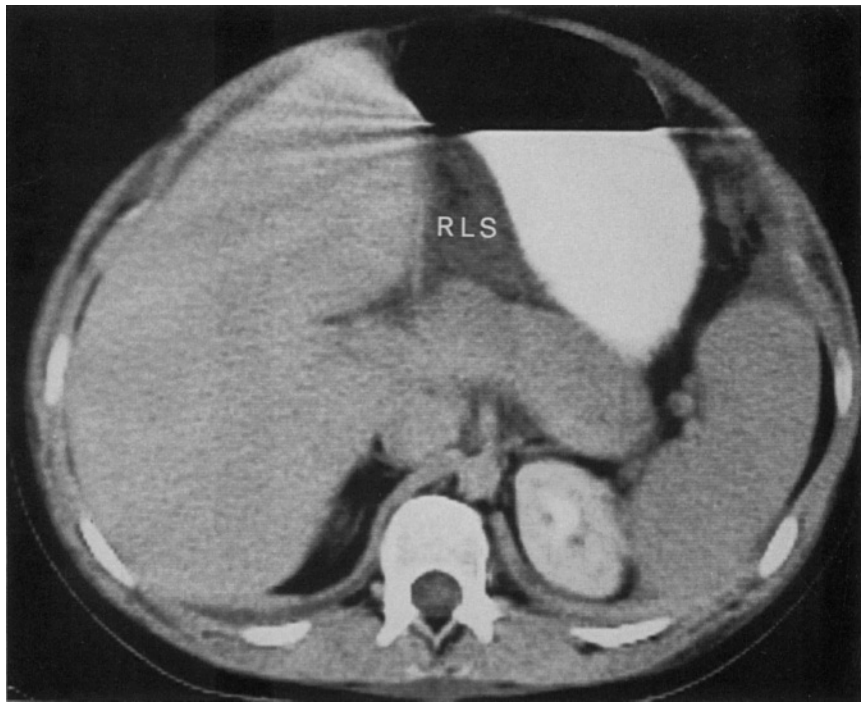


Fig. 3–77. Pancreatic fluid within medial compartment of lesser sac.
In this patient with acute pancreatitis, there is fluid loculation within the right (medial) compartment of the lesser sac *(RLS)*.

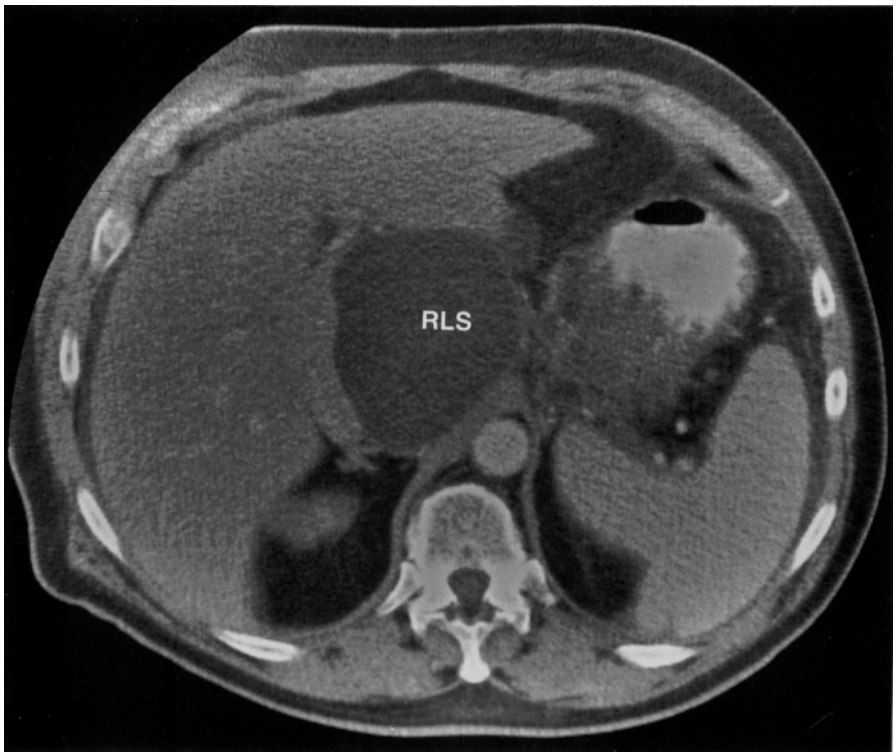


Fig. 3–78. Pancreatic pseudocyst within medial compartment of lesser sac.
The encapsulated collection has localized to the right medial compartment of the lesser sac *(RLS).*
(Courtesy of Richard Gore, M.D., Evanston Hospital, Evanston, IL.)

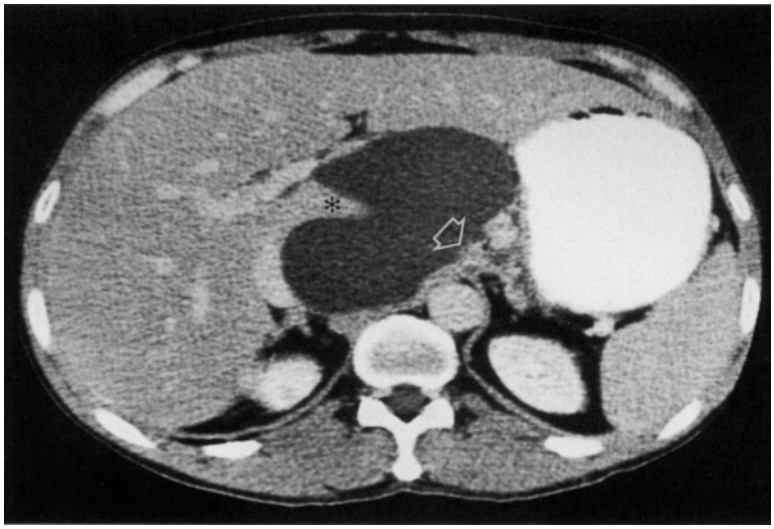


Fig. 3–79. Pancreatic pseudocyst within medial compartment of lesser sac.
The loculation severely compresses the papillary process of the caudate lobe in the superior recess *(asterisk)* and is limited toward the left of the inflammatory reaction at the plane of the gastropancreatic plica *(arrow).*
(Courtesy of Yong Ho Auh, M.D., Asan Medical Center, Seoul, Korea.)

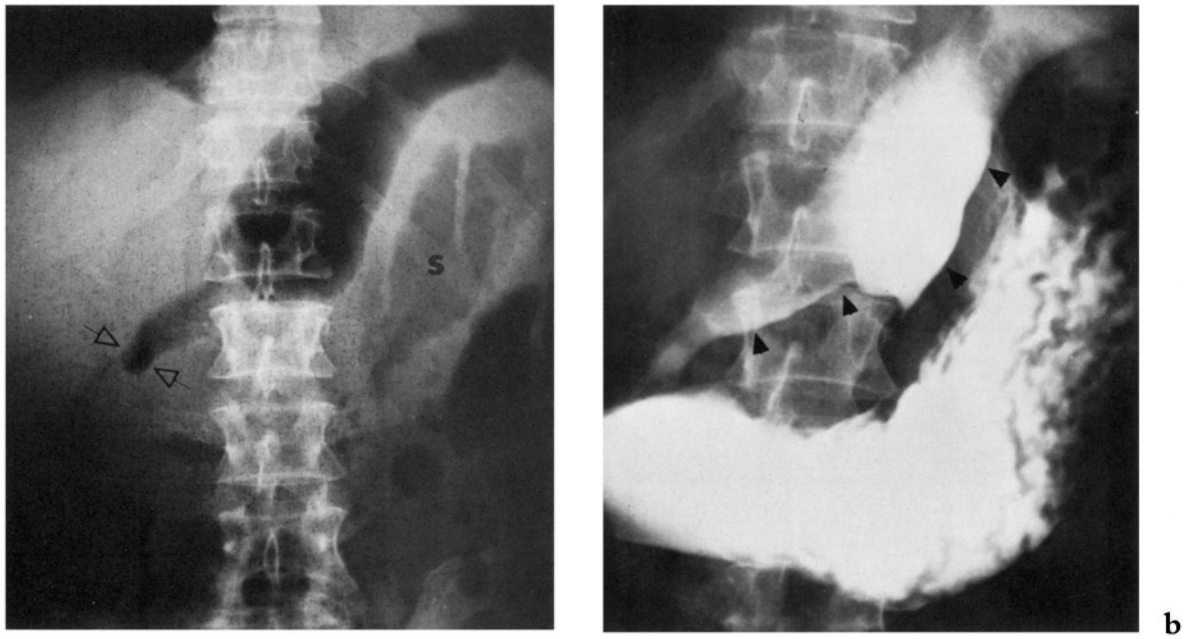


Fig. 3–80. Lesser sac abscess.
(a) Well-defined loculated gas collection superior to the stomach (*S*), identified by its rugal outlines. The collection is continuous with a circular lucency at its base *(arrows).* There are associated changes at the left lung base.
(b) GI series demonstrates extravasation from a large duodenal ulcer accounting for the circular lucency on the plain film, into the medial compartment of the lesser sac, demarcated inferiorly by the fold *(arrowheads)* raised by the left gastric artery.
(Courtesy of Al Berne, M.D., Crouse Hospital, Syracuse, NY.)

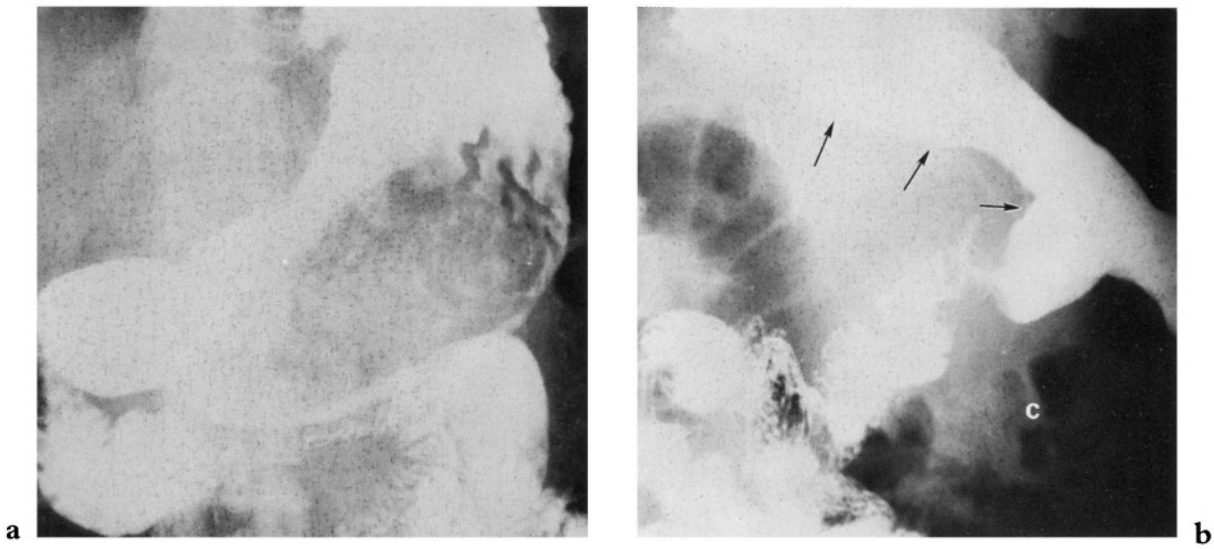


Fig. 3–81. Lesser sac abscess.
Frontal **(a)** and lateral **(b)** projections demonstrate a large retrogastric mass displacing the stomach anteriorly *(arrows)* and depressing the transverse colon (*C*). These changes localize the abscess behind the stomach and gastrocolic ligament and above the transverse mesocolon. The collection is compartmentalized within the lateral compartment of the omental bursa.

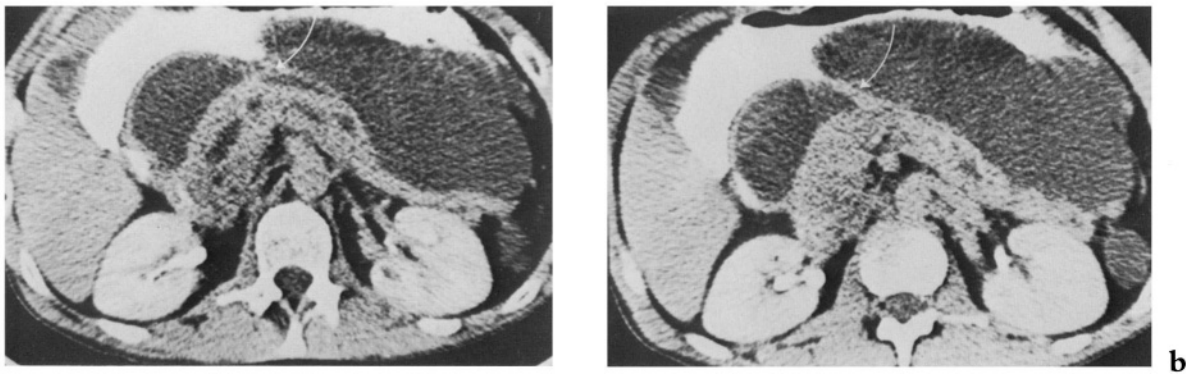


Fig. 3–82. Pancreatic pseudocysts compartmentalized by the left gastric artery.
CT scan at two different levels **(a** and **b)** demonstrates partition of pseudocysts obliterating the lesser sac by attachment *(arrow)* to the posterior wall of the contrast-filled stomach along the plane of the peritoneal fold of the left gastric artery.

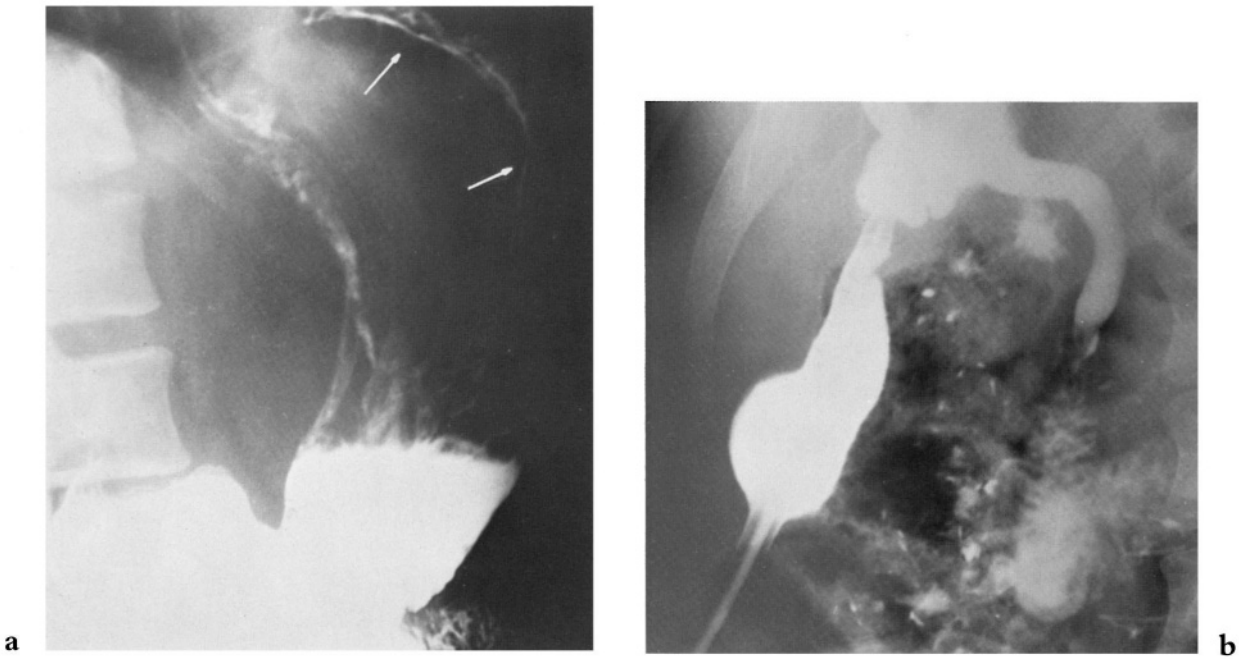


Fig. 3–83. Lesser sac abscess secondary to perforated gallbladder.
(a) Initial upper GI series shows a large retrogastric mass and left pulmonary basilar changes.
(b) Contrast injection through a paracolic drainage tube demonstrates that the catheter has inadvertently entered a site of gallbladder rupture.

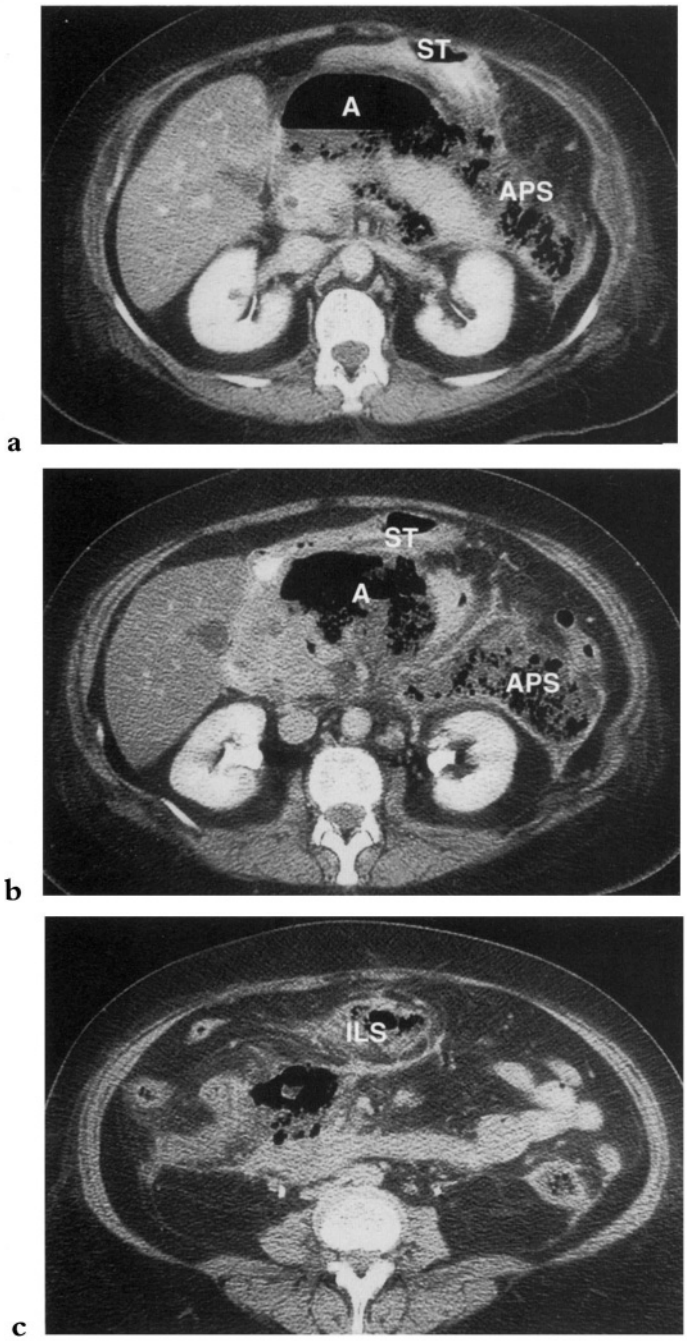


Fig. 3–84. Lesser sac abscess with inferior extension between the layers of the greater omentum.
(**a** and **b**) Large gas-containing abscess (*A*) in the lesser sac secondary to acute pancreatitis displaces the stomach (*ST*) anteriorly. There is also extension into the mesentery and considerably into the anterior pararenal space (*APS*) on the left.
(c) Spread has occurred into the inferior recess of the lesser sac (*ILS*) between the anterior and posterior reflections of the greater omentum.
(Courtesy of David H. Stephens, M.D., Mayo Clinic, Rochester, MN.)

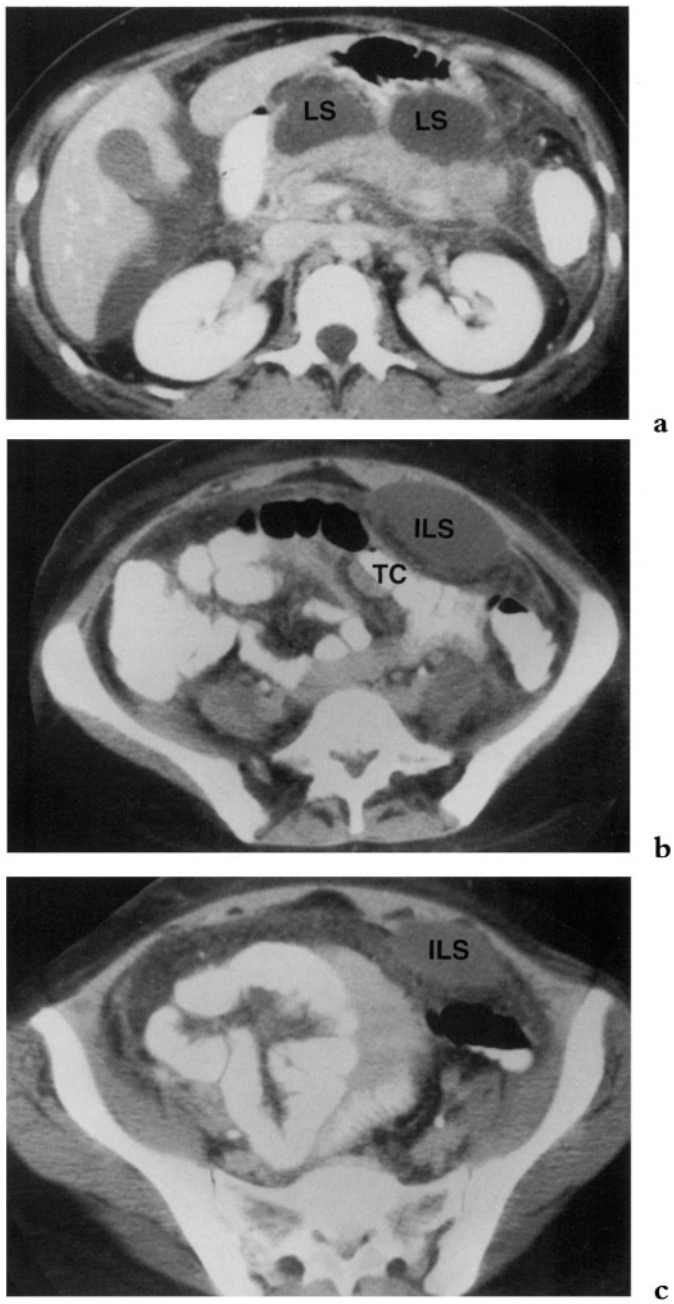


Fig. 3–85. Acute pancreatitis with development of lesser sac pseudocysts and extension into greater omentum.
(a) Loculated fluid collections have developed within the lesser sac (*LS*) separated by the peritoneal fold raised by the left gastric artery. Ascites and extrapancreatic effusion within the left anterior pararenal space are present.
(b and **c)** Pancreatic pseudocyst extends within the inferior recess of the lesser sac (*ILS*) between the reflections of the greater omentum anterior to the transverse colon (*TC*) and into the pelvis.
(Courtesy of Michiel Feldberg, M.D., University of Utrecht, The Netherlands.)

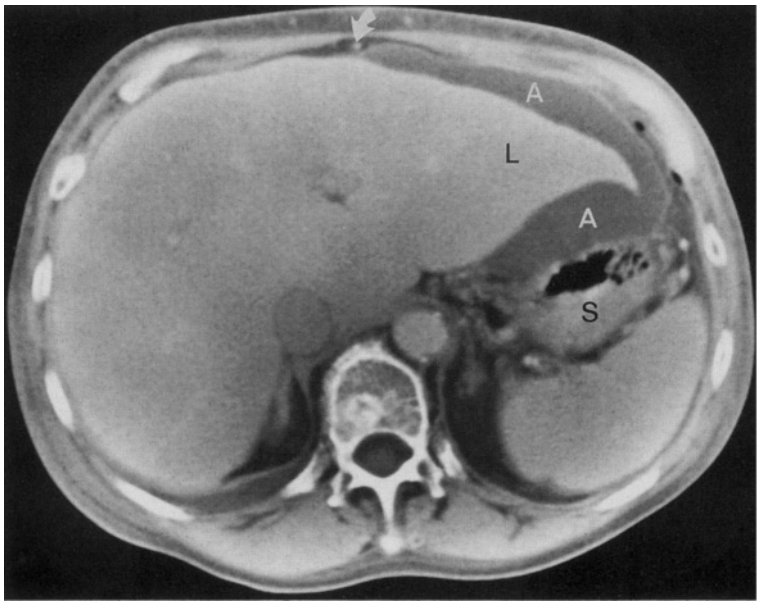


Fig. 3–86. Left subphrenic abscess secondary to anterior perforation of a gastric ulcer. The abscess (*A*) is bordered by the falciform ligament (*arrow*), the anterior peritoneal reflection of the stomach (*S*), and the liver (*L*).
Gas is present around the pars transversus of the left portal vein. (Courtesy of Richard Gore, M.D., Evanston Hospital, Evanston, IL.)

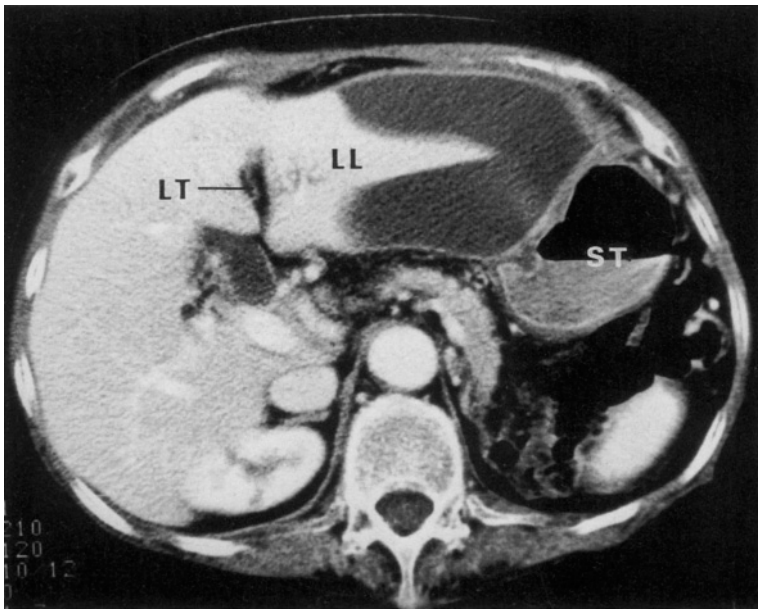


Fig. 3–87. Left perihepatic abscess.
The fluid collection has coalesced around the lateral segment of the left lobe of the liver (*LL*), encapsulated with rim enhancement anterior to the gastrohepatic ligament. In contrast to the right gastrohepatic space, the left perihepatic space communicates freely around the lateral segment of the left lobe. *LT* = ligamentum teres; *ST* = stomach.

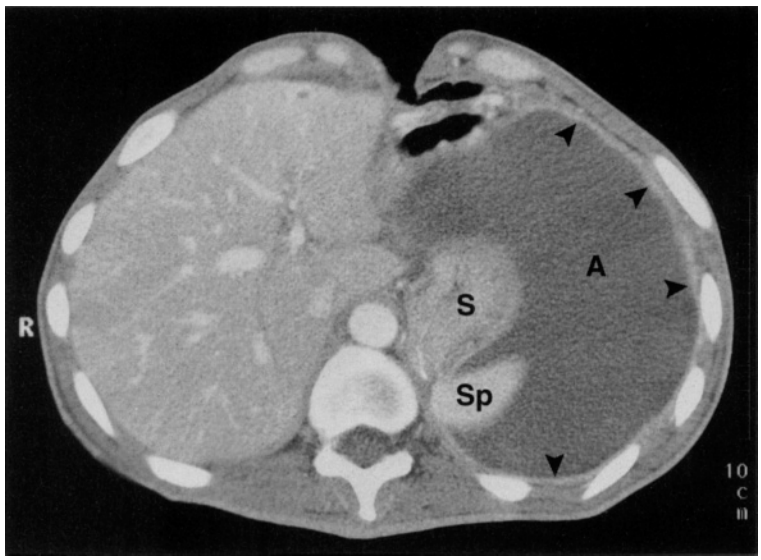


Fig. 3–88. Left subphrenic abscess.
Following left hemicolectomy for a gunshot wound, a huge abscess (*A*) has coalesced in the left subphrenic space. It displaces the fundus of the stomach (*S*) and the spleen (*Sp*) anteromedially. The abscess has a characteristic enhancing rim (arrowheads). (Courtesy of Jay Heiken, M.D., Mallinckrodt Institute of Radiology, St. Louis, MO.)

phrenicocolic ligament had been excised previously, as is done in splenectomy and in surgical mobilization of the splenic flexure of the colon, infection may readily spread from the left paracolic gutter to the subphrenic space (Figs. 3–101 through 3–103).

Summary of Pathways

Figure 3–104 summarizes the major pathways of spread of intraperitoneal infections. Given the source of contamination, an understanding of the dynamics of spread allows the anticipation of a remote abscess at a specific site.

Abscess Localization in Postoperative Neocompartments

Postoperative changes of normal anatomic barriers may cause subsequent development of abscesses in unusual or unexpected locations (Fig. 3–105).[27,58] Surgery with transection of peritoneal ligaments and mesenteries resulted in formation of new and "atypical" abdominal compartments that were the site of 39% of postoperative abscesses in one large series reported by Kumpan.[27] Communication of the lesser sac with the left subphrenic space, infra/paracolic spaces, or gastrohepatic recess was most frequently involved, followed by the fused right subphrenic and subhepatic space, when the coronary ligament was disconnected operatively (Figs. 3–106 through 3–114). This understanding is essential for correct CT localization and CT-guided drainage.[27]

Abscesses Secondary to Retention of Surgical Foreign Bodies

An infrequent but alarming cause of postoperative abscesses is retention of surgical foreign bodies. The objects include various types of sponges, pads, drains, forceps, needles, metallic irrigator tips, and tantalum mesh.[59,60] A laparotomy sponge is the most commonly retained surgical foreign body because of the frequency of its use and the depth of the cavities into which it is placed.[59] The diagnosis of retained towels or sponges in the abdomen is usually difficult because of the rarity and unexpected nature of the complication and because symptoms typically appear only months to many years after surgery.

Surgical sponges are usually made of inert cotton and do not undergo decomposition or biochemical reaction[59]; however, in some cases, they may become distorted by folding, twisting, and partial disintegration.[61] Occasionally, they may cause no apparent problem other than medicolegal liability. Retained sponges may stimulate an inflammatory reaction, with development of fibrosis, adhesions, and foreign-body, granuloma, that can result in bowel obstruction.[61–63] The retained sponge may also serve as the nidus for subsequent abscess formation.[60] In addition, a sinus tract and fistula into a hollow viscus may form in an attempt by the body to extrude the foreign material.[63]

Because of past difficulty in recognizing retained surgical sponges, most institutions now use only sponges that have been manufactured with radiopaque markers.[59] Detection of the opaque marker may be hindered

text continues on page 106

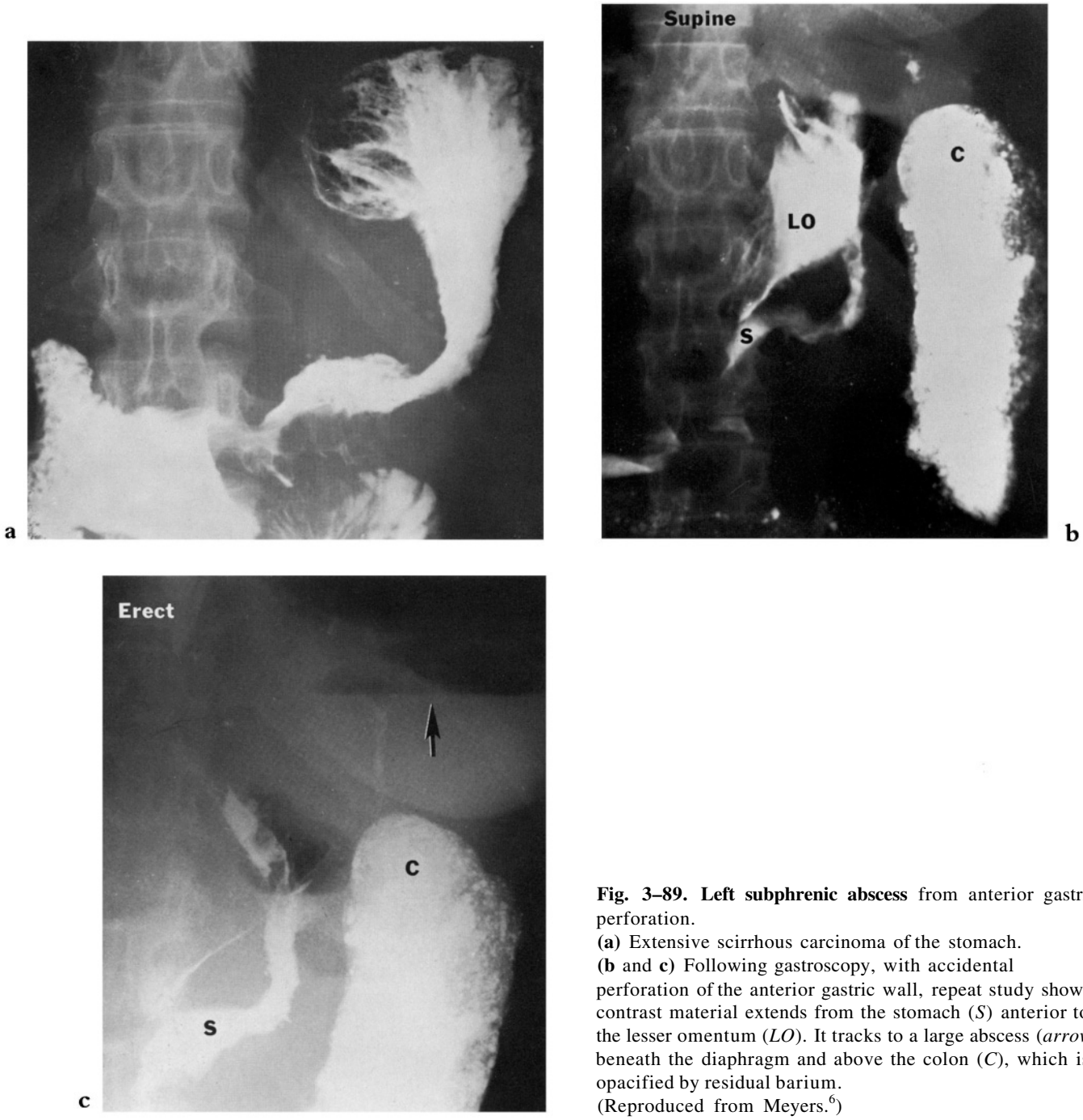


Fig. 3–89. Left subphrenic abscess from anterior gastric perforation.
(a) Extensive scirrhous carcinoma of the stomach.
(b and **c)** Following gastroscopy, with accidental perforation of the anterior gastric wall, repeat study shows contrast material extends from the stomach (*S*) anterior to the lesser omentum (*LO*). It tracks to a large abscess (*arrow*) beneath the diaphragm and above the colon (*C*), which is opacified by residual barium.
(Reproduced from Meyers.[6])

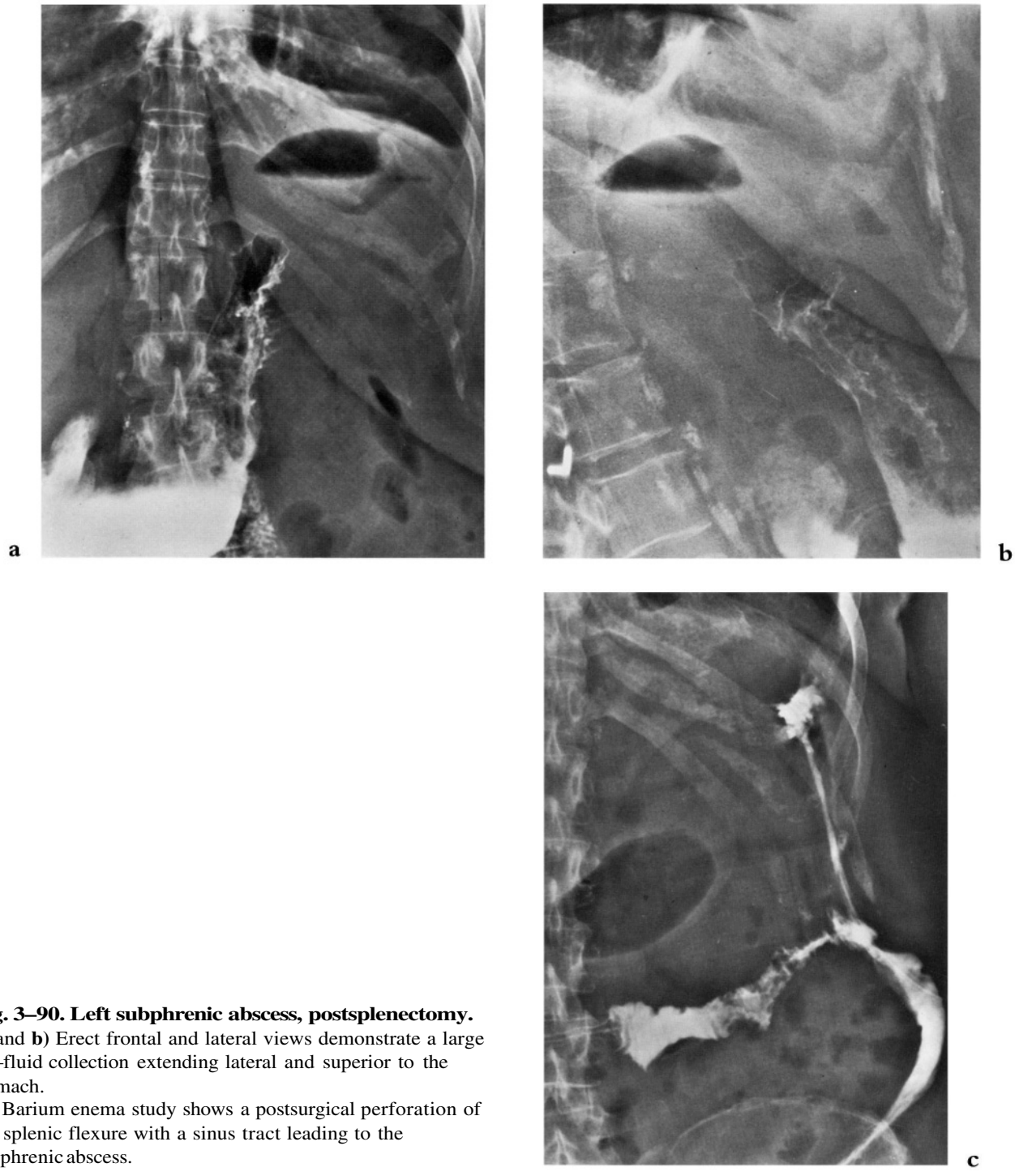


Fig. 3–90. Left subphrenic abscess, postsplenectomy.
(a and **b)** Erect frontal and lateral views demonstrate a large air–fluid collection extending lateral and superior to the stomach.
(c) Barium enema study shows a postsurgical perforation of the splenic flexure with a sinus tract leading to the subphrenic abscess.

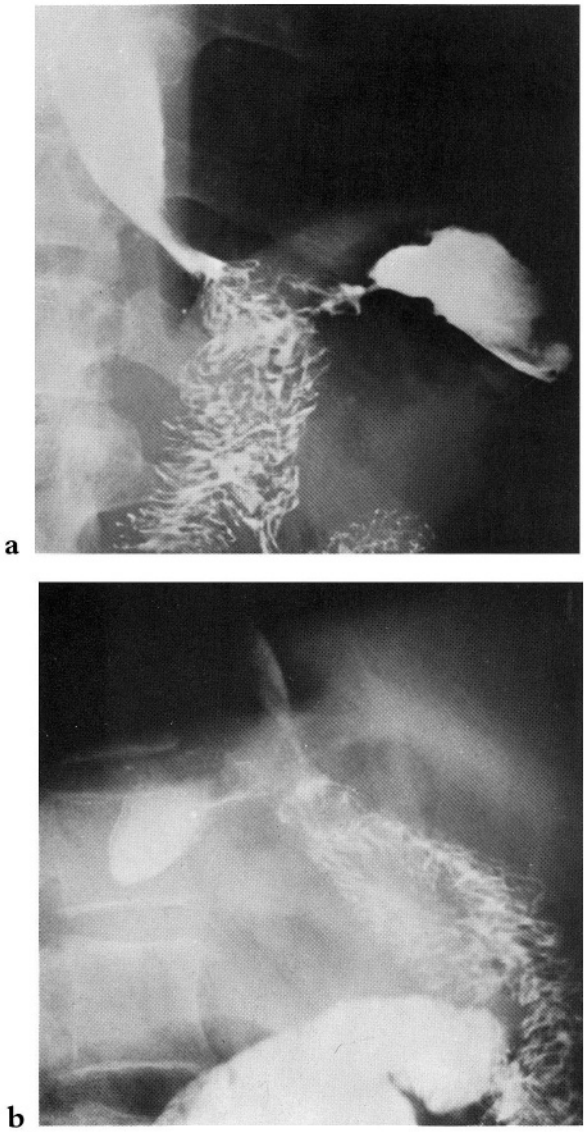


Fig. 3–91. Chronic loculated left subphrenic abscess secondary to anastomotic leak, following gastrectomy and esophagojejunostomy. Frontal **(a)** and lateral **(b)** views.

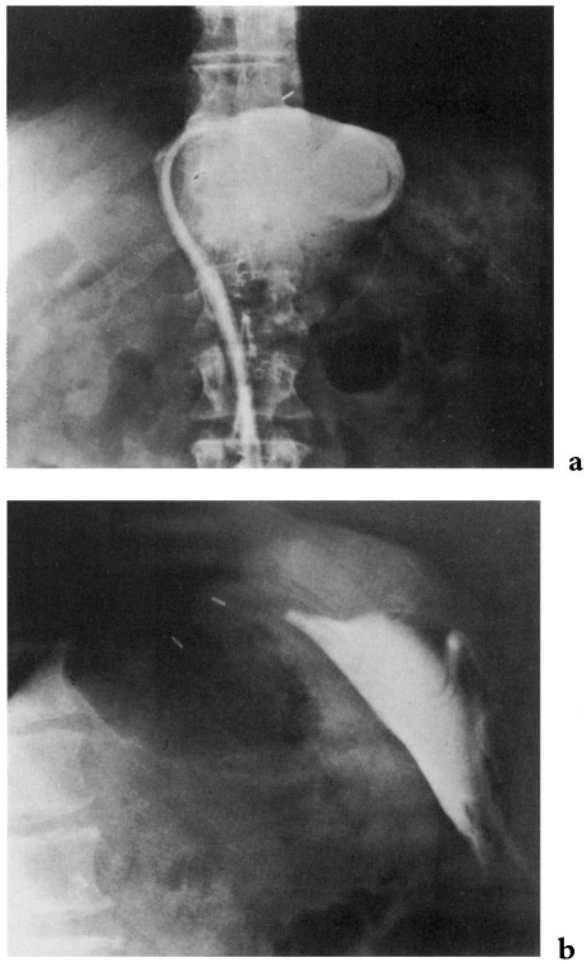


Fig. 3–92. Left subphrenic abscess secondary to anastomotic leak, post-Billroth II.
(**a** and **b**) Contrast injection through drainage tube shows loculated cavity beneath the central tendon of the diaphragm anterior to the left lobe of the liver.

by its distortion and by overlying bony structures.[61,64] In addition, retained sponges may even now be found in patients operated on before the use of radiopaque sponges. Plain film radiography has at least a 25% false-negative rate.[65] Other radiographic signs suggesting the presence of retained surgical sponges include a well-circumscribed mass, whorl-like gas patterns in the sponge's meshwork, abnormal gas collections owing to abscess formation adjacent to the sponge, and rarely, development of calcification around a retained sponge[59–61] (Fig. 3–115). In patients with a sinus tract, injection of contrast material usually identifies the meshwork of the retained sponge, and a bizarre filling defect in the intestinal lumen may be found on contrast examination in patients with sponges that erode into the intestine.

Ultrasonography of retained surgical sponges typically shows a hyperechogenic mass with a well-defined acoustic shadow.[64,66–68] A retained towel may be revealed by a folded appearance of echogenic material inside a cystic mass.[63]

text continues on page 116

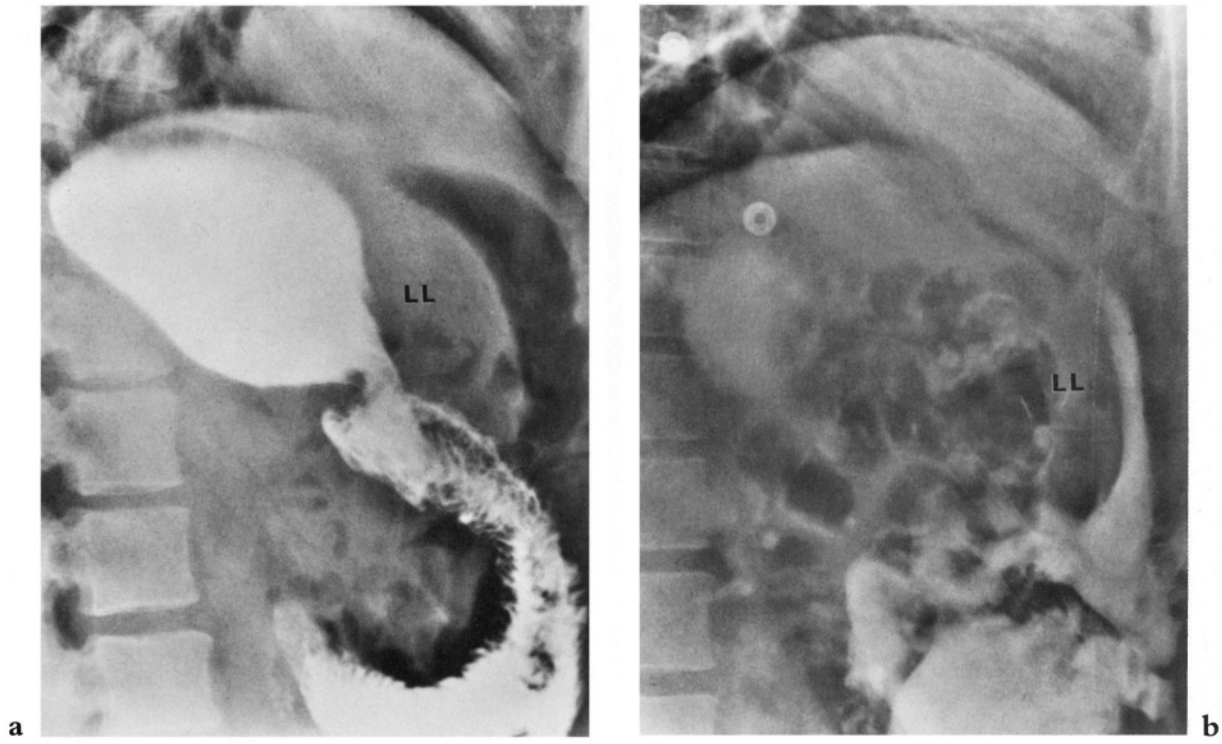


Fig. 3–93. Left subphrenic abscess secondary to anastomotic leak, post-Billroth II.
The collection, first filled with gas and later opacified, seeks the subphrenic area anterior to the left lobe of the liver (*LL*).

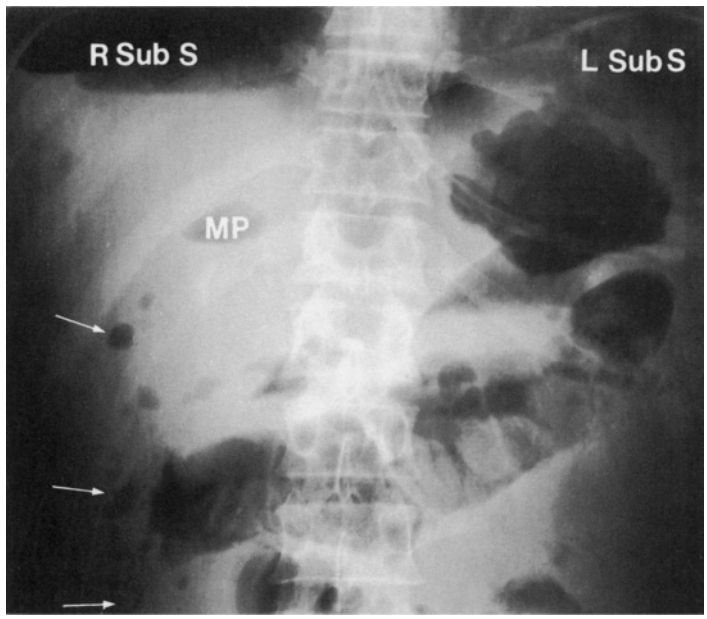


Fig. 3–94. Perforation of an anterior wall gastric ulcer leads to abscesses of the left subphrenic space (*LSubS*), Morison's pouch (*MP*), and the right subphrenic space (*RSubS*). The gas-containing exudate extends along the visceral surface of the liver to the right paracolic gutter (*arrows*). This case illustrates the flow of exudate across three quadrants of the abdomen. (Reproduced from Meyers.[6])

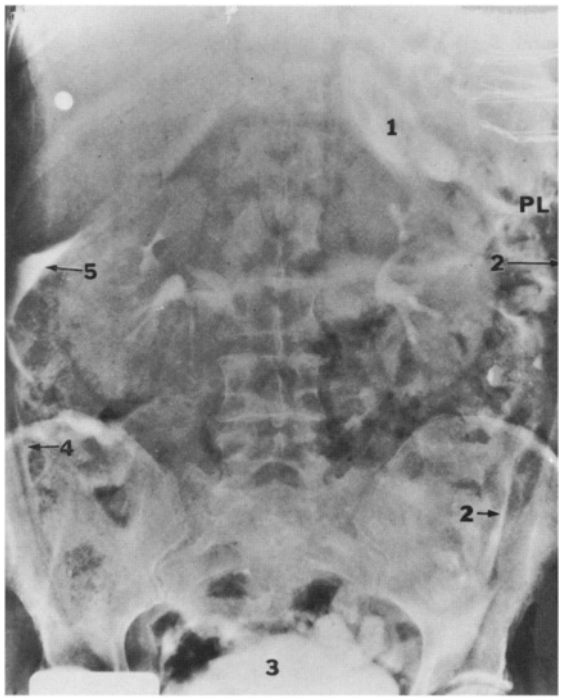


Fig. 3–95. Extravasated contrast material in the left upper quadrant (*1*) at the time of percutaneous splenoportography can be traced to overflow the phrenicocolic ligament (*PL*) and proceed down the left paracolic gutter (*2*) to the pelvis (*3*). From here it ascends the right paracolic gutter (*4*) to the subhepatic spaces (*5*). This illustrates the dynamic pathways of fluid across the four quadrants of the abdomen.

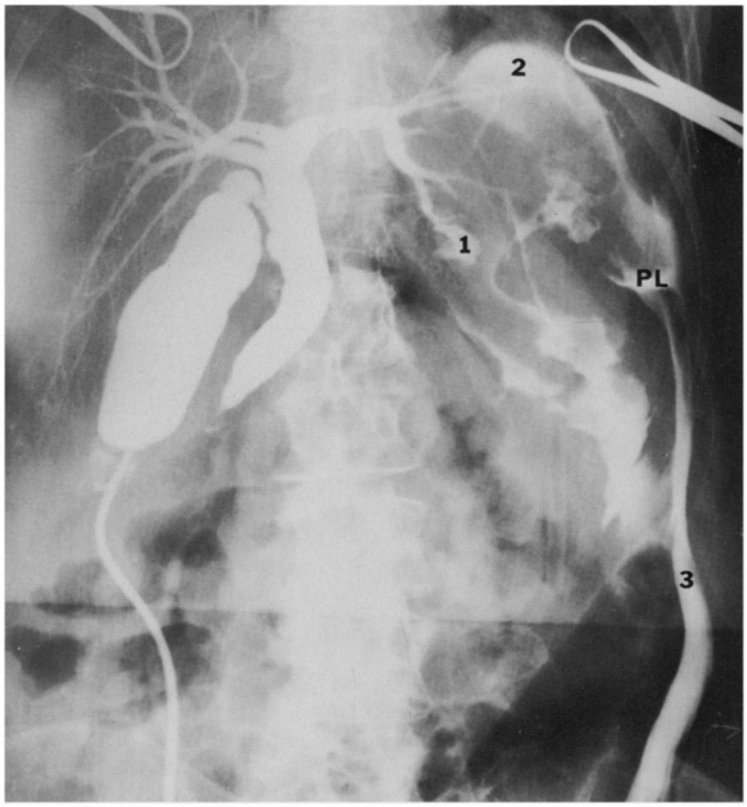
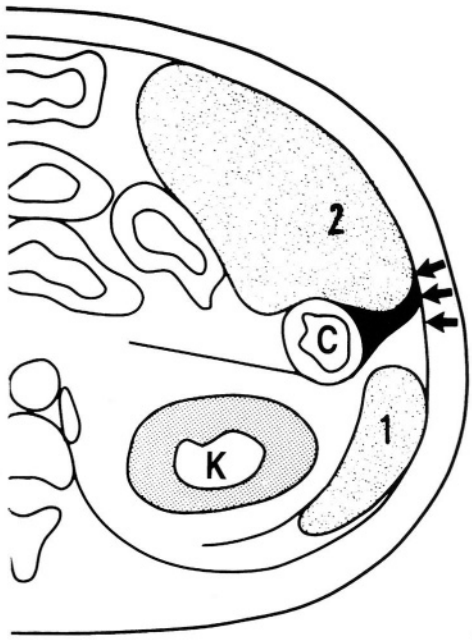
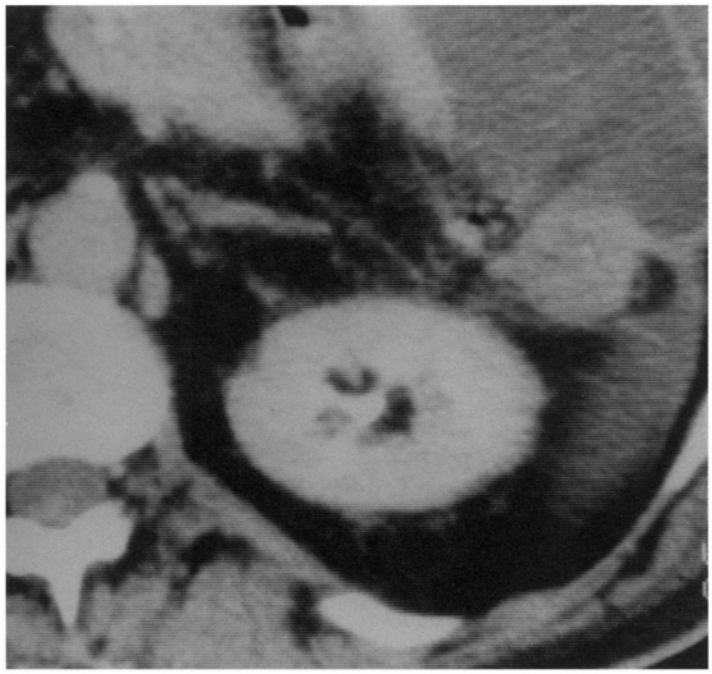


Fig. 3–96. Stab wound of liver.
Injection through cholecystotomy tube shows extravasation from left lobe of liver (*1*). This seeks the left subphrenic space (*2*), overflows the phrenicocolic ligament (*PL*), and progresses down the left paracolic gutter (*3*) to the pelvis.



a



b

Fig. 3–97. Left subphrenic abscess partially separated from abscess in left paracolic gutter by phrenicocolic ligament.
(a) Diagram and (**b**) CT. Following splenectomy, an intact phrenicocolic ligament (*arrows*) through its slanted course partially divides the caudal edge of an abscess in the splenorenal recess (*1*) from a gross abscess in the paracolic gutter overflowing to the infracolic space (*2*). *K* = kidney; *C* = splenic flexure of colon.
(Reproduced from Kumpan.[27])

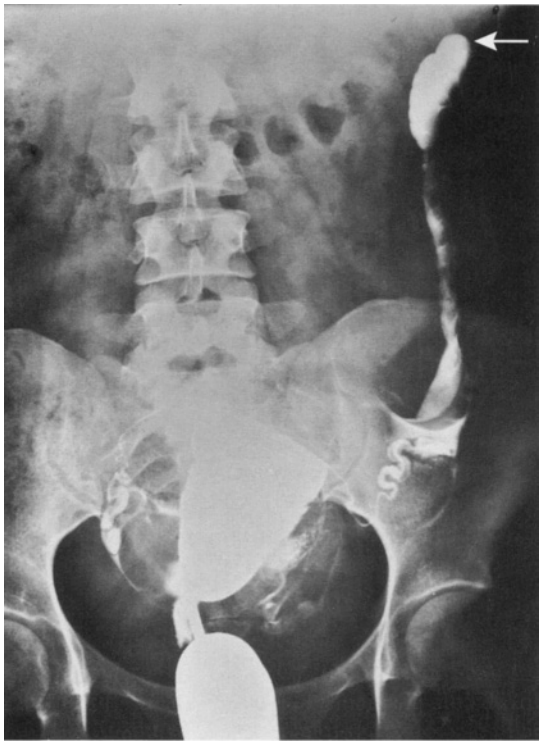


Fig. 3–98. Slow flow up the shallow left paracolic gutter is arrested at the level of the phrenicocolic ligament.
Hysterosalpingography with overzealous contrast injection through patent fallopian tube opacifies the left paracolic gutter. Cephalad flow is arrested at the level of the phrenicocolic ligament (*arrow*).

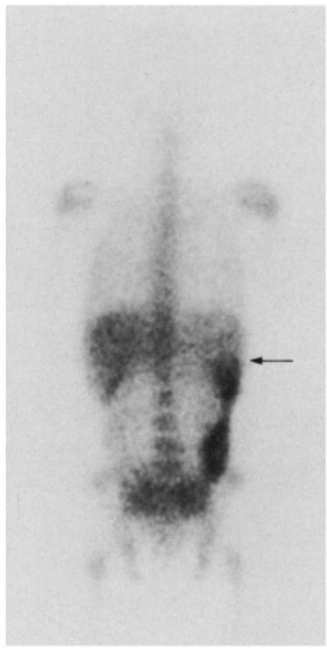


Fig. 3–99. Phlegmon in left paracolic gutter, postappendectomy.
Gallium-67 scan demonstrates activity extending up the left paracolic gutter with an abrupt cutoff at the level of the phrenicocolic ligament (*arrow*). This activity is not in the colon and did not clear following repeated enemas. Activity in the pelvis is associated with surgical drains in this area. (Courtesy of Paul B. Hoffer, M.D., Yale University School of Medicine, New Haven, CT.)

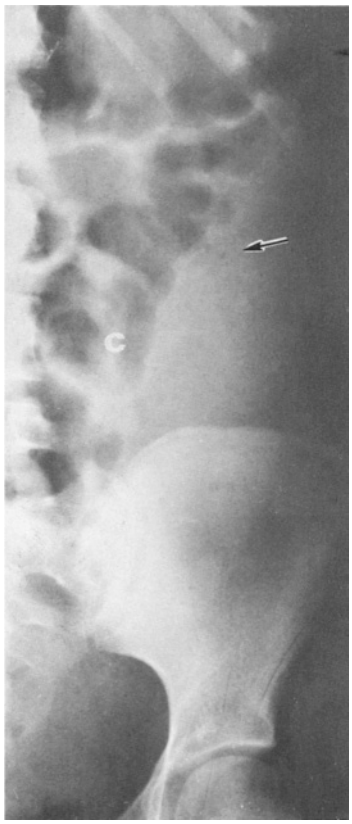


Fig. 3–100. Localized abscess of the left paracolic gutter, 2 weeks after a cesarean section.
The mass displaces the descending colon (*C*) medially and bulges the flank structures laterally. It is ill defined inferiorly and superiorly, at which point several small discrete gas bubbles are present (*arrow*). Cephalad flow to the left subphrenic space is prevented by the phrenicocolic ligament in this case.

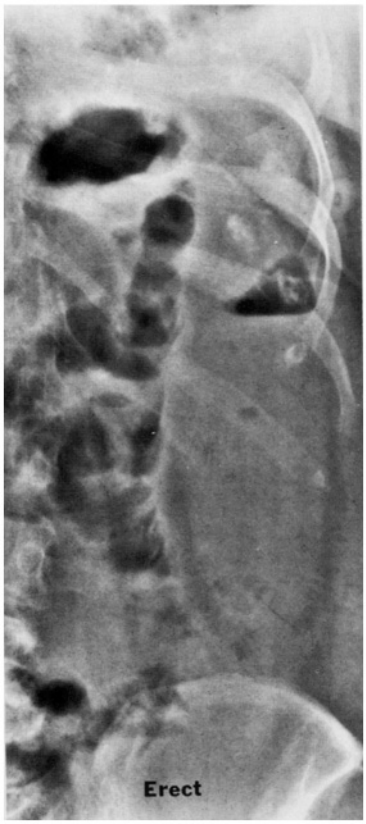


Fig. 3–101. Abscess of left paracolic gutter extending into the perisplenic space. Following a resection of the sigmoid colon with mobilization of the splenic flexure and excision of the phrenicocolic ligament, the large gas-producing infected collection in the gutter is not restrained from progressing into the perisplenic area.



Fig. 3–102. Left paracolic and subphrenic abscesses. Following splenectomy and excision of the phrenicocolic ligament, intestinal infarction within the pelvis leads to infected exudate in the left paracolic gutter (*arrows*). This progresses without interruption to the development of a left subphrenic abscess (*LSA*).

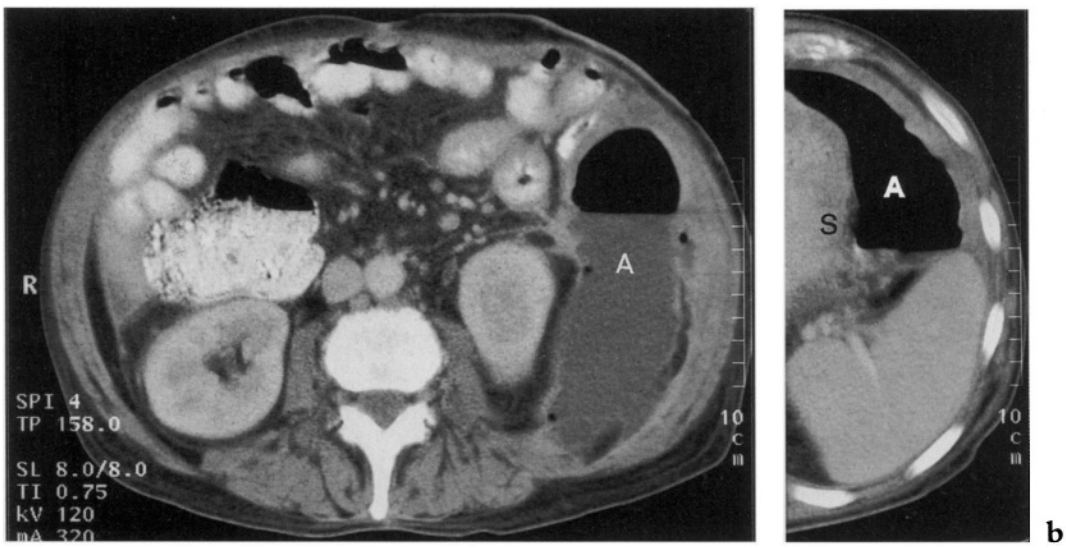


Fig. 3–103. Left paracolic and subphrenic abscesses, following sigmoidectomy with descending colostomy for perforated diverticulitis.
(a) CT shows a large fluid and gas-containing abscess (*A*), displacing bowel and the left kidney.
(b) At a higher level, continuity to a prominent abscess in the left upper quadrant anterior to the gastrosplenic ligament lateral to the stomach (*S*) has developed.
(Courtesy of Ann Singer, M.D., Cleveland Clinic, Cleveland, OH.)

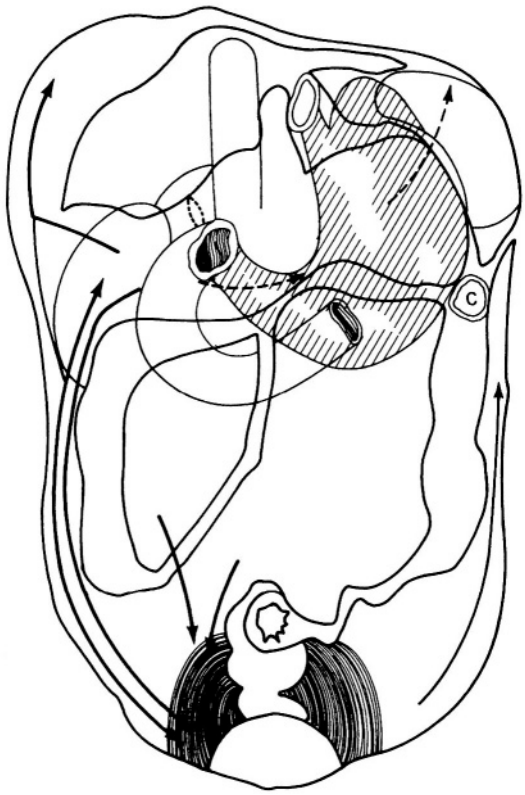


Fig. 3–104. Diagram of the pathways of flow of intraperitoneal exudates.
(See Fig. 3–2) *Broken arrows* indicate spread anterior to the stomach to the left subphrenic area. *C* = splenic flexure of colon
(Modified from Meyers.[6])

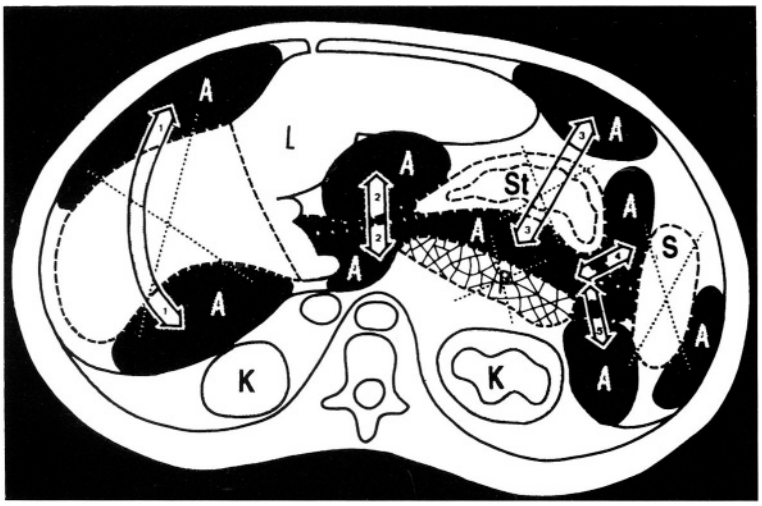


Fig. 3–105. Diagram of abscess localization in intraperitoneal postoperative neocompartments following transection of ligaments and mesenteries.
1 = right posterior subphrenic–subhepatic space; *2–5* = lesser sac–left subphrenic space (gastrohepatic, gastrosplenic, splenorenal recesses); *A* = abscess; *L* = liver; *St* = stomach; *S* = spleen; *K* = kidney; *P* = pancreas.
(Modified from Kumpan.[27])

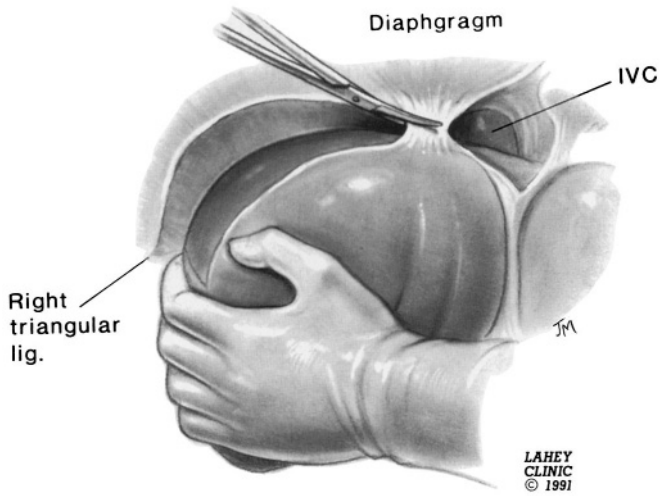


Fig. 3–106. Steps in right hepatic lobectomy with surgical transection of ligaments.
After division of the falciform ligament up to the inferior vena cava (*IVC*), further mobilization of the right lobe is achieved by transection of the right triangular ligament and the coronary ligament. This provides communication between the right subphrenic and subhepatic spaces. (From Braasch JW, Sedgwick CE, Veidenheimer MC, et al: Atlas of Abdominal Surgery. WB Saunders, Philadelphia, 1991. Illustration used with permission of The Lahey Clinic.)

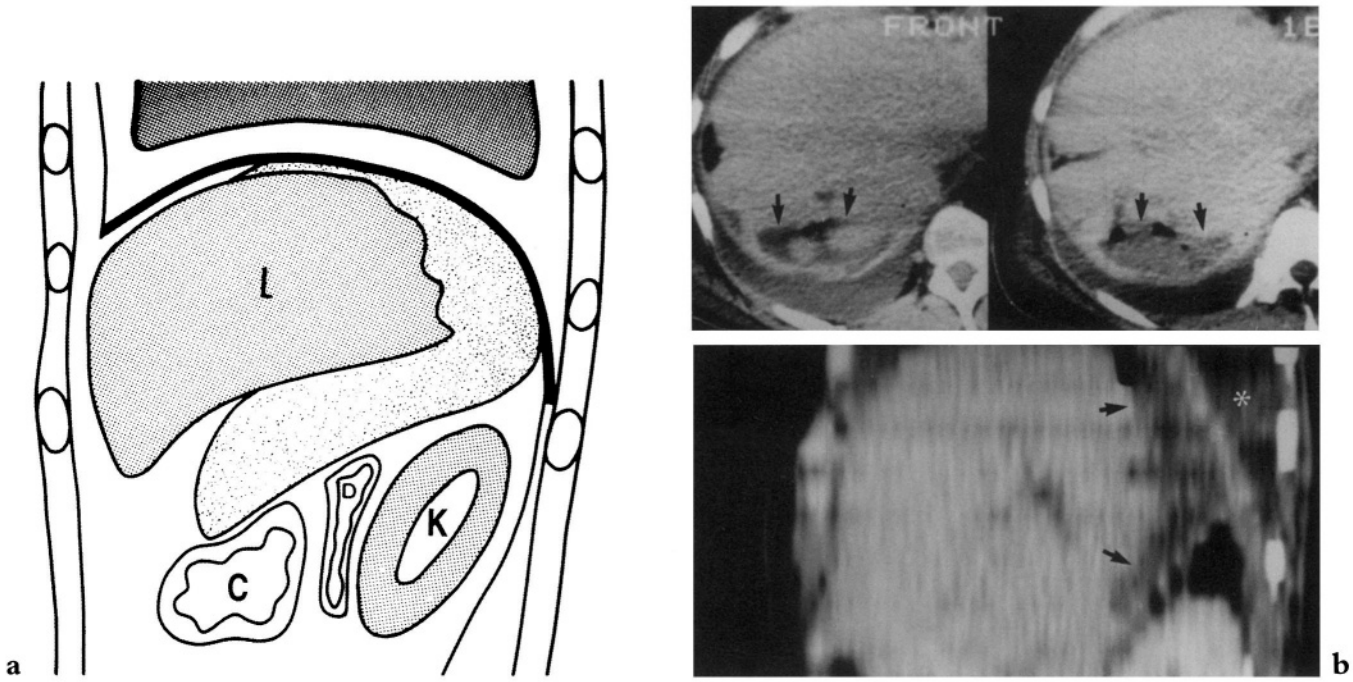


Fig. 3–107. Abscess localization in postoperative neocompartment. Excision of right coronary ligament associated with hemihepatectomy.
(a) Lateral diagram and **(b)** axial CT with sagittal reconstruction demonstrate abscess with gas formation in new right subphrenic–subhepatic compartment (*arrows*). The communication of the right subphrenic space with Morison's pouch may extend anteriorly to involve the right anterior subhepatic space as well. *L* = right lobe of liver; *K* = right kidney; *D* = descending duodenum; *C* = colon; *asterisk* = pleural fluid.
(Reproduced from Kumpan.[27])

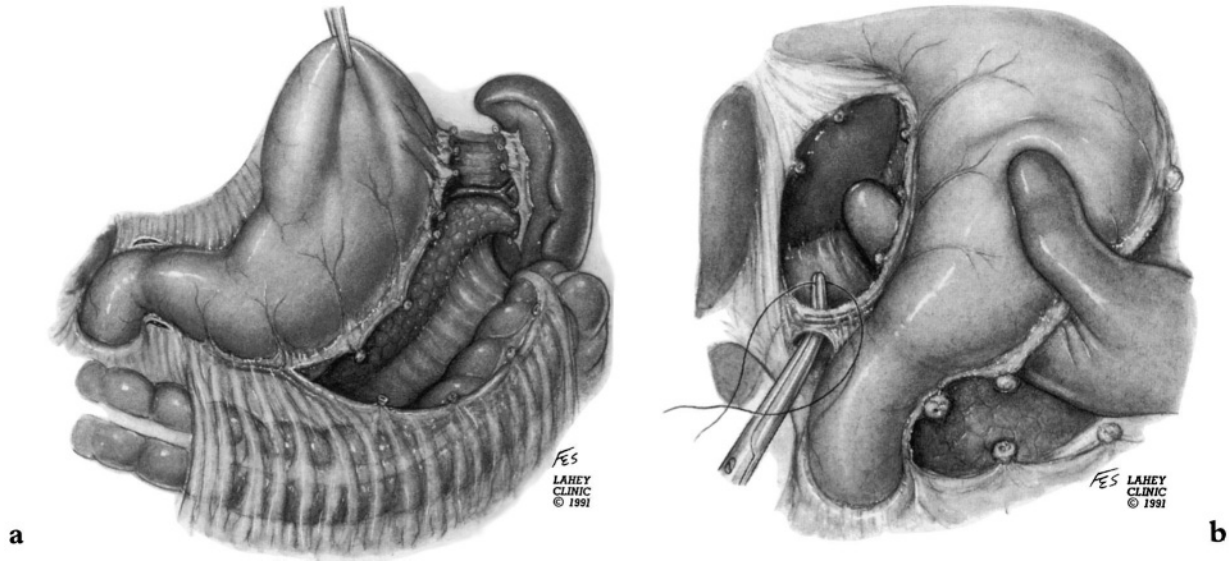


Fig. 3–108. Steps in gastrectomy with surgical transection of ligaments.
(a) With traction on the stomach and transverse colon, the greater curvature of the stomach is mobilized by excising the gastrocolic and gastrosplenic ligaments and dividing the short gastric and gastroepiploic vessels.
(b) The gastrohepatic ligament is entered in order to mobilize the distal stomach and first portion of the duodenum. An avascular plane is developed so that the caudate lobe of the liver is visualized. The right and then the left gastric vessels are ligated. This establishes communication between the lesser sac and the left subphrenic, gastrohepatic, and gastrosplenic spaces. (From Braasch JW, Sedgwick CE, Veidenheimer MC, et al: Atlas of Abdominal Surgery. WB Saunders, Philadelphia, 1991. Illustrations used with permission of The Lahey Clinic.)

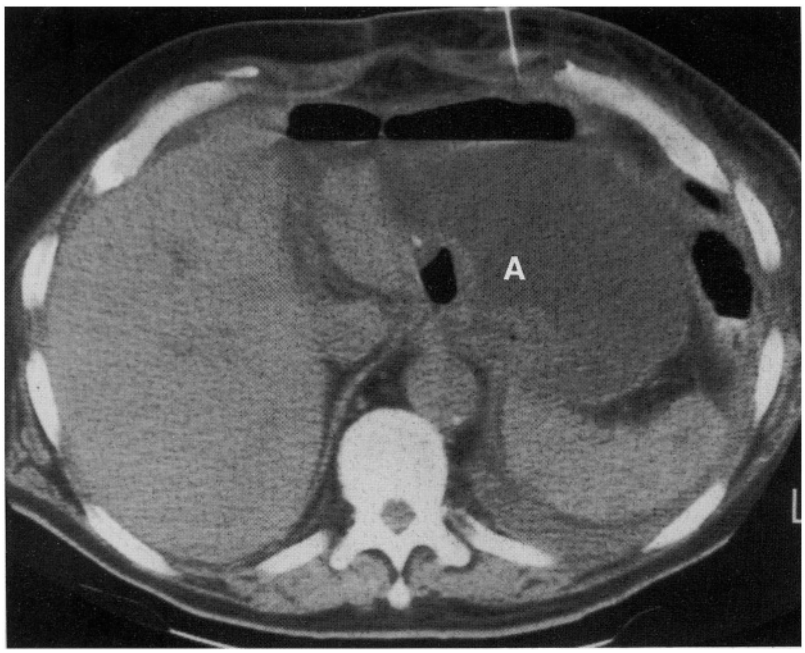
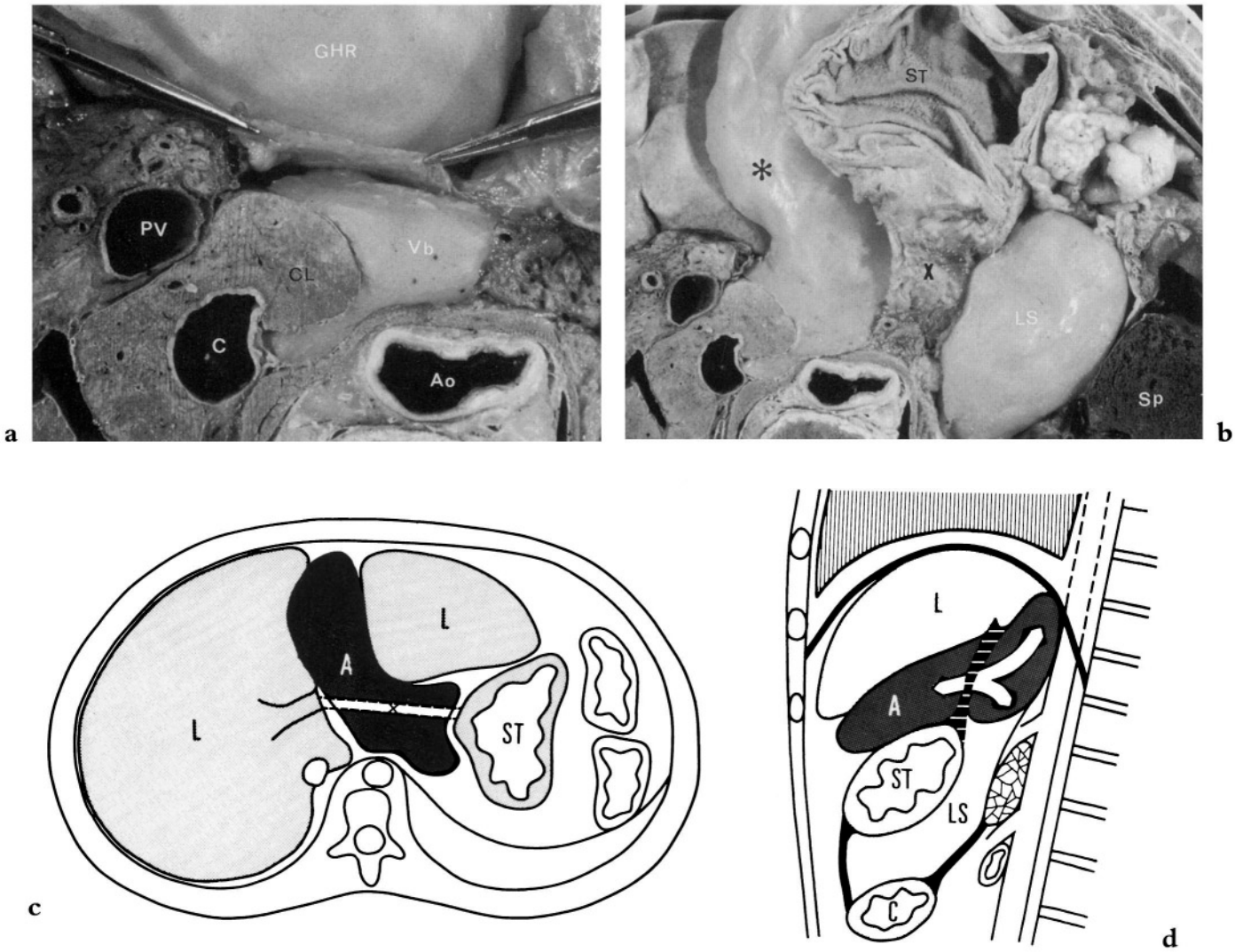


Fig. 3–109. Abscess localization in postoperative neocompartment following subtotal gastrectomy.
CT demonstrates a large abscess (*A*) with multiple air–fluid levels occupying the combined lesser sac and gastrohepatic recess. A drainage needle approaches the abscess. Left pleural fluid is also noted.
(Courtesy of Michael Oliphant, M.D., Crouse Hospital, Syracuse, NY.) (Left)

Fig. 3–110. Abscess localization in postoperative neocompartment following transection of gastrohepatic ligament. (See illustration on opposite page)
(a) Axial anatomic section with injection to simulate abscess formation within the vestibule (*Vb*) of the lesser sac clearly separated by an intact gastrohepatic ligament (between the clamps) from abscess within the gastrohepatic recess (*GHR*) of the greater peritoneal cavity. *CL* = caudate lobe; *Ao* = aorta; *C* = inferior vena cava; *PV* = portal vein. **(This figure also appears in the color insert.)** →



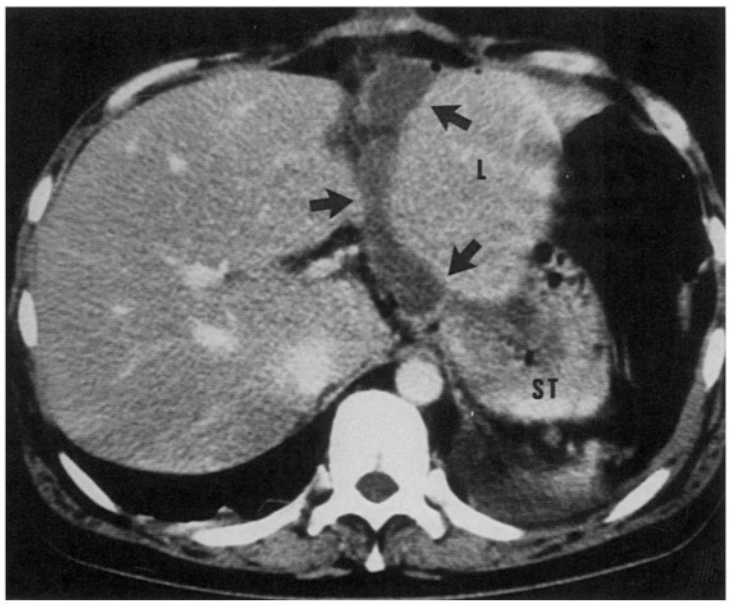


Fig. 3–110. (Continued)
(b) After resection of the gastrohepatic ligament, a neocompartment (*asterisk*) is formed by communication of the gastrohepatic recess and vestibule. *X* = gastropancreatic plica; *ST* = stomach; *LS* = lesser sac; *Sp* = spleen. **(This figure also appears in the color insert.)**
(c and **d)** Cross-sectional and sagittal diagrams showing spread of abscess (*A*) permitted by removal of the anatomic barrier of the gastrohepatic ligament. *C* = colon; *L* = liver; *LS* = lesser sac; *ST* = stomach.
(e) Following operative transection of the gastrohepatic ligament, CT demonstrates spread of abscess (*arrows*) from the ventrally located gastrohepatic recess between the stomach (*ST*) and left lobe of the liver (*L*) to the superior recess of the lesser sac.
(Reproduced from Kumpan[27] and Pokieser et al.[58])

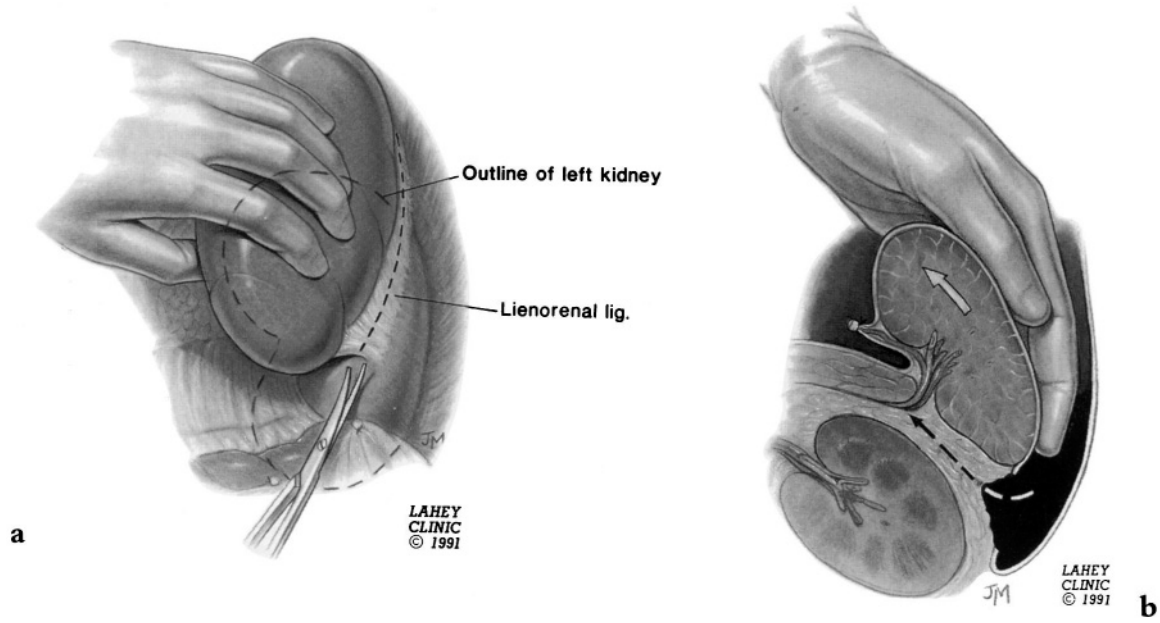


Fig. 3–111. Steps in splenectomy with surgical transection of ligaments.
In an elective splenectomy, the lesser sac is opened via the distal gastrocolic ligament and gastrosplenic ligament. The left gastroepiploic and short gastric vessels are divided and the splenic artery ligated.
(a and **b)** The spleen is then rotated to the right and the splenorenal ligament sectioned. This establishes communication between the lesser sac and the left subphrenic space.
(From Braasch JW, Sedgwick CE, Veidenheimer MC, et al: Atlas of Abdominal Surgery. WB Saunders, Philadelphia, 1991. Illustrations used with permission of The Lahey Clinic.)

Computed tomography demonstrates a generally well-defined mass with a thick wall, internal heterogeneous densities with a wavy or striped appearance, and occasionally mottled calcifications and gas bubbles.[63,66–68] A retained towel may show multiple, thin linear densities with a peculiar infolded[63] or whorled[64] appearance (Fig. 3–116). Similar characteristics with signal intensity differences are evident by MR imaging.[69]

On CT scans, the appearance of an abscess can be closely mimicked by that of retained oxidized cellulose (Surgicel) .[70,71] This is a commonly used knitted fabric used as an agent for intraoperative hemostasis. Unlike traditional surgical sponges, it is bioabsorbable and can be left in the surgical bed.

Spread of Infection via Perihepatic Ligaments

Intraabdominal infections and inflammatory processes may spread and localize not only within the recesses of the peritoneal cavity but along the peritoneal ligaments and mesenteries as well. I have previously recognized that these structures may provide the avenues of spread by direct invasion by malignancies.[14,34,72,73] Mori and colleagues have reported the exophytic spread of hepatobiliary disease along the perihepatic ligaments,[74] and Arenas et al.[75] have further detailed inflammatory and infectious dissemination along these anatomic pathways.

The liver is fixed in the peritoneal cavity by various ligaments, and their radiologic appearance with CT and MR imaging has been well described.[34,35] The perihepatic ligaments are generally identifiable by their locations and relationships to organs or by the landmarks provided by their major constituent vessels along with ligamental fat.

Focal hepatic diseases adjacent to the attachments of the perihepatic ligaments can show contiguous extrahepatic spread along these ligaments. Any hepatic lesion adjacent to the hepatic hilus can exhibit ligamentous spread via the hepatoduodenal ligament and the liga-

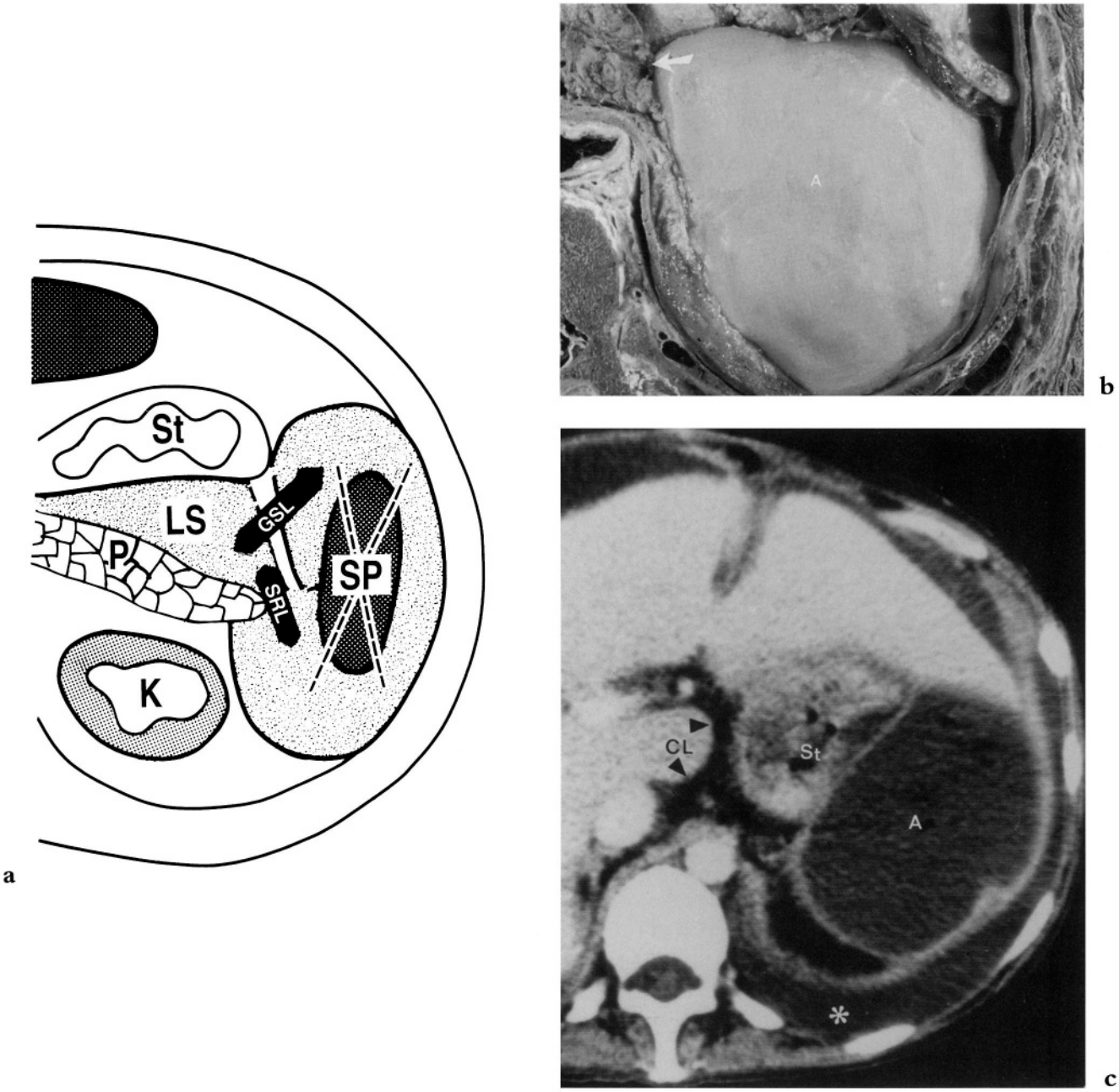


Fig. 3–112. Abscess localization in postoperative neocompartment.
Following splenectomy with resection of the gastrosplenic and splenorenal ligaments, communication is established between the left subphrenic (perisplenic) space and the lesser sac.
(a) Axial diagram. *SP* = spleen; *GSL* = gastrosplenic ligament; *SRL* = splenorenal ligament; *LS* = lesser sac; *St* = stomach; *P* = pancreas; *K* = kidney
(b) Axial anatomic section with injection after removal of spleen to simulate abscess (*A*). *Arrow* = gastropancreatic plica.
(This figure also appears in the color insert.)
(c) CT demonstrates gross abscess (*A*) in postoperative neocompartment. The vestibule of the lesser sac is not involved. At the level of the caudate lobe, the gastropancreatic plica has a fatty triangular configuration, within which course the left gastric artery and vein, extending to the posterior wall of the stomach. *St* = stomach; *CL* = caudate lobe; *arrowheads* = gastropancreatic plica; *asterisk* = pleural fluid.
(Reproduced from Kumpan.[27])

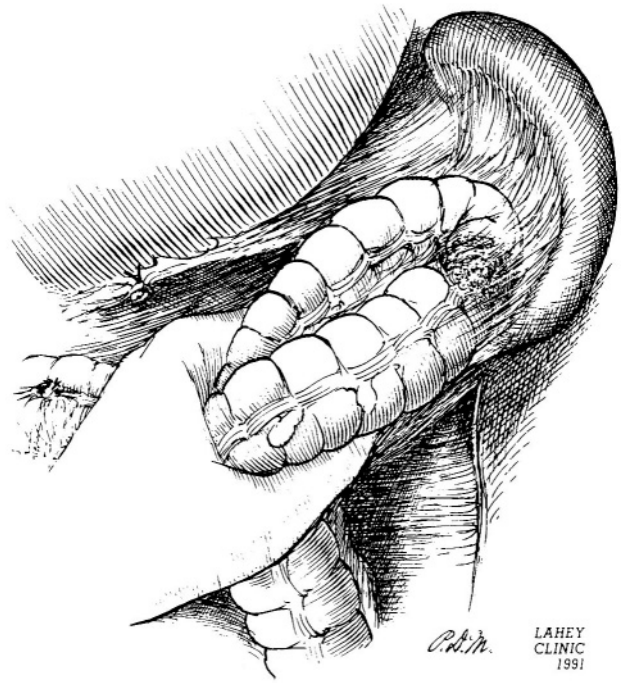


Fig. 3–113. Steps in colectomy of the splenic flexure with surgical transection of ligaments.
After division of the gastrocolic ligament toward the left, the peritoneum of the left paracolic gutter is divided to mobilize the proximal descending colon. This permits gentle traction on the colon and careful dissection of the splenic flexure and its mesentery.
(From Braasch JW, Sedgwick CE, Veidenheimer MC, et al: Atlas of Abdominal Surgery. WB Saunders, Philadelphia, 1991. Illustration used with permission of The Lahey Clinic.)

mentum teres and then can show spread to the gastrohepatic ligament, the gastrocolic ligament, the duodenocolic ligament, the transverse mesocolon, and the falciform ligament. Disease processes of the biliary tract in the hepatic hilus and in the hepatoduodenal ligament can also show the same mode of exophytic spread (Figs. 3–117 through 3–124).

Similarly, a lesion originating in the stomach or pancreas can spread upward along the gastrohepatic ligament to involve the liver (Figs. 3–125 and 3–126).

The Sectional and Isotopic Imaging Modalities

The sectional imaging modalities have not only confirmed the pathways of extension but have provided a striking advance in the diagnosis and localization of intraperitoneal abscesses.[27,40,74,78,79]

Ultrasonography has a sensitivity of almost 95% and a specificity approaching 100% if the study is not limited by bowel gas, obesity, and surgical wounds and bandages.[80–82] The absence of ionizing radiation makes it particularly safe in evaluating children and young women. Abscesses present generally as irregular fluid collections with indistinct margins. Ultrasonography is too time consuming, however, to serve as a survey evaluation of the entire abdomen in suspected abscesses; it is best used when localizing features have been indicated.

Computed tomography may reveal an abscess as a mass with low attenuation value displacing surrounding structures, occasionally with a peripheral rim of higher density that may show contrast enhancement; there may be thickening or obliteration of neighboring fascial planes, and the frequent presence of gas bubbles or air–fluid levels usually allows definitive diagnosis. Computed tomography may diagnose and accurately define the extent of involvement in up to 96–100% of cases, depending on the size of the abscess.[78–81,83,84] It provides precise differentiation with excellent anatomic detail. Radiation dosage is comparable to that from an average barium study. The characteristic signs on ultrasonography and CT usually permit clear distinction from other postoperative fluid collections such as seroma and lymphocysts.

Increasing clinical experience has shown that MR imaging has high diagnostic accuracy in the evaluation

text continues on page 124

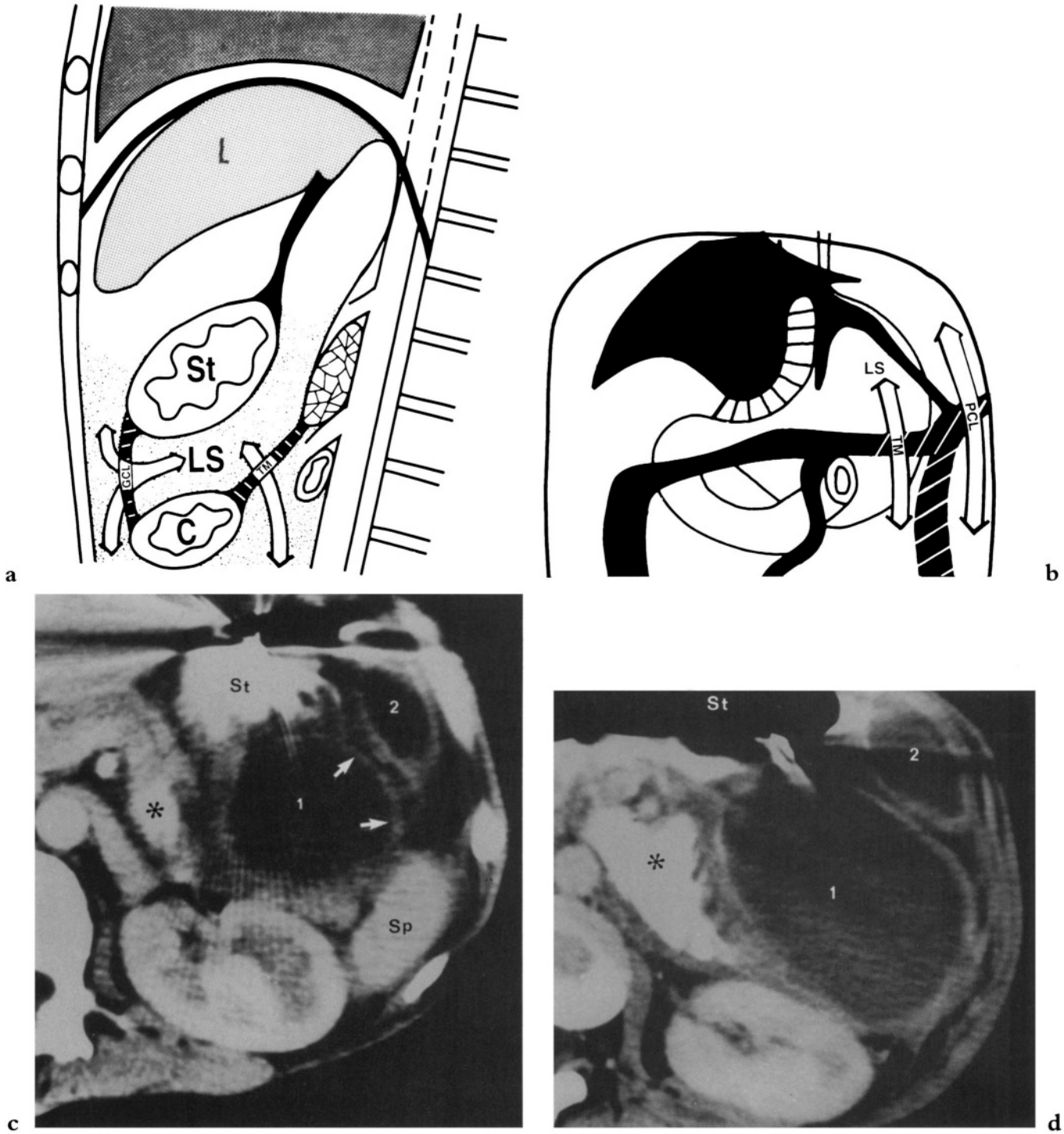


Fig. 3–114. Abscess localization in postoperative neocompartment.
Excision of gastrocolic ligament (*GCL*), transverse mesocolon (*TM*), and phrenicocolic ligament (*PCL*), associated with colectomy. Lateral and frontal diagrams **(a** and **b)** and CT **(c** and **d)** after left colectomy illustrate abscess in a newly established lesser sac plus an infra/paracolic compartment (*1*). An intact gastrosplenic ligament (*arrows*) demarcates this from an abscess in the left subphrenic space (2). *Sp* = spleen; *St* = stomach; *L* = liver; *C* = colon; *LS* = lesser sac; *asterisk* = duodenojejunal flexure.
(Reproduced from Kumpan.[27])

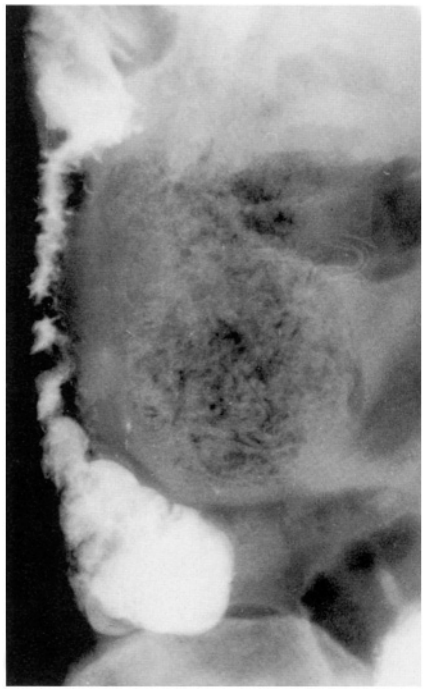
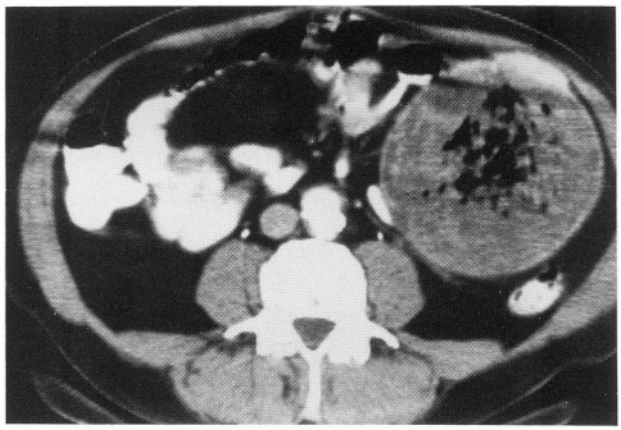
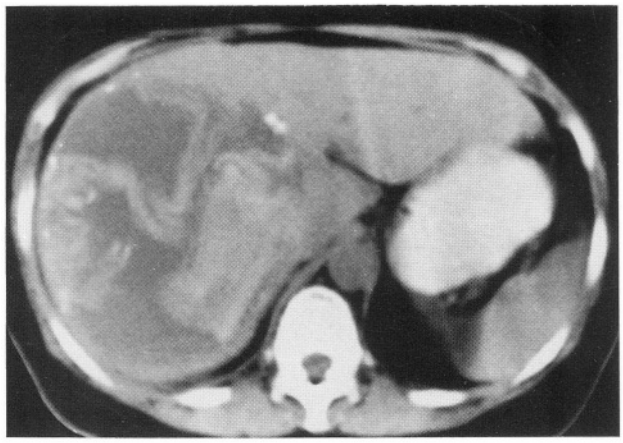


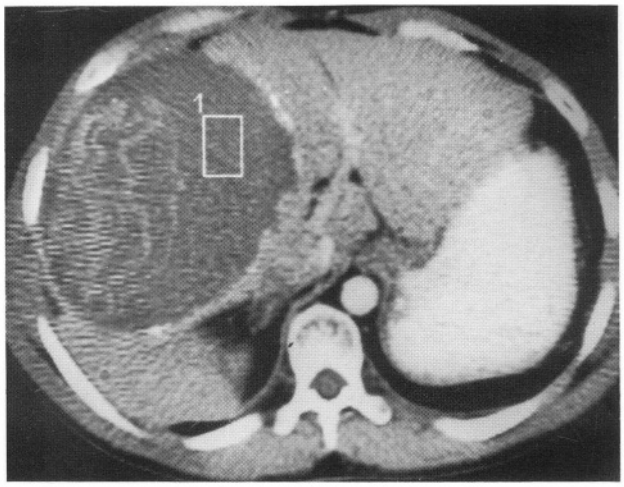
Fig. 3–115. Abscess secondary to retained laparotomy pad.
The abscess is shown by swirled pattern of gas loculations, and the pad demonstrates localized opacities. The abscess distorts and compresses the ascending colon.



a



b



c

Fig. 3–116. Three different examples of retained surgical sponges and towels shown by CT.
(a) Contrast-enhanced CT shows a spherical, sharply defined mass with a thin dense wall and containing multiple gas bubbles in the supramesocolic space beneath the tail of the pancreas. A retained sponge was confirmed at surgery. An aorticoiliac bypass is present.
(b) Contrast-enhanced CT shows a low-density mass containing multiple linear infolded densities. Calcifications in the wall of the mass are present. A retained surgical towel was found at surgery within a subdiaphragmatic abscess penetrating the right lobe of the liver and the right hemidiaphragm.
(c) Contrast-enhanced CT demonstrates a cystic spherical mass with well-defined borders containing dense, linear contiguous shadows having a folded appearance. At surgery, a retained towel in a right subphrenic sterile abscess was discovered.
(Reproduced from Buy et al.[63])

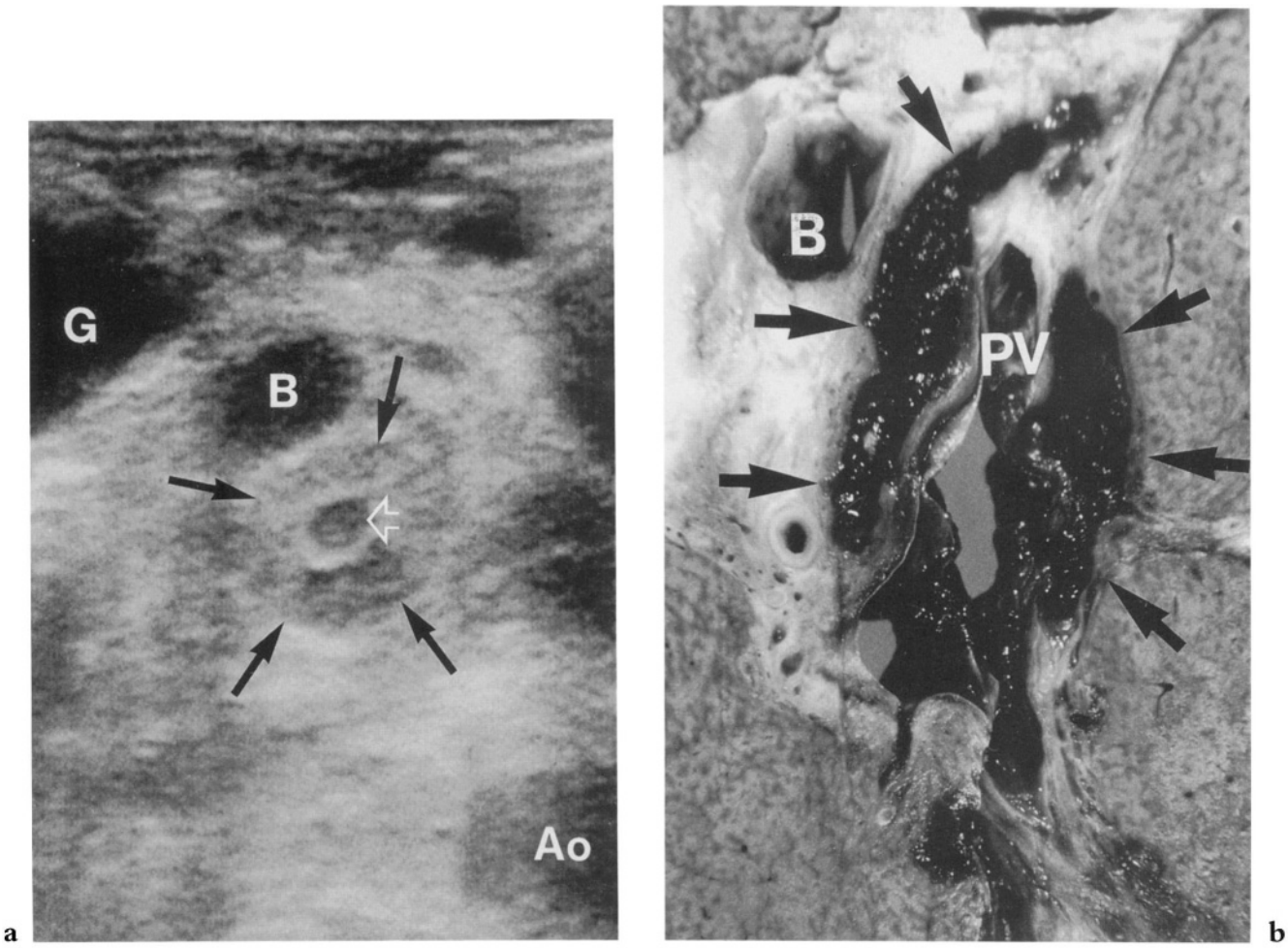


Fig. 3–117. Abscess (infected biloma) of the hepatoduodenal ligament.
(a) Ultrasonography, transverse view, shows echogenic fluid collection (*black arrows*) encasing the main portal vein (*open arrow*). The common bile duct (*B*) is dilated, and cholecysto-choledocholithiasis was noted (not shown). *G* = gallbladder; *A*o = abdominal aorta.
(b) At autopsy, greenish biliary abscess (*arrows*) extends along the portal vein (*PV*) within the hepatoduodenal ligament from the site of a minute disruption of the right hepatic duct. *B* = common bile duct.
(Reproduced from Mori et al.[74])

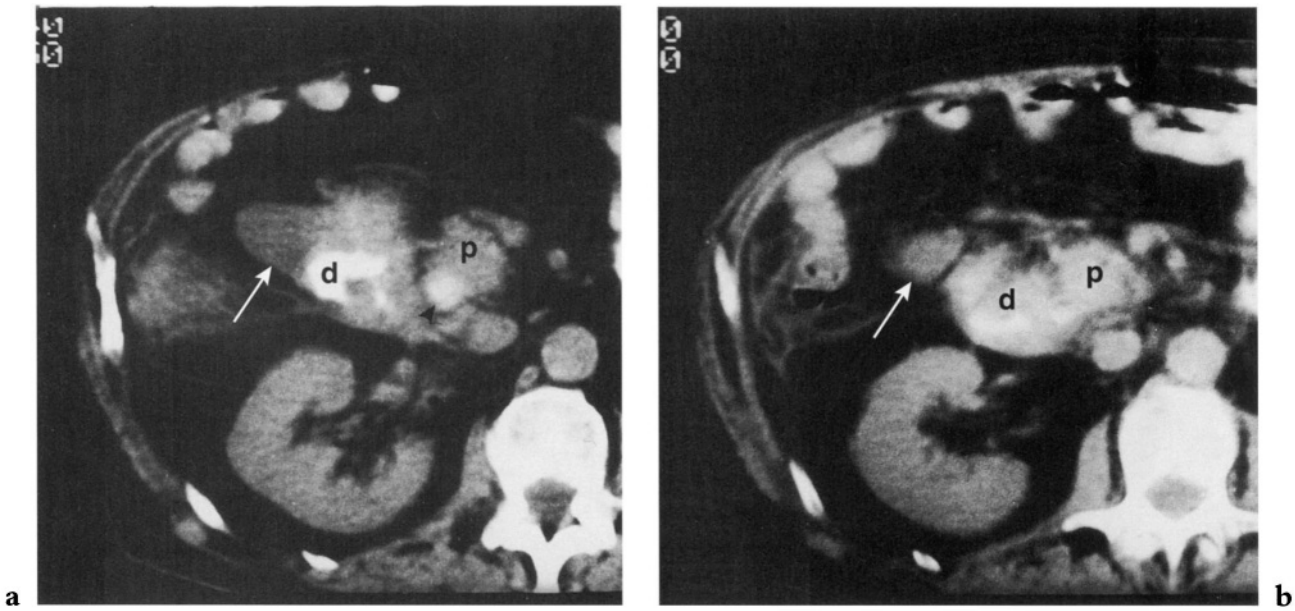


Fig. 3–118. Extension via the hepatoduodenal ligament to the duodenocolic ligament from an infected biloma secondary to acute cholecystitis.
(a) CT through the inferior insertion of the hepatoduodenal ligament shows a collection (*arrow*) around the duodenum(*d*).
A calcified stone (*arrowhead*) is seen in the common bile duct. The fat plane around the pancreas (*p*) is preserved.
(b) In a more caudal section, the collection (*arrow*) lies anterolateral to the descending duodenum, in the duodenocolic ligament.
(Reproduced from Arenas et al.[75])

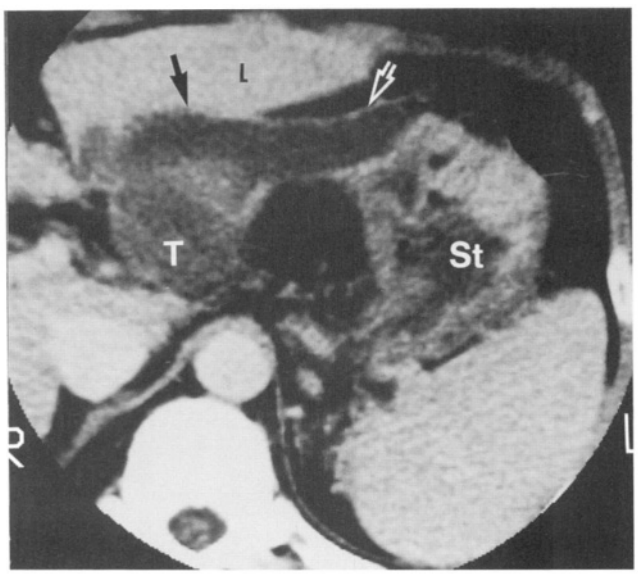


Fig. 3–119. Abscess of the gastrohepatic ligament, extending from a hepatic abscess.
The liver abscess is secondary to transcatheter embolotherapy for a hepatocellular carcinoma located in the posteroinferior portion of the lateral segment of the liver.
Contrast-enhanced CT shows a fluid collection (*arrows*) between the posteroinferior aspect of the left lobe of the liver (*L*) and the lesser curvature of the stomach (*St*) that is contiguous with the necrotic tumor (*T*) of the liver.
(Reproduced from Mori, et al.[74])

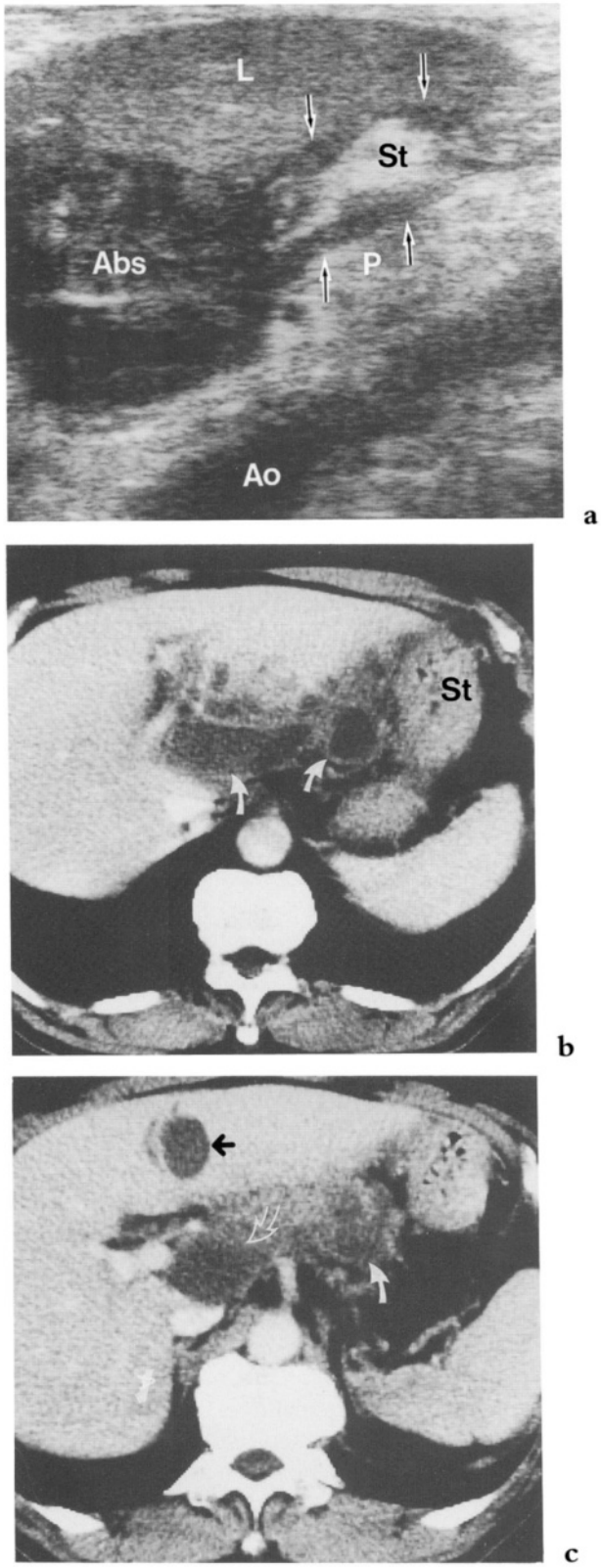


Fig. 3–120. Abscess of the gastrohepatic ligament, hepatoduodenal ligament, and ligamentum teres extending from an abscess in the posteromedial portion of the lateral segment of the liver.
(a) Ultrasonography shows abscess in the posterior portion of the lateral segment (*Abs*) of the left lobe of the liver. Contiguous hypoechoic zones (*arrows*) are present between the left lobe of the liver (L) and the stomach (*St*) and between the stomach and the pancreas (*P*). These zones reflect abscesses (fluid collections) of the gastrohepatic ligament and in the lesser sac, respectively. *Ao* = abdominal aorta.
(b and **c)** CT scans after the administration of contrast medium demonstrate fluid collections in the gastrohepatic ligament (*curved closed arrows*), the hepatoduodenal ligament (*curved open arrow*), and the ligamentum teres (*black arrow*). Collections may lie partially within the fissure for ligamentum teres and the superior recess of the lesser sac. *St* = stomach. (Reproduced from Mori, et al.[74])

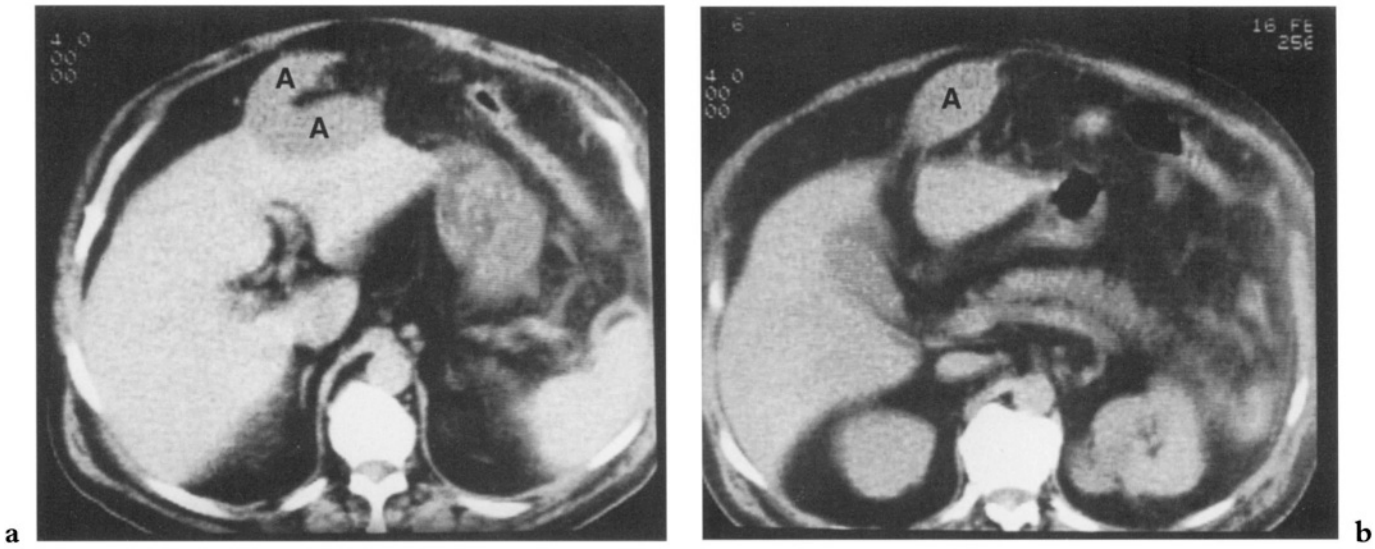


Fig. 3–121. Abscess of the falciform ligament extending from a hepatic abscess.
(a and **b)** CT in a patient with fever and leukocytosis following anal surgery shows a subcapsular hepatic collection *(A)* extending into the falciform ligament. Fine-needle aspiration yielded purulent material.
(Reproduced from Arenas et al.[75])

of acute intraperitoneal abscesses. They are best demonstrated on gadolinium-enhanced T1-weighted fat-suppressed images as well-defined fluid collections with peripheral rim enhancement.[85]

The overall accuracy for gallium-67 examination is highly dependent on the type of patient studied.[82,86–88] The presence of a surgical incision as well as nonspecific uptake in inflammatory but nonsuppurative lesions, bowel, and tumors may be mistaken for an abscess. Despite the use of cleansing enemas for repeated gallium scans, differentiation of an abscess from normal bowel may still occasionally be difficult. The technique provides relatively poor resolution and has a higher false-positive and false-negative rate than either ultrasonography or CT. Although 6-hour delay scans have been advocated,[86] they are difficult to interpret because of high background radioactivity. A reliable diagnosis may be made from the 24-hour study, but 48- and sometimes 72-hour scans are necessary. This contrasts with the immediate results obtainable from ultrasonography and CT.

In^{111}-labeled leukocyte scanning, in contrast, results in superior image quality; moreover, no indium-^{111} normally appears in the gastrointestinal tract or its contents or in the urinary collection system. However, intense uptake may occur in recent hematomas and less intense accumulations in any acute inflammatory lesion and in some noninflammatory states as well.[89]

Isotopic scans are particularly useful as an initial survey in suspected abscesses when there are no localizing clinical signs and plain film findings are negative or equivocal. Newer agents include technetium-99m (99mTc)-HMPAO-labeled leukocytes, 99mTc-labeled chemotactic peptides, 111In-labeled polyclonal immunoglobulin G, and 99mTc-labeled monoclonal antibody.

Currently, patients who are not critically ill and have no focal signs of an abscess may be initially imaged by an indium-labeled leukocyte scan. In critically ill patients, however, CT and ultrasound provide a more rapid and specific diagnosis. Computed tomography obviates many of the practical disadvantages of ultrasound in such patients, displays the relationship of an abscess to surrounding structures, and permits planning of the most appropriate route for percutaneous or surgical drainage.

Management

Precise radiologic identification of an intraabdominal abscess permits the most appropriate route of drainage (Fig. 3–12). Although antibiotics play an important role, drainage remains the cornerstone of therapy. Radiographic localization is particularly important in supramesocolic infections.

An abscess compartmentalized to the right posterior subhepatic space is classically drained surgically by Ochsner's extrapleural approach through the bed of the

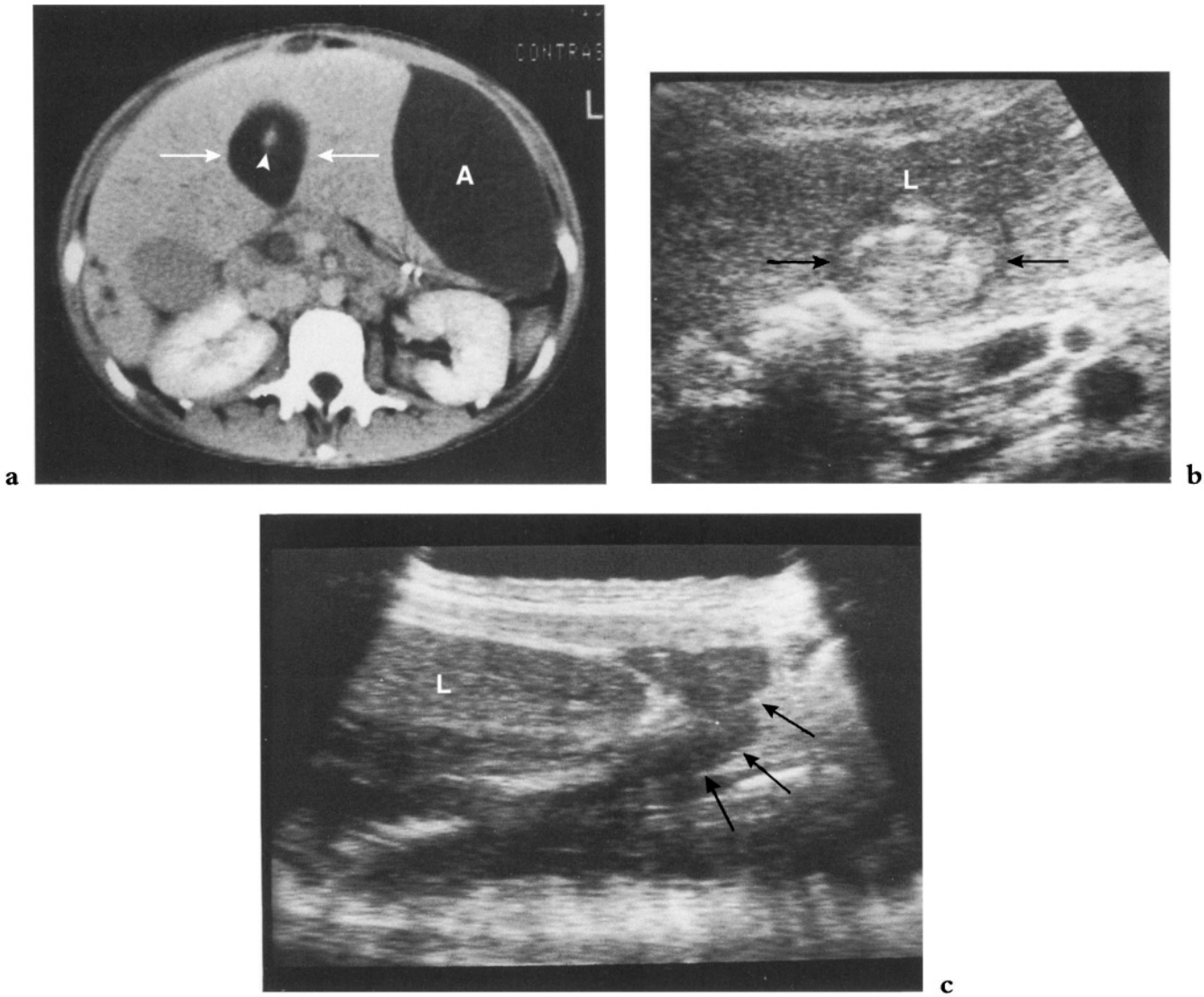


Fig. 3–122. Abscess of the falciform ligament, secondary to suppurative cholangitis.
(a) CT demonstrates a large subphrenic abscess (*A*) and many small intrahepatic lesions. Another collection occupies the left periportal space and spreads into the falciform ligament (*arrows*). *Arrowhead* = ligamentum teres.
(b) Axial ultrasound scan shows the abscess in the falciform ligament as a hyperechoic collection (*arrows*) within the left lobe of the liver (*L*).
(c) Sagittal sonogram demonstrates extension through the ligament (*arrows*) to the anterior abdominal wall, beyond the hepatic edge.
(Reproduced from Arenas et al.[75])

resected 12th rib. The right posterior subphrenic space is drained via Trendelenburg's transpleural route: the 8th, 9th, 10th, or 11th ribs are resected subperiosteally, and the pleural cavity is entered; the diaphragm is tightly sutured around the pleural opening, and the subphrenic abscess is drained after an incision is made through the diaphragm.

A transperitoneal approach is generally employed for surgical drainage of anterior subphrenic and subhepatic, left subphrenic, lesser sac, and multiple abscesses. It is especially advantageous since it permits a thorough evaluation of the extent of the purulent collection and drainage can be undertaken accordingly.

Ultrasound- and CT-guided aspiration and drainage of intraabdominal abscesses represent recent major advantages in management.[90–98] It is generally accepted

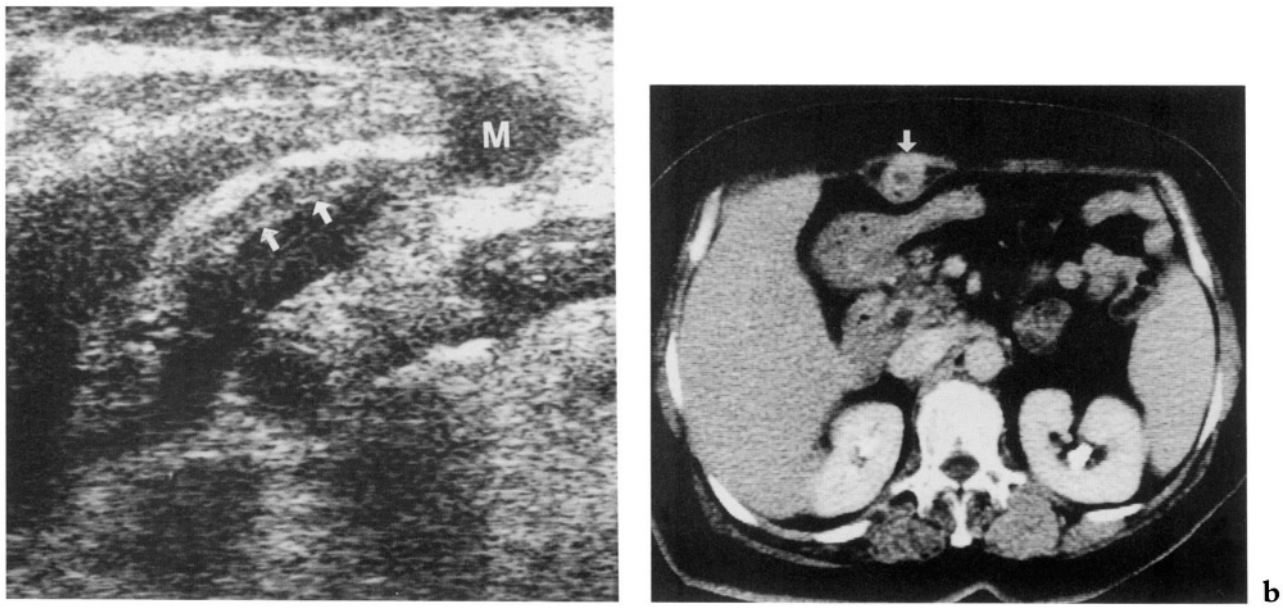


Fig. 3–123. Abscesses of the ligamentum teres and the falciform ligament, secondary to cholecystitis.
(a) Longitudinal sonogram demonstrates a hypoechoic mass (*M*) beneath the abdominal wall, representing a falciform ligament abscess, continuous with a thickened ligamentum teres (*arrows*).
(b) CT shows a mass of soft-tissue attenuation replacing the falciform ligament (*arrow*) and surrounding the remnant of the umbilical vein. The fat of the ligamentum teres was also obliterated and thickened.
(Reproduced from Mori, et al.[74])

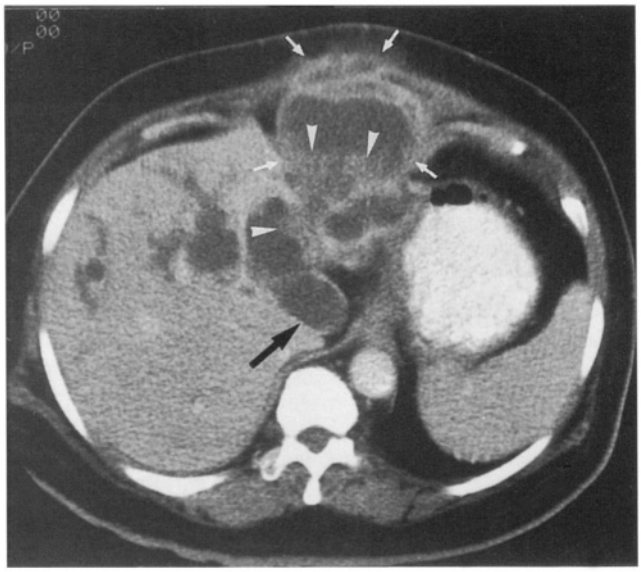
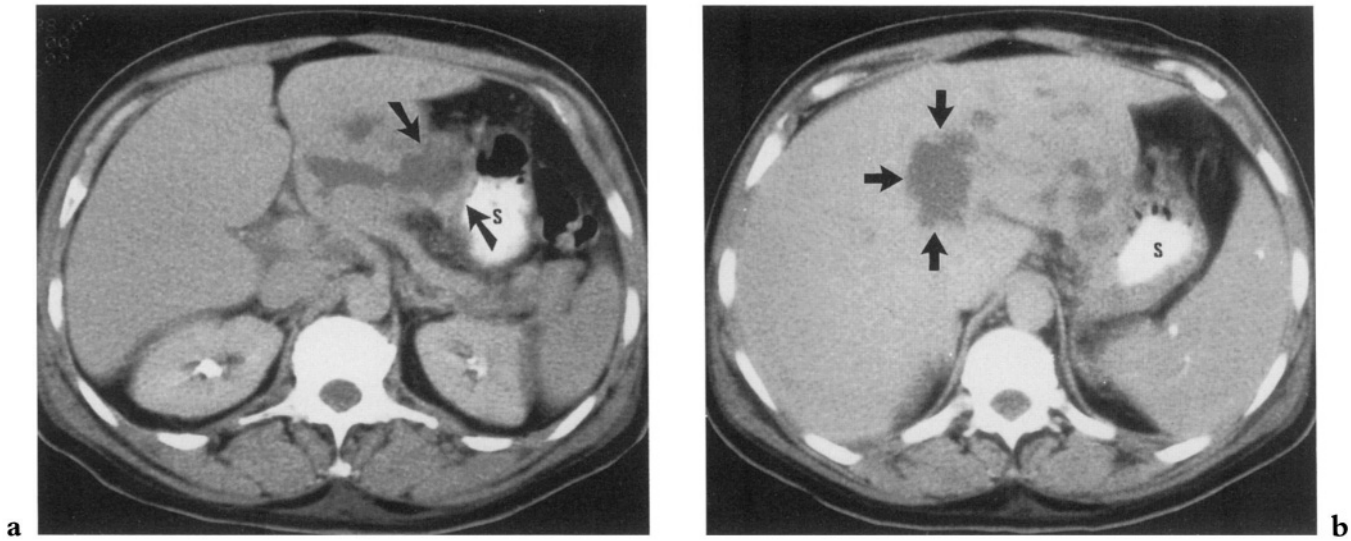
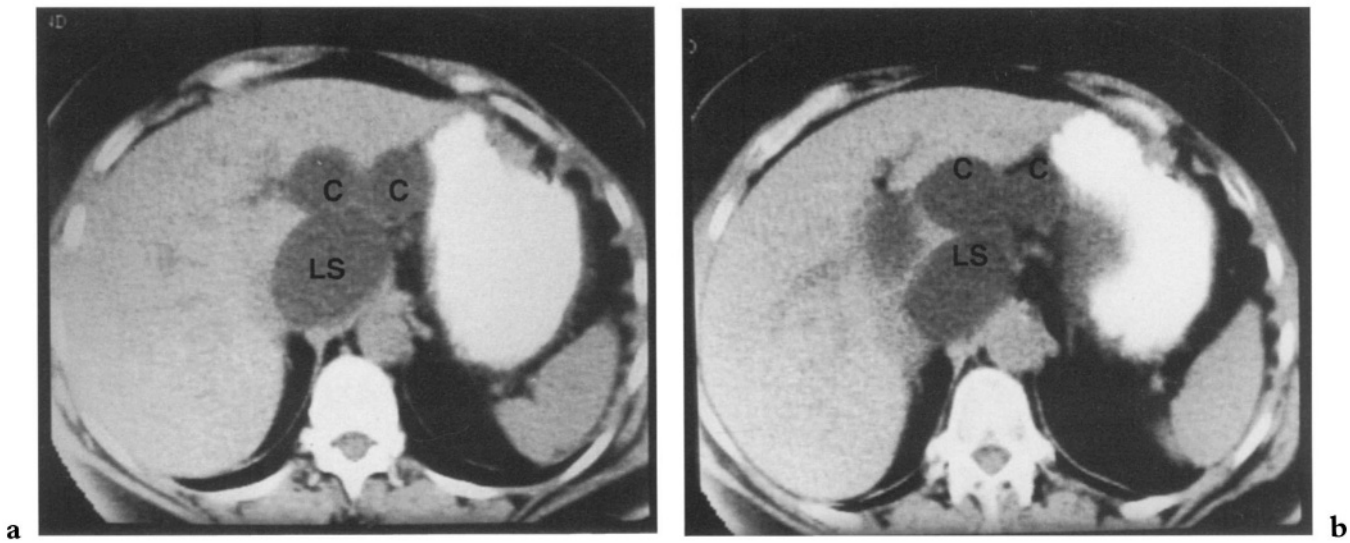


Fig. 3–124. Abscess of the ligamentum teres and anterior abdominal wall consequent to cholangiocarcinoma.
CT shows dilation of the common hepatic duct (*black arrow*) and the left intrahepatic ducts with papillary or nodular soft tissue vegetations (*arrowheads*) characteristic of mucin-hypersecreting papillary cholangiocarcinoma. There is focal liver disruption in the anterior aspect of the atrophic left lateral segment, with an extension of infected biliary fluid to the anterior abdominal wall forming an abscess via the falciform ligament and ligamentum teres (*white arrows*).
(Reproduced from Ko et al.[76])



a b

Fig. 3–125. Hepatic abscess secondary to confined gastric perforation along the gastrohepatic ligament.
(a) An irregular low-attenuation mass (*arrows*) secondary to confined perforation of a lesser curvature gastric ulcer extends from the stomach (*S*) into the gastrohepatic ligament.
(b) CT at a higher level demonstrates a hepatic abscess (*arrows*) in the left lobe. *S* = stomach.
(Reproduced from Jacobs et al.[77])



a b

Fig. 3–126. Intrahepatic pancreatic pseudocysts via the gastrohepatic ligament.
(**a** and **b**) CT after an acute recurrence of chronic pancreatitis shows a bilobed collection (C) in the gastrohepatic ligament and in the fissure for the ligamentum venosum, invading the left hepatic lobe. Another collection is seen in the upper recess of the lesser sac (*LS*), medial to the inferior vena cava, indenting the caudate lobe.
(Reproduced from Arenas et al.[75])

that 80–85% of abscesses can be treated exclusively by percutaneous catheter drainage with a mortality rate of 6%. Percutaneous drainage of abdominal abscesses is less traumatic and disruptive to the normal anatomy than is operative drainage. One-step needle aspiration and lavage has been recently reported as quite effective, when combined with intravenous antibiotic therapy, in curing small abscesses.[99]

References

1. Connell TR, Stephens DH, Carlson HC, et al: Upper abdominal abscess: A continuing and deadly problem. AJR 1980; 134:759–765.
2. Wang SMS, Wilson SE: Subphrenic abscess: The new epidemiology. Arch Surg 1977; 112:934–936.
3. Wetterfors J: Subphrenic abscess: A clinical study of 101 cases. Acta Chir Scand 1959; 117:388–408.
4. Samuel E, Duncan JG, Philip T, et al: Radiology of the postoperative abdomen. Clin Radiol 1963; 14:133–148.
5. Annotation: Subphrenic abscess: A changing pattern. Lancet 1970; 2:301.
6. Meyers MA: The spread and localization of acute intraperitoneal effusions. Radiology 1970; 95:547–554.
7. Morison R: The anatomy of the right hypochondrium relating especially to operations for gallstones. Br Med J 1894; 2:968.
8. Barnard HL: Surgical aspects of subphrenic spaces. Br Med J 1908; 1:371–377.
9. Ochsner A, DeBakey M: Subphrenic abscess: Collective review and an analysis of 3,608 collected and personal cases. Int Abstr Surg 1938; 66:426–438.
10. Harley HRS: Subphrenic abscess, with particular reference to the spread of infection. Hunterian Lecture. Ann R Coll Surg Engl 1955; 17:201–224.
11. Mitchell GAG: The spread of acute intraperitoneal effusions. Br J Surg 1940; 28:291–313.
12. Boyd DP: The anatomy and pathology of the subphrenic spaces. Surg Clin North Am 1958; 38:619–626.
13. Boyd DP: The subphrenic spaces and the emperor's new robes. N Engl J Med 1966; 275:911–917.
14. Meyers MA: Peritoneography: Normal and pathologic anatomy. AJR 1973; 117:353–365.
15. Whalen JP, Bierny JP: Classification of perihepatic abscesses. Radiology 1969; 92:1427–1437.
16. Wooler AH: Subphrenic abscess. Thorax 1956; 11:211–222.
17. Min P-Q, Yang Z-G, Lei Q-F, et al: Peritoneal reflections of left perihepatic region: Radiologic-anatomic study. Radiology 1992; 182:553–557.
18. Meyers MA: Roentgen significance of the phrenicocolic ligament. Radiology 1970; 95:539–545.
19. Auh YH, Lim JH, Kim KW, et al: Loculated fluid collections in hepatic fissures and recesses: CT appearance and potential pitfalls. RadioGraphics 1994; 14: 529–549.
20. va der Zypen E, Revész E: Investigation of development, structure, and function of the phrenicocolic and duodenal suspensory ligaments. Acta Anat 1984; 119:142–148.
21. Winslow JB: Exposition anatomique de la structure du corps humain. Paris, G. Desprez et J. Dessesartz, 1732.
22. Weill FS: Ultrasound Diagnosis of Digestive Diseases. Springer, Heidelberg, 1996.
23. Weill FS, Manco-Johnson ML: Imaging of Abdominal and Pelvic Anatomy. Churchill Livingstone, New York, 1997.
24. Estrada RL: Internal Intra-abdominal Hernias. RG Landes, Austin, TX, 1994.
25. Auh YH, Rosen A, Rubenstein WA, et al: CT of the papillary process of the caudate lobe of the liver. AJR 1984; 142:535–538.
26. Donoso L, Martínez-Noguera A, Zidan A, et al: Papillary process of the caudate lobe of the liver: Sonographic appearance. Radiology 1989; 173: 631–633.
27. Kumpan W: Computertomographische Analyse postoperativer abdomineller Kompartments. Radiologie 1987; 27:203–215.
28. Erenbourg L, Reggiani P: A new ligament: The "gastro-pancreatic". Anat Clin 1985; 7:143–144.
29. De Meo JH, Fulcher AS, Austin RF Jr: Anatomic CT demonstration of the peritoneal spaces, ligaments and mesenteries: Normal and pathologic processes. RadioGraphics 1995; 15: 755–770.
30. Vincent LM, Mauro MA, Mittelstaedt CA: The lesser sac and gastrohepatic recess: Sonographic appearance and differentiation of fluid collections. Radiology 1984, 150:515–519.
31. Weill FS, Perriguey G, Belloir A, et al: Ultrasonic anatomical study of the lesser omental sac: A pictorial essay. Eur J Radiol 1983; 3:142–147.
32. Dodds WJ, Foley DW, Lawson TL, et al: Anatomy and imaging of the lesser peritoneal sac. AJR 1985; 144:567–575.
33. Jeffrey RB, Federle MP, Goodman PC: Computed tomography of the lesser peritoneal sac. Radiology 1981; 141:117–122.
34. Meyers MA, Oliphant M, Berne AS, et al: The peritoneal ligaments and mesenteries: Pathways of intra-abdominal spread of disease. Annual oration. Radiology 1987; 163:593–604.
35. Chou C-K, Liu G-C, Chen L-T, et al: MRI demonstration of peritoneal ligaments and mesenteries. Abdom Imaging 1993; 18:126–130.
36. Meyers MA, Whalen JP: Radiologic aspects of intraabdominal abscesses. *In* The Diagnosis and Treatment of Intraabdominal Abscesses. Edited by I Ariel, K Kazarian. Williams & Wilkins, Baltimore, 1971.

37. Forsby J, Henriksson L: Detectability of intraperitoneal fluid by ultrasonography. Acta Radiol Diagn 1984; 25(Fasc. 5):375–378.
38. Yeh H-C, Wolf BS: Ultrasonography in ascites. Radiology 1977; 124:783–790.
39. Myerson PJ, Myerson D, Spencer RP: Anatomic patterns of Ga–67 distribution in localized and diffuse peritoneal inflammation: Case report. J Nucl Med 1977; 18:977–980.
40. Meyers MA: Abdominal abscesses. *In* Radiology Today. Edited by MW Donner, FHW Heuck. Springer-Verlag, Berlin, 1981, pp 186–190.
41. Wojtowicz J, Rzymski K, Czarnecki R: A CT evaluation of the intraperitoneal fluid distribution. Fortschr Röntgenstr 1982; 137(1):95–99.
42. Douglas J: A description of the peritonaeum, and of that part of the membrana cellularis which lies on its outside. With an account of the true situation of all the abdominal viscera, in respect of these two membranes. London, J Roberts, 1730.
43. Semelka RC, Ascher SM, Reinhold C: MRI of the Abdomen and Pelvis. Wiley-Liss, New York, 1997.
44. Jorulf H: Roentgen diagnosis of intraperitoneal fluid: A physical, anatomic, and clinical investigation. Acta Radiol Suppl 1975; 343.
45. Auh YH, Rubenstein WA, Markisz JA, et al: Intraperitoneal paravesical spaces: CT delineation with US correlation. Radiology 1986; 159:311–317.
46. Hajdu N, deLacy G: The Rutherford Morison pouch: A characteristic appearance on abdominal radiographs. Br J Radiol 1970; 43:706–709.
47. Hellmer H: Die Konturen des rechten Leberlappens beim Ascites. Acta Radiol 1942; 23:533–540.
48. Love L, Demos TC, Reynes CJ, et al: Visualization of the lateral edge of the liver in ascites. Radiology 1977; 122:619–622.
49. Naidich DP, Megibow AJ, Hilton S, et al: Computed tomography of the diaphragm: Peridiaphragmatic fluid collection. J Comput Assist Tomogr 1983; 7:641–649.
50. Rubinstein WA, Auh YH, Whalen JP, et al: The perihepatic spaces: Computed tomographic and ultrasound imaging. Radiology 1983; 149:231–239.
51. Autio V: The spread of intraperitoneal infection. Studies with roentgen contrast medium. Acta Chir Scand Suppl 1964; 321:1–31.
52. Overholt RH: Intraperitoneal pressure. Arch Surg 1931; 22:691–703.
53. Salkin D: Intraabdominal pressure and its regulation. Am Rev. Tubercu 1934; 30:436–457.
54. Drye JC: Intraperitoneal pressure in the human. Surg Gynecol Obstet 1948; 87:472–475.
55. Allen KS, Siskind BN, Burrell MI: Perforation of distal esophagus with lesser sac extension: CT demonstration. J Comput Assist Tomogr 1986; 10(4):612–614.
56. Halvorsen RA, Jones MA, Rice RP, et al: Anterior left subphrenic abscess: Characteristic plain film and CT appearance. AJR 1982; 139:283–289.
57. Livingston EM: A Clinical Study of the Abdominal Cavity and Peritoneum. Paul B Hoeber, New York, 1932.
58. Pokieser H, Czembirek H, Frank W, et al: Septic lesions of the abdomen. *In* Radiology Today 3. Edited by MW Donner, FHW Heuck. Springer–Verlag, New York, 1985.
59. Williams RG, Bragg DG, Nelson JA: Gossypiboma—The problem of the retained surgical sponge. Radiology 1978; 129:323–326.
60. Meyers MA, Ghahremani GG, Gold BM: Postoperative abdominal abscesses. *In* Iatrogenic Gastrointestinal Complications. Edited by MA Meyers, GG Ghahremani. Springer-Verlag, New York, Heidelberg, 1981.
61. Olnick HM, Weens HS, Rogers JV Jr: Radiological diagnosis of retained surgical sponges. JAMA 1955; 159:1525–1527.
62. Carsky EW, Haswell DM: Huge laparotomy pad granuloma simulating a gastric wall tumor. AJR 1978; 131:909–910.
63. Buy J–N, Hubert C, Ghossain MA, et al: Computed tomography of retained abdominal sponges and towels. Gastrointest Radiol 1989; 14:41–45.
64. Sheward JE, Williams AG, Mettler FA, et al: CT appearance of a surgically retained towel (Gossypiboma). J Comp Assist Tomogr 1986; 10:343–345.
65. Revesz G, Siddiqui TS, Buchheit WA, et al: Detection of retained surgical sponges. Radiology 1983; 149:411–413.
66. Kokubo T, Itai Y, Ohtomo K, et al: Retained surgical sponges: CT and US appearance. Radiology 1987; 165:415–418.
67. Yamato M, Ido K, Izutsu M, et al: CT and ultrasound findings of surgically retained sponges and towels. J Comp Assist Tomogr. 1987; 11:1003–1006.
68. Choi BI, Kim SH, Yu ES, et al: Retained surgical sponge: Diagnosis with CT and sonography. AJR 1988; 150:1047–1050.
69. Sigimura H, Tamura S, Kakitsubata S, et al: Magnetic resonance imaging of retained surgical sponges: Case report. Clin Imaging 1992; 16:259–262.

70. Young ST, Paulson EK, McCann RL, et al: Appearance of oxidized cellulose (Surgicel) on postoperative CT scans: Similarity to postoperative abscess. AJR 1993; 160:175–277.
71. Turley BR, Taupmann RE, Johnson PL: Postoperative abscess mimicked by Surgicel. Abdom Imaging 1994; 19:345–346.
72. Meyers MA, McSweeney J: Secondary neoplasms of the bowel. Radiology 1972; 105:1–11.
73. Meyers MA: Intraperitoneal spread of malignancies and its effect on the bowel. Second Annual Leeds Lecture. Clin Radiol 1981; 32:129–146.
74. Mori H, Aikawa H, Hirao K, et al: Exophytic spread of hepatobiliary disease via perihepatic ligaments: Demonstration with CT and US. Radiology 1989; 172:41–46.
75. Arenas AP, Sanchez LV, Albillos JM, et al: Direct dissemination of pathologic abdominal processes through perihepatic ligaments: Identification with CT. RadioGraphics 1994; 14:515–527.
76. Ko S–F, Chen Y-S, Ng S-H, et al: Mucm-hypersecreting papillary cholangiocarcinoma presenting as abdominal abscesses: CT and spiral CT cholangiography. Abdom Imaging 1996; 21:222–225.
77. Jacobs JM, Hill MC, Steinberg WM: Peptic ulcer disease: CT evaluation. Radiology 1991; 178:745–748.
78. Koehler PR, Moss AA: Diagnosis of intra-abdominal and pelvic abscesses by computed tomography. JAMA 1980; 244:49–52.
79. Scneekloth G, Terrier F, Fuchs WA: Computed tomography of intraperitoneal abscesses. Gastrointest Radiol 1982; 7:35–42.
80. McNeil BJ, Sanders R, Alderson PO, et al: A prospective study of computed tomography, ultrasound and gallium imaging in patients with fever. Radiology 1981; 139:647–653.
81. Knochel JQ, Koehler PR, Lee TG, et al: Diagnosis of abdominal abscesses with computed tomography, ultrasound, and ^{111}In leukocyte scans. Radiology 1980; 137:425–432.
82. Taylor KJW, Sullivan DC, Wasson JF, et al: Ultrasound and gallium for the diagnosis of abdominal and pelvic abscesses. Gastrointest Radiol 1978; 3:281–286.
83. Haaga JR, Weinstein AJ: CT-guided percutaneous aspiration and drainage of abscesses. ARJ 1980; 135:1187–1194.
84. Wolverson MR, Jagannadharao B, Sundaram M, et al: CT as a primary diagnostic method in evaluating intraabdominal abscess. AJR 1979; 133:1089–1095.
85. Noone TC, Semelka RC, Worawattankul S, et al: Intraperitoneal abscesses: Diagnostic accuracy of and appearances at MR imagery. Radiology 1998; 208:525–528.
86. Hopkins GB, Kan M, Mende CW: Early ^{67}GA scintigraphy for the localization of abdominal abscesses. J Nucl Med 1975; 16:990–992.
87. Kumar B, Alderson PO, Geisse G: The role of Ga-67 citrate imaging and diagnostic ultrasound in patients with suspected abdominal abscesses. J Nucl Med 1977; 18:534–537.
88. Forgacs P, Wahner HW, Keys TF, et al: Gallium scanning for the detection of abdominal abscesses. AmJ Med 1978; 65:949–954.
89. McAfee JG, Samin A: In-111 labeled leukocytes: A review of problems in image interpretation. Radiology 1985; 155:221–229.
90. Mueller PR, van Sonnenberg E, Ferrucci JT Jr: Percutaneous drainage of 250 abdominal abscesses and fluid collections. II. Current procedural concepts. Radiology 1984; 151:343–347.
91. Mueller PR, Simeone JF, Butch RJ, et al: Percutaneous drainage of subphrenic abscess: A review of 62 patients. AJR 1986; 147:1237–1240.
92. van Sonneberg E, Mueller PR, Ferrucci JT Jr: Percutaneous drainage of 250 abdominal abscesses and fluid collections. I. Results, failures, and complications. Radiology 1984; 151:337–341.
93. Mueller PR, Ferrucci JT Jr, Simeone JE, et al: Lesser sac abscess and fluid collections: Drainage by transhepatic approach. Radiology 1985; 155:615–618.
94. Nunez DJR, Yrizarry JM, Russell E, et al: Transgastric drainage of pancreatic fluid collections. AJR 1985; 145:815–818.
95. Lambiase RE, Deyoe L, Cronan JJ: Percutaneous drainage of 335 consecutive abscesses: Results of primary drainage with 1-year follow-up. Radiology 1992; 184:167–179.
96. van Sonnenberg E, D'Agostino HB, Casola G, et al: Percutaneous abscess drainage: Current concepts. Radiology 1991; 181:617–626.
97. Bennet JD, Kozak MB, Taylor BM, et al: Deep pelvic abscesses: Transrectal drainage with radiologic guidance. Radiology 1992; 185:825–828.
98. Sanchez RB, van Sonnenberg E, D'Agostino H, et al: Transvaginal drainage of pelvic fluid collections. Semin Intervent Radiol 1992; 9:152–158.
99. Wroblicka JT, Kuligowska E: One-step needle aspiration and lavage for the treatment of abdominal and pelvic abscesses. AJR 1998; 170:1197–1203.

Intraperitoneal Spread of Malignancies

4

The spread of neoplasms within the peritoneal cavity occurs by direct invasion, intraperitoneal seeding, embolic metastases, and lymphatic extension.[1,2] Recent insights and basic correlation with the pathogenesis of the intraabdominal spread of malignancies have established that the *pattern* of involvement and the individual effects of secondary malignancies of the bowel often present characteristic radiologic features. [1,3–6] These reflect the mode of dissemination and thereby indicate the primary site. They are based on the application of certain gross anatomic relationships, the dynamic factors of the flow of ascites, and conditions of hematogenous dissemination.

Distinction between the major pathways of spread (Table 4–1) is of critical practical importance for several reasons: (a) It closely correlates the radiologic changes with the pathogenesis and provides a rational system for radiologic analysis, (b) Since it is not rare for a malignant neoplasm to be manifested initially by its gastrointestinal metastasis or extension,[7] recognition of the *type* of secondary involvement can aid in the search for the primary lesion. Confronted with a lesion of the bowel that can be identified as secondary in nature, the clinical radiologist is then in a crucial position—by recognizing the particular mode of dissemination—to determine the further investigation required in the search for the primary lesion. (c) If there is a known primary tumor and gastrointestinal symptomatology develops, particular radiologic attention can be directed to the most likely sites in the abdomen for that type of lesion. In a patient with either a known or clinically occult primary malignancy, only nonspecific abdominal symptomatology may herald the development of intraperitoneal metastases. Not infrequently, these are attributed to other gastrointestinal disorders or perhaps to the side effects of chemotherapeutic drugs. (d) Identification of the type of secondary involvement of the bowel can help in planning treatment. Awareness that involvement of a portion of the alimentary tract is secondary to invasion from an adjacent primary tumor allows for adequate preoperative preparation for wider surgical excision. Localized embolic metastases are subject to segmental resection.[7,8] Radiotherapy and chemotherapy may be reserved for disseminated metastases or implants.

Table 4-1. Classification of Pathways of Spread of Secondary Neoplasms to the Bowel

Direct invasion
From noncontiguous primary tumors
Along mesenteric reflections
By lymphatic permeation
From contiguous primary tumors
Intraperitoneal seeding
Embolic metastases

Analysis of a large proved series[1] has demonstrated that each of the three major pathways of spread (direct invasion, seeding, and hematogenous metastases) accounts for roughly an equal number of cases of secondary neoplastic involvement of the bowel. Occasionally, more than one mechanism of spread may be encountered in any given patient. This is seen most frequently in intraperitoneal primary malignancies with both direct invasion and seeded metastases.

Direct Invasion from Noncontiguous Primary Tumors

Invasion Along Mesenteric Reflections

The mesenteric reflections provide an important natural pathway for extension of primary neoplasms to other sites that may not be in actual contiguity.[1,9]

In the upper abdomen, peritoneal reflections constitute nine major ligaments and mesenteries that provide continuity of anatomic planes for the spread of malignancies (Figs. 4–1 and 4–2; Table 4–2). These not only connect intraperitoneal sites, but also extend between intraperitoneal and extraperitoneal sites.[9–12] Neither the mesenteries nor the ligaments should be thought of as veil-like membranes but rather as connective tissue-laden peritoneal reflections of often considerable substance. The areolar tissue within these planes contains lymphatics accompanying blood vessels so that this interconnecting abdominal network provides discrete pathways of spread of disease. The sites of lymph node metastases from gastric carcinoma, for example, have been meticulously analyzed (Fig. 4–3). Yet, it is apparent that these lymphatics and draining nodal groups constitute an architecture, for the most part, within identifi-

Table 4-2. Major Upper Abdominal Peritoneal Reflections

Gastrohepatic ligament
Hepatoduodenal ligament
Gastrocolic ligament
Transverse mesocolon
Duodenocolic ligament
Gastrosplenic ligament
Splenorenal ligament
Phrenicocolic ligament
Small bowel mesentery

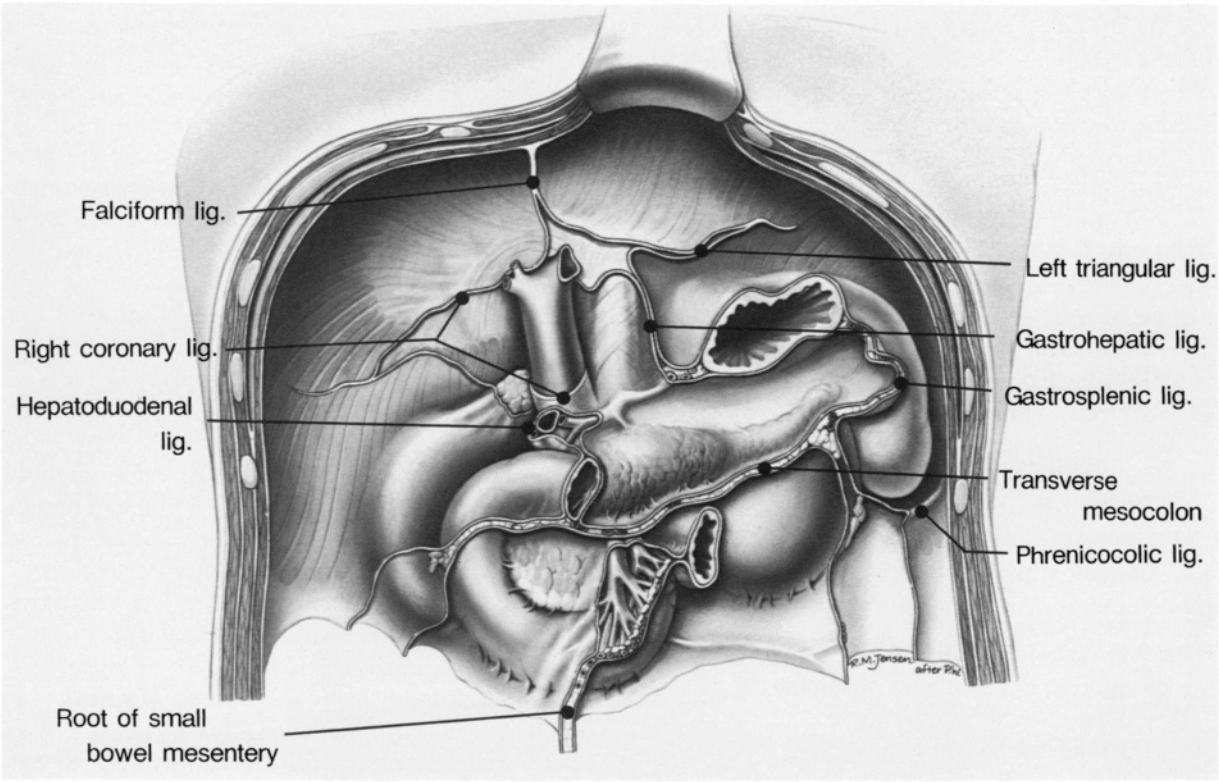


Fig. 4–1. Peritoneal ligaments and mesenteries.
Drawing of the posterior parietal wall of the upper abdomen showing the planes of peritoneal reflections constituting the major ligaments and mesenteries. Anatomic continuity is established along the "bare areas" at the roots of origin between intraperitoneal structures and between extraperitoneal and intraperitoneal sites.
(Reproduced from Meyers et al.[9])

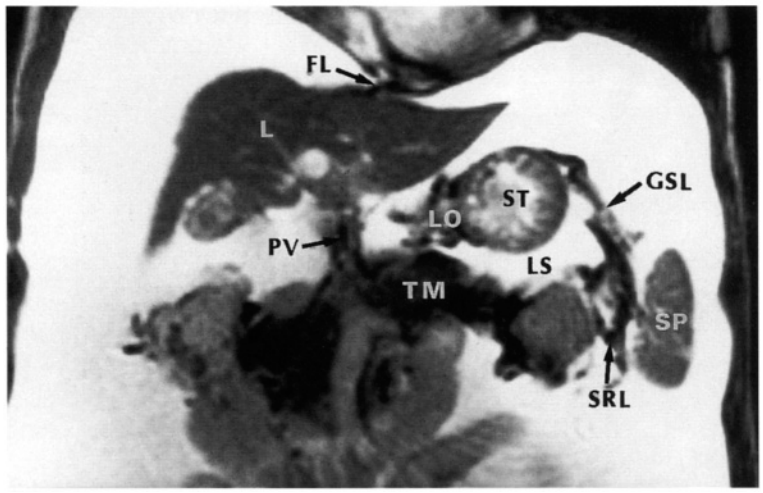


Fig. 4–2. Major mesenteric reflections in the upper abdomen, shown on coronal MR image.
Abdominal organs, mesenteries, and ligaments are floating in a large amount of ascites. The falciform ligament (*FL*) attaches the liver (*L*) superiorly. The portal vein (*PV*) courses within the hepatoduodenal ligament. Further demarcation of the lesser sac (*LS*) is provided by the lesser omentum (*LO*), stomach (*ST*), gastrosplenic (*GSL*), and splenoral (*SRL*) ligaments as they are related to the spleen (*SP*) and the transverse mesocolon (*TM*).
(Reproduced from Auh et al.[10])

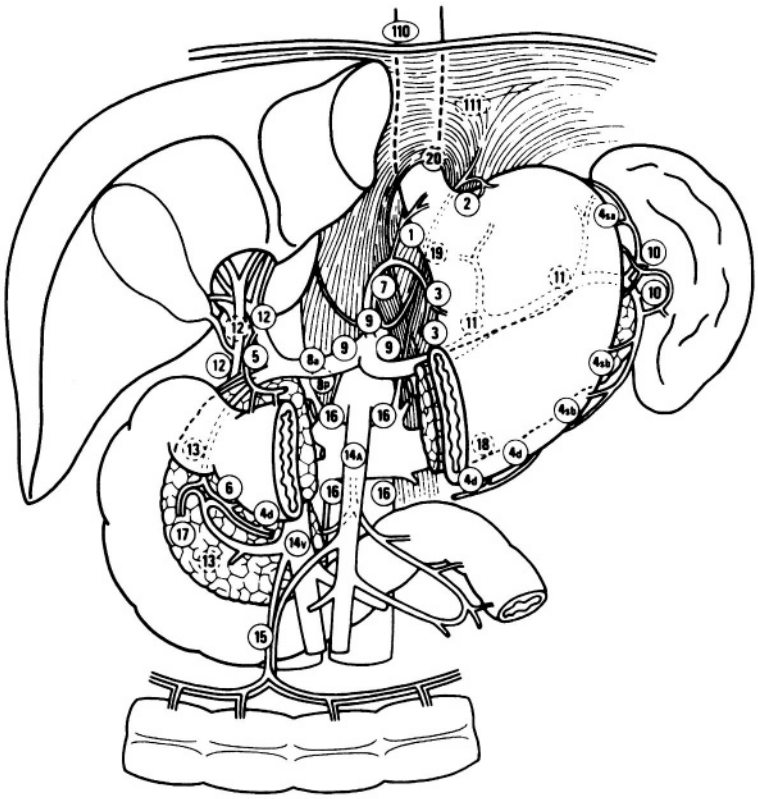


Fig. 4–3. Lymph node stations in gastric cancer as classified by the Japanese Research Society for Gastric Cancer.
Involvement of nodes along the lesser or greater curvature (groups *1–6*) constitutes N1 disease, and the celiac axis and its three branches are N2 (*7–11*), N3 (*12–14*), and N4 (*15,16*). N1: *1* = right paracardial; *2* = left paracardial; *3* = lesser curvature; *4* = greater curvature; *5* = suprapyloric; *6* = infrapyloric. N2: *7* = left gastric artery; *8* = common hepatic artery; *9* = celiac artery; *10* = splenic hilus; *11* = splenic artery. N3: *12* = hepatic pedicle; *13* = retropancreatic; *14* = mesenteric root. N4: *15* = middle colic artery; *16* = paraaortic.
(Data from Japanese Research Society for Gastric Cancer. Japanese Classification of Gastric Carcinoma: General Rules for the Gastric Cancer Study. Tokyo, Kanehara, 1995, pp 1–104.)

able peritoneal reflections. The ligaments and mesenteries are generally readily recognizable on CT and MRI by either their typical location and organ relationships or the landmarks provided by their major constituent vessels.

Gastrohepatic Ligament and Hepatoduodenal Ligament

The lesser omentum is subdivided into the gastrohepatic ligament and the hepatoduodenal ligament. The gastrohepatic ligament extends between the lesser curvature of the stomach and the liver, attached in its upper portion deep within the fissure for the ligamentum venosum and more inferiorly with the porta hepatis. The subperitoneal areolar tissue of the gastrohepatic ligament continues into the liver as Glisson's capsule.[13] The ligament is generally wedge-shaped and contains considerable adipose tissue, through which course the left gastric artery, coronary vein, and the left gastric nodal chain[14] (Fig. 4–4). Identification of the fissure for the ligamentum venosum immediately inferior to the esophagogastric junction determines the CT sections in which the gastrohepatic ligament is readily evident.[14]

The free edge of the gastrohepatic ligament is known as the hepatoduodenal ligament, extending from the flexure between the first and second portions of the duodenum to the porta hepatis and transporting the portal triad. After the common hepatic artery gives off its gastroduodenal branch, the proper hepatic artery courses within the hepatoduodenal ligament anterior to the portal vein in most patients. The common bile duct also lies anterior to the portal vein, but is located lateral to the proper hepatic artery[15–17] (Figs. 4–5 and 4–6). A fibrofatty sheath of tissue invaginates the liver parenchyma from the porta hepatis and continues along the course of the portal vein, hepatic artery, and bile duct branches. It is thus evident that this "edge" is in truth a structure

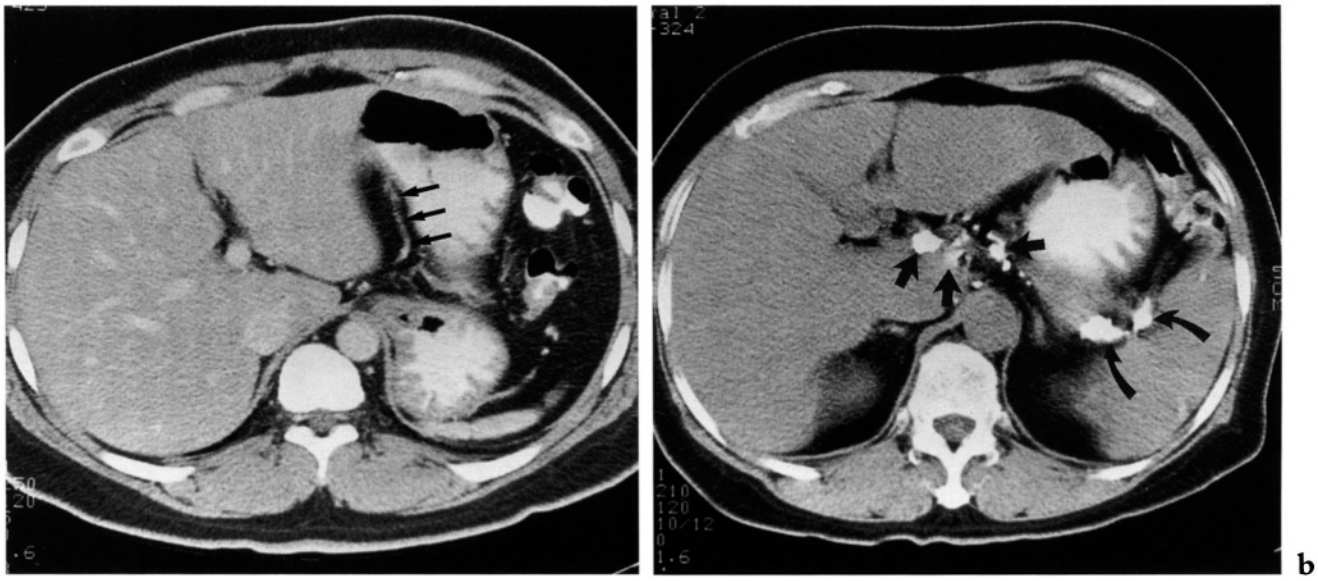
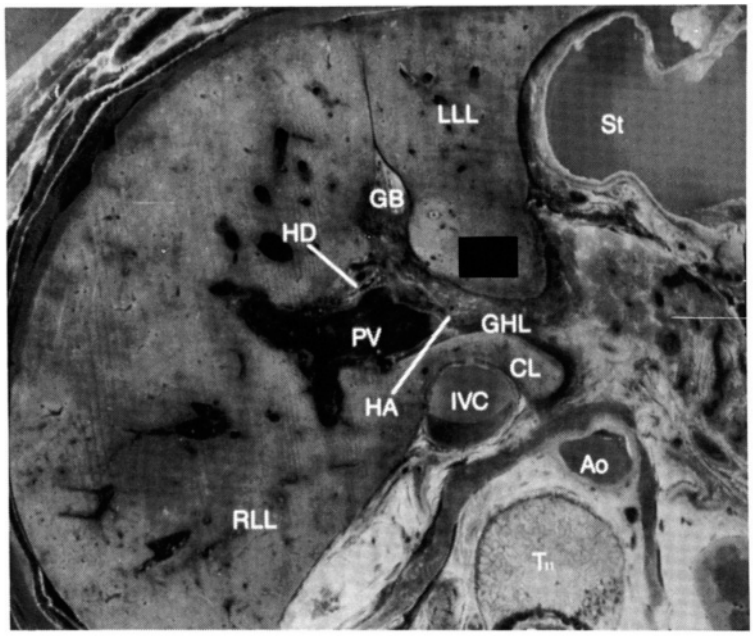
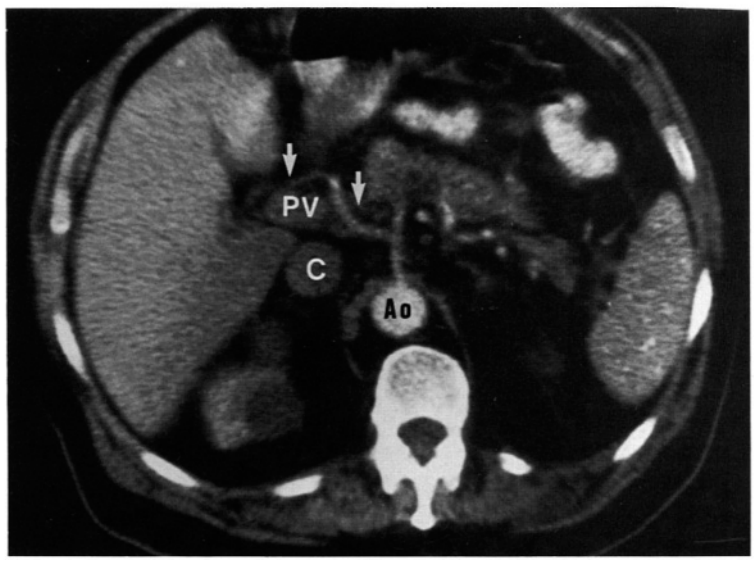


Fig. 4–4. The gastrohepatic, hepatoduodenal, and gastrosplenic ligaments.
(a) The gastrohepatic ligament occupies the wedge-shaped area between the opacified stomach and the liver. The left gastric artery (*arrows*) as well as the coronary vein and accompanying lymphatics course through it. Posteriorly, the ligament inserts in relationship to the bulbous enlargement of the right diaphragmatic crus. At this level, it continues into the fissure for the ligamentum venosum.
(b) In another patient, multiple calcified lymph nodes (*arrows*), presumably from previous tuberculous infection of the abdomen, are localized in the hepatoduodenal ligament. Here, the ligament continues into the porta hepatis, also known as the transverse fissure of the liver. The gastrosplenic ligament is designated by the fatty tissue between the greater curvature of the stomach and the medial contour of the spleen. Another calcified nodal group (*curved arrows*) is seen in the splenorenal ligament.



a



b

Fig. 4–5. The hepatoduodenal ligament.
(a) Anatomic cross-section demonstrates the relationships of the portal triad within the hepatoduodenal ligament at its insertion in the liver. *HA* = hepatic artery; *PV* = portal vein; *HD* = hepatic duct; *RLL* = right lobe of the liver; *LLL* = left lobe of the liver; *CL* = caudate lobe; *GHL* = gastrohepatic ligament; *GB* = gallbladder; *Ao* = aorta; *IVC* = inferior vena cava.
(b) CT scan. The opacified hepatic artery (*arrows*) passes anteriorly to the portal vein (*PV*) as both structures, accompanied by the bile duct, course within the hepatoduodenal ligament. Immediately behind its free edge resides the epiploic foramen of Winslow, deep to which is the inferior vena cava (*C*). Right renal cysts are incidentally present. *Ao* = aorta.
(Reproduced from Meyers et al.[9])

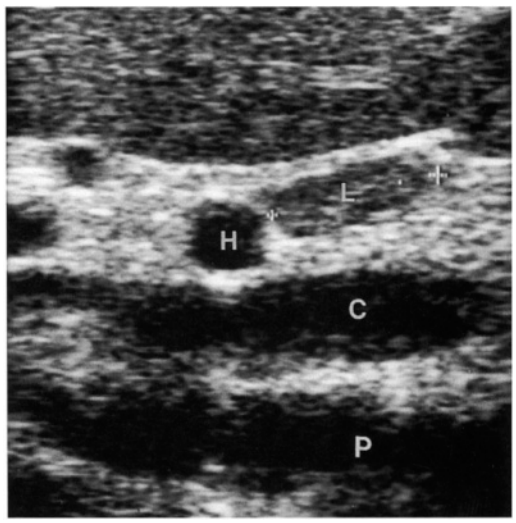


Fig. 4–6. Contents and relationships of hepatoduodenal ligament shown by laparoscopic ultrasonography.
Longitudinal scan of the hepatoduodenal ligament through the liver shows the course and relationships of the portal vein (*P*), common bile duct (*C*), and hepatic artery (*H*). A lymph node (*L*) is adjacent to the hepatic artery. Its benign nature is indicated by its longitudinal shape and echogenicity.
(Reproduced from van Delden et al.[17])

of considerable thickness. Immediately behind it is the epiploic foramen of Winslow leading into the lesser sac.

On CT, identification of the sites of the left gastric artery and the hepatic artery permits precise localization of disease spread to the gastrohepatic and hepatoduodenal ligaments, respectively.

An exception to be noted in these relationships is the variant of an aberrant right hepatic artery that passes dorsal to the portal vein and ventral to the inferior vena cava just medial to the hilus of the liver[18,19] (Fig. 4–7). This variant is to be distinguished from nodes of the foramen of Winslow, or portacaval space, which have an unusual morphology in that their transverse dimension is greater than their anteroposterior dimension[20,21] (Figs. 4–8 and 4–9). Moreover, the medial papillary process of the caudate lobe of the liver, separated by a groove of variable depth from the lateral caudate process, can appear separate from the liver on transverse sections as it protrudes into the portacaval space (Fig. 4–10) and be mistaken for portacaval lymph nodes[20–23] (Fig. 4–11).

Although the lymphatics of the gastrohepatic ligament are frequent sites of metastases in cases of carcinoma of the stomach, distal esophagus, pancreas, breast, and lung, they also may give rise to lymphoma. Discrete

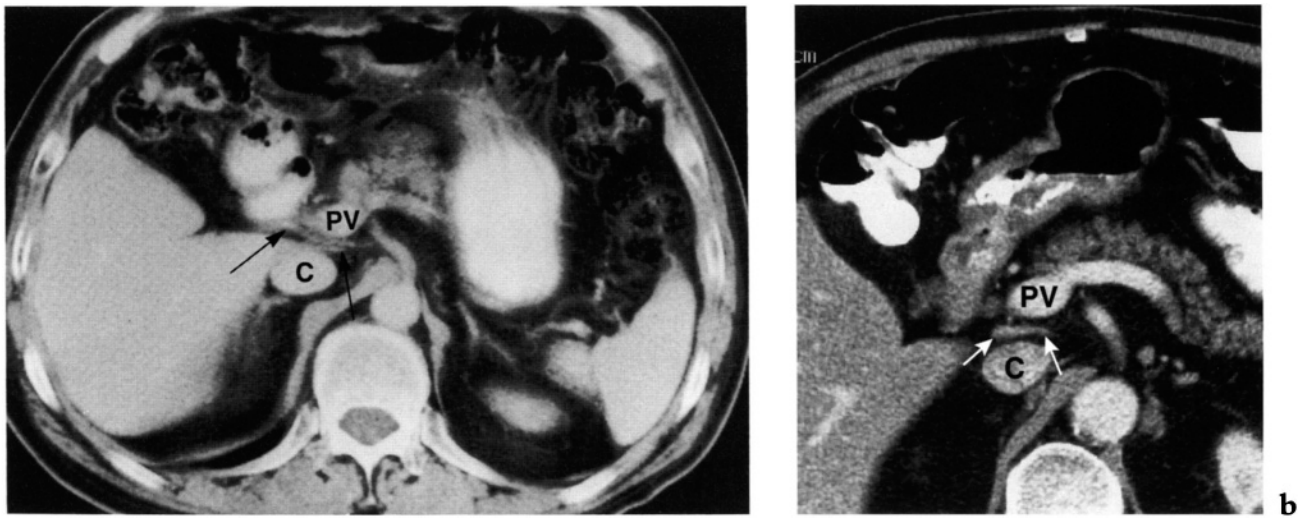


Fig. 4–7. Course and relationships of an aberrant right hepatic artery.
(a and **b)** Contrast-enhanced CT scans in two different cases demonstrate the aberrant right hepatic artery (*arrows*) passing between the portal vein (*PV*) and inferior vena cava (*C*).

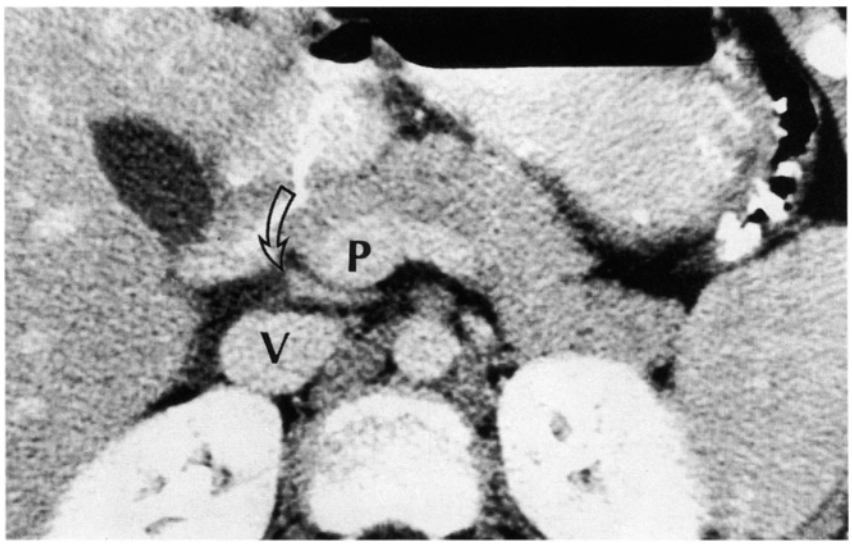


Fig. 4–8. Normal portacaval lymph node.
Contrast-enhanced CT shows a discoid shape of normal-sized node (*arrow*) between the portal vein (*P*) and inferior vena cava (*V*). Some ascites along the course of the foramen of Winslow is seen immediately anterior to this node in this patient with liver cirrhosis.
(Reproduced from Auh and Ha.[21])

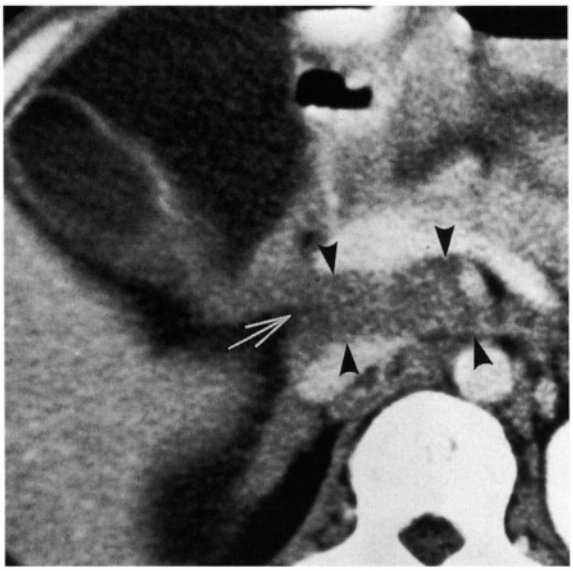


Fig. 4–9. Portacaval lymphadenopathy secondary to lymphoma.
Contrast-enhanced CT shows rectangular shape of enlarged nodes (*arrowheads*) in the portacaval space. A crevice (*arrow*) resulting from fluid collection in the region of the foramen of Winslow may separate a node originating from the hepatoduodenal ligament from that of the paraaortic space. (Reproduced from Auh and Ha.[21])

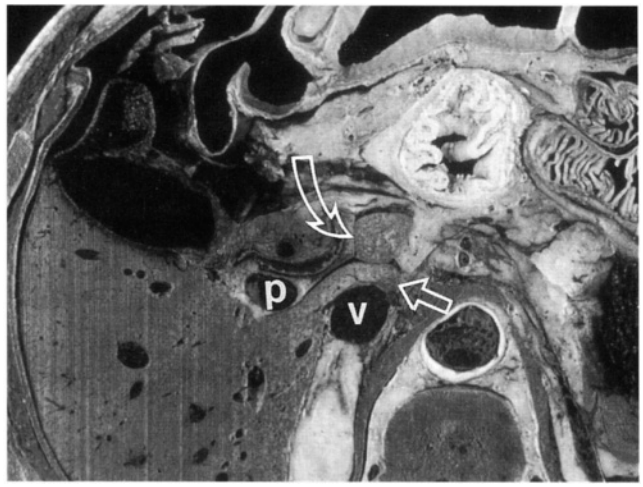


Fig. 4–10. Papillary process simulates enlarged portacaval node.
Anatomic cross-section shows the papillary process (*curved arrow*), separate from the caudate process (*straight arrow*), protruding into the portacaval space, where it ends with a bulbous contour and mimics an enlarged lymph node. *p* = portal vein, *v* = inferior vena cava.
(Reproduced from Auh and Ha.[21])

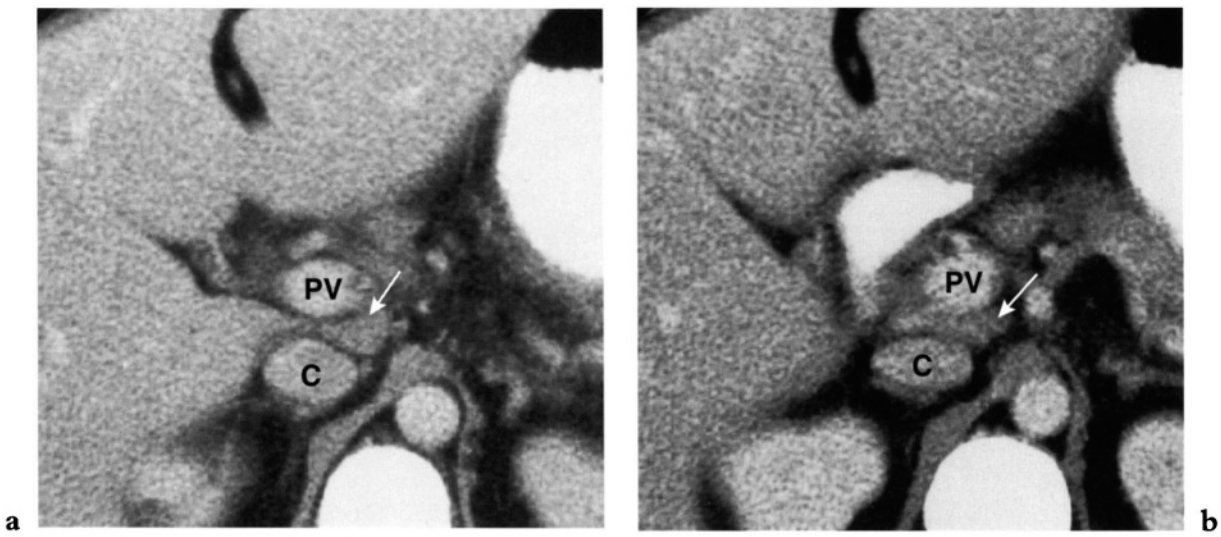


Fig. 4–11. Papillary process of the caudate lobe.
(a and **b)** On contiguous CT scans, the papillary process (*arrow*) appears separate from the liver and presents an appearance mimicking lymph nodes.

nodal enlargement may be identifiable or there may be gross mass involvement expanding the area, separating the stomach and liver, and resulting in organ distortion (Figs. 4–12 and 4–13).

The upper portion of the stomach and the left lobe of the liver bear an intimate relationship connected by the gastrohepatic ligament, the areolar tissue of which is continuous with that constituting Glisson's capsule and its intrahepatic perivascular extensions. This brief pathway permits invasion of the left hepatic lobe by carcinoma of the fundus and pars media of the stomach. The CT findings in such cases include loss of the fat plane and consequent lack of a definite boundary between the two organs[25] (Figs. 4–14 through 4–16). In MR imaging, the extent of hepatic invasion is apparent during the early phase[27] (Fig. 4–17).

Rarely, intraperitoneal involvement of the gastrohepatic ligament can be mimicked by anterior extension of a retroperitoneal process, most commonly pancreatic carcinoma.[28]



Fig. 4–12. Nodal metastases within the gastrohepatic ligament.
Extensive spread of tumor to nodes (*N*) in the gastrohepatic ligament from a carcinoma of the gastric antrum. There is also tumor in the porta hepatis (*arrow*) transmitted by the hepatoduodenal ligament and ascites (*A*). (Reproduced from Gore and Meyers.[24])



Fig. 4–13. Nodal mass within the gastrohepatic ligament.
Lymphomatous mass (*M*) occupies the wedge-shaped site of the gastrohepatic ligament, mildly separating the stomach and the liver.

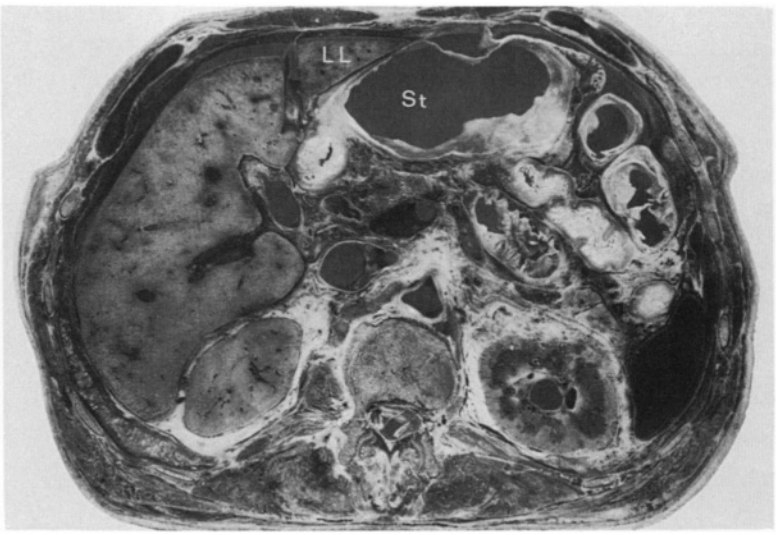


Fig. 4–14. Anatomic cross-section demonstrates the intimate relationship of the stomach (*St*) and the left lobe of the liver (*LL*).
The upper portion of the gastrohepatic ligament extends from the lesser curvature of the stomach to the fissure for the ligamentum venosum. Its areolar tissue is continuous with Glisson's capsule.

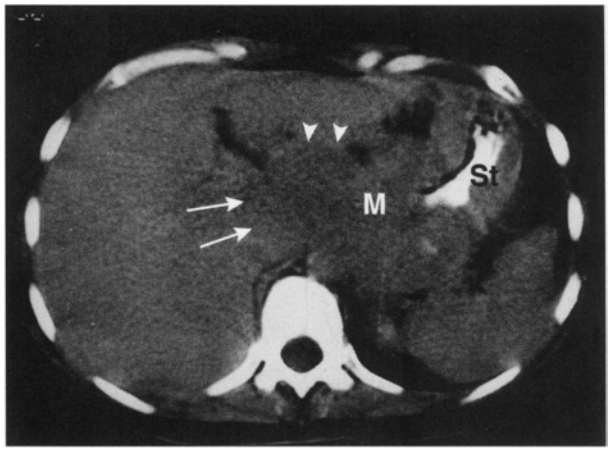


Fig. 4–16. Direct extension of gastric carcinoma to liver.
In a patient with diffusely infiltrating carcinoma of the stomach (*St*), CT demonstrates the tumor mass (*M*) invades the gastrohepatic ligament, penetrates the fissure for the ligamentum venosum, and invades the left hepatic lobe *(arrowheads)* and the caudate lobe (*arrows*). (Reproduced from Arenas et al.[26])

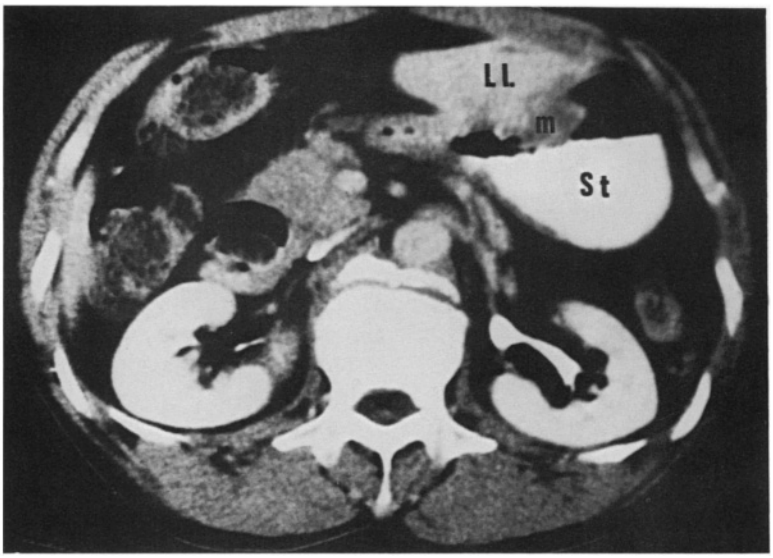


Fig. 4–15. Hepatic invasion across the gastrohepatic ligament.
CT in a patient with an infiltrating polypoid carcinoma of the stomach (*St*), shown as a soft-tissue mass (*m*) projecting into its lumen, demonstrates direct invasion of the overlying left lobe of the liver (*LL*). (Reproduced from Meyers et al.[9])



Fig. 4–17. Hepatic invasion by advanced gastric carcinoma.
Early-phase of dynamic MR imaging demonstrates marked enhancement of invasion of the liver (*arrow*) across the gastrohepatic ligament by a cancer of the stomach.
(Reproduced from Oi et al.[27])

The hepatoduodenal ligament, when thickened, may be seen directly on CT coursing from its intraperitoneal relationships to its extraperitoneal insertion (Fig. 4–18). The portal structures pass into the retroperitoneum through the hepatoduodenal ligament. Lymphadenopathy is readily identifiable by CT[15,29–33] (Fig. 4–19) and by ultrasonography[31,34–36] (Fig. 4–20). Malignant invasions may be further indicated by the demonstration of prominent collateral vessels (Figs. 4–20 and 4–21). Lymphatic drainage from the gallbladder is initially to cystic and common bile duct nodes, then into the pancreaticoduodenal system with later potential spread into the rest of the celiac axis or aortic nodes.[37–40]

Gastrocolic Ligament

The gastrocolic ligament extends inferiorly from the greater curvature of the stomach to suspend the transverse colon and is traversed by the gastroepiploic vessels (Fig. 4–22). It inserts in relationship to the taenia omentalis, and injection studies and clinical observations have documented that spread of gastric lesions down the gas-

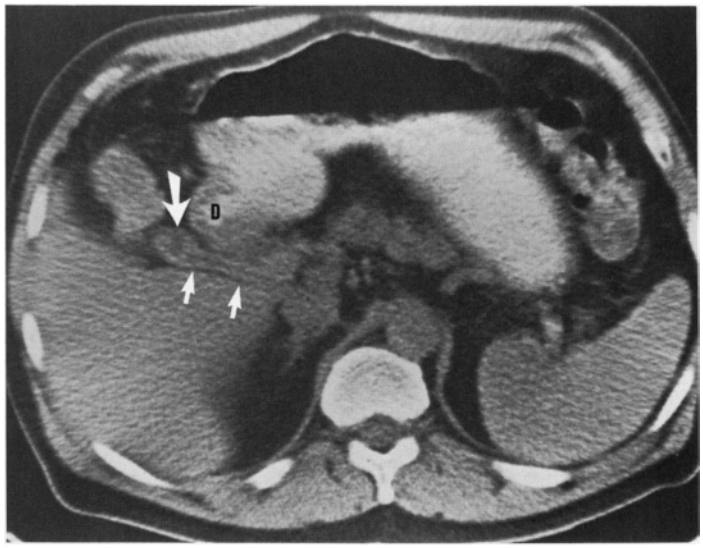


Fig. 4–18. Inflammatory thickening of the hepatoduodenal ligament.
Secondary to a penetrating postbulbar duodenal ulcer with obstructive jaundice, there is mural thickening of the duodenum (*D*) and inflammatory thickening of the hepatoduodenal ligament (*small arrows*), which contains the dilated common bile duct (*large arrow*).
(Reproduced from Meyers et al.[9])

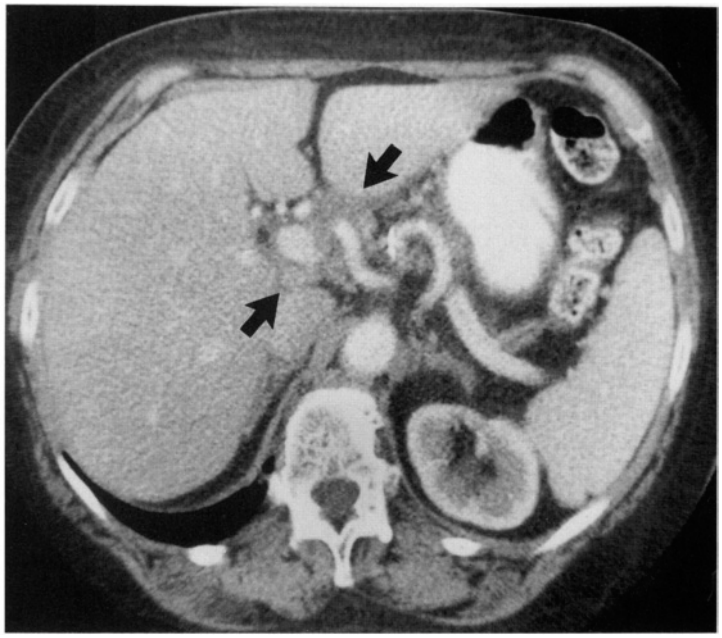


Fig. 4–19. Nodal metastases in the hepatoduodenal ligament from carcinoma of the head of the pancreas.
The pancreatic carcinoma has spread around the hepatic artery and portal vein along the hepatoduodenal ligament to the porta hepatis (*arrows*).

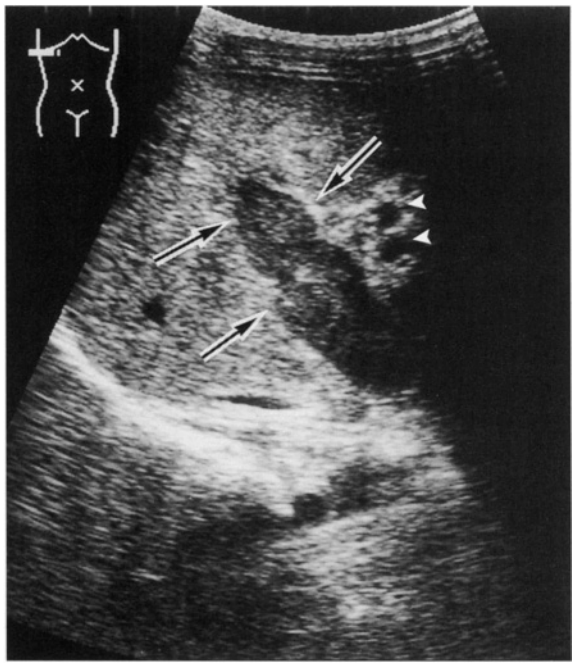


Fig. 4–20. Lymphomatous involvement of the portal vein and hepatoduodenal ligament.
Ultrasonography demonstrates mixed hypo- and hyperechoic mass along the hepatoduodenal ligament (*arrows*). Note the collateral pathways (*arrowheads*). (Reproduced from Fukuda T, et al: Radiologic imaging of perihepatic ligament. Jpn J Diagn Imaging 1997, 17:245–247.)

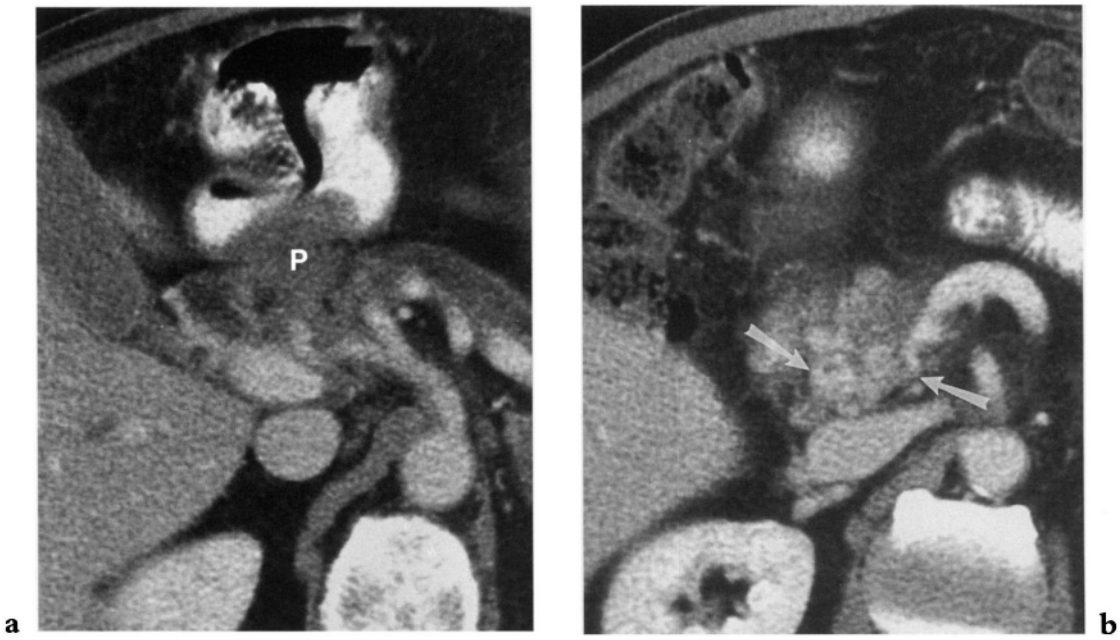


Fig. 4–21. Cavernous transformation of the portal vein within the hepatoduodenal ligament secondary to pancreatic carcinoma.
(a) A carcinoma arising from the neck of the pancreas (*P*) invades the hepatoduodenal ligament as well as the gastric antrum and first portion of the duodenum.
(b) The portal vein, superior mesenteric vein, and splenic vein are also encased by tumor at their confluence with prominent venous collaterals (cavernous transformation of the portal vein) seen as brightly enhancing veins (*arrows*) within the hepatoduodenal ligament.
(Courtesy of James Brink, M.D., Yale University School of Medicine, New Haven, CT.)

trocolic ligament involves first and predominantly the superior haustral row of the transverse colon[1,5,41,42] (Fig. 4–23), with highly characteristic changes on barium enema study. The wall becomes fixed and straightened, with selective loss of the contour of the haustral sacculations and most characteristically, the mucosal folds are conspicuously tethered (Figs. 4–24 through 26). The term "tethering" is used to indicate that the mucosal folds lose their parallel orientation to each other, and their axes, which are normally perpendicular to the lu-

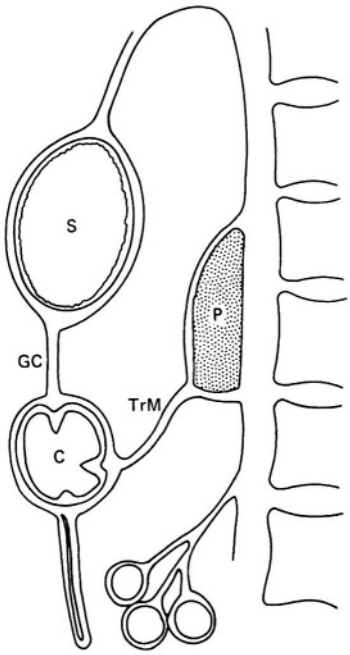


Fig. 4–22. Sagittal section showing the mesenteric reflections to the transverse colon (*C*) from the stomach (*S*) and the pancreas (*P*).
Note that the gastrocolic ligament (*GC*) inserts superiorly and the transverse mesocolon *(TrM)* posteroinferiorly.
(Reproduced from Meyers and McSweeney.[1])

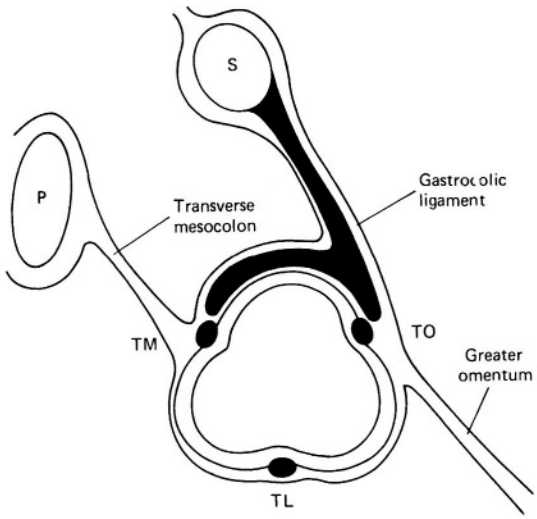


Fig. 4–23. Sagittal section through the transverse colon, demarcated into its three constituent haustral rows by the taenia omentalis (*TO*), taenia mesocolica (*TM*), and taenia libera (*TL*).
Extension of a malignancy from the stomach (*S*) through the gastrocolic ligament spreads preferentially to the TM–TO haustral row. This constitutes the superior border of the transverse colon. *P* = pancreas.
(Reproduced from Meyers et al.[42])

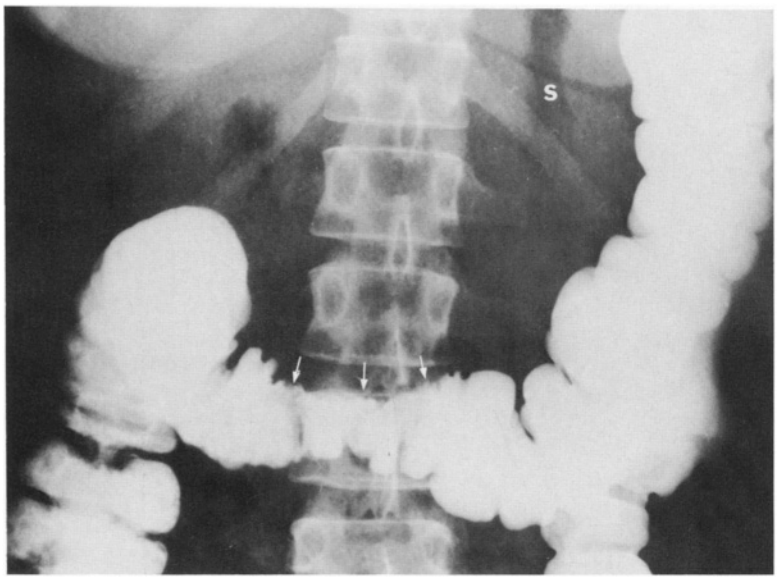


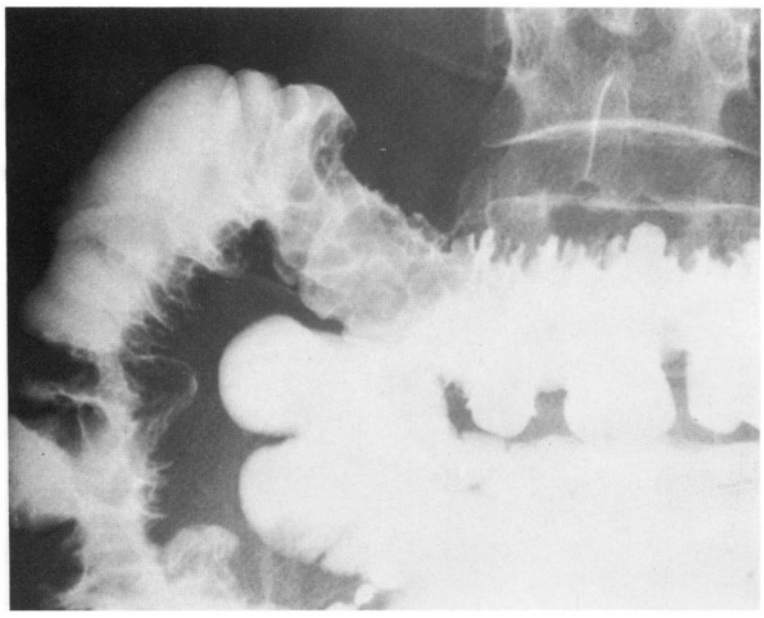
Fig. 4–24. Direct invasion of the transverse colon along the gastrocolic ligament from a scirrhous carcinoma of the stomach (*S*).
There is fixation and angulation of the mucosal folds along the superior contour *(arrows)* involving the TM–TO haustral row. The fixation results in pseudosaccular outpouchings from the uninvolved haustral row on the inferior border.
(Reproduced from Meyers and McSweeney.[1])



Fig. 4–25. Carcinoma of the stomach extending down the gastrocolic ligament involves first the *TM–TO* row on the superior contour of the transverse colon (*arrowheads*). Nodular irregularities are associated with tethering of the mucosal folds.
(Reproduced from Meyers et al.[42])



a



b

Fig. 4–26. Gastric carcinoma spreading down the gastrocolic ligament.
(a) Fixation and mucosal tethering along the entire superior border of the transverse colon. Prominent haustral pseudosacculations project from the uninvolved inferior contour.
(b) Spot film of hepatic flexure shows the appearance of cobblestone linear and transverse ulcers.

men of the bowel, become randomly angulated. This change reflects the associated desmoplastic reaction within the gastrocolic ligament itself, acting in effect as a mass of adhesions. The uninvolved haustral contours of the inferior border of the transverse colon retain their pliability and are thrown into pseudosacculations (Figs. 4–25 and 4–26). Further distortion and fixed buckling of the mucosal pattern may occasionally produce the appearance of cobblestone linear and transverse ulcers (Fig. 4–26). The primary gastric carcinomas are usually scirrhous in nature and are frequently clinically occult. It is said that glandular adenocarcinomas spread mainly in the mucosa and submucosa with little serosal spread, whereas scirrhous carcinomas spread in submucosa and muscle coats, probably via lymphatics.[8] The incidence of involvement of the gastrocolic ligament is over 90% once the cancer reaches the serosa.[43] Initially, the complex of these features on a barium enema examination may be mistaken for an intrinsic inflammatory process, such as granulomatous colitis,[44] since the processes share several pathologic and roentgenographic characteristics. These include unilateral mural involvement, nodular irregularities, pseudosaccular outpouchings, and the occasional appearance of ulcerations. However, the localization specifically to the superior border of the transverse colon and the identification of the tethered mucosal folds, a change not seen in granulomatous colitis, readily lead to the correct diagnosis.

A similar appearance may uncommonly be the result of seeded metastases on the gastrocolic ligaments,[45] but this is almost invariably accompanied by contiguous changes upon the greater curvature of the stomach and characteristic changes at other seeded sites.[46]

Even with extensive circumferential invasion, the greater degree of involvement with fixation and angulation of mucosal folds and mass effects tends to be maintained on the superior contour (Figs. 4–27 and 4–28.)

Computed tomography particularly, and more recently magnetic resonance imaging,[47] documents that gastric carcinoma may extend into the ligament only partially, although certainly a sign of extramural spread, to perhaps only indent the underlying colon (Fig. 4–29), or may spread down its length to invade the upper haustral contour clearly (Fig. 4–30), or progress to an-

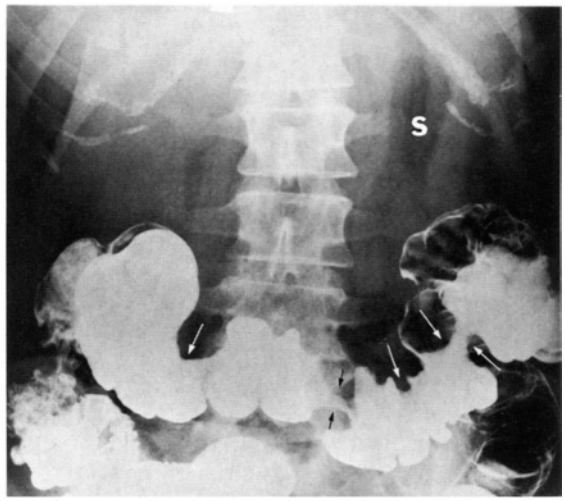


Fig. 4–27. Circumferential invasion of the transverse colon from a scirrhous carcinoma of the stomach (*S*). The nodular masses (*arrows*) remain predominant on the superior contour.

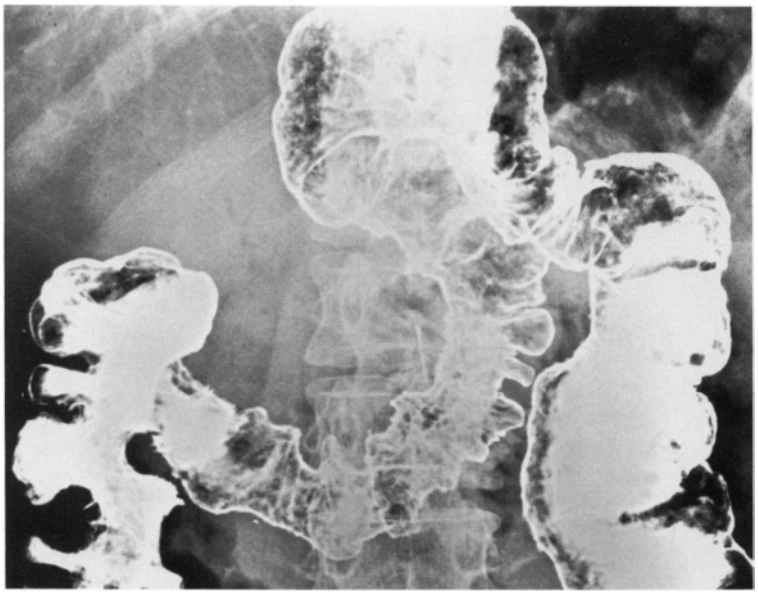


Fig. 4–28. Annular invasion of the transverse colon from gastric carcinoma. Double-contrast study shows nodular masses and infiltration predominate on the superior contour.
(Reproduced from Gore and Meyers.[24])

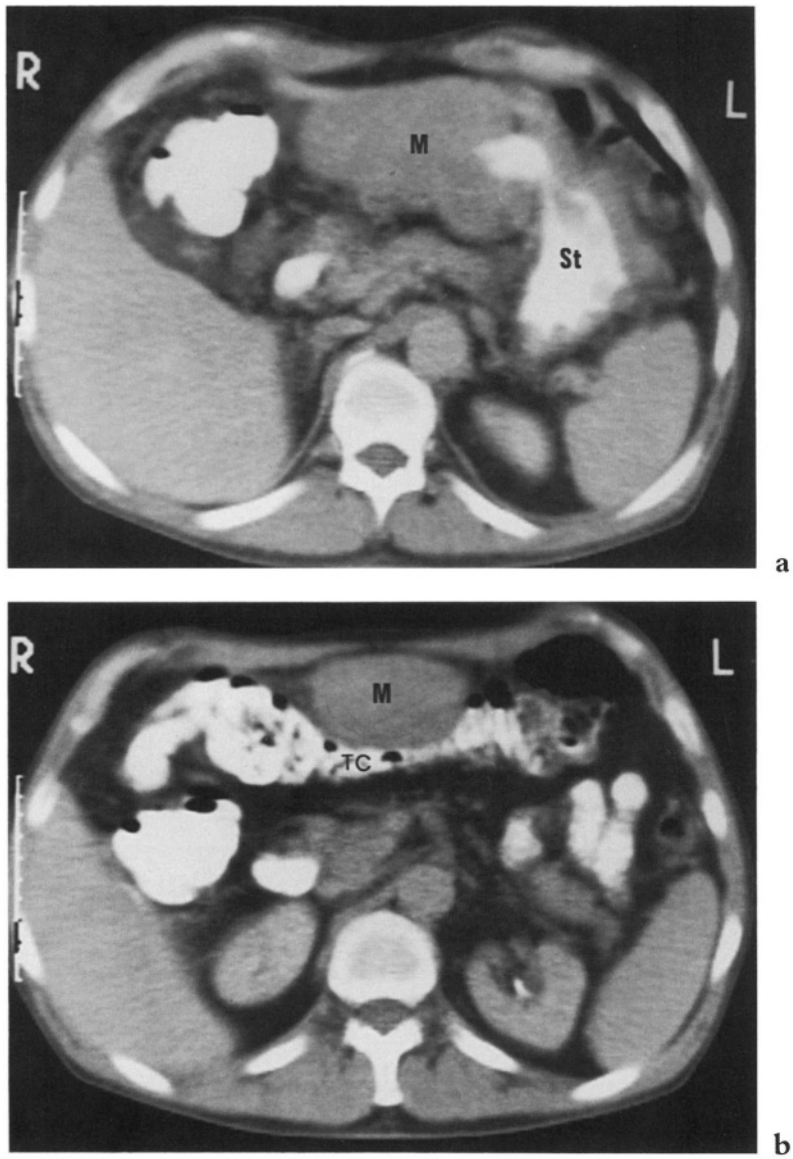


Fig. 4–29. Extension of gastric carcinoma along gastrocolic ligament.
(a) A large mass (*M*) representing carcinoma extends from the stomach (*St*).
(b) The mass extends inferiorly within the gastrocolic ligament to displace and compress the transverse colon (*TC*).
(Reproduced from Meyers et al.[9])

nular involvement of the transverse colon (Figs. 4–31 through 4–33).

The limit of anatomic continuity of the mesenteric reflections toward the left is at the level of the phrenicocolic ligament,[48] which extends from the anatomic splenic flexure to the diaphragm. At this point, the mesenteric transverse colon continues as the extraperitoneal descending colon. Spread of the process thus typically ends abruptly at the anatomic splenic flexure of the colon, just below the tip of the spleen (Figs. 4–34 through 4–36). A mass may further develop within the phrenicocolic ligament itself (Fig. 4–37).

As evidence of the "two-way street" provided by the ligament, carcinoma of the transverse colon can extend superiorly to involve the greater curvature of the stomach[49] (Fig. 4–38). Further invasion may result in a malignant gastrocolic fistula (Fig. 4–39).

Ultrasonography and computed tomography may show not only abnormal mural thickening but also the intraabdominal tumor extension.[50–54] These modalities further refine capabilities in staging tumors, assessing surgical resectability, evaluating tumor response, and detecting postoperative recurrence.

text continues on page 152

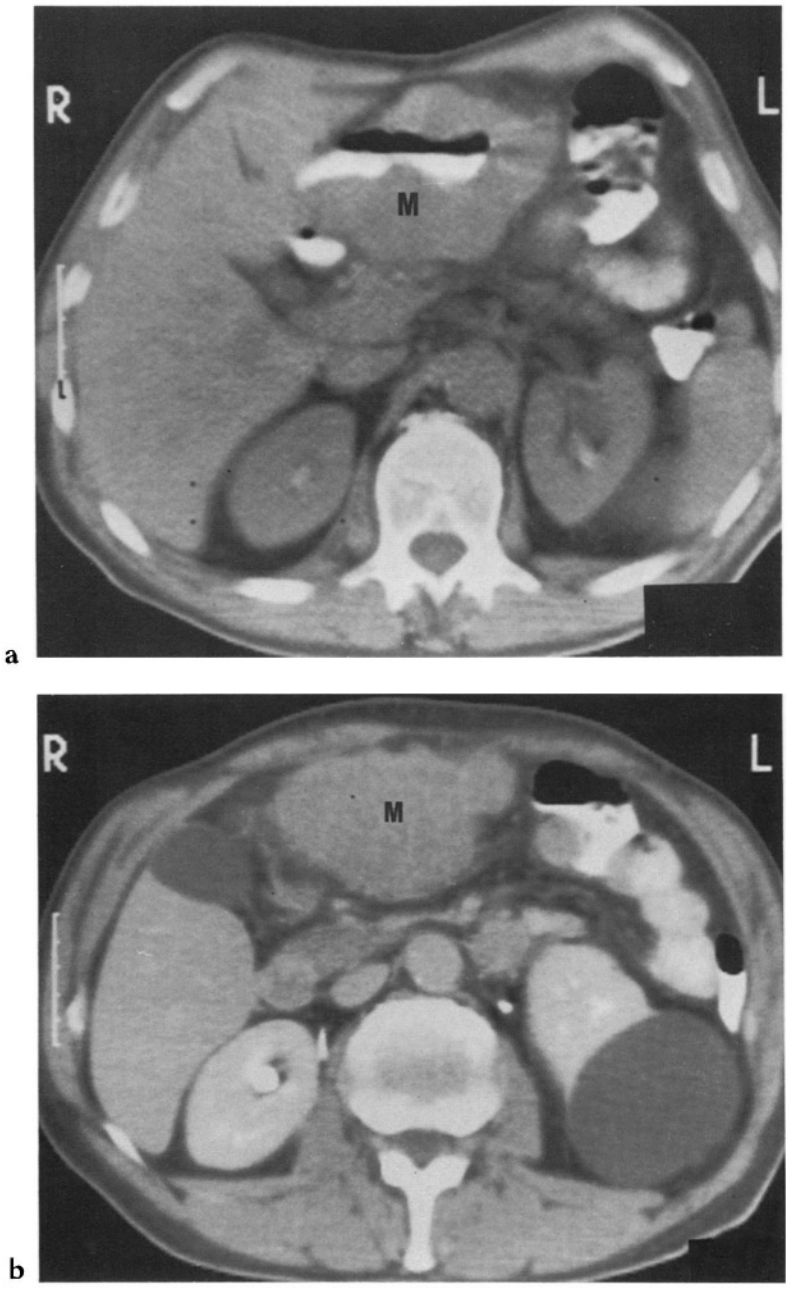
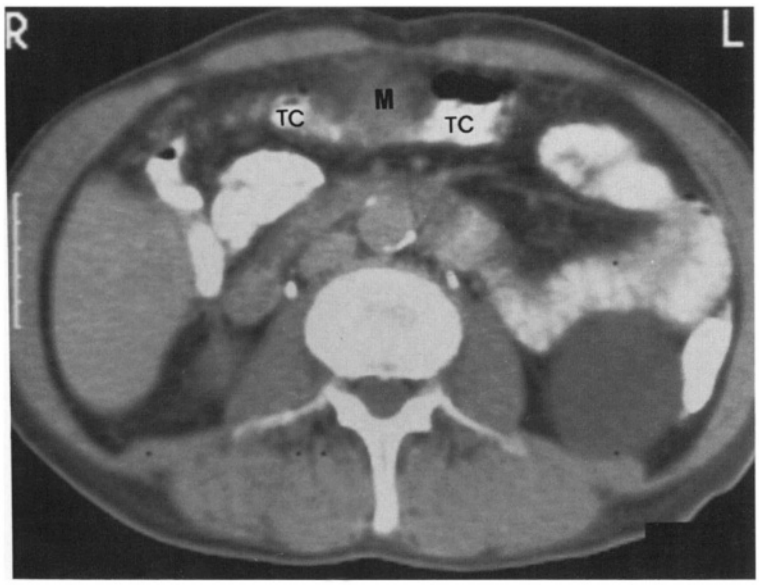
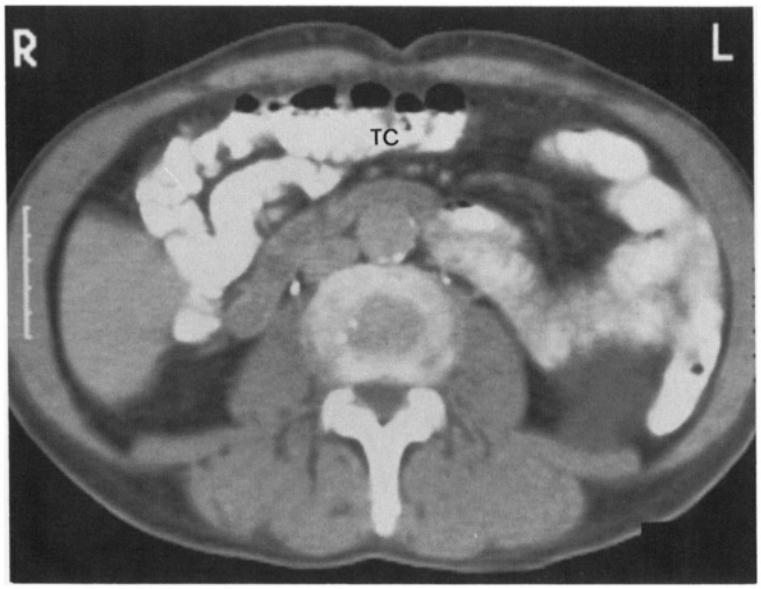


Fig. 4–30. Extension of gastric carcinoma along gastrocolic ligament to the transverse colon with involvement of the upper haustral row.
(a) A prominent mass (*M*) representing an annular carcinoma compresses the gastric lumen.
(b) The mass extends inferiorly into the gastrocolic ligament. An incidental left renal cyst is noted.
(Continued)

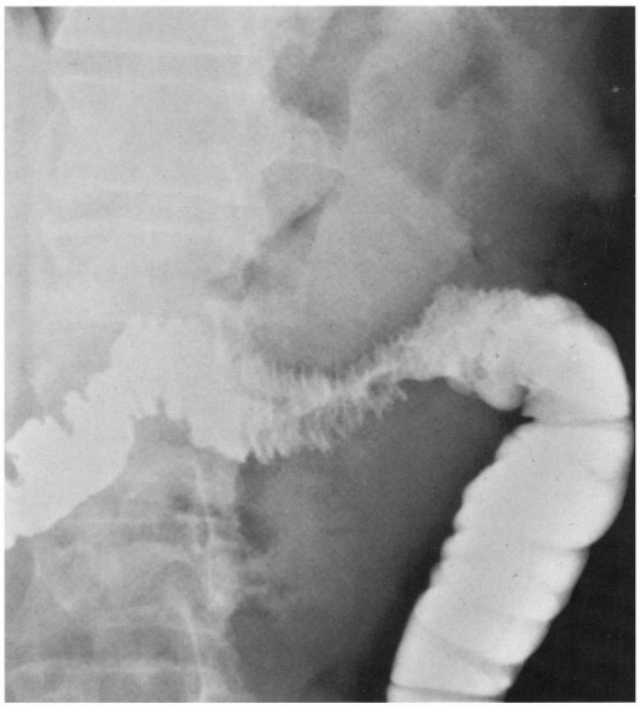


c

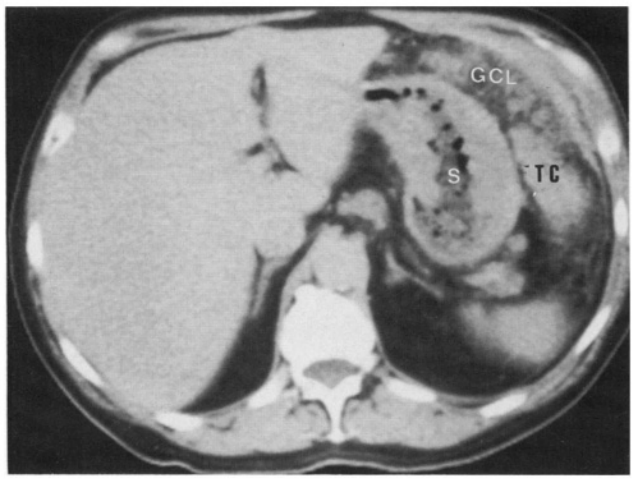


d

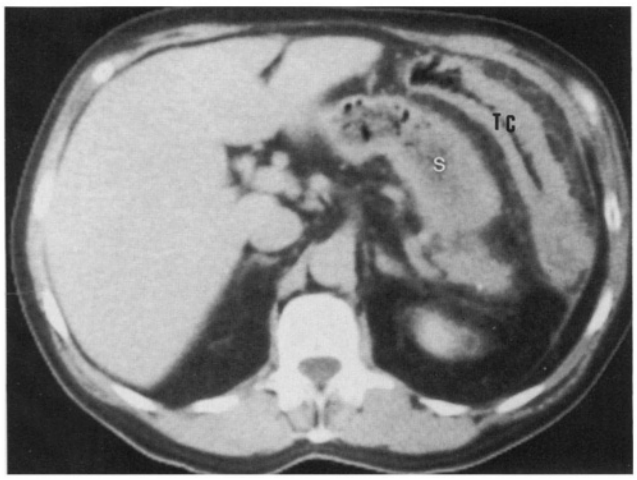
Fig. 4–30. Continued. (c) At a level through the superior haustral row of the midtransverse colon (*TC*), early infiltration by the mass is seen.
(d) At a level through lower haustral sacculations of the transverse colon, no further involvement by the malignant extension is present.



a



b



c

Fig. 4–31. Annular invasion of transverse colon by extension of gastric carcinoma along gastrocolic ligament.
(a) Barium enema demonstrates circumferential mass narrowing of distal transverse colon. Note narrowing and distortion of gastric lumen.
(b and **c)** CT shows the thickened wall of the stomach (*S*) and its progression along the gastrocolic ligament (*GCL*) with direct annular infiltration of the transverse colon (*TC*).
(Courtesy of Gary Ghahremani, M.D., Evanston Hospital, Evanston, IL.)

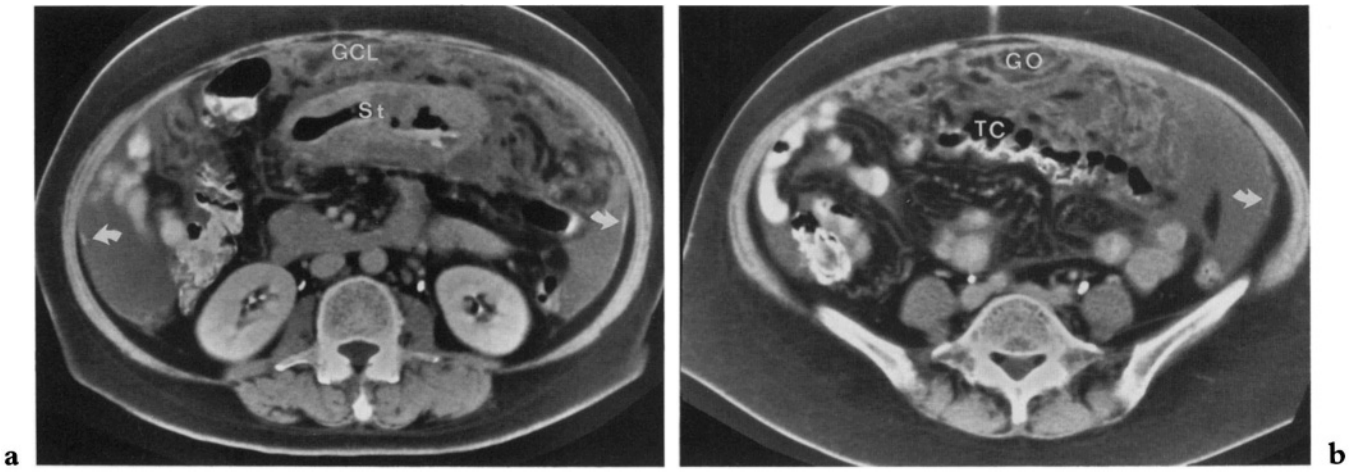
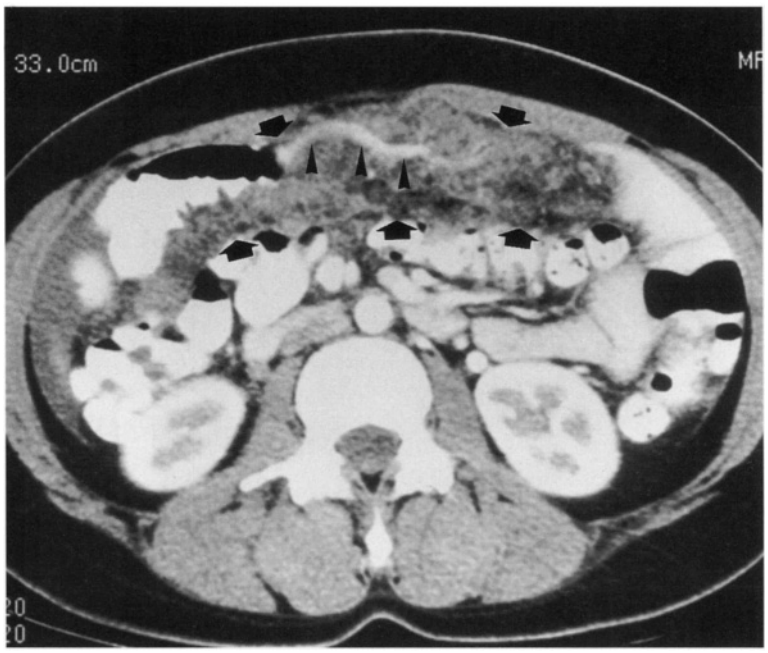


Fig. 4–32. Spread of gastric carcinoma along gastrocolic ligament to the transverse colon and greater omentum. **(a** and **b)** Antral carcinoma causing marked mural thickening of the stomach (*St*) spreads along the gastrocolic ligament (*GCL*) to strangulate the transverse colon (*TC*) and extends into the greater omentum (*GO*). Subtle peritoneal implants highlighted by ascites are noted as well (*arrows*).
(Reproduced from Gore and Meyers.[24])

Fig. 4–33. Spread of gastric carcinoma along the gastrocolic ligament to invade the transverse colon.
An engorged right gastroepiploic vein (*arrowheads*) is embedded in the extensive tumor infiltrate (*arrows*).
(Reproduced from Auh et al.[10])



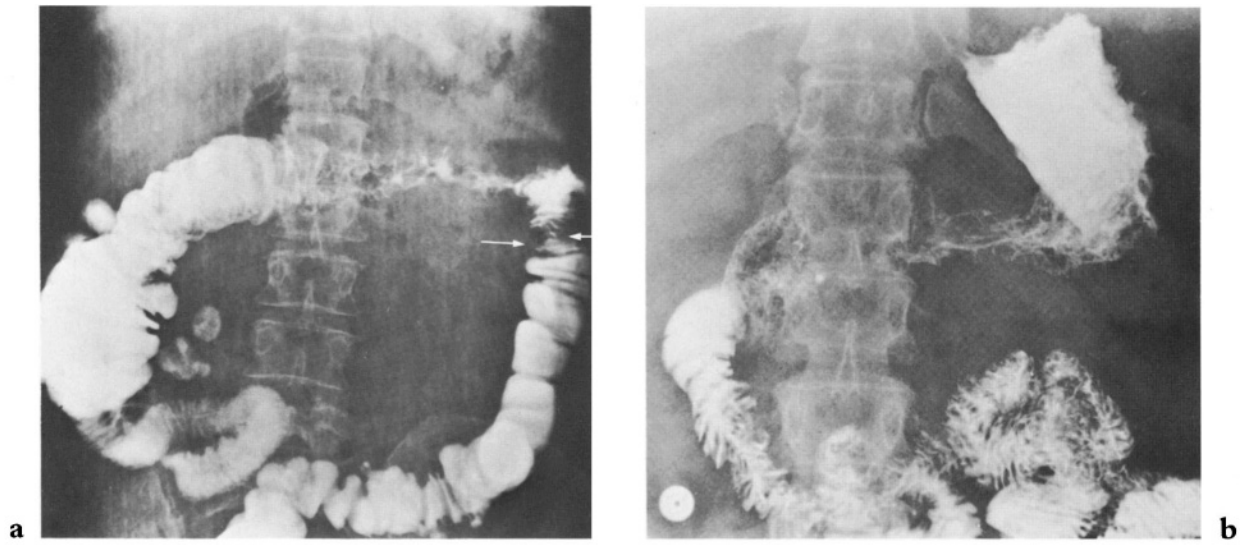


Fig. 4–34. Direct invasion of the transverse colon from gastric carcinoma along the gastrocolic ligament.
(a) Invasive desmoplastic changes involve the distal transverse colon, stopping abruptly at the anatomic splenic flexure (*arrows*).
(b) Upper GI series documents a primary scirrhous carcinoma of the stomach.



Fig. 4–35. Annular strangulation of the transverse colon by spread from gastric carcinoma down the gastrocolic ligament.
The severe extension involves the entire length and typically stops abruptly at the anatomic splenic flexure (*arrows*).



Fig. 4–36. Extension of gastric carcinoma along gastrocolic ligament to anatomic splenic flexure of colon.
(a) Mural thickening *(arrows)* of stomach *(St)* secondary to carcinoma.
(b) Mass extension *(M)* into the gastrocolic ligament to the transverse colon (*TC*) ending on the left at the anatomic splenic flexure of the colon *(SF).*

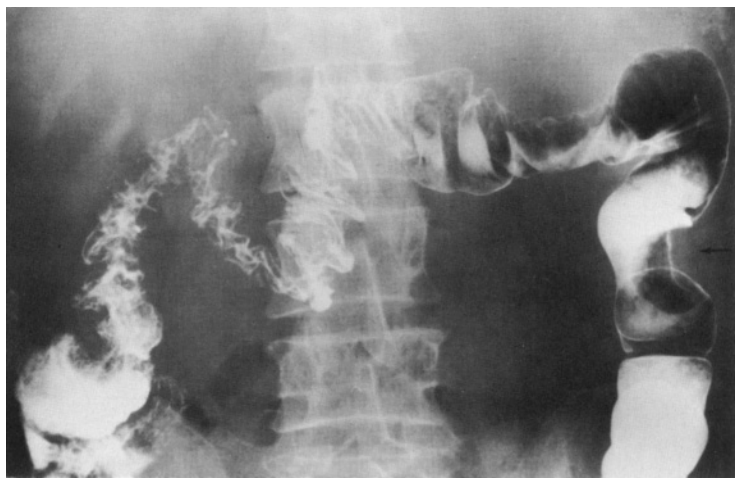


Fig. 4–37. Extensive annular invasion along the length of the transverse colon from gastric carcinoma.
The changes end abruptly at the level of the phrenicocolic ligament. At this point along the lateral aspect of the anatomic splenic flexure of the colon, a prominent serosal mass has developed *(arrow).*
(Reproduced from Meyers and McSweeney.[1])

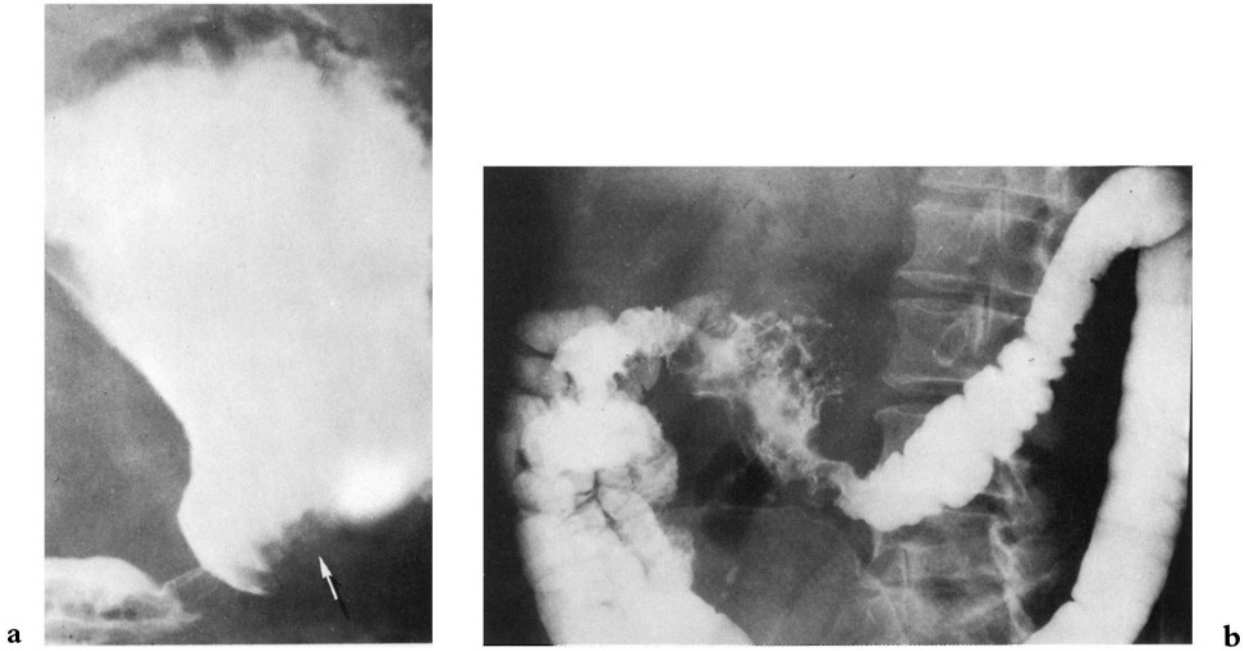


Fig. 4–38. Transmural invasion of the stomach from colonic carcinoma.
(a) There is nodular infiltration along the greater curvature *(arrow).*
(b) Spread has occurred along the gastrocolic ligament from a large primary carcinoma of the transverse colon.

Carcinoma of the pancreas may invade the gastrocolic ligament in exceptional cases, following mass infiltration of the transverse mesocolon (Fig. 4–40).

Transverse Mesocolon and Duodenocolic Ligament

The root of the transverse mesocolon extends across the infraampullary segment of the descending duodenum, the head of the pancreas, and continues along the lower edge of the body and tail of the pancreas anteriorly to bear continuity with the splenorenal and phrenicocolic ligaments[6,56] (Fig. 4–41). Near the uncinate process of the pancreas it becomes confluent as well with the root of the small bowel mesentery. These bare areas thus establish anatomic planes of continuity between (a) the pancreas and (b) the transverse colon up to the anatomic splenic flexure, the spleen, and small bowel loops. The very beginning of the peritoneal reflections on the right, known as the duodenocolic ligament, further establishes continuity to the descending duodenum and posterior hepatic flexure.[6,57]

The transverse mesocolon inserts in relation to the taenia mesocolica, and correlative studies have established that the preferential spread of pancreatic lesions along this mesentery is to the inferior border of the transverse colon[41,42] (Figs. 4–42 through 4–45). The haustral pattern on the uninvolved, pliable superior border may be thrown into a pseudosaccular appearance. Circumferential growth may develop, although usually the degree of invasion and fixation is not as extensive as may occur from indurated carcinoma of the stomach. Nevertheless, the greater involvement of the posteroinferior margin of the transverse colon on a barium enema study generally indicates the pancreas as the primary site. Rarely, similar changes may be encountered from seeded metastases on the greater omentum[58] (Fig. 4–46).

On CT, the transverse mesocolon is identified as the fatty plane extending from the pancreas, particularly at the level of the uncinate process, to the ventrally situated transverse colon with the middle colic vessels coursing through it (Figs. 4–47 and 4–48). In cases of pancreatic carcinoma, masslike or dendritic spread through the mesocolon can be precisely localized (Figs. 4–49 through 4–51).

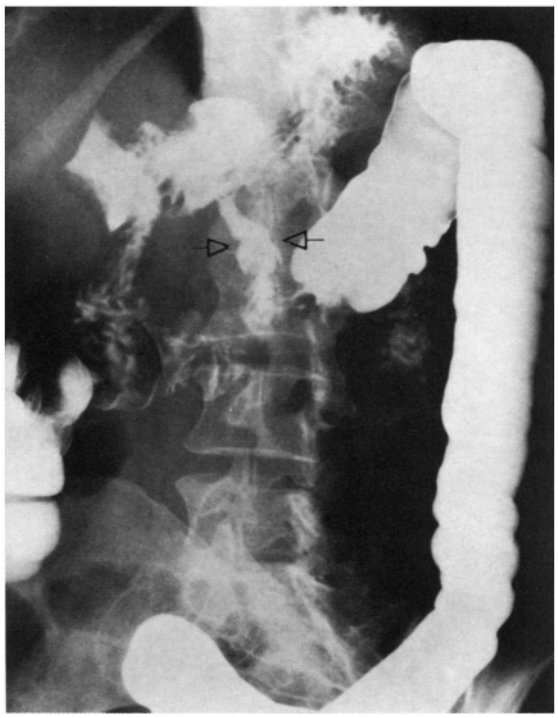


Fig. 4–39. Gastrocolic fistula secondary to carcinoma of the transverse colon.
Barium enema demonstrates that the small primary lesion has established a malignant fistulous tract along the gastrocolic ligament *(arrows).*
(Reproduced from Meyers and McSweeney.[1])

The gastrocolic trunk, which enters the superior mesenteric vein at the level of the uncinate process, may be used as a vascular landmark on CT scans of the pancreas, representing the root of the transverse mesocolon as it becomes confluent with the root of the small bowel mesentery.[60]

These same ligaments provide mesenteric planes for direct extension to and from other sites. As the hepatic flexure of the colon crosses anterior to the descending duodenum, the two structures are in very close anatomic relationship, separated only by the duodenocolic ligament, constituting the short beginning of the transverse mesocolon[6] (Fig. 4–52). In this way, the paraduodenal area may be involved by direct spread from an infiltrating carcinoma of the hepatic flexure across the beginning reflection of the transverse mesocolon[6,57,61–63] (Figs. 4–53 and 4–54). Carcinomas of the right colon are notoriously clinically occult, and the palpation of an epigastric or right upper quadrant mass in such a patient may lead to radiologic investigation being initiated with an upper GI series (Fig. 4–54a). This may be very misleading unless the underlying anatomic relationships are kept in mind and a barium enema study undertaken.

Direct lymphatic extension along the draining chain of lymph nodes may be identified occasionally by barium studies.[6,64] By its relationship to the central lymph nodes draining the colon, the duodenum may reflect changes of lymph node spread from a remote carcinoma of the colon. The lymphatic vessels draining the colon parallel the arterial supply. Those draining the right side of the colon are located near the origin of the superior mesenteric artery, in close relationship to the superior border of the horizontal (third) portion of the duodenum (Fig. 4–52). Those draining the distal transverse and descending colon are partially located in the transverse mesocolon and near the ascending left colic branch of the inferior mesenteric artery, which courses lateral to the ascending (fourth) portion of the duodenum. By radiologically recognizing these changes of nodal impressions upon the superior contour of the third portion

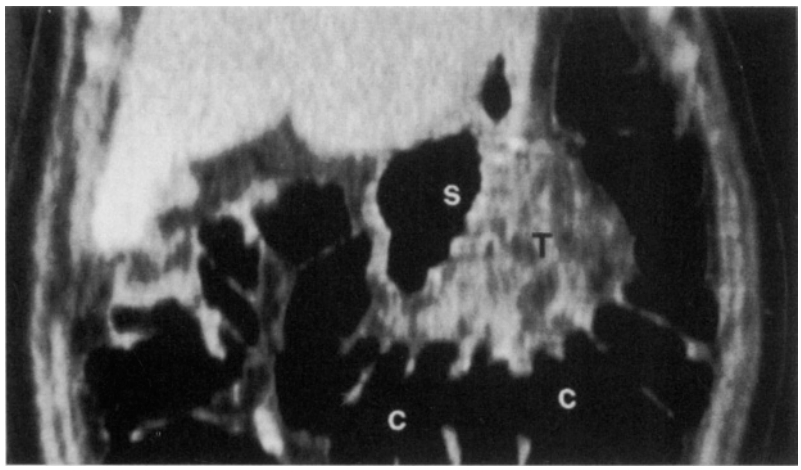
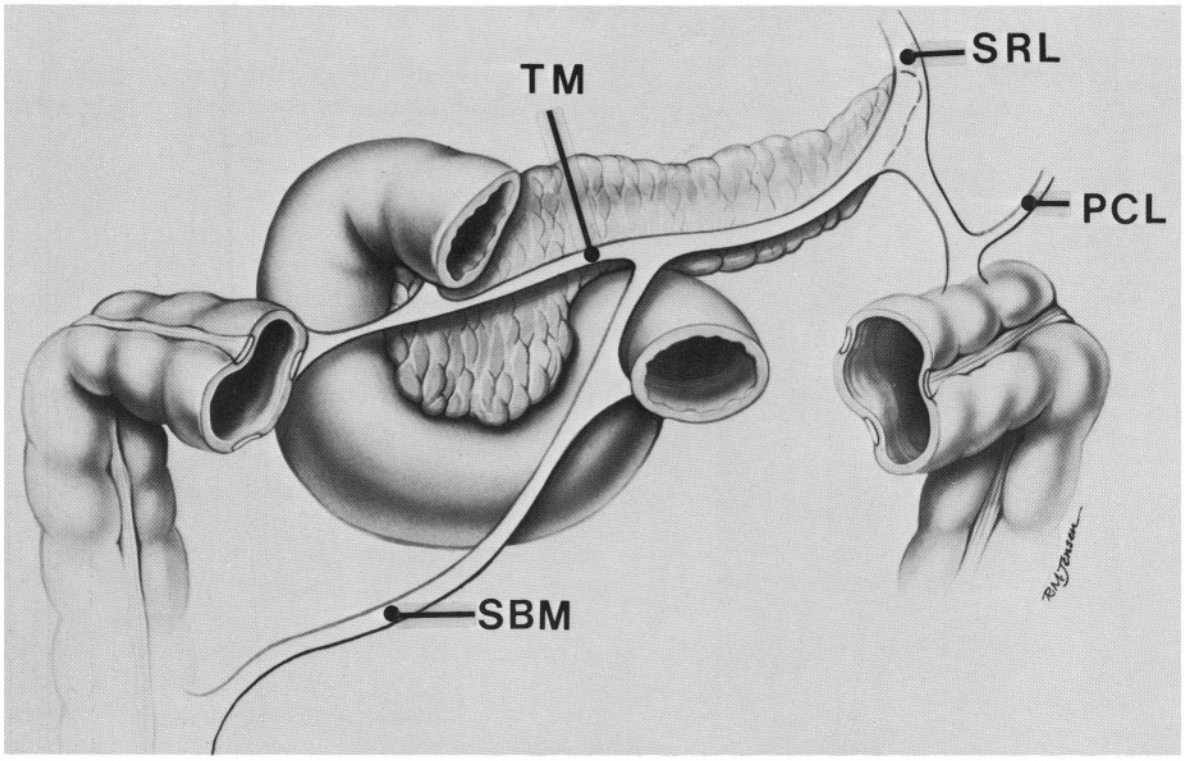
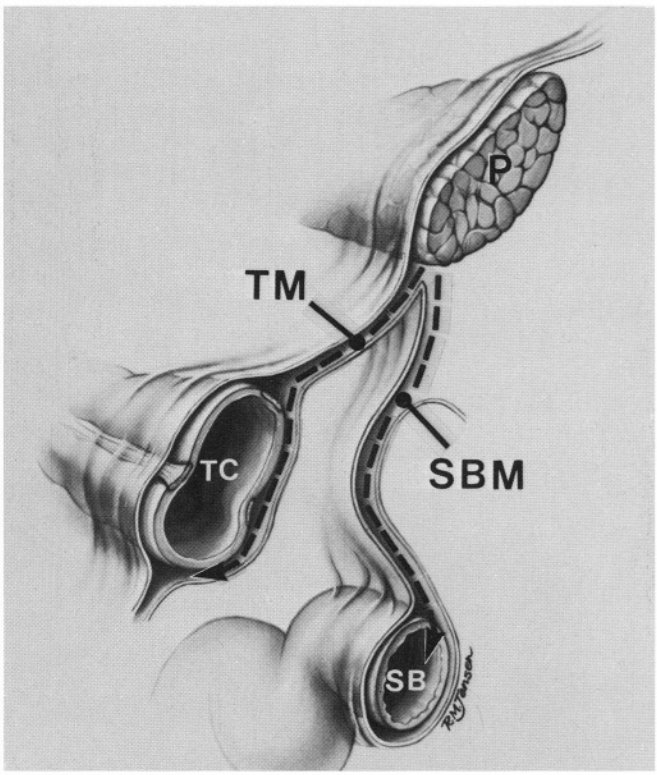


Fig. 4–40. Spread of pancreatic carcinoma into the gastrocolic ligament.
CT coronal reconstruction shows extensive tumor involvement (*T*) of the gastrocolic ligament between the stomach (*S*) and transverse colon (*C*) following invasion of the transverse mesocolon by a carcinoma of the tail of the pancreas.
(Reproduced from Heiken et al.[55])



a



b

Fig. 4–41. The transverse mesocolon: anatomic relationships and planes of spread.
(a) Frontal drawing showing the relationships of the transverse mesocolon *(TM)* and its continuity with the small bowel mesentery *(SBM),* the splenorenal ligament *(SRL),* and the phrenicocolic ligament (*PCL*).
(b) Lateral diagram. The *arrowed-dashed lines* show the planes of spread from the pancreas (*P*) to the transverse colon *(TC)* and small bowel (*SB*).
(Reproduced from Meyers et al.[9])

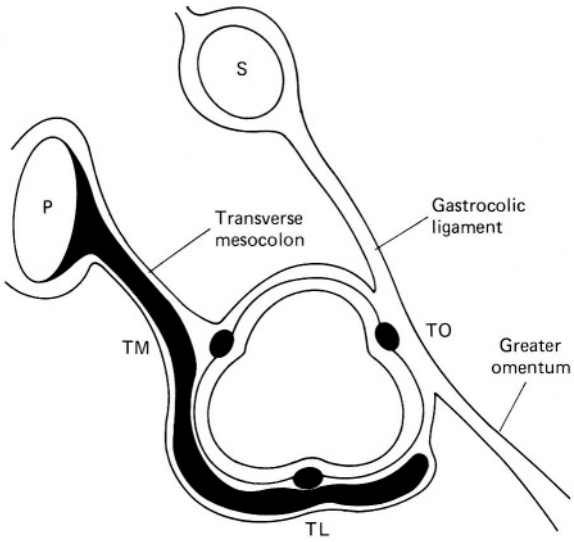


Fig. 4–42. Sagittal section through the transverse colon.
Extension of a malignancy from the pancreas (*P*) through the transverse mesocolon spreads preferentially downward along the TM–TL haustra toward the TO–TL row. This constitutes the inferior border of the transverse colon. *S* = stomach; *TM* = taenia mesocolica; *TO* = taenia omentalis, *TL* = taenia libera.
(Reproduced from Meyers et al.[42])

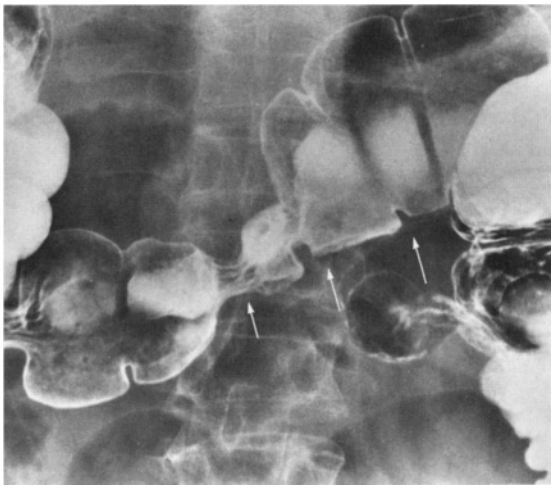


Fig. 4–43. Extension of carcinoma of the pancreas along the transverse mesocolon.
Barium enema documents flattening and fixation along the inferior border of the transverse colon *(arrows).*

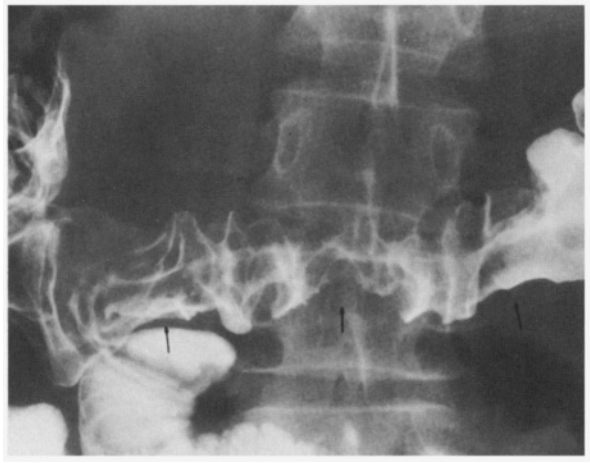


Fig. 4–44. Carcinoma of the pancreas with direct invasion of the transverse colon along the mesocolon.
The major extension is typically along the inferior contour *(arrows),* where multiple nodules are present.



Fig. 4–45. Carcinoma of the pancreas extending along the transverse mesocolon.
This results in fixation and large mass along the inferior border of the transverse colon.
(Reproduced from Meyers and McSweeney.[1])



Fig. 4–46. Seeded metastatic ovarian carcinoma on the greater omentum.
Barium enema shows multinodular infiltration of the inferior border of the transverse colon *(arrows).*
(Reproduced from Krestin et al.[58])

of the duodenum (Fig. 4–55) or upon the lateral aspect of the duodenojejunal junction (Fig. 4–56), it is possible to determine the extent of a colonic carcinoma preoperatively or the development of lymph node metastases postoperatively.[6,64] CT clearly verifies these pathways.[63,65] (Figs. 4–57 through 4–60). Rarely, postoperative lymph node metastases may undergo necrosis and become manifest as duodenoduodenal fistulas[66] (Figs. 4–61 and 4–62).

Gastrosplenic Ligament; Splenorenal Ligament; Phrenicocolic Ligament

The peritoneal reflections in the left upper quadrant of the abdomen are shorter but are certainly no less important in providing avenues of spread of disease. Anatomic continuity between multiple sites is readily established.

The gastrosplenic ligament is continuous with the gastrocolic ligament and extends from the greater curvature of the stomach to the spleen (Fig. 4–63). It contains the left gastroepiploic and short gastric vessels as well as associated lymphatics. The splenorenal ligament (Fig. 4–63) invests the extremity of the pancreatic tail as it inserts toward or within the splenic hilus and also contains the distal splenic artery. Both ligaments form the boundaries of the lesser sac on the left.

The gastrosplenic ligament is identified on CT by its fat and vascular content at the site between the stomach and spleen (Figs. 4–4 and 4–64): It may be arranged into longitudinal pleats or a series of ruffles.[67,68] Radiologic localization of disease spread here can be very precise (Fig. 4–65) and is particularly helpful in the evaluation of extramural spread of gastric malignancies (Figs. 4–66 through 4–68). A tract may be formed in the gastrosplenic ligament to enable spread from the stomach to the development of a splenic abscess (Figs. 4–69 and 4–70). Although neoplasm in a contiguous organ has been considered a rare cause of splenic abscess in the past,[69] this pathogenesis is being increasingly recognized by CT. Continuity with the splenorenal ligament allows spread of disease between the stomach, spleen, and tail of the pancreas (Figs. 4–71 and 4–72). This short ligament is



Fig. 4–47. The transverse mesocolon.
(a) CT scan shows middle colic vessels branching in the fatty space between the uncinate process *(U)* and body of the pancreas (*P*) and the transverse colon (*T*). *D* = duodenum. Some ascites is present adjacent to the liver and spleen.
(Reproduced from Meyers et al.[9])
(b) In a contrast-enhanced CT in another patient, the fat-laden plane of the transverse mesocolon is signalled by the opacified middle colic vessels. *T* = transverse colon.

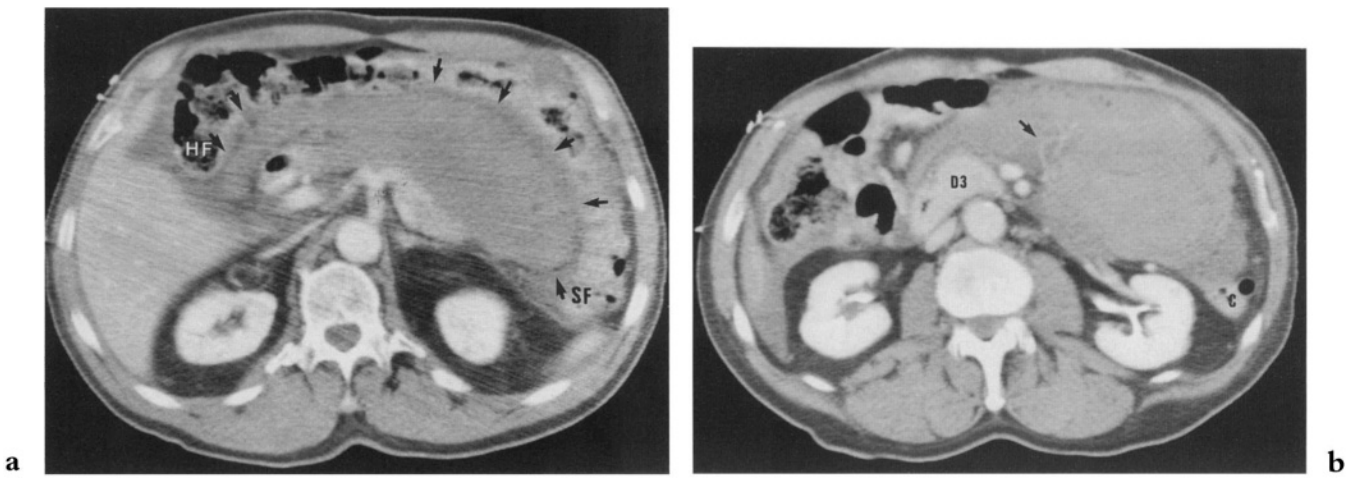


Fig. 4–48. Hematoma of the transverse mesocolon, demonstrating its extent and relationships *in vivo.*
(a) At the level of the celiac axis, a mass of fluid density *(arrows)* extends throughout the mesocolon from the anterior hepatic flexure (*HF*) on the right to the splenic flexure (*SF*) on the left and to the anteriorly displaced transverse colon.
(b) At the level of the third portion of the duodenum *(D3)* and the superior mesenteric vessels, the mesocolic hematoma—containing areas of heterogeneous increased attenuation—extends to the anatomic splenic flexure of the colon (*C*). A middle colic vessel is seen *(arrow).* Hemoperitoneum is also present.
(Courtesy of Gary Ghahremani, M.D., Evanston Hospital, Evanston, IL.)

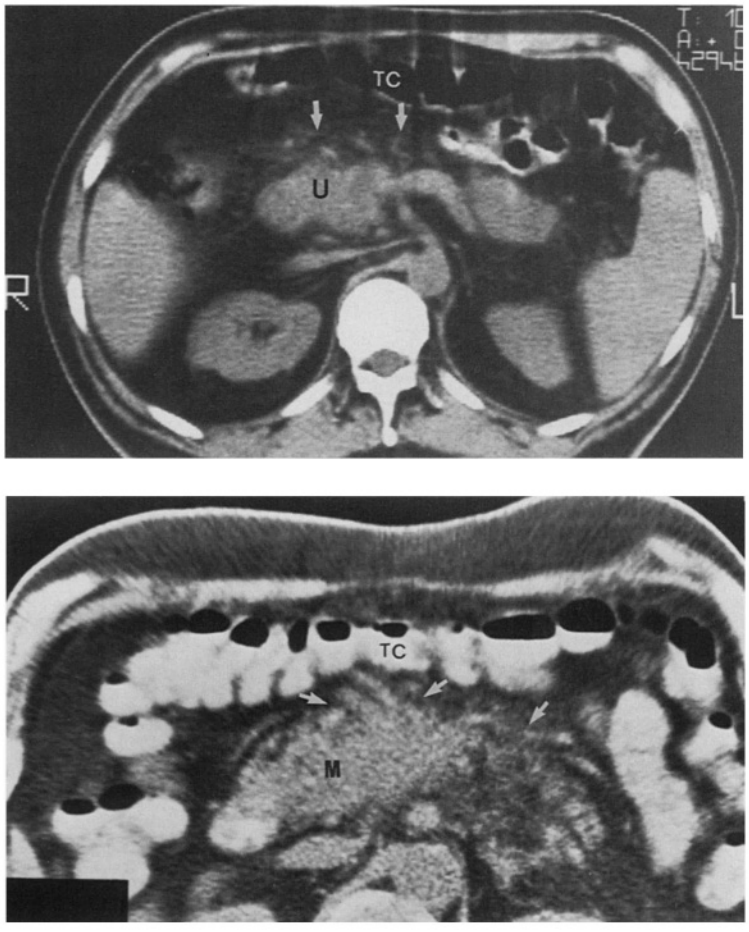


Fig. 4–49. Spread of pancreatic carcinoma into transverse mesocolon.
In two different patients (**a** and **b**), *arrows* show extension of carcinoma of the uncinate process *(U)* and the body of the pancreas (M) as stellate and dendritic infiltrations of the transverse colon *(TC).*
(**a,** courtesy of Nancy O. Whitley, M.D., University of Maryland School of Medicine, Baltimore.)

identified less frequently by CT, but is generally indicated after intravenous contrast injection by the distal splenic artery or the proximal splenic vein.

The phrenicocolic ligament (Fig. 4–73a) extends from the anatomic splenic flexure of the colon to the diaphragm at the level of the 11th rib[48] and serves to support the spleen in the left upper quadrant. It is in most direct continuity with the splenorenal ligament and the transverse mesocolon. It can be identified occasionally on plain films[48] and clearly by peritoneography,[70] and on CT in cases of ascites it may be outlined in its characteristic position (Fig. 4–73b). The avenue of spread facilitated by the ligament's relationships explains the predisposition of carcinoma of the tail of the pancreas to involve the anatomic splenic flexure of the colon (Figs. 4–74 and 4–75).

Small Bowel Mesentery

The small bowel mesentery is a voluminous fat-laden peritoneal reflection. Whereas its root (Fig. 4–41) is only 15 cm long as it extends obliquely from the region of the pancreas to the right lower quadrant, the mesentery itself suspends 20–25 feet of jejunal and ileal loops.[72] This is achieved by its characteristic ruffled nature, which markedly lengthens its intestinal border. The mesenteric ruffles thereby provide routes of spread



Fig. 4–50. Spread of pancreatic carcinoma into the transverse mesocolon.
(a) Transaxial contrast-enhanced CT demonstrates a large mass in the tail of the pancreas encasing the splenic artery *(arrowhead).*
(b) Left-sided sagittal reconstruction shows spread of tumor along the transverse mesocolon *(black arrowheads)* to the gastrocolic ligament *(white arrowheads).* The renal artery *(small arrow)* and ovarian vein *(large arrow)* are also encased by tumor. *M* = pancreatic mass; *P* = normal pancreas; *S* = stomach; *C* transverse colon).
(Reproduced from Heiken et al.[55])

to one or multiple small bowel loops[73] (Figs. 4–76 and 4–77).

The normal small bowel mesentery is best appreciated on CT when its structural components are positioned to be imaged transaxially (Fig. 4–78). Its root is a bare area in continuity with the extraperitoneal anterior pararenal space.

These features also explain many of the characteristic growth patterns of mesenteric lymphoma. This may present or originate within the mesenteric root, and extension may be seen as multiple or conglomerate densities or a stellate infiltration[74,75] of the mesentery. Lymphomatous mural involvement of a small bowel loop specifically on its mesenteric border may then be noted[73] (Fig. 4–79).

When mesenteric lymphoma coexists with paraaortic/paracaval adenopathy, a helpful differential feature on CT relies upon the integrity of the anterior pararenal fat. Even in the presence of a "sandwich sign" of a confluent lymphomatous mass infiltrating the mesenteric leaves and encasing the mesenteric vessels,[76] there remains a visible plane of demarcation from commonly accompanying retroperitoneal adenopathy[9] (Fig. 4–80).

text continues on page 166



Fig. 4–51. Extension of pancreatic carcinoma into the transverse mesocolon, shown by interstitial-phase gadolinium-enhanced fat-suppressed T1-weighted MR images.
(a) A large cancer arises from the body of the pancreas *(arrow).*
(b) Tumor extends along the transverse mesocolon to involve the transverse colon *(arrow).*
(Reproduced from Semelka et al.[59])

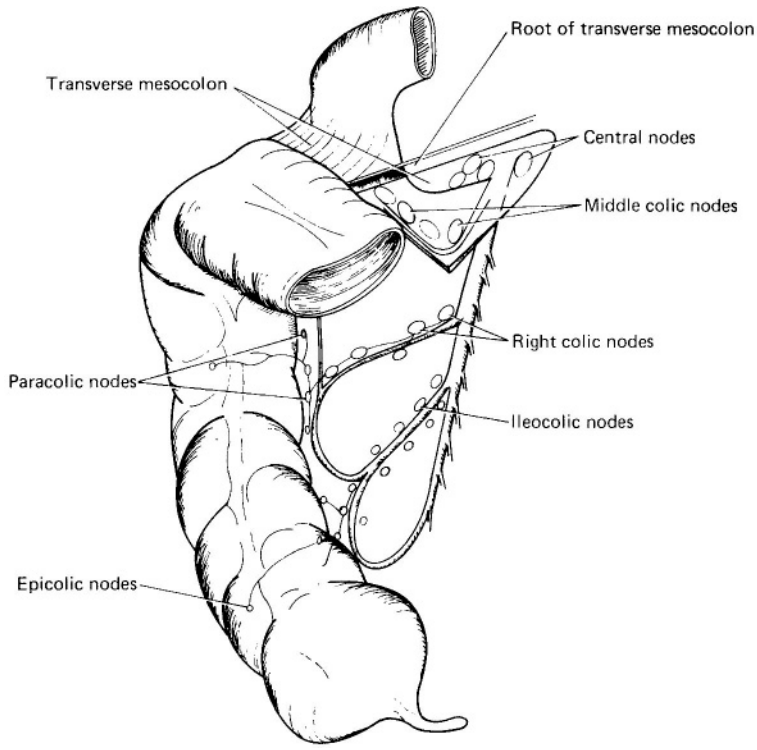


Fig. 4–52. Duodenocolic relationships.
(1) The hepatic flexure of the colon and the descending duodenum are bridged by the transverse mesocolon.
(2) The central lymph nodes draining the right colon are in relationship to the duodenum.



Fig. 4–53. Spread of carcinoma of right colon across duodenocolic ligament.
(a) Barium enema shows an annular carcinoma of the distal ascending colon *(arrow)*.
(b and **c)** CT scans demonstrate the mass (*M*) of the primary carcinoma and its spread across the duodenocolic ligament to paraduodenal–peripancreatic nodal masses (*DC*). *D* = duodenum. (Reproduced from Meyers et al.[9])

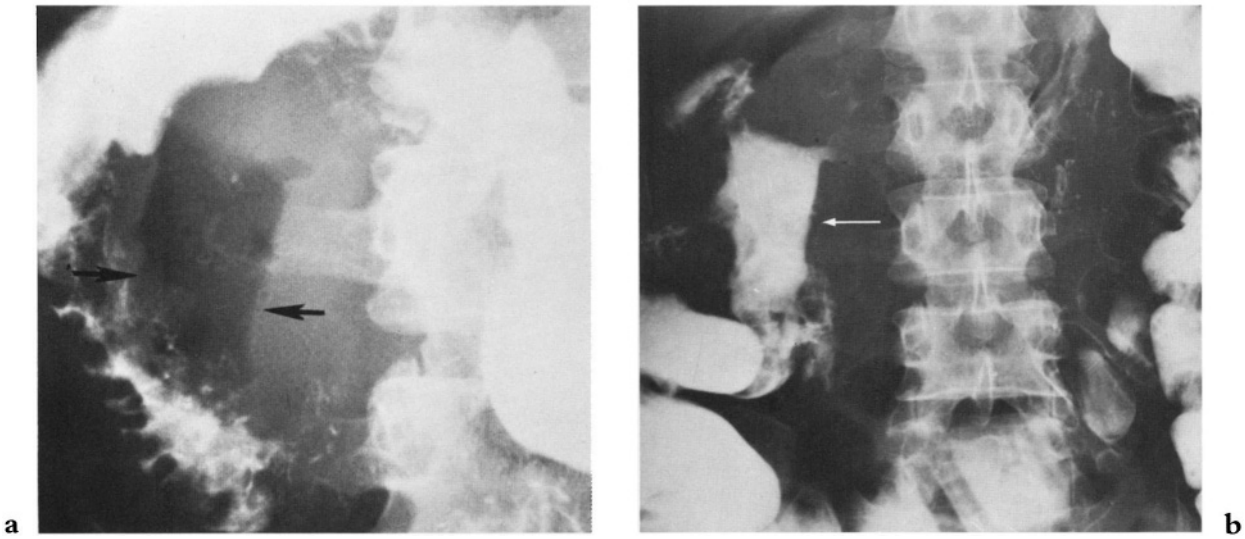


Fig. 4–54. Invasion of paraduodenal area across the mesocolon by colonic carcinoma.
(a) Upper gastrointestinal series demonstrates well-defined gas-containing abscess cavity *(arrows)* within a mass in the area of the head of the pancreas. Mucosal edema of the descending duodenum is present.
(b) A subsequent barium enema reveals a primary infiltrating carcinoma of the anterior hepatic flexure with opacification of a pericolonic–paraduodenal abscess *(arrow).*
(Reproduced from Treitel et al.[57])

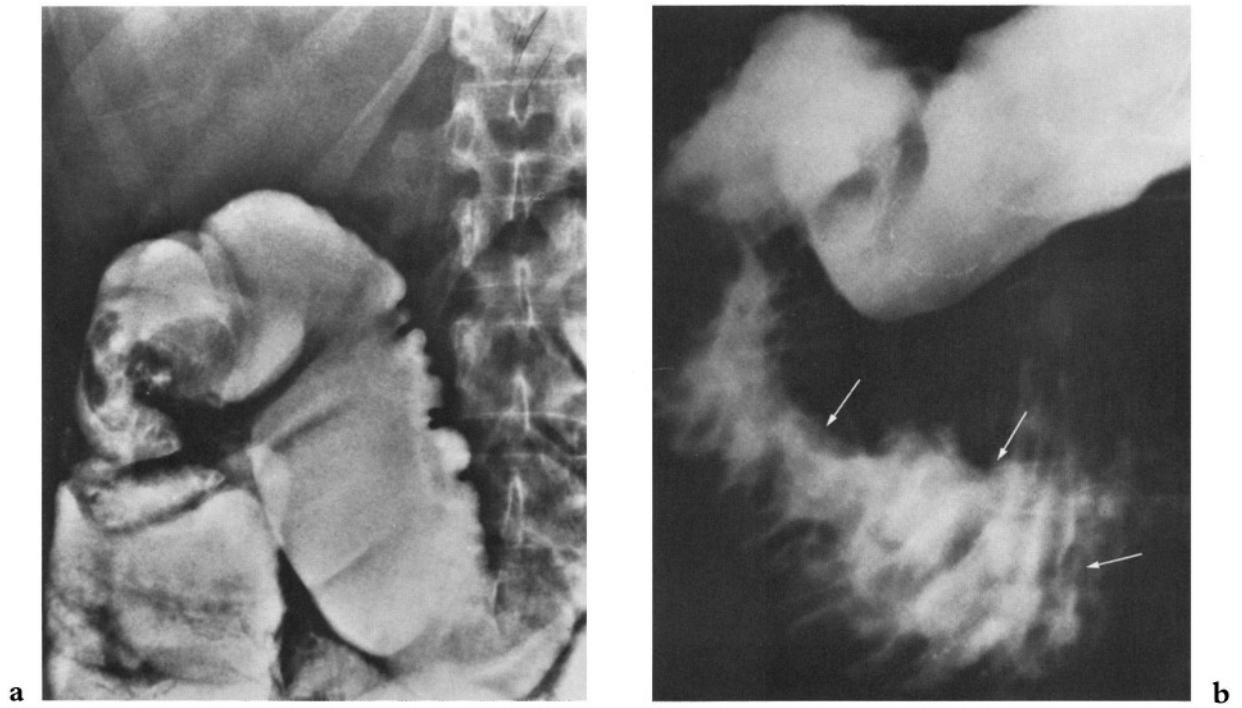


Fig. 4–55. Nodal spread from colonic carcinoma.
(a) Barium enema shows a polypoid carcinoma within the distal ascending colon.
(b) Upper gastrointestinal series documents metastases within the enlarged, draining lymph nodes by virtue of their extrinsic impressions upon the duodenum *(arrows).*

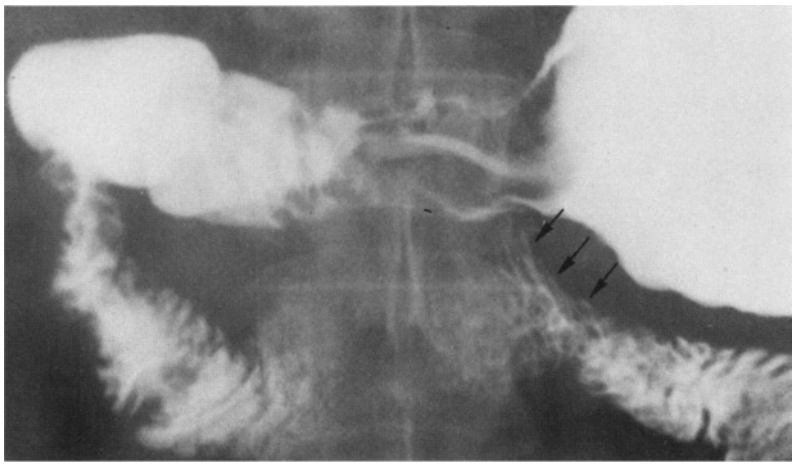


Fig. 4–56. Metastases within the draining central inferior mesenteric lymph nodes from a carcinoma of the left colon.
These are shown by the extrinsic pressure effect on the lateral aspect of the duodenojejunal junction *(arrows).*

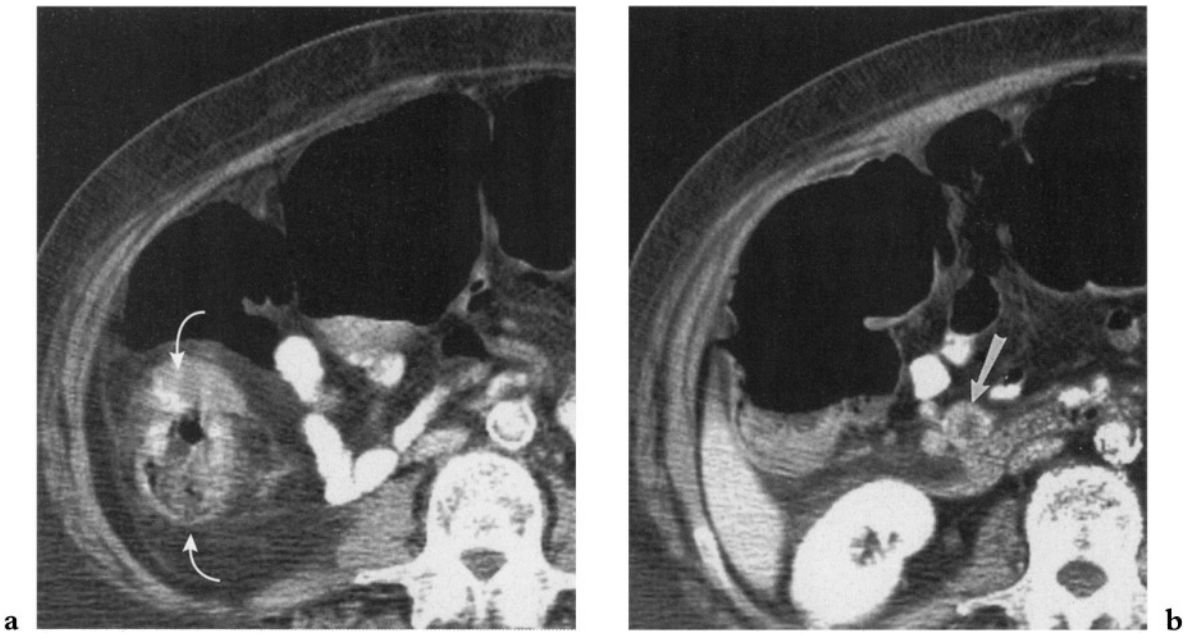


Fig. 4–57. Metastases to paraduodenal lymph nodes from carcinoma of the ascending colon.
(a) Contrast-enhanced CT shows an annular carcinoma of the right colon *(arrows).*
(b) At a higher level, an enlarged paraduodenal lymph node with central necrosis *(arrow)* is evident. This lymphatic metastasis has occurred via the duodenocolic ligament.
(Courtesy of James Brink, M.D., Yale University School of Medicine, New Haven, CT.)

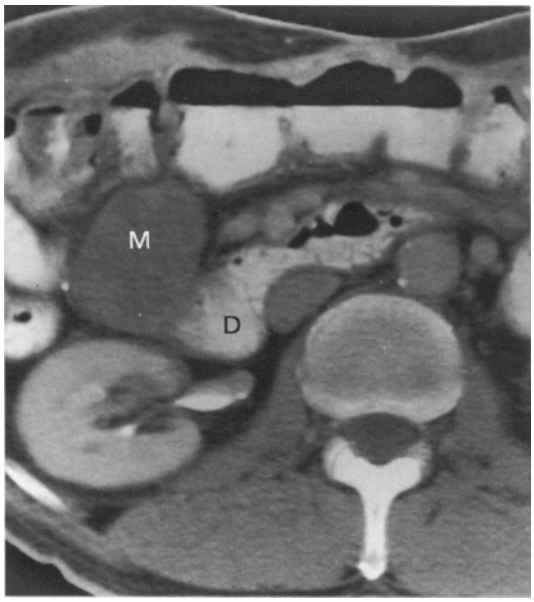


Fig. 4–58. Metastatic paraduodenal node secondary to recurrent carcinoma of ascending colon.
A 6-cm nodal mass *(M)* is present anterior and lateral to the second portion of the duodenum (*D*).
(Reproduced from McDaniel et al.[63])

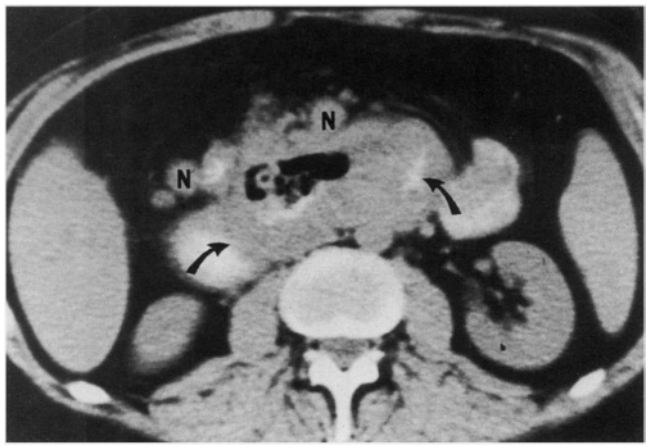


Fig. 4–60. Lymphatic metastases to the duodenum from recurrent colon carcinoma.
CT reveals a large ulcerating lymphatic-borne metastasis in the third portion of the duodenum *(arrows)* associated with regional adenopathy (*N*).
(Courtesy of Kyunghee Cho, M.D., UMD-New Jersey Medical School, Newark, New Jersey.)

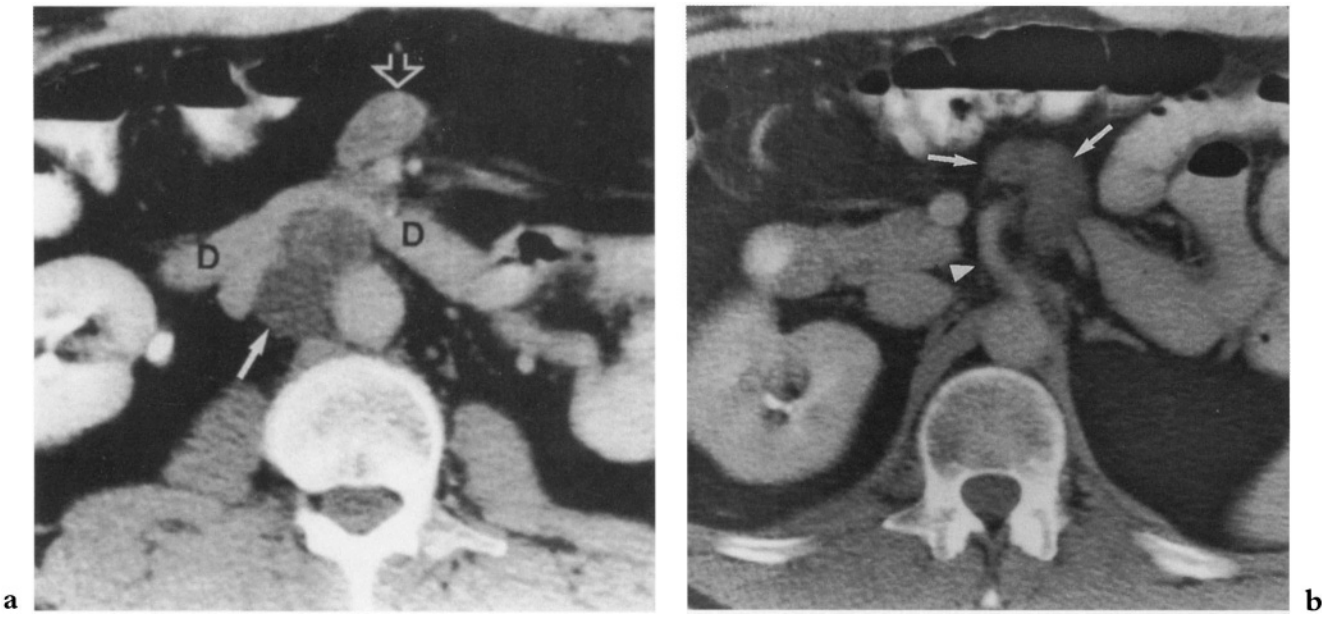


Fig. 4–59. Metastatic nodes along the principal superior mesenteric artery and in aortocaval region and small bowel mesentery with impressions upon duodenum secondary to carcinoma of the cecum.
(a) Metastatic lymph nodes in retroperitoneum, aortocaval nodal group *(solid arrow)* and mesentery *(open arrow).* Note compression upon third portion of duodenum *(D).*
(b) Metastatic nodes *(arrow)* near origin *(arrowhead)* of superior mesenteric artery.
(Reproduced from McDaniel et al.[63])



Fig. 4–61. Duodenoduodenal fistula.
Fifteen months following a right hemicolectomy for carcinoma of the hepatic flexure, upper GI series demonstrates the fistula *(arrowheads),* proved to be secondary to duodenal invasion by paradudodenal lymph node metastases.
(Reproduced from Schabel et al.[66])

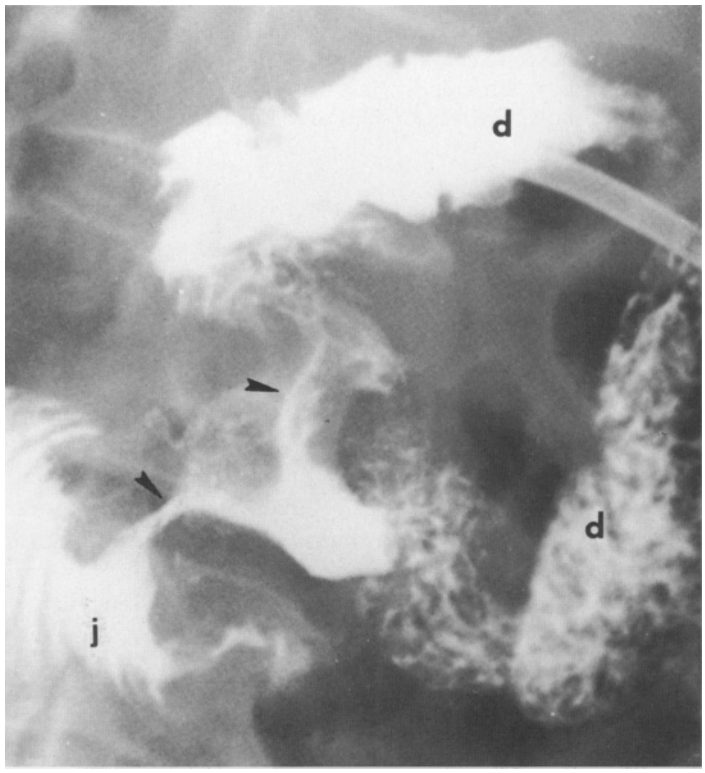


Fig. 4–62. Duodenoduodenal fistula.
Eight years following a right hemicolectomy for carcinoma of the ascending colon, upper GI series shows multiple fistulous tracts *(arrowheads)* between the second and third portions of the duodenum *(d)* and jejunum *(j)* secondary to a large mass of necrotic paraduodenal tumor.
(Reproduced from Schabel et al.[66])

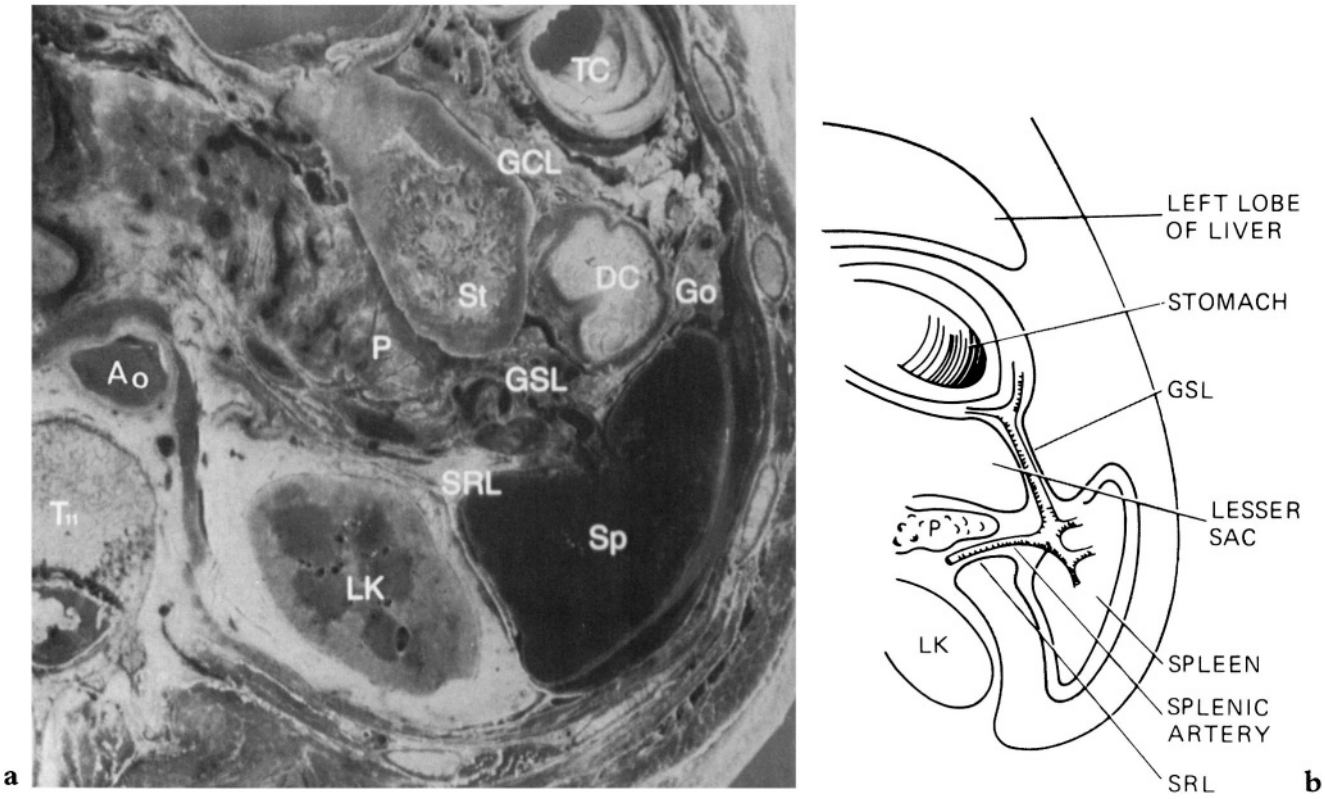


Fig. 4–63. The gastrosplenic and splenorenal ligaments.
(a) Anatomic cross sections at the level of T11 demonstrates the relationships of the gastrosplenic (*GSL*), splenorenal *(SRL),* and gastrocolic (*GCL*), ligaments. *TC* = transverse colon; *DC* = descending colon; *St* = stomach; *P* = pancreas; *Go* = greater omentum; *Sp* = spleen; *LK* = left kidney; *Ao* = aorta.
(b) Transverse diagram of the left upper quadrant shows the relationships of the gastrosplenic ligament (*GSL*) and splenorenal ligament *(SRL).*

Invasion by Lymphatic Permeation

Lymphatic permeation plays an apparently minor role in the dissemination of secondary neoplasms of the bowel. The process refers to lymphatic–borne tumor emboli from a primary neoplasm of the bowel, which may not be arrested in the nearest lymph nodes along the chain of drainage. Rather, complete blockage of a more remote node can occur from cellular impaction, with retrograde passage along other afferent channels to involve a segment of bowel adjacent to, or at some distance from, the primary carcinoma (Fig. 4–81). It has been documented that metastatic tumor cells may be carried for considerable distances beyond the usual route by this altered lymph flow.[77] This process may play a role in anastomotic recurrence following resection of the colon for carcinoma (Fig. 4–82). It appears to be a major factor in some cases of local bowel metastases.[78,79]

The deranged lymph flow in the initial stages may be radiologically demonstrated as edema in the wall of the bowel with mucosal thickening and luminal narrowing (Figs. 4–83 and 4–84). As the metastatic lymphatic edema increases, nodular tumor deposits occur that may be evident as "thumbprinting" in the colon and "cobblestoning" of the small intestine (Fig. 4–85), changes mimicking inflammatory bowel disease.[78.79] Radiologic demonstration of these findings indicates that extensive lymphatic permeation has occurred and that resection will not be curative.[77] The process can also result in diversion of lymph flow into veins through direct lymphaticovenous communications[81] or through shared channels intrinsic to lymph nodes.[82]

Lymphatic permeation also explains the rare form of insidious widespread linitis plastica of the intestines that can follow carcinoma of the stomach.[83]

text continues on page 182

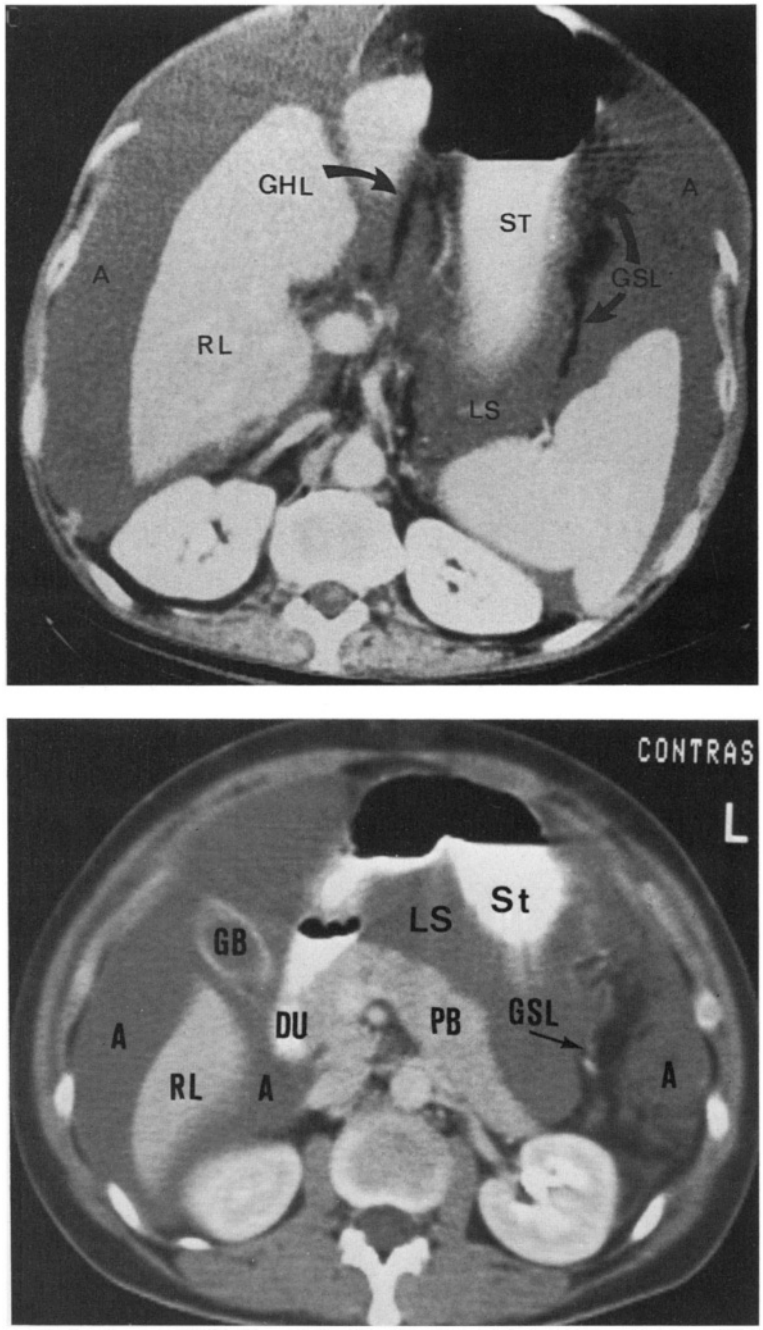


Fig. 4–64. The gastrosplenic ligament.
CT scans on two different patients with ascites (*A*) demonstrate the gastrosplenic ligament (*GSL*) by virtue of its fatty elements and contained blood vessels. *RL* = right lobe of the liver; *GHL* = gastrohepatic ligament; *GB* = gallbladder; *St* = stomach; *DU* = duodenum; *PB* = pancreatic body; *LS* = lesser sac.

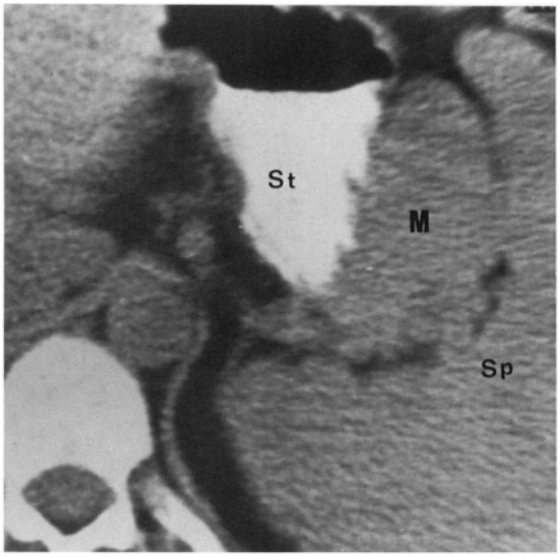
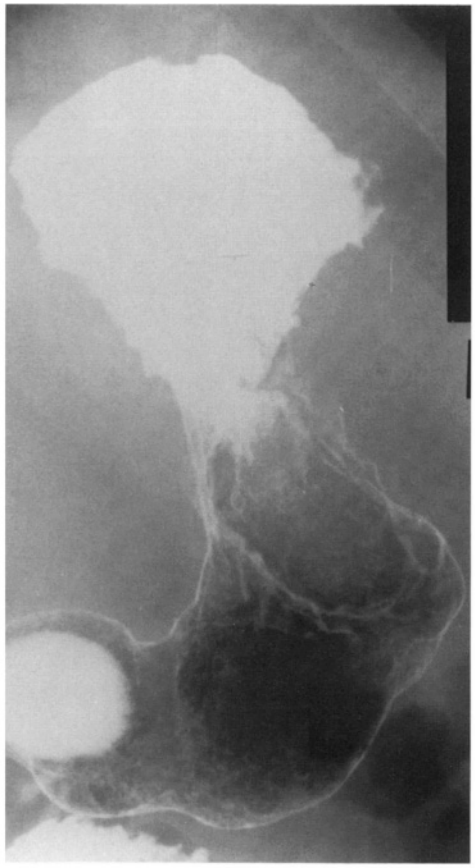
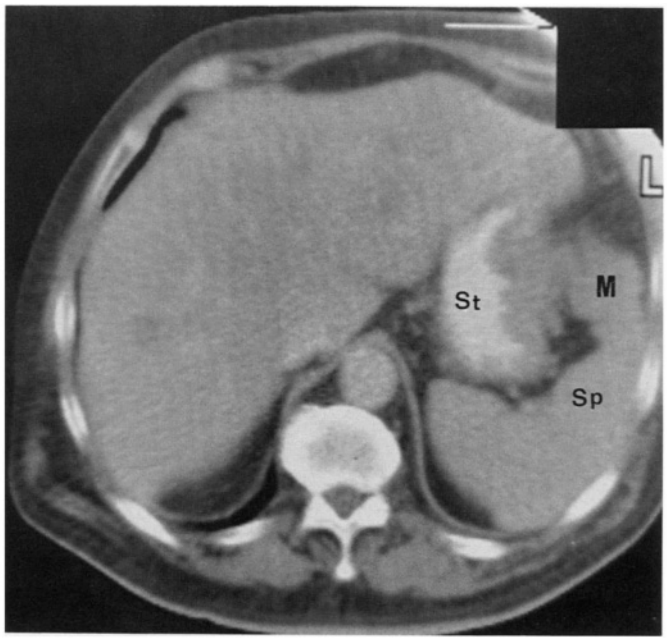


Fig. 4–65. Lymphoma within the gastrosplenic ligament. Nodal mass (*M*) in the gastrosplenic ligament separates the stomach (*St*) from the enlarged spleen *(Sp).*



a



b

Fig. 4–66. Extension of gastric carcinoma into gastrosplenic ligament.
(a) Upper GI series demonstrates an infiltrating carcinoma of the greater curvature of the stomach. Extramural spread cannot be determined.
(b) CT scan documents nodal metastases (*M*) within the gastrosplenic ligament between the thickened irregular wall of the stomach *(St)* and the spleen *(Sp).*
(Reproduced from Meyers et al.[9])

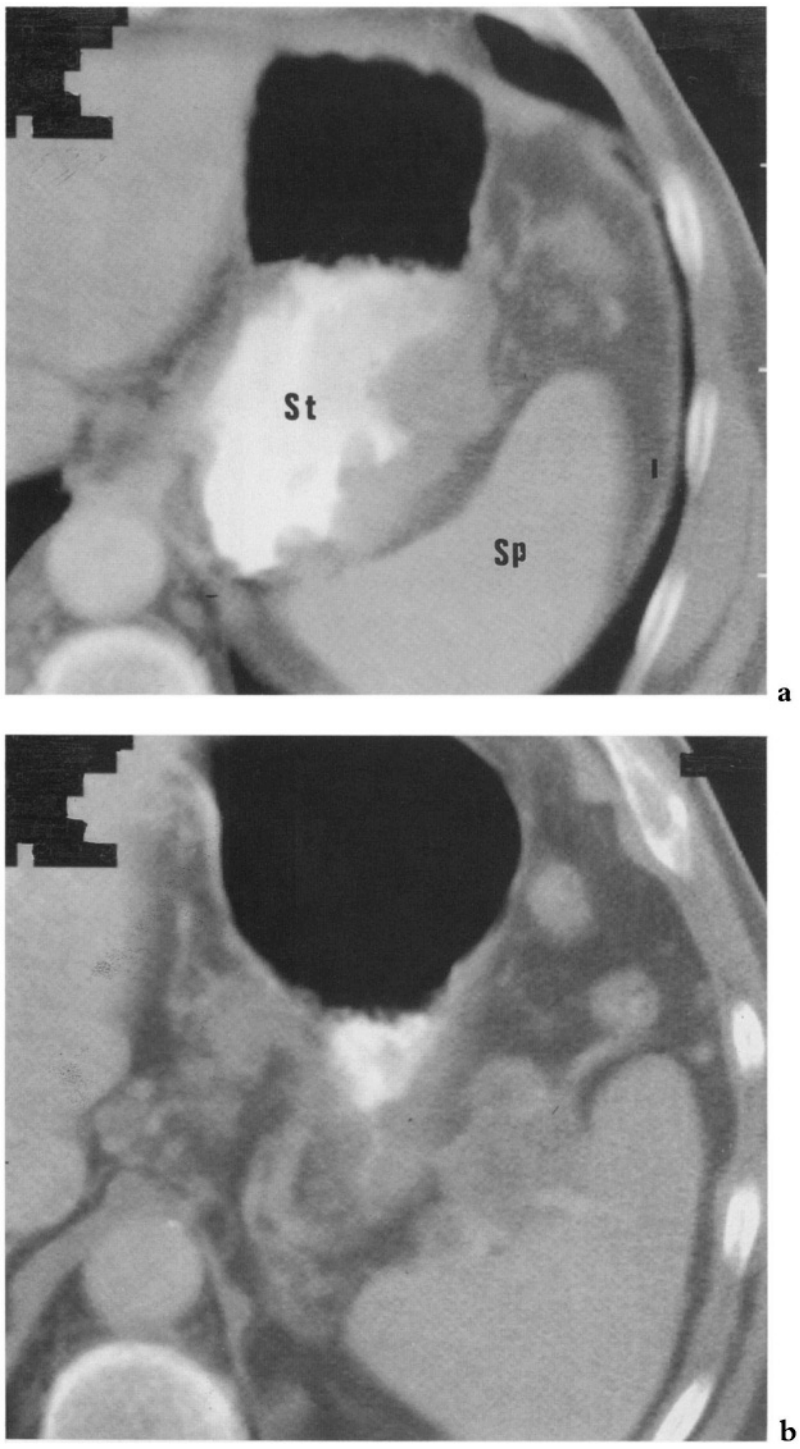


Fig. 4–67. Spread of gastric carcinoma across the gastrosplenic ligament to the spleen.
(a) An ulcerated adenocarcinoma of the stomach (*St*) is shown by the marked thickening of the greater curvature. *Sp* = spleen.
(b) The malignancy has extended across the gastrosplenic ligament to invade the splenic hilar fat. Metastatic lymph nodes are also seen along the lesser curvature.
(Courtesy of Gary Ghahremani, M.D., Evanston Hospital, Evanston, IL.)

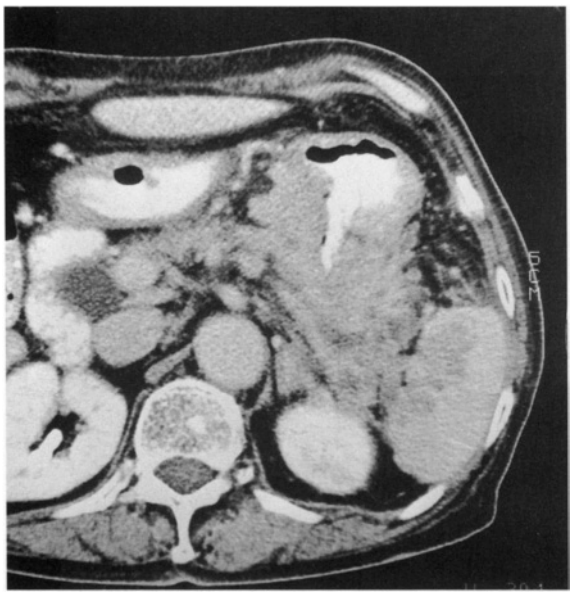


Fig. 4–68. Extension of gastric carcinoma to invade the spleen.
A carcinoma that diffusely involves the stomach with wall thickening and bulky mass spreads widely across the gastrosplenic ligament to infiltrate the spleen.
(Courtesy of Yong Ho Auh, M.D., Asan Medical Center, Seoul, Korea.)

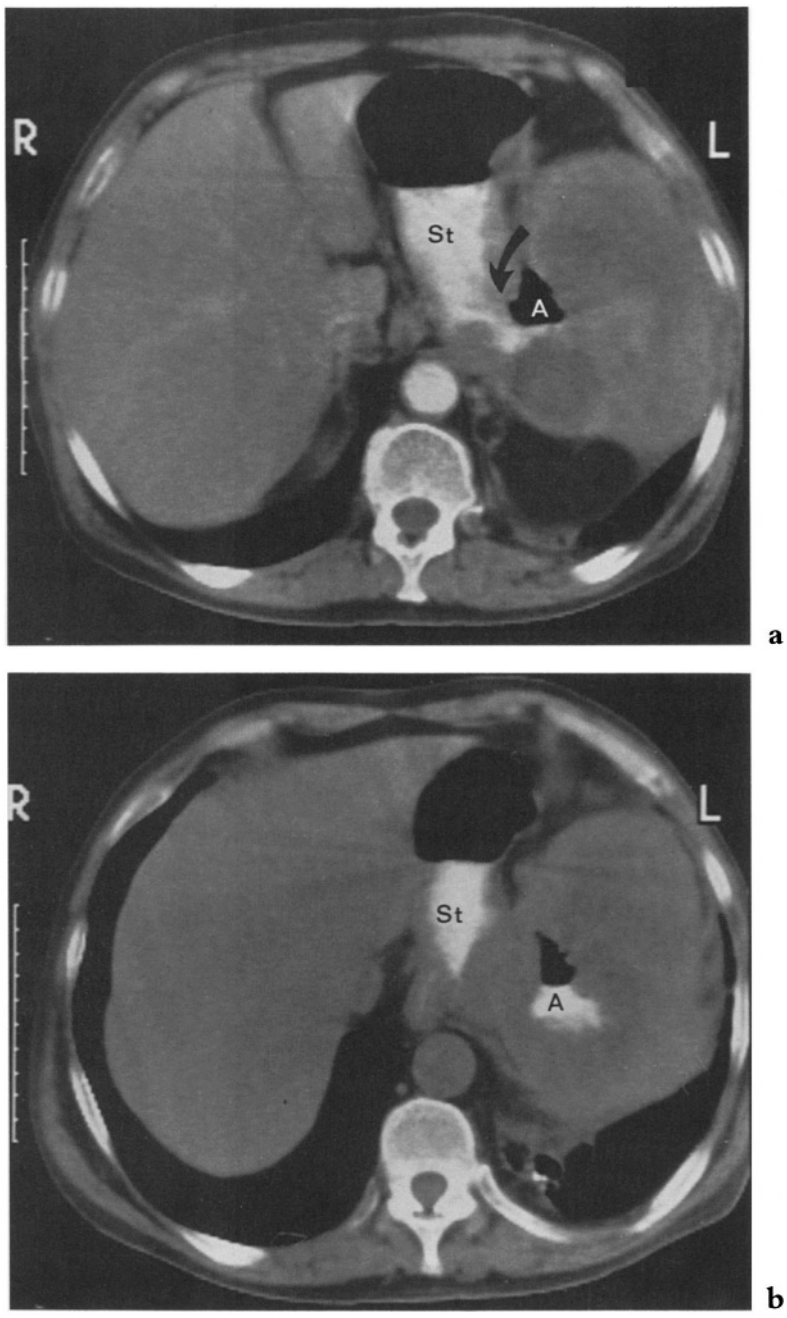
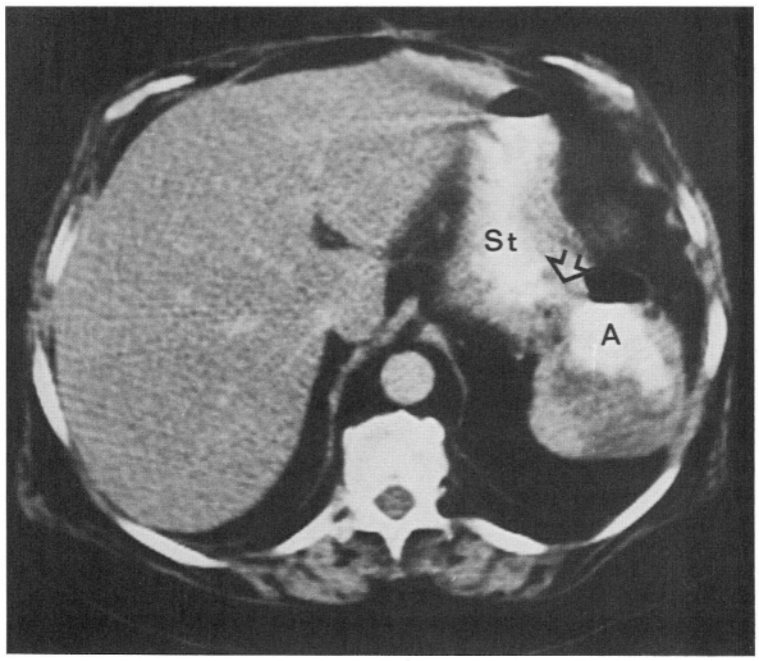
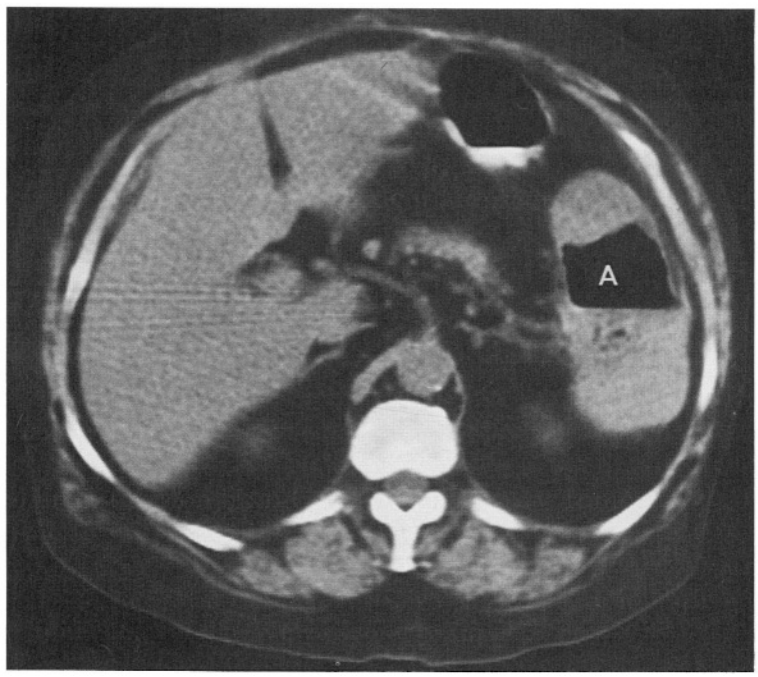


Fig. 4–69. Spread of gastric carcinoma across the gastrosplenic ligament to the spleen. **(a** and **b)** Tract across the gastrosplenic ligament *(arrow)* establishes continuity between infiltrating carcinoma of stomach *(St)* and abscess cavity (*A*) within spleen.



a



b

Fig. 4–70. Spread of gastric lymphoma across the gastrosplenic ligament to the spleen, (a and **b)** Lymphomatous thickening of wall of stomach *(St)* directly continues across gastrosplenic ligament *(arrow)* to the development of a large communicating abscess cavity *(A)* within the spleen.

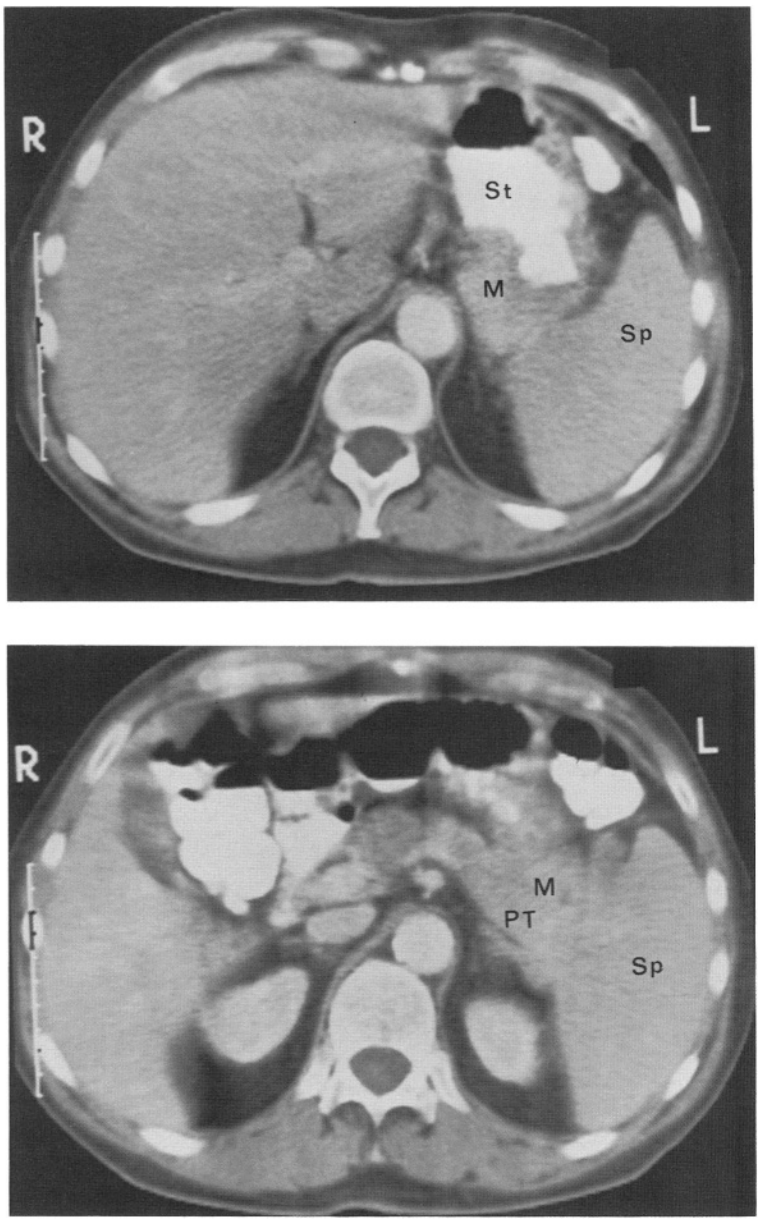


Fig. 4–71. Spread of gastric carcinoma to gastrosplenic and splenorenal ligaments.
(a) An ulcerated carcinoma of the stomach *(St)* extends as a mass *(M)* within the gastrosplenic ligament.
(b) At a lower level, the mass continues into the splenorenal ligament to displace the pancreatic tail (*PT*) posteriorly away from the spleen *(Sp)*.

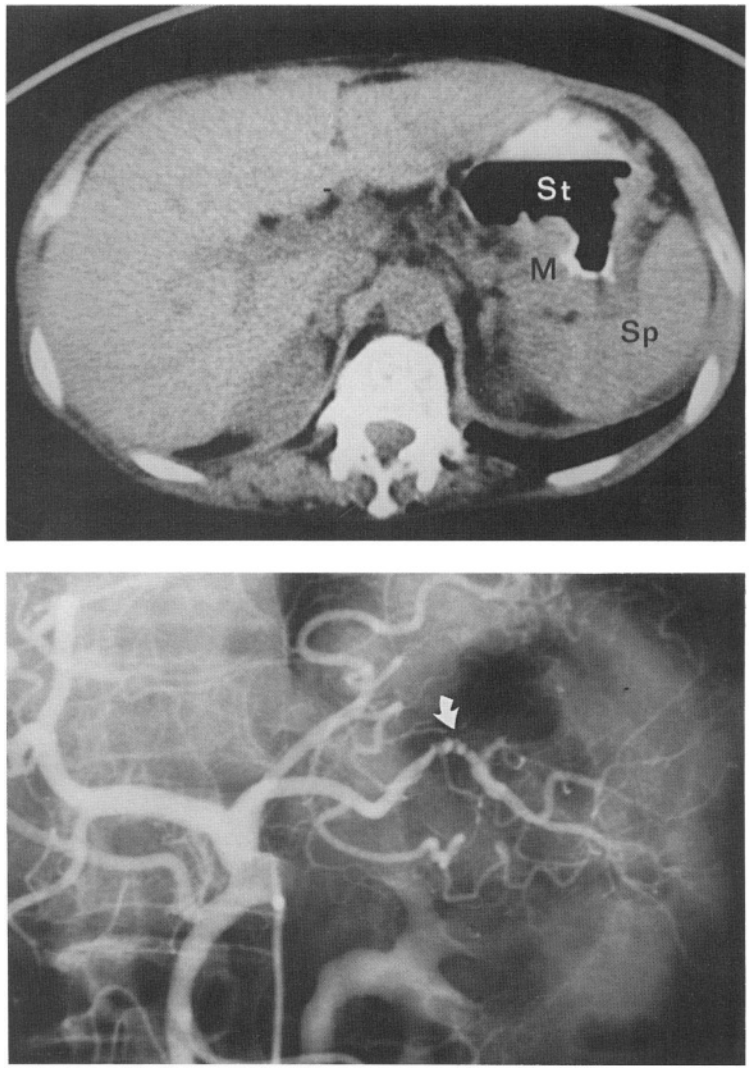
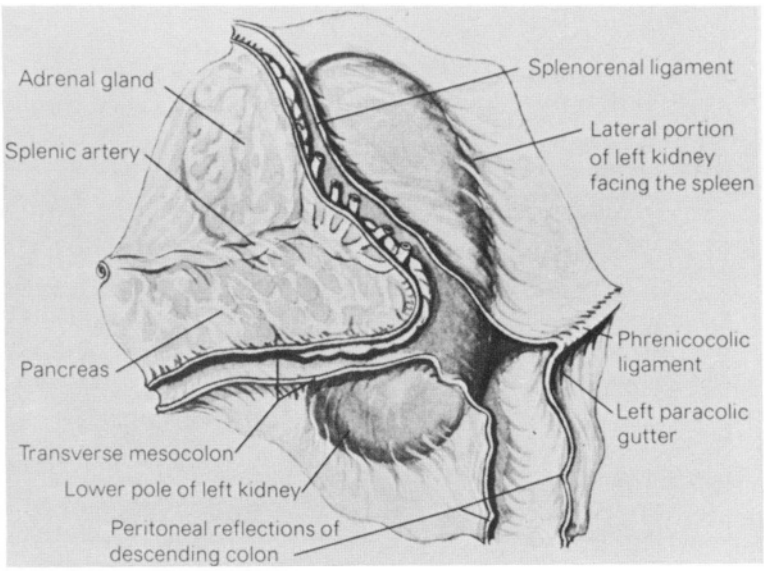
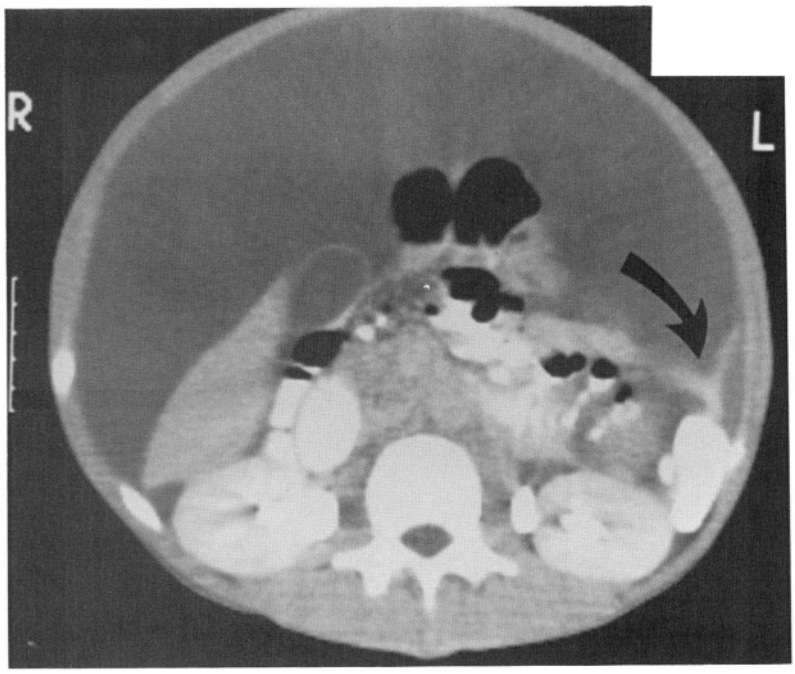


Fig. 4–72. Continuity of gastric carcinoma into gastrosplenic and splenorenal ligaments.
(a) The mass *(M)* of an ulcerated carcinoma of the stomach *(St)* extends into the gastrosplenic ligament in relation to the spleen *(Sp)*.
(b) Celiac arteriogram documents extension into the splenorenal ligament by virtue of neoplastic beading of the splenic artery *(arrow)*.

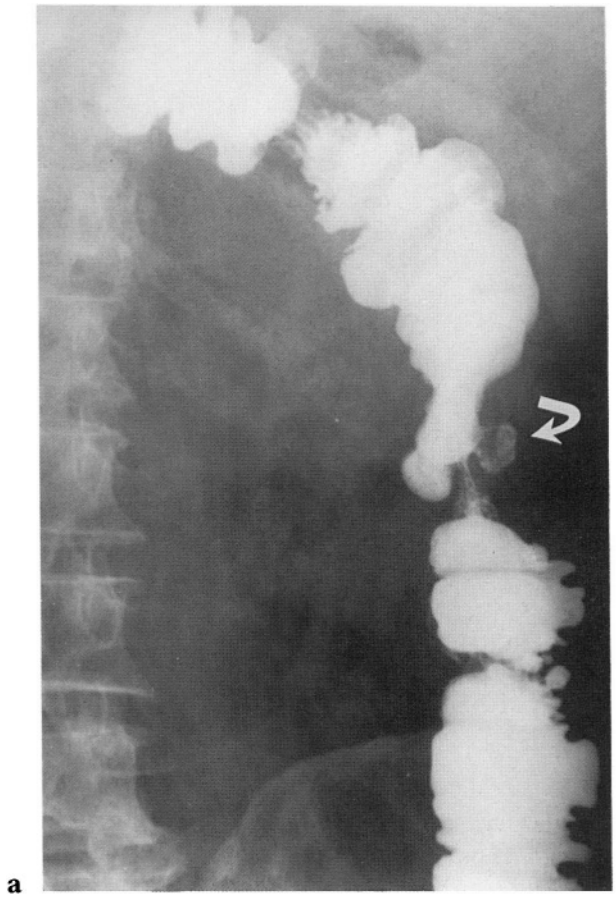


a

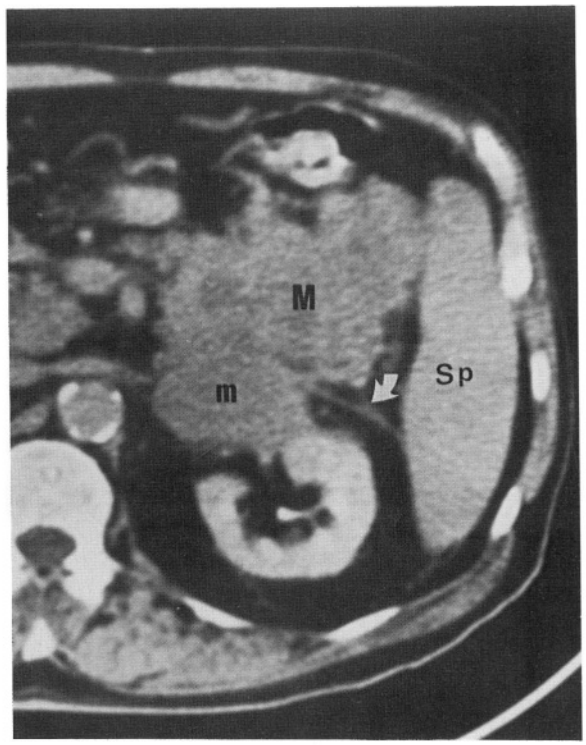


b

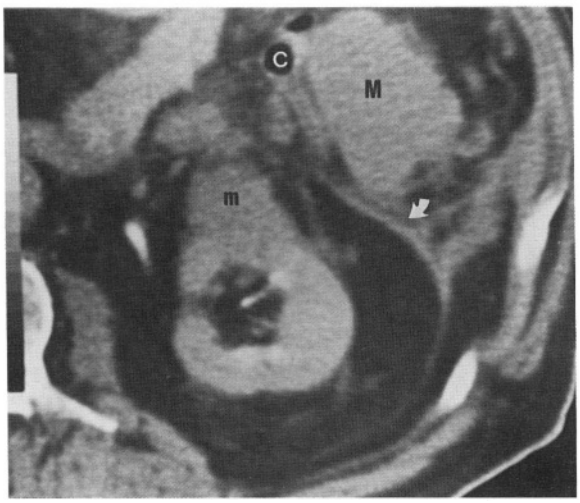
Fig. 4–73. The phrenicocolic ligament.
(a) Frontal drawing of the sites of the major posterior ligaments of the left upper quadrant shows that all have continuity with the phrenicocolic ligament.
(b) In a patient with ascites, CT scan demonstrates the phrenicocolic ligament *(arrow)* extending laterally from the region of the anatomic splenic flexure of the colon.
(Reproduced from Meyers et al.[9])



a



b



c

Fig. 4–74. Spread of pancreatic carcinoma into phrenicocolic ligament.
(a) Barium enema demonstrates lateral mass impression upon the anatomic splenic flexure of the colon *(arrow).* Incidental diverticula are present.
(b) CT scan shows a carcinomatous mass *(M)* arising from the tail of the pancreas anterior to the thickened anterior renal fascia *(arrow)* within the splenorenal ligament approaching the spleen *(Sp).* A component of the mass *(m)* has invaded the perirenal space.
(c) At a lower level, there is spread of the mass *(M)* into the phrenicocolic ligament anterior to the renal fascia *(arrow)* pressing upon the lateral aspect of the anatomic splenic flexure of the colon (*C*), as indicated initially by the barium enema. A component of the mass (*m*) has invaded the left kidney.

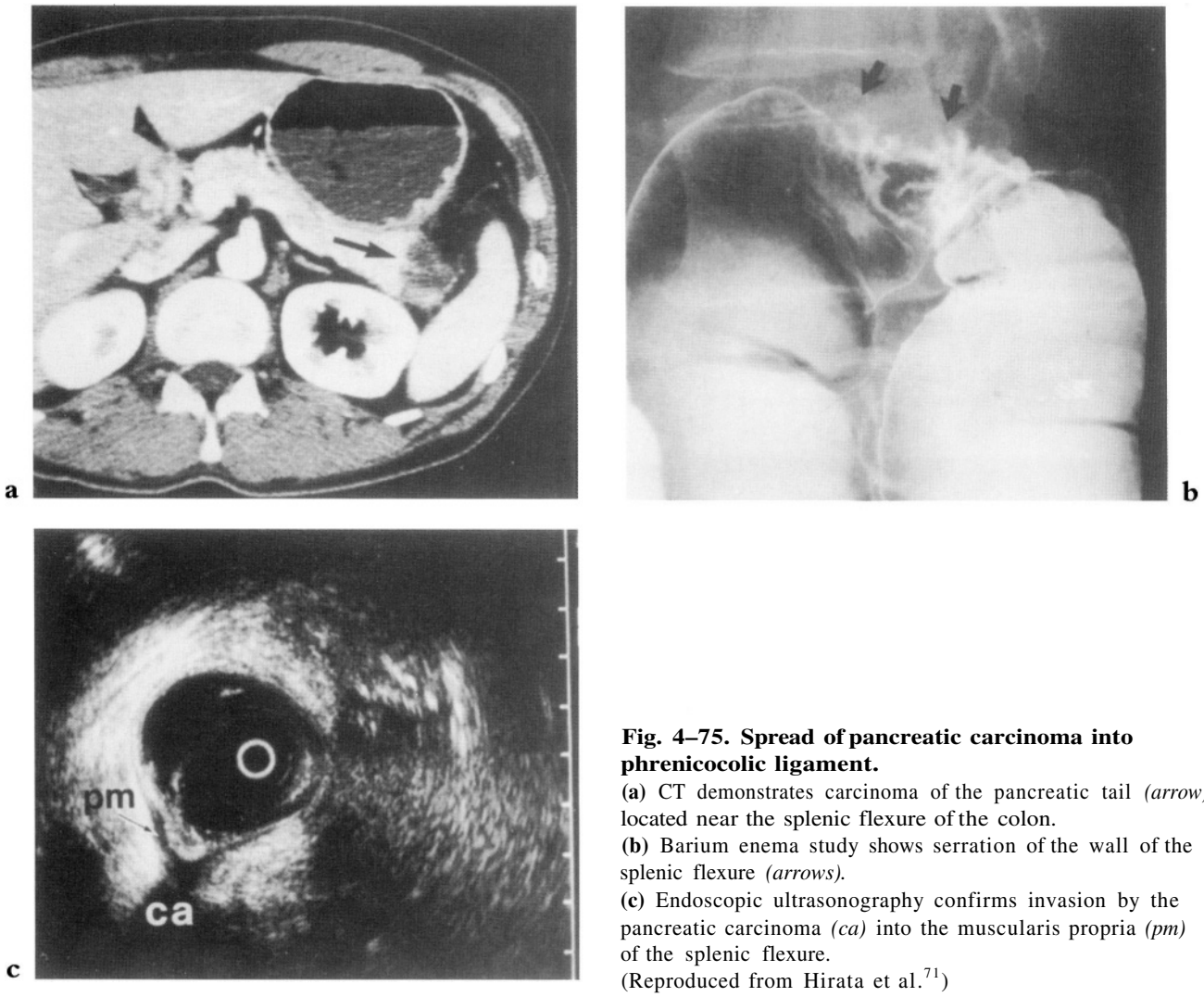


Fig. 4–75. Spread of pancreatic carcinoma into phrenicocolic ligament.
(a) CT demonstrates carcinoma of the pancreatic tail *(arrow)* located near the splenic flexure of the colon.
(b) Barium enema study shows serration of the wall of the splenic flexure *(arrows).*
(c) Endoscopic ultrasonography confirms invasion by the pancreatic carcinoma *(ca)* into the muscularis propria *(pm)* of the splenic flexure.
(Reproduced from Hirata et al.[71])

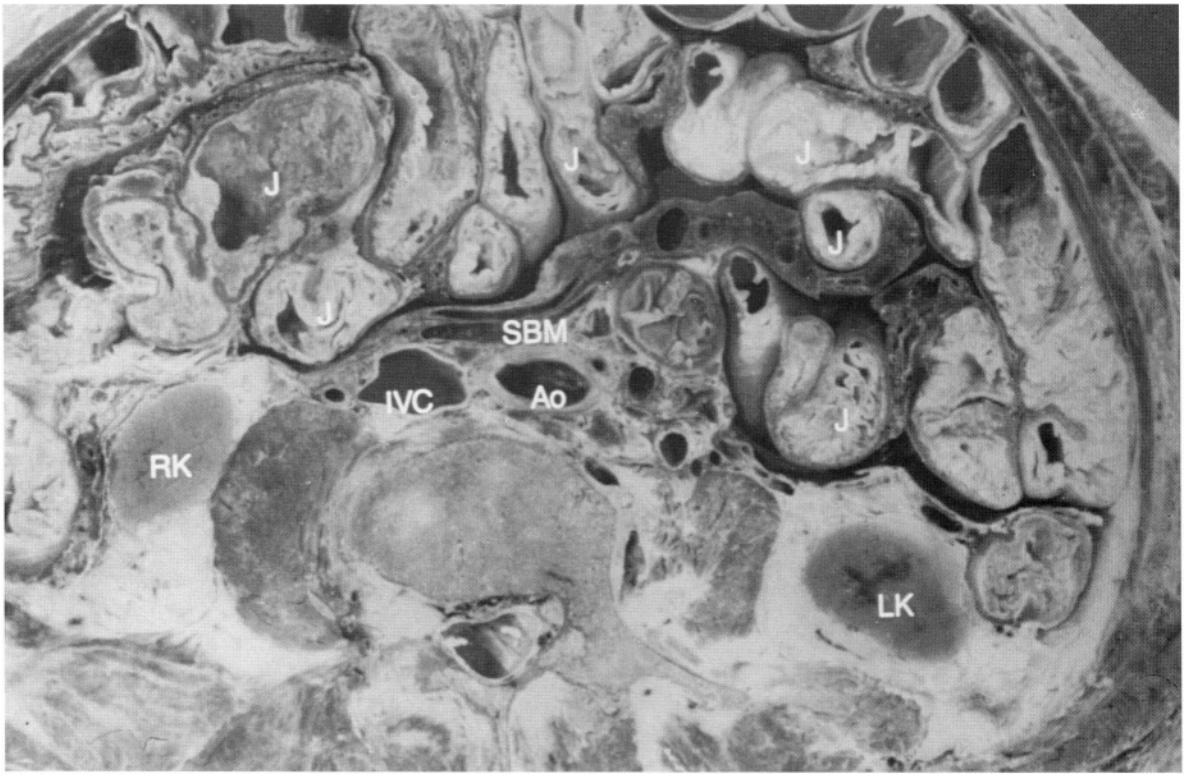


Fig. 4–76. Relationships of the small bowel mesentery.
Anatomic cross-section illustrates an extension of the small bowel mesentery (*SBM*) suspending jejunal loops (*J*). Anatomic continuity is established between the extraperitoneal anterior pararenal space and the intraperitoneal small bowel mesentery. *RK* = right kidney; *LK* = left kidney; *Ao* = aorta; *IVC* = inferior vena cava.
(Reproduced from Meyers et al.[9])

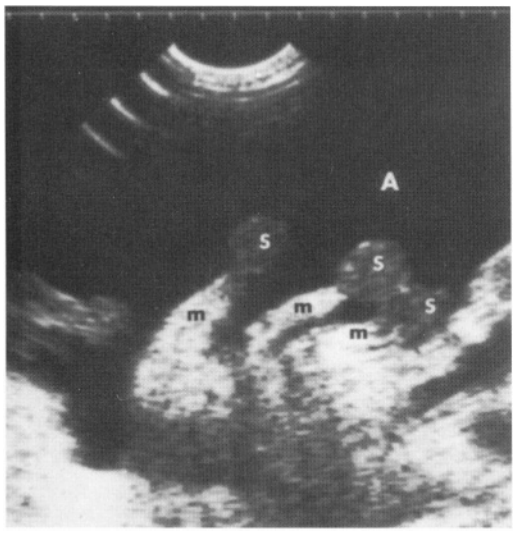


Fig. 4–77. Mesenteric pathways to small bowel loops.
Sagittal ultrasound scan shows loops of small bowel (*s*), floating in massive ascites (*A*), are attached by their mesentery (*m*).
(Courtesy of Francis S. Weill, M.D., University Hospital, Besançon, France.)

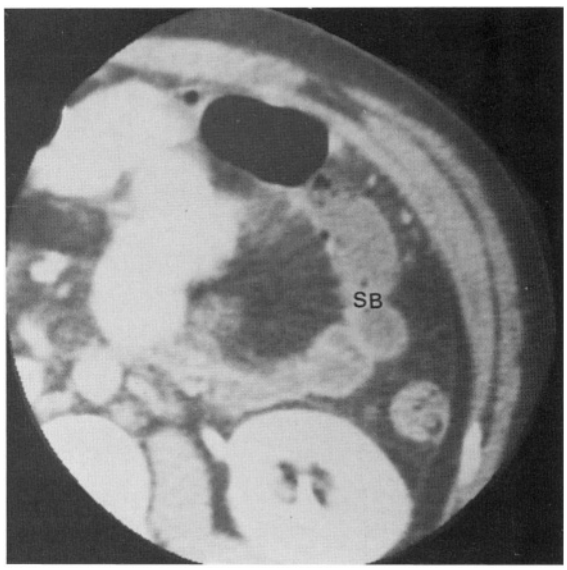


Fig. 4–78. CT identification of the small bowel mesentery.
Discrete vasa recta penetrate the mesenteric border of a small bowel loop (*SB*).

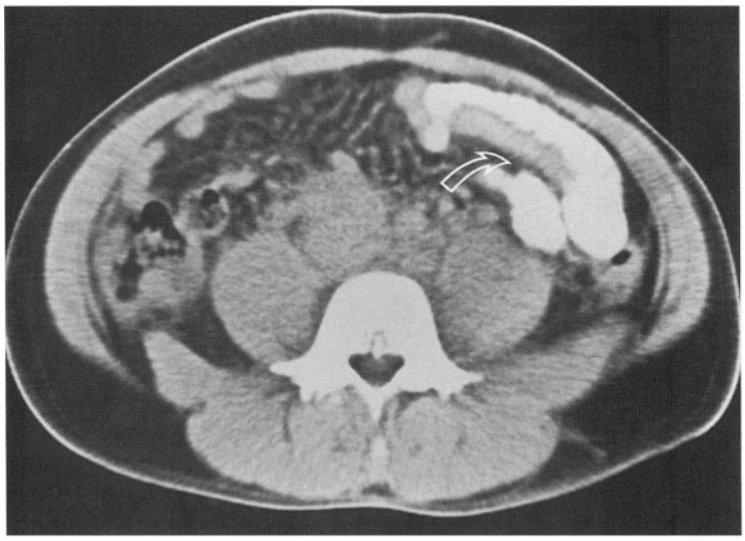


Fig. 4–79. Spread of lymphoma within the mesentery. Hodgkin's lymphoma produces stellate infiltration of the small bowel mesentery and mural thickening of the mesenteric side of an opacified loop (*arrow*). (From Meyers et al.[9])

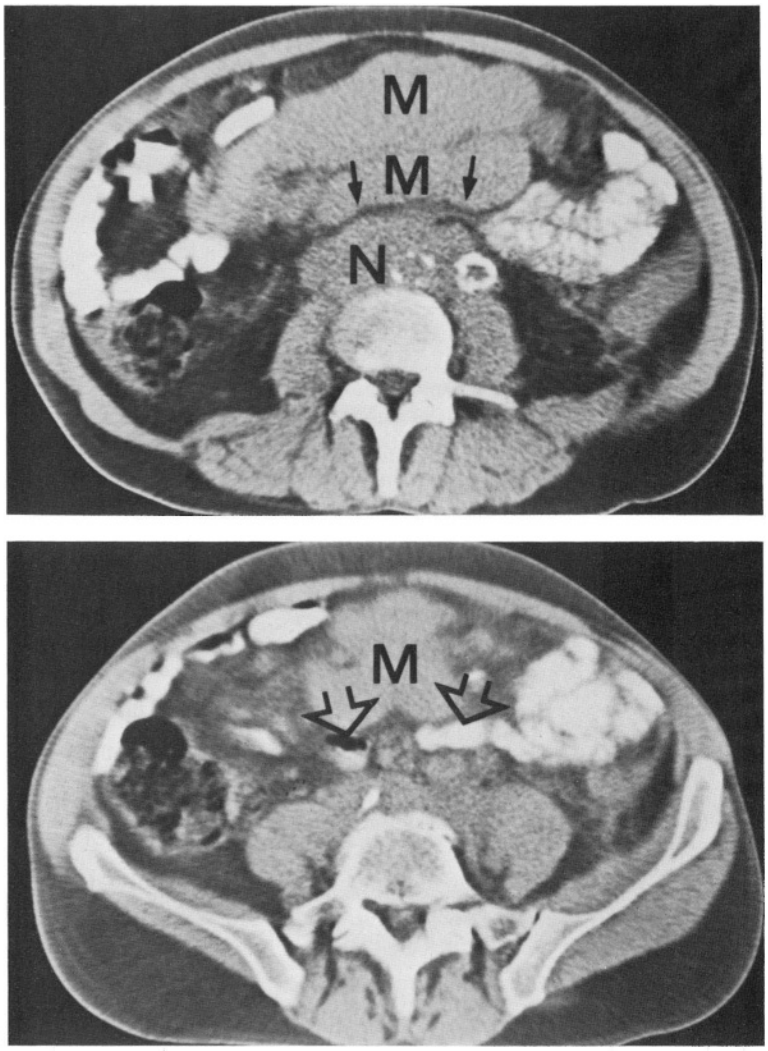


Fig. 4–80. Distinction of mesenteric and retroperitoneal masses.
(a) In a patient with lymphoma, enlarged retroperitoneal nodes (*N*) can be distinguished from extensive mesenteric nodal masses (*M*) by virtue of an intact fat plane *(arrows)* of the anterior pararenal space. The mesenteric masses themselves exhibit the "sandwich" sign.
(b) The distinction between anatomically distinct compartments is further confirmed at a lower level by the partial interposition of opacified small bowel loops (*arrows*) approaching the root of the mesentery between the extraperitoneal tissues and the mesenteric mass (*M*).
(Reproduced from Meyers et al.[9]).

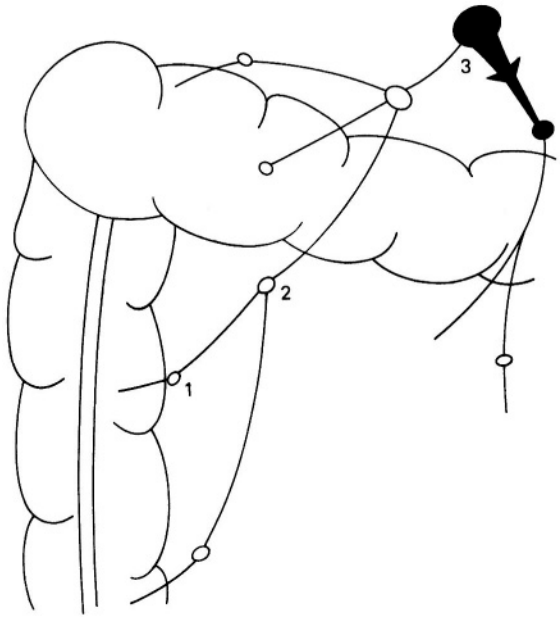


Fig. 4–81. The mechanism of lymphatic permeation.
Tumor cells may be transported through the draining chain of lymph nodes (*1,2*) to impact a more central node (*3*), with retrograde permeation then occurring.

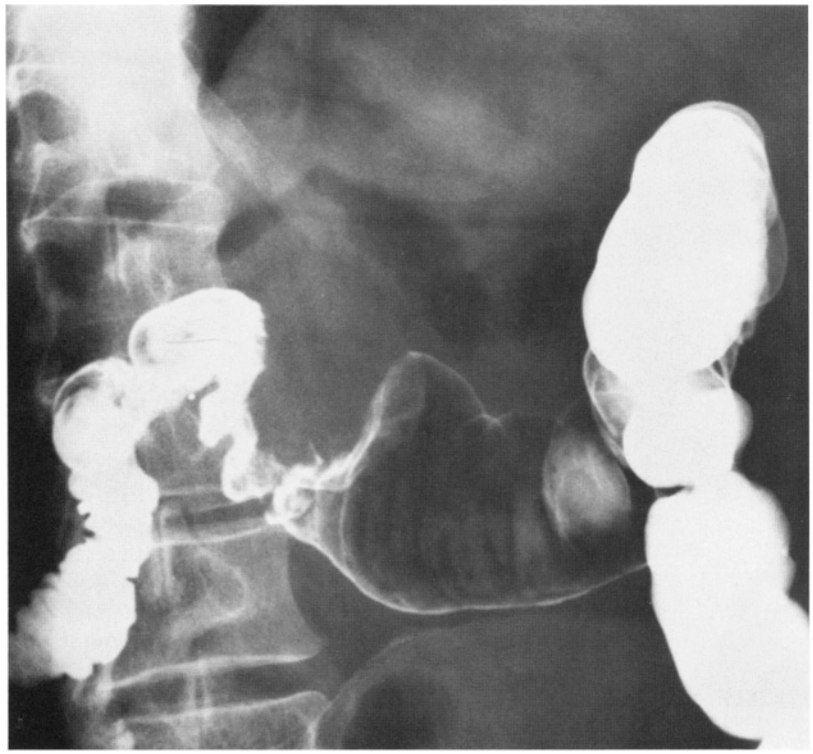


Fig. 4–82. Anastomotic recurrence.
This occurred following right hemicolectomy for carcinoma and ileotransverse colostomy. Lymphatic permeation may be a contributing factor.

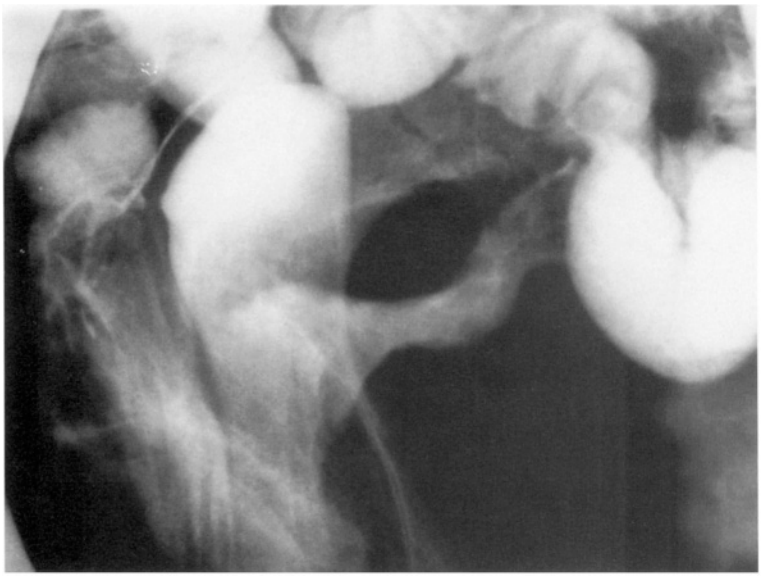


Fig. 4–83. Carcinoma of the cecum with lymphatic permeation.
A spot compression view of the terminal ileum shows a cecal carcinoma exhibiting a short stricture with mucosal destruction and shouldering of the margins. Retrograde lymphatic spread into the terminal ilieum results in a neoplastic mass at this site larger than the primary cecal carcinoma.
(Reproduced from Gourtsoyiannis and Nolan.[80])

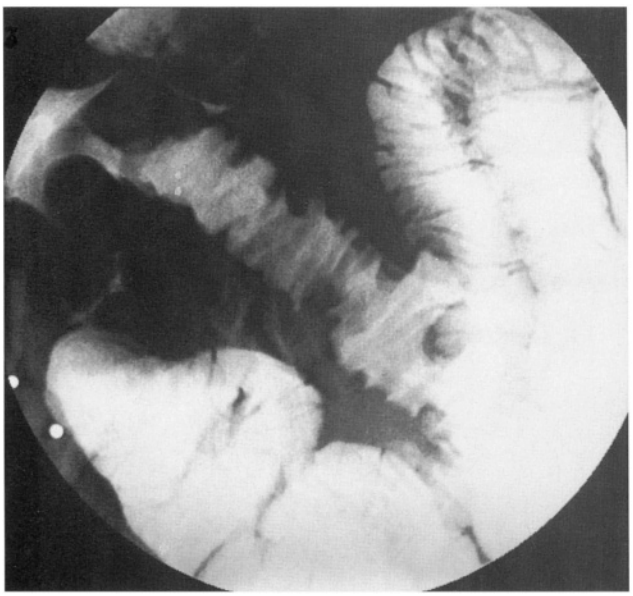


Fig. 4–84. Carcinoma of the cecum with lymphatic permeation.
Enteroclysis study shows thickening of the valvulae conriiventes with narrowing of the lumen of the terminal ileum. Operation disclosed an occult small carcinoma of the cecum with extensive lymphatic spread to the terminal ileum.
(Reproduced from Gourtsoyiannis and Nolan.[80])

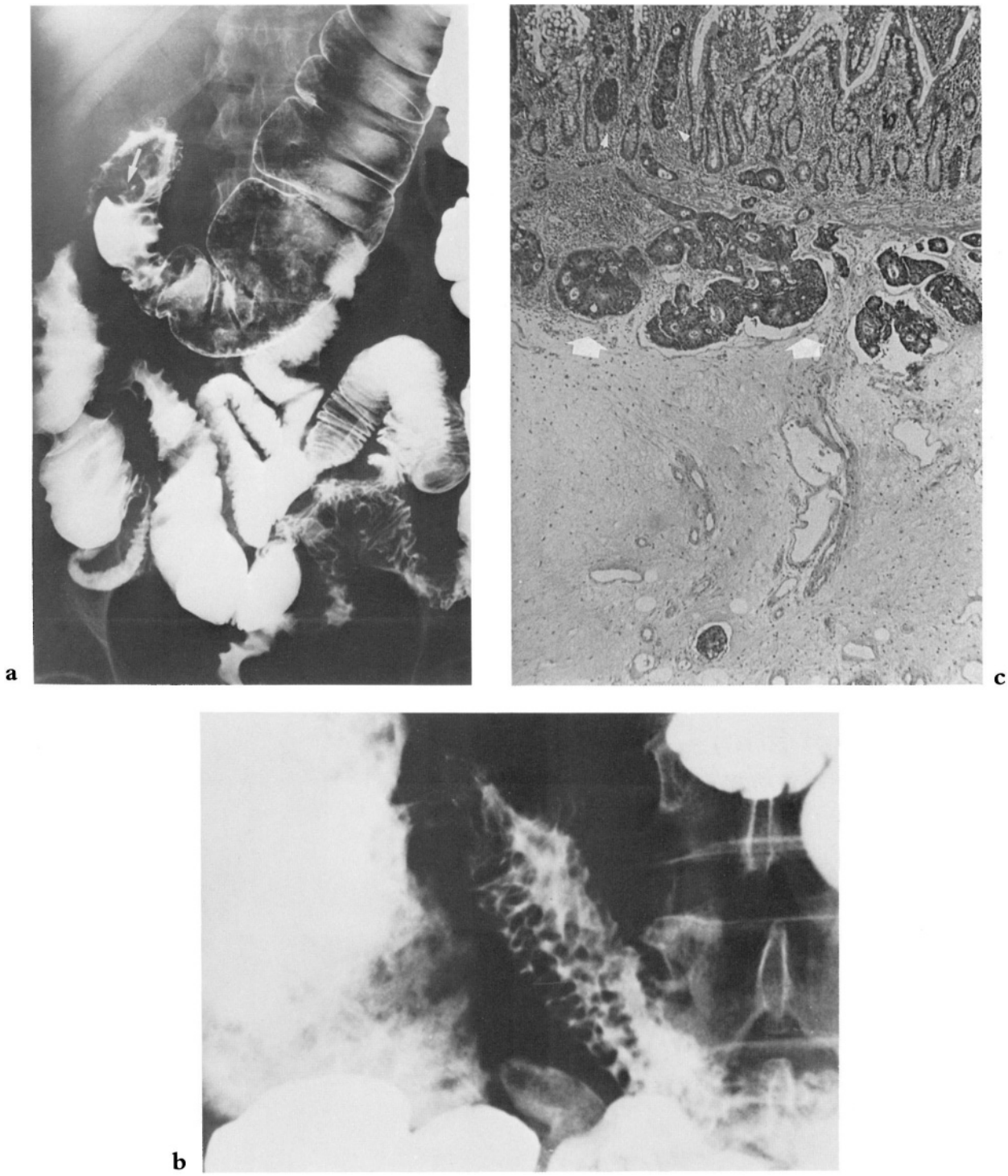


Fig. 4–85. Carcinoma of the hepatic flexure with lymphatic permeation simulating Crohn's disease.
(a) Barium enema shows a severe long stenosis in the hepatic flexure secondary to a primary adenocarcinoma with colocolonic fistulization (*arrow*). "Thumbprinting" is present in the ascending colon and terminal ileum, and the appendix shows spiculation and nodularity.
(b) Small bowel examination demonstrates a "cobblestone" appearance in the terminal ileum and thickening of the ileocecal valve.
(c) Histologic findings include submucous lymphatic infiltration by carcinoma cells (*arrows*). Some metastatic cell groups are invading the normal intestinal mucosa in retrograde fashion (*arrowheads*).
(Reproduced from Perez et al.[79])

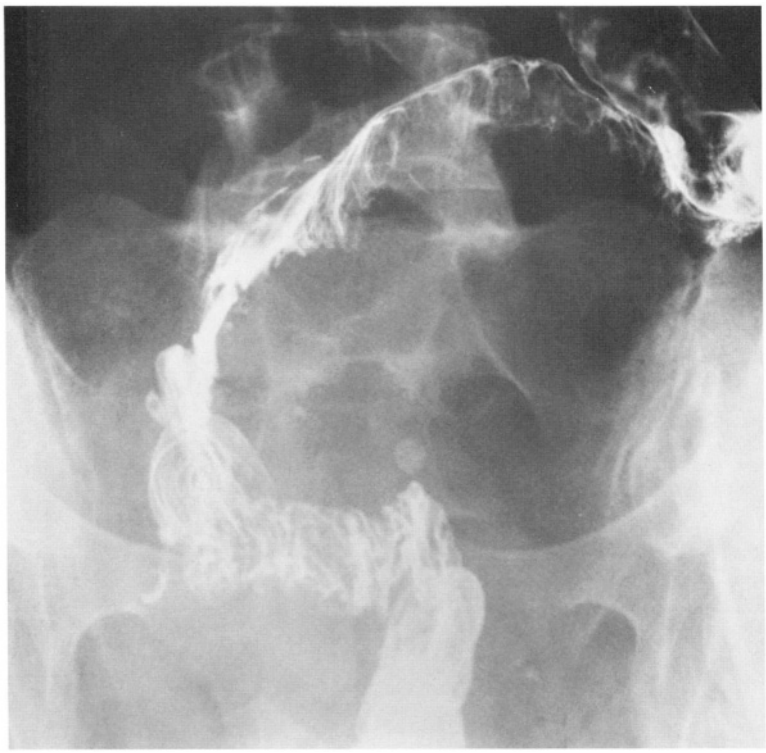


Fig. 4–86. Direct invasion of the sigmoid colon by a leiomyosarcoma (malignant fibroid) of the uterus.
Large pelvic mass displaces and fixes the colon, with gross distortion and tethering of the mucosal folds from the associated desmoplastic reaction. (Reproduced from Meyers and McSweeney.[1])

Direct Invasion from Contiguous Primary Tumors

Intrinsic involvement of the alimentary tract by an immediately contiguous neoplasm indicates that a locally aggressive tumor has usually broken through fascial planes.[84,85] The most common primaries arise in the ovary, uterus, prostate, and kidney.

With pelvic tumors, the cardinal roentgen signs include an identifiable mass and invasion of the wall of adjacent bowel, often over a considerable length, usually without overhanging margins (Fig. 4–86). Tethering of mucosal folds is often a conspicuous feature. In a female, the most common primary that directly invades the large intestine is *carcinoma of the ovary.* On the left, the *inferior* border of the sigmoid colon is characteristically involved first. Stages of involvement range from fixation with nodular irregularities (Figs. 4–87 through 4–89) or gross desmoplastic angulation of mucosal folds (Fig. 4–90) to annular involvement (Fig. 4–91).

Advanced *prostatic carcinoma* can spread across Denonvillier's fascia to invade the rectum anteriorly or circumferentially[86–88] (Figs. 4–92 through 4–94). Winter[89] reported that 26 of 225 (11.6%) patients with carcinoma

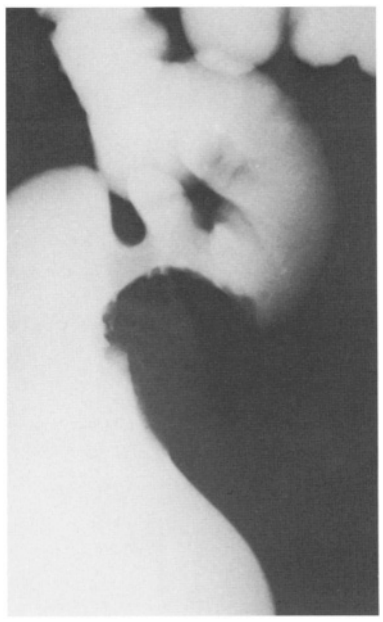


Fig. 4–87. Direct invasion of the sigmoid colon by carcinoma of the left ovary.
A large nodular infiltration involves the inferior border. Pseudosacculations result on the pliable superior border. (Reproduced from Meyers.[5])

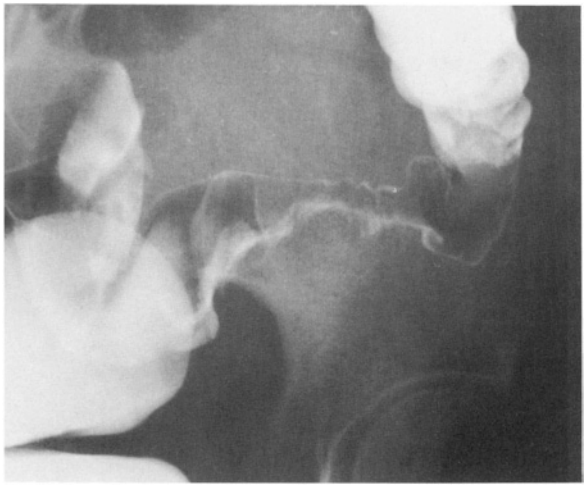
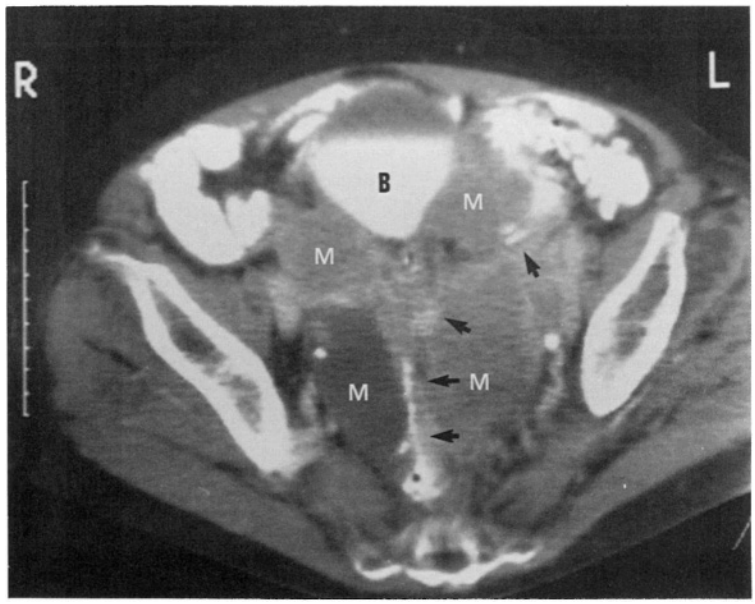


Fig. 4–88. Direct invasion of the sigmoid colon by carcinoma of the left ovary.
Nodular infiltrations involve the inferior border.



a



b

Fig. 4–89. Direct invasion of the sigmoid colon by carcinoma of the left ovary.
(a) Barium enema shows gross nodular invasion extending from inferior border of sigmoid colon. **(b)** CT demonstrates the presence of bilateral ovarian carcinomatous masses (*M*), with those on the left straightening and displacing the markedly narrowed sigmoid colon (*arrows*). *B* = urinary bladder.
(Courtesy of Michiel Feldberg, M.D., Ph.D, University of Utrecht, The Netherlands.)

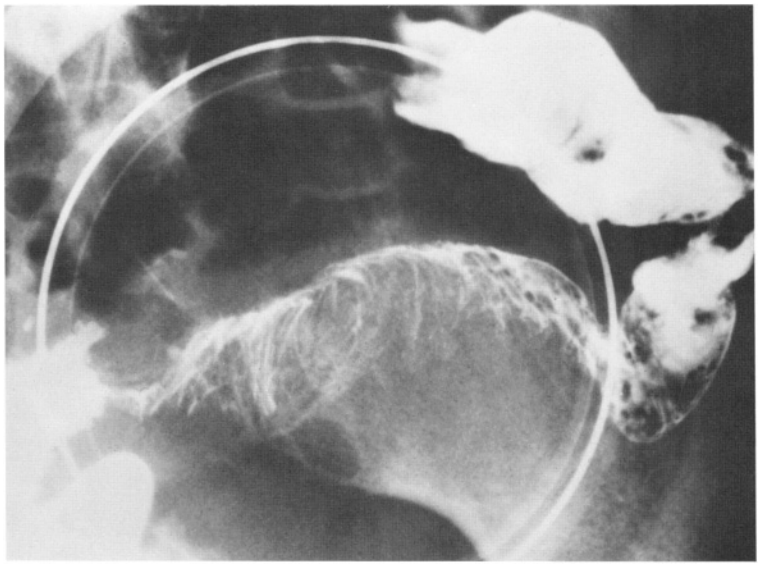


Fig. 4–90. Direct invasion of the sigmoid colon by carcinoma of the left ovary. Mass displacement and fixation of the inferior border are accompanied by striking mucosal tethering.

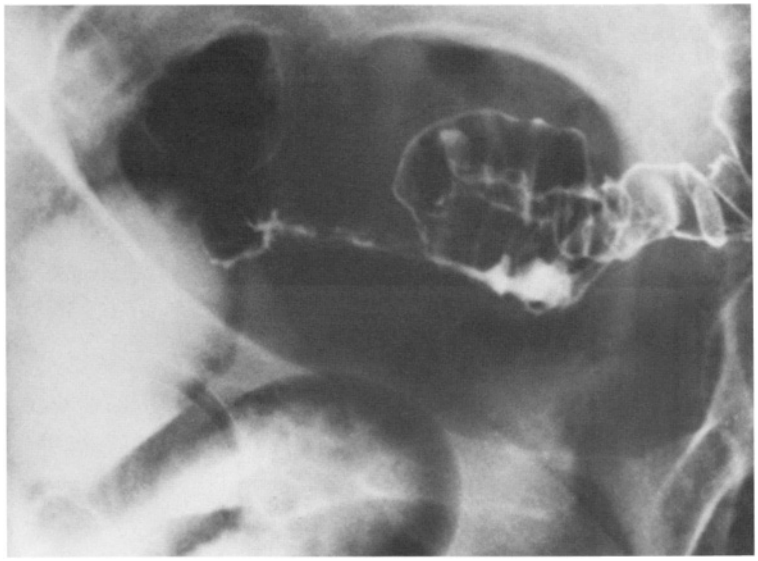


Fig. 4–91. Direct invasion of the sigmoid colon by carcinoma of the left ovary. Extension has progressed to annular involvement.

of the prostate had rectal involvement. Young[90] found 12 instances of rectal mucosal involvement at autopsy in 800 patients with prostatic carcinoma, an incidence of 1.5%. Annular type constriction of the rectum may cause partial to complete obstruction.

Renal neoplasms may invade adjacent segments of bowel directly, possibly as recurrences many years after resection of the primary tumor. The late manifestations of renal metastasis may occur as long as 30 years after diagnosis. The delay in extension from the nephrectomy site may be due to the poor blood supply of the scar.[91] With growth, they tend to produce bulky intraluminal masses without significant obstruction, since they generally do not elicit a desmoplastic response.[1,92,93] Occasionally, they may produce luminal narrowing with mucosal destruction, simulating a primary carcinoma of the bowel (Fig. 4–95). Recognition of the usual sites of involvement and identification of any extraluminal soft-



Fig. 4–92. Annular rectal invasion by prostatic carcinoma.
The surrounding extrinsic mass narrows the rectal lumen.

tissue mass lead to the correct diagnosis. On the right, the descending duodenum (Figs. 4–95 through 4–97) and, on the left, the distal transverse colon or proximal descending colon (Figs. 4–98 and 4–99) are most often involved. At times, jejunal loops may be affected (Figs. 4–100 and 4–101).

Endoscopic ultrasonography has been shown to be useful for evaluating the depth of colonic mural invasion[71] (Figs. 4–102 through 4–104).

text continues on page 192

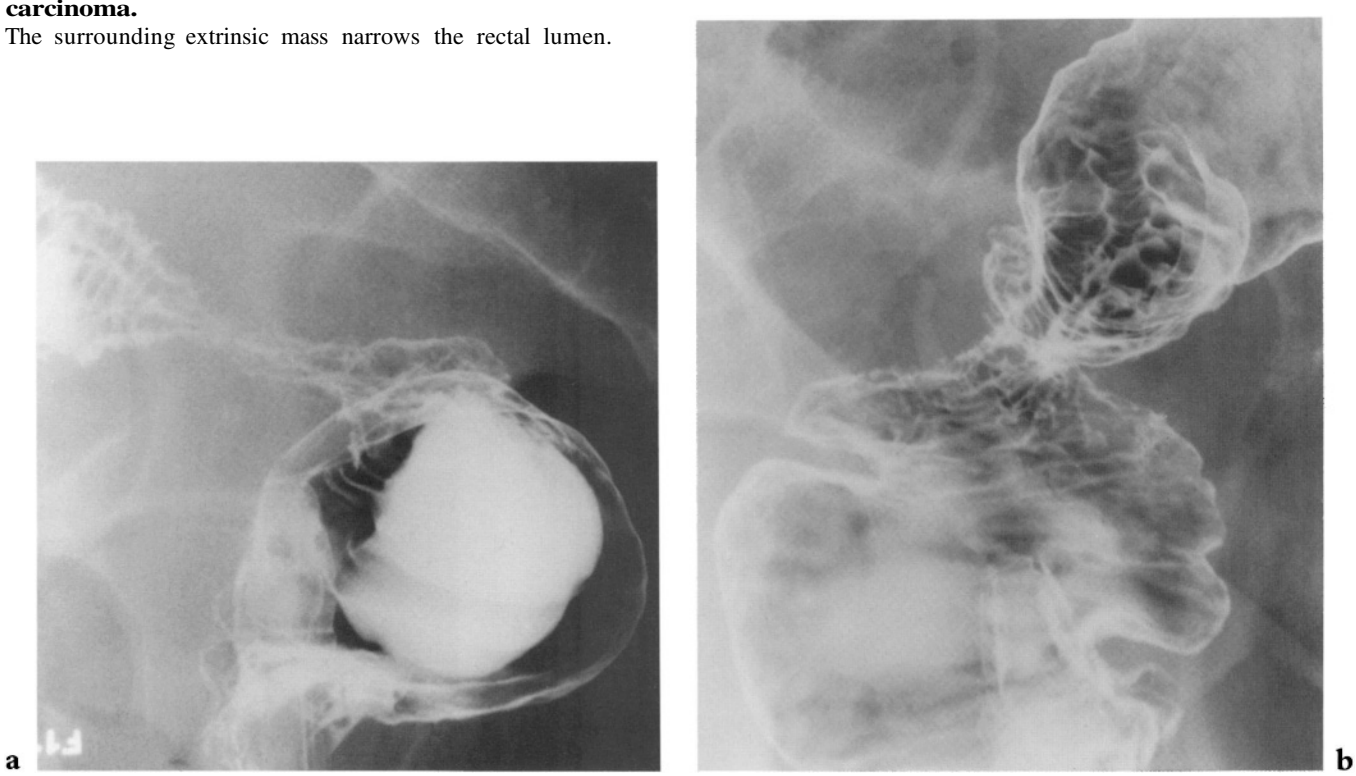


Fig. 4–93. Direct invasion of rectosigmoid colon by prostatic carcinoma.
Lateral **(a)** and mild left posterior oblique **(b)** views of rectum show mass effect and markedly spiculated contour along anterior rectosigmoid junction and sigmoid colon and widening of superior presacral space.
(Reproduced from Rubesin et al.[87])

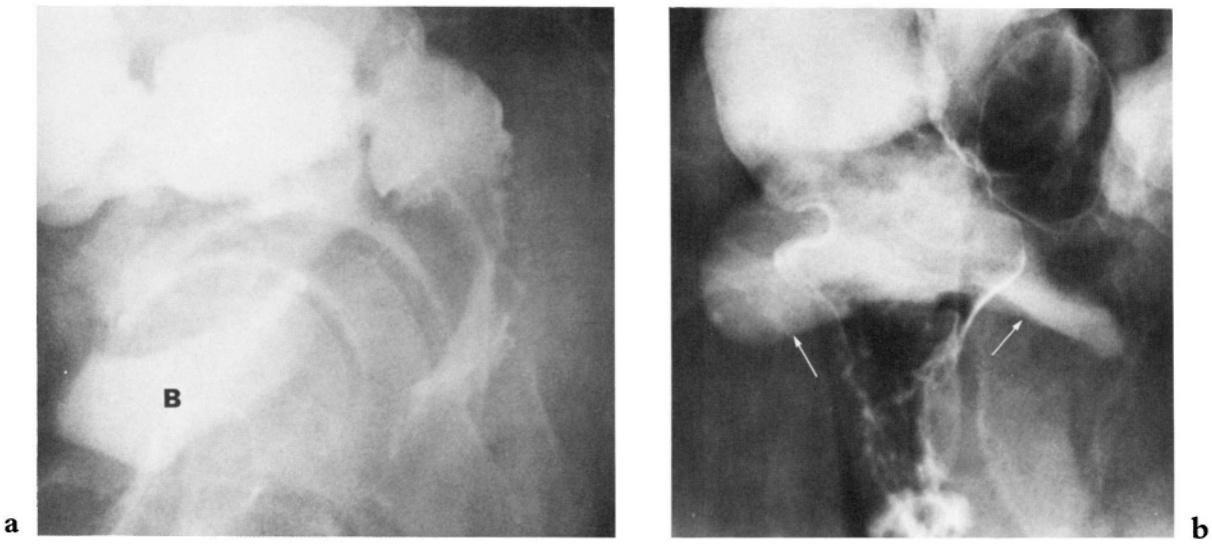


Fig. 4–94. Circumferential invasion of the rectum by carcinoma of the prostate.
(a) Lateral view. Note the widened retrorectal and rectovesical spaces as well as the mucosal alterations in the rectum. Urinary bladder (*B*) opacified by simultaneous intravenous urography.
(Reproduced from Meyers and McSweeney.[1])
(b) Frontal view. The superior border of the annular involvement of the rectum corresponds to the base of the urinary bladder (*arrows*), which is elevated by the enlarged prostate gland.

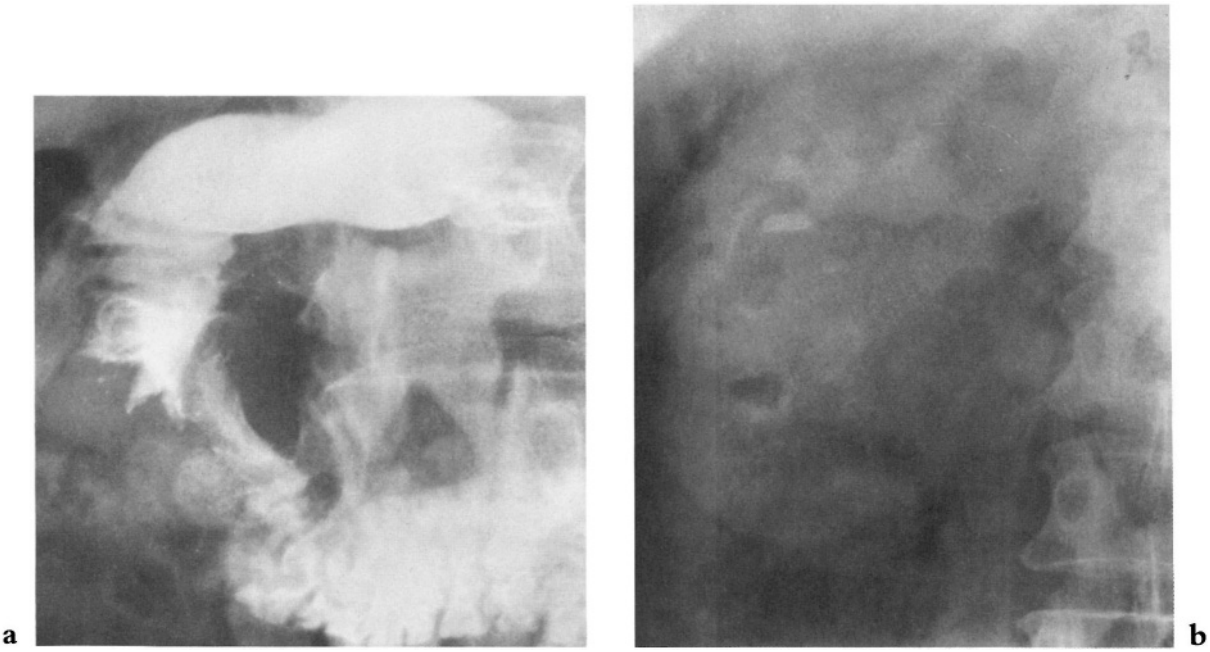
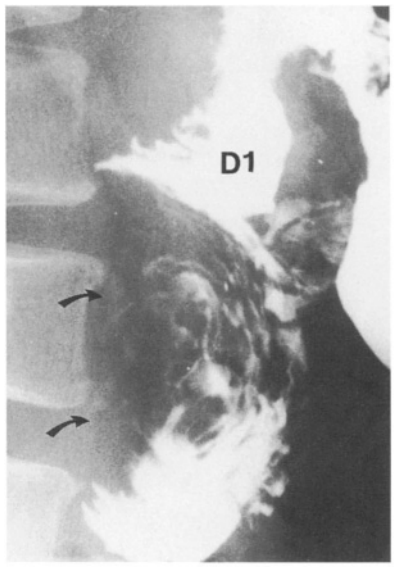


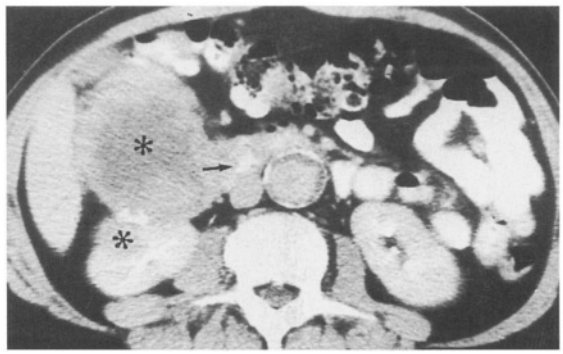
Fig. 4–95. Direct invasion of the descending duodenum by right renal cell carcinoma.
(a) Mucosal destruction simulates a primary neoplasm of the duodenum.
(Reproduced from Meyers and McSweeney.[1])
(b) Intravenous urogram shows large mass with a few faint calcifications within the lower pole of the right kidney, displacing the collecting system.



Fig. 4–96. Direct invasion of the descending duodenum by right renal cell carcinoma.
This results in multiple polypoid intramural masses of varying sizes, without angulation.



a



b

Fig. 4–97. Direct invasion of the descending duodenum by right renal cell carcinoma.
(a) Upper GI series, lateral view, shows a large mass effect upon the posterior wall of the descending duodenum. The *curved arrows* indicate faint tumoral calcification. *D1* = duodenal bulb.
(b) CT demonstrates a large heterogeneous mass (*asterisks*) of the right kidney invading the second portion of the duodenum (*arrow*).
(Reproduced from K. Cho: *In* Gourtsoyiannis and Nolan.[80])

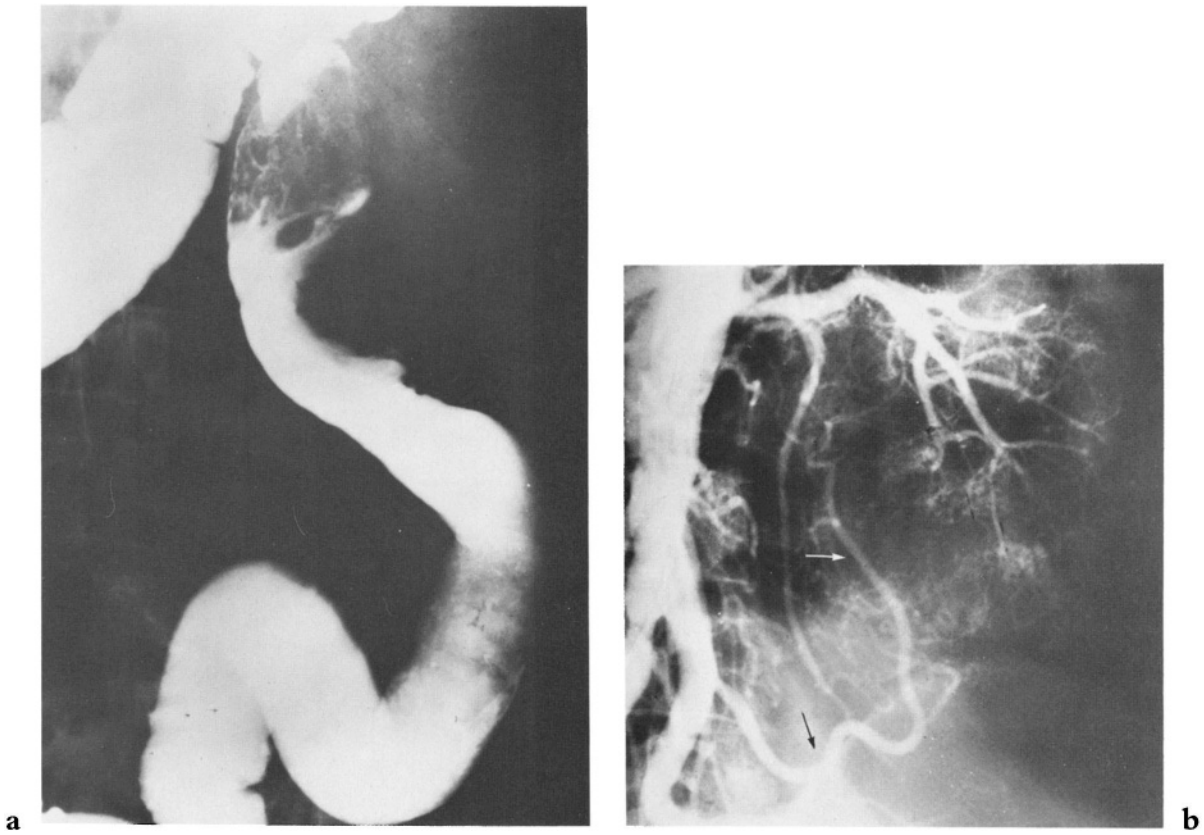


Fig. 4–98. Direct invasion of the colon by left renal carcinoma.
(a) Extrinsic and intramural masses of the distal transverse and proximal descending colon with bulky polypoid intraluminal extensions. There is no obstruction or acute angulation. (Reproduced from Meyers and McSweeney.[1])
(b) Abdominal aortogram shows neovascularity from the renal artery. In addition, a hugely dilated inferior mesenteric artery (*arrows*) contributes blood supply to the tumor invasion of the colon.

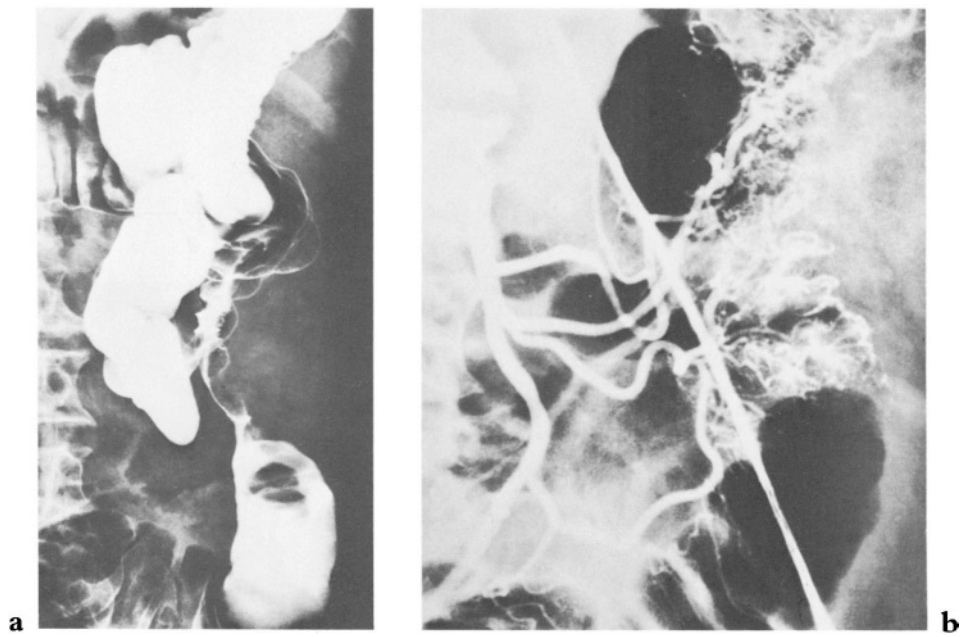
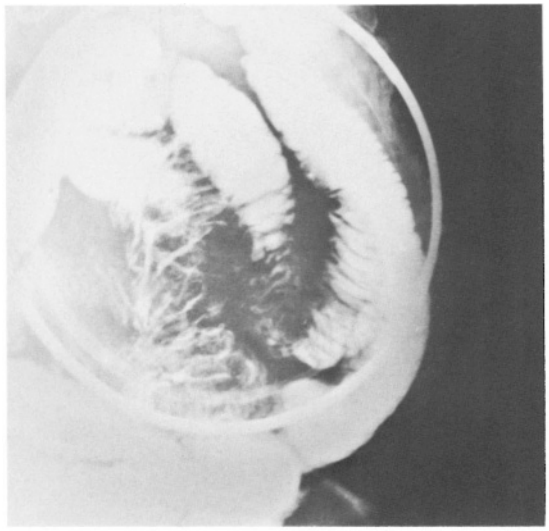


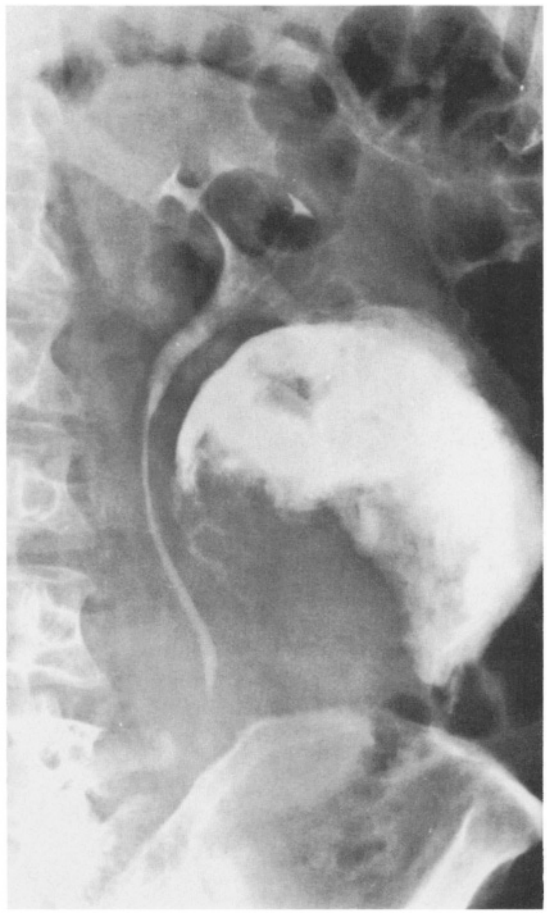
Fig. 4–99. Direct invasion of the colon by left renal cell carcinoma.
(a) Extrinsic masses deform and narrow the descending colon and grow into its lumen.
(b) Selective inferior mesenteric arteriogram demonstrates a plethora of neovascularity within the invaded colon.



Fig. 4–100. Direct invasion of the jejunum by left renal cell carconoma.
Following a nephrectomy, recurrent tumor invades overlying jejunal loops as bulky intramural and intraluminal growths.

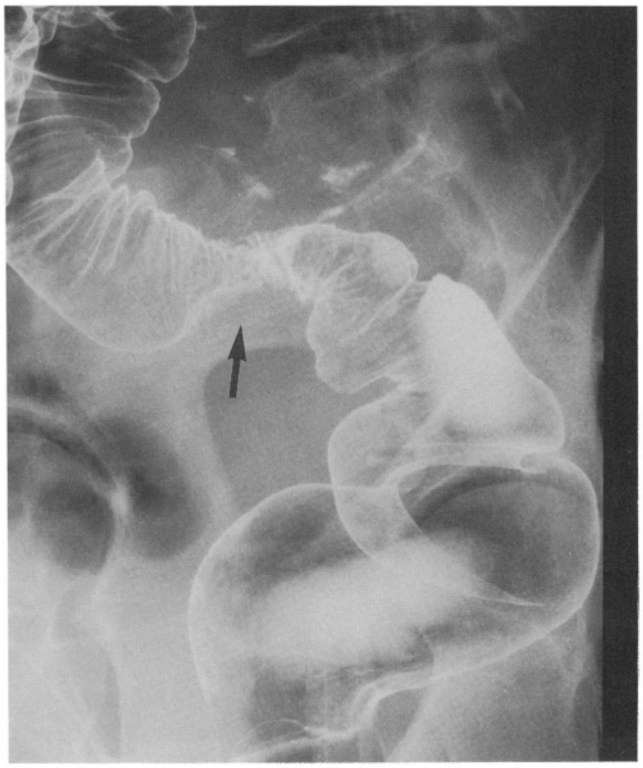


a

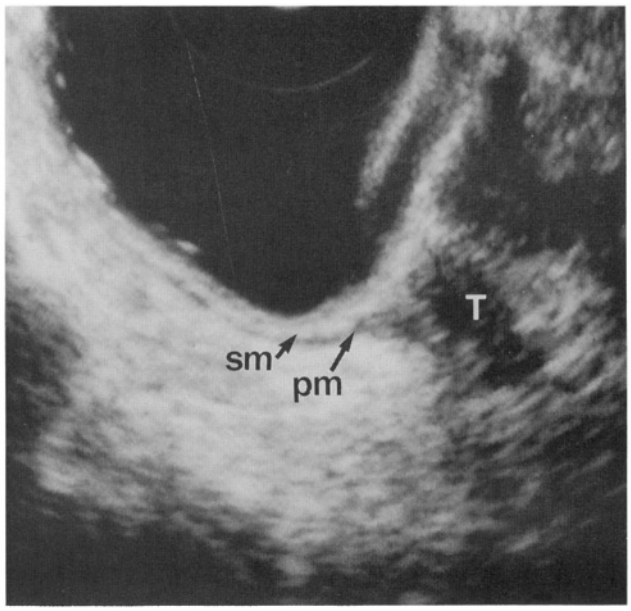


b

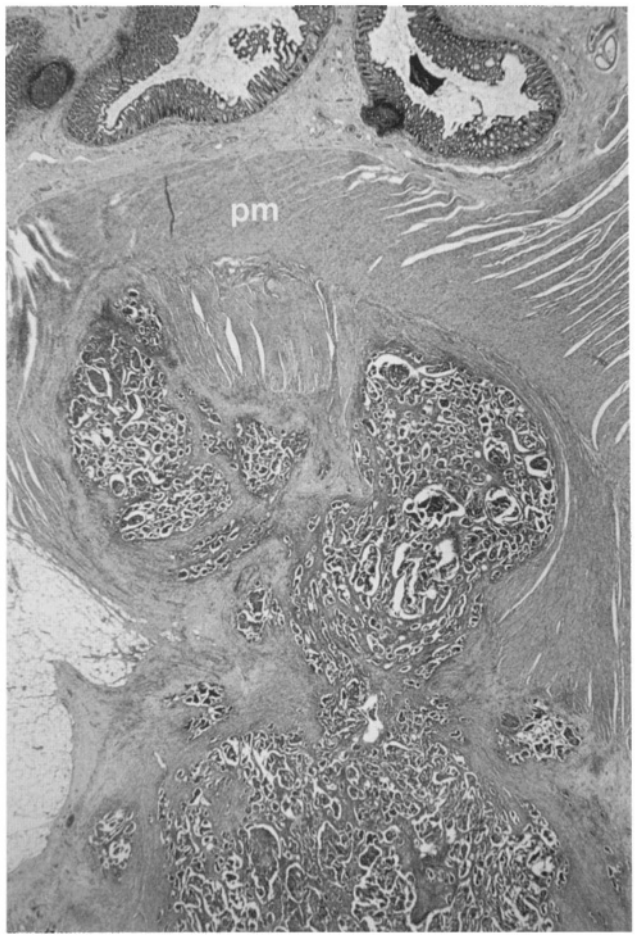
Fig. 4–101. Direct invasion of the jejunum by left renal cell carcinoma.
(a) Compression spot film demonstrates infiltration of the mesentery and jejunal loops.
(b) Percutaneous puncture of neoplastic mass arising from lower pole of left kidney shows its polypoid components.



a



b



c

Fig. 4–102. Depth of direct invasion of the sigmoid colon by ovarian carcinoma shown by endoscopic ultrasonography.
(a) Double–contrast barium enema demonstrates narrowing of the distal sigmoid colon with tethering of mucosal folds (*arrow*).
(b) Endoscopic ultrasonography reveals that the pelvic tumor (*T*) has invaded into the hypoechoic layer representing the muscularis propria (*pm*) but the hyperechoic submucosa (*sm*) is intact.
(c) Microscopic findings document that the ovarian carcinoma has directly invaded into the muscularis propria (*pm*).
(Reproduced from Hirata et al.[71])

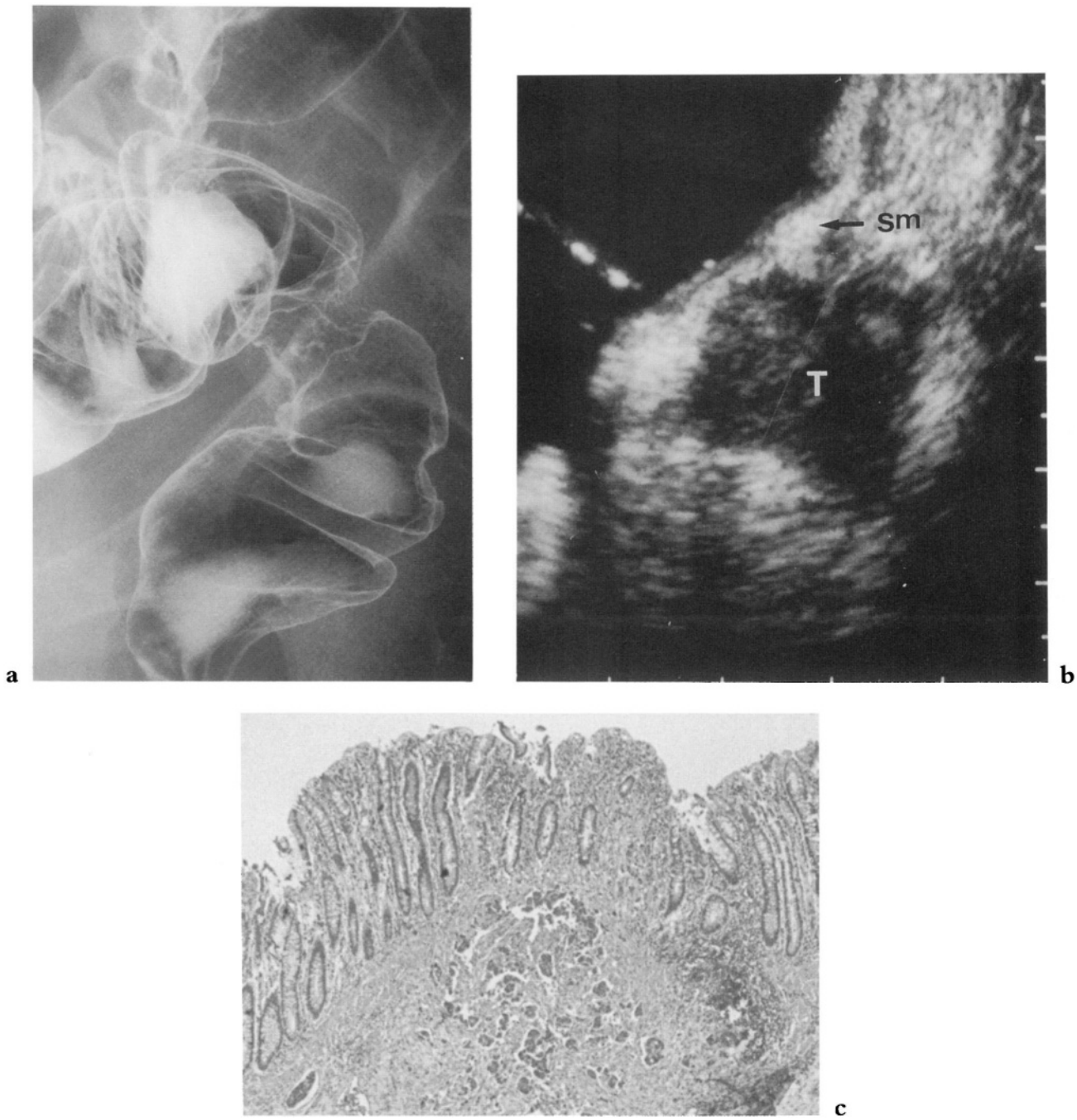


Fig. 4–103. Depth of direct invasion of rectum by carcinoma of the ovary shown by endoscopic ultrasonography.
(a) Double-contrast barium enema shows nodular mural irregularities involving the rectosigmoid junction.
(b) Endoscopic ultrasonography reveals the pelvic tumor (*T*) invading through the wall, extending to the hyperechoic layer of the submucosa (*sm*), which is thin without interruption.
(c) Histologic findings confirm that the depth of invasion by the ovarian carcinoma is to the submucosa.
(Reproduced from Hirata et al.[71])

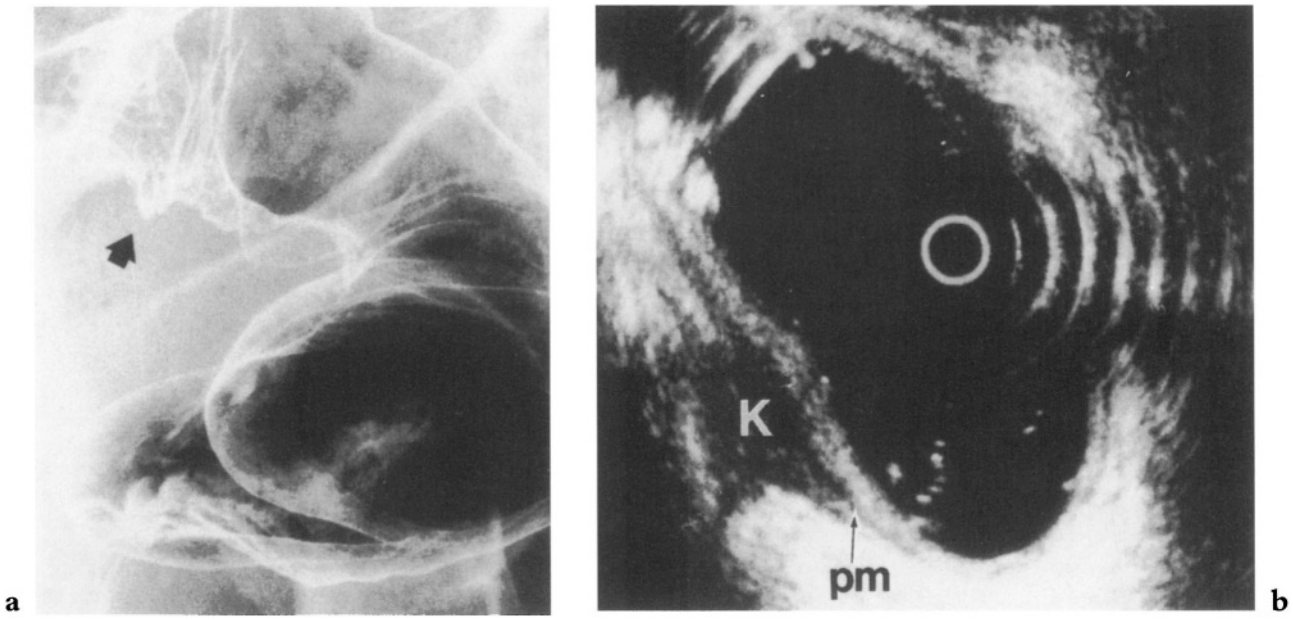


Fig. 4–104. Depth of direct invasion of the sigmoid colon by a Krukenberg tumor of the ovary shown by endoscopic ultrasonography.
(a) Barium enema reveals extrinsic compression with tethering (*arrow*).
(b) On endoscopic ultrasonography, a Krukenberg tumor (*K*) invades into the muscularis propria (*pm*).

Intraperitoneal Seeding

It has been classically assumed that transcoelomic spread is a random event or, at least, a function of serosal implantation in the immediate area of a primary neoplasm. However, I have shown that the deposition and growth of secondarily seeded neoplasms in the abdomen depend on the natural flow of ascites within the peritoneal recesses.[3] A primary neoplasm or even its intraabdominal lymph node metastases, in breaking through into the peritoneal cavity, can shed cells into the ascitic fluid induced. The degree of ascites need not be great for the transportation and deposition of malignant cells. I have documented that intraperitoneal fluid, rather than being static, continually follows a circulation through the abdomen.[3,70,94] These dynamic pathways of distribution and sequential spread depend particularly on mesenteric reflections and peritoneal recesses as well as on the forces of gravity and negative subdiaphragmatic pressure.

Anatomic Features

The peritoneal cavity is subdivided by peritoneal reflections and mesenteric attachments into several compartments and recesses (Fig. 4–105a). These are anatomically continuous, either directly or indirectly.

The major barrier dividing the abdominal cavity is the *transverse mesocolon.* Below this, the obliquely oriented *small bowel mesentery* divides the inframesocolic space into two compartments of unequal size—the *right* and *left infracolic spaces.* Its main axis, nevertheless, is directed toward the right lower quadrant in relation to the terminal ileum and cecum. The right infracolic space terminates at their junction. The left infracolic space is open anatomically to the pelvis to the right of the midline; toward the left, it is restricted from continuity with the pelvic cavity by the sigmoid mesocolon.

The *right* and *left paracolic gutters* are lateral to the attachments of the peritoneal reflections of the ascending and descending colon. They represent potential communications between the lower abdomen and pelvis below with the supramesocolic area above. On the left, however, the phrenicocolic ligament[48] partially separates the paracolic gutter from the perisplenic (left subphrenic) space. This ligament extends from the splenic flexure of the colon to the diaphragm at the level of the 11th rib.

The *pelvis* is the most dependent portion of the peritoneal cavity in either the supine or erect position. Its compartments include the midline cul-de-sac or *pouch of Douglas* (rectovaginal pouch in the female and rectovesical pouch in the male) and the *lateral paravesical recesses.*

Pathways of Ascitic Flow

The transverse mesocolon, small bowel mesentery, sigmoid mesocolon, and the peritoneal attachments of the ascending and descending colon clearly serve as watersheds directing the flow of ascites (Fig. 4–105b). The force of gravity operates to pool peritoneal fluid in dependent peritoneal recesses. Fluid in the inframesocolic compartments preferentially seeks the pelvic cavity. From the left infracolic space, some fluid is temporarily arrested along the superior plane of the sigmoid mesocolon but gradually channels into the pelvis. From the right infracolic space, spread occurs along the small bowel mesentery. It is not until a pool is formed at the apex, at the termination of the ileum with the cecum, that some fluid begins to overflow into the pelvis. The pouch of Douglas is first filled and then, symmetrically, the lateral paravesical recesses (Fig. 4–106). From this point, the fluid ascends both paracolic gutters. Passage up the shallower left one is slow and weak, and cephalad extension is limited by the phrenicocolic gutter. The major flow from the pelvis is up the right paracolic gutter. It continues to the right subhepatic and right subphrenic spaces. The right paracolic gutter serves also as the main communication from the upper to the lower abdominal compartments. Freely movable fluid collecting in the right upper quadrant also continues to be redirected downward along this channel to the pelvis.

Four predominant sites in the lower abdomen are therefore identified clearly as the preferential, repeated, or arrested flow of ascitic fluid: (a) the pelvic cavity, particularly the pouch of Douglas; (b) the right lower quadrant at the termination of the small bowel mesentery; (c) the superior aspect of the sigmoid mesocolon; and (d) the right paracolic gutter. These pathways are illustrated in Fig. 4–105b.

Seeded Sites

Stasis or pooling of ascitic fluid favors the processes of deposition, fixation, and growth of seeded malignant cells. The seeded deposits coalesce and are then fixed to

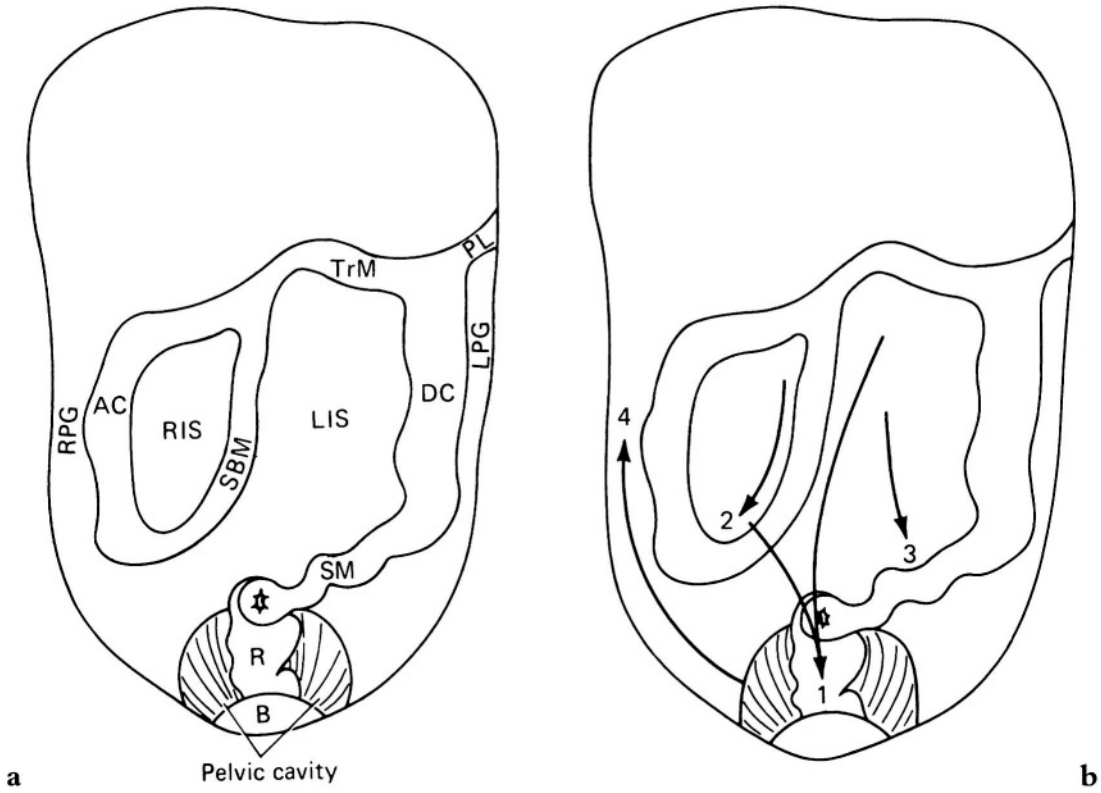


Fig. 4–105. (a) Posterior peritoneal reflections and intraabdominal spaces.
TrM = transverse mesocolon; *PL* = phrenicocolic ligament; *SBM* = small bowel mesentery; *AC* = attachment of ascending colon; *DC* = attachment of descending colon; *SM* = sigmoid mesocolon; *R* = rectum; *B* = urinary bladder; *RIS* = right infracolic space; *LIS* = left infracolic space; *RPG* = right paracolic gutter; *LPG* = left paracolic gutter.
(b) Diagram of the pathways of flow of intraperitoneal fluid and the four predominant sites in the lower abdomen.

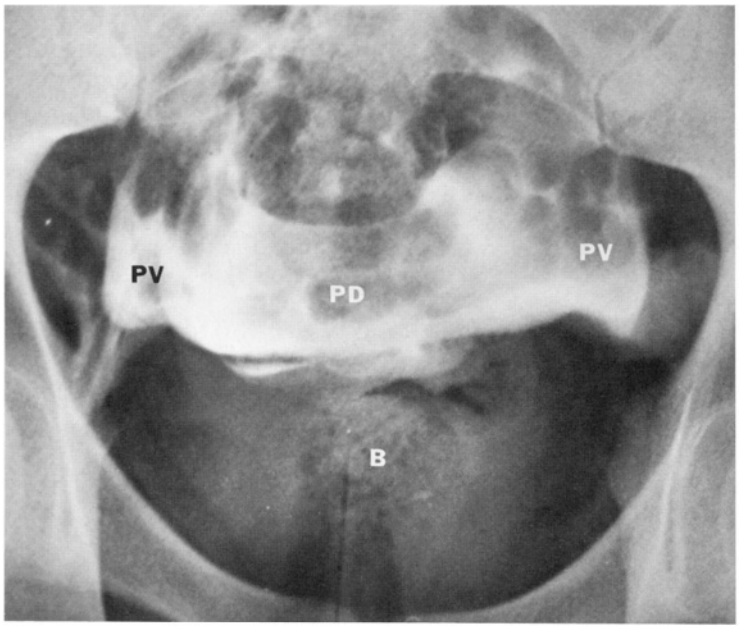


Fig. 4–106. Pelvic drainage of intraperitoneal fluid.
Intraperitoneal opaque contrast material first gravitates to the pelvic cavity, filling the midline pouch of Douglas (*PD*) and then the two paravesical recesses (*PV*). *B* = urinary bladder.

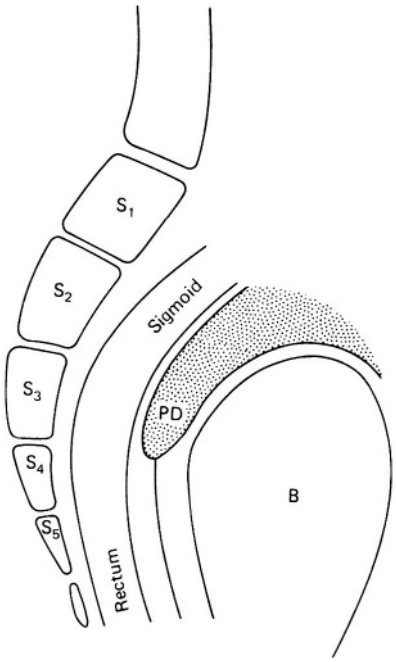


Fig. 4–107. Sagittal view of relationships of pouch of Douglas (*PD*).
This is the lower continuation of the peritoneal cavity between the rectosigmoid and the urinary bladder (*B*). (Reproduced from Meyers.[3])

the serosal surfaces by fibrinous adhesions that quickly become organized.[95]

Analysis of a series of proved cases has shown that the sites of lodgment and growth of intraperitoneal seeded metastases clearly follow the pathways of flow of ascitic fluid.[3] The pouch of Douglas is involved in over 50%, the lower small bowel mesentery in about 40%, the sigmoid mesocolon in about 20%, and the right paracolic gutter in about 20% of cases. In males, the primary carcinoma most often arises in the gastrointestinal tract (stomach, colon, pancreas), and in females, in the genital system (ovary).[96–102] In carcinoma of the pancreas, intraperitoneal seeding appears to be more commonly associated with neoplasms of the tail.[103] Peritoneal metastases from primary neoplasms of the urinary tract are rare.[104–106]

Pouch of Douglas (Rectosigmoid Junction): Radiologic Features

Intraperitoneal fluid consistently seeks the pouch of Douglas, the most caudal and posterior part of the peritoneal cavity, and then the lateral paravesical recesses (Fig. 4–106). The lower extension of the peritoneal reflections, comprising the pouch of Douglas, projects generally at the level of the lower second to upper fourth sacral segment (Fig. 4–107). This variability is determined by the developmental fixation of the peritoneum to Denonvillier's fascia (rectovaginal or rectovesical septum) and the degree to which the urinary bladder and rectum are distended.[99] It is a particularly useful land-

mark, demarcating the junction between the rectum and sigmoid colon. Thus, it is apparent that the ventral surface of the rectosigmoid junction faces the pouch of Douglas.

Seeding at this site is most common. On barium enema study, this results in a characteristic pattern of fixed parallel folds or a nodular indentation on the anterior aspect of the rectosigmoid junction[3,100] (Figs. 4–108

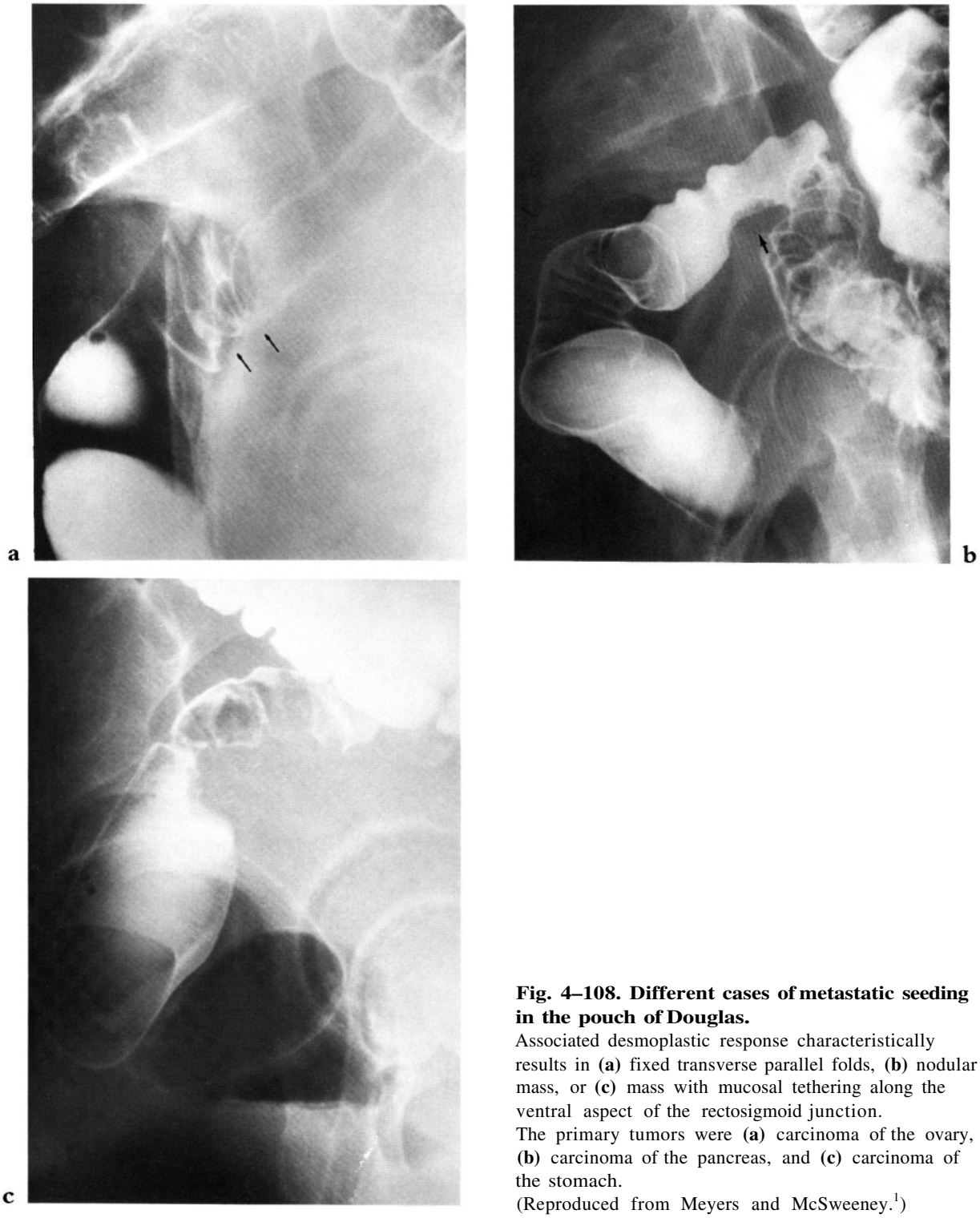


Fig. 4–108. Different cases of metastatic seeding in the pouch of Douglas.
Associated desmoplastic response characteristically results in **(a)** fixed transverse parallel folds, **(b)** nodular mass, or **(c)** mass with mucosal tethering along the ventral aspect of the rectosigmoid junction.
The primary tumors were **(a)** carcinoma of the ovary, **(b)** carcinoma of the pancreas, and **(c)** carcinoma of the stomach.
(Reproduced from Meyers and McSweeney.[1])

through 4–110). These changes reflect the coalescence of deposits with a dense fibrous reaction. This may be clinically palpable as the classic Blumer's shelf.[99,101] It is thought that the factor essential to the development of a rectal shelf tumor is pathologic fixation of the uppermost part of Denonvillier's fascia.[99] Sectional imaging readily demonstrates seeding as this site (Figs. 4–111 and 4–112). The nodular impression on the ventral aspect of the rectosigmoid junction from seeding in the pouch of Douglas may be duplicated by endometriosis, periproctitis, tumors, inflammation of the seminal vesicles,[99,100] or postirradiation changes. The presence of ascites, however, indicates these findings as part of peritoneal carcinomatosis.

Lower Small Bowel Mesentery (Terminal Ileum and Cecum): Radiologic Features

The root of the small bowel mesentery extends from the left side of the second lumbar vertebra downward to the right, across the aorta and inferior vena cava, to the right sacroiliac joint, a distance of only about 15 cm. From the root, a series of mesenteric ruffles support the small bowel loops (Figs. 4–113 and 4–114). These fanlike mesenteric extensions contribute to the characteristic undulating nature and position of the coils of small bowel, which averages 15–20 ft in length. Distally, the mesentery inserts most often at the cecocolic junction. A series of peritoneal recesses is thus formed extending along the right side of the ruffled small bowel mesentery obliquely toward the right lower quadrant of the abdomen. I have shown that these also serve to pool collections of ascitic fluid[1,3,4] (Figs. 4–115 and 4–116). Spread here occurs in a series of cascades or rivulets from one mesenteric ruffle to the next, directed along the axis of the small bowel mesentery toward the right lower quadrant in relation to distal ileal loops and the cecum (Fig. 4–117). It is here, within the lower recesses of the small bowel mesentery, that the most consistent pool of fluid forms before overflow into the pelvis occurs.

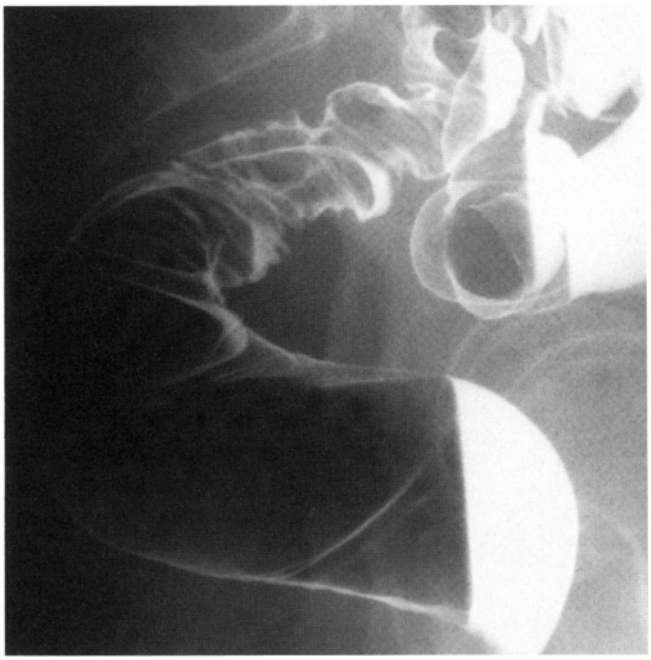


Fig. 4–109. Metastatic seeding in the pouch of Douglas.
Double-contrast study demonstrates infiltrations and mucosal tethering involving the rectosigmoid junction anteriorly from metastatic ovarian carcinoma.
(Courtesy of Stephen Rubesin, M.D., Hospital of the University of Pennsylvania, Philadelphia.)

Seeded deposits lodging within the lower recesses of the small bowel mesentery in the right infracolic space are clinically identifiable in over 40% of cases by their displacement of distal ileal loops, perhaps with pressure effects also upon the medial contour of the cecum and ascending colon.

Symmetric growth within multiple adjacent mesenteric recesses results in discrete separation of ileal loops in the right lower quadrant. Angulated tethering of mucosal folds indicates associated fibrous response. Significantly, these and any serosal masses are therefore identifiable on the concave borders, which are suspended by the mesenteric ruffles.[4] The narrowed loops may be aligned in a parallel configuration that I describe as "palisading" (Fig. 4–118). The axis of the serosal masses as well as of the affected intestinal loops conforms to the axis of the small bowel mesentery. As the seeded growths become somewhat larger, they may displace the bowel loops in a gently arcuate manner (Fig. 4–119). The striking symmetry of size, mass displacement from the mesenteric border of the loops, and orientation to the mesenteric ruffles in the right lower quadrant characterize the process. The seeded metastases on the serosal aspect of ileal loops in the right lower quadrant are typically localized to the concave mesenteric borders.

If the desmoplastic response to the seeded metastases is severe, marked fixation and angulation of ileal loops in the right lower quadrant result (Figs. 4–120 and 4–121). The most extreme fibrous reaction has been encountered in metastatic seeding from pancreatic carcinoma and mucin-producing gastric carcinoma. Serosal mass displacement may remain evident. The points of acute angulation tend to conform to the axis of the mesentery. Despite the narrowing and sharp course, obstruction may not be conspicuous.

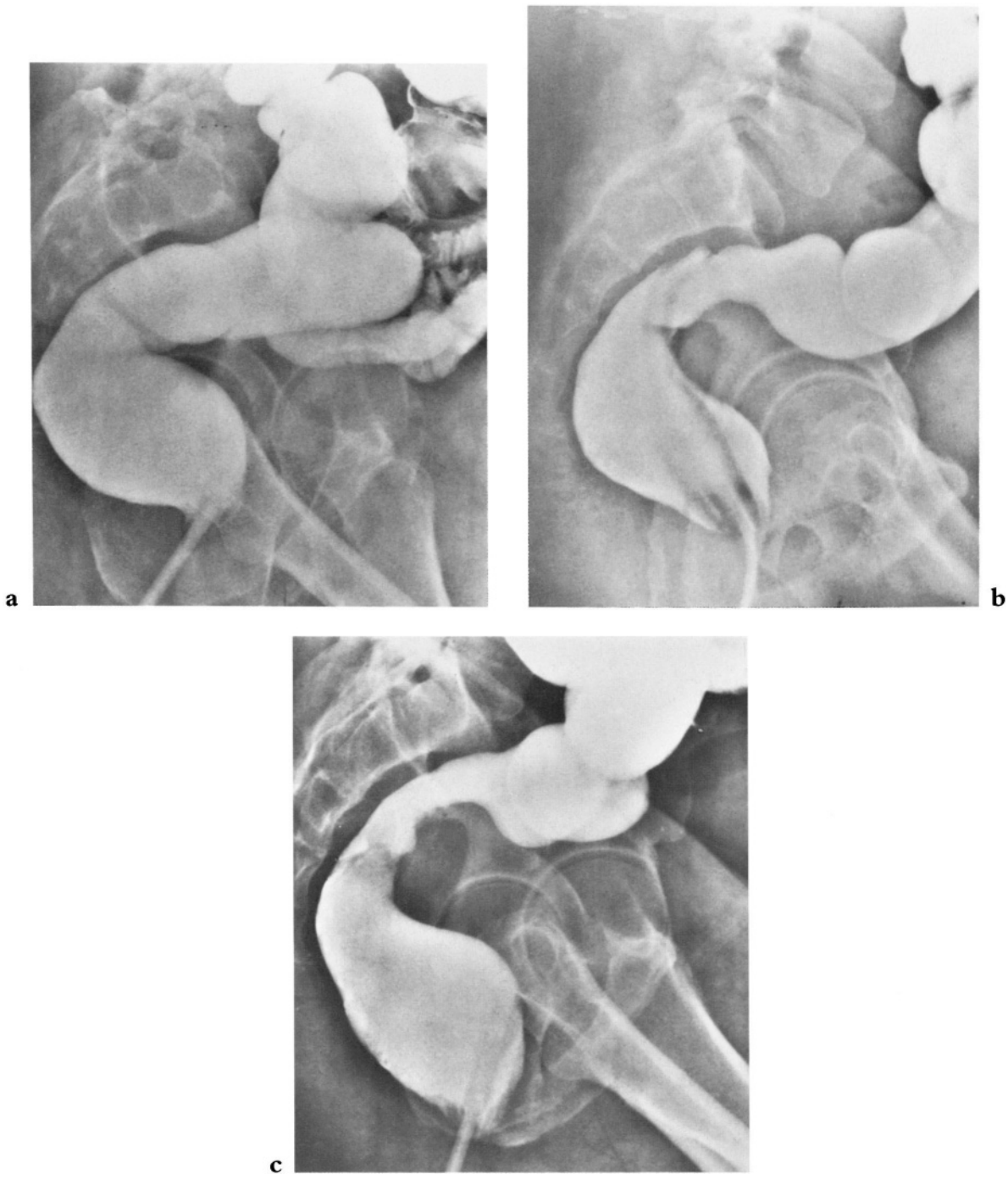


Fig. 4–110. Progressive changes of metastatic seeding in the pouch of Douglas.
Deposits from a primary carcinoma of the splenic flexure of the colon result in increasing mass impression on the rectosigmoid.
(b and **c)** 5 months and 1 year, respectively, after **(a).**

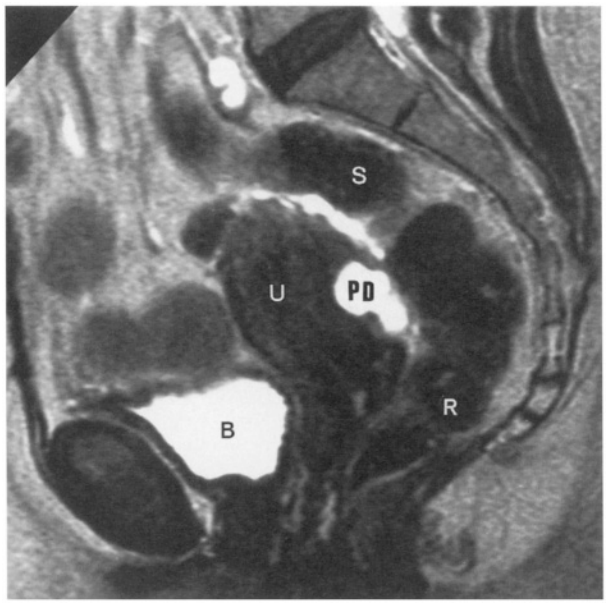


Fig. 4–111. Metastatic seeding in the pouch of Douglas.
Sagittal MR image shows seeded deposits from a primary carcinoma of the ovary in the rectouterine pouch of Douglas (*PD*). *R* = rectum; *S* = sigmoid colon; *U* = uterus; B = urinary bladder.
(Courtesy of Michiel Feldberg, M.D., Ph.D., University of Ultrecht, The Netherlands.)

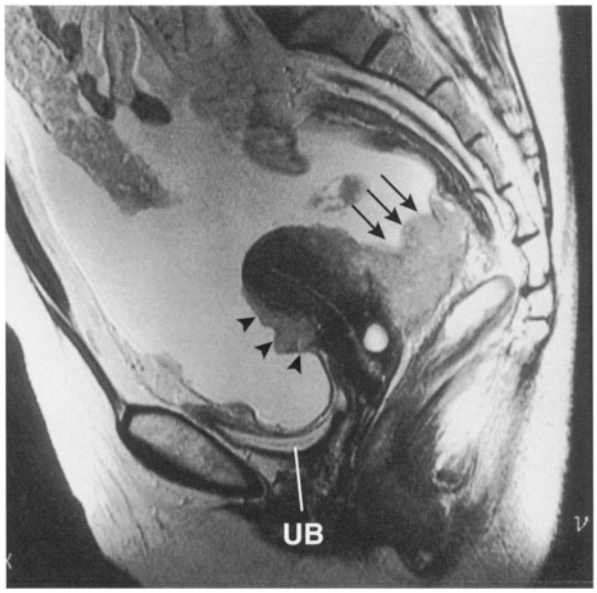


Fig. 4–112. Metastatic seeding in the pouch of Douglas.
Sagittal MR image in a patient with ovarian carcinomatosis shows implanted tumor filling the rectouterine pouch (*arrows*) and tumor plaques adhered to the anterior uterine wall (*arrowheads*). The urinary bladder (*UB*) is collapsed and compressed by a large amount of ascites.
(Reproduced from Auh et al.[10])



Fig. 4–113. The small bowel mesentery, illustrating its ruffled nature.
A series of peritoneal recesses is formed along its right side.
(Reprinted with permission from Kelly HA: Appendicitis and Other Diseases of the Vermiform Appendix. Lippincott, Philadelphia, 1909.)



Fig. 4–114. The small bowel mesentery.
CT section through the lower abdomen containing ascites clearly shows the fat-laden small bowel mesentery with its vessels (*arrows*).
In the right lower quadrant, mesenteric ruffles support loops of ileum (*I*).

If no significant fibrous reaction is elicited as the metastases increase in size, gross extrinsic mass displacement may be shown (Figs. 4–122 through 4–124). The mesenteric masses, however, tend to be multiple, and they maintain their relationship to the lower small bowel mesentery (Fig. 4–125). They displace ileal loops predominantly inferiorly and medially and may exert pressure on the ascending colon medially and the proximal transverse colon inferiorly.

Since the small bowel mesentery most commonly inserts at the cecocolic junction, the effects of seeded metastases on the cecum are shown typically on its medial and inferior contours.[4] The level of involvement is thus usually below the ileocecal valve in the caput of the cecum. The extrinsic mass indenting the cecum may be smooth or lobulated (Figs. 4–126 and 4–127), of variable size (Fig. 4–128), and at times, may encircle the cecum (Fig. 4–129). The mass changes on the cecum are not, in themselves, specific for seeded metastases and may simulate appendiceal abnormalities, other mesenteric masses, or even primary lesions of the cecum. However, they are almost invariably accompanied by the more characteristic changes involving distal small bowel loops. If first appreciated on a barium enema study, these can be identified by reflux into the terminal ileum (Figs. 4–127 and 4–128) or in a subsequent small bowel series. The association of findings may occasionally closely simulate granulomatous enterocolitis.[44] (Fig. 4–130). The small bowel alterations are usually not difficult to distinguish from other common disease states. The lack of inflammatory features, such as spasm, ulcerations, and sinus tracts, and the characteristic spectrum of changes help in the differential diagnosis from regional enteritis, tuberculosis, amebiasis, and peritoneal adhesions. When the seeded metastases are diffuse throughout the small bowel (Fig. 4–131), the changes secondary to the desmoplastic process may resemble carcinoid or radiation enteritis. Fixed angulation and alternating areas of narrowing and dilatation are accompanied by serosal masses identifiable on the mesenteric borders and conspicuous tethering of mucosal folds.

Sigmoid Colon: Radiologic Features

The sigmoid mesocolon reflects obliquely off the level of the left sacroiliac joint to suspend the redundant sigmoid loops anteriorly. It forms an inverted V with its apex located at the division of the left common iliac artery. The left portion descends medial to the left psoas major muscle.[107,108] The right segment descends into the

text continues on page 205

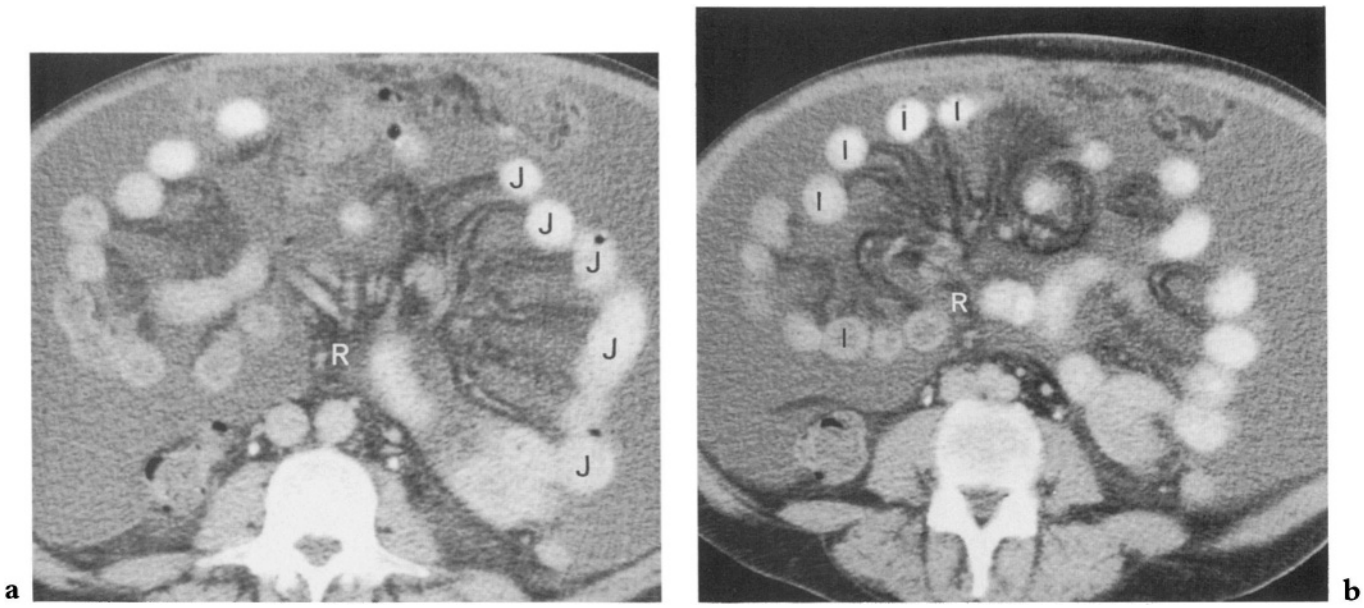


Fig. 4–115. Ascitic fluid collecting between mesenteric folds.
(a and **b)** CT documents ascitic fluid pooling between the folds of the small bowel mesentery. The latter are seen as lucent bands, reflecting their adipose nature, with their contained vessels radiating from the root (*R*) to opacified loops of jejunum (*J*) and ileum (*I*).

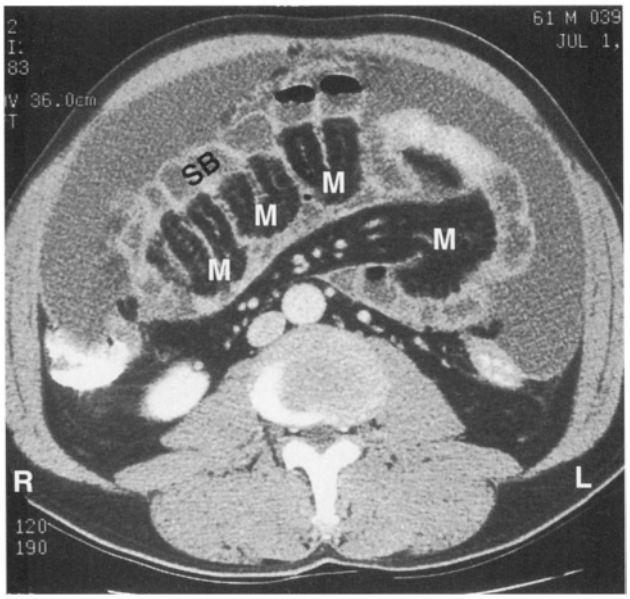


Fig. 4–116. Relationships of small bowel mesentery to pooled ascites.
CT in a patient with a large amount of ascites and peritoneal thickening shows multiple mesenteric leaves that are separated from each other clearly by thickened peritoneum and pools of ascites. Linear vessels course with the fat-laden mesenteric leaves that display U-shapes reflecting their ruffled nature as they extend from the evident broad-based root. *SB* = small bowel, *M* = mesentery.

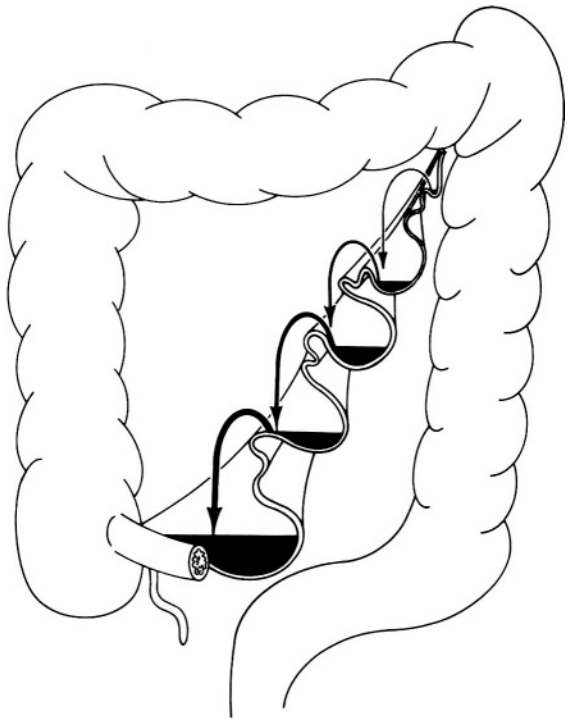


Fig. 4–117. The flow of ascites forms a series of pools within the recesses of the small bowel mesentery.
The most consistent drainage is to its lower end, in relation to distal ileal loops and the cecum.
(Reproduced from Meyers.[4])

Fig. 4–118. Seeded gastric carcinoma along lower small bowel mesentery.
There is palisaded separation of ileal loops in the right lower quadrant (*arrows*). Mucosal folds are mildly tethered. (Sites of obstruction are also present proximally.) (Reproduced from Meyers.[4])



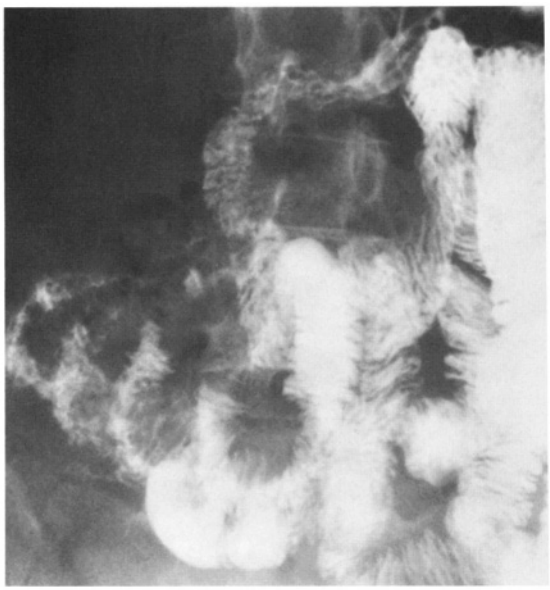


Fig. 4–119. Seeded ovarian carcinoma along lower small bowel mesentery.
There is striking scalloped displacement of multiple ileal loops in the right lower quadrant, following the axis of the mesenteric recesses. The mucosal folds are mildly tethered. (Reproduced from Meyers and McSweeney.[1])



Fig. 4–120. Seeded ovarian carcinoma along lower small bowel mesentery.
Nodular serosal masses on the mesenteric borders of distal ileal loops are associated with fibrotic narrowing and angulation. These produce some proximal obstruction.



Fig. 4–121. Seeded pancreatic carcinoma along lower small bowel mesentery.
Mass separation and striking angulation of fixed ileal loops in right lower quadrant from extensive desmoplastic reaction.
(Reproduced from Meyers.[4])

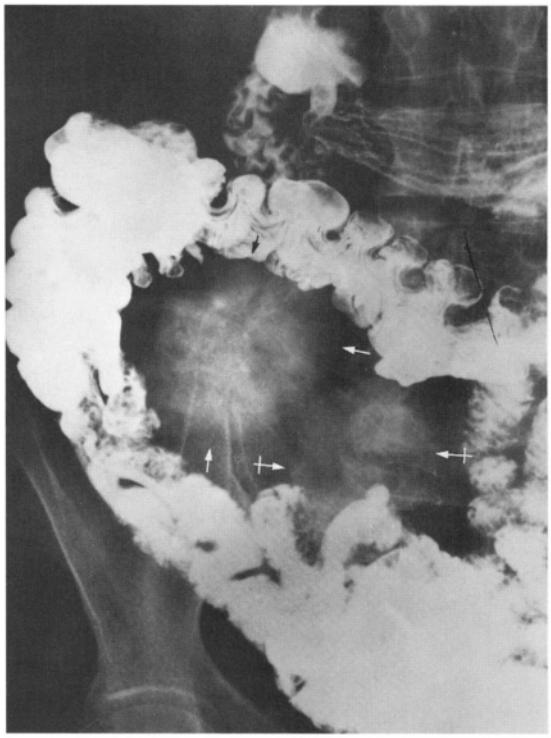


Fig. 4–122. Seeded ovarian carcinoma along lower small bowel mesentery.
Two masses with psammomatous calcifications in the right lower quadrant displace ileal loops and press on the ascending and transverse colon.
(Reproduced from Meyers and McSweeney.[1])

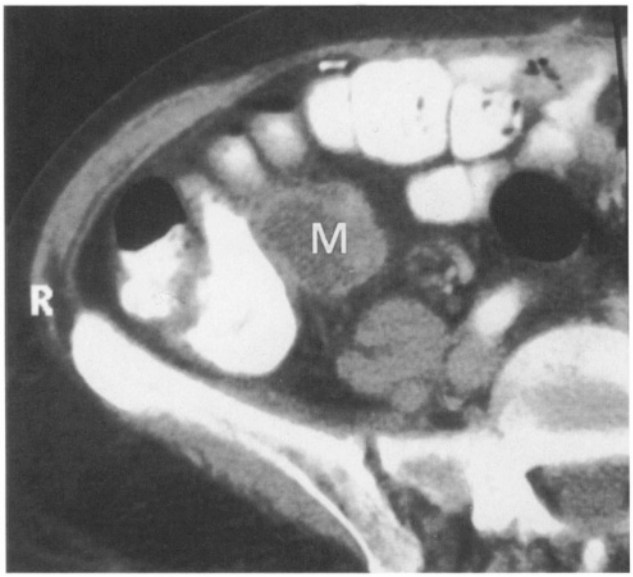


Fig. 4–123. Seeded ovarian carcinoma along lower small bowel mesentery.
CT demonstrates a necrotic seeded metastasis (*M*), displacing bowel in the right lower quadrant.

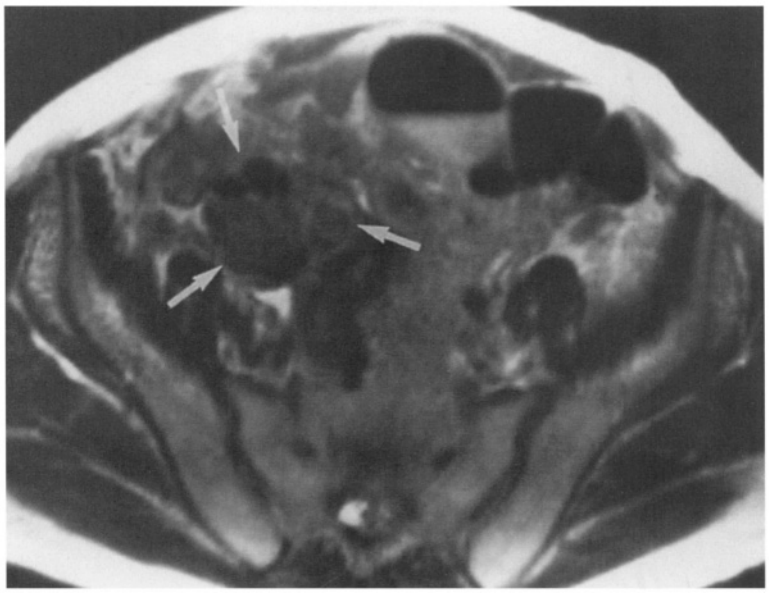


Fig. 4–124. Seeded pancreatic carcinoma along lower small bowel mesentery.
T2-weighted MR image shows a metastatic deposit in the right lower quadrant (*arrows*), displacing bowel loops.
(Reproduced from Semelka et al.[59])

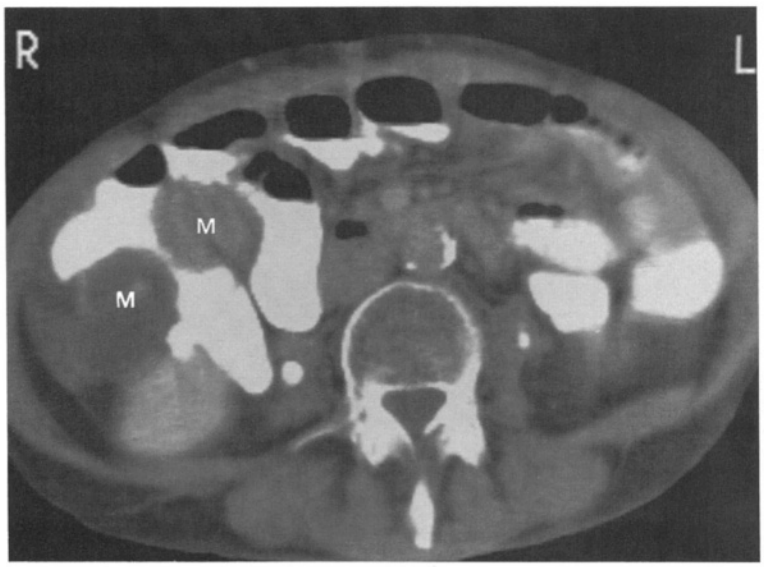


Fig. 4–125. Seeded ovarian carcinoma along lower small bowel mesentery.
Metastatic masses (*M*) compress the ileocecal region and an adjacent ileal loop. There is early tethering of mucosal folds. Ascites is present.

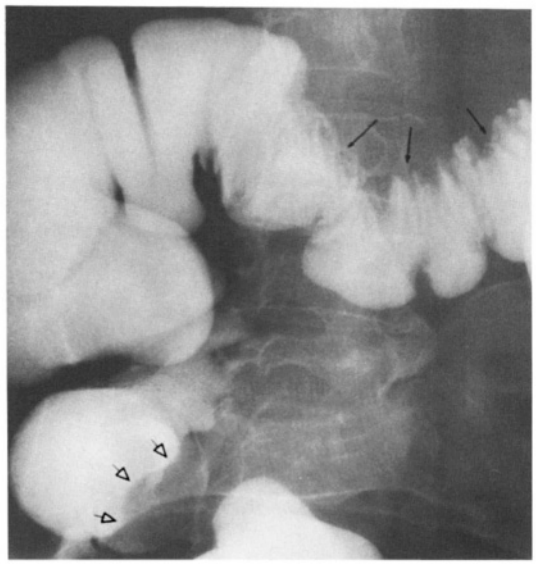


Fig. 4–126. Seeded carcinoma of the gallbladder along lower small bowel mesentery.
This results in a mass eccentrically indenting the medial contour of the cecum (*open arrows*). There is also direct invasion of the transverse colon (*black arrows*).
(Reproduced from Meyers.[4])

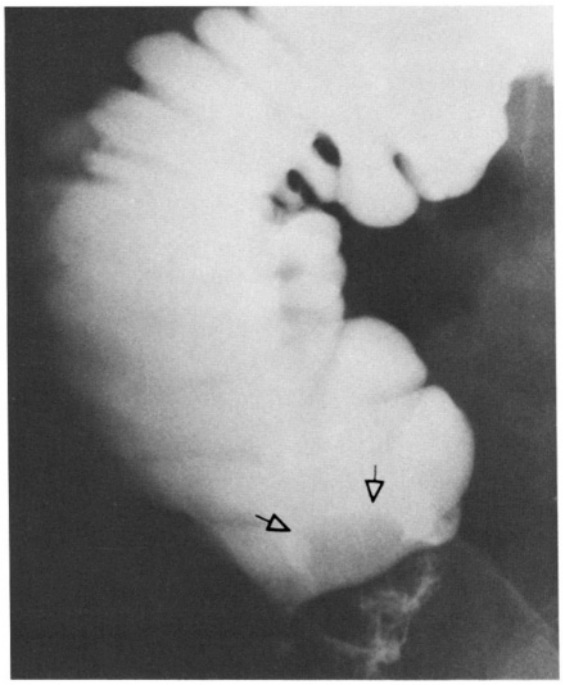


Fig. 4–127. Seeded gastric carcinoma along lower small bowel mesentery.
Lobulated mass indents the inferior contour of the cecum (*arrows*). The distal ileum is angulated and deformed by mass impressions.
(Reproduced from Meyers.[4])

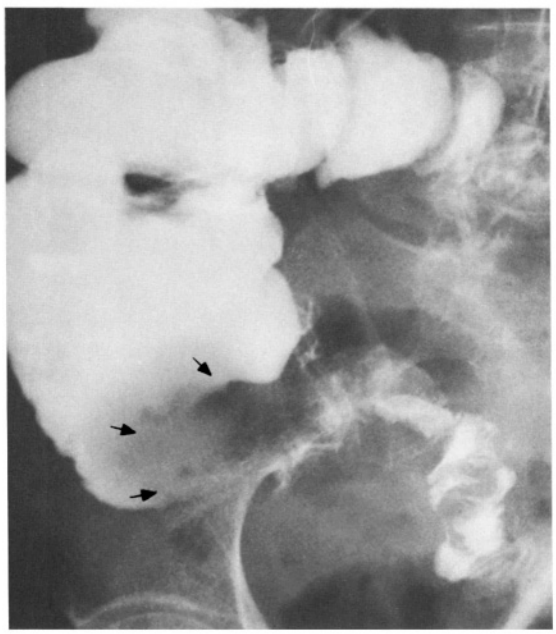


Fig. 4–128. Seeded pancreatic carcinoma along lower small bowel mesentery.
Large lobulated mass with nodular excrescences grossly indents the inferior contour of the cecum (*arrows*). There is also mass pressure on the terminal ileum with fibrous angulation.
(Reproduced from Meyers.[4])

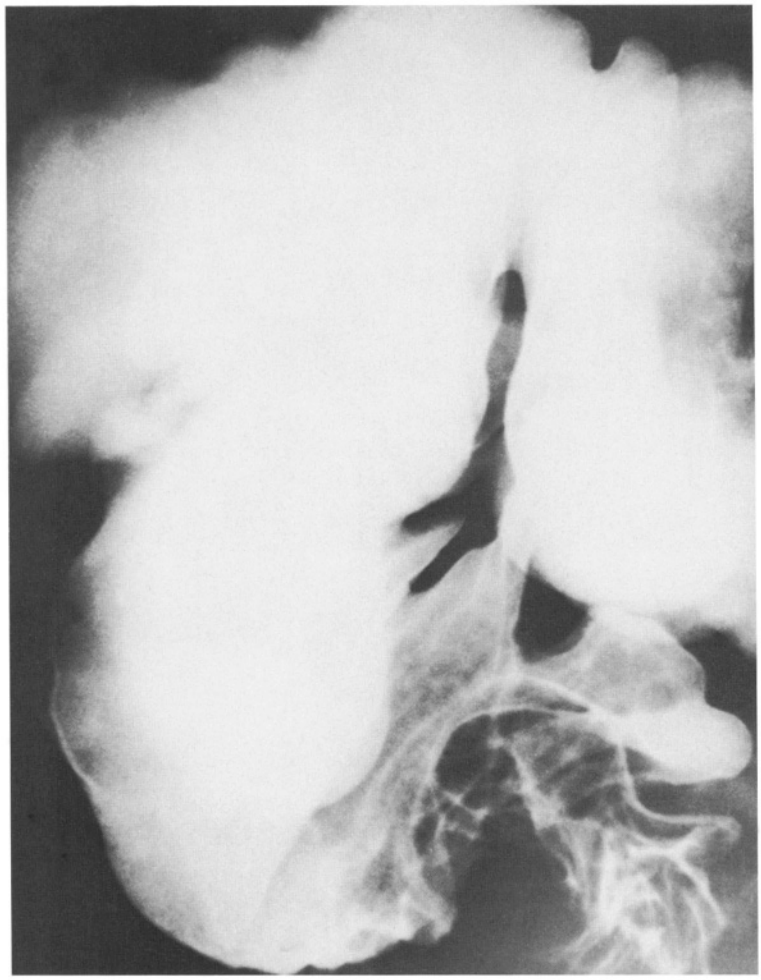


Fig. 4–129. Seeded ovarian carcinoma along lower small bowel mesentery.
Annular mass narrowing of apex of cecum.
(Reproduced from Meyers.[4])

pelvis and ends at the level of the third sacral vertebra. Considerable fat is normally present within the sigmoid mesocolon, allowing visualization of sigmoid and superior rectal vessels, which course between the two peritoneal layers (Fig. 4–132). Ascitic fluid and thus metastatic seeding commonly collect adjacent to the sigmoid mesocolon in the "intersigmoid" recess.

Lodgment and growth of deposits arrested along the barrier of the sigmoid mesocolon in the left lower quadrant result in changes characteristically localized to the superior border of the sigmoid colon (Figs. 4–133 through 4–135). The associated desmoplastic reaction causes tethering of the mucosal folds. These lose their axis normally perpendicular to the lumen of the bowel and become angulated, often toward a common point in the mesentery at the site of the secondary lesion (Figs. 4–136 through 4–138). Even when annular invasion from the seeded metastases has occurred, the sigmoid colon tends to show preponderant changes on its superior border (Figs. 4–139 and 4–140). This localization occurs in more than 20% of cases of metastatic seeding.

Right Paracolic Gutter (Cecum and Ascending Colon) and Morison's Pouch: Radiologic Features

Following the flow of ascitic fluid from the pelvis preferentially upward within the right paracolic gutter, deposition and growth in this peritoneal recess are shown by mass changes lateral and posterior to the cecum and proximal ascending colon (Figs. 4–141 through 4–144). Tethering of mucosal folds or angulated fixation of a small bowel loop in this area may occur as a consequence of an associated fibrous reaction (Fig. 4–145). This localization in the right paracolic gutter occurs in 18% of cases. More cephalad deposition in the right subhepatic space may occasionally be identified (Figs. 4–146 and 4–147).

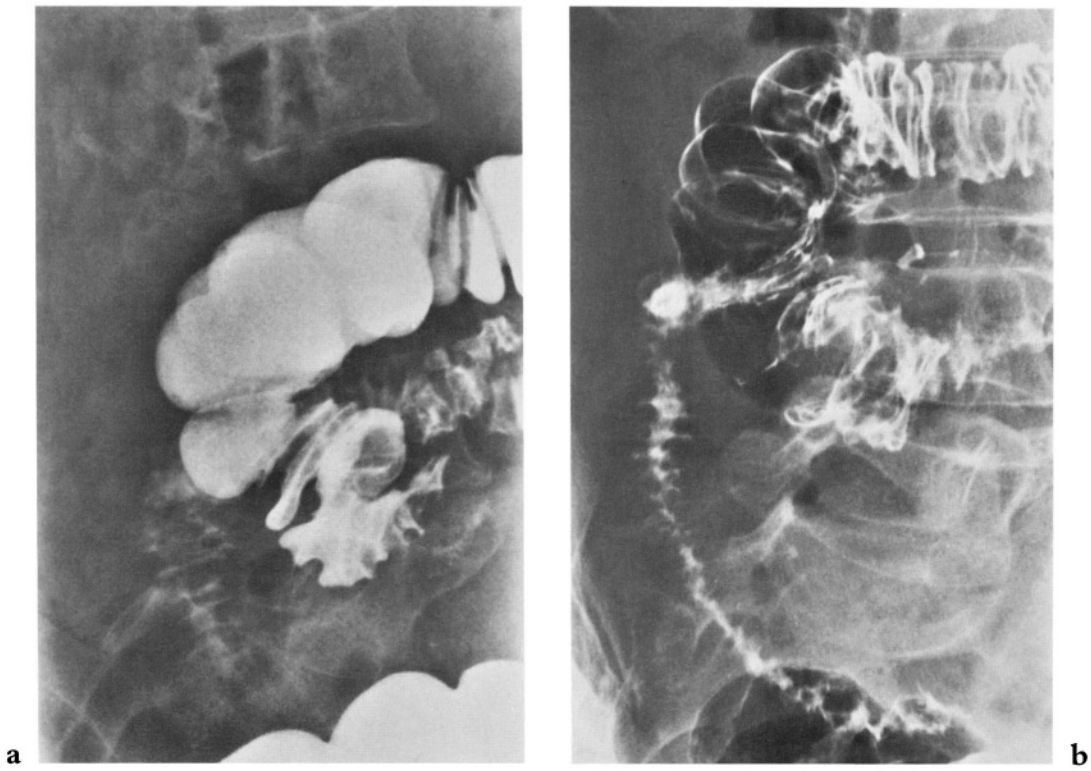


Fig. 4–130. Seeded pancreatic carcinoma along lower small bowel.
(a) Barium enema with **(b)** air-contrast studies demonstrate changes involving the cecum and terminal ileum closely simulating granulomatous enterocolitis.
(Reproduced from Meyers.[4])

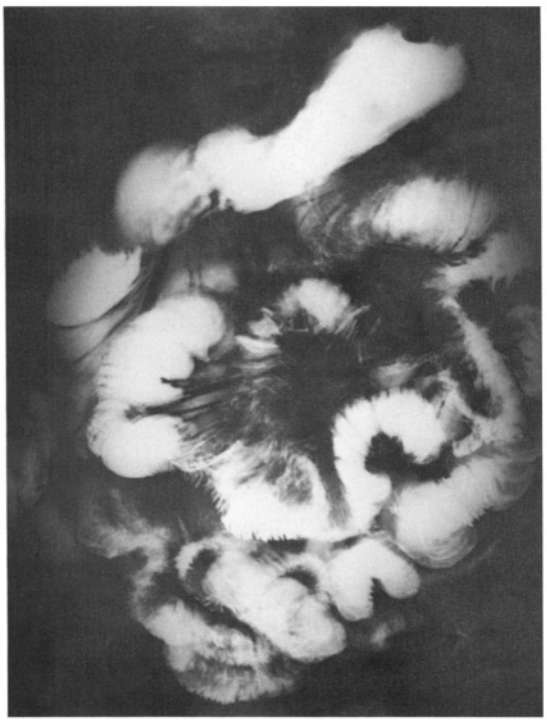


Fig. 4–131. Diffuse seeded metastases from gastric carcinoma along small bowel mesentery.
Serosal masses are present predominantly on the mesenteric borders of small bowel loops, including the ileum in the right lower quadrant. The mucosal folds are tethered, and there are angulations and alternating constrictions of loops. These changes are consequent to the fibrotic reaction.

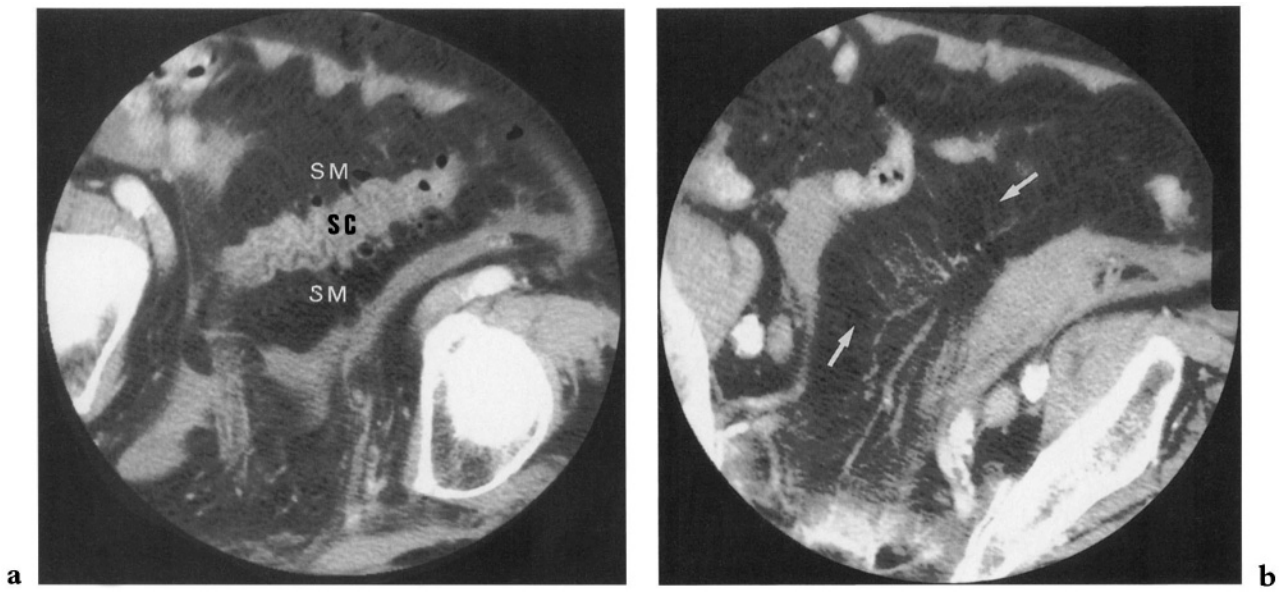


Fig. 4–132. The sigmoid mesocolon.
(a and **b)** CT identifies the fat-laden sigmoid mesocolon (*SM*) and its relationship to the sigmoid colon (*SC*), which in this case bears diverticula, and to sigmoid and superior rectal vessels (*arrows*).

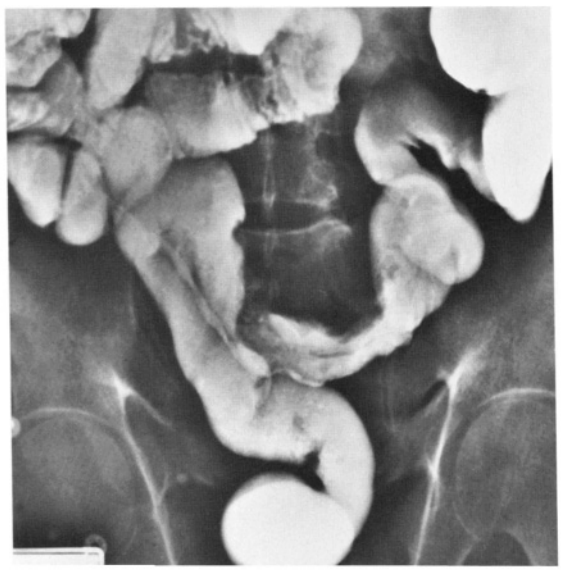


Fig. 4–133. Seeding in the sigmoid mesocolon from colonic carcinoma.
Metastatic mass impresses the superior contour of the sigmoid colon.



Fig. 4–134. Seeding on the sigmoid mesocolon from pancreatic carcinoma.
CT identifies metastatic deposits (*arrows*) on the fatty sigmoid mesocolon. Massive ascites is present.

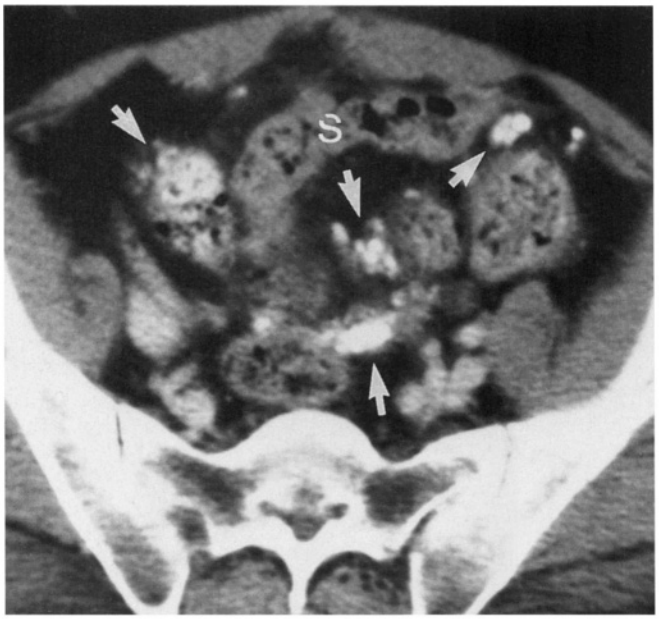


Fig. 4–135. Calcified seeded metastases on the sigmoid mesocolon.
Calcified deposits (*arrows*) from a serous cystadenocarcinoma of the ovary have lodged on the mesocolon adjacent to the sigmoid colon (*S*).
(Courtesy of Michiel Feldberg, M.D., Ph.D., University of Utrecht, The Netherlands.)

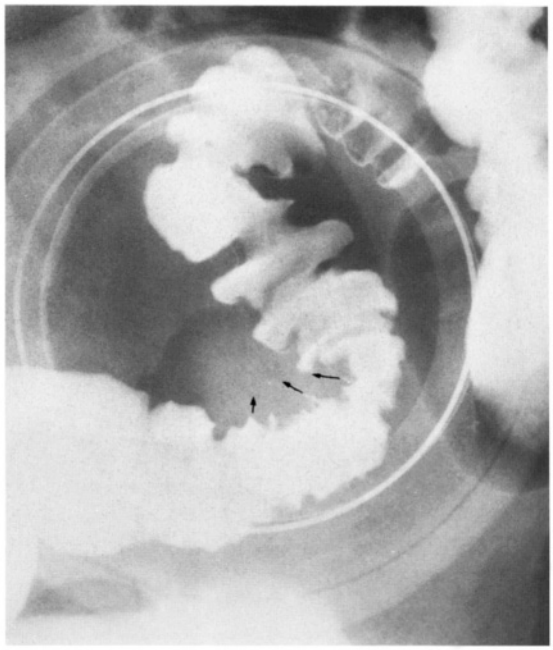


Fig. 4–136. Intraperitoneal seeding in the sigmoid mesocolon from pancreatic carcinoma.
The desmoplastic reaction accompanying the deposits causes tethering of the mucosal folds along the superior border of the sigmoid colon, angulated (*arrows*) toward a common site in the mesentery.
(Reproduced from Meyers.[3])

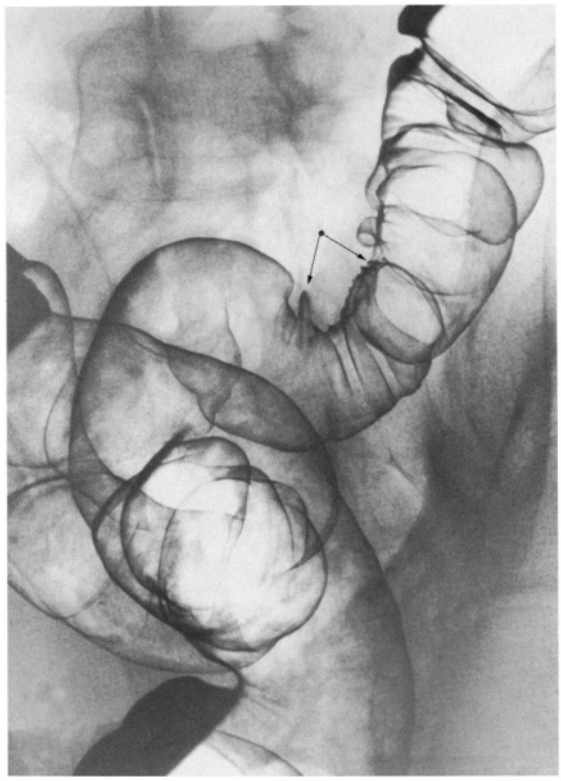


Fig. 4–137. Intraperitoneal seeding in the sigmoid mesocolon from gastric carcinoma.
The desmoplastic response tethers mucosal folds along the superior border of the sigmoid colon (*arrows*).
(Reproduced from Maruyama M: Radiologic Diagnosis of Polyps and Carcinoma of the Large Bowel. Igaku-Shoin, Tokyo, 1977.)

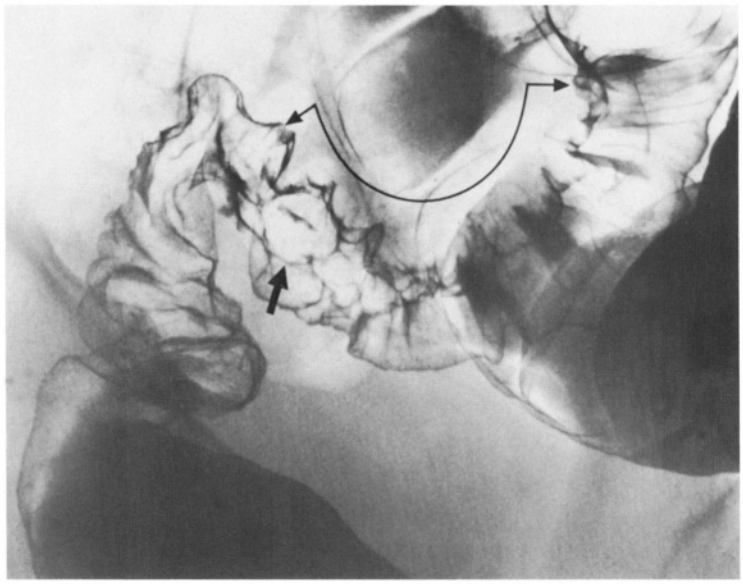


Fig. 4–138. Metastatic seeding in sigmoid mesocolon.
The superior margin of the sigmoid colon is involved over a considerable length with infiltrative and desmoplastic mucosal changes (*arrow line*). Mucosal elevation seen *en face* suggests submucosal tumor (*arrow*).
(Reproduced from Maruyama M: Radiologic Diagnosis of Polyps and Carcinoma of the Large Bowel. Igaku–Shoin, Tokyo, 1977.)

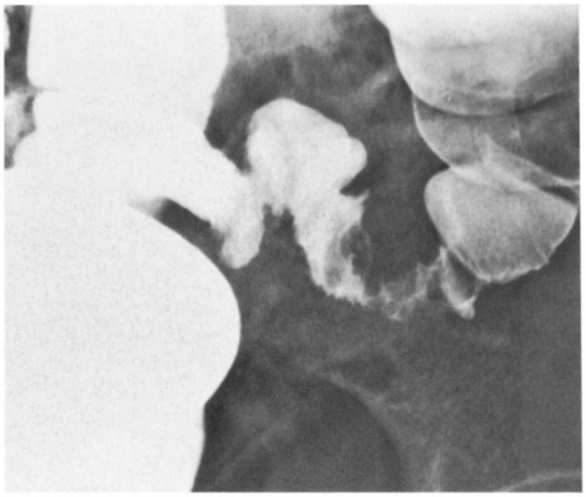


Fig. 4–139. Metastatic seeding in the sigmoid mesocolon from gastric carcinoma.
Circumferential invasion has occurred but the predominant effect can be identified on the superior contour of the sigmoid colon.
(Reproduced from Meyers et al.[44])



Fig. 4–140. Metastatic seeding in the sigmoid mesocolon from pancreatic carcinoma.
Double-contrast study demonstrates that seeded deposits accompanied by desmoplastic reaction result in mass compression with tethered mucosal folds on the superior border of the sigmoid colon (*arrows*). At one point, the process has become annular (*curved arrow*).
(Courtesy of Stephen Rubesin, M.D., Hospital of the University of Pennsylvania, Philadelphia.)

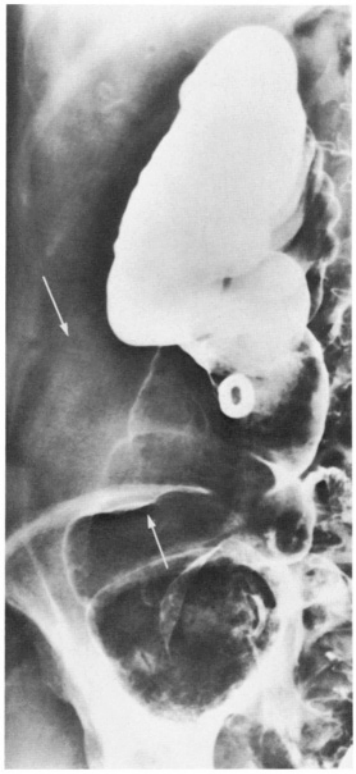


Fig. 4–141. Seeding in right paracolic gutter from ovarian carcinoma.
Metastatic mass displaces the lateral aspect of the ascending colon (*arrows*).

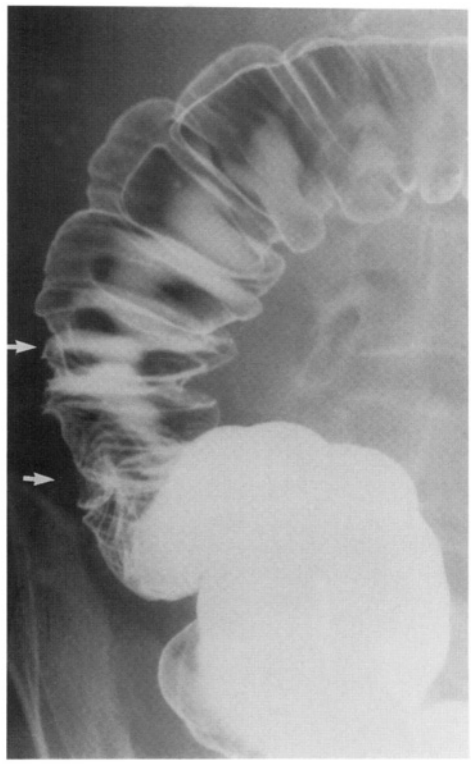


Fig. 4–142. Metastatic seeding in right paracolic gutter from ovarian carcinoma.
Double-contrast study demonstrates infiltration of the lateral contour of the ascending colon (*arrows*).
(Reprinted with permission from Laufer I, Levine MS: Double-Contrast Gastrointestinal Radiology. WB Saunders, Philadelphia, 1992.)

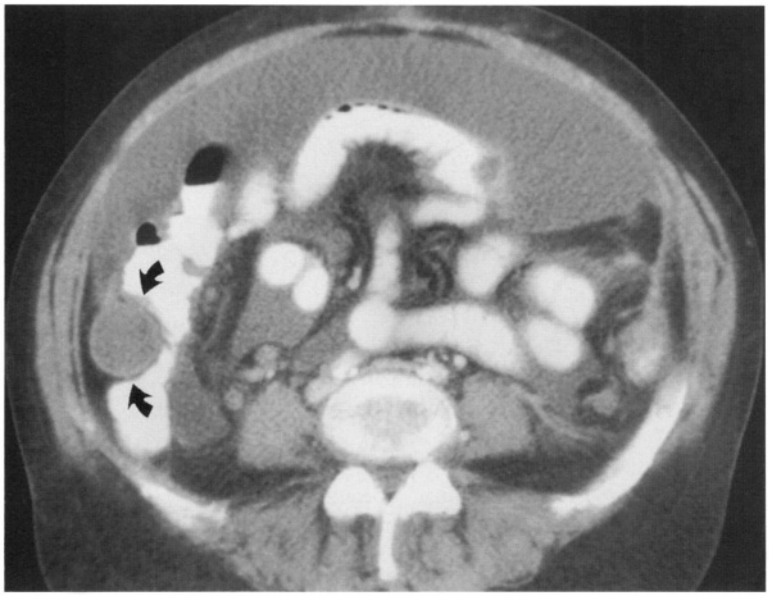


Fig. 4–143. Intraperitoneal seeding in right paracolic gutter from ovarian carcinoma.
A cystic metastatic implant (*arrows*) indents the lateral aspect of the ascending colon. Ascites is present.
(Courtesy of Michiel Feldberg, M.D., University of Utrecht, The Netherlands.)

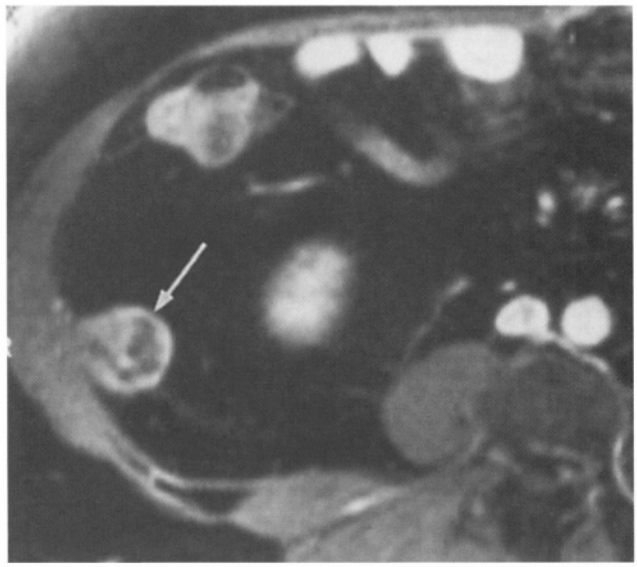


Fig. 4–144. Seeded ovarian carcinoma in the right paracolic gutter.
Gadolinium-enhanced fat-suppressed T1-weighted MR image demonstrates the implant with heterogeneous speckled enhancement (*arrow*).
(Reproduced from Semelka et al.[59])



Fig. 4–145. Intraperitoneal seeding in the right paracolic gutter from gastric carcinoma.
Nodular masses displace the ascending colon anteriorly and medially, and cause angulated fixation of a small bowel loop.
(Reproduced from Meyers and McSweeney.[1])

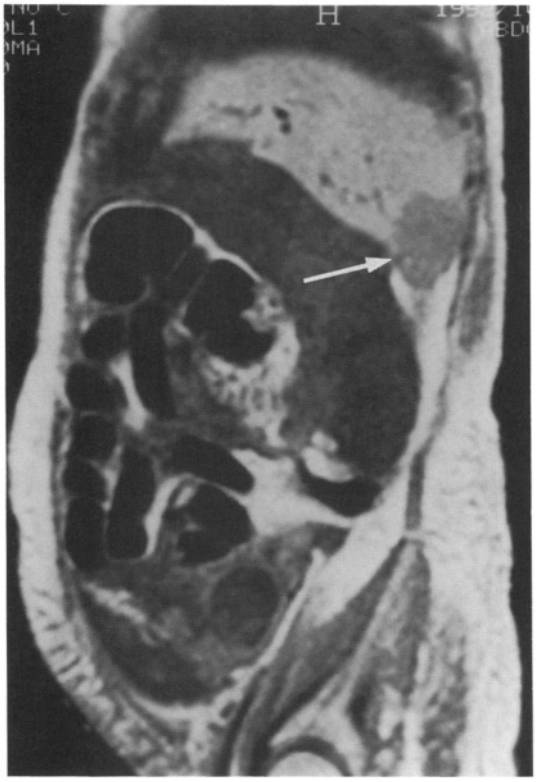


Fig. 4–146. Intraperitoneal seeding in Morison's pouch from ovarian carcinoma.
MRI, T1-weighted sagittal image, demonstrates a prominent implant in the right posterior subhepatic space (*arrow*).
(Reproduced from Chou et al.[102])



Fig. 4–147. Seeded deposit in Morison's pouch from ovarian carcinoma.
Sagittal gadolinium-enhanced T1-weighted MR image displays an implant discretely in Morison's pouch (*arrow*).
(Reproduced from Forstner et al.[109])

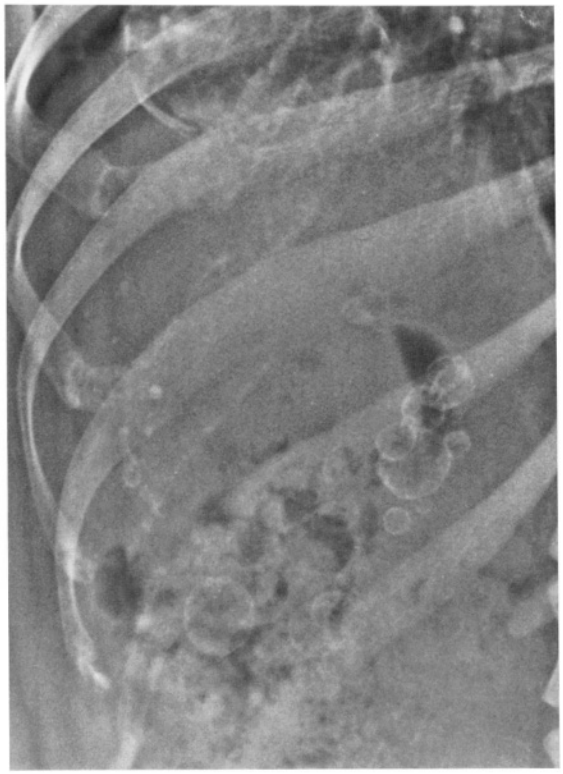
Seeded Perihepatic and Subdiaphragmatic Metastases

Conventional radiologic studies have disclosed the intraperitoneal spread of seeded metastases to the supramesocolic compartment only on occasion. This pathway of spread is illustrated graphically in Figure 4–148 in an instance of a spilled ovarian dermoid cyst.[110] The avenue and characteristic sites of implantation are clearly mapped out in the patient studied by CT in Figure 4–149. Seeded deposits in both Morison's pouch and the right subphrenic space are therefore not uncommon (Fig. 4–150).

Transcoelomic migration of fluid, particles, and cells cephalad toward the undersurface of the diaphragm is caused by changes in intraperitoneal pressure during breathing and the topographic arrangement of the peritoneal recesses.[3,94] In ovarian carcinoma, free tumor cells are shed from gross or microscopic tumor excrescenses on the capsule of the primary tumor. These free-floating cells have been shown to be removed from the peritoneal cavity through lymphatic channels located in the diaphragm.[112,113] However, absorption does not take place evenly over the whole diaphragmatic surface, but is more extensive on the right side, overlying the liver.[114,115] Drainage occurs into submesothelial lymphatic capillaries of the diaphragm, which penetrate through the muscle to intercommunicate with a comparable plexus arising on the pleural surface. From the diaphragm, lymphatic drainage primarily occurs to the anterior mediastinal lymph nodes[114,116–119] (Fig. 4–151). The uppermost scan levels in CT of the abdomen should be routinely evaluated for this transit of malignant spread (Fig. 4–152). This pathway is quantitatively the most significant, accounting for 80% of the clearance from the peritoneal cavity. Partial or complete obstruction of the diaphragmatic lymph channels by ovarian carcinoma tumor cells facilitates the accumulation of malignant ascites and creates favorable conditions for the implantation of tumor cells at other sites in the peritoneal cavity.[112] Nearly 90% of patients with ovarian carcinoma



a



b



c

Fig. 4–148. Perihepatic spread of ruptured ovarian dermoid cyst.
(a) Plain film of the pelvis identifies the fatty radiolucency of a large dermoid cyst of the ovary. It contains toothlike and multiple small cystic calcifications.
(b) Plain film. Multiple cystlike calcifications in the right subphrenic and subhepatic areas.
(c) Intravenous cholangiogram with tomography verifies the location of the calcified structures. These represent perihepatic satellite cysts implanted from the ruptured dermoid of the ovary.



a



b



c

Fig. 4–149. Extension of seeded deposits from primary carcinoma in the pelvis to Morison's pouch and the right subphrenic space. Calcifications in the primary ovarian serous cystadenocarcinonia and seeded implants following chemotherapy facilitate the documentation of the avenue of spread.
(a) The calcified primary ovarian mass (*arrows*), deep to opacified small bowel loops, is identified.
(b) Following cephalad passage up the right paracolic gutter, deposits are lodged in Morison's pouch (*arrow*).
(c) Responding to the subatmospheric pressure below the diaphragms, spread occurs in the perihepatic right subphrenic space (*arrows*). Note that the medial extent of these lesions typically ends at the level of the falciform ligament.

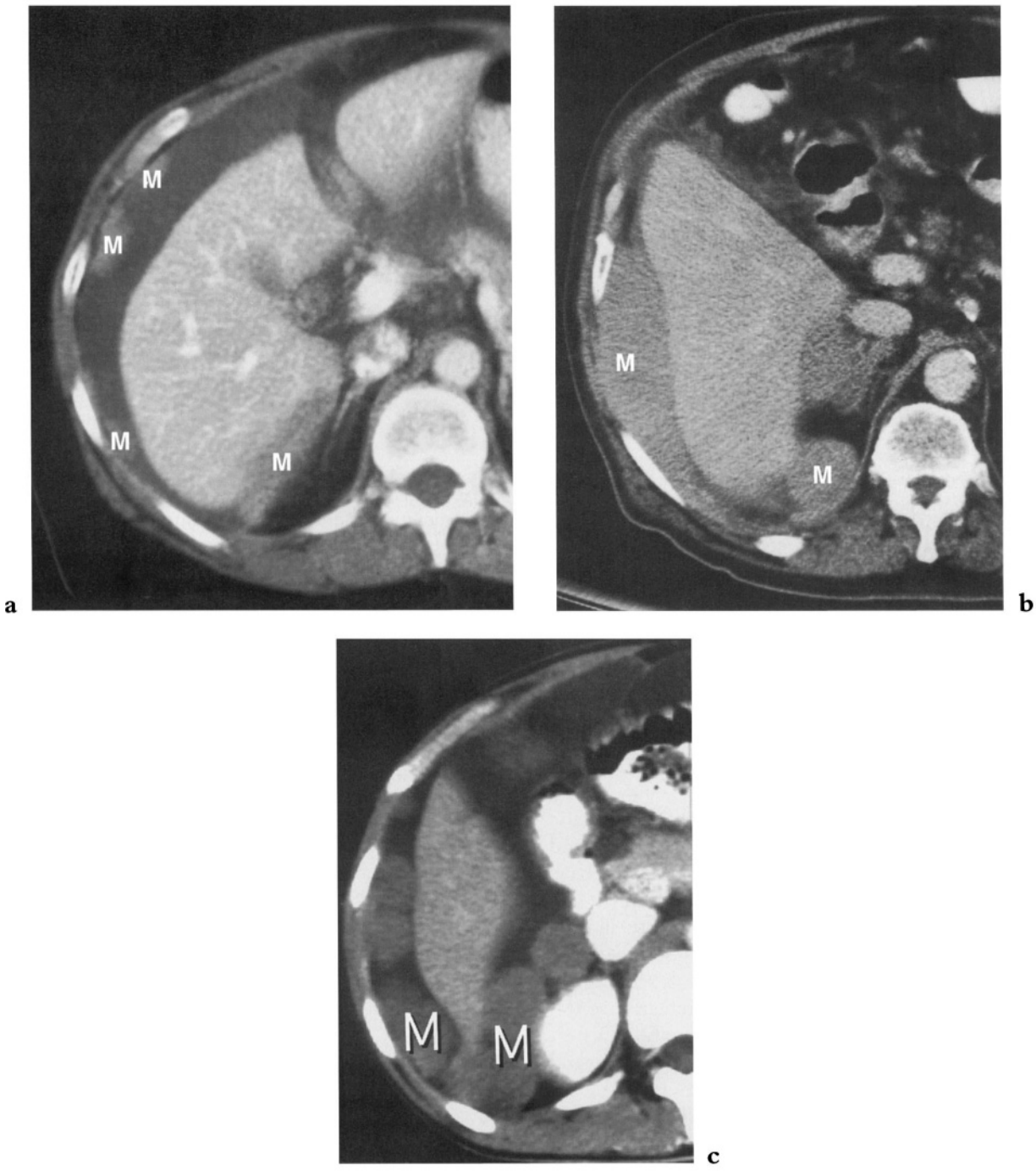


Fig. 4–150. Simultaneous metastatic seeding in Morison's pouch and the right subphrenic space.
Three different examples illustrate the range of magnitude from minimal deposits to masses (*M*) of varying sizes and shapes. The primary tumors were:
(a) Endometrial carcinoma.
(b) Carcinoma of the ovary. (Reproduced from De Meo, et al.[111])
(c) Pineal germinoma, with peritoneal dissemination via a ventriculo-peritoneal shunt. (Courtesy of Hiromu Mori, M.D., Oita Medical Center, Oita, Japan.)

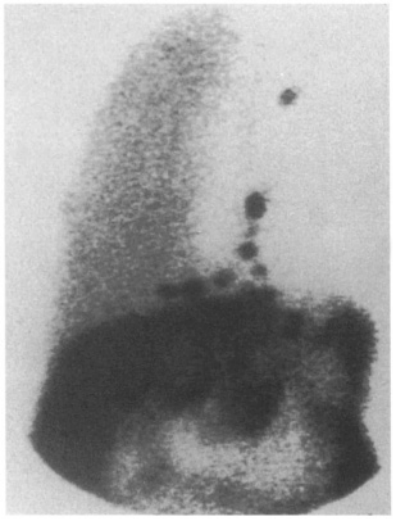


Fig. 4–151. Peritoneal–pleural communication.
Anterior scinti-image of upper abdomen and chest 2 hours after instillation of Tc99m sulphur colloid into the peritoneal cavity demonstrates visualization of anterior mediastinal lymphatic channels and passage of radiotracer into the right hemothorax.
(Reproduced from Mittal, et al.[119])

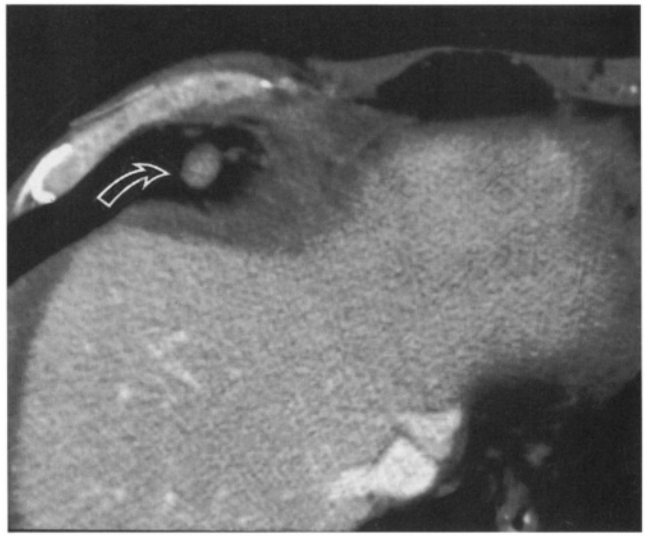


Fig. 4–152. Pericardiac lymphadenopathy secondary to metastatic pancreatic carcinoma.
CT demonstrates an enlarged anterior mediastinal lymph node (*arrow*).

have peritoneal implants at autopsy, and 60–70% have ascites.[120]

It is being increasingly recognized that metastatic ovarian implants along the right hemidiaphragm and liver capsule are frequent. Peritoneoscopic studies have shown metastatic diaphragmatic involvement in 61% of patients with ovarian carcinoma,[121] and, more significantly, that in 21–34% of patients otherwise diagnosed as having stage I or stage II disease, there is seeding on the undersurface of the diaphragm, particularly on the right.[122–125] These implants are generally only 2–3 mm in diameter (Fig. 4–153), but may reach a size of several centimeters[126] (Figs. 4–154 and 4–155).

The perihepatic dissemination of ovarian carcinoma is now being increasingly detected by CT. Peritoneal implants may be seen as nodular, plaquelike, or sheetlike masses[127,128] (Figs. 4–150, 4–156 through 4–159), and deposits as small as 5 mm from ovarian carcinoma may be detected, often outlined by ascites.[126,128–130] High-resolution ultrasonography may demonstrate even minute metastases when they are seeded on the anterior peritoneum[131] (Fig. 4–160). Notable sites of implantation are the falciform ligament and interhepatic fissures (Figs. 4–161 and 4–162). Accurate identification of peritoneal implants is particularly important since cytoreductive surgery is of value in improving survival if all intraabdominal masses greater than 1.5 cm in diameter can be removed.[133–135] Implants in the porta hepatis and interlobar fissure indicate tumor nonresectability.[136]

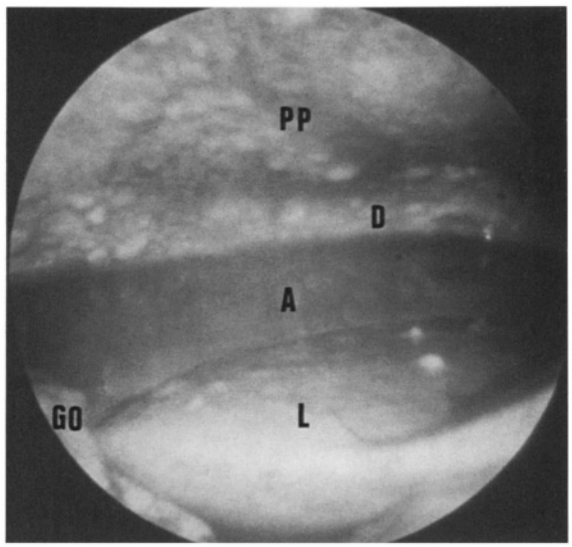


Fig. 4–153. Perihepatic seeded ovarian carcinoma shown by peritoneoscopy.
Multiple small nodules are present on the liver (*L*) and the parietal peritoneum (*PP*) of the abdominal wall and diaphragm (*D*). *A* = ascites; *GO* = greater omentum.
(Courtesy of Charles Lightdale, M.D., New York.)

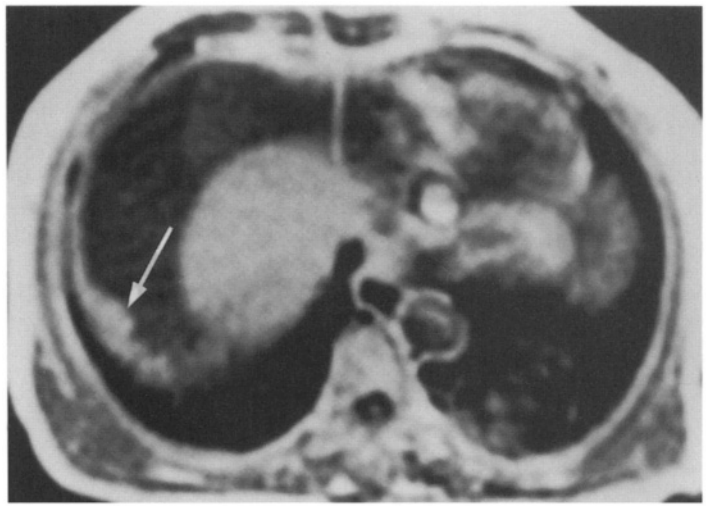


Fig. 4–154. Right subdiaphragmatic implants from ovarian carcinoma.
MRI, T1-weighted axial image, demonstrates seeded metastases from ovarian carcinoma on the diaphragmatic parietal peritoneum on the right (*arrow*). (Reproduced from Chou et al.[102])

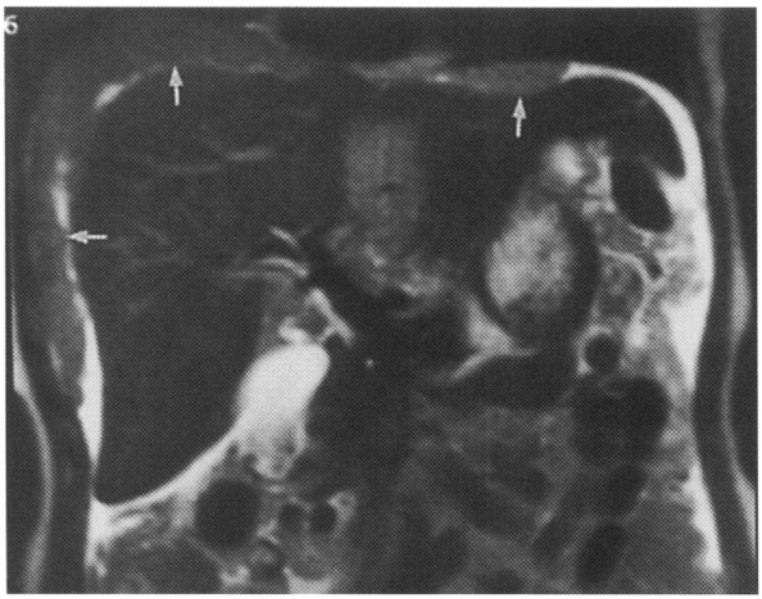


Fig. 4–155. Seeded implants along the diaphragmatic surface and the liver capsule from fallopian tube carcinoma.
Coronal T2-weighted MR image demonstrates an irregular layer of metastatic deposit measuring up to 2 cm in thickness along the parietal peritoneum of the diaphragm and the liver capsule (*arrows*). (Reproduced from Semelka et al.[59])

Parietal peritoneal thickening with contrast enhancement of the peritoneum, making the peritoneum visible as a smooth or nodular line along the abdominal wall, representing confluent seeded deposits, may be conspicuous (Fig. 4–163). In one series of patients with peritoneal tumor spread studied by CT, it was evident in 62%.[137] Refinements in MR imaging, in which the examination protocol focuses on T1-weighted fat-saturated sequences after application of gadolinium, similarly lead to detection of peritoneal carcinomatosis[59,138–141] (Fig. 4–164). It has also been reported in tuberculous peritonitis[137, 142–147] (Figs. 4–165 and 4–166), other infectious processes of the peritoneum[148,149] (Fig. 4–167), mesothelioma,[150] and peritoneal endometriosis.[151]

In mucinous cystadenocarcinoma of the ovary, the gelatinous material produced by seeded metastases may be first seen as a mantle over the right lobe of the liver (Figs. 4–168 and 4–169).

With progression to the condition known as pseudomyxoma peritonei,[152] the characteristic findings of scalloping of the liver edge by the cystic collections and

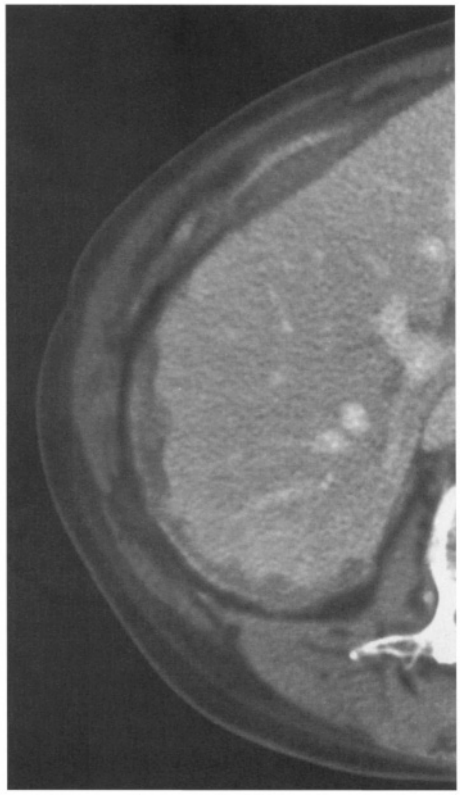


Fig. 4–156. Perihepatic seeded implants from ovarian carcinoma.
Multiple deposits on the liver capsule result in a scalloped contour.

septated ascites may be evident[153–155] (Figs. 4–170 through 4–173). In this entity, the primary tumor usually occurs within the appendix or ovary. Related to the surface adherence of the high-grade cells, there is a notable lack of tumor on bowel surfaces that are active in peristalsis. Thus, the greatest volumes of cancer are beneath the diaphragms and in the pelvis. The greater and lesser omentum also contain a relatively larger volume of tumor.[156]

Delineation by the falciform ligament is a characteristic landmark of the process of intraperitoneal seeding.[70,94]

Dense, punctate perihepatic calcifications in a case of pseudomyxoma peritonei from mucinous adenocarcinoma of the appendix following intraperitoneal chemotherapy has been reported.[157] Diffuse intraperitoneal gelatinous metastases from mucin-producing teratocarcinoma of the testis in which the peritoneal cavity was seeded during retroperitoneal lymphadenectomy has been observed.[158]

In serous cystadenocarcinoma of the ovary, calcified perihepatic metastatic implants may be detected.[128,137,159–161] This is the most common type of ovarian carcinoma and contains histologic calcification, psammoma bodies, in approximately 30% of cases.[162] The perihepatic calcifications are seen related to the right hemidiaphragm (Fig. 4–174) and liver surface (Figs. 4–175 and 4–176), even up to the immediate subphrenic region (Fig. 4–177), as well as on the falciform ligament (Figs. 4–162b and 4–176). Calcified implants have also been noted in the right paracolic gutter, in

text continues on page 229

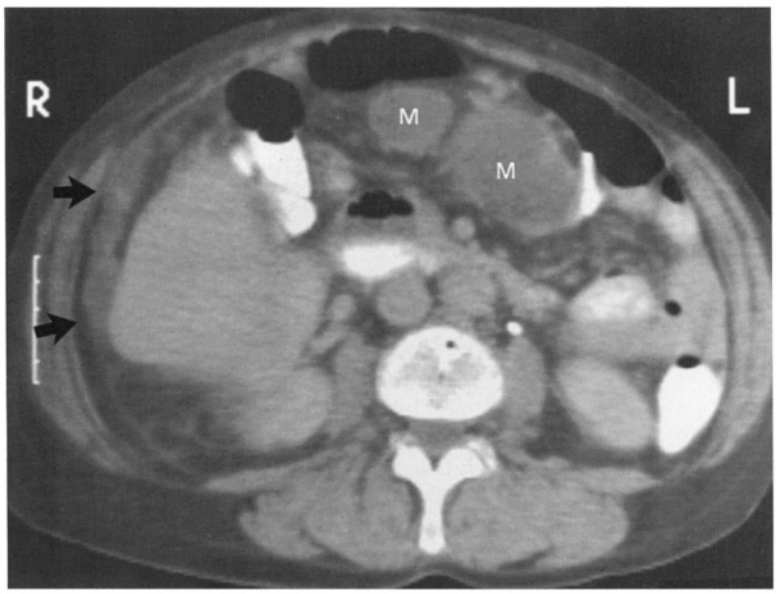


Fig. 4–157. Metastatic "caking" of the parietal peritoneum.
Seeded metastases from ovarian carcinoma have resulted in plaquelike thickening of the parietal peritoneum lateral to the right lobe of the liver (*arrows*). Mesenteric masses (*M*) are also present.
(Courtesy of Michiel Feldberg, M.D., Ph.D., University of Utrecht, The Netherlands.)

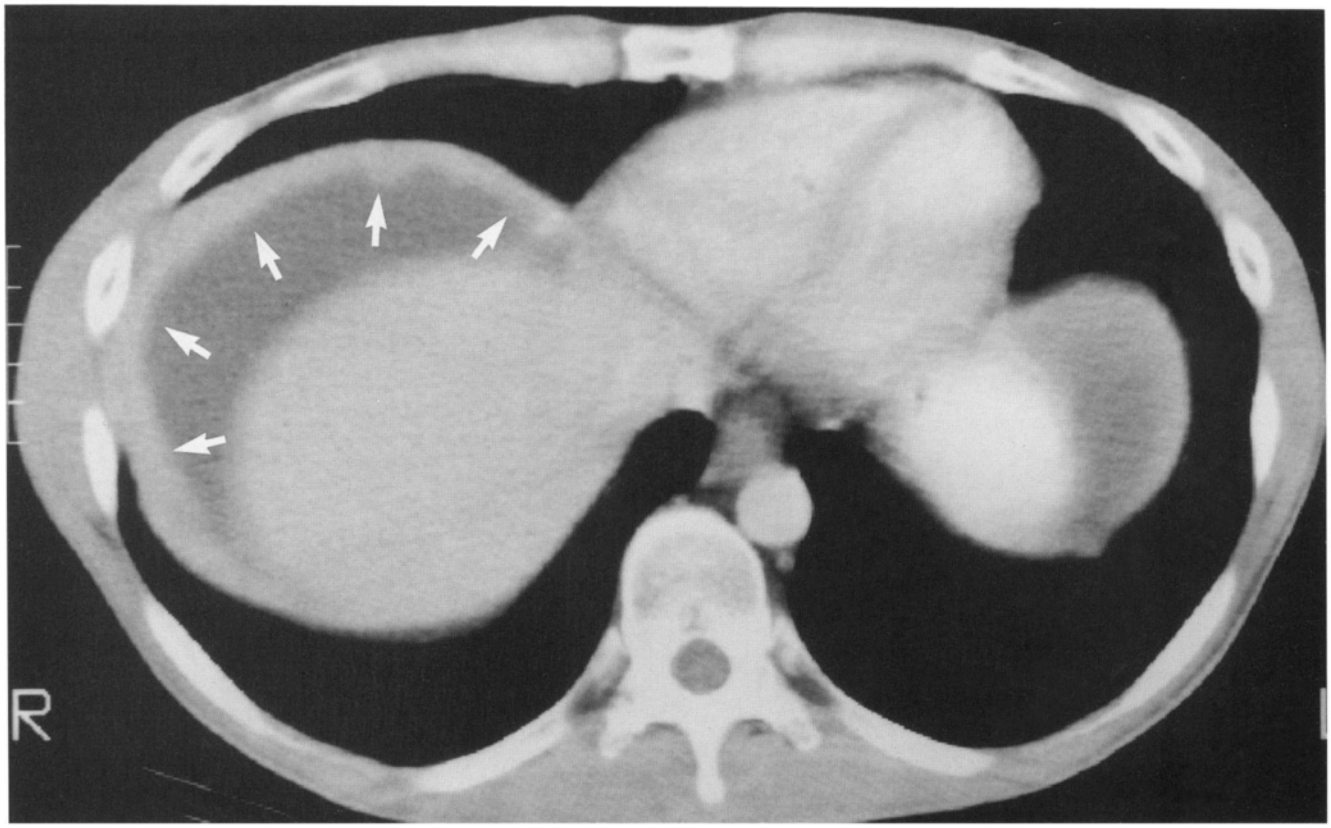


Fig. 4–158. Plaquelike seeding on diaphragmatic peritoneum.
Intraperitoneal seeding from an anaplastic carcinoma, site unknown, results in marked thickening of the diaphragmatic parietal peritoneum, particularly on the right (*arrows*). Ascites is present.
(Courtesy of Emil Balthazar, M.D., Bellevue Hospital—New York University School of Medicine, New York.)

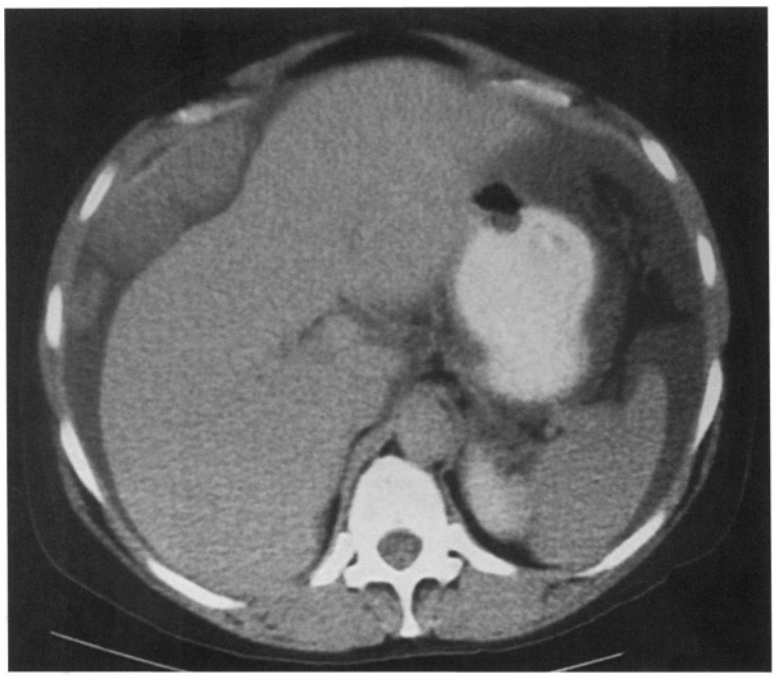


Fig. 4–159. Perihepatic diaphragmatic metastatic nodules.
Seeded implants from ovarian carcinoma are seen as prominent nodular masses on the parietal peritoneum overlying the diaphragm impressing upon the liver. Ascites is present.

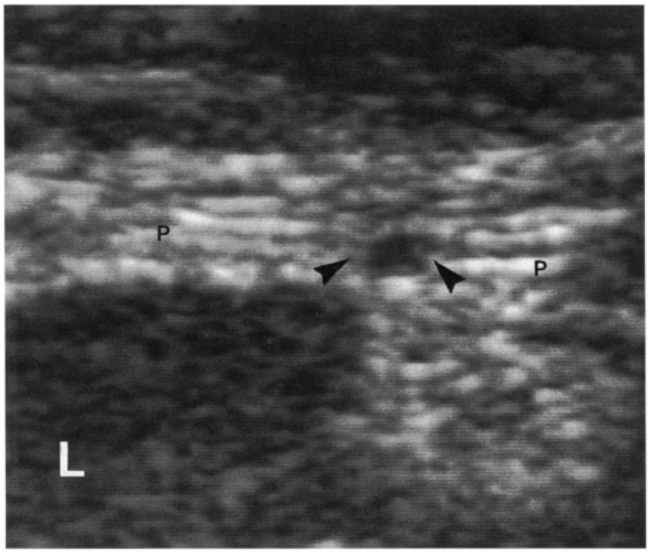


Fig. 4–160. Small anterior peritoneal implant.
Ultrasonography shows a 3-mm implant (between *arrowheads*), revealed as a focal hypoechoic linear interruption of the normally hyperechoic parietal peritoneum (*p*). *L* = liver.
(Reproduced from Rioux and Midlaud.[131])

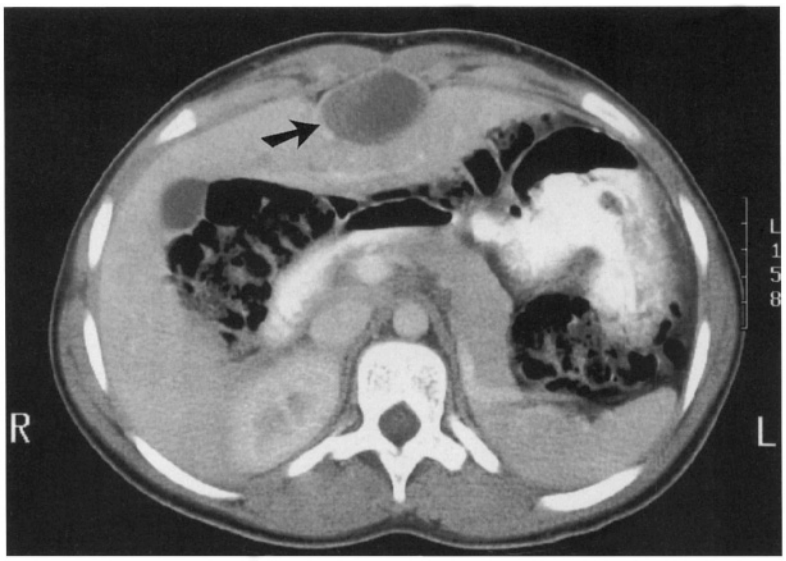


Fig. 4–161. Falciform ligament implant.
A large metastasis from a myxoid liposarcoma of the pelvis has deposited on the falciform ligament (*arrow*).

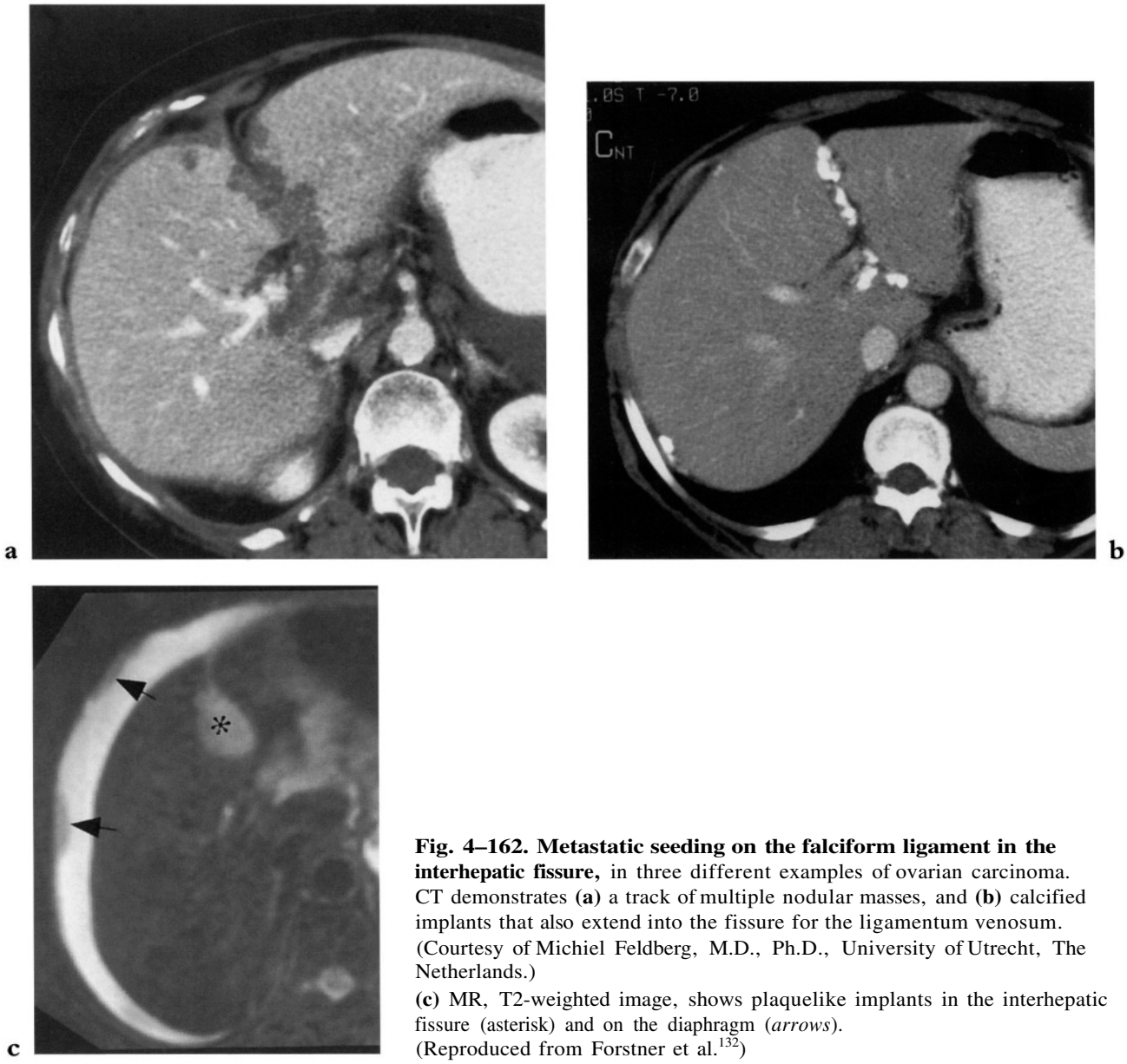
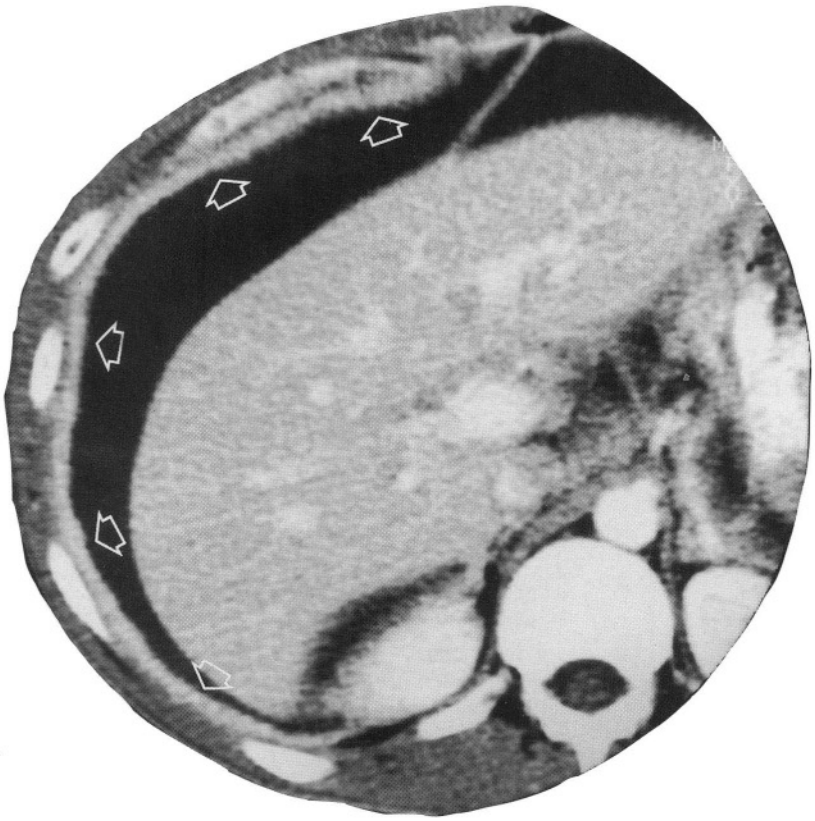
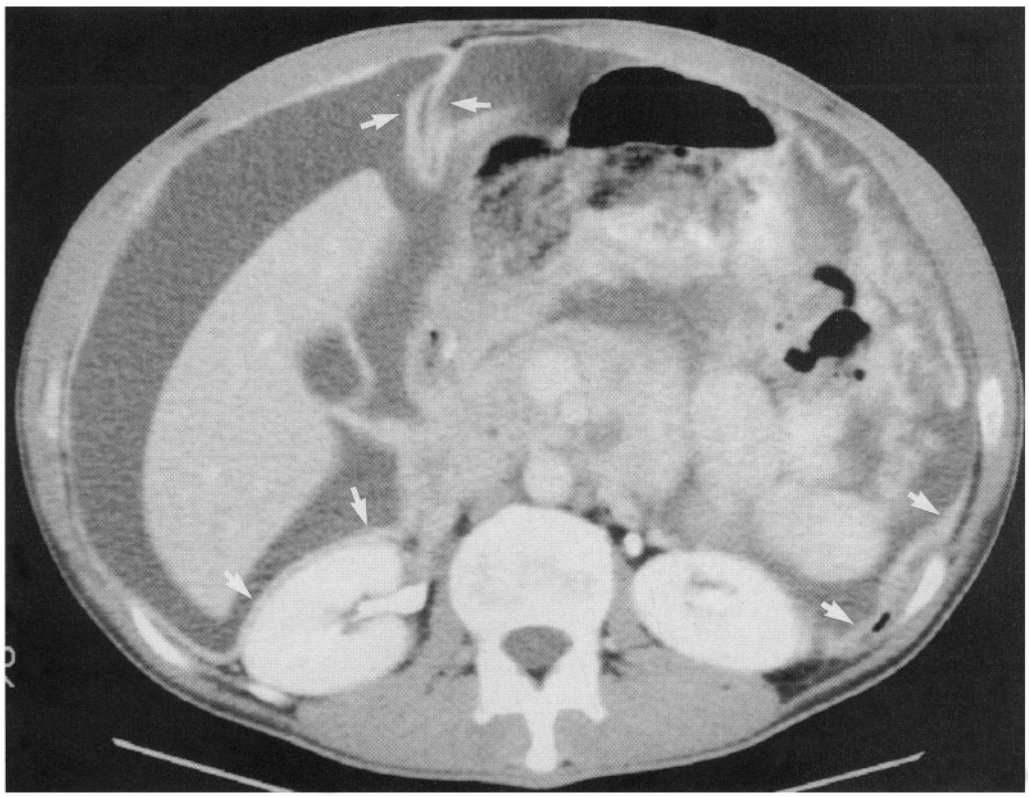


Fig. 4–162. Metastatic seeding on the falciform ligament in the interhepatic fissure, in three different examples of ovarian carcinoma. CT demonstrates **(a)** a track of multiple nodular masses, and **(b)** calcified implants that also extend into the fissure for the ligamentum venosum. (Courtesy of Michiel Feldberg, M.D., Ph.D., University of Utrecht, The Netherlands.)

(c) MR, T2-weighted image, shows plaquelike implants in the interhepatic fissure (asterisk) and on the diaphragm (*arrows*). (Reproduced from Forstner et al.[132])



a



b

Fig. 4–163. Enhancement of peritoneum thickened by seeded metastases.
(a) There is striking contrast enhancement of the perihepatic thickened parietal peritoneum (*arrows*).
(b) In addition to changes in the parietal peritoneum lateral to the liver, enhancement is also seen in the thickened parietal peritoneum on the left side, overlying the right kidney, and constituting the falciform ligament (*arrows*). Metastatic caking of the greater omentum, ascites, and retroperitoneal adenopathy are also present. The primary carcinoma is an anaplastic lesion, site unknown.
(Courtesy of Emil Balthazar, M.D., Bellevue Hospital—New York University School of Medicine, New York.)

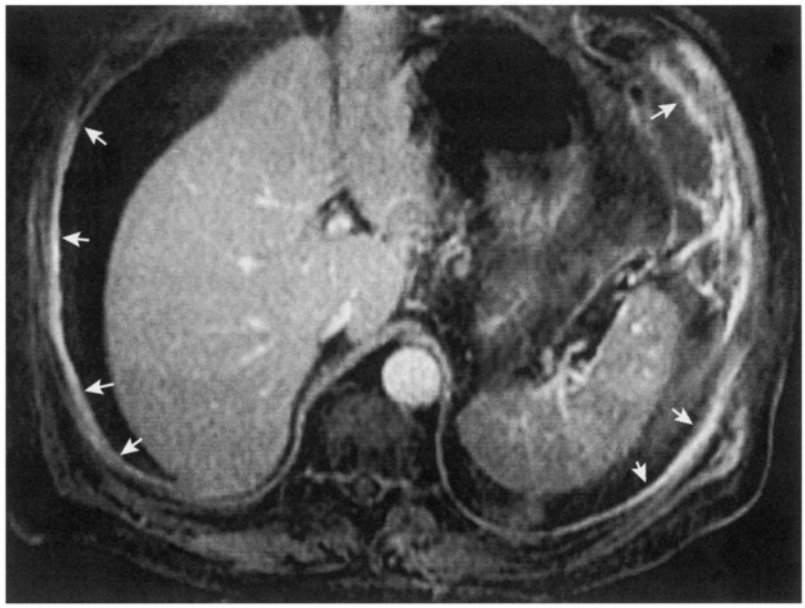


Fig. 4–164. Peritoneal carcinomatosis.
Gadolinium-enhanced MR image with fat saturation shows a thin rim of abnormally enhancing peritoneum in the right and left subphrenic spaces (*arrows*). Ascites is present. At laparoscopy, carcinomatosis with diffuse miliary tumor nodules was confirmed.
(Reproduced from Low et al.[138])



Fig. 4–165. Tuberculous peritonitis.
Contrast-enhanced CT shows massive ascites and marked thickening of the visceral and parietal peritoneum, further demarcated by contrast enhancement (*arrows*).
(Courtesy of Hiromu Mori, M.D., Oita Medical Center, Oita, Japan.)

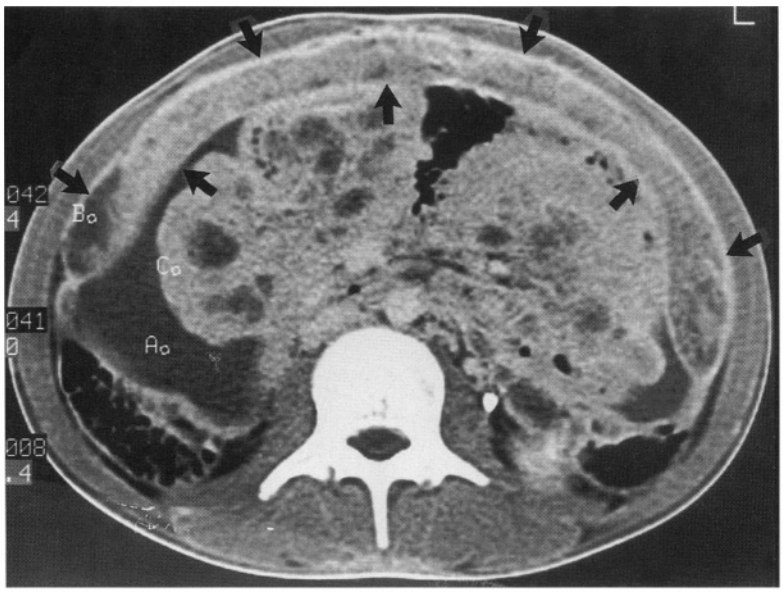


Fig. 4–166. Tuberculosis peritonitis.
Contrast-enhanced CT demonstrates a conspicuous omental cake (*arrows*) demarcated by enhanced thickened peritoneum. The small bowel mesentery is matted and conglomerated by the inflammatory process. (Reproduced from Auh et al.[10])

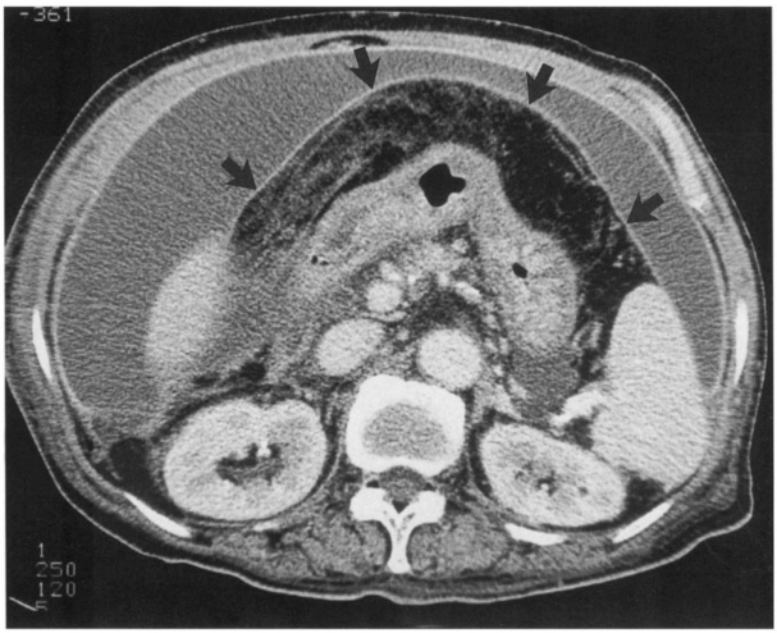


Fig. 4–167. Spontaneous bacterial peritonitis.
Peritoneum lining the greater omentum, which is displaced posteriorly by a large loculated ascites, is conspicuously thickened and enhanced (*arrows*). Similar changes demarcate the parental peritoneum of the anterior abdominal wall. (Reproduced from Auh et al.[10])

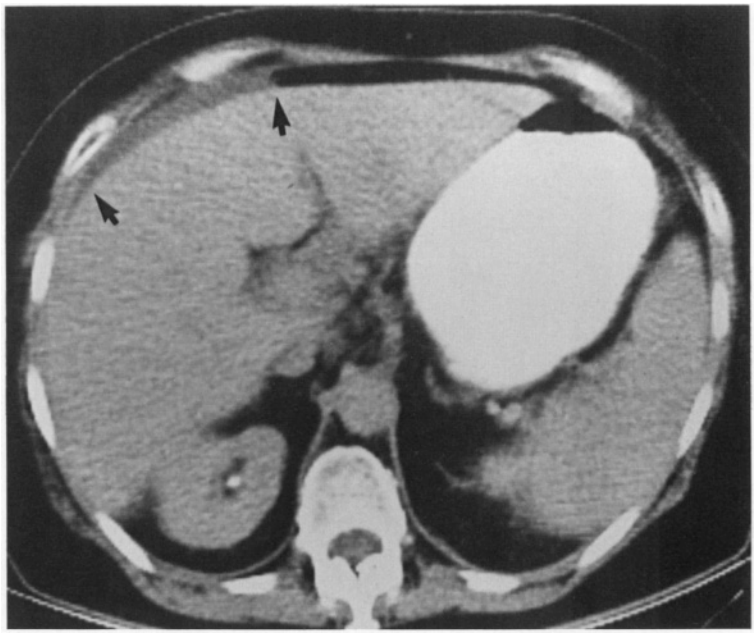


Fig. 4–168. Perihepatic mantle of seeded metastases.
A thin mantle of low-density material representing early seeding from a mucinous ovarian carcinoma is adjacent to the liver (*arrows*). It extends anteriorly to the level of the falciform ligament. There is no appreciable ascites.



Fig. 4–169. Perihepatic mantle of seeded metastases.
Seeded metastases from an ovarian mucinous cystadenocarcinoma are deposited on the liver capsule (*arrows*). This process extends from the level of the falciform ligament anteriorly to the level of the right coronary ligament posteriorly at the bare area of the liver. There is no appreciable ascites. In the older anatomic pathology literature, such thickening of the visceral peritoneum over the liver is termed "sugar-icing" (*Zuckergussleber*).

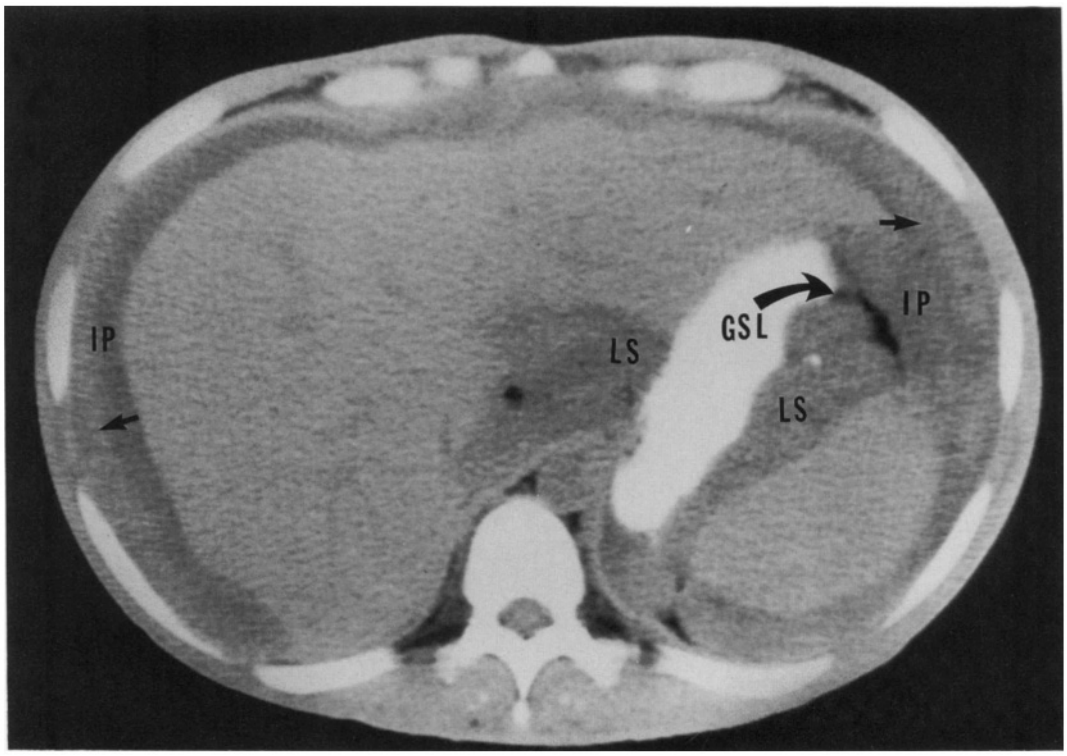


Fig. 4–170. Pseudomyxoma peritonei.
Mild scalloping of the liver contour is related to conspicuous fluid collections in the greater peritoneal cavity (*IP*) and lesser sac (*LS*). These are inhomogeneous, with some areas showing increased density (*arrows*). *GSL* = gastrosplenic ligament. (Reproduced from Churchill and Meyers.[154])

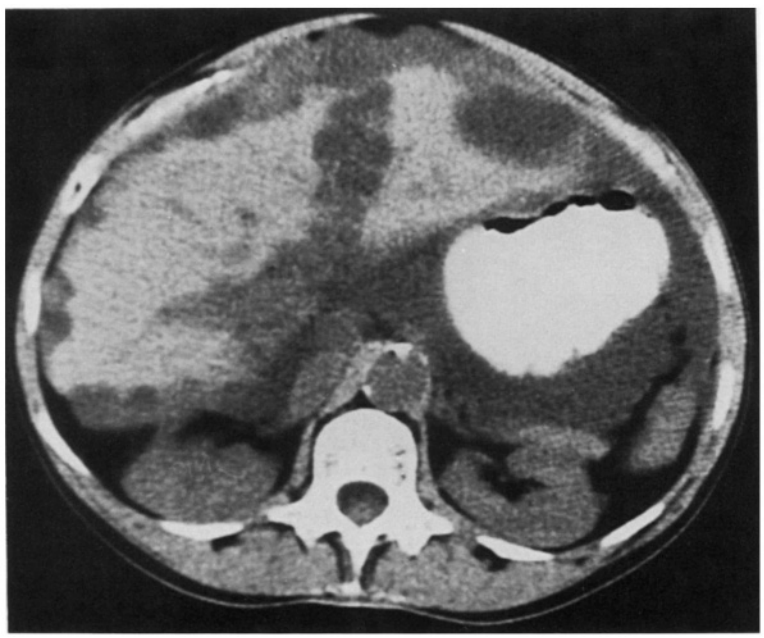


Fig. 4–171. Pseudomyxoma peritonei secondary to mucinous cystadenocarcinoma of the ovary.
Gelatinous cysts of varying densities produce scalloped indentations upon the liver. Discrete cysts bound the falciform ligament. Fluid collections in both the greater peritoneal cavity and lesser sac are inhomogeneous.

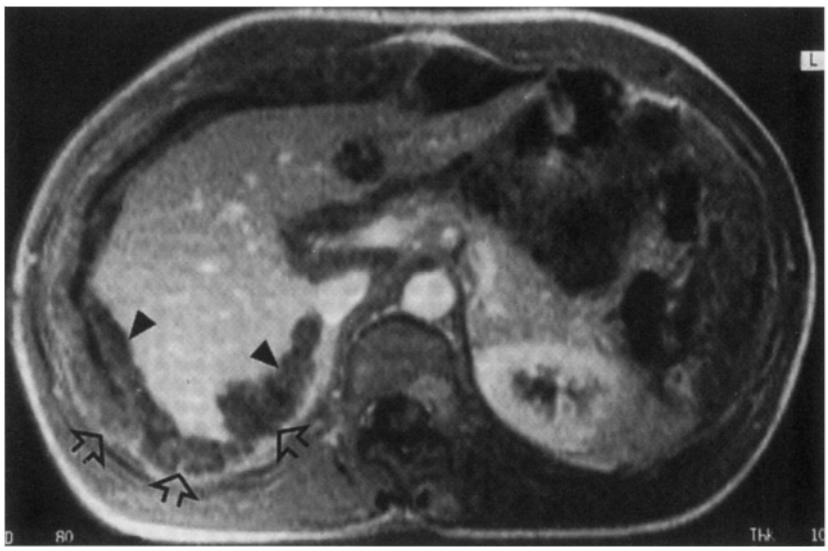


Fig. 4–172. Pseudomyxoma peritonei secondary to appendiceal mucinous cystadenocarcinoma.
T1-weighted gadolinium enhanced MR image demonstrates scalloping of the liver margin *(arrowheads)* and enhancement of the gelatinous material (*open arrows*).
(Reproduced from Semelka et al.[59])



Fig. 4–173. Pseudomyxoma peritonei secondary to appendiceal mucinous cystadenocarcinoma.
Gadolinium-enhanced T1-weighted MR image with fat suppression demonstrates a rim of enhancing right subphrenic tumor *(white arrows)* and bulky tumor encasing the stomach, spleen, and splenic flexure of the colon. Enhancing tumor is also evident in the superior recess of the lesser sac (*black arrow*).
(Reproduced from Low et al.[139])

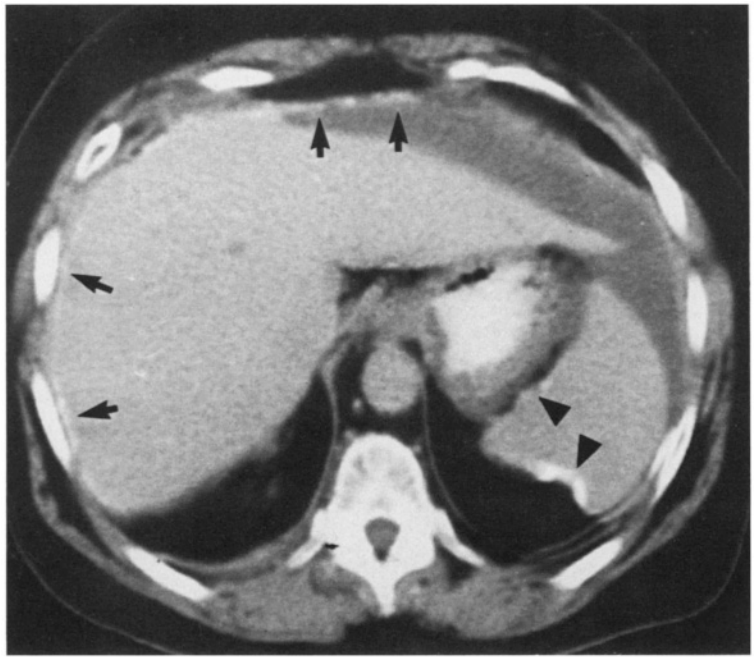


Fig. 4–174. Calcified perihepatic implants from ovarian carcinoma.
CT shows calcification along the right border of the liver that extends anteriorly along the diaphragm *(arrows),* where it is separated from the liver by ascites. Perisplenic calcification is also present (*arrowheads*).
(Reproduced from Mitchell et al.[159])

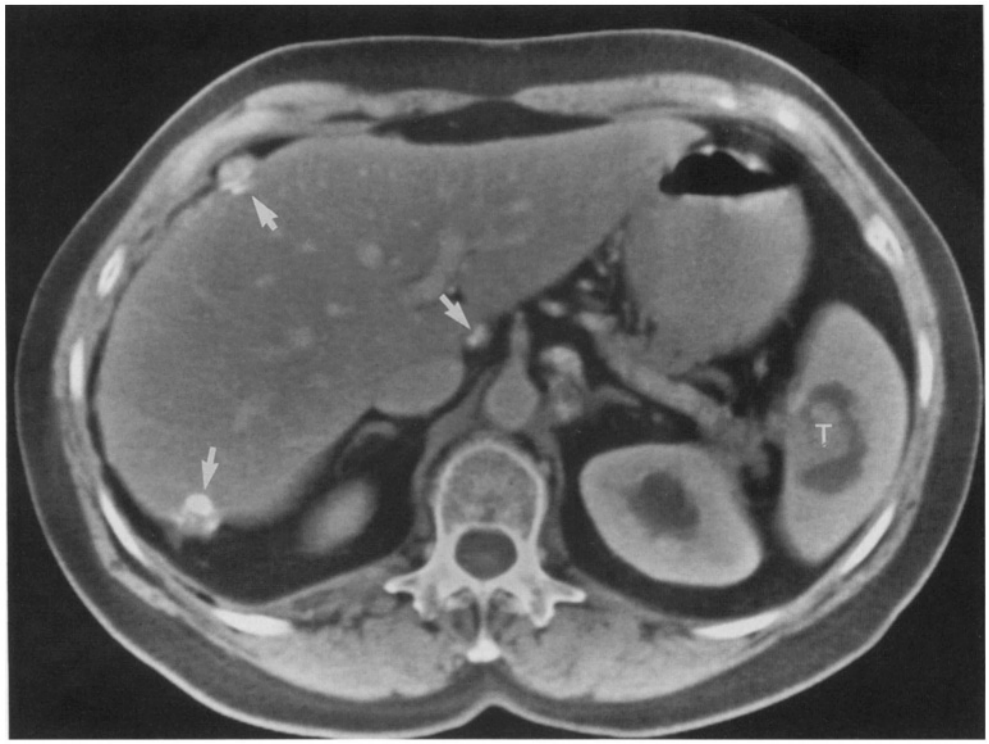


Fig. 4–175. Calcified perihepatic implants from ovarian carcinoma.
Calcified seedings are seen on the liver surface (*arrows*). Metastatic tumor is present in the splenic hilum *(T).*
(Reproduced from Gore and Meyers.[24])

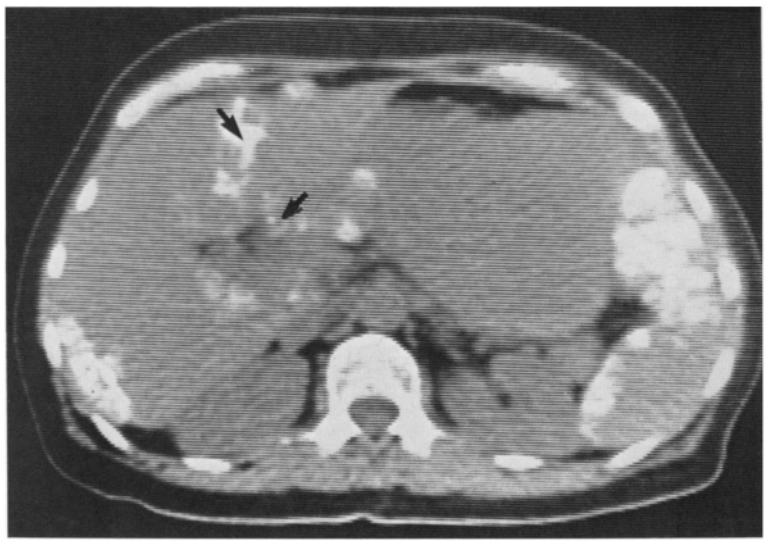


Fig. 4–176. Calcified perihepatic implants from ovarian carcinoma.
Calcified metastatic deposits are seen along the liver surface, the ligamentum teres and falciform ligament *(arrows),* and spleen. (Reproduced from Solomon and Rubinstein.[161])

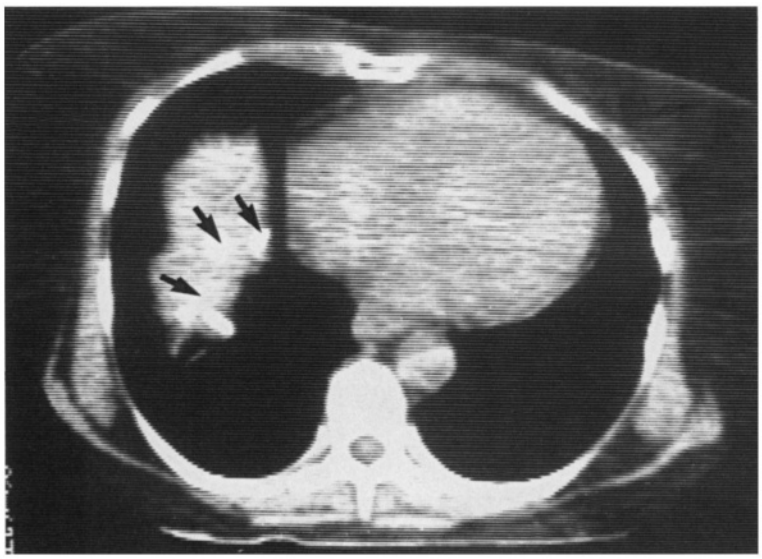


Fig. 4–177. Calcified perihepatic metastases from ovarian carcinoma.
The secondary malignancies have been transported and implanted in the immediate subdiaphragmatic region *(arrows).* (Reproduced from Solomon and Rubinstein.[161])

Morison's pouch, and adjacent to the spleen.[137,159,161] Peritoneal calcifications secondary to gastric carcinoma are rare.[163,164]

Subcapsular liver metastases have been observed by CT in 13 cases of ovarian carcinoma by Triller et al.[126] These are seen on CT and MR imaging as rounded or oval low-density or high-signal-intensity lesions between the liver capsule and the liver parenchyma, generally of 0.5–1 cm diameter and infrequently approaching 8 cm (Figs. 4–178 through 4–180). They are characteristically located in the dorsomedial and dorsolateral parts of the right liver lobe and may be associated with peritoneal metastases in Morison's pouch. Presumably, cancer cells implanted on the liver surface infiltrate the capsule as well as the liver parenchyma and develop at these sites as subcapsular metastases.[95,126] The lesion may regress after chemotherapy.

Distinction between subcapsular metastases and intraparenchymal liver metastases by CT and MR imaging is important because the former do not represent a contraindication for cytoreductive surgery. It may be difficult preoperatively to differentiate between parenchymal liver metastases (potentially curable with liver resection), serosal liver lesions, and diaphragmatic peritoneal implants, the latter two representing peritoneal metastatic growth[126,137,165,166] (Figs. 4–181 and 4–182). Subcapsular

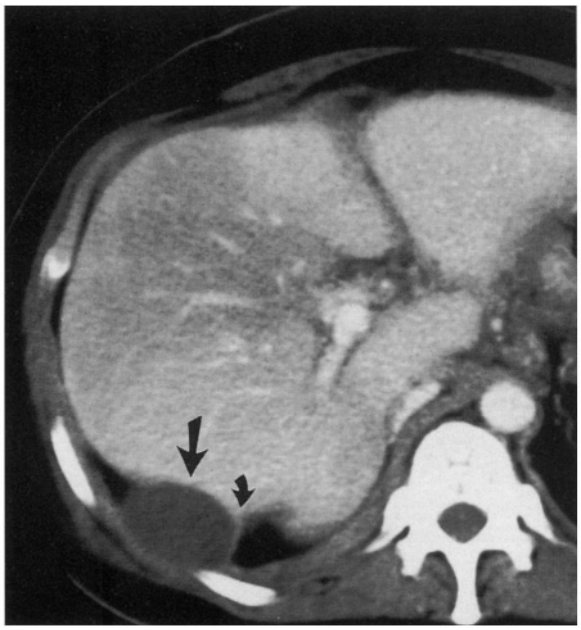


Fig. 4–178. Subcapsular liver metastasis from ovarian carcinoma.
A cystic mass *(large arrow)* indents the posterior contour of the right lobe of the liver. A "claw-sign" *(small arrow)* along one of its margins indicates its relationship to the parenchyma.

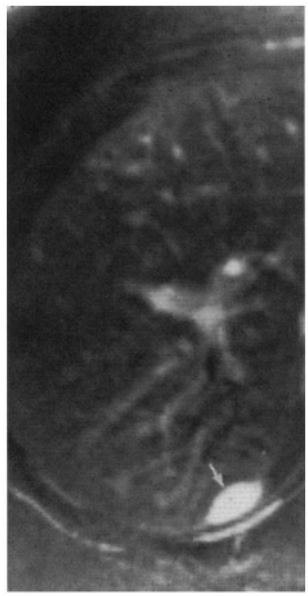


Fig. 4–180. Subcapsular liver metastasis from ovarian carcinoma.
T2-weighted fat suppressed MR image demonstrates a Subcapsular liver metastasis *(arrow).* It presents a characteristic biconvex lens shape.
(Reproduced from Semelka et al.[59])

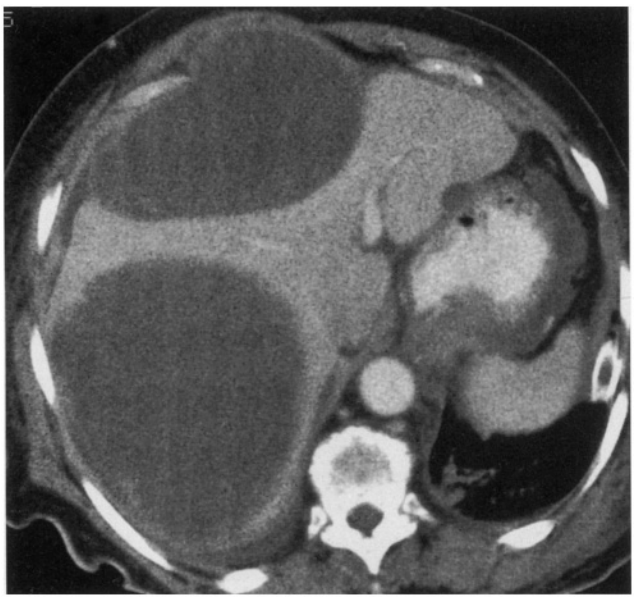


Fig. 4–179. Subcapsular liver metastases from ovarian carcinoma.
Large lesions involve the liver.
(Courtesy of Jay Heiken, M.D., Mallinckrodt Institute of Radiology, St. Louis, MO.)

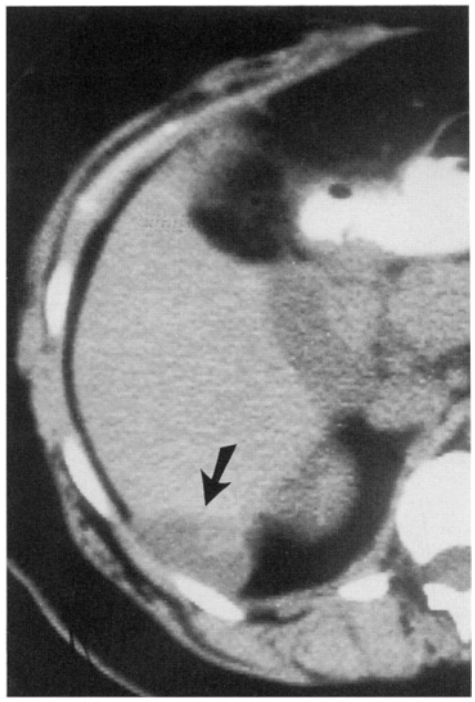
liver metastases may present a characteristic "claw" sign (Fig. 4–178), analogous to that seen in superficial renal cysts, or a biconvex lens shape (Fig. 4–180).

Seeded Metastases on the Greater Omentum

A characteristic feature of the greater omentum, projecting as the fatty apron of the abdomen, is its associated lymphoid tissue, known as *milky spots.* These are composed of numerous macrophage and lymphocyte aggregations surrounding a capillary convolution.[167,168] The mesothelial cells overlying these areas are loosely connected and lack basement membranes.[169–171] They act as open lymphatic lacunae that absorb peritoneal fluid and thereby bring tumor cells in large quantity to this structure.[172,173] The secretion of angiogenetic factors by omental tissue may result in early vascularization of the seeded tumors and, therefore, their more rapid growth.[174] This results in the *omental cake.*

In disseminated carcinomatosis, most commonly from ovarian carcinoma, seeded metastases on the greater omentum may be readily evident by sectional imaging. The lesions range from soft-tissue permeation

Fig. 4–181. Intrahepatic metastasis simulated by extracapsular lesion.
A lesion is seen dorsally seemingly involving the right lobe *(arrow).* This was proved to be a metastasis to the diaphragm from ovarian carcinoma. The liver parenchyma and the liver capsule were both free from tumor in this area. (From Lundstedt et al.[166])



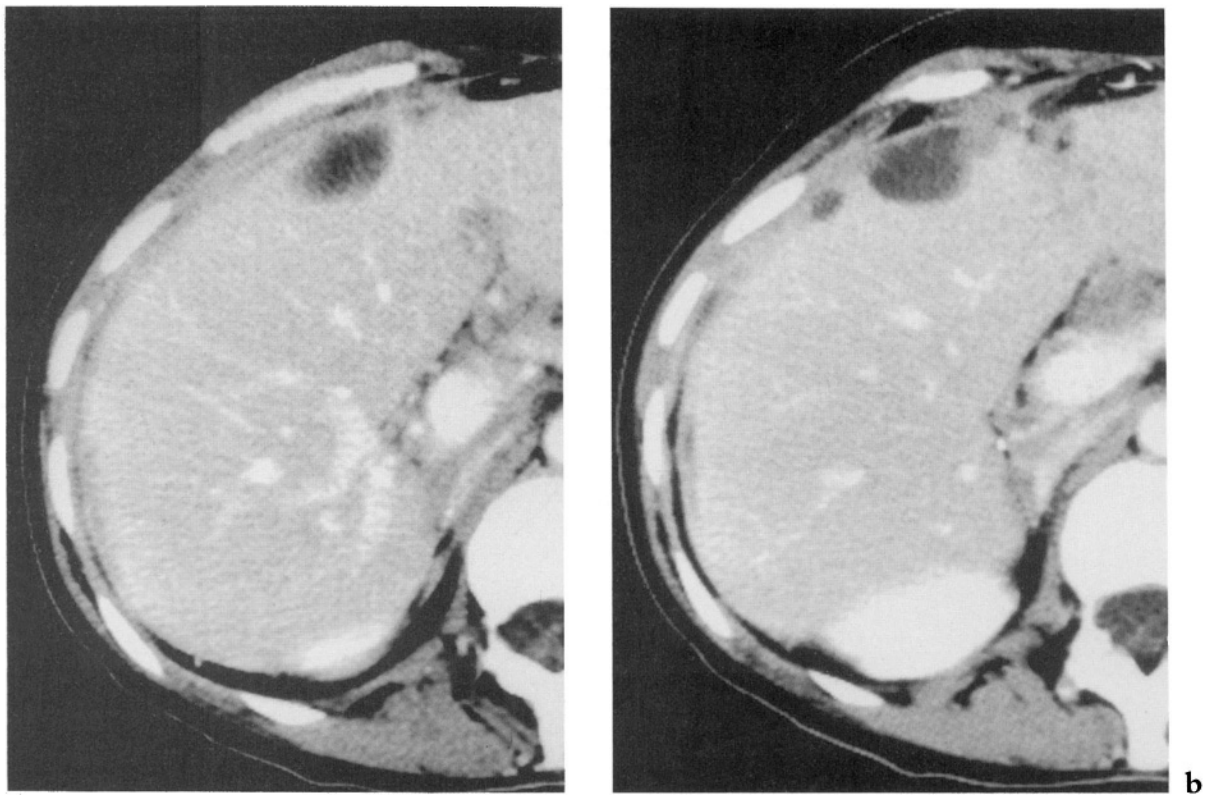


Fig. 4–182. Intrahepatic metastasis mimicked by extracapsular lesion.
(a) CT shows an appearance strongly suggesting a peripheral intrahepatic cystic metastasis, secondary to ovarian carcinoma. **(b)** Lower level more clearly indicates true nature of extracapsular metastases, associated with diaphragmatic peritoneal thickening.

of omental fat to discrete linear and nodular densities (Fig. 4–183) to thick, solid omental masses described as "caking"[137,175,176] (Figs. 4–184 and 4–185). Widespread peritoneal metastasis, including omental infiltration, is a rare consequence of a retroperitoneal malignancy such as renal cell carcinoma.[177] A densely calcified omental cake secondary to a metastatic serous cystadenocarcinoma of the ovary rich in psammoma bodies has been reported.[160]

Heavily seeded metastatic deposits on the greater omentum are to be distinguished from primary neoplasms,[178,179] infection and inflammation (Fig. 4–186), consequences of trauma, varices (Fig. 4–187), and infarction.[179,180]

Two Unusual Sites of Peritoneal Carcinomatosis

Sister Mary Joseph's Nodule. A dynamic occurrence of metastatic spread is the umbilical lesion known as Sister Mary Joseph's nodule. Named by Sir Hamilton Baily[181,182] after the surgical assistant to Dr. William Mayo, who first called his attention to this sign of intraabdominal malignancy,[183] many hundreds of cases have now been reported.[184,185] They are secondary, most commonly, to carcinomas of the stomach, ovary, colon, and pancreas. The umbilical nodules are usually 1–1.5 cm in diameter[184] (Fig. 4–188), but lesions as large as 10 cm in diameter have been reported[186] (Fig. 4–189). Frequently, the umbilical nodule is the initial presentation of the internal primary malignancy.[187,188] Most patients die within months of its appearance.[187,188] Various modes of spread to the umbilicus have been proposed, ranging from lymphatic or hematogenous dissemination via the abdominal folds to seeded implants.[184,185,187] The entity should be distinguished from seeded implantation during a surgical incision[189] (Fig. 4–190) or implants of endometriosis.[184]

Krukenberg Tumors. A striking targeted pathway of seeding is occasionally encountered as the entity of Krukenberg tumors of the ovaries.[190–194] These are usually secondary to gastric or colon mucinous adenocarcinomas, are usually bilateral, and are associated with ascites (Fig. 4–191). Their likely pathogenesis has been recently elucidated as fixation and entrance of seeded cells at sites

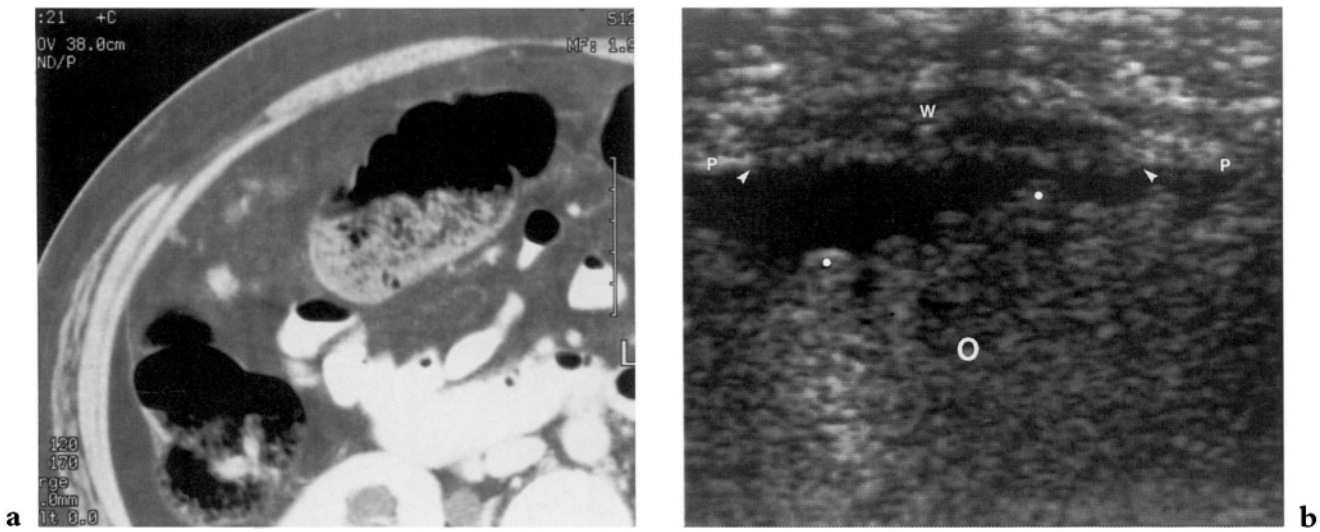


Fig. 4–183. Discrete nodular metastases on the greater omentum, demonstrated in two different cases.
(a) Contrast-enhanced CT shows multiple focal enhancing lesions on the fat-laden greater omentum anterior to the colon, metastatic from ovarian carcinoma.
(Courtesy of Robert E. Mindelzun, M.D., Stanford University School of Medicine, Palo Alto, CA.)
(b) High-resolution ultrasonography, magnified view, shows a thick, hypoechoic, homogeneous, and completely infiltrated omentum (*O*). A micronodular anterior surface *(white dots)* is further outlined by the ascites present. Also evident is an implant on the parietal peritoneum (*P*), shown by its acoustic interruption (between *arrowheads*).
(Reproduced from Riioux and Michaud.[131])



Fig. 4–184. Omental caking from seeded pancreatic carcinoma.
CT in this patient following a Whipple operation demonstrates confluent soft tissue masses *(arrows)* separating the transverse colon from the anterior abdominal wall.

of ovarian follicular rupture and perigonadal fat milky spots.[195] In a study of Krukenberg tumors by MRI, most showed a characteristic finding of varied hypointense solid components from a dense desmoplastic reaction.[194]

Multiple Sites

Multiple sites of seeded deposition are somewhat more common than a solitary focus. They may be appreciated on a barium enema study with reflux into the terminal ileum or in a subsequent small bowel series. Computed tomography or MR imaging may readily demonstrate these. Seeding in other disparate sites may be related to adhesions from previous inflammation or abdominal operations.

Mimicry of Carcinomatosis

Many of the imaging findings of peritoneal carcinomatosis may be closely mimicked by tuberculosis peritonitis[145–147] and the rare conditions of peritoneal mesothelioma,[150] (Fig. 4–192) peritoneal lymphomatosis[196] (Fig. 4–193) leiomyomatosis peritonealis disseminata,[197–199] peritoneal leiomyosarcomatosis,[200,201] sclerosing mesenteritis,[201a] and peritoneal serous papillary carcinoma.[202,203]

Instrumental, Operative, and Needle Track Seeding

Implantation of tumor cells may be a rare consequence of endoscopic surgical techniques and percutaneous biopsy or therapy. In a European review of 90,000 cases of fine-needle biopsies, only 6 cases of needle-track seeding were reported,[204] whereas an American review reported a needle-track seeding rate of 1 in 20,000.[205] Plaquelike subcutaneous infiltration may superficially resemble omental caking[206] (Fig. 4–194), or discrete peritoneal nodules[207] may be evident (Fig. 4–195).

Developments and Advances in Imaging

Multiple approaches have been applied in pursuit of refining the diagnostic accuracy of peritoneal carcino-

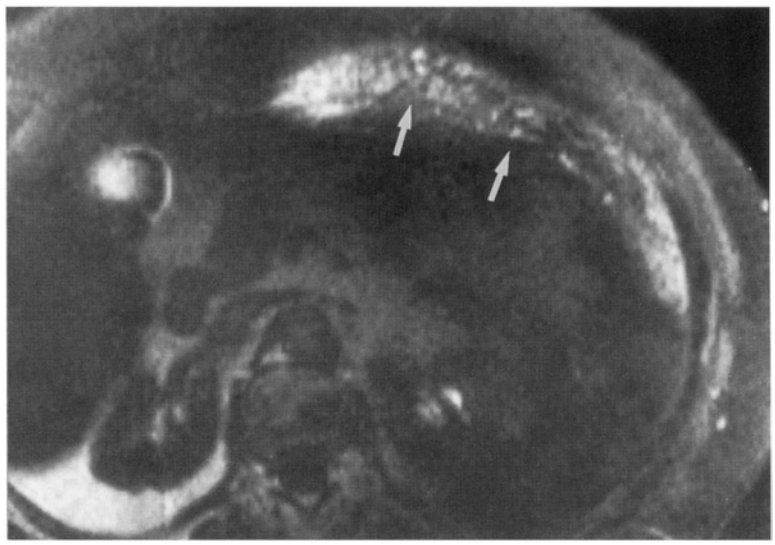


Fig. 4–185. Omental caking demonstrated secondary to ovarian carcinoma.
T1-weighted gadolinium-enhanced fat-saturated MR image demonstrates enhancement of tumor implants on the greater omentum (*arrows*).
(Reproduced from Ricke and Hosten.[141])

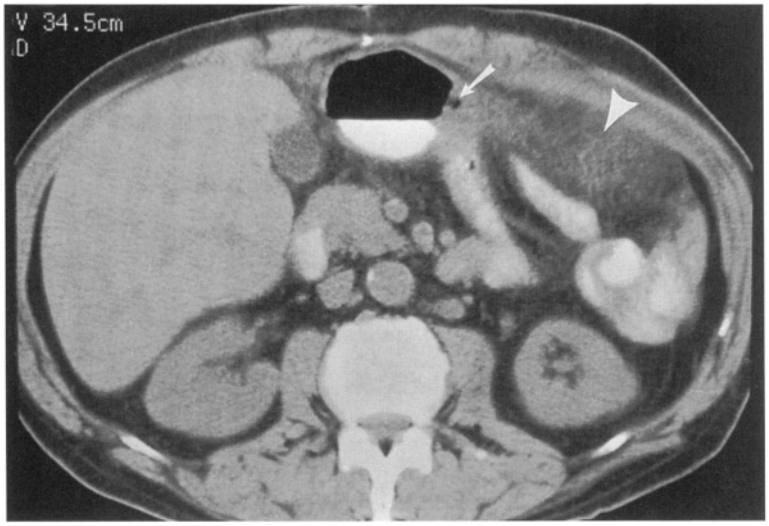


Fig. 4–186. Omental inflammation.
CT demonstrates inflammatory infiltration of the greater omentum *(arrowhead),* consequent to a perforated gastric ulcer *(arrow)* arising from the greater curvature of the stomach.
(Courtesy of James Drink, M.D., Yale University School of Medicine, New Haven, CT.)

Fig. 4–187. Omental varices.
The greater omentum, in contrast to the small bowel mesentery, has scanty vascular structures. In this patient with portal hypertension and ascites, omental varices (*arrows*) may mimic omental infiltration from carcinomatosis or peritonitis.

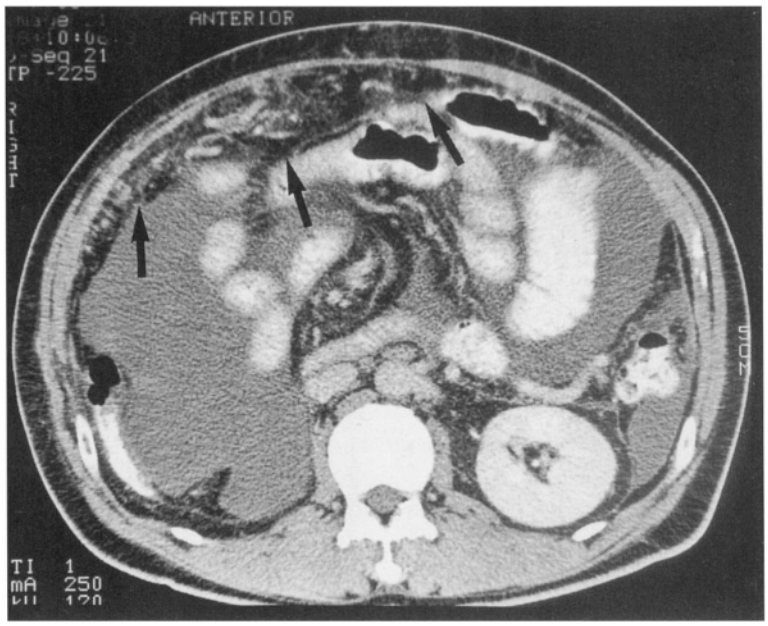




Fig. 4–188. Sister Mary Joseph's nodule.
A soft tissue mass *(arrows)* is present in the subcutaneous tissue at the level of the umbilicus, metastatic from a primary gastric adenocarcinoma. Note that it causes no discernible bulge of the skin surface. Generalized ascites is seen.
(Courtesy of Michiel Feldberg, M.D., Ph.D., University of Utrecht, The Netherlands.)

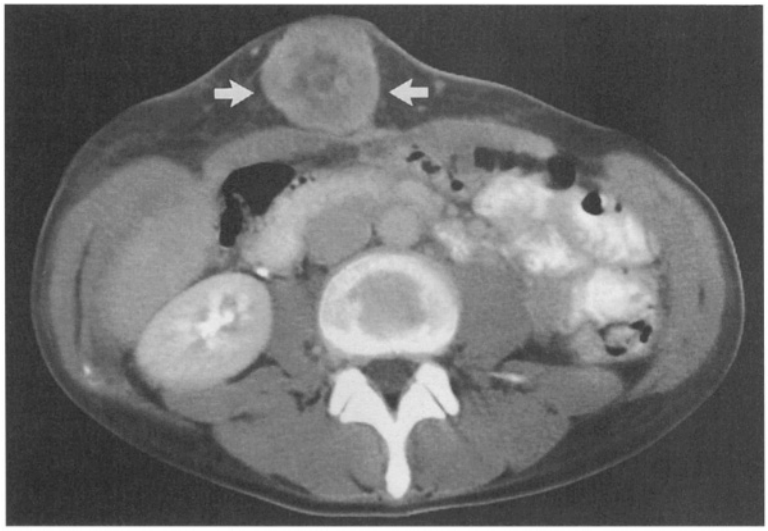


Fig. 4–189. Sister Mary Joseph's nodule.
CT demonstrates a large umbilical nodule with central necrosis *(arrows).* In this 33-year-old male with adenocarcinoma of the esophagogastric junction, carcinomatosis included a lesser omental mass (coronary lymphadenopathy) and bilateral adrenal metastases.

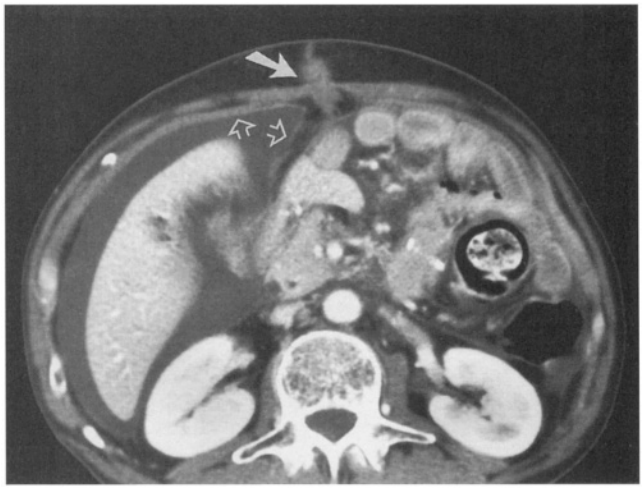


Fig. 4–190. Incisional recurrence mimicking a Sister Mary Joseph's nodule.
Tumor cells seeded at a surgical incision yield a subcutaneous mass *(closed arrow)* that appears to extend into the fat pad of the falciform ligament. This is associated with enhancement and thickening of the peritoneum *(open arrows)* and ascites in this patient with peritoneal carcinomatosis. It remains questionable whether the mass truly represents an umbilical metastasis that developed after the surgical procedure.

matosis. Whereas CT may clearly demonstrate localized or diffuse involvement of the peritoneum and its reflections and recesses, it is not reliable for low-volume tumor on peritoneal surfaces, and its greatest inaccuracies have been recorded in the pelvis.[208] Contrast enhancement of ascites in peritoneal carcinomatosis on delayed images in CT[209–211] may obscure peritoneal implants of soft tissue density. This enhancement probably results from increased vascular–peritoneal permeability.[210,212–214] Similar results have been reported for MRI using delayed gadolinium-enhanced sequences.[138,215] Positive-contrast peritoneography has been used in the demonstration of abdominal metastases.[70,216,217] When coupled with CT,[218–222] it may further enhance the demonstration of small peritoneal lesions (Fig. 4–196), but small implants in curved recesses may be missed on axial sectional imaging. CT with induced pneumoperitoneum with CO_2 has been reported with disclosure of implants even <2 mm in size (Fig. 4–197), but with significant limitations.[223] Abdominal ultrasonography has revealed signs for peritoneal carcinomatosis that account for malignant ascites in 78–92% of cases.[224–227] Using high-resolution ultrasonography, Rioux and Michaud[132] documented omental, serosal, and peritoneal implants. Following early reports,[102,228] MRI detection of peritoneal implants has been accelerated with technological

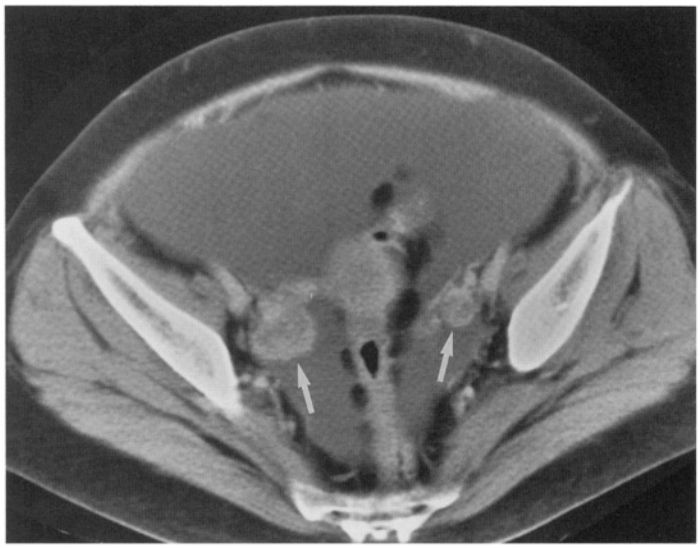
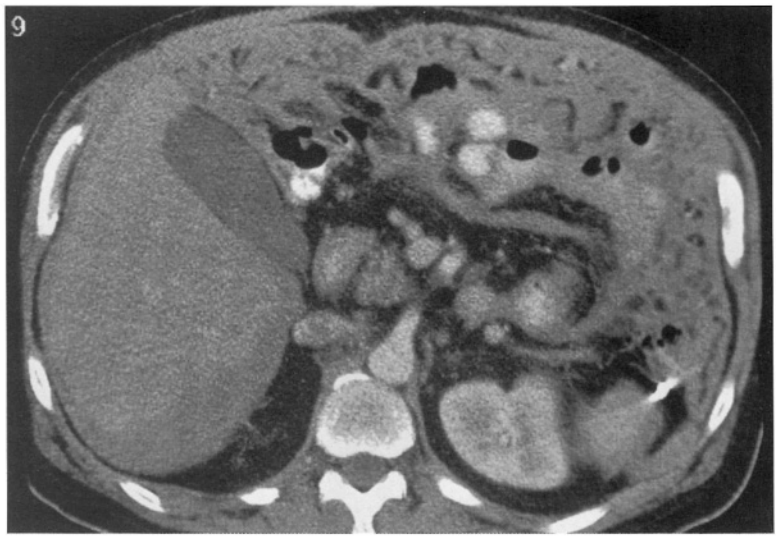
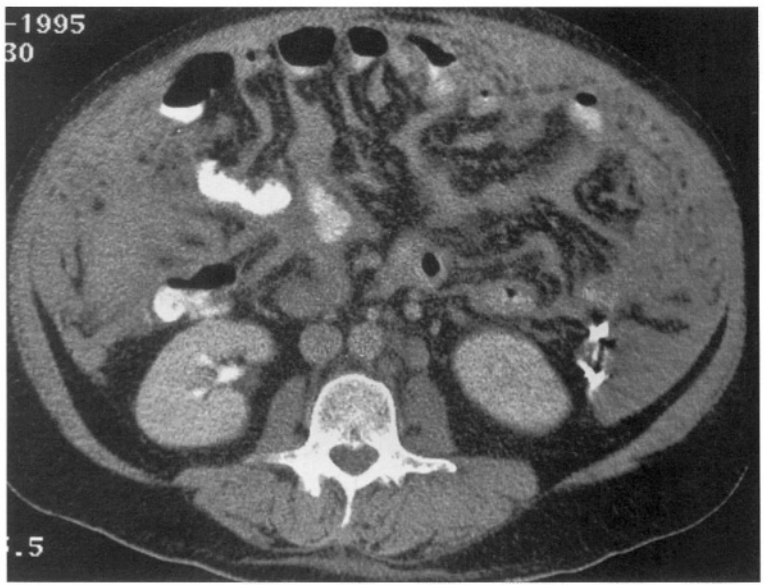


Fig. 4–191. Bilateral Krukenberg tumors of the ovaries secondary to gastric carcinoma.
The ovarian masses are clearly evident *(arrows),* highlighted by massive ascites.
(Reproduced from Gore and Meyers.[24])



a



b

Fig. 4–192. Peritoneal mesothelioma.
(a and **b)** Contrast-enhanced CT reveals diffuse infiltration of the greater omentum and small bowel mesentery with tumor. Ascites is a less impressive finding with peritoneal mesothelioma than it is with peritoneal carcinomatosis.
(Courtesy of James Brink, M.D., Yale University School of Medicine, New Haven, CT.)



Fig. 4–193. Peritoneal lymphomatosis.
Extensive tumor spreads along the peritoneal and mesenteric surfaces. Despite prominent compression of the mesenteries, the intrinsic intramesenteric fat is preserved. (Courtesy of Robert Mindelzun, M.D., Stanford University School of Medicine, Palo Alto, CA.)

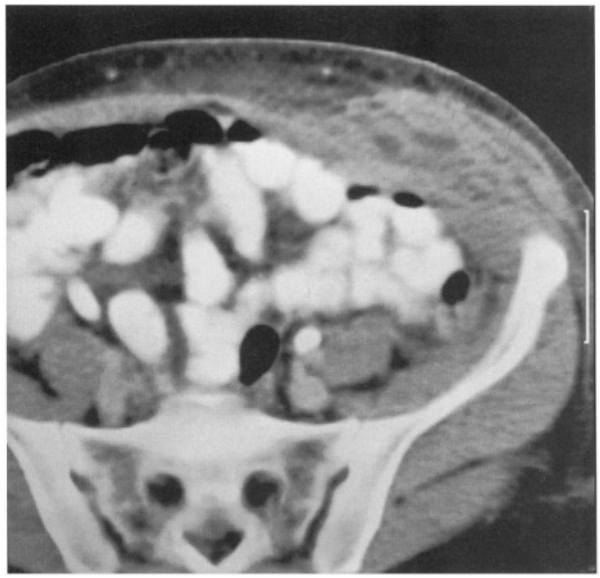


Fig. 4–194. Subcutaneous implant tumor from serous ovarian carcinoma following paracentesis.
Four months after paracentesis with an intraperitoneal catheter that was left *in situ* for 24 hours, CT shows a large solid inhomogeneous mass in the subcutaneous tissue in the paracentesis site. Part of its margins infiltrate fatty tissue. This was proved to be an infiltrative metastatic implant. (Reproduced from La Fianza, et al.[206])

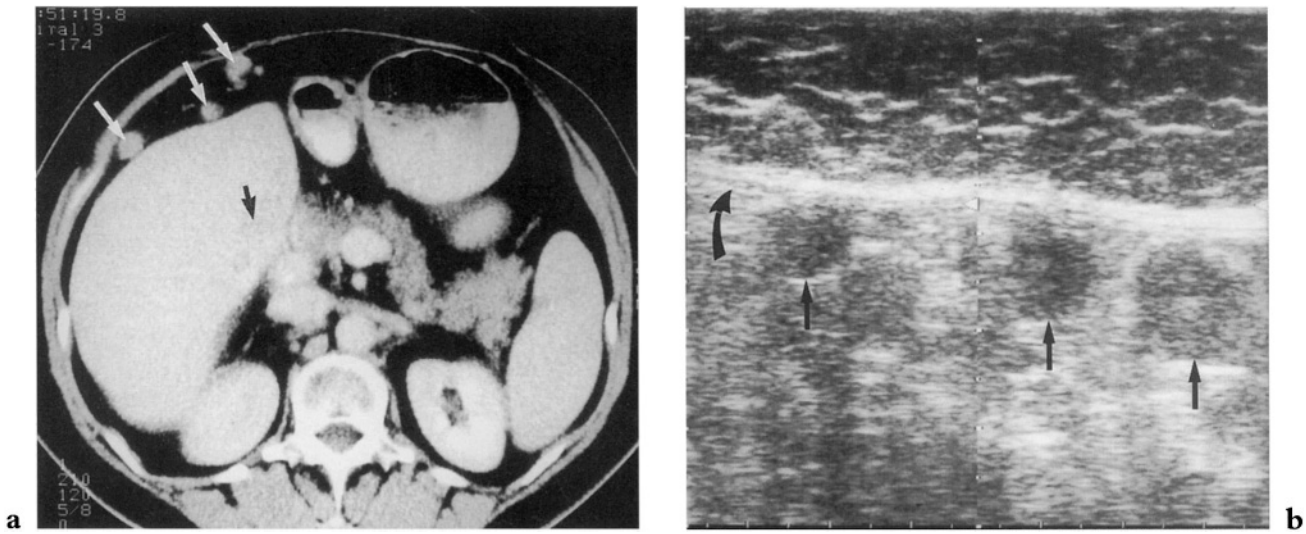


Fig. 4–195. Peritoneal seeding at site of needle track.
Eight months after percutaneous ethanol ablation therapy for hepatocellular carcinoma.
(a) CT shows small firm nodules at the sites of the punctures attached to the peritoneum *(white arrows).* Part of the primary tumor is indicated *(black arrow).*
(b) Ultrasound demonstrates the three small inhomogeneous nodules *(arrows)* attached to the peritoneum *(curved arrow).*
(Reproduced from Kurl et al.[207])

improvements. Seeded peritoneal metastases may be evident as discrete nodules[59,106,132,140] or as peritoneal thickening and enhancement.[138] Saline MR peritoneography, heavily T2-weighted images in conjunction with intraperitoneally instilled saline, may enhance the detection of small implants on peritoneal surfaces.[229] Radioimmunoscintigraphy[230] may be applied to the detection of peritoneal carcinomatosis.

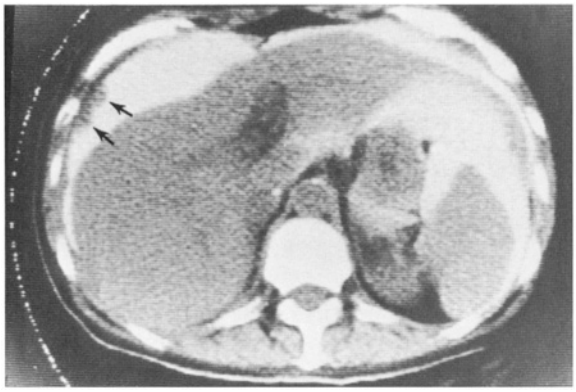


Fig. 4–196. Peritoneal seeded metastases.
CT after intraperitoneal infusion of contrast medium demonstrates filling defects in right upper quadrant *(arrows)* representing studding of peritoneal surface from metastases. (Reproduced from Dunnick et al.[218])

Embolic Metastases

Malignancies shed as many as 4 million cells per gram of tumor tissue into the bloodstream per day. Of these, greater than 90% are cleared rapidly from the circulation.[231,232] Despite this "metastatic inefficiency," the abdominal organs and bowel are a common site of hematogenous metastases from both intraabdominal and extraabdominal primary sites.[231,232]

The most common primary neoplasms that embolize to bowel include melanoma and tumors of the breast and lung. The presenting picture is usually one of incomplete obstruction or bleeding, often occurring several years after treatment of the original neoplasm. At times, the symptoms of the bowel metastases may be the first clinical manifestation of an occult primary malignancy.[7,8,233,234] Partial or complete obstruction is the result of the bulk of the metastatic mass, accompanied by either angulation of the bowel from a fibrotic response or intussusception. The appearance of a hematogenous metastasis to bowel depends on the characteristics of the lesions.[1] These include both the degree of vascularity relative to the rate of growth and the desmoplastic capabilities.

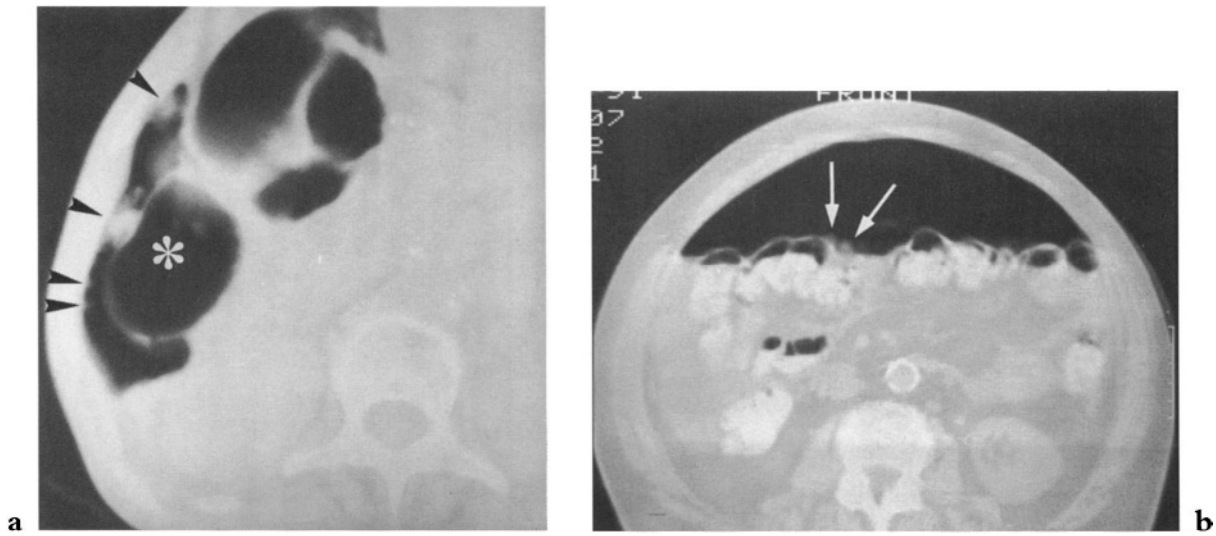


Fig. 4–197. Demonstration of small seeded deposits by CT after induced pneumoperitoneum, using a "pulmonary-type window."
(a) Pinpoint metastatic ovarian lesions *(arrowheads)* are detected. *Asterisk* = ascending colon.
(b) Two ovarian carcinomatous nodular lesions outside the bowel lumen *(arrows)* are shown. (Reproduced from Caseiro-Alves et al.[223])

Metastatic Melanoma

Metastatic melanoma is by far the most common of these tumors to be encountered clinically, and it may be taken as a particular prototype. The hematogenous deposition is usually in the submucosal layer where it may be seen early as small mural nodules, and growth typically results in polypoid masses with a bulky extension into the lumen.[7,8,235–237] There is no significant desmoplastic response. Central ulceration is especially common as the metastasis outgrows its blood supply. In smaller lesions, this may be identified as a "bull's eye" or "target" lesion (Figs. 4–198 and 4–199), in which, characteristically, the borders of the filling defect are well defined and the ulcer is quite large in proportion to the metastatic mass (Fig. 4–200). Linear fissures over the surface of the mass, radiating distinctly to the central collection, produce a "spokewheel" pattern[1,235] (Fig. 4–201). In the larger lesions, necrosis may be reflected as a large excavating lesion (Fig. 4–202) yielding an appearance of aneurysmal dilatation[235–240] (Figs. 4–203 through 4–207). Intussusception may be associated with the larger polypoid masses[235] (Figs. 4–205 and 4–206).

Dissemination may be single (Fig. 4–208) but is more often multiple. Although metastatic melanomas may involve any portion of the alimentary tract, they tend to be more numerous and more frequent in the small bowel. In an autopsy series of 1,000 cases, secondary small bowel involvement was found in 58%.[241] When multiple, they may be either widespread (Fig. 4–209) or confined to a segment of intestine (Figs. 4–198 and 4–210). This reflects their mode and periodicity of vascular distribution.[1] Diffuse metastases are infrequently of different sizes (Fig. 4–209), indicating periodic embolic showers. At times, the secondary deposits are present within the field of a specific arterial distribution when, typically, the nodules are of approximately the same size

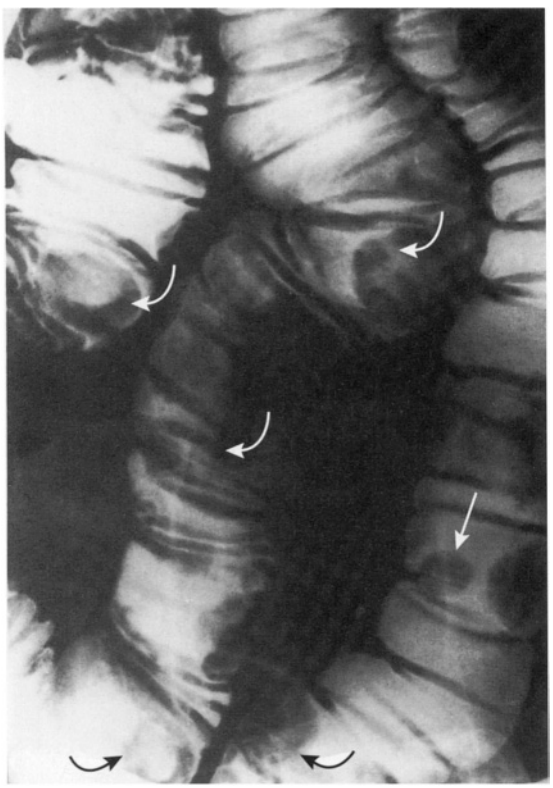


Fig. 4–198. Metastatic melanoma to small bowel.
Multiple submucosal nodular masses, some with prominent central ulceration (*arrows*), are present throughout a length of small intestine. These are described as *bull's-eye* or *target lesions.*
(Reproduced from Herlinger and Maglinte.[237])

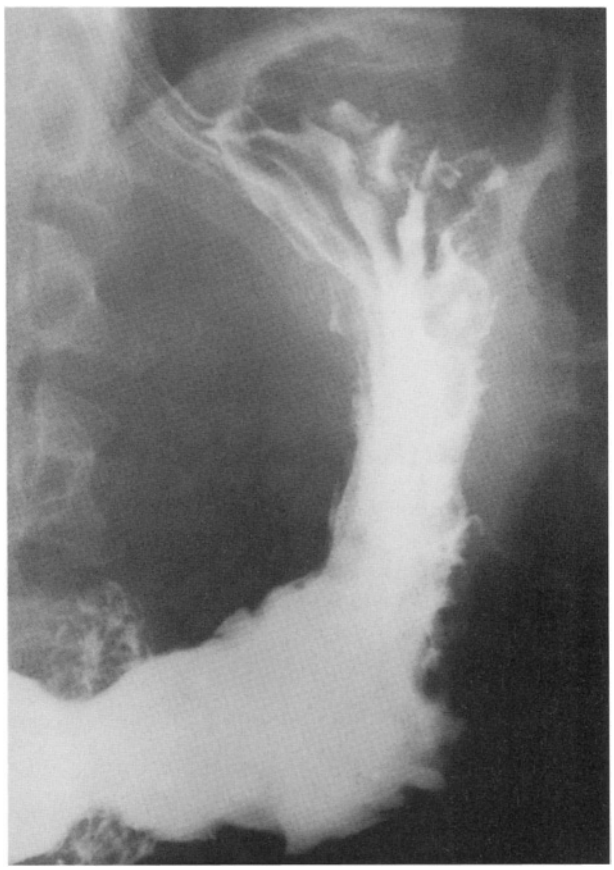


Fig. 4–199. Metastatic melanoma to stomach.
The multiple, centrally ulcerated submucosal lesions are seen *en face* and tangentially along the curvatures as *bull's-eye* lesions.
(Reproduced from Meyers and McSweeney.[1])

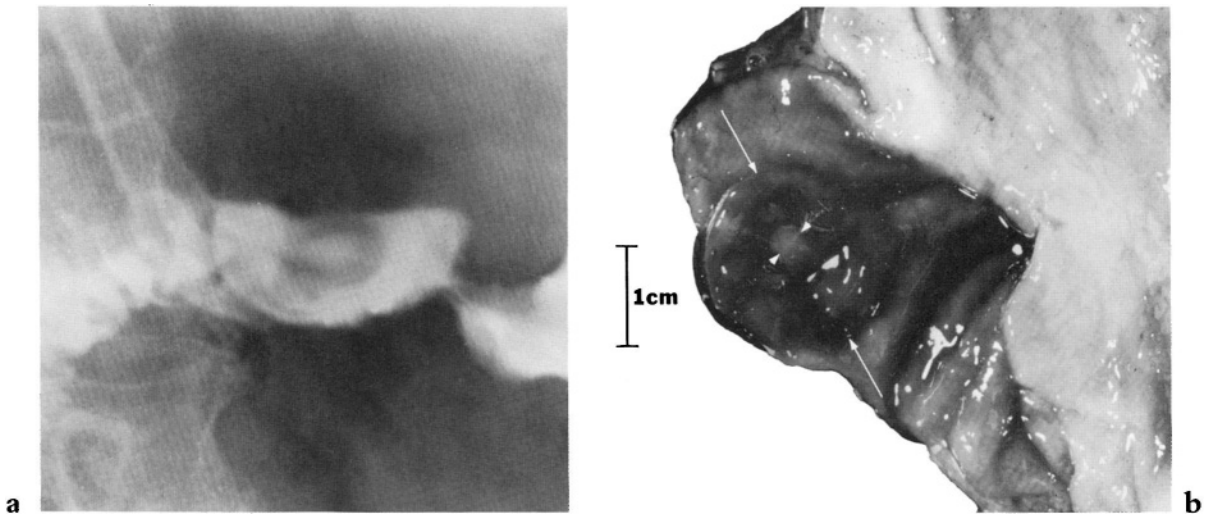


Fig. 4–200. Metastatic melanoma to duodenal bulb.
(a) A filling defect with sharply demarcated borders contains a proportionately large ulcer crater. These features are helpful in identifying this lesion as a submucosal nodule with secondary central ulceration, in contrast to a benign peptic ulcer with surrounding edema, the borders of which usually fade away gradually.
(b) Gross specimen demonstrates prominent submucosal mass *(arrows)* with central ulceration *(arrowheads).* Pathologically, this type of hematogenous metastasis is described as a "buttercup" lesion.
(Reproduced from Meyers and McSweeney.[1])

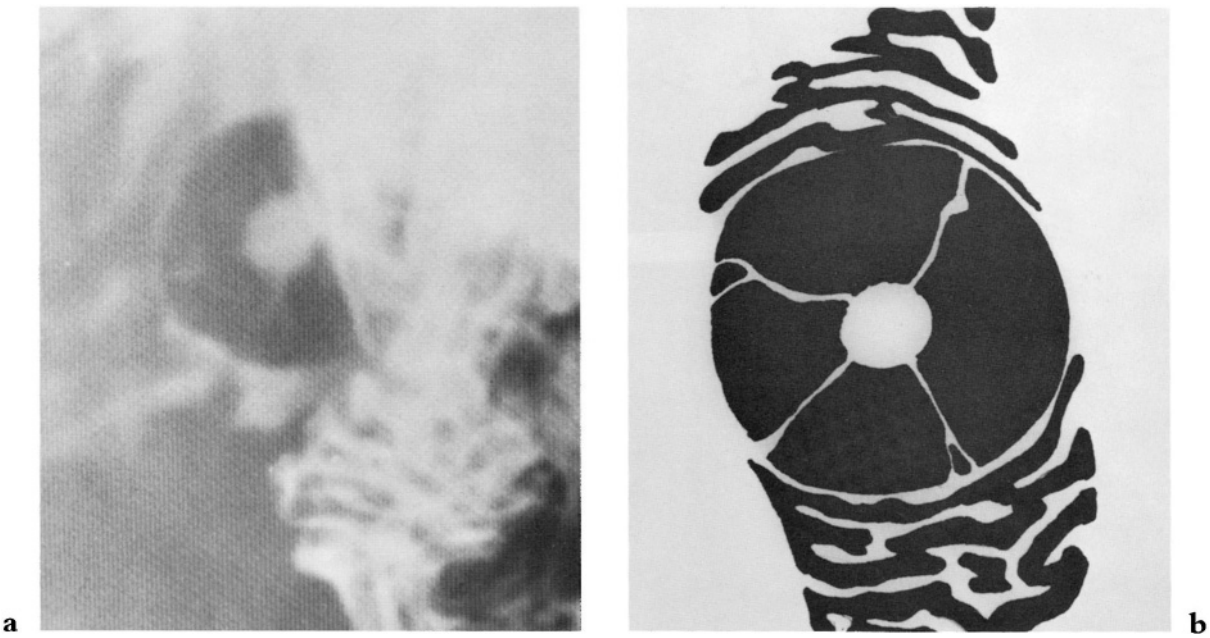


Fig. 4–201. Metastatic melanoma to stomach.
(a) On the greater curvature, there is a centrally ulcerated submucosal mass. Radiating linear fissure ulcerations result in a distinctive "spokewheel" configuration.
(b) Diagrammatic representation of **(a).**
(Reproduced from Meyers and McSweeney.[1])

Fig. 4–202. Metastatic melanoma to small bowel.
A moderate-sized irregular cavity with multiple nodules replaces the lumen of a short segment of ileum. Reflecting its submucosal location, it is non-obstructive in nature.
(Reproduced from Gourtsoyiannis and Nolan.[80])

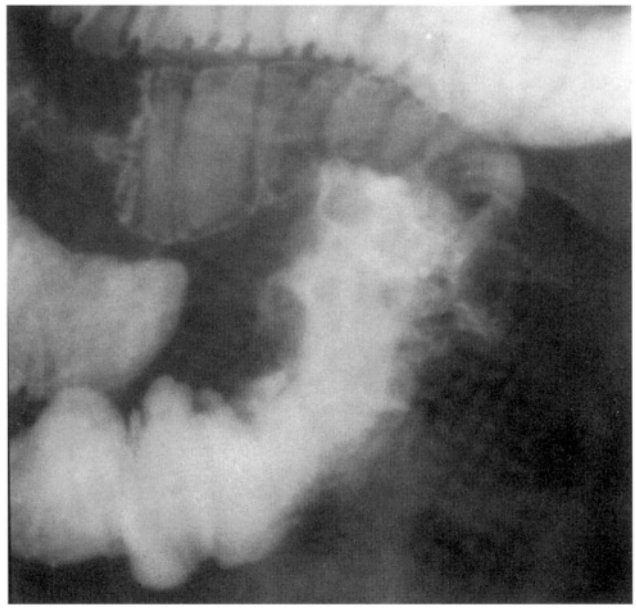




Fig. 4–203. Metastatic melanoma to small bowel.
Several bulky polypoid masses involve the mid-small bowel *(black arrows).* Some have undergone large ulcerations (*curved arrows*).
(Reproduced from Oddson et al.[235])

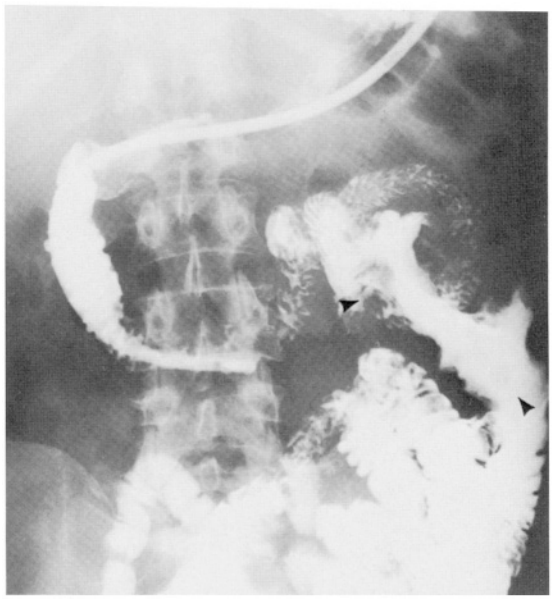


Fig. 4–204. Metastatic melanoma to small bowel.
A large cavitating mass is present in the proximal jejunum (*arrowheads*).
(Reproduced from Oddson et al.[235])



Fig. 4–205. Metastatic melanoma to small bowel.
A huge cavitating mass with intussusception is present in the ileum.
(Reproduced from Oddson et al.[235])



Fig. 4–206. Metastatic melanoma to small bowel.
CT shows a submucosal metastasis (*M*) is the lead point of an ileal–ileal intussusception in the right lower quadrant.

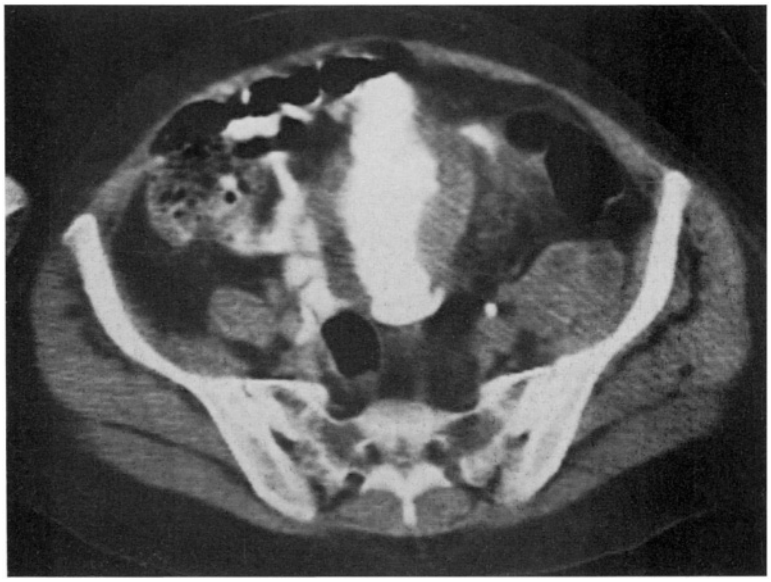


Fig. 4–207. Metastatic melanoma to small bowel.
CT demonstrates aneurysmal dilatation with submucosal masses, a widened lumen, and grossly ulcerated mucosa. Enlarged iliac nodes are also present.

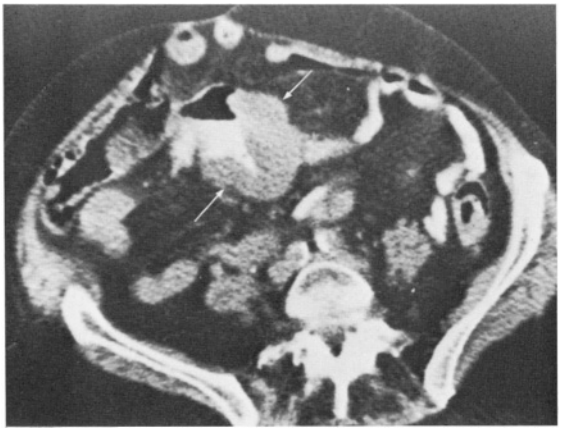


Fig. 4–208. Metastatic melanoma to small bowel.
CT demonstrates an ulcerated submucosal mass involving an opacified mid-small bowel loop *(arrows).*



Fig. 4–209. Metastatic melanoma to small bowel.
Numerous submucosal masses are scattered throughout the small intestine. Their varying sizes indicate probable embolic metastatic showers at different times. (Reproduced from Meyers and McSweeney.[1])

(Figs. 4–210 and 4–211). A further observation that is useful in identifying such submucosal masses at embolic metastases relates to their specific sites on the bowel wall.[1,72,73] When the lesion is localized to one wall of the bowel, a distinct predilection is shown for the antimesenteric border. In the small intestine, this is readily identified as the convex margin of the loop (Figs. 4–212 through 4–214), since the mesentery supports the concave surface. In the ascending and descending colon, the lateral borders constitute the antimesenteric margins (Fig. 4–211). These findings are apparently related to the entrance of the intestinal vessels on the mesenteric border and their intramural ramifications toward the antimesenteric side. They are in agreement with Coman's experimental work, which revealed that strictly mechanical and circulatory factors can account for the distribution of some secondary tumors.[242]

A patient with melanoma with small bowel involvement, a stage III designation, now has available surgical treatment complemented by adjuvant therapy and immunotherapy, with an improved survival rate.[243–245]

Breast Metastases

Breast metastases to the gastrointestinal tract result in a different pattern. Autopsy series record an incidence of breast metastases to the gastrointestinal tract as high as 8.2%[246] to 16.4%.[233] The need for surgical intervention for an abdominal complication of the metastasis is not uncommon.[234] Asch and associates[233] collected a group of 18 cases of metastatic breast lesions requiring surgery, often many years after a mastectomy.



Fig. 4–210. Metastatic melanoma to small bowel.
Multiple submucosal masses of approximately equal size confined to one segment of small bowel indicate embolic metastases within a discrete arterial distribution.

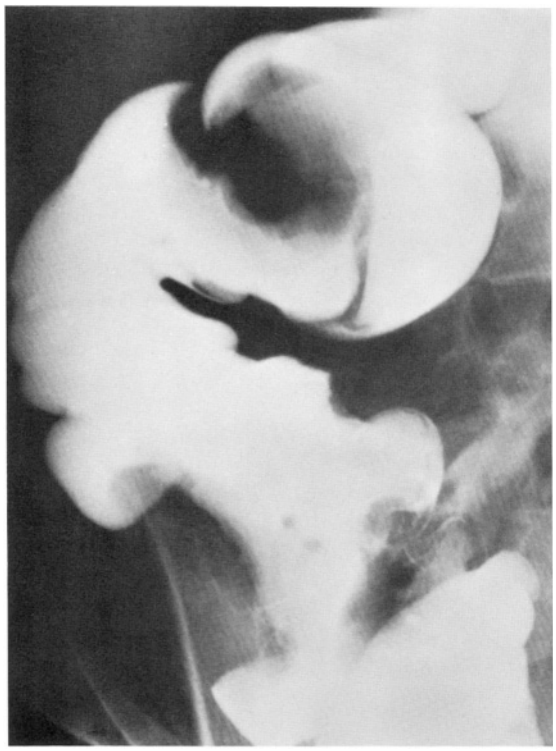


Fig. 4–211. Metastatic melanoma to the ascending colon.
Its embolic nature is revealed by the two large submucosal masses of approximately equal size on the antimesenteric border in the field of distribution of the right colic artery. (Reproduced from Meyers and McSweeney.[1])

The type that gives rise to gastrointestinal metastases and symptoms most often is the poorly differentiated breast cancer that grows in rows of small anaplastic cells.[246] No significant desmoplastic response accompanies the highly cellular secondary deposits. Infiltrating lobular carcinoma, while considerably less common than infiltrating ductal carcinoma, metastasizes significantly more often to the gastrointestinal tract.[247–249] Although all layers of the bowel wall may be diffusely infiltrated, most of the embolic deposits reside in the submucosa,[234] where they are more readily subject to radiologic identification.

While widespread peritoneal metastases may be present, a linitis plastica appearance often dominates the radiologic findings, commonly in the stomach [1,250–254] (Figs. 4–215 and 4–216). Although no desmoplastic response is elicted by breast metastases, the highly cellular submucosal deposits may narrow and deform the lumen, presenting a scirrhous appearance. Rigidity and thickening with markedly diminished or absent peristalsis are associated with spiculation and angulation of the folds. Pseudoulcerations are produced by buckling or redundancy of the mucosa. The changes may be diffuse or localized but are more common and prominent in the distal two-thirds of the stomach. Despite the occasional severe circumferential narrowing of the antrum, some degree of luminal patency is maintained so that gastric outlet obstruction is not a characteristic feature. The linitis plastica appearance produced is indistinguishable from that of a primary scirrhous carcinoma or lymphoma. Osteoblastic metastases, however, are frequently

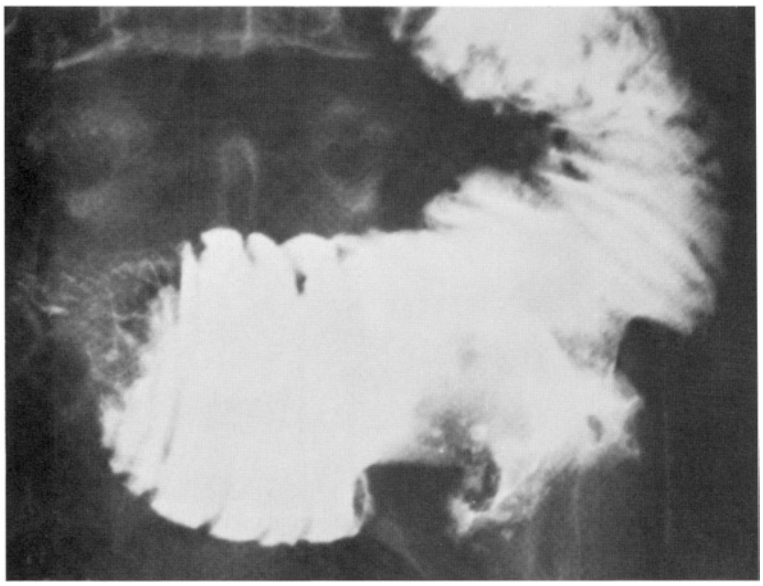


Fig. 4–212. Metastatic melanoma to small bowel.
There is a nonobstructing submucosal mass with a large ulcerated excavation in a distal jejunal loop. The hematogenous metastasis is distinctly localized to the antimesenteric border of the loop.
(Reproduced from Meyers and McSweeney.[1])

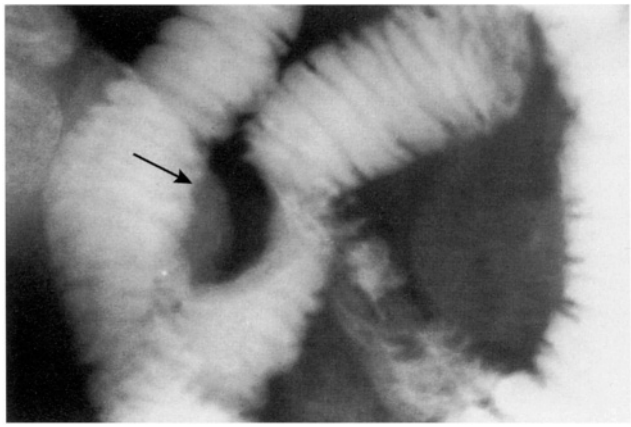


Fig. 4–213. Metastatic melanoma to small bowel.
A prominent submucosal metastasis is present on the antimesenteric border of the ileum (*arrow*).
(Reproduced from Gourtsoyiannis and Nolan.[80])

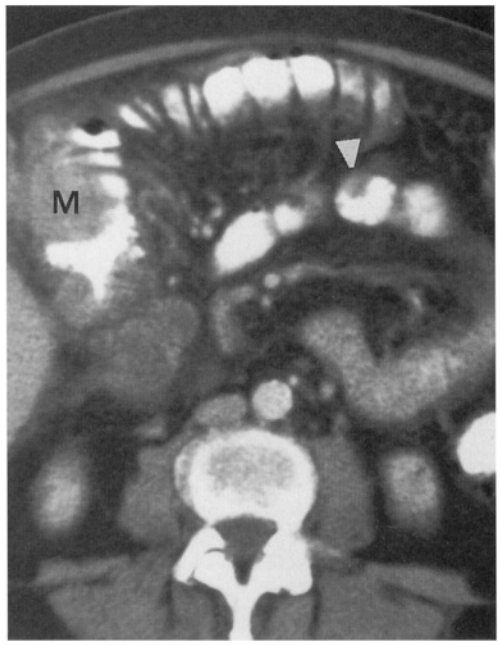


Fig. 4–214. Metastatic melanoma to small bowel.
CT demonstrates a large submucosal mass (*M*) in the antimesenteric wall of a jejunal loop. Another loop shows a smaller metastasis (*arrowhead*).
(Courtesy of Michiel Feldberg, M.D., Ph.D., University of Utrecht, The Netherlands.)

present[1,255] (Fig. 4–215a). Secondary ulceration may be encountered as a prominent feature[236,253] (Fig. 4–217).

Breast metastases to the small bowel may result in a focal stricture (Fig. 4–218) alternating areas of narrowing with interval dilatations (Fig. 4–219), or, rarely, a localized submucosal mass (Fig. 4–220).

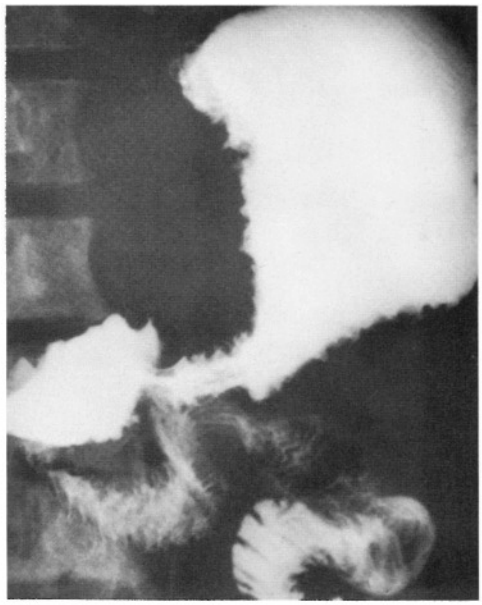
Carcinoma of the breast is the most common source of hematogenous spread to the colon. In a series of 337 autopsies in patients with breast carcinoma, Asch and associates[233] observed metastases to the colon in 4.5%. Of a group of 75 patients with advanced breast carcinoma who had laparotomy or autopsy, Graham[234] noted that 16% demonstrated colonic metastases. These may present clinically many years after a radical mastectomy.[44] The spread to the large intestine may be easily mistaken for primary inflammatory processes, such as granulomatous or ulcerative colitis, both clinically and radiologically.[44] Diarrhea may be a conspicuous clinical presentation, occasionally of several years' duration, and perhaps associated with some blood and mucus. Characteristic radiologic findings (Figs. 4–221 through 4–227), include mucosal thickening, nodular masses, multiple and eccentric strictures, asymmetric involvement, pseudosacculations, spiculations of contour, and frequent associated terminal ileal involvement.[44] The findings may be limited to the right colon (Figs. 4–221 and 4–222), diffuse (Figs. 4–223 through 4–226), or rarely confined to the rectum[256,257] (Fig. 4–227). It is apparent that these changes share many common features with inflammatory colitis, particularly Crohn's disease. Deep biopsy and cytologic analysis of any ascitic fluid may be confirmatory.

Bronchogenic Carcinoma

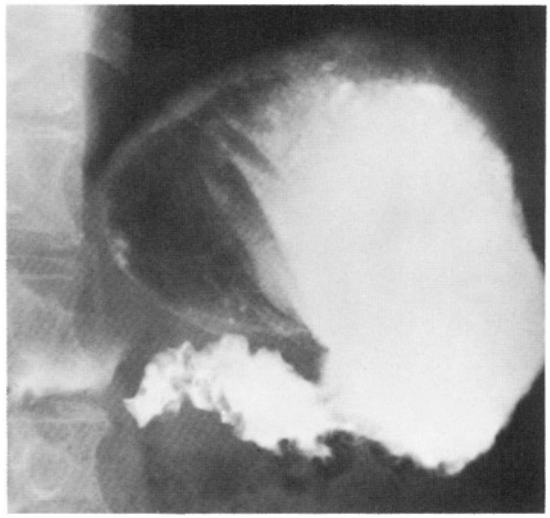
Metastatic involvement of the large intestine by bronchogenic carcinoma is rare.[258] Luomanen and Watson[259] report that of 676 patients who died of lung cancer, only 2.2% revealed metastases to the colon at autopsy. These were often small, serosal deposits. Metastases may infrequently be seen as focal stenosis, mural rigidity, or annular narrowing[260] (Figs. 4–228 through 4–230). Occasionally, they result in large mesenteric masses with infiltration of the bowel wall and fixation and angulation of the bowel and its mucosal folds (Fig. 4–231). In such cases, the findings are indistinguishable from those in widespread intraabdominal metastases from other sources. Rarely, central ulceration may be seen in the submucosal deposits (Fig. 4–232), which may lead to perforation.[236,258]

Renal Carcinoma

Hematogenous metastasis to bowel from a renal carcinoma is rare. In some cases, Batson's vertebral venous plexus is a possible route.[261] It typically presents as a solitary bulky intramural lesion[92] (Fig. 4–233).



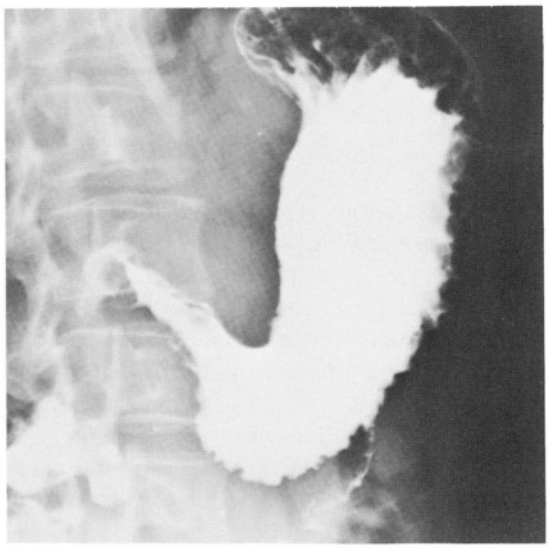
a



b



c



d



e

Fig. 4–215. Different cases of breast metastases to stomach. (Opposite page)
These are characterized by rigidity and narrowing with markedly decreased peristalsis and fixation, spiculation, and angulation of folds. Although any portion of the stomach may be involved, the changes are more common and prominent in the distal two-thirds. The findings are indistinguishable from those of a primary linitis plastica. Note, however, the osteoblastic metastases in **(a).**
(a and **b** reproduced from Meyers and McSweeney.[1])

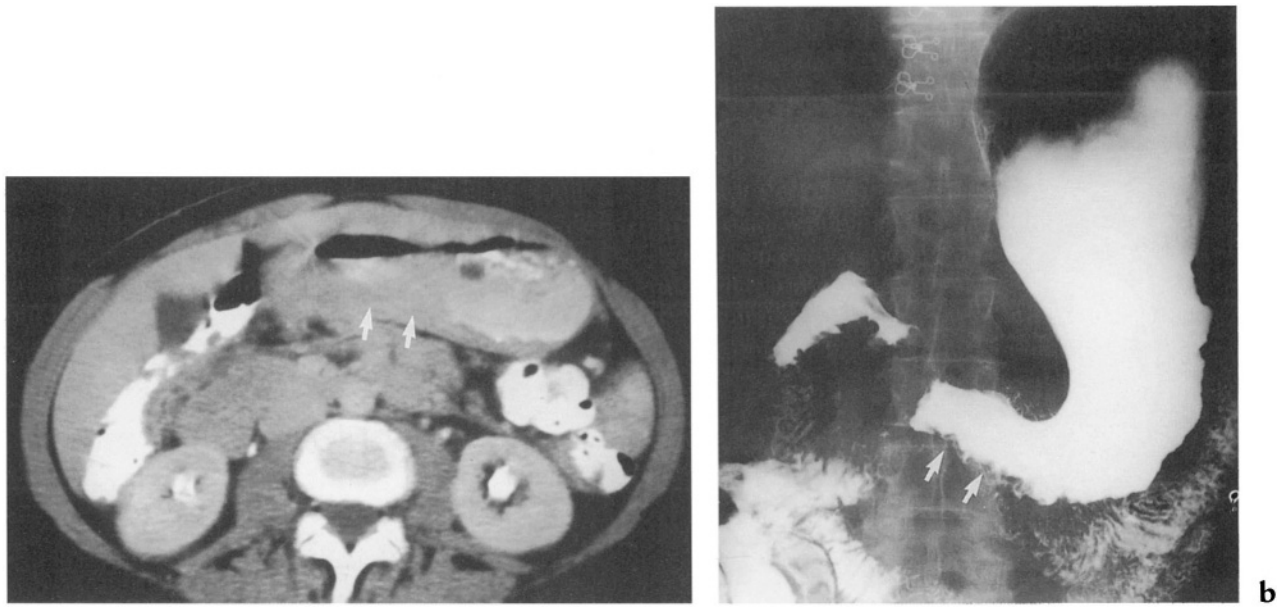


Fig. 4–216. Metastatic breast carcinoma to stomach.
(a) CT shows marked gastric antral wall thickening *(arrows).*
(b) Upper GI series demonstrates an irregular linitis plastica appearance involving the distal two-thirds of the stomach (*arrows*).
(Reproduced from Kidney, et al.[249])



Fig. 4–217. Breast metastasis to stomach.
A large submucosal mass in the distal stomach and antrum has undergone prominent ulceration.

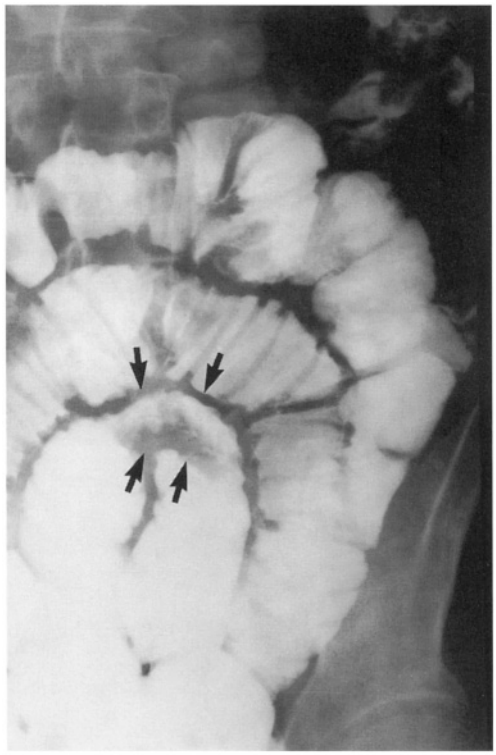


Fig. 4–218. Metastatic breast carcinoma to small bowel.
Small bowel series shows a short, fixed nonobstructing stenotic lesion in the ileum (*arrows*).
(Reproduced from Kidney, et al.[249])



Fig. 4–219. Metastatic breast carcinoma to small bowel.
There are multiple skip areas of strictures with intervening dilatation. Diffuse submucosal metastases are also present within the stomach.
(Reproduced from Meyers et al.[44])

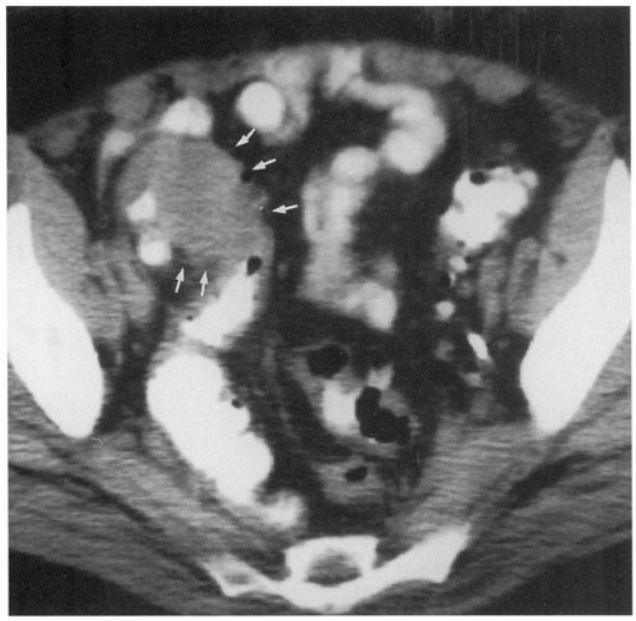


Fig. 4–220. Metastatic breast carcinoma to ileocecal junction.
CT demonstrates a prominent soft tissue mass at the ileocecal junction *(arrows),* presumably representing embolic metastasis via the ileocolic artery.
(Reproduced from Kidney, et al.[249])

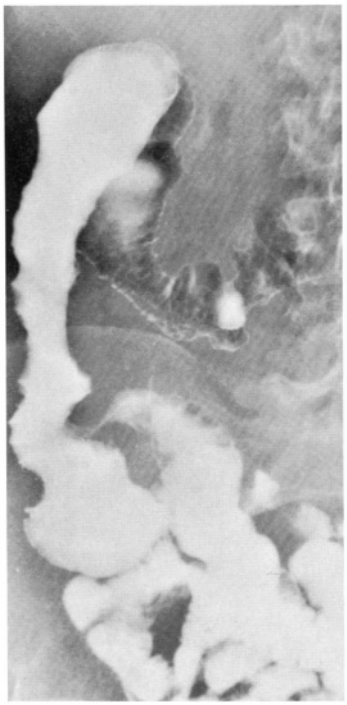


Fig. 4–221. Metastatic breast carcinoma to right colon.
The entire ascending colon is encased by densely cellular submucosal secondary deposits. It is diffusely and irregularly narrowed, the mucosal and haustral patterns are effaced, and occasional nodular filling defects and serrations resembling minute ulcers are present. The ileocecal valve is widely patulous. The lesion strikingly resembles granulomatous colitis.
(Reproduced from Meyers al.[44])

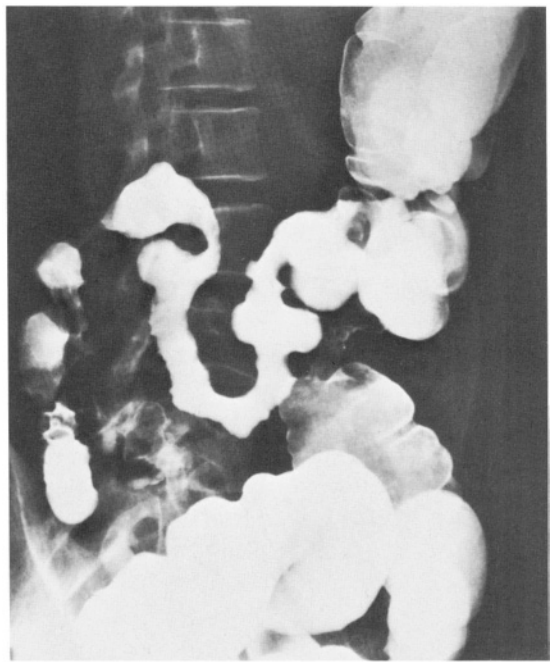


Fig. 4–222. Metastatic breast carcinoma to right colon.
The ascending and proximal transverse colon show asymmetric narrowing, scattered pseudosaccular formation, loss of the normal haustral and mucosal pattern, and the appearance of marginal ulcerations. The terminal ileum is also involved.
(Reproduced from Meyers et al.[44])



Fig. 4–223. Metastatic breast carcinoma to colon. Skip areas of narrowing with localized loss of haustral and mucosal pattern involving the ascending, transverse, sigmoid, and rectosigmoid colon. Pseudosacculations reflect the asymmetric nature of the process. Deep transverse ulcers appear to project from the narrowed segment in the transverse colon.
(Reproduced from Meyers et al.[44])

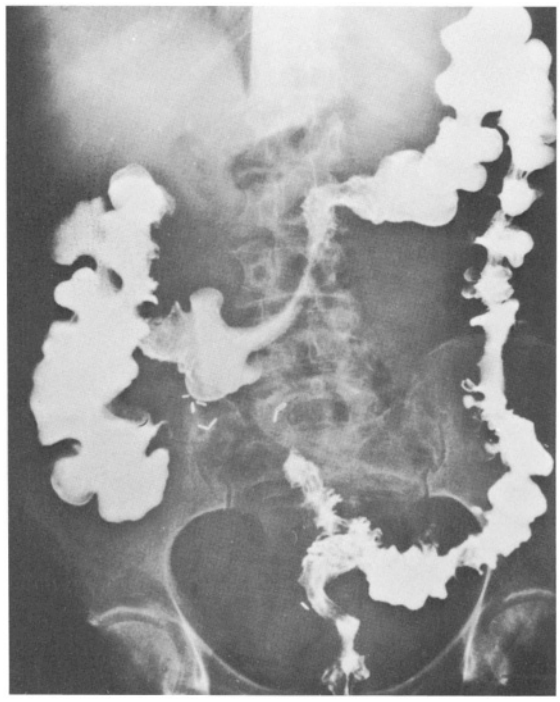
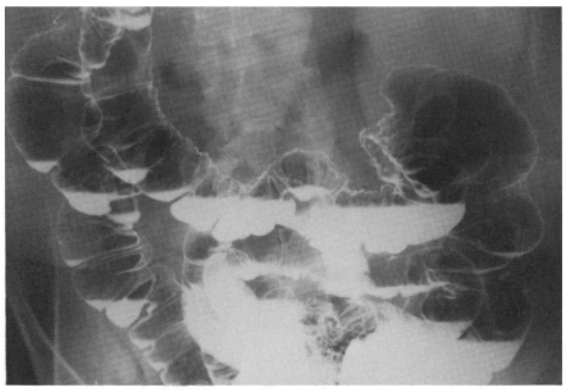
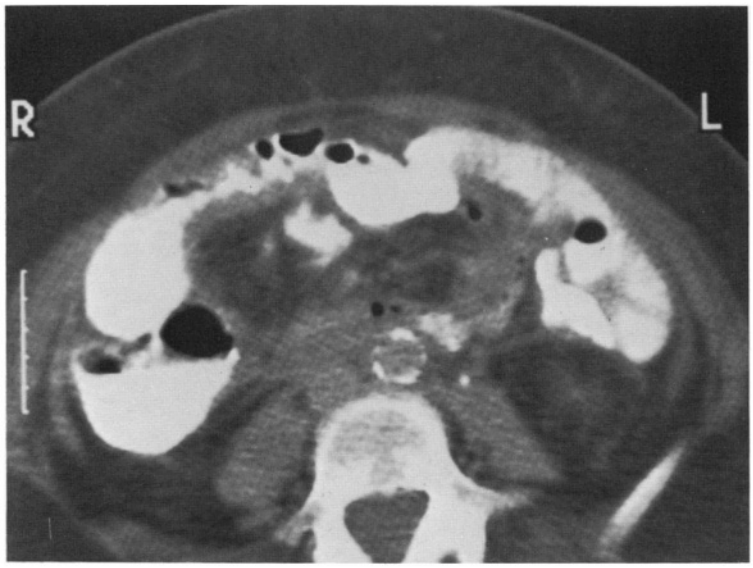


Fig. 4–224. Metastatic breast carcinoma to colon. The entire large intestine is involved by multiple sites of narrowing and rigidity, with pseudosacculations.



a



b

Fig. 4–225. Metastatic breast carcinoma to colon.
(a) Barium enema shows narrowing, angulation, fixation, and buckling of the mucosa in the transverse colon.
(b) CT documents mural thickening with luminal narrowing and mucosal speculations. (Courtesy of Michiel Feldberg, M.D., Ph.D., University of Utrecht, The Netherlands.)

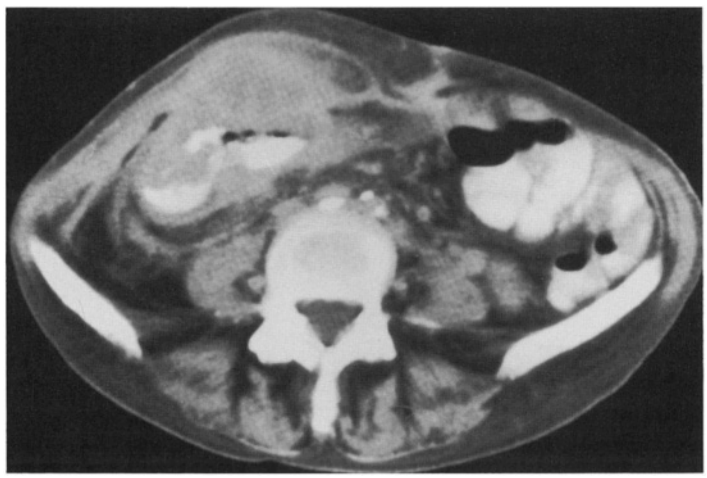


Fig. 4–226. Extramural extension of colonic breast metastasis.
The proximal transverse colon is markedly thickened and its lumen is narrowed and distorted by hematogenous metastases from breast carcinoma. Direct invasion of the anterior abdominal wall has occurred.



Fig. 4–227. Metastatic breast carcinoma to rectum. There is narrowing of the rectum with nodularity and distortion of the mucosal folds and the appearance of multiple cobblestone ulcerations. There is a gradual transition to normal, distended sigmoid segment. (Reproduced from Meyers et al.[44])

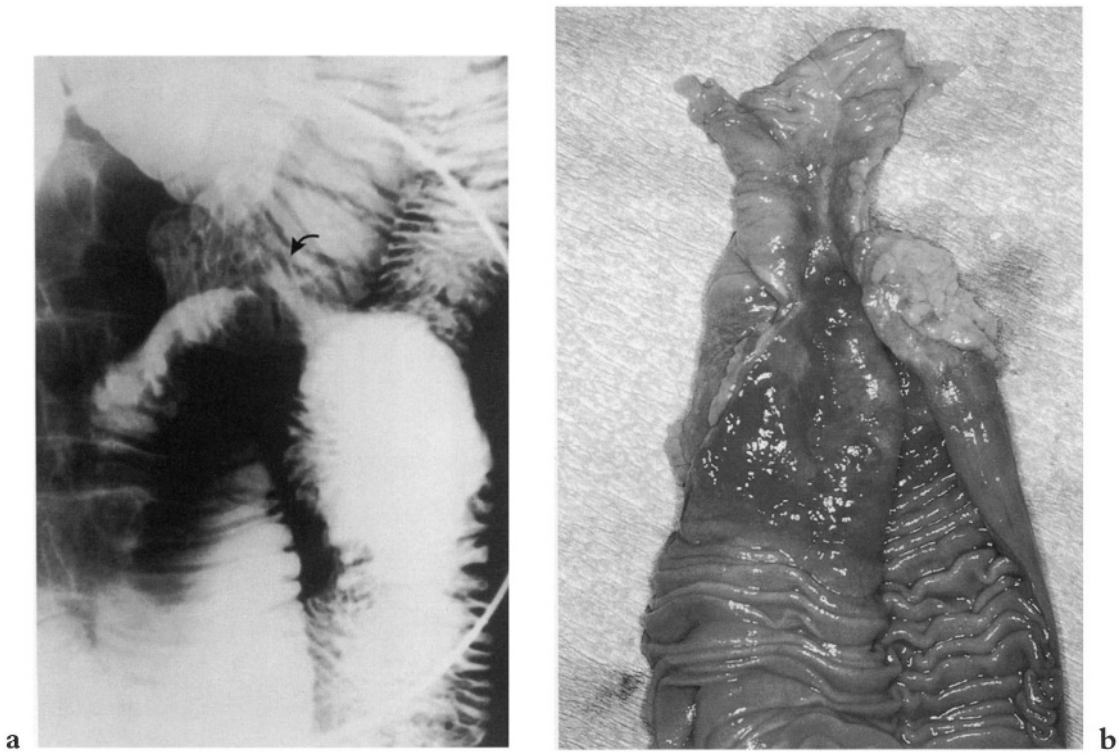


Fig. 4–228. Metastatic bronchogenic carcinoma to small bowel.
(a) A focally stenotic lesion with fixation and angulation of a jejunal loop *(arrow)* causes proximal dilatation.
(b) The operative specimen confirms the submucosal nature of the metastasis.
(Reproduced from Gourtsoyiannis and Nolan.[80])

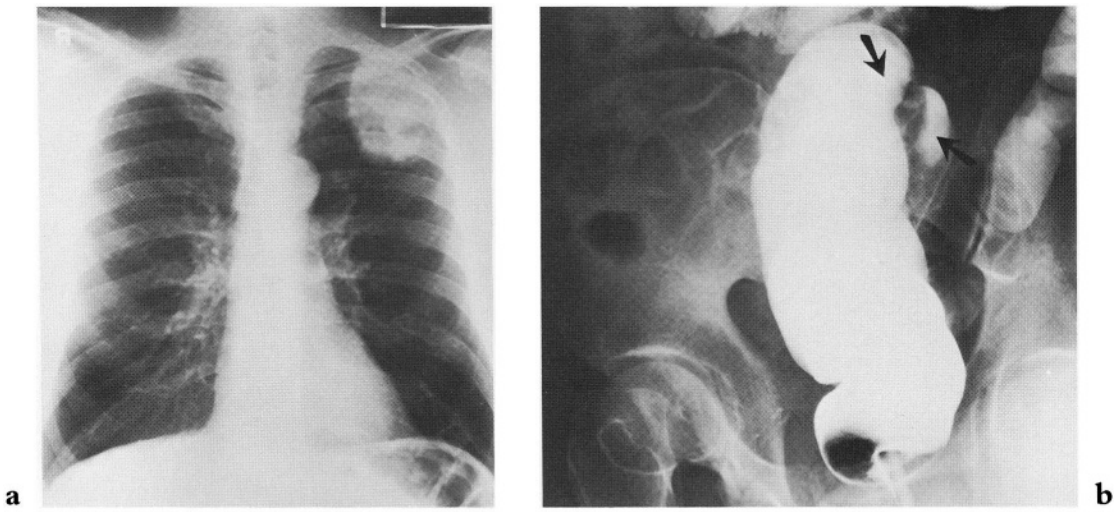


Fig. 4–229. Metastatic bronchogenic carcinoma to colon.
(a) Chest film shows peripheral left upper lobe squamous cell carcinoma with pleural extension and partial excavation.
(b) Barium enema study shows metastatic annular narrowing in the sigmoid colon *(arrows).*
(Reproduced from Smith and Vlasak.[260])

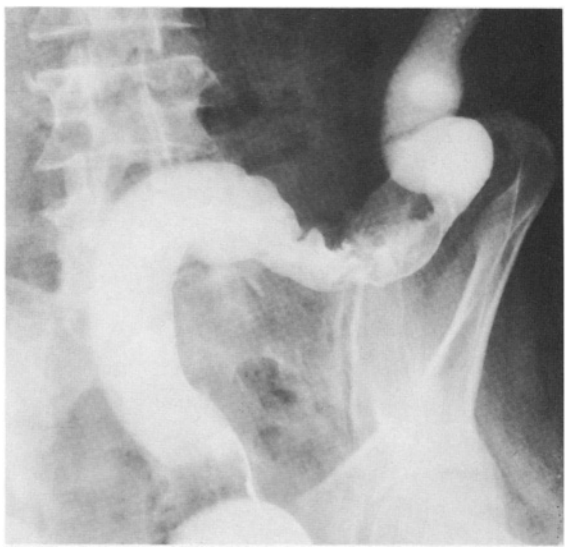


Fig. 4–230. Metastatic bronchogenic carcinoma to colon.
Submucosal deposition results in an eccentrically narrowed segment of the sigmoid colon.
(Reproduced from Smith and Vlasak.[260])

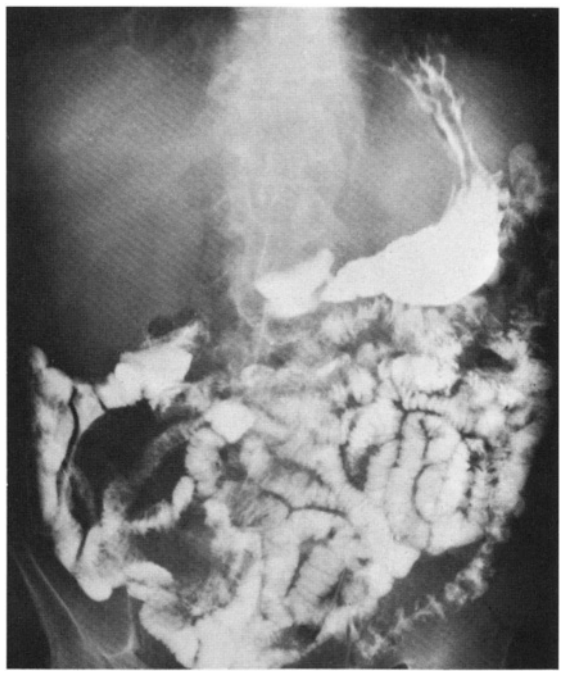


Fig. 4–231. Metastatic lung carcinoma.
Large mesenteric and serosal mass displaces distal small bowel and right colon.

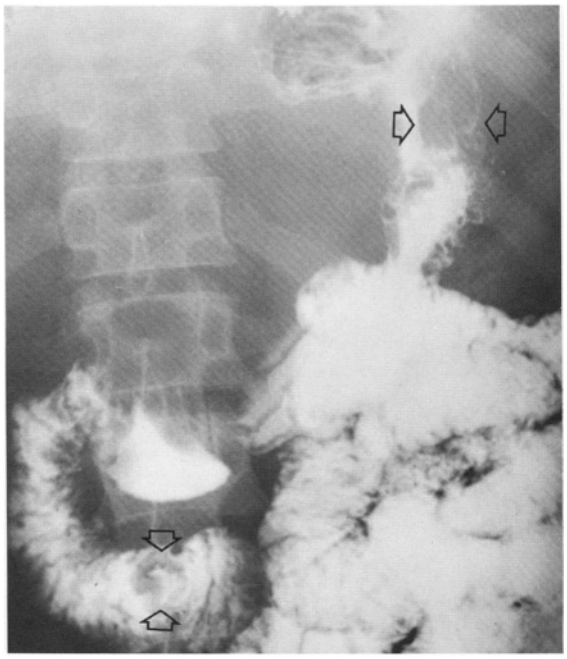


Fig. 4–232. Hematogenous metastases of carcinoma of lung to stomach and third portion of the duodenum (*arrows*).
The duodenal metastasis shows irregular central ulceration. (Reproduced from Meyers and McSweeney.[1])

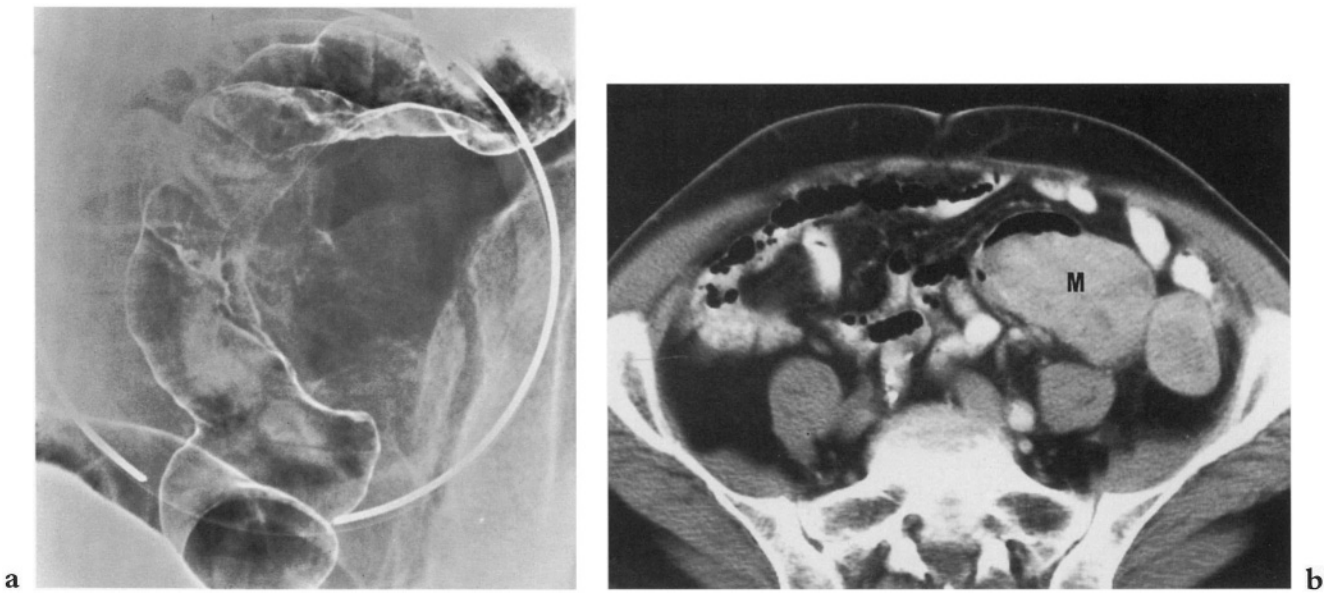


Fig. 4–233. Metastatic renal cell carcinoma to sigmoid colon.
Two and one-half years after nephrectomy for renal cell carcinoma, barium enema study **(a)** shows a large transmural tumor of the sigmoid colon with both extrinsic and intraluminal components. CT **(b)** confirms a large secondary mass (*M*) with displacement and compression upon the colon.

References

1. Meyers MA, McSweeney J: Secondary neoplasms of the bowel. Radiology 1972; 105:1–11.
2. Willis RA: The Spread of Tumours in the Human Body, 2nd ed. Butterworth, London, 1952.
3. Meyers MA: Distribution of intra-abdominal malignant seeding: Dependency on dynamics of flow of ascitic fluid. AJR 1973; 119:198–206.
4. Meyers MA: Metastatic seeding along small bowel mesentery: Roentgen features. AJR 1975; 123: 67–73.
5. Meyers MA: Intraperitoneal spread of malignancies and its effect on the bowel. Second Annual Leeds Lecture. Clin Radiol 1981; 32:129–146.
6. Meyers MA, Whalen JP: Roentgen significance of the duodenocolic relationships: An anatomic approach. AJR 1973; 117:263–274.
7. De Castro CA, Dockerty MB, Mayo CW: Metastatic tumors of the small intestines. Int Abstr Surg 1957; 105:159–165.
8. Farmer RG, Hawk WA: Metastatic tumors of the small bowel. Gastroenterology 1964; 47:496–504.
9. Meyers MA, Oliphant M, Berne AS, et al: The peritoneal ligaments and mesenteries: Pathways of intra-abdominal spread of disease. Annual oration. Radiology 1987; 163:593–604.
10. Auh YH, Lim JH, Jeong YK, et al: Anatomy of the peritoneal cavity and reflections. *In* Abdominal and Gastrointestinal Imaging Multimedia Virtual Textbook. Edited by NC Gourtsoyiannis, R. Yamada, Y Itai, MA Meyers, D Nolan, P Ros, G Stevenson (*http://medic-online.net/abdo/*).
11. Oliphant M, Berne A, Meyers MA: Subperitoneal spread of intraabdominal disease. *In* Computed Tomography of the Gastrointestinal Tract Including the Peritoneal Cavity and Mesentery. Edited by MA Meyers. Springer-Verlag, New York, 1986, pp 95–137.
12. Oliphant M, Berne AS: Computed tomography of the subperitoneal space: Demonstration of direct spread of intraabdominal disease. J Comput Assist Tomogr 1982; 6(6):1127–1137.
13. Glisson F: Anatomia Hepatitis, 2nd ed. London, Hagae, 1654.
14. Balfe DM, Mauro MA, Koehler RE, et al: Gastrohepatic ligament: Normal and pathologic CT anatomy. Radiology 1984, 150:485–490.
15. Weinstein JB, Heiken JP, Lee JKT, et al: High resolution CT of the porta hepatis and hepatoduodenal ligament. Radiographics 1986; 6(1):55–73.
16. Rothlin M, Largiadèr F: The anatomy of the hepatobiliary ligament in laparoscopic sonography. Surg Endosc 1994; 8:173–180.
17. van Delden OM, deWit LT, Bemelman WA, et al: Laparoscopic ultrasonography for abdominal tumor staging: Technical aspects and imaging findings. Abdom Imaging 1997; 22:125–131.
18. Michels NA: Blood Supply and Anatomy of the Upper Abdominal Organs with a Descriptive Atlas. Lippincott, Philadelphia, 1995.
19. Kuhns LR, Borlaza G: Normal roentgen variant: Aberrant right hepatic artery on computed tomography. Radiology 1980; 135:392.
20. Ito K, Choji T, Fujita T, et al: Imaging of the portacaval space. AJR 1993; 161:329–334.
21. Auh YH, Ha HK: Foramen of Winslow adenopathy. Abdom Imaging 1996; 21:278–281.
22. Auh YH, Rosen A, Rubenstein WA, et al: CT of the papillary process of the caudate lobe of the liver. AJR 1984; 142:535–538.
23. Donoso L, Martinez-Noguera A, Zidan A, et al: Papillary process of the caudate lobe of the liver: Sonographic appearance. Radiology 1989; 173: 631–633.
24. Gore RM, Meyers MA: Pathways of abdominal and pelvic disease spread (Chapter 131). *In* Textbook of Gastrointestinal Radiology. Edited by RM Gore, MS Levine, I Laufer. WB Saunders, Philadelphia, 1993.
25. Dehn CB, Reznek RH, Nockler B, et al: The preoperative assessment of advanced gastric cancer by computed tomography. Br J Surg 1984; 71:413–417.
26. Arenas A, Sanchez LV, Albillos JM, et al: Direct dissemination of pathologic abdominal processes through perihepatic ligaments: Identification with CT. RadioGraphics 1994; 14:515–527.
27. Oi H, Matsushita M, Murakami T, et al: Dynamic MR imaging for extraserosal invasion of advanced gastric cancer. Abdom Imaging 1997; 22:35–40.
28. Wechsler RJ, Miller CL, Kurtz AB, et al: Anterior protrusion of retroperitoneal processes: A mimic of lesser sac or gastrohepatic masses. Clin Imaging 1990, 14:146–151.
29. Engels JT, Balfe DM, Lee JKT: Biliary carcinoma: CT evaluation of extrahepatic spread. Radiology 1989; 172:35–40.
30. Baker ME, Silverman PM, Halvorsen RA, et al: Computed tomography of masses in periportal/ hepatoduodenal ligament. J Comput Assist Tomogr 1987; 11:258–263.
31. Zeman RK, Schiebler M, Clark LR, et al: The clinical and imaging spectrum of pancreaticoduodenal lymph node enlargement. AJR 1985; 144:1223–1227.
32. Zirinsky K, Auh YH, Rubenstein WA, et al: The

portacaval space: CT with MR correlation. Radiology 1985; 156:453–460.
33. Gore RM, Vogelzang RL, Nemcek AA: Lymphadenopathy in chronic active hepatitis: CT observations, AJR 1988; 151:75–78.
34. Weill FS, Costaz R, Racle A, et al: Ultrasound study of adenopathies within the hepatoduodenal ligament: The "Rosebud" pattern. Gastrointest Radiol 1986; 11:142–144.
35. Forsberg L, Floren CH, Hederstrom E, et al: Ultrasound examination in diffuse liver disease. Clinical significance of enlarged lymph nodes in the hepatoduodenal ligament. Acta Radiol Diagn (Stockh) 1987; 28:281–290.
36. Lyttkens R, Forsberg L, Hederstrom E: Ultrasound examination of lymph nodes in the hepatoduodenal ligament. Br J Radiol 1990; 63:26–30.
37. Fahim RB, McDonald JR, Richards JC, et al: Carcinoma of the gallbladder: A study of its modes of spread. Ann Surg 1962; 156:114–124.
38. Vaittinen F: Carcinoma of the gallbladder: A study of 390 cases diagnosed in Finland 1953–1967. Ann Chir Gynecol Fenn 1970; 29(suppl 168): 7.
39. Richard PF, Cantin J: Primary carcinoma of the gallbladder: Study of 108 cases. CanJ Surg 1976; 10:27–32.
40. Ohtani T, Shirai Y, Hatakeyama K: Diagnosis and staging of gallbladder carcinoma by computed tomography. *In* Neoplasms of the Digestive Tract: Imaging, Staging and Management. Edited by MA Meyers. Lippincott-Raven, Philadelphia, 1998, pp 485–492.
41. Meyers MA, Volberg F, Katzen B, et al: Haustral anatomy and pathology: A new look. I. Roentgen identification of normal pattern and relationships. Radiology 1973; 108:497–504.
42. Meyers MA, Volberg F, Katzen B, et al: Haustral anatomy and pathology: A new look. II. Roentgen interpretation of pathologic alterations. Radiology 1973; 108:505–512.
43. Kajitan T, Kyuno K, Nishi M: Pathology of gastric cancer. Gendaig, 1974; 35B:19–81.
44. Meyers MA, Oliphant M, Teixidor H, et al: Meta–static carcinoma simulating inflammatory colitis. AJR 1975; 123:67–83.
45. Rubesin SE, Levine MS: Omental cakes: Colonic involvement by omental metastases. Radiology 1985; 154:593–596.
46. Rubesin SE, Levine MS, Glick SN: Gastric involvement by omental cakes: Radiographic findings. Gastrointest Radiol 1986; 11:223–228.
47. Chou C-K, Liu G-C, Chen L-T, et al: MRI demonstration of peritoneal ligaments and mesenteries. Abdom Imaging 1993; 18:126–130.
48. Meyers MA: Roentgen significance of the phrenicocolic ligament. Radiology 1970; 95:539–545.
49. Bachman AL: Roentgen appearance of gastric invasion from carcinoma of the colon. Radiology 1954; 63:814–822.
50. Lee KR, Levine E, Moffat RE, et al: Computed tomographic staging of malignant gastric neoplasms. Radiology 1979; 133:151–155.
51. Moss AA, Schnyder P, Marks W, et al: Gastric adenocarcinoma: A comparison of the accuracy and economics of staging by computed tomography and surgery. Gastroenterology 1981; 80:45–50.
52. Kiyota YK, Mukai H, et al: Endoscopic ultrasonography (EUS) in the diagnosis of upper digestive tract diseases. Determination of the depth of cancer invasion. Gastroenterol Endosc 1986; 28:253–263.
53. Komaki S: Gastric carcinoma. *In* Computed Tomography of the Gastrointestinal Tract: Including the Peritoneal Cavity and Mesentery. Edited by MA Meyers, Springer-Verlag, New York, 1986, pp 23–54.
54. Machi J, Takeda J, Sigel B, et al: Normal stomach wall and gastric cancer: Evaluation with high-resolution operative US. Radiology 1986; 159:85–87.
55. Heiken JP, Brink JA, Vannier MW: Spiral (helical) CT. Radiology 1993; 189:647–656.
56. Meyers MA, Evans JA: Effects of pancreatitis on the small bowel and colon: Spread along mesenteric planes. AJR 1973; 119:151–165.
57. Treitel H, Meyers MA, Maza V: Changes in the duodenal loop secondary to carcinoma of the hepatic flexure of the colon. Br J Radiol 1970; 43:209–213.
58. Krestin GP, Beyer D, Lorenz R: Secondary involvement of the transverse colon by tumors of the pelvis: Spread of malignancies along the greater omentum. Gastrointest Radiol 1985; 10:283–288.
59. Semelka RC, Ascher SM, Reinhold C: MRI of the Abdomen and Pelvis: A Text-Atlas. Wiley-Liss, New York, 1997.
60. Mori H, McGrath FP, Malone DE, et al: The gastrocolic trunk and its tributaries: CT evaluation. Radiology 1992; 182:871–877.
61. Vieta JO, Blanco R, Valentini GR: Malignant duodenocolic fistula: Report of two cases, each with one or more synchronous gastrointestinal cancers. Dis Colon Rectum 1976; 19:542–552.
62. Diamond RT, Greenberg HM, Boult IF: Direct metastatic spread of right colonic adenocarcinoma to duodenum: Barium and computed tomographic findings. Gastrointest Radiol 1981; 6:339–341.

63. McDaniel KP, Charnsangavej, DuBrow RA, et al: Pathways of nodal metastasis in carcinomas of the cecum, ascending colon, and transverse colon: CT demonstration. AJR 1993; 161:61–64.
64. McCort JJ: Roentgenographic appearance of metastases to central lymph nodes of superior mesenteric artery in carcinoma of right colon. Radiology 1953; 60:641–646.
65. Charsangavej C, Whitley NO: Metastases to the pancreas and peripancreatic lymph nodes from carcinoma of the right side of the colon: CT findings in 12 patients. AJR 1993; 160:49–52.
66. Schabel SI, Rogers CI, Rittenberg GM: Duodeno-duodenal fistula—A manifestation of carcinoma of the colon. Gastrointest Radiol 1978; 3:15–17.
67. Jeffrey RB, Federle MP, Goodman PC: Computed tomography of the lesser peritoneal sac. AJR 1985; 144:567–575.
68. Dodds WJ, Foley WD, Lawson TL, et al: Pictorial essay. Anatomy and imaging of the lesser peritoneal sac. AJR 1985; 144:567–575.
69. Chun CH, Raff MF, Conteras L, et al: Splenic abscess. Medicine (Baltimore) 1980; 59:50–65.
70. Meyers MA: Peritoneography: Normal and pathologic anatomy. AJR 1973; 117:353–365.
71. Hirata N, Kawamoto K, Ueyama T, et al: Endoscopic ultrasonography in the assessment of colonic wall invasion by adjacent diseases. Abdom Imaging 1994; 19:21–26.
72. Meyers MA: Clinical involvement of mesenteric and anti-mesenteric borders of small bowel. I. Normal pattern and relationships. Gastrointest Radiol 1976; 1(1):41–48.
73. Meyers MA: Clinical involvement of mesenteric and anti-mesenteric borders of small bowel. II. Radiologic interpretation of pathologic alterations. Gastrointest Radiol 1976; 1(1):49–58.
74. Whitley NO, Bohlman ME, Baker LP: CT patterns of mesenteric disease. J Comput Assist Tomogr 1982; 6(3):490–496.
75. Whitley NO: Mesenteric disease. *In* Computed Tomography of the Gastrointestinal Tract Including the Peritoneal Cavity and Mesentery. Edited by MA Meyers. Springer-Verlag, New York, 1986, pp 139–178.
76. Mueller PR, Ferrucci JT, Harbin WP, et al: Appearance of lymphomatous involvement of the mesentery by ultrasonography and body computed tomography: The "sandwich sign." Radiology 1980; 134:467–473.
77. Grinnel RS: Lymphatic block with atypical and retrograde lymphatic metastasis and spread in carcinoma of the colon and rectum. Ann Surg 1966; 163:272–280.
78. Moffat RE, Gourley WK: Ileal lymphatic metastases from cecal carcinoma. Radiology 1980; 135:55–58.
79. Perez C, Cacares J, Vails J: Carcinoma of the hepatic flexure with proximal lymphatic invasion mimicking Crohn's disease. Gastrointest Radiol 1984; 9:365–367.
80. Gourtsoyiannis NC, Nolan DJ: Imaging of Small Intestinal Tumours. Elsevier, Amsterdam, 1997.
81. Threefoot SA: Gross and microscopic anatomy of the lymphatic vessels and lymphaticovenous communications. Cancer Chemother Rep 1968; 52:1–20.
82. Pressman J, Dunn RF, Burtz M: Lymph node ultrastructure related to direct lymphaticovenous communication. Surg Gynecol Obstet 1967; 124:963–973.
83. Correia JP, Baptista AS, Antonio JF: Slowly evolving widespread diffuse alimentary tract carcinoma (linitis plastica). Gut 1968; 9:485–488.
84. Khilnani MT, Marshak RH, Eliasoph J, et al: Roentgen features of metastases to the colon. AJR 1966; 96:302–310.
85. Wigh R, Tapley Ndu V: Metastatic lesions to the large intestine. Radiology 1958; 70:222–228.
86. Gengler L, Baer J, Finby N: Rectal and sigmoid involvement secondary to carcinoma of the prostate. AJR 1975; 125:910–917.
87. Rubesin SE, Levine MS, Bezzi M, et al: Rectal involvement by prostatic carcinoma: Barium enema findings. AJR 1989; 152:53–57.
88. Lawrence SP, Shimek CM, Deutsch JC: Prostate cancer masquerading as a large rectal cancer: Diagnosis by endoscopic ultrasound. Gastrointest Endosc 1998; 48:88–89.
89. Winter CC: The problem of rectal involvement by prostatic cancer. Surg Gynecol Obstet 1957; 105:136–140.
90. Young HH: The cure of cancer of the prostate by radical perineal prostatectomy (prostato-seminal vesiculectomy). History, literature, and statistics of Young's operation. J Urol 1945; 53:188–252.
91. Kradjian RM, Bennington JL: Renal carcinoma recurrent 31 years after nephrectomy. Arch Surg 1965; 90:192–195.
92. Khilnani MT, Wolf BS: Late involvement of the alimentary tract by carcinoma of the kidney. Am J Dig Dis 1960; 5:529–540.
93. Shoemaker CP, Hoyle CL, Levine SB, et al: Late solitary recurrence of renal carcinoma. Am J Surg 1970; 120:99–100.

94. Meyers MA: The spread and localization of acute intraperitoneal effusions. Radiology 1970; 95:547–554.
95. Sampson JA: Implantation peritoneal carcinomatosis of ovarian origin. Am J Pathol 1931; 7:423–443.
96. Buie LA, Jackman RJ, Vickers PM: Extrarectal masses caused by tumors of the recto-uterine or rectovesical space. JAMA 1941; 117:167–169.
97. Raiford TS: Tumors of small intestine. Arch Surg 1932; 25:321–355.
98. Walther HE: Krebsmetastasen. Benno Schwabe, Basel, 1948.
99. Hultborn KA, Morales O, Romanus R: The so-called shelf tumour of the rectum. Acta Radiol Suppl 1955; 124.
100. Theander G, Wehlin L, Langeland P: Deformation of the rectosigmoid junction in peritoneal carcinomatosis. Acta Radiol Diagn 1963; 1:1071–1076.
101. Blumer G: Rectal shelf: Neglected rectal sign of value in diagnosis of obscure malignant and inflammatory disease within abdomen. Albany Med Ann 1909; 30:361.
102. Chou C-K, Liu G-C, Su J-H, et al: MRI demonstration of peritoneal implants. Abdom Imaging 1994; 19:95–101.
103. Lee M-G, Auh YH, Cho KS, et al: CT of carcinoma of the pancreas: Different mode of spread according to lesion site. Clin Imaging 1993; 17:269–273.
104. Pevarski DJ, Mergo PJ, Ros PR: Peritoneal carcinomatosis due to transitional cell carcinoma of the bladder: CT findings in two patients. AJR 1995; 164:929–930.
105. Chrysikopoulos H, Maniatis V, Roussakis A, et al: Peritoneal metastases from transitional cell carcinoma of the urinary tract: CT and MR imaging. Abdom Imaging 1998; 23:91–95.
106. Tartar VM, Heiken JP, McClennan BL: Renal cell carcinoma presenting with diffuse peritoneal metastases: CT findings. J Comput Assist Tomogr 1991; 15:450–453.
107. Charnsangavej C, DuBrow R, et al: CT of the mesocolon. Part 1. Anatomic considerations. RadioGraphics 1993; 13:1035–1046.
108. Charnsangavej C, DuBrow R, et al: CT of the mesocolon. Part 2. Pathologic considerations. RadioGraphics 1993; 13:1309–1322.
109. Forstner R, Hricak H, Powell CB, et al: Ovarian cancer recurrence: Value of MR imaging. Radiology 1995; 196:715–720.
110. Esenstein ML, Shaw SL, Pak HY, et al: CT demonstration of multiple intraperitoneal teratomatous implants. J Comput Assist Tomogr 1983; 7:1117–1118.
111. De Meo GH, Fulcher AS, Austin RF Jr: Anatomic CT demonstration of the peritoneal spaces, ligaments and mesenteries: Normal and pathologic processes. RadioGraphics 1995; 15:755–770.
112. Feldman GB, Knapp RC: Lymphatic drainage of the peritoneal cavity and its significance in ovarian cancer. Am J Obstet Gynecol 1974; 119:991–994.
113. Simer PH: The drainage of particulate matter from the peritoneal cavity by lymphatics. Anat Rec 1944; 88:175–192.
114. Feldman GB, Knapp RC, Order SE: The role of lymphatic obstruction in the formation of ascites in a murine ovarian carcinoma. Cancer Res 1972; 32:1663–1666.
115. Higgins GM, Graham AS: Lymphatic drainage from the peritoneal cavity in the dog. Arch Surg 1929; 19:453–465.
116. Bettendorf U: Lymph flow mechanism of the subperitoneal diaphragmatic lymphatics. Lymphology 1978; 11:111–116.
117. French GE, Florey HW, Morris BL: The absorption of particles by the lymphatics of the diaphragm. QJ Exp Biol 1960; 45:88–103.
118. Vock P, Hodler J: Cardiophrenic angle adenopathy: Update of causes and significance. Radiology 1986; 159:395–399.
119. Mittal BR, Maini A, Das BK: Peritoneopleural communication associated with cirrhotic ascites: Scintigraphic demonstration. Abdom Imaging 1996; 21:69–70.
120. Bergman F: Carcinoma of the ovary: A clinicopathological study of 86 autopsied cases with special reference to mode of spread. Acta Obstet Gynecol Scand 1966; 45:211–231.
121. Rosenoff SH, DeVita VT, Hubbard S, et al: Peritoneoscopy in staging and follow-up of ovarian cancer. Semin Oncol 1975; 2(3):223–228.
122. Dagnini G, Marin G, Caldironi MW, et al: Laparoscopy in staging, follow-up, and restaging of ovarian carcinoma. Gastrointest Endosc 1987; 33:80–83.
123. Ozols RF, Fisher RI, Anderson T, et al: Peritoneoscopy in the management of ovarian cancer. Am J Obstet Gynecol 1981; 140:611–619.
124. Piver MS, Barlow JJ, Lele SB: Incidence of subclinical metastasis in stage I and II ovarian carcinoma. Obstet Gynecol 1978; 52:100–104.
125. Young RC, Decker DG, Wharton JT, et al: Staging laparotomy in early ovarian cancer. JAMA 1983; 250(22):3072–3076.

126. Triller J, Goldnirsch A, Reinhard J-P: Subcapsular liver metastasis in ovarian cancer: Computed tomography and surgical staging. Eur J Radiol 1985; 5:261–266.
127. Jeffrey RB Jr: CT demonstration of peritoneal implants. Am J Roentgenol 1980; 135:323–326.
128. BuyJ-N, Moss AA, Ghossain MA, et al: Peritoneal implants from ovarian tumors: CT findings. Radiology 1988; 169:691–694.
129. Megibow AJ, Bosniak MA, Ho AG, et al: Accuracy of CT in detection of persistent or recurrent ovarian carcinoma: Correlation with second-look laparotomy. Radiology 1988; 166:341–345.
130. Kalovidouris A, Gouliamos A, Pontifex GR, et al: Computed tomography of ovarian carcinoma. Acta Radiol Diagn 1984; 25:203–208.
131. Rioux M, Michaud C: Sonographic detection of peritoneal carcinomatosis: A prospective study of 37 cases. Abdom Imaging 1995; 20:47–51.
132. Forstner R, Hricak H, White S: CT and MRI of ovarian cancer. Abdom Imaging 1995; 20:2–8.
133. Fiorica JV, Hoffman MS, La Polla JP, et al: The management of diaphragmatic lesions in ovarian carcinoma. Obstet Gynecol 1989; 74:927–929.
134. Prayer L, Kainz C, Kramer J, et al: CT and MR accuracy in the detection of tumor recurrence in patients treated for ovarian cancer. J Comput Assist Tomogr 1993; 17(4):626–632.
135. Meyer JI, Kennedy AW, Friedman R, et al: Ovarian cancer: Value of CT in predicting success of debulking surgery. AJR 1995; 165:875–878.
136. Forstner R, Hricak H, Occhipinti KA, et al: Ovarian cancer: Staging with CT and MR imaging. Radiology 1995; 197:619–626.
137. Walkey MM, Friedman AC, Sobotra P, et al: CT manifestations of peritoneal carcinomatosis. AJR 1988; 150:1035–1041.
138. Low RN, Sigeti JS: MR imaging of peritoneal disease: Comparison of contrast-enhanced fast multiplanar spoiled gradient-recalled and spin-echo imaging. AJR 1994; 163:1131–1140.
139. Low RN, Barone RM, Lacey C, et al: Peritoneal tumor: MR imaging with dilute oral barium and intravenous gadolinium-containing contrast agents compared with unenhanced MR imaging and CT. Radiology 1997; 204:513–520.
140. Low RN, Francis IR: MR imaging of the gastrointestinal tract with IV gadolinium and diluted barium oral contrast media compared with unenhanced MR imaging and CT. AJR 1997; 169:1051–1059.
141. Ricke J, Hosten N: Peritoneal carcinomatosis. Abdom Imaging 1997; 22:235–236.
142. Epstein BM, Mann JH: CT of abdominal tuberculosis. AJR 1982; 139:861–866.
143. Zirinsky K, Auh YH, Kneeland JB, et al: Computed tomography, sonography, and MR imaging of abdominal tuberculosis. J Comput Assist Tomogr 1985; 9:961–963.
144. Hulnick DH, Megibow AJ, Naidich DP, et al: Abdominal tuberculosis: CT evaluation. Radiology 1985; 157:199–204.
145. Ha HK, Jung JI, Lee MS, et al: CT differentiation of tuberculous peritonitis and peritoneal carcinomatosis. AJR 1996; 167:743–748.
146. Rodriguez E, Pombo F: Peritoneal tuberculosis versus peritoneal carcinomatosis: Distinction based on CT findings. J Comput Assist Tomogr 1996; 20(2):269–272.
147. Jadvar H, Mindelzun RE, Orcott EW, et al: Still the great mimicker: Abdominal tuberculosis. AJR 1997; 168:1455–1460.
148. Hamrick-Turner JE, Chiechi MV, Abbit PL, et al: Neoplastic and inflammatory processes of the peritoneum, omentum, and mesentery: Diagnosis with CT. RadioGraphics 1992; 12:1051–1068.
149. Thoeni RF: The role of imaging in patients with ascites. AJR 1995; 165:16–18.
150. Reuter K, Raptopoulos V, Reale F, et al: Diagnosis of peritoneal mesothelioma: Computed tomography, sonography, and fine-needle aspiration biopsy. AJR 1983; 140:1189–1194.
151. Nardi PM, Ruchman RB: CT appearance of diffuse peritoneal endometriosis. J Comput Assist Tomogr 1989; 13(6):1075–1077.
152. Ronnett BM, Zahn CM, Kurman RJ, et al: Disseminated peritoneal adenomucinosis and peritoneal mucinous carcinomatosis: A clinicopathologic analysis of 109 cases with emphasis on distinguishing pathologic features, site of origin, prognosis, and relationship to "pseudomyxoma peritonei." Am J Surg Pathol 1995; 19:1390–1408.
153. Seshul MB, Coulam CM: Pseudomyxoma peritonei: Computed tomography and sonography. AJR 1981; 136:803–806.
154. Churchill R, Meyers MA: Intraperitoneal fluid collections (Chapter 7). *In* Computed Tomography of the Gastrointestinal Tract: Including the Peritoneal Cavity and Mesentery. Edited by MA Meyers. Springer-Verlag, New York, 1986.
155. Walensky RP, Venbrux AC, Prescott CA, et al: Pseudomyxoma peritonei. AJR 1996; 167:471–474.
156. Sugarbaker PH: Peritoneal Carcinomatosis: Principles of Management. Kluwer Academic Publ, Boston, 1996, pp 85, 86, 94.

157. Miller DL, Udelsman R, Sugarbaker PH: Case report: Calcification of pseudomyxoma peritonei following intraperitoneal chemotherapy: CT demonstration. J Comput Assist Tomogr 1985; 9:1123–1124.
158. Barakos JA, Jeffrey RB Jr, McAninch JW, et al: Computerized tomography diagnosis of diffuse intraperitoneal metastases after retroperitoneal lymphadenectomy for testicular carcinoma. J Urol 1986; 136:680–681.
159. Mitchell DG, Hill MC, Hill S, et al: Serous carcinoma of the ovary: CT identification of metastatic calcified implants. Radiology 1986; 158: 649–652.
160. Pandolfo I, Blandino A, Gaeta M, et al: Calcified peritoneal metastases from papillary cystadenocarcinoma of the ovary: CT features. J Comput Assist Tomogr 1986; 10(3):545–546.
161. Solomon A, Rubinstein Z: Importance of the falciform ligament, ligamentum teres, and splenic hilus in the spread of malignancy as demonstrated by computed tomography. Gastrointest Radiol 1984; 9:53–56.
162. Ferenczy A, Talens M, Zoghby M, et al: Ultrastructural studies on the morphogenesis of psammoma bodies in ovarian serous neoplasia. Cancer 1977; 39:2451–2459.
163. Kunieda K, Okuhira M, Nonaka T, et al: A case of calcified gastric cancer—review of Japanese literature. Jpn J Gastroenterol 1990; 87:1236–1242.
164. Matsuoka Y, Itai Y, Ohtomo K, et al: Calcification of peritoneal carcinomatosis from gastric carcinoma: A CT demonstration. Eur J Radiol 1991; 13:207–208.
165. Hughes KS, Miller DL, Neuman R, et al: Extrahepatic tumor deposits misdiagnosed as intrahepatic metastases. Arch Surg 1988; 123(8):1013–1015.
166. Lundstedt C, Holmin T, Thorvinger B: Peritoneal ovarian metastases simulating liver parenchymal metastases. Gastrointest Radiol 1992; 17:250–252.
167. Liebermann-Meffert D, White H: The Greater Omentum: Anatomy, physiology, pathology, surgery, with an historical survey. Springer-Verlag, New York, 1983, 1–173.
168. Shimotsuma M, Kawarta M, Hagiwara A, et al: Milky spots in the human greater omentum: Its macroscopic and histological identification. Acta Anat 1989; 136:211–216.
169. Shimotsuma M, Hagiwara A, Takahashi T, et al: Surface structure and cell zonation in human omental milky spots. Lymphology 1990; 23:207–208.
170. Hodel C: Ultrastructural studies on the absorption of protein markers by the greater omentum. Eur Surg Res 1970; 2:435–449.
171. Cranshaw ML, Leak LV: Milky spots on the omentum: A source of peritoneal cells in the normal and stimulated animal. Arch Histol Cytol 1990; 53:165–177.
172. Shimatsuma M, Sakuyama A, Sirasu M, et al: The role of the lymphatic system of the greater omentum and diaphragm in intraperitoneal cancer dissemination, Jpn J Lymphol 1993; 26:90–101.
173. Shimatsuma M, Shields JW, Simpson-Morgan MW, et al: Morpho-physiological function and role of omental milky spots as omentum-associated lymphoid tissue (OALT) in the peritoneal cavity. Lymphology 1993; 26:90–101.
174. Holm-Nielsen P: Pathogenesis of ascites in peritoneal carcinomatosis. Acta Pathol Microbiol Scand 1953; 33:10–21.
175. Cooper C, Jeffrey RB, Silverman PM, et al: Computed tomography of omental pathology. J Comput Assist Tomogr 1986; 10(1):62–66.
176. Levitt RG, Sagel SS, Stanley RJ: Detection of neoplastic involvement of the mesentery and omentum by computed tomography. AJR 1978; 131:835–838.
177. Tartar VM, Heiken JP, McClennan BL: Renal cell carcinoma presenting with diffuse peritoneal metastases: CT findings. J Comput Assist Tomogr 1991; 15(3):450–453.
178. Schwartz RW, Reams M, McGrath PC, et al: Primary solid neoplasms of the greater omentum. Surgery 1990; 109:543–549.
179. Sompayrac SW, Mindelzun RE, Silverman PM, et al: The greater omentum. AJR 1997; 168:683–687.
180. Karak PK, Millmond SH, Neumann D, et al: Omental infarction: Report of three cases and review of the literature. Abdom Imaging 1998; 23:96–98.
181. Bailey H: Demonstration of Physical Signs in Clinical Surgery, 13th ed. Williams & Wilkins, Baltimore, 1960.
182. Key JD, Shephard DAE, Walters W: Sister Mary Joseph's nodule and its relationship to diagnosis of carcinoma of the umbilicus. Minn Med 1976; 59:561–566.
183. Mayo WJ: Metastasis in cancer. Proc Staff Meet Mayo Clin 1928; 3:327.
184. Barrow MV: Metastatic tumors of the umbilicus. J Chron Dis 1966; 19:1113–1117.
185. Shetty MR: Metastatic tumors of the umbilicus: A review 1830–1989. J Surg Oncol 1990; 45:212–215.

186. Cullen TS: Embryology, Anatomy and Diseases of the Umbilicus. WB Saunders, Philadelphia, 1916, pp 118–458.
187. Powell FC, Cooper AJ, Massa MC, et al: Sister Mary Joseph's nodule: A clinical and histologic study. J Am Acad Dermatol 1984; 10:610–615.
188. Steck WD, Helwig EB: Tumors of the umbilicus. Cancer 1965; 18:907–915.
189. Weiss SM, Wengert PA, Harkavy SE: Incisional recurrence of gallbladder cancer after laparoscopic cholecystectomy. Gastrointest Endosc 1994; 40: 244–246.
190. Krukenberg F: Ueber das Fibrosarcoma ovarii mucocellulare (Carcinomatodes). Arch Gynecol 1896; 50:287–321.
191. Cho KC, Gold BM: Computed tomography of Kruckenberg tumors. AJR 1985; 145:285–288.
192. Choi BI, Choo IW, Han MC, et al: Sonographic appearance of Kruckenberg tumor from gastric carcinoma. Gastrointest Radiol 1988; 13:15–18.
193. Mata JM, Inaraja L, Rams A, et al: CT findings in metastatic ovarian tumors from gastrointestinal tract neoplasms (Krukenberg tumors). Gastrointest Radiol 1988; 13:242–246.
194. Ha HK, Baek SY, Kim SH, et al: Krukenberg's tumor of the ovary: MR imaging features. AJR 1995; 164:1435–1439.
195. Sugarbaker PH, Averbach AM: Krukenberg syndrome as a natural manifestation of tumor cell entrapment. *In* Peritoneal Carcinomatosis: Principles of Management. Edited by PH Sugarbaker Kluwer, Boston, 1996, pp 163–191.
196. Kim Y.-S., Cho O.-K., Song S.-Y., et al: Peritoneal lymphomatosis: CT findings. Abdom Imaging 1998; 23:87–90.
197. Hardman WJ, Majmudar B: Leiomyomatosis peritonealis disseminata: Clinicopathologic analysis of five cases. Southern Med J 1996; 89(3):291–294.
198. Papadatos D, Taourel P, Bret PM: CT of leiomyomatosis peritonealis disseminata mimicking peritoneal carcinomatosis. AJR 1996; 167:475–476.
199. Fulcher AS, Szucs RA: Leiomyomatosis peritonealis dissemination complicated by sarcomatous transformation and ovarian torsion: Presentation of two cases and review of the literature. Abdom Imaging 1998; 23:640–644.
200. Choi BI, Lee WJ, Chi JG, et al: CT manifestations of peritoneal leiomyosarcomatosis. AJR 1990; 155:799–801.
201. Villanueva A, Pérez C, Sabaté JM, et al: CT manifestations of peritoneal leiomyosarcomatosis. Eur J Radiol 1993; 17:166–169.
201a. Sabaté JM, Torrubia S, Maideu J, et al: Sclerosing mesenteritis: Imaging findings in 17 patients, AJR 1999; 172:625–629.
202. Stafford-Johnson DB, Bree RL, Francis IR, et al: CT appearance of primary papillary serous carcinoma of the peritoneum. AJR 1998; 171:687–689.
203. Furukawa T, Ueda J, Takahashi S, et al: Peritoneal serous papillary carcinoma: Radiologic appearance. Abdom Imaging 1999; 24:78–81.
204. Goletti O, De Negri F, Pucciarelli M, et al: Subcutaneous seeding after percutaneous ethanol injection of liver metastases. Radiology 1992; 183:785–786.
205. Smith E: Complications of needle biopsy. Radiology 1991; 178:253–258.
206. La Fianza A, Di Maggio EM, Preda L, et al: Infiltrative subcutaneous metastases from ovarian carcinoma after paracentesis: CT findings. Abdom Imaging 1997; 22:522–523.
207. Kurl S, Farin P, Rytkohen H, et al: Intraperitoneal seeding from hepatocellular carcinoma following percutaneous ethanol ablation therapy. Abdom Imaging 1997; 22:261–263.
208. Jacquet P, Jelinek JS, Steves MA: Evaluation of computed tomography in patients with peritoneal carcinomatosis. Cancer 1993; 72:1631–1636.
209. Minutoli A, Volta S, Gaeta M: Delayed enhancement of ascites following high-dose contrast CT for liver metastases. J Comput Assist Tomogr 1989; 13:916–917.
210. Cooper C, Silverman PM, Davros W, et al: Delayed contrast enhancement of ascitic fluid on CT: Frequency and significance. AJR 1993; 161:787–790.
211. Wise SW, DeMeo JH, Austin RF: Enhancing ascites: An aid to CT diagnosis. Abdom Imaging 1996; 21:67–68.
212. Garrison RN, Kaelin LD, Heuser LS, et al: Malignant ascites: Clinical and experimental observations. Ann Surg 1986; 203:644–649.
213. Heuser LS, Miller FN, Gilley-Pietsch C: Protein leak from normal vasculature due to human malignant ascites. Am J Surg 1988; 155:765–769.
214. Runyon BA, Hoefs JC, Morgan TR: Ascitic fluid analysis in malignancy-related ascites. Hepatology 1988; 8:1104–1109.
215. Arai K, Makino H, Morioka T, et al: Enhancement of ascites on MRI following intravenous administration of GD-DTPA. J Comput Assist Tomogr 1993; 17:617–622.
216. Meyers MA: Clinical report: A new view of the peritoneal cavity. Mod Med 1976; 44(6):51–56.
217. Meyers MA: Peritoneography: Normal and path-

ologic anatomy (Chapter 3). *In* Dynamic Radiology of the Abdomen: Normal and Pathologic Anatomy. Springer-Verlag, New York, 1976.
218. Dunnick NR, Jones RB, Doppman JL, et al: Intraperitoneal contrast infusion for assessment of intraperitoneal fluid dynamics. AJR 1979; 133:221–223.
219. Roub LW, Drayer BP, Orr DP, et al: Computed tomographic positive contrast peritoneography. Radiology 1979; 131:699–704.
220. Giunta S, Tipaldi L, Diotellevi F, et al: CT demonstration of peritoneal metastases after intraperitoneal injection of contrast media. Clin Imaging 1990; 14:31–34.
221. Halvorsen RA, Panushka C, Oakley GJ, et al: Intraperitoneal contrast material improves the CT detection of peritoneal metastases. AJR 1991; 157:37–40.
222. Nelson RC, Chezmar JL, Hoel MJ, et al: Peritoneal carcinomatosis: Preoperative CT with intraperitoneal contrast. Radiology 1992; 182:133–138.
223. Casiero-Alves G, Goncalo M, Abraul E, et al: Induced pneumoperitoneum in CT evaluation of peritoneal carcinomatosis. Abdom Imaging 1995; 29:52–55.
224. Weill FS, Costaz R, Guetarni S, et al: Le diagnostic échographique des métastases péritonéales chez les malades ascitiques. J Radiol 1990; 71:365–368.
225. Derchi LE, Solbiati L, Rizzatto G, et al: Normal anatomy and pathologic changes of the small bowel mesentery: US appearance. Radiology 1987; 164:649–652.
226. Goerg C, Schwerk W-B: Malignant ascites: Sonographic signs of peritoneal carcinomatosis. Eur J Cancer 1991; 27:720–723.
227. Goerg C, Schwerk W-B: Peritoneal carcinomatosis with ascites. AJR 1991; 156:1185–1187.
228. Chou CK, Liu GC, Chen LT, et al: MRI manifestations of peritoneal carcinomatosis. Gastrointest Radiol 1992; 17:336–338.
229. Magre GR, Terk M, Colletti P, et al: Saline MR peritoneography. AJR 1996; 167:749–751.
230. Carrasquillo JA, Sugarbaker P, Colcher D, et al: Peritoneal carcinomatosis: Imaging with intraperitoneal injection of 1-131-labeled B72.3 monoclonal antibody. Radiology 1988; 167:35–40.
231. Weiss L: Metastatic inefficiency: Causes and consequences. Cancer Rev 1986; 3:1–24.
232. Weiss L: Cancer cell traffic from lungs to liver: An example of metastatic inefficiency. Int J Cancer 1980; 25:385–392.
233. Asch MJ, Wiedel PD, Habif DV: Gastrointestinal metastases from carcinoma of the breast: Autopsy study and 18 cases requiring operative intervention. Arch Surg 1968; 96:840–843.
234. Graham WP III: Gastrointestinal metastases from carcinoma of the breast. Ann Surg 1964; 159:477–480.
235. Oddson TA, Rice RP, Seiler HF, et al: The spectrum of small bowel melanoma. Gastrointest Radiol 1978; 3:419–423.
236. Kadakia SC, Parker A, Canales L: Metastatic tumors to the upper gastrointestinal tract: Endoscopic experience. Am J Gastroenterol 1992; 87:1418–1423.
237. Herlinger H, Maglinte D: Clinical Radiology of the Small Intestine. WB Saunders, Philadelphia, 1989.
238. Goldstein HM, Beydoun MT, Dodd GD: Radiologic spectrum of melanoma metastatic to the gastrointestinal tract. AJR 1977; 129:605–612.
239. Smith SJ, Carlson HC, Gisvold JJ: Secondary neoplasms of the small bowel. Radiology 1977; 125:29–33.
240. Kawashima A, Fishman EK, Kuhlman JE, et al: CT of malignant melanoma: Patterns of small bowel and mesenteric involvement. J Comput Assist Tomogr 1991; 15(4):570–574.
241. Das Gupta T, Brasfield R: Metastatic melanoma: Clinico-pathologic study. Cancer 1969; 17:1323–1339.
242. Coman DR, De Long KP, McCutcheon M: Studies on the mechanism of metastasis: The distribution of tumors in various organs in relation to the distribution of arterial emboli. Cancer Res 1951; 11:648–651.
243. Einhorn LH, Burgess MA, Vallejos C, et al: Prognostic correlations and response to treatment in advanced metastatic malignant melanoma. Cancer Res 1974; 34:1995–2004.
244. Branum GD, Seigler HF: The role of surgical intervention in the management of intestinal metastases from malignant melanoma. Am J Surg 1991; 162:428–431.
245. Lejeune FJ, Chaudhuri PK, Das Gupta TK: Malignant Melanoma: Medical and Surgical Management. McGraw-Hill, New York, 1994.
246. Choi SH, Sheehan FR, Pickren JW: Metastatic involvement of the stomach by breast cancer. Cancer 1964; 17:791–797.
247. Dixon AR, Ellis IO, Elston CW, et al: A comparison of the clinical metastatic patterns of invasive lobular and ductal carcinomas of the breast. Br J Cancer 1991; 63(4):34–35.
248. Lamovec J, Bracko M: Metastatic pattern of infiltrating lobular carcinoma of the breast: An autopsy study. J Surg Oncol 1991; 48:28–33.

249. Kidney DD, Cohen AJ, Butler J: Abdominal metastases of infiltrating lobular breast carcinoma: CT and radiographic findings. Abdom Imaging 1997; 22:156–159.
250. Eker R, Etskind J: Investigations on the intramural spread of gastric carcinoma. Acta Pathol Microbiol Scand 1952; 30:371–383.
251. Cormier JC, Gaffey TA, Welch JM, et al: Linitis plastica caused by metastatic lobular carcinoma of the breast. Mayo Clin Proc 1980; 55:747–753.
252. Caskey CI, Scatarige JC, Fishman EK: Distribution of metastases in breast carcinoma: CT evaluation of the abdomen. Clin Imaging 1991; 15: 166–171.
253. Taal BG, den Hartog Jager FCA, Steinmetz R, et al: The spectrum of gastrointestinal metastases of breast carcinoma: I. Stomach. Gastrointest Endosc 1992; 38:130–135.
254. Elliott LA, Hall GD, Perren TJ, et al: Metastatic breast carcinoma involving the gastric antrum and duodenum: Computed tomography appearances. Br J Radiol 1995; 68:970–972.
255. Joffe N: Metastatic involvement of the stomach secondary to breast carcinoma. 1975; AJR 123: 512–521.
256. Taal BG, den Hartog Jager FCA, Steinmetz R, et al: The spectrum of gastrointestinal metastases of breast carcinoma: II. The colon and rectum. Gastrointest Endosc 1992; 38:136–141.
257. Thaler W: Rectal metastases from carcinoma of the breast: A case report and a review of the literature. GI Cancer 1995; 1:75–78.
258. Antler AS, Ough Y, Pitchumoni CS, et al: Gastrointestinal metastases from malignant tumors of the lung. Cancer 1982; 49:170–172.
259. Luomanen RKJ, Watson WL: Autopsy findings (Chapter 20). *In* Lung Cancer: A Study of Five Thousand Memorial Hospital Cases. Edited by WL Watson. Mosby, St. Louis, 1968.
260. Smith HJ, Vlasak MG: Metastasis to the colon from bronchogenic carcinoma. Gastrointest Radiol 1977; 2:393–396.
261. Hayes HT, Burr HB: Hypernephroma of the sigmoid colon. Am J Surg 1951; 81:98–100.

Staging of Gastrointestinal Cancers 5

A basic understanding of the spread of cancers of the gastrointestinal tract relies upon the depth of mural penetration. Originating in the epithelial layer, the cancer's invasion of the wall may variously extend into the lamina propria, muscularis mucosae, submucosa, muscularis propria, and subserosal connective tissue or through the serosa with or without direct invasion of adjacent structures. This determination forms the basis of the universally adopted TNM staging classification,[1–3] encompassing all three prognostic factors of tumoral mural penetration (T), nodal involvement (N), and distant metastatic spread (M) in one staging system.

Staging is the process by which the anatomic extent of a tumor is defined at a certain point of time. Oncoradiology has had a major influence on the TNM staging system, which has incorporated changes to accommodate the information available by the widening spectrum of diagnostic and interventional imaging and endosonography.[4] Depth of tumor invasion (T) is the main criterion for clinical classification, replacing factors such as tumor size, circumferential extent of involvement, and gross morphology. In carcinoma of the esophagus and stomach, depth of invasion as the major determinant of prognosis was clearly established in Japanese studies of more than 3000 cases[5] and 15,000 cases,[6] respectively. This was achieved because of developments in endosonography (EUS) and CT. Similarly, the current TNM classification for colorectal carcinomas is based on the accuracy of cross-sectional images. Developments in sectional imaging contribute significantly to the earlier detection of disease, to determine the stage of a malignancy, to substantiate criteria for resectability and nonresectability of a cancer, to monitor posttreatment tumor response, and to evaluate residual or recurrent disease. Fundamental to the staging system is the concept of possible independence of the TNM states. Because lymph node involvement (N) is designated as a separate category, there is no assumption that the full thickness of the gut wall must be penetrated before lymph node involvement occurs, as is the assumption behind the Dukes classification of rectal carcinoma.[7] The concept of the stages of a cancer does not imply a regular progression from stage I to stage IV.

Importance of Staging

Carcinoma of the Esophagus

Patients with esophageal carcinoma should be stratified to determine whether palliative treatment or attemptive curative therapy is appropriate. The importance of the staging of esophageal cancer (Table 5–1) lies in judging the resectability of the tumor and evaluating the prognosis of the patient. The stage of the disease has a direct effect on survival.[8–11]

Lymph node metastases are seldom present with a T1 mucosal (T1m) tumor, whereas the incidence with a T1 submucosal (T1sm) tumor is approximately 33%[12] to 45%.[13,14] Submucosal invasion by esophageal carcinoma is a decidedly advanced lesion, compared, for example, to a similar depth of penetration in gastric carcinoma. For patients with mucosal-type cancers, endoscopic resection or laser ablation is being used in many centers, particularly in Japan. In the United States and Europe, esophageal carcinomas are generally far advanced at the time of presentation.

Table 5–1. TNM Clinical Classification System for Staging Esophageal Cancers

Primary tumor (T)			
TX			Primary tumor cannot be assessed
T0			No evidence of primary tumor
Tis			Carcinoma *in situ*
T1			Tumor invades lamina propria or submucosa
T2			Tumor invades muscularis propria
T3			Tumor invades adventitia
T4			Tumor invades adjacent structures
Regional lymph nodes (N)			
NX			Regional lymph nodes cannot be assessed
N0			No regional lymph node metastasis
N1			Regional lymph node metastasis
Distant metastasis (M)			
MX			Distant metastasis cannot be assessed
M0			No distant metastasis
M1			Distant metastasis
Tumors of the lower thoracic esophagus:			
M1a			Metastasis in celiac lymph nodes
M1b			Other distant metastasis
Tumors of the midthoracic esophagus:			
M1a			Not applicable
M1b			Nonregional lymph nodes and/or other distant metastasis
Tumors of the upper thoracic esophagus:			
M1a			Metastasis in cervical nodes
M1b			Other distant metastasis
Stage grouping			
Stage 0	Tis	N0	M0
Stage I	T1	N0	M0
Stage IIA	T2	N0	M0
	T3	N0	M0
Stage IIB	T1	N1	M0
	T2	N1	M0
Stage III	T3	N1	M0
	T4	Any N	M0
Stage IV	Any T	Any N	M1
Stage IVA	Any T	Any N	M1a
Stage IVB	Any T	Any N	M1b

Carcinoma of the Stomach

In the TNM classification of gastric cancer[1–3] (Table 5–2), depth of invasion is the main criterion, as in esophageal carcinoma. The current T staging system is illustrated in Figure 5–1.

The classification presents some limitations. The T1 designation does not distinguish mucosal and submucosal invasion. In the definition of a T2 cancer, no distinction is made as to whether the muscularis propria is merely invaded or there is extension to involve the subserosa. Invasion of the serosa is the main criterion of a T3 cancer.

The Japanese Research Society for Gastric Cancer has used a detailed classification based on meticulous surgical and pathologic findings,[15] mostly translatable to the TNM system, providing an anatomic basis for systematic lymph node dissection in the surgical treatment of gastric cancer.

There is a distinct correlation between the T stage

Table 5–2. TNM Clinical Classification System for Staging Gastric Carcinoma

Primary tumor (T)			
TX	Primary tumor cannot be assessed		
T0	No evidence of primary tumor		
Tis	Carcinoma *in situ:* intraepithelial tumor, without invasion of lamina propria		
T1	Tumor invades lamina propria or submucosa		
T2	Tumor invades muscularis propria or subserosa		
T3	Tumor penetrates serosa (visceral peritoneum) without invasion of adjacent structures		
T4	Tumor invades adjacent structures		
Regional lymph nodes (N)			
NX	Regional lymph nodes cannot be assessed		
N0	No regional lymph node metastasis		
N1	Metastasis in 1–6 regional lymph nodes		
N2	Metastasis in 7–15 regional lymph nodes		
N3	Metastasis in >15 regional lymph nodes		
Distant metastasis (M)			
MX	Presence of distant metastasis cannot be assessed		
M0	No distant metastasis		
M1	Distant metastasis		
Stage grouping			
Stage 0	Tis	N0	M0
Stage IA	T1	N0	M0
Stage IB	T1	N1	M0
	T2	N0	M0
Stage II	T1	N2	M0
	T2	N1	M0
	T3	N0	M0
Stage IIIA	T2	N2	M0
	T3	N1	M0
	T4	N0	M0
Stage IIIB	T3	N2	M0
Stage IV	T4	N1	M0
	T1	N3	M0
	T2	N3	M0
	T3	N3	M0
	T4	N2	M0
	T4	N3	M0
	Any T	Any N	M1

and the number and sites of invaded lymph nodes.[16] Increases in either the number of positive nodes or the extent of nodal involvement adversely influence survival.[17]

Early Gastric Cancer

As a result of advances in diagnostic procedures, there are increasing numbers of reports concerning the detection of early-stage gastric cancer, particularly in Japan with the application of mass gastric screening,[18–20] where almost one-half of all gastric cancer diagnoses refer to early lesions.

Early gastric cancer is defined as a tumor confined to the mucosa and submucosa, regardless of the presence or absence of perigastric lymph node metastasis.

Depth of invasion is the most important prognostic factor in early gastric carcinoma. Patients with lesions confined to the mucosa have a <5% chance of having nodal metastases and a nearly 100% 5-year survival. This

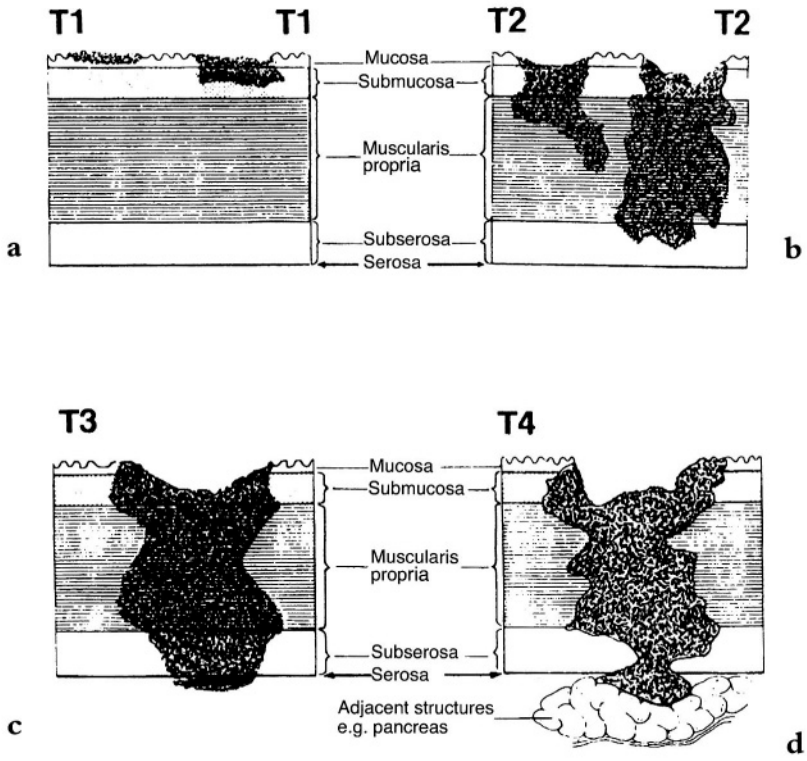


Fig. 5–1. TNM classification of gastric cancer.
Increasing T stages correlate with depth of penetration of wall of stomach.
(a) T1 cancers (early gastric cancer) may be limited to the mucosa or may also invade the submucosa.
(b) T2 cancers may be limited to the muscularis propria or may also invade the subserosa.
(c) T3 cancers penetrate the serosa.
(d) T4 lesions further invade adjacent structures.
(Reproduced from Spiessel et al.[2])

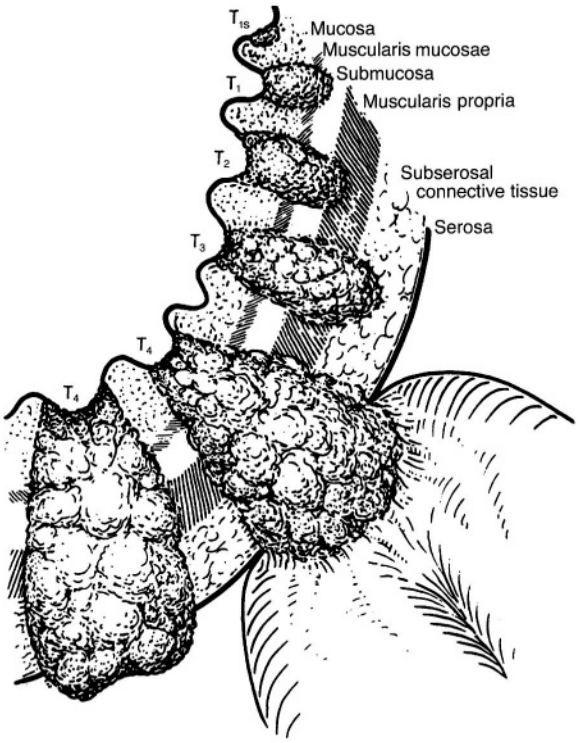


Fig. 5–2. T stages of colonic mural penetration.
(Reproduced from Fielding LP: Staging systems. *In* Cancer of the Colon, Rectum and Anus. Edited by AM Cohen, SJ Winawer. McGraw-Hill, New York, 1995, p 210.)

outstanding survival is related to the fact that the stomach has a paucity of lymphatic channels in the lamina propria, in contrast to the esophagus and small intestine. These early carcinomas may be treated by endoscopic mucosectomy[21–23] or by endoscopic laser treatment.[24] Invasion through the muscularis mucosae into the submucosa is associated with a 10–20% likelihood of nodal metastases and a 90–95% 5-year survival.

Colorectal Carcinoma

Few investigators have applied imaging methods to staging of suprarectal colonic carcinomas.[25–28] The vast majority of clinical studies have been directed to the diagnosis, staging, and management of carcinomas of the rectum.

The TNM classification for colorectal cancer (Table 5–3 and Fig. 5–2) of the American Joint Committee on Cancer (AJCC) and the Union Internationale Contra le Cancer (UICC)[1,3] is compatible with the Dukes classification.

The most important independent pathologic factor for survival or recurrence after potentially curative surgery is the depth of the cancer's penetration through the bowel wall and the presence and number of positive lymph nodes.[29–31] The status of the cancer in relation to the muscularis propria demarcates T2 and T3 tumors. The classification stratifies regional nodal involvement by one to three compared with four or more positive nodes, a dichotomy of prognostic significance, with a 5-year survival rate of 66% and 37%, respectively.[32]

Table 5–3. TNM Clinical Classification System for Staging Colorectal Cancers

Primary tumor (T)

TX	Primary tumor cannot be assessed
T0	No evidence of primary tumor
Tis	Carcinoma *in situ:* confined within the glandular basement membrane (intraepithelial) or lamina propria (intramucosal)
T1	Tumor invades the submucosa
T2	Tumor invades the muscularis propria
T3	Tumor invades through the muscularis propria into the subserosa or into nonperitonealized pericolic or perirectal tissues
T4	Tumor directly invades other organs or structures and/or perforates the visceral peritoneum

Regional lymph nodes (N)

NX	Regional lymph nodes cannot be assessed
N0	No regional lymph node metastasis
N1	Metastasis in 1–3 pericolic or perirectal lumph nodes
N2	Metastasis in ≥4 pericolic or perirectal lymph nodes

Distant metastasis (M)

MX	Presence of distant metastasis cannot be assessed
M0	No distant metastasis
M1	Distant metastasis

Stage grouping

	AJCC/UICC			Dukes[a]
Stage 0	Tis	N0	M0	—
Stage I	T1	N0	M0	A
	T2	N0	M0	—
Stage II	T3	N0	M0	B
	T4	N0	M0	—
Stage III	Any T	N1	M0	C
	Any T	N2	M0	—
Stage IV	Any T	Any N	M1	—

[a]The Dukes classifications do not encompass all three prognostic factors in one staging system. Dukes B is a composite of better (T3, N0, M0) and worse (T4, N0, M0) prognostic groups, as is Dukes C (any T, N1, M0 and any T, N2, M0).

Delineation of Normal Mural Components by Sectional Imaging

Five discrete layers of the wall are shown by conventional endoscopic ultrasonography. The first hyperechoic and second hypoechoic layers represent the mucosa, the third hyperechoic layer represents the submucosa, the fourth hypoechoic layer is the muscularis propria, and the fifth hyperechoic layer reflects the subserosa and serosa (Figs. 5–3 and 5–4). In the esophagus, lacking a serosa, the latter represents adventitia. With the development of small 15–20 MHz ultrasonic probes, nine distinct layers of the normal esophageal and gastric wall may be clearly visualized,[33,34] permitting delineation of the lamina propria and muscularis mucosae in addition to a three-layered muscularis propria (Fig. 5–5).

Recent investigations have advanced the accuracy of CT in the detection and staging of gastric cancer. Minami et al.[35] and Cho et al.[36] refined a protocol in which the normal gastric wall showed a two- or three-layered structure: an inner mucosal layer with marked enhancement, an outer submucosal layer with lower attenuation, and another outer muscular-serosal layer with moderate enhancement. Improving the protocol further with the use of dual-phase spiral CT with narrow collimation and close interscan spacing may increase the accuracy of CT.

In dynamic multiphasic MR imaging of the stomach, a decisive feature is a low-signal-intensity band that shows irregularity in an area of extraserosal invasion by an advanced carcinoma (Fig. 5–6). This band is not a morphologic structure but rather a chemical shift misregistration artifact and a phase-cancellation artifact between fat and water.[37]

Identification of the layers of the circumference of the rectal wall is accomplished by plain and contrast-enhanced MR imaging with the endorectal surface coil[38] (Fig. 5–7).

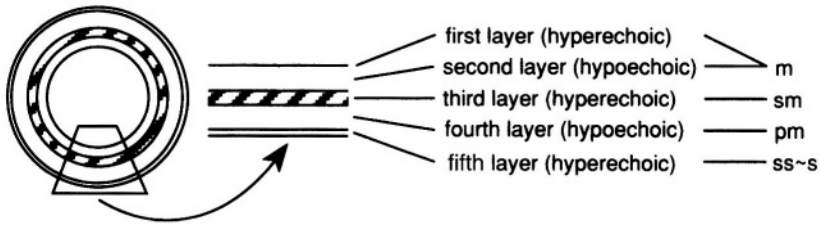


Fig. 5–3. Diagram showing the normal layers of the colon.
m = mucosa; *sm* = submucosa; pm = muscularis propria; ss ~ s = subserosa ~ serosa.
(Reproduced from Hirata et al: Endoscopic ultrasonography in the assessment of colonic wall invasion by adjacent diseases. Abdom Imaging 1994; 19:21–26.)

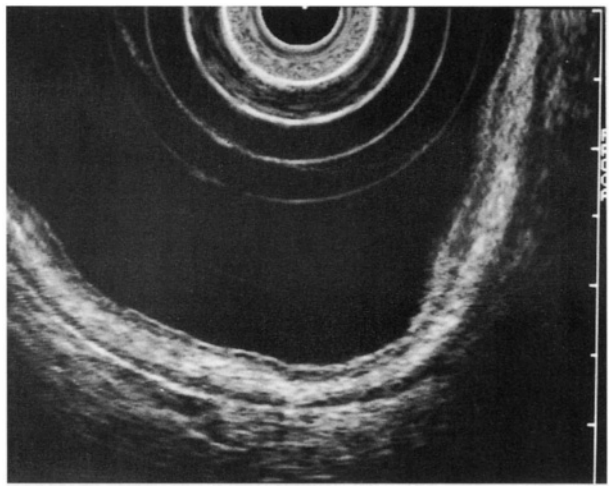


Fig. 5–4. Normal gastric wall demonstrated by EUS with a 20-MHz transducer showing the layered structure of the gastrointestinal wall.

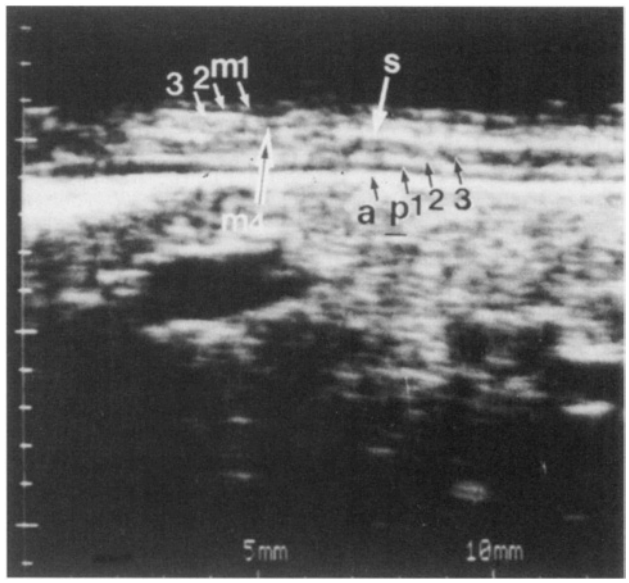


Fig. 5–5. Nine distinct layers of the normal esophageal wall demonstrated in a patient with a small 20-MHz ultrasonic probe.
The mucosa consists of four layers: the first and second layers *(m1* and *m2)* represent the epithelium, the third layer *(m3)* the lamina propria, and the fourth layer *(m4)* the muscularis mucosae. The submucosa *(s)* is seen as the hyperechoic fifth layer. The muscularis propria is imaged as three layers: the sixth layer *(p1)* is the circular muscle, the seventh layer *(p2)* is an interface of connective tissue, and the eighth layer *(p3)* is the longitudinal muscle. The adventitia *(a)* is represented by the hyperechoic ninth layer.
(Reproduced from Murata et al.[33])

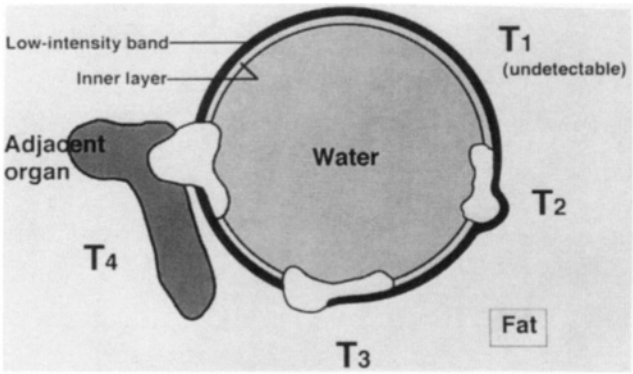


Fig. 5–6. T staging of gastric cancer by MR imaging.
T1 = Lesion is undetectable since there is no abnormal enhancement. *T2* = A clear, smooth low-intensity band surrounds the enhanced lesion. *T3* = The low-intensity band is interrupted. *T4* = The low-intensity band has disappeared, and there is contiguous extension of the enhanced lesion to adjacent organs.
(Reproduced from Oi et al.[37])

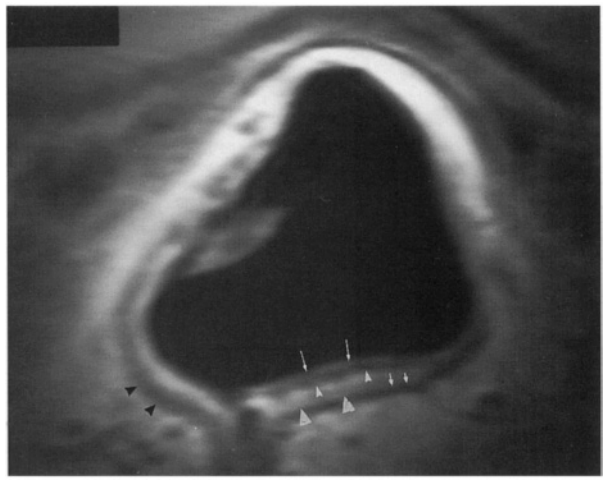


Fig. 5–7. Endorectal MR image of the normal rectal wall.
Multiple layers are visualized: high-signal-intensity mucus within the rectal lumen *(thin white arrows),* low-signal-intensity mucosal layer (mucosa and muscularis mucosae) *(small white arrowheads),* high-signal-intensity submucosal layer *(large white arrowheads),* low-signal-intensity muscularis propria *(small white arrows),* and high-signal-intensity perirectal fat *(black arrowheads).*
(Reproduced from Pegios et al.[38])

T Staging

In the diagnosis and staging of esophageal cancer, CT is highly accurate for detecting distant metastases, especially to the liver, and for determining advanced local spread involving vital mediastinal structures. It cannot, however, distinguish tumors that invade only the mucosa or submucosa (T1) from tumors that invade the muscularis propria (T2). Consequently, CT is much more reliable for classifying stage III and stage IV lesions than stage I and stage II lesions. In contrast, EUS is very accurate for diagnosing stage I and stage II lesions, often good for stage III lesions, and of limited accuracy for stage IV lesions.

T1 Stage

In the esophagus, the distinction of cancer involving only the mucosa (T1m) (Fig. 5–8) from cancer invading the submucosa (T1sm) (Figs. 5–9 and 5–10) may guide the application of endoscopic resection.[33]

Early gastric cancer may be defined on contrast-enhanced dynamic CT as an enhancing lesion with an intact low-density stripe at its base (Fig. 5–11).

Figure 5–12 illustrates a thickening limited to the mucosal layer of the rectum with a normal muscularis mucosae representing a sessile adenoma, shown by endorectal MRI. In contrast, Figure 5–13 shows mucosal thickening secondary to carcinoma with preservation of the submucosal layer but with a small regional metastatic lymph node.

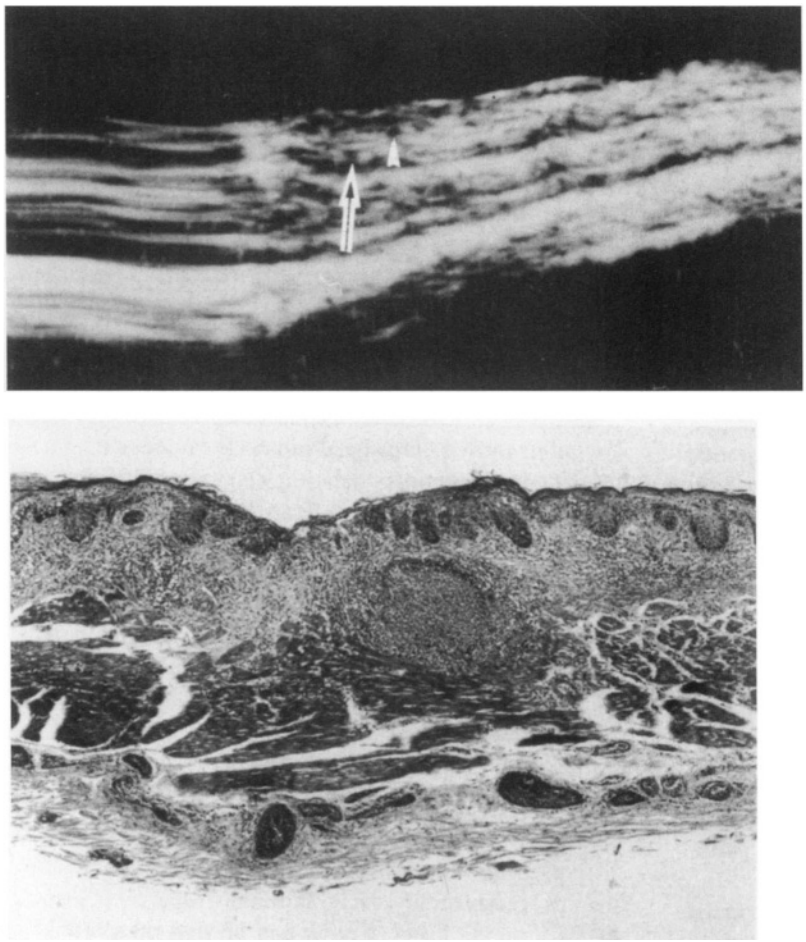


Fig. 5–8. Esophageal cancer limited to the lamina propria shown with a small 20-MHz EUS probe.
(a) The *white arrowhead* indicates cancer invading the lamina propria. The *outlined black arrow* demonstrates an intact muscularis mucosae.
(b) The endoscopic mucosal resection specimen.
(Reproduced from Murata et al.[33])

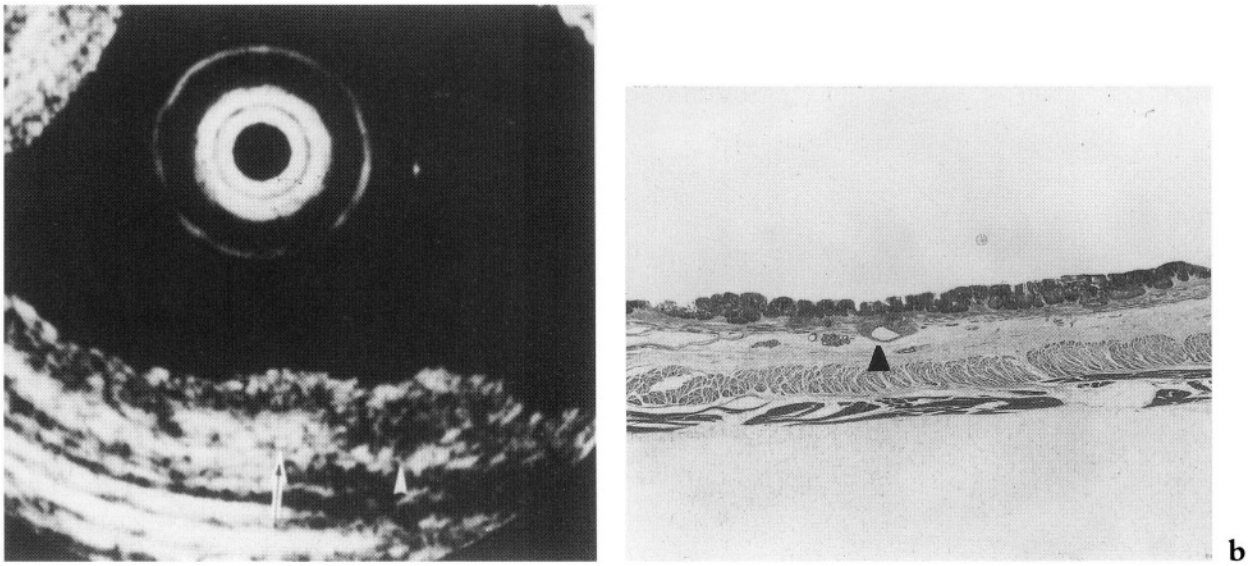


Fig. 5–9. Esophageal cancer invading the muscularis mucosae shown with a small 20-MHz EUS probe.
(a) The *outlined black arrow* indicates the muscularis mucosae and the *white arrowhead* designates the point at which the m4 layer is destroyed by tumor infiltration.
(b) The resected specimen. The *black arrowhead* shows the point of cancerous destruction of the muscularis mucosae.
(Reproduced from Murata et al.[33])

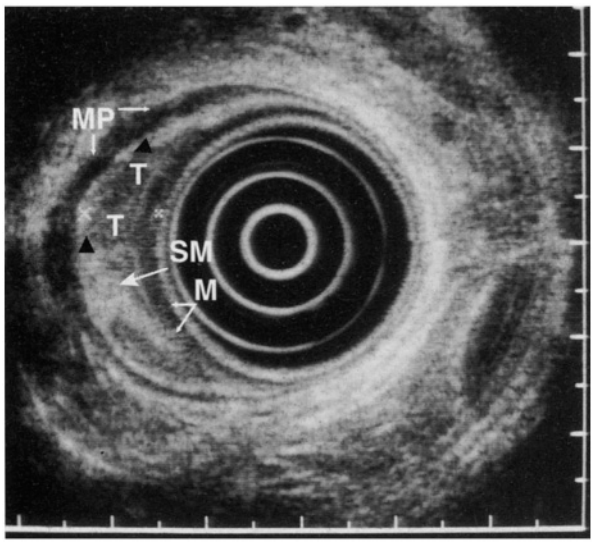


Fig. 5–10. T1sm esophageal cancer.
EUS reveals a hypoechoic tumor *(T)* limited to the mucosa *(M)* and submucosa *(SM).* A portion of the submucosa beyond the tumor is still intact *(arrowheads).* *MP* = muscularis propria.
(Reproduced from Tio TL.[39])



Fig. 5–11. Early gastric cancer (T1).
Early phase of bolus-enhanced dynamic CT of water-distended stomach shows a small, well-defined, elevated lesion *(arrowheads)* with moderate enhancement in the posterior wall of gastric antrum. Low-attenuation stripe of the submucosa *(arrows)* is clearly seen at base of tumor.
(Reproduced from Cho et al.[36])

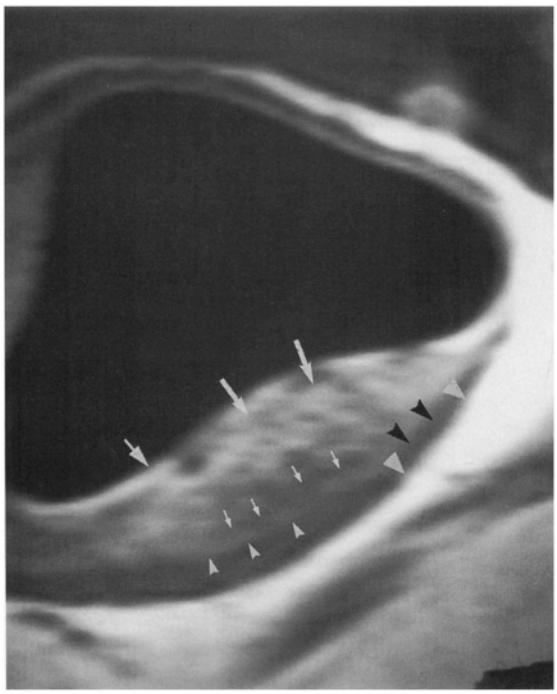


Fig. 5–12. Sessile tubulovillous adenoma of the rectum. Endorectal T1-weighted contrast-enhanced MR image demonstrates the tumor. The different layers of the rectal wall can be identified. From lateral to medial: the high signal intensity of the perirectal fat tissue *(white arrowheads),* the low signal intensity of the muscularis propria *(black arrowheads),* a layer of high signal intensity representing the submucosal core *(small white arrowheads),* and the low signal intensity of the muscularis mucosae *(thin white arrows).* Note the high signal intensity of the thickened mucosal layer *(large white arrows).*
(Reproduced from Pegios et al.[38])

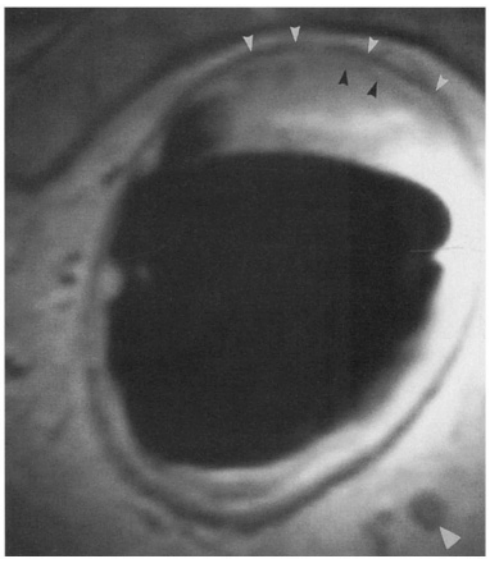


Fig. 5–13. T1N1 rectal carcinoma. Endorectal T2-weighted MRI demonstrates a sessile lesion of the rectum showing focal mucosal thickening with a high-signal-intensity submucosal core *(black arrowheads).* The muscularis propria *(small white arrowheads)* layer has not been involved. One small, 3-mm-diameter perirectal lymph node is completely replaced by soft tissue *(large white arrowhead).*
(Reproduced from Pegios W, et al: MRI diagnosis and staging of rectal carcinoma. Abdom Imaging 21:211–218, 1996.)

T2 Stage

Extension into the muscularis propria establishes a carcinoma as stage T2 (Figs. 5–14 through 5–16).

T3 Stage

In esophageal carcinoma, the hallmark of a T3 lesion is penetration into the adventitia (Figs. 5–17 and 5–18).

In the stomach, T3 tumors show a reticular or an irregular outer border of thickened gastric wall and/or a blurred fat plane around the lesion (Figs. 5–19 through 5–22).

T3 rectal cancers invade through the muscularis propria to extend into the perirectal fat (Fig. 5–23).

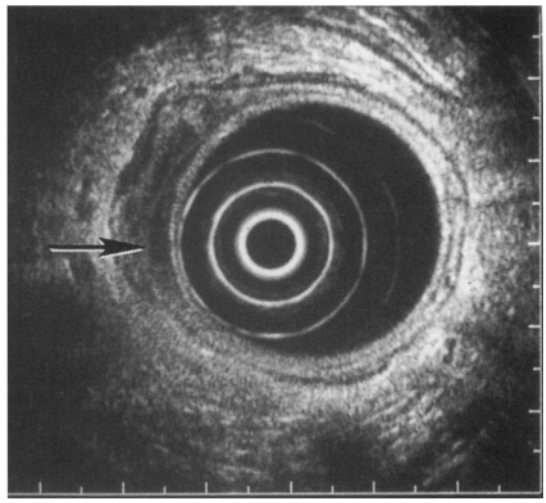


Fig. 5–15. T2 rectal carcinoma.
EUS demonstrates a hypoechoic tumor deeply invading the muscularis propria layer *(arrow).*

T4 Stage

In esophageal carcinoma, direct invasion of mediastinal structures can be predicted using criteria of mass effect or localized loss of fat planes[39,42–47] (Figs. 5–24 through 5–30). Actual unresectability, however, remains difficult to predict with CT or MRI.[47-52] In the assessment of unresectability by EUS, criteria include tumor invasion into the left atrium, the wall of the descending aorta, the pulmonary vein and/or artery, the tracheobronchial system, and a vertebral body.[39]

T4 gastric cancers show obliteration of the fat plane between the gastric tumor and the adjacent organ (Figs. 5–31 and 5–32).

text continues on page 283

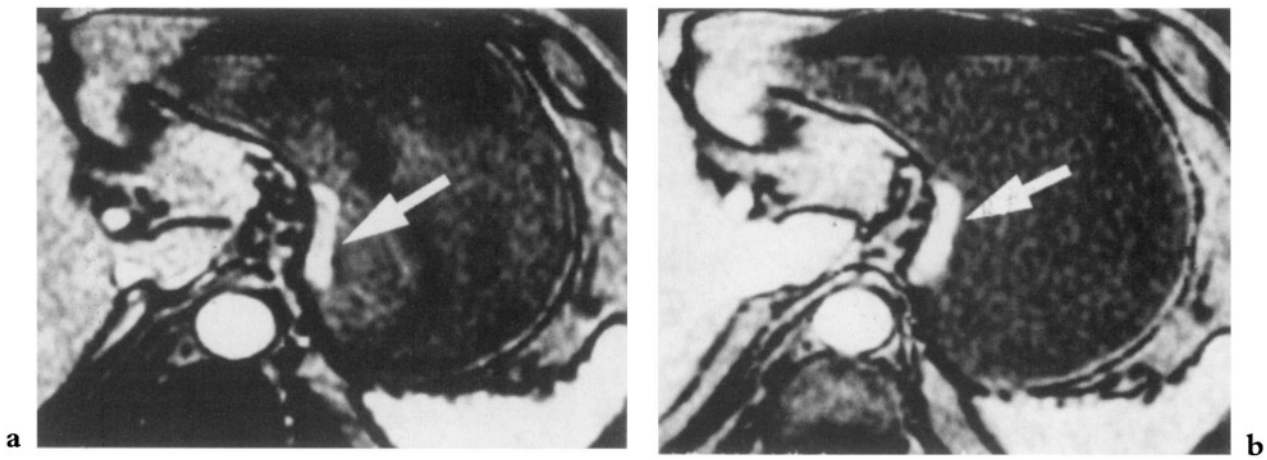
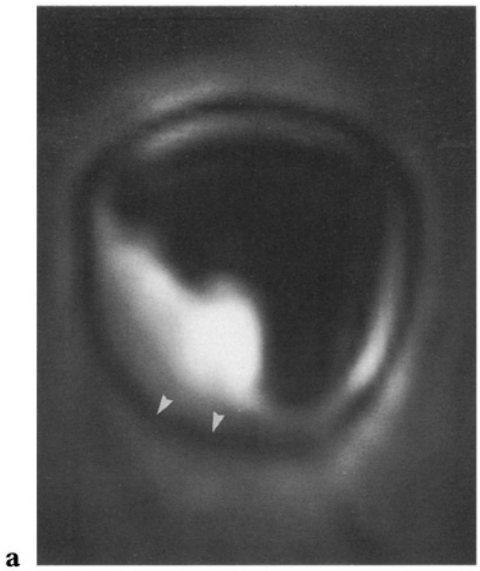
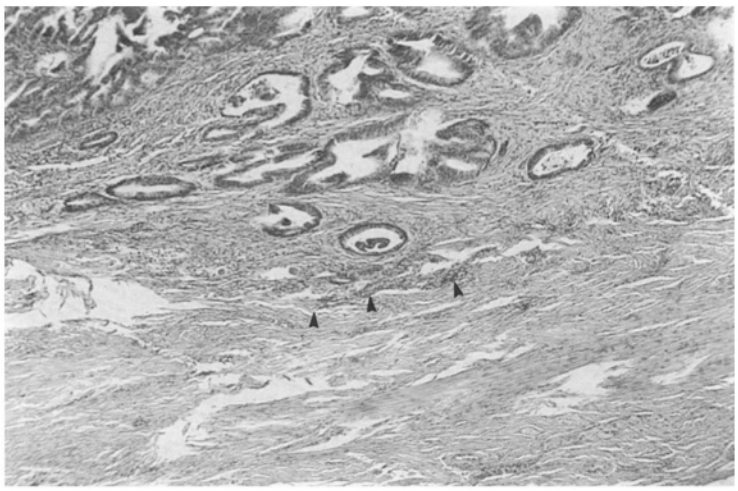


Fig. 5–14. T2 gastric cancer demonstrated by dynamic MR imaging.
(a) Early-phase (25 sec) and **(b)** late-phase (120 sec) images show the gastric cancer in the subcardia *(arrow)* as a highly enhanced thickened wall. A low-intensity band is observed around the stomach, and that of the lesion remains clear and smooth.
(Reproduced from Oi et al.[37])



a



b

Fig. 5–16. T2 rectal cancer demonstrated by endorectal MR image.
(a) Dynamic turbo FLASH sequence after Gd-DTPA administration demonstrates a depressed lesion and complete disruption of the submucosa with an involved but not disrupted muscularis propria *(white arrowheads).*
(b) Histopathology demonstrates tumor invading into but not through the muscularis propria *(black arrowheads)* (hematoxylin-eosin stain, × 20).
(Reproduced from Pegios et al.[38])

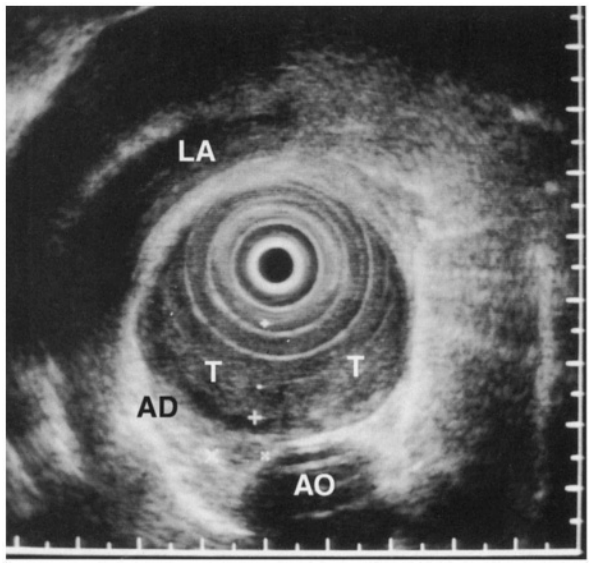


Fig. 5–17. T3 esophageal cancer.
EUS obtained from the midesophagus approximately at the level of the carina reveals a hypoechoic semicircular tumor *(T)* with penetration into the adventita *(AD).* The border between the tumor and the aortic wall *(AO)* is still intact. *LA* = left atrium.
(Reproduced from Tio.[39])

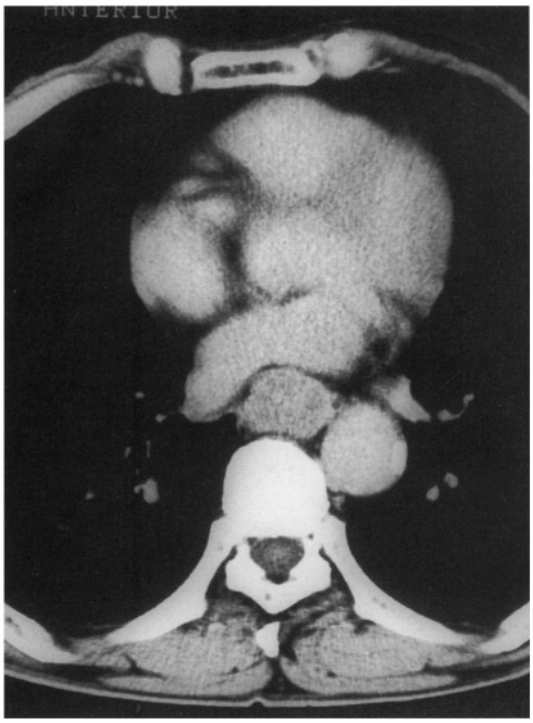


Fig. 5–18. T3 carcinoma of the lower esophagus.
On CT, the slightly irregular outlines of the tumor are due to invasion of the periesophageal fat.
(Reproduced from van Overhagen and Becker.[40])

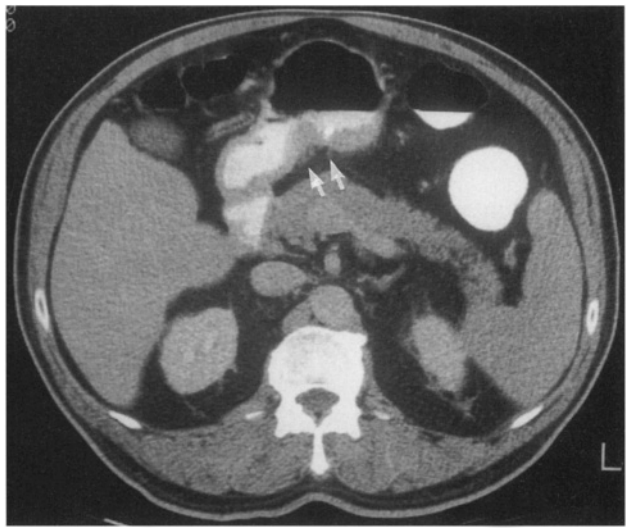


Fig. 5–19. T3 carcinoma of the gastric antrum.
CT demonstrates focal nodular thickening of the posterior wall with mild irregularity of the outer contour *(arrows),* indicating direct extension of tumor into the perigastric fat.
(Reproduced from Yee and Halvorsen.[41])

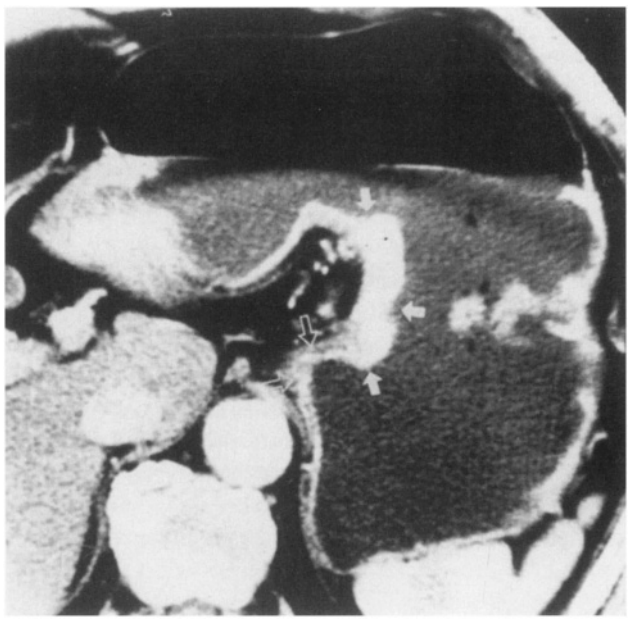


Fig. 5–20. T3 gastric cancer.
Early phase of bolus-enhanced dynamic CT of water-distended stomach shows a well defined, protruding lesion *(solid arrows),* with destruction of the multilayered pattern and marked enhancement at lesser curvature of upper body of stomach. The lesion has a reticular outer margin in contrast to the normal three-layered pattern of uninvolved gastric wall *(open arrows)* at cardia.
(Reproduced from Cho et al.[36])

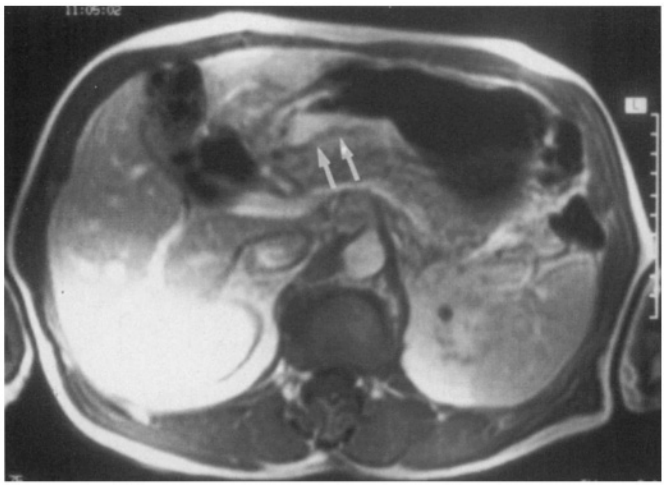
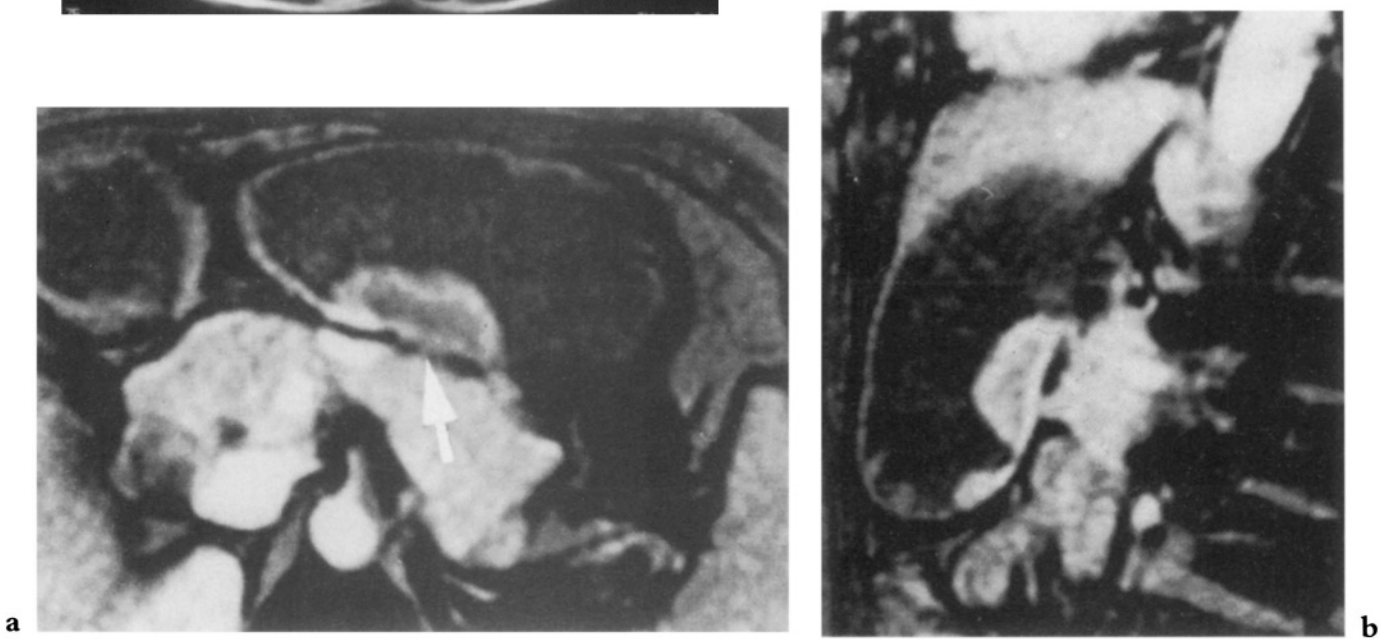
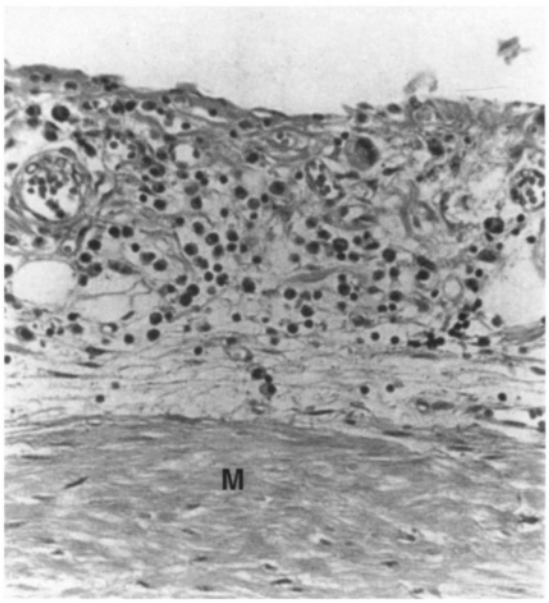


Fig. 5–21. T3 gastric carcinoma.
T1-weighted gradient-echo MR image following intravenous administration of Gd-DTPA shows marked enhancement of the thickened antral wall with evidence of irregularity and blurring of the low-signal band along the posterior border of the stomach *(arrow).* This reflects tumor infiltration through all layers of the gastric wall as well as extraserosal extension.
(Reproduced from Yee and Halvorsen.[41])



a **b**



c

Fig. 5–22. T3 gastric cancer demonstrated by dynamic MR imaging.
(a) Late phase image shows that the low-intensity band at the base of the enhancing tumor is interrupted *(arrow).*
(b) Sagittal image during delayed phase (10 min) shows the enhanced elevated lesion in the posterior wall of the gastric body.
(c) Microscopic section of this interrupted-band lesion reveals extraserosal invasion by the gastric cancer. *M* = muscularis propria. (hematoxylin-eosin stain, × 400.)
(Reproduced from Oi et al.[37])

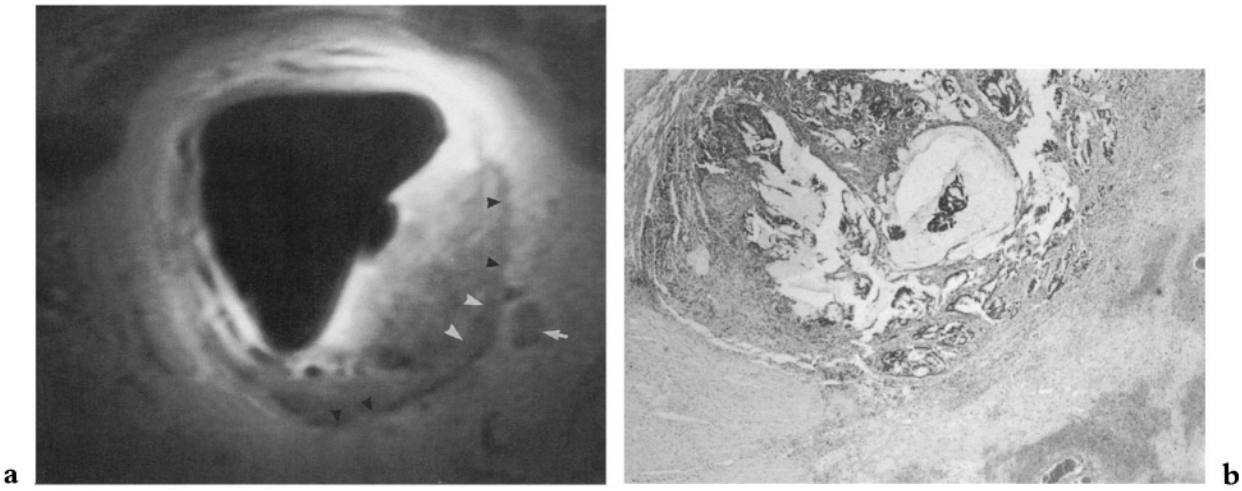


Fig. 5–23. T3 polypoid carcinoma of the rectum.
(a) Endorectal T1-weighted MR image after Gd-DTPA administration demonstrates the inhomogeneous mucosal thickening of a rectal cancer that completely disrupts the submucosa *(white arrowheads)* and the muscularis propria *(black arrowheads).* Additionally, one 5-mm-diameter perirectal lymph node *(white arrow)* was positive for carcinoma at pathologic examination.
(b) Resected specimen shows tumor invading completely through the muscularis propria with focal strands extending into perirectal fat (hematoxylin-eosin stain, × 30).
(Reproduced from Pegios et al.[38])

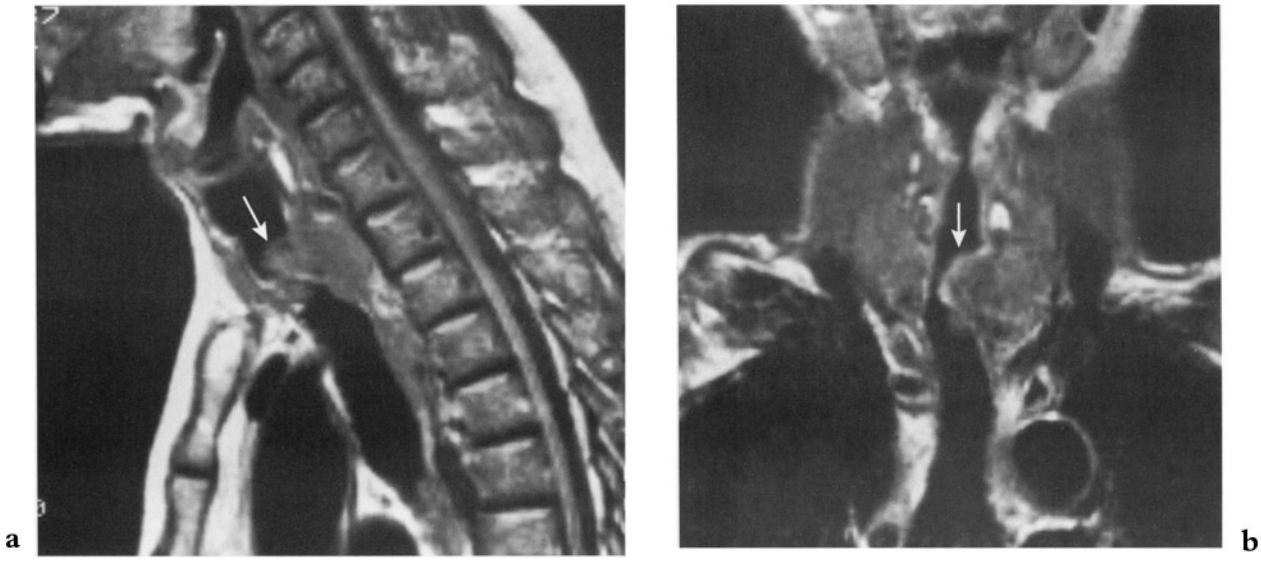


Fig. 5–24. T4 esophageal carcinoma.
(a) Sagittal and **(b)** coronal MR views at the level of the cervicothoracic junction reveal direct invasion of an esophageal neoplasm into the lumen of the trachea *(arrow).*
(Reproduced from Balzarini et al.[42])

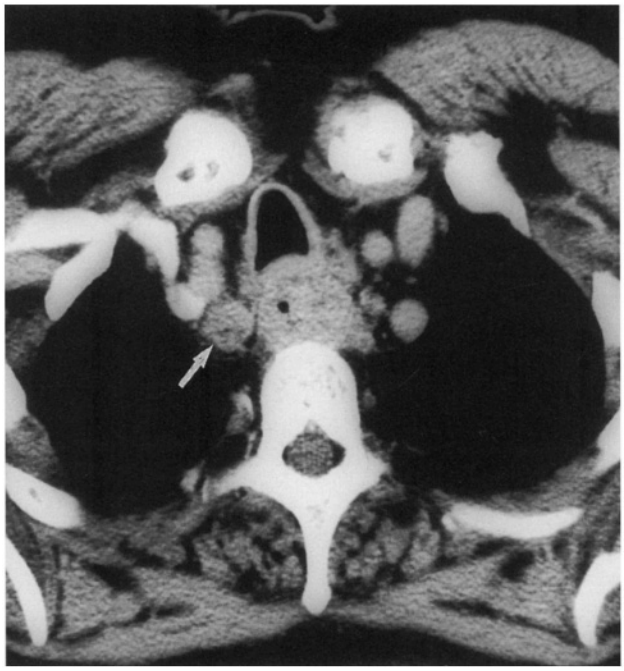


Fig. 5–25. Unresectable squamous cell carcinoma of the upper thoracic esophagus with indentation of the posterior wall of the trachea indicating neoplastic invasion (T4).
Note the enlarged periesophageal lymph node adjacent to the tumor *(arrow).*
(Reproduced from van Overhagen and Becker.[40])

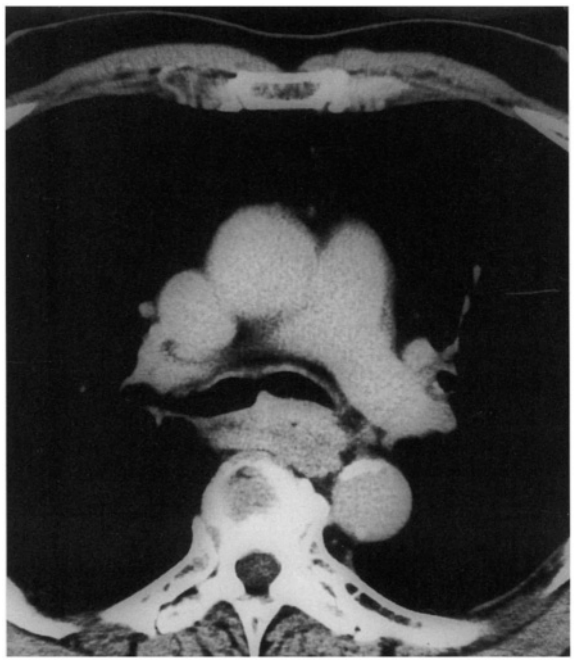


Fig. 5–26. Squamous cell carcinoma of the middle thoracic esophagus.
A large esophageal mass (T4) indents the posterior wall of the left mainstem bronchus. Tracheobronchial invasion and resectability were confirmed at surgery.
(Reproduced from van Overhagen and Becker.[40])

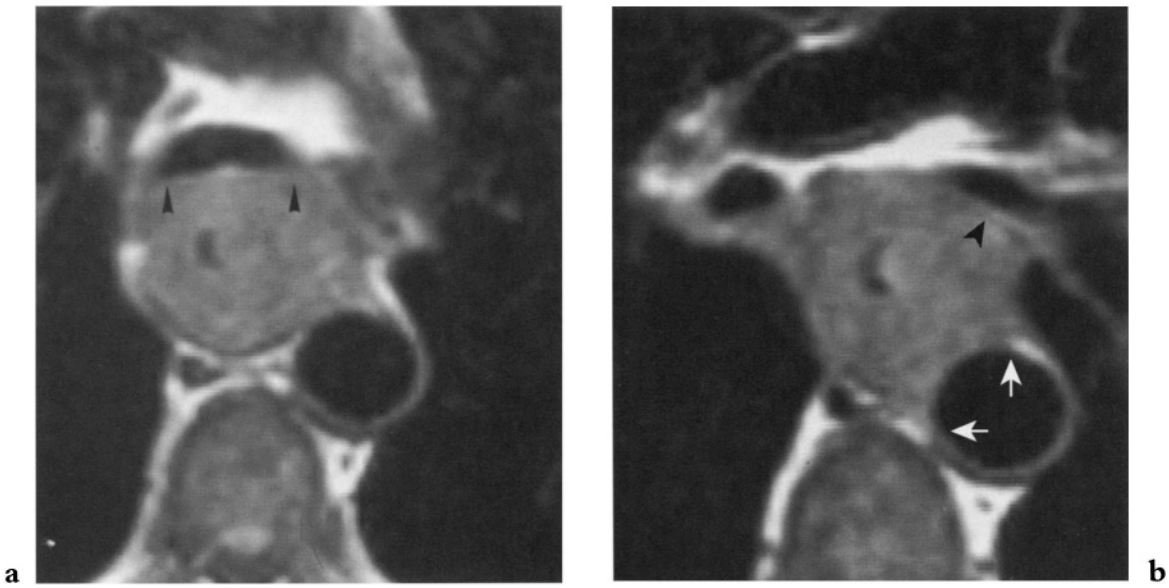


Fig. 5–27. T4 esophageal carcinoma with invasion of mediastinal structures.
Axial MR images at the level of the tracheal bifurcation **(a)** and subcarinal space **(b).**
(a) Extraluminal extension of the tumor mass has obliterated the fat adjacent to the wall of the main bronchi *(arrowheads).*
(b) With neoplastic invasion of the subcarinal space, the left main bronchus is displaced anteriorly and compressed *(arrowhead).* The angle of contact between the tumor and aorta is approximately 100° *(white arrows).* The triangular fat plane between the esophagus, spine, and aorta has been obliterated. All criteria of aortic invasion are present.
(Reproduced from Balzarini et al.[42])

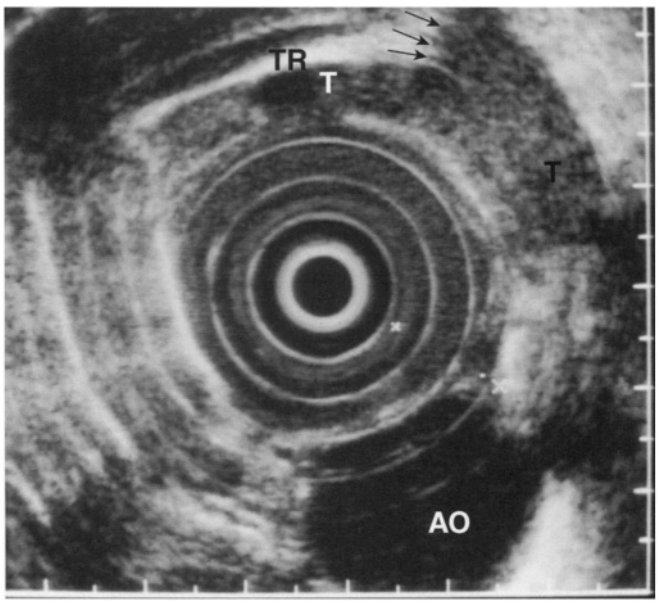


Fig. 5–28. T4 esophageal cancer.
EUS at the level of the carina shows a transmural hypoechoic tumor *(T)* with deep penetration into and beyond *(arrows)* the posterior wall of the trachea *(TR). AO* = aorta.
(Reproduced from Tio.[39])

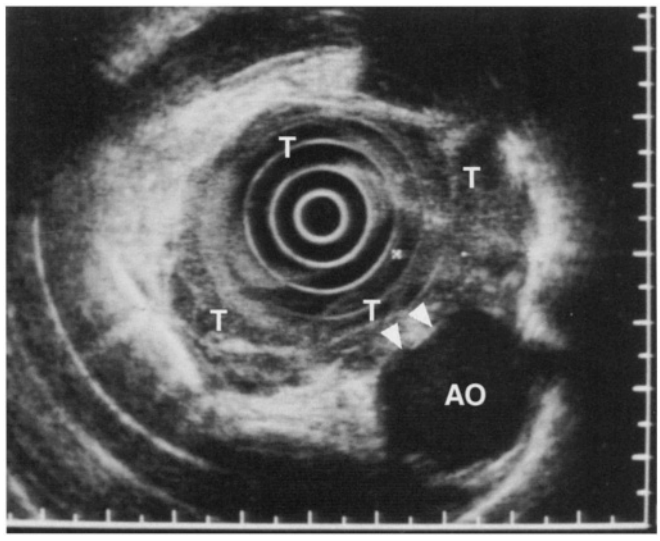


Fig. 5–29. T4 esophageal cancer.
EUS obtained from the level of the distal esophagus reveals a circular hypoechoic tumor *(T)* with deep infiltration *(arrowheads)* into the aortic wall *(AO).*
(Reproduced from Tio.[39])

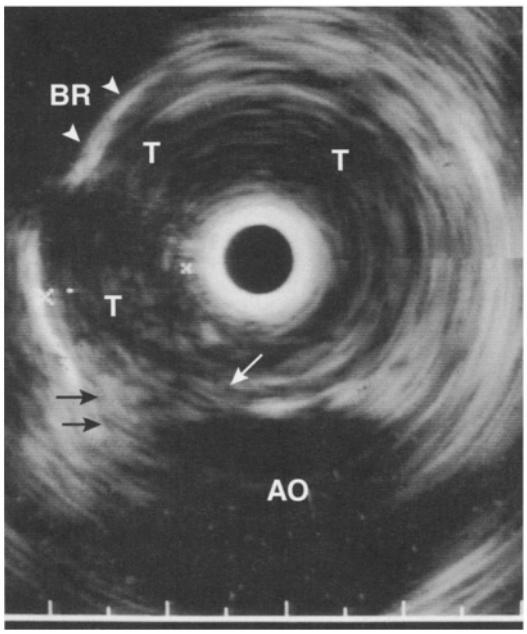


Fig. 5–30. T4 esophageal cancer demonstrated with catheter echoprobe.
EUS obtained with 7.5-MHz miniature catheter echoprobe reveals a transmural hypoechoic tumor *(T)* with multiple invasion into the aortic wall *(AO)* at 7 o'clock *(arrows)* and into the right bronchus *(BR)* and the bifurcation *(arrowheads)* of the bronchus seen as hyperechoic *(white)* lines between the esophagus and the left atrium.
(Reproduced from Tio.[39])

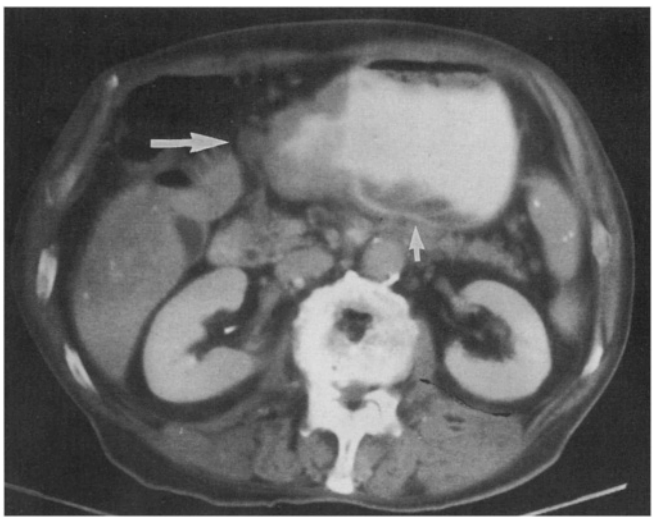


Fig. 5–31. T4 gastric carcinoma.
CT demonstrates loss of the normal fat plane between the diffuse thickening of the wall of the antrum and the body of the pancreas *(small arrow),* indicating pancreatic invasion. Metastatic perigastric adenopathy is present *(large arrow),*
(Reproduced from Yee and Halvorsen.[41])

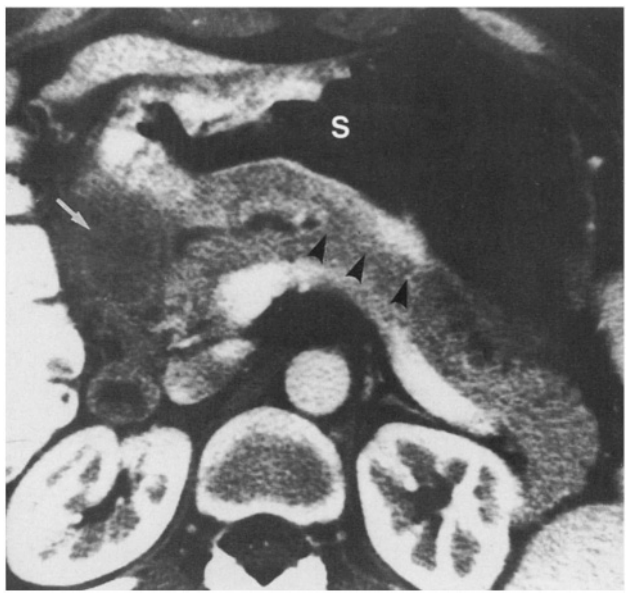


Fig. 5–32. T4 gastric cancer.
Bolus-enhanced dynamic CT in early phase shows diffuse wall thickening and destruction of multilayered pattern involving antrum and body of stomach (*S*) with strong heterogeneous enhancement. Focal obliteration of the fat plane *(arrowheads)* between thickened gastric wall and pancreatic body, indicating pancreatic invasion, as well as an enlarged metastatic subpyloric lymph node *(arrow)* are clearly identified.
(Reproduced from Cho et al.[36])

Lymph Node Metastases

Detection of lymphadenopathy is difficult by sectional imaging. Normal-sized lymph nodes may harbor micrometastases (Fig. 5–33), and some enlarged nodes are due to benign reactive hyperplasia.

The original EUS criteria of distinguishing between benign reactive and metastatic lymph nodes on the basis of echo texture, size, and margination (Fig. 5–34) is now undergoing intense doubt.[53–56]

In the past, the diagnosis of lymph node abnormalities on CT scans has been based on size criteria, with the upper limits of normal in the upper abdomen reported as varying from 6 mm to 11 mm.[57,58] However, accuracy is limited by the presence of micrometastases and reactive nodal hyperplasia. A recent report of improved detection using thin-sector contrast enhanced helical CT offers additional criteria to size alone in diagnosing metastatic lymph nodes, based on attenuation and configuration.[59] The nodal pathways in gastrointestinal cancers are documented in Chapter 6.



Fig. 5–33. Micrometastases in lymph node.
Histologic section demonstrates that metastatic cells in a small zone of a lymph node *(arrows)* would be undetectable by sectional imaging.
(Courtesy of Clive Bartram, M.D., St. Mark's Hospital, Northwick Park, England.)

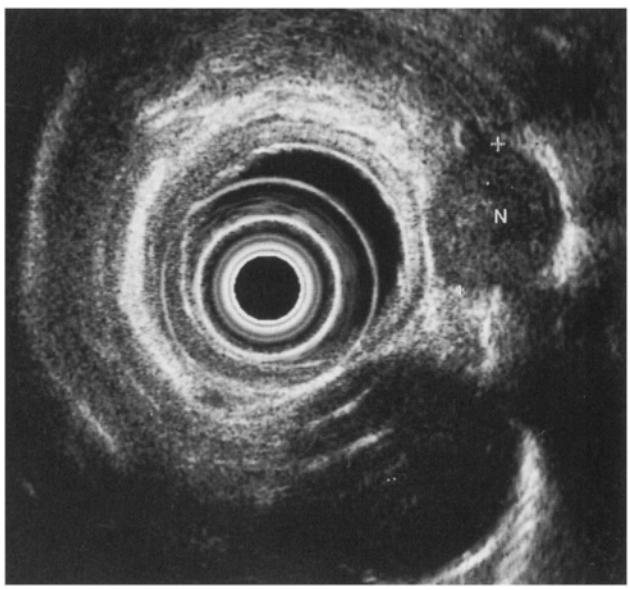


Fig. 5–34. Metastatic lymph node shown by EUS.
Enlarged, spherical hypoechoic, sharply marginated node *(N)* in a case of esophageal carcinoma fulfills the original criteria. (Courtesy of Paul Fockens, M.D., Academic Medical Center, Amsterdam, The Netherlands.)

References

1. Hermanek P, Sobin LH: UICC: TNM Classification of Malignant Tumours, 4th ed., 2nd rev. Springer-Verlag, Berlin, 1992.
2. Spiessel B, Beahrs OH, Hermanek P, et al: UICC: TNM Atlas: Illustrated Guide to the TNM/pTNM Classification of Malignant Tumours, 3rd ed., 2nd rev. Springer-Verlag, Berlin, 1992.
3. Fleming ID, Cooper JS, Henson DE, et al: Manual for Staging of Cancer, 5th ed. Lippincott-Raven, Philadelphia, 1997.
4. Sobin LH, Ros PR: Radiology and the new TNM classification of tumors: The future. Radiology 1990; 176:1–4.
5. Japanese Committee for Registration of Esophageal Cancer: A proposal for a new TNM classification of esophageal carcinoma. Jpn J Clin Oncol 1985; 14:625–636.
6. Miwa K, Japanese Research Society for Gastric Cancer: Evaluation of the TNM classification of stomach cancer and proposal for its rational stage-grouping. Jpn J Clin Oncol 1984; 14:385–410.
7. Dukes CE: The classification of cancer of the rectum. J Pathol Bacteriol 1932; 35:323–332.
8. Iizuka T, Isono K, Kakegawa T, et al: Parameters linked to ten-year survival in Japan of resected esophageal carcinoma. Chest 1989; 96:1005–1011.
9. Siewert JR, Holscher AH, Dittler HJ: Preoperative staging and risk analysis in esophageal carcinoma. Hepatogastroenterology 1990; 37:382–387.
10. Skinner DB, Ferguson MK, Soriano A, et al: Selection of operation for esophageal cancer based on staging. Ann Surg 1986; 204:391–401.
11. Gertsch P, Vauthey J-N, Lustenberger AA, et al: Long-term results of transhiatal esophagectomy for esophageal carcinoma. Cancer 1993; 72:2312–2319.
12. Sugimachi K, Kitamura K, Matsuda H, et al: Proposed new criteria for early carcinoma of the esophagus. Surg Gynecol Obstet 1991; 173:303–308.
13. Japanese Society for Esophageal Diseases: Guidelines for the Clinical and Pathologic Studies on Carcinoma of the Esophagus, 8th ed. Kanehara, Tokyo, 1992.
14. Natusgoe S, Aikou T, Yoshinaka H, et al: Lymph node metastasis of early stage carcinoma of the esophagus and of the stomach. J Clin Gastroenterol 1995; 20:325–328.
15. Japanese Research Society for Gastric Cancer: Japanese Classification of Gastric Carcinoma: General Rules for the Gastric Cancer Study. Kanehara, Tokyo, 1995; 1–104.
16. Maruyama K, Gunvén P, Okabayashi K, et al: Lymph node metastases of gastric cancer. Ann Surg 1989; 210:596–602.
17. Ichikura T, Tomimatsu S, Okusa Y, et al: Comparison of the prognostic significance between the number of metastatic lymph nodes and nodal stage based on their location in patients with gastric cancer. J Clin Oncol 1993; 11:1894–1900.
18. Hisamichi S, Fukao A, Sugawara N, et al: Evaluation of mass screening programme for stomach cancer in Japan. *In* Cancer Screening. Edited by AB Miller, J Chamberlain, NE Day, et al. Cambridge University Press, Cambridge, 1991; pp 357–370.
19. Kaneko E, Nakamura T, Umeda N, et al: Outcome of gastric carcinoma detected by gastric mass survey in Japan. Gut 1997; 18:626–630.
20. Kawai K, Watanabe Y: The impact of mass screening on gastric cancer mortality in Japan. Gastrointest Endosc 1998; 47:320–322.
21. Torii A, Sakai M, Kajiyama T, et al: Endoscopic aspiration mucosectomy as curative endoscopic surgery: Analysis of 24 cases of early gastric cancer. Gastrointest Endosc 1995; 42:475–479.
22. Yanai H, Matsumoto Y, Harada T, et al: Endoscopic ultrasonography and endoscopy for staging depth of invasion in early gastric cancer: A pilot study. Gastrointest Endosc 1997; 46:212–216.
23. Kojima T, Parra-Blanco A, Takahashi H, et al: Outcome of endoscopic mucosal resection for early gastric cancer: Review of the Japanese literature. Gastrointest Endosc 1998; 48:550–554.
24. Sibille A, Descamps C, Jonard P, et al: Endoscopic Nd:YAG treatment of superficial gastric carcinoma: Experience in 18 Western inoperable patients. Gastrointest Endosc 1995; 42:340–345.
25. Keeney G, Jafri SZ, Mezwa DG: Computed tomographic evaluation and staging of cecal carcinoma. Gastrointest Radiol 1989; 14:65–69.
26. Tio TL, Coene PPLO, van Delden OM, et al: Colorectal carcinoma: Preoperative TNM classification with endosonography. Radiology 1991; 179:165–170.
27. Yoshida M, Tsukamoto Y, Niwa Y, et al: Endoscopic assessment of invasion of colorectal tumors with a new high-frequency ultrasound probe. Gastrointest Endosc 1994; 41:587–592.
28. Hamada S, Kazuya A, Chijiiwa X, et al: Preoperative staging of colorectal cancer by a 15 MHz ultrasound miniprobe. Surgery 1998; 123:264–269.
29. Minsky BD, Mies C, Recht A, et al: Resectable adenocarcinoma of the rectosigmoid and rectum. I: Patterns of failure and survival. Cancer 1988; 61:1408–1416.

30. Minsky BD, Mies C, Rich TA, et al: Potentially curative surgery of colon cancer. I: Patterns of failure and survival. J Clin Oncol 1988; 6:106–118.
31. Krook JE, Moertel CG, Gunderson LL, et al: Effective surgical adjuvant therapy for high-risk rectal carcinoma. N Engl J Med 1991; 324:709–715.
32. Cohen AM, Tremittera S, Candela F, et al: Prognosis of node-positive colon cancer. Cancer 1991; 67:1859–1861.
33. Murata Y, Suzuki S, Ohta M, et al: Small ultrasonic probes for determination of the depth of superficial esophageal cancer. Gastrointest Endosc 1996; 44:23–28.
34. Akahoshi K, Chijiiwa Y, Hamada S, et al: Pretreatment staging of endoscopically early gastric cancer with a 15 MHz ultrasound catheter probe. Gastrointest Endosc 1998; 48:470–476.
35. Minami M, Kawauchi N, Itai Y: Gastric tumors: Radiologic-pathologic correlation and accuracy of CT staging with dynamic CT. Radiology 1992; 185:173–178.
36. Cho J, Kim J-K, Rho S, et al: Preoperative assessment of gastric carcinoma: Value of two-phase dynamic CT with mechanical IV injection of contrast material. AJR 1994; 163:69–75.
37. Oi H, Matsushita M, Murakami T, et al: Dynamic MR imaging for extraserosal invasion of advanced gastric cancer. Abdom Imaging 1997; 22:35–40.
38. Pegios W, Vogl Th. J, Hünerbein M, et al: Diagnosis and staging of rectal carcinoma by magnetic resonance imaging. *In* Neoplasms of the Digestive Tract: Imaging, Staging and Management. Edited by MA Meyers. Lippincott-Raven, Philadelphia, 1998, pp 269–276.
39. Tio TL: Diagnosis and staging of esophageal carcinoma by endoscopic ultrasonography. *In* Neoplasms of the Digestive Tract: Imaging, Staging and Management. Edited by MA Meyers. Lippincott-Raven, Philadelphia, 1998, pp 61–70.
40. van Overhagen H, Becker CD: Diagnosis and staging of carcinoma of the esophagus and gastroesophageal junction, and detection of postoperative recurrence by computed tomography. *In* Neoplasms of the Digestive Tract: Imaging, Staging and Management. Edited by MA Meyers. Lippincott-Raven, Philadelphia, 1998, pp 31–48.
41. Yee G, Halvorsen RA Jr: Diagnosis and staging of gastric carcinoma by computed tomography and magnetic resonance imaging. *In* Neoplasms of the Digestive Tract: Imaging, Staging and Management. Edited by MA Meyers. Lippincott-Raven, Philadelphia, 1998, pp 125–136.
42. Balzarini L, Potepan P, Musumeci RN: Diagnosis and staging of esophageal carcinoma by magnetic resonance imaging. *In* Neoplasms of the Digestive Tract: Imaging, Staging and Management. Edited by MA Meyers. Lippincott-Raven, Philadelphia, 1998, pp 49–60.
43. Quint LE, Glazer GM, Orringer MB: Esophageal imaging by MR and CT: Study of normal anatomy and neoplasms. Radiology 1985; 156:727–731.
44. Quint LE, Francis IR, Glazer GM, et al: CT and MR staging of tumors of the esophagus and gastroesophageal junction and detection of postoperative recurrence. *In* Margulis and Burhenne's Alimentary Tract Radiology, 5th ed. Edited by P Freeny, G Stevenson. Mosby, St Louis, 1994, pp 272–281.
45. Halvorsen RA, Thompson WM: Computed tomographic staging of gastrointestinal tract malignancies. Part I: Esophagus and stomach. Invest Radiol 1987; 22:2–16.
46. Picus D, Balfe DM, Koehler RE, et al: Computed tomography in the staging of esophageal carcinoma. Radiology 1983; 146:433–438.
47. Takashima S, Takeuchi N, Shiozaki H, et al: Carcinoma of the esophagus: CT vs MR imaging in determining resectability. AJR 1991; 156:297–302.
48. Holscher AH, Dittler HJ, Siewert JR: Staging of squamous esophageal cancer: Accuracy and value. World J Surg 1994; 18:312–320.
49. van den Hoed RD, Feldberg MAM, vanLeeuwen MS, et al: CT prediction of irresectability in esophageal carcinoma: Value of additional patient positions and relation to patient outcome. Abdom Imaging 1997; 22:132–137.
50. Koch J, Halvorsen RA Jr: Staging of esophageal cancer: Computed tomography, magnetic imaging, and endoscopic ultrasound. Semin Roentgenol 1994; 29:364–372.
51. Hirai T, Otsuji H, Hirohashi S, et al: Evaluation of MRI for the staging of esophageal cancer. Jpn J Clin Radiol 1990; 35:141–146.
52. Thompson WM, Halvorsen RA Jr: Staging esophageal carcinoma II: CT and MRI. Semin Oncol 1994; 21:447–452.
53. Heintz A, Wahl W, Mildenberger P, et al: Endosonographie beim Oesophaguscarcinom: Ergebnisse einer klinischen Untersuchiung und einer In-vitro-Analyse. Chirurg 1992; 63:629–633.
54. Heintz A, Mildenberger P, Georg M, et al: In vitro studies of lymph node analysis. Gastrointest Endosc Clin N Am 1995; 5:577–586.
55. Hildebrandt U, Klein G, Schwartz HP, et al: Endosonography of pararectal lymph nodes: In vitro and in vivo evaluation. Dis Colon Rectum 1990; 33:863–868.

56. Nielsen MD, Qvitzau S, Pedersen JF: Detection of pericolonic lymph nodes in patients with colorectal cancer: An in vitro and in vivo study of the efficacy of endosonography. AJR 1993; 161:57–60.
57. Balfe DM, Mauro MA, Koehler RE: Gastrohepatic ligament: Normal and pathological CT anatomy. Radiology 1984; 150:485–490.
58. Dorfman RE, Alpern MB, Gross BH, et al: Upper abdominal lymph nodes: Criteria for normal size determined with CT. Radiology 1991; 180:319–322.
59. Fukuya T, Honda H, Hayasha T, et al: Lymph-node metastases: Efficacy of detection with helical CT in patients with gastric cancer. Radiology 1995; 197: 705–711.

Pathways of Lymph Node Metastases in Cancer of the Gastrointestinal and Hepatobiliary Tracts

6

Chusilp Charnsangavej, M.D.

Lymph node metastasis from malignant tumors of the gastrointestinal tract and abdominal organs generally follows lymphatic pathways in the peritoneal ligaments and mesentery or mesocolon that attach the organs to the retroperitoneum and abdominal wall.[1] The pathways of lymphatic drainage accompany the blood vessels supplying or draining the organs, and they are located within the peritoneal ligaments, mesentery, or mesocolon. These blood vessels serve as anatomic landmarks on imaging studies such as CT and MRI. Understanding the pathways of lymph node metastasis helps to identify the expected sites of lymph node metastasis in the staging of cancers originating from the abdominal organs, for surgical planning, and for evaluating patients with suspected recurrent disease after the treatment.

This chapter defines the anatomy of the blood vessels within the peritoneal ligaments, mesentery, and mesocolon as seen on CT or MR imaging and describes the pathways of lymph node metastasis from malignant tumors originating from the gastrointestinal tract and hepatobiliary tracts. The discussion focuses on the organs in the supramesocolic compartment, which include the liver, stomach, and spleen, and in the inframesocolic compartment, which include the colon and small bowel.

The Supramesocolic Compartment

Anatomic Consideration

The liver, stomach, and spleen are the organs in the supramesocolic compartment of the abdomen. The spleen and the liver develop within the peritoneal ligaments known as the dorsal mesogastrium and ventral mesogastrium, respectively. The dorsal mesogastrium attaches the primitive foregut to the retroperitoneum while the ventral mesogastrium attaches the foregut to the anterior abdominal wall and the diaphragm.[2] The foregut later develops to form the stomach and duodenum. Part of the dorsal mesogastrium fuses with the posterior abdominal wall anterior to the left kidney to anchor the body of the pancreas, the spleen, and the stomach as the *splenorenal* and *gastrosplenic ligaments.* The remainder of the dorsal mesogastrium evaginates to create a recess that separates from the peritoneal cavity, known as the omental bursa or lesser sac. The caudal recess of the bursa fuses with the transverse colon and forms the *gastrocolic ligament* and the *greater omentum.*

Thus, the dorsal mesogastrium gives rise to several peritoneal ligaments, including the *splenorenal, gastrosplenic* and *gastrocolic ligaments* and the *greater omentum.*

The ventral mesogastrium develops to form (a) the lesser omentum *(gastrohepatic* and *hepatoduodenal ligaments)* with the free edge defining the epiploic foramen of the lesser sac; (b) the *falciform ligament* between the liver and anterior abdominal wall; and (c) the *coronary ligament* between the liver and the diaphragm.

Peritoneal Ligaments of the Liver

Because the liver is developed in the ventral mesentery attaching the foregut to the anterior abdominal wall and the transverse septum, it is covered almost completely by the peritoneum derived from the ventral mesentery. The peritoneal reflections between the liver and the diaphragm, the anterior abdominal wall, and the stomach form peritoneal ligaments around the liver.[2,3] Along the diaphragmatic surface, the liver is attached to the hemidiaphragm by the coronary ligaments and triangular ligaments. The coronary ligaments are formed by two single layers of peritoneum, the anterior–superior and the posterior–inferior layer. The anterior–superior layer extends across the dome of the right hemidiaphragm from the midline to the right and fuses with the posterior–inferior layer that extends along the posterior surface of the right hemidiaphragm to form the right triangular ligament. These ligaments attach the right liver to the right hemidiaphragm. Similarly, the anterior–superior and posterior–inferior layers of the left coronary ligament extend across the undersurface of the left hemidiaphragm and fuse to form the left triangular ligament laterally attaching the left liver to the left hemidiaphragm. The area of the liver between the anterior–superior and the posterior–inferior layers of the coronary ligament is closely applied to the diaphragm and is known as the bare area.

The anterior surface of the liver is attached to the anterior abdominal wall by the falciform ligament. The cranial portion of the falciform ligament is formed by the fusion of the right and left leaves of the anterior–superior layer of the coronary ligament. The falciform ligament extends caudally, and its free edge becomes the ligamentum teres (the round ligament). This ligament carries the obliterated umbilical vein from the umbilicus to the left portal vein via the umbilical fissure of the left liver.

Along the inferior and medial surface, the liver is attached to the lesser curvature of the stomach by the gastrohepatic ligament. The gastrohepatic ligament is formed by two peritoneal layers that cover the stomach. It extends from the lesser curvature of the stomach and inserts into a horizontal fissure of the liver separating the left liver from the caudate sector. This ligament, also known as the lesser omentum, forms the anterior boundary of the lesser sac or the omental bursa. Caudally, the free edge of the gastrohepatic ligament is the hepatoduodenal ligament, which attaches to the duodenal bulb and inserts into the hilum of the liver (transverse fissure) carrying the hepatic artery, portal vein, and bile duct into the liver. The hepatoduodenal ligament forms the anterior boundary of the epiploic foramen (foramen of Winslow), which is where the lesser sac communicates with the peritoneal cavity.

Peritoneal Ligaments of the Stomach

The peritoneal ligaments serve as supportive structures suspending the stomach in the peritoneal cavity. They are formed by two layers of peritoneal lining covering the blood vessels, lymphatic vessels and lymph nodes, nerve, and fat.

The Gastrohepatic and Hepatoduodenal Ligament

The gastrohepatic ligament suspends the cardia and the lesser curvature of the stomach from the inferior surface of the liver. It inserts deep into the fissure of the ligamentum venosum anterior to the caudate lobe of the liver. It separates the lesser sac from the perihepatic space posterior to the lateral segment of the left lobe and forms the anterior boundary of the lesser sac. Caudally, the free edge of the gastrohepatic ligament becomes the hepatoduodenal ligament.

The vascular landmarks of the gastrohepatic ligament are the left gastric artery and vein and the right gastric artery and vein that form an anastomotic arcade along the lesser curvature of the stomach.[4] It should be noted that the segment of the left gastric artery where it originates from the celiac axis and the left gastric (coronary) vein where it drains into the splenic–portal venous confluence run in the cephalocaudal direction in the gastropancreatic fold in the retroperitoneum before branching into the gastrohepatic ligament along the lesser curvature of the stomach. Within the ligament, the left gastric artery bifurcates into the ascending esophageal branch and a descending gastric branch. The latter supplies the superior portion of the lesser curvature.

The hepatoduodenal ligament is the free edge of the gastrohepatic ligament, extending from the duodenum to the hilum of the liver carrying the hepatic artery, bile

duct, and portal vein. The right gastric vein usually drains into the portal vein in this ligament.

The Gastrosplenic Ligament

The gastrosplenic ligament extends from the posterolateral wall of the fundus and the greater curvature of the stomach to the splenic hilum. It forms the lateral boundary of the lesser sac. The vascular landmarks of the gastrosplenic ligament are the short gastric artery and vein at the fundus and the segment of the left gastroepiploic artery and vein branching from the splenic artery and vein at the hilum of the spleen along the body of the stomach.

The Gastrocolic Ligament and the Omentum

The gastrocolic ligament attaches the greater curvature of the stomach to the anterior surface of the transverse colon and extends anteriorly as an apron to become the omentum covering the colon and small bowel in the peritoneal cavity. The gastrocolic ligament is in continuity with the gastrosplenic ligament on the left side of the abdomen, and it is fused with the transverse mesocolon on the right side of the abdomen as it is inserted and attached to the retroperitoneum behind the pylorus and anterior to the head of the pancreas.

The vascular landmarks of the gastrocolic ligament are the left and right gastroepiploic vessels that course along the greater curvature of the stomach. The left gastroepiploic vessels are branches of the distal splenic artery and vein. They run from the splenic hilum in the gastrosplenic ligament, which continues to be the gastrocolic ligament, and run along the greater curvature of the stomach to anastomose with the right gastroepiploic artery and vein. The right gastroepiploic artery is a branch of the gastroduodenal artery arising anterior to the head of the pancreas and coursing anteriorly in the fused gastrocolic ligament and transverse mesocolon, then continuing in the gastrocolic ligament along the greater curvature of the stomach. The right gastroepiploic vein joins the middle colic vein to form the gastrocolic trunk and drain into the superior mesenteric vein anterior to the head of the pancreas[5] and, in most cases, medial to the origin of the right gastroepiploic artery.

Tables 6–1 and 6–2 summarize the vessels within the peritoneal ligaments in the supramesocolic compartment. These vessels serve as anatomic landmarks to follow the pathways of lymphatic drainage of the liver, stomach, and spleen.

Table 6–1. Peritoneal Ligaments Derived from the Dorsal Mesogastrium and their Vascular Landmarks

Peritoneal ligaments	Vascular landmarks
Splenorenal ligament	Splenic artery and vein
Gastrosplenic ligament	Short gastric artery and vein
	Left gastroepiploic artery and vein
Gastrocolic ligament	Left gastroepiploic artery and vein
	Right gastroepiploic artery and vein
	Gastrocolic trunk
Omentum	Epiploic artery and vein

Table 6–2. Peritoneal Ligaments Derived from the Ventral Mesogastrium and their Vascular Landmarks

Peritoneal ligaments	Vascular landmarks
Gastrohepatic ligament	Left gastric artery and vein
	Right gastric artery and vein
	Aberrant left hepatic artery
Hepatoduodenal ligament	Hepatic artery
	Portal vein and parabillary plexus
Falciform ligament	Vessels in the falciform ligament

Lymphatic Drainage of the Liver and Pathways of Lymph Node Metastasis

The lymphatic drainage of the liver consists of two major pathways: the deep pathways and the superficial pathways.[1] The lymphatic vessels in the liver are believed to originate in the perilobular connective tissue. The perilobular lymphatic vessels from the lobules deep inside the parenchyma drain into the deep networks along the periportal space in the Glisson's sheath toward the porta hepatis and along the hepatic veins. The perilobular lymphatic vessels from the lobules near the surface of the liver drain into the numerous superficial lymphatic networks under the capsule of the liver (Fig. 6–1).

Table 6–3 summarizes various pathways of lymphatic drainage and potential pathways of lymph node metastasis of the liver based on anatomic study by Rouvier and various clinical studies.[1,6–8]

The deep lymphatic networks follow the portal veins, drain into the lymph nodes at the hilum of the liver (known as the hepatic or hilar lymph nodes), and then drain to the nodes in the hepatoduodenal ligament (Fig.

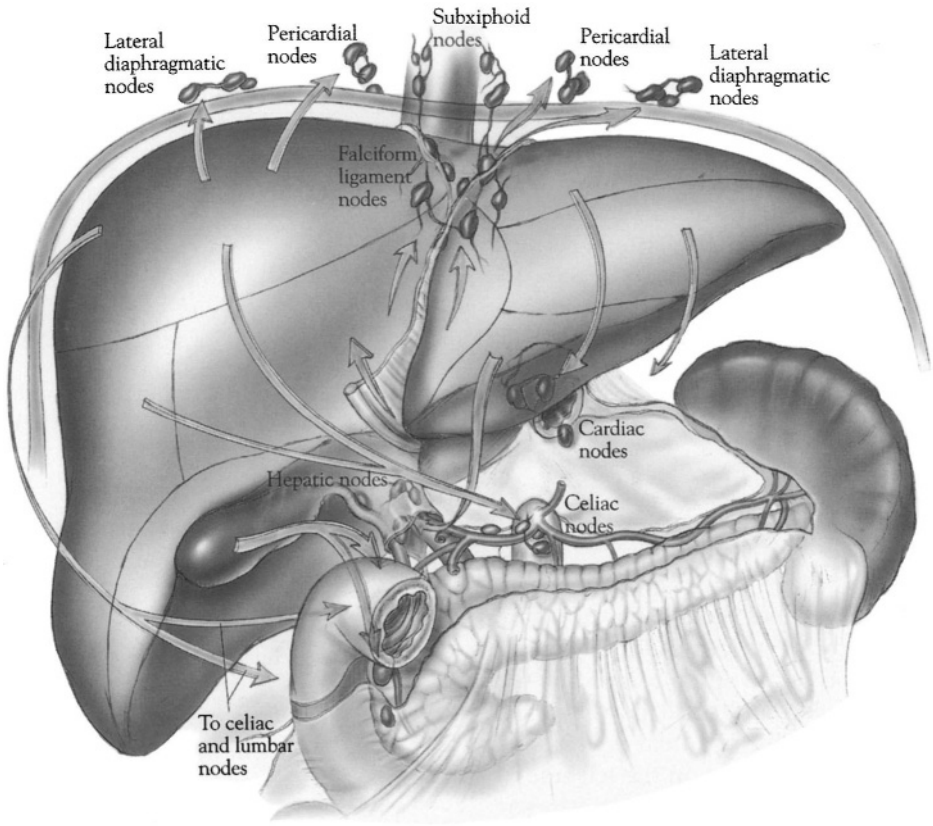


Fig. 6–1. Superficial pathways of lymphatic drainage of the liver.
Note that the anterior diaphragmatic nodes consist of two groups: the lateral anterior diaphragmatic group and the medial group, which includes the pericardiac nodes and the subxiphoid nodes behind the xiphoid cartilage. The nodes in the falciform ligament drain into the anterior abdominal wall along the superficial epigastric and deep epigastric lymph nodes. The epigastric and the subxiphoid nodes drain into the internal mammary nodes.
(This figure also appears in the color insert.)

Table 6–3. Pathways of Lymphatic Drainage of the Liver

Deep lymphatic network
Descending chains (hepatoduodenal ligament)
Hepatic hilar nodes
Anterior periportal chains: hepatic artery and celiac nodes
Posterior periportal chains: portocaval, superior retropancreatic, and inferior retropancreatic nodes
Descending chains (hepatic vein): Inferior vena cava terminal nodes
Superficial lymphatic network
Anterior ascending chain (falciform ligament): anterior diaphragmatic nodes
Posterior descending chain (bare areas): right and left inferior phrenic nodes
Paracardial chain (gastrohepatic ligament): left gastric nodes
Anterior descending chain (falciform ligament): deep superior epigastric nodes

6–2). The nodes in the hepatoduodenal ligament can be separated into two major chains; the anterior periportal (hepatic artery) chain and posterior periportal chain. The anterior periportal chain (Figs. 6–3 and 6–4) begins at the hepatic artery nodes, follows the common hepatic artery to the nodes at the celiac axis, and drains into the cisterna chyli. The posterior periportal chain (Fig. 6–3), which begins at the portocaval nodes, is located posterior to the portal vein in the hepatoduodenal ligament. This chain drains into the superior and inferior retropancreatic nodes and the aortocaval nodes before draining into the cisterna chyli and ascending to the thoracic duct.

The deep networks along the hepatic veins drain into the lymph nodes around the inferior vena cava (IVC) above the diaphragmatic opening through which the IVC passes (Fig. 6–5). This nodal group is known as the IVC terminal nodes or juxtaphrenic nodes.

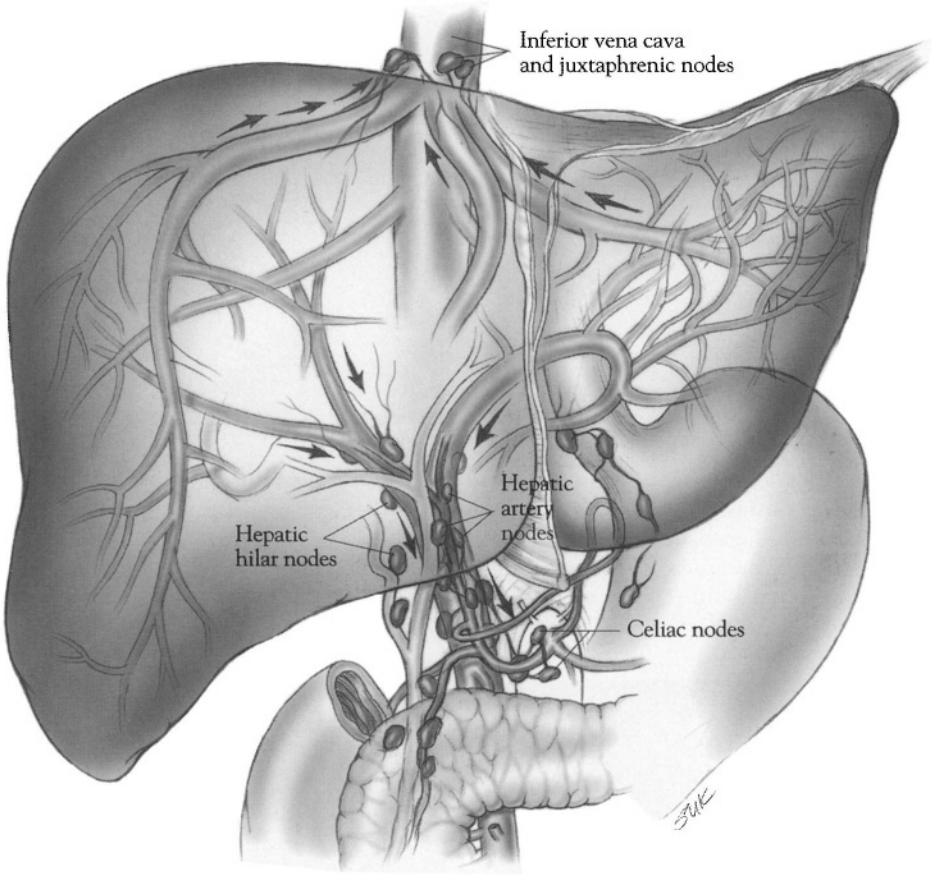


Fig. 6–2. Deep pathways of lymphatic drainage of the liver.
The deep pathways follow the hepatic veins to the inferior vena cava nodes and the juxtaphrenic nodes that follow along the phrenic nerve. These nodal groups are considered as the middle diaphragmatic nodes. The pathways that follow the portal vein drain to the hepatic hilar nodes and the nodes in the hepatoduodenal ligament. They drain into the celiac node and the cisterna chyli.
(This figure also appears in the color insert.)

Superficial Lymphatic Pathways

The numerous superficial lymphatic networks are located under the capsule of the liver. They form several collecting trunks draining in various directions along the ligaments that attach to the liver.

Along the anterior surface, several collecting trunks follow the falciform ligament, ascending to the anterior diaphragmatic nodes above the diaphragm (Fig. 6–5). These trunks can also descend and join the lymphatic networks at the inferior surface to drain into the hepatic hilar nodes. On rare occasions, a collecting trunk can be identified in the falciform ligament that drains downward into a lymph node in the deep superior epigastric chain in the anterior abdominal wall (Fig. 6–6).

From the superior surface, the collecting trunks follow the triangular and coronary ligaments and penetrate the diaphragm to several nodal groups above the diaphragm, including the anterior diaphragmatic nodes, retrosternal or retroxiphoid nodes, IVC terminal or juxtaphrenic nodes, and paraesophageal nodes.

Along the posterior surface of the liver are several collecting trunks that follow the IVC to the IVC terminal nodes and that follow the inferior leaf of the coronary ligaments and join the right and left inferior phrenic arteries to drain to the inferior phrenic nodes and the paraaortic nodes.

Along the inferior surface are the collecting trunks that drain mostly into the hepatic hilar nodes and that join the lymphatic vessels in the hepatoduodenal ligament and gastrohepatic ligament. The group in the gastrohepatic ligament may drain into the paracardial chain

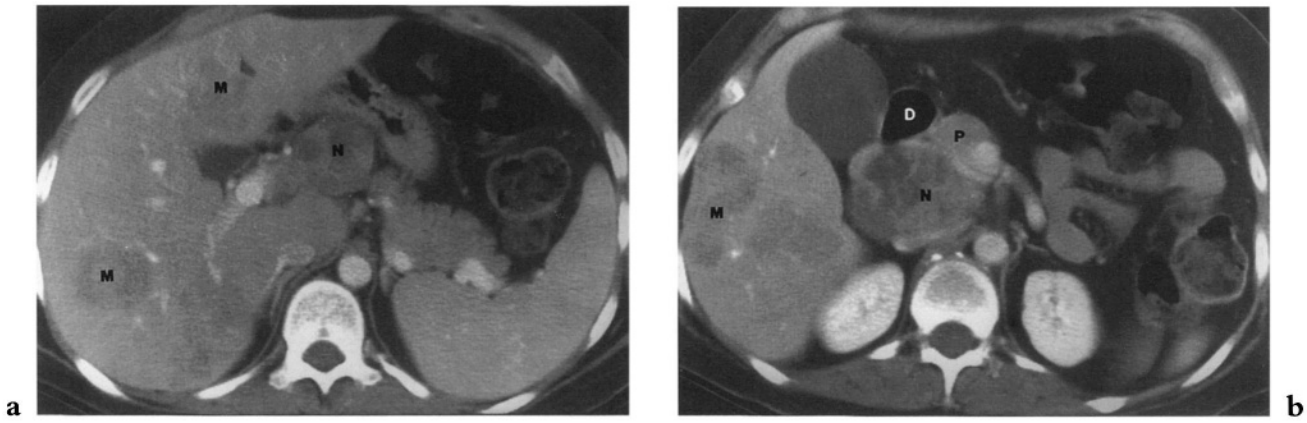


Fig. 6–3. Metastatic colon carcinoma to the liver and lymph node metastasis to the common hepatic and posterior periportal nodes.
(a) Node *(N)* at the common hepatic artery. *M* = hepatic metastasis.
(b) Node *(N)* at the posterior periportal chain or node at the foramen of Winslow. Note that the nodal mass displaces pancreas *(P)* and duodenum *(D)* anteriorly.

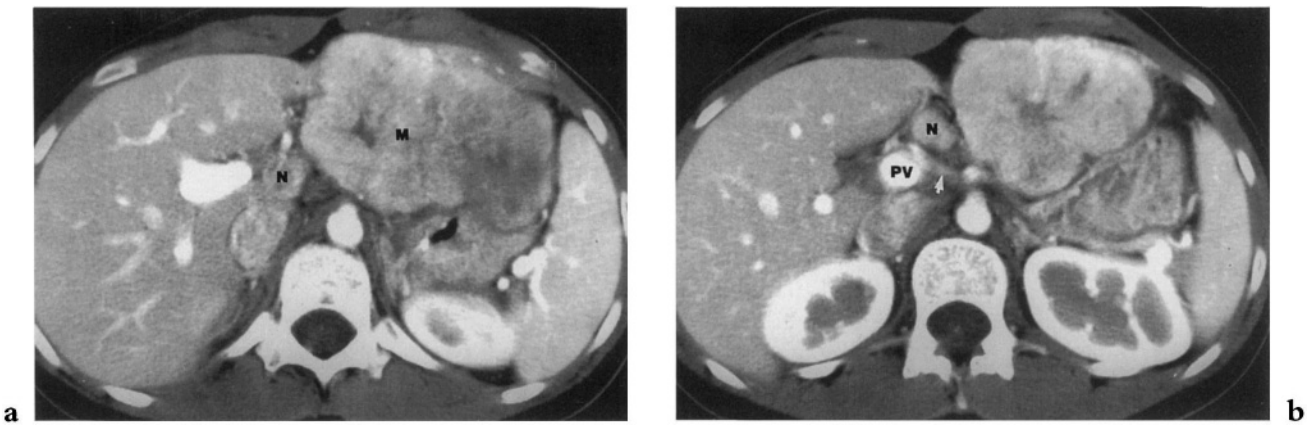
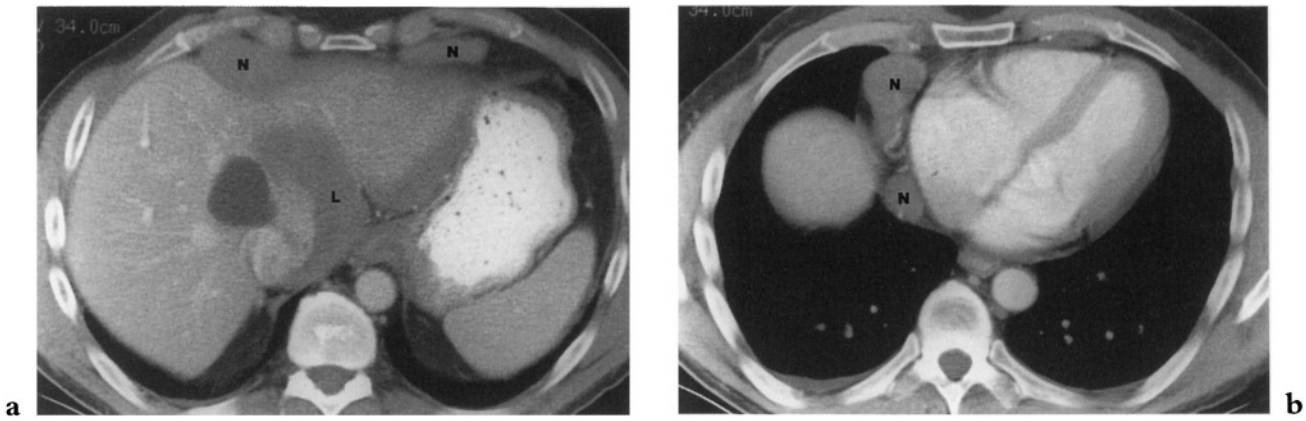


Fig. 6–4. Fibrolamellar hepatocellular carcinoma (HCC) with lymph node metastasis to hepatic hilar node and common hepatic artery node where gastrohepatic ligament attaches. Proved at surgery.
(a) Metastatic node *(N)* at hepatic hilum from large primary fibrolamellar HCC *(M)* in lateral segment (segment 2 and 3). Node is located at junction between the cystic duct and common hepatic duct.
(b) Metastatic node *(N)* at common hepatic artery *(arrow).* Note that node is also anterior to portal vein *(PV).*

of the left gastric nodes. The lymphatic network at the surface of the caudate lobe frequently follows the IVC to the IVC terminal nodes.

Lymphatic Drainage of the Stomach and Pathways of Lymph Node Metastasis

The lymphatic drainage of the stomach consists of intrinsic and extrinsic systems. The intrinsic system includes intramural submucosal and subserosal networks, and the extrinsic system forms lymphatic vessels outside the stomach and generally follows the course of the arteries in various ligaments around the stomach.[9,10] These lymphatic vessels drain into the lymph nodes at nodal stations in the corresponding ligaments and drain into the central collecting nodes at the root of the cellac axis and the superior mesenteric artery (Table 6–4 and Fig. 6–7). Various classification systems have been developed involving complex numerical schemes to define nodal



a b

Fig. 6–5. Primary lymphoma *(L)* of the liver with nodal involvement of anterior diaphragmatic nodes and juxtaphrenic or inferior vena cava node.
(a) Note right and left anterior diaphragmatic nodes *(N).*
(b) Right juxtaphrenic nodes *(N)* along phrenic nerve are also involved.

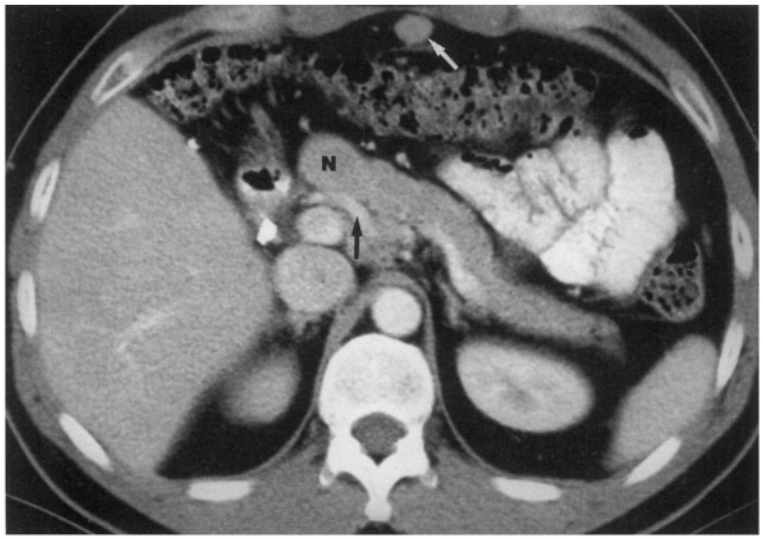


Fig. 6–6. Recurrent hepatocellular carcinoma after resection of primary tumor in left lobe.
Note enlarged node *(N)* at common hepatic artery *(black arrow)* and node *(white arrow)* at deep superior epigastric vessels. This node drains lymphatics along vessels in the falciform ligament. Nodes are proved metastatic by biopsy and progression on follow-up.

stations based on the location and the distance of the nodal stations from the primary tumors, such as local group I (N1), intermediate group II (N2), and distant group III (N3).[10] These nodal stations are used for correlation with prognosis and for planning treatment. In general, metastases to the nodal station closer to the primary tumor have a better prognosis than those found at the station further away from the primary.[10,11]

Nodal Metastases in the Gastrohepatic Ligament

Tumors arising from the area of the stomach along the lesser curvature and the esophagogastric junction, supplied by the left gastric artery, generally metastasize to the lymph nodes in the gastrohepatic ligament. The primary nodal group (N1 station) consists of nodes along

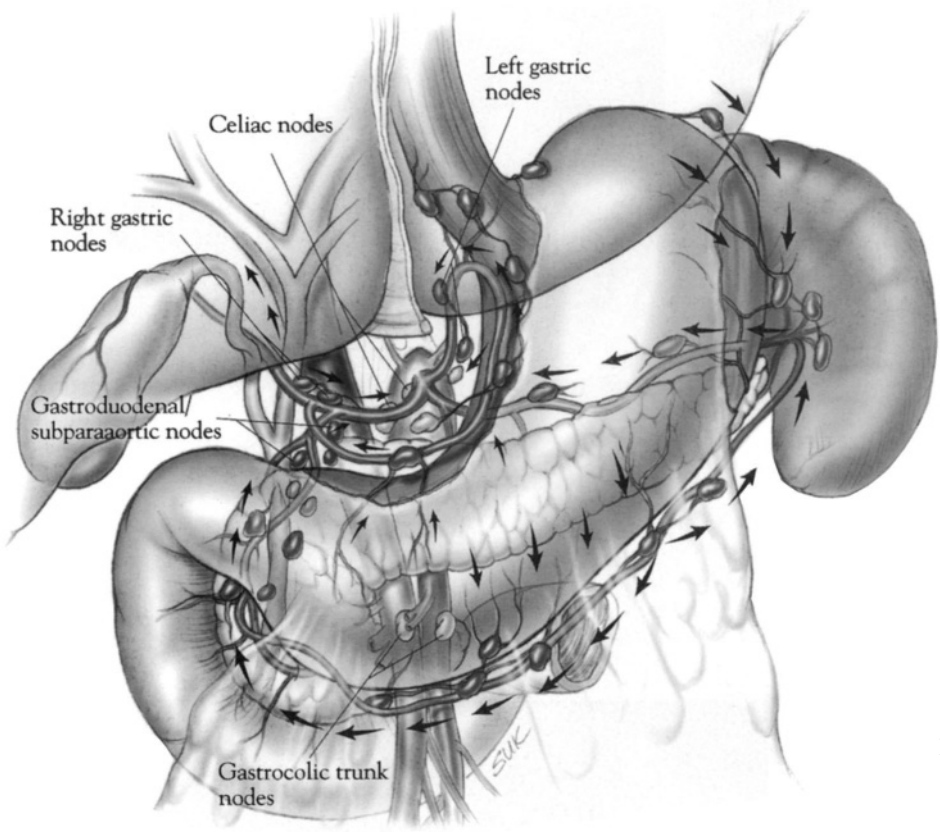


Fig. 6–7. Pathways of lymphatic drainage of the stomach. (This figure also appears in the color insert.)

Table 6–4. Pathways of Lymphatic Drainage of the Stomach

	Primary nodes (N1)	Intermediate nodes (N2)	Principal nodes (N3)
Esophagogastric junction	Perigastric nodes	Left gastric nodes	Celiac nodes
		Left inferior phrenic nodes (rare)	Paraaortic nodes
Fundus, posterior wall	Perigastric nodes	Suprapancreatic nodes	Celiac nodes
Body, lesser curvature	Perigastric nodes	Left gastric nodes	Celiac nodes
	(left and right gastric vessels)	Right gastric node	Celiac nodes
Antrum, lesser curvature	Perigastric nodes	Right gastric nodes	Celiac nodes
Body, greater curvature	Perigastric nodes	Splenic hilum nodes	Celiac nodes
	(left gastroepiploic vessels)		
Body, greater curvature	Perigastric nodes	Nodes at the gastrocolic trunk	SMA nodes
	(right gastroepiploic vessels)		
Body, greater curvature	Perigastric nodes	Gastroduodenal (subpyloric nodes)	Celiac nodes

the left and right gastric artery anastomosis along the lesser curvature. The N2 station includes the nodes along the left gastric artery and vein in the gastropancreatic fold (Figs. 6–8 and 6–9) that drain toward the suprapancreatic nodes along the superior border of the body of the pancreas (Fig. 6–8) and then the celiac axis (N3 station).

Tumors arising from the area of the stomach supplied by the right gastric artery, including the lesser curvature of the antrum and pylorus, drain into the nodes in the hepatoduodenal ligament (Fig. 6–8), where the right gastric artery originates from the hepatic artery or the right gastric vein drains into the portal vein. From these nodes, drainage continues along the hepatic artery toward the celiac axis.

Nodal Metastases in the Gastrocolic Ligament

Primary tumors involving the greater curvature of the antrum of the stomach in the distribution of the right gastroepiploic artery spread to the perigastric nodes (N1 station) accompanying the right gastroepiploic vessels that course along the greater curvature of the stomach. They drain into the nodes at the gastrocolic trunk (N2 station) (Fig. 6–10) or the nodes at the origin of the right gastroepiploic artery and the nodes along the gastroduodenal artery (the subpyloric or retropyloric node). From there, they can proceed to the celiac axis or the root of the superior mesenteric artery.

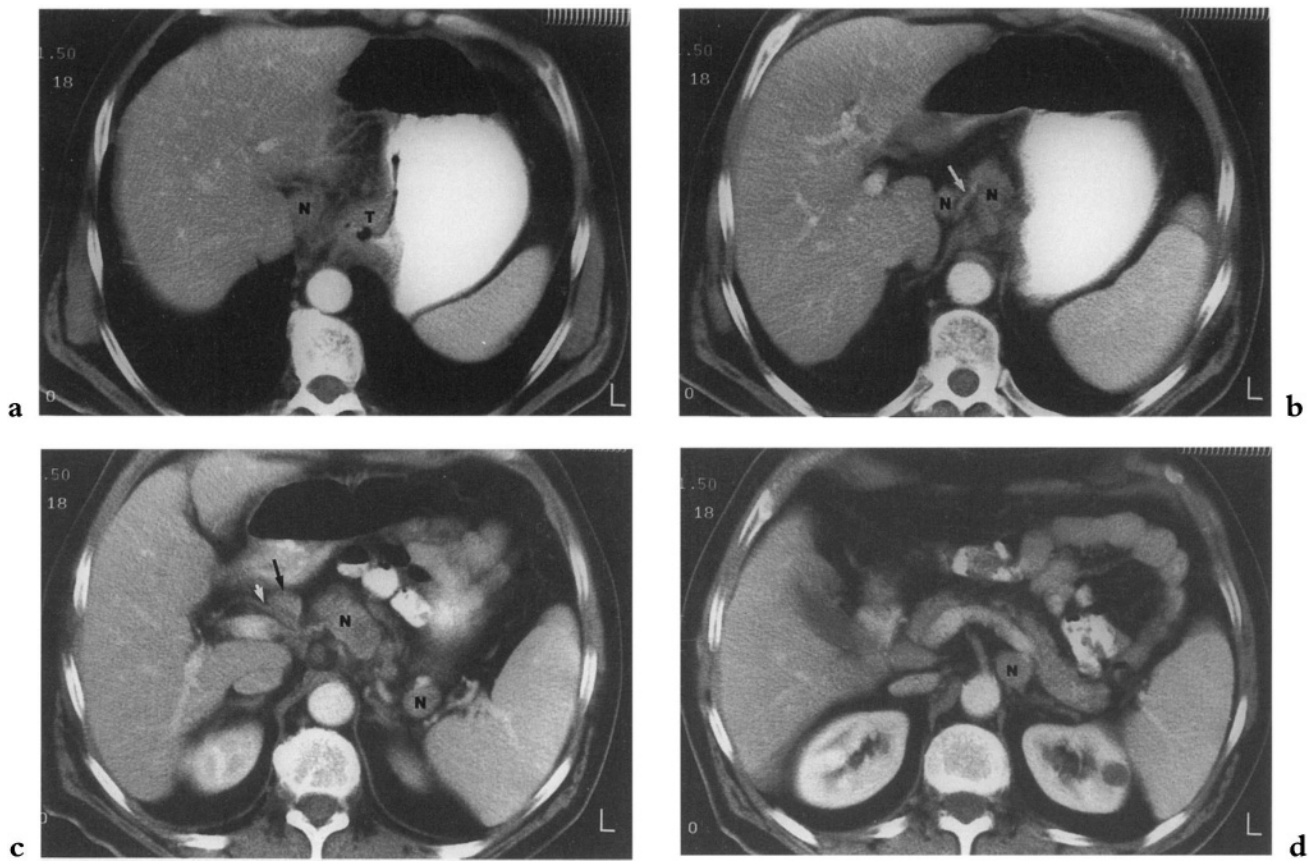


Fig. 6–8. Adenocarcinoma at esophagogastric (EG) junction with nodal metastases.
(a) Primary tumor *(T)* at EG junction with metastatic perigastric node *(N)* in gastrohepatic ligament, an N1 station.
(b) Nodes (N) in gastropancreatic fold along left gastric vessel *(white arrow),* an N2 station.
(c) Nodes *(N)* at suprapancreatic nodes, N2 station, along splenic artery draining from posterior wall of fundus to splenic hilum via gastrosplenic ligament. Also note common hepatic artery node *(black arrow),* N2 station, anterior to common hepatic artery *(white arrow)* draining along left and right gastric anastomosis.
(d) Left inferior phrenic node *(N),* N3 station, located at apex of adrenal gland draining from left diaphragm at esophageal hiatus along left inferior phrenic vessels where they drain into left renal vein.

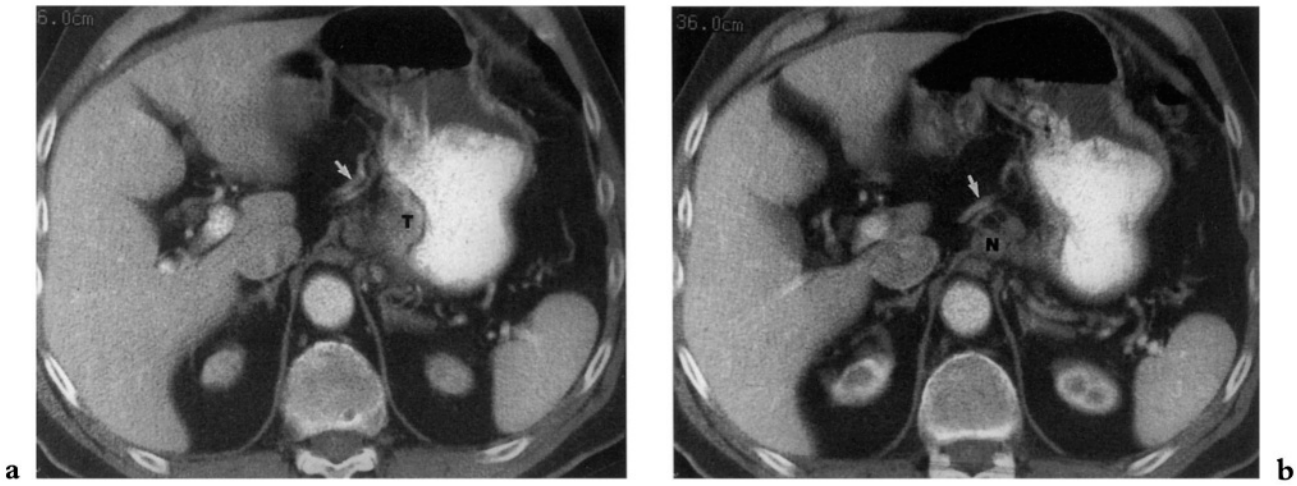


Fig. 6–9. Carcinoma of the stomach.
(a) Tumor *(T)* involves lesser curvature of the fundus.
(b) Note enlarged nodes *(N)* along left gastric vessels *(arrow).*

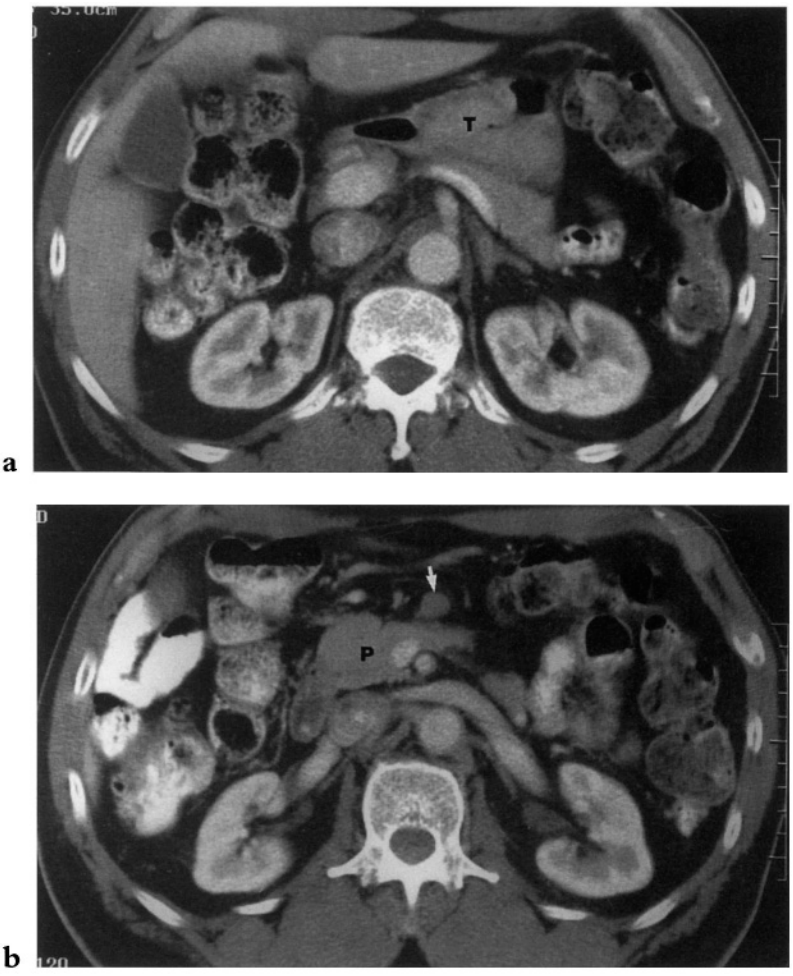


Fig. 6–10. Carcinoma of stomach.
(a) Tumor mass *(T)* arises in the gastric antrum.
(b) Note metastatic node *(arrow),* N2 station in gastrocolic ligament anterior to pancreas *(P)* where gastrocolic trunk drains into superior mesenteric vein.

Nodal Metastases in the Gastrosplenic Ligament

Primary tumors from the greater curvature of the body of the stomach spread along the left gastroepiploic vessels and drain into the lymph nodes in the splenic hilum by following the left gastroepiploic vessels via the gastrocolic ligament and gastrosplenic ligament. From the posterior wall of the fundus of the stomach, they can also spread along the superior extent of the gastrosplenic ligament to the splenic hilum. From the splenic hilum, they can spread along the splenic artery to the celiac axis. This nodal group is known as the suprapancreatic nodes or the nodes in the splenorenal ligament. These nodes are also the primary site of lymphatic drainage from the spleen (Fig. 6–11).

Unusual Pathways

Tumors involving the esophagogastric junction or the fundus of the stomach may invade the diaphragm as they grow beyond the serosa. The lymphatic drainage of the peritoneal surface of the diaphragm is via the nodes along the inferior phrenic artery and vein that run along the left crus of the diaphragm toward the celiac axis or the left renal vein (Fig. 6–9).

The Inframesocolic Compartment

Anatomic Consideration

The large intestine consists of the cecum, ascending colon, transverse colon, descending colon, sigmoid colon, and rectum. The ascending colon, descending colon, and rectum are considered extraperitoneal organs because the ascending and descending colon lie in the anterior pararenal space and are covered by a single layer of the posterior peritoneum, while the rectum is surrounded by extraperitoneal perirectal fat in the pelvis. The transverse colon and sigmoid colon are suspended in the peritoneal cavity by the mesocolon, which is formed by two layers of the peritoneal linings, and the cecum is attached to the ileocolic mesentery in the right iliac fossa.[12]

The arterial supply to the cecum, ascending colon, and transverse colon derives from the superior mesenteric artery (SMA), whereas the blood supply to the descending colon, sigmoid colon, and upper rectum is from the inferior mesenteric artery (IMA) and that to the lower rectum from the internal iliac arteries. Similarly, the venous drainage of the cecum, ascending co-



Fig. 6–11. Splenic lymphoma with involvement of nodes *(arrows)* along splenic artery in splenorenal ligament. These nodes drain into the celiac node and left inferior phrenic node *(N).*

lon, and transverse colon drains into the superior mesenteric vein (SMV), and that of the descending colon, sigmoid colon, and rectum drains into the inferior mesenteric vein (IMV). In general, the artery and vein supplying and draining each segment of the colon accompany each other in the mesocolon, with the marginal artery and vein forming the arcade along the mesocolic side of the colonic wall before giving off the branches of vasa recta to penetrate into the colonic wall. These vessels in the mesocolon and the marginal vessels along the mesocolic side of the colonic wall form the anatomic landmarks to localize the mesocolon.

Cecum, Ascending Colon, Ileocolic Mesentery, and Descending Colon and Mesocolon

Along the mesocolic margin of the ascending colon and the descending colon lie the marginal vessels. As these vessels course in the cephalocaudal direction, the vessels can be identified as "dots" of vessels medial to the ascending and descending colon on axial images, with branches of the vasa recta supplying the colon (Fig. 6–12). These vessels can be better defined on CT images scanned at 3- to 5-mm scanning collimation. Medial to

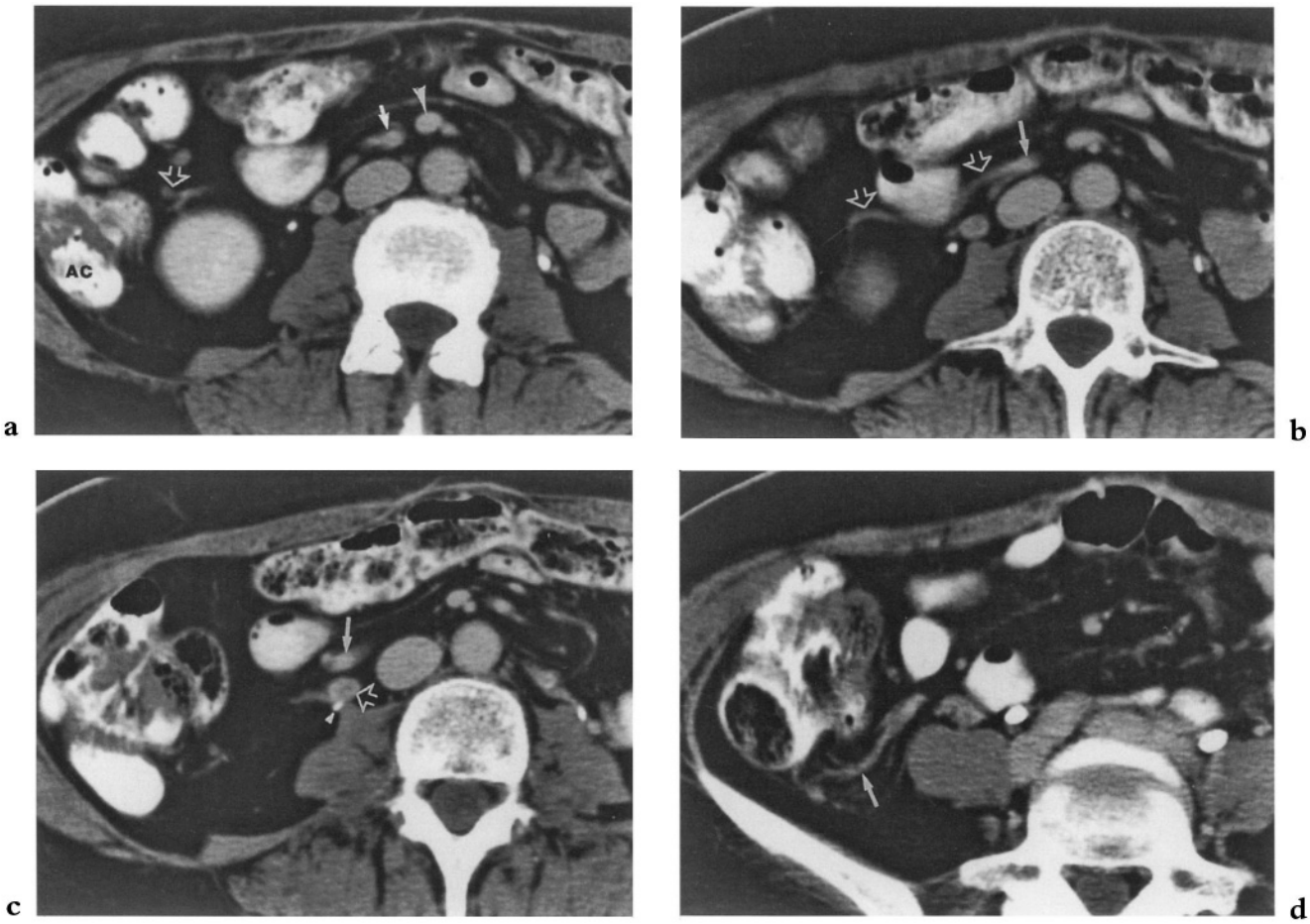


Fig. 6–12. CT anatomy of the ascending mesocolon.
(a) The ileocolic vein *(arrow),* a branch of the superior mesenteric vein (SMV) *(arrowhead),* and the marginal vessels *(open arrow)* of the ascending colon *(AC)* form the plane of the ascending mesocolon.
(b) The right colic vein *(open arrows)* is a branch of the ileocolic vein *(arrow),* communicating with the marginal vessels.
(c) The plane of the ileocolic vein *(arrow)* is anterior to the right gonadal vein *(open arrow)* and the right ureter *(arrowhead).* Note thrombosis of the gonadal vein.
(d) The distal branches of the ileocolic vessels *(arrow)* terminate in the cecum, appendix, and the terminal ileum.

the marginal vessels, we should identify the ileocolic vessels for the ascending mesocolon and mesocecum, and the inferior mesenteric vessels for the descending mesocolon.[13–15]

The ileocolic vessels are the branches of the superior mesenteric vessels located near the base of the mesentery. They run in the oblique direction from near the midline, anterior to the third portion of the duodenum, toward the cecum in the right iliac fossa. As they are located near the base of the mesentery, their course is constant and not flopping in the peritoneal cavity like other branches of the SMA or SMV supplying the ileum or the jejunum. After crossing the third portion of the duodenum, they can be identified anterior to the right ureter and the gonadal vessels and can be traced toward the cecum. The plane between the marginal vessels of the ascending colon and the ileocolic vessels defines the plane of the ascending mesocolon.[13–14]

The inferior mesenteric vessels run in the cephalocaudal direction in the anterior pararenal space slightly anterior and left to the aorta. The vessels can be identified anterior to the left ureter and the gonadal vessels and the left renal vein.[15] The IMV drains into the splenic vein, the confluence of the SMV and splenic vein, or directly into the SMV. Before it enters that vein, it forms the left duodenomesocolic fold at the left paraduodenal space, which is where the duodenum exits the retroperitoneum and enters into the peritoneal cavity. Therefore, the anatomic landmarks for the left paraduodenal space include the inferior mesenteric vein forming the left and superior boundaries, the superior mesenteric artery and vein forming the right boundary, with the duodenum at the center. The plane between the inferior mesenteric vein and the marginal vessels of the descending colon forms the plane of the descending mesocolon.

The Transverse Colon and Mesocolon

The transverse colon is suspended in the peritoneal cavity by the transverse mesocolon. The transverse mesocolon is formed by two posterior peritoneal layers, with the root of the transverse mesocolon traversing across the second portion of the duodenum and the head of the pancreas and along the inferior border of the body and the tail of the pancreas. Within the transverse mesocolon are branches of the middle colic artery, which most commonly arises from the anterior surface of the proximal segment of the SMA, and branches of the middle colic veins, which drain into the SMV or IMV.

The marginal vessels along the mesocolic side of the colon can be identified as longer segments of the vessels as compared to dots of marginal vessels of the ascending or descending colon. This is because the marginal vessels of the transverse mesocolon run in the transverse direction. The position of the vessels varies depending upon the position of the transverse colon. If the transverse colon hangs down toward the umbilicus as most of the midportion of the transverse colon does, the marginal vessels can be seen cephalad to the wall of the colon. However, if the transverse colon suspends or floats up toward the diaphragm as most splenic flexure does, the marginal vessels will be caudal to the colonic wall.

The transverse mesocolon can be traced toward the root of the mesocolon by following the marginal vessels to the middle colic vein draining into the SMV. The typical anatomy will show the marginal vessels from the right and left transverse colon forming the middle colic vein and joining the right gastroepiploic vein to become the gastrocolic trunk draining into the SMV anterior to the head of the pancreas.[5,14] However, there are many anatomic variations that demonstrate several isolated branches of the middle colic vessels in the transverse mesocolon draining into the SMV or IMV, but these vessels are all coursing toward the head and the body of the pancreas into which the root of the transverse mesocolon inserts.

The Sigmoid Colon and Mesocolon

The sigmoid colon is another segment of the colon that is suspended in the peritoneal cavity. The sigmoid mesocolon is formed by the two peritoneal layers attached to the third sacral segment and extending in the cephalad direction toward the left external iliac vessel where it joins another leaf of the sigmoid mesocolon, which extends from the descending mesocolon, suspending the proximal sigmoid colon. These two leaves of sigmoid mesocolon ascend toward the anterior surface of the abdominal aorta where the IMA arises. The length and arrangement of the mesocolon vary depending upon the length and redundancy of the sigmoid colon.

The anatomic landmarks of the sigmoid mesocolon are the superior hemorrhoidal vessels, the marginal vessels, the sigmoidal vessels, and the IMA and IMV.[13,14] The superior hemorrhoidal vessels are plexuses of vessels on both sides of the rectum ascending to form the inferior mesenteric vessels. The IMV is located anterior to the left external iliac vessels, the left ureter, and the left gonadal vein. The marginal vessels form the arcade along the mesocolic side of the colon with multiple branches of the sigmoidal vessels communicating the marginal vessels to the IMV. However, because of anatomic variations in the length and redundancy of the sigmoid colon, the positions of the marginal vessels and the sigmoidal vessels are not constant. On the other hand, the anatomy of the IMA and IMV is more con-

stant. The origin of the IMA almost always arises from the anterior wall of the abdominal aorta at approximately the level of L3, then courses to the left and gives off a branch, the left ascending colic artery, that ascends along the IMV toward the left paraduodenal space. The other branches form the sigmoidal arteries and the superior hemorrhoidal artery.

Lymphatic Drainage of the Colon and Pathways of Lymph Node Metastasis

Regional nodal metastasis is one of the most common modes of tumor spread in carcinoma of the colon. The lymph nodes draining lymphatics from the colon can be classified into four groups: the epicolic nodes, the paracolic nodes, the intermediate mesocolic nodes, and the principal nodes.[16,17] The epicolic nodes lie on the wall of the colon beneath the peritoneum covering the colon, generally on the antimesocolic side of the colonic wall. The paracolic nodes lie along the marginal vessels along the mesocolic side of the colon. The intermediate mesocolic nodes lie in the mesocolon accompanying the vessels in the mesocolon and draining into the principal nodes at the root of the mesocolon. In general, the pathway of lymphatic drainage follows these groups of nodes from the epicolic to paracolic, intermediate, and principal nodes, respectively.

Table 6–5 and Figure 6–13 show the pathways of nodal spread to the intermediate mesocolic nodes and the principal nodes from various segments of the colon. These pathways follow the course of the arterial supply and venous drainage of those colonic segments.[14,18–20]

Pathway of Nodal Metastases from Carcinoma of the Cecum and Ascending Colon

The primary nodal group draining lymphatics from tumors of the cecum and the ascending colon is the paracolic nodes along the marginal vessels of the cecum and ascending colon (Figs. 6–14 and 6–15). Further spread would follow along the ileocolic vessels toward the root of the SMA. Progression of nodal disease along the base of the mesentery may cause obstruction of the right ureter because of their close proximity and nodal spread could progress to the paraaortic nodal group. The principal nodes of this segment of the colon are the nodes at the root of the SMA.

Similarly, nodal metastasis from tumors of the distal ileum shares a similar pathway to the cecum or ascending colon (Fig. 6–16).

Pathway of Nodal Metastases from Carcinoma of the Transverse Colon

After the paracolic nodes, lymphatic spread from carcinoma of the transverse colon may follow along the branches of the middle colic vessels in the transverse mesocolon toward the root of the mesocolon (Figs. 6–17 through 6–20). From the hepatic flexure, the spread would follow the right colic vessels or right middle colic vessels to the nodal group at the gastrocolic trunk where it drains into the SMV anterior to the head of the pancreas. From the splenic flexure, the lymphatic drainage would follow along the left middle colic vessels toward

Table 6–5. Intermediate and Principal Nodes of Various Segments of the Colon

	Intermediate nodes	Principal nodes
Cecum	Ileocolic mesentery	Root of SMA
Ascending colon	Right colic vessels	Root of SMA
	Ascending mesocolon	
	Ileocolic mesentery	
Right transverse colon	Transverse mesocolon	Pancreatic head
	Middle colic vessels	Root of SMA
Left transverse colon	Transverse mesocolon	Pancreatic body
	Left middle colic vessels	Root of SMA
Descending colon	Descending mesocolon	Left paraduodenal space
	Left colic vessels, IMV	Root of IMA
Sigmoid colon	Sigmoid mesocolon	Root of IMA
	Sigmoidal vessels	

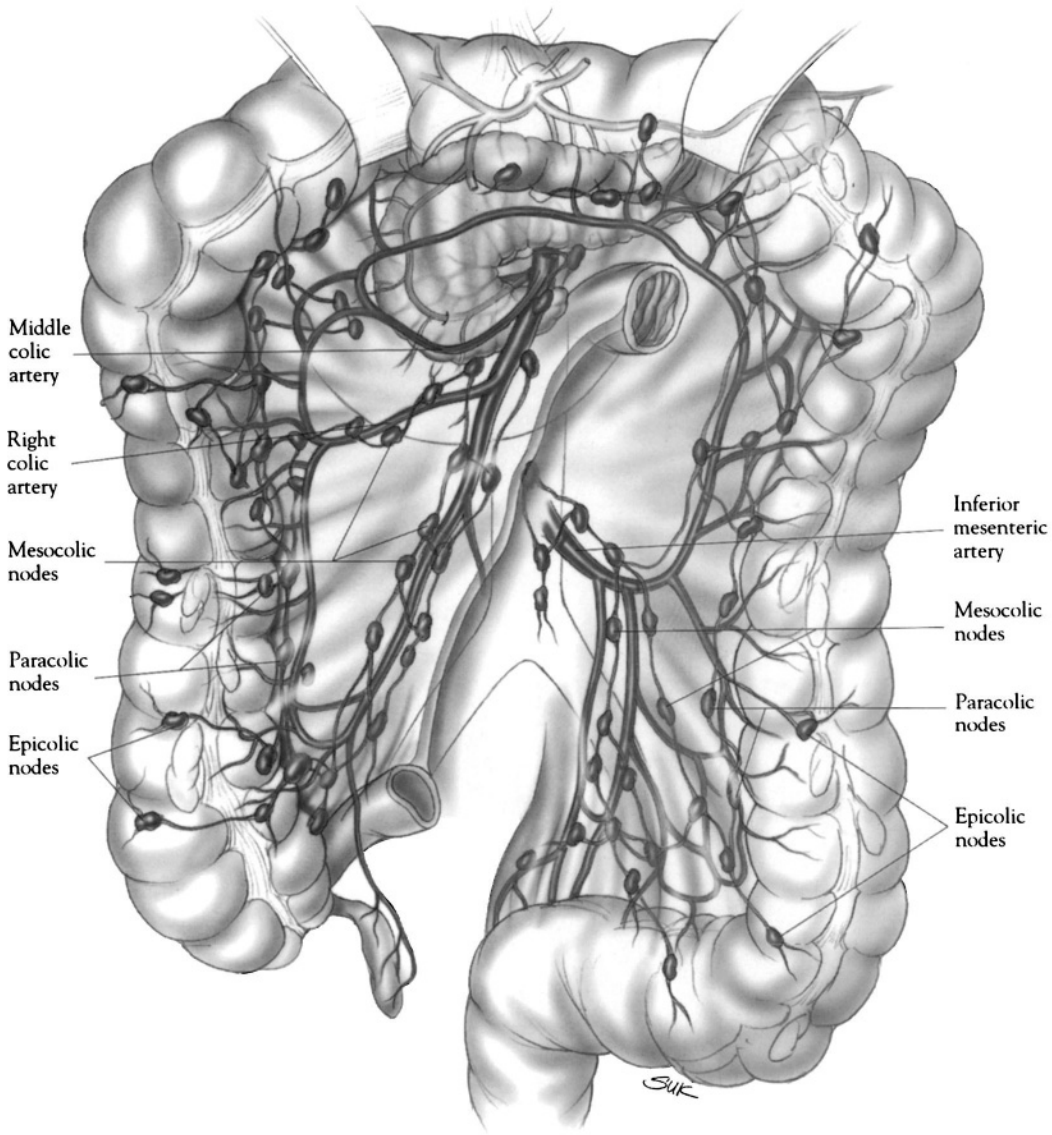


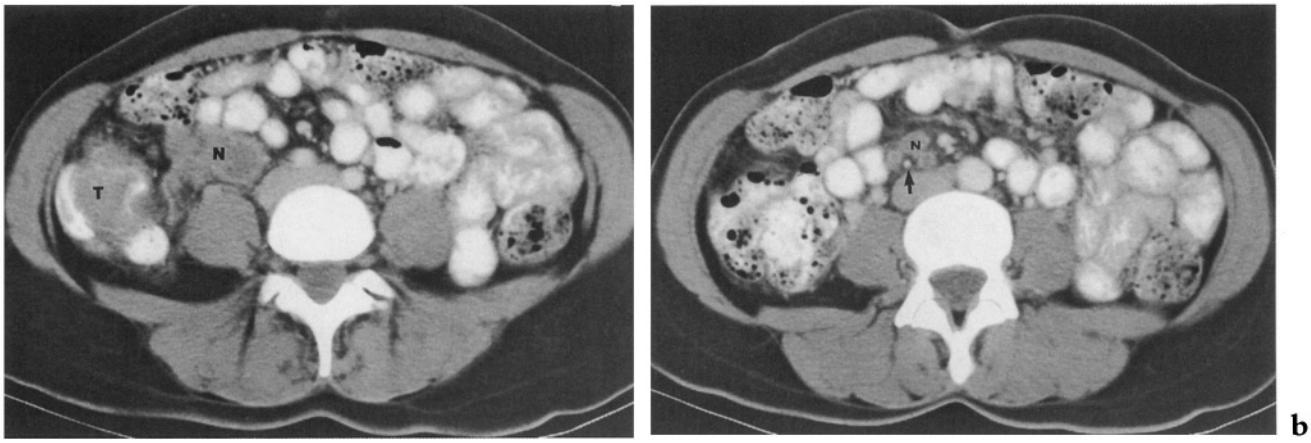
Fig. 6–13. Pathways of lymphatic drainage of the colon. (This figure also appears in the color insert.)

the IMV just caudal to the body and tail of the pancreas. On occasion, lymphatic spread may follow the left middle colic vein to the confluence of the IMV and the junction of the splenic vein and the SMV. Since the root of the transverse mesocolon is covering over the head of the pancreas and it is inserted caudal to the body and tail of the pancreas, progression of nodal metastasis or recurrent disease could involve the pancreas and not infrequently be mistaken as a pancreatic mass.

Pathway of Nodal Metastasis from Carcinoma of the Descending Colon and Sigmoid Colon

Lymphatic drainage of the descending colon and the sigmoid mesocolon follows along the vessels such as the sigmoidal vessels, the superior hemorrhoidal vessels, and the left ascending colic vessels in the mesocolon toward

text continues on page 306



a b

Fig. 6–14. Carcinoma of cecum with metastatic nodes along ileocolic vessels in the ascending mesocolon at base of the mesentery.
(a) CT at level of cecum shows primary tumor *(T)* with metastatic nodes *(N)* at paracolic nodal group. Nodes are posterior to distal ileum.
(b) CT at level 3 cm cephalad to **a** shows metastatic nodes *(N)* along ileocolic vessel *(arrow)* at base of mesentery.



a b

Fig. 6–15. Lymphoma of redundant cecum that is suspended in the pelvis.
(a) CT shows primary tumor *(T)* in cecum in pelvis.
(b) Enlarged nodes *(N)* can be identified along ileocolic vessels *(arrow)* at base of mesentery that is attached to right iliac fossa.

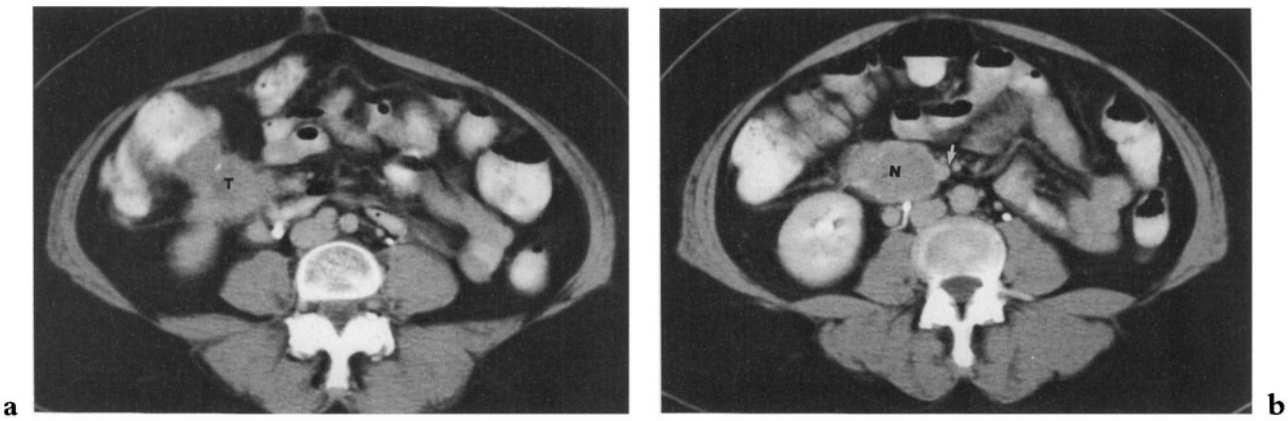


Fig. 6–16. Carcinoid of terminal ileum.
(a) The primary tumor (*T*) is evident.
(b) Metastatic node (*N*) at base of mesentery along ileocolic vessels *(arrow)*.

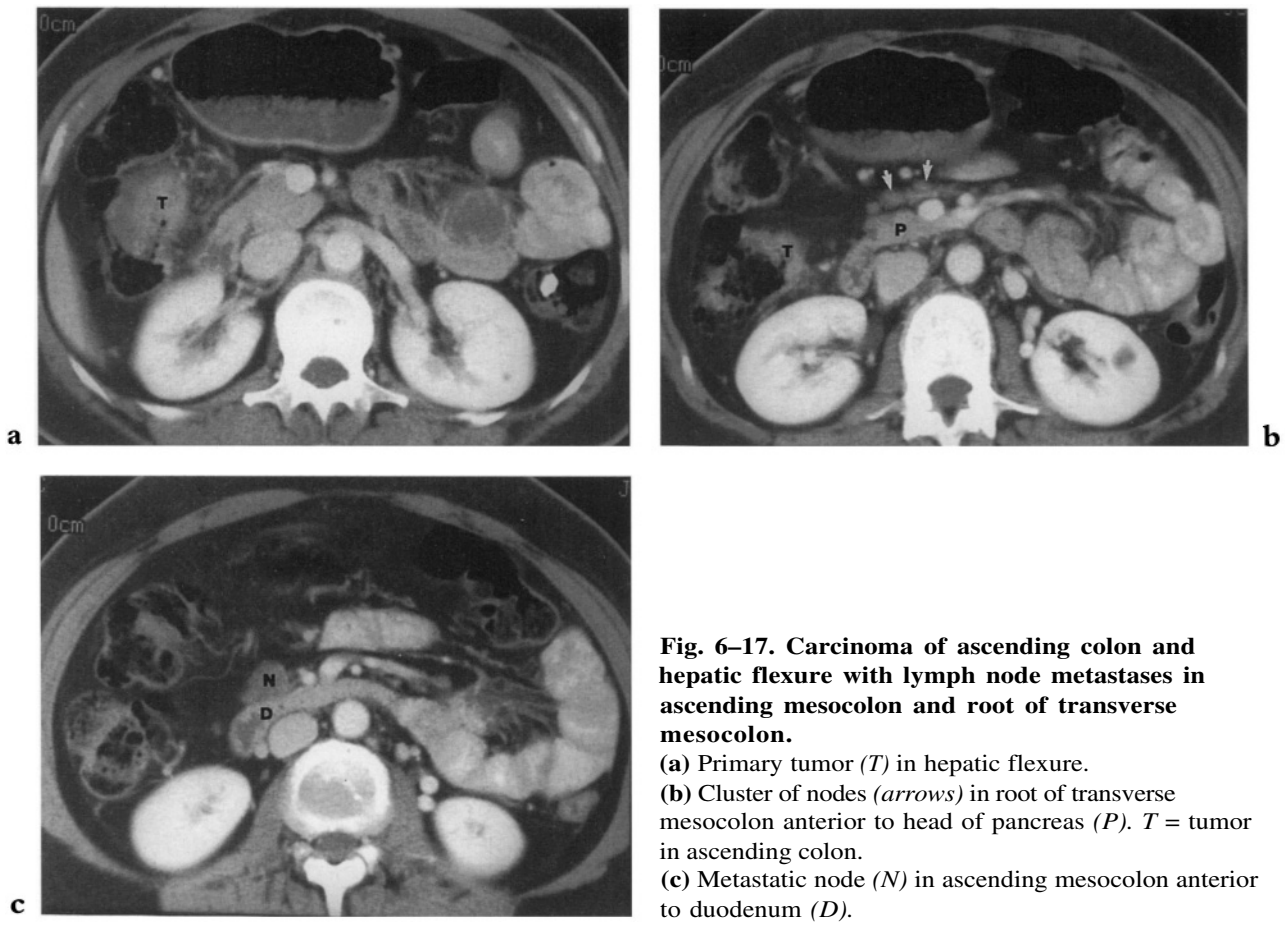


Fig. 6–17. Carcinoma of ascending colon and hepatic flexure with lymph node metastases in ascending mesocolon and root of transverse mesocolon.
(a) Primary tumor *(T)* in hepatic flexure.
(b) Cluster of nodes *(arrows)* in root of transverse mesocolon anterior to head of pancreas *(P)*. *T* = tumor in ascending colon.
(c) Metastatic node *(N)* in ascending mesocolon anterior to duodenum *(D)*.

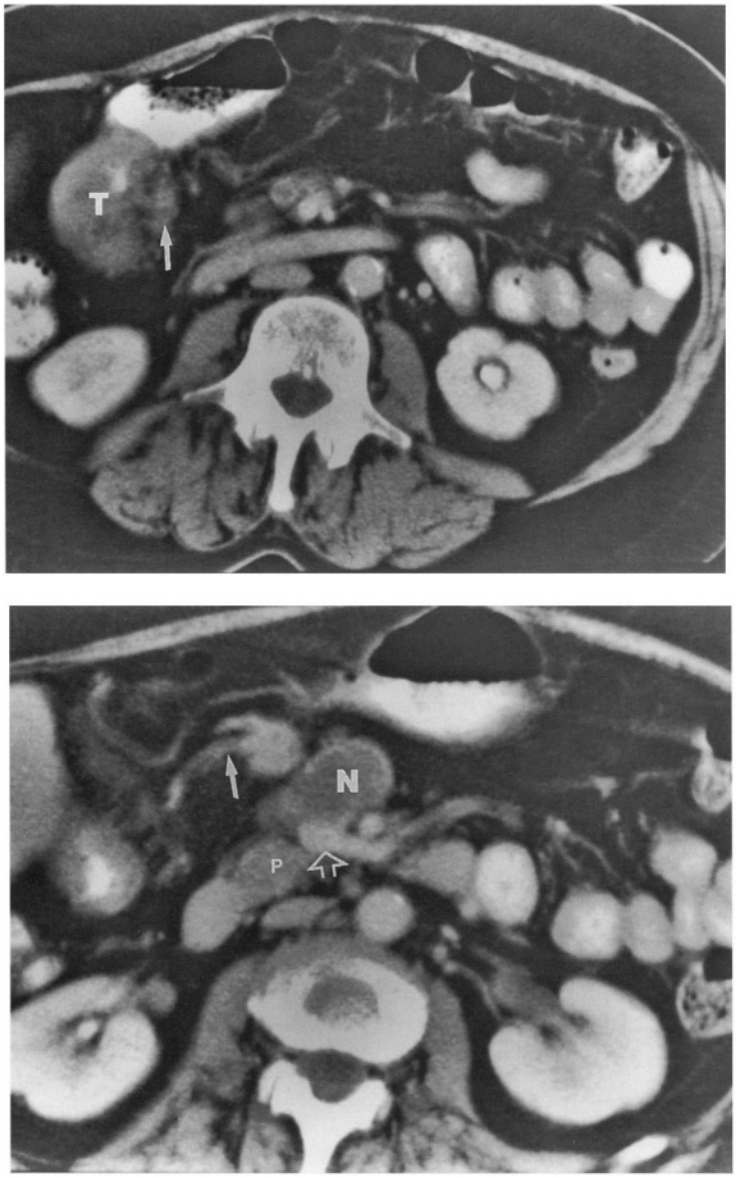


Fig. 6–18. Carcinoma of hepatic flexure of transverse colon with metastatic nodes in mesocolon and nodes at gastrocolic trunk.
(a) Primary tumor *(T)* at hepatic flexure. Note metastatic nodes *(arrow)* at paracolic nodal group.
(b) Note metastatic nodes *(N)* where right middle colic vein *(arrow)* drains into SMV *(open arrow)* anterior to head of pancreas *(P)*.

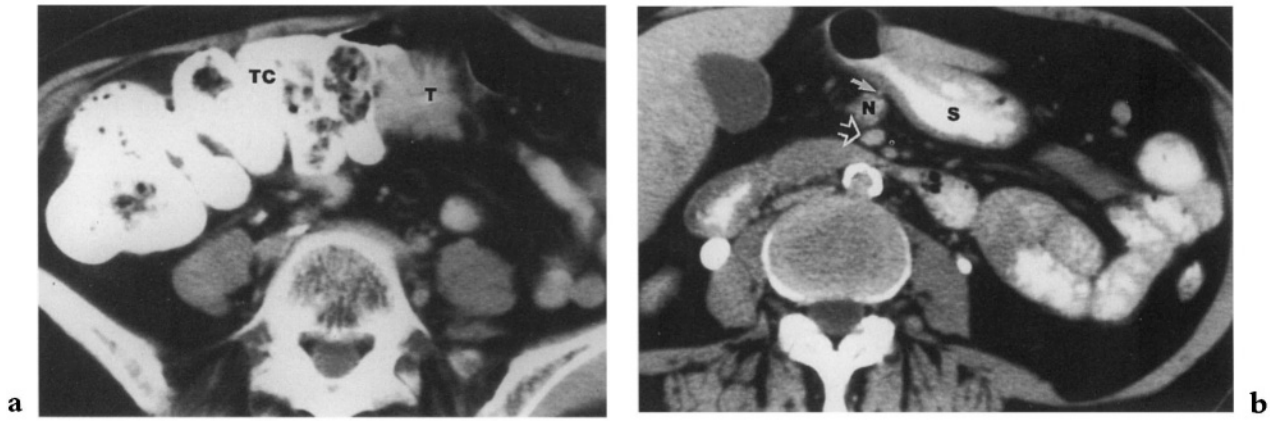


Fig. 6–19. Carcinoma of mid transverse colon with metastatic node in transverse mesocolon.
(a) Primary tumor *(T)* at midtransverse colon *(TC).* Note transverse colon suspended inferiorly to level of umbilicus.
(b) Because transverse colon is hanging down to lower abdomen, transverse mesocolon can be traced in cephalad direction toward the pancreas and, in this case, a metastatic node (*N*) can be identified along middle colic vein *(arrow)* behind the stomach *(S),* before the middle colic vein drains into SMV *(open arrow).*

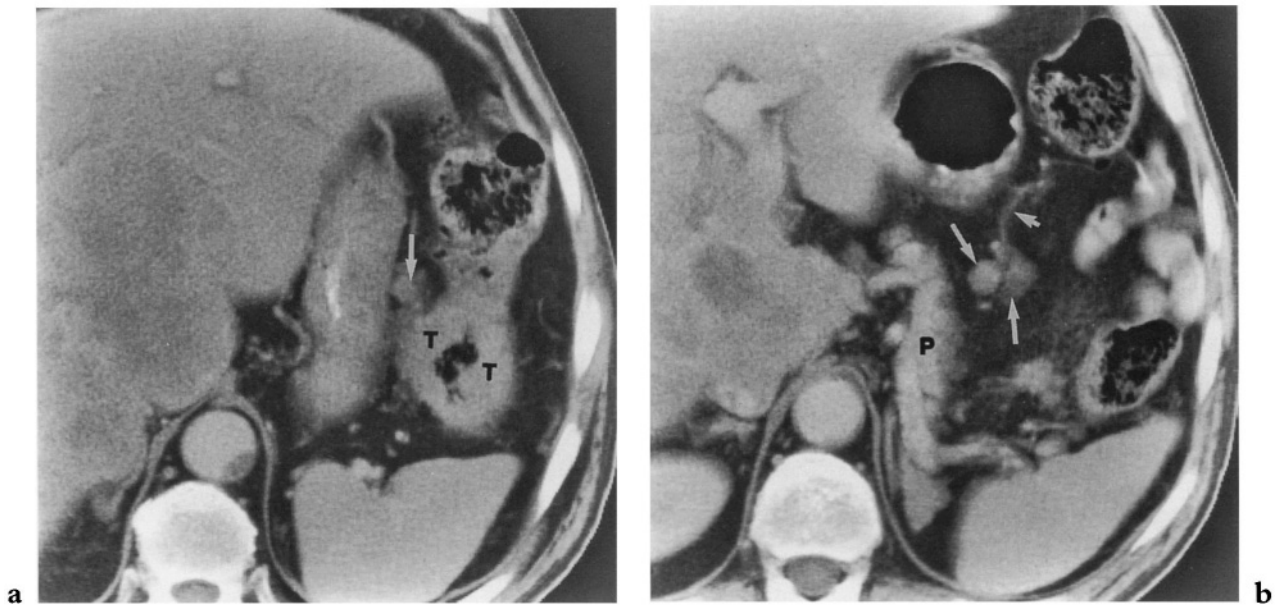


Fig. 6–20. Carcinoma of left transverse colon with metastatic nodes in left transverse mesocolon.
(a) Primary tumor *(T)* at left transverse mesocolon near surgical splenic flexure. Note metastatic paracolic nodes *(arrow)* along marginal vessels.
(b) Note nodes *(long arrows)* in transverse mesocolon along branches of left middle colic vessels *(short arrow).* Pancreas *(P)* is vertically oriented because of the absence of the left kidney.

the principal nodes at the origin of the IMA[18,19] (Figs. 6–21 and 6–22). Progression of nodal metastasis at the root of the sigmoid mesocolon, particularly the one that crosses the left ureter, may cause hydronephrosis of the left kidney. On rare occasion, metastasis may be observed along the IMV at the left duodenomesocolic fold lateral to the fourth portion of the duodenum because there are lymphoid aggregates along the IMV (Fig. 6–

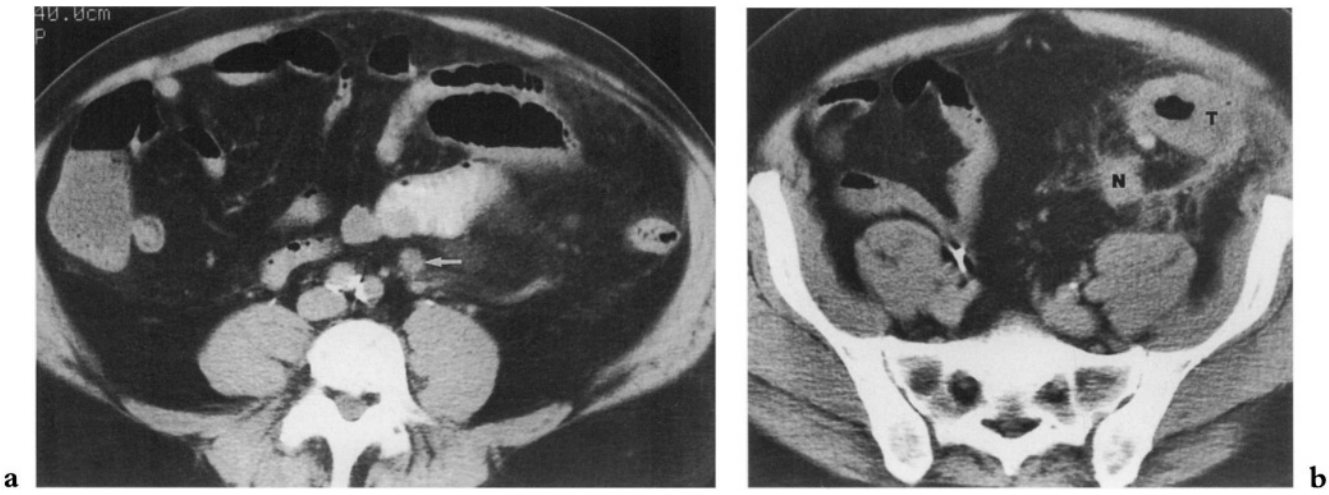


Fig. 6–21. Metastatic adenopathy *(arrow)* in sigmoid mesocolon, shown in **(a)** from primary tumor *(T)* in sigmoid colon shown in **(b).** Also note enlarged paracolic node *(N)* in **(b).**

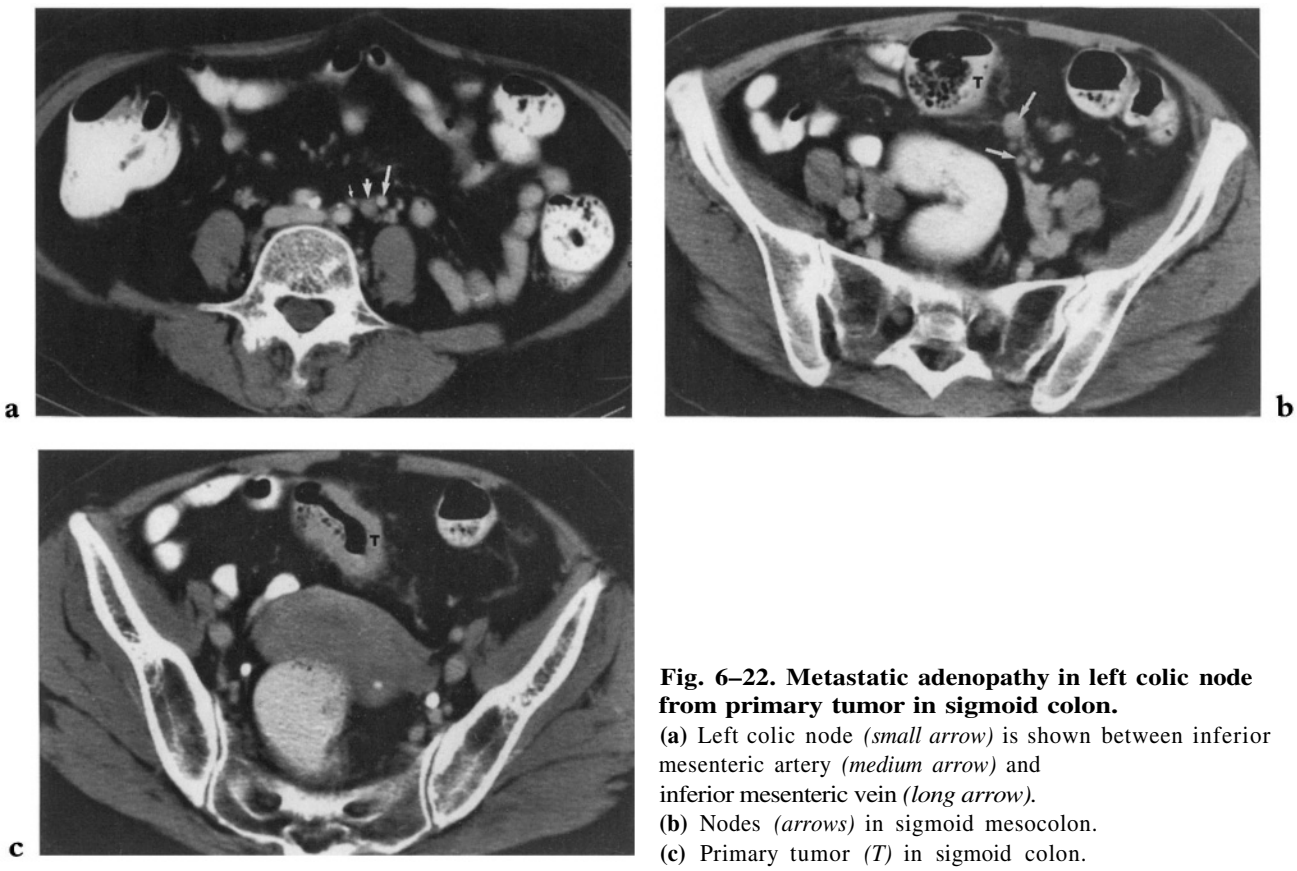


Fig. 6–22. Metastatic adenopathy in left colic node from primary tumor in sigmoid colon.
(a) Left colic node *(small arrow)* is shown between inferior mesenteric artery *(medium arrow)* and inferior mesenteric vein *(long arrow).*
(b) Nodes *(arrows)* in sigmoid mesocolon.
(c) Primary tumor *(T)* in sigmoid colon.



Fig. 6–23. Recurrent adenopathy (*M*) at left paraduodenal space with involvement of pancreas simulating pancreatic cancer.
Patient had primary tumor in sigmoid colon resected. Recurrent disease was confirmed by aspiration biopsy.

23). Metastasis to this area may involve the pancreas and simulate the pancreatic mass.[21]

References

1. Rouvier H, Toblas MJ (trans): Lymphatic system of the abdomen and pelvis. *In* Anatomy of the Human Lymphatic System. Edwards Brothers, Ann Arbor, MI, 1938, pp 158–237.
2. Collins P: Embryology and development. *In* Gray's Anatomy, 38th ed. Edited by PL Williams, LH Bannister, MM Berry, et al. Churchill Livingstone, London, 1995, pp 186–190.
3. Netter FH: Normal anatomy of the liver, biliary tract and pancreas. *In* The Ciba Collection of Medical Illustrations, vol 3: Digestive System: Liver, Biliary Tract and Pancreas. Ciba, Summit, NJ, 1979, pp 2–31.
4. Balfe DM, Mauro MA, Koehler RE, et al: Gastrohepatic ligament: Normal and pathologic CT anatomy. Radiology 1984; 150:485–490.
5. Mori H, McGrath FP, Malone DE, et al: The gastrocolic trunk and its tributaries: CT evaluation. Radiology 1992; 182:871–877.
6. Watanabe J, Nakashima O, Kojiro M: Clinicopathologic study of lymph node metastasis of hepatocellular carcinoma: A retrospective study of 660 consecutive autopsy cases. Jpn J Clin Oncol 1994, 24:37–41.
7. Tanaka T, Nakamura H, Choi S, et al: CT diagnosis of abdominal lymph node metastases in hepatocellular carcinoma. Eur J Radiol 1985; 5:175–177.
8. Araki T, Hihara T, Karikomi M, et al: Hepatocellular carcinoma: Metastatic abdominal lymph nodes identified by computed tomography. Gastrointest Radiol 1988; 13:247–252.
9. Coller FA, Kay EB, MacIntyre RS: Regional lymphatic metastases of carcinoma of the stomach. Arch Surg 1941; 43:748–761.
10. Adachi Y, Oshiro T, Okuyama T: A simple classification of lymph node level in gastric carcinoma. Am J Surg 1995; 169:382–385.
11. Fukuya T, Honda H, Hayashi T, et al: Lymph node metastases: Efficacy of detection with helical CT in patients with gastric cancer. Radiology 1995; 197:705–711.
12. Meyers MA, Oliphant M, Berne AS: The peritoneal ligaments and mesenteries: Pathways of intraabdominal spread of disease. Radiology 1987; 163:593–604.
13. Netter FH: Atlas of Human Anatomy. Ciba Medical Education Division, Summit, NJ, 1989, plate 261–267 and 286–301.
14. Charnsangavej C, Dubrow RA, Varma DGK, et al: CT of the mesocolon: Anatomic considerations. RadioGraphics 1993; 13:1035–1045.
15. Shapir J, Rubin J: CT appearance of the inferior mesenteric vein. J Comput Assist Tomogr 1984; 8:877–880.

16. Goligher J. Surgery of the Anus, Rectum and Colon, 5th ed. Balliere Tindall, Eastbourne, England, 1984, pp 25–26 and 439–460.
17. Rouviere H: The lymphatics of the intestines. *In* Anatomy of the Human Lymphatic System. Edited by H Rouviere. Edwards Brothers, Ann Arbor, MI, 1938, pp 188–196.
18. Granfield CAJ, Charnsangavej C, Dubrow RA, et al: Regional lymph node metastases in carcinoma of the left side of the colon and rectum: CT demonstration. AJR 1992; 159:757–761.
19. Charnsangavej C, Dubrow RA, Varma DGK, et al: CT of the mesocolon: Pathologic considerations. RadioGraphics 1993; 13:1309–1322.
20. McDaniel K, Charnsangavej C, Dubrow RA, et al: Pathway of nodal metastasis in carcinomas of the cecum, ascending colon, and transverse colon: CT demonstration. AJR 1993; 161:61–64.
21. Charnsangavej C, Whitley NO: Metastases to the pancreas and peripancreatic lymph nodes from carcinoma of the right side of the colon: CT findings in 12 patients. AJR 1993; 160:49–52.

Manifestations of Intraperitoneal Air

7

Kyunghee C. Cho, M.D.
Stephen R. Baker, M.D.

A spontaneous pneumoperitoneum usually indicates perforation of a hollow viscus and requires undelayed operative intervention. A plain film examination is often performed before surgery to establish a definitive diagnosis. With careful attention to technique and localizing anatomic features, it can be a valuable examination, capable of detecting even a very small collection of free air.

Detection of Intraperitoneal Air

The upright chest film has long been considered to be the most sensitive plain film view for the recognition of tiny amounts of free air.[1–3] Miller and Nelson showed that as little as 1 mL of free gas could be demonstrated in an erect patient using a horizontal x-ray beam.[1] However, the real sensitivity of the upright projection has not yet been scrutinized by a prospective study. The supine film, obtained with a vertical beam, has been generally considered to be of relatively limited utility, useful only for the recognition of a relatively large amount of air. Actually, more current studies have demonstrated that the supine film is in fact extremely incisive, revealing even less than 1 mL of free air in some cases.[4–7] Yet its true sensitivity also awaits confirmation by prospective analysis.

The CT scan is generally regarded as the gold standard for the recognition of free air.[8–10] In a recent investigation, CT detected all small pneumoperitoneums introduced during diagnostic peritoneal lavage, whereas upright chest films missed almost two thirds of cases.[8] Sonography can occasionally demonstrate extraluminal gas, but it rarely demonstrates very small accumulations of free air.[11,12]

Supine Abdominal Films

In the past decade, the utility of the supine film for the detection of free air has been reassessed, and several new observations have been reported.[4–6,13–18] The right upper quadrant is the most fruitful place to look for a small pneumoperitoneum,[5,6,18,19] because CT studies have shown that free air most commonly accumulates in this abdominal region.[8,20] Moreover, the homogeneous shadow of the liver provides an excellent background, enabling small deposits of air to stand out clearly.

The conventional abdominal film, colloquially known as a KUB, often excludes from view the uppermost abdomen, the locus of most collections of free air. This is because the abdomen in many adults is often too long to be encompassed in its entirety on one supine film. This geometric limitation partly explains the 59% detection rate of pneumoperitoneum on supine films in a recent study by Levine et al.[18] To recognize subtle signs of free air, the entire right upper quadrant must be carefully scrutinized, sometimes on a separate film. Any lucency inconsistent with the expected pattern of gas in the stomach, duodenum, distal small bowel, and colon must be regarded with suspicion.

Supine Film Signs of Pneumoperitoneum

Supine film signs of pneumoperitoneum can be divided into four categories (Table 7–1): (a) Depiction of ligaments protruding into the peritoneal cavity; (b) Visualization of the peritoneal surface of intraabdominal organs; (c) Detection of free air confined in specific peritoneal recesses; and (d) Recognition of free air superimposed on the liver shadow.

Depiction of Ligaments Protruding into the Peritoneal Cavity

Falciform Ligament

The falciform ligament is a sickle-shaped or triangular fold of peritoneum that affixes the liver to the anterior abdominal wall and the diaphragm (Fig. 7–1). When air collects anteriorly abutting both sides of the ligament, it can be visualized as a vertical paramedian line curving slightly to the right, directed inferiorly toward the umbilicus (Figs. 7–2 through 7–7). The falciform ligament varies in thickness from 1–15 mm. It usually has a thin edge superiorly but may have a bulbous caudal end (Figs. 7–5 through 7–7). The attachment of the upper portion of the falciform ligament to the anterior surface of the liver extending from the ligamentum teres notch caudally to the diaphragm superomedially may be also delineated by air (Figs. 7–7 and 7–8).

Table 7–1. Supine film signs of pneumoperitoneum

A. Depiction of ligaments protruding into the peritoneal cavity
Falciform ligament
Ligamentum teres
Medial umbilical folds, inverted V sign
Urachus
B. Visualization of peritoneal surface of abdominal organs
Rigler's sign
Triangle sign
Hepatic edge
Hepatic notch
Gallbladder
C. Detection of free air confined in specific peritoneal recesses
Cupola sign
Diaphragm muscle slip sign, leaping dolphins sign
Ligamentum teres fissure sign
Morison's pouch air (doge's cap sign)
Football sign
Lesser sac gas
Left upper quadrant gas
Pneumoscrotum
D. Recognition of free air superimposed on the liver shadow
Lucent liver
Anterior superior bubble
Ill-defined pereiduodenal lucency

Ligamentum Teres

The ligamentum teres is a fibrous cord representing an obliterated left umbilical vein.[21] Lying in the free edge of the triangular falciform ligament, the ligamentum teres ascends from the umbilicus to the ligamentum teres notch at the inferior border of the liver (Figs. 7–1 and 7–9). It then enters the liver, traverses the fissure for the ligamentum teres, and terminates by joining the left portal vein at the left extremity of the porta hepatis opposite the attachment of the ligamentum venosum.[22]

The extrahepatic segment of the ligamentum teres is located within the anterior peritoneal cavity and can be discerned when outlined by free air. It appears in the inferomedial aspect of the right upper quadrant, directed obliquely between the umbilicus and the ligamentum teres notch of the liver. It describes a straight or gently curved oblique interface with a clearly defined inferolateral margin, or it is configured as a well-defined band of increased density of varying length[13,23] (Figs. 7–3, 7–6, 7–7, 7–10). Its presentation on supine films depends on the quantity and position of free air as well as the shape and size of the ligament. The falciform ligament, if also delineated by air, can be seen together with the ligamentum teres as they merge caudally near the umbilicus (Figs. 7–3, 7–6, 7–7). The ligamentum teres sign requires a moderate to large amount of free air. Hence, it is nearly always accompanied by other signs of pneumoperitoneum.

Inverted V Sign

The inverted V sign refers to visualization of the medial umbilical folds (they are also known as umbilical ligaments, but folds are the preferred term), which together form an inverted V-shaped increased density in the pelvis outlined by free air[24,25] (Fig. 7–11). Anatomically, there are actually two pairs of folds in the lower abdominal wall that can create an inverted V; the medial umbilical folds representing the obliterated umbilical arteries, and the lateral umbilical folds containing the inferior epigastric vessels.[22]

text continues on page 316



Fig. 7–1. Falciform ligament and ligamentum teres.
The gross specimen of the upper abdominal contents demonstrates the falciform ligament with its attachment to the resected anterior abdominal wall *(arrowheads)* and the ligamentum teres *(arrows)* lying along the free margin of the sickle-shaped fold of the peritoneum, the falciform ligament. Note also the hepatic attachment of the falciform ligament.
(From Gosling JA, Harris PF, Humpherson JR: Human Anatomy: Text and Colour Atlas. Brower Medical, London, 1990, pp 4–28.)

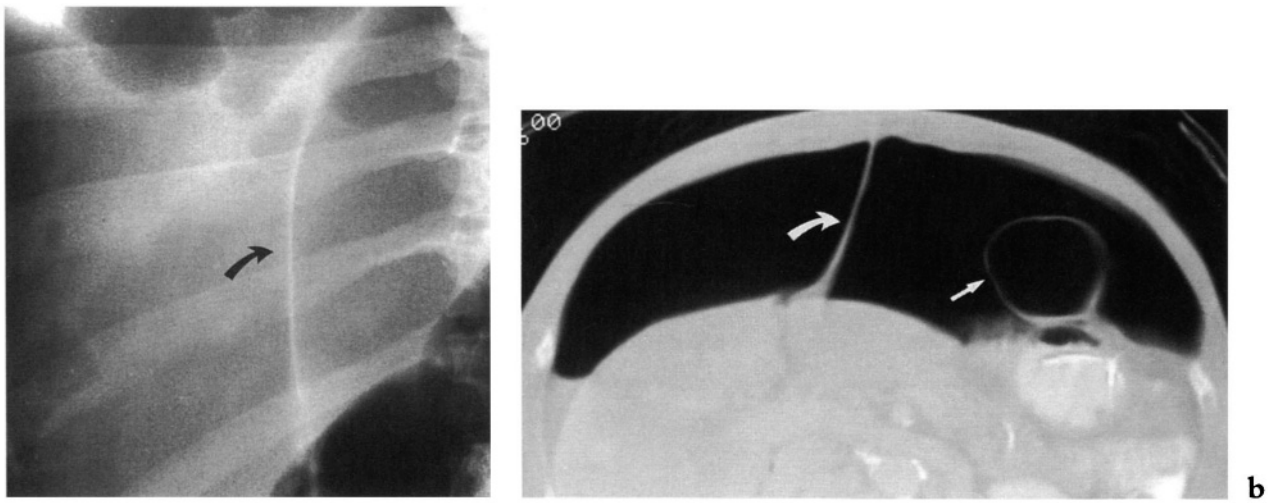


Fig. 7–2. Falciform ligament.
(a) A thin vertical paramedian line represents the falciform ligament *(curved arrow)* delineated by free air on both sides.
(b) CT reveals the falciform ligament *(curved arrow)* and a gas-distended colonic loop *(straight arrow)* within the anterior peritoneal cavity surrounded by a large pneumoperitoneum.

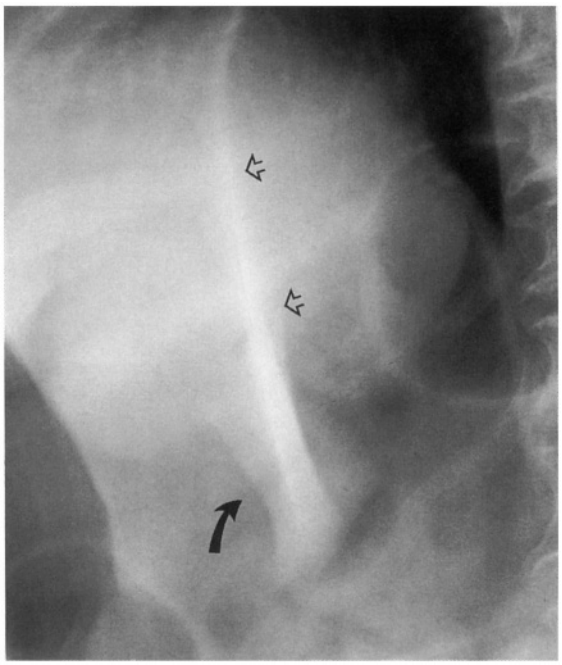
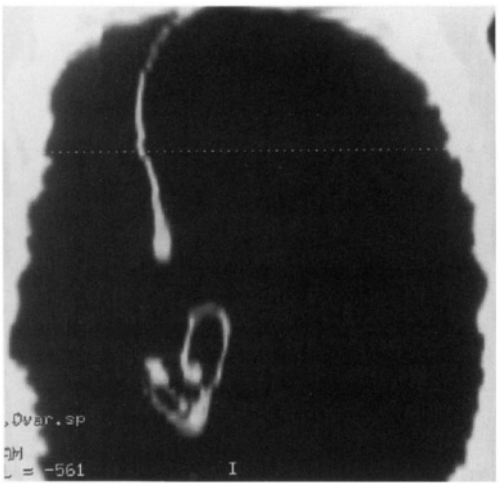
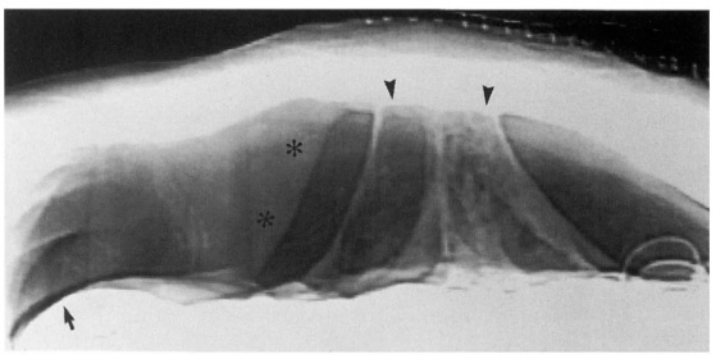


Fig. 7–3. Falciform ligament.
A slightly rotated supine film shows a large pneumoperitoneum delineating a long falciform ligament *(open arrows),* thin in its superior aspect but much thicker distally. Note also the ligamentum teres *(curved arrow)* directed obliquely toward the liver. Rigler's sign is also present.



a



b

Fig. 7–4. Falciform ligament.
(a) A coronal reformatted image of the anterior abdomen from a CT scan reveals a large pneumoperitoneum outlining the falciform ligament in the right upper quadrant. The amorphous rounded structure caudal to the ligament represents adhesive bands extending between the anterior abdominal wall and the underlying abdominal contents within the anterior peritoneal cavity, also delineated by free air.
(b) A digital radiograph in cross-table lateral projection demonstrates the falciform ligament as a broad fold of peritoneum *(asterisks)* and multiple adhesive bands *(arrowheads)* caudally within the anterior peritoneal cavity surrounded by free air. Diaphragm muscle slips are also delineated *(arrow).*

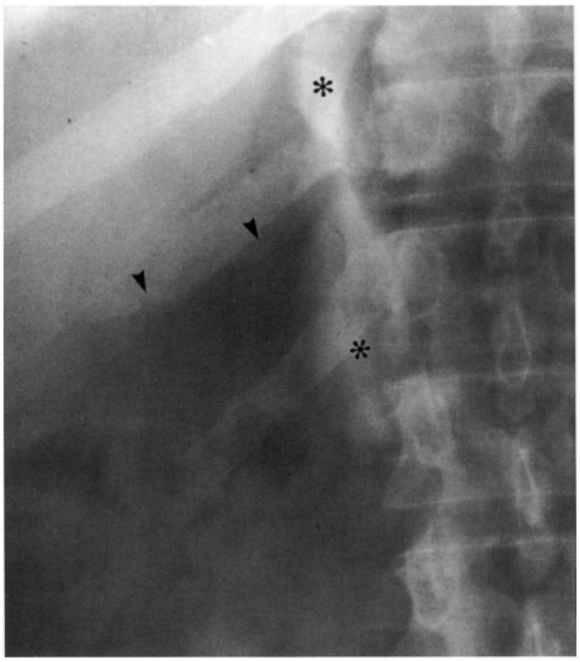


Fig. 7–5. Falciform ligament.
An unusually thick falciform ligament *(asterisk)* having a bulbous lower end is outlined by free air. Note also the hepatic edge seen as a smooth, oblique interface *(arrowheads).*



Fig. 7–6. Ligamentum teres, falciform ligament, and hepatic notch.
A supine film during an upper GI series demonstrates juxtaposition of the ligamentum teres *(arrows),* the falciform ligament *(arrowheads),* and the ligamentum teres notch *(curved arrow).* The ligamentum teres is seen as a long curved interface entering the liver. Note also the nodular thickening of the falciform ligament near the umbilicus *(asterisk).*
(From Cho and Baker.[13])



Fig. 7–7. Ligamentum teres sign.
A slightly rotated supine film during a water soluble contrast study of the bowel reveals the extrahepatic ligamentum teres presenting as a thick oblique band of soft tissue density *(long arrows).* It joins the vertically oriented, thin linear falciform ligament *(arrowheads)* caudally. The ligamentum teres notch is denoted by the *open curved arrow. Small arrows* highlight the hepatic attachment of the triangular "anatomic" falciform ligament stretching between the anterior abdominal wall and its free inferior edge, the ligamentum teres. Contrast fills the esophagus.
(From Cho and Baker.[13])



Fig. 7–8. Morison's pouch air (doges's cap sign.) A digital radiograph shows air trapped in Morison's pouch posteriorly below the 11th rib *(arrow)* and air overlying the liver anteriorly, which has a more diffuse presentation. The hepatic attachment of the falciform ligament is also visualized as an oblique curvilinear interface overlying the 10th rib *(arrowheads).*
(From Cho.[16])

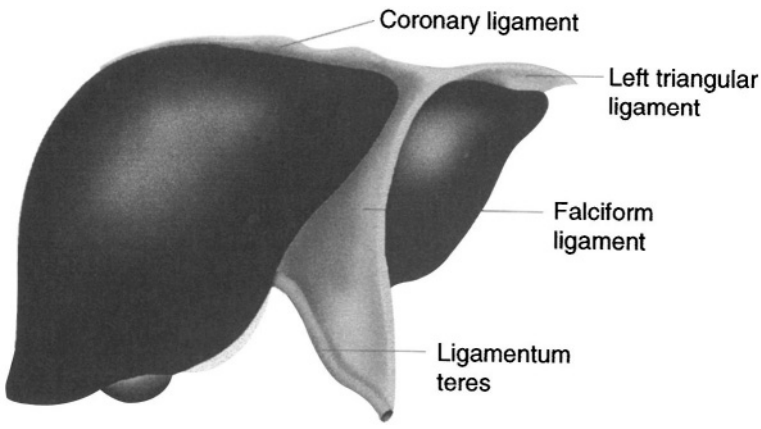


Fig. 7–9. Illustration of the anterior surface of the liver. Note the spatial relationship between the ligamentum teres, the falciform ligament, the coronary ligament, and the left triangular ligament with their attachments to the liver.
(From Cho and Baker.[14])

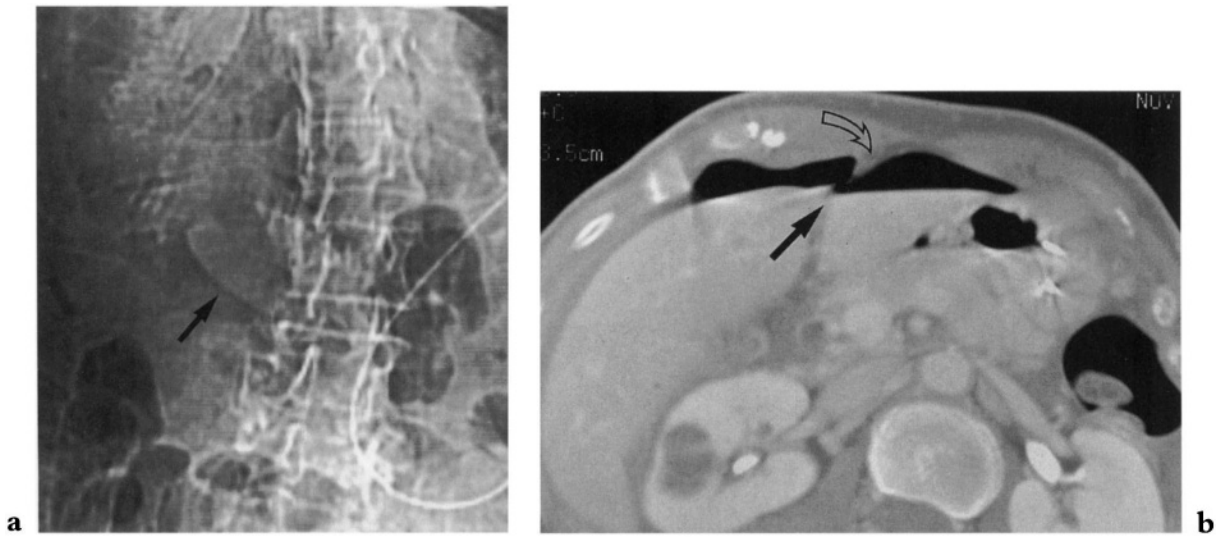


Fig. 7–10. Ligamentum teres sign.
(a) A supine digital radiograph shows a distinct oblique interface *(arrow)* representing the extrahepatic segment of the ligamentum teres visualized by adjacent free air.
(b) A corresponding CT image shows a ventral collection of free air outlining the ligamentum teres *(open arrow).* The *black arrow* points to the ligamentum teres notch between the medial and lateral segments of the left hepatic lobe.
(From Cho and Baker.[13])

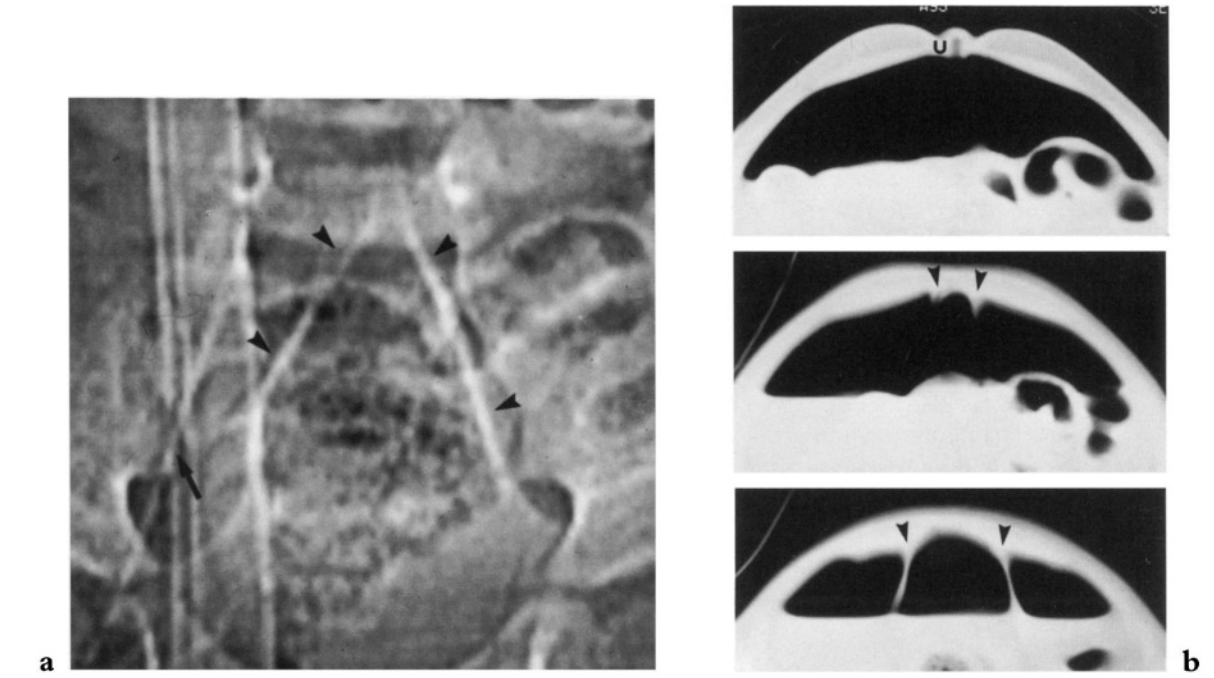


Fig. 7–11. Inverted V sign in an infant with massive pneumoperitoneum from child abuse.
(a) On a digital scout radiograph at the time of CT scan, an inverted V *(arrowheads)* representing the medial umbilical folds is seen with its apex at the umbilicus. A femoral venous catheter is seen laterally *(arrow).*
(b) Three CT images with the most superior, at the level of the umbilicus *(u)* and the other two more caudad, show the medial umbilical folds *(arrowheads)* outlined by free air converging into the umbilicus.
(From Cho et al.[5])

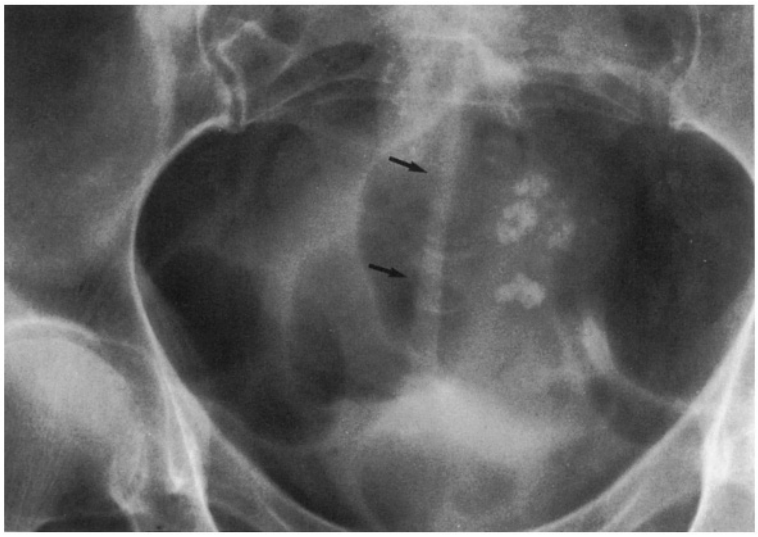


Fig. 7–12. Urachus.
The urachus is seen as an elongated density slightly wider inferiorly situated between the umbilicus and the bladder visualized by virtue of free air *(arrows).* Calcifications in a uterine fibroid are incidentally evident.
(From Cho and Baker.[17])

There has been some confusion in the literature regarding the nomenclature of the umbilical ligaments and with respect to the inverted V sign. In older texts and in the original article describing this sign,[24] the medial umbilical ligament was erroneously labeled as the lateral umbilical ligament. Moreover, Bray[25] in 1984 reported that the inverted V represented the medial umbilical ligaments (obliterated umbilical arteries) in infants and the lateral umbilical ligaments (inferior epigastric arteries) in adults. Some investigators, however, believe that even in adults the medial umbilical ligaments are usually responsible for this sign because they are the more prominent fold pair.[5,26] Nonetheless, the inverted V sign requires a large pneumoperitoneum and is never the sole indicator of free air. The sign is often subtle, and only one fold or even only part of one may be visible.

Urachus

The median umbilical ligament containing the obliterated urachus can be outlined by free air as an elongated tubular or slightly triangular density located in the midline between the umbilicus and the bladder (Fig. 7–12). A massive pneumoperitoneum is also needed to demonstrate this interesting, albeit rare sign.

Visualization of the Peritoneal Surface of Intraabdominal Organs

Rigler's Sign

Also known as the bas relief or double wall sign, Rigler's sign is the most frequently cited plain film manifestation of free air. It refers to the demarcation of both the inner and outer surface of the bowel wall by the simultaneous presence of air in the lumen and outside the serosa (Fig. 7–13). Sometimes, only the serosal surface of the bowel is delineated because its lumen is completely filled with fluid. Large accumulations of air are needed to demonstrate the bas relief sign. Furthermore, it is nonspecific, sometimes simulated by abundant abdominal fat and by distended adjacent bowel loops (Fig. 7–14).



Fig. 7–13. Rigler's sign.
A large pneumoperitoneum allows clear demarcation of the bowel walls on plain film.

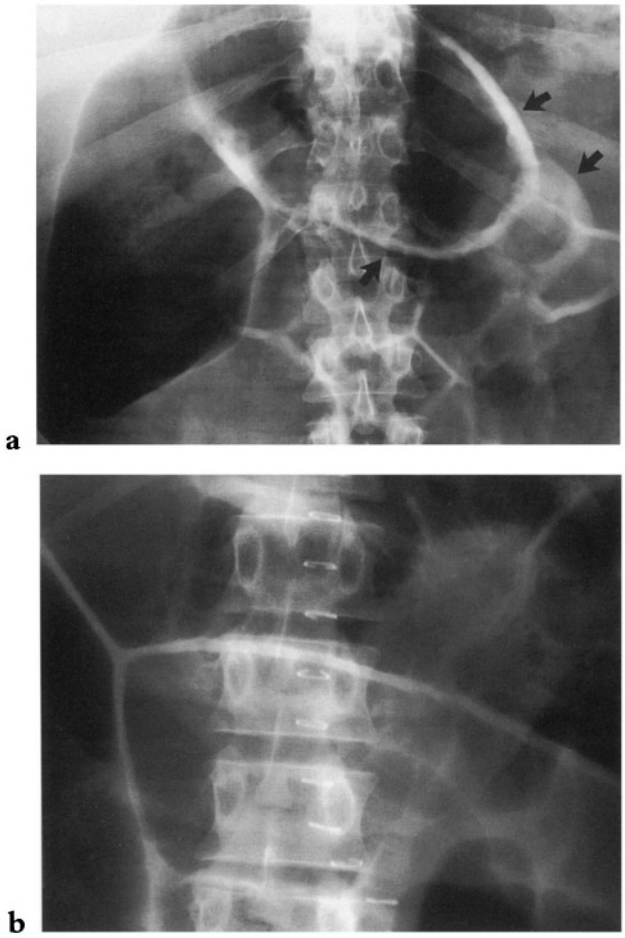


Fig. 7–14. Pseudo Rigler's sign.
(a) The serosal surface of markedly dilated, thick-walled ileal loops *(arrows)* is visualized by abundant "creeping fat" of the mesentery in this young man with long-standing Crohn's disease with ileal stricture.
(b) Adjacent gas-distended bowel loops produce an appearance resembling Rigler's sign.

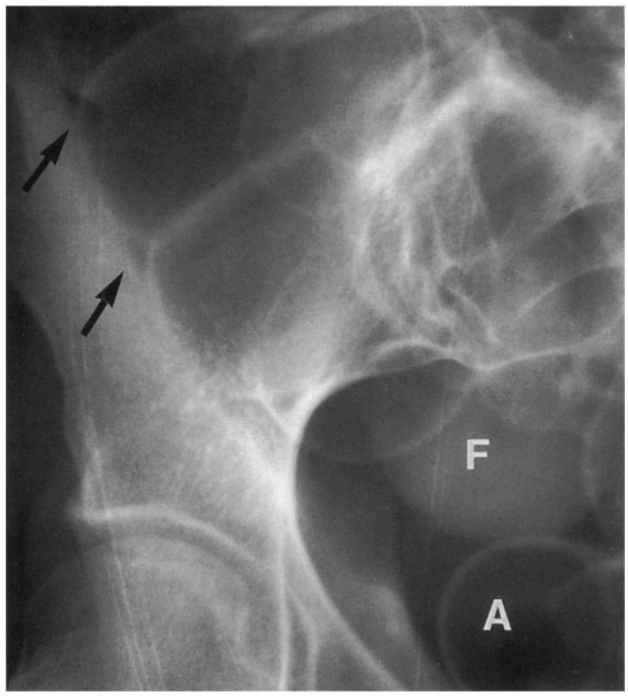


Fig. 7–15. Triangle sign.
Small triangular collections of free air *(arrows)* are usually best depicted in the right lower quadrant. Note Rigler's sign of two ileal loops: one distended with fluid *(F)* and the other with air *(A)*.
(From Cho.[16])

Triangle Sign

Air trapped between two bowel loops and also abutting the nearby lateral edge of the peritoneal cavity or a third bowel loop appears as a sharply outlined, triangular lucency (Fig. 7–15). Sometimes only two sides of the triangle are well delineated, with the border of the third one less distinct (Fig. 7–16). Although it is not a very sensitive indicator of free air, the triangle sign is highly specific and is best depicted at the periphery of the lower abdomen. The triangle sign is also valuable for confirming that a coincident Rigler's double wall sign is a true manifestation of free air rather than merely a delineation of the mural surface by the juxtaposition of a separate bowel loop or by adjacent fat.

Hepatic Edge

The anterior inferior margin of the liver, either the right or left lobe, may be revealed as a slitlike or crescentic lucency (Fig. 7–17) or an oblique interface with a well-defined superolateral margin (Figs. 7–5 and 7–18).

Hepatic Notch

The ligamentum teres notch is an indentation in the inferior hepatic margin situated between the lateral and medial segments of the left lobe. Consequently, it can be visualized as an inverted V-shaped lucency in the right upper quadrant, with its superior borders delimiting the liver edge[5,16] (Fig. 7–18). The ligamentum teres, if outlined with air, may be seen directed toward the notch.

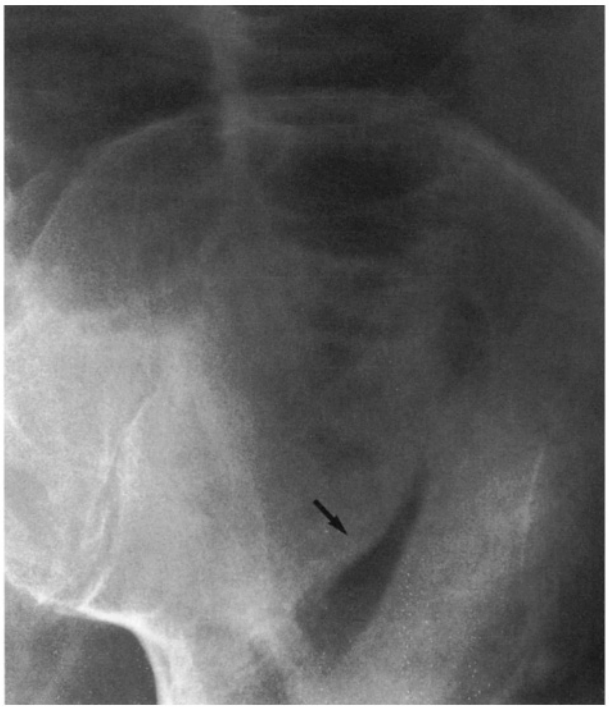


Fig. 7–16. Triangle sign.
A lucent collection in the left lower quadrant *(arrow)* represents free air between a bowel loop and the lateral peritoneal wall. The "base" of the extraluminal triangle is less distinct than the other two borders.

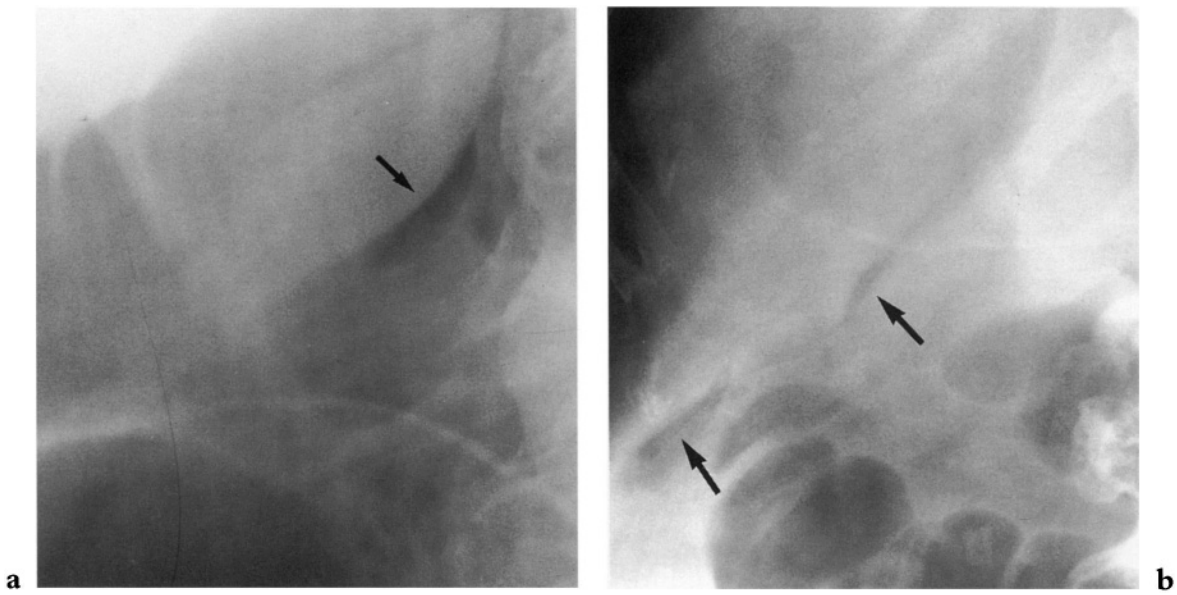


Fig. 7–17. Hepatic edge.
Two examples of free air depicting an outline of a portion of the anterior inferior hepatic edge, manifested by a crescentic lucency *(arrow)* in **a** and slitlike lucencies *(arrows)* in **b.** Note also the bas relief sign in **a** and the diffuse lucency over the liver in **b.**



Fig. 7–18. Hepatic notch.
Inverted V-shaped gas collection delineates the ligamentum teres notch *(curved arrow) in* the inferior border of the liver between the medial and lateral segments of the left lobe. Note also the well-defined hepatic edges *(arrowheads).*

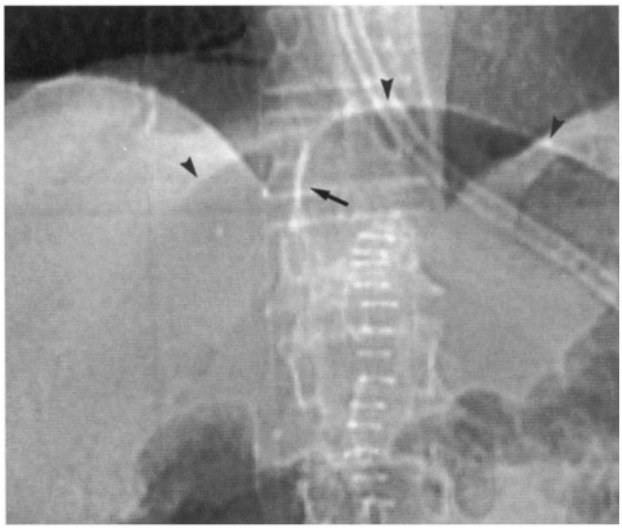


Fig. 7–19. Cupola sign.
A large free air collection in the midsubphrenic space is clearly seen as a diffuse lucency high in the epigastrium with a sharply defined superior border curving downward *(arrowheads).* Inferiorly, the lucency is typically open without a demarcation. Note that the falciform ligament *(arrow)* is contiguous with the superior border.

Gallbladder

The fundus or body of the gallbladder can be outlined by a large pneumoperitoneum.[27]

Detection of Free Air Confined in Specific Peritoneal Recesses

Cupola Sign

An anterior free air collection in the midsubphrenic space underneath the middle leaf of the central tendon of the diaphragm can be detected on supine films by its characteristic location and configuration.[5,16,28] The cupola sign, also known as visualization of the inferior border of the heart, appears as a radiolucency of varying size, sharply defined above but poorly delimited below, overlying and extending lateral to the spine just caudad to the heart (Figs. 7–19 through 7–21). Its upper margin is straight or slightly concave downward. Within its lucent shadow may be seen the falciform ligament (Fig. 7–19). The appearance of this intraperitoneal collection is affected by the volume of air defining it and by the orientation of the diaphragm. A small linear free air deposit can be simulated by extraperitoneal air near the

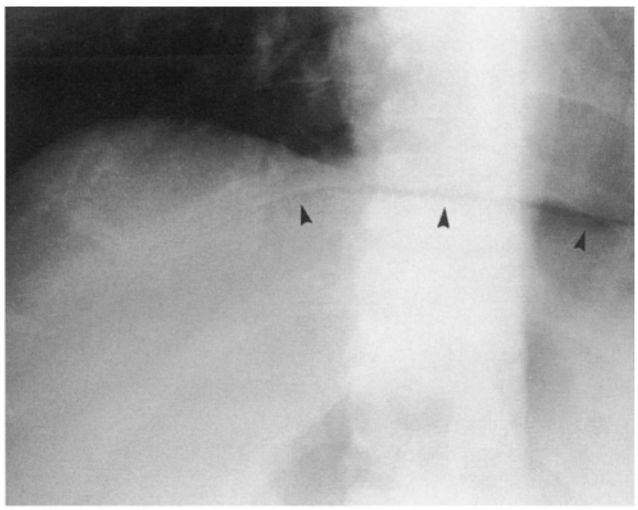


Fig. 7–20. Cupola sign.
A supine film reveals a thin transverse line of lucency *(arrowheads)* delineating the undersurface of the central tendon of the diaphragm beneath the pericardium, mimicking an extraperitoneal air collection. Note the smooth downward deflection of the superolateral border, characteristic for the cupola sign.
(From Baker and Cho.[6])

diaphragm[29] (Fig. 7–20). A gas-filled stomach or transverse colon situated high in this space should not be mistaken for free air.

The cupola sign, described by Mindelzun and McCort[28] in 1986, is one of the most valuable manifestations of free air on plain films, but it has been underemphasized. The middle leaf of the central tendon, ventrally positioned with respect to either the right or left leaf,[30] is the preferred site for free air accumulation in the supine position. On portable chest radiographs, especially in immobile patients confined in the intensive care units, this upper abdomen should be carefully evaluated to diagnose pneumoperitoneum that may be clinically unsuspected.[16,17,31]

Diaphragm Muscle Slip Sign, Leaping Dolphins Sign

The diaphragm muscle slip sign is a recently recognized, yet surprisingly common, right upper quadrant sign that refers to visualization of the costal muscle slips of the diaphragm outlined by a relatively large pneumoperitoneum. It appears in the superior half of the right upper quadrant as sharply defined, long arcuate interfaces or curved bands of increased density[14] (Figs. 7–4b, 7–21 through 7–23). Generally, two to four elongated, parallel curves can be seen, each gently arching convex upward, and all merge together superomedially. Resembling the

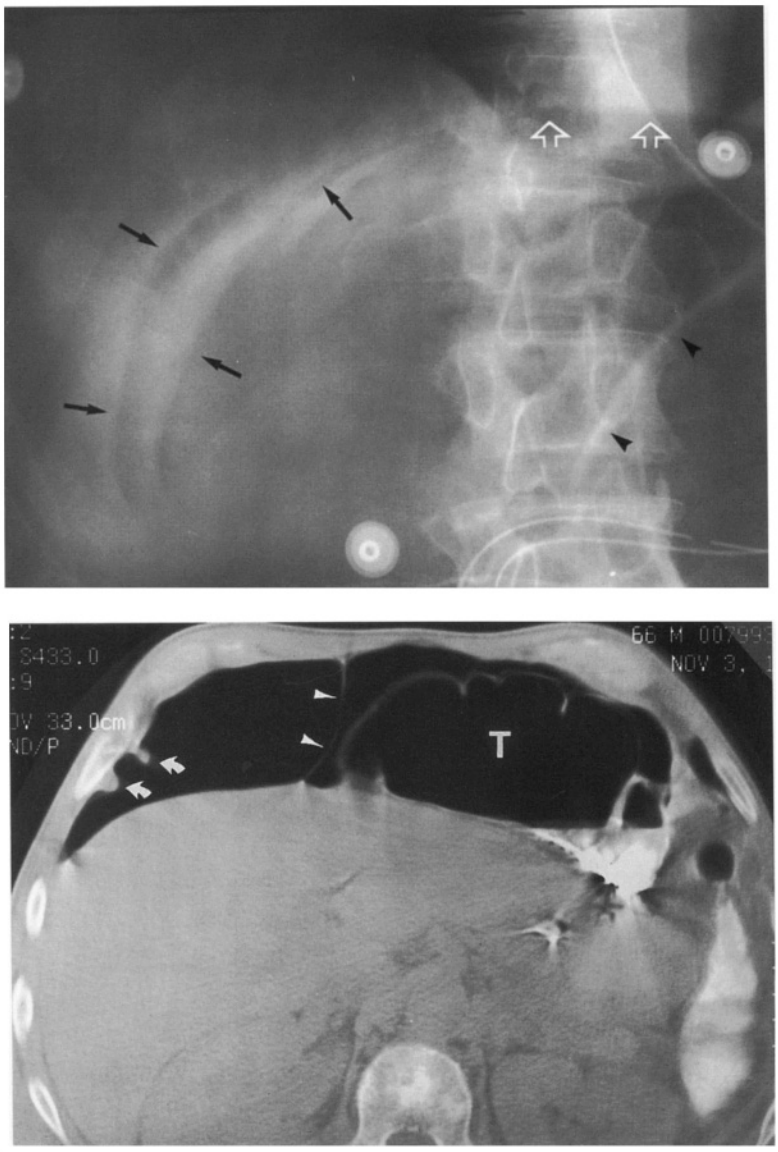


Fig. 7–21. Diaphragm muscle slip sign in a patient with infarcted small intestine and pneumoperitoneum.
(a) Two long arcuate interfaces, paralleling each other *(arrows),* represent the costal muscle slips of the diaphragm indenting the parietal peritoneum, thus delineated by adjacent free air. Superomedially, they converge into the central tendon of the diaphragm, outlined also by pneumoperitoneum—the cupola sign *(open arrows).* The wall of the markedly gas-distended colon is indicated by the *arrowheads.*
(b) Corresponding CT image confirms the presence of two muscle slips anteromedially *(arrows).* The serosal surface of the transverse colon *(T)* and the falciform ligament *(arrowheads)* are well delineated by free air.
(From Cho and Baker.[14])

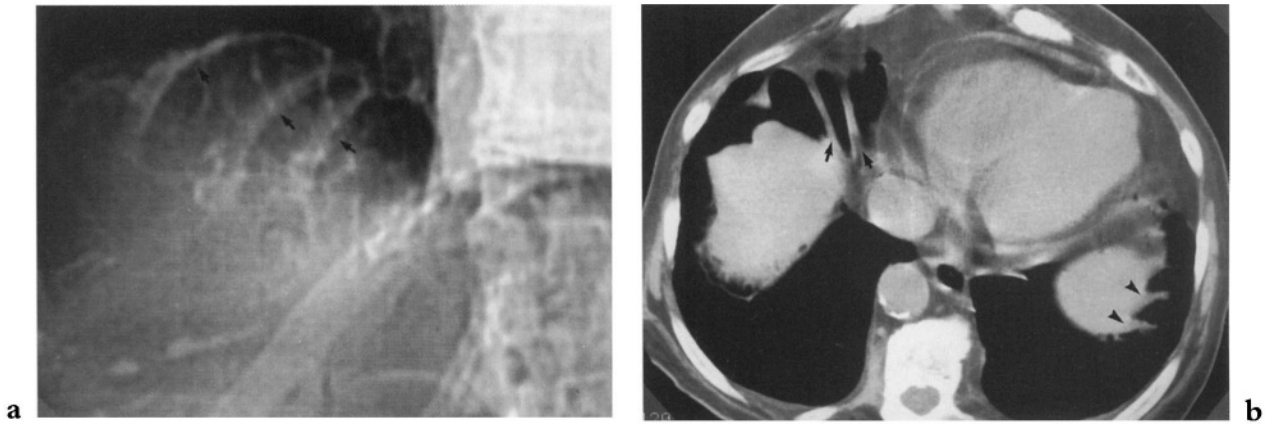


Fig. 7–22. Diaphragm muscle slip sign.
A massive pneumoperitoneum developed following endoscopic biopsy of a gastric ulcer.
(a) On a spine digital radiograph, three diaphragm muscle slips are depicted as distinct curved bands merging together superomedially.
(b) A CT image through the dome of the diaphragm reveals two discrete muscle slips *(arrows)* separating free air into three ovoid pockets. Muscle slips are also seen on the left *(arrowheads).*
(From Cho and Baker.[14])

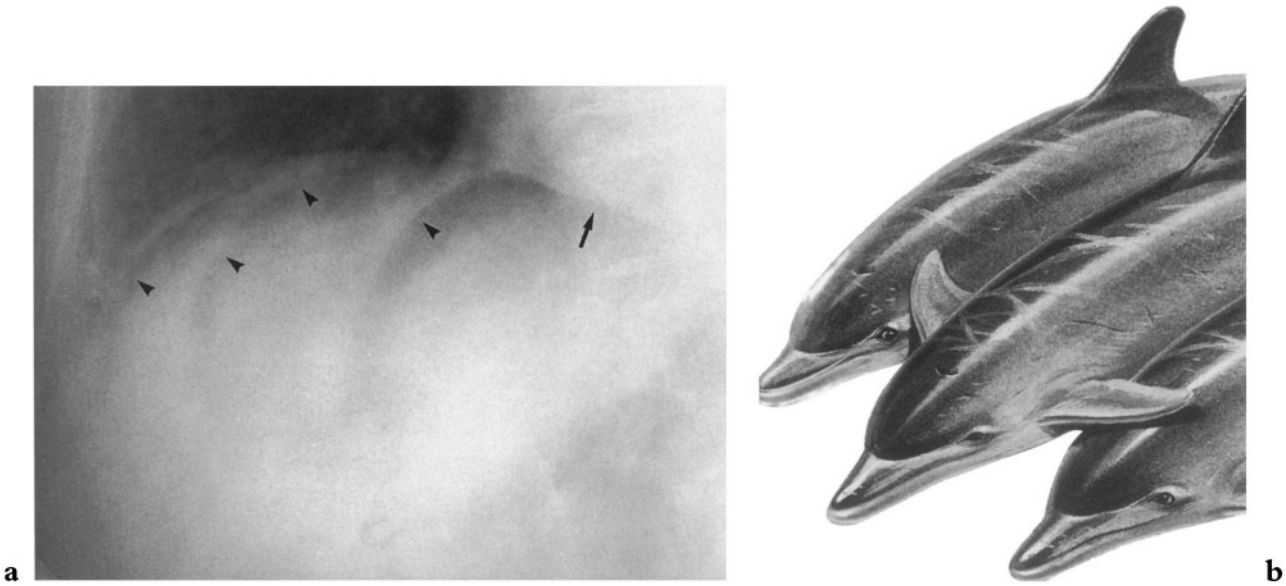
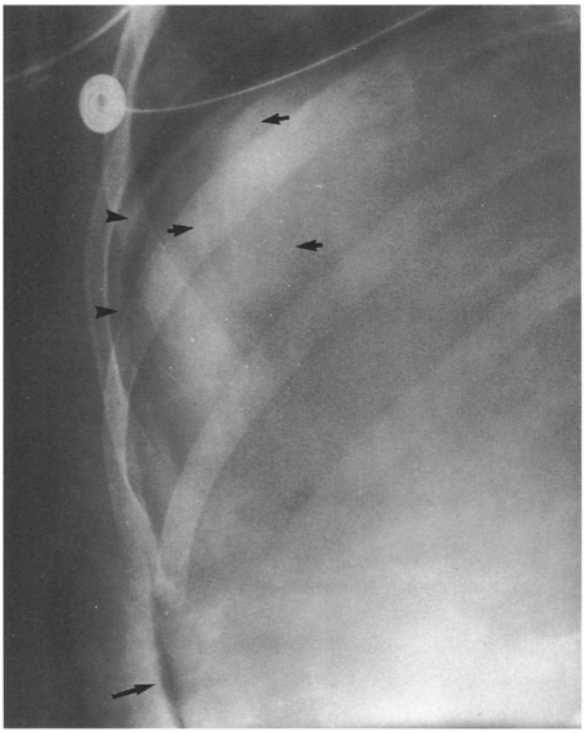


Fig. 7–23. Diaphragm muscle slip sign; leaping dolphins sign.
(**a**) Three diaphragm muscle slips *(arrowheads)* converging superomedially into the central tendon *(arrow)* are visualized by free air on a supine chest radiograph. (**b**) It has an appearance reminiscent of the graceful bending of dolphins leaping in unison.
(From Baker and Cho.[6])



graceful dorsal curvature of the dolphins leaping in unison, the pattern is also named the leaping dolphins sign[6] (Fig. 7–23).

The muscle slip sign for pneumoperitoneum should not be confused with the less distinct, more numerous curvilinear shadows that are depicted as a result of extraperitoneal air infiltrating the diaphragmatic muscle itself[32] (Fig. 7–24). In chronic obstructive pulmonary disease, the supporting edge of the costal muscle slips may occasionally be visualized by overinflated lung that may even indent the underlying hepatic surface. In general,

Fig. 7–24. Visible muscle of the diaphragm due to extraperitoneal air.
A supine film reveals diaphragmatic muscle fibers depicted by infiltrating extraperitoneal air as several gently curved, vertical lines *(short arrows).* They are indistinct, short, and accompanied by crescentic deposits of retroperitoneal air under the diaphragm *(arrowheads)* as well as in the flank *(long arrow).*
(From Cho and Baker.[14])

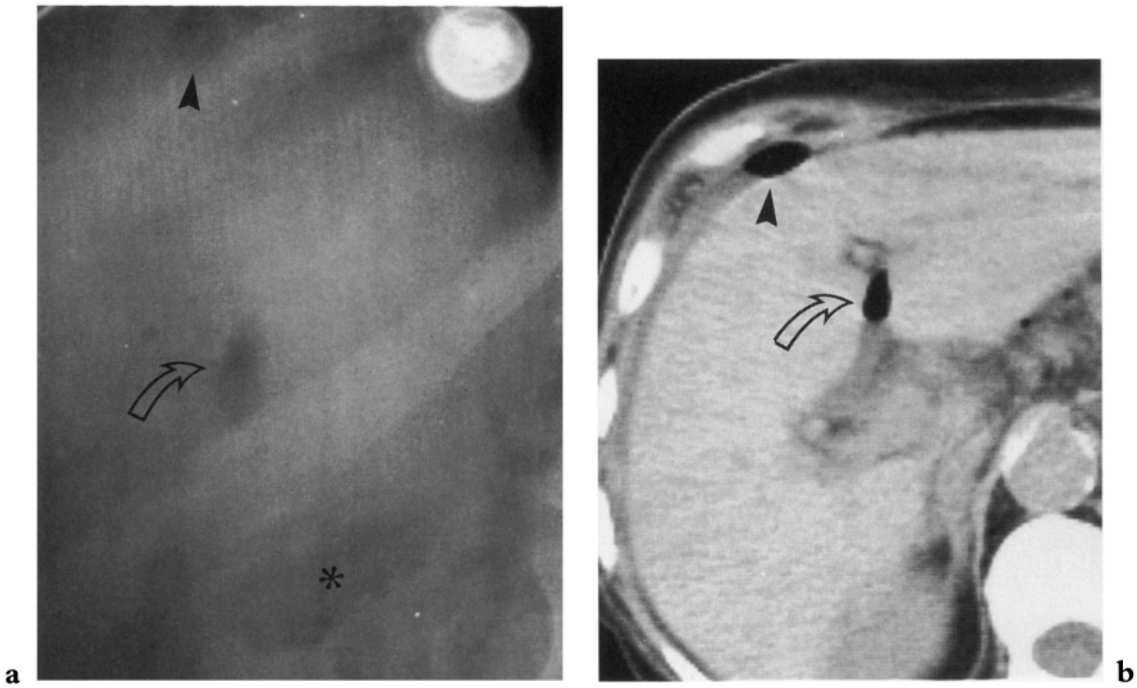


Fig. 7–25. Ligamentum teres fissure sign from antral ulcer perforation.
(a) The *open arrow* points to free air trapped in the peritoneal recess within the fissure for the ligamentum teres, and the *arrowhead* highlights the anterior superior bubble sign. The *asterisk* indicates air in the duodenal bulb. **(b)** Corresponding CT image reveals a tiny amount of air trapped within the fissure *(open arrow)* and a small anterior superior bubble over the liver *(arrowhead).*
(From Cho and Baker.[4])

such superior protrusions of muscle slips abutting pulmonary air are situated more superolaterally than the "leaping dolphin" lucencies indicative of intraperitoneal air.

Ligamentum Teres Fissure Sign

Another distinctive sign of pneumoperitoneum is free air confined in the intrahepatic fissure for the ligamentum teres. It appears on supine films as a small but sharply defined vertically oriented slitlike or ovoid lucency projecting upon the medial half of the right upper quadrant[4] (Figs. 7–25 and 7–26). The fissure for the ligamentum teres is a crevice in the liver that contains fat, the ligament itself, and a variable protrusion of peritoneum. It is situated anterior and superior to the gastroduodenal junction. Consequently, gas liberated from the duodenal lumen by a perforated anterior ulcer often collects in this intrahepatic peritoneal recess.

The ligamentum teres fissure sign is very sensitive, and even less than 1 mL of air trapped within this narrow space can be clearly delineated. The reason for such a high sensitivity is based on the particulars of its anatomy. The fissure is oriented anteroposteriorly, parallel to the x-ray beam on supine film. The ligamentum teres fissure sign may be the only manifestation of pneumoperitoneum, but more often there is air in other locations superimposed on the liver shadow.

Fat within the fissure, normally seen in 30% of patients[33] (Fig. 7–27), and air in the common bile duct may mimic this sign, but they are easily distinguishable. However, a tiny amount of free air occupying only a portion of this peritoneal recess (Fig. 7–28) cannot be differentiated from a small collection of pneumobilia in the left hepatic duct (Fig. 7–29).

Morison's Pouch Air (doge's Cap Sign)

Triangular or linear collection of air in the posterior intraperitoneal recess bounded anteriorly by the liver and posteriorly by the right kidney may simulate the conformation of the tip of a doge's cap, the ceremonial headgear worn only by the doges of Venice[34] (Fig. 7–8). Potential simulators include gas in the duodenal bulb, a gas-filled gallbladder, and intraperitoneal abscess, or a malrotated bowel.

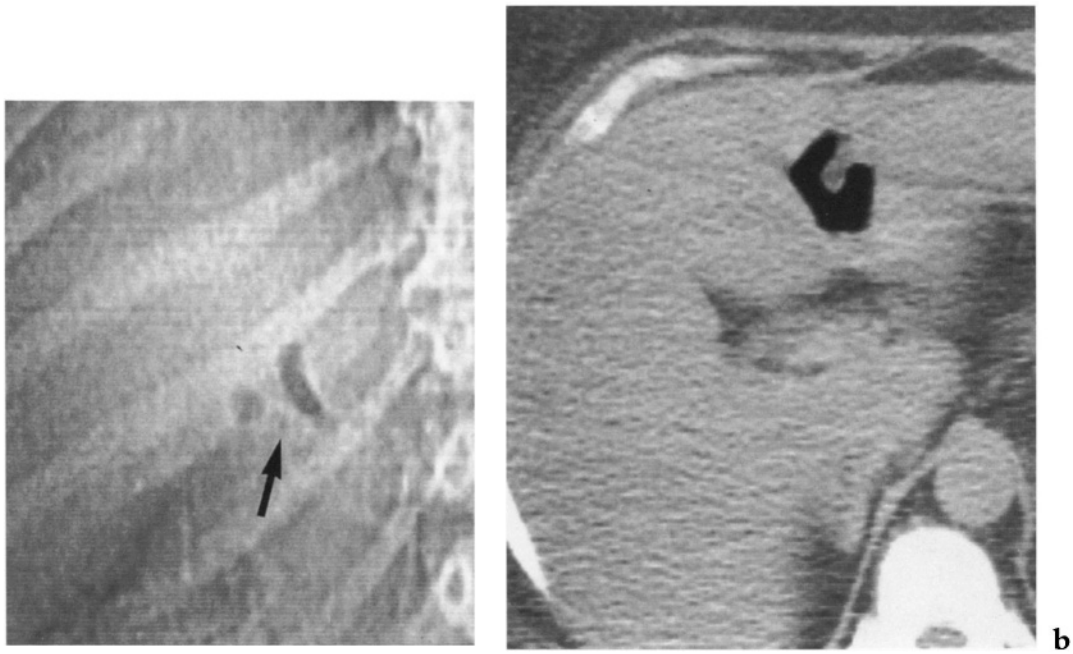


Fig. 7–26. Ligamentum teres fissure sign.
(a) Free air in the fissure in a patient with a perforated duodenal ulcer. This was the only sign of free air on plain films and CT scan. A digital radiograph shows two distinct small round and tubular lucencies *(arrow)* representing free air trapped within this V-shaped fossa, a variant configuration of this peritoneal recess.
(b) CT confirms the plain film findings.
(From Cho and Baker.[4])

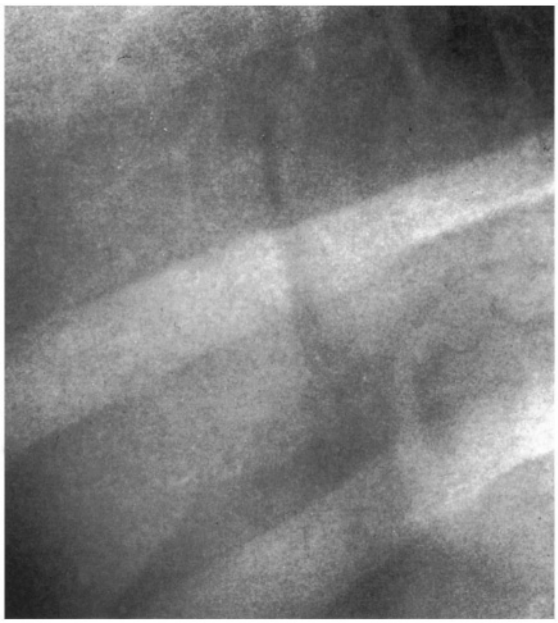


Fig. 7–27. Fat in the ligamentum teres fissure.
This vertical lucency is longer, less lucent, and not as sharply defined as a free air collection within this space.

Football or Air-Dome Sign

An ovoid, distended air-filled anterior peritoneal cavity resembles the configuration of an American football, with the falciform ligament as the bisecting seam. It is seen predominantly in children, being exceedingly uncommon in adults.

Lesser Sac Air

Rarely, gas collects in the lesser sac configured as a homogeneous round lucency with sharply defined upper and lower margin in the epigastrium. Its right border is smooth, describing a slightly convex curve, usually in the same sagittal plain as the falciform ligament. The commonest cause of isolated lesser sac gas is perforation of a posterior gastric or duodenal ulcer. Herniated bowel into the lesser sac or an abscess may mimic this sign.

Left Upper Quadrant Gas

Although most signs of upper abdominal free air appear over the liver, on occasion, perhaps because of preexisting adhesions, gas may accumulate only on the left side, either lateral to the stomach or between the gastric air bubble and the left hemidiaphragm (Fig. 7–30).

Pneumoscrotum

Rarely, free air can extend into the scrotum through the open processus vaginalis (Fig. 7–31). This unusual sign of large pneumoperitoneum occurs only in males. It is anatomically interesting but never crucial for the diagnosis.

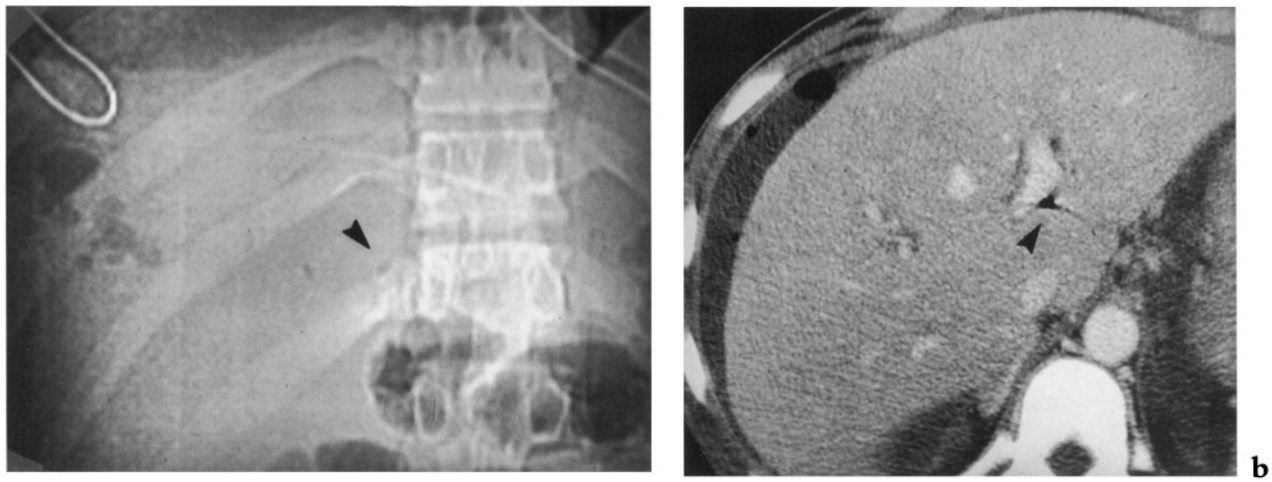


Fig. 7–28. Ligamentum teres fissure sign with less than 1 mL of air seen on supine film.
(a) On this plain radiograph, a tiny lucency above the 12th rib medially *(arrowhead)* represents free air trapped in the fissure. Anterior superior bubbles are also seen laterally.
(b) On CT, note the posterior position of air *(arrowhead)* in the fissure, behind the left portal vein. Small anterior superior bubbles are also present, separated from each other and situated ventral to fluid in the peritoneal space. (From Cho et al.[5])

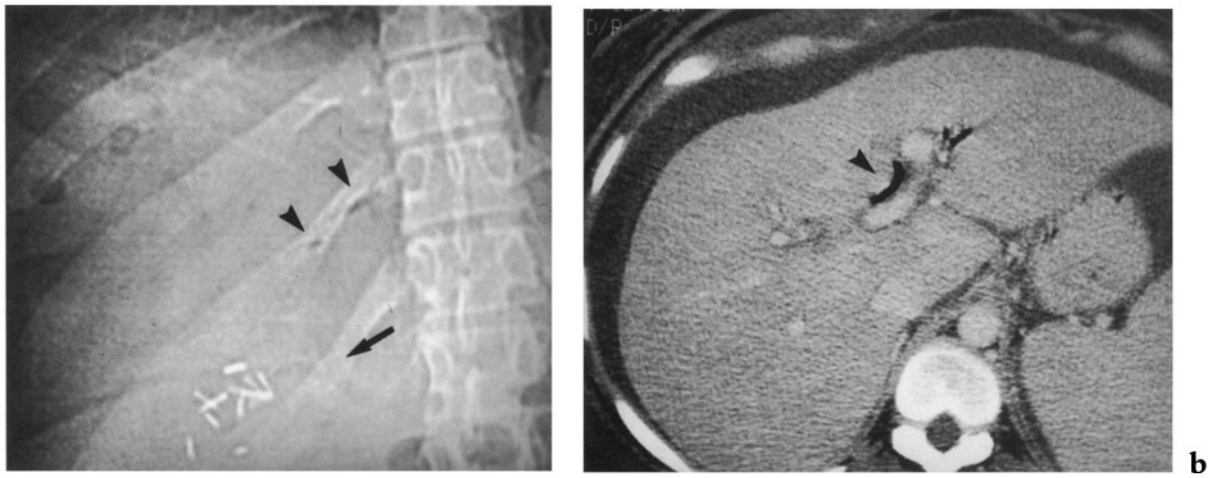


Fig. 7–29. Air in the left hepatic bile duct.
(a) The two tiny lucencies overlying the 11th rib *(arrowheads)* on supine film represent air within the left bile duct, indistinguishable from a tiny free air collection in the ligamentum teres fissure. Note pneumobilia in the common bile duct seen as a subtle tubular lucency *(arrow)* and also two small anterior superior bubbles of free air superolaterally.
(b) CT scan confirms the location of air in the left bile duct *(arrowhead).* Note its anterior position relative to the portal vein.

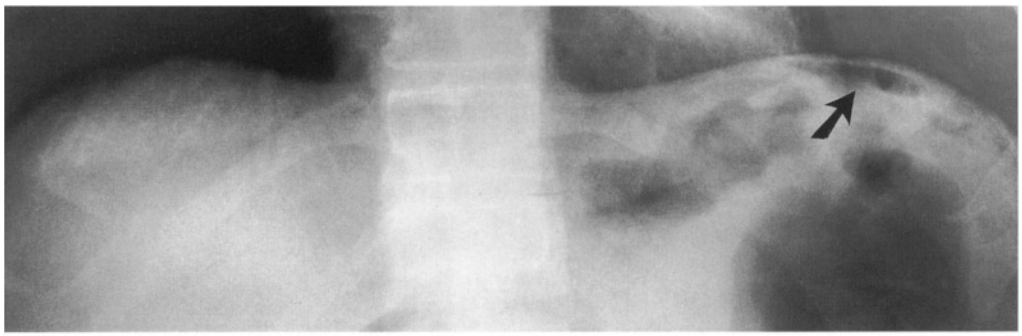


Fig. 7–30. Isolated left upper quadrant free air.
Free air has collected under the left hemidiaphragm but within the peritoneal cavity *(arrow).*

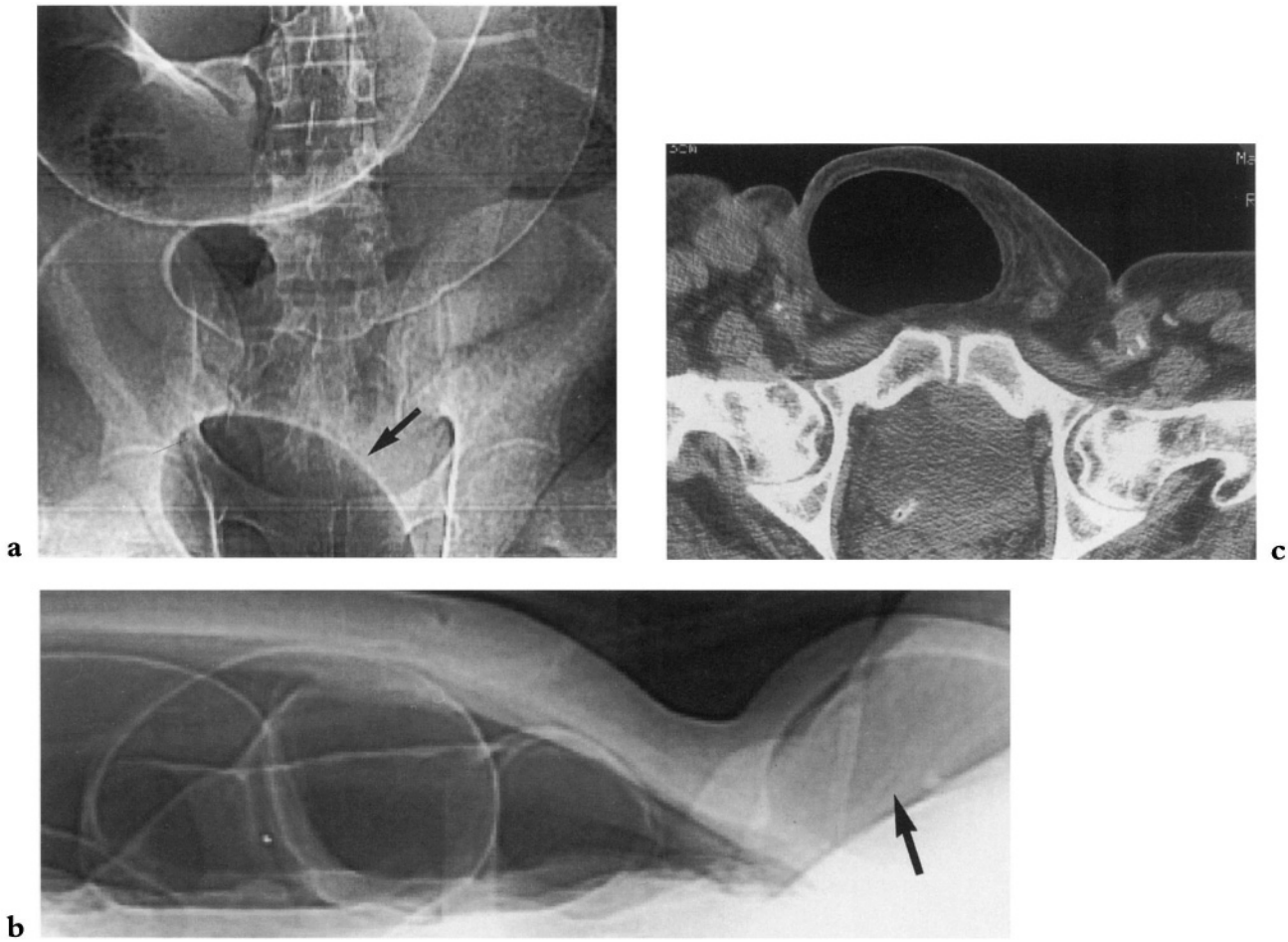


Fig. 7–31. Pneumoscrotum.
(a) A digital supine radiograph demonstrates a large rounded gas collection overlying the right pubic bone *(arrow).* It was confined in the scrotum and represents an extension of intraperitoneal free air. Rigler's sign is demonstrated as well.
(b) Digital cross-table lateral radiograph demonstrates that the caudal gas collection is within the scrotum.
(c) On a corresponding CT image, the pneumoscrotum is seen projecting anterior to the symphysis pubis.
(From Baker and Cho.[6])

Recognition of Free Air Superimposed on the Liver

Lucent Liver

A diffuse increase in lucency superimposed on the liver by free air can be a crucial but subtle finding (Figs. 7–8 and 7–32). Depending on the habitus of the patient, the right lateral border of the lucency may be straight. This observation was formerly considered a sign of hydropneumoperitoneum.[35] However, it may be caused by air alone because the straight lateral border can reflect the interface of the curving anterolateral abdominal wall and the ventral collection of free air even without the presence of associated ascites.

Anterior Superior Bubble

This sign refers to a small isolated aggregation of gas situated anterior to the upper hepatic surface. It is the most frequent, therefore the most important, among the various right upper quadrant gas signs.[5,6,15,17] The anterior superior bubble may be single or multiple, with the gas describing an oval or circular shadow, ranging from a few millimeters to several centimeters in diameter



Fig. 7–32. Lucent liver.
There is diffuse lucency over the liver with a straight lateral border *(arrowheads)* from a large pneumoperitoneum.

(Figs. 7–25, 7–28, 7–29, 7–33 through 7–35). It often appears in the medial half of the right upper quadrant, but small deposits of free air may be positioned more laterally. Its location varies depending on the shape and size of the liver in relation to the contour of the anterior abdominal wall. Occasionally, an abscess in and near the liver, bowel gas, and an atelectatic streak of lung projecting under the dome of the diaphragm can closely simulate the anterior superior bubble.

Ill-Defined Periduodenal Lucency

Another anterior collection of free air but situated more inferiorly, ill-defined periduodenal lucency appears as an agglomeration of bubbles or slitlike lucency in the periduodenal region. It is more difficult to detect than the anterior superior bubble due to nearby duodenal and colonic gas. It also may resemble localized retroperitoneal gas collections.[6]

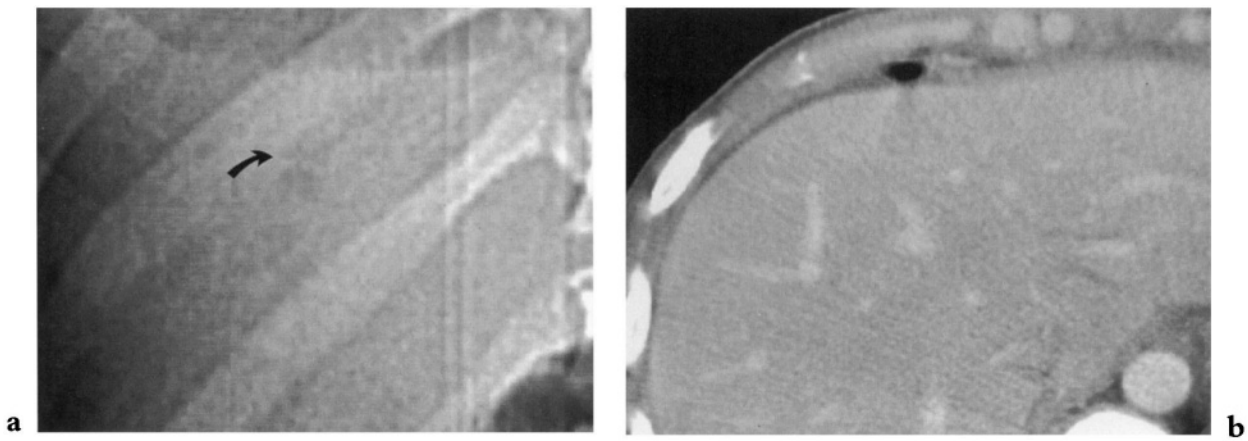


Fig. 7–33. Anterior superior bubble.
Free air is aggregated as a small lucency ventral to the liver *(curved arrow)* on a supine digital radiograph (**a**) and on a corresponding CT section (**b**).

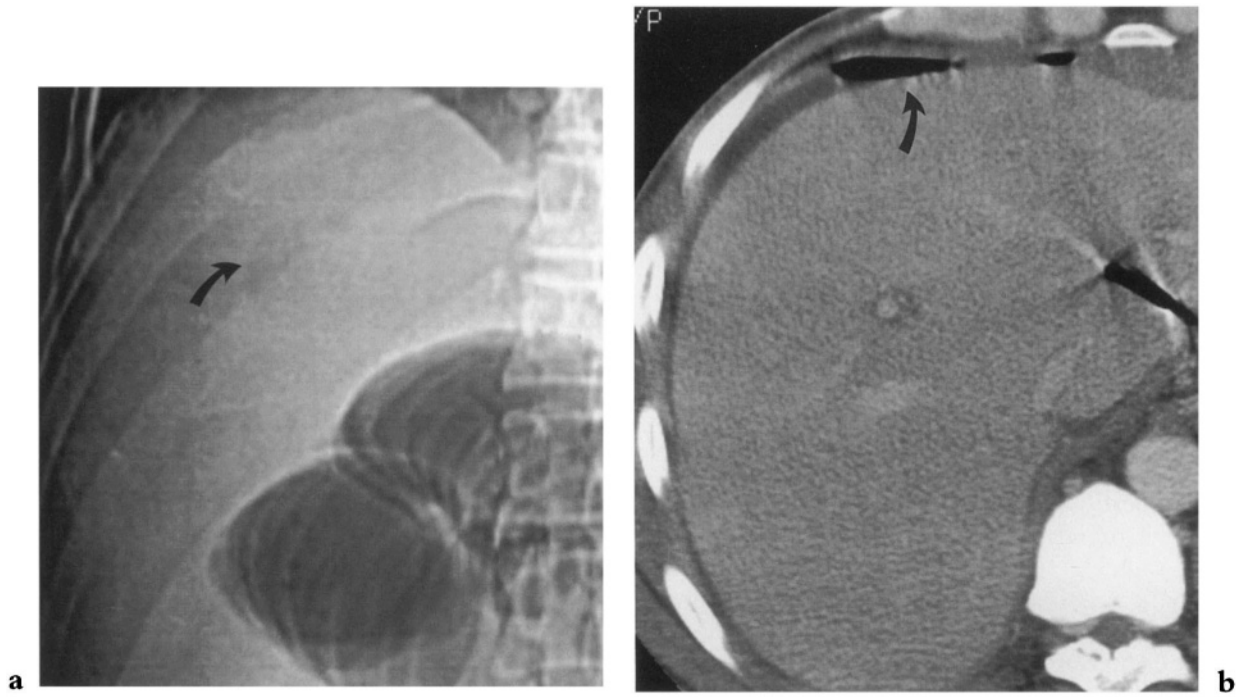


Fig. 7–34. Anterior superior bubble.
A small pneumoperitoneum *(curved arrow)* visualized on both a supine film (**a**) and on a CT scan (**b**) in a patient with small bowel obstruction and perforation. The anterior superior bubble is the only plain film sign of free air. There is also air trapped within the fissure for the ligamentum venosum demonstrated on CT, but not discerned on the plain film.

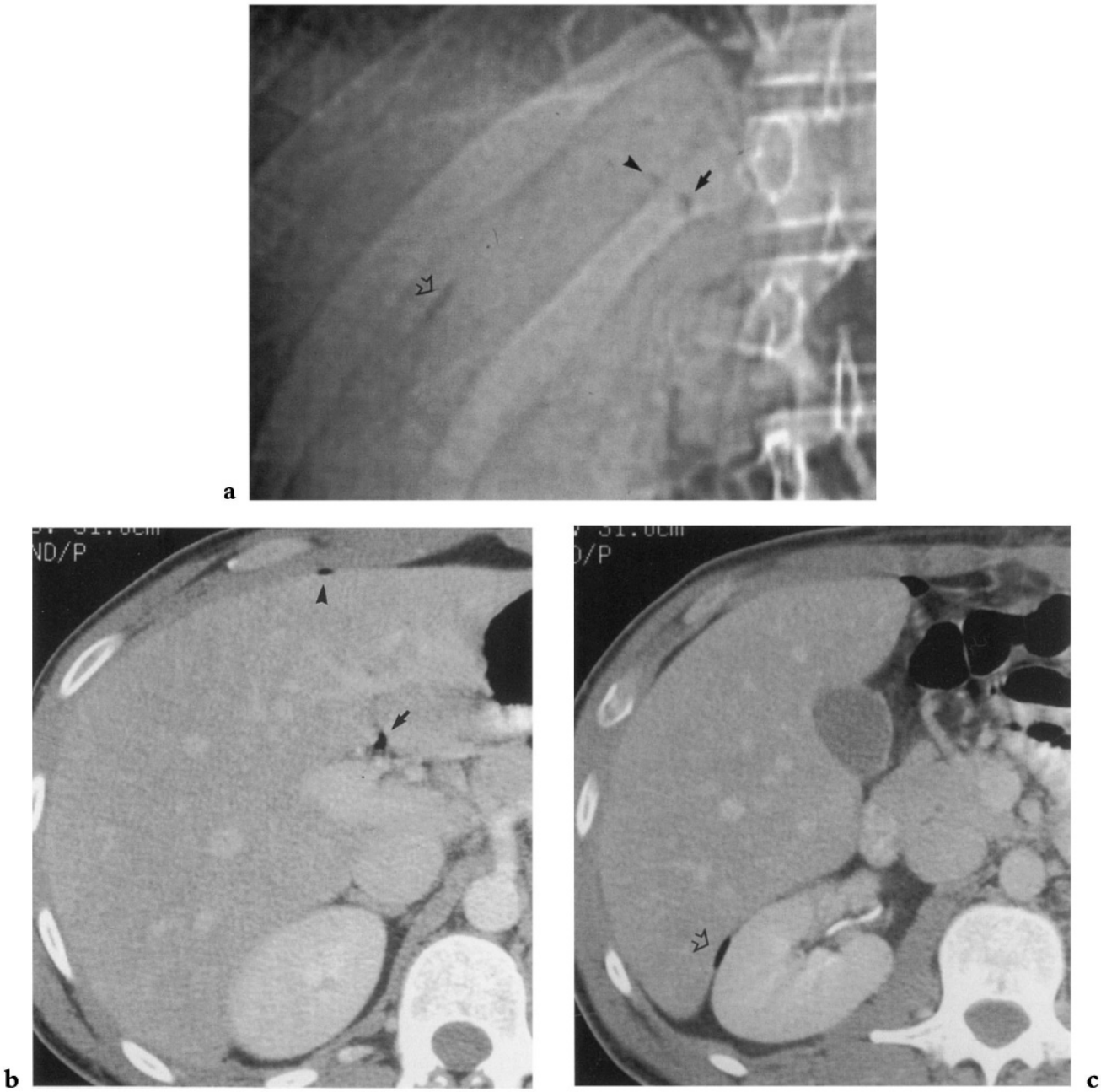


Fig. 7–35. Pneumoperitoneum less than 1 mL.
(a) A digital radiograph reveals three tiny air collections. The most medial air bubble *(arrow)* is in volume a less than 0.5 mL deposit of free air in the fissure for the ligamentum teres. The lucency lateral and cephalad to it *(arrowhead)* is a less than 1 mL anterior superior bubble, and the oblique slit inferolaterally *(open arrow)* is in the posterior subhepatic space, Morison's pouch. It, too, is less than 1 mL.
(b) CT at the level of the fissure for the ligamentum teres. Air in the fissure *(arrow)* and a separate bubble of free air anteriorly *(arrowhead)* correspond to the plain film lucencies.
(c) CT section 3 cm caudad reveals a tiny amount of air trapped between the liver and the kidney *(open arrow),* corresponding to the oblique slit seen on the digital scout. The amount of air is so small it occupies only a portion of Morison's pouch. Therefore, it appears as an atypical lucency and not the expected triangular doge's cap configuration.
(From Baker and Cho.[6])

References

1. Miller RE, Nelson SW: The roentgenological demonstration of tiny amounts of free intraperitoneal gas: Experimental and clinical studies. AJR 1971; 112:574–585.
2. Woodring JH, Heiser MJ: Detection of pneumoperitoneum on chest radiographs: Comparison of upright lateral and posterior-anterior projections. AJR 1995; 165:45–47.
3. Markowitz SK, Ziter FMH Jr: The lateral chest film and pneumoperitoneum. Ann Emerg Med 1986; 15:425–427.
4. Cho KC, Baker SR: Air in the fissure for the ligamentum teres: New sign of intraperitoneal air on plain radiographs. Radiology 1991; 178:489–492.
5. Cho KC, Baker SR, Lum C, et al: Pneumoperitoneum: New observations on plain films and CT scans. *In* Selected Scientific Exhibits in Gastrointestinal Radiology: RSNA 1996. RadioGraphics, November 1997; 17 (suppl 2, pt 2, CD-ROM) 1616–1620 (abstr).
6. Baker SR, Cho KC: The Abdominal Plain Film with Correlative Imaging, 2nd ed. Appleton and Lange, Stamford, CT, 1999.
7. Baker SR: Diagnosis of minimal to moderate pneumoperitoneum (the query corner). Abdom Imaging 1995; 20:492–494.
8. Stapakis JC, Thickman D: Diagnosis of pneumoperitoneum: Abdominal CT vs. upright chest film. J Comput Assist Tomogr 1992; 16:713–716.
9. Earls JP, Dachman AH, Colon E, et al: Prevalence and duration of postoperative pneumoperitoneum: Sensitivity of CT vs left lateral decubitus radiography. AJR 1993; 161:781–785.
10. Lee FT Jr, Leahy-Gross KM, Hammond TG, et al: Pneumoperitoneum in peritoneal dialysis patients: Significance of diagnosis by CT. J Comput Assist Tomogr 1994; 18:439–442.
11. Braccini G, Lamacchia M, Boraschi P, et al: Ultrasound versus plain film in the detection of pneumoperitoneum. Abdom Imaging 1996; 21:404–412.
12. Baker SR: Imaging of pneumoperitoneum. Abdom Imaging 1996; 21:413–414.
13. Cho KC, Baker SR: Visualization of the extrahepatic segment of the ligamentum teres: A sign of free air on plain radiographs. Radiology 1997; 202:651–654.
14. Cho KC, Baker SR: Depiction of diaphragmatic muscle slips on supine plain radiographs: A sign of pneumoperitoneum. Radiology 1997; 203:431–433.
15. Cho KC, Baker SR, Thornhill BA, et al: Supine film diagnosis of pneumoperitoneum: New observations in the right upper quadrant. Radiology 1988; 169(p):405.
16. Cho KC: Manifestations of intraperitoneal air *(http: // medic-online.net/abdo/kcho/index.html).* *In* Abdominal and Gastrointestinal Imaging Multimedia Virtual Textbook *(http://medic-online.net/abdo/index.html).* Edited by NC Gourtsoyiannis, R Yamada, Y Itai, MA Meyers, D Nolan, P Ros, G Stevenson, SA Euromultimedia, Luxembourg, 1998.
17. Cho KC, Baker SR: Extraluminal air: Diagnosis and significance. *In* Imaging the Acute Abdomen. Edited by EJ Balthazar. Radiol Clin North Am 1994; 32:829–844.
18. Levine MS, Scheiner JD, Rubesin SE, et al: Diagnosis of pneumoperitoneum on supine abdominal radiographs. AJR 1991;156:731–735.
19. Menuck L, Siemers PT: Pneumoperitoneum: Importance of right upper quadrant features. AJR 1976; 127:753–756.
20. Jeffrey RB, Federle MP, Wall S: Value of CT in detecting occult gastrointestinal perforation. J Comput Assist Tomogr 1983; 7:825–827.
21. Cho KC, Baker SR: Umbilical vein nomenclature. Radiology 1997; 204:874 (letter to the editor).
22. Williams PL, Warwick R: Anatomy of the Human Body, 38th ed. WB Saunders, Philadelphia, 1995, pp 1376–1378.
23. Grassi R, Pinto F, Rotonda A, et al: Pneumoperitoneo. Gnocchi, Napoli, Italy, 1996.
24. Weiner CI, Diaconis JN, Dennis JM: The "inverted V": A new sign of pneumoperitoneum. Radiology 1973; 107:47–48.
25. Bray JF: The "inverted V" sign of pneumoperitoneum. Radiology 1984; 151:45–46.
26. Eguchi N, Saida Y, Itai Y: CT of the medial umbilical folds. J Comput Assist Tomogr 1997; 21:723–725.
27. Radin R, Van Allan RJ, Rosen RS: The visible gallbladder: A plain film sign of pneumoperitoneum AJR 1996; 167:69–70.
28. Mindelzun RE, McCort JJ: The cupola sign of pneumoperitoneum in the supine patient. Gastrointest Radiol 1986; 11:283–285.
29. Balthazar EJ, Moore SL: CT evaluation of infradiaphragmatic air in patients treated with mechanically assisted ventilation: A potential source of error. AJR 1996; 167:731–734.

30. Agur AM: Grant's Atlas of Anatomy, 9th ed. Williams & Wilkins, Baltimore, 1991, p 137.
31. Baker SR, Cho KC, Lum C: The supine plain film and pneumoperitoneum: A revisionist approach. Asian Oceanian J Radiol 1997; 2:15–19.
32. Christensen EE, Landay MJ: Visible muscle of the diaphragm: Sign of extraperitoneal air. AJR 1980; 135:521–523.
33. Haswell DM, Berne AS, Schneider B: Plain film recognition of the ligamentum teres hepatis. Radiology 1975; 114:263–267.
34. Hajdu N, deLacey G: The Rutherford Morison pouch. A characteristic appearance on abdominal radiographs. Br J Radiol 1970; 43:706–709.
35. Han SY, Shin MS, Tishlar JM: Plain film findings of hydropneumoperitoneum. AJR 1981; 136:1195–1197.

The Extraperitoneal Spaces: Normal and Pathologic Anatomy

8

The extraperitoneal portion of the abdomen has always been considered a difficult region in terms of anatomic definitions, clinical evaluation, and radiologic diagnosis. Anatomically, it has been vaguely considered as occupying the posterior half of the abdomen, without well-defined fascial boundaries. Clinically, it is commonly recognized that extraperitoneal effusions are difficult to diagnose. The area is not accessible to the bedside modalities of auscultation, palpation, or percussion. Symptoms and signs may be obscure, delayed, nonspecific, or misleading.

Extraperitoneal tissues do not react as acutely and severely to bacterial contamination as does the peritoneal cavity.[1] Known amounts of bacteria introduced intraperitoneally result in acute peritonitis and dramatic constitutional signs. When introduced into the extraperitoneal tissues, however, they cause a more smoldering infection. This explains the prolonged duration of the symptoms of extraperitoneal abscess before operation or death, often as long as 2 months.[2]

Several reports emphasize the difficulties in clinically recognizing even severe extraperitoneal infection. Indeed, in large series, the diagnosis has been completely overlooked in 25–50% of the patients.[2,3] Unless diagnosed early and treated adequately, extraperitoneal abscess is associated with prolonged morbidity and high mortality.

Extraperitoneal infection is usually secondary, a complication of infection, injury, or malignancy in adjacent retroperitoneal or intraperitoneal organs. Only rarely is it a consequence of bacteremia or suppurative lymphadenitis.

The predominant symptoms of an extraperitoneal infection are chills, fever, abdominal or flank pain, nausea, vomiting, night sweats, and weight loss. The clinical course is usually insidious, and the initial symptoms are so nonspecific that the correct diagnosis is usually not considered. Constitutional symptoms may be present for weeks to months before localizing signs develop. With pressure on the extraperitoneal nerves, pain may be referred to the groin, hip, thigh, or knee, with little or no complaint of abdominal or back pain. Urologic symptoms are rare, even with perirenal abscess.

A mass or swelling of the flank is palpable about 50% of the time,[3] but only if it is large or localizes inferiorly below the costal margin. Almost all patients exhibit tenderness to palpation over the abscess. Scoliosis, psoas spasm, and a sinus tract may be other clinical signs. Although there is invariably leukocytosis, urinalysis may be normal, even in perirenal abscess.

Unusual complications of extraperitoneal abscess include rupture into the free peritoneal cavity and progressive dissection in the soft tissues. Spread may involve the anterior abdominal wall, subcutaneous tissues of the back or flank, subdiaphragmatic spaces, mediastinum, thoracic cavity, psoas muscle, thigh, or hip. A fistula may extend from the kidney into the extraperitoneal portion of the bowel or into a bronchus.

Extraperitoneal blood is usually caused by trauma, ruptured aneurysm, malignancy, bleeding diathesis, or overanticoagulation.

Extraperitoneal gas is most often the result of bowel perforation secondary to inflammatory or ulcerative disease, blunt or penetrating trauma, a foreign body, iatrogenic manipulation, or a gas-producing infection originating in extraperitoneal organs. The underlying condition may be chronic, occult, or only suspected clinically. Often it is not until the gas is recognized ra-

diologically that attention is directed to or confirms the presence of an acute process in the abdomen. Extraperitoneal gas is seen as mottled lucencies within the tissues or as linear shadows tracking along fascial planes.

Radiologically, loss of visualization of the lateral margin of the psoas muscle has been considered the hallmark of extraperitoneal effusions. This sign, however, is unreliable since 25–44% of normal individuals show unequal visualization of the psoas borders.[4,5]

An editorial in *Lancet* has woefully highlighted the problem:[6]

> Many a clinical reputation lies buried behind the peritoneum. In this hinterland of straggling mesenchyme with . . . its shadowy fascial boundaries, the clinician is often left with only his flair and his diagnostic first principles to guide him.

It is essential to realize that this is no longer true. Rather, roentgen-anatomic studies by Meyers et al. have clarified the fascial relationships that clearly demarcate the region into three distinct compartments.[7–12] Each has specific boundaries and relationships that can be recognized. Radiologic identification by retroperitoneal pneumography of the renal fascia enclosing the contents of the perirenal space was described by Meyers,[13] and the structure was subsequently noted on urography and nephrotomography[11,12,14–16] and then definitively on computed tomography.[7,17–19] The pathways of flow, preferential routes of spread from various sites, and margination of infection or other effusions within a particular extraperitoneal compartment are guided primarily by the fixed fascial planes and paths of least resistance. This information permits the recognition of the presence, extent, and localization of fluid and gas collections in the extraperitoneal tissues and often pinpoints the precise site of origin and nature of the fluid.

Anatomic Considerations

Basic to an understanding of the clinical and radiologic criteria is precise knowledge of the anatomy of the extraperitoneal fascial planes, compartments, and relationships. The retroperitoneal space is bounded anteriorly by the posterior parietal peritoneum and posteriorly by the transversalis fascia. It extends from the pelvic brim inferiorly to the diaphragm superiorly. The major organs and structures within it include (a) the adrenal glands, kidneys, and ureters; (b) the descending, transverse, and ascending portions of the duodenum, and the pancreas; (c) the great vessels and branches; and (d) the ascending and descending colon.

The intraperitoneal structures do not simply occupy the anterior half of the abdomen and the extraperitoneal structures the posterior half. Rather, the extraperitoneal space is mildly C-shaped, with its convexity projecting anteriorly in the midline. This is a function of both the particular relationships of the abdominal organs and their accommodation to the lordotic curvature of the lumbar spine. In this way, segments of the extraperitoneal region (e.g., the body of the pancreas and the duodenal loop) lie considerably anterior to portions of intraperitoneal viscera (e.g., the spleen and posterior aspects of the liver).

The Three Extraperitoneal Compartments and Perirenal Fasciae

Detailed evaluation shows that the extraperitoneal region, rather than being composed of amorphous "straggling mesenchyme," is distinctly demarcated by well-defined fascial planes. Figure 8–1a is an enlarged horizontal cross-section through the flank at the lower pole of the kidney. Central to the division of the extraperitoneal region are the conspicuous anterior and posterior layers of renal fascia. (The posterior renal fascia was first described by Zuckerkandl[21] [Fig. 8–2] and the anterior renal fascia subsequently by Gerota[22] [Fig. 8–3], but the two layers have since been known collectively as Gerota's fascia.[23])

The renal fascia is a dense, collagenous, elastic connective tissue sheath that envelops the kidney and perirenal fat. Its two layers fuse behind the ascending or descending colon to form the single lateroconal fascia, which then continues around the flank to blend with the peritoneal reflection forming the paracolic gutter. Figure 8–1b illustrates these important fascial relationships by computed tomography. In this way, I have defined precisely three individual extraperitoneal compartments. Their major fascial marginations are illustrated in Figure 8–1c.

1. The *anterior pararenal space* extends from the posterior parietal peritoneum to the anterior renal fascia. Significantly, it is confined laterally by the lateroconal fascia.

2. The *perirenal space* encompasses the kidney and its investing fat. A conspicuous anatomic feature is the perirenal fat, which is most abundant behind and somewhat

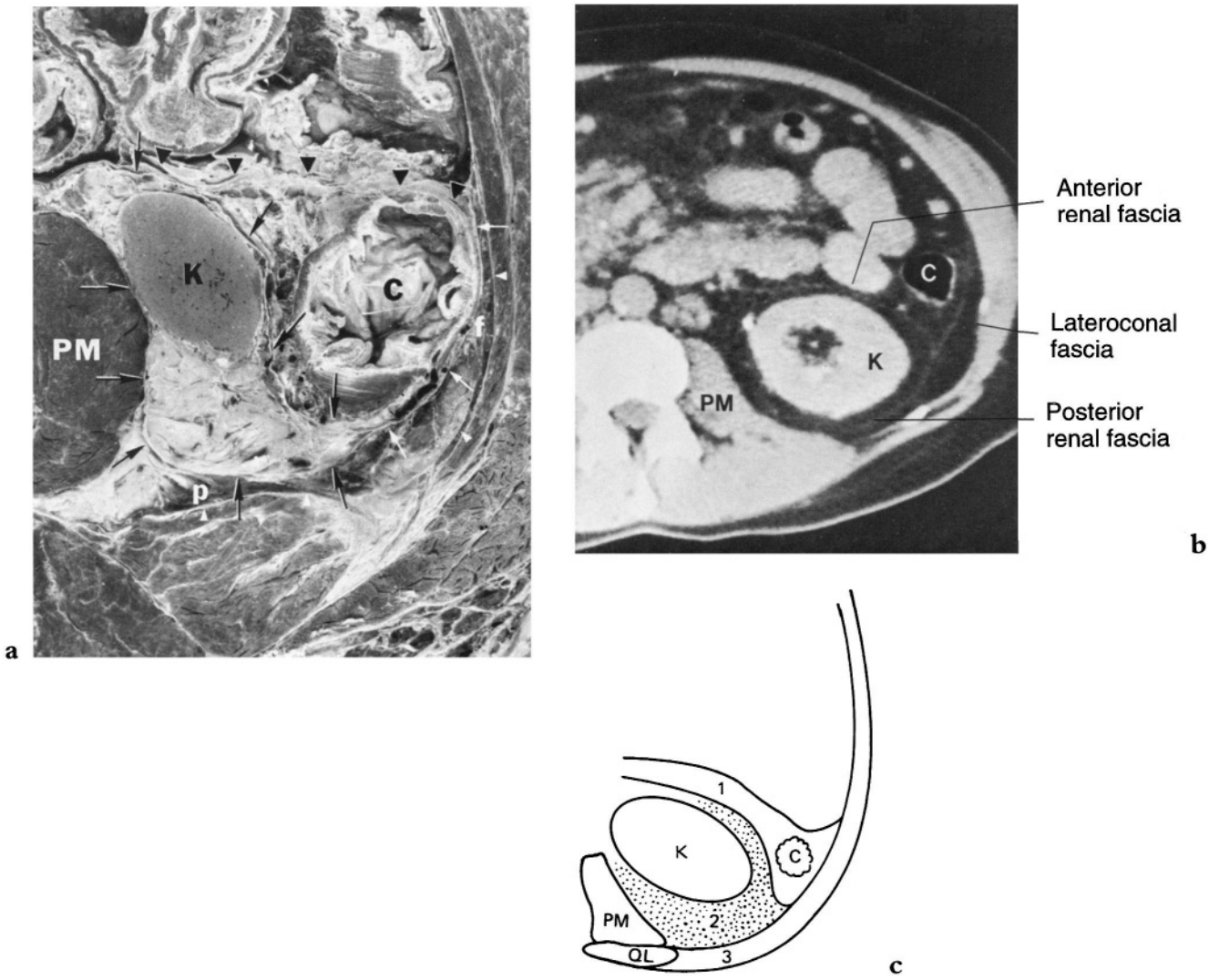


Fig. 8–1. Extraperitoneal anatomy of the flank.
(a) Transverse cross section. The anterior and posterior renal fasciae *(black arrows)* envelop the kidney *(K)* and perirenal fat. From their line of fusion, the lateroconal fascia *(white arrows)* continues behind the descending colon *(C)* to the parietal peritoneum *(black arrowheads).* The posterior pararenal fat *(p)* is continuous with the flank fat *(f)* deep to the transversalis fascia *(white arrowheads). PM* = psoas muscle.
(b) Computed tomography demonstrates the anterior and posterior renal fasciae and the lateroconal fascia, which demarcate the extraperitoneal fat. Note their relationships to the kidney *(K)* and descending colon *(C).*
(c) The three extraperitoneal spaces: *1* = the anterior pararenal space; *2* = the perirenal space; *3* = the posterior pararenal space; *QL* = quadratus lumborum muscle. As evident in the cross-section at the level of the lower renal pole in **a,** this depicts an acute angle between the anterior and posterior renal fasciae at their junction lateral to the kidney. At this level, the junction is indeed more posteriorly located compared with the level of the renal hilus.[20] Imaging studies, as in **b**, generally show the leaves and their junction smoothly curved and parallel to the renal contour.[20]
(Modified from Meyers.[9])



Fig. 8–2. Emil Zuckerkandl (1849–1910), at the age of 25.
The Austrian Zuckerkandl was the favorite pupil of the eminent Professor of Anatomy Josef Hyrtl in Vienna, and he subsequently became Professor of Anatomy in Graz and Vienna. He was a universal and productive anatomist, especially active in the field of otorhinology. Among his many publications, of special interest are his descriptions of collections of chromaffin tissue near the origin of the inferior mesenteric artery in 1901, called the *organ of Zuckerkandl* and the posterior renal fascia in 1883, sometimes called the *fascia of Zuckerkandl.*
(Courtesy of the Institut für Geschichte der Medizin der Universität Wien, Museum Josephinum, Vienna.)

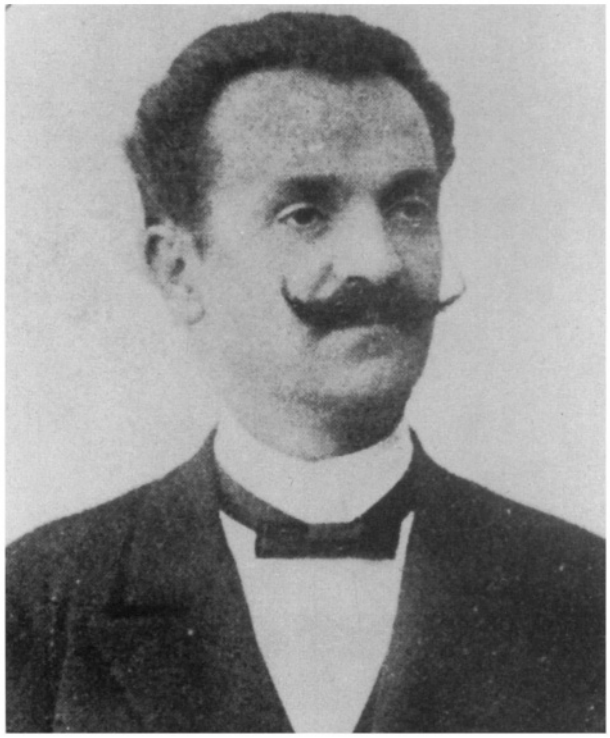


Fig. 8–3. Dimitrie Gerota (1867–1939).
Gerota received his medical education in Bucharest and published his classic article in 1895 on the fixation of the kidneys and the presence of the anterior renal fascia, sometimes selectively called *Gerota's fascia.* In 1898, he wrote the book *The Röntgen Rays or the X-rays.* He initiated academic radiologic education in Romania but was obliged to abandon radiology because of radiodermatitis and epithelioma of the hand, which required amputation. From 1913 onward, he continued as Professor of Anatomy in Bucharest and owner and principal of the leading private hospital at that time, The Gerota Sanitorium.
(Courtesy of Prof. dr Nicolae Marcu, University of Bucharest.)

lateral to the lower pole of the kidney. This becomes of practical importance in the diagnosis of coalescent perirenal abscesses and hematomas.

3. The *posterior pararenal space* extends from the posterior renal fascia to the transversalis fascia. It consists of a thin layer of fat, and its most notable feature is that it continues uninterruptedly external to the lateroconal fascia as the properitoneal fat of the abdominal wall. It is important to recognize that it is the posterior pararenal fat, as it courses laterally external to the lateroconal fascia and deep to the transversalis fascia, that is radiologically visualized as the "flank stripe" (Figs. 8–4 and 8–5).

Figure 8–6a is a horizontal diagram illustrating the major relationships and components of the three extraperitoneal compartments.

The *anterior pararenal space* includes the ascending and descending colon, the duodenal loop, and the pancreas. In other words, the extraperitoneal portions of the alimentary tract reside within this compartment. While the space is potentially continuous across the midline, fluid volumes even under pressure typically reach only the midline (Fig. 8–7) or shortly beyond (Fig. 8–8). Clinically, moreover, I have observed that collections of fluid or gas are generally confined to their side of origin. A notable exception includes pancreatic extravasations, probably for two reasons: (a) the pancreas itself straddles

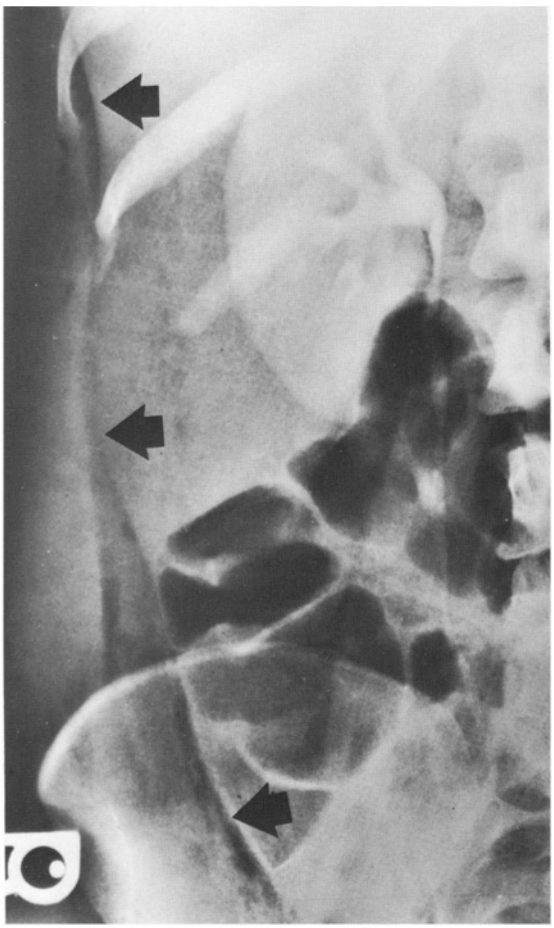


Fig. 8–4. Flank stripe highlighted by air postlaparoscopy.
Following laparoscopy, air inadvertently entering the anterior abdominal wall is seen as it courses around the flank extraperitoneally *(arrows).* Here, it lies deep to the transversalis fascia, within the flank extension of the posterior pararenal fat.

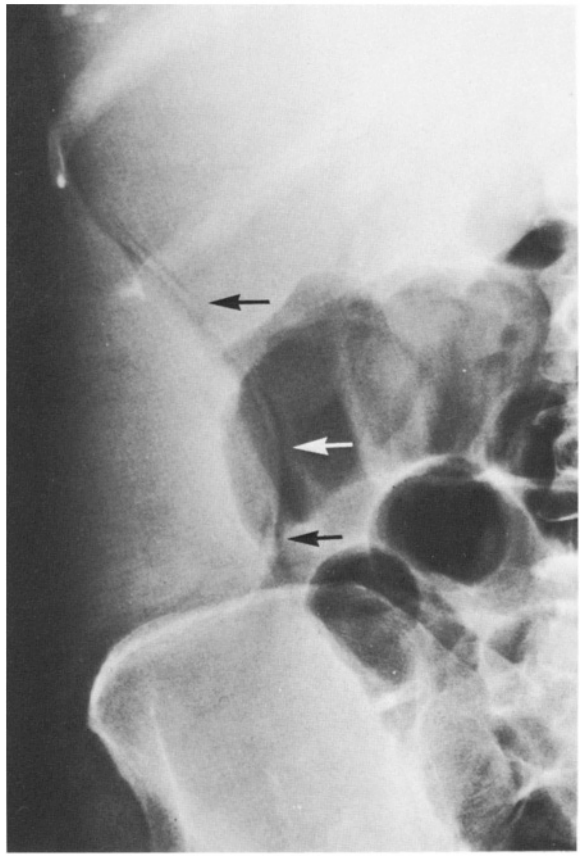


Fig. 8–5. Flank hematoma.
The blood is seen as a prominent soft-tissue mass displacing the intact flank stripe medially *(arrows).* These features localize the hematoma to be superficial to the transversalis fascia and therefore subcutaneous in position.

the midline and (b) liberated pancreatic enzymes, particularly trypsin, dissect the fascial planes and permit freer dissemination. Ventrally, the anterior pararenal space is anatomically continuous with the roots of the small bowel mesentery and transverse mesocolon.[24,43]

The *perirenal spaces* generally have no continuity across the midline. Medially, the posterior fascial layer fuses with the psoas or quadratus lumborum fascia,[25] and the anterior renal fascia blends into the dense mass of connective tissue surrounding the great vessels in the root of the mesentery and behind the pancreas and duodenum[44] (Fig. 8–9). Originally, Gerota[22] claimed bilateral continuity of the perirenal compartments deep to the anterior renal fasciae. When pressure markedly increases within the perirenal space acutely, rupture occurs in the hilar region, the anterior renal fascia first giving way and then perhaps the peritoneum.[27] Most precise dissections and injection experiments and meticulous CT observations have shown that the two perirenal spaces have no actual or direct communications generally throughout most of their courses.[8,9,12,17] At the level of the renal hilum, CT seems to confirm the work of Martin,[26] namely, that the anterior and posterior ipsilateral fasciae occasionally fuse and blend with the hilar vessels, preventing communications between both perirenal spaces across the midline[17] (Fig. 8–10). Lower, however, at the levels of L3 to L5, there is evidence that indicates potential communication across the midline[27–29] (Figs. 8–11 through 8–13). Contralateral extension of fluid, when the disease process originates in the kidney, is impeded by fibrous septa and by the narrowness of the potentially communicating channel.[27,30] Indeed, recent

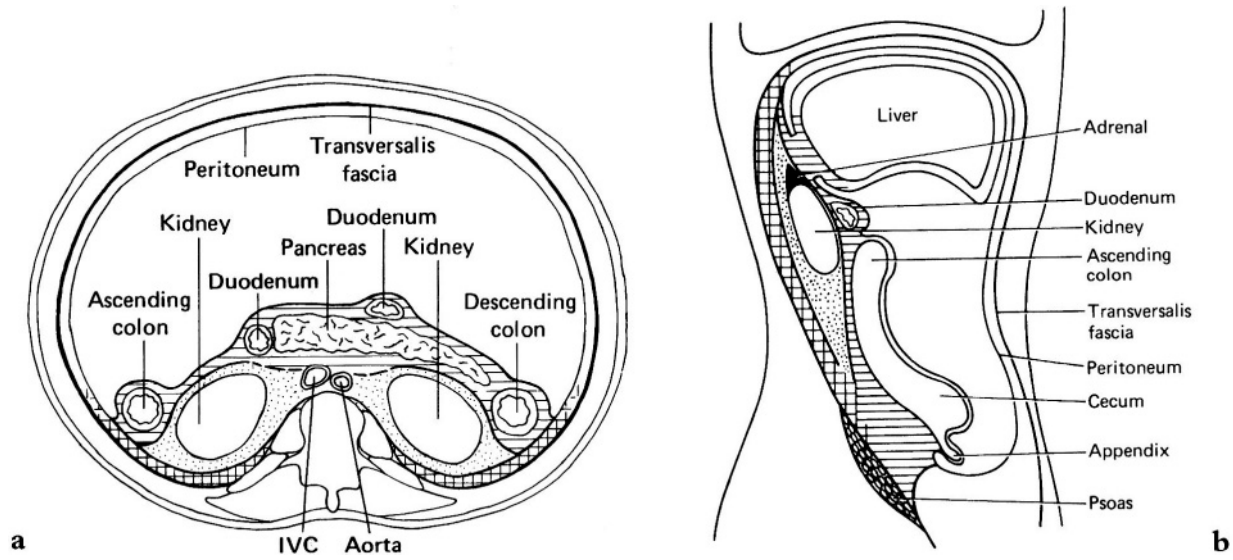


Fig. 8–6. The three extraperitoneal compartments.
(a) and **(b)** *Striped areas* = anterior pararenal space; *stippled areas* = perirenal space; *cross-hatched areas* = posterior pararenal space; *IVC* = inferior vena cava.
(Reproduced from Meyers.[8])

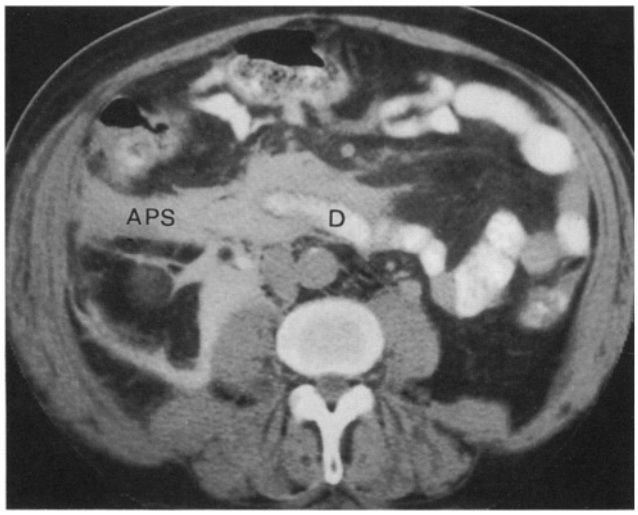


Fig. 8–7. Hemorrhage in anterior pararenal space extending to midline.
Owing to complications in a nephrostomy procedure, extravasation has occurred not only within the perirenal space but also of considerable volume within the anterior pararenal space *(APS),* where it spreads to the third portion of the duodenum *(D)* in the midline but not to the contralateral side.
(Courtesy of Michiel Feldberg, M.D., University of Utrecht, The Netherlands.)

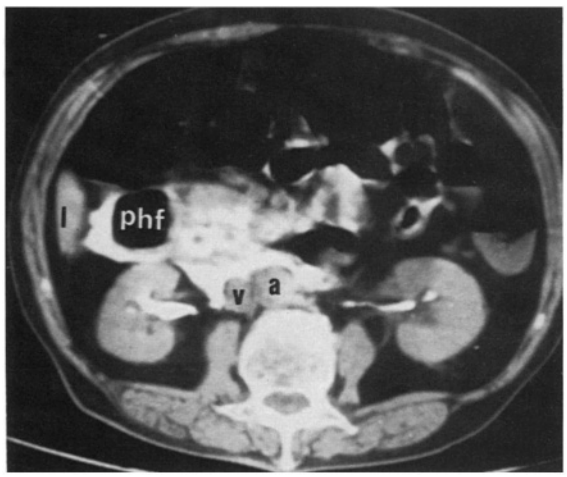


Fig. 8–8. *In vivo* opacification of right anterior pararenal space.
This occurred from extravasation of contrast medium from a ruptured pseudocyst in the head of the pancreas during ERCP. Note that there is extension in this plane across the midline. Laterally, the extravasate is in relationship to the posterior hepatic flexure *(phf)* and angle of the liver *(l). a* = aorta; *v* = inferior vena cava.

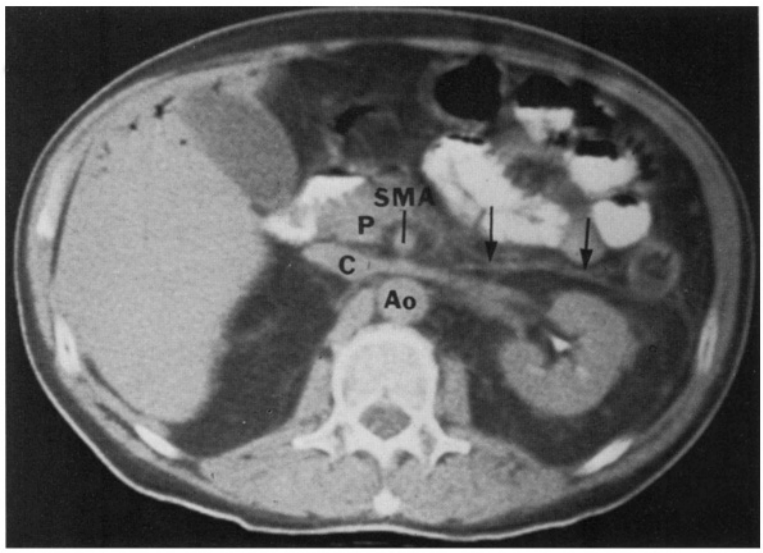


Fig. 8–9. Midline termination of the anterior renal fascia. CT shows thickened anterior renal fascia *(arrows)* blending into tissues near the midline around the renal pedicle in relationship to the superior mesenteric artery *(SMA).* There is no evidence of continuity across the midline. *Ao* = aorta; *P* = pancreas; *C* = inferior vena cava.

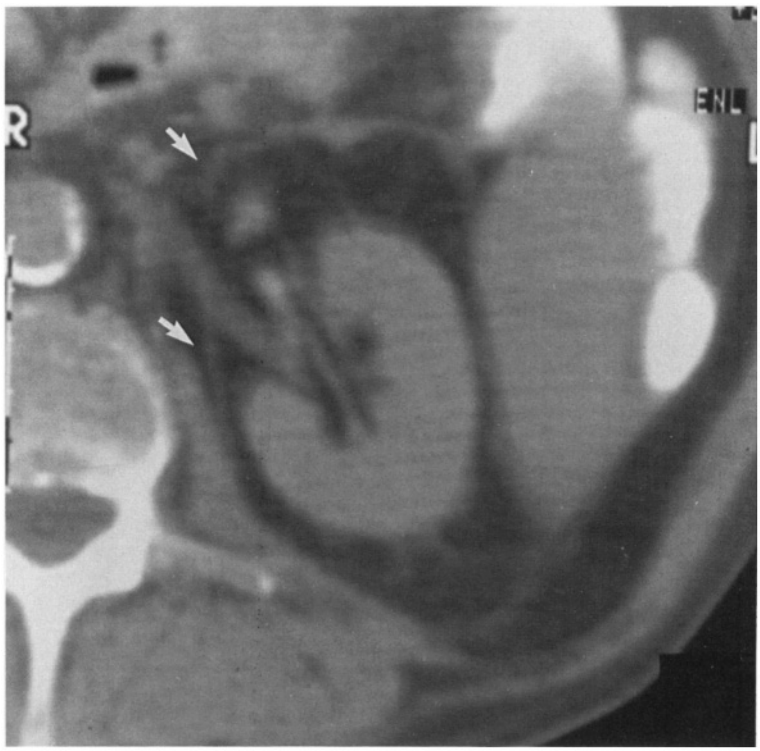


Fig. 8–10. Medial fascial closure of the perirenal space. CT demonstrates accentuated renal fascial planes fusing medially around the renal pedicle *(arrows).* (Courtesy of Michiel Feldberg, M.D., University of Utrecht, The Netherlands.)

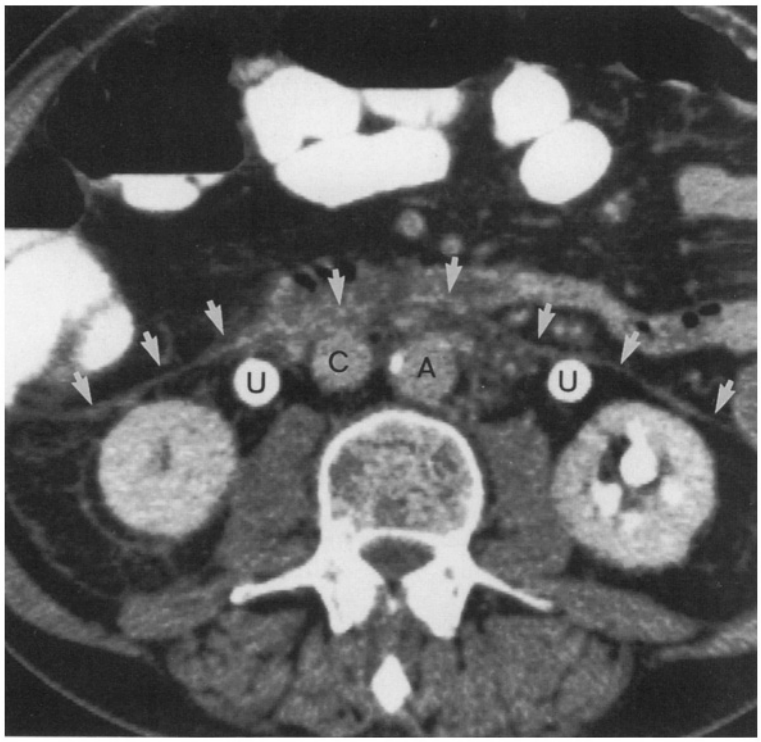


Fig. 8–11. Midline continuity of the anterior renal fascia. At the level of the lower renal poles, the anterior renal fascia is identified to be continuous across the midline *(arrows),* anterior to the ureters *(U),* inferior vena cava (*C*), and aorta *(A).* (Reproduced from Pistolesi GF, Procacci C, Tonegutti N, et al: Analyse des différents espaces des régions extrapéritonéales. Radiologie J CEPUR 1990; 10:195–204.)

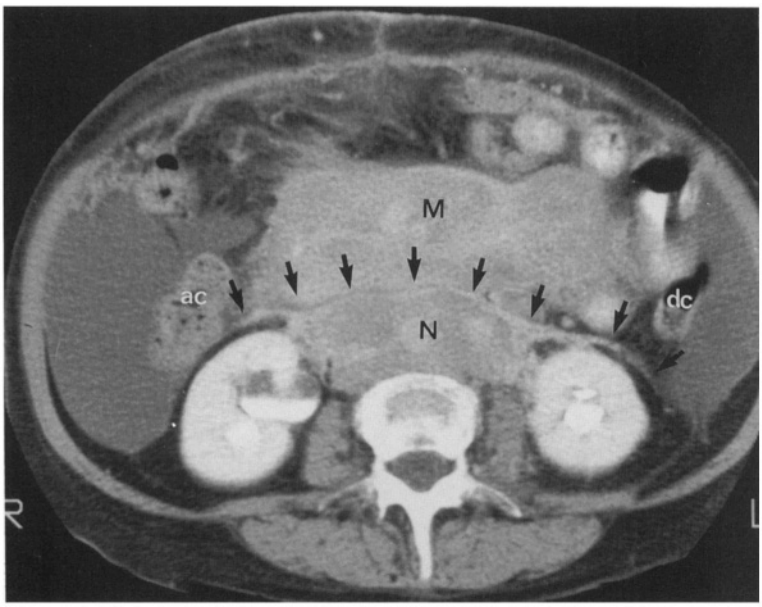


Fig. 8–12. Midline continuity of the anterior renal fascia. At a level 6-cm caudal to the renal vessels, reactive thickening allows clear identification of the anterior renal fascia as continuous across the midline *(arrows).* In this patient with lymphoma, the fascia is seen between retroperitoneal nodal masses *(N)* and mesenteric adenopathy *(M),* both of low attenuation. It extends posterior to the ascending *(ac)* and descending colon *(dc),* which are displaced medially by intraperitoneal fluid. (Courtesy of Michael Oliphant, M.D., Crouse Hospital, Syracuse, NY.)

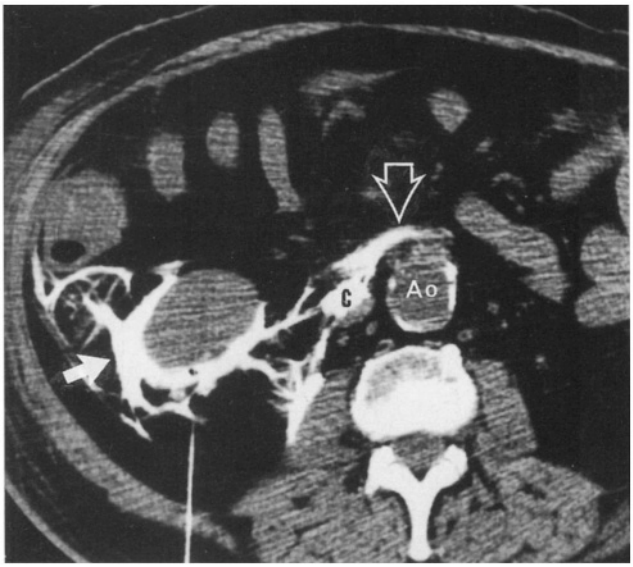


Fig. 8–13. Potential midline communication of perirenal spaces.
CT scan of prone cadaver at the level of the lower renal pole following injection of 200 mL of contrast medium into the right perirenal space *(closed arrow)* shows narrow channel to the midline *(open arrow)* anterior to the inferior vena cava *(C)* and aorta *(Ao).*
(Reproduced from Mindell et al.[29])

clinical investigations strongly suggest that such infrequently encountered midline communications are actually within the *retromesenteric plane.* Dissection of fluids within this anatomic plane of the anterior pararenal space, based on embryologic fascial fusions,[31–33] has received renewed appreciation.[34,35] At levels just inferior to the origin of the superior mesenteric artery, fluid can track anterior to the aorta, inferior vena cava, and left renal vein and posterior to the root of the mesentery. This is the characteristic location in which retroperitoneal collections cross the midline.

It has been recently reported that the anterior renal fascia may be deficient over the upper portion of the right kidney and adrenal gland so that the superior aspect of the perirenal space is open toward the bare area of the liver[36–38] (Fig. 8–14). Whether this is a variation in extent and attachments or actual rupture through the fascia creating a communication remains to be further determined. These anatomic relationships may be of considerable clinical significance. In the occasional circumstance of a hepatic injury involving the posterior segment of the right lobe of the liver with the capsular extent of laceration limited to the bare area, retroperitoneal rather than intraperitoneal bleeding may occur[39,40] (Fig. 8–15). Thus, the classic peritoneal findings may be absent, and peritoneal lavage may not show intraabdominal blood. Rupture of amoebic liver abscess into the retroperitoneum along this precise anatomic route has also been documented.[41]

The *posterior pararenal space* is demarcated on each side of the body by the fusion of the transversalis fascia medially with the muscle fascia. It is therefore limited by and parallels the margin of the psoas muscle. The space is open laterally toward the flank and inferiorly toward the pelvis (Fig. 8–16). Bilaterally they are potentially in communication only via the properitoneal fat of the anterior abdominal wall deep to the transversalis fascia. As opposed to the other two extraperitoneal spaces, the posterior pararenal spaces contain no organs.

Figure 8–17 displays several anatomic features particularly relevant to clinical imaging and an understanding of disease processes.

Figure 8–6b is a sagittal view of a few more anatomic features that have particular diagnostic significance:

1. The lines of fusion of the anterior and posterior renal fascial layers are unique and contribute distinctly to the spread and confinement of extraperitoneal effusions. The perirenal space on each side narrows as it extends inferiorly, resembling an inverted cone. (For this reason, the single layer of fascia extending laterally from the cone of renal fascia has been designated as the lateroconal fascia.) Inferiorly, the layers fuse weakly or blend with the iliac fascia; as they narrow medially, they also blend loosely with the periureteric connective tissue. Investigators differ regarding patency of the apex of the cone. Some describe a multilaminar fusion,[42] whereas others have documented ready communication toward the iliac fossa.[29] However, it has been consistently observed clinically that infections and other effusions arising in the kidney or perirenal tissues are confined to the perirenal space. It may also be postulated that there is early inflammatory sealing of the potential outlet or that acute distention of the cone results in a self-sealing mechanism. Superiorly, the two layers are firmly fixed to each other above the adrenal glands to the diaphragmatic fascia.[13] (Fig. 8–18).

2. At the level of the iliac crest, below the cone of renal fascia, the anterior and posterior pararenal spaces are in potential communication.

3. At this same level, the lateroconal fascia disappears as a distinct boundary so that the anterior pararenal space communicates laterally with the properitoneal fat of the flank stripe.

4. Superiorly, posterior pararenal fat continues as a thin subdiaphragmatic layer of extraperitoneal fat.

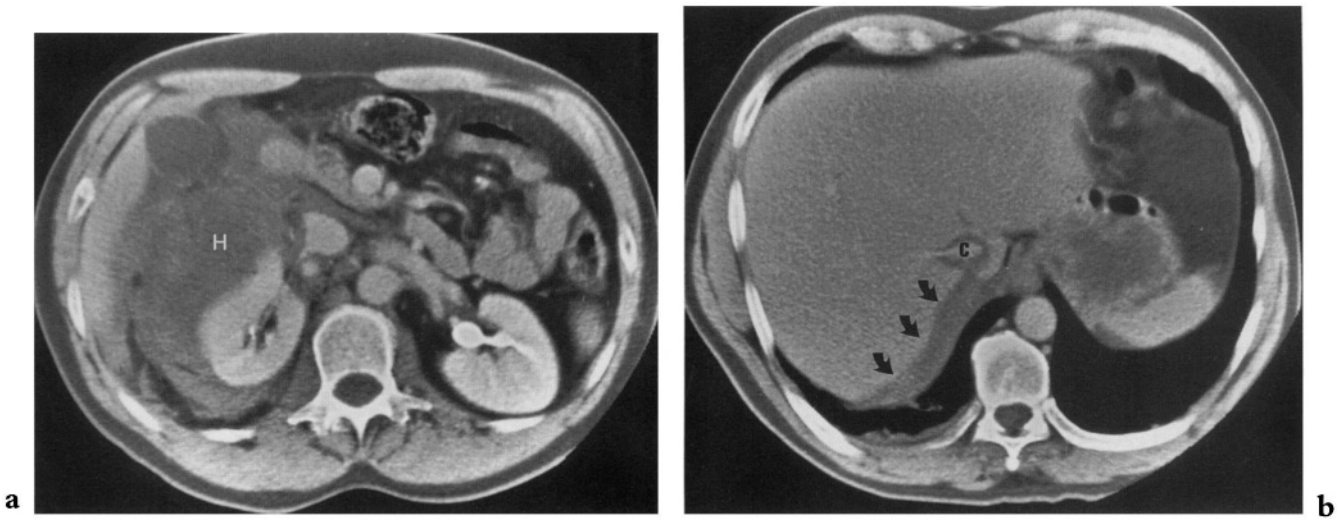


Fig. 8–14. Communication between the right perirenal space and the bare area of the liver.
(a) Occult right renal cell carcinoma *(not shown)* results in massive perirenal hemorrhage *(H).*
(b) At a higher level, the blood has risen to the site of the bare area of the liver *(arrows)* and encircles the inferior vena cava *(C).*

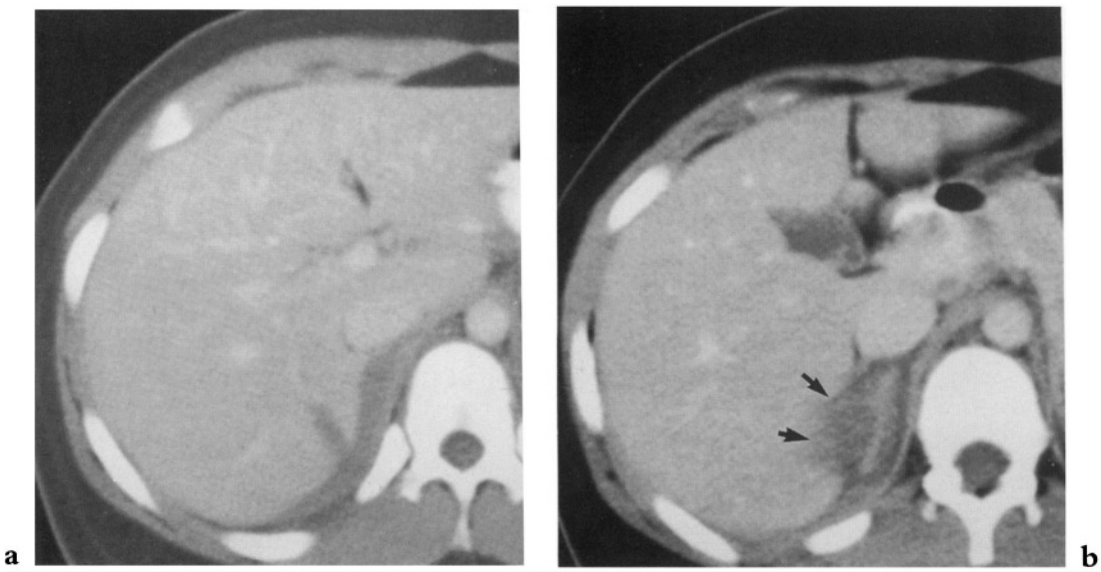


Fig. 8–15. Traumatic laceration of bare area of liver with communication to periadrenal tissues.
(a) CT shows that simple hepatic laceration involving the bare area is associated with hemorrhage, which is presumably subcapsular. No free fluid was seen in Morison's pouch or in the pelvis.
(b) At a level 2 cm inferiorly, a hematoma *(arrow)* surrounds and obscures the right adrenal gland. This had resolved at follow-up CT performed 6 days later.
(Reproduced from Patten et al.[39])

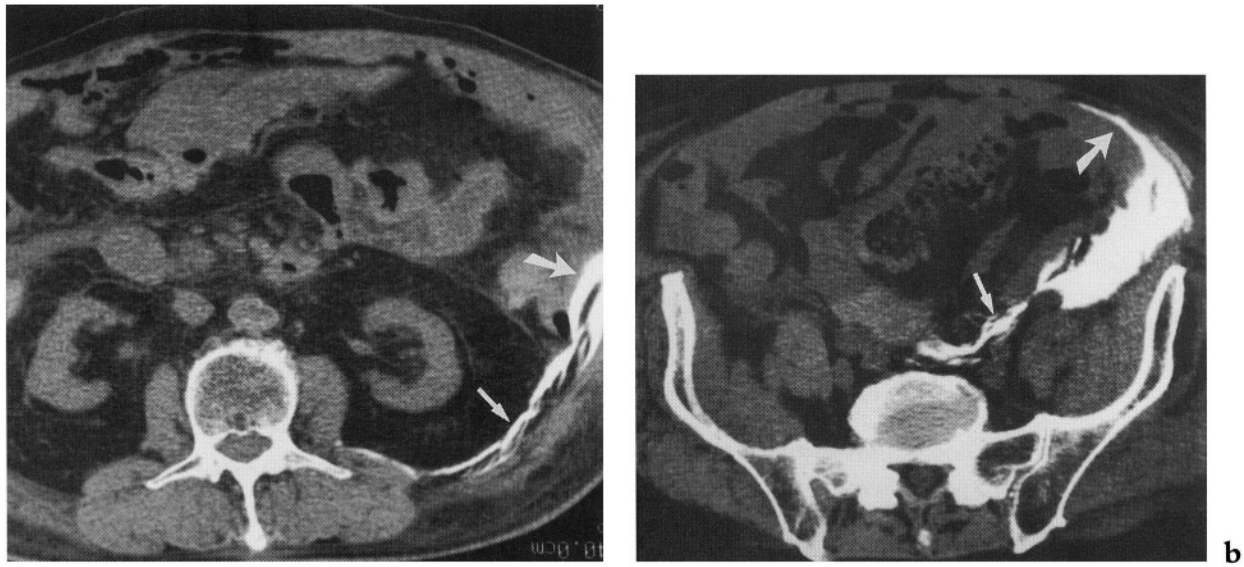


Fig. 8–16. Anterolateral extension of posterior pararenal space and its communication to extraperitoneal spaces in the pelvis.
(a) CT scan of prone cadaver after injection of 100 mL of contrast medium into the left posterior pararenal space *(small arrow)* documents its anterolateral extension around the flank within the properitoneal fat *(large arrow).*
(b) CT scan of prone cadaver after injection of 300 mL of contrast medium into the left posterior pararenal space shows its connection with infrarenal space *(small arrow)* and its extension anterolaterally *(large arrow)* en route to prevesical space.
(Reproduced from Mindell et al.[29])

At the level of the renal hilum, the posterior renal fascia terminates at the midportion of the psoas muscle. Further down it withdraws toward the quadratus lumborum muscle (Fig. 8–19), only to fuse again with the posterolateral margin of the psoas muscle at the level of the inferior apex of the cone.[17,25,26,45]

The normal thickness of the fascial planes is 1–2 mm. On CT, the posterior renal fascia is normally seen far more often than the anterior. A fascia that is focally thickened or greater than 2–3 mm in width is usually abnormal[19,46] (Figs. 8–20 and 8–21). Renal fascial thickening may be caused by edema, hyperemia, fibrosis, or lipolysis.[47] It has been reported in a large variety of pathologic conditions,[46,48,49] including inflammatory, malignant, and traumatic processes, and it is further nonspecific in not allowing diagnostic localization to a primary extraperitoneal site since it may be related to disease in the kidney, perirenal space, or pararenal compartments,[7,8,11,19,50] or even intraperitoneal structures.[51]

Rarely, the appearance of thickened fascia may be simulated on CT supine scans by intraperitoneal fluid within posterior peritoneal recesses, particularly on the left.[17,52,53] Fluid layering in a deep left paracolic gutter may mimic thickening of the lateroconal fascia and a portion of the posterior renal fascia. As the fluid continues superiorly into the inferior extension of the splenorenal recess, and perhaps to some degree medially within the unusual variant of a retropancreatic recess, the appearance of a thickened anterior renal fascia may result (Fig. 8–22). In those cases where distinction from intrinsic involvement of the anterior pararenal space may be difficult.[53] I have noted that two further findings may be of value; (a) intraperitoneal fluid would be expected to shift position on decubitus or prone CT scans; and (b) although there is some variability in the peritoneal fixation of the descending colon[54,55] (Figs. 8–23 and 8–24) evidence of involvement of the extraperitoneal attachment of the descending colon indicates fluid in the anterior pararenal space (Fig. 8–25).

The posterior renal fascia has been shown by dissection studies to be divided into two laminae at a variable point from the kidney.[20] The thinner anterior leaf extends anteriorly to be continuous with the anterior renal fascia. The thicker posterior lamina becomes the

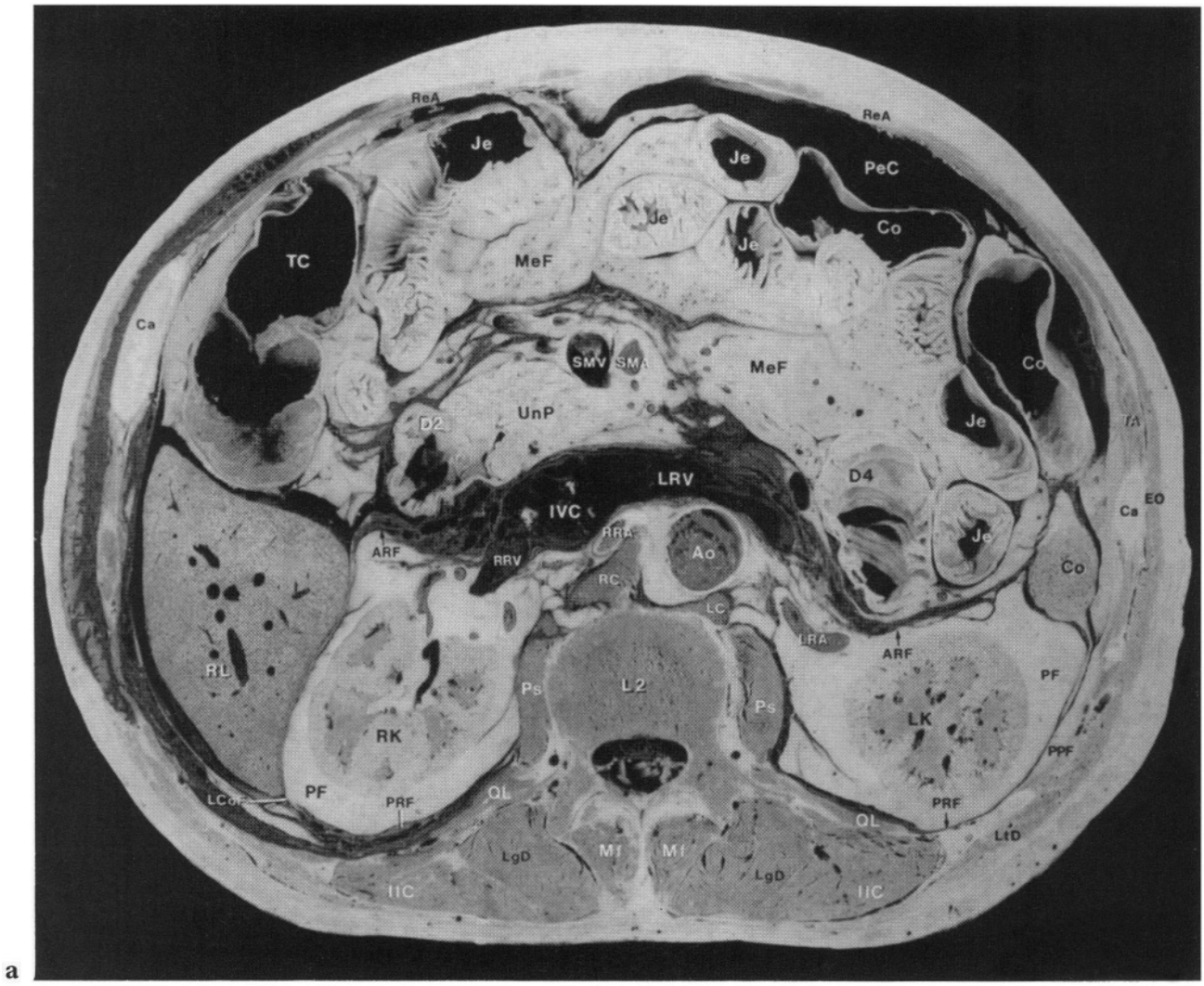
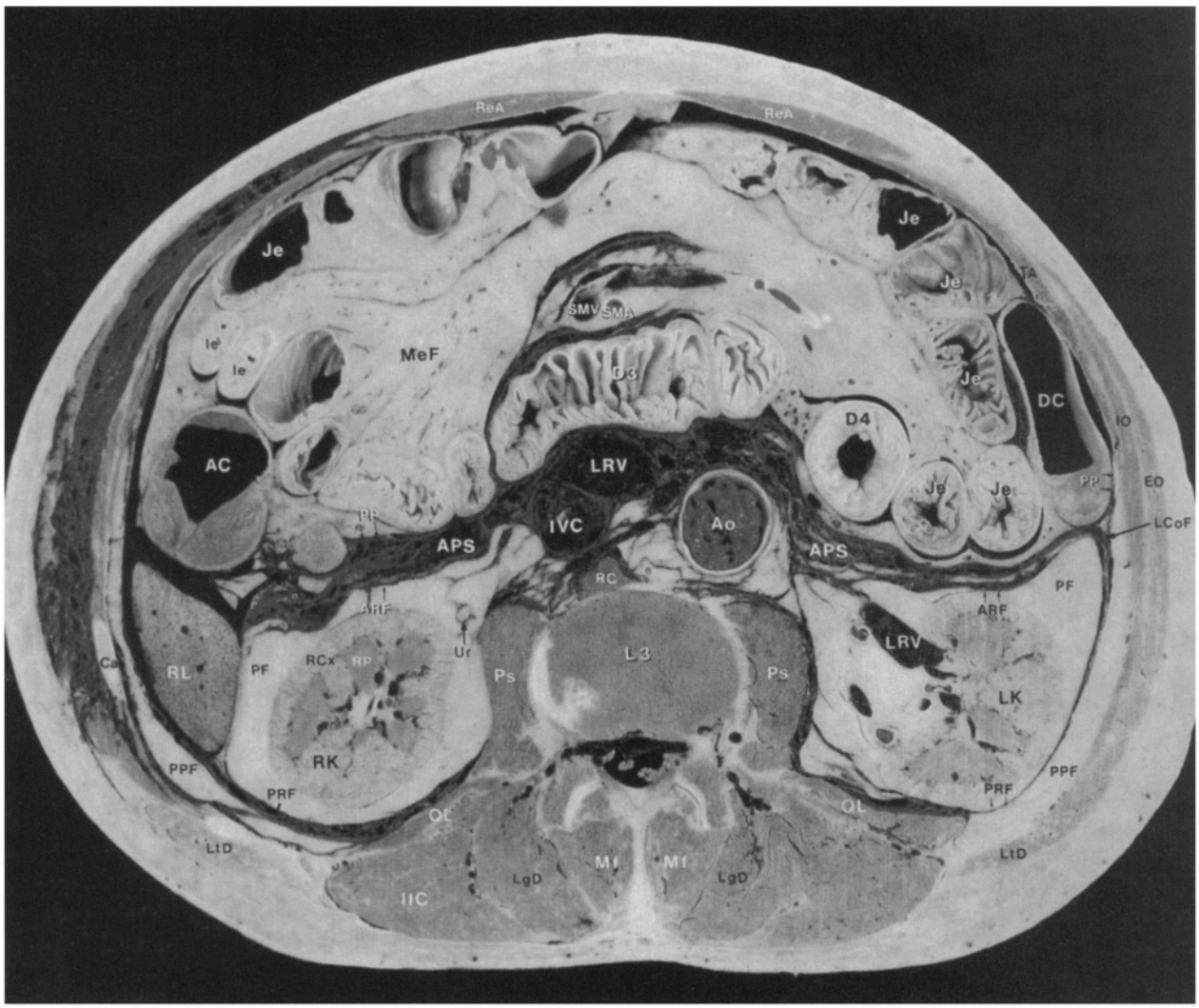


Fig. 8–17. Transverse anatomic cross-sections.
Connective tissues of spaces as well as mesenteries and fasciae are stained by dye permeation. **(This figure also appears in the color insert.)**
(a) Level of uncinate process of pancreas and renal arteries.
(b) Level of third portion of duodenum and the infrarenal abdominal aorta.
These stained sections demonstrate particularly relevant features:
1. Anatomically, the anterior pararenal space is potentially continuous across the midline.
2. The perirenal spaces at these levels share no bilateral continuity; there is midline termination of the anterior renal fascia.
3. The anterior pararenal space ventrally is anatomically continuous with the roots of the small bowel mesentery and similarly of the transverse mesocolon. Lesions of the perirenal contents, including the kidneys and adrenals, are provided anatomic continuity along their major vessels to the aorta and inferior vena cava and thereby to the small bowel mesentery and transverse mesocolon. Extraperitoneal and intraperitoneal structures constitute the continuum designated as the subperitoneal space. This is fully discussed in Chapter 13.
4. Rupture of an abdominal aortic aneurysm can be anticipated as likely occurring into the perirenal space or dissecting into the posterior pararenal space or psoas muscle on the left. Anatomic considerations include the point of rupture both on the circumference of the aorta and on the cephalocaudal level. Other factors include the acuity, force, and volume of the rupture and preexisting adhesions.
(Reprinted with permission from Han M-C, Kim C-W: Sectional Human Anatomy, 2nd ed. Ilchokak, Seoul, Korea, 1989.)



b

AC = Ascending colon
APS = Anterior pararenal space
ARF = Anterior renal fascia
Ao = Aorta
Ca = Cartilage
Co = Colon
D2 = Second portion of duodenum
D3 = Third portion of duodenum
D4 = Fourth portion of duodenum
DC = Descending colon
EO = External oblique muscle
IO = Internal oblique muscle
IVC = Inferior vena cava
IE = Ileum
IlC = Iliocostalis muscle
Je = Jejunum
L1-2 = L1-2 intervertebral disc
L2 = L2 vertebral body
L3 = L3 vertebral body
LC = Left diaphragmatic crus
LCoF = Lateroconal fascia
LK = Left kidney
LRA = Left renal artery
LRV = Left renal vein
LgD = Longissimus dorsi muscle
LtD = Latissimus dorsi muscle
MeF = Mesenteric fat
Mf = Multifidus muscle
PF = Perirenal fat
PP = Parietal peritoneum
PPE = Posterior pararenal fat
PRE = Posterior renal fascia
PeC = Peritoneal cavity
Ps = Psoas muscle
OL = Quadratus lumborum muscle
RC = Right diaphragmatic crus
RCx = Renal cortex
RK = Right kidney
RL = Right lobe of liver
RP = Renal pelvis
RRA = Right renal artery
RRV = Right renal vein
ReA = Rectus abdominis muscle
Ri = Rib
SMA = Superior mesenteric vein
TA = Transversus abdominis muscle
TC = Transverse colon
UnP = Uncinate process of pancreas, head
Ur = Ureter

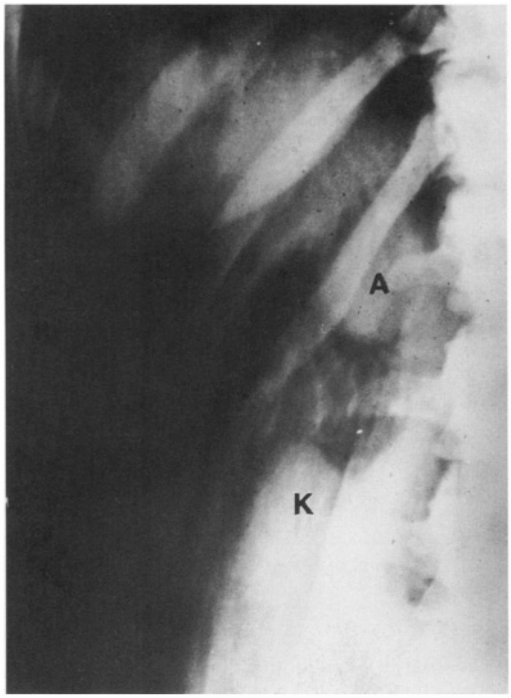


Fig. 8–18. Attachment of adrenal gland to renal fascia superiorly.
The distinction of an adrenal mass from an upper renal pole mass can be readily made on erect films. Highlighted by retroperitoneal pneumography, the upright position allows the kidney *(K)* to fall, but the adrenal gland *(A)* harboring a pheochromocytoma remains fixed by its fascial attachment. (Reproduced from Meyers.[13])

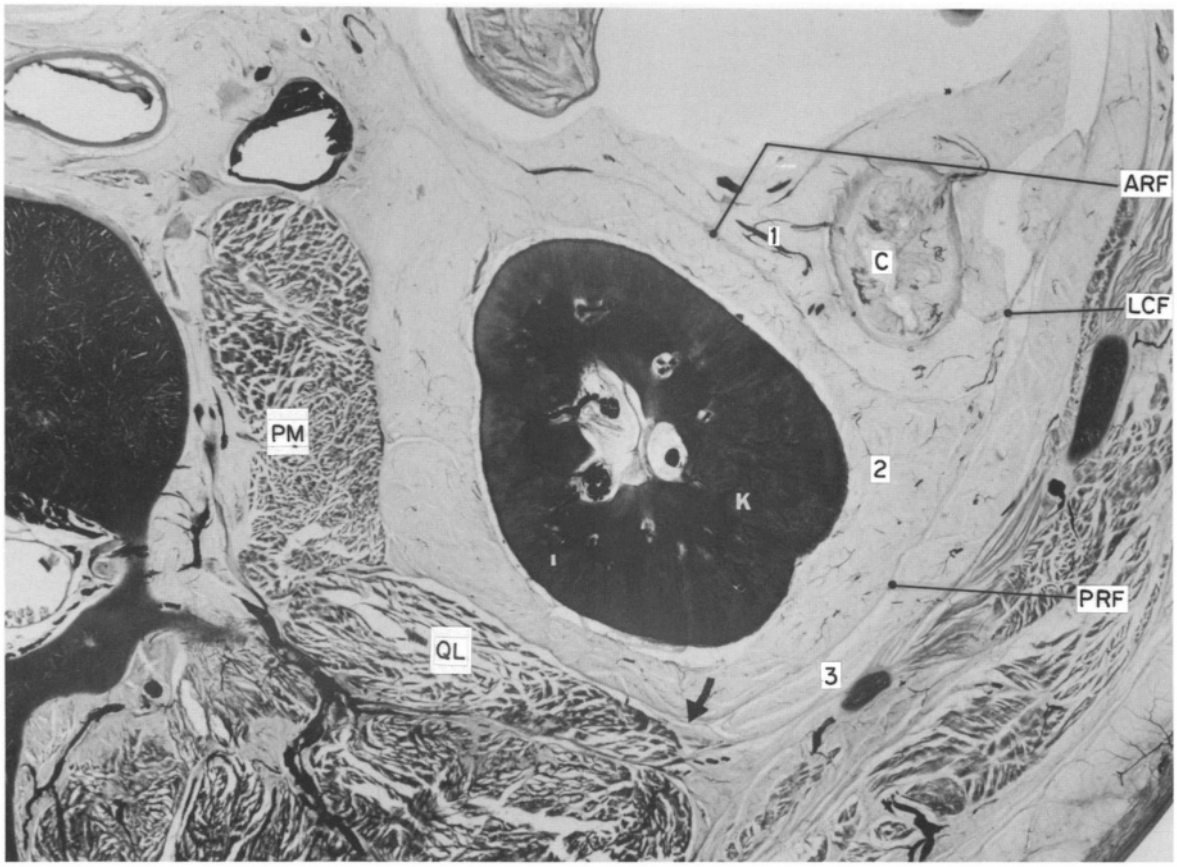
lateroconal fascia. Figures 8–26 through 8–29 clearly display these laminae in four different patients. A potential space between the two laminae is thus anatomically continuous with the anterior pararenal space[20] (Fig. 8–30). The laminated, potentially expansile fascial planes of the extraperitoneal tissues provide pathways of spread.[35]

On plain films of the abdomen, the lateroconal fascia sometimes appears as a thin line lateral to the kidney (Fig. 8–31). It is more commonly seen on the right, where it projects inferior to the hepatic angle. Characteristically, it is slightly angled medially as it extends inferiorly. The lateral fusion of the renal fascial layers at the level of the lateroconal fascia demarcates the perirenal fat medially from the posterior pararenal fat laterally as it extends into the flank stripe. These fascial layers are more frequently visualized in nephrotomography. In the past, this fascial line has been mistaken for the peritoneal reflection itself, leading to considerable confusion in the radiologic localization of disease processes. Its significance lies in the fact that it is truly an extraperitoneal structure that provides a boundary.

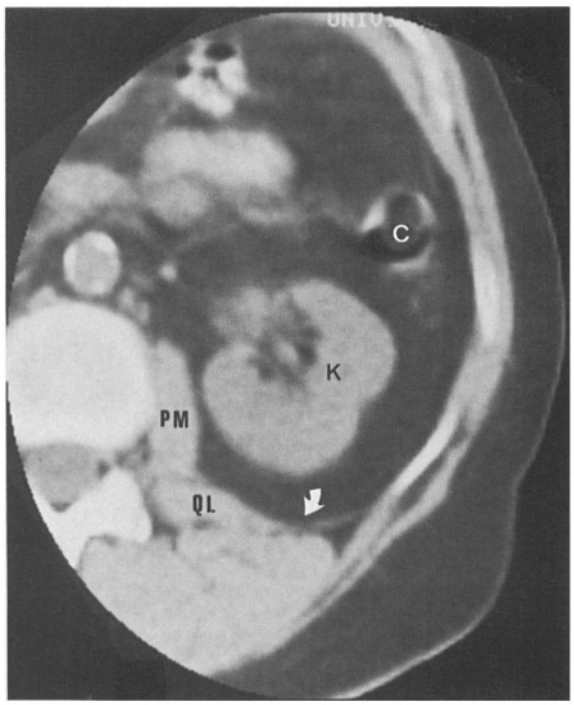
Variations in the origin of the lateroconal fascia may explain the uncommon occurrence of retrorenal colon (Fig. 8–32) or extension of ascitic fluid.[56–58] The site of blending of the lateroconal fascia with the perirenal fascia varies from patient to patient as well as from side to side and from cephalad to caudad, and ranges from a location anterior to a location posterior to the kidney.[20] It has been pointed out that abundant perirenal fat is much more common in men than in women and that a lack of this adipose tissue may contribute to the colon lying lateral to, or even behind, the kidney.[59] Recognition of retrorenal colon may have practical applications when an invasive renal procedure is contemplated.

Kunin has called attention to three groups of bridging connective tissue septa that may divide the perirenal space into relatively discrete compartments. These include fibrous lamellae that connect the renal capsule to the perirenal fascia and some that connect the anterior and posterior renal fasciae, but the most commonly visible in well-fatted patients is the posterior renorenal bridging septum.[60] This is attached only to the renal capsule and runs parallel to the surface of the kidney. It is variable in extent somewhere between the posteromedial and posterolateral margins (Figs. 8–33 and 8–34). The septa may course over a considerable distance (Fig. 8–35) and may thicken in response to the same stimuli that cause thickening and increased visibility of the

text continues on page 353



a



b

Fig. 8–19. Medial insertion of posterior renal fascia. Anatomic cross-section (**a**) and CT **(b)** below midlevel of left kidney *(K)* show termination of the posterior renal fascia in relationship to the quadratus lumborum muscle *(arrow).* The quadratus lumborum has variable width and thus the medial extent of the posterior pararenal space varies from patient to patient.[20] *PM* = psoas muscle; *C* = descending colon; *ARF* = anterior renal fascia; *LCF* = lateroconal fascia; *PRF* = posterior renal fascia; *1* = anterior pararenal space; *2* = perirenal space; *3* = posterior pararenal space.

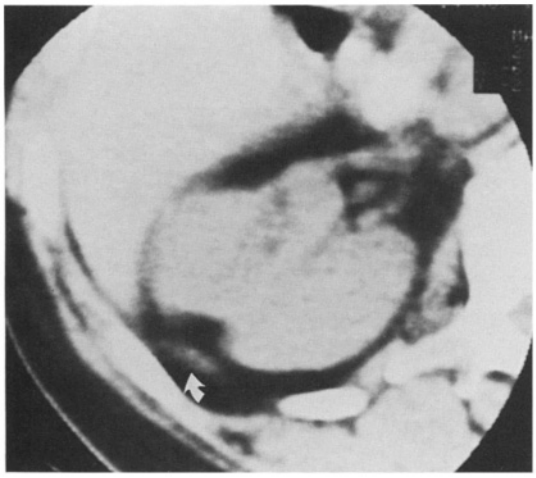


Fig. 8–20. Localized thickening of the renal fascia *(arrow)* at the site of a pyelonephritic cortical scar. (Courtesy of Roger Parienty, M.D., Neuilly, France.)

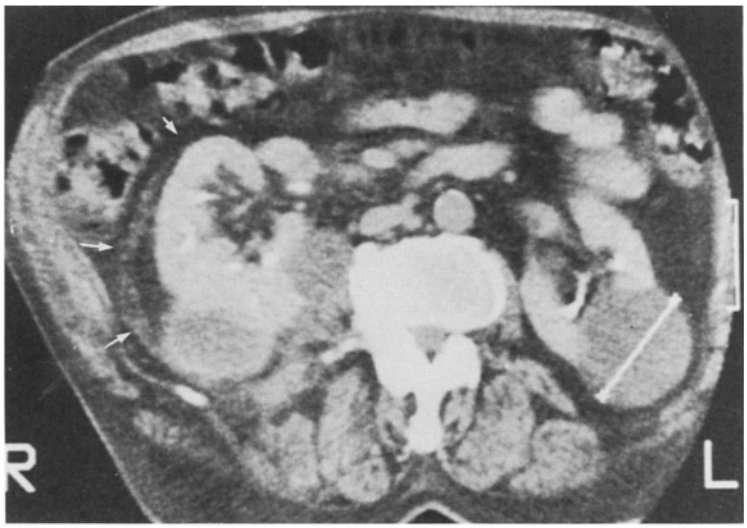


Fig. 8–21. Thickening of the renal fascia *(arrows)* in conjunction with an infected right renal cyst. An uninvolved simple renal cyst is present on the left. (Courtesy of Roger Parienty, M.D., Neuilly, France.)

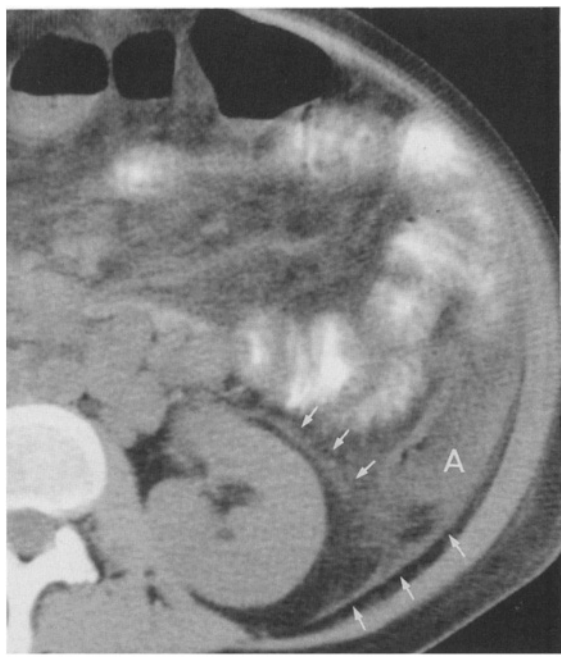


Fig. 8–22. Thickened fascia simulated by intraperitoneal fluid.
In this cirrhotic patient with portal hypertension and widespread varices, ascitic fluid *(A)* occasions the appearance of thickening of the anterior renal fascia, lateroconal fascia, and a segment of the posterior renal fascia *(arrows).*

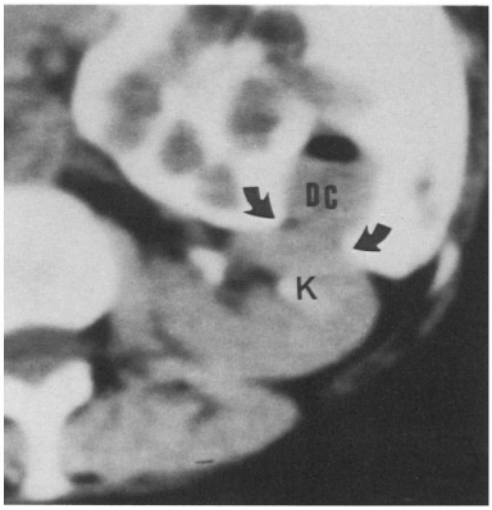


Fig. 8–23. The peritoneal reflection over the descending colon *(arrows)* is shown on this CT study by intraperitoneal contrast medium. The bare area of the descending colon *(DC)* is contiguous with the adipose tissue of the anterior pararenal space ventral to the left kidney *(K).*

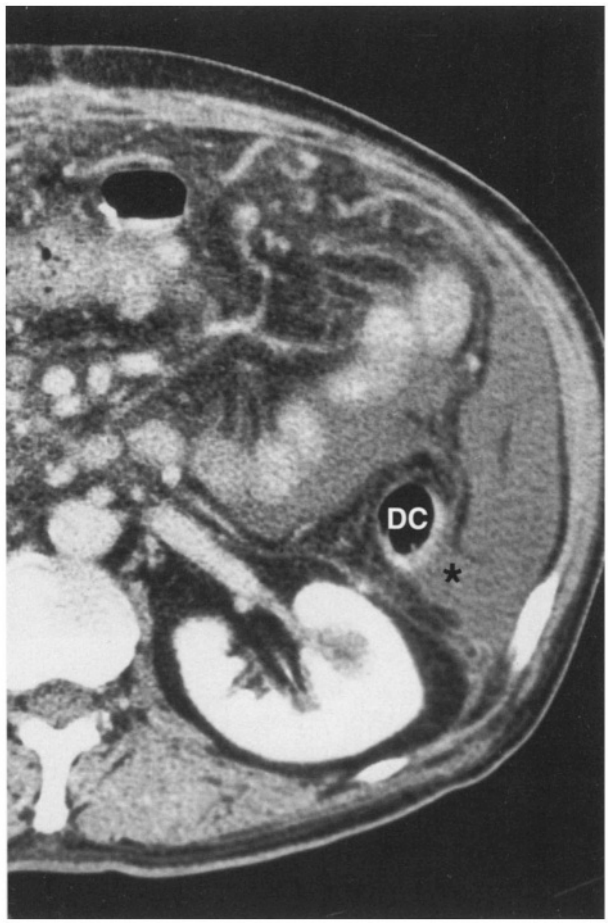


Fig. 8–24. Partial peritonealization of the descending colon.
CT shows the descending colon *(DC)* in this case is partially peritonealized, secondary to incomplete posterior fusion of the descending mesocolon, allowing posterior extension of the left paracolic gutter *(asterisk).*

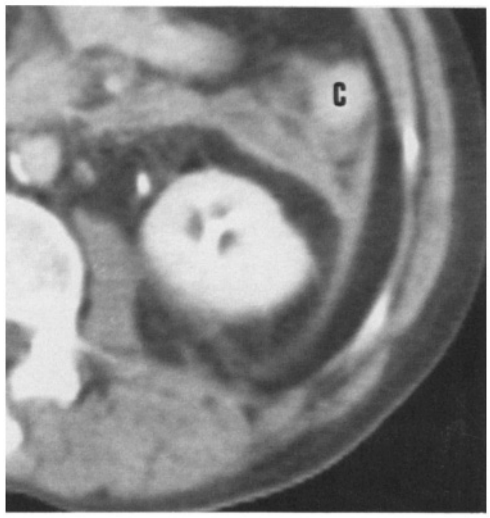


Fig. 8–25. Involvement of descending colon's extraperitoneal bare area.
In a case of thickened renal fascia secondary to acute pancreatitis, CT demonstrates inflammatory involvement of the extraperitoneal fat related to the bare area of the descending colon *(C).* This localizes the process to the anterior pararenal space and distinguishes the changes from intraperitoneal fluid.

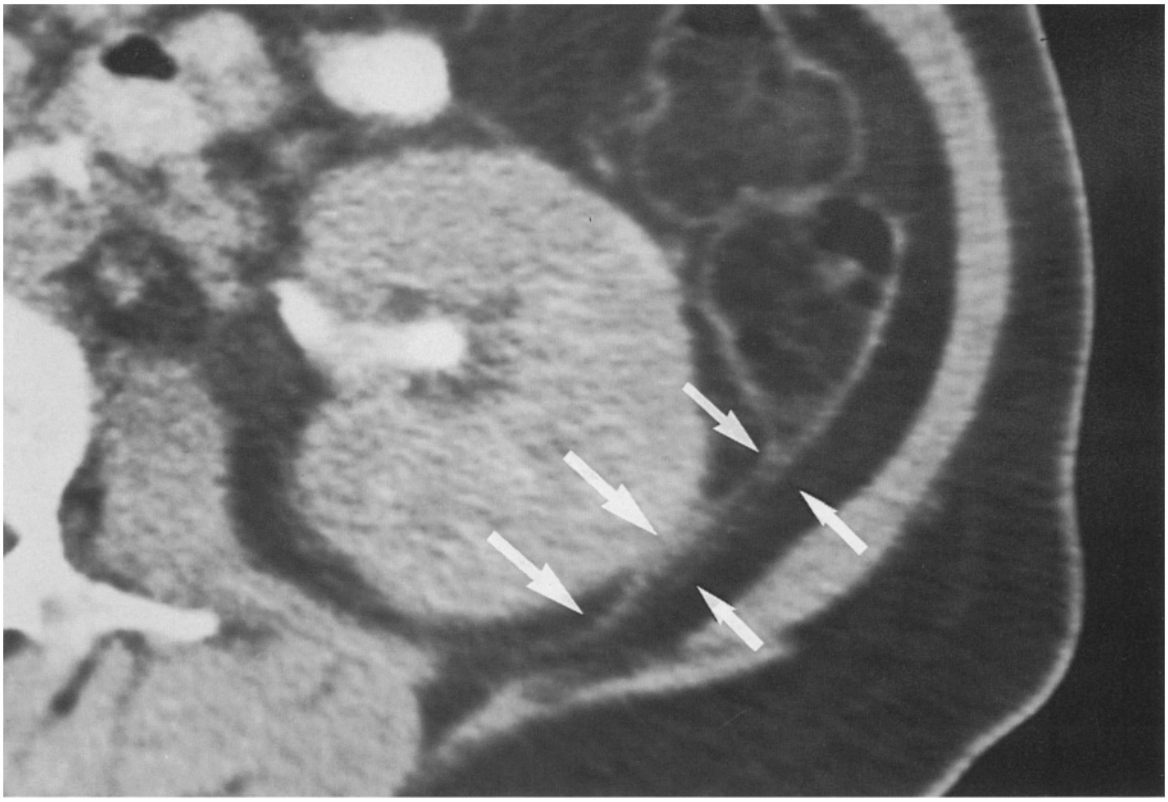


Fig. 8–26. *In vivo* identification of the two layers of the posterior renal fascia.
CT demonstrates an enlarged left kidney, secondary to acute pyelonephritis, abutting the posterior renal fascia and the presence of a double line of the posterior renal fascia *(arrows).* The inner line adjacent to the kidney is thickened, and the potential space between the two leaves of the posterior renal fascia is now seen.
(Courtesy of Michael Oliphant, M.D., Syracuse, NY.)

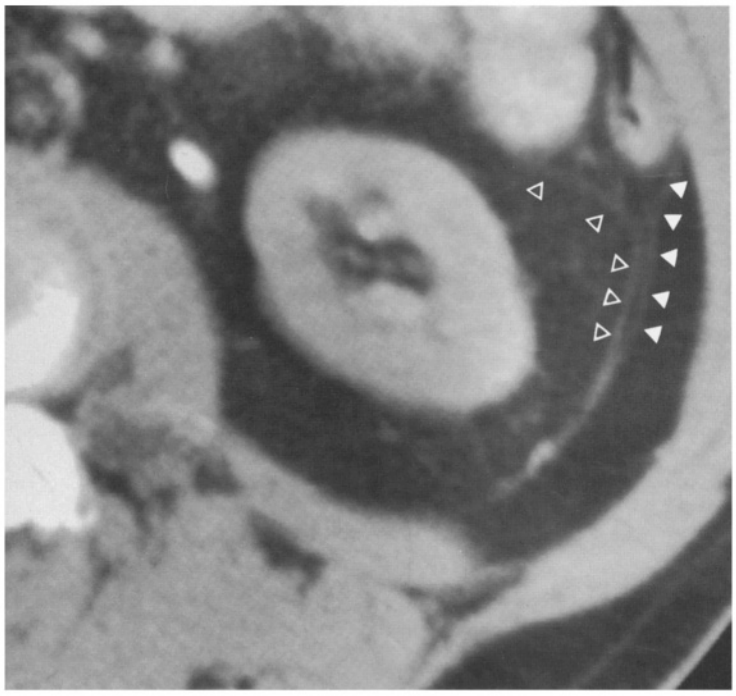


Fig. 8–27. *In vivo* identification of the two laminae of the posterior renal fascia.
CT demonstrates continuity of the inner layer with the anterior renal fascia *(open arrowheads)* and of the outer layer with the lateroconal fascia *(closed arrowheads).* The anterior pararenal space thus extends between the two laminae.
(Courtesy of Jay P. Heiken, M.D., Mallinckrodt Institute of Radiology, St. Louis, MO.)

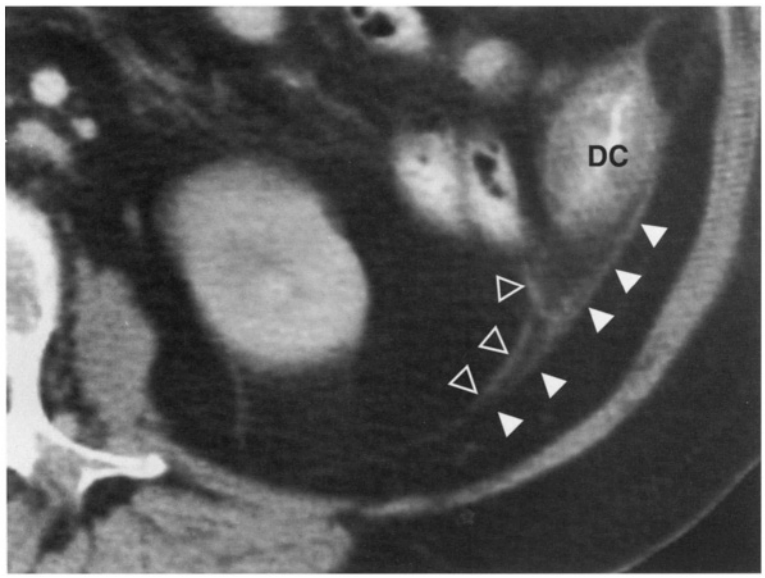


Fig. 8–28. *In vivo* identification of the two laminae of the posterior renal fascia.
CT demonstrates the inner layer of the posterior renal fascia merging with the anterior renal fascia *(open arrowheads)* and the outer layer continuing as the lateroconal fascia *(closed arrowheads).* Mural thickening with luminal narrowing of the descending colon *(DC)* in this instance is due to ischemic colitis.

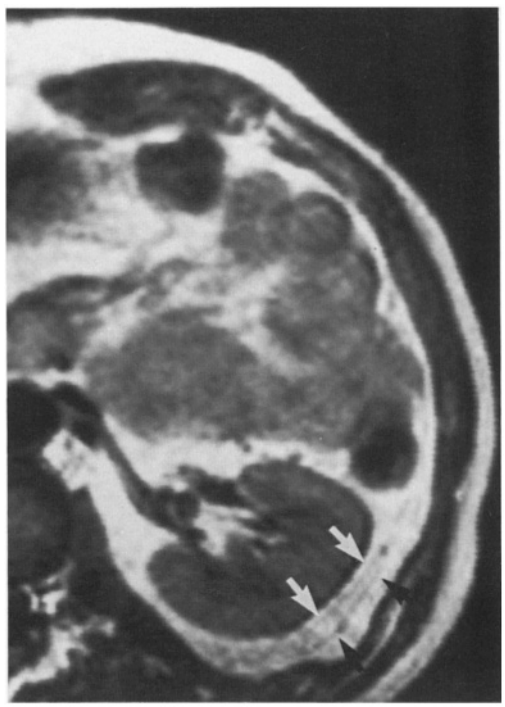


Fig. 8–29. Two layers of the posterior renal fascia *(arrows)* shown discretely by magnetic resonance imaging.

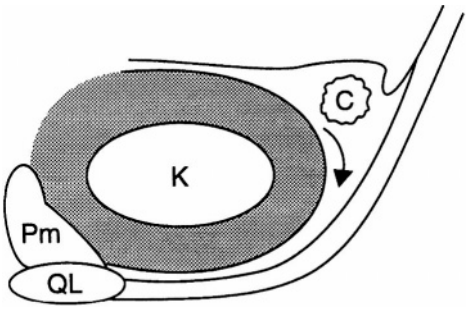


Fig. 8–30. Anatomic continuity of the anterior pararenal space between the two leaves of the posterior renal fascia, as described by Raptopoulos et al.[20] *K* = kidney; *C* = descending colon; *PM* = psoas muscle; *QL* = quadratus lumborum muscle.

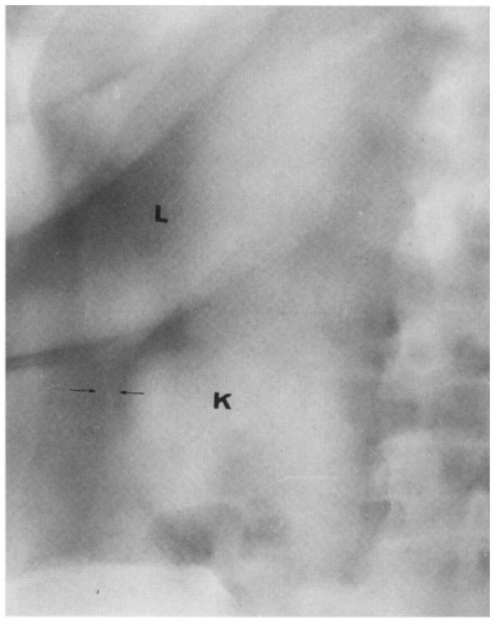


Fig. 8–31. Plain film demonstration of the edge of the lateroconal fascia *(arrows).*
This projects as a thin density inferior to the angle of the liver *(L)* and lateral to the kidney *(K).* This demarcates the extraperitoneal adipose tissue into the perirenal fat medially and posterior pararenal fat laterally, extending into the flank fat.
(Reproduced from Meyers et al.[12])



Fig. 8–32. Retrorenal colon.
The transverse colon and hepatic flexure are insinuated deeply lateral and posterior to the right kidney. This is explained by the variable origin of the lateroconal fascia.
(Courtesy of Jay P. Heiken, M.D., Mallinckrodt Institute of Radiology, St. Louis, MO.)

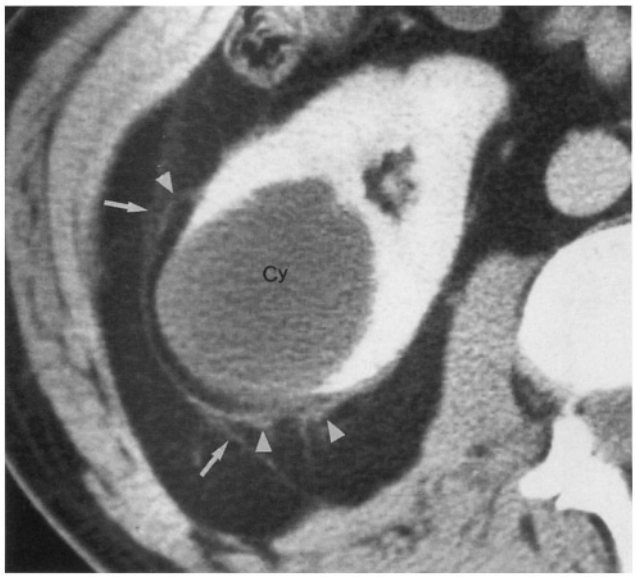


Fig. 8–33. Deflection of the posterior renorenal septum.
A large renal cyst *(Cy)* displaces the adjacent renorenal bridging septum *(arrowheads)* outward to the renal fascia *(arrows).*
(Courtesy of Michiel Feldberg, M.D., University of Utrecht, The Netherlands.)

anterior and posterior renal fasciae[61,62] (Figs. 8–36 and 8–37). Venous collaterals in the perirenal fat secondary to renal vein occlusion[46,63] or simply the hypervascularity associated with a neoplasm[46] should be distinguished from thickened bridging renal septa.

The Psoas Muscle

I have clarified the radiographic anatomy of the psoas muscle by anatomic sections through the extraperitoneal tissues at different levels.[8] The upper and lower segments of the psoas muscle are visualized by virtue of the contrast provided by different aspects of the extraperitoneal fat.

At the level of the kidney, it is the perirenal fat that predominantly marginates the lateral border of the psoas muscle. However, below the kidney, secondary to the lines of fusion of the cone of renal fascia, posterior pararenal fat provides the contrast margination of the muscle.

Loss of visualization of the complete muscle border is often misleading and must be carefully evaluated. It is often not seen unilaterally in normal individuals.[4,5] Furthermore, the psoas outline may disappear with only very minimal rotation or scoliosis of the lumbar spine,[64] and extraperitoneal fat may be scanty in emaciated patients or in those who have lost weight.

A reliable sign, however, is *segmental* loss of visualization of the psoas border. Such asymmetry in properly centered films immediately localizes a fluid collection to a specific extraperitoneal compartment. Thus, localized perirenal processes tend to obliterate only the upper margin, whereas fluid collection in the posterior pararenal spaces obliterates the psoas muscle in its lower segment (Fig. 8–38) or throughout, depending on its extent. Two qualifications must be appreciated: (a) on frontal films, a large collection within the anterior pararenal space may, by superimposition of the density, obscure the psoas border, but well-penetrated oblique projections will nevertheless demonstrate its intact mar-



Fig. 8–34. Localized retraction of the thickened renorenal septum *(arrow)* at the site of a cortical scar. The renal fascia is also thickened *(open arrows).*
(Courtesy of Michiel Feldberg, M.D., University of Utrecht, The Netherlands.)

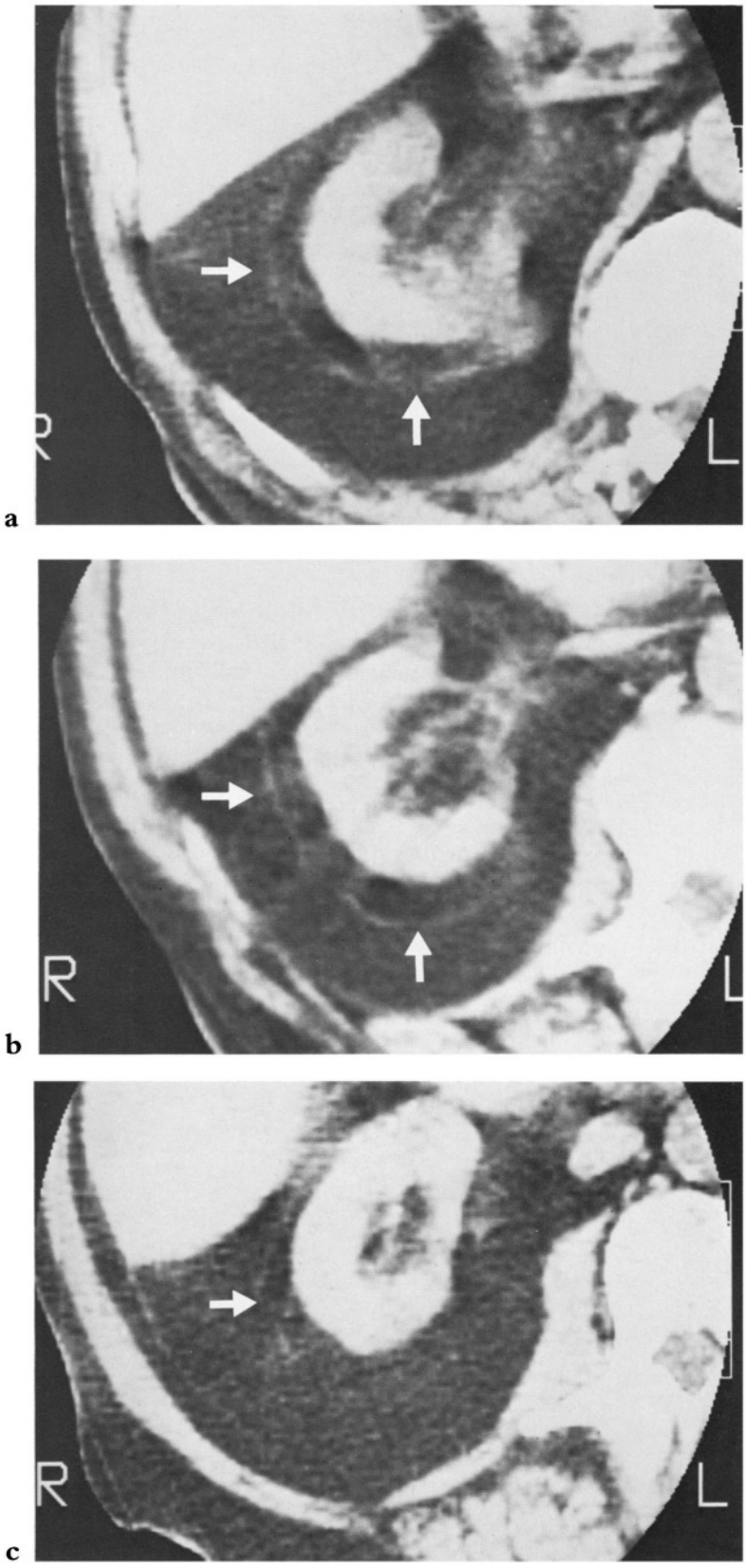


Fig. 8–35. Perirenal bridging septa.
(a–c) CT shows the posterior lamella *(arrows)* over a vertical extent of 4.5 cm.

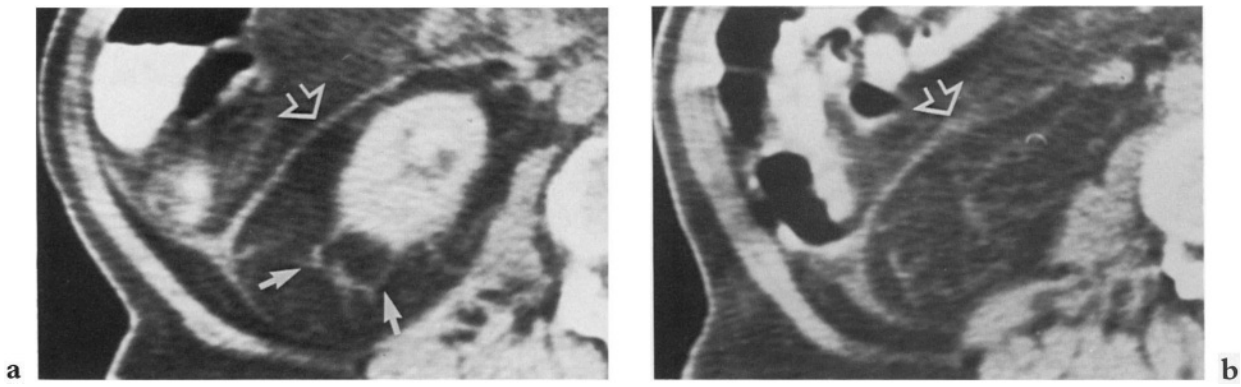


Fig. 8–36. Bridging renal septa.
(a) Among multiple bridging septa, the most conspicuous is a dorsal renorenal septum *(arrows).* These are associated with a thickened anterior renal fascia *(open arrow).*
(b) At a level below the lower renal pole, the septa continue within the fat in the cone of fascia.

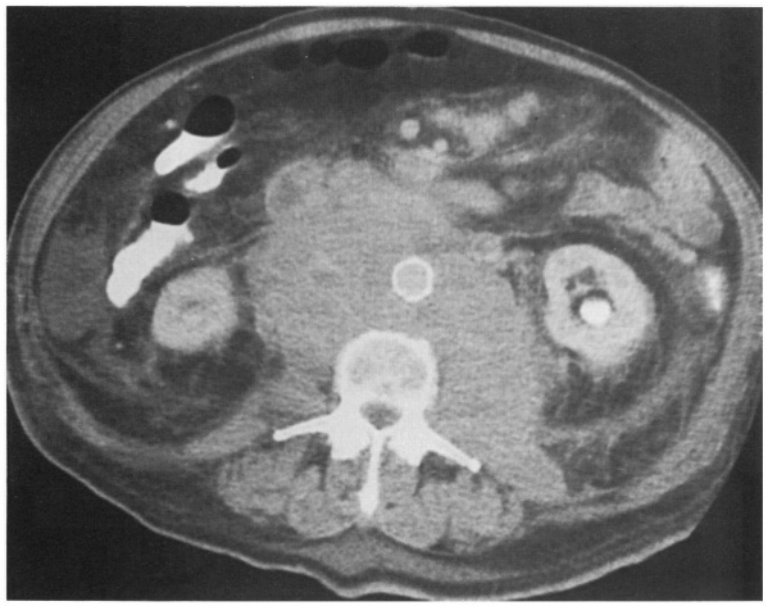


Fig. 8–37. Lymphatic stranding through the extraperitoneal spaces.
In a patient with non-Hodgkin's lymphoma with gross paraaortic/paracaval adenopathy, CT demonstrates extraperitoneal lymphedema with thickening of fasciae and septa.

gin; (b) extraperitoneal gas localized within the posterior pararenal compartment will sharply outline the lateral border of the psoas muscle at all levels.

The Hepatic and Splenic Angles

The hepatic and splenic angles, the posterior and inferior contours of these intraperitoneal organs, are outlined normally by the contrast provided by the subjacent extraperitoneal fat.[65] Figure 8–39 shows that the lateral aspects of the angles are adjacent to the lateral extension of the posterior pararenal fat, while the medial aspects are related to the anterior pararenal and perirenal fat. Loss of their visualization, however, is a nonlocalizing abnormality. Either intraperitoneal (subhepatic) fluid collections or infiltration within any of the three extraperitoneal compartments may act as a mass to displace the angle out of the bed of fat.



Fig. 8–38. Right posterior pararenal abscess in a patient with fever of unknown origin.
Plain film of the abdomen demonstrates visualization of the psoas muscle margins bilaterally *(arrows)* except for segmental loss of the lower aspect on the right. Despite multiple contrast studies, this was the sole finding indicating and localizing the underlying infection, which was proved at surgery.

Anterior Pararenal Space

Roentgen Anatomy of Distribution and Localization of Collections

Selective opacification of the anterior pararenal space in the cadaver permits identification of the preferential pathway of spread and the characteristic localizing features, as shown in Figure 8–40. Preferential flow is downward to the iliac fossa, and the collection demonstrates several diagnostic features:

1. The general axis is vertical.
2. Medially, the collection overlaps the lateral border of the psoas muscle and approaches the spine.
3. Laterally, the lucent flank stripe is preserved, since flow is restricted by the lateroconal fascia.
4. Superiorly, the renal outline remains demarcated where the space lies anterior to the kidney. The hepatic or splenic outline, displaced from its bed of contrasting extraperitoneal fat, is lost. On the right, communication may be established across the reflections of the coronary ligament to the bare area of the liver. The occasional development of abscess in the bare area of the liver secondary to extraperitoneal infection, most commonly from appendicitis, is explained by this anatomic continuity with the anterior pararenal space (Fig. 8–41).

Figure 8–42 exquisitely confirms these findings *in vivo*. Figure 8–43 clarifies these relationships in the horizontal plane.



Fig. 8–39. Transverse anatomic section shows the hepatic angle embedded in extraperitoneal fat. Infiltration of any of the three compartments as well as of the intraperitoneal space may result in loss of radiographic visualization of the hepatic angle. *1* = anterior pararenal fat; *2* = perirenal fat; *3* = posterior pararenal fat; *4* = intraperitoneal space; *K* = kidney; *L* = liver.

The significant criteria for the radiologic localization and distinction of collections within the anterior pararenal space are outlined in Table 8–1.

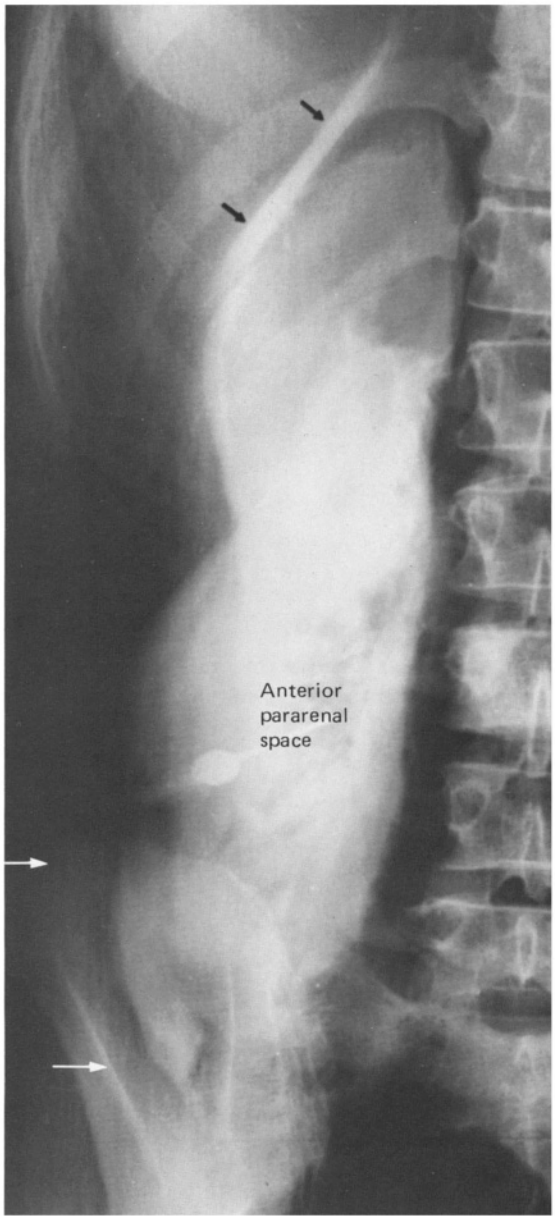
Sources of Effusions

The anterior pararenal compartment is the most common site of extraperitoneal infection. Of 160 patients with extraperitoneal abscess reviewed by Altemeier and Alexander,[3] the process was confined to the anterior pararenal space in 84 (52.5%). Most arise from primary lesions of the alimentary tract, especially the colon, extraperitoneal appendix, pancreas, and duodenum. The exudates originate from perforating malignancies, inflammatory conditions, penetrating peptic ulcers, and accidental or iatrogenic trauma.[3,67] Hemorrhage from a ruptured abdominal aortic aneurysm is rarely localized to this space (Fig. 8–44). I have also recognized localization to this compartment in hemorrhage from the bare area of the spleen, the hepatic and splenic arteries, and in some cases of spontaneous extraperitoneal bleeding.

Extraperitoneal Perforations of the Colon and Appendix

Figure 8–45 illustrates that extraperitoneal perforations of the colon can be identified as clearly localized to the anterior pararenal space, even on plain films. The extraperitoneal collection of mottled gaseous lucencies is oriented with a general vertical axis, medially overlaps the psoas muscle and approaches the spine, and does not obscure the flank stripe laterally. In this patient, who

text continues on page 362



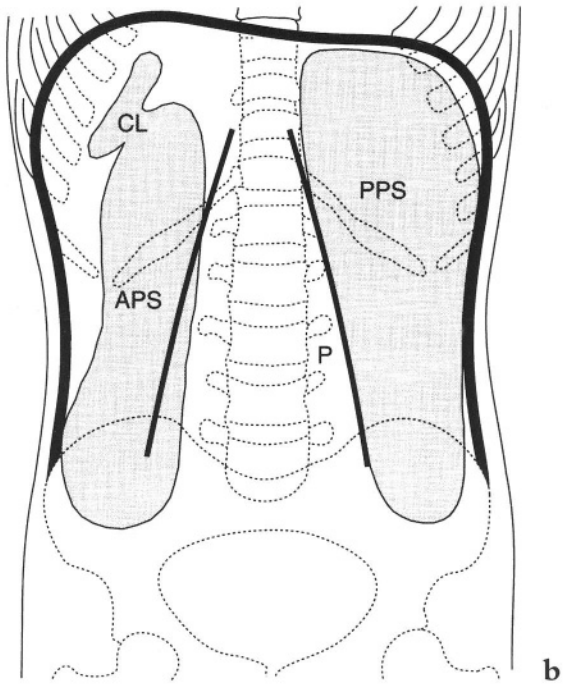


Fig. 8–40. (a) Postmortem injection into the anterior pararenal space.
The collection has a generally vertical axis. Laterally, the lucent flank stripe is intact *(white arrows).* Medially, spread approaches the spine over the psoas muscle. Superiorly, it follows the obliquity of the kidney, and there is extension to the bare area of the liver at the site of reflection of the coronary ligament *(black arrows).*
(From Meyers et al.[12])
(b) Diagram showing the characteristic spread and configuration of extraperitoneal fluid and/or gas collections in the anterior pararenal space *(APS).*
Superiorly, there is continuity to the bare area of the liver at the reflections of the right coronary ligament *(CL). P* = psoas muscle margin.
Configuration of collection within the posterior pararenal space *(PPS)* on the opposite side is shown for comparison.

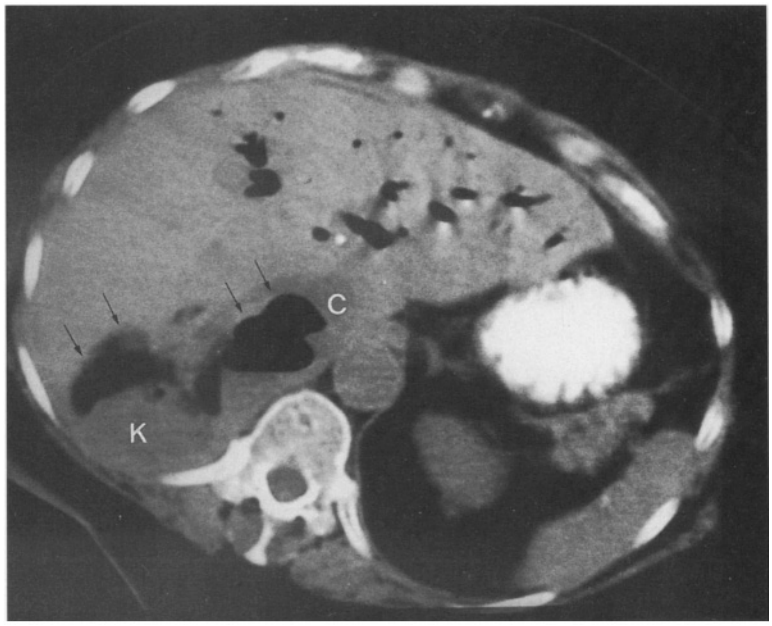


Fig. 8–41. Anterior pararenal abscess, secondary to duodenal perforation, extending cephalad to bare area of liver.
CT in a patient with abdominal pain and fever following an endoscopic papillotomy shows air in the biliary tract and a gas-containing collection, secondary to perforation of the descending duodenum, in the anterior pararenal space, extending cranially to the bare area *(arrows). K* = kidney; *C* = inferior vena cava. (Reproduced from Arenas et al.[66])

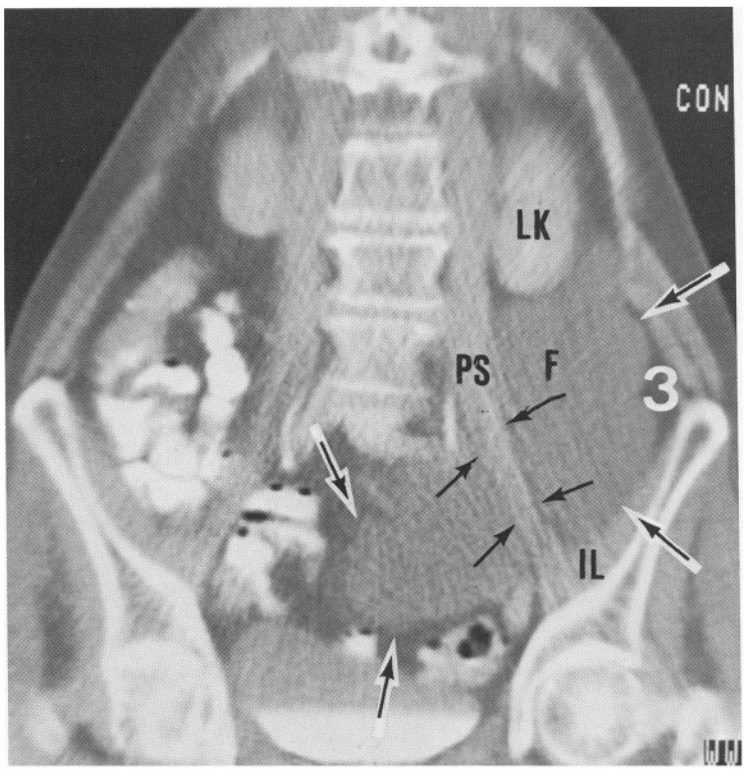


Fig. 8–42. Fluid in the anterior pararenal space.
Direct coronal CT section reveals a fluid collection *(F)* in the left anterior pararenal space *(arrows)* with a vertical axis and medial extension inferiorly. The outlines of the kidney and of the psoas muscle *(PS)* are preserved *(black arrows),* and the flank fat *(3)* of the posterior pararenal space is not infiltrated. The descending colon is not visible since it has been displaced ventrally. *LK* = left kidney; *IL* = iliacus muscle.
(Reproduced from Feldberg.[17])

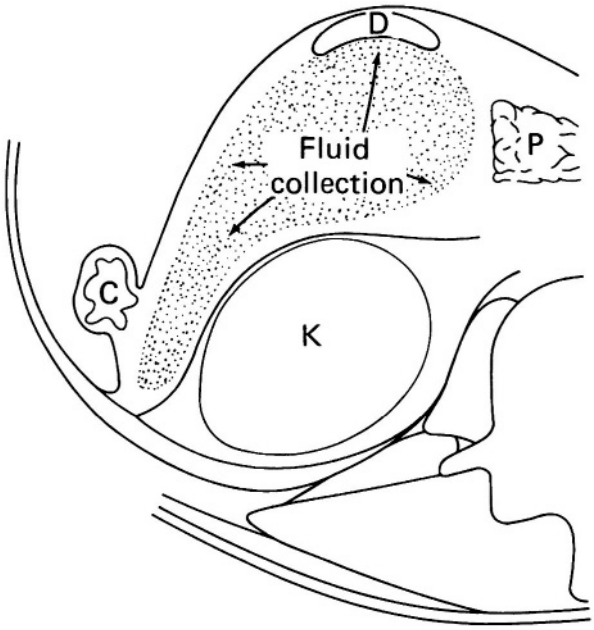


Fig. 8–43. Fluid collection in the right anterior pararenal compartment with viscus displacement. *K* = kidney; *P* = pancreas; *D* = duodenum; *C* = colon. (Reproduced from Meyers et al.[12])

Table 8–1. Radiologic criteria for localizing extraperitoneal effusions

Radiologic features	Anterior pararenal space	Perirenal space	Posterior pararenal space
Perirenal fat and renal outline	Preserved	Obliterated	Preserved
Axis of density	Vertical	Vertical (acute) Inferomedial (chronic)	Inferolateral (parallel to psoas margin)
Kidney displacement	Lateral and superior	Anterior, medial, and superior	Anterior, lateral, and superior
Psoas muscle outline	Preserved	Upper half obliterated	Obliterated in lower half or throughout
Flank stripe	Preserved	Preserved	Obliterated
Hepatic and splenic angles	Obliterated	Obliterated	Preserved or obliterated
Displacement of ascending or descending colon	Anterior and lateral	Lateral	Anterior and medial
Displacement of descending duodenum or duodenojejunal junction	Anterior	Anterior	Anterior

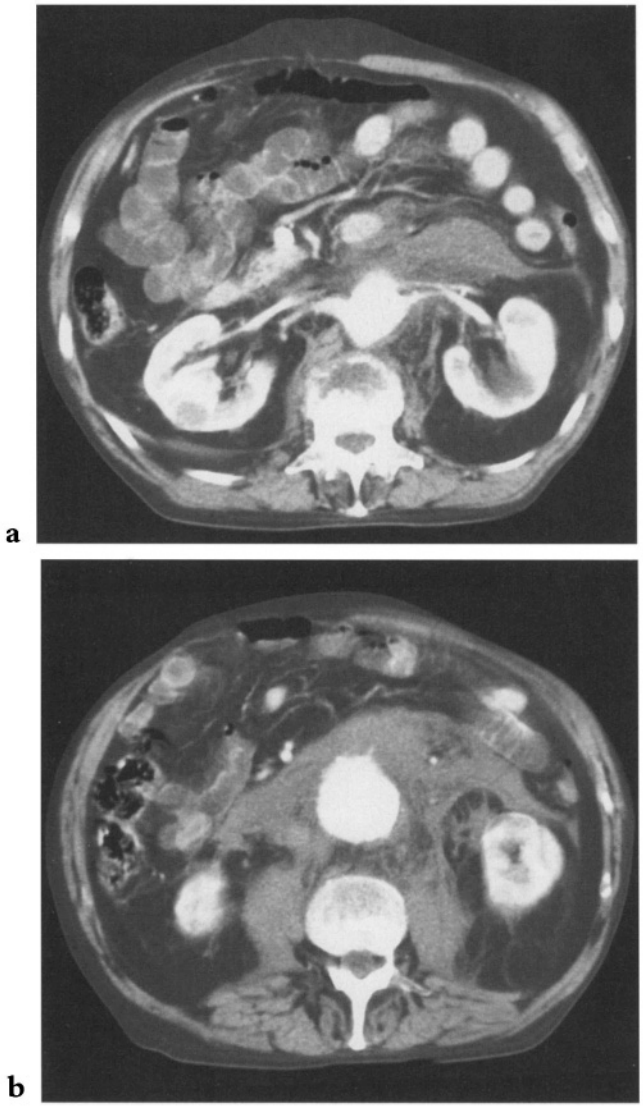


Fig. 8–44. Anterior pararenal space blood from leaking abdominal aortic aneurysm.
CT scans demonstrate that the extravasate is localized to the left side at the level of the renal hila **(a)** and extends across the midline at the level of the lower renal poles **(b).** Retroaortic and perirenal reaction are evident. (Courtesy of Michiel Feldberg, M.D., University of Utrecht, The Netherlands.)

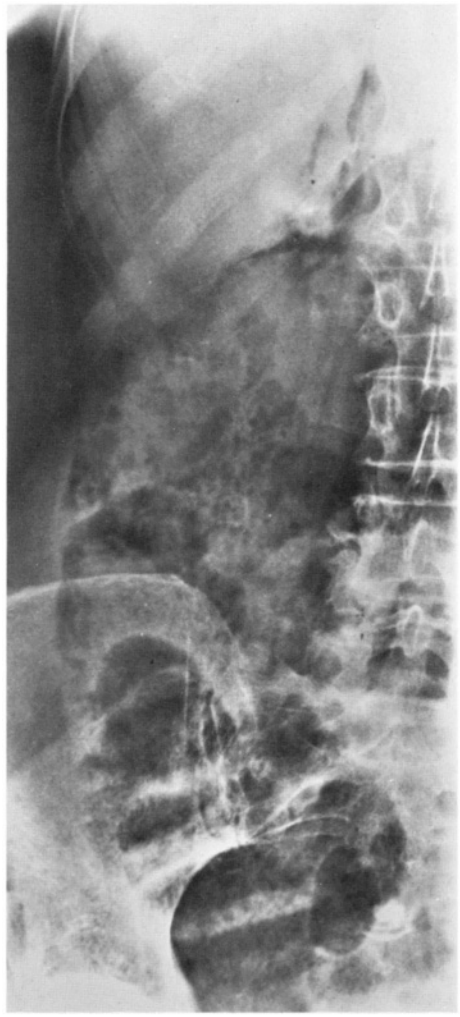


Fig. 8–45. Perforation of the hepatic flexure.
Mottled lucent areas on the right represent collections of gas extending medially over the psoas muscle and approaching the spine. The flank stripe is intact. These changes localize the extraperitoneal gas to the anterior pararenal space.

developed fever after numerous scattered polyps were removed by colonoscopic cautery, the characteristic findings localize the site of perforation to the ascending colon.

Abscesses secondary to perforated lesions of the ascending or descending colon are localized by the characteristic fascia] boundaries[68] (Figs. 8–46 through 8–48).

The appendix in an ascending retrocecal position is frequently an extraperitoneal structure.[69] Perforation then leads to an abscess, which may be localized within the right anterior pararenal space[18,70] (Fig. 8–49).

Because the structures and connective tissue behind the anterior pararenal space are relatively unyielding, massive accumulations within it tend to distend the space anteriorly, bulging forward into the peritoneal cavity and displacing small intestinal loops. Figure 8–50 illustrates a huge abscess originating from a perforated extraperitoneal appendicitis. Its dimensions in an anterior–posterior plane approach its vertical extent from the cecal area to the transverse colon.

In children, extraperitoneal appendicitis and its associated abscess within the anterior pararenal space commonly produce pressure on the right ureter after it has emerged from the cone of the renal fascia. This typically occurs at the L5 or lumbosacral level, producing localized obstruction and hydronephrosis (Fig. 8–51). In adults, similar changes may be due to perforated carcinoma or diverticulitis of the colon but more frequently are secondary to granulomatous ileocolitis[71] with extension of the infection into the anterior pararenal space (Fig. 8–52). Indeed, this localization explains the ureteral complications of Crohn's disease.

I have confirmed by postmortem injections the anatomic continuity of the right anterior pararenal space with the nonperitonealized bare area of the right lobe of the liver (Fig. 8–40) at the site of reflection of the right coronary ligament.[12] This pathway permits the spread of disease from extraperitoneal perforations of the bowel precisely to the bare area of the liver[24] (Fig. 8–53).

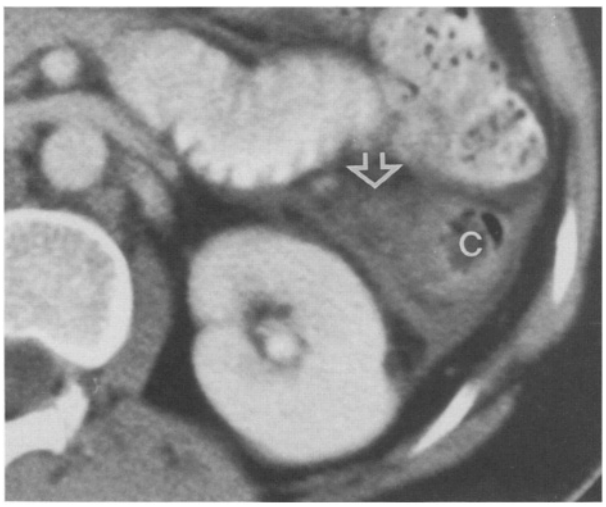


Fig. 8–46. Left anterior pararenal space inflammatory changes secondary to diverticulitis of the descending colon.
Soft-tissue stranding through the anterior pararenal fat *(arrow)* adjacent to the descending colon *(C)* is accompanied by reactive thickening of the fascia.
(Courtesy of Jay P. Heiken, M.D., Mallinckrodt Institute of Radiology, St. Louis, MO.)



Fig. 8–47. Left anterior pararenal space abscess secondary to a perforated diverticulum of the mid-descending colon.
The gas-producing infection has coalesced deep to the peritoneum between the anterior renal fascia and the lateroconal fascia *(arrows).*

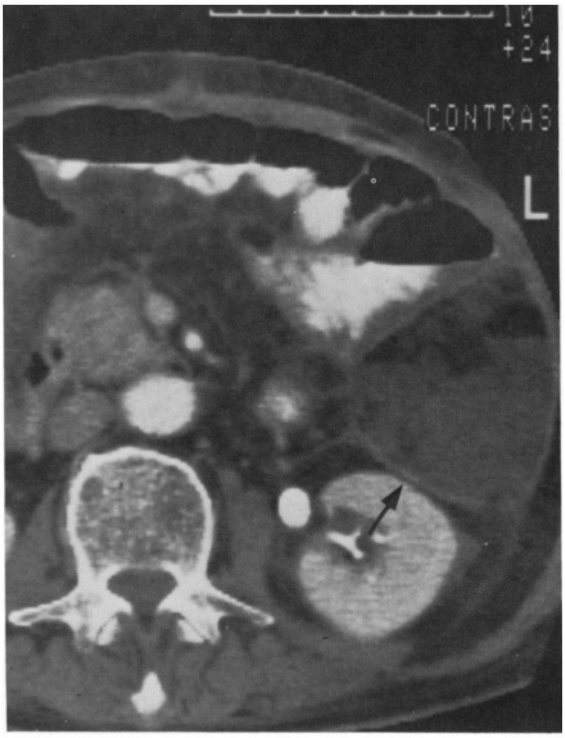


Fig. 8–48. Left anterior pararenal abscess following left hemicolectomy.
The gas-producing infection is bounded by thickened anterior renal *(arrow)* and lateroconal fascia.

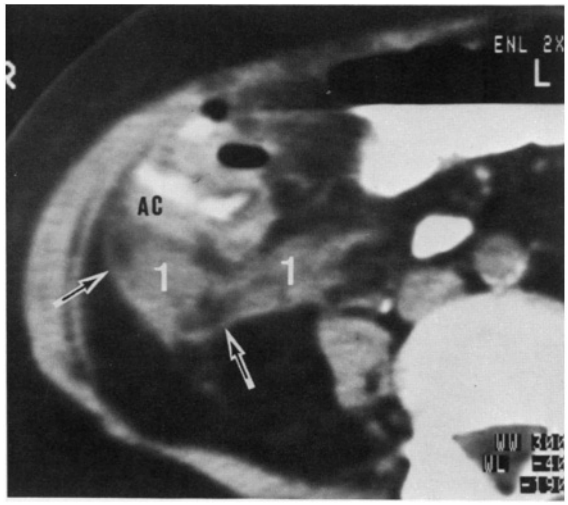


Fig. 8–49. Anterior pararenal phlegmon secondary to extraperitoneal appendicitis.
CT shows infiltrate in right anterior pararenal space *(1)* secondary to an inflamed appendix in an ascending retrocecal position. There is thickening of the lateroconal and anterior renal fasciae *(arrows).* The ascending colon *(AC)* shows bowel wall thickening.
(Reproduced from Feldberg.[17])

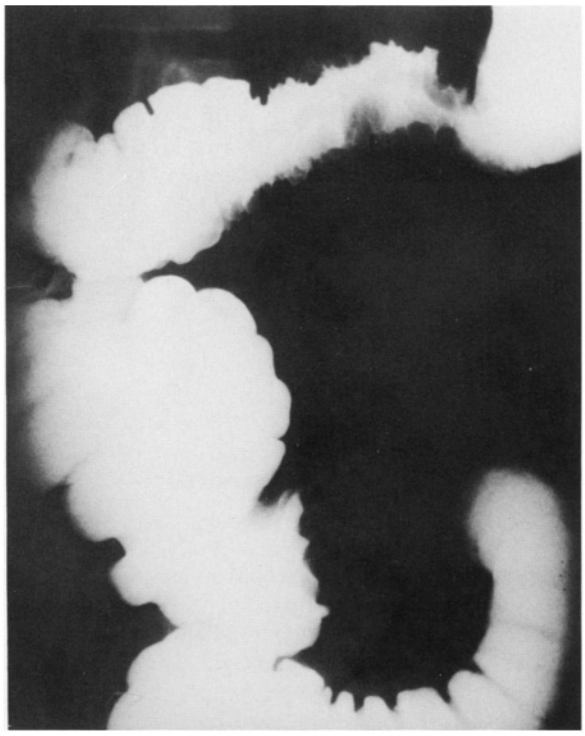


Fig. 8–50. Large anterior pararenal space abscess originating from extraperitoneal appendicitis.
Barium enema. Note deformity of the medial contour of the cecum and the abscess extending to the transverse colon.
(Reproduced from Meyers.[8])

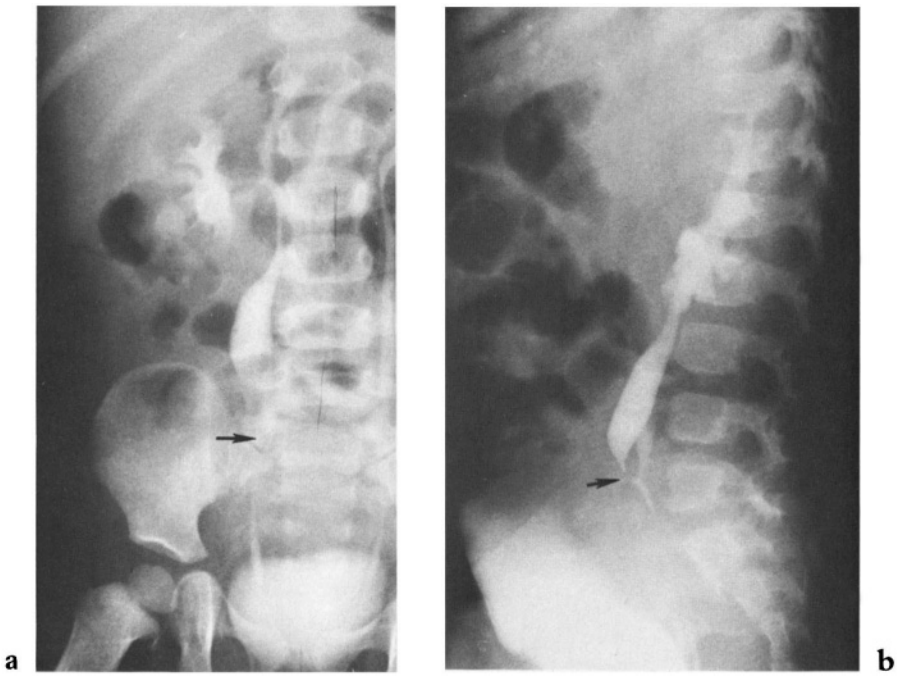


Fig. 8–51. Extraperitoneal appendicitis.
The associated abscess within the anterior pararenal space partially obstructs the right ureter *(arrow).*

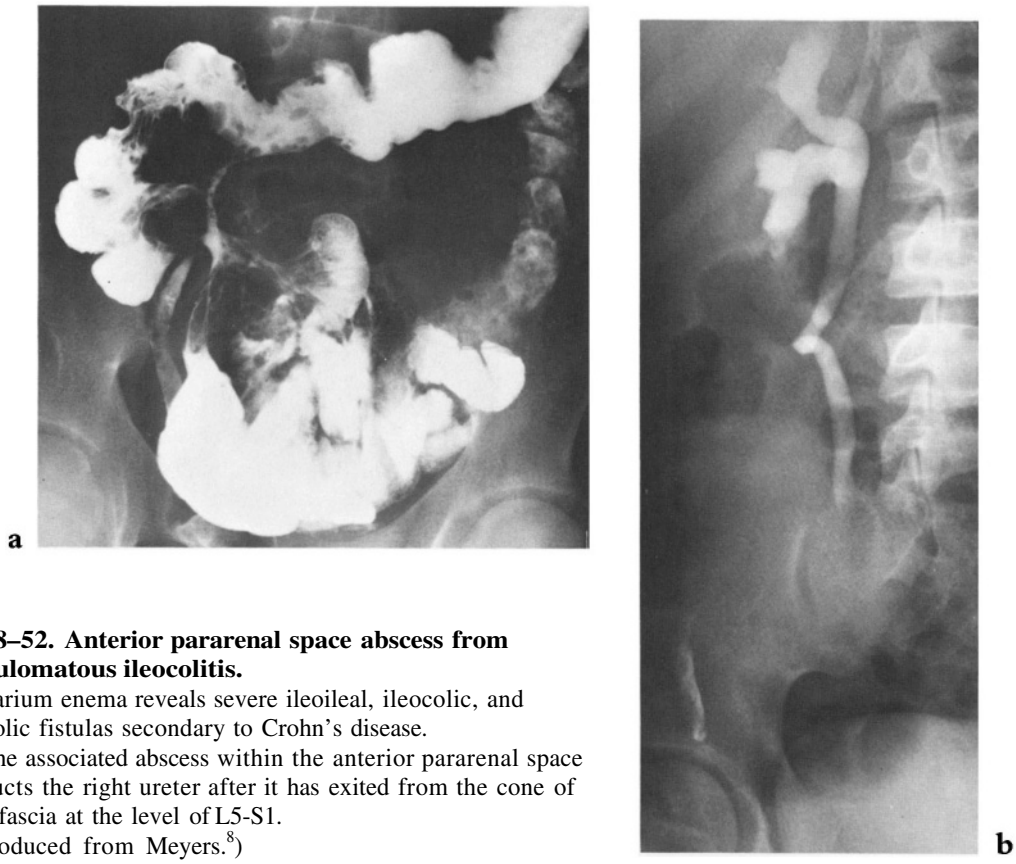


Fig. 8–52. Anterior pararenal space abscess from granulomatous ileocolitis.
(a) Barium enema reveals severe ileoileal, ileocolic, and colocolic fistulas secondary to Crohn's disease.
(b) The associated abscess within the anterior pararenal space obstructs the right ureter after it has exited from the cone of renal fascia at the level of L5-S1.
(Reproduced from Meyers.[8])

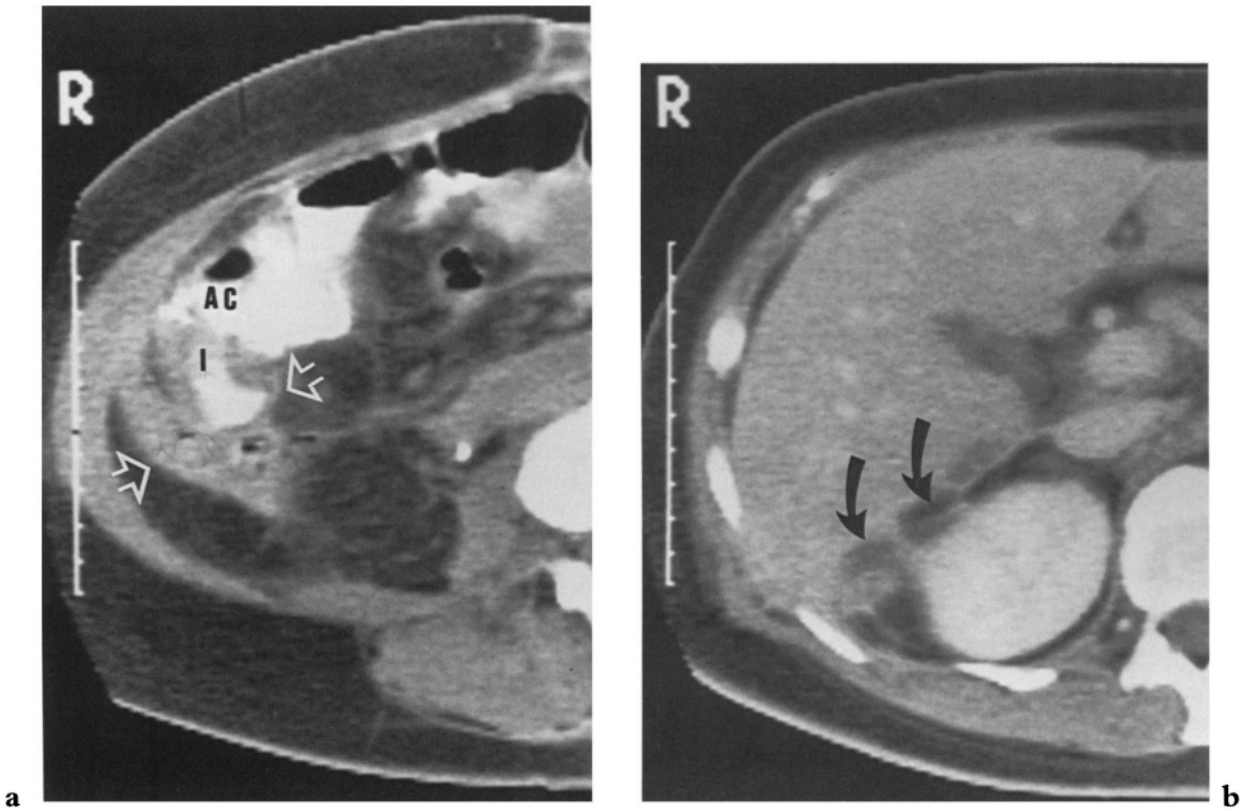


Fig. 8–53. Extension of anterior pararenal inflammation to bare area of liver.
(a) After an ileocecal resection for Crohn's disease, inflammatory changes *(arrows)* within the anterior pararenal space surround the anastomotic site between the ileum (*I*) and the ascending colon *(AC)*.
(b) The inflammatory changes have extended cephalad within the anterior pararenal extraperitoneal space to the bare area of the liver *(arrows)*.
(Reproduced from Meyers et al.[24])

Perforation of the Duodenum

Perforation of the duodenum is usually caused by blunt trauma to the abdomen and is now being encountered as an automobile lap-belt deceleration injury. The duodenum bears the brunt of the injury because of its firm attachment, acutely angled flexures, and compression against the vertebral column. It is of interest to note that the structure derives its name from the term "dodekadactilon"[72] by Herophilus of Chalcedon, who lived in Alexandria from 335 to 280 B.C., because it is about 12 fingerbreadths in length. Comparatively few patients are greatly inconvenienced by the original trauma. Only when the effects of the extravasation become evident do the symptoms become marked. Rupture usually occurs at the junction of the second and third portions; multiple perforations are possible, and there may be accompanying traumatic pancreatitis. Early recognition is important because unrecognized duodenal perforation has a 65% mortality rate as opposed to a 5% mortality rate in those patients operated upon within the first 24 hours after injury.[73]

The extraperitoneal gas with the extravasated bile and pancreatic juices is limited to the right anterior pararenal space and takes a characteristic distribution (Figs. 8–54 and 8–55). CT is considerably more sensitive than plain films in detecting the extraluminal gas[74–77] (Fig. 8–56).

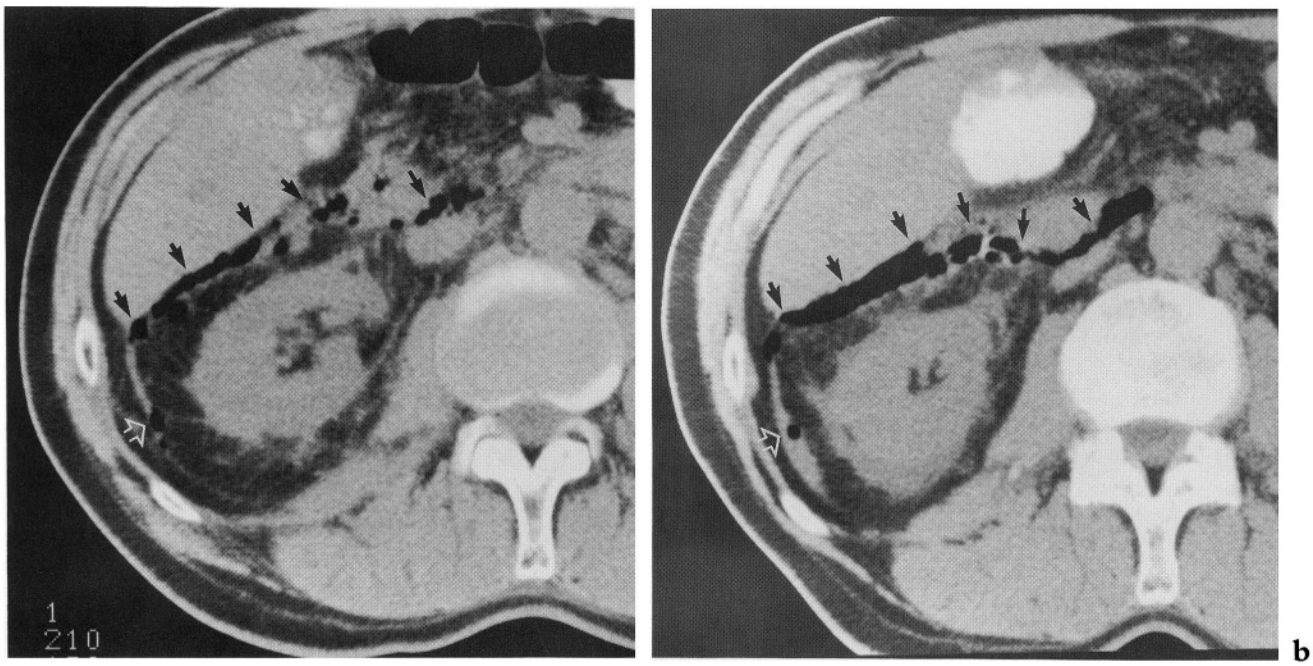
Figure 8–57 illustrates another striking finding. Only when the infection progresses inferiorly, below the apex of the cone of renal fascia and the limitation of the lateroconal fascia, can the gas proceed directly to the properitoneal fat. Gaseous lucencies can then be identified in the extraperitoneal tissues, with local extension into the flank, specifically at the level of the iliac crest and



Fig. 8–54. Extraperitoneal perforation of the duodenum after blunt trauma.
Several gas bubbles associated with a fluid soft-tissue density are present in the right anterior pararenal space. These cause loss of the hepatic angle, but the flank stripe *(arrows)* is intact. The upper GI series shows medial displacement of the descending duodenum but does not demonstrate the site of extravasation.



Fig. 8–55. Extraperitoneal perforation of the descending duodenum following blunt trauma, with spread through the right anterior pararenal space.
The mottled gas shadows continue over the psoas muscle medially but do not extend into the flank fat laterally. (Reproduced from Meyers.[9])



a b

Fig. 8–56. Extraperitoneal perforation of the duodenum following ERCP.
(a and **b)** CT demonstrates gas loculations precisely within the right anterior pararenal space *(black arrows).* Note that a few extend into the potential space between the two layers of the thickened posterior renal fascia *(white arrow).*
(Courtesy of Jay P. Heiken, M.D., Mallinckrodt Institute of Radiology, St. Louis, MO.)

progressing cephalad. The finding is typical of gaseous spread down the right anterior pararenal compartment and is seen most commonly in perforation of the extraperitoneal duodenum.

An upper gastrointestinal series may demonstrate the perforation site (Fig. 8–57a), but not always (Fig. 8–54).

Violation of the fascial boundaries in cases of blunt retroperitoneal duodenal rupture may result in the appearance of gas surrounding the right kidney[78,79] and is associated with other findings that indicate extensive retroperitoneal cellulitis. However, CT has shown that the exudate may not truly enter the perirenal space but extend from the anterior to the posterior pararenal space around the renal fascial cone.[18,74]

Retroduodenal and Intramural Duodenal Hematoma

Blunt trauma or acute deceleration may also cause rupture of the small blood vessels behind the fixed second portion of the duodenum. The hematoma resides within the right anterior pararenal space. It results in a characteristic spiculation of the mucosal folds of the posterior margin of the descending duodenum and may displace that structure anteriorly (Fig. 8–58).

Confirmation of its presence, precise localization, and extent is readily shown by CT, which is also useful in follow-up to document the usual course of spontaneous resolution of the hematoma.

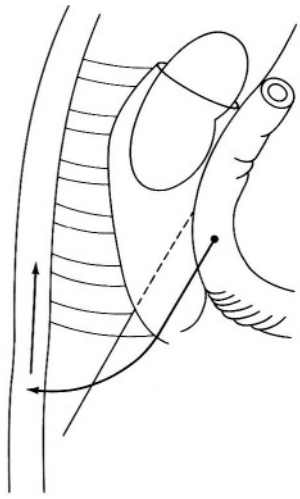
Intramural duodenal hematoma may be associated with and is also seen secondary to blunt abdominal trauma, anticoagulant therapy, bleeding disorders, ruptured aneurysm, aortoenteric fistula, and acute pancreatitis.[80,81]

Pancreatitis

The fascial reactions in acute pancreatitis have been meticulously studied by CT.[17] Thickening of the anterior renal fascia is commonly seen (Fig. 8–59), and the inflammatory process often extends to involve typically the anterior pararenal space[7,8,12,82–87] (Fig. 8–60). This usually spreads to the left from the tail of the pancreas. Reactive thickening of Gerota's fascia and perhaps the lateroconal fascia may remain after resolution of the pancreatitis (Fig. 8–61).



a



b

Fig. 8–57. Extraperitoneal perforation of the descending duodenum following blunt trauma with anterior pararenal space infection.

(a) Gastrografin GI series shows extravasation from the duodenum. Mottled gaseous lucencies extend inferiorly and laterally. Below the level of the cone of the renal fascia and the lateroconal fascia, the infection reaches and then ascends the flank fat *(arrows)*.

(b) Pathway of spread inferior to the lateroconal fascia to communicate with the flank fat. (Reproduced from Meyers.[8])

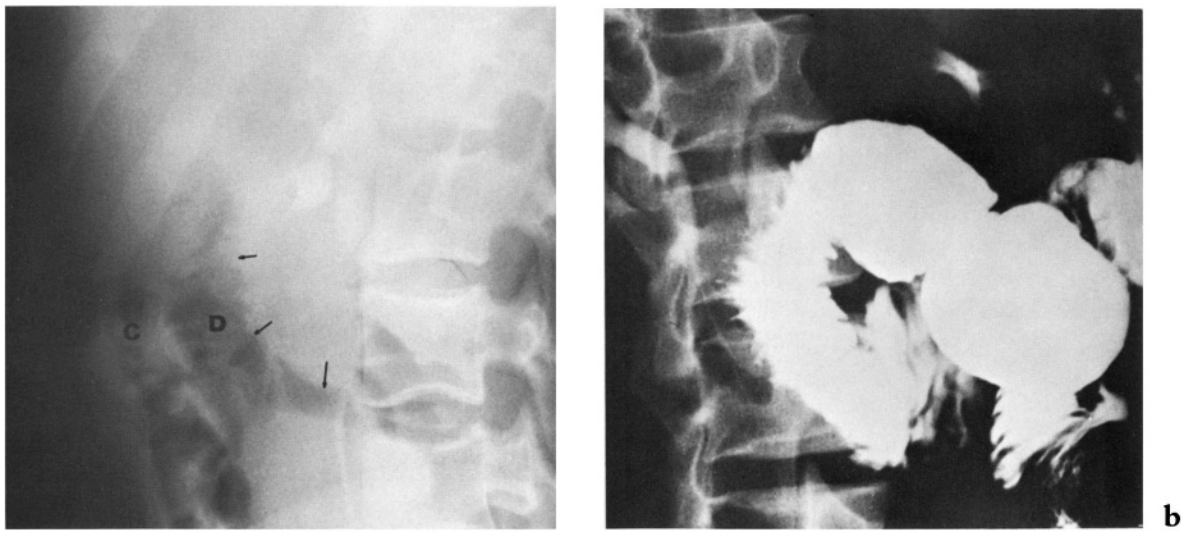
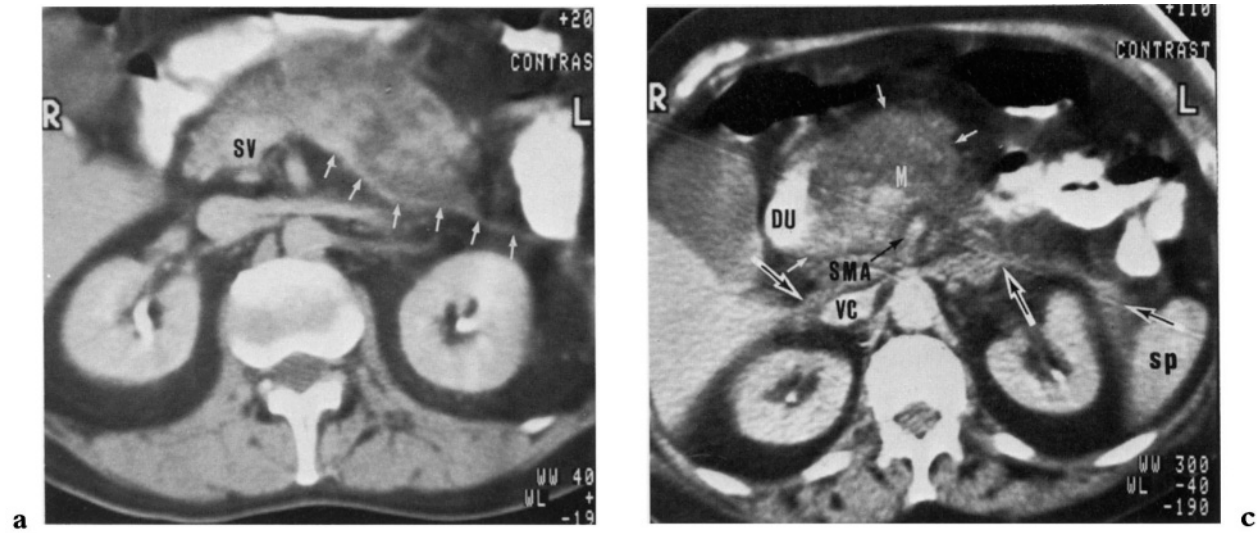


Fig. 8–58. Retroduodenal anterior pararenal hemorrhage.
(a) Lateral excretory urogram shows a mass separating the right kidney from the anteriorly displaced descending duodenum *(D). C* = colon.
(b) Upper GI series shows spiculation of mucosal folds along the posterior aspect of the descending duodenum.
(Reproduced from Meyers et al.[12])



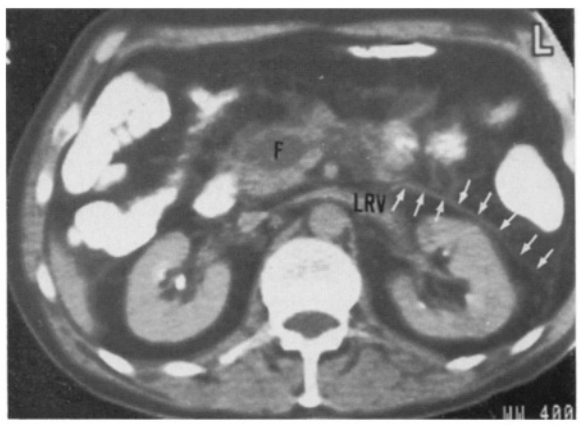


Fig. 8–59. Anterior renal fascial reactions in pancreatitis in three different patients.
(a) A thickened left anterior renal fascia converges behind the pancreas *(arrows),* which is swollen with intrapancreatic fluid. *SV* = splenic vein.
(b) Intrapancreatic fluid collection *(F)* with thickened left anterior renal fascia blending into posterior pancreatic tissue *(arrows). LRV* = left renal vein.
(c) Inflammatory pancreatic mass *(M)* with very thickened anterior renal fascial planes bilaterally *(black-and-white arrows). DU* = duodenum; *SMA* = superior mesenteric artery; *sp* = spleen; *VC* = vena cava.
(Reproduced from Feldberg.[17])

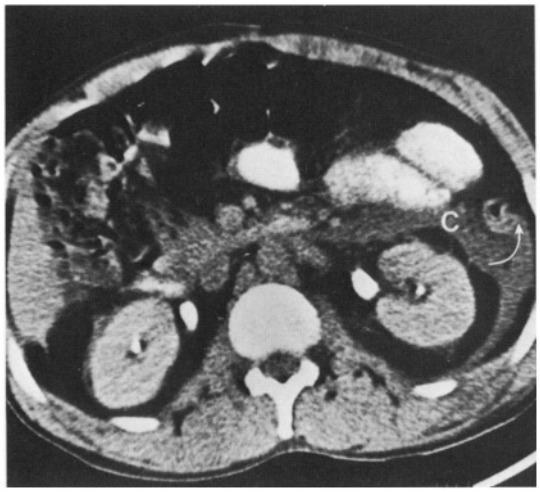


Fig. 8–60. Pancreatitis extending through anterior pararenal space.
CT scan shows fluid collection *(C)* extending from tail of pancreas through the anterior pararenal space on the left. Note its continuation to the bare area posteriorly of the descending colon *(curved arrow),* where it is bounded laterally by the lateroconal fascia. There is fluid interposition within the posterior renal fascia, tapering posteriorly. The perirenal space and flank fat remain uninvolved.

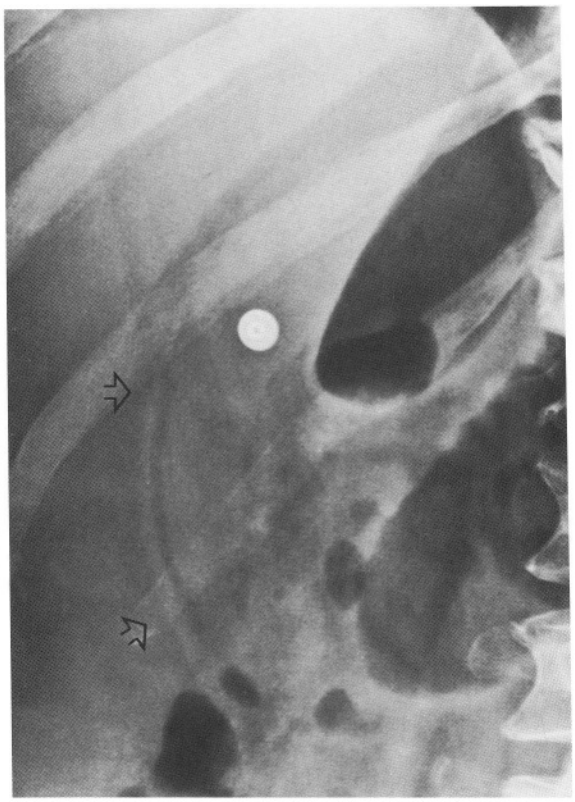


Fig. 8–61. Thickened renal fascia *(arrows).*
This is identified on plain film as a curvilinear soft-tissue band separated by lucent perirenal fat from the lateral contour of the kidney. This finding persisted after resolution of acute pancreatitis.

On plain films, in the presence of an exudate in the left anterior pararenal space, a radiolucent halo about the left kidney may rarely be evident, secondary to enhanced visualization of the peripheral margin of the uninvolved perirenal fat.[87,88]

Solitary or predominant involvement of the anterior pararenal space on the right is seen in pancreatitis involving the head, typically severe in nature (Figs. 8–62 and 8–63). Bilateral involvement of the anterior pararenal spaces reflects advanced or fulminating pancreatitis (Figs. 8–64 through 8–66). The extrapancreatic collection may readily extend within the posterior renal fascia on either or both side as well as along mesenteric pathways.

Extraperitoneal spread of a pancreatic abscess may be extensive but usually follows recognizable planes. Drainage from the head of the pancreas tends to be downward and to the right. Figure 8–67 illustrates the typical localization found at surgery in cases of extensive pancreatic infections within the anterior pararenal compartment. The large abscess pictured has come into contact with the ascending colon and has not crossed the midline. Figure 8–68 demonstrates identical characteristic features *in vivo.* Figure 8–69 shows the operative findings when the process has continued inferiorly to the level of the iliac crest. The drainage here has led to a discrete collection external to the peritoneum. Although this pathway has not been previously explained in the surgical literature, it is clearly the result of the process extending below the level of the lateroconal fascia and then gaining immediate access to the properitoneal flank fat. This is basically the same pathway as outlined in Figure 8–57.

Emphysematous or fulminating pancreatitis is a principal exception to unilateral confinement within the anterior pararenal space from a process arising in the upper abdomen. Figure 8–70 illustrates a gas-producing infection of the pancreas with spread downward within both sides of the compartment. The gaseous lucencies overlie the psoas muscles, but there is no evidence of direct continuity across the midline. This indicates that the in-

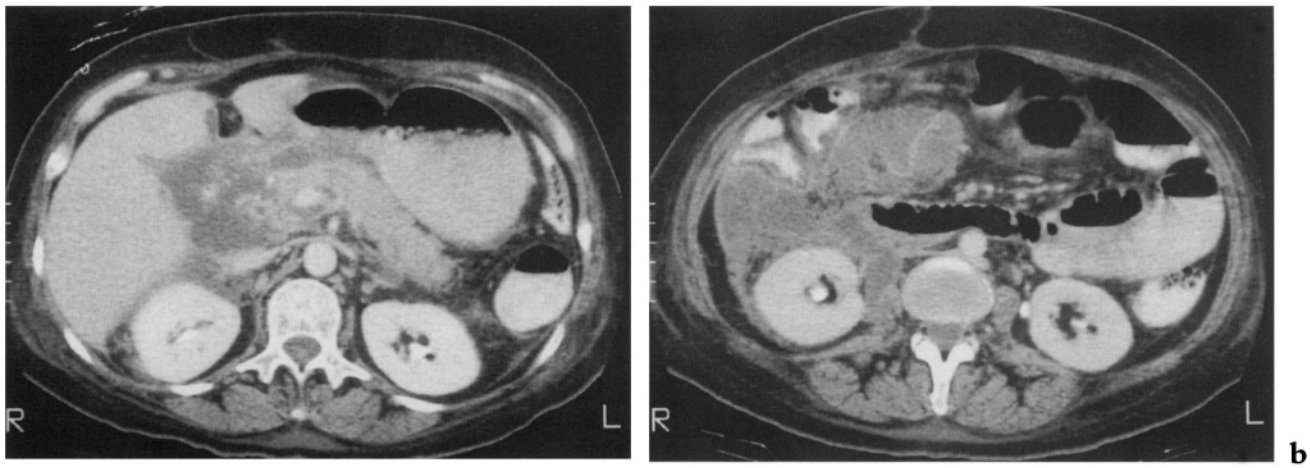


Fig. 8–62. Right anterior pararenal space fluid secondary to necrotizing pancreatitis.
(a) While there is enhancement of the body and tail of the pancreas, high-resolution bolus CT shows there is lack of enhancement of the area of the head, which is surrounded by fluid. These changes indicate necrosis.
(b) There is extension of fluid loculating predominantly within the anterior pararenal space on the right as well as within the transverse mesocolon.
(Courtesy of Emil Balthazar, M.D., Bellevue Hospital, New York University School of Medicine, New York, NY.)

fection has dissected separately down both sides from the pancreas. Figure 8–71 shows similar bilateral changes of large infected pseudocysts of the pancreas in an alcoholic male. Yet, the anatomic planes of the anterior pararenal space may allow direct extension across the midline, particularly in cases of liberated pancreatic enzymes (Fig. 8–72).

A potential space into which fluid collections from the anterior pararenal space can extend is created by the division of the posterior renal fascia into two laminae (Figs. 8–73 and 8–74). In moderate to severe cases of pancreatitis, retrorenal extension of pancreatic effusion or phlegmon into this potential space is common[20,34,35] (Figs. 8–64 through 8–66). Raptopoulos and colleagues have emphasized the typical appearance of this posterior extension of pancreatitis as a widening of the posterior renal fascia that tapers posteriorly[20] (Fig. 8–60). However, I have observed that variability in the origin of the division into two leaves in the horizontal plane as well as apparently in the vertical dimensions of the cleavage account for the varied appearances of fluid accumulation in this plane (Figs. 8–75 and 8–76).

Posteriorly, these collections at some axial level generally become contiguous with the lateral edge of the quadratus lumborum muscle. Instances of extension of severe pancreatitis toward the structures of the posterior wall without cutaneous signs are not uncommonly observed by CT.[12,34,90,91] Sites of anatomic weakness in the flank wall may contribute to more ready passage in some

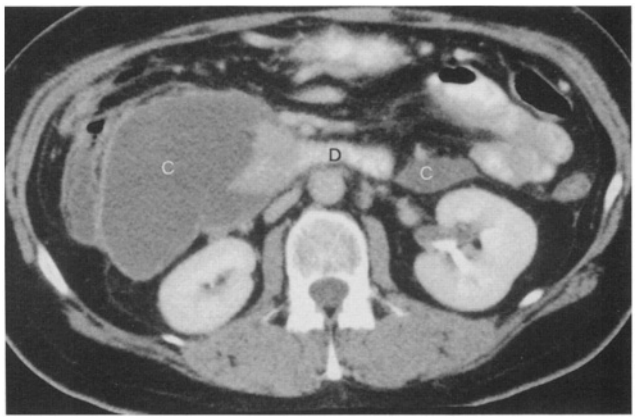


Fig. 8–63. Pancreatitis with anterior pararenal space fluid collections.
A huge fluid collection *(C)* is encapsulated on the right, and a smaller one has localized on the left lateral to the transverse duodenum *(D).*
(Courtesy of Jay P. Heiken, M.D., Mallinckrodt Institute of Radiology, St. Louis, MO.)

individuals. The lumbar region is an area defined superiorly by the 12th rib, inferiorly by the iliac crest, medially by erector spinae muscle group, and laterally by the posterior border of the external oblique muscle as it extends from the 12th rib to the iliac crest.[92] Defects

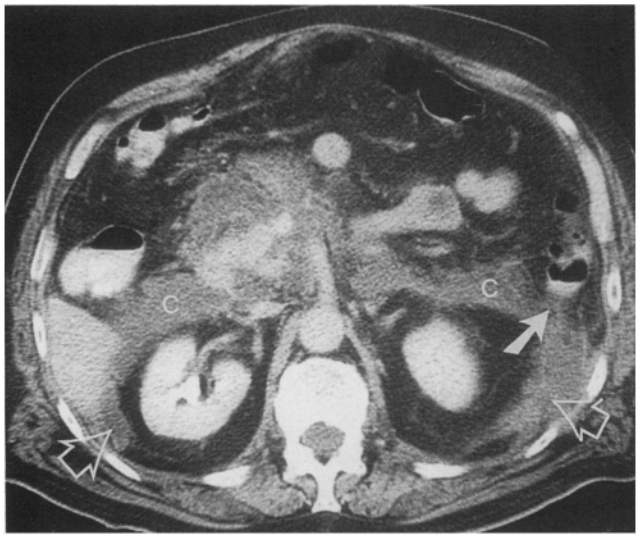


Fig. 8–64. Pancreatitis extending through the anterior pararenal spaces bilaterally.
Fluid collection *(C)* extends to both anterior pararenal spaces and between the lamellae of the posterior renal fasciae *(open arrows).* On the left, the process involves the extraperitoneal fat of the bare area of the descending colon *(white arrow).* A mesocolic phlegmon is also present.
(Courtesy of David H. Stephens, M.D., Mayo Clinic, Rochester, MN.)

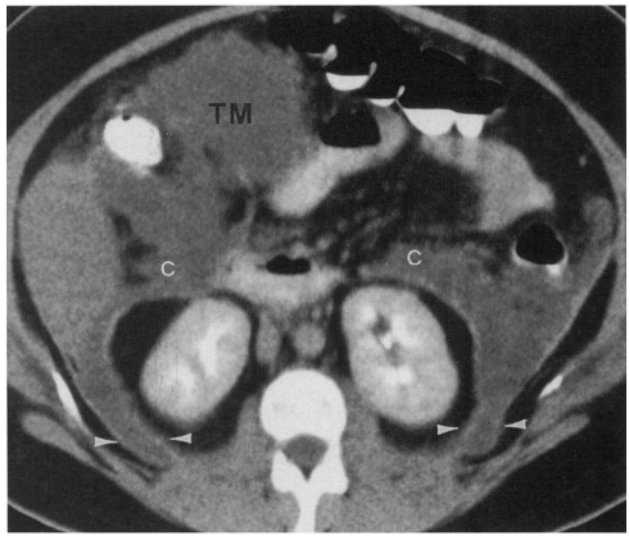


Fig. 8–65. Bilateral spread of fulminating acute pancreatitis.
The extrapancreatic fluid collections *(C)* in both anterior pararenal spaces dissect between the two layers of the posterior renal fascia bilaterally *(arrowheads).* No direct communication across the midline is evident. The process extends into the transverse mesocolon *(TM)* on the right and to the extraperitoneal fat of the bare area of the descending colon.
(Courtesy of Jay P. Heiken, M.D., Mallinckrodt Institute of Radiology, St. Louis, MO.)

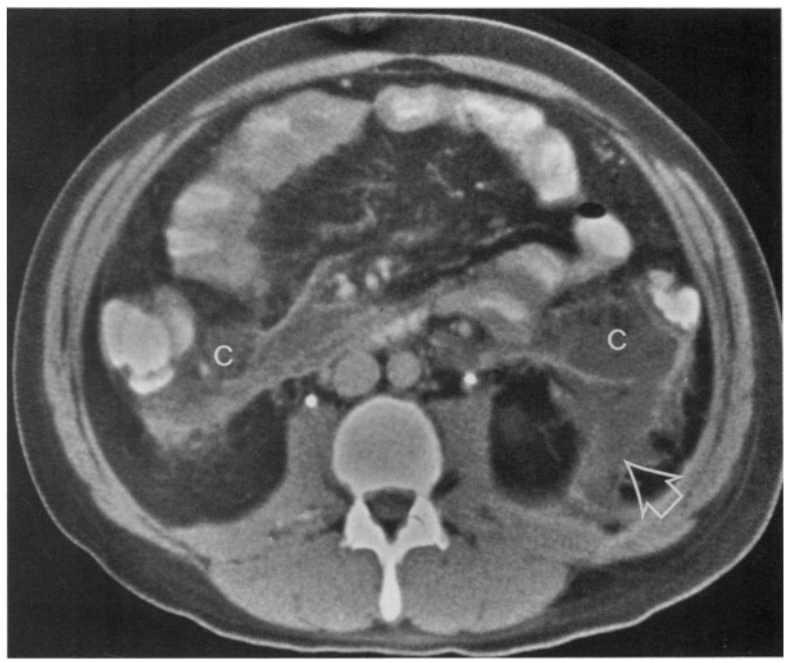


Fig. 8–66. Pancreatitis involving both anterior pararenal spaces.
Fluid collections *(C)* are evident bilaterally. It is difficult to ascertain whether this has occurred simultaneously on each side or is the result of midline communication. The process has reached both the ascending and descending colon and, on the left, has interposed within the posterior renal fascia *(arrow).*

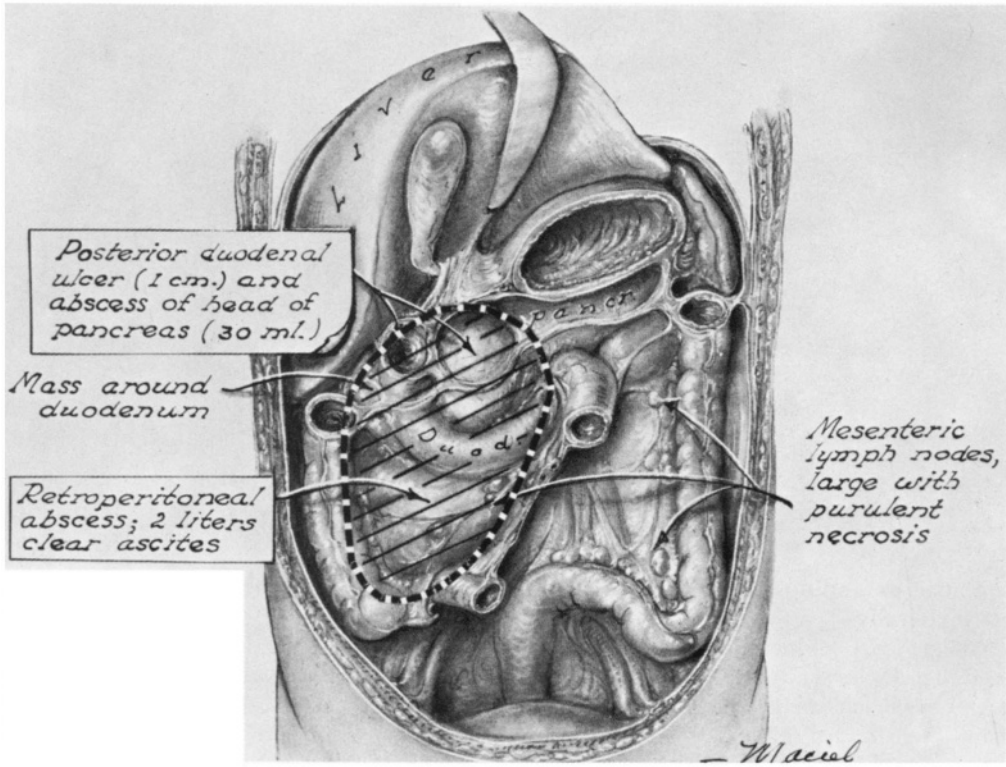


Fig. 8–67. Inferior drainage of infection from pancreatic abscess within anterior pararenal space secondary to penetration of a posterior duodenal ulcer, as depicted in the surgical literature.
(Reproduced from Wulsin.[89])

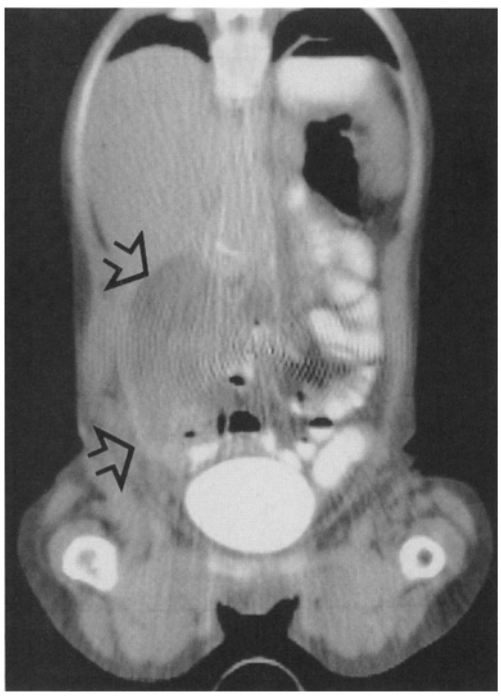


Fig. 8–68. Inferior extension of abscess from head of pancreas within right anterior pararenal space *(arrows)* shown in a coronal CT section.
(Courtesy of Michiel Feldberg, M.D., University of Utrecht, The Netherlands.)

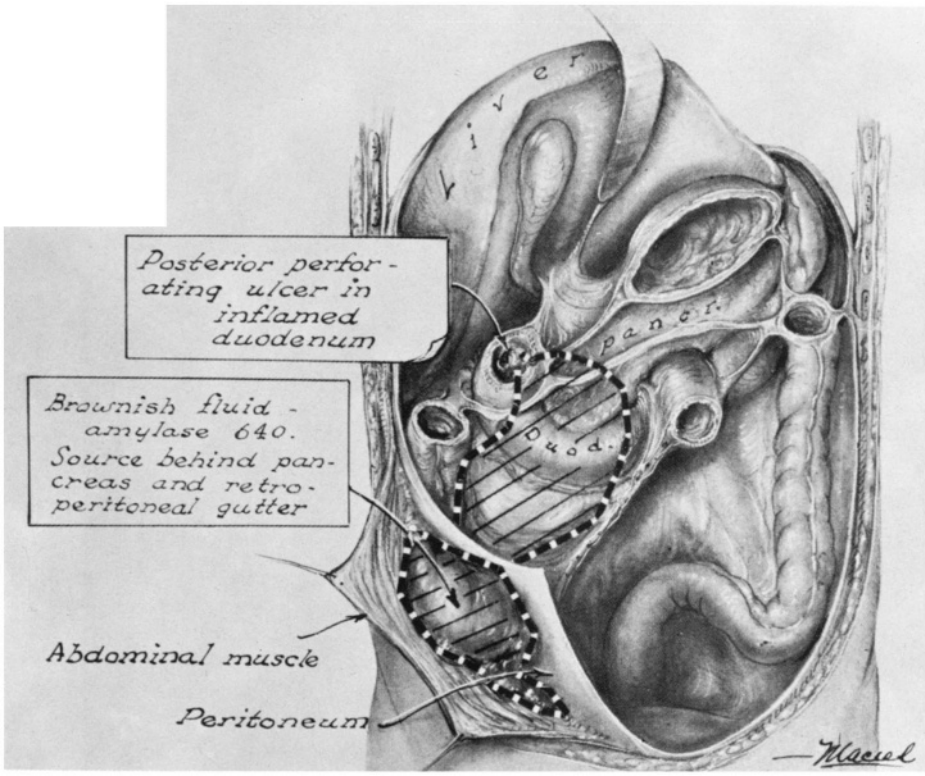


Fig. 8–69. Pancreatitis secondary to duodenal ulcer, as depicted in the surgical literature.
The anterior pararenal extension reaches the flank fat external to the peritoneum below the level of the cone of renal fascia.
(Reproduced from Wulsin.[89])

in the lumbar musculature or aponeurosis in this region result in two sites known as the larger and more constant superior triangle of Grynfeltt-Lesshaft inferior to the 12th rib[93,94] and the smaller inferior lumbar triangle of Petit just cephalad to the iliac crest[95] (Fig. 8–77). Figure 8–78 clearly depicts the relationship of the superior lumbar triangle to the extraperitoneal structures and fascial planes of the flank. The floor of Petit's triangle is composed of the underlying internal oblique and transversus abdominis muscles. While these triangles have been recognized as anatomic areas of weakness that may lead to unusual lumbar hernias,[96–98] it is also apparent that these structural defects may predispose to the ready transmission of extravasated pancreatic enzymes or blood-stained fluid to the subcutaneous tissues of the flanks. Thus, fluid in the retrorenal plane that lies behind the perirenal fat often tracks along the lumbar triangle pathway through a cleft between the medial border of the posterior pararenal space and the lateral border of the quadratus lumborum fat pad lying just anterior to the quadratus lumborum muscle (Figs. 8–79 through 8–81). Hemorrhage (Figs. 8–82) and infection (Fig. 8–83) may also course along this pathway.

I have shown[12,91] that these pathways provide an anatomic–radiologic explanation for the classic clinical sign of subcutaneous discoloration in the costovertebral

text continues on page 377

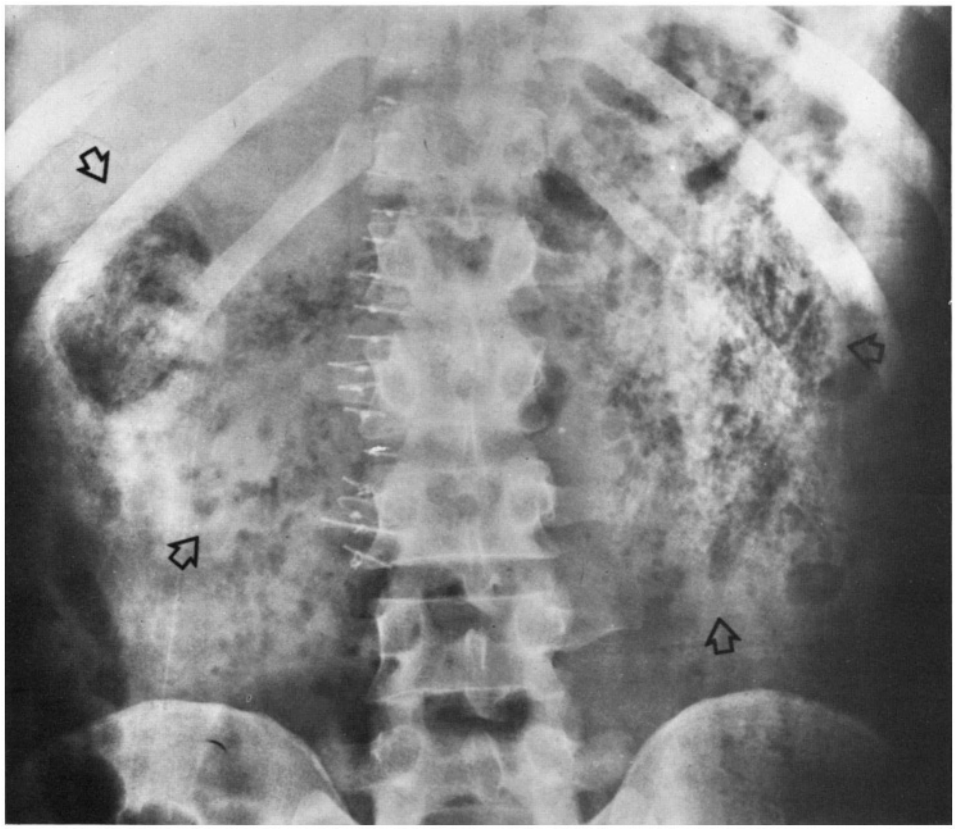
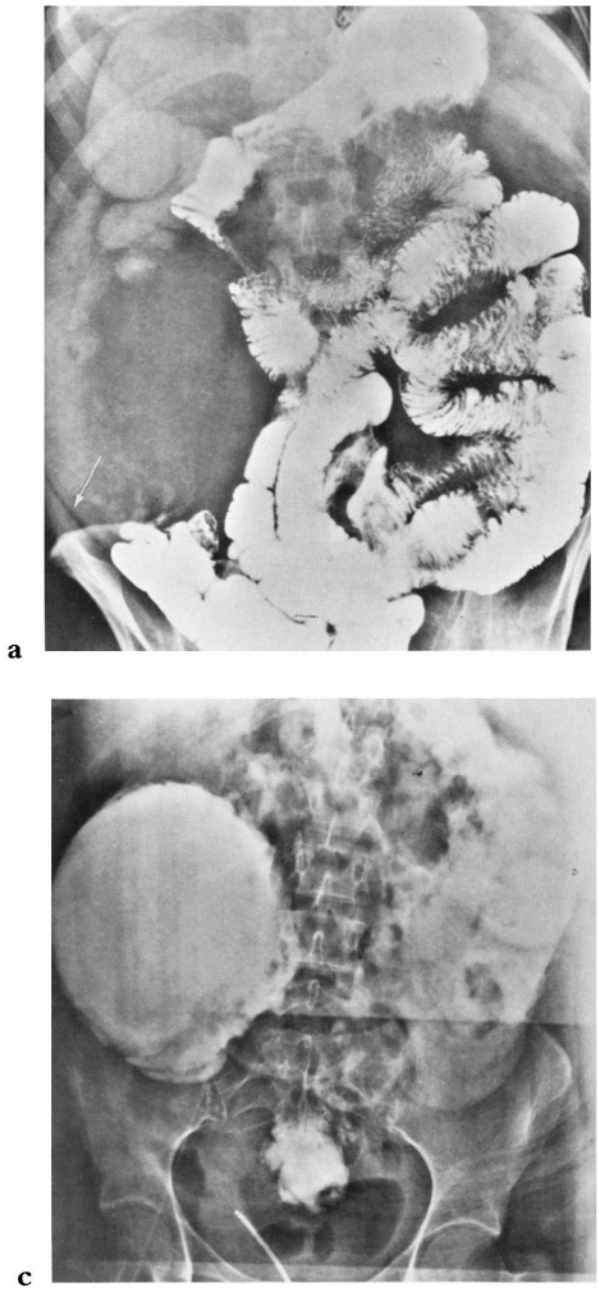


Fig. 8–70. Gas-producing infection of the pancreas.
Mottled lucencies are present diffusely throughout the pancreas and progress down both sides within the anterior pararenal spaces *(arrows),* overlying the psoas muscle. The flank stripes are maintained.
(Reproduced from Meyers.[9])



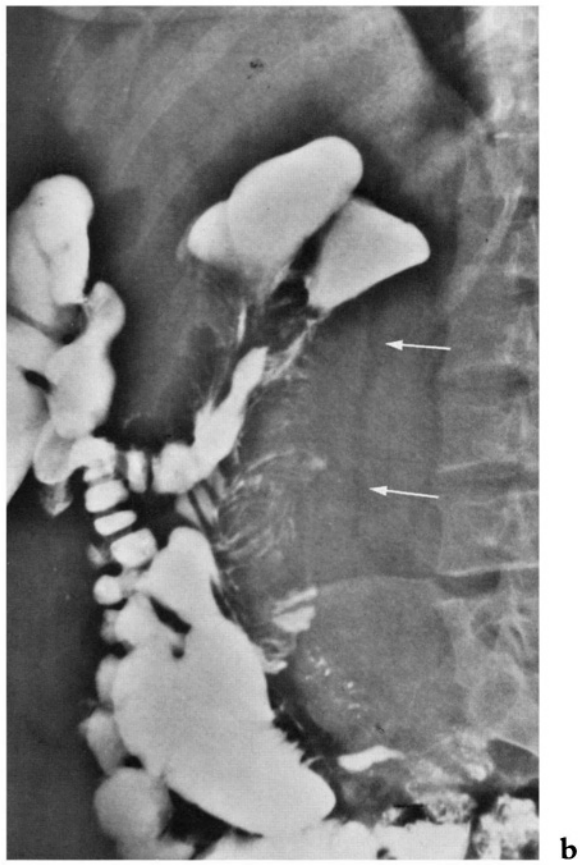


Fig. 8–71. Bilateral infected pancreatic pseudocysts within the anterior pararenal compartments.
(a) On the right, a large mass with a vertical axis displaces bowel toward the midline. The flank stripe is intact *(arrow).* Another extraperitoneal abscess is present on the left, draping small bowel loops.
(b) Steep oblique projection shows bowel displaced anteriorly and intact perirenal fat on right *(arrows).*
(c) Contrast injections of the huge pseudocysts verify their bilateral anterior pararenal compartmentalization.

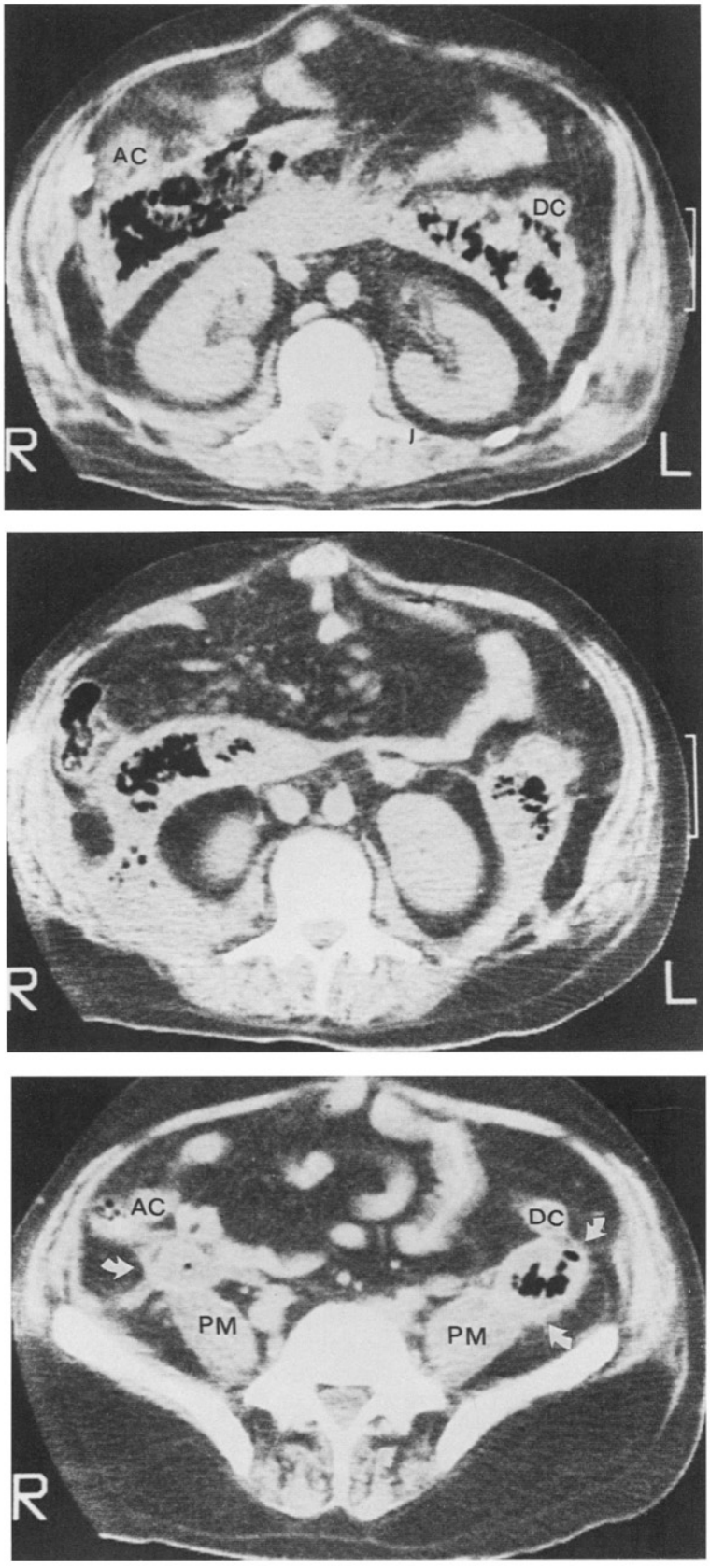


Fig. 8–72. Bilateral spread of emphysematous pancreatitis within anterior pararenal spaces.
(a) CT displays a gas-producing pancreatic phlegmon extending across the midline throughout both anterior pararenal spaces. *AC* = ascending colon; *DC* = descending colon.
(b) More inferiorly, the collection has fused into the anterior and posterior pararenal spaces.
(c) At the level of the iliac crests, CT shows the apex of the renal fascial cones *(arrows),* where anterior and posterior pararenal spaces communicate, just in front of and slightly lateral to the psoas muscles *(PM)* and immediately behind the ascending *(AC)* and descending colon *(DC).* (Courtesy of Roger Parienty, M.D., Neuilly, France.)

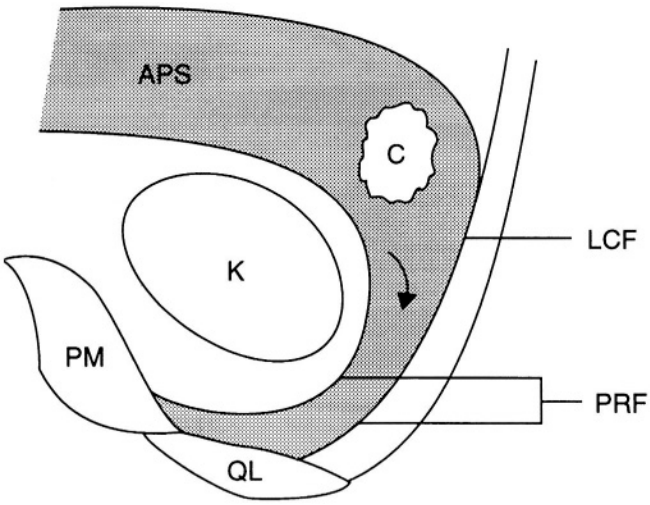


Fig. 8–73. Fluid in the anterior pararenal space may extend posteriorly between the two lamellae of the posterior renal fascia.
K = kidney; *C* = descending colon; *PM* = psoas muscle; *QL* = quadratus lumborum muscle; *APS* = anterior pararenal space; *PRF* = posterior renal fascia; *LCF* = lateroconal fascia.

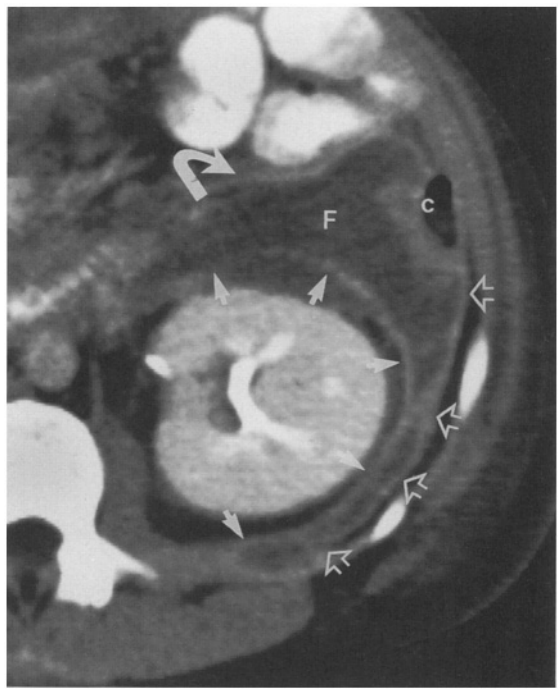


Fig. 8–74. Extrapancreatic fluid collection *(F)* in the left anterior pararenal space between the posterior parietal peritoneum *(curved arrow)* and the anterior renal fascia cleaves into the space between the two lamellae of the posterior renal fascia and extends behind the kidney toward the quadratus lumborum muscle. It can be seen that the inner layer of the posterior renal fascia is continuous with the anterior renal fascia *(white arrows)* and the outer layer is continuous with the lateroconal fascia *(open arrows).* The perirenal and posterior pararenal spaces are preserved. *C* = descending colon.
(Reprinted with permission from Pistolesi GF, Procacci C, Tonegutti, N, et al.: Analyses des différents espaces des régions extra-péritonéales. Radiologie J CEPUR 1990; 10: 195–204.)

angle (Grey Turner's sign) that may be associated with acute pancreatitis[99,100] (Figs. 8–84 and 8–85). The characteristic radiologic changes are readily distinguished from the subcutaneous soft tissue densities occasionally seen in the flanks and gluteal region by CT in severe pancreatitis secondary to the extravascular movement of fluid.[101] Three days to a week after the onset of symptoms, hemorrhagic changes (characteristically slate blue to yellow-brown discoloration) may be apparent in the flank, more frequently on the left.[99,100,102,103] The discoloration indicates extravasation of blood in the subcutaneous tissue and further resembles ecchymosis in that the color is typically at first a bluish black, fading through greenish and finally yellowish tints before disappearing.[102] The fat deep to the subcutaneous fascial plane[103a,103b] is predominantly involved. Grey Turner's sign has been observed in about 2% of patients with acute pancreatitis.[100,104]

Grey Turner's sign is frequently accompanied by periumbilical discoloration (Cullen's sign).[100,104,105] Cullen's sign is secondary to the tracking of liberated pancreatic enzymes to the anterior abdominal wall from the inflamed hepatoduodenal ligament and across the falciform ligament.[24,91] The subperitoneal tissue within the falciform ligament and ligamentum teres communicates with the properitoneal fatty tissue[106] in the abdominal wall, with the left periportal space, with the hepatic hilum, and with the hepatoduodenal ligament and gastrohepatic ligament[107] (Figs. 8–86 and 8–87). Therefore, a continuous pathway is established between the pancreatoduodenal area in the retroperitoneum and the anterior abdominal wall. Early investigations explored this route. Podlaha noted that gas formed from subserous injections of hydrogen peroxide at the pylorus in dogs and human cadavers diffused into the hepatoduodenal ligament, fat of porta hepatis, ligamentum teres, and subsequently to the subcutaneous tissues in the region of the umbilicus.[110] This pathway of gas from the pancreatoduodenal area to the porta hepatis can be documented clinically

text continues on page 385

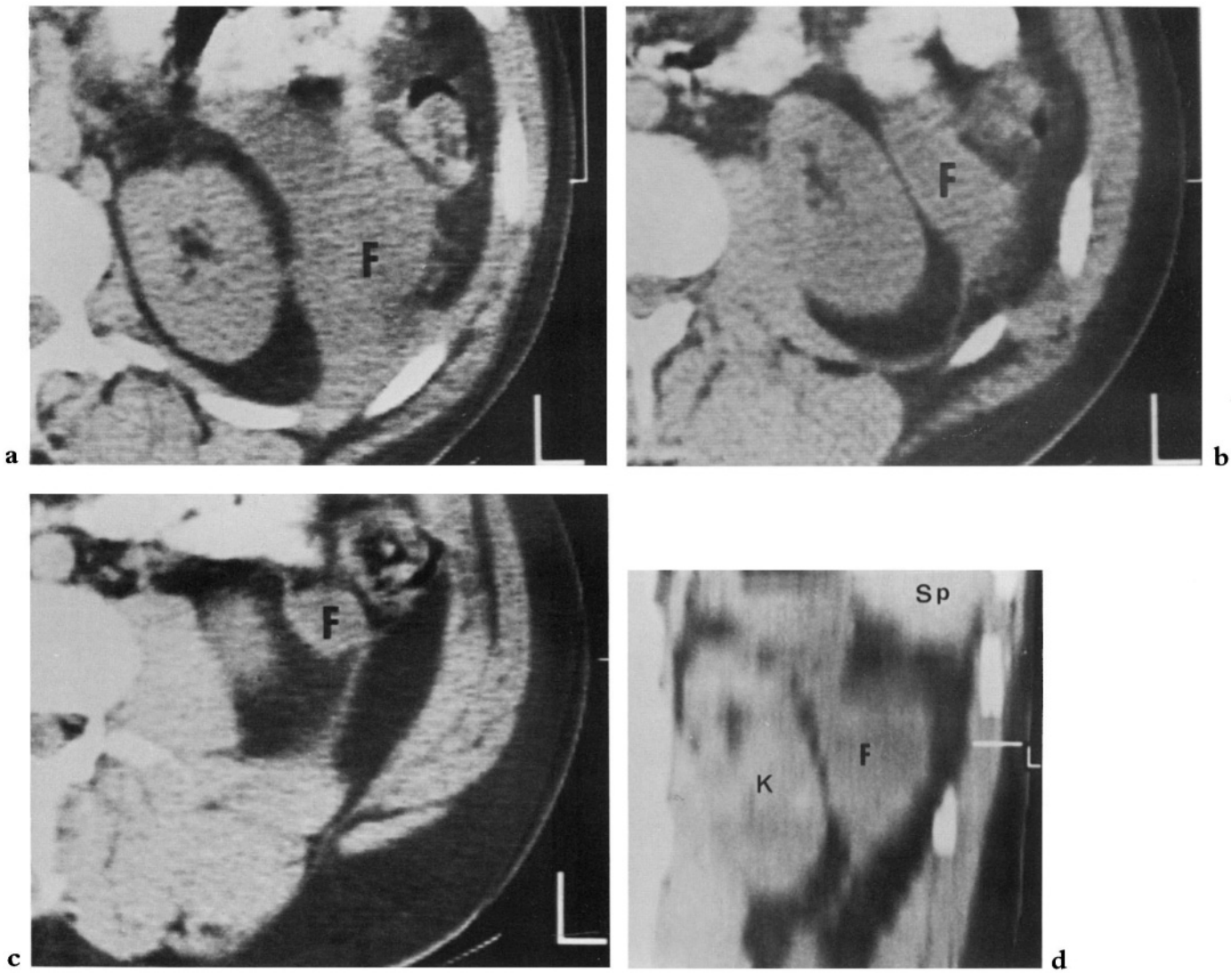


Fig. 8–75. Pancreatitis extending from anterior pararenal space to within the leaves of the posterior renal fascia.
(a–c) Three axial CT levels demonstrate pancreatic fluid collection *(F)* spreading from the left anterior pararenal space to the potential space between the bilaminated posterior renal fascia. Inferiorly the collection tapers to remain as a small loculated intrafascial collection. Dissection through the posterior renal fascia thus appears most prominent in the portion related to the upper renal pole.
(d) Reconstructed CT image demonstrates in the coronal plane the size, position, and relationships of the fluid collection within the posterior renal fascia. *K* = left kidney; *Sp* = spleen.

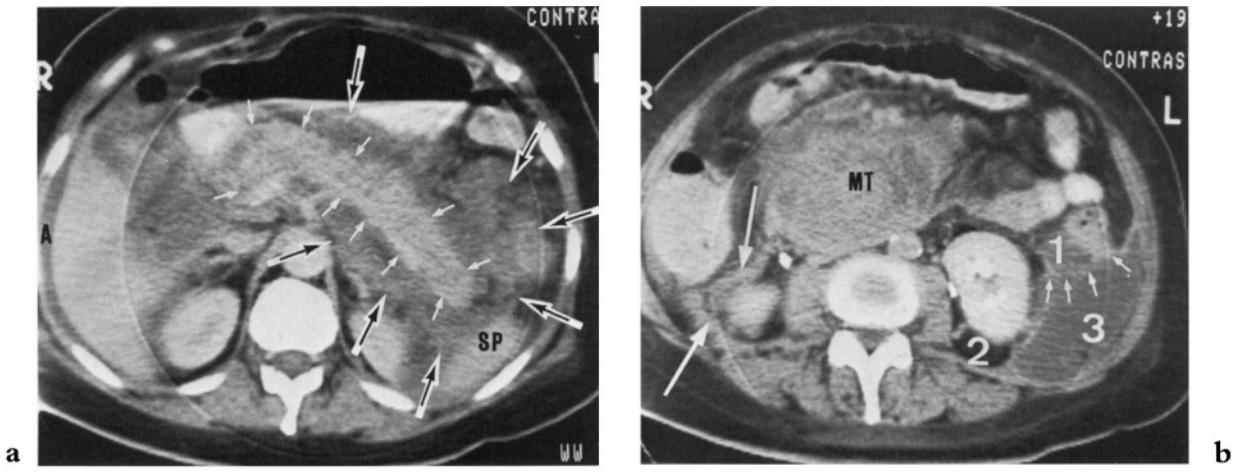


Fig. 8–76. Extension of pancreatitis to posterior pararenal space.
(a) Extensive phlegmonous infiltrate in anterior pararenal space *(black-and-white arrows)* surrounds pancreas whose preserved contours are identifiable after bolus contrast injection *(white arrows). A* = ascitic fluid; *Sp* = spleen.
(b) The extrapancreatic inflammatory process with fluid has extended from the anterior pararenal space (*1*) to the posterior pararenal space *(3).* At this particular level, the lateroconal fascia remains visible (*small arrows*). The perirenal space (*2*) is preserved. On the right, renal fasciae are also thickened *(large arrows).* Pancreatic abscess extends into small bowel mesentery (*MT*).
(Reproduced from Feldberg.[17])

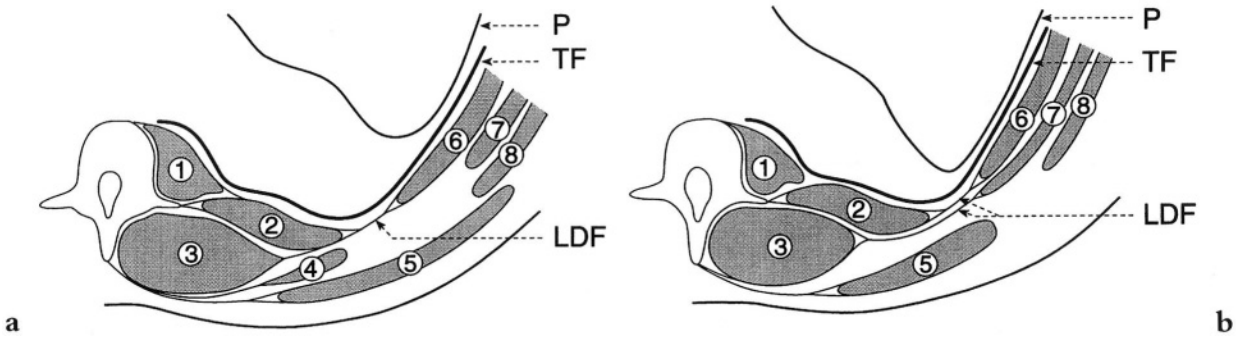


Fig. 8–77. Superior lumbar triangle (a) and inferior lumbar triangle (b).
1 = psoas muscle
2 = quadratus lumborum muscle
3 = sacrospinalis muscle
4 = serratus posterior inferior muscle
5 = latissimus dorsi muscle
6 = transverse abdominis muscle
7 = internal oblique muscle
8 = external oblique muscle
P = peritoneum
TF = transversalis fascia
LDF = lumbodorsal fascia

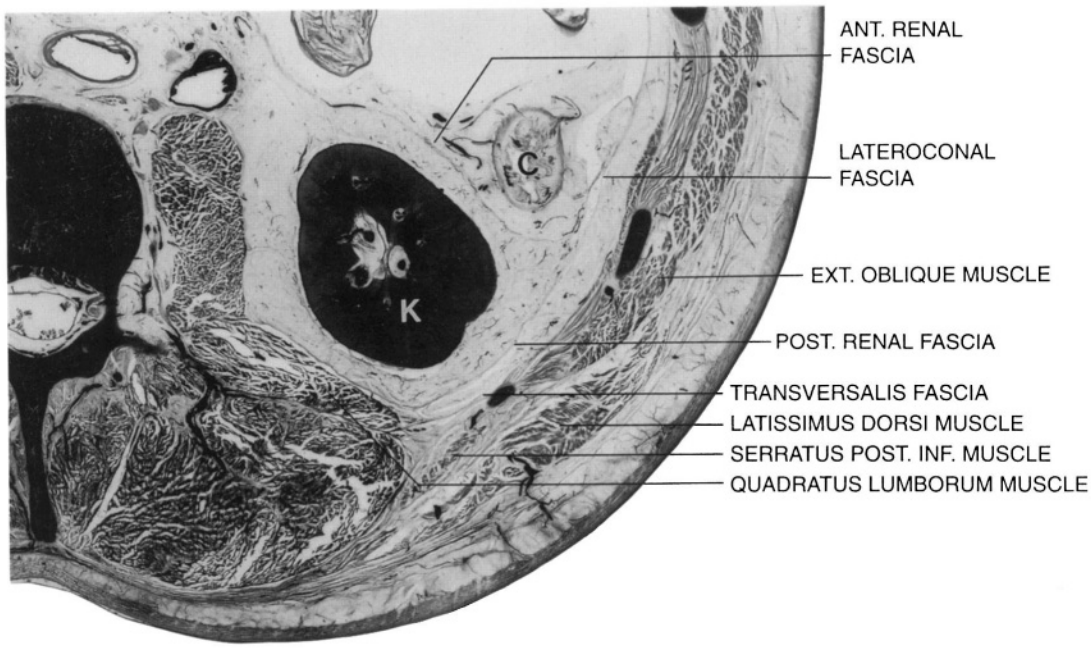


Fig. 8–78. The lumbar triangle.
Anatomic section of the left flank through the base of the superior lumbar triangle. Note the anatomic defect of the flank wall lateral to the quadratus lumborum muscle. *K* = kidney; *C* = descending colon.

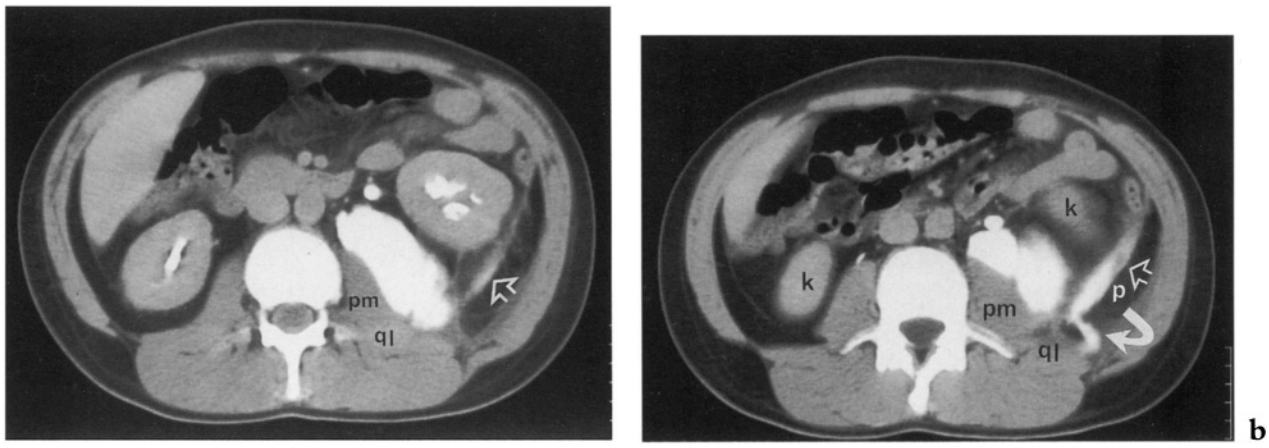


Fig. 8–79. Opacification of lumbar triangle pathway.
Contrast-enhanced CT shows extravasation from the left kidney after stone extraction.
(a) Gross extravasation localizes adjacent to the psoas major (*pm*) and quadratus lumborum *(ql)* muscles. Extravasated contrast has also dissected along perirenal bridging septa to the interlaminar plane of the posterior renal fascia *(open arrow).*
(b) At a lower level, fluid tracks through the lumbar triangle *(curved arrow)* through a defect between the posterior pararenal space (*p*) and the quadratus lumborum fat pad. *k* = kidney.
(Courtesy of Michiel Feldberg, M.D., University of Utrecht, The Netherlands.)

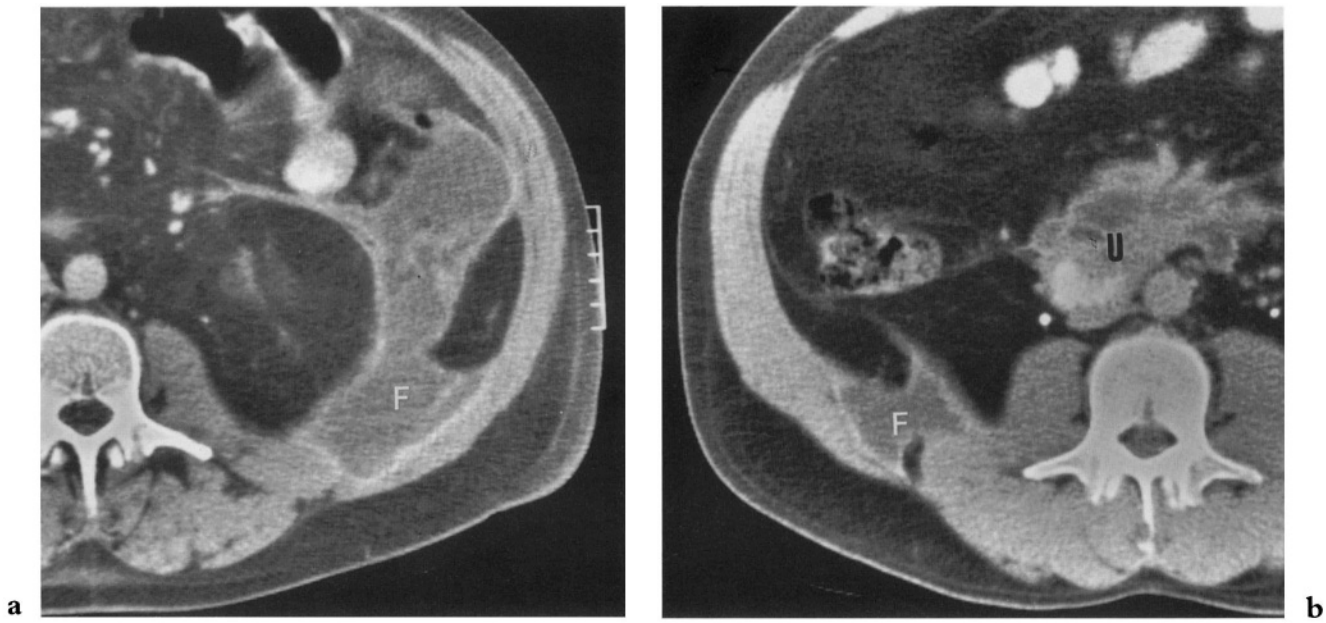


Fig. 8–80. Extension of pancreatitis to posterior abdominal wall in two different patients.
(a) Fluid collection (*F*) progressing through the posterior renal fascia intrudes upon the flank wall lateral to the quadratus lumborum muscle.
(b) In another patient, pancreatitis is manifested at this level by inflammatory tumefaction of the uncinate process (*U*). Secondary fluid collection (*F*) has dissected in relationship with the posterior abdominal wall lateral to the quadratus lumborum muscle.
Note that in both instances, the extravasated pancreatic enzymes are approaching the lumbar triangle and subcutaneous fat.
(Courtesy of Richard Gore, M.D., Evanston Hospital, Evanston, IL.)

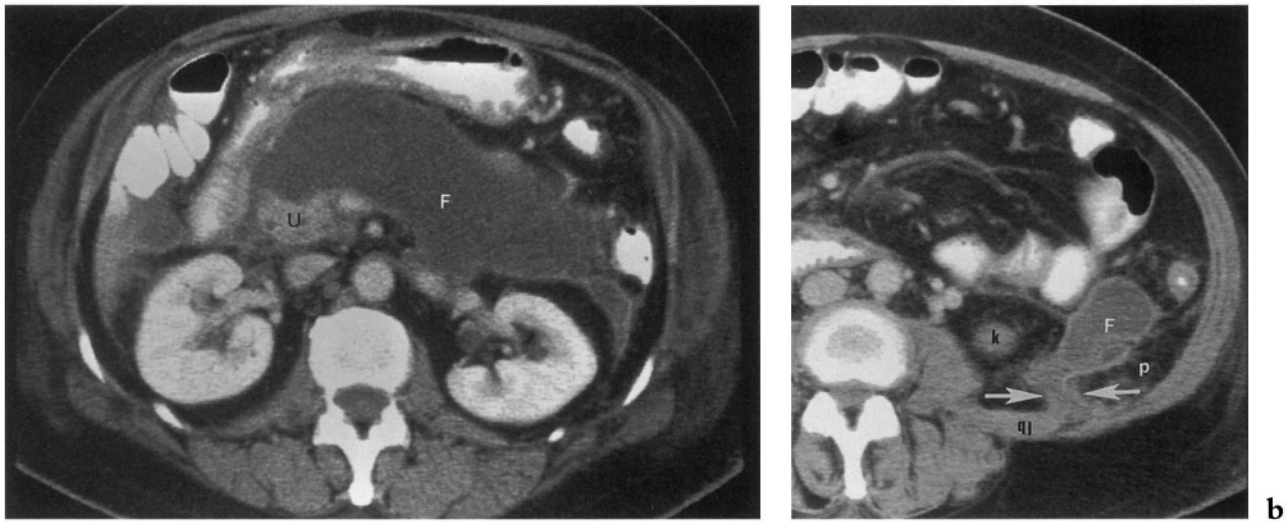


Fig. 8–81. Extension of pancreatitis to lumbar triangle pathway.
(a) Contrast-enhanced CT shows that the pancreas is largely liquified with voluminous fluid (*F*). A small amount of viable pancreas remains in the uncinate process (*U*).
(b) Pancreatic fluid (*F*) dissects along the posterior interfascial plane through the lumbar triangle *(arrows)* between the posterior pararenal fat (*p*) and the fat anterior to the quadratus lumborum muscle *(ql)* to contact the transversalis fascia. *k* = kidney.
(Courtesy of James Brink, M.D., Yale University School of Medicine, New Haven, CT.)

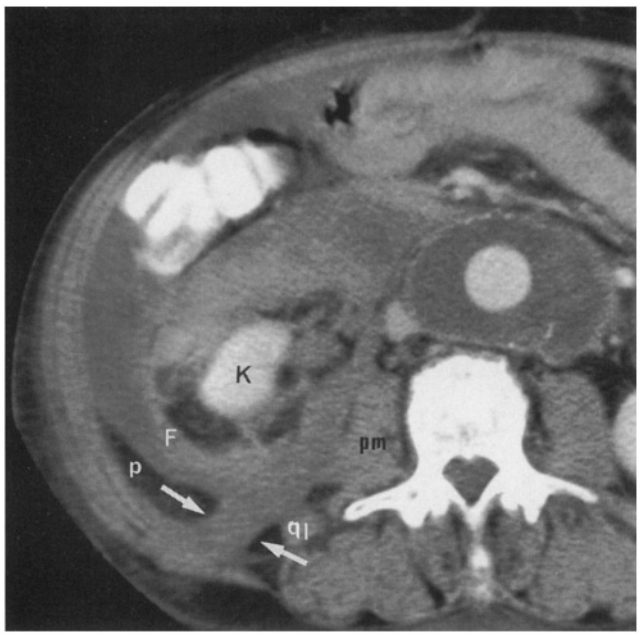


Fig. 8–82. Extension of retrorenal blood to lumbar triangle pathway.
After aortic prosthesis for aneurysmal rupture, contrast-enhanced CT demonstrates blood in the anterior pararenal space progressing through the retrorenal interfascial pathway (*F*) to the lumbar triangle *(arrows).* This is the site of a defect between the posteromedial boundary of the posterior pararenal space (*p*) and the anterolateral margin of the fat pad adjacent to the quadratus lumborum muscle (*ql*). *K* = kidney; pm = psoas muscle.
(Courtesy of Michiel Feldberg, M.D., University of Utrecht, The Netherlands.)

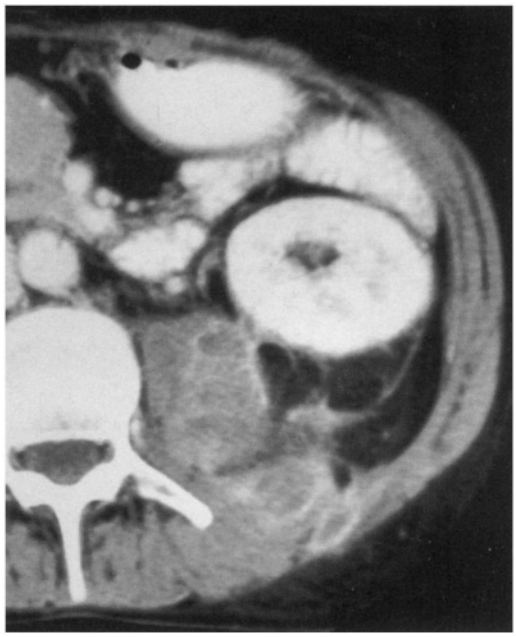


Fig. 8–83. Extension of psoas and posterior pararenal abscess to lumbar triangle pathway.
Contrast-enhanced CT demonstrates abscesses with rim enhancement in the psoas muscle and posterior pararenal space directly extending through the lumbar triangle.
(Courtesy of Michiel Feldberg, M.D., University of Utrecht, The Netherlands.)

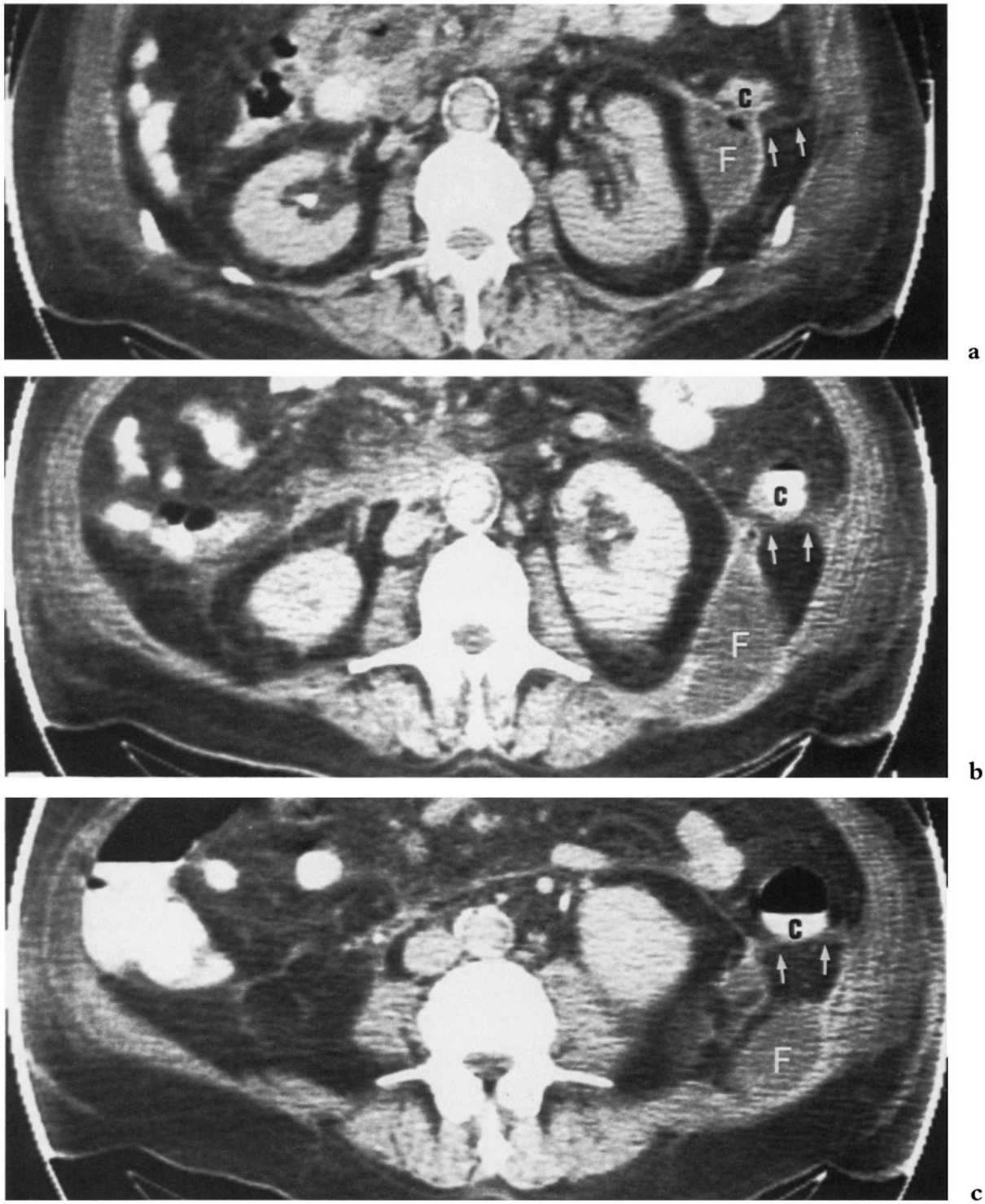


Fig. 8–84. Extension of pancreatitis to posterior abdominal wall presenting with Grey Turner's sign.
(a) Accompanying thickening of the renal fasciae and of the lateroconal fascia (*arrows*), there is a loculadon of fluid (*F*) between the leaves of the posterior renal fascia immediately behind the descending colon (*C*). **(b)** At a lower level, the fluid collection has dissected more posteriorly and comes into relationship with the posterior abdominal wall, presumably effacing the intervening segment of the posterior pararenal space. **(c)** More inferiorly, while some fluid distention of the posterior renal fascia remains evident, a loculated fluid collection intrudes upon the flank lateral to the quadratus lumborum muscle at the site of cutaneous discoloration that is clinically evident.

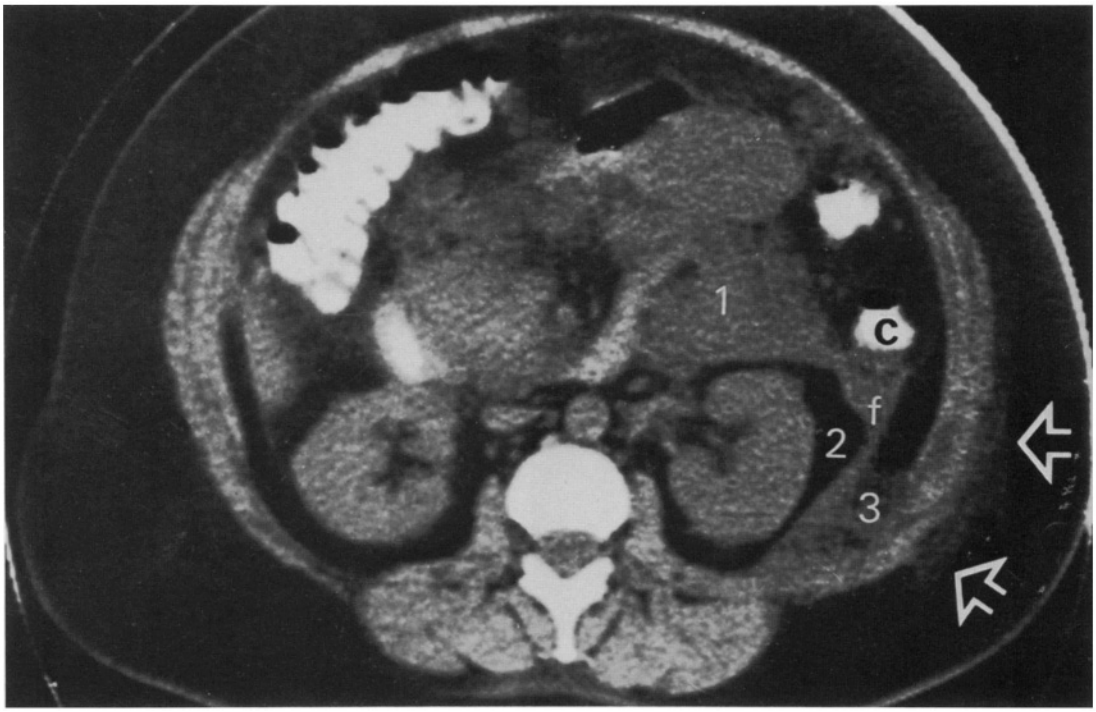


Fig. 8–85. The Grey Turner sign secondary to pancreatitis.
Extravasated pancreatic fluid in the left anterior partrenal space (*1*) dissects between the leaves of the posterior renal fascia with a loculated fluid collection (*f*) near the descending colon (*c*). The perirenal space (*2*) is maintained.
Inflammatory changes have reached an adjacent portion of the posterior pararenal space *(3)* and the subcutaneous tissues in the left flank (*arrows*) at the clinical site of discoloration.

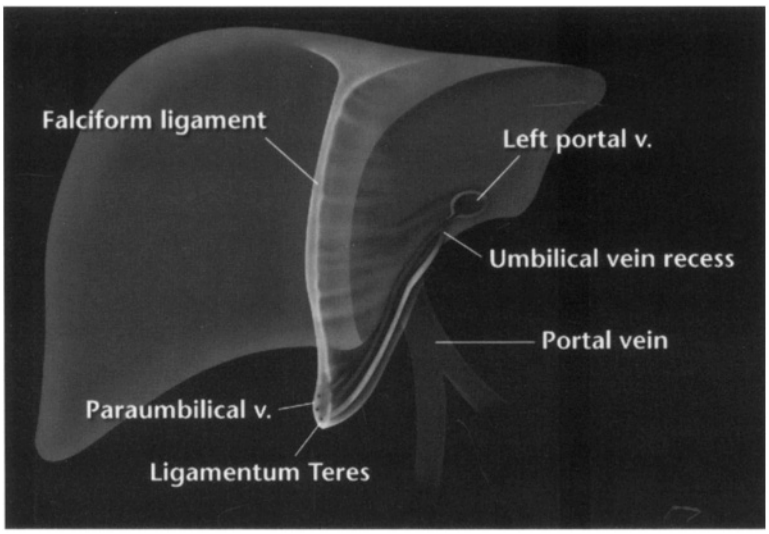


Fig. 8–86. Ligamentum teres and falciform ligament with vascular relationships.
Illustration depicts the paraumbilical veins running in the falciform ligament with the obliterated umbilical vein. The relationship to the left portal vein is also demonstrated. (Reproduced from Horton and Fishman.[108])

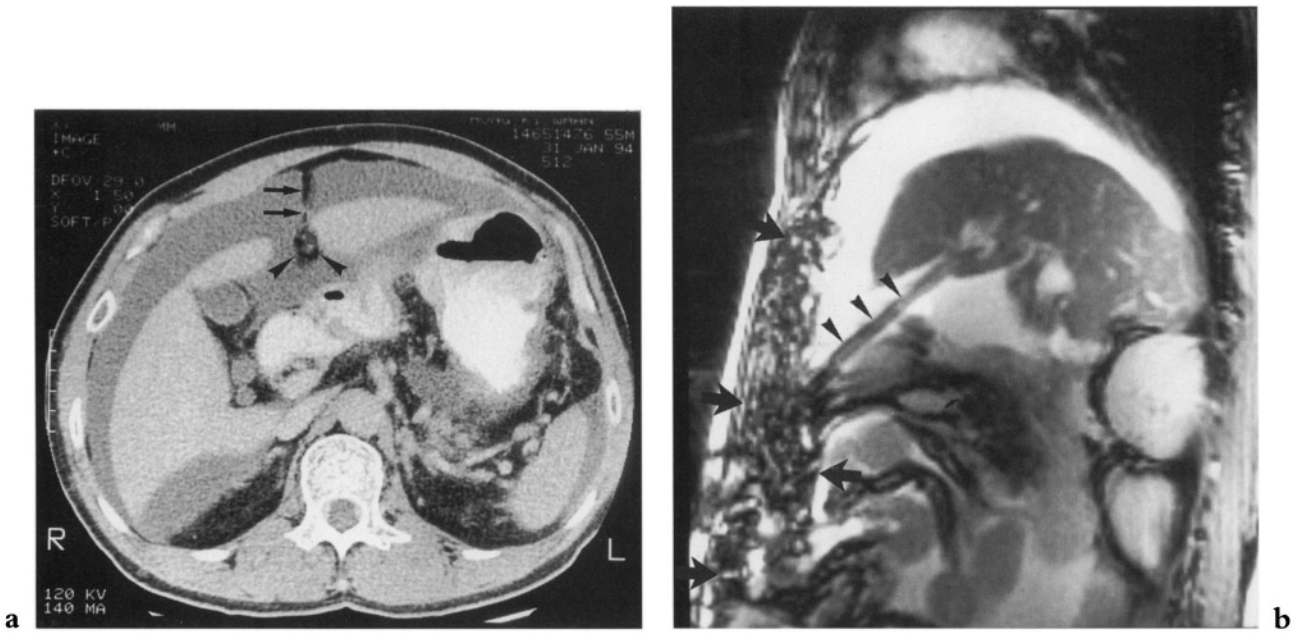


Fig. 8–87. Falciform ligament and ligamentum venosum in a patient with ascites.
(a) Fat-containing falciform ligament *(arrows)* extends from the anterior abdominal wall to the ligamentum teres *(arrowheads).* The falciform ligament is uneven in thickness, and the ligamentum teres contains small vessels.
(b) Sagittal MRI in a patient with liver cirrhosis shows entire extent of the ligamentum teres (*arrowheads*). Falciform ligament may be too thin to be visualized. The greater omentum *(arrows)* floats underneath the anterior abdominal wall.
(Reproduced from Auh et al.[109])

by CT (Fig. 8–88). Similarly, intrahepatic pancreatitis[107] (Figs. 8–89 and 8–90) even with pseudocyst formation[111] extending to localize in the falciform ligament (Fig. 8–91) and involve the properitoneal fat of the periumbilical region (Fig. 8–92) can be observed. By way of the same anatomic continuity, a cutaneous discoloration of the medial upper abdominal wall after infusion of chemotherapeutics in the hepatic artery can occur because the falciform ligament artery originating from the left or middle hepatic artery may bring the drugs to the properitoneal fat.[112,112a] Another, more direct pathway may be extension from inflammatory changes of the small bowel mesentery or greater omentum to the round ligament and then to properitoneal fat deep to the umbilicus.

The liberated digestive enzymes of severe pancreatitis may dissect within fascial planes to result in an interesting extension to the posterior pararenal space from the anterior pararenal space without the contamination of the intervening perirenal compartment. This may be a consequence either of violation of the lateroconal fascia[7,18] or the process spreading from the pancreas down the anterior pararenal space and then rising posterior to the cone of renal fascia within the posterior pararenal space,[8,12](Fig. 8–93). The kidney and colon are pushed forward, and the psoas muscle and flank stripe are obliterated.

Despite the digestive effects of pancreatic fluid, the renal fascia almost invariably is not transgressed so that the perirenal fat and kidney retain their integrity. Indeed, in acute pancreatitis, CT documentation of extrapancreatic fluid collections with perirenal spread and without renal involvement is rare[52,113–120] (Figs. 8–94 through 8–96).

Ranson has defined a set of laboratory and clinical criteria that are commonly used to judge the severity of an attack of acute pancreatitis and have some prognostic significance in predicting complications, including abscess development and hemorrhage.[121,122] Several investigators, most notably Balthazar, have recently reported the use of CT early in the course of pancreatitis as a predictor of outcome. In most reports, the presence and

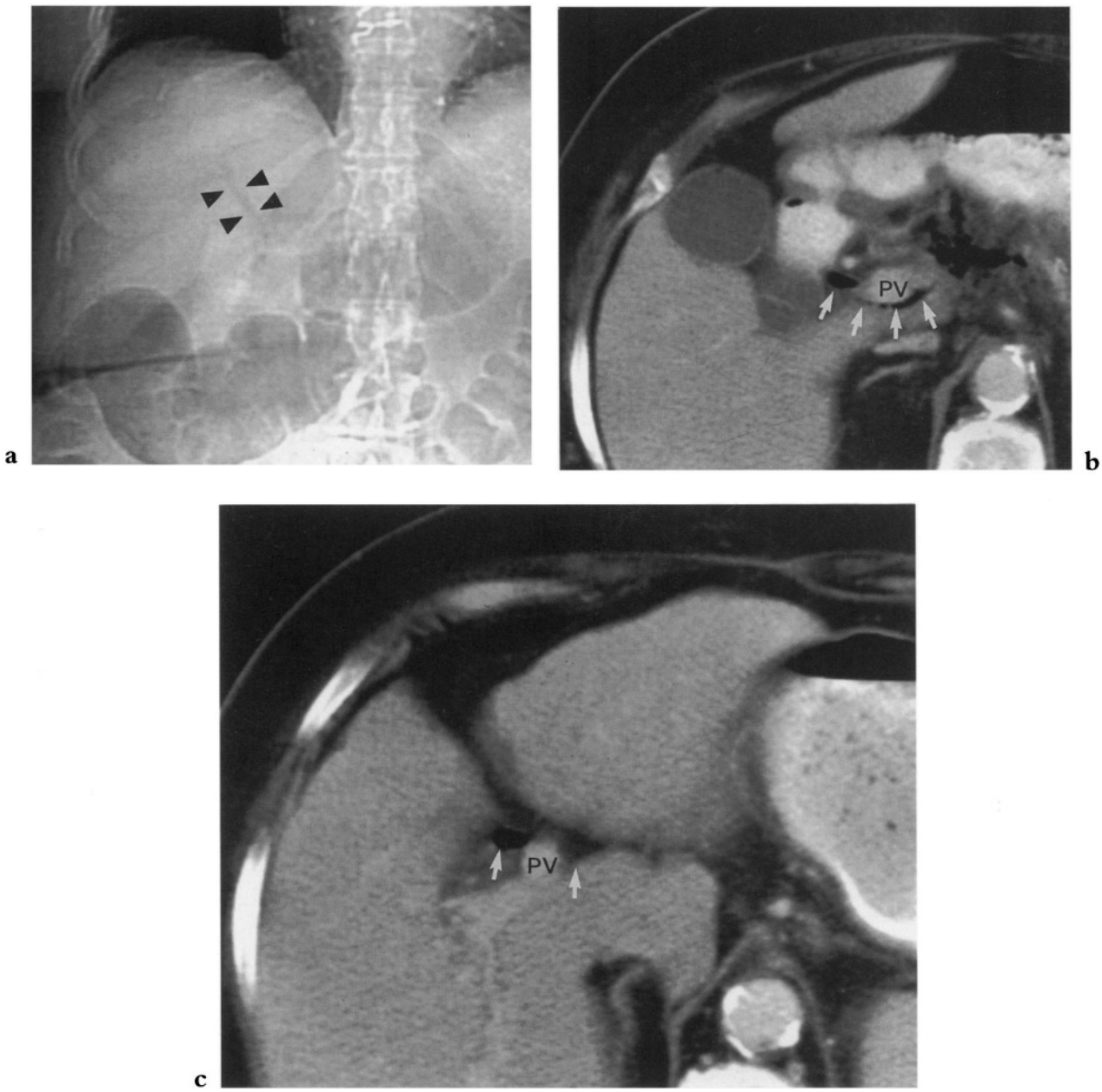


Fig. 8–88. Intrahepatic extension via the hepatoduodenal ligament.
ERCP with sphincterotomy resulted in duodenal rupture.
(a) Digital scout film shows periductal/periportal gas tracking cephalad within the hepatoduodenal ligament (*arrowheads*).
(b) CT demonstrates gas *(arrows)* deep to the portal vein (*PV*), anterior to the caudate lobe.
(c) At a higher level, gas is in the upper hilum near the falciform ligament.

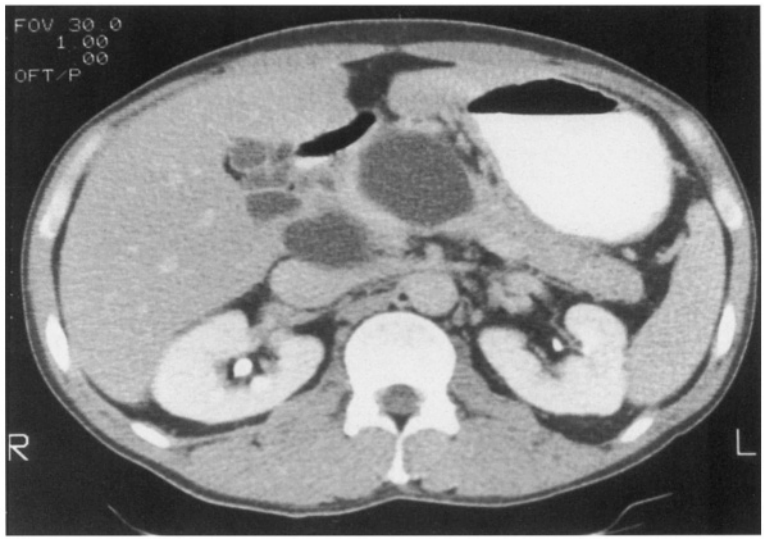


Fig. 8–89. Tracking of pancreatic pseudocysts along hepatoduodenal ligament.
Multiple extrapancreatic loculations course along the hepatoduodenal ligament toward the ligamentum teres fissure, from which the potential pathway may further extend along this edge of the falciform ligament to the umbilical region to present as Cullen's sign.
(Courtesy of Yong Ho Auh, M.D., Asan Medical Center, Seoul.)

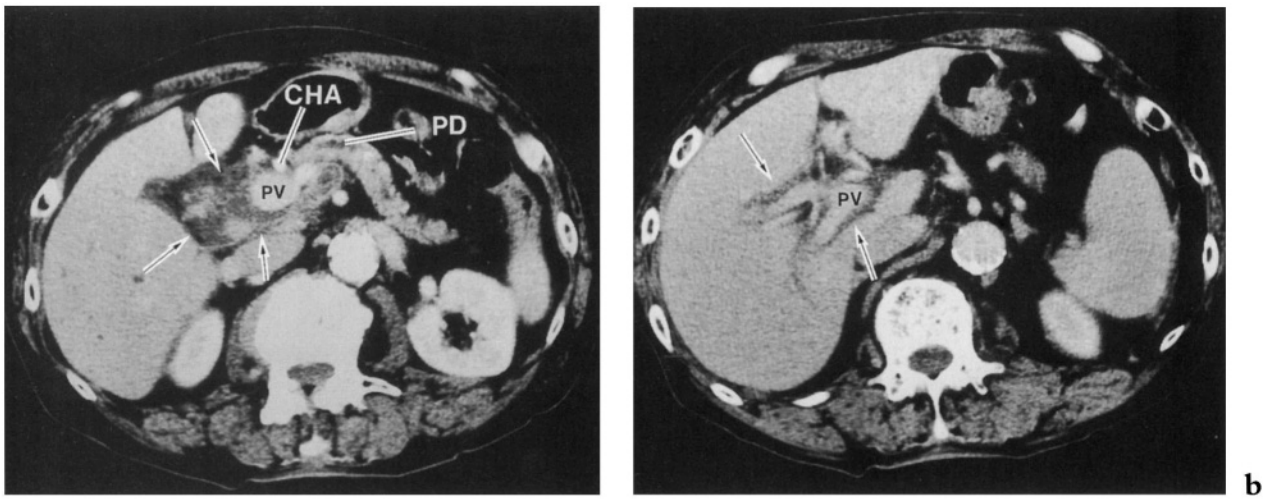


Fig. 8–90. Direct extension of pancreatitis into the liver.
Fluid collection secondary to pancreatitis has extended along the hepatoduodenal ligament.
(a) Contrast-enhanced CT shows pancreatic fluid *(arrows)* around the portal vein (*PV*). The pancreatic duct (*PD*) is dilated. *CHA* = common hepatic artery.
(b) At a higher level, the fluid collection extends upward along the portal vein at the hepatic hilum.
(Courtesy of Toshio Fukuda, M.D., Nagasaki University School of Medicine, Japan.)



Fig. 8–91. Pancreatic fluid in falciform ligament.
This patient presented with a palpable epigastric mass after an episode of acute pancreatitis.
(a and **b)** CT images show a fluid collection (*F*) between the left hepatic lobe and the abdominal wall, within the falciform ligament *(arrow).* There is inflammatory thickening of the intrahepatic portion of the ligament (*arrowheads*), which communicates with the hepatic hilum and the hepatoduodenal ligament, through the left periportal space. Fine-needle aspiration yielded dark fluid with high amylase content.
(Reproduced from Arenas et al.[66])

extent of extrapancreatic abnormalities as detected by CT have correlated with Ranson's criteria and the subsequent development of complications.[123–129]

Bleeding from Bare Area of Spleen, Splenic Artery, or Hepatic Artery

The hilum of the spleen receives the reflections of its supporting mesenteries, the gastrosplenic and splenorenal ligaments (Fig. 8–97). The bare area of the spleen is the nonperitonealized area representing the fusion of the splenorenal ligament to the surface of the perirenal fat. It bears a constant relationship to the upper anterior part of the left kidney. Its length is usually about 2–3 cm, and its width is about 2 cm.[130] The splenorenal ligament provides an anatomic bridge for bleeding to extend from the bare area of the spleen to the left anterior pararenal space[51,130a] (Fig. 8–98). In a review of CT scans in 23 cases with splenic trauma, hematoma in the left anterior pararenal space was seen in 3 (13%).[131]

The hepatic and splenic arteries are located anatomically within the anterior pararenal compartments. When these vessels rupture from trauma or aneurysm, the bleeding may be discretely localized to the extraperitoneal space on the side of origin.

Bleeding from the hepatic artery is clearly shown in the following case history. A 70-year-old man was examined because of a 1-month history of colicky right upper quadrant pain. His past medical history included acute rheumatic fever at the age of 5 and an episode of acute staphylococcal endocarditis at the age of 56. Oral cholecystography revealed moderate opacification of the gallbladder, and the hepatic angle, flank fat, and psoas muscle were clearly visualized (Fig. 8–99a) at this time. However, 24 hours later, the patient's colicky right upper quadrant pain increased suddenly, with abdominal distention. Initial diagnostic considerations included acute cholecystitis, acute pancreatitis, and penetrating peptic ulcer. An abdominal radiograph now showed a density throughout the right abdomen, with loss of the

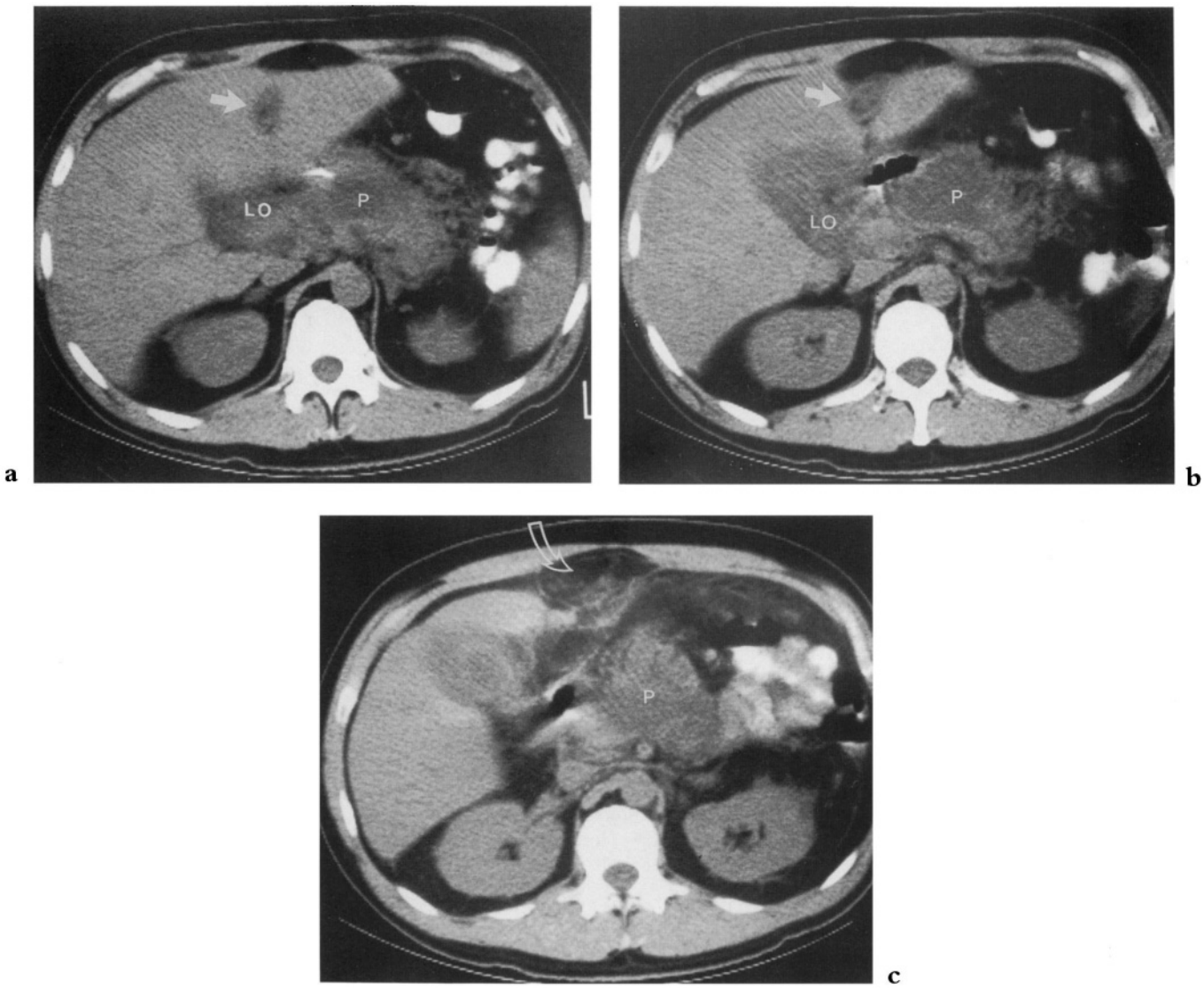


Fig. 8–92. Cullen's sign secondary to spread of pancreatitis along falciform ligament.
(a–c) Inflammatory process of pancreas (*P*) has extended into the lesser omentum (*LO*) toward the liver and porta hepatis. There is extension of disease to the ligamentum teres as shown by increased density of fat in region *(white arrow).* Inflammatory densities extend throughout the falciform ligament and involve the properitoneal fat of the anterior abdominal wall *(open arrow)* immediately deep to the site of clinical periumbilical discoloration. Inflammatory changes consequent to the pancreatitis also involve the greater omentum lateral to the falciform ligament. Incidentally noted is mural thickening of the gallbladder.
(a and **c,** reproduced from Meyers et al.[24])

hepatic angle, although the flank fat was clearly maintained (Fig. 8–99b). These changes indicated an acute fluid collection extraperitoneally, specifically within the anterior pararenal compartment. On the basis of these plain film abnormalities, a ruptured hepatic artery aneurysm was diagnosed radiologically. The patient's condition deteriorated rapidly, however, and he died on the second hospital day. Postmortem examination revealed a 10-cm aneurysm involving the proximal hepatic artery and celiac axis (Fig. 8–99c), containing a laminated bland thrombus. Rupture had occurred with massive hemorrhage extraperitoneally on the right.

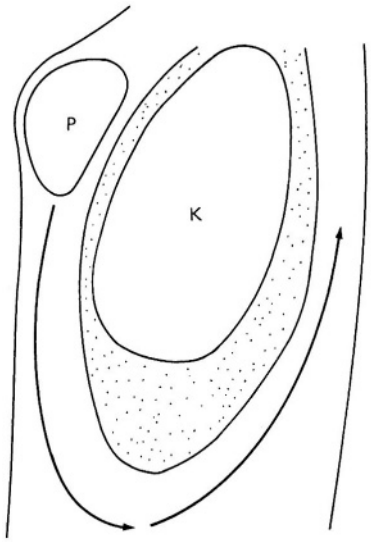


Fig. 8–93. Pancreatic extravasation with extension down the anterior pararenal space and then upward into the posterior pararenal compartment.
Sagittal diagram illustrates fluid collection in the left anterior pararenal space from the pancreas (*P*), and continuity under and around the cone of renal fascia into the posterior pararenal compartment.
(Reproduced from Meyers.[8])

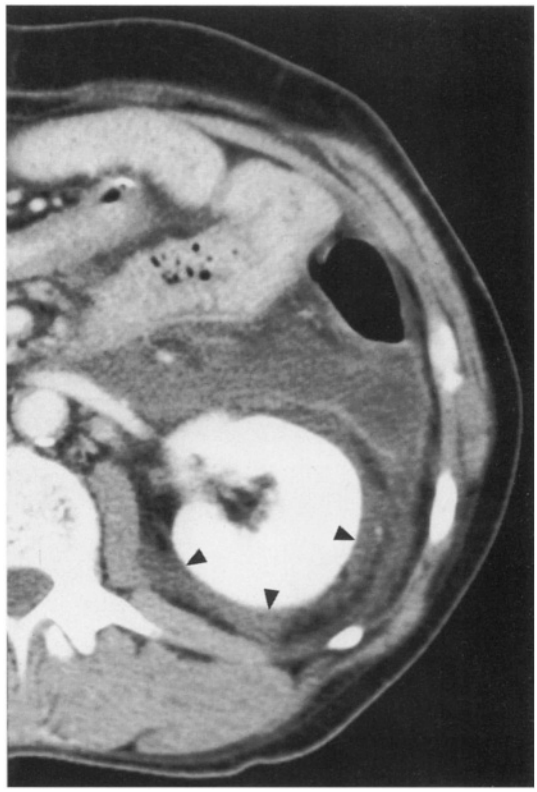


Fig. 8–94. Perirenal fat involvement in acute pancreatitis.
Anterior pararenal space fluid has dissected posteriorly between the layers of the posterior renal fascia. Fluid collections are also present within the perirenal fat (*arrowheads*).
(Courtesy of Michiel Feldberg, M.D., University of Utrecht, The Netherlands.)

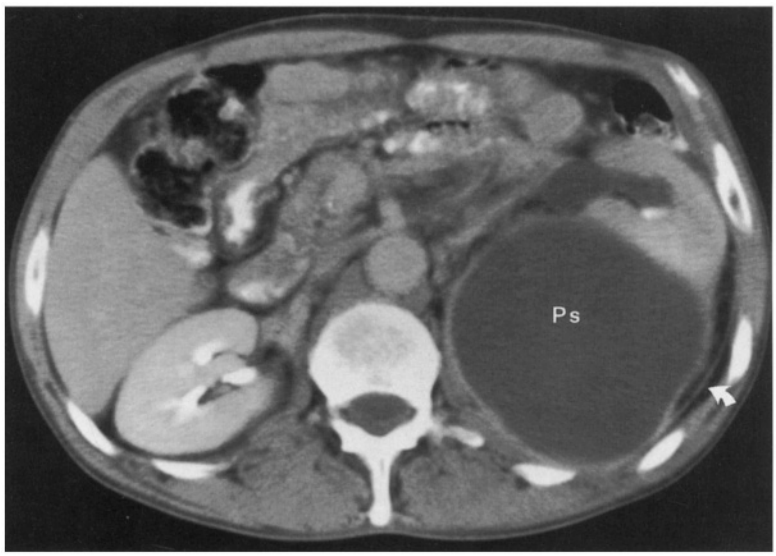


Fig. 8–95. Perirenal pancreatic pseudocyst.
A huge pancreatic pseudocyst (*Ps*) distends the perirenal space posteriorly, displacing the kidney. Posterior renal fascia remains evident (*arrow*). Fluid from the cyst was aspirated, diluted × 120, and had an amylase content of 25,870 IU/L.

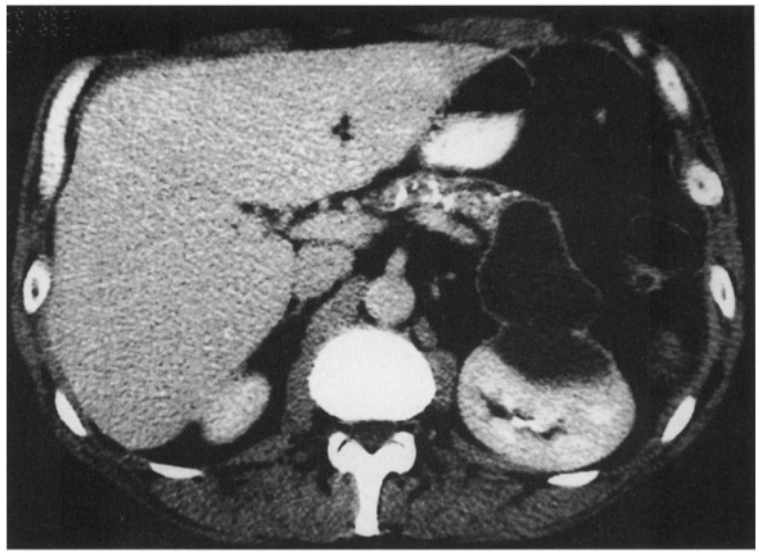


Fig. 8–96. Subcapsular pancreatic pseudocyst of the kidney.
CT demonstrates a pseudocyst originating from the pancreatic tail entering the subcapsular space through the focally disrupted renal capsule. The pancreatic body and tail are shrunken and exhibit stones and dilated ducts.
(Reproduced from Blandino et al.[120])

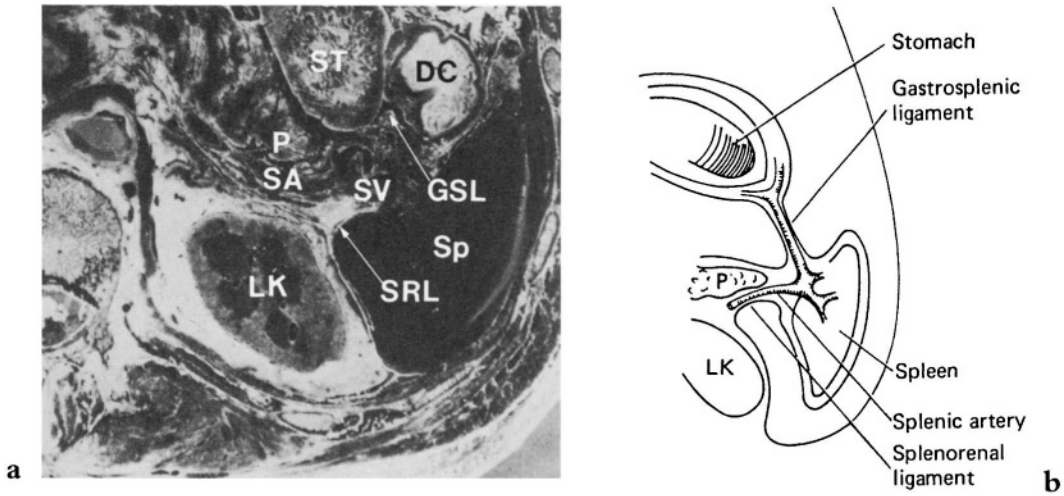


Fig. 8–97. Peritoneal attachments of the spleen.
(a) Transverse anatomic section demonstrates gastrosplenic ligament (*GSL*), within which course the short gastric and left gastroepiploic vessels, and the splenorenal ligament (*SRL*), which envelops the pancreatic tail and the proximal splenic vein (*SV*) and splenic artery (*SA*). *Sp* = spleen; *ST* = stomach; *P* = pancreas, *DC* = descending colon; *LK* = left kidney.
(b) Transverse drawing illustrates the intraperitoneal suspension of the spleen by the gastrosplenic and splenorenal ligaments.



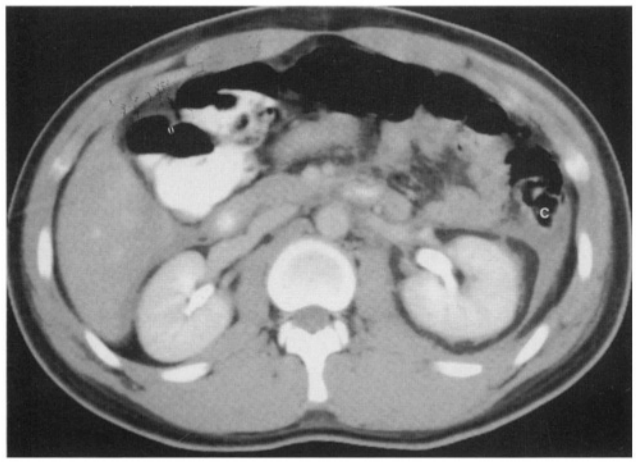


Fig. 8–98. Splenic bleeding extending through the splenorenal ligament to the anterior pararenal space.
Following a motor vehicle accident, peritoneal lavage showed no intraperitoneal blood in a patient with a falling hematocrit.
(a) CT demonstrates lacerations of the spleen extending into its bare area *(arrows)* with the blood within the left anterior pararenal space *(asterisk).*
(b) At the level of the kidneys, blood is evident within the anterior pararenal space extending to the descending colon *(c)* and posteriorly between the two lamellae of the posterior renal fascia.
(Courtesy of S. Balachandran, M.D., University of Texas Medical Branch, Galveston, TX.)

Bleeding from the splenic artery assumes a similar distribution, but a frequent associated finding is a localized change in the region of the splenic flexure of the colon, especially along its lateral margin (Fig. 8–100a). This is secondary to extension of the hemorrhage into the phrenicocolic ligament[132] at this level (Fig. 8–l00b).

A specific structural lesion can be identified ultimately in most instances of bleeding into the anterior pararenal space. I have only rarely encountered a case of spontaneous, nontraumatic hemorrhage in which neither a vascular source nor a bleeding dyscrasia could be diagnosed (Fig. 8–101).

An unusual instance demonstrating urine leakage into the anterior pararenal space from a traumatic tear of the ureter after its exit from the cone of renal fascia is shown in Figure 8–102.

Pelvic and Mesenteric Continuities

Clinical instances of the anatomic continuity of the extraperitoneal conjoined anterior and posterior pararenal spaces below the cone of renal fascia with the extraperitoneal spaces within the pelvis[29,133,134] provide striking evidence of the continuum of the subperitoneal space and the potential for bidirectional spread between the abdomen and the pelvis.[9,12,18,135,136] Figures 8–103 and 8–104 demonstrate direct cephalad extension into the anterior pararenal space and small bowel mesentery from pelvic hemorrhage. As a complication of femoral vascular catheterization procedures, bleeding from the femoral sheath may open directly into the prevesical extraperitoneal compartment and then spread superiorly and posteriorly, deep to the parietal peritoneum into the

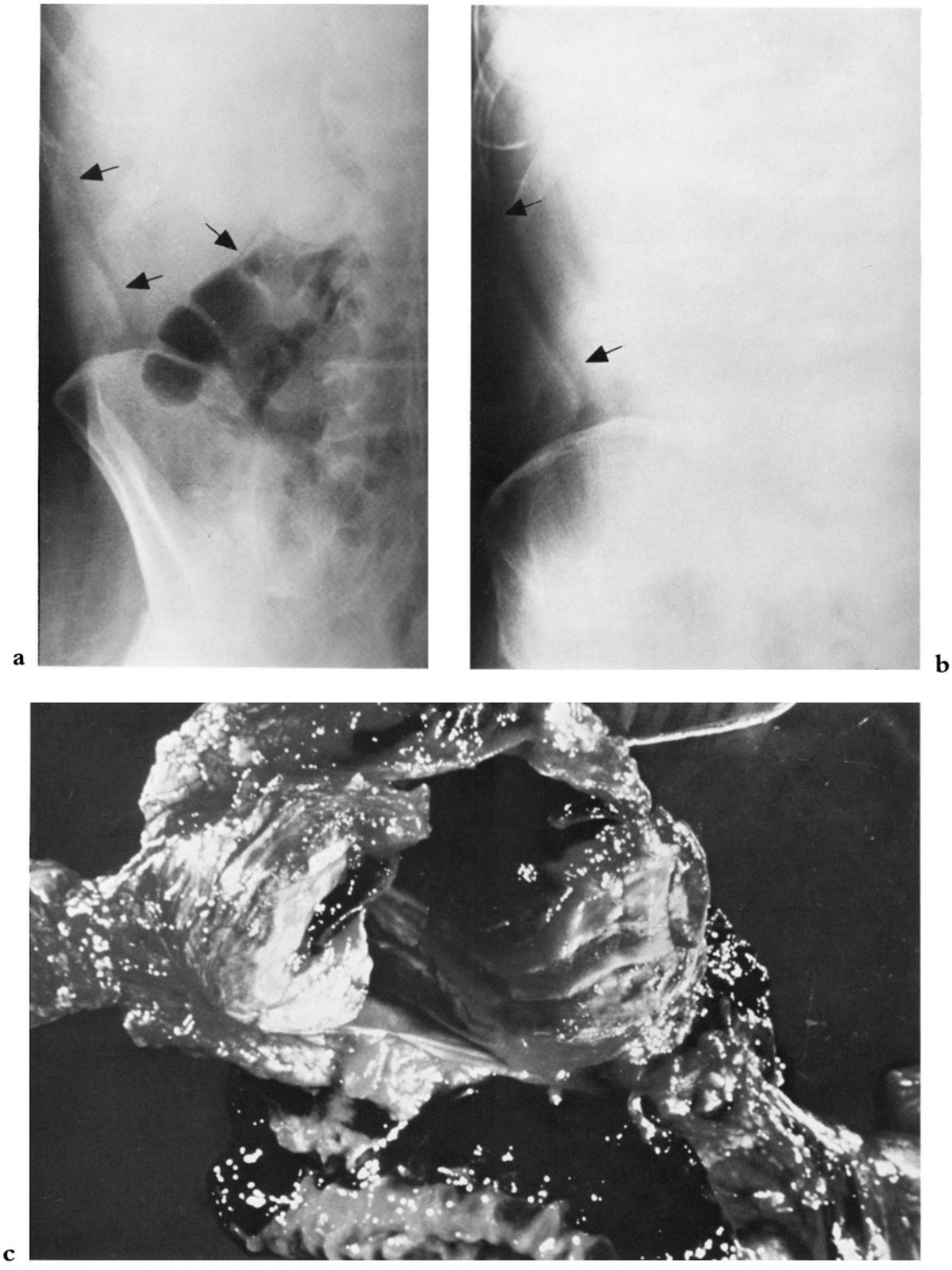


Fig. 8–99. Acute bleeding in right anterior pararenal space.
(a) At the time of initial oral cholecystogram, extraperitoneal fat is intact, allowing visualization of the hepatic angle and flank stripe *(arrows)* and psoas muscle.
(b) Film obtained the next day during abdominal catastrophe documents acute loss of the hepatic angle associated with a diffuse density throughout the right abdomen. Significantly, the flank stripe *(arrows)* is preserved.
(c) Gross specimen. Ruptured hepatic artery aneurysm, thrombus removed.

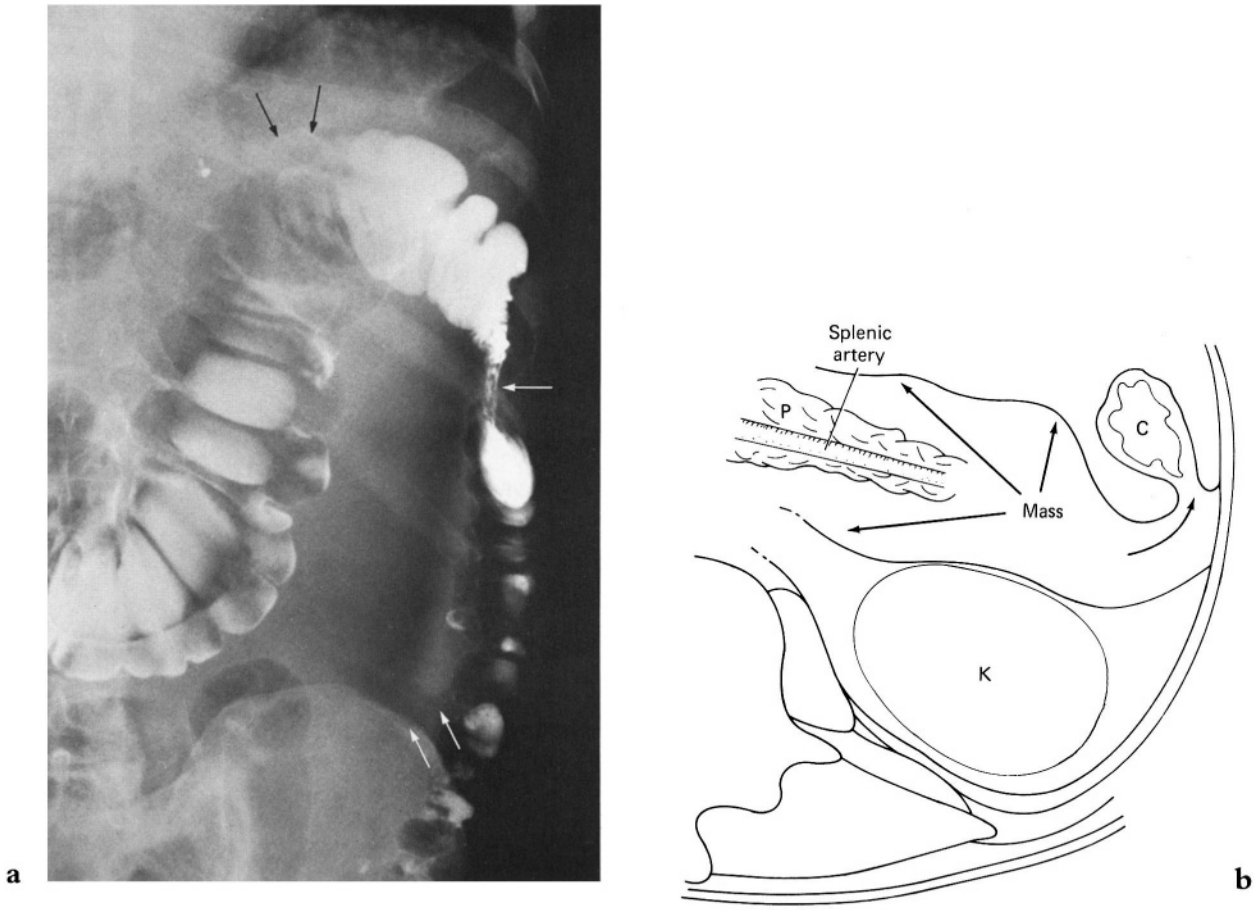


Fig. 8–100. Anterior pararenal hemorrhage from a ruptured calcified splenic artery aneurysm (*black arrows).*
(a) The fluid mass displaces the descending colon laterally as it extends downward within the anterior compartment *(white arrows).* The prominent localized changes of hematoma in the phrenicocolic ligament on the anatomic splenic flexure of the colon *(single white arrow)* further localize the effusion to the anterior pararenal space.
(b) Extension from ruptured splenic artery into the anterior pararenal space and into the phrenicocolic ligament. *C* = colon; *P* = pancreas; *K* = kidney.
(Reproduced from Meyers.[132])

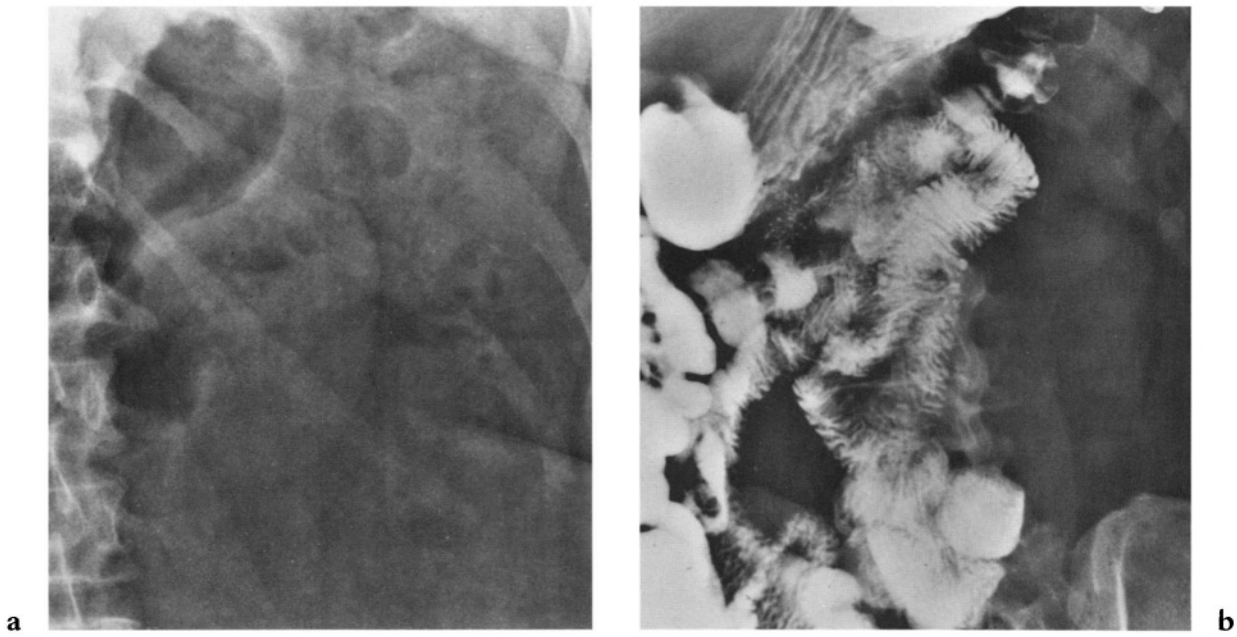


Fig. 8–101. Spontaneous left anterior pararenal hemorrhage in a middle-aged female with a fall in hematocrit from 34–20% within 10 days. No specific etiology could be identified.
(a) A left-sided mass is evident but the contours of the kidney and psoas muscle are clearly maintained.
(b) Small bowel series. Oblique view demonstrates that the intestine is displaced anteriorly.

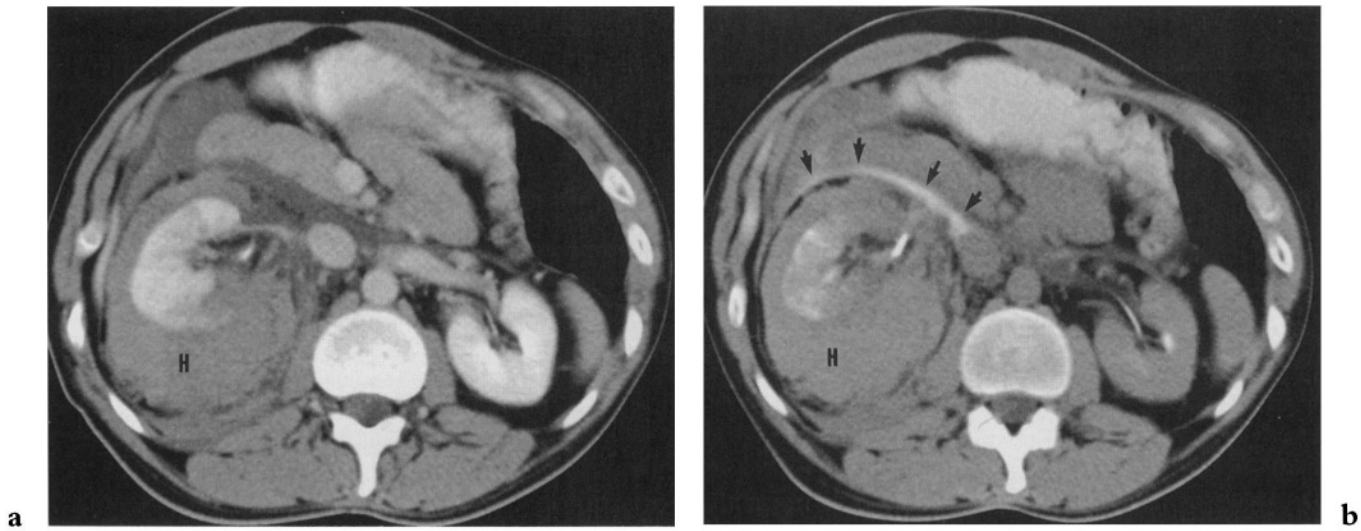


Fig. 8–102. Anterior pararenal space urine extravasation accompanying perirenal hematoma.
(a) Fractured right kidney with acute perirenal hematoma (*H*) after fall from a ladder. Fluid is also present in the right anterior pararenal space.
(b) On delayed image, this is shown to be due to leak of urine from the ureter *(arrows).* Both CT images are in the right decubitus position.
(Courtesy of Jay P. Heiken, M.D., Mallinckrodt Institute of Radiology, St. Louis, MO.)

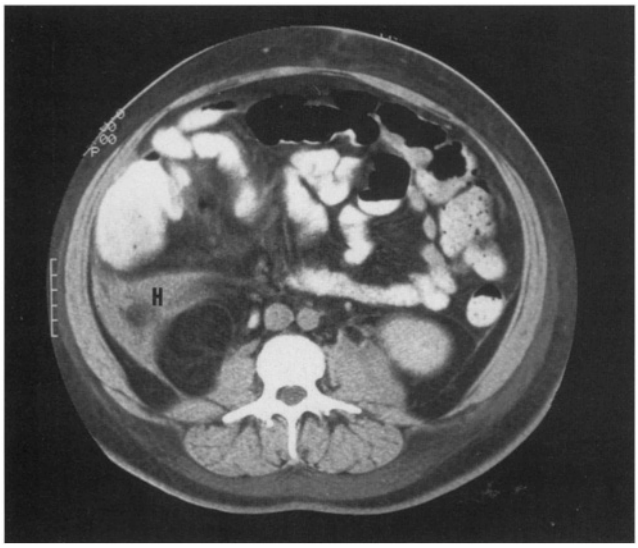


Fig. 8–103. Ascent of pelvic bleeding into anterior pararenal space.
Following pelvic surgery in this female patient receiving anticoagulants, severe pelvic hemorrhage is shown to rise into the anterior pararenal space on the right (*H*) to the level of the lower cone of renal fascia.

combined pararenal space of the abdomen.[137,138] On the other hand, Figure 8–105 documents extension from the anterior pararenal space into the prevesical pelvic space by a pancreatic inflammatory process.

Compartmentalization of the Anterior Pararenal Space

Maarten S. van Leeuwen, M.D.
Michiel A.M. Feldberg, M.D.

The space based on fascial boundaries, enclosed by the posterior parietal peritoneum anteriorly, the anterior renal fascia posteriorly, and the lateroconal fascia laterally, has been termed the *anterior pararenal space* by Meyers et al.[12] It contains the extraperitoneal alimentary structures, namely the pancreas, duodenum, and ascending and descending colon. Because the spread of fluids, inflammation, and gas does not always conform to the anterior pararenal space as a distinct compartment, Dodds et al.[31] stressed the importance of the embryologic development of the anterior pararenal space from three major compartments: the bilateral pericolonic spaces and the pancreaticoduodenal space. They stated that the secondary or anterior retroperitoneuni is a laminated space, bounded by folded, fused leaves of mesentery that contain the distinct and generally separate colonic and pancreaticoduodenal subcompartments. Whereas the anterior renal fascia and similarly the lateroconal fascia, although fusional in nature,[139] have been considered as single laminae, Molmenti et al.[34] recently emphasized the existence of a dissectable set of planes on CT. The fact that these fusion planes of the mesenteric surfaces with the primary retroperitoneum may reopen by the entrance of fluid supports the clinical identification and extent of fluid collections, seen occasionally in pancreatitis, less frequently in duodenal lesions, and rarely in appendicitis, diverticulitis, or colitis.

Anatomic Considerations

Since the first descriptions by Toldt (Fig. 8–106) in 1879,[140] the fusion of contiguous peritonealized surfaces and blending of the connective layers of the apposed peritoneal sheets forming a fibrous layer strong enough to call a fascia has been widely accepted.[139,141] The sheet of tissue behind the head of the pancreas and the duodenal loop has been called the *retroduodenopancreatic fascia of Treitz,* following his description in 1853.[142] Its embryologic basis, however, of mesoduodenum fused to the posterior wall after bowel rotation was later clearly established by Toldt.[140,143] Toldt also described the fusion fascia behind the body of the pancreas as a result of the fixation of the dorsal wall of the lesser sac, which subsequently has been named the *retropancreatic fascia of Toldt* (Fig. 8–107). In addition, he described the fusion fascia of the right and left mesocolon of the ascending and descending colon respectively, which since then are named *right* and *left retrocolic fascia of Toldt* (Fig. 8–107). In 1900, Fredet[144] described thoroughly these processes of fusion with numerous cross-sectional drawings and coined the French term *fascia d'accolement,* which means joining or fusion fascia: a unique layer, more or less defined from surrounding tissue, with mobilization often remaining possible. Others have confirmed the ease of identification and surgical mobilization of these fusion fasciae.[145,146] Yet, some have called this fascia a misuse of the term fascia,[147] denied its existence,[148] or hardly ever found a real fusion fascia at operation.[149] Congdon et al.[139] found these fusion fasciae to be very thin (0.1 to 0.6 mm) and sometimes bilaminar with a separable-looser stratum, ranging from similar thickness as the two lamina to several millimeters thick. They described the fused segments of the adult mesocolon as somewhat mobile, and not fixed, despite the fusions. According to Hureau et al.,[32,33] the real anterior pararenal space is the potential space between the fusion fascia of mesoduodenum and mesocolons and the perirenal fascia extending from diaphragm to pelvis.

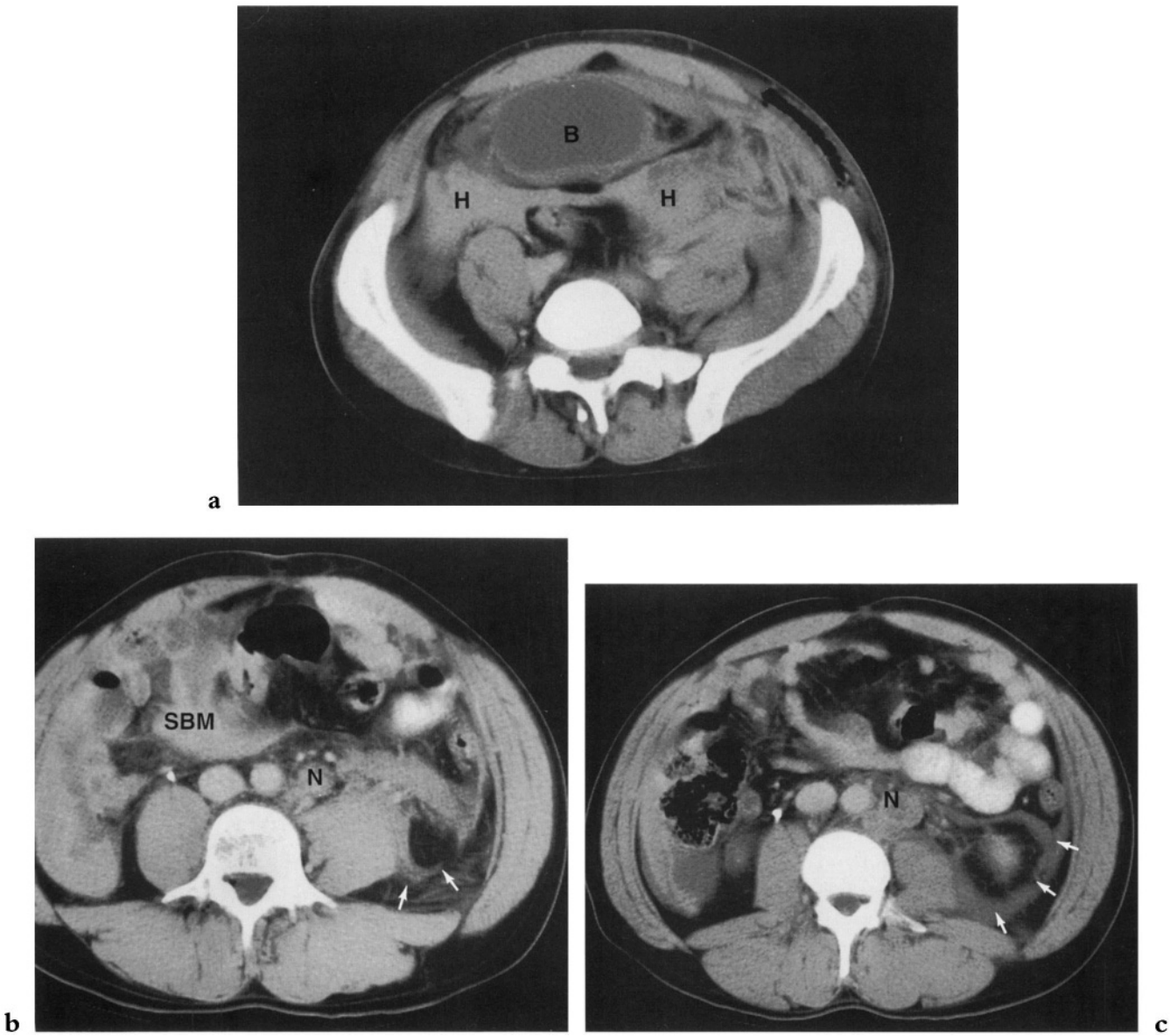


Fig. 8–104. Extension of pelvic hemorrhage into the anterior pararenal space and small bowel mesentery.
Following a left orchiectomy for seminoma, this 31-year-old man had a falling hematocrit.
(a) CT demonstrates extraperitoneal hemorrhage (*H*) with increased attenuation in the pelvis extending across the midline deep to the urinary bladder (*B*). Postoperative subcutaneous emphysema is evident on the left.
(b and **c)** The blood rises into the anterior pararenal space within the abdomen. On the left, it extends within the two laminae of the posterior renal fascia *(arrows).* On the right, it continues into the lower small bowel mesentery (*SBM*). *N* = nodal metastasis.
The hemorrhage apparently originated from inadequate ligature of the testicular artery.

The effects of pancreatitis on small bowel and colon by spread along mesenteric planes were first noted by Meyers et al.[84] In 1981, Strax et al.[150] reported the correlation of barium enema and CT in acute pancreatitis. Later, Raptopoulos et al.[20] reported the posterior extension of pancreatic effusions arising in the anterior pararenal space into the so-called retrorenal space, formed by dissection of the posterior renal fascia in two parts: the anterior part, continuous with the anterior renal fascia, and the posterior part, continuous with the latero-

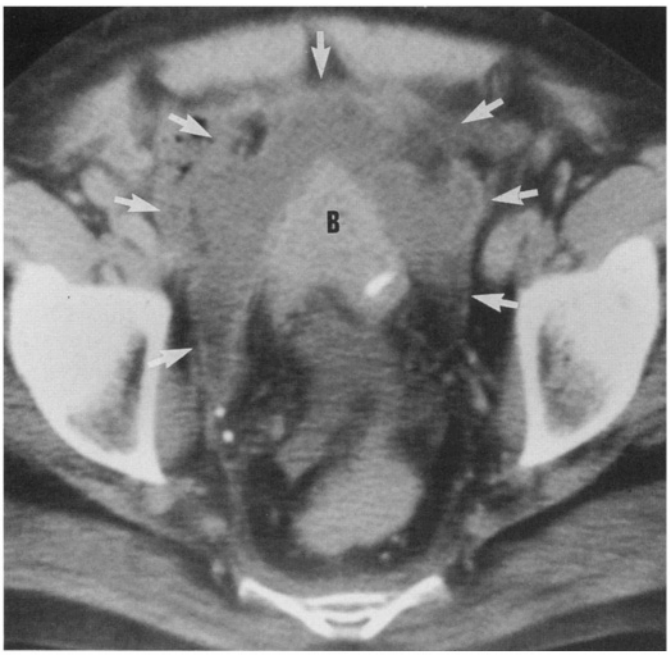


Fig. 8–105. Caudad extension of pancreatitis from the anterior pararenal space to the pelvis.
In a patient with fluid collection in the right anterior pararenal space secondary to severe acute pancreatitis, CT scan of the pelvis demonstrates the inflammatory process has descended into the extraperitoneal prevesical space assuming a characteristic "molar-tooth" configuration *(arrows)* in relation to the urinary bladder (*B*).
(Courtesy of Michiel Feldberg, M.D., University of Utrecht, The Netherlands.)

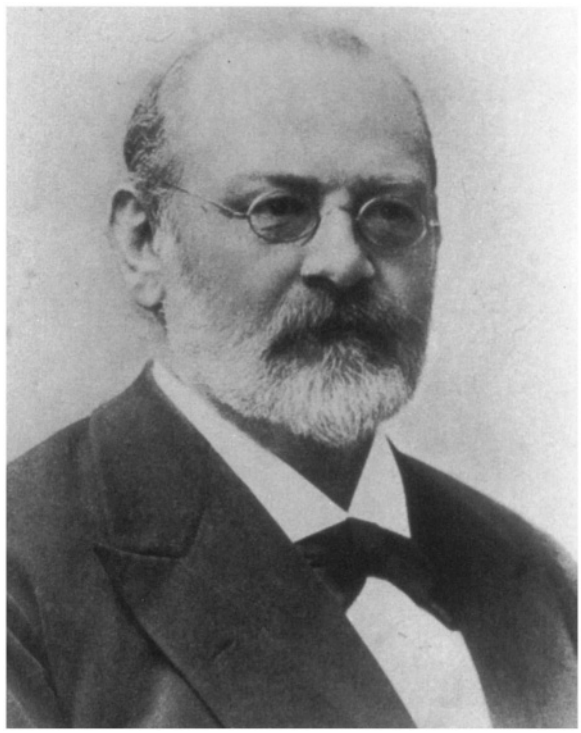


Fig. 8–106. Carl Toldt (1840–1920).
Carl Toldt was appointed to the Chair of Anatomy first in Prague and then in Vienna. His most important work is the widely accepted concept that during embryologic development, the secondary fusion of various mesenteries to the primitive parietal peritoneum is decisive for the definitive shape and location of mesenteries and different segments of the alimentary tract in adults.
(Courtesy of the Institut für Geschichte der Medizin der Universität Wien.)

conal fascia.[151] Recent injection studies[29,34] of the pancreatic and peripancreatic tissues on the left further confirm extension from a retromesenteric plane, posterior to the fused mesocolon and anterior to the renal fascia, to the retrorenal plane. With volume and force, extension can occur across the midline, superiorly to the diaphragm and inferiorly to the pelvis.[34,152] Fredet[153] considered the posterior renal fascia embryologically as a result of a reinforcement by outcoming fibers of the peritoneal fascia, whereas Paturet[154] viewed it as coming from fusion of the primitive retrorenal cul-de-sac to the posterior wall. Both concepts can explain the communication of the retromesenteric to the retrorenal plane through mobilization of these loose connections by fluid collections. Aizenstein et al.[35] mention the so-called interfascial plane, indicating the potential space between the layers of renal and lateroconal fascia, to be the result of incomplete fusion of embryonic mesentery. The ease

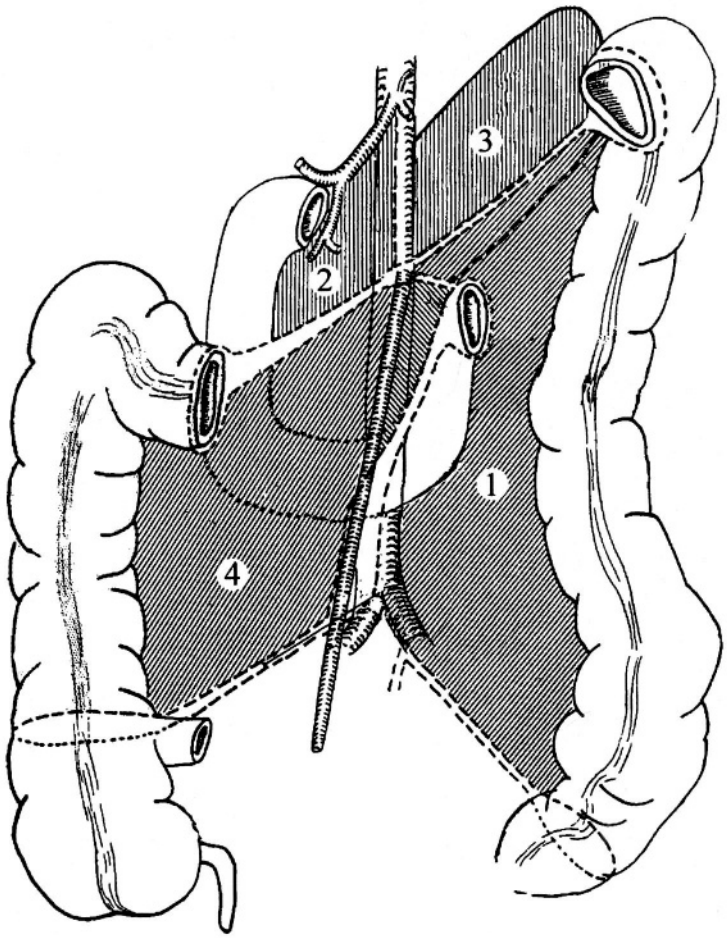


Fig. 8–107. Frontal diagram of the fusion fasciae of left and right colon and duodenal loop.
The fusion fascia of the left colon (*1*) fixes the meso of the descending colon to the posterior primitive parietal peritoneum. The superior limit, which covers part of the retroperitonealized pancreatic body and tail, is the line connecting the origin of the superior mesenteric artery to the left angle of the transverse mesocolon. The medial limit is in front of the aorta. The inferior limit begins a little left from the midline, in front of the promontory, and descends along the inner border of the psoas muscle, at the upper root of the sigmoid mesocolon. The retroduodenopancreatic fusion fascia of the duodenal loop *(2)* fixes the mesoduodenum and pancreatic head to the posterior primitive parietal peritoneum and to the fusion fascia of the left mesocolon, respectively, right and left from the midline. The superior limit above the root of the transverse mesocolon is the common hepatic artery. The medial limit is in front of the aorta. The left limit, below the radix of the transverse mesocolon, is short, starting below the superior mesenteric artery and extending to the duodenojejunal angle. The retropancreatic fusion *fascia (3)* fixes the dorsal mesogastrium, containing pancreatic body and part of the tail, to the posterior primitive parietal peritoneum. The fusion fascia of the right colon *(4),* located between cecum and transverse mesocolon, fixes the meso of the ascending colon to the posterior primitive parietal peritoneum and the duodenum and its fused meso, containing the caudal part of the pancreatic head. The superior limit is the line from the origin of the superior mesenteric artery across the second portion of the duodenum to the right angle of the transverse mesocolon. The inferior limit is the oblique line from the level of the aortic bifurcation to the ileocecal angle and the medial limit is close to the midline.
(Adapted from Grégoire R, Oberlin S: Précis d'anatomie, 10th ed. J.B. Ballière, Paris, 1991.)

for surgeons to perform mobilization of the duodenum by blunt dissection, after incising the peritoneum lateral to the duodenal loop (Kocher maneuver), or mobilization of the colon after incising along the line of Toldt,[140] laterally behind the ascending and descending colon where the fusion took place first,[155] may simulate the manner rapidly accumulating fluid and gas collections may loosen the fusion fasciae. Anatomic cross–sections demonstrate these loose connections well (Fig. 8–108).

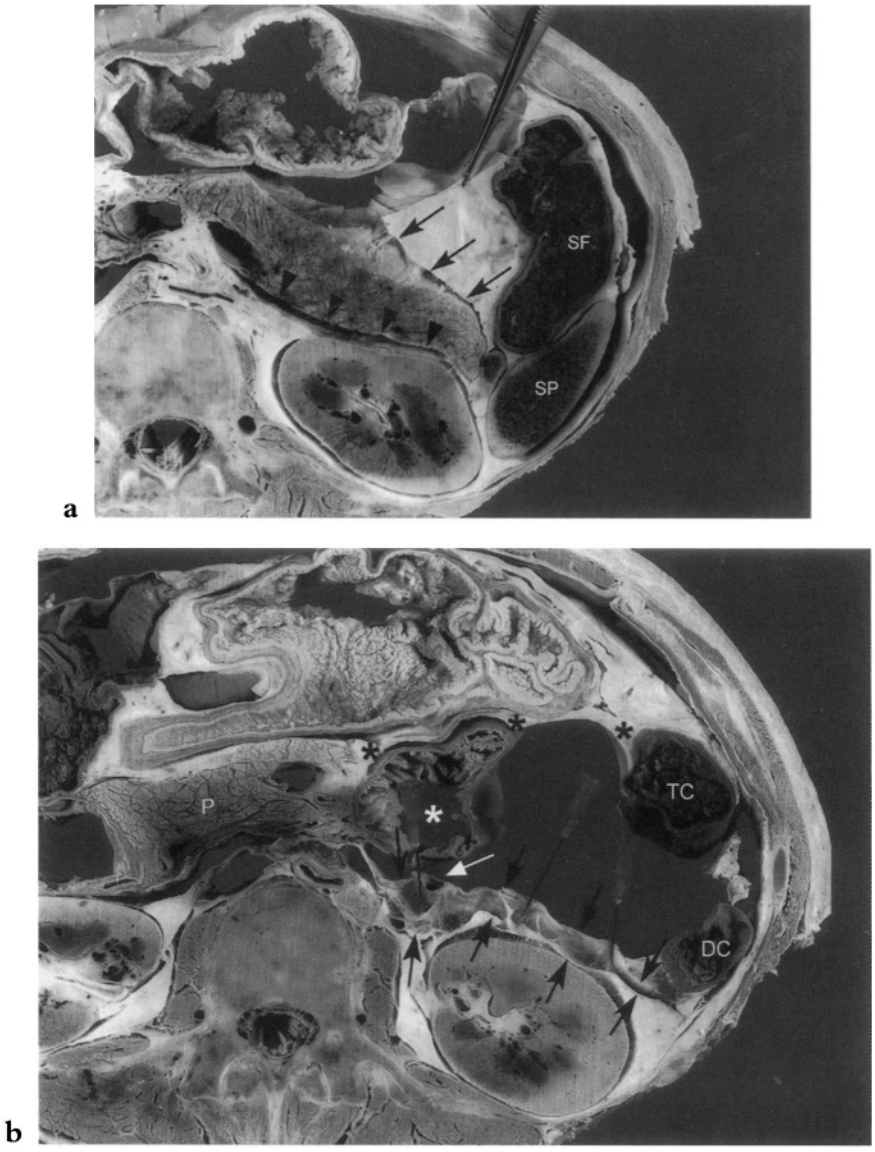
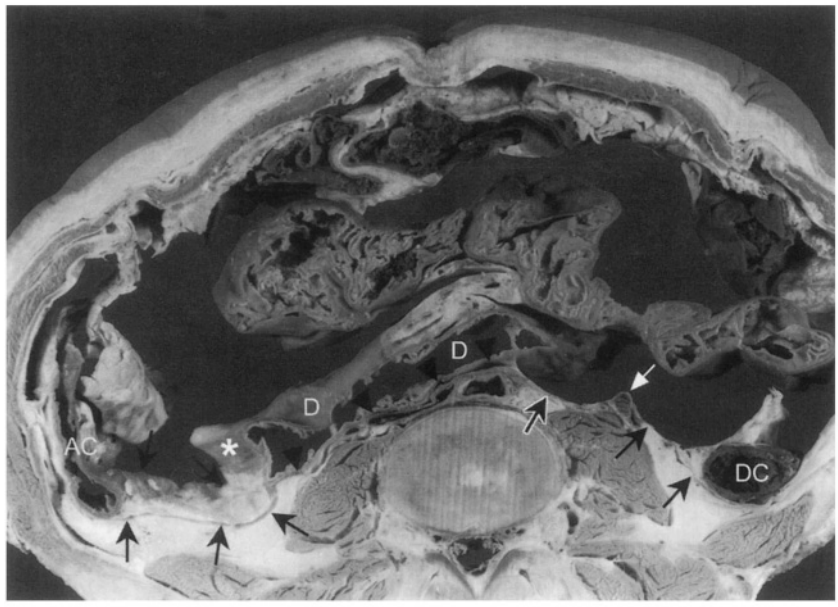


Fig. 8–108. Anatomic sections of fusion fasciae.
(a) Section at the level of the pancreatic tail, with slight anterior traction on the left colonic fat. The mesenteric fat medial to the splenic flexure (*SF*) of the colon portrays the continuity between transverse mesocolon mediocranially and left colonic compartment laterocaudally. Note the loose areolar tissue *(arrows)* between this mesenteric fat and the pancreatic tail, representing the fusion fascia posterior to the transverse mesocolon medially and the cranial extension of the left retromesenteric plane, also called left fascia of Toldt, laterally. A space, also bridged by loose areolar tissue *(arrowheads),* appears between the pancreatic tail and perirenal space, representing the fusion fascia between the left pancreaticoduodenal compartment and primitive retroperitoneum. *SP* = spleen.
(This figure also appears in the color insert.)
(b) Section at the level of pancreatic head (*P*) and neck, with traction on the left colonic compartment. The left colonic compartment is demarcated from the primitive retroperitoneum by loose areolar tissue representing the left retromesenteric plane *(black arrows).* Anteriorly, the transverse mesocolon *(black asterisks)* attaches to the pancreatic neck, posterior to the stomach, and anterior to the duodenojejunal junction *(white asterisk)* in the left paraduodenal fossa. *White arrow* = inferior mesenteric vein; *DC* = descending colon; *TC* = transverse colon.
(This figure also appears in the color insert.)

Continued on opposite page



c



d

Fig. 8–108. (Continued) (c) Section at the level of the pancreatic head *(P).* The right pancreaticoduodenal compartment is demarcated posteriorly by the loose areolar tissue of the retropancreaticoduodenal fusion fascia *(arrowheads),* also called fascia of Treitz, and anteriorly by the loose areolar tissue of the cranial extension of the right retromesenteric plane, also called right fascia of Toldt *(arrows).* Note the continuity of the transverse mesocolon *(asterisks)* with the right colonic compartment, located anterior to the right perirenal space. *White arrow* = inferior mesenteric vein; *HF* = hepatic flexure.
(This figure also appears in the color insert.)
(d) Section below the level of the pancreatic head, demonstrating the slender right and left colonic compartments at this level *(black arrows).* Note how the right colonic compartment covers the right side of the pancreaticoduodenal compartment *(white asterisk),* while the medial extension of the left colonic compartment *(black-and-white arrow)* lies posterior to the left extension of the horizontal part of the duodenum *(D).* The retropancreaticoduodenal fusion fascia is located posterior to the duodenum and anterior to the primitive retroperitoneum, aorta, and inferior caval vein. *AC* = ascending colon; *DC* = descending colon.
(This figure also appears in the color insert.)

Normal Imaging Features

On cross-sectional imaging, the right and inferior extensions of the pancreaticoduodenal compartment are demarcated by the duodenal loop surrounding the pancreatic head (Figs. 8–108 and 8–109). Its left and midportion are demarcated by the pancreatic body and tail. The retroperitoneal colonic compartments are recognizable by the presence of the ascending and descending colon with mesenteric vessels: on the left side the left colic vessels and the inferior mesenteric vein and side branches, and on the right side the right colic and ileocolic vessels (Figs. 8–108 and 8–109). The continuity of the right, middle, and left colic vessels, indicating the transition between the right colonic compartment, transverse mesocolon, and left colonic compartment, can be appreciated on most CT scans[156,157] (Fig. 8–109). The lower edge of the right colonic compartment is indicated by the ileocolic vessels and cecum; on the left it is indicated by the junction of the fused descending colon and its mesentery to the intrapelvic sigmoid colon and its unfused mesentery. The inferior mesenteric vessels can be followed down into the mesocolon of the sigmoid, its side branches anastomosing with the left colic vessels along the medial border of the descending colon. Cranially, the junction of the left colonic compartment to the transverse mesocolon can be appreciated as the thin sheet of colonic fat widens medial to the splenic flexure, anterior to the pancreatic tail and body, at the level of the left angle of the transverse mesocolon (Figs. 8–108 and 8–109). Medially, the left colonic compartment is indicated by the inferior mesenteric vein, as it ascends, posterior to the duodenojejunal angle and left paraduodenal fossa, before it drains into the splenic or superior mesenteric vein (Figs. 8–108 through 8–110).

Abnormal Imaging Features

Extensions of Fluid Collections Originating in the Pancreaticoduodenal Compartment

Fluid originating from the body and tail of the pancreas in the pancreaticoduodenal compartment is generally not limited to this area but may transgress into the left retroperitoneal colonic compartment or dissect into the left retromesenteric colonic plane (Figs. 8–110 through 8–112). From there onward it may communicate with the retrorenal space (Fig. 8–112) at the level of the pancreaticoduodenal compartment or more cranially surround the superior part of the perirenal space (Fig. 8–113), and it may sometimes communicate with the lateroconal interfascial space posterior to the ascending and descending colon. It may also spread into the root of the transverse mesocolon (Figs. 8–110 and 8–112) and continue along the splenorenal and phrenicocolic ligaments. Fluid originating from the head of the pancreas may spread via the transverse mesocolon into the right colonic compartment at the hepatic flexure and inferiorly (Fig. 8–112). Also, it can dissect into the right retromesenteric colonic plane (Figs. 8–110, 8–112, 8–114, 8–115). Finally, fluid can dissect into the retropancreaticoduodenal plane posterior to the pancreatic head and duodenum (Figs. 8–112 and 8–114) and along mesenteric vessels into the small bowel mesentery.

Retromesenteric Plane Fluid Collections

Retromesenteric plane fluid collections are well-defined planes anterior to the perirenal spaces and posterior to the pancreas, duodenum, and right and left colonic compartments. Because of the presence of primitive roots of the dorsal mesenteries in the midline, communication across the midline is only possible where fusion planes cross the midline, as especially occurs behind the horizontal portion of the duodenum, just inferior to the superior mesenteric artery (Figs. 8–114 and 8–116). Cranially, the extension of the retromesenteric fluid is usually to the bare area of the stomach (Fig. 8–113) and dorsally around the lateral border of the perirenal space into the retrorenal space and/or the lateroconal space (Figs. 8–112, 8–113, 8–115).

Retrorenal Plane Fluid Collections

The dissectable, potential planes of the bilateral posterior renal fascia communicate with the bilateral retromesenteric planes and lateroconal space, typically without involving perirenal fat and posterior pararenal fat (Figs. 8–112, 8–113, 8–115). In the presence of ascites, fluid in the posterior peritoneal recesses may have a forktailed or wishbone configuration posterior to the kidney mimicking retrorenal and lateroconal plane fluid collections.[34,53,57,158] This is probably related to the extent in which the colon and mesocolon fuse laterally with the primary posterior peritoneum. Cranially, the retrorenal plane extends medially, posterior to the perirenal fat. Caudally, its medial extent is more laterally, adjacent to the quadratus lumborum muscle. Distally, the continuation of either the combined interfascial plane, formed by the inferior blending of the anterior renal, posterior renal, and lateroconal fascia or the retrorenal plane, is to

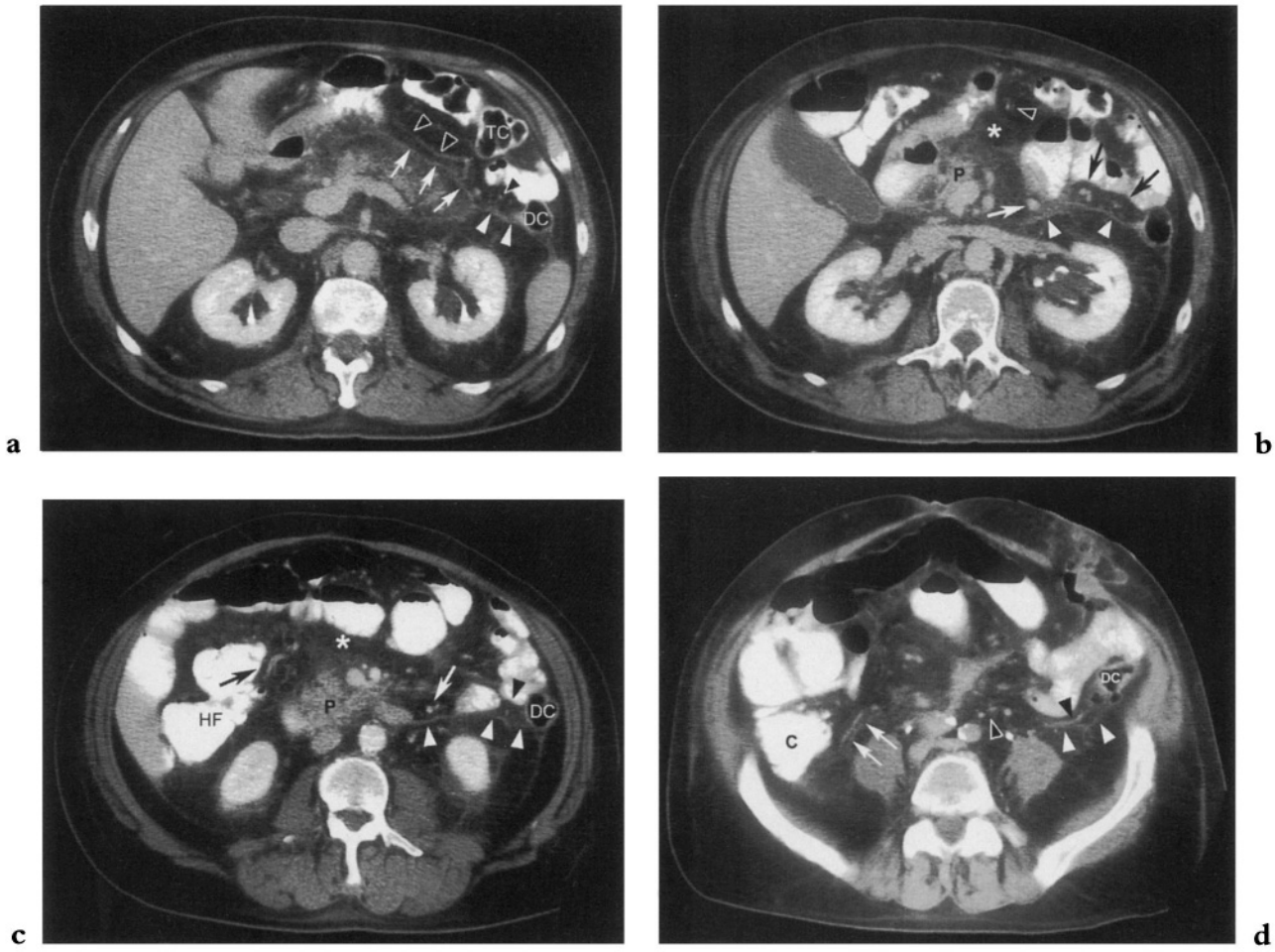


Fig. 8–109. Anatomic landmarks of the different components of the anterior pararenal space in a patient with pancreatitis.

(a) At the level of the pancreatic tail, the fusion fascia *(arrows)* dorsal to the transverse mesocolon is continuous with the left retromesenteric plane *(white arrowheads),* behind the cranial extent of the left colonic compartment. Note the vessels within the fat *(black-and-white arrowheads)* representing the continuity between middle colic vessels in the transverse mesocolon and left colic vessels within the left colonic compartment. *DC* = descending colon; *TC* = transverse colon.

(b) More caudally, at the level of the renal veins, the left colonic compartment contains the left colic vessels laterally *(black arrows)* and the inferior mesenteric vein medially *(white arrow).* Note the accentuated left retromesenteric plane *(white arrowheads).* The transverse mesocolon *(asterisk),* containing the middle colic vessels *(black-and-white arrowhead),* is attached anterior to the pancreatic neck *(P).*

(c) At the level of the lower pole of the kidneys, the upper extension of the right colonic compartment is indicated by the vessels *(black arrow)* medial to the hepatic flexure *(HF),* representing the continuity between middle and right colic vessels. The pancreatic head *(P)* is located posterior to the right colonic compartment and transverse mesocolon *(asterisk).* Note left colic vessels *(black arrowhead)* in the left colonic compartment medial to the descending colon *(DC). White arrow* = inferior mesenteric vein; *white arrowheads* = left retromesenteric plane.

(d) At the level of the aortic bifurcation, the right colic vessels are continuous with the ileocolic vessels *(white arrows),* located medial to the cecum *(C),* within the caudal extension of the right colonic compartment. The left colic vessels *(black arrowheads),* within the left colonic compartment, are continuous with the branches from the inferior mesenteric vein *(black-and-white arrowhead)* within the cranial extension of the mesosigmoid. *DC* = descending colon; *white arrowheads* = caudal extent of left retromesenteric plane.

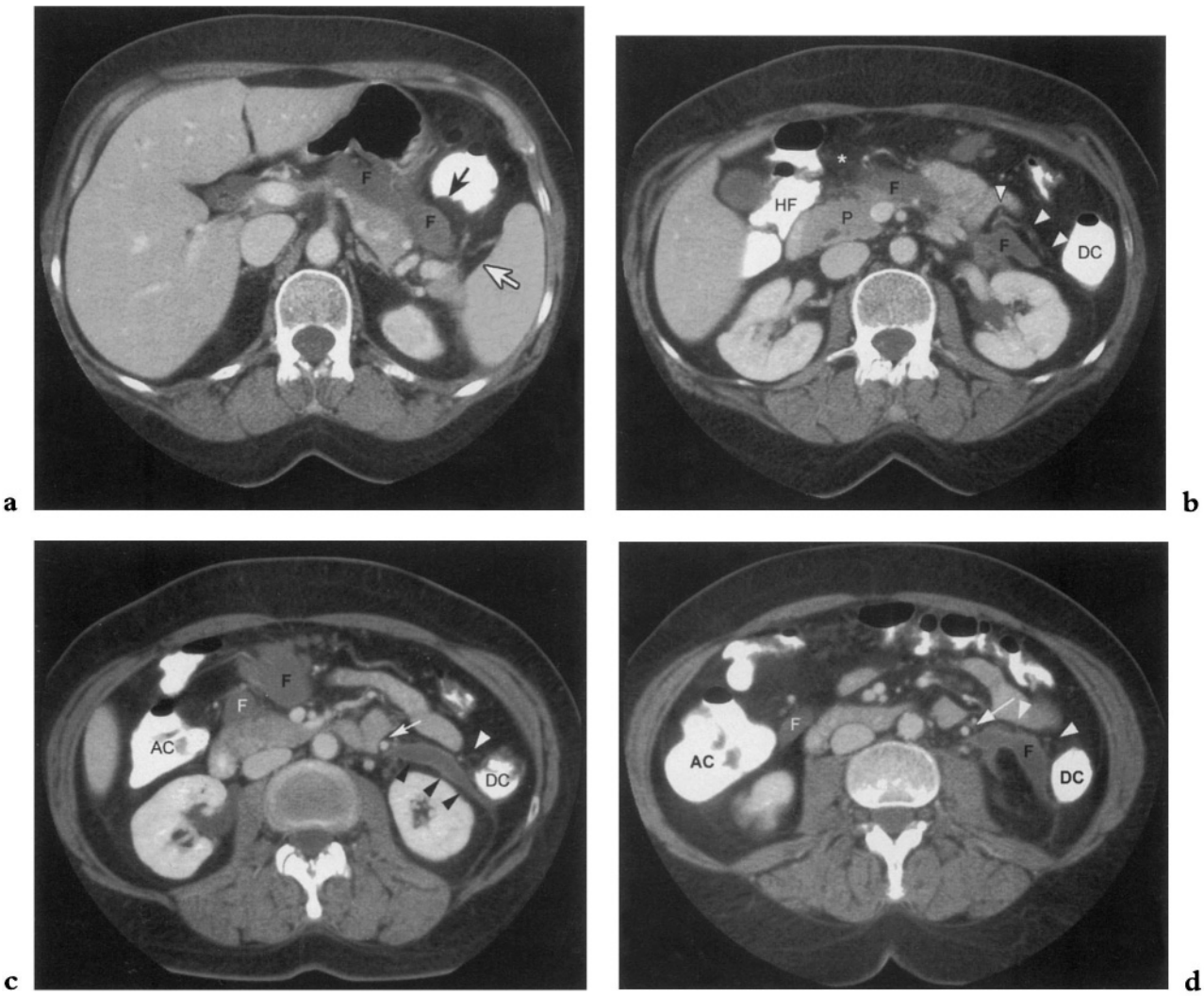


Fig. 8–110. Patient with resolving exudative pancreatitis.
(a) Cranially, fluid *(F)* is located anterior to the pancreatic tail within the left pancreaticoduodenal compartment. Note the transverse mesocolon *(black arrow)* and upper extension of the left colonic compartment *(black-and-white arrow),* anterior and lateral to the fluid collection, respectively.
(b) At the level of the pancreatic head *(P),* the fluid collection *(F)* is continuous with the left retromesenteric plane laterally and with the base of the transverse mesocolon *(asterisk)* medially. *HF* = hepatic flexure; *white arrowheads* = vessels in left colonic compartment, medial to descending colon *(DC).*
(c) More caudally, the collection *(black F)* within the base of the transverse mesocolon extends anteriorly and continues laterally within the cranial extension of the right retromesenteric plane *(white F).* The left retromesenteric collection *(arrowheads)* demarcates the left perirenal space posteriorly from the left colonic compartment anteriorly. Note the inferior mesenteric vein *(white arrow)* within the medial extension of the left colonic compartment. *AC* = ascending colon; *DC* = descending colon; *white arrowhead* = left colic vessels in left colonic compartment.
(d) Below the pancreatic head, the right and left retromesenteric fluid collections *(F)* continue posterior to the right and left colonic compartment, respectively. *AC* = ascending colon; *DC* = descending colon; *white arrow* = inferior mesenteric vein; *white arrowheads* = left colic vessels in left colonic compartment.

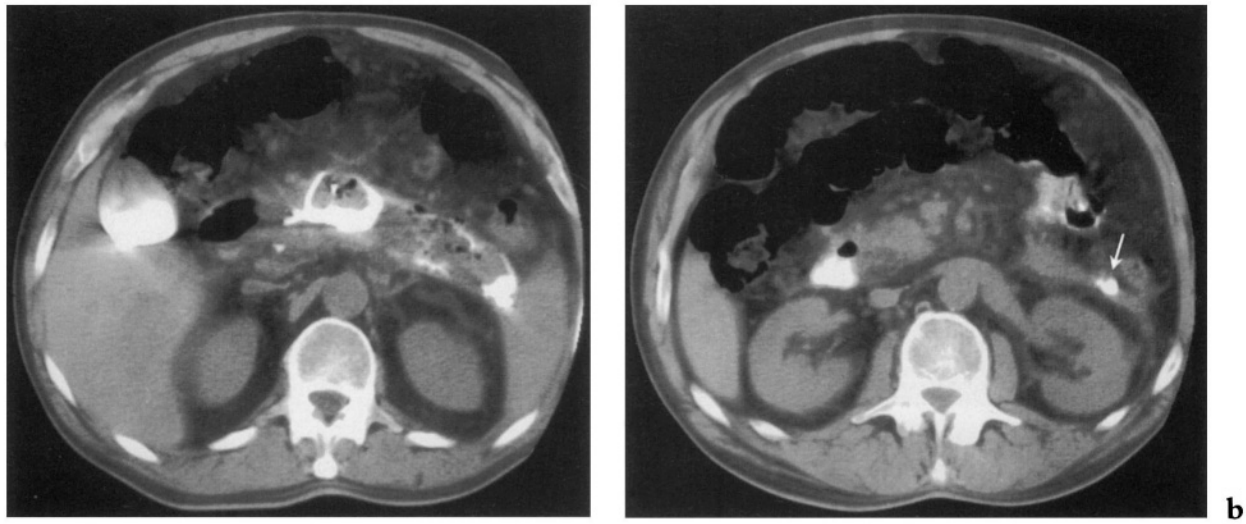


Fig. 8–111. Communications of left pancreaticoduodenal space to left retromesenteric colonic space. After catheter drainage of pancreatic abscess, contrast around the pancreas in **(a)** has spread in **(b)** to the left retromesenteric space *(arrow).*

the infraconal compartment[133] or lateral pathway,[159] abutting the psoas muscle, lateral from the ureter and the sigmoid mesocolon into the pelvis[134] (Fig. 8–112). Inferior to the cone of perirenal fat, posterior extension of retrorenal fluid between the quadratus lumborum fat pad and posterior pararenal fat can frequently be seen on CT through a well-defined defect near the lumbar triangle, the so-called inferior lumbar pathway[34] (Fig. 8–112). If the subcutaneous tissues in the flank are reached via this route or the nearby posterior pararenal space,[91] the spread of fluid may be responsible for flank discoloration (Grey Turner sign).

text continues on page 409

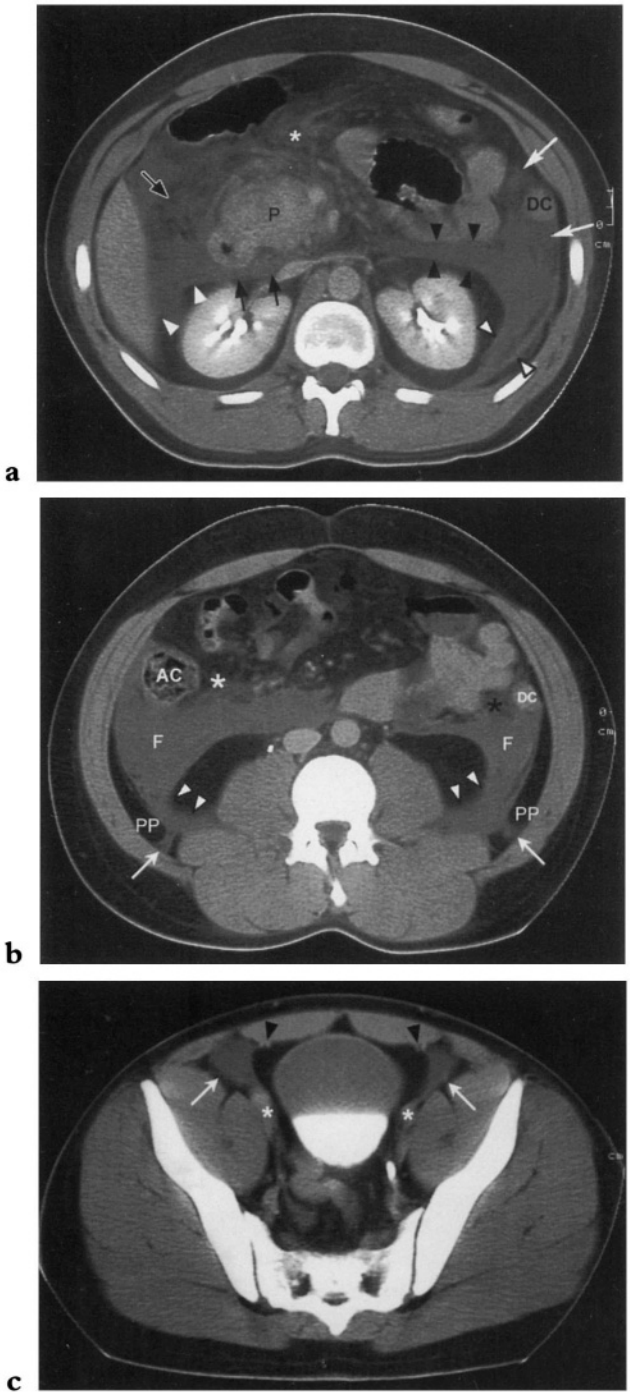


Fig. 8–112. Extensive spread of pancreatic fluid to retromesenteric and retrorenal spaces, with caudal extent.
(a) At the level of the pancreatic head *(P),* fluid is present within the left colonic compartment *(white arrows),* surrounding the descending colon *(DC),* and in the left retromesenteric plane *(black arrowheads),* left retrorenal space *(black-and-white arrowheads),* right colonic compartment *(black-and-white arrow),* right retromesenteric plane *(white arrowheads),* and retropancreaticoduodenal fusion fascia *(black arrows).* Fluid is also located ventrally in the transverse mesocolon *(asterisk).*
(b) Bilateral extension of the retrorenal spaces *(arrowheads)* through a well-defined defect *(arrows)* at the posteromedial boundary of the posterior pararenal *(PP)* space, the lumbar triangle pathway. There is no extension in the flank tissues. Although the right and left retromesenteric planes have acquired large amounts of fluid *(F),* little fluid is present within the right *(white asterisk)* and left *(black asterisk)* colonic compartments, medial to the ascending *(AC)* and descending colon *(DC),* respectively.
(c) Distal extension of fluid *(arrows)* lateral to the inferior epigastric vessels *(arrowheads)* and ventral to the external iliac vessels *(asterisks).*

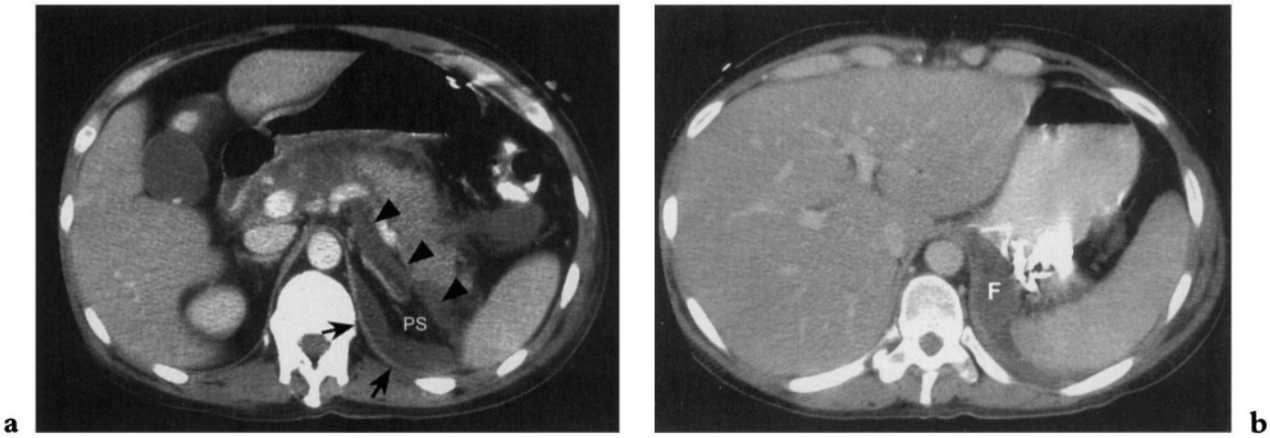


Fig. 8–113. Spread along the fusion fascia of the dorsal mesogastrium in pancreatitis.
The fusion of the dorsal mesogastrium, containing the body and part of the pancreatic tail, to the posterior primitive parietal peritoneum extends from the gastrophrenic ligament, behind the pancreatic body and over the transverse mesocolon, to the greater omentum. The lateral and medial limits are the posterior reflections of the lesser sac.
(a) At the level of the pancreatic tail, spread of fluid is discernible within the left retropancreatic fusion fascia *(arrowheads)* behind the pancreatic body and tail and in the retrorenal space *(arrows),* posterior to the superior part of the perirenal space *(PS).*
(b) At the level of the bare area of the stomach, fluid *(F)* has spread to the gastrophrenic ligament.

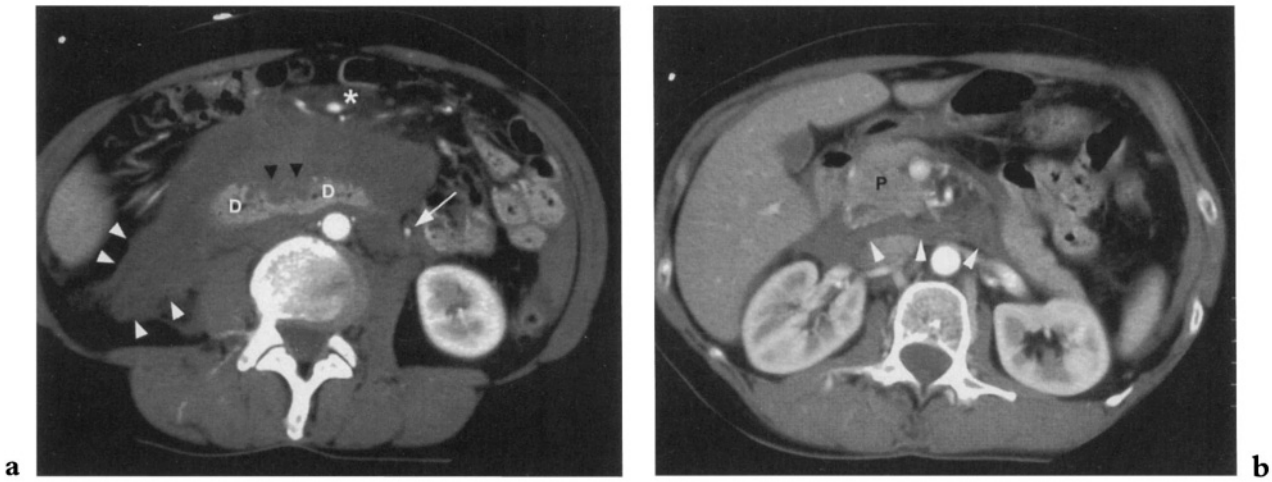


Fig. 8–114. Retroperitoneal hemorrhage due to traumatic duodenal rupture.
(a) At the level of the duodenum *(D),* a large fluid collection in the pancreaticoduodenal compartment, posterior to the mesenteric root *(asterisk),* surrounds the duodenum *(D)* and extends into the right retromesenteric plane *(arrowheads). Black arrowheads* indicate traumatic disrupture of duodenal wall. *White arrow* = inferior mesenteric vein.
(b) Cranially, at the level of the pancreatic head *(P),* midline continuation *(arrowheads)* is present within the cranial extension of the retropancreaticoduodenal fusion fascia.

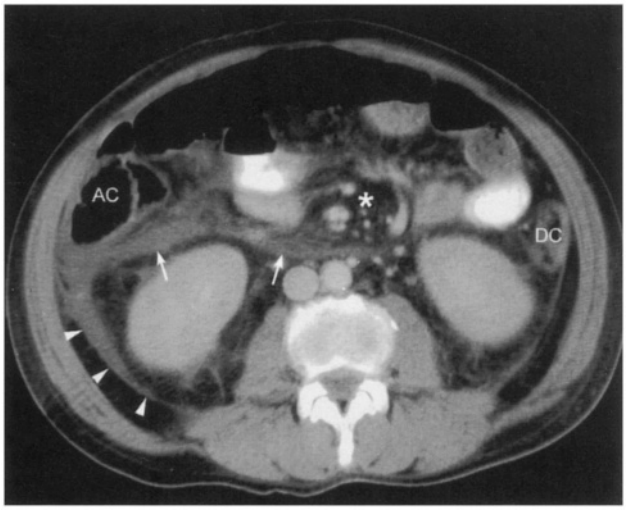


Fig. 8–115. Duodenal perforation during ERCP.
Note the right retromesenteric plane involvement *(arrows)* with midline continuation posterior to the mesenteric root *(asterisk).* Note also the extension within the right retrorenal space *(arrowheads). AC* = ascending colon; *DC* = descending colon.

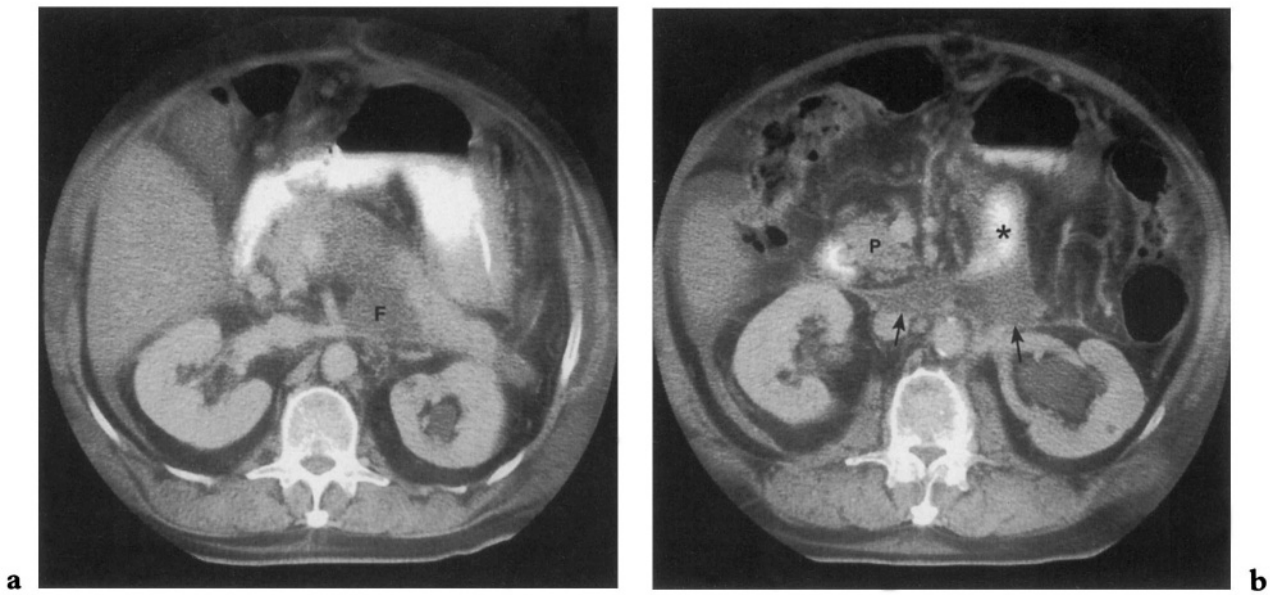


Fig. 8–116. Left–right communication in a patient with pancreatitis.
(a) At the level of the origin of the superior mesenteric artery, only left-sided dorsal fluid *(F)* is present behind the pancreatic body and tail.
(b) Below this level, fluid *(F)* within the retropancreaticoduodenal fusion fascia indicates left–right communication *(arrows)* in the midline. *Black asterisk* = duodenojejunal junction; *P* = pancreatic head.

Perirenal Space

Roentgen Anatomy of Distribution and Localization of Collections

The perirenal space on each side is distinctly defined by the cone of renal fascia (Figs. 8–117 through 8–119).

Selective opacification of this compartment in the cadaver permits identification of the preferential pathway of spread and the characteristic localizing features. This is shown in Figure 8–120. The space is surprisingly capacious, and distention yields a typical outline. The injection study demonstrates that the lower border of the distended cone of renal fascia presents a diagnostic silhouette, inferiorly convex, overlying the region of the iliac crest. Some acute traumatic episodes provide an *in vivo* model and confirm these investigational observations (Figs. 8–121 and 8–122). This outline is the hallmark of perirenal collections, and its identification, therefore, on plain films as well as on other studies (Fig. 8–123) serves reliably to localize a disease process immediately.

The significant criteria for the localization and distinction of collections within the perirenal space are outlined in Table 8–1 on page 360.

Sources of Effusions

The overwhelming majority of perirenal *abscesses* are secondary to a renal infection. The underlying condition is most often pyelonephritis, tuberculosis, or carbuncle. Perforation of the renal capsule then leads to contamination of the perirenal space.

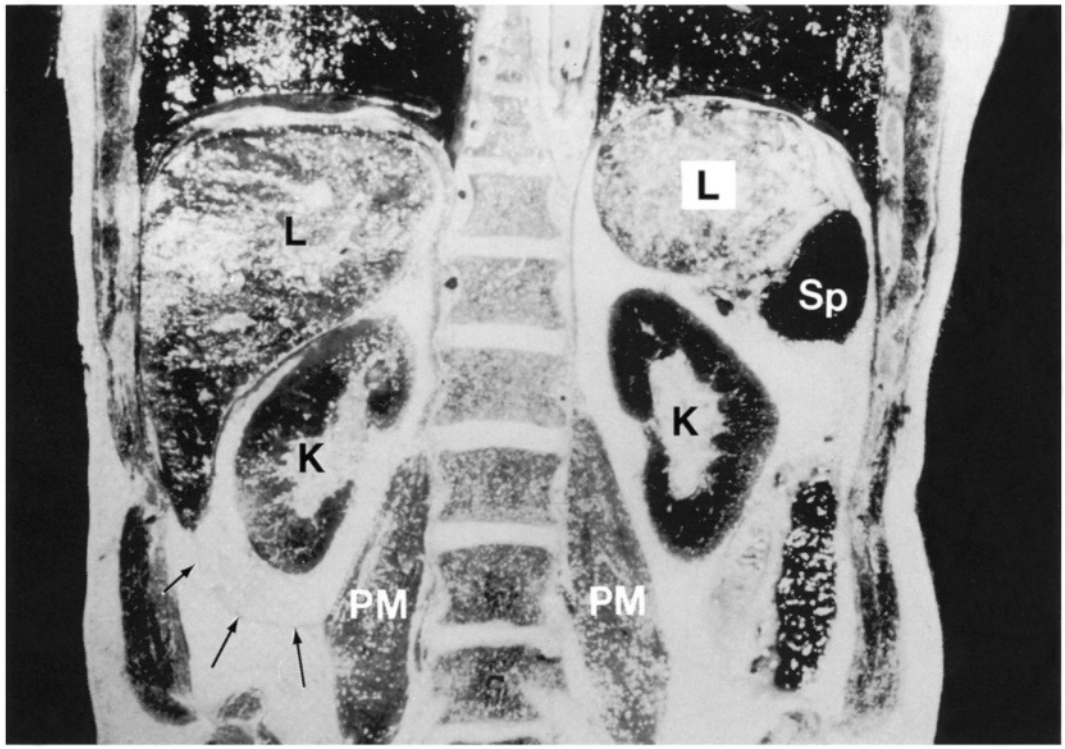


Fig. 8–117. Coronal anatomic section.
The cone of renal fascia *(arrows)* envelops the adrenal gland, kidney *(K),* and perirenal fat. Medially it blends with the fascia of the psoas muscle *(PM).* The perirenal fat is particularly abundant in relationship to the lower pole of the kidney. The hepatic angle abuts on pararenal and perirenal fat. *L* = liver; *Sp* = spleen.
(Courtesy of Manuel Viamonte, Jr., M.D., Mt. Sinai Hospital, Miami Beach, FL.)

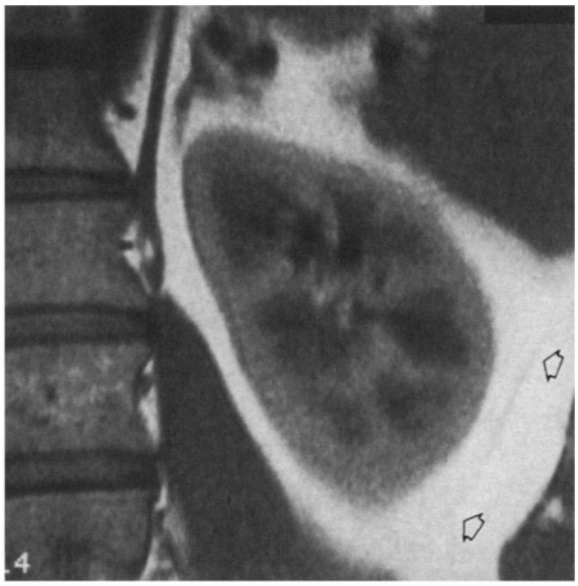
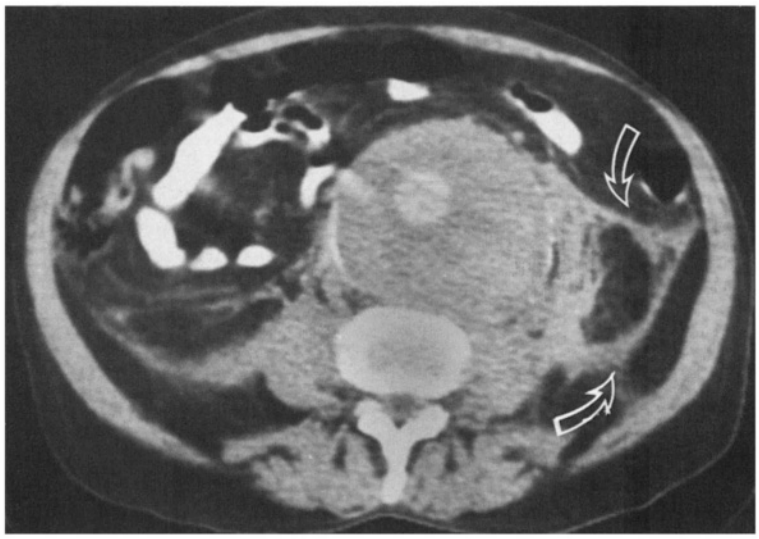
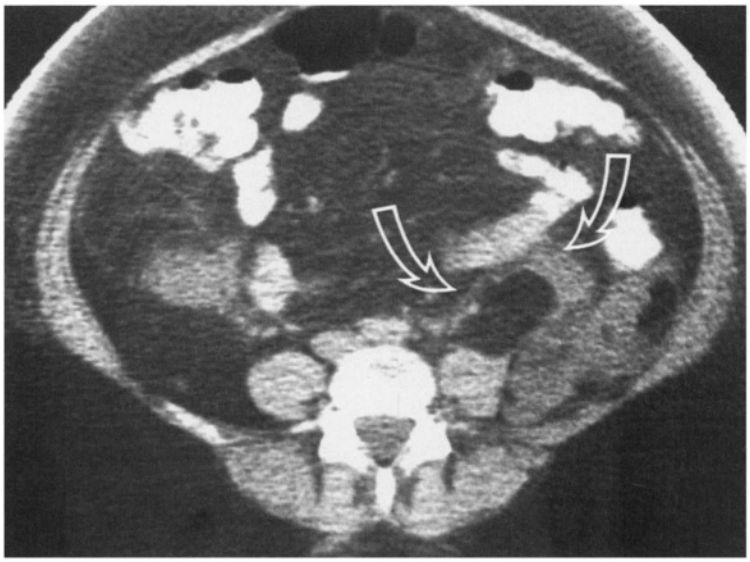


Fig. 8–118. The edge of the cone and lateroconal fascia *(arrows)* seen by magnetic resonance imaging on coronal plane.



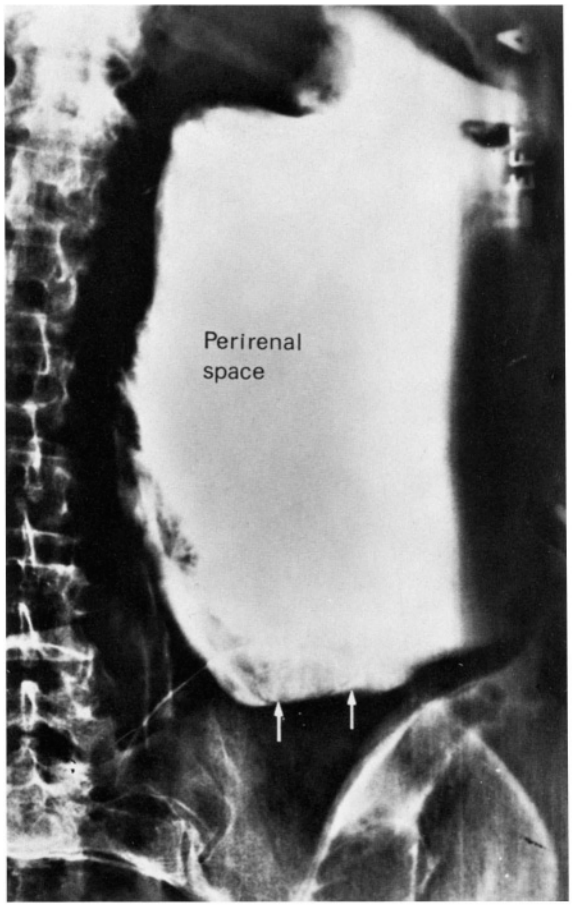
a



b

Fig. 8–119. The lower cone of renal fascia.
CT shows the narrowed cone of renal fascia on the left near its inferior apex *(arrows)* just above the level of the iliac crests in two different patients. Thickening and adjacent changes render it visible secondary to **(a)** a leaking abdominal aortic aneurysm and **(b)** pancreatitis.

Fig. 8–120. Postmortem injection into the perirenal space.
After the introduction of 450 mL of contrast medium, the distended cone of renal fascia is vertical and presents an inferiorly convex border overlying the iliac crest *(arrows).* This contour is highly characteristic of acute fluid distention of the perirenal space.
(Reproduced from Meyers et al.[12])



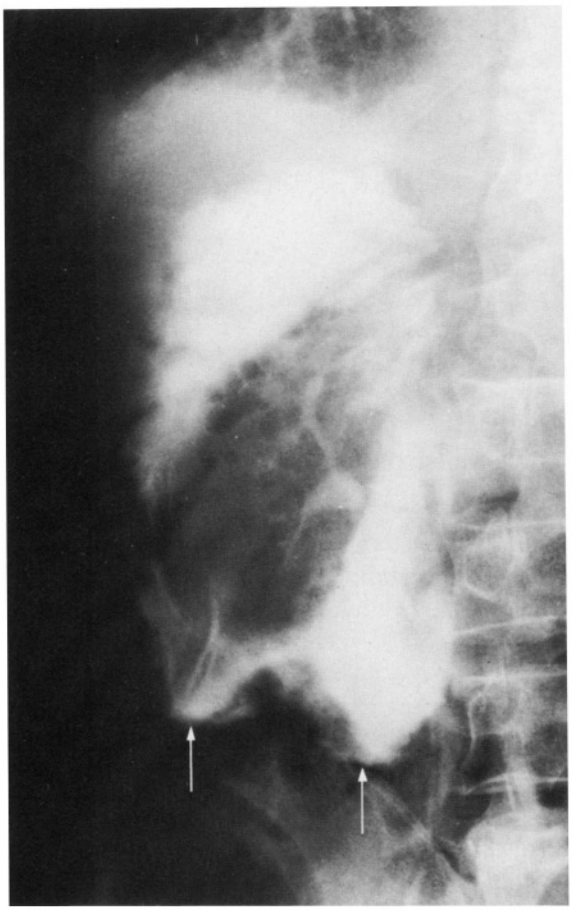


Fig. 8–121. Opacification of the perirenal space, occurring as a complication of attempted selective renal venography.
The distended cone extends to the level of the iliac crest. At this level, pressure from the overlying hepatic flexure disrupts the typical inferiorly convex border *(arrows).*

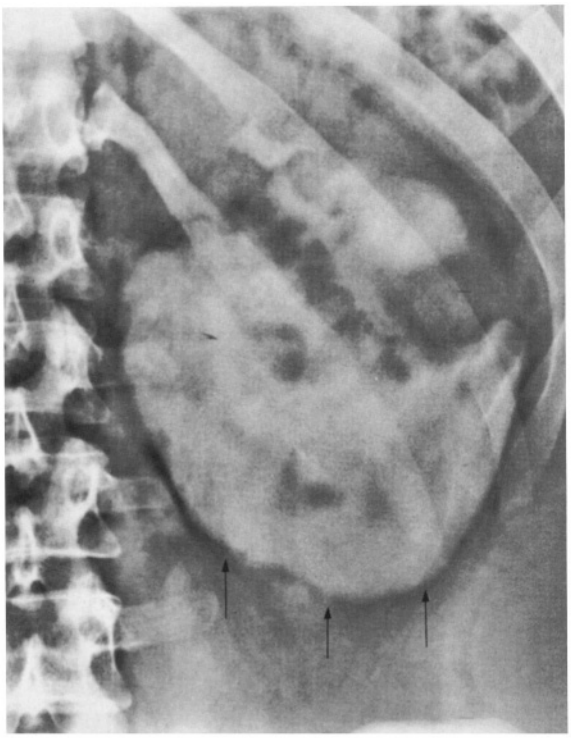


Fig. 8–122. Opacification of the perirenal space.
Gross extravasation during high-dose urography in a case of traumatic fracture of the kidney opacifies the distended perirenal space, demonstrating its convex lower contour *(arrows).*

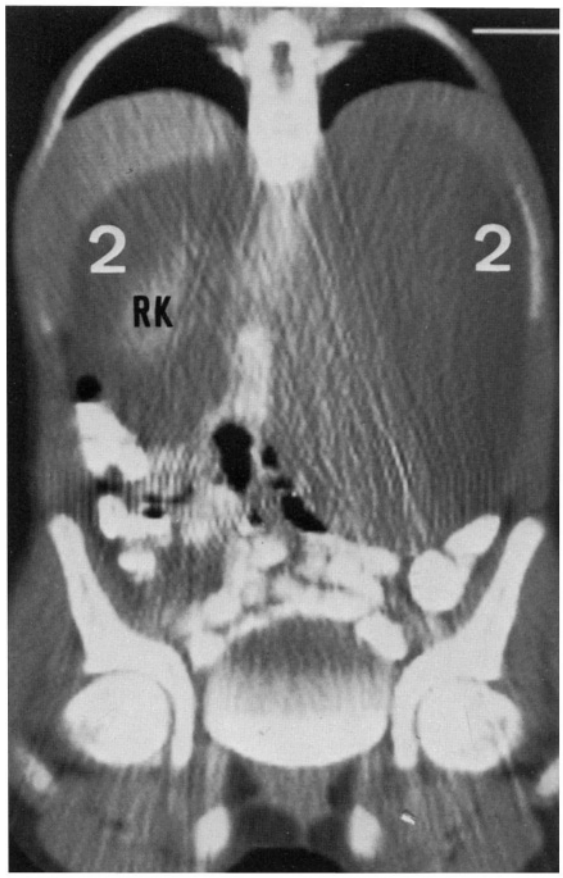


Fig. 8–123. The distended perirenal space.
Direct coronal CT section reveals fluid collections in both perirenal spaces *(2).* The distended cone of renal fascia on the left extends more inferiorly to the level of the iliac crest. *RK* = right kidney.
(Reproduced from Feldberg.[17])

Two predominant forms are encountered. An acute gas-producing infection can diffusely involve the perirenal compartment. It is secondary to *Escherichia coli, Aerobacter aerogenes,* or, rarely, *Clostridium* and develops especially in diabetics. Or, the infection may localize within the perirenal fat as a coalescent abscess. The offending organism is usually *E. coli, B. proteus,* or a streptococcus. Bilateral involvement is rare and is secondary to bilateral renal infections. In children, hematogenous spread occasionally occurs to the perirenal fat from remote sites of infection, such as furunculosis, wound infection, or upper respiratory disease.[160]

Chronic extravasation of *urine* into the perirenal compartment is a result of perforation of the collecting system. The collection develops as a uriniferous perirenal pseudocyst (urinoma).

Hematomas within the perirenal space as well as within the subcapsular zone, are secondary to trauma or to lesions of the kidneys and their blood vessels, ranging from neoplasms to periarteritis nodosa.[161]

Perirenal Gas-Producing Infection

The radiologic features of a perirenal space gas-producing infection are distinctive. Its recognition is related directly to an understanding of the characteristic appearance of the acutely distended cone of renal fascia and the preferential spread through the rich perirenal fat dorsal to the kidney.

The gas may encircle the kidney or present as a mottled collection of radiolucencies within the shadows of the perirenal fat. Figure 8–124 illustrates the typical distribution in a diabetic female. Three characteristic features localize the infection to the perirenal space:

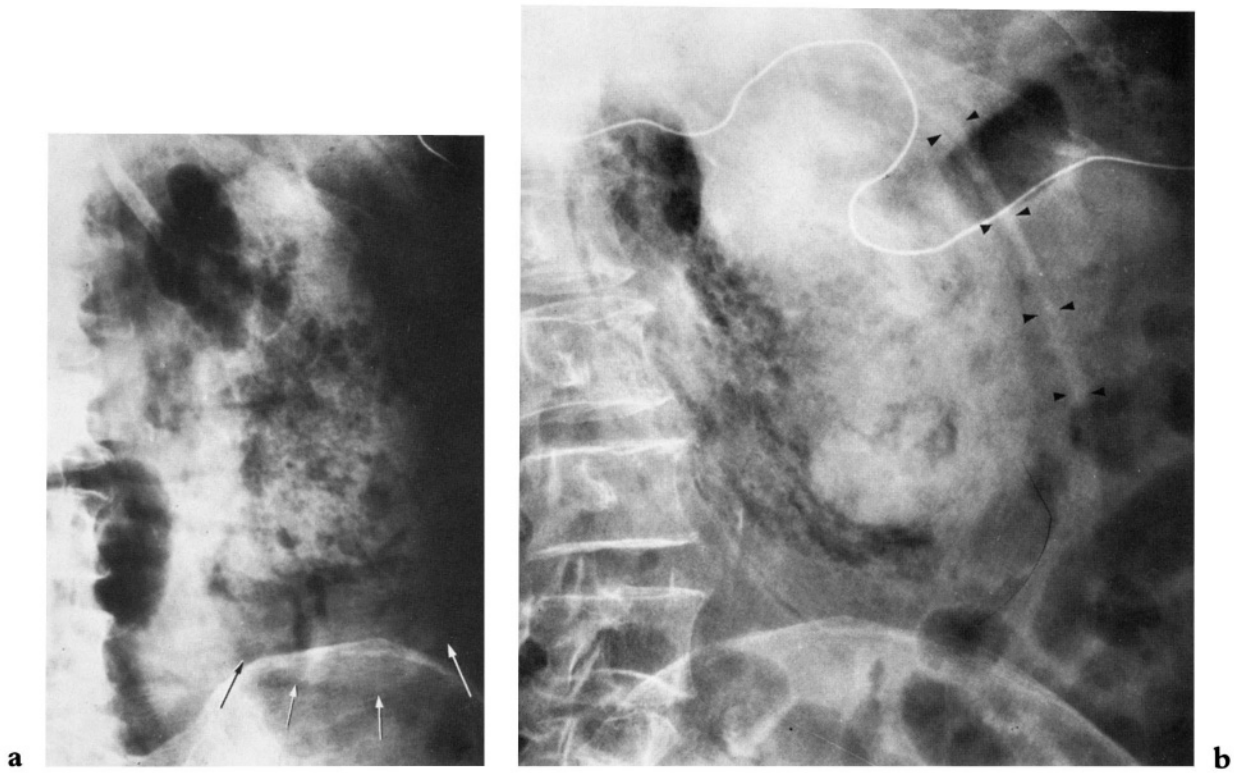


Fig. 8–124. Acute gas-producing left perirenal abscess.
(a) In addition to the mottled gaseous radiolucencies, fluid distention of the renal fascial cone overlies the iliac crest, presenting a typical convex inferior border *(arrows).*
(b) Oblique view demonstrates the preponderance of gas and fluid in the perirenal fat dorsal to the kidney. Inflammatory thickening of the anterior renal fascia is shown as a striplike density *(arrowheads).*
(Reproduced from Meyers.[8])

1. Associated exudate distends the cone of renal fascia so that its lower border can be identified as an inferiorly convex shadow overlying the iliac crest.
2. The gas is most prominent within the rich fat posterior to the kidney.
3. Inflammatory thickening of the renal fascia itself may be seen.

The inferiorly convex border of the distended perirenal space is a highly reliable localizing sign (Fig. 8–125). Figure 8–126a demonstrates this finding at an early stage in a diabetic patient with pyelonephritis and fever. Twenty-four hours later (Fig. 8–126b), a diffuse gas-producing infection of the perirenal space becomes apparent. When localization occurs, it preferentially develops posterior to the kidney (Fig. 8–127).

Fulminating infection may disrupt the perirenal fascial boundaries, allowing the gas to escape to other compartments. Figure 8–128 demonstrates acute fascial violation with direct extension into the flank fat. The resulting decompression of the perirenal space may not distend it to the level of the iliac crest, but it tends to maintain a diagnostic silhouette with an inferiorly convex lower border.

Bilateral perirenal gas-producing infections are unusual but their contours are again distinctive (Fig. 8–129). In such instances, septic emboli or retrograde pyelonephritis from the bladder should be particularly considered.

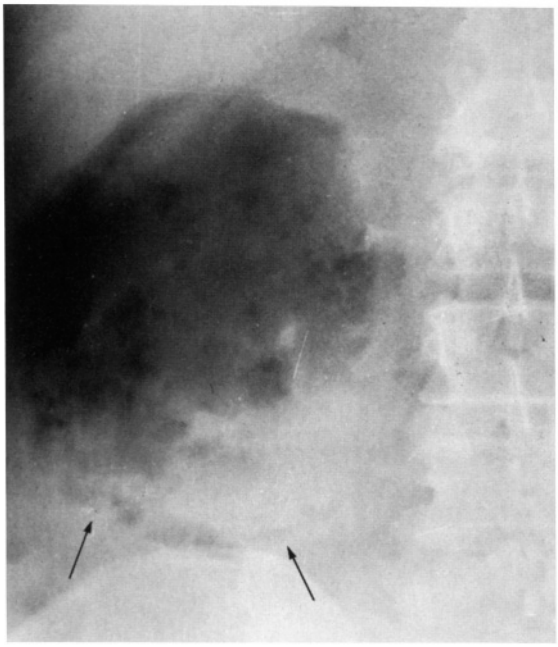


Fig. 8–125. Right perirenal gas-producing infection in a diabetic.
A convex lower border *(arrows)* at the level of the iliac crest characterizes the distended cone of renal fascia.



Fig. 8–126. Acute gas-producing perirenal infection.
(a) In addition to a few ill-defined mottled lucencies in the right flank, a crescentic gas collection *(arrows)* overlies the iliac crest.
(b) The next day, extensive infection developed throughout the perirenal space.



Fig. 8–127. Localized gas-producing perirenal infection.
The process has localized behind the kidney, displacing it anteriorly (lateral view, retrograde study).

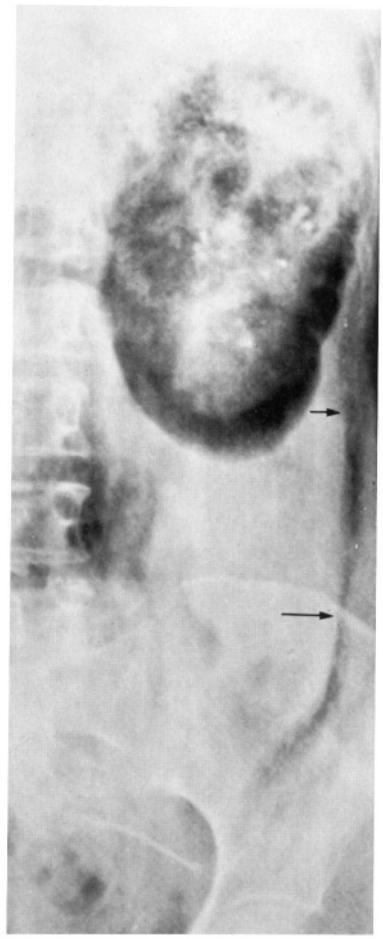


Fig. 8–128. Perirenal gas-producing infection.
The process has broken into and extends down the flank fat *(arrows).*

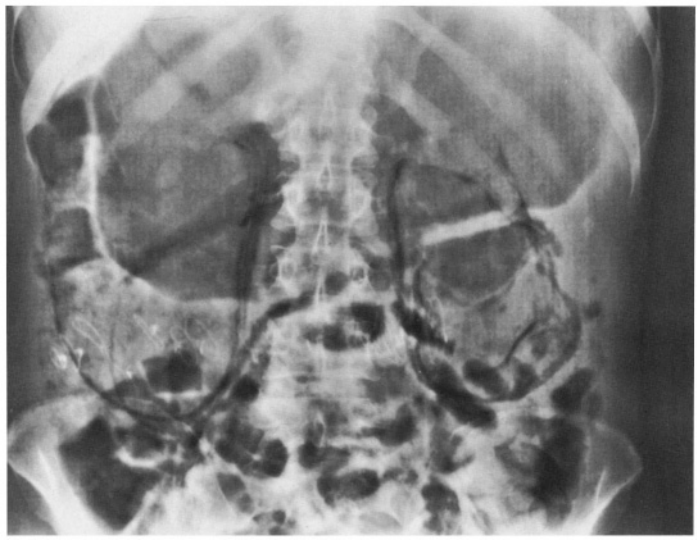


Fig. 8–129. Bilateral perirenal gas-producing infections.

Perirenal Abscess

Initially, fluid introduced into the perirenal space is evenly dispersed throughout the perirenal fat. Preferential flow then seeks the abundant fat dorsolateral to the lower pole of the kidney[8,12] (Figs. 8–130 through 8–133). The exudate is guided by gravity along the path of least resistance. This natural drainage is also illustrated in Figure 8–134, in which a portion of a large staghorn calculus has eroded through the kidney to ultimately seek out the area of rich fat behind and lateral to the lower pole. It is important to understand that the coalescence at this particular site forms the basis for the radiologic identification of most perirenal abscesses.[8,12]

As a rule, a single finding is nonspecific because it may be due to some other disease. But in combination, radiologic signs usually permit the correct diagnosis.[162]

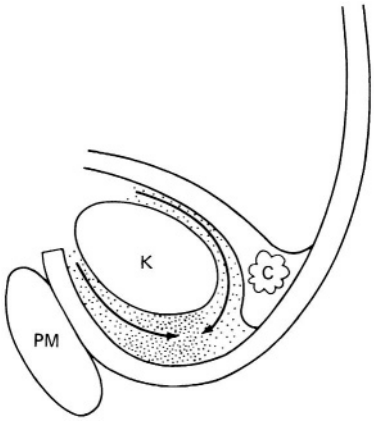


Fig. 8–130. Coalescence of perirenal effusions.
This typically develops behind and somewhat lateral to the lower pole of the kidney. *K* = kidney; *C* = colon; *PM* = psoas muscle.

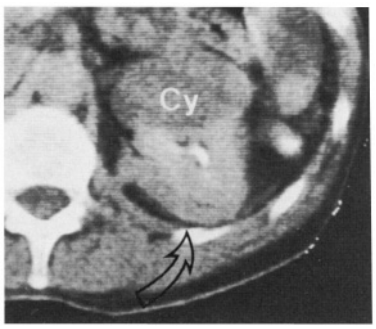


Fig. 8–131. Perirenal hematoma.
This clinical case, in the early CT experience, serves as an *in vivo* model documenting the flow and coalescence of perirenal effusions. Following percutaneous puncture of a left renal cyst (*Cy*), CT scan shows a collection of blood *(arrow)* localized to the perirenal fat behind the kidney.

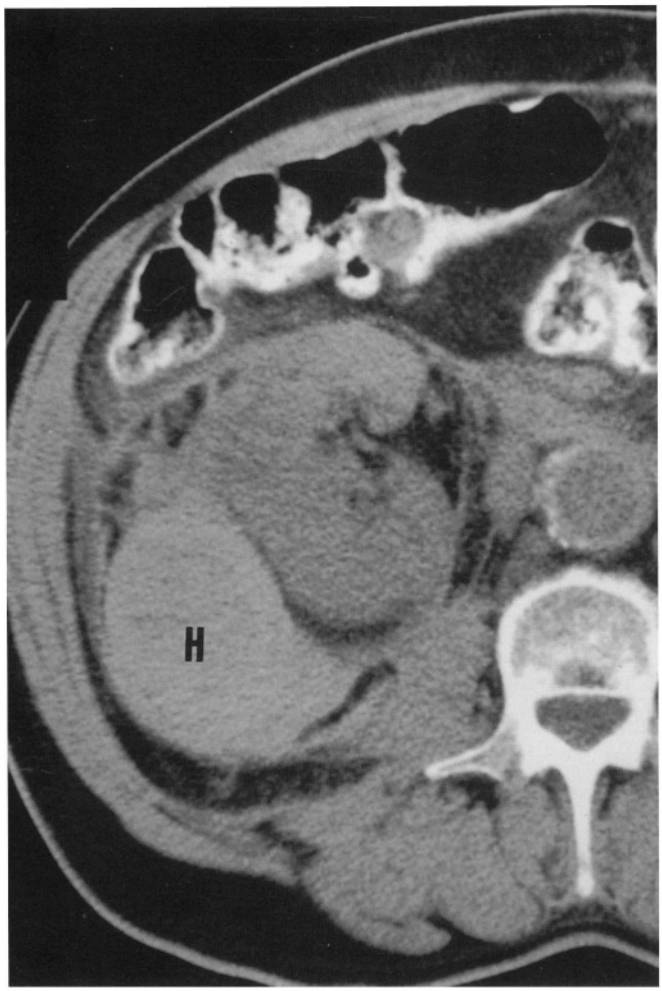


Fig. 8–132. Acute perirenal hematoma.
Unenhanced CT shows a high attenuation hematoma (*H*) posterolateral to the kidney, displacing it anteriorly, medially, and superiorly. The perirenal fascia is thickened, and there is tracking of blood along some of the bridging renal septa.
(Courtesy of Jay P. Heiken, M.D., Mallinckrodt Institute of Radiology, St. Louis, MO.)

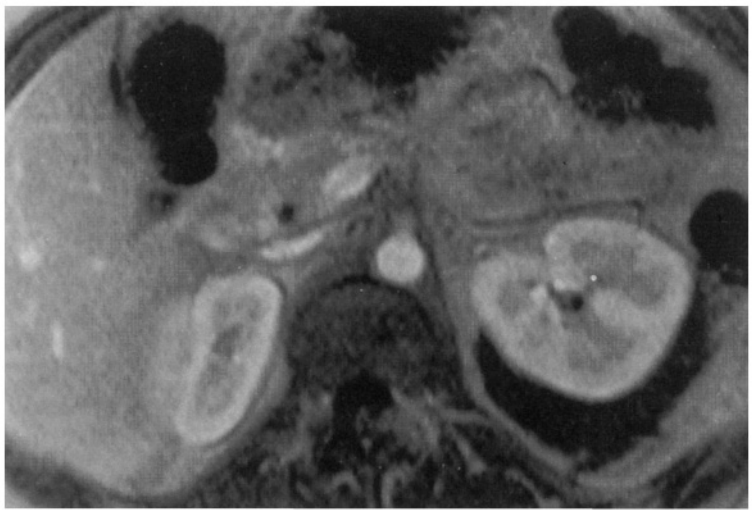


Fig. 8–133. Perirenal hematoma after biopsy.
T1-weighted fat-suppressed postgadolinium MR image demonstrates subacute blood, low in signal intensity, localized in the perirenal fat behind the left kidney.
(Reproduced from Semelka RC, Ascher SM, Reinhold C: MRI of the Abdomen and Pelvis: A Text-Atlas. Wiley-Liss, New York, 1997, with permission.)

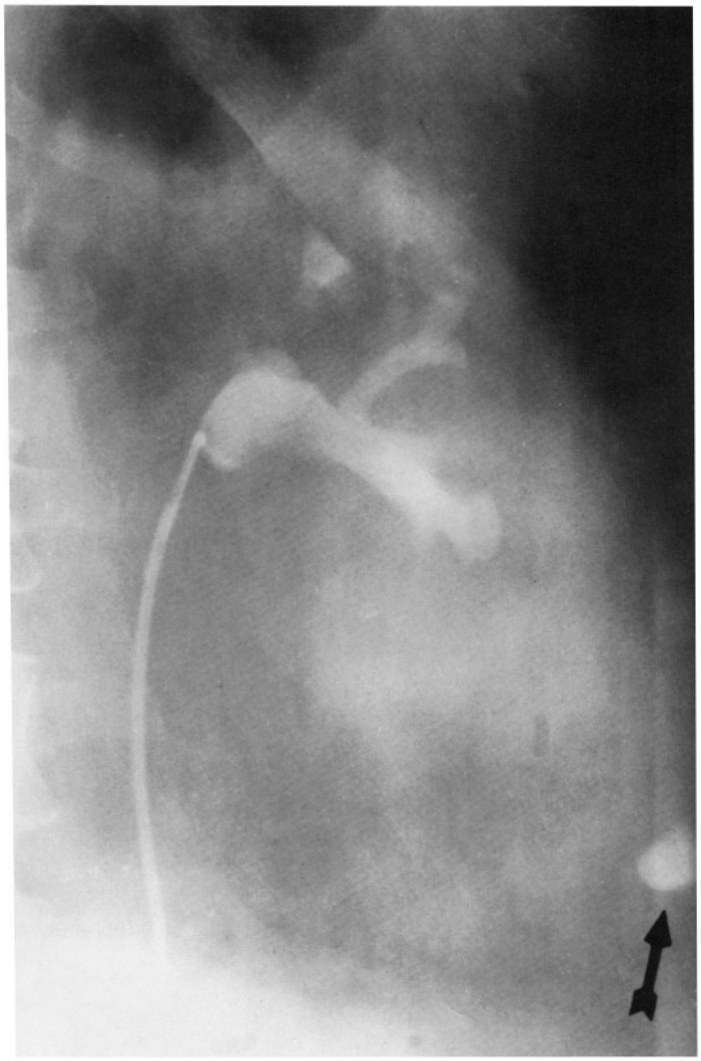


Fig. 8–134. Chipped piece of staghorn calculus *(arrow).*
This has gravitated to the rich perirenal fat behind and lateral to the lower pole of the kidney. Plain film with opaque ureteral catheter.

For practical application, roentgen signs may be divided into primary and secondary groups. *Primary roentgen signs* include the following (Figs. 8–135 through 8–140):

1. *Loss of definition of the lower renal outline* with increased density or an identifiable discrete mass in the region of the kidney.

2. *Displacement and, perhaps, axial rotation of the kidney.* The lower pole is displaced medially, upward, and anteriorly, and the kidney may be rotated about its vertical axis. On frontal supine films, the affected kidney may appear larger because of magnification; a lateral film will then document its anterior displacement. The suspected side should be dependent for the lateral view since in this position a kidney in its normal location does not project anterior to the lumbar spine.

3. *Loss of the upper segment of the psoas muscle margin.*

4. *Extrinsic compression of the renal pelvis and proximal ureter.* The mass tends to press from the lateral aspect so that the proximal ureter may also be displaced anteriorly over the psoas muscle as well as medially. Compression may be severe enough to cause dilatation of the upper collecting system.

5. *Fixation of the kidney.* Normal renal mobility of 2–6 cm can be shown on erect views or with respiratory excursions.[163] A perirenal process tends to fix the kidney in most patients.

6. *Extravasation into the perirenal space.* Communication of the collecting system with the perirenal compartment is presumptive evidence of a perirenal abscess in all but the most acute circumstances. The extravasation may be demonstrated by retrograde pyelography or fistulography.

7. *Displacement of contiguous bowel.* A collection of pus in the perirenal compartment may produce a mass effect on adjacent intestine. On the right, the descending duodenum may be displaced medially and anteriorly and the hepatic flexure of the colon downward. On the left, the distal transverse colon may be displaced superiorly or inferiorly and the duodenojejunal junction medially.

8. *Arteriographic findings.* Arteriography has been of particular value in the past in cases where the conventional radiographic findings are uncertain or where primary renal infection is suspected to extend through the capsule. The angiogram may define the size and location of the abscess. Characteristically, the findings include an

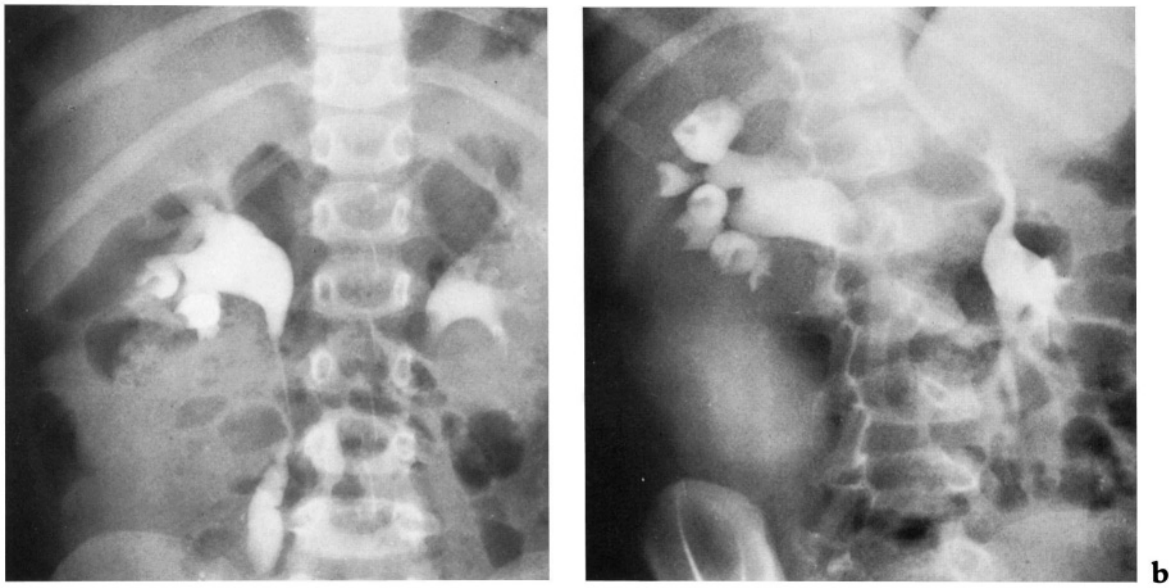


Fig. 8–135. Right perirenal abscess.
The infection is localized behind the lower pole, resulting in anterior, medial, and superior displacement of the kidney.
(a) The affected kidney appears larger because of the magnification resulting from its anterior displacement. There is loss of the renal outline and the hepatic angle. Extension of the infection along the ureter has caused mild ureteropelvic obstruction.
(b) On oblique projection, the abscess itself is visualized as a mass density.
(Reproduced from Meyers.[8])

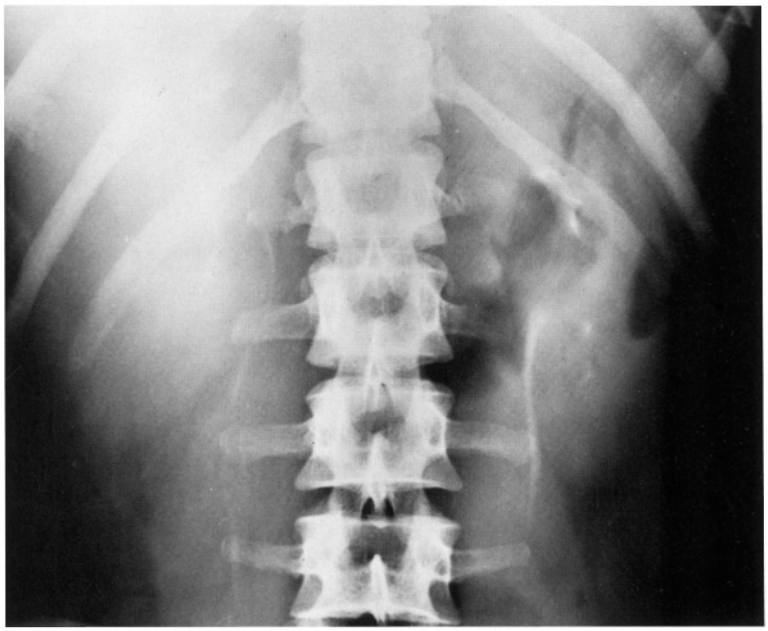


Fig. 8–136. Right perirenal abscess.
The collection in the dorsolateral fat near the lower pole displaces the kidney upward and medially, deflects the upper ureter medially, and obscures the proximal psoas margin. Note the loss of contrast of the perirenal fat and renal outline. (Reproduced from Evans et al.[162])



Fig. 8–137. Perirenal abscess.
Retrograde pyelogram shows characteristic upward and medial displacement of the kidney and proximal ureter with axial rotation of the kidney by a large mass. There is loss of visualization of the renal outline and psoas margin. (Reproduced from Evans et al.[162])

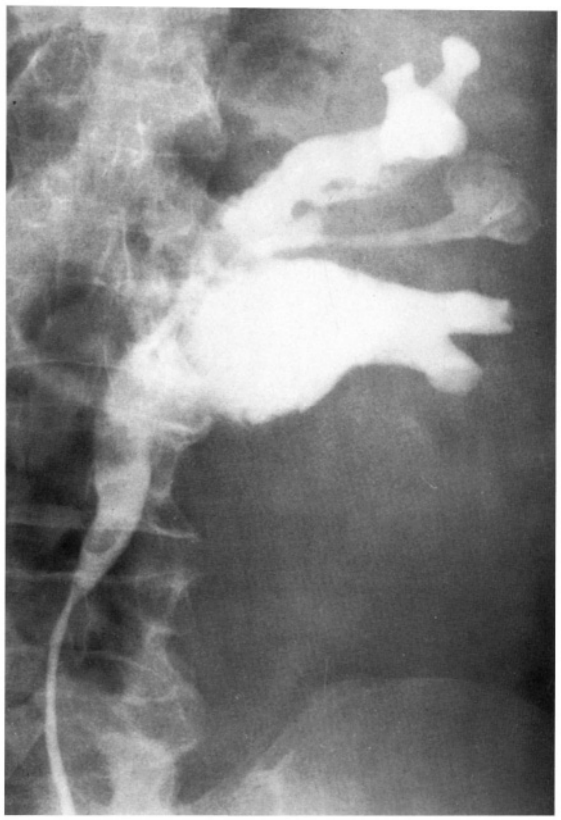


Fig. 8–138. Large left perirenal abscess.
This displaces the lower pole anteromedially and results in renal magnification. Gross inflammatory disease involves the collecting system.
(Reproduced from Meyers.[8])



Fig. 8–139. Extensive perirenal abscess draining into the iliac fossa beyond the confines of the renal fascia.
The abscess originated from a lower calyx *(arrow)* in a kidney involved by severe pyonephrosis.

increased number and size of perforating arteries extending from the kidney, stretching of tortuous and prominent capsular and, perhaps, pelvic arteries around the margin of the abscess, and a contrast blush.

9. *Infiltration of flank stripe.* This indicates fulminating and widespread extension into the adjacent tissues.

Secondary roentgen signs include the following:

1. *Scoliosis.* This occurs in less than half the patients with perirenal abscess.

2. *Restriction of diaphragmatic motility and pulmonary basilar changes.* Nesbit and Dick[164] showed that of 85 patients with perirenal abscess, 14 (16.5%) had pulmonary complications. These may vary from a minimal pleuritis to effusion, pneumonia, and nephrobronchial fistula. Excursion of the ipsilateral hemidiaphragm, especially its posterior segment, may be restricted or absent.

Other localization may be encountered (Fig. 8–141).

Treatment of perirenal abscesses is included in the discussion on pages 439 and 444.

Uriniferous Perirenal Pseudocyst (Urinoma)

A unique type of perirenal collection is acutely extravasated urine secondary to ureteral obstruction or laceration[165] (Figs. 8–142 and 8–143). It has been long established that chronic partial obstruction with repeated pyelosinus backflow may lead to uriniferous pseudocyst formation.[166]

The chronic extravasation of urine into the extraperitoneal tissues around the kidney and upper part of the ureter, leading to an encapsulated collection, is a distinct clinical and radiologic entity. The condition has been given a variety of confusing names, including

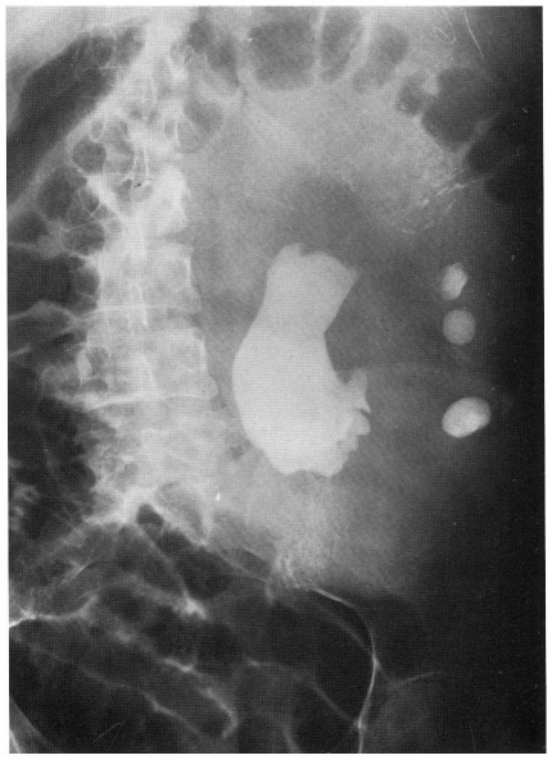


Fig. 8–140. Massive perirenal abscess secondary to calculous pyonephrosis.
Plain film shows increased density, loss of kidney outline, and numerous renal calculi. The abscess has displaced the transverse and descending colon.

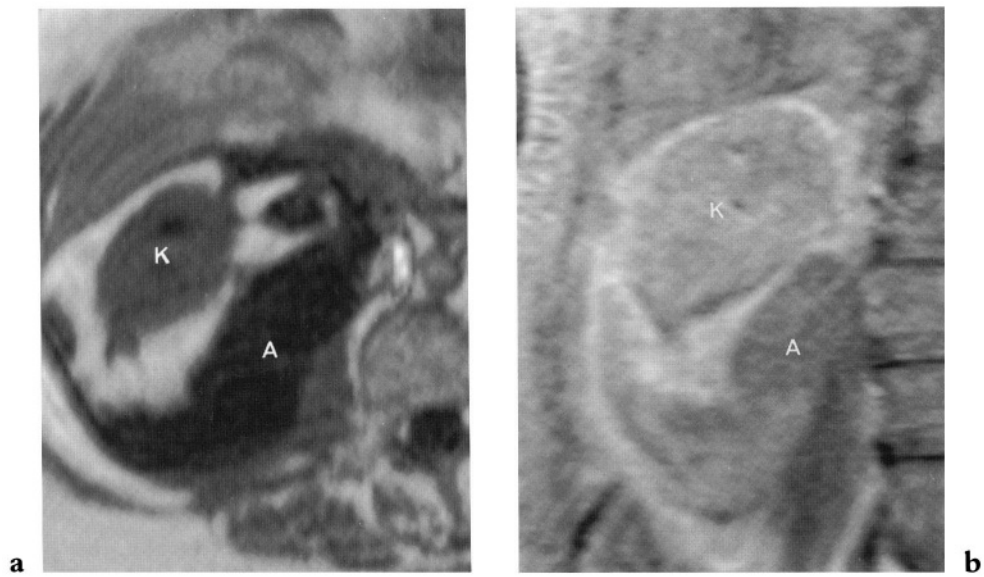


Fig. 8–141. Perirenal abscess.
In this case, MRI demonstrates the perirenal abscess *(A)* has loculated medially in relation to the lower renal pole. Note how it is precisely confined inferiorly by the cone of renal fascia. The kidney (*K*) is displaced laterally, anteriorly, and upward.
(a) T1-weighted axial view.
(b) T2-weighted coronal view.
(Courtesy of Jay P. Heiken, M.D., Mallinckrodt Institute of Radiology, St. Louis, MO.)

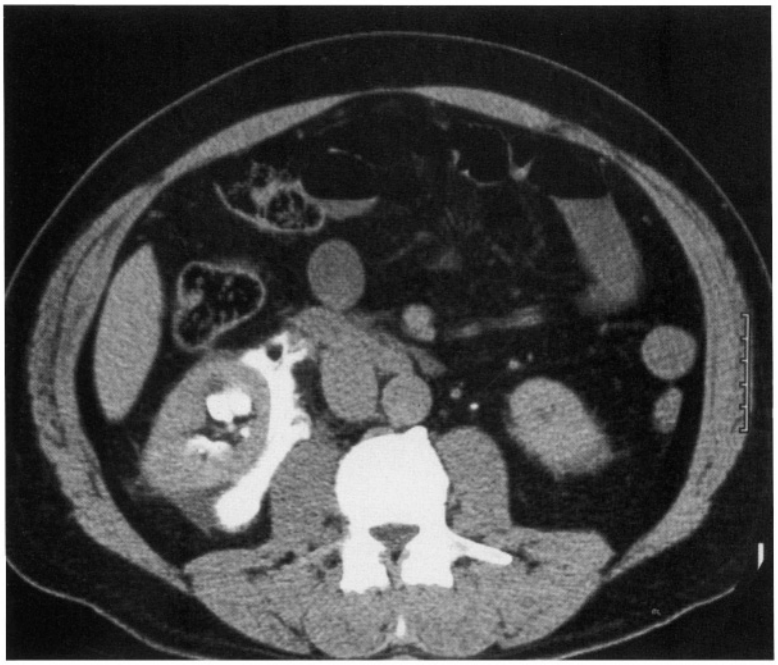


Fig. 8–142. Perirenal extravasated urine.
Enhanced CT scan shows opacified urine extravasating medially within the perirenal space.



Fig. 8–143. Early development of uriniferous perirenal pseudocyst.
CT scan at level of both kidneys shows right kidney *(K)* with mild hydronephrosis displaced anteriorly by perirenal urine collection *(arrows).* This occurred as a consequence of pyelosinus backflow secondary to partial distal ureteral obstruction from a retroperitoneal mass.

pseudohydronephrosis, hydrocele renalis, perirenal cyst, perinephric cyst, pararenal pseudocyst, and urinoma. Unfortunately, each of these terms is misleading, nonspecific, or inaccurate. To indicate its pathogenesis and characteristic morphology, I believe the most accurate designation for this condition should be uriniferous perirenal pseudocyst.[10]

Since the chronic urine extravasation occurs into the perirenal space, with aseptic inflammation and dissolution of its fat, the contents of the pseudocyst are confined by the cone of renal fascia that comes to constitute its walls.[10]

Etiology and Pathogenesis. Most cases of chronic urinary extravasation are secondary to accidental or iatrogenic trauma. Early reports stress renal and ureteral trauma from automobile accidents, football injuries, blows, falls, etc. At the time of clinical presentation, the nature of the original injury may not be recognized or may be remote in nature. More recently, instances are being encountered after surgical operations on the kidney or ureter, diagnostic cystoscopic procedures with perforation of the ureter or renal pelvis, or inadvertent trauma to the lower ureter during pelvic operations.[10] In infants and children, a congenital obstruction in the urinary tract may be an underlying factor.[167]

Three factors are necessary to produce the lesion:[168]

1. A transcapsular tear of the renal parenchyma must extend into the calyx or pelvis. Perforations of the pelvis or ureter alone are often sufficient.

2. The injury must fail to heal or fail to be sealed off with a blood clot before leakage of urine in any quantity can take place. Urinary extravasation into the perirenal fat results in rapid lipolysis, and a definite fibrous sac (false capsule or pseudocyst) is formed within 12 days.[169] Pseudocysts of up to 2,500 mL of urine have been reported. There may also be fatty, fibrous, or oily debris, altered blood clot, or deposits of urinary salts.

3. Ureteral obstruction must be present. It may be caused by a previous pathologic condition, by a transient blood clot within the ureter or a periureteral hematoma, or from fibrosis secondary to the injury. Indeed, the tissue reaction itself results in a continuing element of obstruction establishing a vicious cycle. The ureter may be bound down by scar tissue as it lies embedded in the newly formed sac wall. The necessarily slow development of scar tissue readily explains the typically delayed formation of the mass. The hydrokinetic system then reaches stability only when autonephrectomy occurs.

Clinical Signs and Symptoms. The usual clinical presentation of a uriniferous perirenal pseudocyst is a palpable flank mass associated with some degree of abdominal distress, often mild in nature. The mass is generally only slightly tender to palpation and there is little, if any, increase in temperature. Urinalysis is often completely negative. A typical sequence is general improvement after the original abdominal trauma, followed by the delayed appearance of a flank mass. The latent period between the traumatic episode and the appearance of symptoms and a mass is often 1 to 4 months.[170] The mass has occasionally been noted to increase rapidly in size.[168,171] Sauls and Nesbit[172] observed a latent period of 2 years, and Johnson and Smith reported an unusual case of a calcified pseudocyst diagnosed 37 years after the presumed trauma.[173]

Radiologic Findings. Since perirenal effusions localize according to the effect of gravity and planes of least resistance, extravasated urine seeks out the portion of the cone of renal fascia caudad to the kidney. Basic to an appreciation of the characteristic complex of radiographic abnormalities is the fact that the pseudocyst typically conforms to the axis and dimensions of the cone of renal fascia (Fig. 8–144), as encountered at surgery (Fig. 8–145). Slow, persistent effusion within the cone of renal fascia distends the perirenal space but allows it to retain its characteristic axis. This phenomenon accounts for the diagnostic changes[10] (Fig. 8–146).

The characteristic complex of radiographic abnormalities involves features of the soft tissue mass of the

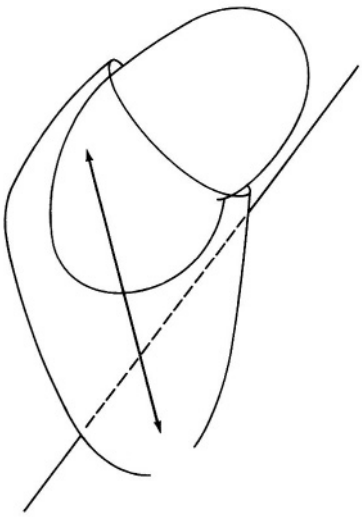


Fig. 8–144. Cone of renal fascia.
The two layers of renal fascia completely envelop the kidney and perirenal fat. They fuse in such a manner that the perirenal space bears an axis inferiorly (to the level of the iliac crest) and medially (overlying the lower segment of the psoas muscle).
(Reproduced from Meyers.[8])

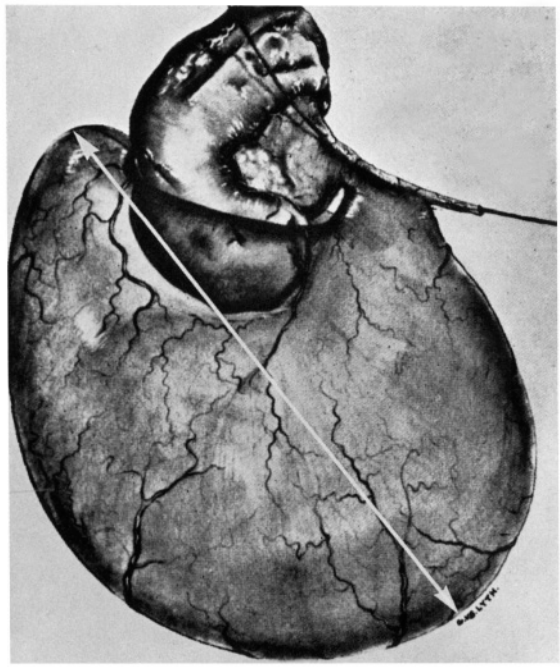


Fig. 8–145. Surgical specimen of uriniferous perirenal pseudocyst and nonfunctioning hydronephrotic kidney.
Operation was performed 3 months after a traumatic pelvilithotomy. Note that the findings show massive urine distention of the thickened cone of renal fascia, which nevertheless maintains its characteristic axis downward and medially.
(Reproduced from Pyrah and Smiddy.[174])

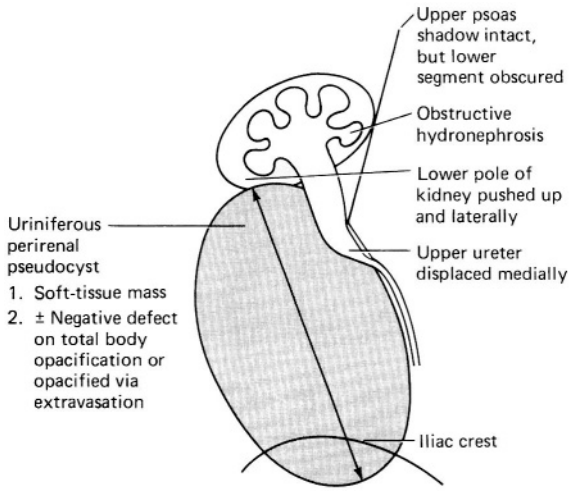


Fig. 8–146. Major characteristic radiologic changes secondary to uriniferous perirenal pseudocyst.
Basic are the axis and relationships of the chronically distended cone of renal fascia.
(Reproduced from Meyers.[10])

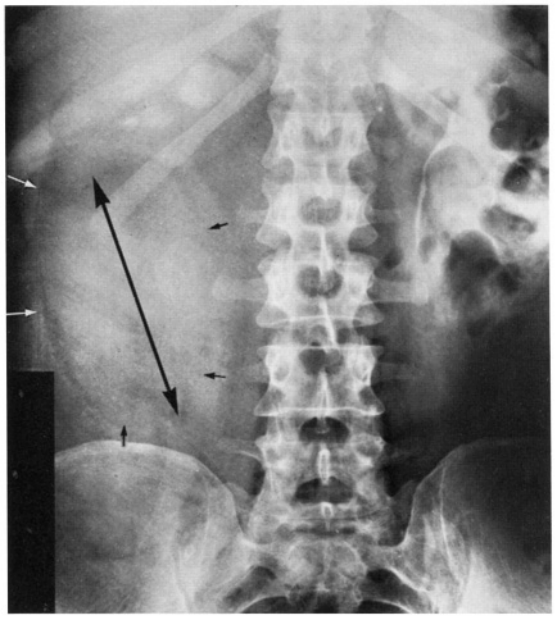


Fig. 8–147. Uriniferous perirenal pseudocyst after pelvilithotomy.
Intravenous urogram shows the lower pole of the partially obstructed right kidney displaced upward and laterally by a large elliptical soft-tissue mass *(small arrows).* The axis of the mass is characteristically oriented inferomedially. Its contours are further highlighted by the contrast provided by posterior pararenal fat into which it bulges posteriorly. The proximal ureter is displaced medially and is dilated, associated with caliectasis and a mild obstructive nephrogram. Incision and drainage of 1,500 mL of urine, nephrostomy, and a splinted ureterostomy were followed by marked improvement.
(Reproduced from Meyers.[10])

pseudocyst and its effects on the kidney and ureter (Figs. 8–147 through 8–151). In addition, extravasation into the pseudocyst may confirm the actual point of leakage or indicate gross communication with the collecting system.

The most typical and consistent feature of the pseudocyst is that its axis conforms to the distended cone of renal fascia. Thus, it is elliptical in outline and obliquely oriented inferomedially. Its upper border is lateral in the flank as it comes into relationship to the lower pole of the kidney and its lower border is more medial as it overlaps the psoas muscle near the level of the iliac crest. Its contours may be further outlined on plain films by the contrast of other extraperitoneal fat (specifically within the posterior pararenal compartment) into which the pressure of the pseudocyst bulges. With huge collections, the cone of renal fascia may become so distended that its axis appears more vertical.

The pseudocyst can be identified as a soft-tissue density or as a lucent defect during the phase of total body opacification. Needle opacification of the pseudocyst may outline precisely its contour, size, and characteristic axis.

The kidney is usually displaced upward and its lower pole characteristically deviated laterally. The fat immediately around the kidney and upper third of the psoas muscle can be visualized intact, but the lower margin of the psoas muscle is obscured by the pseudocyst. The involved kidney shows poor and delayed function or absent excretion on intravenous urography. Hydronephrosis is apparent on delayed films or on retrograde pyelography. The upper ureter is usually deviated medially, occasionally across the midline, but this may require retrograde studies for demonstration. The catheter is often arrested in the upper third of the ureter.

Extravasation into the area of the pseudocyst may be seen on excretory urography or on retrograde pyelography. Opacification of the mass may be noted at the same time as the nephrogram during intravenous urography or as the patient's position is changed from supine to prone.

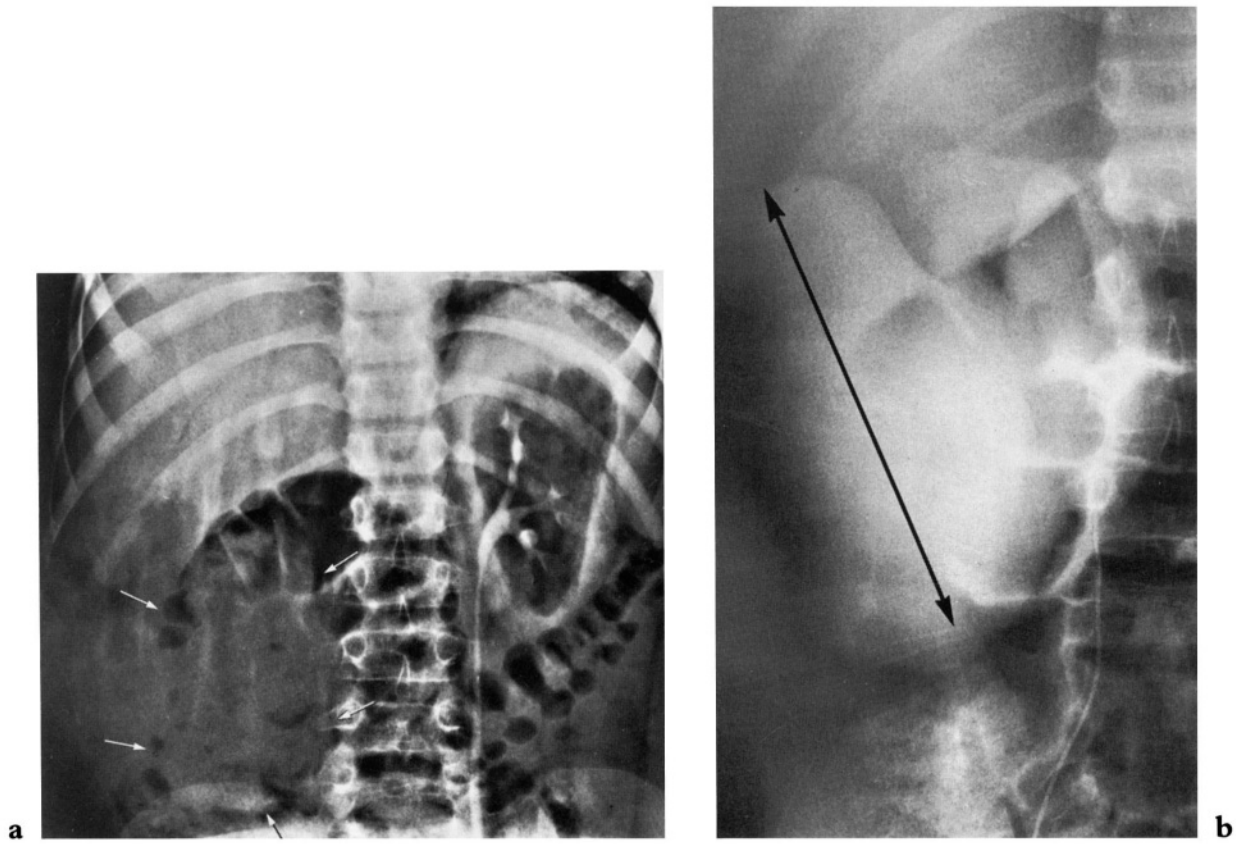


Fig. 8–148. Uriniferous perirenal pseudocyst postpelvilithotomy.
(a) Total body opacification during intravenous urography outlines a lucent mass *(arrows).* The right kidney is partially obstructed and is displaced upward and laterally.
(b) Contrast opacification of pseudocyst through drainage needle confirms its inferomedial axis. Residual contrast from retrograde pyelography shows obstructive uropathy proximal to the strictured and displaced ureter.
(Reproduced from Meyers.[10])

Arteriography demonstrates no inflammatory or neoplastic hypervascularity associated with the mass and may be helpful in further evaluating the position and state of function of the kidney.

Ultrasonography may demonstrate the cystic nature of the mass, its size and position, and the presence of hydronephrosis and the level of obstruction.[175,176] Isotopic studies may also reveal the characteristic findings[176,177] (Fig. 8–152).

Computed tomography clearly demonstrates the size, position, and relationships of the pseudocyst and may document continuing extravasation by virtue of its opacification[178] (Figs. 8–153 through 8–157).

Unusual sites of development of uriniferous pseudocyst may be a consequence of surgery, instrumentation, or penetrating injury with interruption of anatomic planes.[178]

Treatment. It is important to diagnose the condition early so that it can be corrected surgically before inoperable damage to the kidney occurs. The best results have been obtained when surgical intervention occurred within 2–3 weeks after injury. Later, marked fibrosis of the tissues and cicatrization of the ureter make it difficult or impossible to repair or bridge the defect. Nephrostomy drainage with intubation of the repaired ureter is the procedure of choice.[179] If renal function has been lost and the contralateral kidney is normal, nephrectomy is advisable.

text continues on page 430

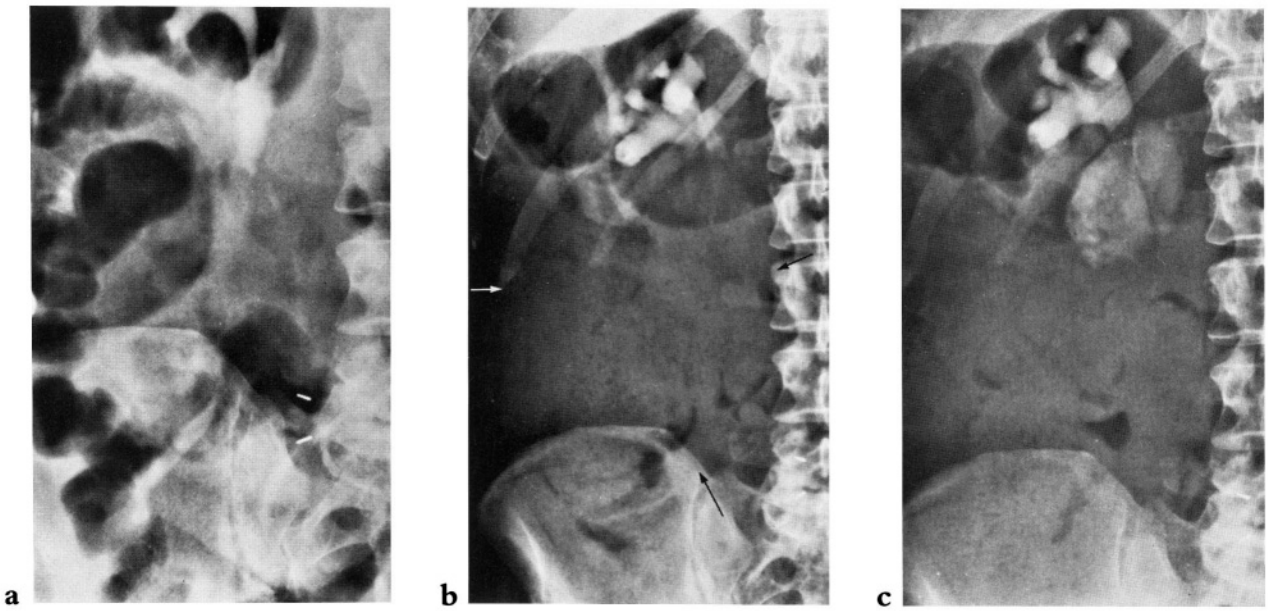


Fig. 8–149. Uriniferous perirenal pseudocyst.
(a) Following accidental partial interruption of the right ureter at the time of retroperitoneal lymph node dissection, intravenous urography demonstrates extravasation of urine.
(b) Three weeks later, there is evidence of a large encapsulated mass *(arrows)* extending to the level of the iliac crest, with obstruction of the proximal right ureter and hydronephrosis. The lower pole of the kidney is displaced superiorly and laterally.
(c) Later radiograph shows localized extravasation into the pseudocyst.
(Reproduced from Meyers.[10])

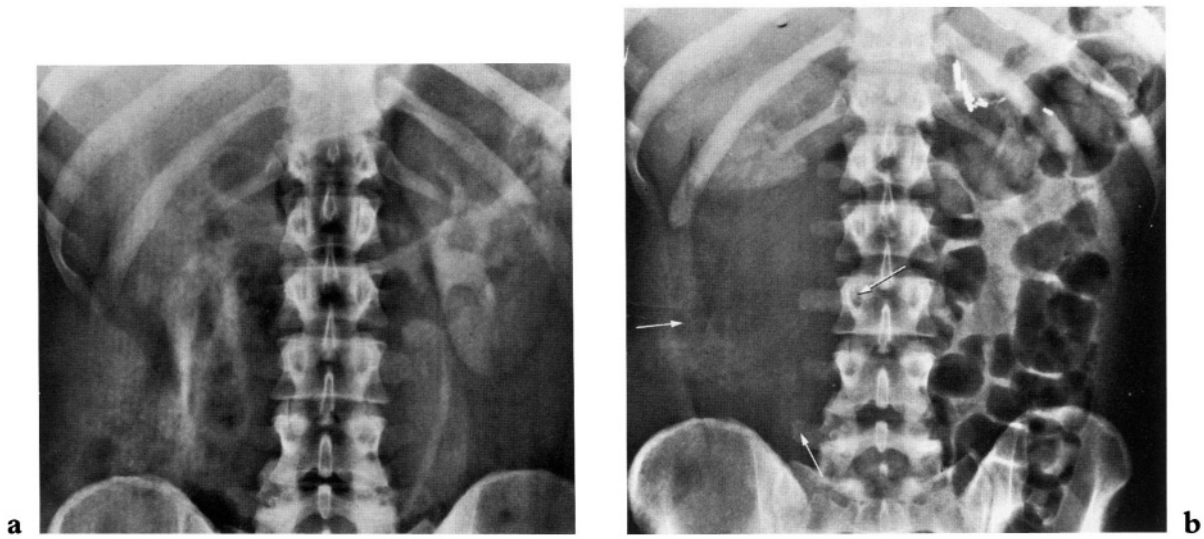


Fig. 8–150. Uriniferous perirenal pseudocyst.
(a) Following abdominal trauma from an automobile accident, intravenous urography demonstrates extravasation from a poorly functioning right kidney.
(b) Ten days later, after emergency gastrectomy and splenectomy, there is evidence of a large soft-tissue mass *(arrows)* displacing the obstructed kidney upward and laterally and the colon medially. The mass is oriented somewhat inferomedially, extends to the level of the iliac crest, and is outlined as relatively lucent by the effect of total-body opacification.
(Reproduced from Meyers.[10])

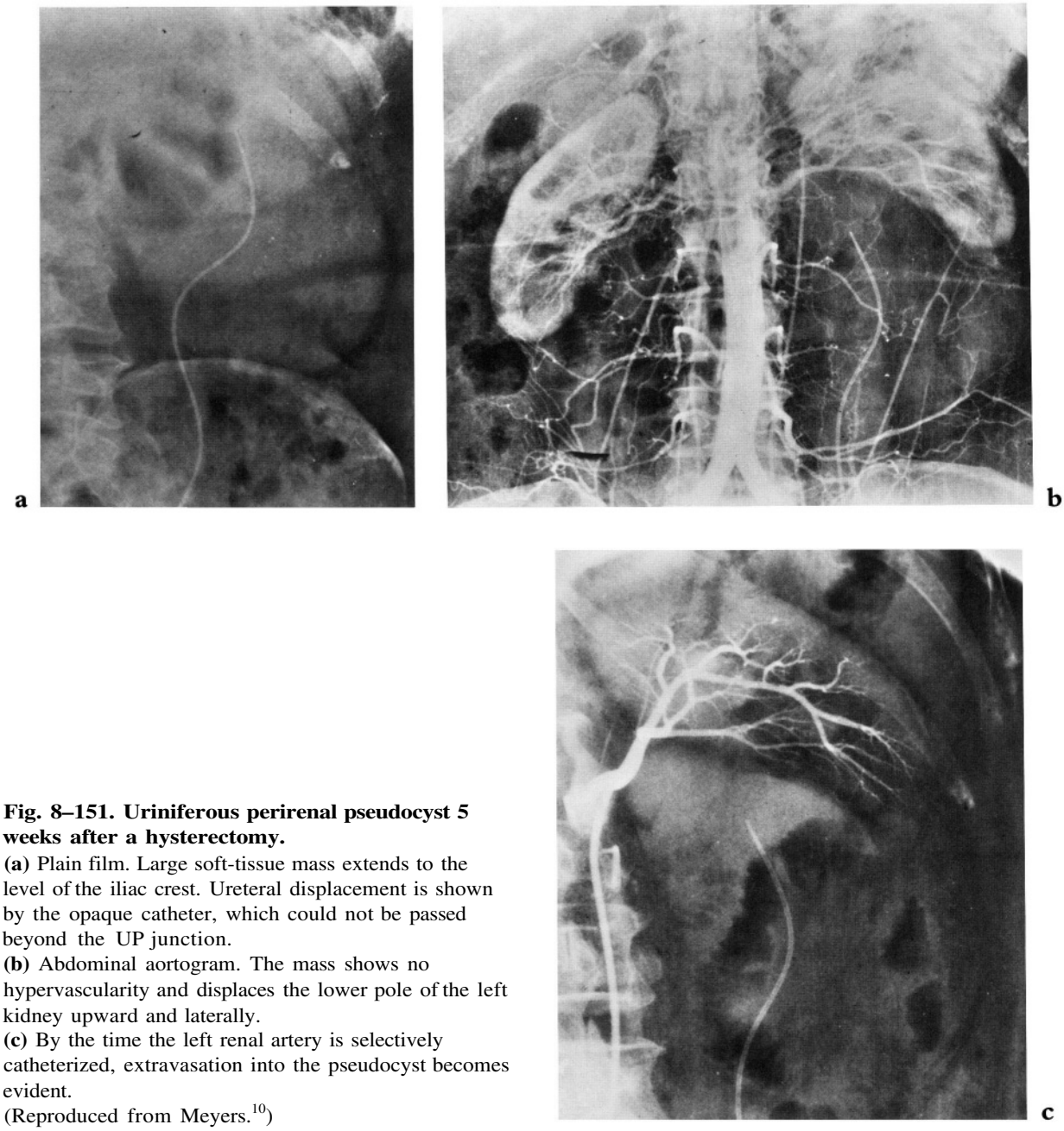


Fig. 8–151. Uriniferous perirenal pseudocyst 5 weeks after a hysterectomy.
(a) Plain film. Large soft-tissue mass extends to the level of the iliac crest. Ureteral displacement is shown by the opaque catheter, which could not be passed beyond the UP junction.
(b) Abdominal aortogram. The mass shows no hypervascularity and displaces the lower pole of the left kidney upward and laterally.
(c) By the time the left renal artery is selectively catheterized, extravasation into the pseudocyst becomes evident.
(Reproduced from Meyers.[10])

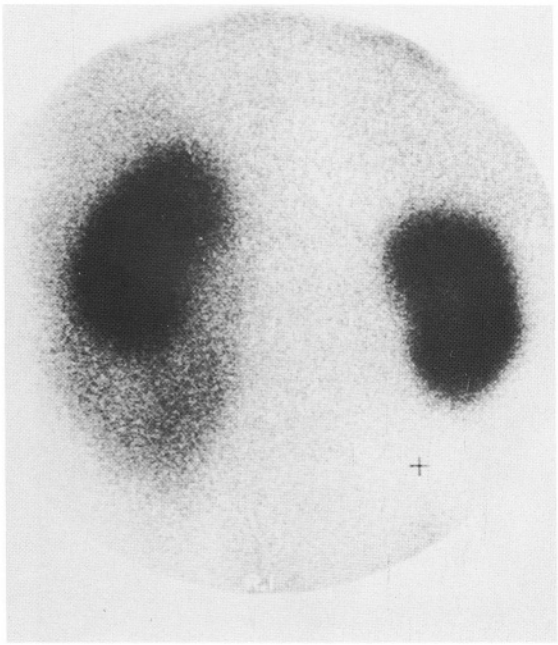


Fig. 8–152. Uriniferous perirenal pseudocyst, secondary to obstruction from recurrent invasive carcinoma of the rectum. Posterior radionuclide image demonstrates the left kidney elevated and its lower pole deviated laterally by an elliptical extrarenal urine collection of lesser activity. The axis of this is obliquely oriented inferomedially. (Reproduced from Suzuki et al.[177])

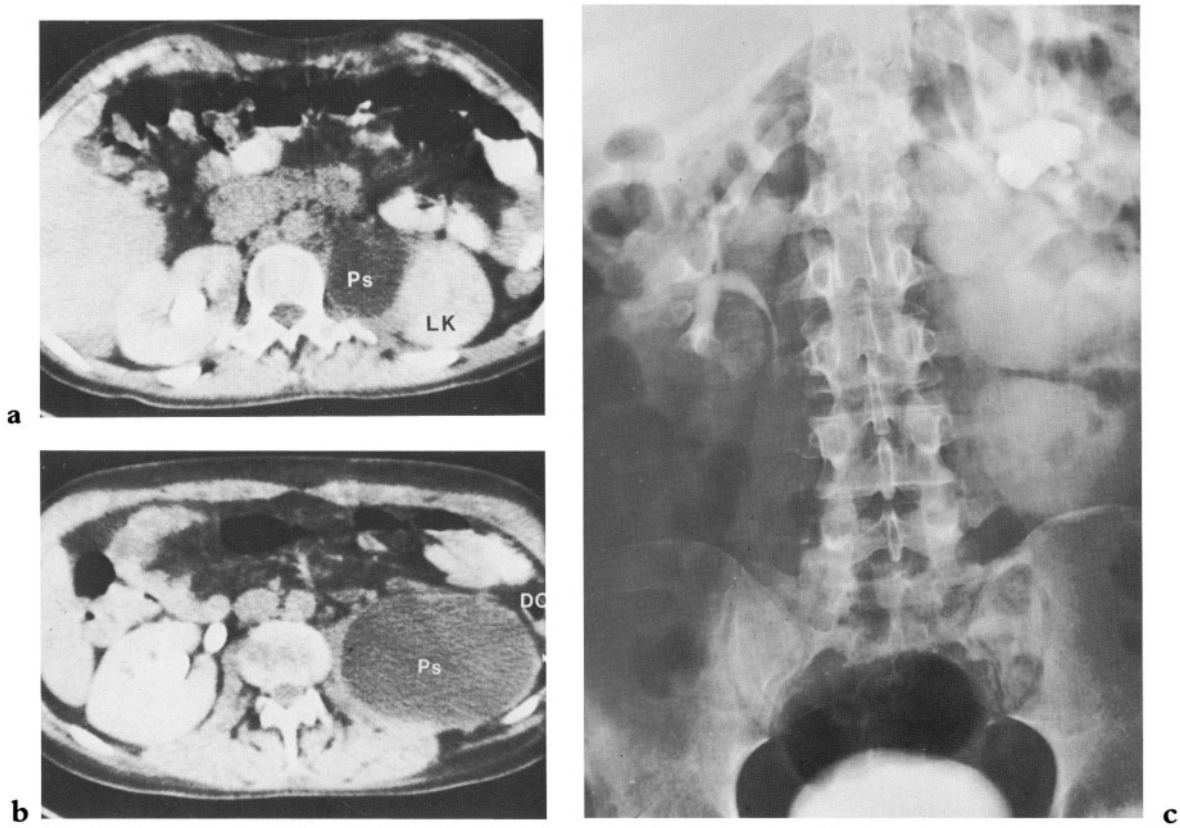


Fig. 8–153. Uriniferous perirenal pseudocyst.
(a) CT scan after intravenous injection of contrast medium shows encapsulated pseudocystic collection of extravasated urine (*Ps*) displacing the left kidney (*LK*) laterally.
(b) At a lower level, it distends the cone of renal fascia medial to the descending colon (*DC*). The anterior and posterior pararenal fat and the lateroconal fascia (*arrow*) remain intact. At this stage in the study, there is no opacification of the extravasated urine.
(c) Delayed radiograph demonstrates opacification of the pseudocyst, which bears a typical axis and renal displacement.

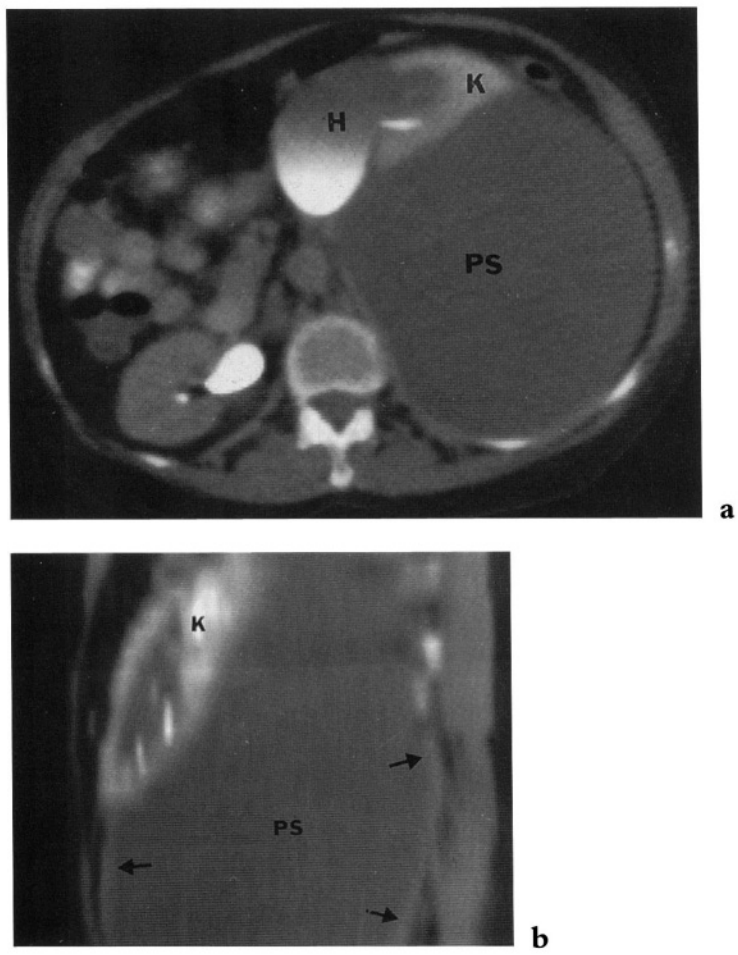


Fig. 8–154. Uriniferous perirenal pseudocyst presenting 2 months after a fall.
(a) CT shows large uriniferous pseudocyst within the left perirenal space *(PS),* anterior displacement of the kidney (*K*), and a severely hydronephrotic renal pelvis (*H*).
(b) Sagittal reconstruction demonstrates anterior and superior displacement of the kidney (*K*) by the large uriniferous pseudocyst (*Ps*) confined within the cone of thickened renal fascia (*arrows*).
(Reproduced from Healey et al.[178])

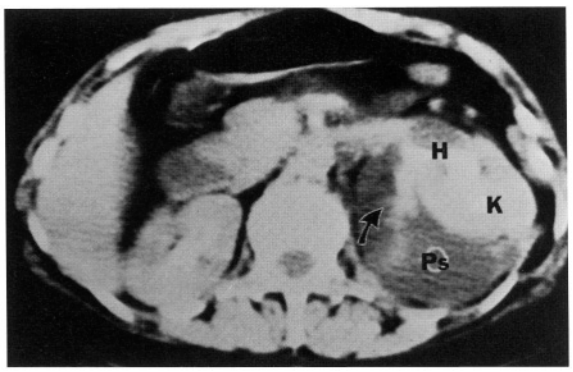


Fig. 8–155. Uriniferous perirenal pseudocyst.
CT in a patient with recurrent carcinoma of the cervix and paraaortic adenopathy demonstrates the left kidney (*K*) with hydronephrosis (*H*) displaced anteriorly and laterally by a uriniferous perirenal pseudocyst (*Ps*). There is extravasation of contrast medium *(arrow)* into the encapsulated urine collection, decompressing the hydronephrosis.

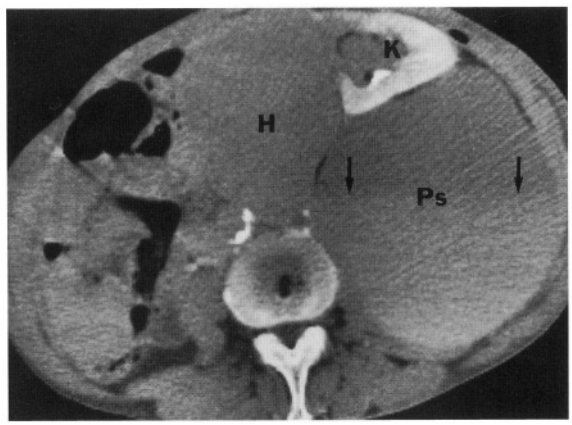


Fig. 8–156. Uriniferous perirenal pseudocyst.
CT in a 60-year-old woman 10 weeks after a "fall" demonstrates a large uriniferous pseudocyst within the perirenal space (*Ps*), with contrast medium in its dependent portion (*arrows*). Anterior displacement of the left kidney (*K*) and a severely hydronephrotic renal pelvis (*H*) are also present.
(Reproduced from Healy et al.[178])

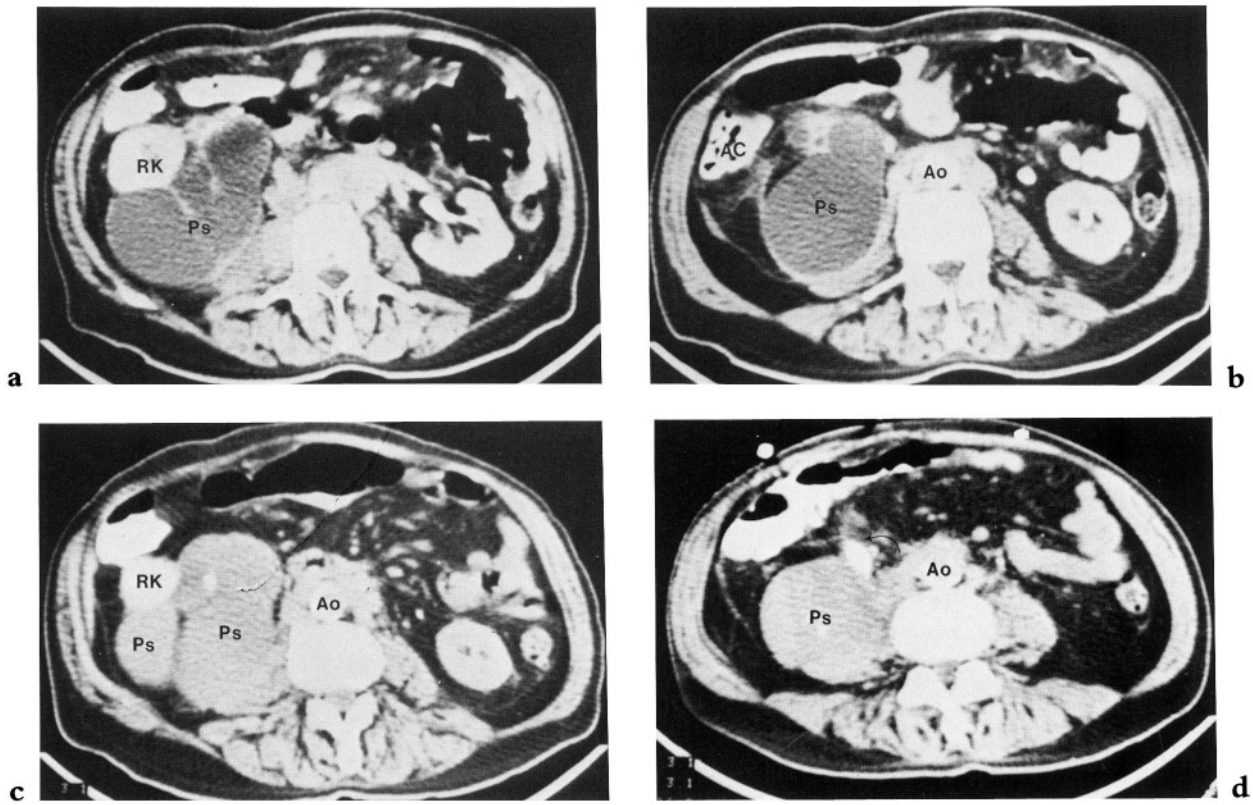


Fig. 8–157. Uriniferous perirenal pseudocyst, secondary to obstruction from metastatic carcinoma of the urinary bladder. **(a** and **b)** CT scans after intravenous injection of contrast medium show large pseudocystic collection of extravasated urine (*Ps*) extending from the right kidney (*RK*), which it displaces laterally and anteriorly from the medial border of the psoas muscle. As it extends inferiorly, it remains confined within the cone of renal fascia medial to the ascending colon *(AC),* Adhesions or bridging renal septa within the pseudocyst contribute to mild septation. Metastatic tumor in lymph nodes around the calcified abdominal aorta *(Ao)* and inferior vena cava is seen as soft-tissue masses.
(c and **d)** Six-hour delayed scans demonstrate a significantly higher CT number within the pseudocyst, reflecting active extravasation. It is because of this decompression that although the right ureter is dilated *(curved arrow),* the collecting system does not appear obstructed.
(Courtesy of Michael Oliphant, M.D., Crouse Hospital, Syracuse, NY.)

Distinction Between Perirenal and Subcapsular Collections

Abscesses or hematomas in the perirenal space and in the subcapsular region of the kidney can simulate each other and a host of other conditions closely. Identification of their specific localization may be very important in the clinical diagnosis and in determining the most appropriate therapy. Advances in establishing the characteristic features of abscesses or hematomas are based on the anatomic structures that define their collection.[11]

Anatomic Considerations. The renal capsule (Fig. 8–158) is a thin tunic that forms an intimate, firm, smooth investment for the kidney. It is composed predominantly of fibrous tissue, but there is some smooth muscle within its inner layer. No adipose tissue is found between the renal parenchyma and the capsule. The capsule can be stripped off easily; when this is done, numerous fine processes of connective tissue and small blood vessels are torn through.

The capsular arteries course through and supply primarily the perirenal fat, which is located between the renal capsule and the renal fascia. The somewhat confusing designation of these vessels as "capsular" is apparently derived from the old nomenclature of the perirenal fat as the "adipose capsule of the kidney." They are composed of three basic pathways: superior, middle (recurrent and perforating), and inferior capsular arteries. A prominent arterial arcade is formed within the

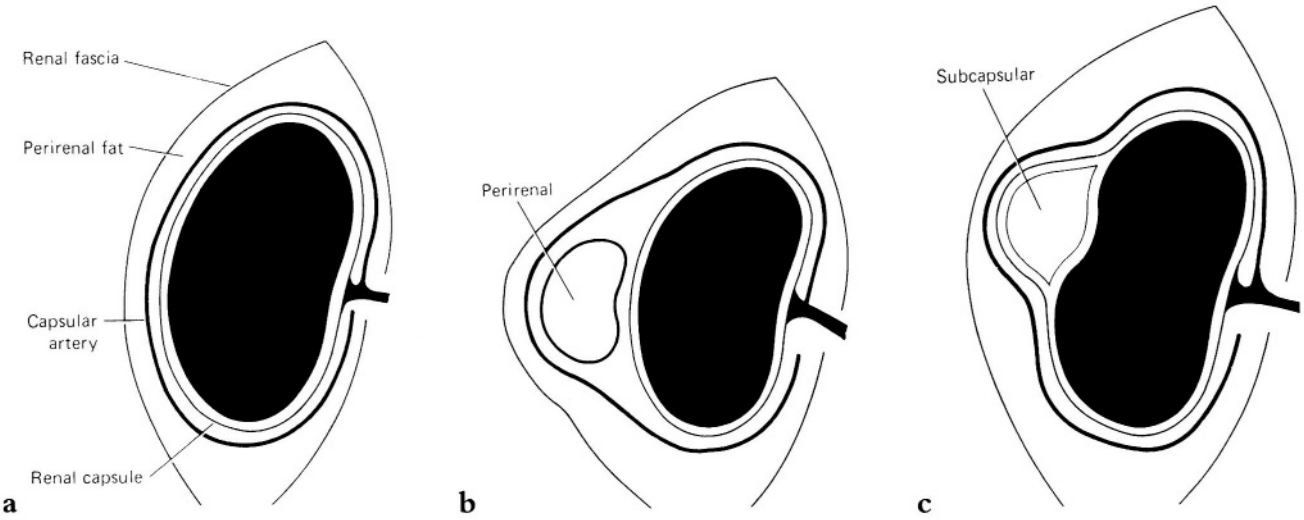


Fig. 8–158. Normal relationships of investing structures of kidney and major findings distinguishing a perirenal from a subcapsular collection.
Note particularly the relationships of the displaced renal capsule, perirenal fascia, and capsular arteries at the borders of the mass. Flattening of the underlying renal parenchyma is more commonly found in subcapsular collections.
(From Meyers et al.[11])

perirenal fat lateral to the kidney that communicates with renal branches perforating through the capsule.

Etiology and Pathogenesis. Perirenal *abscesses,* as we have seen, are almost invariably secondary to a site of renal infection that perforates through the capsule to contaminate the perirenal fatty compartment.

Extrarenal *hematomas,* whether subcapsular or perirenal in location, are generally considered either traumatic or spontaneous (nontraumatic). In a classic review of the world literature in 1933, Polkey and Vynalek[161] reported a comprehensive study of the causes of spontaneous hematomas. Of 178 cases reviewed, the location was subcapsular in 18.5% and extracapsular (perirenal or pararenal or a combination of the two) in 81.5%. Lesions of the kidneys and its blood vessels accounted for 92% of the cases. The underlying etiologies, in the order of their relative frequencies, included nephritis, neoplasms, aneurysms of the renal artery, arteriosclerosis, hydronephrosis, periarteritis nodosa, tuberculosis, renal cysts, and blood dyscrasias.

An increasing number of cases of extrarenal hemorrhage owing to periarteritis nodosa and occult, often surprisingly small, renal tumors have been reported.[180–185] Many of the earlier cases diagnosed as nephritis may have actually been periarteritis nodosa or lupus erythematosus. Current experience with spontaneous subcapsular or perirenal hematomas indicates that renal cell carcinoma and renal angiomyolipoma are the cause in 30–60%[180,186]; the remaining cases are caused by a variety of vascular, inflammatory, cystic, and hematologic disorders.[186]

Rarely, metastatic disease to the kidneys, especially from vascular tumors such as choriocarcinoma, can cause perirenal hemorrhage.[187] Melanoma and lung cancer tend to involve the kidney and perirenal space contiguously,[188,189] but these do not tend to hemorrhage.

Percutaneous renal biopsy results in subcapsular hematoma in approximately 28% and in some degree of perirenal hemorrhage in over 90% of patients. Very few of these hematomas, however, are clinically significant.[190–192] Subcapsular hematomas have been identified in 15% of patients after extracorporeal shock wave lithotripsy.[193]

One mechanism of hematoma formation begins with cortical infarcts.[184] The hemorrhage may be confined by the relatively rigid capsule; at other times the blood breaks through the capsule immediately but is confined within the dimensions of the renal fascia. A hematoma within the distensible perirenal compartment can develop to an enormous size before pressure becomes sufficient to cause tamponade of the bleeding site.

The spread of hemorrhage from ruptured abdominal aortic aneurysms depends upon the anatomic level and site of leaking and the amount of extravasated blood. At the level of the kidneys, the aorta lies behind the anterior

renal fascia. Thus, aortic bleeding occurs most commonly directly into the perirenal space.[194–196] In ruptured abdominal aortic aneurysms, a localized disruption of the calcified or noncalcified wall of the aneurysm is identifiable by CT and indicates the site of extravasation (Fig. 8–159). Aortic wall indistinctness, however, is not always a specific indication of rupture.[196,197] The extent of lack of conspicuity of the portion of wall seen on CT is generally greater than the true extent of any rupture.[198] On CT, a crescent of increased attenuation is a reliable sign of acute or impending rupture.[199,200] Rarely, an aortic aneurysm may rupture into the inferior vena cava resulting in a high-output aortocaval fistula[201–203] (Fig. 8–160). Color Doppler sonography may demonstrate the actual site of the fistula to the distended cava in selected patients.

Clinical Signs and Symptoms. The clinical diagnosis of subcapsular or perirenal abscess or bleeding is rarely made. Signs and symptoms are often subtle, delayed, nonspecific, or misleading.

With acute bleeding, the clinical picture may consist of pain, tenderness, and rigidity, which may be associated with nausea, vomiting, and abdominal distention. Concomitant signs of internal bleeding may be present, but this may be manifested only by a drop in hemoglobin or hematocrit. A mass may not be palpable, especially if the hematoma lies posteriorly to the kidney. If the hematoma is subcapsular, it may not become particularly large because of the confining effect of the renal capsule, but occasionally the collection may approximate the size of the kidney itself. With sudden and profuse hemorrhages, many types of retroperitoneal and intraperitoneal catastrophes may be mimicked. If the hematoma extends downward in the retrocecal region, the patient may be explored for an acute appendicitis.[204] Rarely, perforation into the peritoneal cavity may occur, causing a generalized peritonitis or a massive intraperitoneal hemorrhage.

With subacute or chronic bleeding, pain may not be a conspicuous feature, and the principal findings may be only anemia and, perhaps, a palpable mass.

Hypertension may result from the constrictive renal effects of a large subcapsular[11,205–207] or less commonly a perirenal hematoma, producing the *Page kidney*.[208] If the condition is not particularly chronic, the hypertension may be easily corrected by decompression or nephrectomy.

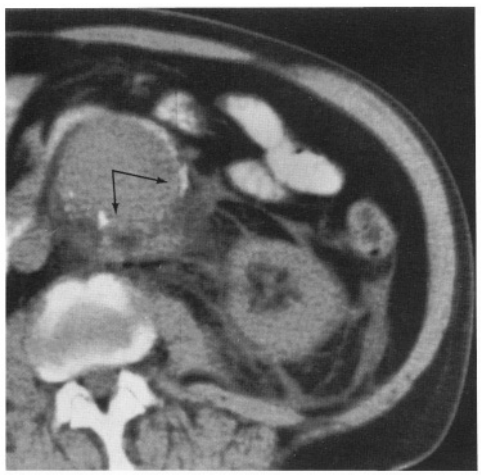


Fig. 8–159. Perirenal bleeding from ruptured aneurysm of the abdominal aorta.
Rupture from the posterolateral wall of the aorta *(arrows)* results in bleeding tracking along the bridging renal septa within the perirenal fat.

Radiologic Findings. Supcapsular or perirenal hemorrhage or abscess can be indicated on plain films or intravenous urography and can be clearly documented by nephrotomography or angiography. While such studies are performed less commonly in the era of sectional imaging, the fundamental changes remain diagnostic. I have shown that localization of the process to a specific extrarenal compartment is based on recognizing characteristic changes involving the renal capsule, renal fascia, kidney margin, and capsular arteries[11] (Fig. 8–158).

1. *Visualization of the displaced renal capsule or fascia.* Either of these structures, displaced outward from the renal margin, can be seen as a striplike density 1–4 mm thick. The renal fascia can be visualized by plain film roentgenography and urography in cases of perirenal abscess or hematoma (Figs. 8–161 through 8–163). In diffuse processes of the perirenal space, it can be recognized over a considerable length. At times, a displaced renal capsule may be demonstrated by urography (Fig. 8–164).

Opacification of the displaced renal capsule (Fig. 8–165) and fascia is achieved in nephrotomography and arteriography.[11,183,209,210] Contrast is further afforded by the nonopaque abscess or hematoma on one side and radiolucent fat on the other.

I have noted a type of displacement, which, when present, distinguishes subcapsular from perirenal collections. The renal capsule is sharply deflected over the margin of a subcapsular mass. Even with huge collec-



Fig. 8–160. Aortocaval fistula.
(a) Contrast-enhanced CT shows marked extraperitoneal hemorrhage on the right with gross displacement of the kidney. There is simultaneous enhancement of both the enlarged inferior vena cava *(C)* and the conspicuous abdominal aorta. Discrepant renal function is noted.
(b) At a lower level, rupture of the calcified abdominal aortic aneurysm into the cava is evident *(arrow).*

tions, its point of displacement intimately conforms to the border of the hematoma (Fig. 8–165). It appears that this is a consequence of the relatively rigid, inelastic nature of the renal capsule. In contrast, renal fascia is often displaced laterally from the margin of the kidney at some distance from a coalescent perirenal collection. Its maximum deflection is at the site of the perirenal hematoma or abscess, but it can be seen to depart from close to the renal border both above and below (Fig. 8–161). It is a reflection of the yielding perirenal fat and renal fascia.

At times, simultaneous displacement of both the renal capsule and fascia can be identified (Fig. 8–166).

2. *Visualization of the hematoma or abscess.* The subcapsular or perirenal collection is easily seen as a nonopaque mass between the opacified renal parenchyma on one side and the elevated renal capsule or fascia on the other. This is most often seen in relationship to the lower pole posterolaterally.

3. *Flattening and compression of the kidney.* While this may occur with tense perirenal collections, it is more typical of subcapsular hematoma. The pressure exerted by a confined subcapsular hematoma typically causes flattening of the subjacent renal parenchyma.

4. *Displacement of capsular arteries.* The capsular arteries may be displaced externally in either condition. Examples of conspicuous arcuate displacements and stretching of the capsular artery system in cases of both subcapsular and perirenal hematomas and abscesses have been amply documented in the literature. Rather, I have noted that the level of displacement of the capsular arterial arcade is the angiographic key to the differential

text continues on page 438

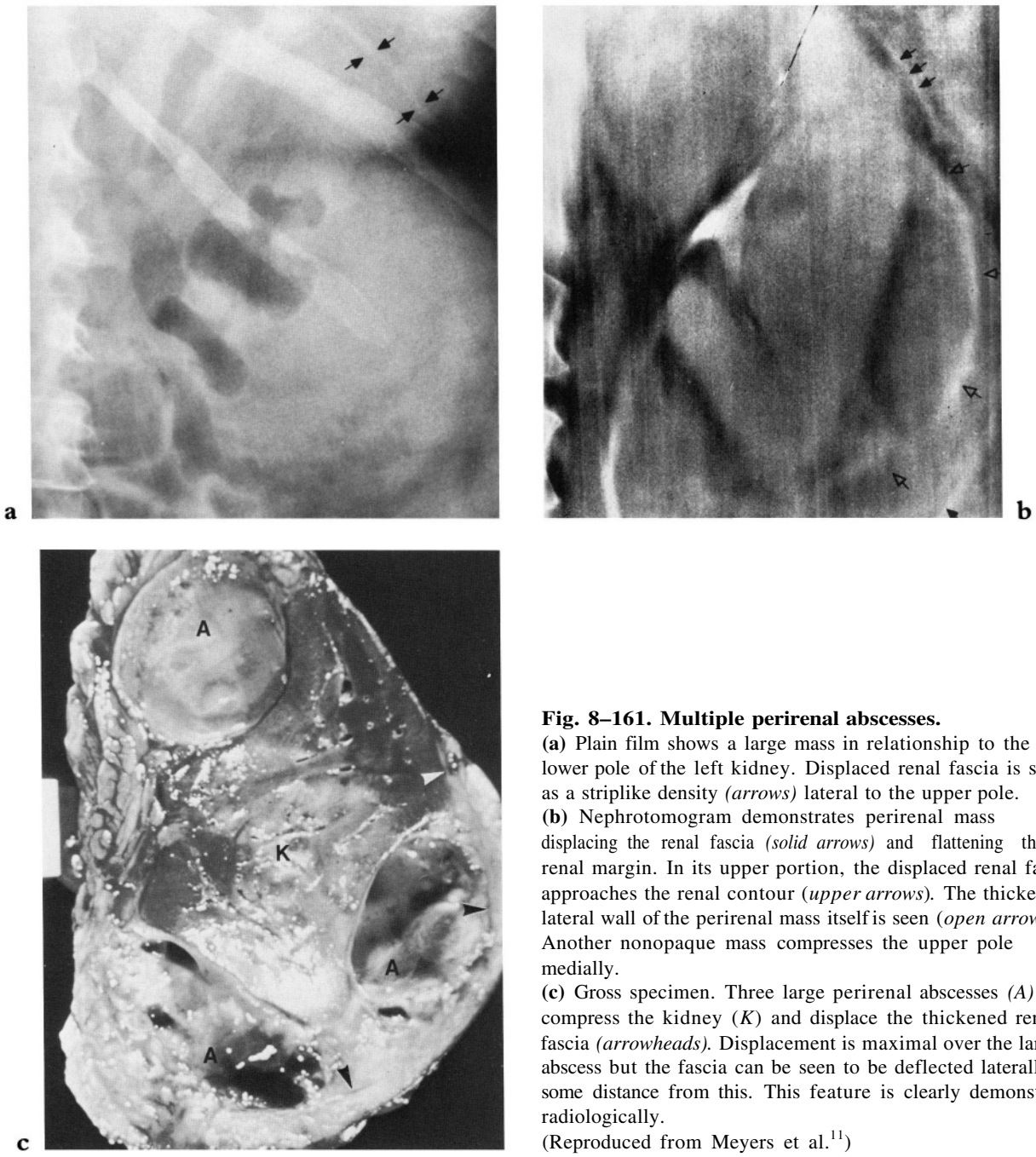


Fig. 8–161. Multiple perirenal abscesses.
(a) Plain film shows a large mass in relationship to the lower pole of the left kidney. Displaced renal fascia is seen as a striplike density *(arrows)* lateral to the upper pole.
(b) Nephrotomogram demonstrates perirenal mass displacing the renal fascia *(solid arrows)* and flattening the renal margin. In its upper portion, the displaced renal fascia approaches the renal contour (*upper arrows*). The thickened lateral wall of the perirenal mass itself is seen (*open arrows*). Another nonopaque mass compresses the upper pole medially.
(c) Gross specimen. Three large perirenal abscesses *(A)* compress the kidney (*K*) and displace the thickened renal fascia *(arrowheads)*. Displacement is maximal over the largest abscess but the fascia can be seen to be deflected laterally at some distance from this. This feature is clearly demonstrated radiologically.
(Reproduced from Meyers et al.[11])

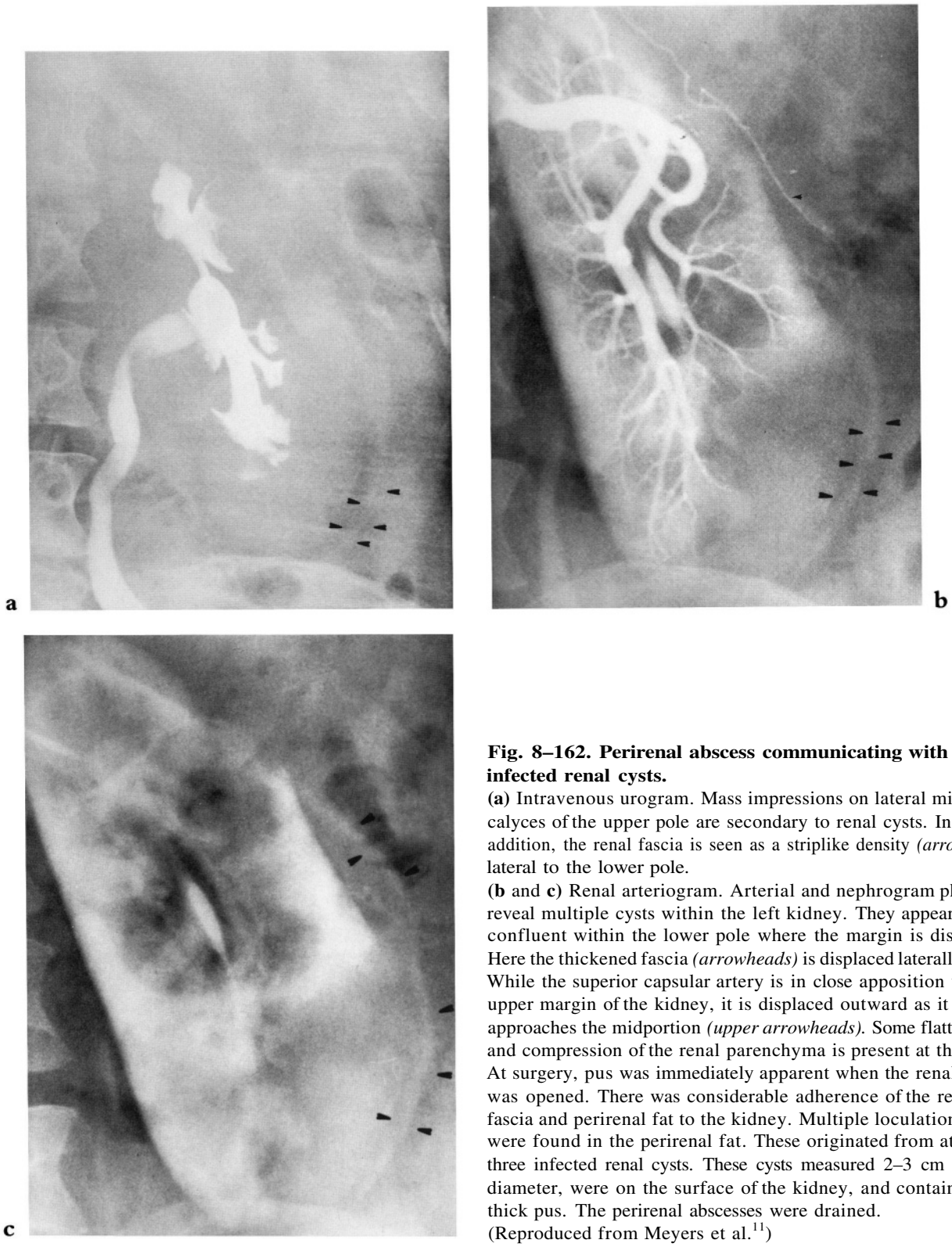


Fig. 8–162. Perirenal abscess communicating with infected renal cysts.
(a) Intravenous urogram. Mass impressions on lateral minor calyces of the upper pole are secondary to renal cysts. In addition, the renal fascia is seen as a striplike density *(arrowheads)* lateral to the lower pole.
(b and **c)** Renal arteriogram. Arterial and nephrogram phases reveal multiple cysts within the left kidney. They appear most confluent within the lower pole where the margin is disrupted. Here the thickened fascia *(arrowheads)* is displaced laterally. While the superior capsular artery is in close apposition to the upper margin of the kidney, it is displaced outward as it approaches the midportion *(upper arrowheads).* Some flattening and compression of the renal parenchyma is present at this site. At surgery, pus was immediately apparent when the renal fascia was opened. There was considerable adherence of the renal fascia and perirenal fat to the kidney. Multiple loculations of pus were found in the perirenal fat. These originated from at least three infected renal cysts. These cysts measured 2–3 cm in diameter, were on the surface of the kidney, and contained thick pus. The perirenal abscesses were drained.
(Reproduced from Meyers et al.[11])

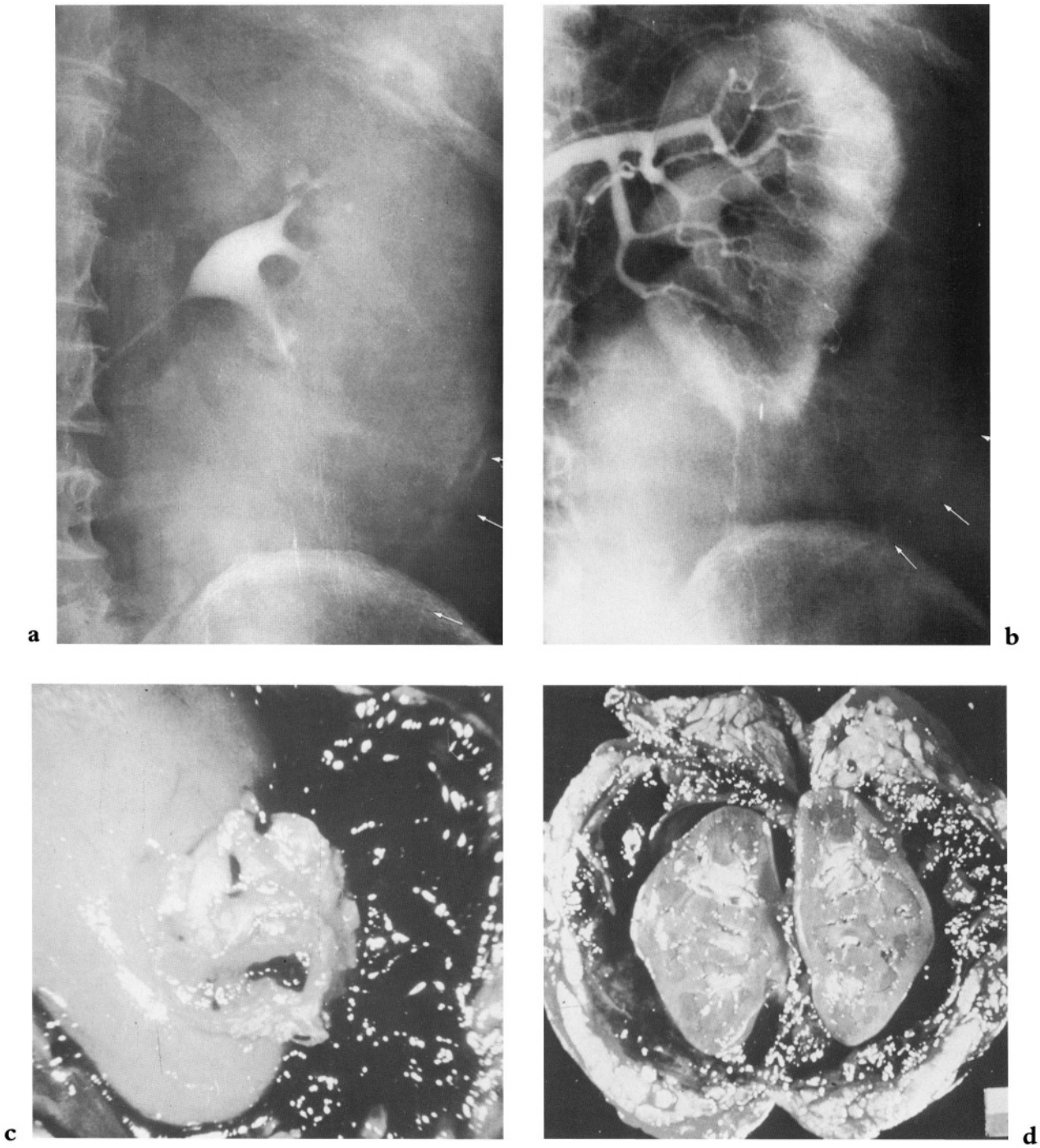


Fig. 8–163. Perirenal hemorrhage secondary to occult renal tumor.
(a) Intravenous urogram. Renal fascia is seen as a striplike density *(arrows)* displaced laterally by a large mass. This also results in loss of definition of the lateral and inferior borders of the kidney.
(b) Renal arteriogram. Perforating capsular arteries extend through the mass to its lateral limit by the displaced renal fascia *(arrows).* No definite abnormal intrarenal vasculature is identified.
(c) At surgery, a large collection of blood distended the perirenal space, contained within the cone of renal fascia. Nephrectomy was performed and the pathologic examination disclosed a 3 × 5 × 4 cm infiltrating papillary adenocarcinoma of the lower renal pole.
(d) Bivalved specimen. Extension through the renal capsule had resulted in gross perirenal hemorrhage within the thickened cone of renal fascia.
(Reproduced from Meyers et al.[11])

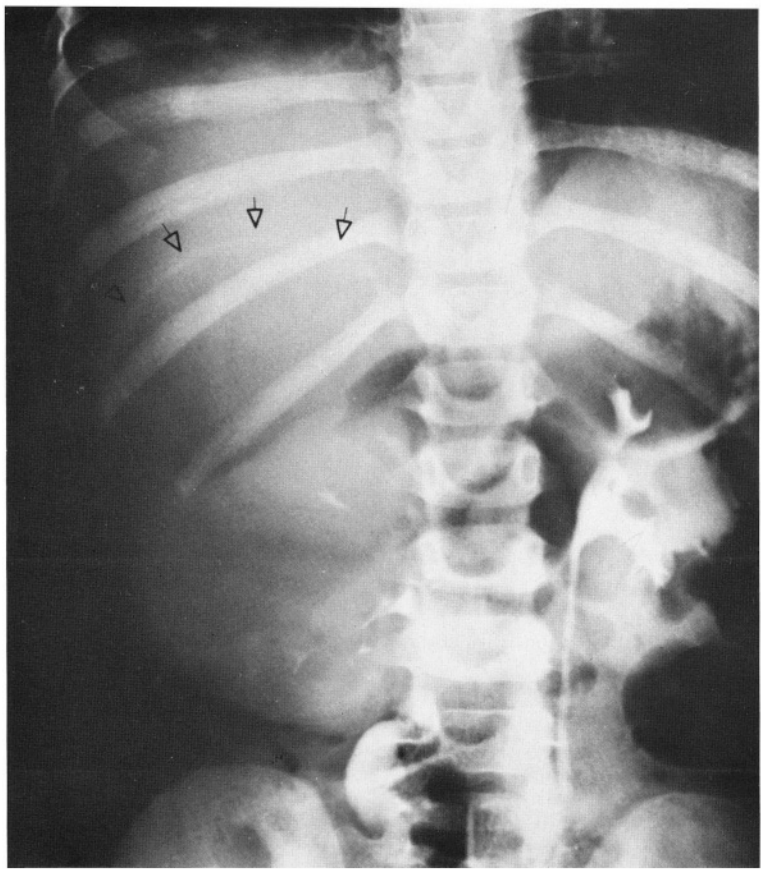


Fig. 8–164. Subcapsular abscess.
On the right, the calyces are displaced by a large, relatively lucent mass in the lower half of the kidney. The renal capsule *(arrows)* is displaced superiorly by a prominent collection that also results in mild compression of the underlying renal margin. The apparent enlargement of the right kidney is secondary to magnification since the kidney is also pushed forward. Decreased function is evident.
At surgery, a large subcapsular abscess containing creamy white pus and some old blood clot was found. The abscess had clearly dissected the capsule off the kidney. It communicated with a large infected thick-walled intrarenal cyst through a small tract along the lateral border of the kidney. It was evident that the cyst accounted for the calyceal deformity and the subcapsular collection also posterior to the kidney accounted for the renal magnification. Drainage and excision of both were accomplished.
(Reproduced from Meyers et al.[11])

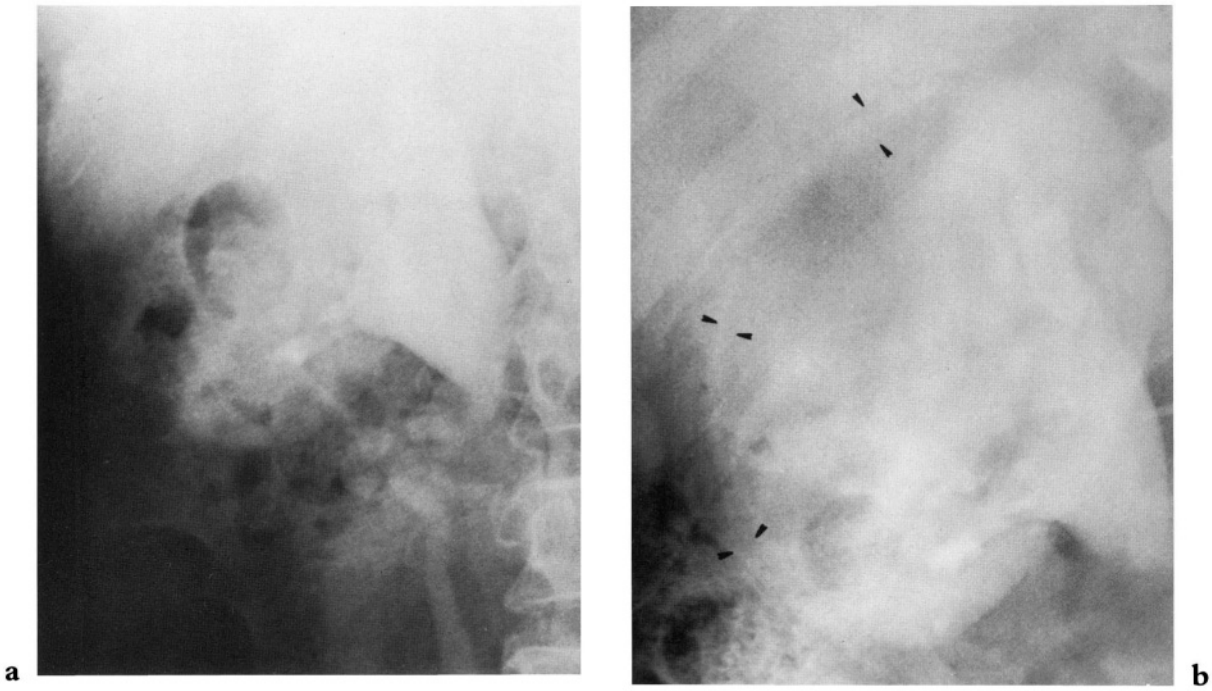


Fig. 8–165. Subcapsular hematoma resulting in hypertension ("Page kidney").
(a) Intravenous urogram. The right kidney is displaced medially. Dilatation of the collecting system and ureter is present.
(b) Nephrotomogram demonstrates the displaced and thickened renal capsule *(arrowheads)* confining a nonopaque mass that is compressing the lateral contour of the kidney.

Illustration continued on opposite page

diagnosis. If the vessel conforms closely to the border of the mass, a subcapsular collection is indicated (Fig. 8–165c). If deviation of the capsular artery begins at some distance from the extrarenal mass, a perirenal collection is indicated (Fig. 8–162b).

As a differential point, it must be recognized that the capsular arteries will be separated from the cortical margin in cases of renal atrophy.[211] Perirenal adipose replacement in instances of acquired shrinkage of the kidney tends to increase the distance between the capsular artery and the atrophied kidney. This separation can be distinguished easily from a subcapsular or perirenal mass displacing the capsular artery.

The marked increase in intrarenal vascular resistance produced particularly by a large subcapsular hematoma may result in striking slowing of arterial flow with failure of opacification of the small intrarenal and capsular vessels.[184]

5. *Structure and function of the renal collecting system.* Distortion of the calyces and renal pelvis may accompany any gross displacement of the kidney itself. Since perirenal abscesses result from a site of renal infection that has perforated through the capsule, chronic inflammatory changes involving the calyces may be evident. An intrarenal abscess or hematoma may produce mass displacement upon the collecting system. Failure of excretion of contrast medium on the involved side ("unilateral anuria") can result from the compression of either a perirenal or subcapsular hematoma.[212]

Computed tomography provides a rapid, noninvasive, and highly accurate method to evaluate and distinguish the presence of subcapsular and perirenal bleeding.[7,213–217] By virtue of its ability to discriminate very small differences in tissue density, CT confirms and readily makes apparent the characteristic anatomic features permitting localization of the collections (Figs. 8–167 through 8–172). Magnetic resonance imaging may also be useful. (Fig. 8–173).

Bridging Renal Septa. The distribution of perirenal fluid may be limited by the bridging renal septa. Compartmentalization of a fluid collection by this internal architecture of the perirenal fat, particularly the posterior

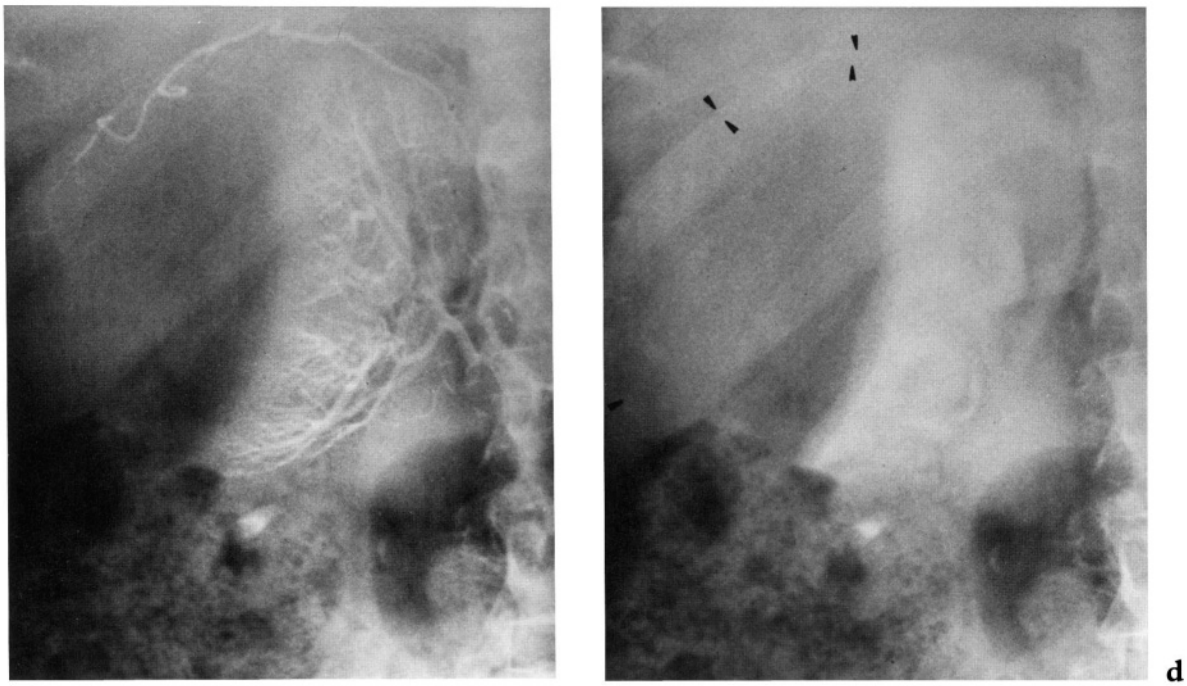


Fig. 8–165. Subcapsular hematoma resulting in hypertension ("Page kidney"). Continued.
(c) Renal arteriogram, arterial phase. The avascular mass compresses the renal parenchyma and vessels, producing a pronounced concave lateral border to the kidney, and displaces the superior capsular artery.
(d) Renal arteriogram, nephrogram phase. The renal capsule *(arrowheads)* is displaced to the same extent as the capsular artery. The renal parenchyma, while markedly compressed, appears intrinsically intact.
At surgery, a large subcapsular hematoma was confirmed, and deep pyelonephritic scars were evident on the surface of the kidney. A right nephrectomy was performed. Pathologic examination confirmed a large, partially organized subcapsular hematoma. A thickened capsule measuring up to 8 mm was present. A 1.2cm resolving abscess in the midportion of the kidney communicated with the hematoma. Hydronephrosis and generalized pyelonephritis were present. Blood pressure returned to normal after operation.
(Reproduced from Meyers et al.[11])

renorenal bridging septum, may mimic a subcapsular collection[60] (Figs. 8–174 and 8–175). At times, on CT, a black line separating the renal parenchyma from the hematoma may be seen (Fig. 8–176a), initially described as representing the swollen renal capsule but probably due to a CT boundary artifact.[219] I have observed two further differential features in that fluid may further extend within continuous branching septa (Figs. 4–176 and 4–177) and the collection may taper to a beak-shape along one contour at the site of traction by an attached septum (Fig. 8–176). This illustrates that the septa may serve to decompress rapidly accumulating collections.

Treatment. These observations on the localization of subcapsular and perirenal collections are of considerable help in planning the most appropriate therapy.[186,220–223] Whether the underlying cause is predominandy unilateral kidney disease or a systemic condition involving both kidneys must be considered.[224] With the recognition that most extrarenal abscesses are secondary to an infection of the kidney, conservative treatment perhaps with surgical drainage or nephrectomy is determined by the extent of involvement. Percutaneous drainage is being currently recommended as the therapeutic procedure of choice for perirenal abscesses.[220] For small lesions, catheter placement is best accomplished under image guidance. A trochar technique can be used in large collection; if no critical anatomy intervenes.[221] Separate drains may be required for multifocal or multiloculated lesions. Percutaneous drainage is frequently curative.[221,223] About one third of perirenal abscesses show communication with the urinary collecting system;

text continues on page 444

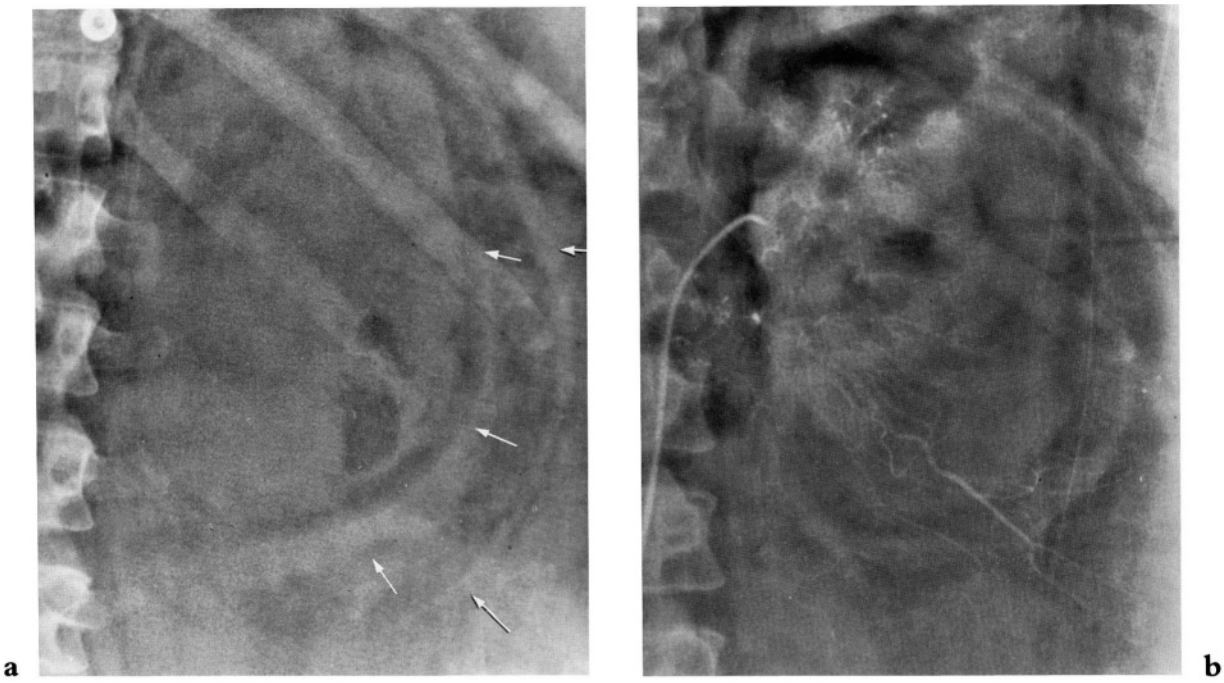


Fig. 8–166. Subcapsular and perirenal hematomas secondary to overanticoagulation.
(a) Plain film. Two discrete curvilinear densities are seen external to an apparently enlarged renal silhouette. These represent displaced renal capsule *(inner arrows)* and renal fascia *(outer arrows).*
(b) Renal arteriogram. The kidney itself is not enlarged but rather is compressed by a prominent subcapsular hematoma. Blood in the perirenal space also displaces the renal fascia.

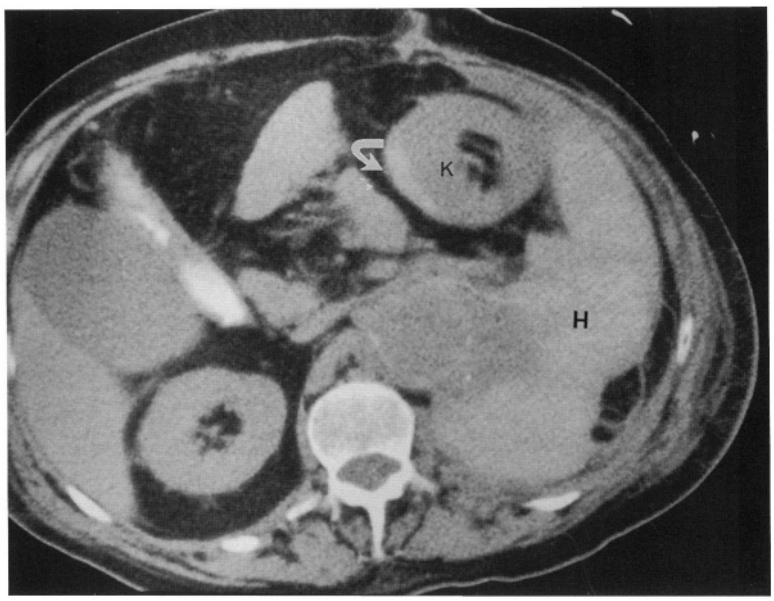
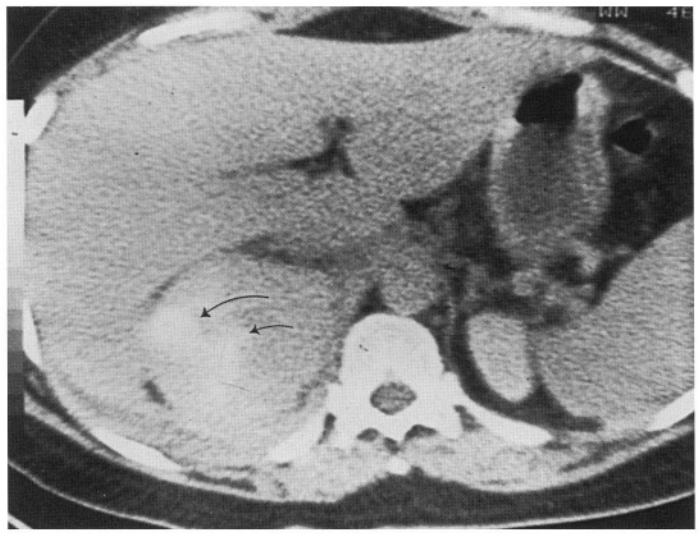
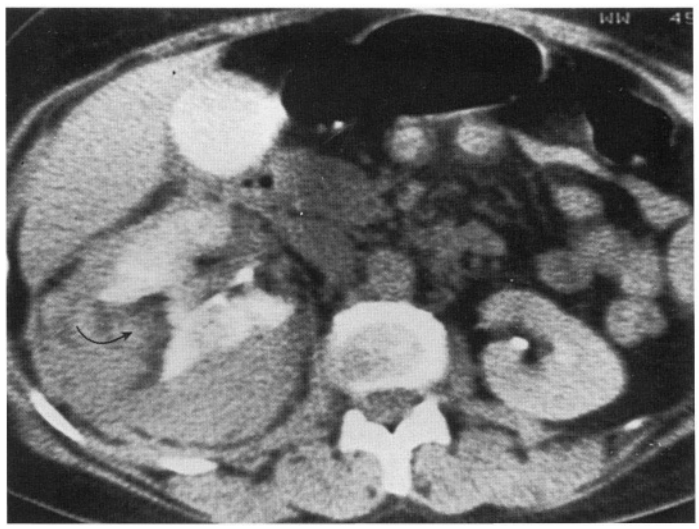


Fig. 8–167. Perirenal hemorrhage.
Following repair of a thoracoabdominal aortic aneurysm, noncontrast CT demonstrates a prominent acute hematoma (*H*) shown by high attenuation fluid, which collects in the posterior and lateral aspects of the left perirenal space. The kidney (*K*) is displaced anteriorly and medially. A small acute subcapsular hematoma is present medially *(arrow).*
(Courtesy of Jay P. Heiken, M.D., Mallinckrodt Institute of Radiology, St. Louis, MO.)


a


b

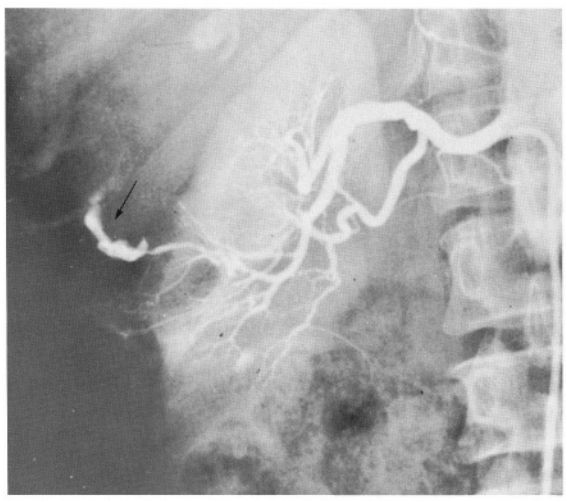

c

Fig. 8–168. Perirenal hemorrhage secondary to renal angiomyolipoma.
(a) CT scan after intravenous contrast medium demonstrates active bleeding *(arrows)* into hemorrhagic collection within right perirenal space.
(b) At a lower level, blood distends the perirenal space. A structure of low attenuation density *(arrow)* corresponds to a defect in the nephrogram. This represents the fatty nature of the parenchymal tumor from which bleeding has occurred.
(c) Selective right renal arteriogram demonstrates active bleeding *(arrow)* into the perirenal space from vessels associated with the tumor mass. (Courtesy of Daniel Wise, M.D., Toronto Western Hospital, Toronto, Canada.)

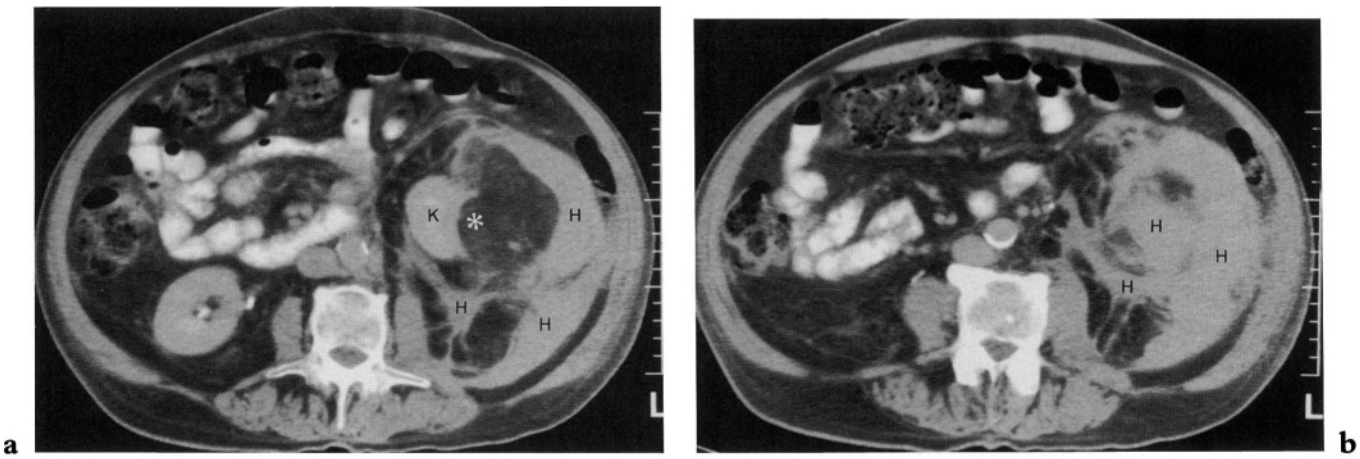


Fig. 8–169. Compartmentalization of perirenal blood by bridging renal septa.
This 78-year-old man, receiving Coumadin therapy for cardiac problems, fell and developed left flank pain and discoloration.
(a and **b)** Multiple sites of acute perirenal hemorrhage (*H*), secondary to unsuspected bleeding angiomyolipoma *(asterisk)* of the left kidney (*K*), are loculated by bridging renal septa. The left kidney is displaced. Bleeding into the flank wall and a segment of the posterior pararenal fat from the fall is also noted.
(Courtesy of Gary Ghahremani, M.D., Evanston Hospital, Evanston, IL.)

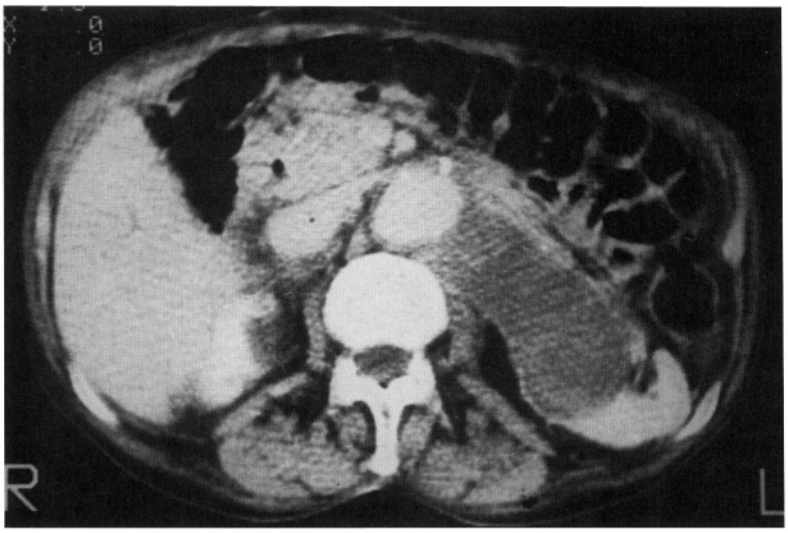


Fig. 8–170. Intrarenal rupture of abdominal aortic aneurysm.
Enhanced CT scan shows a low-density tubular mass extending from the aorta directly into the left renal hilus. This originated from a localized aortic aneurysm that ruptured along the renal vascular pedicle. The posterior perirenal and pararenal spaces are intact. This case indicates that the renal vascular pedicle may provide an avenue for dissection of blood into the perirenal space. (Reproduced from Gavant et al.[218])

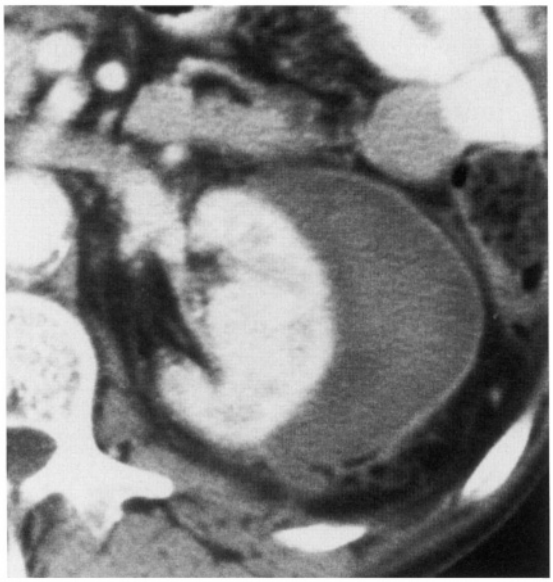


Fig. 8–171. Subcapsular hematoma.
CT demonstrates that a tense collection of blood has stripped the renal capsule, which is thickened and enhanced. The perirenal fat and Gerota's fascia are maintained.

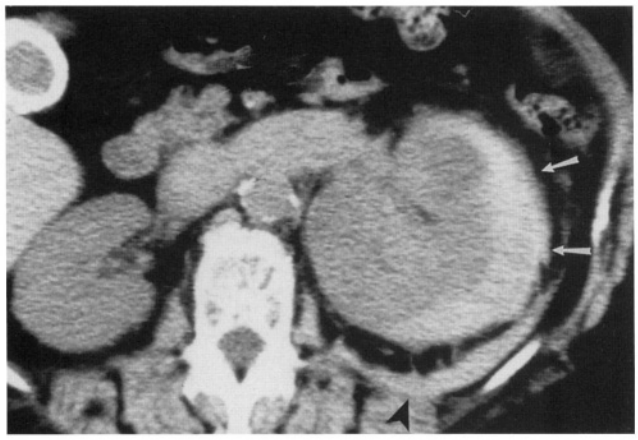


Fig. 8–172. Subcapsular and perirenal hemorrhage secondary to renal cell carcinoma.
CT demonstrates a high attenuation Subcapsular hematoma *(arrows)* and bleeding gravitating to the posterior contour of the perirenal space (*arrowhead*). The enlarged left renal vein is tumor-filled.
(Reproduced from Zagoria et al.[216])

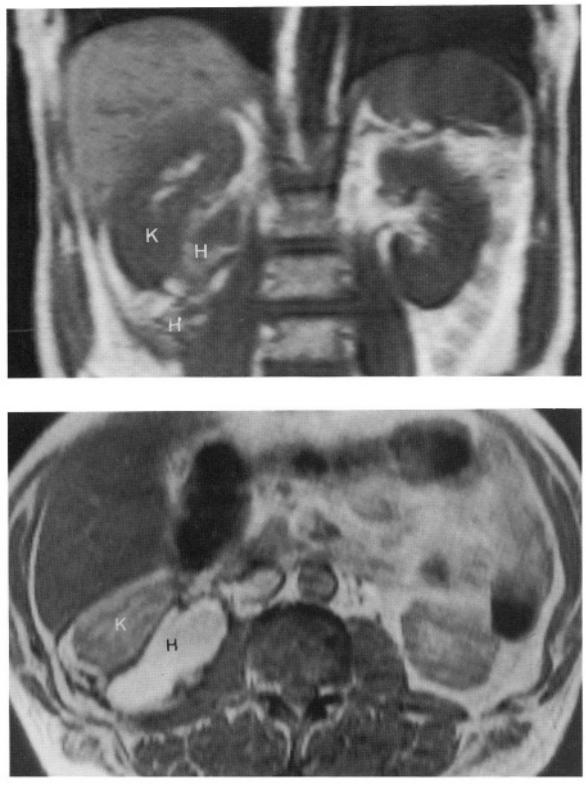


Fig. 8–173. Perirenal hematoma.
MRI demonstrates perirenal hemorrhage (*H*) that has loculated medially and inferiorly. It is discretely confined by the thickened perirenal fascia. The kidney (*K*) is displaced anteriorly, laterally and superiorly.
(a) T1-weighted coronal view.
(b) T2-weighted axial view.
(Courtesy of Jay P. Heiken, M.D., Mallinckrodt Institute of Radiology, St. Louis, MO.)

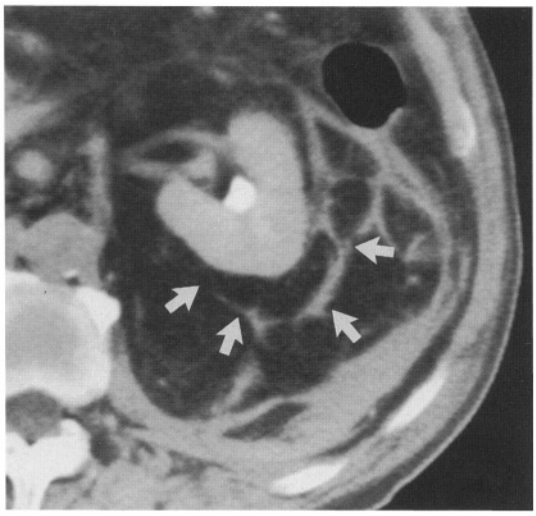


Fig. 8–174. The bridging dorsal renorenal septum.
Acute perirenal bleeding tracking along the bridging renal septa outlines clearly the dorsal renorenal septum *(arrows).* Loculation of blood deep to this can simulate a subcapsular renal hematoma.

successful treatment requires concurrent drainage of the collecting system of it is obstructed.[225] In subcapsular or perirenal hematoma in the presence of a renal tumor, hydronephrosis, renal artery aneurysm, lithiasis, or unilateral renal tuberculosis, nephrectomy does not present any significant long-term problem. On the other hand, if the etiology is nephritis, arteriosclerosis, periarteritis nodosa, or a blood dyscrasia and nephrectomy must be performed as a life-saving procedure, careful follow-up observation of the remaining kidney must be maintained. If the hematoma is not large and adequate visualization of the bleeding site can be obtained, so that it can be controlled with sutures, a biopsy of the involved renal tissue may be preferable to nephrectomy.

Staging of Renal Cell Carcinoma

Survival rates in patients with renal cell carcinoma have been correlated with the extent of tumor at the time of presentation.[226–229] The Robson system of staging[226] is still used by most urologists, but the TNM system[230] is also used, especially in Europe (Table 8–2).

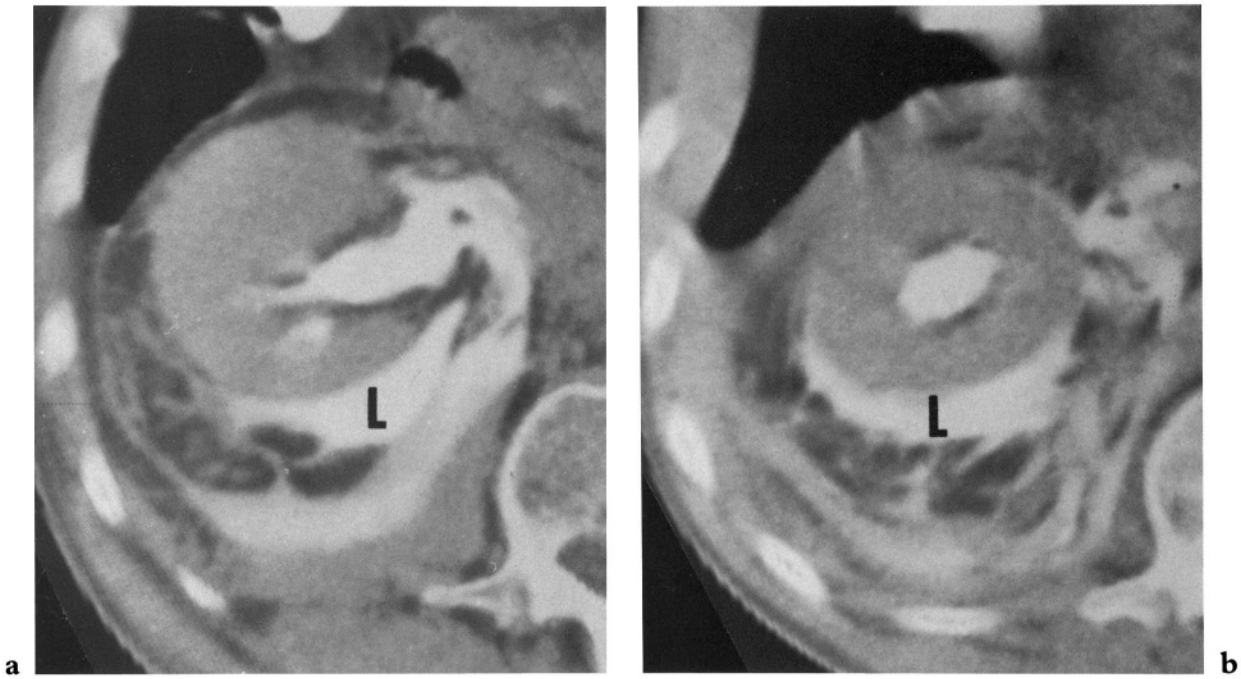


Fig. 8–175. Contrast extravasation during percutaneous nephrostomy outlines bridging perirenal septa.
(**a** and **b**) Fortuitous *in vivo* CT observations at two levels show multiple septa through the perirenal fat and contrast loculation (*L*) by a bridging dorsal renorenal septum. Note that the medial and lateral insertions of this septum vary somewhat at different levels. The fluid loculation may mimic a subcapsular collection. (Courtesy of Michiel Feldberg, M.D., University of Utrecht, The Netherlands.)

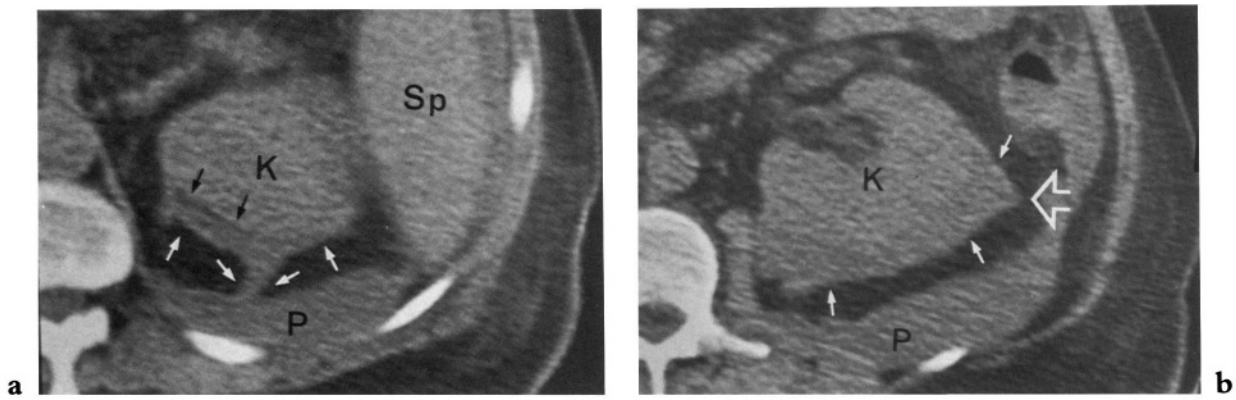


Fig. 8–176. Bleeding deep to renorenal septum mimicking a subcapsular hematoma.
(a) Small hematoma confined by the posterior renorenal bridging septum. Dark line *(black arrows)* between renal parenchyma (*K*) and hematoma *(white arrows)* is thought by some to represent swollen renal capsule and by others a CT artifact. The blood extends within another thickened septum to the posterior renal fascia, which bounds a collection of blood within the posterior pararenal space (*P*). *Sp* = spleen.
(b) The hematoma extends external to the renal capsule from the posteromedial to the posterolateral aspect of the kidney. Laterally it becomes beak-shaped where it is tethered by another septum bridging to the renal fascia *(open arrow).* Tension within the hematoma deep to the renorenal septum displaces the kidney anteriorly.
These findings were proved at autopsy.

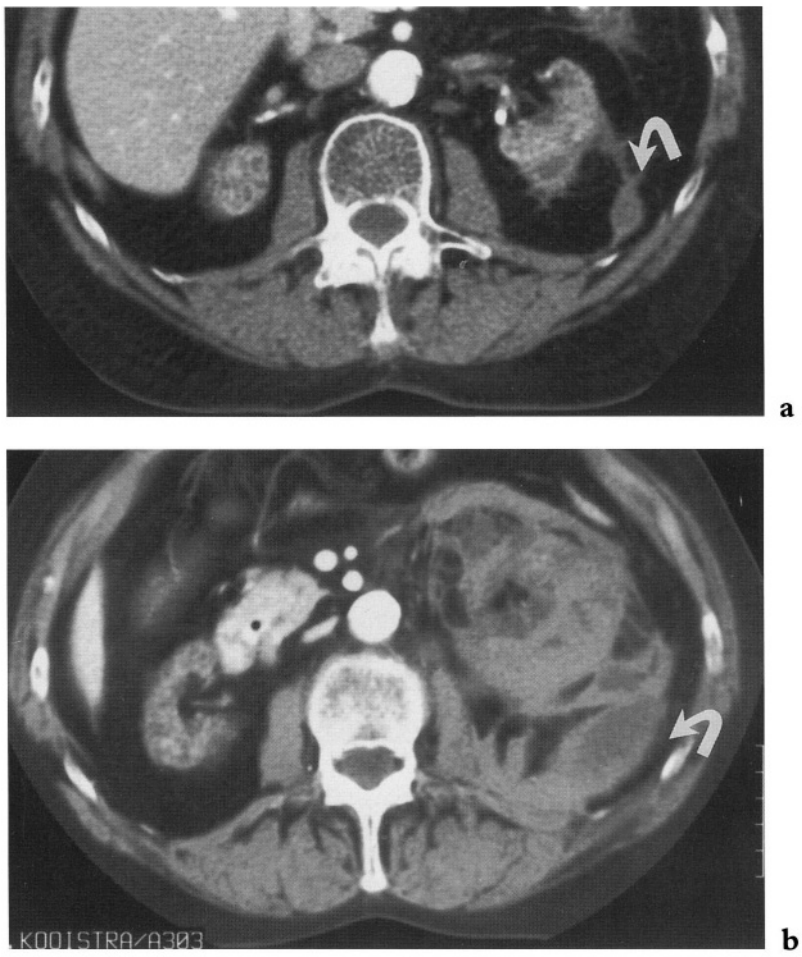


Fig. 8–177. Loculated perirenal blood along bridging septa to the interfascial space.
(a and **b)** In a patient with acquired renal cystic disease secondary to dialysis, CT demonstrates the pathway of perirenal hemorrhage to the intralaminar posterior renal fascia via a bridging septum *(arrow).*
(Courtesy of Michiel Feldberg, M.D., University of Utrecht, The Netherlands.)

Table 8–2. Staging renal cell carcinoma: Robson's classification versus TNM

Robson	Disease extent	TNM
I	Tumor confined to kidney (small, intrarenal)	T1
	Tumor confined to kidney (large)	T2
II	Tumor spread to perirenal fat, but within Gerota's fascia	T3a
IIIA	Tumor spread to renal vein or cava	T3b
IIIB	Tumor spread to local lymph nodes	N1-N3
IIIC	Tumor spread to local vessels and lymph nodes	T3b, N1-N3
IVA	Tumor spread to adjacent organs (excluding ipsillateral adrenal)	T4
IVB	Distant metastasis	M1a-d, N4

Stage I denotes lesions entirely confined within the renal capsule (Fig. 8–178). Stage II indicates extension through the capsule into the perirenal fat but not beyond the renal fascia (Fig. 8–179). Distinction between stages I and II by CT or MRI may be difficult. Thickening of the renal fascia or bridging septa and dilated tortuous perirenal vessels are not reliable signs of tumor extension. However, both stage I and stage II tumors are resectable, and both have good prognoses.

Stage III designates involvement of the renal veins or inferior vena cava or lymph nodes. Venous extension is very uncommon with tumors smaller than 4.5 cm[232] (Figs. 8–180 and 8–181). Since enlarged nodes may be secondary to reactive hyperplasia without harboring tumor,[233] nephrectomy is often done despite the presence of enlarged nodes.

Stage IV denotes either distant metastases or direct invasion of adjacent visceral structures (Figs. 8–182 and 8–183). Local extension can be detected by MRI more accurately than CT, because the most accurate imaging plane can be selected to avoid volume averaging.[234]

Computed tomography often readily provides helpful information in preoperative staging, with an accuracy of over 90%.[235–237] Extracapsular extension is shown by an indistinct tumor margin with strands of soft-tissue density extending into or obliterating the perirenal fat. Color Doppler sonography may be used as a complementary technique for assessing venous extension in patients with an equivocal CT examination.[238] Magnetic resonance imaging appears generally similar to CT in staging renal cell carcinoma,[239–241] but appears superior in differentiating lymphadenopathy from small vascular

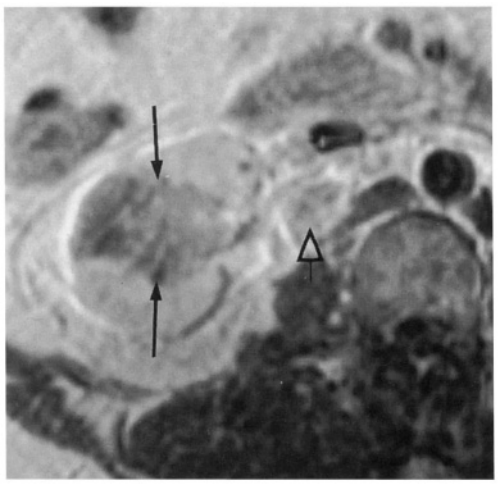


Fig. 8–178. Stage I renal cell carcinoma.
Gadolinium-enhanced T1-weighted MR image demonstrates the tumor *(arrows)* confined within the renal capsule. An enlarged paracaval lymph node *(arrowhead)* proved to be hyperplastic at pathology.
(Reproduced from Narumi et al.[231])

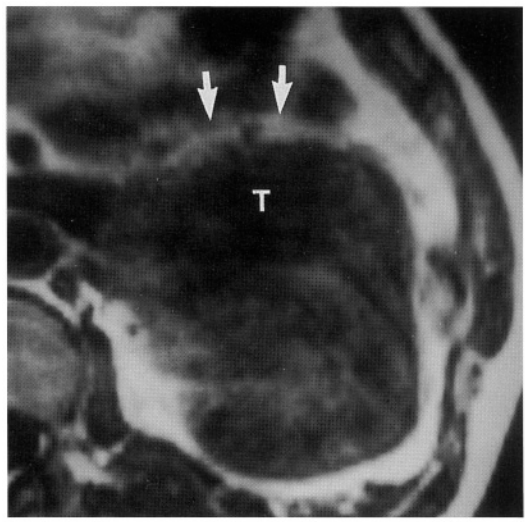


Fig. 8–179. Stage II renal cell carcinoma.
Unenhanced T1-weighted MR image demonstrates the tumor (*T*) extending into the perirenal fat, but the fat plane between the mass and a bowel loop is preserved *(arrows).*
(Reproduced from Narumi et al.[231])

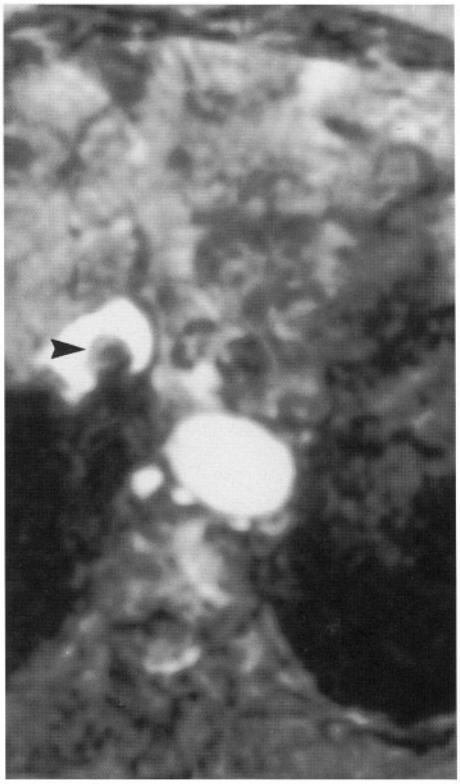
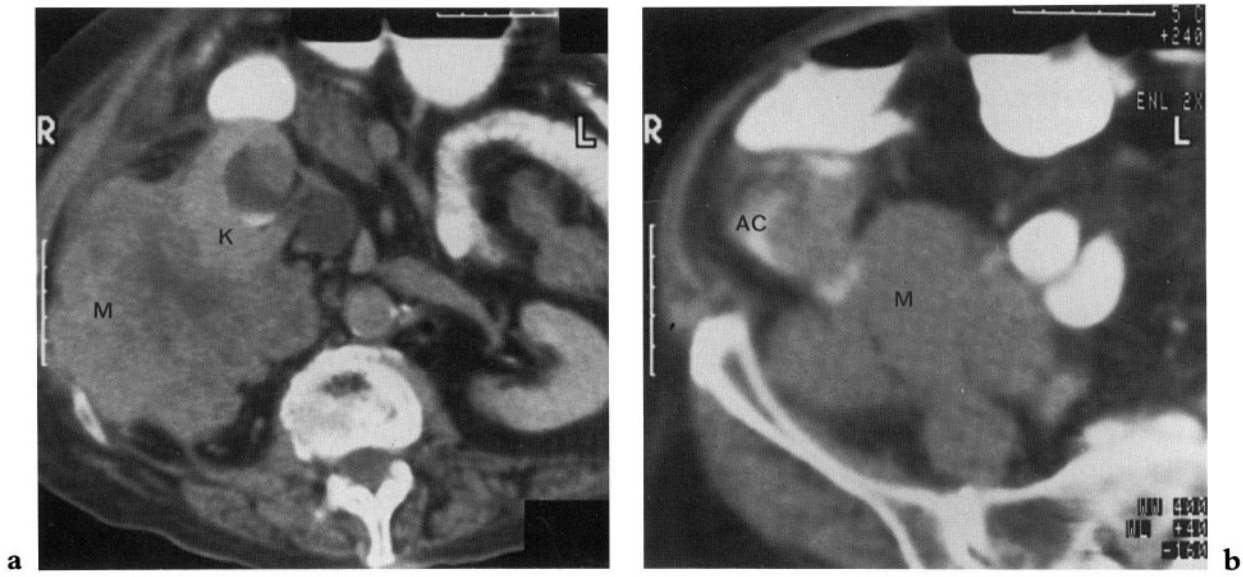


Fig. 8–180. Stage IIIa renal cell carcinoma.
Cine-GRE MR image shows tumor thrombus *(arrowhead)* in the intrahepatic inferior vena cava, arising from a tumor of the right kidney.
(Reproduced from Narumi et al.[231])



Fig. 8–181. Stage IIIa right renal cell carcinoma with IVC thrombus.
T1-weighted MR image demonstrates that the thrombus shows two different signal intensities: an intermediate signal anteriorly *(arrowhead)* and a low signal posteriorly *(arrows),* which proved pathologically to be tumor thrombus and bland thrombus, respectively.
(Reproduced from Narumi et al.[231])



a b

Fig. 8–182. Stage IVa renal cell carcinoma.
(a and **b)** CT shows the large lobulated tumor mass *(M)* extending posteriorly from the displaced right kidney (*K*) and inferiorly where it invades the ascending colon *(AC).*
(Courtesy of Michiel Feldberg, M.D., University of Utrecht, The Netherlands.)

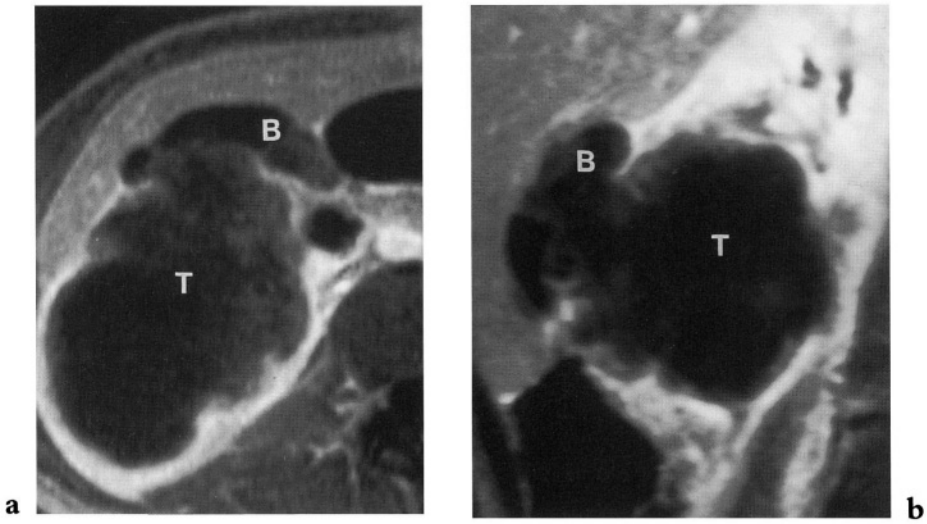


Fig. 8–183. Stage IVa right renal carcinoma.
Gadolinium-enhanced T1-weighted axial **(a)** and sagittal **(b)** MR images show direct extension of the tumor (*T*) to a loop of bowel (*B*), a distinct plane between the tumor and liver, and intratumoral necrosis. (Reproduced from Narumi et al.[231])

structures and in the detection of venous invasion.[231,232,242–244] MRI may be capable in some cases of distinguishing bland thrombus from tumor thrombus (Fig. 8–181), since only the latter will enhance with Gd-DTPA.

Five-year survival decreases with advancing stage, approximating 60% for stage I lesions and decreasing to less than 10% with stage IV tumors.

Stage I and stage II tumors can be approached by a retroperitoneal incision, whereas stage III and stage IV tumors require an abdominal approach. If the vena cava is involved, a thoracoabdominal approach is required.

The prognosis in patients with vena cava extension depends on whether the tumors can be excised completely.[245,246] In patients who have renal vein or vena cava extension without extension outside the renal parenchyma itself and without nodal or distant metastases, the survival at 5 years is 50%. Nodal spread is a poor prognostic indicator, and only 5–10% of these patients survive 5 years.[247]

Perirenal Lymphoma

Lymphomatous involvement of the perirenal space is generally caused by transcapsular extension of parenchymal disease or by direct spread from extraperitoneal disease. The CT appearance of perirenal lymphoma is variable and is dependent on several factors, including the pattern of growth and the mechanism of spread to the perirenal space. It may present diversely, including soft-tissue nodules or plaques, thickening of Gerota's fascia, small curvilinear densities, or a mass contiguous with underlying parenchymal or retroperitoneal disease[40,248–253] (Fig. 8–184). Isolated perirenal involvement without either parenchymal or retroperitoneal disease is unusual and tends to appear as a plaque or "rind" of tissue partially or completely surrounding the kidney. These rinds are typically higher in attenuation than normal renal parenchyma on unenhanced CT but lower in attenuation on contrast-enhanced CT.

Perirenal Retroperitoneal Fibrosis

Retroperitoneal fibrosis has multiple causes and consists of abnormal proliferation of fibrous tissue in the retroperitoneum that may encase the aorta, inferior vena cava, or the ureters.[254] The fibrosis may extend laterally to envelop the renal pelvis, invade the perirenal space to surround the kidney, or both. Perirenal involvement by retroperitoneal fibrosis may appear as nodular masses[253,255] or as a rind or plaque of fibrous tissue surrounding the kidney.[40,256] (Fig. 8–185).

Perirenal Extramedullary Hematopoiesis

Extramedullary hematopoiesis in myelofibrosis is widely distributed, involving organs such as the pleura, lungs,

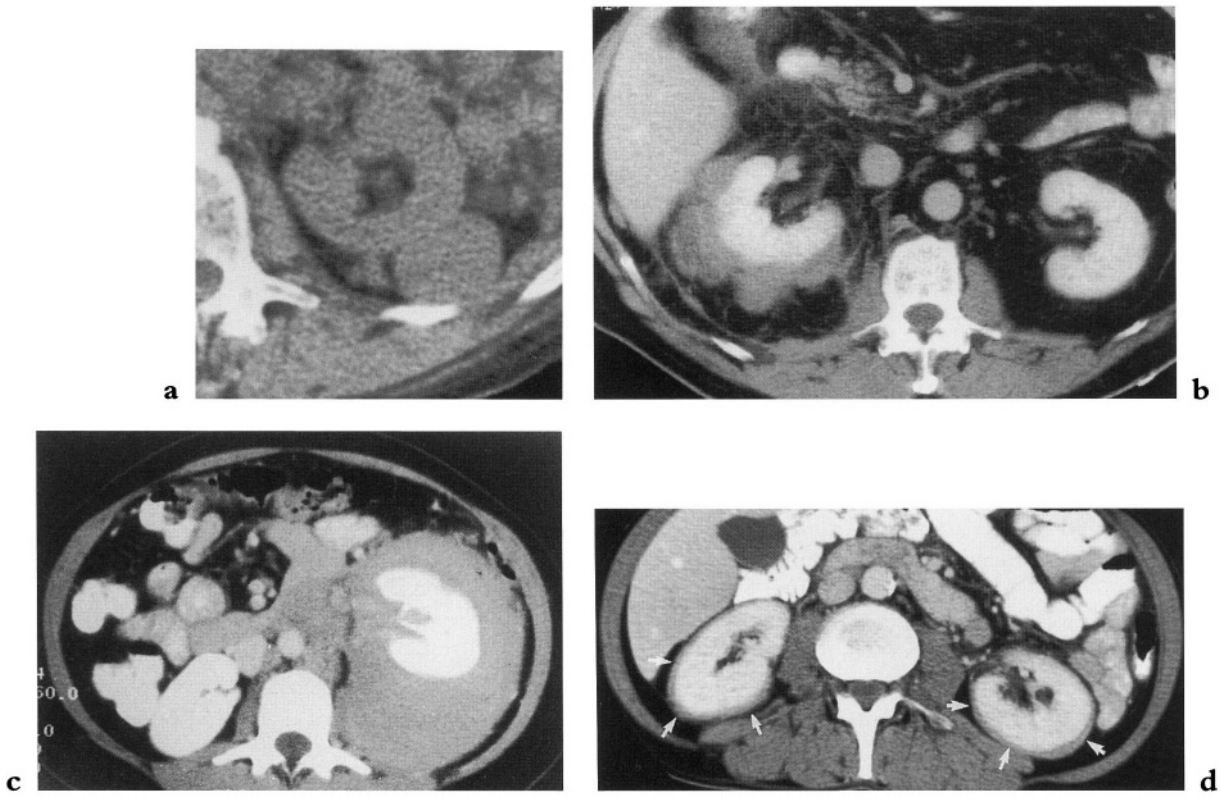


Fig. 8–184. Perirenal lymphoma.
Spectrum of findings illustrated in four different patients.
(a) Several discrete soft tissue nodules in the perirenal fat.
(b) Confluent lobulated perirenal masses are associated with parenchymal involvement on the right. Note plaquelike thickening of Gerota's fascia and the bridging septa.
(Reproduced from Bailey et al.[252])
(c) Massive perirenal lymphomatous mass on the left with displacement of the kidney, contiguous with retroperitoneal adenopathy.
(Courtesy of S. S. Doda, M.D., Diwan Chand Aggarwal Imaging Research Centre, New Delhi, India.)
(d) Bilateral perirenal "rinds" *(arrows).* They are of lower attenuation than adjacent enhancing renal parenchyma. This patient is postsplenectomy for Hodgkin's lymphoma.
(Courtesy of Michiel Feldberg, M.D., University of Utrecht, The Netherlands.)

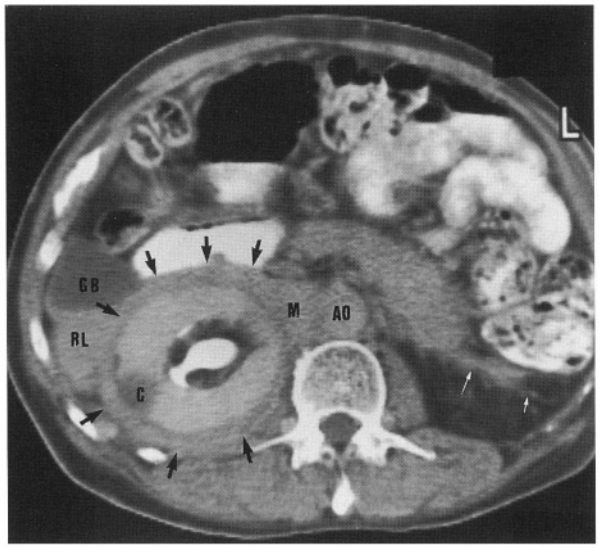


Fig. 8–185. Retroperitoneal fibrosis in perirenal space. Mass *(black arrows)* around right kidney in perirenal space originates from fibrous mass (*M*) adjacent to aorta *(AO).* Behind the pancreas, a linear fibrosis extends along the remnant of the left anterior renal fascia *(white arrows).* C = renal cyst; *GB* = gallbladder; *RL* = right liver. (Courtesy of Michiel Feldberg, M.D., University of Utrecht, The Netherlands.)

gastrointestinal tract, breast, skin, dura matter, kidneys, and adrenal glands. The pathogenesis is not completely understood. Reversion of the liver and spleen to their fetal hemopoietic function after an unidentified stimulus has been proposed. More recently, extramedullary hematopoiesis has been suggested to result from hematogenous spread of multipotential stem cells, with consequent infiltration of organs and tissues. Perirenal localization is a rare finding (Fig. 8–186), and only a few cases have been reported in the literature.[251,257,258]

Perirenal Metastases

The perirenal space because of its perforating capsular vessels and lymphatics may be a site for the metastatic deposits of many malignant conditions. Common sources of perirenal metastatic disease include melanoma, lung, breast, renal cell, or transitional cell carcinoma[189,259] (Fig. 8–187). In cases in which the primary is not of renal origin, the metastases are generally present without the involvement of either kidney.

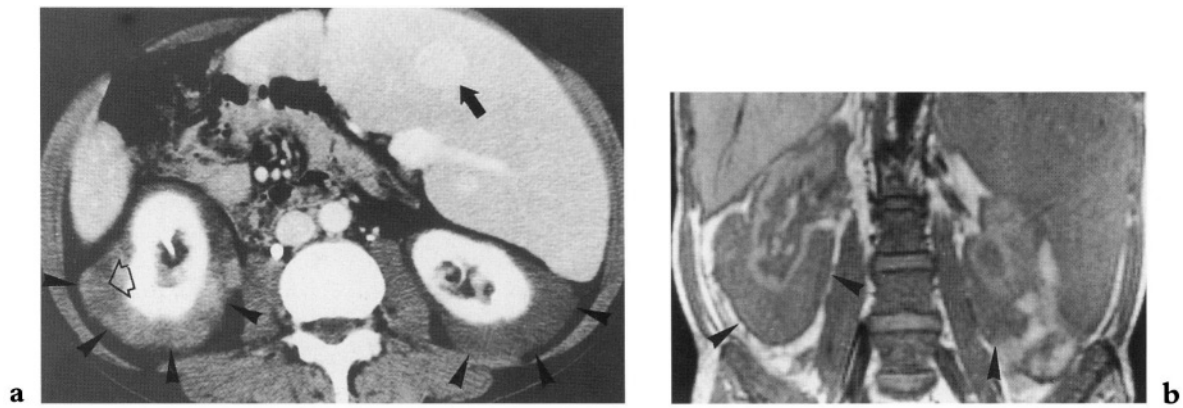


Fig. 8–186. Perirenal extramedullary hematopoiesis in a patient with agnogenic myeloid metaplasia (idiopathic myelofibrosis).
(a) CT and **(b)** coronal T1-weighted MR scan demonstrate bilateral perirenal tissue *(arrowheads)* with distinguishable nodules of extramedullary hematopoiesis (*open arrow).* Needle biopsy confirmed the presence of hemopoietic tissue. There is severe splenomegaly with splenic nodules of extramedullary hematopoiesis *(black arrow),* hepatomegaly, and osteomyelosclerosis of the vertebral bodies. (Reproduced from Rapezz et al.[257])

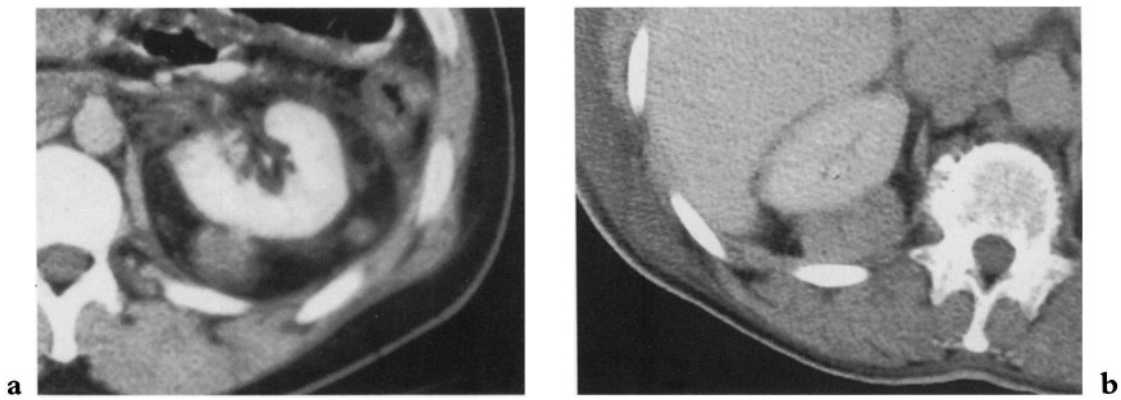


Fig. 8–187. Perirenal metastases.
Multiple soft-tissue masses are present in the perirenal fat in a case of **(a)** metastatic melanoma and **(b)** metastatic lung carcinoma. (Reproduced from Wilbur et al.[259]).

Posterior Pararenal Space

Roentgen Anatomy of Distribution and Localization of Collections

Selective opacification of the posterior pararenal space in the cadaver permits identification of the preferential pathway of spread and the characteristic localizing features. This is shown in Figure 8–188. The natural spread is inferior and lateral because of gravity, lumbar lordosis, and the fact that this space is open toward the flanks. The fluid density thus assumes an axis paralleling that of the psoas muscle and tends to displace the lower pole of the kidney laterally as well as anteriorly and upward. The kidney outline and perirenal fat shadows tend to be preserved. These features further distinguish these collections from effusions within the perirenal space. The psoas muscle shadow is obliterated by fluid collections, although it may actually be highlighted by gas collections. Further progression is shown by anterior and medial displacement of the ascending or descending colon and then encroachment on, or obliteration of, the flank stripe (Fig. 8–189).

The significant criteria for the localization and distinction of collections within the posterior pararenal space are outlined in Table 8–1 on page 360.

Clinical Sources of Effusions

The posterior pararenal space is a common site of spontaneous retroperitoneal hemorrhage in conditions such as a bleeding diathesis or overanticoagulation. Hemorrhage from ruptured abdominal aneurysms also may typically localize within this compartment. Trauma (including stab wounds and rib fractures) and retroperitoneal lymphatic extravasation are other sources of effusions.

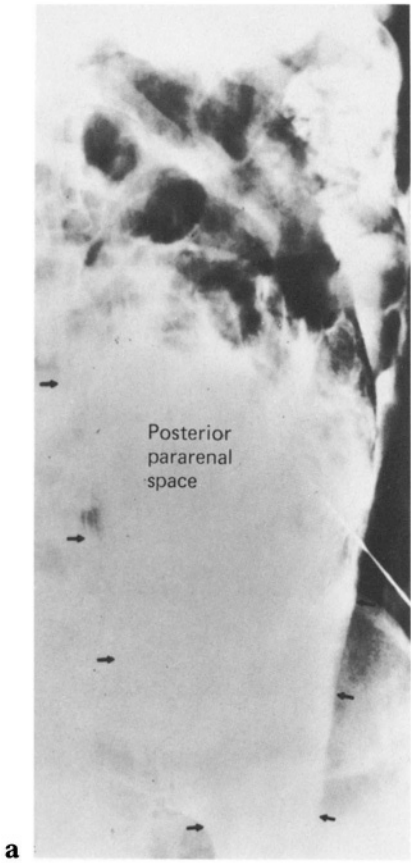
Infection limited solely to this compartment is rare. The posterior pararenal space itself does not include organs from which infection can arise directly. Except for the unusual case caused by bacteremia, infection here may develop as a complication of osteomyelitis of the vertebral column or 12th rib or of an aortic graft. Abscess behind the transversalis fascia is not, strictly speaking, extraperitoneal, but retrofascial abscess (largely of osseous origin from infection in the spine or 12th rib, often from tuberculosis or actinomycosis) occasionally may transgress fascial planes to involve the posterior pararenal space. Fulminating perirenal infection rarely does this.

Extravasates originating in the pelvis, as in perforation of the rectum or sigmoid colon, may spread upward into this compartment.

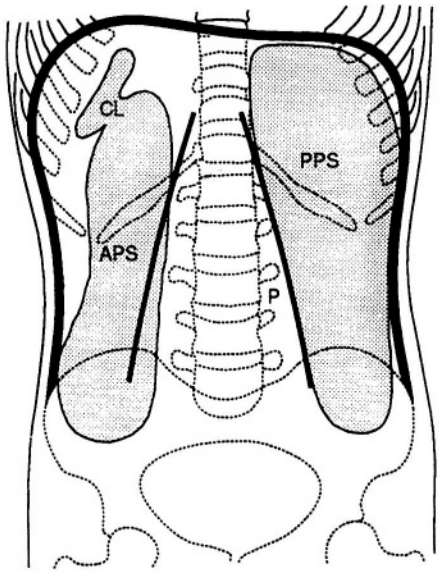
Hemorrhage

Retroperitoneal bleeding accompanying renal trauma or fractures of the spine or posterior ribs may be identified as residing largely within this space (Fig. 8–190).

Many cases of extraperitoneal hemorrhage due to bleeding dyscrasias (Fig. 8–191) or overanticoagulation (Fig. 8–192) can be identified precisely as developing within the posterior pararenal compartment. The distinctive complex of findings is evaluated easily, and the



a



b

Fig. 8–188. (a) Postmortem injection into the left posterior pararenal space.
Medially the collection parallels the psoas muscle and obliterates its outline. Laterally there is direct extension into the flank fat. The axis of the collection is inferior and lateral.
(Reproduced from Meyers et al.[12])
(b) Diagram showing the characteristic spread and configuration of extraperitoneal fluid and/or gas collections in the posterior pararenal space (PPS).
Configuration of collection within the anterior pararenal space *(APS)* on the opposite side is shown for comparison. *P* = psoas muscle margin; *CL* = coronary ligament.

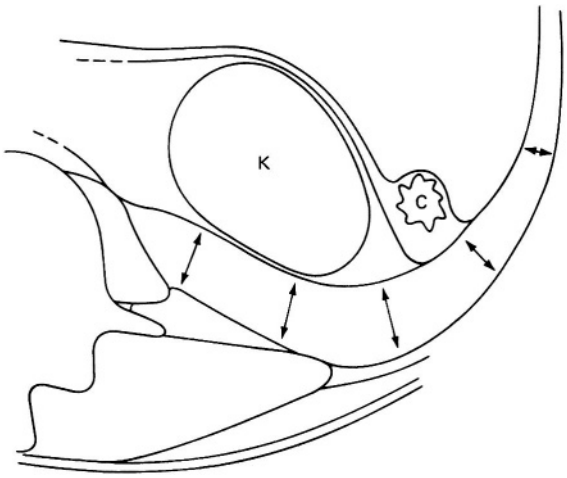


Fig. 8–189. Fluid collection in the posterior pararenal compartment with viscus displacement and extension into the properitoneal fat.
K = kidney; *C* = colon.
(Reproduced from Meyers et al.[12])

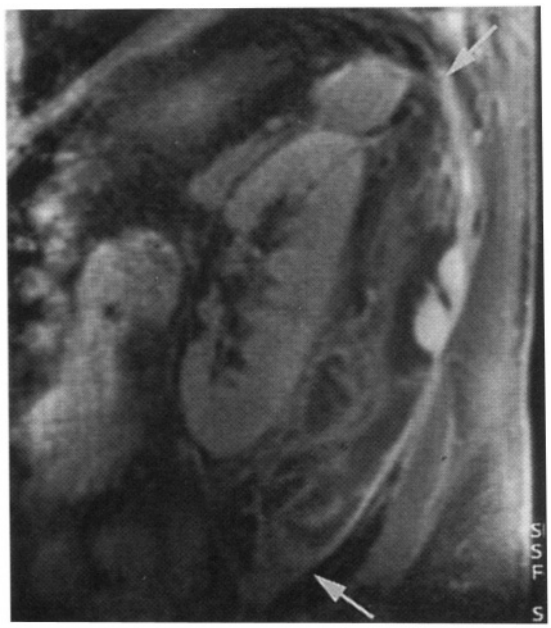


Fig. 8–190. Posterior pararenal hemorrhage following abdominal trauma.
Sagittal T1-weighted post-gadolinium MR image demonstrates a large volume of posterior pararenal blood *(arrows)* of mixed signal intensity, indicating blood products of varying age.
(Reproduced from Semelka RC, Ascher SM, Reinhold C: MRI of the Abdomen and Pelvis: A Text-Atlas. Wiley-Liss, New York, 1997, with permission.)

radiologic evaluation may be crucial in uncovering the primary disorder. Figure 8–193 illustrates the case of a 58-year-old man with chronic bilateral hematomas identified within the posterior pararenal compartments; further investigation then led to the diagnosis of a hemophiliac disorder.

Bleeding from a ruptured aortic aneurysm frequently extends to this compartment. Plain films may show a large extraperitoneal fluid collection with occasional findings localizing the process to the posterior pararenal space, such as alterations of the properitoneal flank stripe[260] or lucent streaks through the fat[261] (Figs. 8–194 and 8–195). Acute diffuse extravasation from a ruptured abdominal aortic aneurysm selectively within the posterior pararenal space has been documented by dynamic contrast-enhanced CT.[262] In a low leak of an abdominal aortic aneurysm, CT often demonstrates that bleeding may preferentially rise upward within the posterior pararenal space (Figs. 8–196 and 8–197). Aneurysms may also rupture first into the psoas muscle and then into the posterior pararenal space.[263]

Bleeding from the femoral sheath as a complication of femoral vascular catheterization procedures[137,138] may open into the pelvic extraperitoneal spaces and then spread superiorly and posteriorly within the posterior peritoneal space, at times as high as the diaphragm (Fig. 8–198).

Abscess

Infection of this space consequent to osteomyelitis (Fig. 8–199) is now much less common than it has been in the past. Fascial transgression with infection may be seen as a complication of bowel or renal surgery (Figs. 8–200 and 8–201) or severe renal disease. Other sources include perforations of the colon (Figs. 8–202 and 8–203) and unusual extraperitoneal positions of the appendix (Figs. 8–204 and 8–205) and infections complicating aortic grafts[18,264–266] (Fig. 8–206).

Lymphatic Extravasation

Extraperitoneal extravasation of lymph often selectively involves the posterior pararenal compartment (Fig. 8–207). Drainage laterally may coalesce into a flank lymphocyst (Fig. 8–208).

At times, circumscribed solid masses of extraperitoneal lymph node origin can be identified clearly as localized to the posterior pararenal space. Figure 8–209 illustrates this in an instance of reticulum cell sarcoma.

text continues on page 463

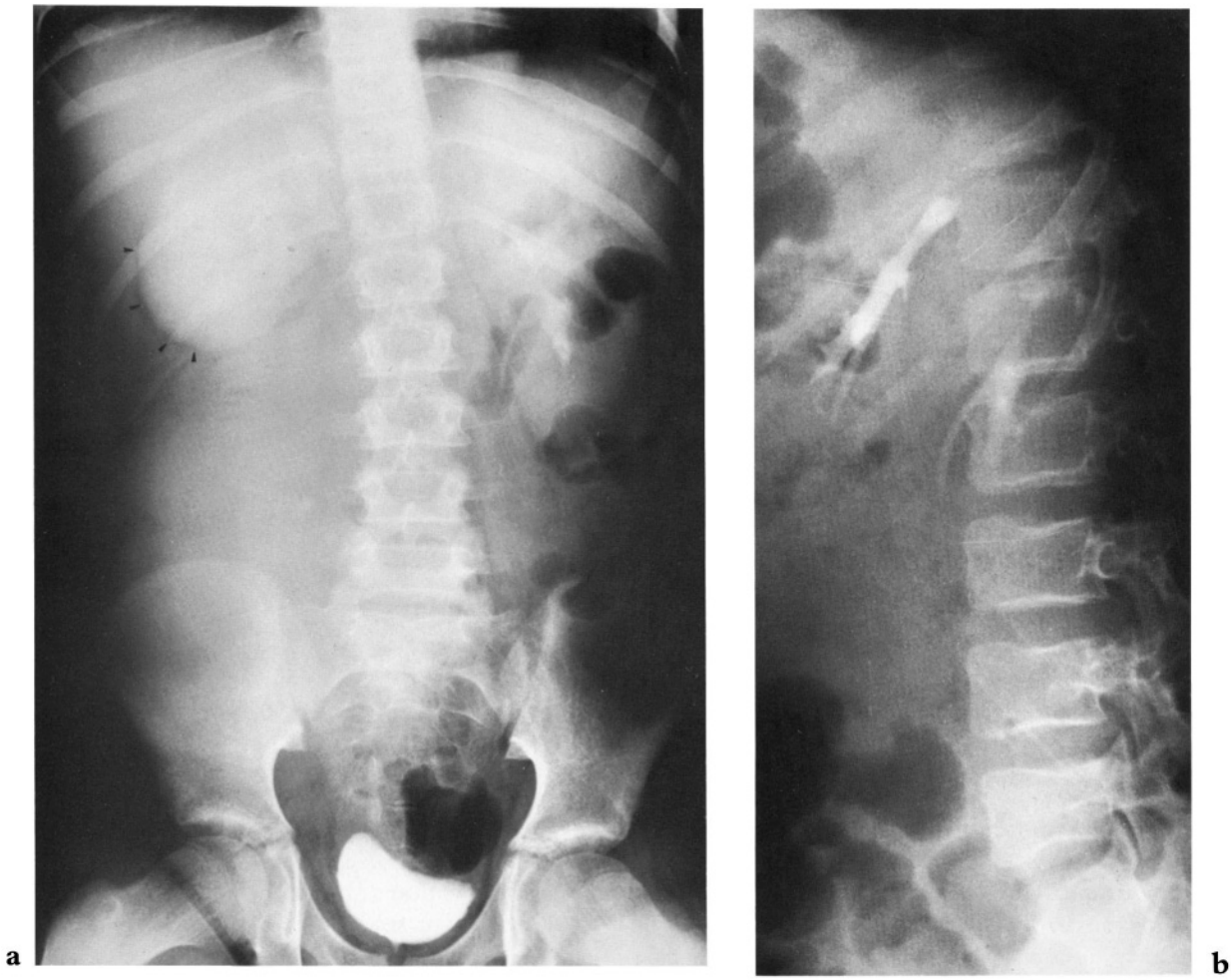


Fig. 8–191. Posterior pararenal hemorrhage in a hemophiliac.
(a) Intravenous urogram. The axis of the extraperitoneal density on the right is oriented inferolaterally. The psoas shadow is obliterated and the flank stripe obscured. The collection displaces the kidney laterally and superiorly. The obstructive nephrogram is outlined further by intact perirenal fat *(arrowheads).*
(b) Right lateral projection. The posterior collection displaces the kidney anteriorly.
(Reproduced from Meyers et al.[12])

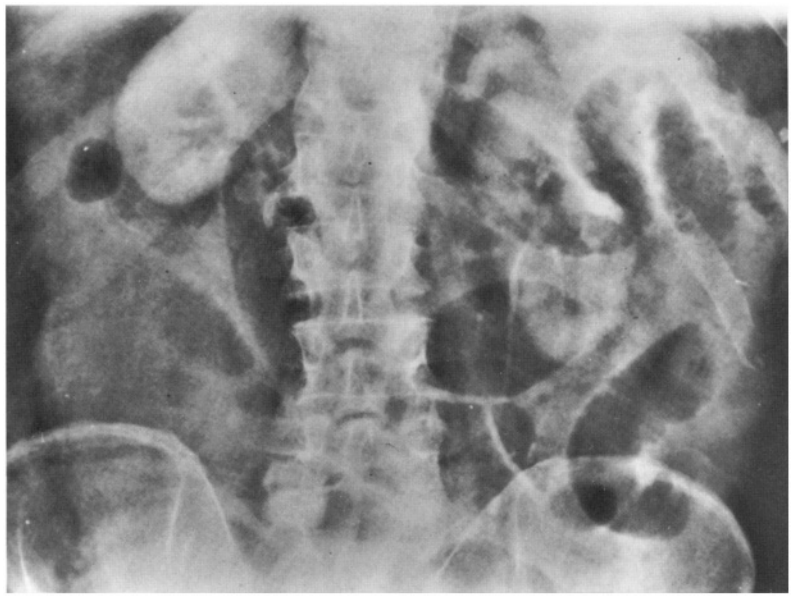


Fig. 8–192. Posterior pararenal hemorrhage secondary to overanticoagulation.
The partially obstructed kidney on the right is displaced superiorly and laterally by the collection of blood that extends in an inferolateral axis. The hemorrhage obscures the psoas muscle margin but has not yet extended into the flank fat. The perirenal fat is not involved.



Fig. 8–193. Chronic bilateral hematomas in the posterior pararenal spaces in an adult hemophiliac.
(**a** and **b**) Intravenous urography demonstrates a calcified mass on the right and a soft-tissue density on the left. The lower segments of the psoas muscles are obliterated. The larger blood collection on the left displaces the lower pole of the kidney superiorly and laterally and the ureter medially and anteriorly.

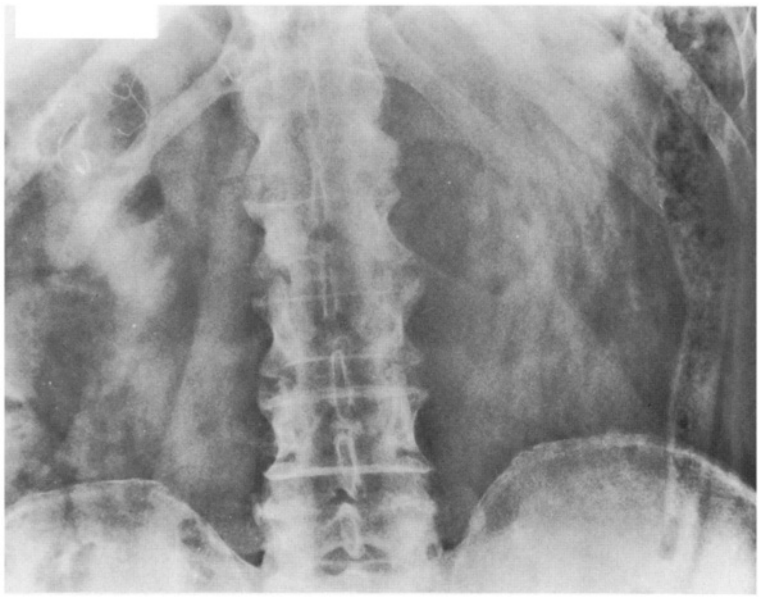


Fig. 8–194. Posterior pararenal hemorrhage from ruptured aneurysm of the abdominal aorta.
Plain film demonstrates streaky radiolucent lines on the left in an area of an ill-defined mass that also causes loss of visualization of the psoas muscle border. These changes are secondary to blood dissecting, often in sheets, through the posterior pararenal fat.

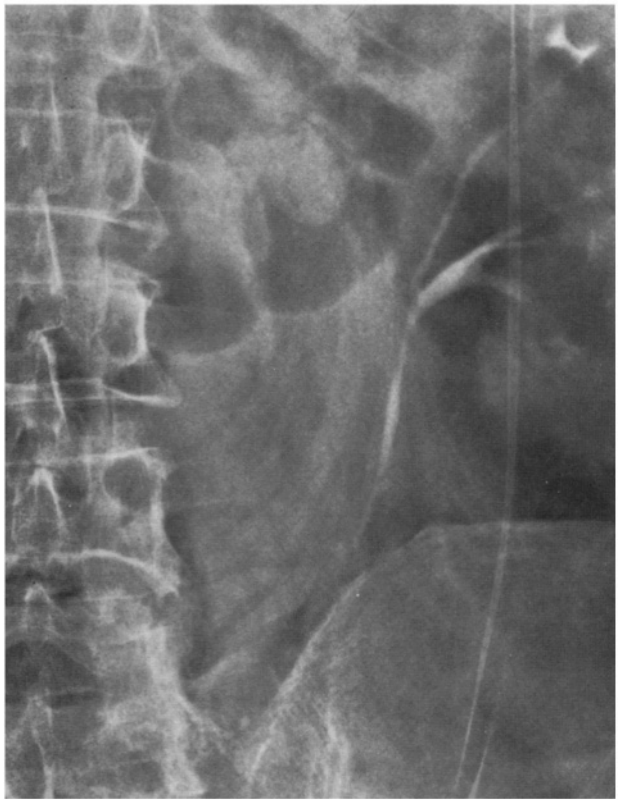


Fig. 8–195. Posterior pararenal hemorrhage from ruptured abdominal aortic aneurysm.
Intravenous urogram demonstrates streaky radiolucent lines in an ill-defined extraperitoneal soft-tissue mass that obscures the psoas muscle margin and displaces the kidney laterally.

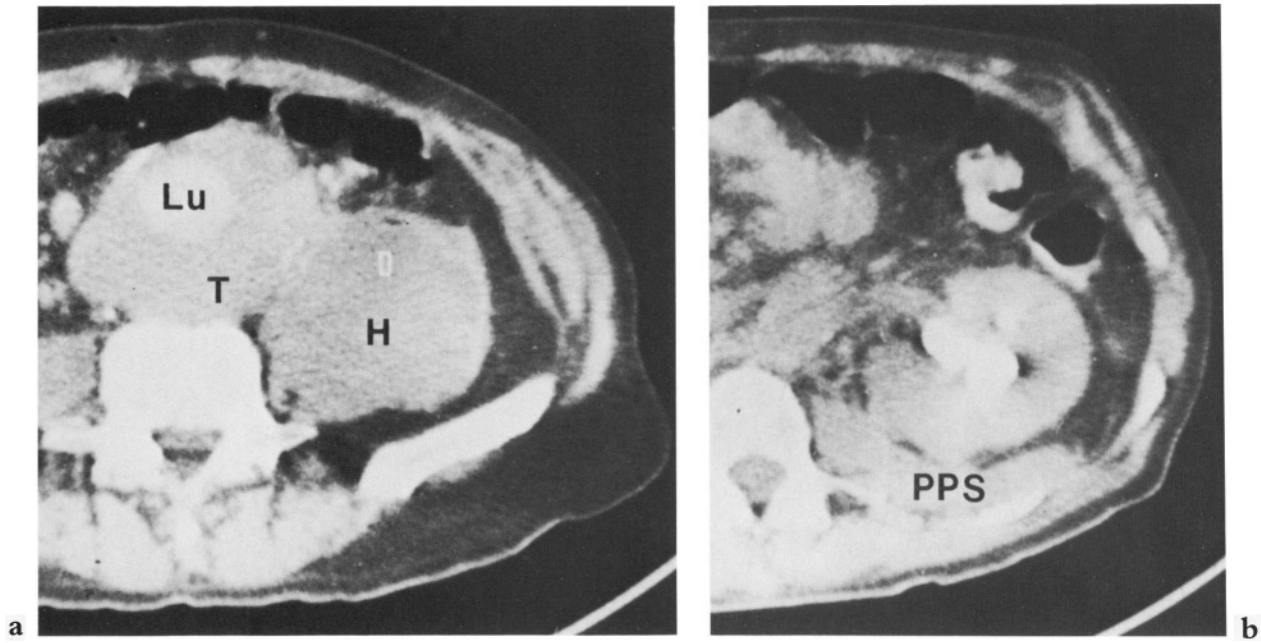


Fig. 8–196. Posterior pararenal hemorrhage from leaking aneurysm of the abdominal aorta.
(a) CT scan after intravenous contrast medium demonstrates a large aneurysm of the abdominal aorta containing thrombus *(T)* surrounding its residual opacified lumen *(Lu).* Hemorrhage *(H)* has extended from a site of rupture into the adjacent tissues on the left.
(b) At a higher level, the hemorrhage has risen into the posterior pararenal space *(PPS),* displacing the kidney anteriorly and laterally.

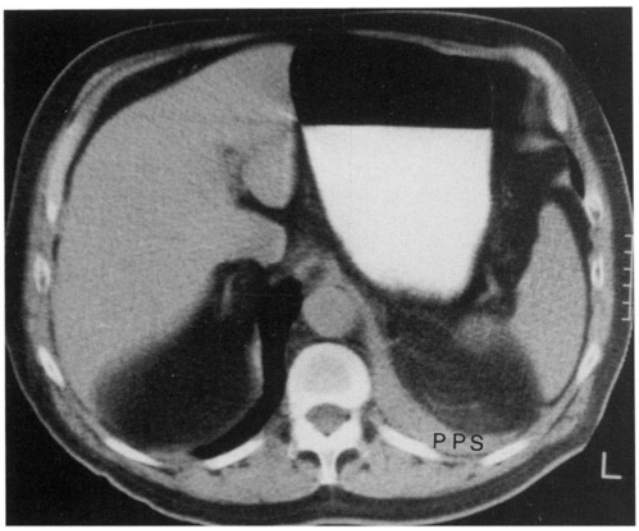


Fig. 8–197. Posterior pararenal hemorrhage from ruptured abdominal aortic aneurysm.
From the site of extravasation from the infrarenal aorta, the hemorrhage has risen toward the left diaphragm within the posterior pararenal space *(PPS).*

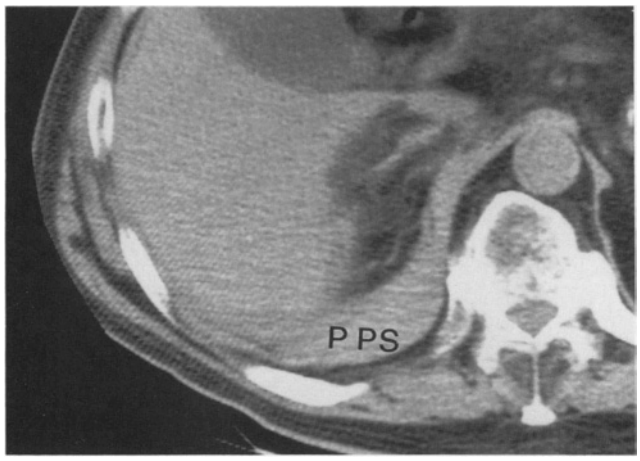


Fig. 8–198. Posterior pararenal hemorrhage from bleeding complication of femoral catheterization.
Postcatheterization bleeding on the right has risen from the pelvis to the diaphragm within the posterior pararenal space *(PPS).* Some perirenal blood tracks along upper bridging septa.

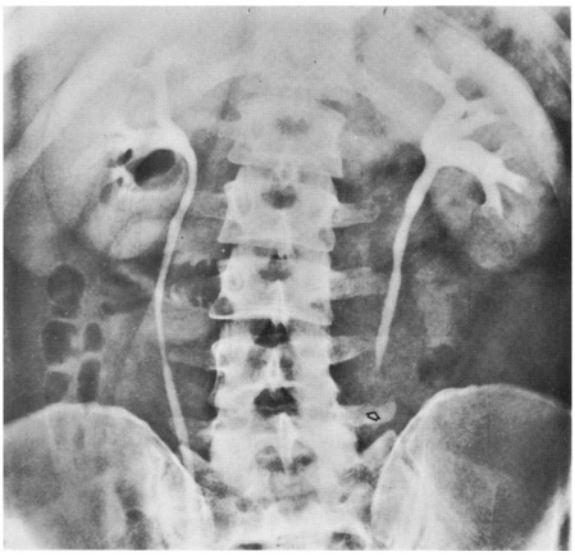


Fig. 8–199. Posterior pararenal abscess secondary to spinal osteomyelitis.
Staphylococcal osteomyelitis involves the left transverse process of L5 *(arrow).* Infection in the posterior pararenal space is revealed by the characteristic displacement of the lower pole of the left kidney upward and outward. Loss of visualization of the psoas margin may be due to the abscess as well, or it may be a consequence only of the scoliosis present.

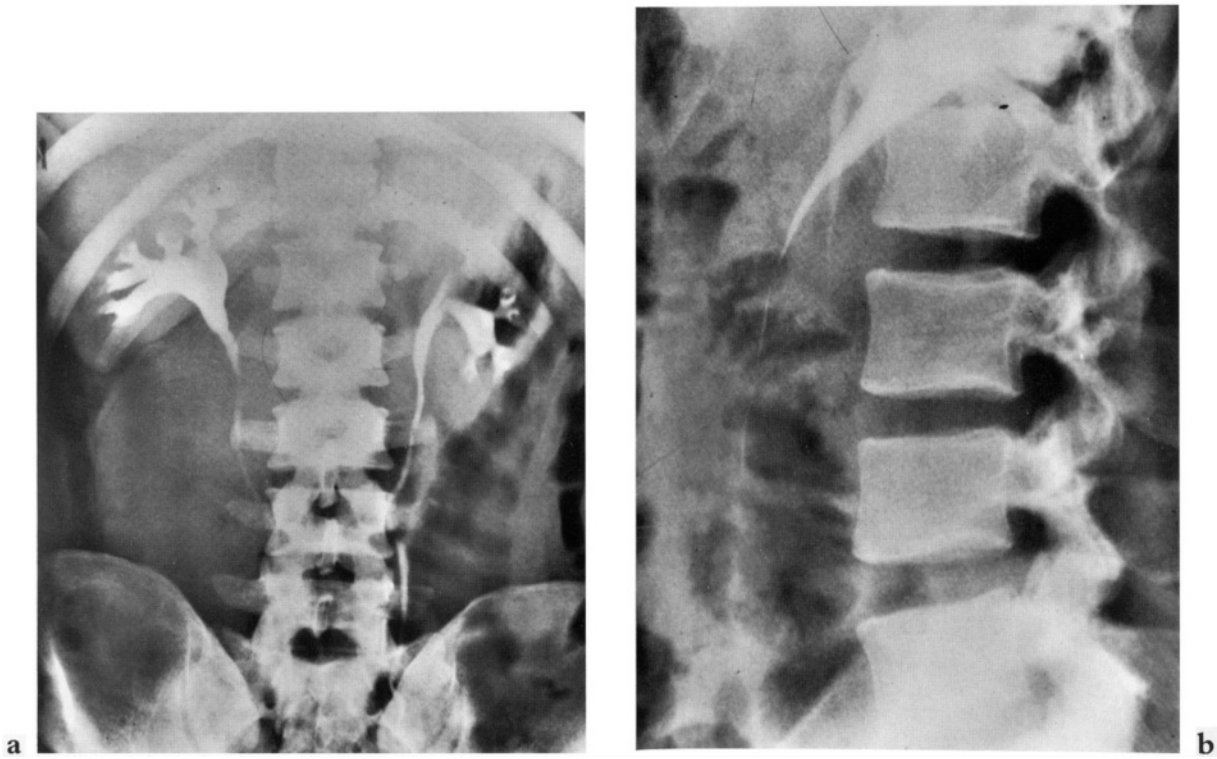


Fig. 8–200. Posterior pararenal abscess following bowel resection for regional enteritis.
(a) The density on the right is directed inferiorly and laterally, obscures the psoas margin, and displaces the lower pole of the kidney upward and outward.
(b) Right lateral view confirms the extreme posterior position of the abscess, which displaces the kidney and ureter forward.

Fig. 8–201. Posterior pararenal infection postnephrectomy.
Following left nephrectomy for renal cell carcinoma, hematoma infected with gas-producing organisms occupies the renal bed and progresses across the posterior pararenal space to involve the flank and abdominal wall.
(Courtesy of Gary Ghahremani, M.D., Evanston Hospital, Evanston, IL.)

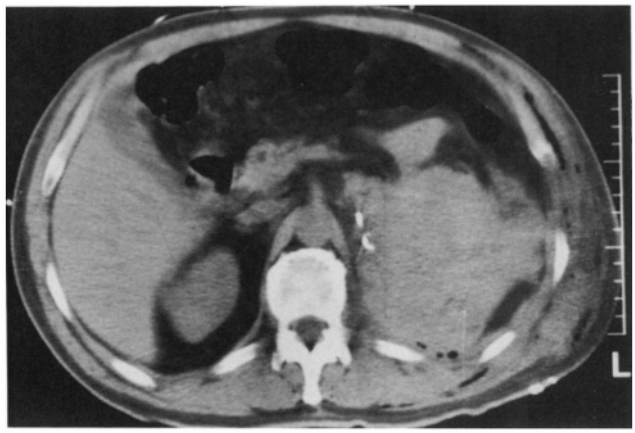




Fig. 8–202. Posterior pararenal abscess secondary to sigmoid colon perforation.
This patient received pelvic irradiation for carcinoma of the cervix. Sigmoid perforation results in an extensive gas and fluid collection throughout the posterior pararenal space on the left, displacing the obstructed kidney and descending colon medially.
(Courtesy ofJay P. Heiken, M.D., Mallinckrodt Institute of Radiology, St. Louis, MO.)

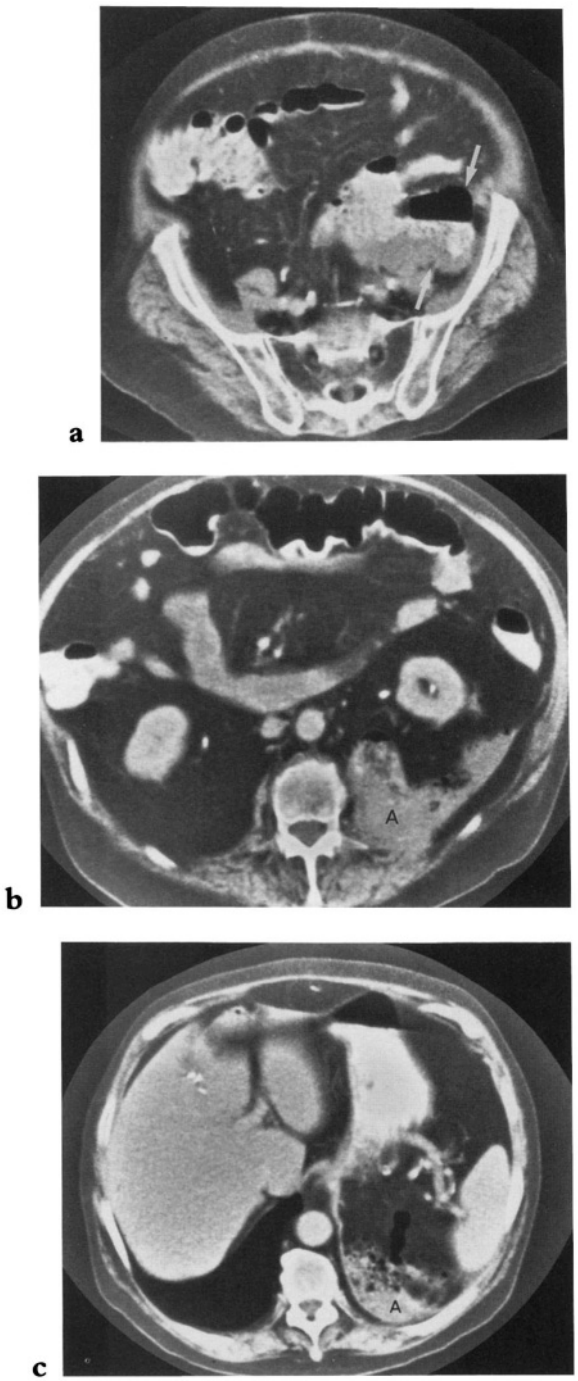


Fig. 8–203. Posterior pararenal abscess secondary to diverticulitis of the sigmoid colon.
In this 72-year-old man, contrast- and gas-containing infection can be traced in continuity throughout the posterior pararenal space.
(a) Diverticular abscess *(arrows)* of the descending colon–sigmoid colon junction has penetrated into the posterior pararenal space.
(b) Scan at the level of the kidneys shows superior continuation of the abscess *(A)* within the posterior pararenal space. The abscess is displacing the left perirenal space anteriorly.
(c) The posterior pararenal abscess *(A)* continues superiorly to reach the diaphragm.
(Reprinted with permission from Gore RM, Meyers MA: Pathways of abdominal and pelvic disease spread. *In* Textbook of Gastrointestinal Radiology. Edited by RM Gore, MS Levine, I Laufer. WB Saunders, Philadelphia, 1993.)

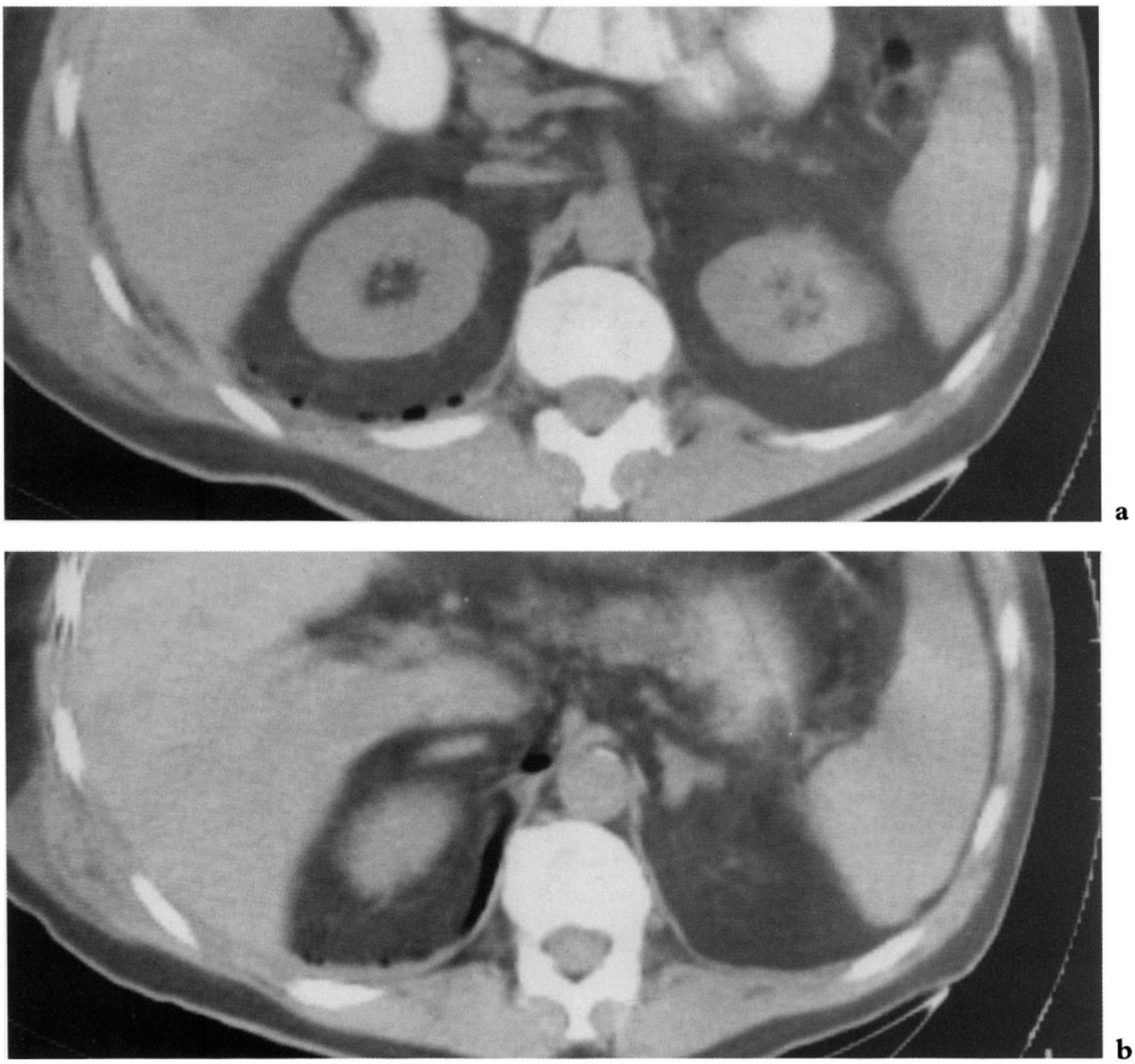


Fig. 8–204. Perforated retrocecal extraperitoneal appendicitis.
(**a** and **b**) Gas has risen into the posterior pararenal space on the right.
(Courtesy of Emil Balthazar, M.D., Bellevue Hospital, New York University School of Medicine, New York, NY.)

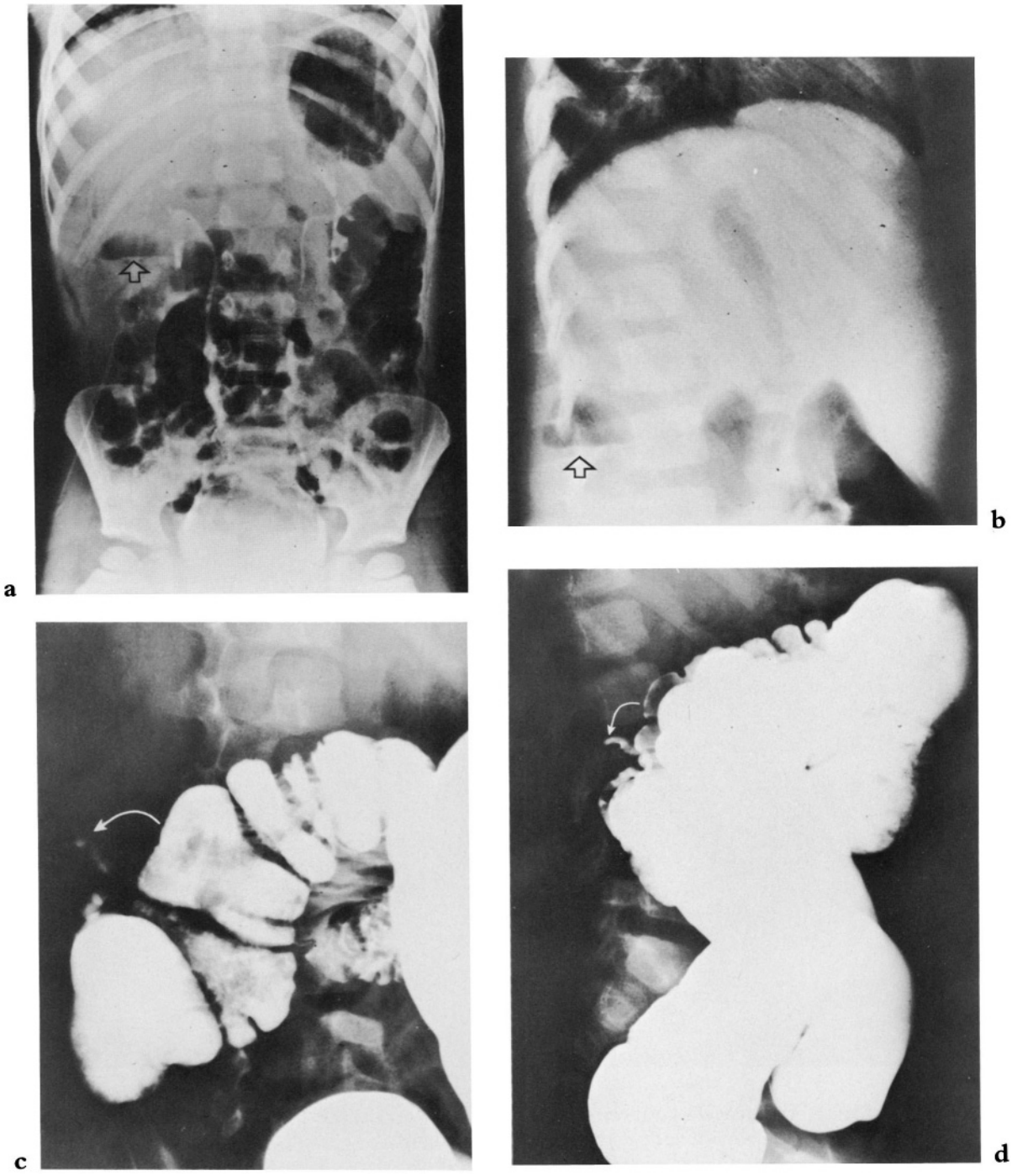


Fig. 8–205. Posterior pararenal abscess secondary to extraperitoneal appendicitis.
(**a** and **b**) Erect AP urogram and lateral plain film in a child demonstrate an air-fluid level in an abscess *(arrows)* behind and a little lateral to the right kidney.
(**c** and **d**) Frontal and lateral views of barium enema study demonstrate an undescended subhepatic cecum from which arises an ascending appendix *(curved arrows).* In this situation, the appendix is extraperitoneal in location, and its perforation can then lead to infection in unusual sites.

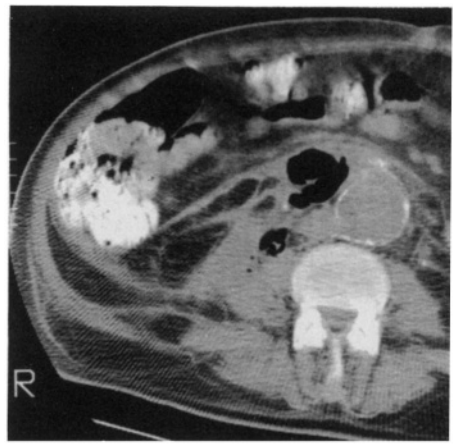


Fig. 8–206. Posterior pararenal abscess secondary to an infected abdominal aortic graft.
The gas-producing infection extends from the paraaortic tissues on the right predominantly to the posterior pararenal space adjacent to the psoas muscle.



Fig. 8–207. Posterior pararenal lymphocyst after sympathectomy.
A mass density on the right displaces the lower pole of the kidney superiorly and laterally and obscures the psoas margin.

Diffuse Extraperitoneal Gas

Radiologic localization of diffuse extraperitoneal gas to a specific compartment is greatly advanced by anatomic knowledge gained from careful study of body sections, postmortem injections, and retroperitoneal pneumography.[9] Fascial boundaries and tissue planes direct the spread and localization of extraperitoneal gas, depending on its source.

In presacral pneumography, if the needle is inserted in the midline behind the rectum, the gas ordinarily rises symmetrically up both sides.[13] While the kidneys and adrenal glands are shown with striking clarity, much of the extraperitoneal gas is outside the perirenal space. A considerable part undoubtedly enters this compartment through its inferior communication with the iliac fossa, but there is also significant distribution into the posterior pararenal space in particular, outlining the contours of the liver, spleen, upper poles of the kidneys, medial crura of the diaphragm, and subphrenic extraperitoneal tissues (Fig. 8–210). Furthermore, because of the fusion of the renal fascial layers with the diaphragm superiorly, perirenal gas alone does not lead to pneumomediastinum and cervical emphysema, whereas gas in the posterior pararenal compartment frequently does.

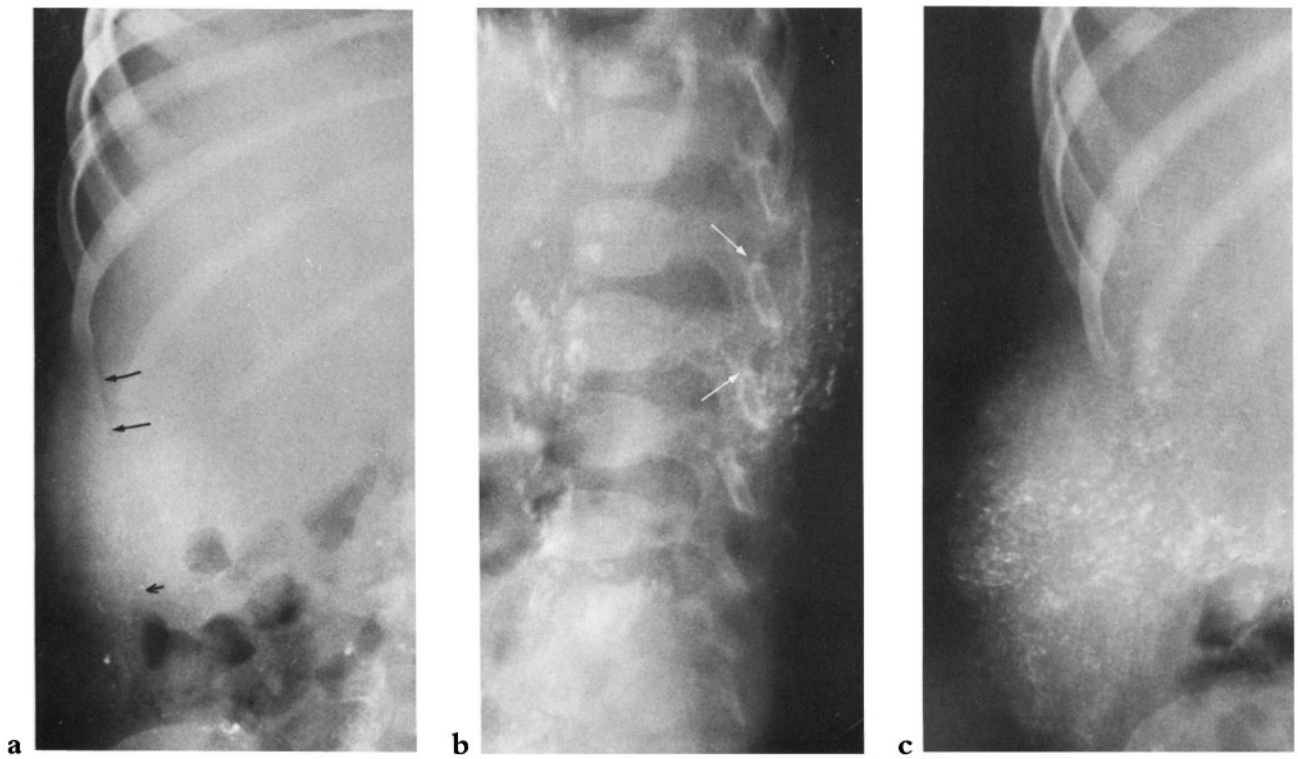


Fig. 8–208. Posterior pararenal lymphatic extravasation in a child presenting with a cystic flank mass.
(a) Lymphangiogram. Extravasated droplets of contrast material extend laterally toward flank mass. At this site, the flank-stripe fat is discretely lost and is maintained only in segments bordering the lymphocyst *(arrows).* The posterior collection also causes loss of visualization of the hepatic angle.
(b) Lateral projection documents the extreme posterior extravasation *(arrows).*
(c) Later film shows that with further extravasation into the enlarged mass all of the flank fat is effaced. (Reproduced from Meyers et al.[12])

It is also apparent that extraperitoneal gas is not truly fixed in position but retains some mobility through the tissues. This is demonstrable clinically by the changeable distribution between supine and erect films (Figs. 8–211 and 8–212).

The general extraperitoneal region can be thought of as Y-shaped in the frontal and lateral planes of the body. In an anteroposterior plane, continuity from the pelvis extends to both sides. It appears that extraperitoneal gaseous extravasation originating from disease processes in the pelvis or at the level of the iliac fossa does not typically enter the perirenal space; rather, it extends into the anterior and posterior pararenal spaces, presumably because the inferior apex of the cone of renal fascia is rapidly sealed off by associated inflammatory adhesions. Figure 8–213 illustrates an example of lateral leak from acute rectal perforation leading to extraperitoneal gas identifiable in each of the three spaces.

These considerations provide a rationale for the observation that bilateral spread of gas through the extraperitoneal tissue planes originates most often in the pelvic region. Extraperitoneal gas arising in the upper abdomen does not generally descend enough to cross over the midline to the opposite side at the level of the lumbosacral junction. An exception to unilateral confinement in the upper abdomen has been seen in gas-producing pancreatitis, presumably by virtue of the digestive enzymes involved. Extraperitoneal gas originating in and confined to the left upper quadrant is rare but may follow a perforated carcinoma or diverticulitis of the proximal descending colon or an abscess of the tail of the pancreas. If both intraperitoneal and extra-

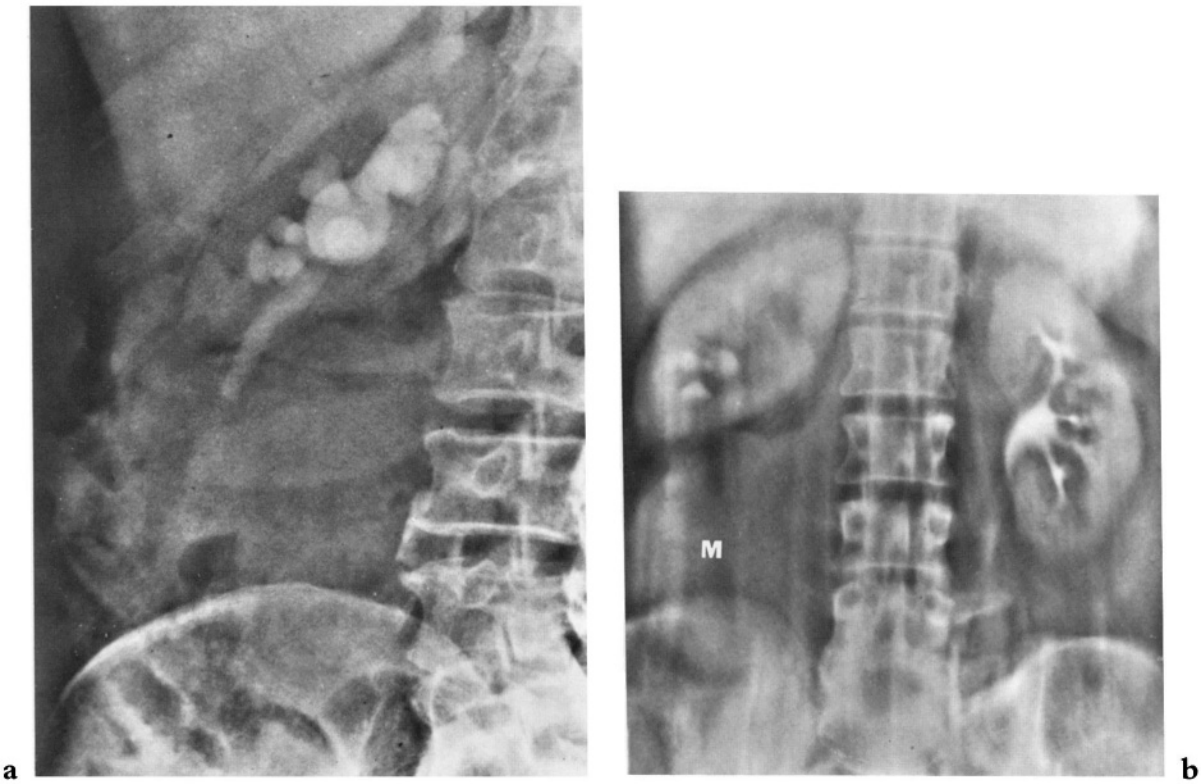


Fig. 8–209. Posterior pararenal development of reticulum cell sarcoma.
(a) Excretory urogram, oblique projection. Large circumscribed mass displaces the right ureter and the lower pole of the right kidney anteriorly. Obstructive hydronephrosis is present.
(b) Nephrotomogram. The sarcomatous mass *(M)* results in loss of visualization of the lower psoas segment and lateral displacement of the lower renal pole. The perirenal fat and upper psoas segment are intact. These changes localize the lymphoma to the posterior pararenal space.

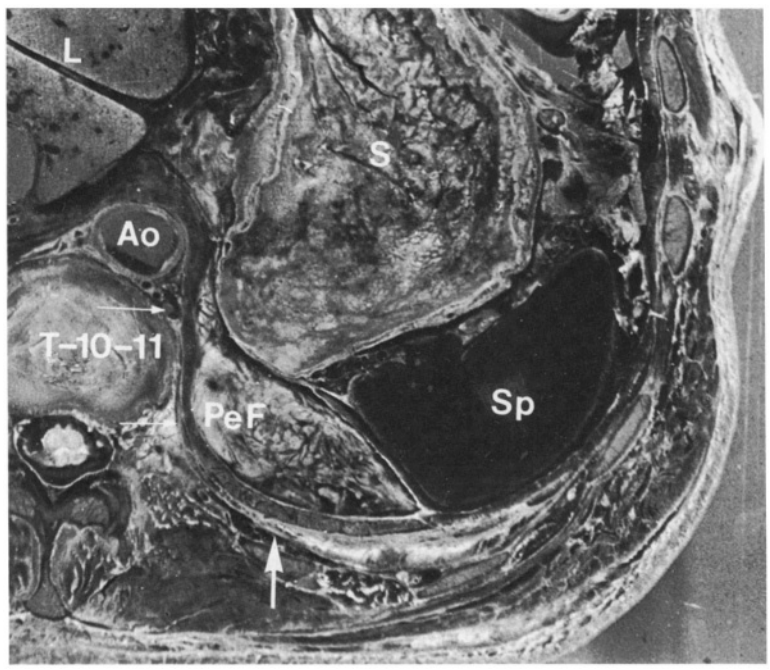


Fig. 8–210. Posterior pararenal fat (PeF).
This provides contrast to the medial crus *(small arrows)* and inferior margin *(large arrow)* of the diaphragm, and to the posteromedial border of the spleen *(Sp)*. *S* = stomach; *L* = liver; *Ao* = aorta.

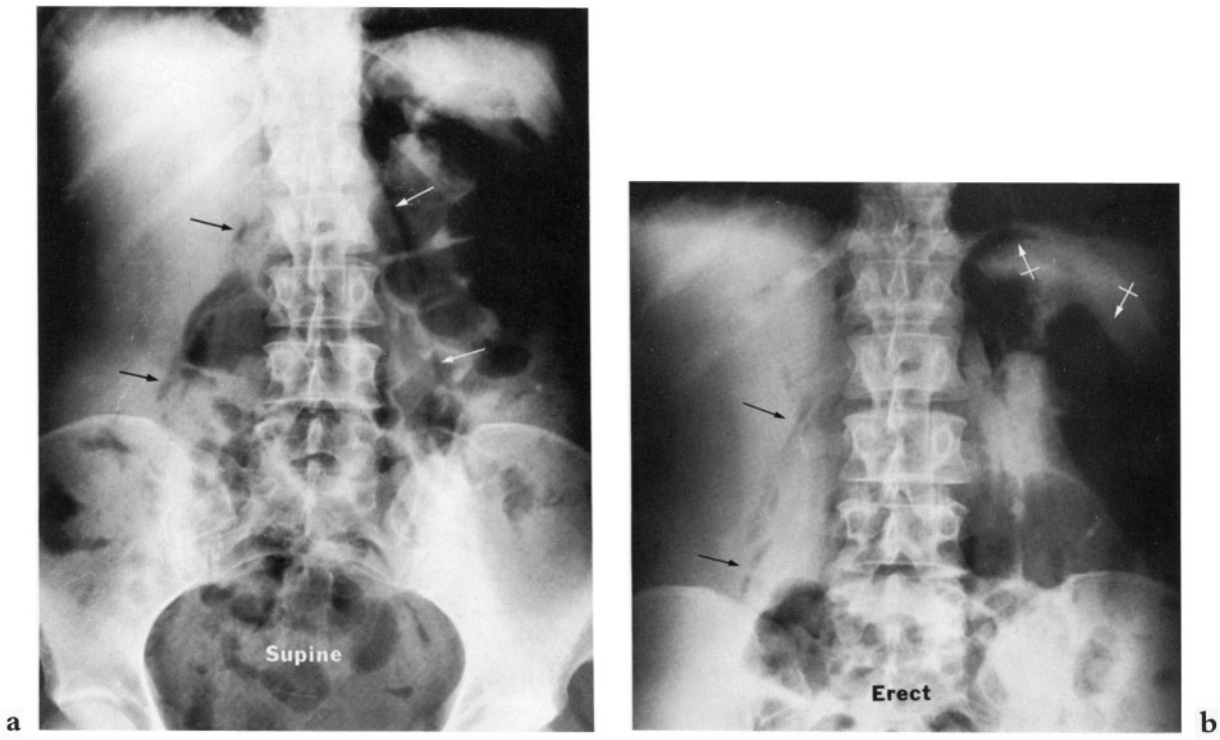


Fig. 8–211. Rectal perforation.
Supine and erect films demonstrate extraperitoneal gas paralleling the lateral borders of the psoas muscles *(arrows).* Cephalad extension on the left outlines the upper pole of the kidney, the adrenal gland, the medial border of the spleen, the medial crus of the diaphragm, and the immediate subphrenic tissues *(crossed arrows).* These findings localize the gas to the posterior pararenal compartments. The suprarenal and subphrenic gas collection increases in the erect position.
(Reproduced from Meyers.[9])

peritoneal gas are present, it can be confidently assumed that the source is a perforation of an extraperitoneal structure that has broken through the posterior parietal peritoneum[268] (Fig. 8–213b,c).

Rectal Perforation

Since the rectum is subperitoneal and lies in the midline, gas that escapes from its lumen rises up both sides within the extraperitoneal tissues. Depending primarily on the exact site of perforation, the gas may predominate on one side, but bilateral spread remains evident. In my experience, spread has preferentially been to the posterior compartments. The gas may then parallel the lateral contour of the psoas muscles, outlining the suprarenal and subdiaphragmatic tissues (Figs. 8–211 and 8–214).

Sigmoid Perforation

The sigmoid colon lies below the limits of the cone of renal fascia where it is in anatomic continuity with both the anterior and posterior pararenal spaces (Fig. 8–215). Gas from a sigmoid perforation may therefore enter either or both compartments.

Studies by Meyers et al.[269,270] have confirmed that only one of the four rows of colonic diverticula faces the peritoneal cavity and that fully 75% of sigmoid diverticula are related to the extraperitoneal tissues. Extraperitoneal gas associated with perforated sigmoid diverticulitis typically progresses up the left side. The gas may extend medially over the psoas muscle in the form of mottled radiolucencies (Fig. 8–212), but extension into the posterior compartment often dominates the radiologic findings. The gas may enter the properitoneal

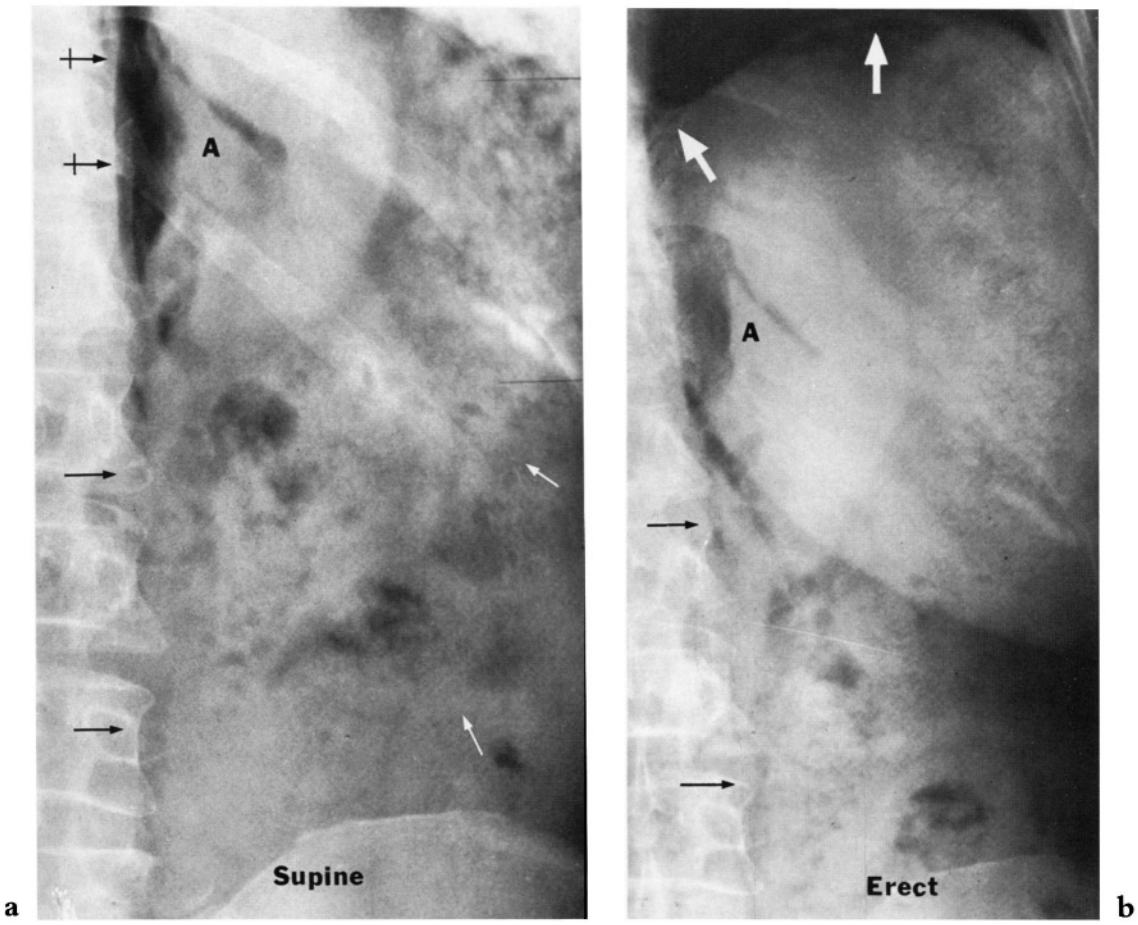


Fig. 8–212. Perforated sigmoid diverticulitis.
Extraperitoneal gas *(arrows)* extends anterior to the psoas muscle toward the spine within the anterior pararenal space. Superiorly, the gas extends within the posterior pararenal space outlining the adrenal gland *(A)* and the posteromedial border of the spleen, the medial crus of the diaphragm *(crossed arrows),* and segments of the extraperitoneal subdiaphragmatic tissue *(large white arrows).* Note that the latter do not follow the highest plane of the diaphragm, in contradistinction to free intraperitoneal air.
(Reproduced from Meyers.[9])

flank fat directly, but superiorly is characterized by its outlining of the left adrenal gland and upper renal pole, the medial crus of the diaphragm, the medial contour of the posterior aspect of the spleen, and the extraperitoneal subdiaphragmatic plane (Fig. 8–212). The relationships of these localizations are lucidly displayed by computed tomography (Fig. 8–216).

Only if the sigmoid perforation occurs between the leaves of the mesocolon does the extraperitoneal gas rise bilaterally within the anterior pararenal spaces[9] (Fig. 8–217).

Extraperitoneal Gas of Supradiaphragmatic Origin

Gas arising above the diaphragm may pass down the mediastinum through the diaphragmatic hiati and directly into the posterior pararenal space. If the gas gains entrance to structures of the chest wall, its extension to the extraperitoneal tissues of the abdomen may pursue a characteristic course. The endothoracic fascia of the chest is continuous with the transversalis fascia of

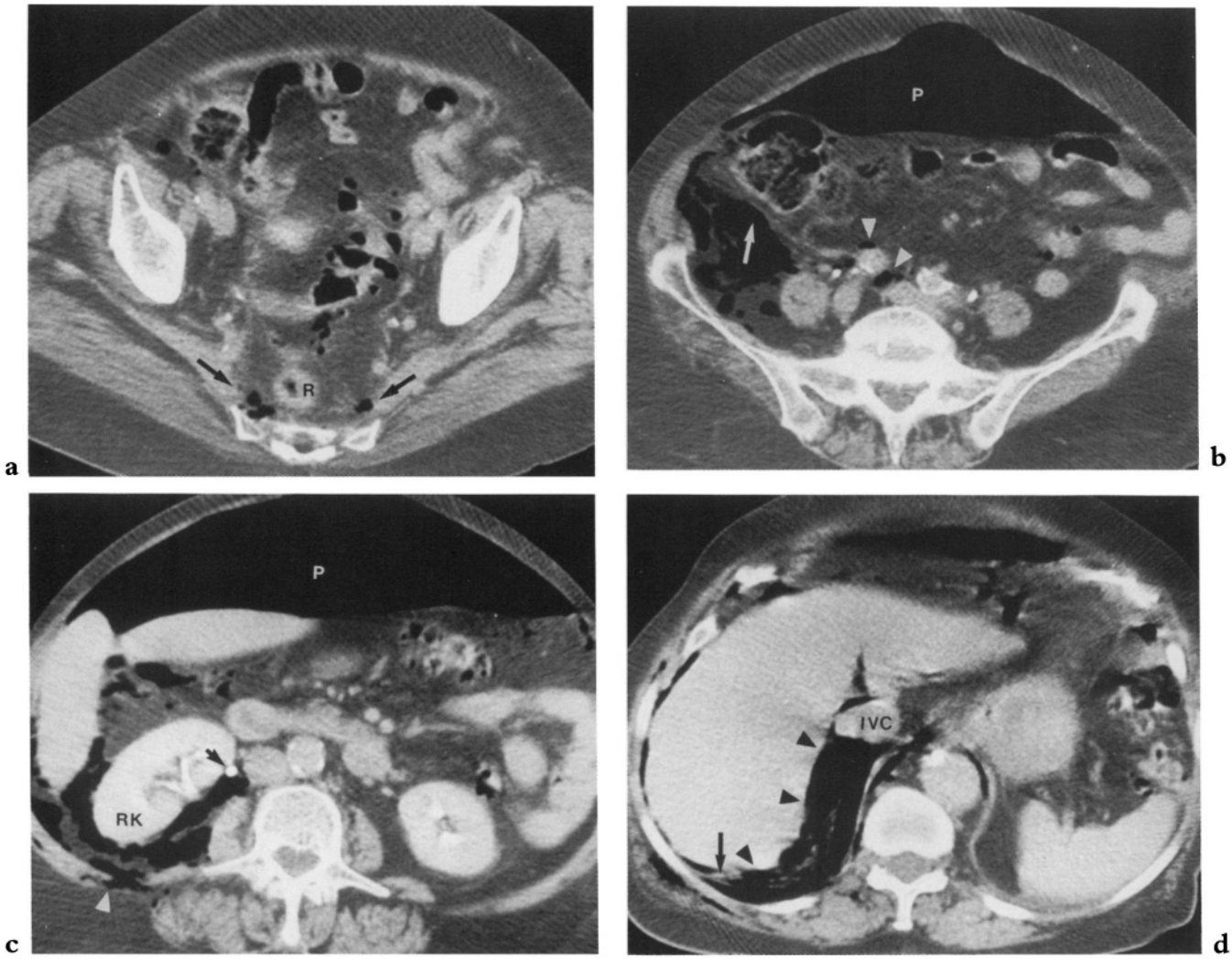


Fig. 8–213. Extraperitoneal gas in all three spaces secondary to rectal perforation from colonoscopic polypectomy.
(a) CT scan shows gas in the perirectal and presacral space following rectal perforation *(arrows). R* = rectum.
(b) Extraperitoneal gas is noted in the retrocecal area *(arrows)* and around the right iliac vessels *(arrowheads). P* = pneumoperitoneum, most likely secondary to perforation of the posterior parietal peritoneum.
(c) Gas is evident in the perirenal space outlining the right kidney *(RK)* and ureter *(arrow)* and in the posterior pararenal space. There is dissection of the properitoneal fat with subcutaneous emphysema developing in the region of the superior lumbar triangle *(arrowhead). P* = pneumoperitoneum.
(d) Scan through the liver shows anterior pararenal space gas outlining the superior coronary ligament *(arrow),* bare area of the liver *(arrowheads),* and inferior vena cava *(IVC).* Retrocrural gas spreads to the mediastinum.
(Reproduced from Nguyen and Beckman.[267])

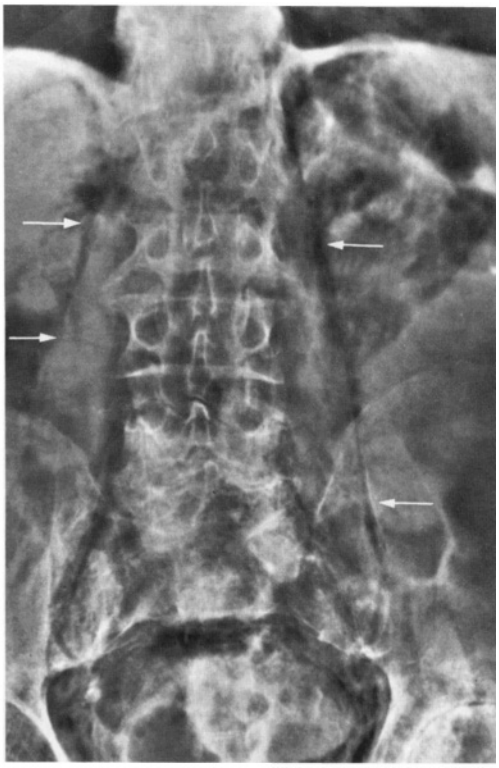


Fig. 8–214. Rectal perforation.
Bilateral gas in the posterior pararenal compartments outlines the complete lateral borders of the psoas muscles *(arrows)* and the upper poles of the kidneys and immediate subphrenic tissues.

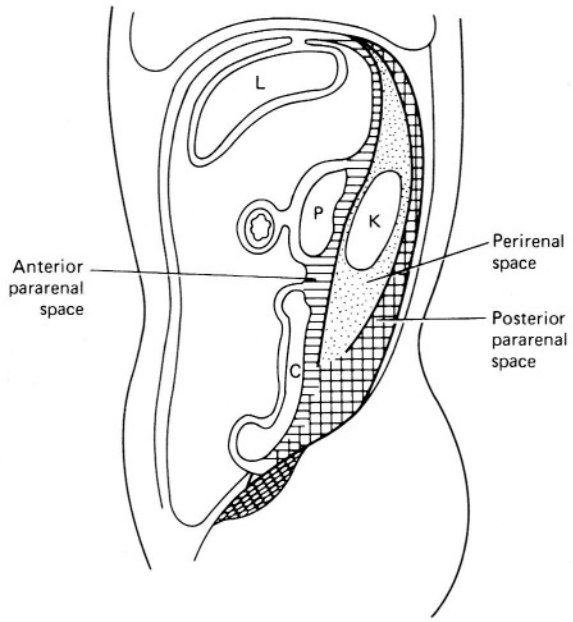


Fig. 8–215. Relationships and structures of the three extraperitoneal spaces on the left.
The sigmoid colon is in continuity with the posterior and anterior pararenal compartments. *L* = liver; *P* = pancreas; *K* = kidney; *C* = colon.
(Reproduced from Meyers.[8])



Fig. 8–216. Perforated sigmoid diverticulitis.
CT displays gas in the posterior and anterior pararenal spaces on the left, enveloping the cone of the renal fascia.

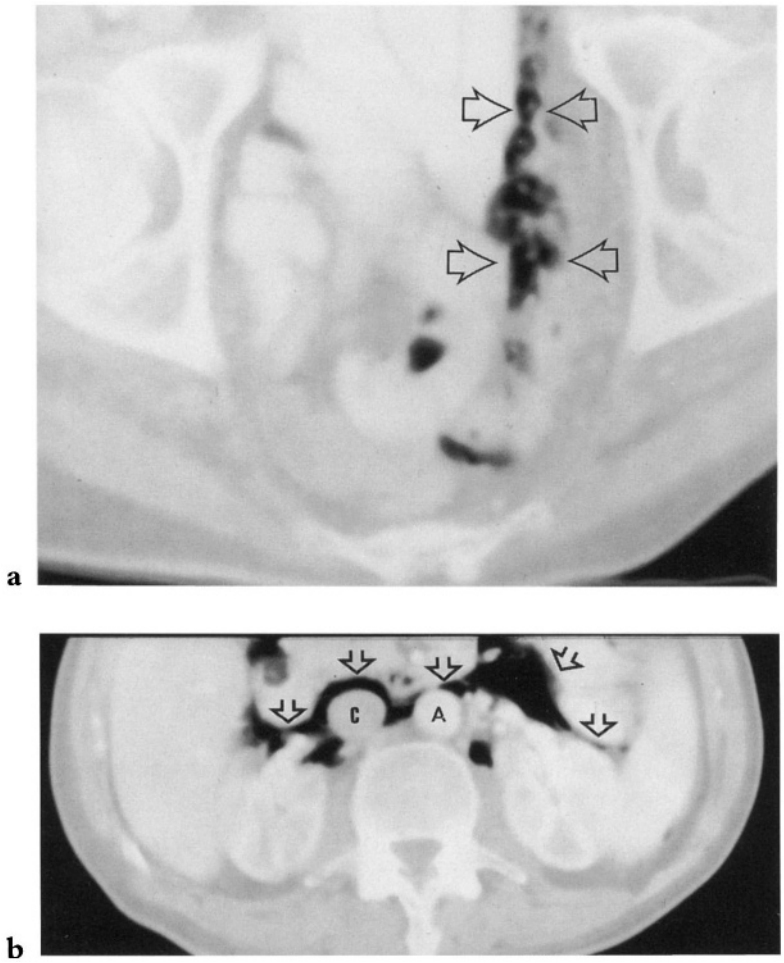


Fig. 8–217. Sigmoid perforation into mesocolon.
CT scans, imaged with wide window settings, demonstrate in the pelvis **(a)** that gas has dissected between the leaves of the sigmoid mesocolon *(arrows)* and at the level of the kidneys **(b)** the gas has arisen bilaterally in the anterior pararenal spaces *(arrows),* outlining the aorta *(A)* and inferior vena cava *(C).*
(Courtesy of Michiel Feldberg, M.D., University of Utrecht, The Netherlands.)

the abdomen. Gas originating in the chest or even in the neck may pass deep to the endothoracic fascia, external to the parietal pleura, and continue directly into the abdominal wall.[9,271,272] The lucencies may then extend preferentially within the flank fat (Fig. 8–218), although some gas may be seen in the deeper portions of the posterior pararenal compartment. Rarely, gas has been noted to dissect inferiorly as scrotal subcutaneous emphysema.[273]

Differential Diagnosis of Small Amounts of Subdiaphragmatic Gas

The predominant extraperitoneal gas within the posterior pararenal fat may seek the immediate subdiaphragmatic tissue planes. While occasionally extraperitoneal air may be distinguished by its outlining of individual diaphragmatic muscle bundles,[274] I have observed two further characteristics at this site on erect films that are particularly useful in differentiating even small amounts of extraperitoneal gas from free intraperitoneal air:

1. Free intraperitoneal air always conforms to the highest curvature of the dome of the diaphragm and may have a flat lower border. Gas in the subphrenic extraperitoneal tissues often parallels a lower plane of the diaphragmatic curvature, medial or lateral to its apex, and invariably demonstrates a crescentic outline (Figs. 8–211 and 8–212).

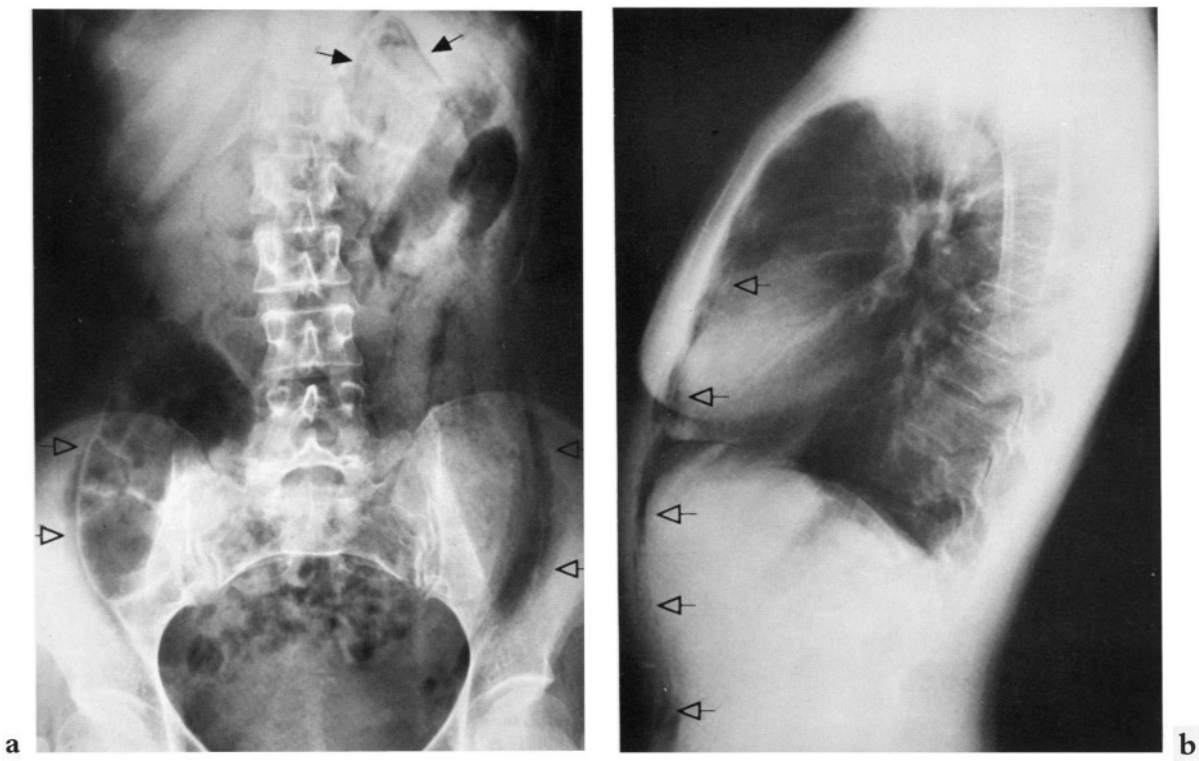


Fig. 8–218. Extraperitoneal gas following tracheostomy.
(a) Preferential spread into the flank fat *(open arrows).* A minimal amount outlines the left psoas muscle and suprarenal area *(solid arrows).*
(b) Lateral chest film demonstrates the continuous channel of gas from the chest to the abdomen deep to the endothoracic fascia and transversalis fascia *(arrows).*
(Reproduced from Meyers.[9])

2. The amount of free intraperitoneal subdiaphragmatic air increases on inspiration and decreases on expiration, presumably reflecting the influence of the greater negative intraabdominal pressure beneath the diaphragm during inspiration. In contrast, extraperitoneal subdiaphragmatic gas appears to increase on expiration and decrease on inspiration on erect frontal films (Fig. 8–219). The extraperitoneal tissues are not affected by respiratory variations in intraperitoneal pressure so that with descent of the diaphragm, extraperitoneal gas is simply compressed more diffusely, resulting in a thinner crescentic collection.

The anatomic boundaries of the three extraperitoneal spaces and the dynamics of the spread of extraperitoneal gas clearly explain its distribution and localization. The radiologic criteria that allow identification of the likely primary source of extraperitoneal gas are summarized in Table 8–3.

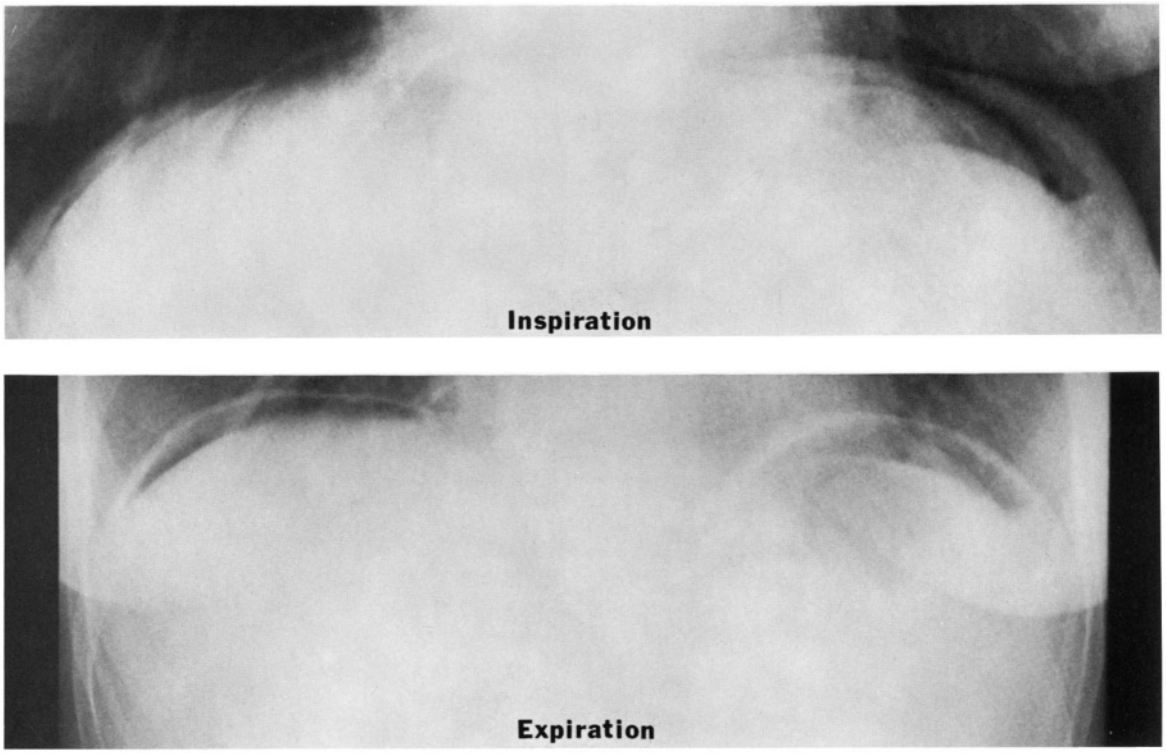


Fig. 8–219. Subdiaphragmatic extraperitoneal gas.
Erect films demonstrate a greater accumulation of subdiaphragmatic extraperitoneal gas within the posterior pararenal spaces during expiration.
(Reproduced from Meyers.[9])

Table 8–3. Spread and localization of extraperitoneal gas

Extraperitoneal compartment	Localizing roentgen features	Side of abdomen	Most likely sources
Anterior pararenal	Medially: gas extends beyond the lateral border of the psoas muscle toward the spine; on oblique projections the outline of the muscle may be preserved.	Right	Perforation of the descending duodenum
		Left	Perforated sigmoid diverticulitis
	Laterally: there is no extension into the flank stripe except possibly inferiorly, below the cone of renal fascia.	Bilateral	Sigmoid perforation into mesocolon; fulminating pancreatitis
	Superiorly: the renal outline may be preserved.		
Perirenal	Gas collection presents an inferiorly convex border overlying the iliac crest.	Right	Renal infection
	Most prominent within the rich far posterior to the kidney.		Occasionally, perforation of the descending duodenum
	Renal outline is enhanced.	Left	Renal infection
	Inflammatory thickening and displacement of the renal fascia.		
Posterior pararenal	Medially: gas is limited by and parallels the margin of the psoas muscle.	Left	Sigmoid diverticulitis
	Laterally: gas extends into the flank stripe.	Bilateral	Rectal perforation
	Superiorly: gas outlines the suprarenal area, diaphragm, and posterior aspects of the liver and spleen.		Supradiaphragmatic origin
	Extension above the diaphragm leads to pneumomediastinum and cervical subcutaneous emphysema.		

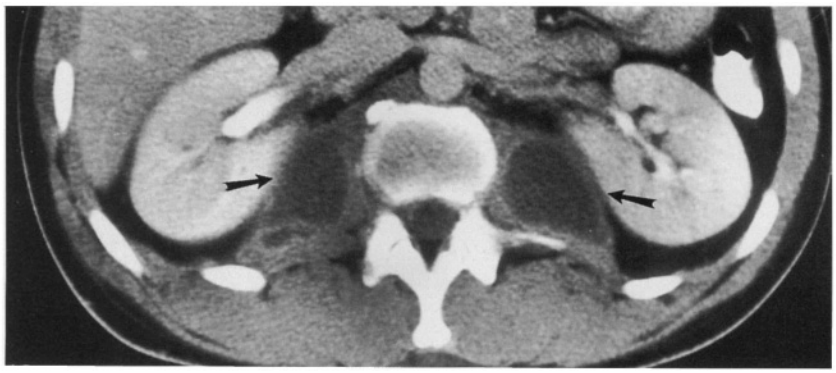
Psoas Abscess and Hematoma

Spontaneous dissection from a primary site in the retrofascial space deep to the transversalis fascia into the extraperitoneal compartments is rare.[3] The iliopsoas compartment is an extraperitoneal space covered by the iliopsoas fascia. The greater psoas muscle originates from the transverse processes of T12 and the lumbar vertebrae and extends inferiorly to merge with the iliac muscle at the L5-S2 level, becoming the iliopsoas muscle. The iliopsoas muscle passes beneath the inguinal ligament to insert on the lesser trochanter of the femur via the psoas tendon.[275–278] Psoas abscesses generally do not originate within the psoas compartment but spread here from neighboring intraabdominal structures.[275] Most psoas abscesses have a pyogenic origin and generally are due to direct spread from spinal or epidural infections, bowel conditions such as Crohn's disease, diverticulitis, appendicitis, perforated colon cardinoma, and perirenal abscesses. Primary abscesses rarely occur and are usually idiopathic. The organisms are typically *Staphylococcus aureus* and mixed gram-negative organisms. Tuberculous psoas abscesses are increasing in incidence because of the AIDS epidemic, and they are frequently associated with evidence of Pott's disease. When it is localized in a paraspinal location, a psoas abscess may be revealed by its effacement of the lateral border of the muscle and its lateral displacement of the kidney and ureter (Fig. 8–220). CT and MR images show enlargement of the muscle with fluid collections, ring enhancement, and perhaps gas[275–281] (Figs. 8–221 through 8–223).

Injection studies confirm clinical observations that the strong psoas fascia confines collections within it (Fig. 8–224). Indeed, this may provide a pathway for extension of the process to the hip and thigh (Figs. 8–225 and 8–226), as discussed in Chapter 17. Hemorrhage into the psoas muscle can be spontaneous (arteriosclerosis) or secondary to trauma, bleeding diathesis, anticoagulant therapy, inflammatory disease, tumor, or recent surgery or biopsy (Fig. 8–227).



Fig. 8–220. Right psoas abscess secondary to osteomyelitis ofL2.
Intravenous urogram demonstrates mass density displacing the right kidney laterally and effacing the upper segment of the psoas muscle.



a



b

Fig. 8–221. Psoas abscesses secondary to tuberculous infection.
(a) Contrast-enhanced CT shows bilateral central lesions of low attenuation with rim enhancement *(arrows)* in the psoas muscles.
(b) Sagittal gadolinium-enhanced fat-suppression MR image demonstrates the localized bilateral low-signal intensity psoas abscesses with rim enhancement *(arrows).*
(Reproduced from Torres et al.[278])

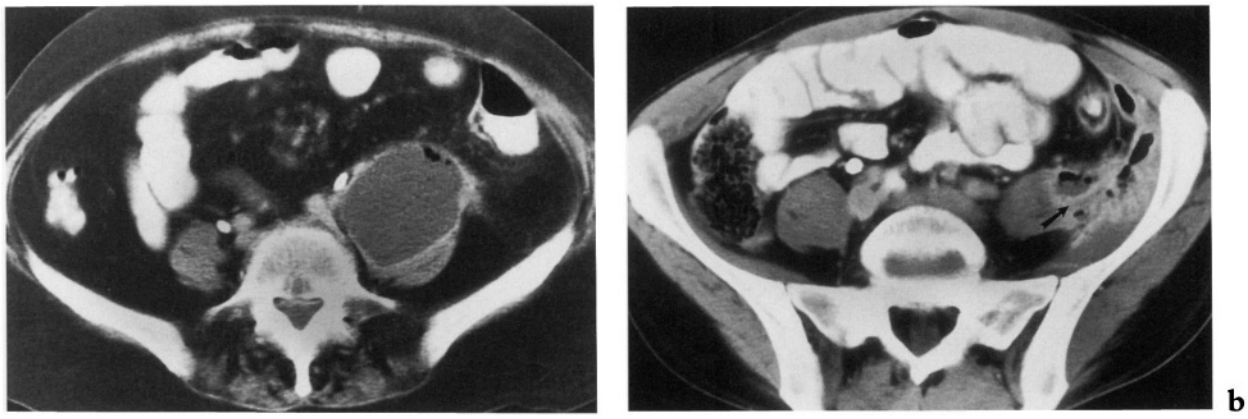


Fig. 8–222. Pyogenic psoas abscess secondary to fistulization from Crohn's enteritis.
(a) CT demonstrates a large fluid-filled abscess with small gas loculi and contrast material within the enhancing rim of the left psoas and iliopsoas muscles.
(b) At a lower level, a fistula between the bowel involved by Crohn's disease and the iliopsoas muscle *(arrow)* is revealed.
(Reproduced from Torres et al.[278])

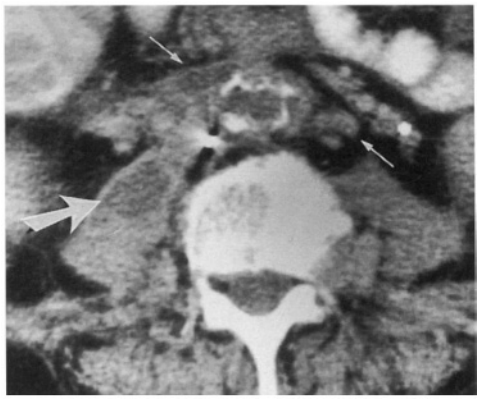


Fig. 8–223. Pyogenic psoas abscess after graft infection.
Contrast-enhanced CT demonstrates an abscess of the right psoas muscle *(large arrow),* consequent to graft infection developing after a recent aortofemoral graft. The latter is indicated by periaortic and mesenteric inflammatory changes and adenopathy *(small arrows).*
(Reproduced from Torres et al.[278])

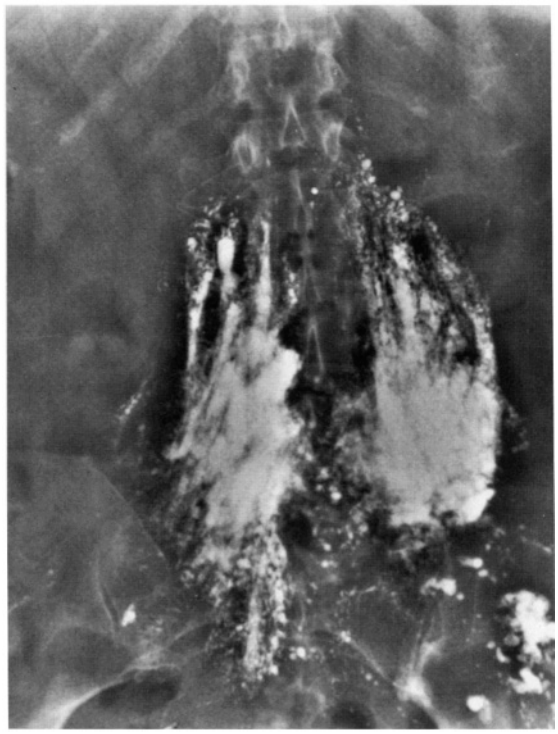


Fig. 8–224. Contrast injection into the psoas muscles.
The collections are restrained by the strong psoas fascia.

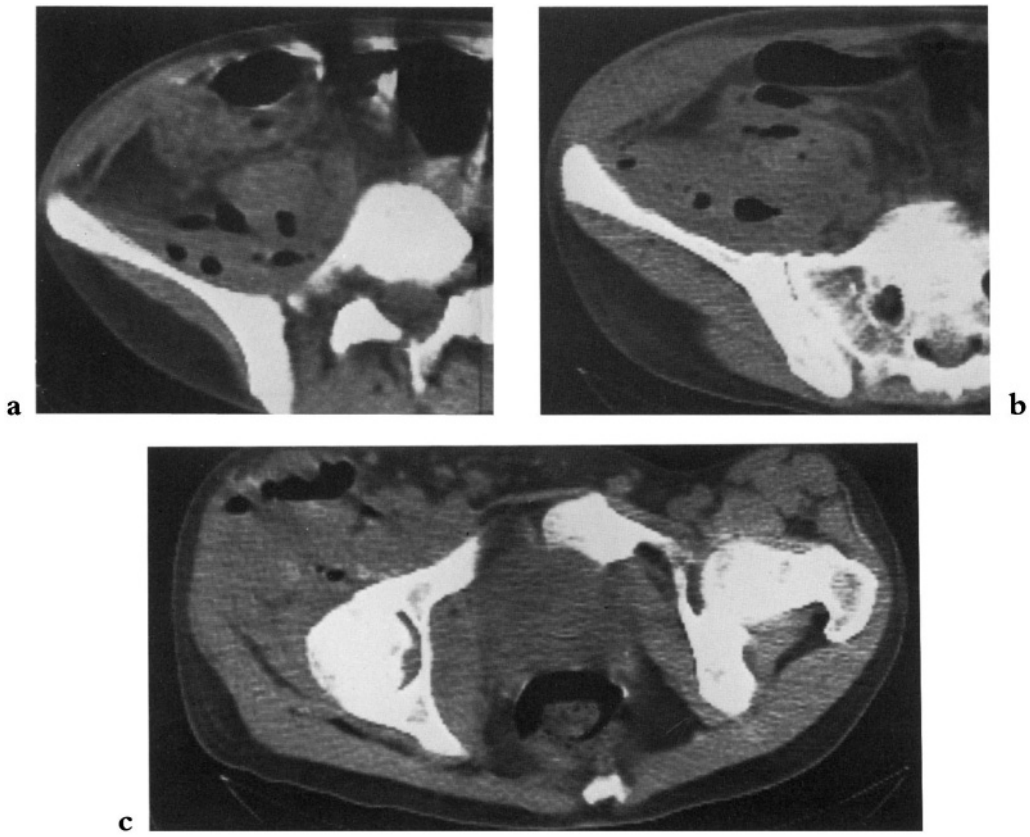


Fig. 8–225. Iliopsoas abscess.
(a–c) CT shows a gas-producing infection of the iliopsoas muscle tracking to a large abscess in the groin.



Fig. 8–226. Tuberculous psoas abscess and Pott's disease with inguinal extension.
(a) Contrast-enhanced CT shows an extensive fluid collection with ring enhancement *(white arrow)* in the left psoas muscle adjacent to associated vertebral bone destruction and extension to the epidural space *(black arrow).* The left kidney is displaced anteriorly and laterally.
(b) The abscess extends down the iliopsoas compartment to the left inguinal area *(arrows).*
(Reproduced from Torres et al.[278])



Fig. 8–227. Psoas hematomas and aortoenteric fistula from ruptured abdominal aortic aneurysm.
Contrast-enhanced CT demonstrates gross rupture of an aortic aneurysm with bleeding extending to the psoas muscles *(white arrows)* and a duodenal clot *(black arrows)* from an aortoenteric fistula.
(Reproduced from Torres et al.[278])

The Extraperitoneal Paravesical Pelvic Spaces

Catherine Roy, M.D.

Spread and localization of fluid collections in the extraperitoneal paravesical pelvic spaces may arise from many causes and from a variety of sites. Disease states and interventional procedures include coagulation defects, abscesses of the pelvic organs, pelvic or inguinal surgery, and trauma. Extrapelvic sites of origin include the extraperitoneal region of the abdomen, groin, and rectus sheath. An understanding of these spaces supports the clinical identification of the extension and characteristic configuration of fluid collections in the pelvis.

Anatomic Considerations[282,283]

The pelvic cavity, covered by the visceral peritoneal layer, is composed of the pelvic organs in the middle with vessels and nerves laterally. It is divided by fasciae developed from vascular sheaths. There are three groups (Fig. 8–228):

1. The visceral pelvic fascia is oriented in a sagittal plane and is composed of two symmetric fasciae. It courses along the lateral borders of the pelvic organs and the medial borders of the vessels, thinning as it extends anteriorly. In the axial plane it can be seen only posteriorly as a thin continuous line enveloping the perirectal fat (Fig. 8–229).

2. The second group is oriented in a frontal plane and is composed of two fasciae originating from the genital artery sheaths and from the inferolateral extension of the peritoneal layer of the cul-de-sac. The anterior one separates the urinary bladder and genital tract; the posterior one, the genital tract from the rectum. Generally, there is a paucity of fat at these sites and the fasciae are not imaged.

3. The umbilicovesical fascia, located anterior to the peritoneum and posterior to the transversalis fascia, has a triangular configuration with its apex at the umbilicus. It is on a more cephalad plane than the anterior portion of the visceral pelvic fascia (Fig. 8–228a,b). Inferiorly, its base joints the pubovesical ligament medially, blends with the pelvic visceral fascia laterally, and then with the parietal pelvic fascia lining the pelvic muscles in continuity with the transversalis fascia. It courses around the anterior part of the bladder and surrounds the urachus. These superior edges are occupied by the obliterated umbilical arteries, extending anteriorly from the internal iliac arteries. The obliterated urachus is often visible in the axial plane as a median fold. The lateral segment of the umbilicovesical fascia including the obliterated umbilical arteries covered by the peritoneum is identifiable as a thin line (Fig. 8–229). Below the peritoneal reflection, the umbilicovesical fascia extends to the pelvic floor on each side of the urinary bladder, but here it is too thin to be demonstrated by CT.

The anterior extraperitoneal fat of the pelvis is divided by the umbilicovesical fascia into three spaces (Figs. 8–229 and 8–230):

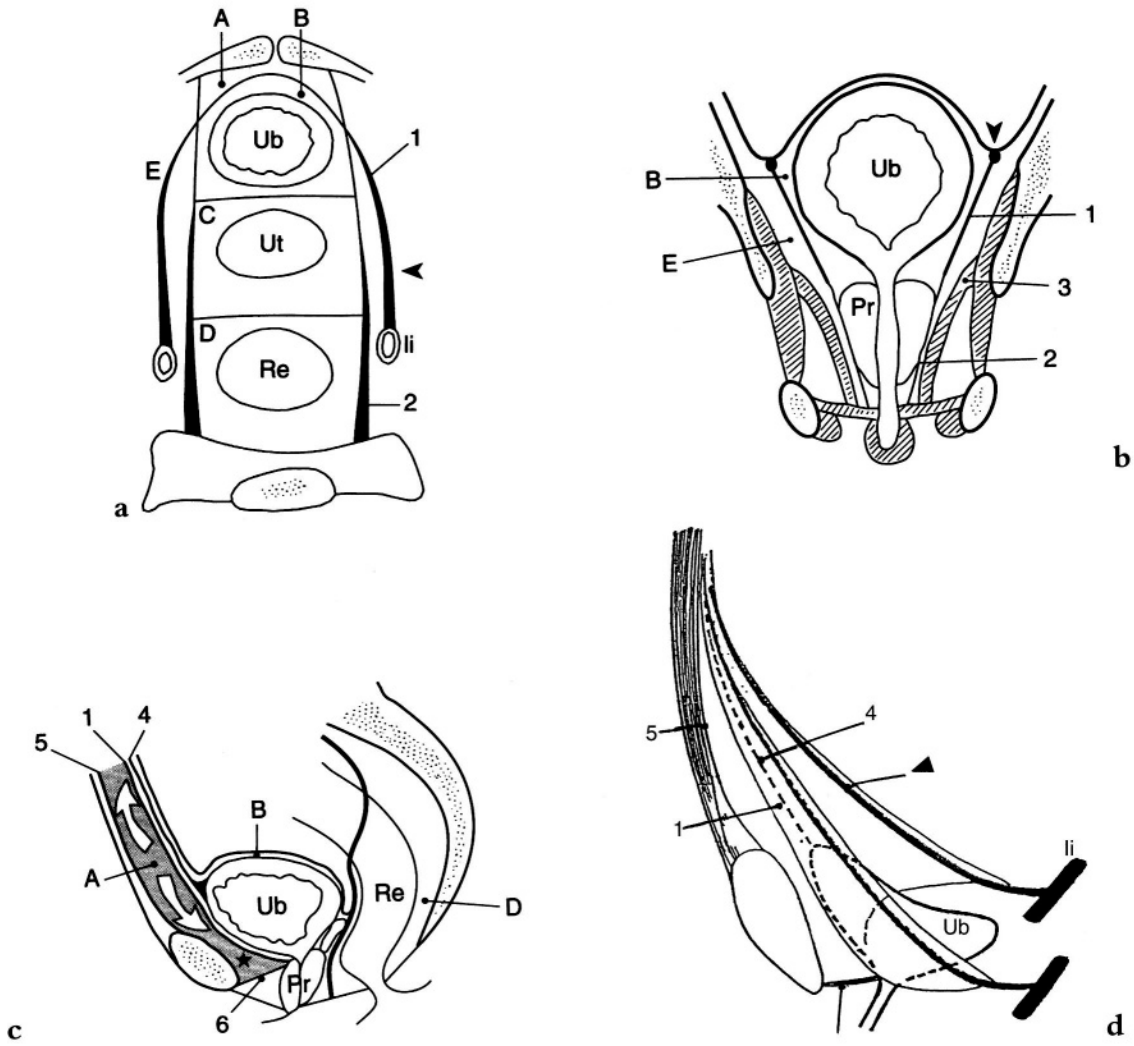
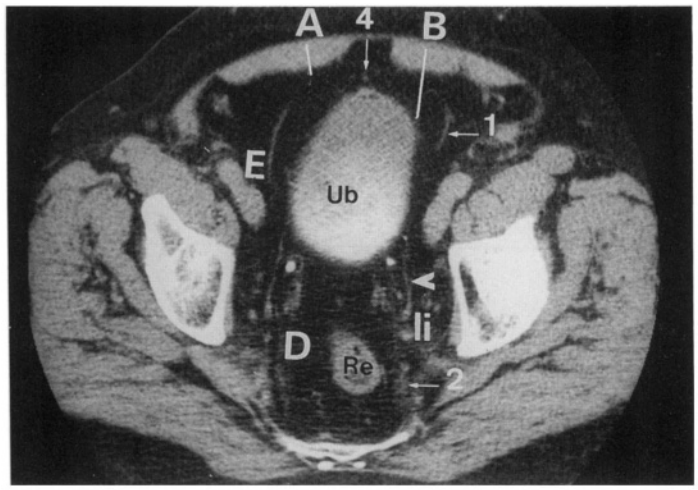
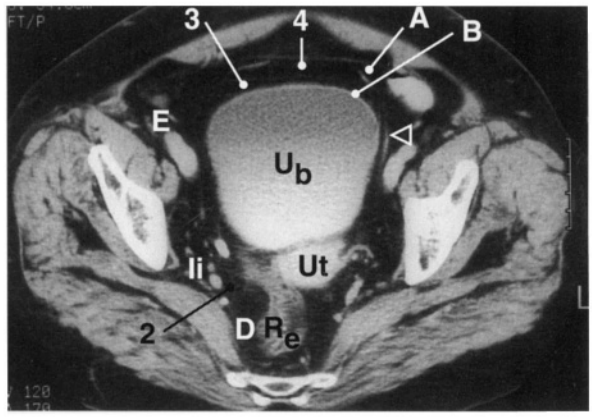


Fig. 8–228. The extraperitoneal paravesical pelvic spaces.
(a) Axial diagram in a female. The upper lateral border of the umbilicovesical fascia surrounds the obliterated umbilical arteries *(arrowhead).* While diagrammatically shown together here, the umbilicovesical fascia is on a more cephalad plane than the anterior part of the visceral pelvic fascia.
(b) Frontal diagram in a male.
(c) Sagittal diagram in a male. *Star* = space of Retzius.
(d) Sagittal oblique view.

Ub = urinary bladder
Ut = uterus
Re = rectum
Pr = prostate
Ii = internal iliac artery
1 = umbilicovesical fascia
2 = visceral pelvic fascia
3 = muscles lined by parietal pelvic fascia
4 = obliterated urachus
5 = transversalis fascia
6 = pubovesical ligament
A = prevesical space
B = perivesical space
C = genital space
D = perirectal space
E = paravesical space



a



b

Fig. 8–229. The prevesical (A), perivesical (B), perirectal (D), and paravesical (E) spaces and landmarks shown by axial CT in a male (a) and in a female (b).
The obliterated urachus *(4)* is visible anterior to the urinary bladder *(Ub).* Only the posterior part of the visceral pelvic fascia *(2)* can be seen on these images. *Re* = rectum; *Ii* = internal iliac artery; *Ut* = uterus; *arrowhead* = obliterated umbilical artery; *1* = umbilicovesical fascia; *3* = peritoneal layer.

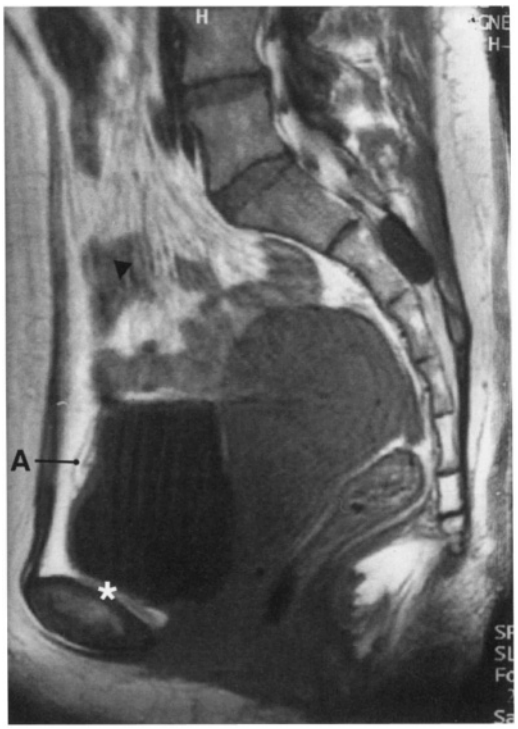


Fig. 8–230. The prevesical space.
T1-weighted sagittal MR image in a female shows the prevesical space with abundant fat *(A)* and the space of Retzius *(asterisk).* The low-signal intensity line is composed of the obliterated urachus and the umbilicovesical fascia.

1. *The prevesical space* lies anterior and lateral to the umbilicovesical fascia, deep to the transversalis fascia, and inferiorly to the posterior part of the pubic bone. It is a huge potential compartment that extends superiorly, becoming progressively thinner as it approaches the umbilicus, and communicates with the properitoneal fat and the posterior pararenal space around the abdominal wall and flanks. Its fat is more abundant anteroinferiorly, especially behind the pubis, where the prevesical space is also called the retropubic space or *space of Retzius.* This space has posterior extensions surrounding the urinary bladder laterally. It is limited laterally by the thin anterior portion of the visceral pelvic fascia and then by the perineal muscles.

2. *The paravesical space* lies between the lateral pelvic wall lined by the parietal pelvic fascia and the visceral pelvic fascia. Superiorly, it is limited by the peritoneum. This compartment's fatty tissue has a large tortuous venous network and loose connective tissue.

3. *The perivesical space* is bounded by the umbilicovesical fascia, within the confines of which lie the bladder, urachus, and obliterated umbilical arteries. It is a thin space with little fat. A small amount of fat is present between the peritoneum and the dome of the bladder. Posterior to the bladder, the supravaginal portion of the cervix and anterior portion of the vagina are continuous with the perivesical space in women. In men, there is similar continuity with the prostate and seminal vesicles.[284]

An additional space in the pelvis is the *perirectal space.* It is limited by the posterior part of the visceral pelvic fascia, which is thick at this level. It continues into the abdominal extraperitoneal spaces.

Abnormal Imaging Features[284–288]

Paravesical Fluid Collection

Because of its extensive venous system, hematomas within this space often become very large. The collection lies in the lateral part of the pelvic cavity and compresses the bladder and genital tract. Its shape is ovoid with a long anteroposterior axis (Fig. 8–231). Large postpartum hematomas and gynecologic hematomas or abscesses may extend via the broad ligament through the paravesical space.[287]

Prevesical Fluid Collection

Because of the orientation of the umbilicovesical fascia, a prevesical fluid collection has a "molar tooth" configuration in an axial plane.[285] The "crown" portion of the tooth lies anterior to the urinary bladder between the umbilicovesical fascia and transversalis fascia of the anterior abdominal wall and displaces the bladder posteriorly. The "roots" portion extends posteriorly between the fascia and either the peritoneum superiorly or the parietal pelvic fascia inferiorly, displacing the bladder medially (Fig. 8–232). or away from the midline if the roots are asymetrical in size (Fig. 8–233). When there is a very large collection, the upper portion extends toward the umbilicus and appears as a round, midline mass displacing the bowel.

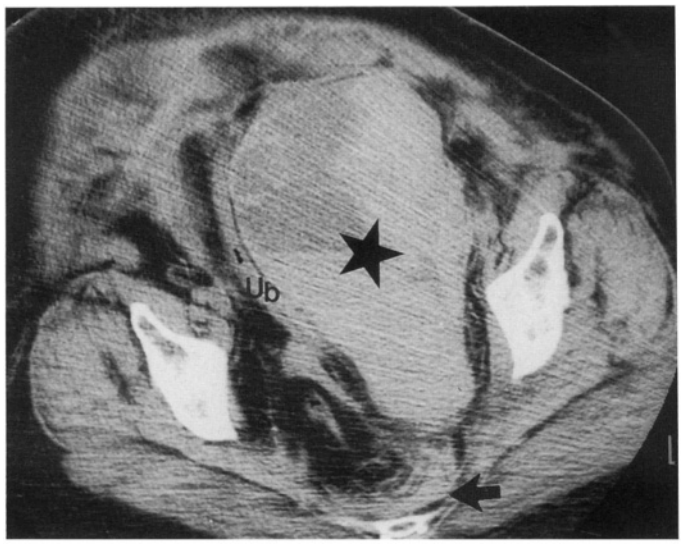


Fig. 8–231. Paravesical hematoma due to coagulation defect.
CT in a female patient demonstrates that the hematoma is localized in the left paravesical space *(star)* with compression of the urinary bladder *(Ub)* to the right and extension posteriorly into the presacral fat *(arrow).* Note the hematoma in the right anterolateral abdominal wall.

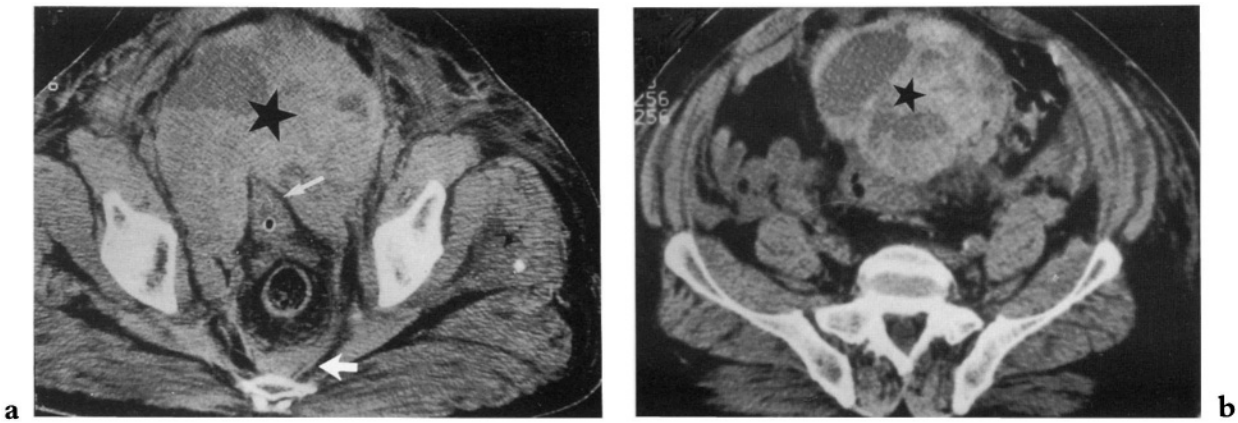


Fig. 8–232. Prevesical hematoma secondary to crash injury.
CT scan in a male.
(a) "Molar tooth" configuration *(star).* The "crown" portion of the tooth lies anterior to the urinary bladder, displacing it posteriorly. The "root" portion of the molar extends posteriorly and symmetrically compresses the lateral portions of the bladder. Note that the normal perivesical space is maintained *(small arrow).* There is an extension into the presacral fat *(large arrow).*
(b) Cephalad extension into the prevesical space *(star).*

As many as 3 L of fluid may occupy the prevesical space and its extensions without evidence of a palpable abdominal wall mass. The space has multiple potential extensions and communications. These include extensions into the extraperitoneal region of the abdomen (such as the posterior pararenal space), into the rectus sheath, along the round ligaments or the vas deferens and spermatic cord, into the femoral sheath, and posteriorly into the presacral space (Fig. 8–231). Many of these communications allow bidirectional spread. Rectus sheath hematomas below the arcuate line extend into the prevesical space to displace and compress the pelvic viscera, and postpuncture hematomas in the femoral sheath can expand rapidly to fill the prevesical space.[284]

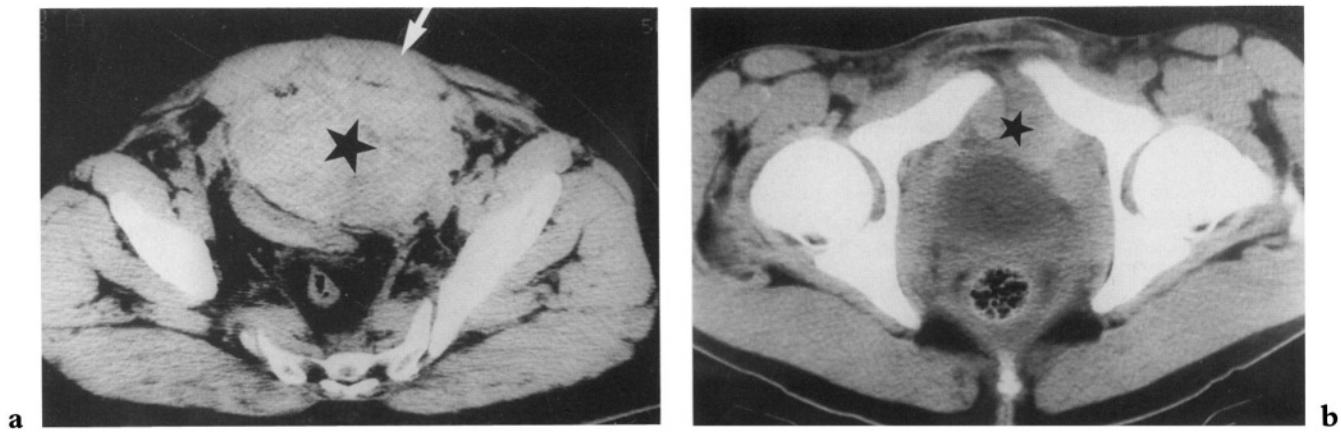


Fig. 8–233. Prevesical hematoma secondary to crash injury.
(a) A large hematoma asymmetrically occupies the prevesical space *(star).* Bleeding into the anterior abdominal wall has also occurred *(arrow).*
(b) Caudal extension is defined within the space of Retzius *(star).*

Perivesical Fluid Collection

A perivesical fluid collection is always small because it is compressed by the umbilicovesical fascia. It may be confused on CT with a thickening of the bladder wall, and when the fluid is localized in the posterior portion of the perivesical space it may mimic a collection in the cul-de-sac. Perivesical fluid collections are better visualized by MRI.

Mixed Collections

As a rule, large pelvic collections occupy several spaces with multiple possibilities: involvement of several extraperitoneal spaces or association of intraperitoneal and extraperitoneal collections (Figs. 8–234 through 8–236). In patients with large amounts of fluid in the infrarenal extraperitoneal space, extension into the pelvic extraperitoneal space is not rare. The dorsal extension medial to the iliac vessels and/or a more medial extension into the prevesical space are the most common pathways[42,134,136] Mixed collections of both intraperitoneal and extraperitoneal fluid are rare, with the exception of major crash injury with rupture of different organs. Differentiation between intraperitoneal and extraperitoneal pelvic collections can be readily made, but it can be difficult to distinguish whether the fluid originated in the pelvic spaces or the retroperitoneum.

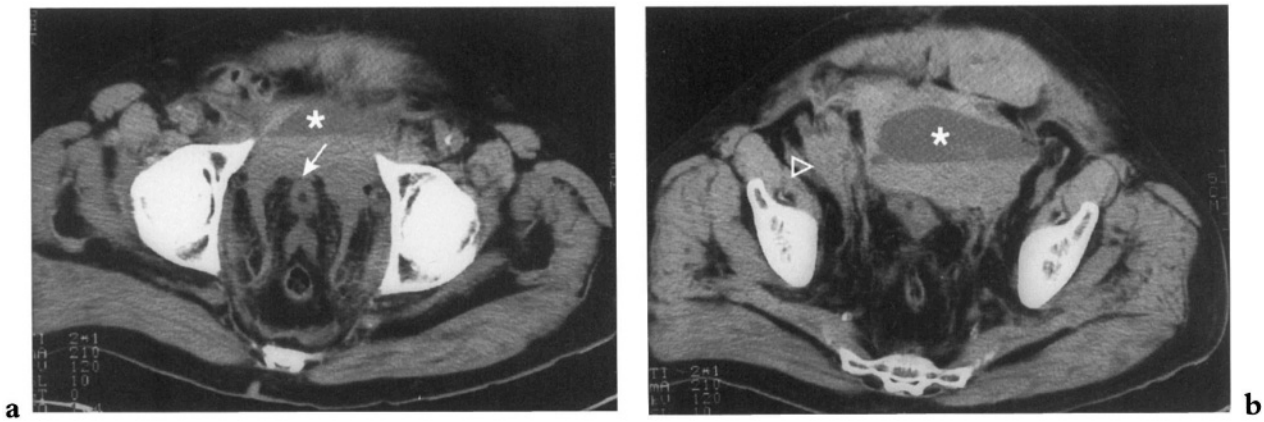


Fig. 8–234. Prevesical hematoma secondary to crash injury in a male.
(a) Typical "molar tooth" configuration with "crown" posterior portion *(asterisk).* There is a small disruption of the anterior part of the perivesical space *(arrow).* Note the fluid–fluid level of subacute hemorrhage.
(b) Cephalad extension into the prevesical space. Small hematoma in the laterovesical space *(arrowhead).* Note hematoma inside left rectus muscle.

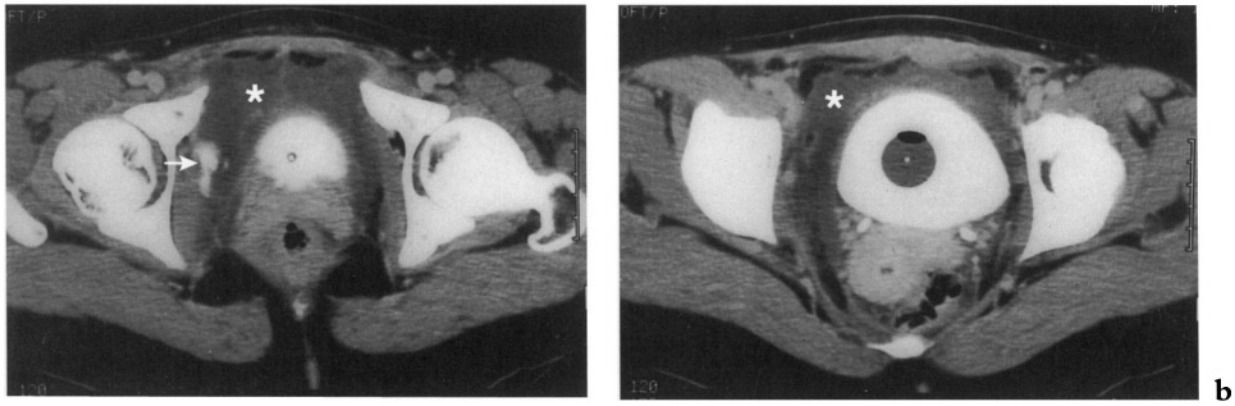


Fig. 8–235. Disruption of the bladder secondary to crash injury in a female.
(a) Liquid in the prevesical space with extension in the perivesical space *(asterisk)* (there is no space between fluid collection and bladder wall). Contrast medium in the collection *(arrow).* "Molar tooth" configuration.
(b) Cephalad portion. The perivesical space is occupied by fluid collection.

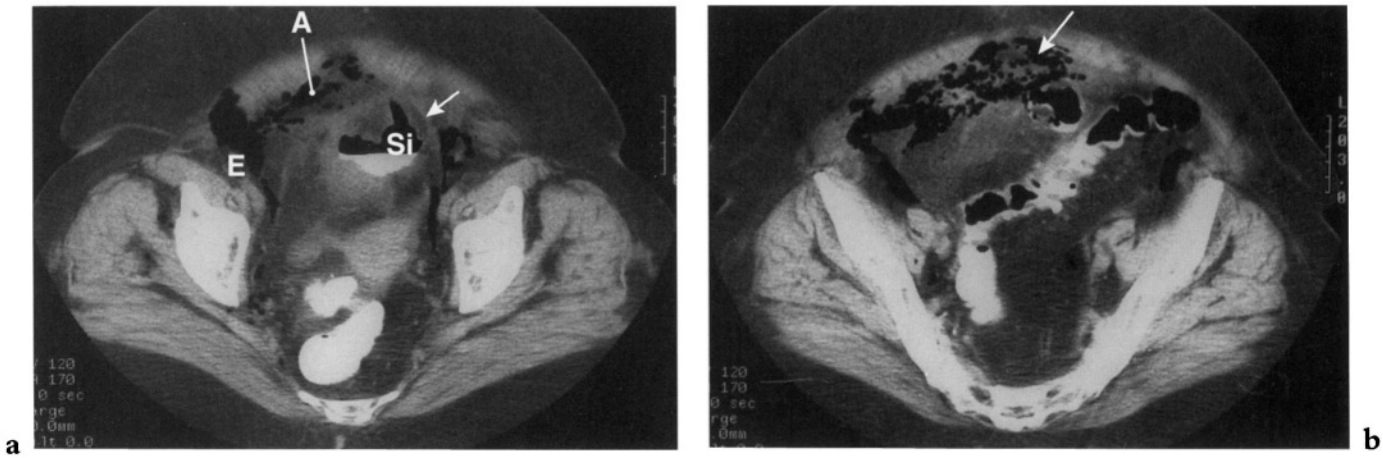


Fig. 8–236. Prevesical and paravesical gas collection secondary to disruption of a sigmoidal abscess in a female.
(a) Gas in the prevesical *(A)* and paravesical *(E)* space with anterior extension into the inguinal canal. Thickening of the umbilicovesical fascia *(arrow). Si* = sigmoid.
(b) Cephalad extension of gas with disruption of transversalis fascia *(arrow).*

References

1. Meyer HI: The reaction of retroperitoneal tissue to infection. Ann Surg 1934; 99:246–250.
2. Stevenson EO, Ozeran RS: Retroperitoneal space abscesses. Surg Gynecol Obstet 1969; 128:1202–1208.
3. Altemeier WA, Alexander JW: Retroperitoneal abscess. Arch Surg 1961; 83:512–524.
4. Elkin M, Cohen G: Diagnostic value of the psoas shadow. Clin Radiol 1962; 13:210–217.
5. Williams SM, Harned RK, Hultman SA, et al: The psoas sign: A reevaluation. Radiographics 1985; 5(4):525–536.
6. Editorial: Periureteric fibrosis. Lancet 1957; 2:780–781.
7. Love L, Meyers MA, Churchill RJ, et al: Computed tomography of extraperitoneal spaces. AJR 1981; 136:781–789.
8. Meyers MA: Acute extraperitoneal infection. Semin Roentgenol 1973; 8:445–464.
9. Meyers MA: Radiologic features of the spread and localization of extraperitoneal gas and their relationship to its source: An anatomical approach. Radiology 1974; 111:17–26.
10. Meyers MA: Uriniferous perirenal pseudocyst: New observations. Radiology 1975; 117:539–545.
11. Meyers MA, Whalen JP, Evans JA: Diagnosis of perirenal and subcapsular masses: Anatomic-radiologic correlation. AJR Rad Ther Nucl Med 1974; 121:523–538.
12. Meyers MA, Whalen JP, Peelle K, et al: Radiologic features of extraperitoneal effusions: An anatomic approach. Radiology 1972; 104:249–257.
13. Meyers MA: Diseases of the Adrenal Glands: Radiologic Diagnosis with Emphasis on the Use of Presacral Retroperitoneal Pneumography. Charles C Thomas, Springfield, IL, 1963, pp 11–15, 20.
14. Barbaric Z: Renal fascia in urinary tract diseases. Radiology 1976; 118:561–565.
15. Kochkodan EJ, Haggar AM: Visualization of the renal fascia: A normal finding in urography. AJR 1983; 140:1243–1244.
16. Whalen JP, Ziter FMH Jr: Visualization of the renal fascia: A new sign in localization of abdominal masses. Radiology 1967; 80:861–863.
17. Feldberg MAM: Computed Tomography of the Retroperitoneum: An Anatomical and Pathological Atlas with Emphasis on the Fascial Planes. Martinus Nijhoff, Boston, 1983.
18. Meyers MA: Dynamic Radiology of the Abdomen: Normal and Pathologic Anatomy, 2nd ed. Springer-Verlag, New York, 1982.
19. Parienty RA, Pradel J, Picard J-D, et al: Visibility and thickening of the renal fascia on computed tomograms. Radiology 1981; 139:119–124.
20. Raptopoulos V, Kleinman PK, Marks S Jr, et al: Renal fascial pathway: Posterior extension of pancreatic effusions within the anterior pararenal space. Radiology 1986; 158:367–374.
21. Zuckerkandl E: Beitrage zur Anatomie des Menschlichen Korpers. Ueber den Fixationsapparat der Nieren. Med Jahr 1883; 13(2):59–67.
22. Gerota D: Beiträge zur Kenntnis des Befestigungsapparates der Niere. Arch Anat Entwicklungsgesch 1895; pp 265–286.
23. Chesbrough RM, Burkhard TK, Martinez AJ, et al: Gerota versus Zuckerkandl: The renal fascia revisited. Radiology 1989; 173:845–846.
24. Meyers MA, Oliphant M, Berne AS, et al: The peritoneal ligaments and mesenteries: Pathways of intra-abdominal spread of disease. Annual oration. Radiology 1987; 163:593–604.
25. Congdon ED, Edson JN: The cone of renal fascia in the adult white male. Anat Rec 1941; 80:289–313.
26. Martin CP: Anatomical notes: A note on the renal fascia. J Anat 1942; 77:101–103.
27. Somogyi J, Cohen WN, Omar MM, et al: Communication of right and left perirenal spaces demonstrated by computed tomography. J Comput Assist Tomogr 1979; 3:270–273.
28. Kneeland JB, Auh YH, Rubenstein WA, et al: Perirenal spaces: CT evidence for communication across the midline. Radiology 1987; 164:657–664.
29. Mindell HJ, Mastromatteo JF, Dickey KW, et al: Anatomic communications between the three retroperitoneal spaces: Determination by CT-guided injections of contrast material in cadavers. AJR 1995; 164:1173–1178.
30. Raptopoulos V, Touliopoulos P, Lei QF, et al: Medial border of the perirenal space: CT and anatomic correlation. Radiology 1997; 205:777–784.
31. Dodds WJ, Darweesh RMA, Lawson TL, et al: The retroperitoneal spaces revisited. AJR 1986; 147:1155–1161.
32. Hureau J, Pradel J, Agossou-Voyeme AK, et al: Les espaces interpariéto-péritoneaux postérieurs ou espaces rétropéritonéaux: Anatomie tomodensitometrique normale. J Radiol 1991; 72:101–106.
33. Hureau J, Pradel J, Agossou-Voyeme AK, et al: Les espaces interpariéto-péritonéaux postérieurs

ou espaces rétropéritonéaux: Anatomie tomodensitometrique pathologique. J Radiol 1991; 72:205–227.
34. Molmenti EP, Balfe DM, Kanterman RY, et al: Anatomy of the retroperitoneum: Observations of the distribution of pathologic fluid collections. Radiology 1996; 200:95–103.
35. Aizenstein RI, Wilbur AC, O'Neil HK: Interfascial and perinephric pathways in the spread of retroperitoneal disease: Refined concepts based on CT observations. AJR 1997; 168:639–643.
36. Lim JH, Yoon Y, Lee SW, et al: Superior aspect of the perirenal space: Anatomy and pathological correlation. Clin Radiol 1988; 39:368–372.
37. Lim JH, Auh YH, Suh SJ, et al: Right perirenal space: Computed tomography evidence of communication between the bare area of the liver. Clin Imag 1990; 14:239–244.
38. Kim KW, Auh YH, Chi HS, et al: CT of retroperitoneal extension of hepatoma mimicking adrenal tumor. J Comput Assist Tomography 1993; 17(4):599–602.
39. Patten RM, Spear RP, Vincent LM, et al: Traumatic laceration of the liver limited to the bare area: CT findings in 25 patients. AJR 1993; 160:1019–1022.
40. Bechtold RE, Dyer RB, Zagoria RJ, et al: The perirenal space: Relationship of pathologic processes to normal retroperitoneal anatomy. RadioGraphics 1996; 16:841–854.
41. Tandon N, Karak PK, Mukhopadhyay S, et al: Amoebic liver abscess: Rupture into retroperitoneum. Gastrointest Radiol 1991; 16:240–242.
42. Raptopoulos V, Lei QF, Touliopoulos P, et al: Why perirenal disease does not extend into the pelvis: The importance of closure of the cone of renal fasciae. AJR 1995; 164:1179–1184.
43. Oliphant M, Berne AS, Meyers MA: Spread of disease via the subperitoneal space: The small bowel mesentery. Abdom Imaging 1993; 18:109–116.
44. Mitchell GAG: The renal fascia. Br J Surg 1950; 37:257.
45. Southam AH: Fixation of the kidney. Q J Med 1923; 16:283–308.
46. Parienty RA, Pradel J: Radiological evaluation of the peri- and pararenal spaces by computed tomography. Crit Rev Diagn Imaging 1983; 20:1–26.
47. Nicholson RL: Abnormalities of the perinephric fascia and fat in pancreatitis. Radiology 1981; 139:125–127.
48. Chintapalli K, Lawson TL, Foley WD, et al: Renal fascial thickening in pancreatitis. J Comput Assist Tomogr 1982; 6(5):983–986.
49. Hadar H, Meiraz D: Thickened renal fascia: A sign of retroperitoneal pathology. J Comput Assist Tomogr 1981; 5:193–198.
50. Jeffrey RB, Federle MP, Crass RA: Computed tomography of pancreatic trauma. Radiology 1983; 147:491–494.
51. Sutton CS, Haaga JR: CT evaluation of limited splenic trauma. J Comput Assist Tomogr 1987; 11:167–169.
52. Feldberg MAM, Hendriks MJ, van Waes P, et al: Pancreatic lesions and transfascial perirenal spread: Computed tomographic demonstration. Gastrointest Radiol 1987; 12:121–127.
53. Rubenstein WA, Auh YH, Zirinsky K, et al: Posterior peritoneal recesses: Assessment using CT. Radiology 1985; 156:461–468.
54. William PL, Warwick R (eds): Gray's Anatomy, 36th ed. Churchill Livingstone, Edinburgh, 1980.
55. Saunders BP, Phillips RKS, Williams CB: Intraoperative measurement of colonic anatomy and attachments with relevance to colonoscopy. Br J Surg 1995; 82:1491–1493.
56. Hopper KD, Sherman JL, Juethke J, et al: The retrorenal colon in the supine and prone patient. Radiology 1987; 162:443–446.
57. Love L, Demos TC, Posniak H: CT of retrorenal fluid collections. AJR 1985; 145:87–91.
58. Sherman JL, Hopper KD, Greene AJ, et al: The retrorenal colon on computed tomography: A normal variant. J Comput Assist Tomogr 1985; 9:339–341.
59. Hadar H, Gadoth N: Positional relations of colon and kidney determined by perirenal fat. AJR 1984; 143:773–776.
60. Kunin M: Bridging septa of the perinephric space: Anatomic, pathologic, and diagnostic considerations. Radiology 1986; 158:361–365.
61. Feuerstein IM, Zeman RK, Jatte MH, et al: Perirenal cobwebs: The expanding CT differential diagnosis. J Comput Assist Tomogr 1984; 8:1128–1130.
62. McLennan BL, Lee JKT, Peterson RR: Anatomy of the perirenal area. Radiology 1986; 158:555–557.
63. Winfield AC, Gerlock AJJL, Shaff MI: Perirenal cobwebs: A CT sign of renal vein thrombosis. J Comput Assist Tomogr 1981; 5:705–708.
64. Skarby HG: Beiträge zur Diagnostik der Paranephritiden mit besonderer Berucksichtigung des Röntgenverfahrens. Acta Radiol Suppl 1946; 62:1–165.

65. Whalen JP, Berne AS, Riemenschneider PA: The extraperitoneal perivisceral fat pad. I. Its role in the roentgenological visualization of abdominal organs. Radiology 1969; 92:466–472.
66. Arenas AP, Sanchez LV, Albillos JM, et al: Direct dissemination of pathologic abnormal processes through perihepatic ligaments: Identification with CT. RadioGraphics 1994; 14:515–527.
67. McCort J: Anterior pararenal-space infection. Mt Sinai J Med 1984; 51:482–490.
68. Feldberg MAM, Hendriks MJ, van Waes P: Role of CT in diagnosis and management of complications of diverticular disease. Gastrointest Radiol 1985; 10:370–377.
69. Meyers MA, Oliphant M: Ascending retrocecal appendicitis. Radiology 1974; 110:295–299.
70. Feldberg MAM, Hendriks MJ, van Waes P: Computed tomography in complicated acute appendicitis. Gastrointest Radiol 1985; 10:289–295.
71. Ginzburg L, Oppenheimer GD: Urological complications of regional ileitis. J Urol 1948; 59:948–952.
72. Galen C: On the Usefulness of the Parts of the Body. Translated by May MT. Cornell University Press, Ithaca, NY, 1968.
73. Roman E, Silva Y, Lucas C: Management of blunt duodenal injury. Surg Gynecol Obstet 1971; 132:7–14.
74. Glazer GM, Buy JN, Moss AA, et al: CT detection of duodenal perforation. AJR 1981; 137:333–336.
75. Rizzo MJ, Federle MP, Griffiths BG: Bowel and mesenteric injury following blunt abdominal trauma: Evaluation with CT. Radiology 1989; 173:143–148.
76. Mirvis SE, Gens DR, Shanmuganathan K: Rupture of the bowel after blunt abdominal trauma: Diagnosis with CT. AJR 1992; 159:1217–1221.
77. Kunin JR, Korobkin M, Ellis JH, et al: Duodenal injuries caused by blunt abdominal trauma: Value of CT in differentiating perforation from hematoma. AJR 1993; 160:1221–1223.
78. Sperling L, Rigler LG: Traumatic retroperitoneal rupture of duodenum: Description of valuable roentgen observations in its recognition. Radiology 1937; 29:521–524.
79. Toxopeus MD, Lucas CE, Krabbenhoft KL: Roentgenographic diagnosis in blunt retroperitoneal duodenal rupture. AJR 1972; 115:281–288.
80. Vellacott KD: Intramural haematoma of the duodenum. Br J Surg 1980; 67:36–38.
81. Zeppa M, Forrest JV: Aortoenteric fistula manifested as an intramural duodenal hematoma. AJR 1991; 157:47–48.
82. Dembner AG, Jaffe CC, Simeone J, et al: A new computed tomographic sign of pancreatitis. AJR 1979; 133:477–479.
83. Mendez G Jr, Isikoff MB, Hill MC: CT of acute pancreatitis: Interim assessment. AJR 1980; 135:463–469.
84. Meyers MA, Evans JA: Effects of pancreatitis on the small bowel and colon: Spread along mesenteric planes. AJR 1973; 119:151–165.
85. Myerson PJ, Berg GR, Spencer RP, et al: Gallium-67 spread to the anterior pararenal space in pancreatitis: Case report. J Nucl Med 1977; 18:893–895.
86. Siegelman SS, Copeland BE, Saba GP, et al: CT of fluid collections associated with pancreatitis. AJR 1980; 134:1121–1132.
87. Griffin JF, Sekiya T, Isherwood I: Computed tomography of pararenal fluid collections in acute pancreatitis. Clin Radiol 1984; 35:181–184.
88. Susman N, Hammerman AM, Cohen E: The renal halo sign in pancreatitis. Radiology 1982; 142:323–327.
89. Wulsin JH: Peptic ulcer of the posterior wall of the stomach and duodenum with retroperitoneal leak. Surg Gynecol Obstet 1972; 134:425–429.
90. Hashimoto T, Gokan T, Munechika H, et al: Pathway to the lumbar triangle from the posterior pararenal space: CT evaluation of the spread of disease (abstr). Radiology 1994; 193 (P):398.
91. Meyers MA, Feldberg MAM, Oliphant M: Grey Turner's sign and Cullen's sign in acute pancreatitis. Gastrointest Radiol 1989; 14:31–37.
92. Geis WP, Hodakowski GT: Lumbar hernia. *In* Hernia, 4th ed. Edited by LM Nyhus, RE Condon. JB Lippincott, Philadelphia, 1995, pp 412–423.
93. Grynfeltt, J: Quelques mots sur la hernie lombaire. Montpellier Med 1866; 16:323.
94. Lesshaft P: Lumbalgegren in anatomisch-chirurgischer Himsicht. Anat Physiol Wissensch Med 1870; 264.
95. Petit JL: Traité des maladies chirurgicales, et des opérations qui leur convenient. 3 vols. Paris, T.F. Didot, 1774; 2:256–258.
96. Lawdahl RB, Moss CN, Van Dyke JA: Inferior lumbar (Petit's) hernia. AJR 1986; 147:744–745.
97. Baker ME, Weinerth JL, Andriani RT, et al: Lumbar hernia: Diagnosis by CT. AJR 1987; 148:565–567.
98. Siffring PA, Forrest TS, Frick MP: Hernias of the inferior lumbar space: Diagnosis with US. Radiology 1989; 170:190.

99. Grey Turner G: Local discoloration of the abdominal wall as a sign of acute pancreatitis. Br J Surg 1919; 7:394–395.
100. Dickson AP, Imrie CW: The incidence and prognosis of body wall ecchymosis in acute pancreatitis. Surg Gynecol Obstet 1984; 159:343–347.
101. Ghiatas AA, Nguyen VD, Perusek M: Subcutaneous soft tissue densities: A computed tomography indicator of severe pancreatitis. Gastrointest Radiol 1990; 15:17–21.
102. Fallis LS: Cullen's sign in acute pancreatitis. Ann Surg 1937; 106:54–57.
103. Cox HT: Discoloration of abdominal wall in acute pancreatitis. Br J Surg 1945; 33:182–184.
103a. Markman B, Barton FE: Anatomy of the subcutaneous tissue of the trunk and lower extremity. Plast Reconstr 1987; 80:248–254.
103b. Johnson D, Dixon AK, Abrahams PH: The abdominal subcutaneous tissue: Computed tomographic, magnetic resonance, and anatomical observations. Clinical Anatomy 1996; 9:19–24.
104. Reid BG, Kune GA: Accuracy in diagnosis of acute pancreatitis. Med J Aust 1978; 1:583–587.
105. Cullen TS: A new sign in ruptured extrauterine pregnancy. Am J Obstet 1918; 7:457.
106. Feldberg MAM, van Leeuwen MS: The properitoneal fat pad associated with the falciform ligament: Imaging of extent and clinical relevance. Surg Radiol Anat 1990; 12:193–202.
107. Oliphant M, Berne AS, Meyers MA: Direct spread of subperitoneal disease into solid organs: Radiologic diagnosis. Abdom Imaging 1995; 20:141–147.
108. Horton KM, Fishman, EK: Paraumbilical vein in the cirrhotic patient: Imaging with 3D CT angiography. Abdom Imaging 1998; 23:404–408.
109. Auh YH, Lim JH, Jeong YK, et al: Anatomy of the peritoneal cavity and reflections. *In* Abdominal and Gastrointestinal Imaging Medical Virtual Textbook. Edited by NC Gourtsoyiannis, R Yamada, GW Stevenson, et al. (*http://medic-online.net/abdo/*)
110. Podlaha J: Zur Frage des subkutanen Emphysems bei perforierten gastroduodenalen Geschwüren. Zentralbl Chir 1926; 53:2793–2841.
111. Scappaticci F, Markowitz SK: Intrahepatic pseudocyst complicating acute pancreatitis: Imaging findings. AJR 1995; 165:873–874.
112. Williams DM, Cho KJ, Ensminger WD, et al: Hepatic falciform artery: Anatomy, angiographic appearance and clinical significance. Radiology 1985; 156:339–340.
112a. Kim DE, Yoon H-K, Ko GY, et al: Hepatic falciform artery: Is prophylactic embolization needed before short-term hepatic arterial chemoinfusion? AJR 1999; 172:1597–1599.
113. Casolo F, Bianco R, Franceschelli N: Perirenal fluid collection complicating chronic pancreatitis: CT demonstration. Gastrointest Radiol 1987; 12:117–120.
114. Weill F, Brun P, Rohmer P, et al: Migrations of fluid of pancreatic origin: Ultrasonic and CT study of 28 cases. Ultrasound Med Biol 1983; 9(5):485–496.
115. Morehouse HT, Thornhill BA, Alterman DD: Right ureteral obstruction associated with pancreatitis. Urol Radiol 1985; 7:150–152.
116. Fishman M, Talner LB: Pancreatitis causing focal caliectasis. AJR 1991; 156:1005–1006.
117. Baker MK, Kopecky KK, Wass JL: Perirenal pancreatic pseudocyst: Diagnostic management. AJR 1983; 140:729–732.
118. Chen H-C, Tsang Y-M, Wu C-H, et al: Perirenal fat necrosis secondary to hemorrhagic pancreatitis, mimicking retroperitoneal liposarcoma: CT manifestation. Abdom Imaging 1996; 21:546–548.
119. Rauch RF, Korobkin M, Silverman PM, et al: Subcapsular pancreatic pseudocyst of the kidney. J Comput Assist Tomogr 1983; 7:536–538.
120. Blandino A, Scribano E, Aloisi G, et al: Subcapsular renal spread of a pancreatic pseudocyst. Abdom Imaging 1996; 21:73–74.
121. Ranson JHC, Pasternak BS: Statistical methods for qualifying the severity of clinical acute pancreatitis. J Surg Res 1977; 22:79–91.
122. Ranson JHC: Etiological and prognostic factors in human acute pancreatitis: A review. Am J Gastroenterol 1982; 77:633–638.
123. Kivisaari L, Somer K, Standertskjold-Nordenstam CG, et al: A new method for diagnosis of acute hemorrhagic-necrotizing pancreatitis using contrast-enhanced CT. Gastrointest Radiol 1984; 9:27–30.
124. Schröder T, Kivisaari L, Somer K, et al: Significance of extrapancreatic findings in computed tomography (CT) of acute pancreatitis. Eur J Radiol 1985; 5:273–275.
125. Block S, Maier W, Bittner R, et al: Identification of pancreas necrosis in severe acute pancreatitis: Imaging procedures versus clinical staging. Gut 1986; 27:1035–1042.
126. Balthazar EJ, Ranson JHC, Naidich DP, et al: Acute pancreatitis: Prognostic value of CT. Radiology 1985; 156:767–772.
127. Balthazar EJ: CT diagnosis and staging of acute pancreatitis. Radiol Clin North Am 1989; 27(1):19–37.
128. Balthazar EJ, Robinson DL, Megibow AJ, et al: Acute pancreatitis: Value of CT in establishing prognosis. Radiology 1990; 174:331–336.
129. Johnson CD, Stephens DH, Sarr MG: CT of acute pancreatitis: Correlation between lack of contrast enhancement and pancreatic necrosis. AJR 1991; 156:93–95.
130. Vibhakar SD, Bellow EM: The bare area of the spleen: A constant CT feature of the ascitic abdomen. AJR 1984; 142:953–955.

130a. Sivit CJ, Frazier AA, Eichelberger MR: Prevalence and distribution of extraperitoneal hemorhage associated with splenic injury in infants and children. AJR 1999; 172:1015–1017.
131. Balachandran S, Leonard MH Jr, Kumar D, et al: Patterns of fluid accumulation in splenic trauma: Demonstration by computed tomography. Abdom Imaging 1994; 19:515–520.
132. Meyers MA: Roentgen significance of the phrenicocolic ligament. Radiology 1970; 95:539–545.
133. Beaulieu CF, Mindelzun RE, Dolph J, et al: The infraconal compartment: A multidirectional pathway for spread of disease between the extraperitoneal abdomen and pelvis. J Comput Assist Tomgr 1997; 21:223–228.
134. Aikawa H, Tanone S, Okino Y, et al: Pelvic extension of retroperitoneal fluid: Analysis in vivo. AJR 1998; 171:671–677.
135. Oliphant M, Berne AS, Meyers MA: The subperitoneal space of the abdomen and pelvis: Planes of continuity. AJR 1996; 167:1433–1439.
136. Mastromatteo JF, Mindell HJ, Mastromatteo MF, et al: Communications of the pelvic extraperitoneal spaces and their relation to the abdominal extraperitoneal spaces: Helical CT cadaver study with pelvic extraperitoneal injections. Radiology 1997; 202:523–530.
137. Trerotola SO, Kuhlman JE, Fishman EK: Bleeding complications of femoral catheterization: CT evaluation. Radiology 1990; 174:37–40.
138. Trerotola SO, Kuhlman JE, Fishman EK: CT and anatomic study of postcatheterization hematomas. Radiographics 1991; 11:247–258.
139. Congdon ED, Blumberg R, Henry W: Fasciae of fusion and elements of the fused mesenteries in the human adult. Am J Anat 1942; 70:251–279.
140. Toldt C: Bau und Wachsthumveränderungen der Gekröse des Menslichen Darmkanales. Denkschr d math naturwissensch Kl d Kaiserl Akad d Wissensch, Wien 1879; 41:1–56.
141. Hayes MA: Abdominopelvic Fasciae. Am J Anat 1950; 87:119–161.
142. Treitz W: Ueber einen neuen Muskel am Duodenum des Menschen, ueber elastische Sehnen, und einige andere anatomische Verhältnisse. Vierteljahrsch f d prakt Heilkunde, Prag 1853; 37:113–144.
143. Toldt C: Bauchfell und Gekröse. Anat Hefte, 2 Abt, Ergebn d Anat u Entwickl Gesch 3: 1893; 263–273.
144. Fredet P: Péritoine Morphogenèse et Morphologie. Fascias d'accolement. Anomalies péritonéales resultant d'un vice ou d'un arrêt de developpement. *In* Traite d'Anatomie Humaine de Poirrier P, Charpy A: Masson, Paris, 1900, pp 863–1053.
145. Duval PA: Traitement chirurgical du cancer du colon pelvien. Indications, technique, operatoire. Thèse, Paris, 1902.
146. Descomps P: Les zones accolées du péritoine. Leur décollement operatoire. Revue de Chirurgie 1922; 451–498.
147. Popp O: Ueber die Struktureigentümlichkeiten des Peritoneum und der Tela subperitonealis und deren Bedeutung fur die Befestigung der Bauch-eingeweide. Anat Anz 1936; 81:369–93.
148. Drouhet Th: Le tissu souspéritonéal. Thèse, Montpellier, 1942.
Couinaud C: Anatomie de 1'Abdomen: 186. Doin Ed, Paris, 1963.
150. Strax R, Toombs BD, Rauschkolb EN: Correlation of barium enema and CT in acute pancreatitis. AJR 1981; 138:1219–1220.
151. Marks SC Jr, Raptopoulos V, Kleinman P, et al: The anatomical basis for retrorenal extensions of pancreatic effusions: The role of the renal fasciae. Surg Radiol Anat 1986; 8:89–97.
152. Aikawa H, Tanoue S, Okino y, et al: Pelvic extension of retroperitoneal fluid: Analysis in vivo. AJR 1998; 171:671–677.
153. Fredet P: Documents sur la formation des capsules du rein chez l'embryon humain. Bull et mem de la societé anat 1904; 285–288.
154. Paturet G: La gaine urinaire. Thèse, Paris, 1923.
155. Colley H: De la mobilisation de fascias d'accolement en chirurgie abdominale. Thèse, Lyon, 1907.
156. Charnsangavej C, DuBrow RE, Varma DGK, et al: CT of the mesocolon. Radiographics 1993; 13:1035–1045.
157. Stallard DJ, Tu RK, Gould MJ, et al: Minor vascular anatomy of the abdomen and pelvis: A CT atlas. Radiographics 1994; 14:493–513.
158. Korobkin M, Silverman PM, Quint LE, et al: CT of the extraperitoneal space: Normal anatomy and fluid collections. AJR 1992; 159:933–941.
159. Oliphant M, Berne AS, Meyers MA: Bidirectional spread of disease via the subperitoneal space: The lower abdomen and pelvis. Abdominal Imaging 1993; 18:117–125.
160. Vermooten V: The mechanism of perinephric and perinephritic abscesses: A clinical and pathological study. J Urol 1933; 30:181–193.
161. Polkey HJ, Vynalek WJ: Spontaneous nontraumatic perirenal and renal hematomas: Experimental and clinical study. Arch Surg 1933; 26:196–218.
162. Evans JA, Meyers MA, Bosniak MA: Acute renal and perirenal infections. Semin Roentgenol 1971; 6:274–291.
163. Bacon RD: Respiratory pyelography: A study of renal motion in health and disease. AJR 1940; 44:71.

164. Nesbit RM, Dick VS: Pulmonary complications of acute renal and perirenal suppuration. AJR 1940; 44:161–169.
165. Kawashima A, Sandler CM, Corriere JN Jr, et al: Ureteropelvic junction injuries secondary to blunt abdominal trauma. Radiology 1997; 205:487–492.
166. Friedenberg RM, Moorehouse H, Gade M: Urinomas secondary to pyelosinus backflow. Urol Radiol 1983; 5:23–29.
167. Morgan CL Jr, Grossman H: Posterior urethral valves as a cause of neonatal uriniferous perirenal pseudocyst (urinoma). Pediatr Radiol 1978; 7:29–32.
168. Crabtree EG: Pararenal pseudo-hydronephrosis: With report of three cases. Trans Am Assoc Genitourinary Surg 1935; 28:9–40.
169. Razzaboni G: Richerche sperimentali sulla pseudoidronefrosi. Arch Ital Chir 1922; 6:365–372.
170. Hudson HG, Hundley RR: Pararenal pseudocyst. J Urol 1967; 97:439–443.
171. Weintrab HD, Rall KL, Thompson IM, et al: Pararenal pseudocysts: Report of three cases. AJR 1964; 92:286–290.
172. Sauls CL, Nesbit RM: Pararenal pseudocysts: A report of four cases. J Urol 1962; 87:288–296.
173. Johnson CM, Smith DR: Calcified perirenal pseudohydronephrosis: Hydronephrosis with communicating perirenal cyst with calcification. J Urol 1941; 45:152–164.
174. Pyrah LN, Smiddy FG: Pararenal pseudohydronephrosis: A report of two cases. Br J Urol 1953; 25:239–246.
175. Itoh S, Yoshioka H, Kaeriyama M, et al: Ultrasonographic diagnosis of uriniferous perirenal pseudocyst. Pediatr Radiol 1982; 12:156–158.
176. Macpherson RI, Gordon L, Bradford BF: Neonatal urinomas: Imaging considerations. Pediatr Radiol 1984; 14:396–399.
177. Suzuki Y, Sugihara M, Kuribayashi S, et al: Uriniferous perirenal pseudocyst detected by 99m-Tc-dimercaptosuccinic acid renal scan. AJR 1979; 133:306–308.
178. Healey ME, Teng SS, Moss AA: Uriniferous pseudocyst: Computed tomographic findings. Radiology 1984; 153:757–762.
179. Hurwitz SP, Weisenthal CL: Pararenal pseudocyst. J Urol 1967; 97:8–15.
180. Belville JS, Morgentaler A, Loughlin KR, et al: Spontaneous perinephric and subcapsular renal hemorrhage: Evaluation with CT, US, and angiography. Radiology 1989; 172:733–738.
181. Cinman AC, Farrer J, Kaufman JJ: Spontaneous perinephric hemorrhage in a 65-year old man. J Urol 1933; 133:829–832.
182. Mukamel E, Nissenkorn I, Avidor I, et al: Spontaneous rupture of renal and ureteral tumors presenting as acute abdominal condition. J Urol 1979; 122:696–698.
183. Pollack HJ, Popky G: Spontaneous subcapsular renal hemorrhage: Its significance and roentgenographic diagnosis. J Urol 1972; 108:530–533.
184. Watnick M, Spindola-Franco H, Abrams HL: Small hypernephroma with subcapsular hematoma and renal infarction. J Urol 1972; 108:534–536.
185. Sherman JL, Hartman DS, Friedman AC, et al: Angiomyolipoma: Computed tomography—pathologic correlation of 17 cases. AJR 1981; 137:1221–1226.
186. Bosniak MA: Spontaneous subcapsular and perirenal hematomas (editorial). Radiology 1989; 172:601–602.
187. Mastrodomenico L, Korobkin M, Silverman PM, et al: Perinephric hemorrhage from metastatic carcinoma to the kidney. J Comput Assist Tomogr 1983; 7(4):727–729.
188. Choyke PL, White EM, Zeman RK, et al: Renal metastases: Clinicopathologic and radiologic correlation. Radiology 1987; 162:359–363.
189. Shirkhoda A: Computed tomography of perirenal metastases. J Comput Assist Tomogr 1986; 10(3):435–438.
190. Rails PW, Barakos JA, Kaptein EM, et al: Renal biopsy-related hemorrhage: Frequency and comparison of CT and sonography. J Comput Assist Tomogr 1987; 11(6): 1031–1034.
191. Castoldi MC, Del Moro RM, D'Urbano ML, et al: Sonography after renal biopsy: Assessment of its role in 230 consecutive cases. Abdom Imaging 1994; 19:72–77.
192. Cronan JJ, Dorfman GS, Amis ES, et al: Retroperitoneal hemorrhage after percutaneous nephrostomy. AJR 1985; 144:801–803.
193. Rubin JI, Arger PH, Pollack HM, et al: Kidney changes after extracorporeal shock wave lithotripsy: CT evaluation. Radiology 1987; 162:21–24.
194. Rosen A, Korobkin M, Silverman PM, et al: CT diagnosis of ruptured abdominal aortic aneurysm. AJR 1984; 143:265–268.
195. Sandier CM, Jackson H, Kaminsky RI: Case report: Right perirenal hematoma secondary to a leaking abdominal aortic aneurysm. J Comput Assist Tomogr 1981; 5(2):264–266.
196. Siegel CL, Cohan RH: CT of abdominal aortic aneurysms. AJR 1994; 163:17–29.

197. Morehouse HT, Hochstztein JG, Lonwie W, et al: Pitfalls in the CT diagnosis of ruptured abdominal aortic aneurysm (abstr). Radiology 1992; 185 (P):181.
198. Raptopoulos V, Cumming I, Smith EH: Computed tomography of life-threatening complications of abdominal aortic aneurysm: The disrupted aortic wall. Invest Radiol 1986; 22:372–376.
199. Siegel CL, Cohan RH, Korobkin M, et al: Abdominal aortic aneurysm morphology: CT features in patients with ruptured and nonruptured aneurysms. AJR 1994; 163:1123–1129.
200. Mehard WB, Heiken JP, Sicard GA: High-attenuating crescent in abdominal aortic aneurysm wall at CT: A sign of acute or impending rupture. Radiology 1994; 192:359–362.
201. Cohen LJ, Sukov RJ, Boswell W, et al: Spontaneous aorto-caval fistula: Report of 2 cases. Radiology 1981; 138:357–359.
202. Middleton WD, Smith WD, Foley WD: CT detection of aortocaval fistula. J Comput Assist Tomogr 1987; 11:344–347.
203. Koslin DB, Kenney PJ, Stanley RJ, et al: Aortocaval fistula: CT appearance with angiographic correlation. J Comput Tomogr 1987; 11(2):348–350.
204. Mackenzie AR: Spontaneous subcapsular renal hematoma: Report of case misdiagnosed as acute appendicitis. J Urol 1960; 84:243–245.
205. Engel WJ, Page IH: Hypertension due to renal compression resulting from subcapsular hematoma. J Urol 1955; 73:735–739.
206. Marshall WH Jr, Castellino RA: Hypertension produced by constricting capsular renal lesions ("Page" kidney). Radiology 1971; 101:561–565.
207. Takahashi M, Tamakawa Y, Shibata A, et al: Computed tomography of "Page" kidney. J Comput Assist Tomogr 1977; 1:344–348.
208. Page IH: Production of persistent arterial hypertension by cellophane and perinephritis. JAMA 1939; 113:2046–2048.
209. Frank IN, Wieche DR: Nephrotomographic appearance of spontaneous subcapsular hemorrhage. Radiology 1967; 89:477–482.
210. Pollack HM, Popky GL: Roentgenographic manifestations of spontaneous renal hemorrhage. Radiology 1974; 110:1–6.
211. Meyers MA, Friedenberg RM, King MC, et al: The significance of the renal capsular arteries. Br J Radiol 1967; 40:949–956.
212. Koehler PR, Talner LB, Friedenberg MJ, et al: Association of subcapsular hematomas with nonfunctioning kidney. Radiology 1973; 101:537–542.
213. Schaner EG, Barlow JE, Doppman JL: Computed tomography in the diagnosis of subcapsular and perirenal hematoma. AJR 1977; 129:83–88.
214. Federle MP, Kaiser JA, McAninch JW, et al: The role of computed tomography in renal trauma. Radiology 1981; 141:455–460.
215. Sandler CM, Toombs BD: Computed tomographic evaluation of blunt renal injuries. Radiology 1981; 141:461–466.
216. Zagoria RJ, Dyer RB, Assimos DG et al: Spontaneous perinephric hemorrhage: Imaging and management. J Urol 1991; 145:468–471.
217. Antonopoulos P, Drossos CH, Triantopoulou CH, et al: Complications of renal angiomyolipomas: CT evaluation. Abdom Imaging 1996; 21:357–360.
218. Gavant ML, Salazar JE, Ellis J: Intrarenal rupture of the abdominal aorta: CT features. J Comput Assist Tomogr 1986; 10(3):516–518.
219. McClennan BL, Lee JKT, Peterson RR: Anatomy of the perirenal area. Radiology 1986; 158:555–557.
220. Sacks D, Banner MP, Meranze SG, et al: Renal and related retroperitoneal abscesses: Percutaneous drainage. Radiology 1988; 167:447–451.
221. Bernardino ME, Baumgartner BR: Abscess drainage in the genitourinary tract. Radiol Clin North Am 1986; 24:539–549.
222. Morehouse HT, Weiner SN, Hoffman-Tretin JC: Inflammatory disease of the kidney. Semin Ultrasound CT MR 1986; 7:246–258.
223. Deyoe LA, Cronan JJ, Lambiase RE, et al: Percutaneous drainage of renal and perirenal abscesses: Results in 30 patients. AJR 1990; 155:81–83.
224. Presman D, Rolnick D, Portney F: Spontaneous perinephric hematoma secondary to renal tumor. AmJ Surg 1961; 102:586–593.
225. Lambiase RE, Deyoe L, Cronan JJ, et al: Percutaneous drainage of 335 consecutive abscesses: Results of primary drainage with 1-year follow-up. Radiology 1992; 184:167–178.
226. Robson CJ, Churchill BM, Anderson W: The results of radical nephrectomy for renal cell carcinoma. J Urol 1969; 101:297–301.
227. Skinner DG, Colvin RB, Vermillion CD, et al: Diagnosis and management of renal cell carcinoma: A clinical and pathologic study of 309 cases. Cancer 1979; 28:1165–1177.
228. Waters WB, Richie JP: Aggressive surgical approach to renal cell carcinoma: Review of 130 cases. J Urol 1979; 122:306–309.
229. Zagoria RJ, Bechtold RE, Dyer RB: Staging of

renal adenocarcinoma: Role of various imaging procedures. AJR 1995; 164:363–370.
230. Spiessl B, Beahrs OH, Hermanek P, et al: TNM Atlas: Illustrated Guide to the TNM/pTNM Classification of Malignant Tumours, 3rd edition, 2nd revision. New York, Springer-Verlag, 1992.
231. Narumi Y, Hricak H, Forstner R, et al: MR imaging evaluation of renal cell carcinoma. Abdom Imaging 1997; 22:216–225.
232. Kallman DA, King BF, Hattery RR, et al: Renal and inferior vena cava tumor thrombus in renal cell carcinoma: CT, US, MRI, and venacavography. J Comput Assist Tomogr 1992; 16:240–247.
233. Studer UE, Scherz S, Scheidegger J, et al: Enlargement of regional lymph nodes in renal cell carcinoma is often not due to metastases. J Urol 1990; 144:243–245.
234. Kabala JE, Gillatt DA, Persad RA, et al: Magnetic resonance imaging in the staging of renal cell carcinoma. Br J Radiol 1991; 64:683–689.
235. Johnson CD, Dunnick NR, Cohan RH, et al: Renal adenocarcinoma: CT staging of 100 tumors. AJR 1987; 148:59–63.
236. Zeman RK, Cronan JJ, Rosenfield AT, et al: Renal cell carcinoma: Dynamic thin-section CT assessment of vascular invasion and tumor vascularity. Radiology 1988; 167:393–396.
237. Kopka L, Fischer U, Zoeller G, et al: Dual-phase helical CT of the kidney: Value of the corticomedullary and nephrographic phase for evaluation of renal lesions and preoperative staging of renal cell carcinoma. AJR 1997; 169:1573–1578.
238. Habboub HK, Abu-Yousef MM, Williams RD, et al: Accuracy of color Doppler sonography in assessing venous thrombus extension in renal cell carcinoma. AJR 1997; 168:267–271.
239. Fein AB, Lee JKT, Balfe DM, et al: Diagnosis and staging of renal cell carcinoma: A comparison of MR imaging and CT. AJR 1987; 148:749–753.
240. Hricak H, Thoeni RF, Carroll PR, et al: Detection and staging of renal neoplasms: A reassessment of MR imaging. Radiology 1988; 166:643–649.
241. Semelka RC, Shoenut JP, Kroeker MA, et al: Renal lesions: Controlled comparison between CT and 1.5-T MR imaging with non-enhanced and gadolinium-enhanced fat-suppressed spin-echo and breath-hold FLASH techniques. Radiology 1992; 182:425–430.
242. Roubidoux MA, Dunnick NR, Sostman HD, et al: Renal carcinoma: Detection of venous extension with gradient-echo MR imaging. Radiology 1992; 182:269–272.
243. Nguyen BD, Westia WH, Zerhouni EA: Renal cell carcinoma and tumor thrombus neovascularity: MR demonstration with pathologic correlation. Abdom Imaging 1996; 21:269–271.
244. Choyke PL, Walter MM, Wagner JR, et al: Renal cancer: Preoperative evaluation with dual-phase three-dimensional MR angiography. Radiology 1997; 205:767–771.
245. Cherrie RJ, Goldman DG, Lindner A, et al: Prognostic implications of vena cava extension of renal cell carcinoma. J Urol 1982; 128:910–912.
246. Sogani PC, Herr HW, Bains MS, et al: Renal cell carcinoma extending into inferior vena cava. J Urol 1983; 130:660–663.
247. DeKirnion JB, Berry D: The diagnosis and treatment of renal cell carcinoma. Cancer 1980; 45:1947–1956.
248. Jafri SZH, Bree RL, Amendola MA, et al: CT of renal and perirenal non-Hodgkin lymphoma. AJR 1982; 138:1101–1105.
249. Reznek RH, Mootoosamy I, Webb AW, et al: CT in renal and perirenal lymphoma: A further look. Clin Radiol 1990; 42:233–238.
250. Villalon FC, Fernandez JE, Garcia TR: The hypoechoic halo: A finding in renal lymphoma. J Clin Ultrasound 1995; 23:379–381.
251. Hauser M, Krestin GP, Hagspiel KD: Bilateral solid multifocal intrarenal and perirenal lesions: Differentiation with ultrasonography, computed tomography and magnetic resonance imaging. Clin Radiol 1995; 50:288–294.
252. Bailey J, Roubidoux MA, Dunnick NR: Secondary renal neoplasms. Abdom Imaging 1998; 23:266–274.
253. Sheeran SR, Sussman SK: Renal lymphoma: Spectrum of CT findings and potential mimics. AJR 1998; 171:1067–1072.
254. Amis ES Jr: Retroperitoneal fibrosis. AJR 1991; 157:321–329.
255. Rominger MB, Kenney PJ: Perirenal involvement by retroperitoneal fibrosis: The usefulness of MRI to establish diagnosis. Urol Radiol 1992; 13:173–176.
256. Yancey JM, Kaude JV: Diagnosis of perirenal fibrosis by MR imaging. J Comput Assist Tomogr 1988; 12:335–337.
257. Rapezzi D, Racchi O, Ferraris AM, et al: Perirenal extramedullary hematopoiesis in agnogenic myeloid metaplasia: MR imaging findings (letter to the editor). AJR 1997; 168:1388–1389.
258. Wright RE: Case report: Pararenal extramedullary haematopoietic tissue—an unusual manifestation of myelofibrosis. Clin Radiol 1991; 44:210–211.

259. Wilbur AC, Turk JN, Capek V: Perirenal metastases from lung cancer: CT diagnosis. J Comput Assist Tomogr 1992; 16:589–591.
260. Loughran CF: A review of the plain abdominal radiography in acute rupture of abdominal aortic aneurysms. Clin Radiol 1986; 37(4):383–387.
261. Nichols GB, Schilling PJ: Pseudo-retroperitoneal gas in rupture of aneurysm of abdominal aorta. AJR 1975; 125:134–137.
262. Jeffrey RB Jr, Cardoza JD, Olcott EW: Detection of active intraabdominal arterial hemorrhage: Value of dynamic contrast-enhanced CT. AJR 1991; 156:725–729.
263. Hopper KD, Sherman JL, Ghaed N: Aortic rupture into retroperitoneum. Letter to the editor. AJR 1985; 145:435–437.
264. Kam J, Patel S, Ward RE: Computed tomography of aortic and aortoiliofemoral grafts. J Comput Assist Tomogr 1982; 6(2):298–303.
265. Mark A, Moss AA, Lusby R, et al: CT evaluation of complications of abdominal aortic surgery. Radiology 1982; 145:409–414.
266. Low RN, Wall SD, Jeffrey RB Jr, et al: Aortoenteric fistula and perigraft infection: Evaluation with CT. Radiology 1990; 175:157–162.
267. Nguyen B, Beckman I: Silent rectal perforation after endoscopic polypectomy: CT features. Gastrointest Radiol 1992; 17:271–273.
268. Calenoff L, Poticha SM: Combined occurrence of retropneumoperitoneum and pneumoperitoneum. AJR 1973; 17:366–372.
269. Meyers MA, Volberg F, Katzen B, et al: Haustral anatomy and pathology: A new look. I. Roentgen identification of normal patterns and relationships. Radiology 1973; 108:497–504.
270. Meyers MA, Volberg F, Katzen B, et al: Haustral anatomy and pathology: A new look. II. Roentgen interpretation of pathologic alterations. Radiology 1973; 108:505–512.
271. Kleinman PK, Brill PW, Whalen JP: Anterior pathway for transdiaphragmatic extension of pneumomediastinum. AJR 1978; 131:271–275.
272. Balthazar EJ, Moore SL: CT evaluation of infradiaphragmatic air in patients treated with mechanically assisted ventilation: A potential source of error. AJR 1996; 167:731–734.
273. McCourtney JS, Molloy RG, Anderson JR: Endoscopic esophageal perforation presenting as surgical emphysema of the scrotum (letter to the editor). Gastrointest Endosc 1994; 40:121–122.
274. Christensen EE, Landay MJ: Visible muscle of the diaphragm: Sign of extraperitoneal air. AJR 1980; 135:521–523.
275. Feldberg MAM, Koehler PR, van Waes P: Psoas compartment disease studied by computed tomography: Analysis of 50 cases and subject review. Radiology 1983; 148:505–512.
276. Donovan JP, Zerhouni EA, Siegelman SS: CT of the psoas compartment of the retroperitoneum. Semin Roentgenol 1981; 16:241–250.
277. Van Dyke JA, Holley HC, Anderson SD: Review of the iliopsoas anatomy and pathology. RadioGraphics 1987; 7:53–85.
278. Torres GM, Cernigliaro JG, Abbitt PL, et al: Iliopsoas compartment: Normal anatomy and pathologic processes. RadioGraphics 1985; 15:1285–1297.
279. Williams MP: Non-tuberculous psoas abscess. Clin Radiol 1986; 37:253–256.
280. Lee JKT, Glazer HS: Psoas muscle disorders: MR imaging. Radiology 1986; 160:683–687.
281. Lenchik L, Dovgan DJ, Kier R: CT of the iliopsoas compartment: Value in differentiating tumor, abscess, and hematoma. AJR 1994; 162:83–86.
282. Testut L, Jacob O: Traité d'Anatomie Topographique, Abdomen, bassin, membres. Doin Ed, Paris, 1992, Tome II: pp 247–542.
283. Vasile N: Tomodensitométrie du corps entier. Vigot Ed, Paris, 1990, pp 417–479.
284. Normal abdominal and pelvic anatomy. *In* Computed Body Tomography with MRI Correlation, 3rd ed. Edited by JKT Lee, SS Sagel, RJ Stanley. Lippincott-Raven, Philadelphia, 1998, pp 623–626.
285. Auh YH, Rubenstein WA, Schneider M, et al: Extraperitoneal paravesical spaces: CT delineation with US correlation. Radiology 1986; 159:319–328.
286. Roy C, Dupuis M, Sick H, et al: Imagerie normale et pathologique des espaces de la cavité pelvienne. Feuillets de Radiologie 1992; 2:227–238.
287. Korobkin M, Silverman PM, Quint LE, et al: Retroperitoneal fluid collections: Controversies and changing concepts. AJR 1992; 159:933–941.
288. Yamashita Y, Torashima M, Harada M, et al: Post-partum extraperitoneal pelvic hematoma: Imaging findings. AJR 1993; 161:805–808.

The Renointestinal Relationships: Normal and Pathologic Anatomy

9

Many patients with renal disease present with symptoms that seem to arise from the digestive tract. Practically every case of urinary tract disease is known to be accompanied by some gastrointestinal complaint of a transitory or permanent character, particularly nausea, vomiting, epigastric distress, constipation, or diarrhea.[1] Gastrointestinal symptoms alone have been noted in up to 43% of patients. Since clinical investigation of such patients is often started with barium contrast studies, it is important to recognize that characteristic effects on specific portions of the bowel may uncover the primary renal disease and redirect the course of evaluation.[2]

Basic to a radiologic appreciation of the characteristic bowel changes is an understanding of the renointestinal anatomic relationships.

Anatomic Considerations

The Right Kidney

The right kidney is in intimate relationship to two segments of the gastrointestinal tract: the descending duodenum and the hepatic flexure of the colon. Figures 9–1 and 9–2 illustrate these relationships and the reflections of the posterior parietal peritoneum in the right flank. Virtually all of the right kidney is invested anteriorly by peritoneum except at two sites constituting its "bare areas":

1. Medially, the second portion of the duodenum descends immediately in front of the right kidney. Here the peritoneum reflects to continue anterior to the duodenum and pancreas.

2. Inferiorly, the extraperitoneal colon courses obliquely over the lower pole of the kidney. This occurs precisely at its level between (a) the distal ascending colon and the posterior hepatic flexure, which is related superiorly to the deep inferior visceral surface of the liver, and (b) the anterior hepatic flexure as it crosses the descending duodenum; this segment marks the beginning of the transverse mesocolon and is related superiorly to the gallbladder.

A common variant exists in the extent of peritonealization of the second portion of the duodenum. Frequently, the postapical segment of the duodenum remains intraperitoneal for several centimeters, even as it courses inferiorly, suspended by the lesser omentum. The point at which it penetrates the posterior parietal peritoneum to descend extraperitoneally as a straight segment is marked characteristically by a mild junctional flexure. An exaggerated form of this is seen as the "hammock" duodenum.

Because of the oblique position of the kidney along the lateral edge of the psoas muscle, its medial surface projects somewhat anterior to its lateral border. Thus, it can be appreciated that both anterior and medial displacement of the descending duodenum, distal to its postapical segment, would result from a right renal mass.

While some variation occasionally exists, the descending duodenum usually lies on a more posterior plane than the duodenojejunal junction at the ligament of Treitz. In a standard right lateral projection of an upper GI series, therefore, projection of the second duodenum anterior to the fourth (ascending) duodenum and duodenojejunal junction should be viewed with suspicion of a right renal mass.

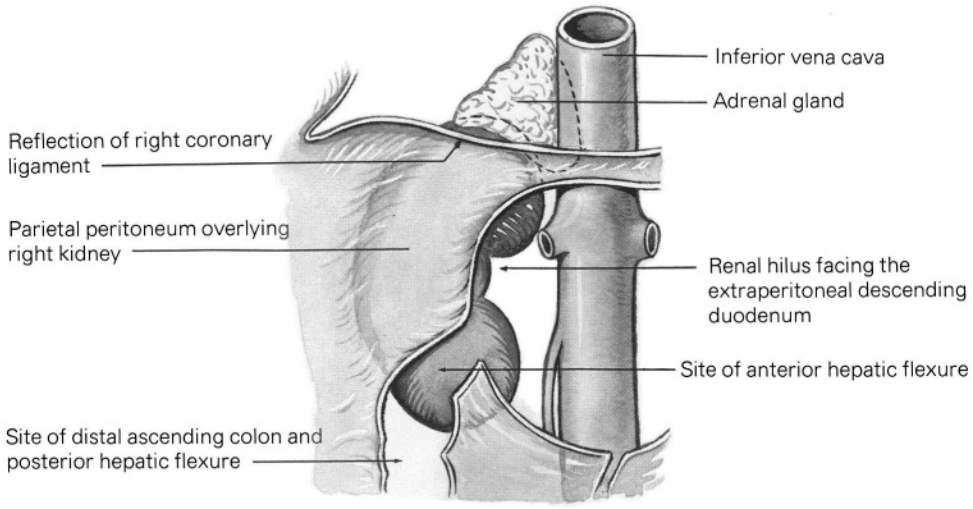


Fig. 9–1. Frontal drawing emphasizing relationships of right kidney to descending duodenum and hepatic flexure of the colon by virtue of their peritoneal reflections.

The upper two-thirds of the right kidney are related to the right colon between its two flexures, whereas the lower pole is inframesocolic and is related laterally and anteriorly to the distal ascending colon.

The Left Kidney

The relationships of the left kidney to the bowel are most intimate to the distal transverse and proximal descending colon. Figure 9–3 illustrates these relationships and the complex peritoneal reflections in the left flank. The reflections of the transverse mesocolon cross the left kidney anteriorly along a narrow "bare area" at the junction of its middle and lower thirds to continue with the peritoneal reflections over the descending colon. At the junction of the transverse and the descending colon, the peritoneum reflects from the anatomic splenic flexure to form the phrenicocolic ligament that inserts on the left diaphragm at the level of the 10th and 11th ribs. The distal transverse colon is related to the anterior surface of the lower half of the left kidney, although at variable distances, depending upon the length of the transverse mesocolon. The lower pole is fully inframesocolic. The extraperitoneal descending colon passes

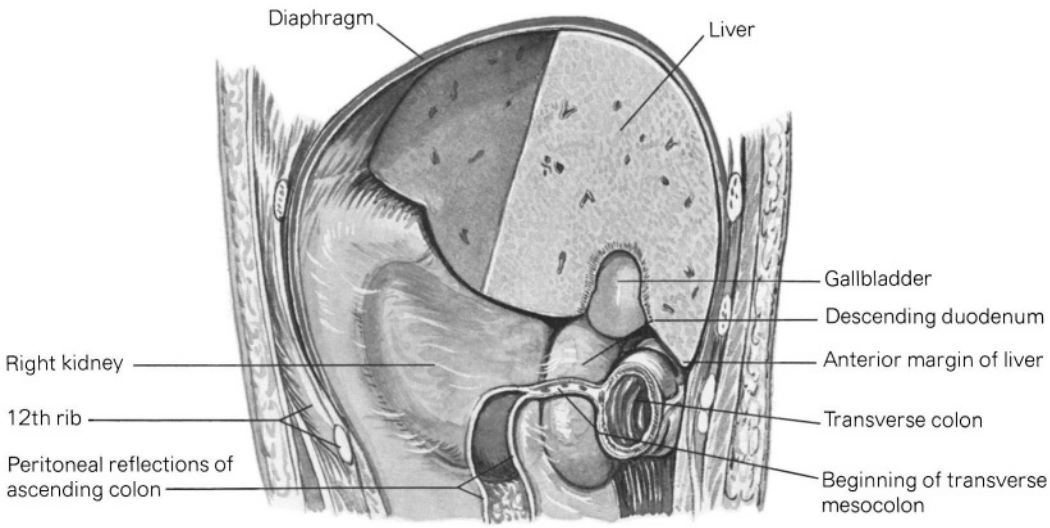


Fig. 9–2. Right parasagittal drawing showing anatomic relationships to the right kidney.

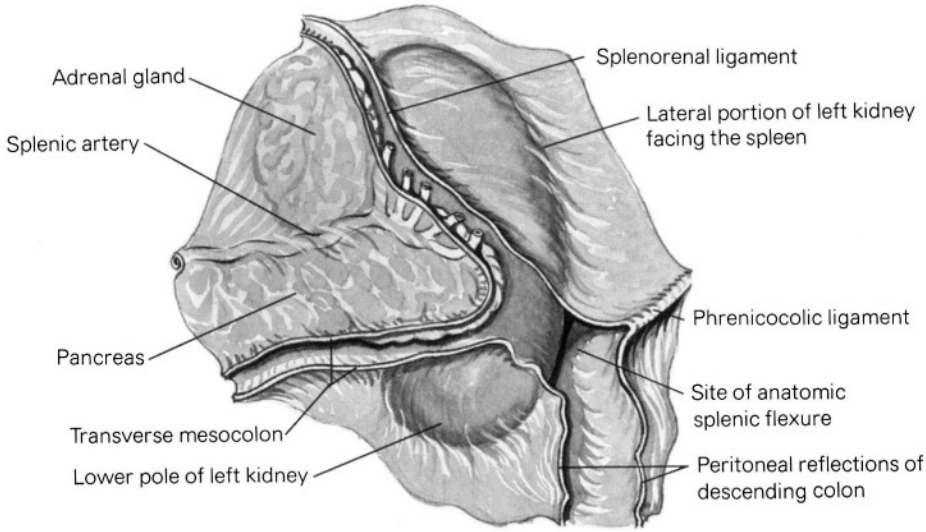


Fig. 9–3. Frontal drawing emphasizing the relationship of the left kidney to the colon by virtue of their peritoneal reflections.

downward along the lateral border of the left kidney, turning somewhat medially toward the lower border of the psoas muscle at the lower pole. Other peritoneal reflections account for the splenorenal ligament, within which the tail of the pancreas inserts and the splenic vessels course. More anterior to the medial surface of the left kidney lie the greater curvature of the stomach, and inferiorly, the duodenojejunal junction and jejunal loops. Figure 9–4 clarifies these relationships in a parasagittal dimension.

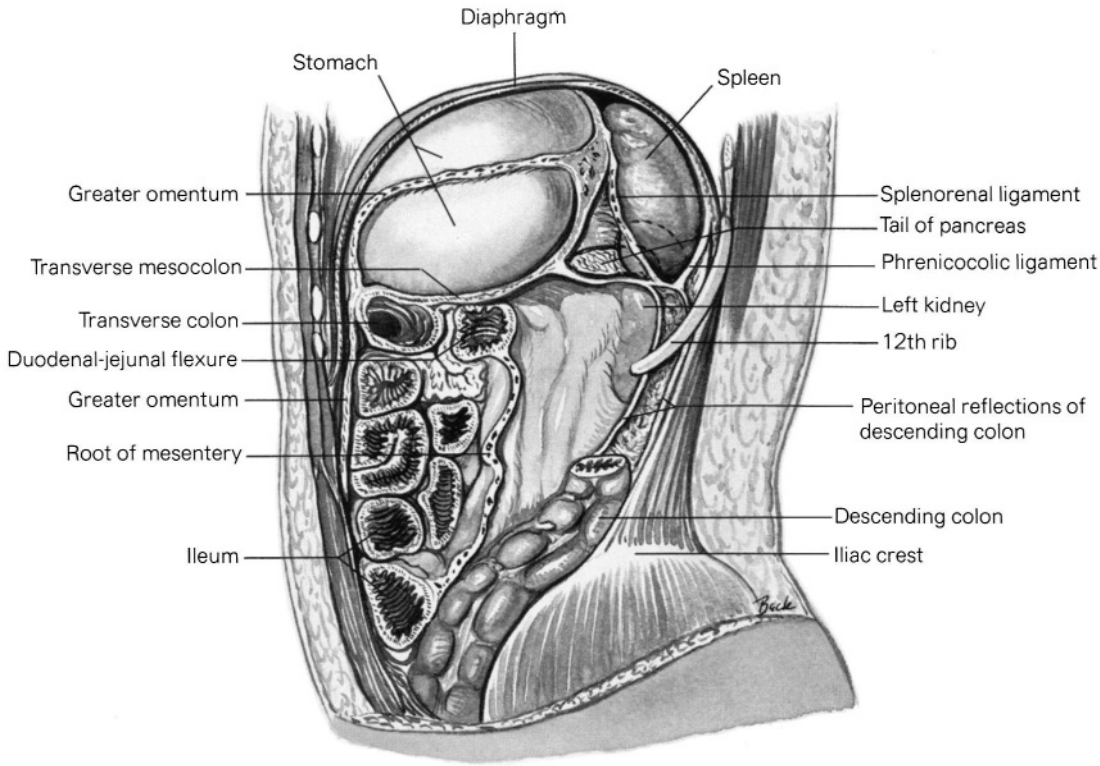


Fig. 9–4. Left parasagittal drawing showing anatomic relationships of the left kidney.

Radiologic Observations

The intimate anatomic relationships of the kidneys to specific portions of the gastrointestinal tract precisely account for characteristic changes of deformity, displacement, or distortion.[2]

Characteristic Mass Displacements

The Right Kidney

Duodenum. Right renal masses typically cause medial and anterior displacement of the descending duodenum, while the immediate postapical segment tends to be unaffected. This produces a characteristic appearance on frontal and lateral projections. In anteroposterior or posteroanterior views, the immediately proximal second portion of the duodenum descends vertically, but the

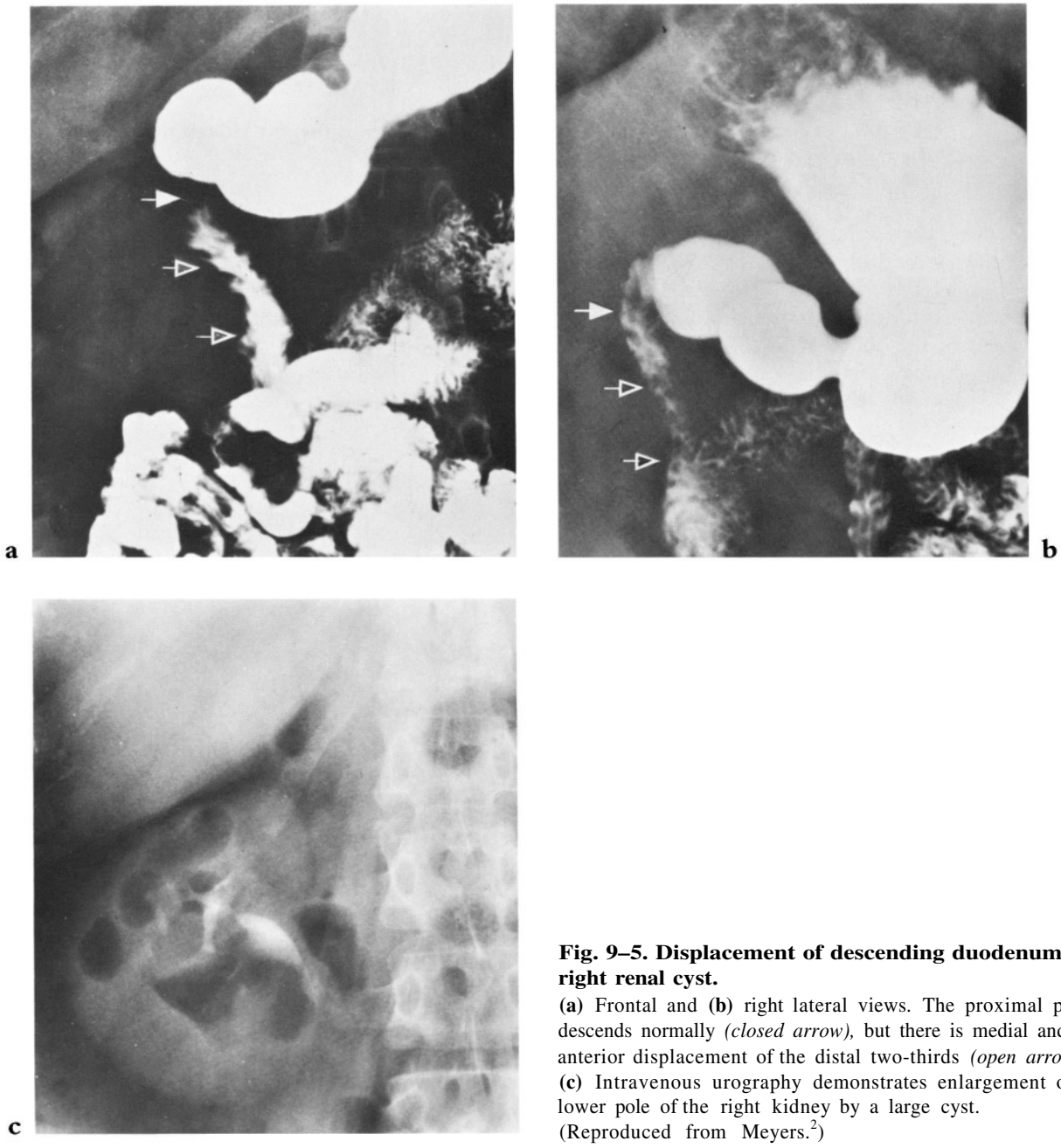


Fig. 9–5. Displacement of descending duodenum by right renal cyst.
(a) Frontal and **(b)** right lateral views. The proximal portion descends normally *(closed arrow),* but there is medial and anterior displacement of the distal two-thirds *(open arrows).* **(c)** Intravenous urography demonstrates enlargement of the lower pole of the right kidney by a large cyst.
(Reproduced from Meyers.[2])

distal two-thirds is deflected medially (Figs. 9–5 through 9–8). In right lateral projections, correspondingly, the normal descent of the proximal segment is maintained but the distal portion is displaced anteriorly; this may result in a gentle axis inferiorly and anteriorly (Figs. 9–5b and 9–6b) or in a striking ventral bowing (Figs. 9–7 and 9–8b). Extrinsic pressure on the mucosal folds themselves may be best appreciated in only one view. This may be shown as mass flattening of the normal mucosal contour, undulations, or gross mass distortion on the lateral or posterior wall.

These changes in the descending duodenum are usually easily distinguishable from other extrinsic masses. Right adrenal masses may attain a size to affect the postapical segment (Fig. 9–9). Enlargement of the right lobe of the liver typically produces a more uniform medial displacement (Fig. 9–10).

Small Bowel. Massive kidney enlargement displaces jejunal loops anteriorly and inferiorly. With progression, particularly if the process is bilateral as in poly cystic renal disease, the small bowel may be crowded into the midline (Fig. 9–11).

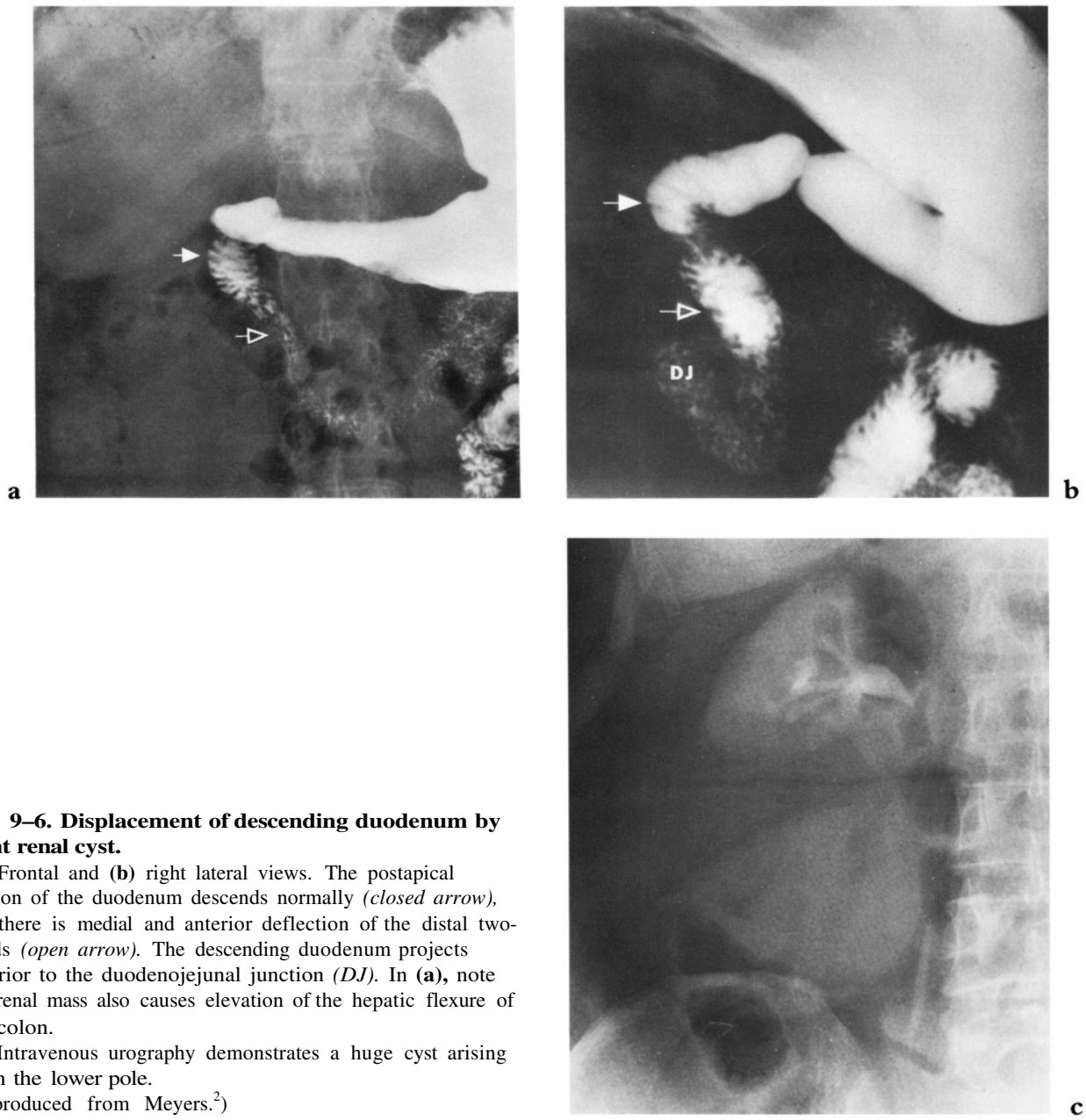


Fig. 9–6. Displacement of descending duodenum by right renal cyst.
(a) Frontal and **(b)** right lateral views. The postapical portion of the duodenum descends normally *(closed arrow),* but there is medial and anterior deflection of the distal two-thirds *(open arrow).* The descending duodenum projects anterior to the duodenojejunal junction *(DJ).* In **(a),** note the renal mass also causes elevation of the hepatic flexure of the colon.
(c) Intravenous urography demonstrates a huge cyst arising from the lower pole.
(Reproduced from Meyers.[2])

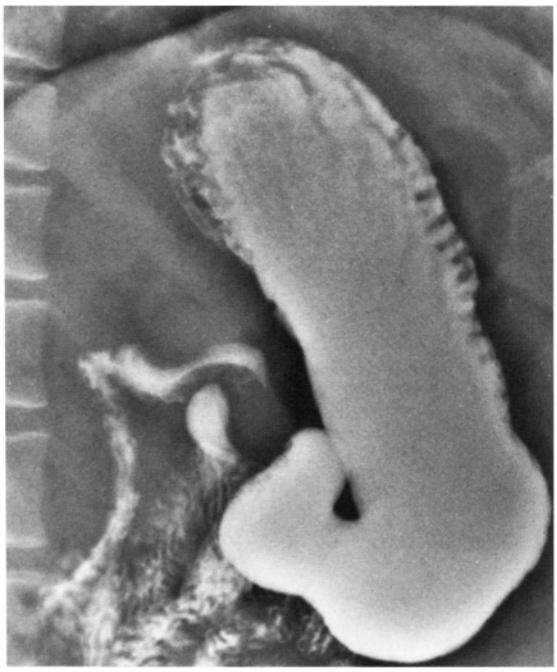


Fig. 9–7. Displacement of descending duodenum by right renal cyst.
Bowed anterior displacement of the second portion of the duodenum.

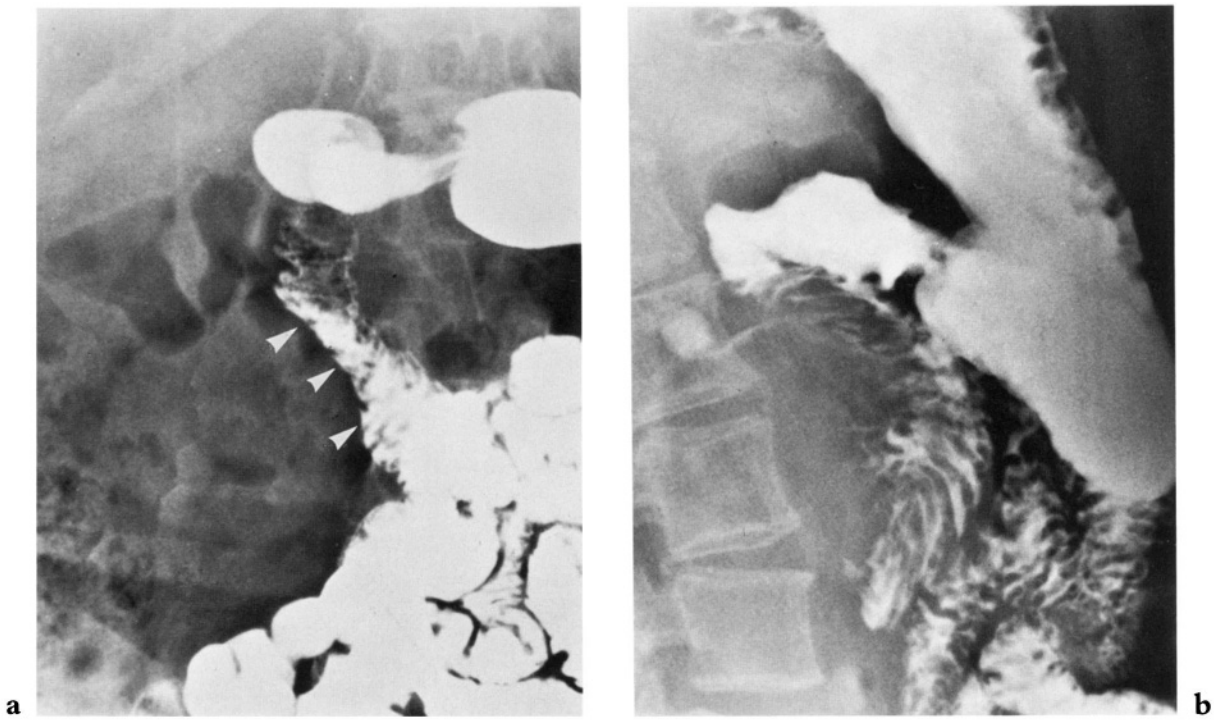


Fig. 9–8. Displacement of descending duodenum by right renal cyst.
The proximal second portion of the duodenum descends normally. While the frontal projection **(a)** shows only relatively mild medial displacement of the distal two-thirds with flattening of the mucosal folds laterally (*arrowheads),* the lateral view **(b)** demonstrates striking anterior bowing and extrinsic mucosal distortion. In **(a),** note that the renal mass also elevates the hepatic flexure of the colon.
(Reproduced from Meyers.[2])

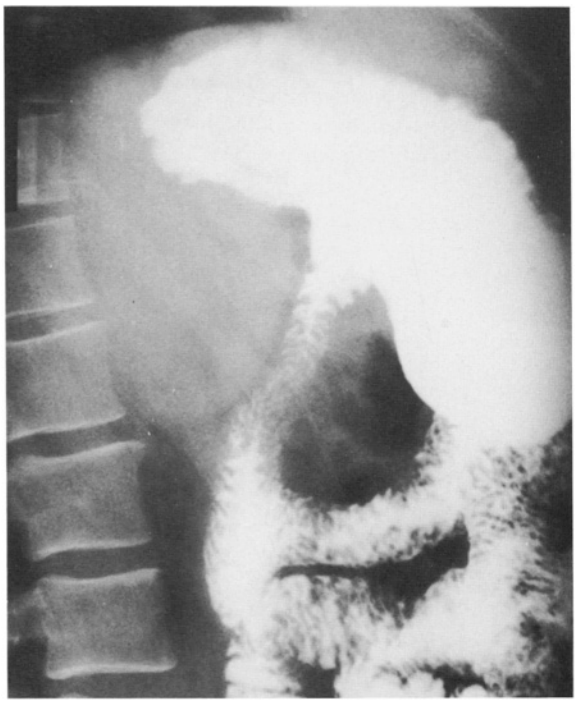


Fig. 9–9. Displacement of descending duodenum by right adrenal mass.
The proximal portion of the descending duodenum is displaced anteriorly by an adrenal mass. Its soft-tissue outline distinctly conforms to its effect upon the duodenum.

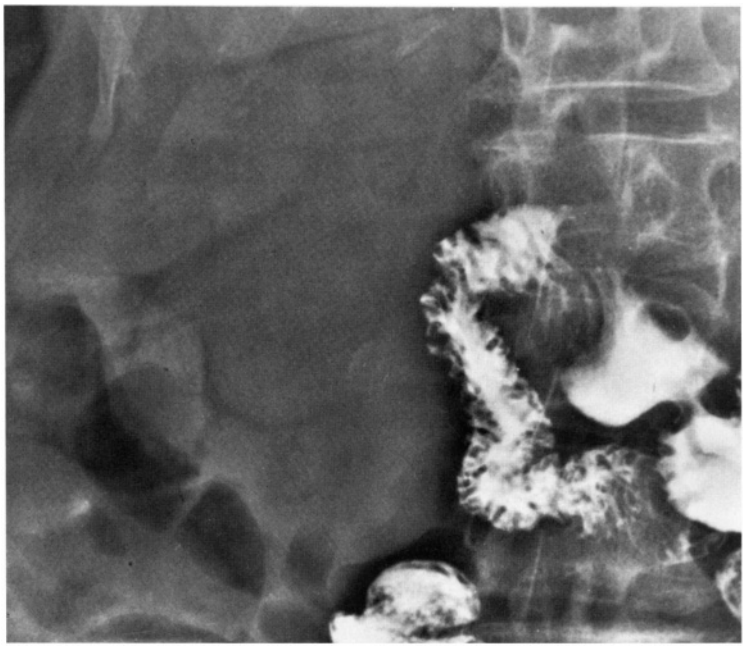


Fig. 9–10. Displacement of descending duodenum by liver enlarged with metastases.
There is mild medial displacement of the descending duodenum and compression upon the gas-filled hepatic flexure of the colon.

Colon. In masses originating within the upper two-thirds of the right kidney, the right colon segment most typically involved is that extending between the posterior and anterior hepatic flexures. This demonstrates displacement inferiorly, medially, and anteriorly (Figs. 9–12 through 9–14). Extrinsic pressure may be further shown by flattening and compression of the superior and posterior haustral rows at this site. Dilatation of an extrarenal pelvis in some cases of obstructive hydronephrosis may produce a more generalized mass effect extending to the anterior hepatic flexure (Fig. 9–15).

Occasionally, similar changes may be produced by a liver mass projecting downward from the visceral surface of the right lobe of the liver (Fig. 9–16).

Extension of a renal mass laterally into the flank displaces the posterior hepatic flexure inferiorly (Figs. 9–12 through 9–14). Further progression may result in striking displacement of the ascending colon medially and anteriorly (Figs. 9–17 and 9–18). Maintenance of the lateral haustral contours with extrinsic flattening of the posterior haustral sacculations (Fig. 9–18b) characterize the mass effects as extraperitoneal in site, rather than those from a mass within the intraperitoneal lateral paracolic gutter.[3,4]

A mass originating in the lower pole of the right kidney characteristically elevates the colon between the two hepatic flexures (Figs. 9–19 and 9–20). Extrinsic compression occurs on the inferior haustral rows at this site,

text continues on page 504

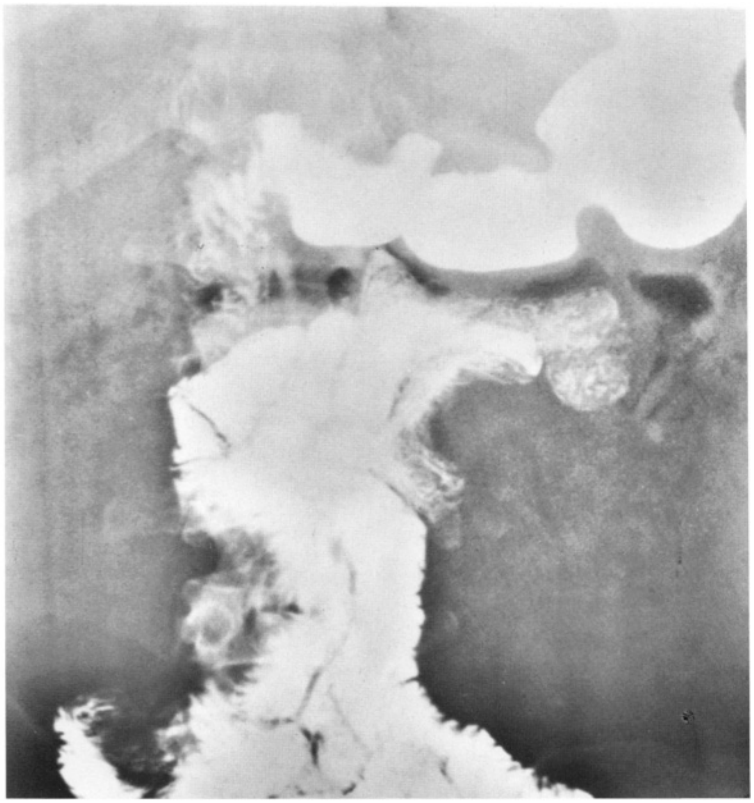


Fig. 9–11. Displacement of small bowel by polycystic renal disease.
Massive renal enlargement bilaterally crowds jejunal loops toward the midline.
(Reproduced from Meyers.)

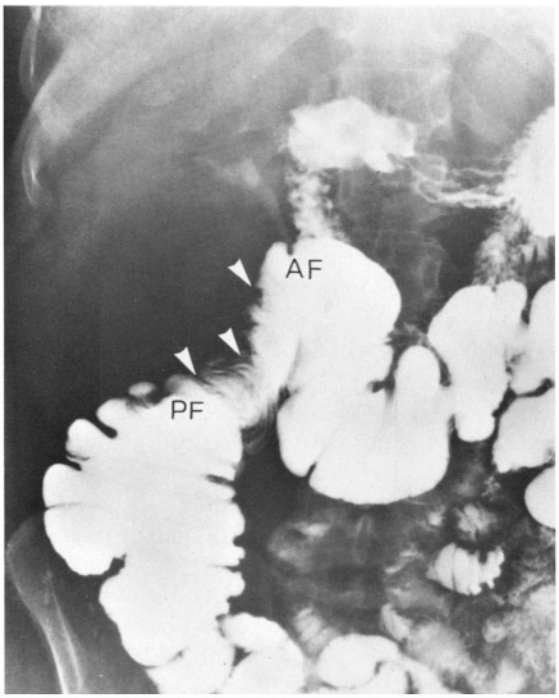


Fig. 9–12. Displacement of right colon by right renal cyst.
The large intestine between the posterior *(PF)* and anterior *(AF)* hepatic flexures is displaced inferiorly and medially, with extrinsic compression of its superior haustral row *(arrowheads).* The posterior flexure is mildly displaced downward as the mass, originating in the middle third of the kidney, extends laterally into the flank. Note that there is no displacement of the descending duodenum.
(Reproduced from Meyers.[2])

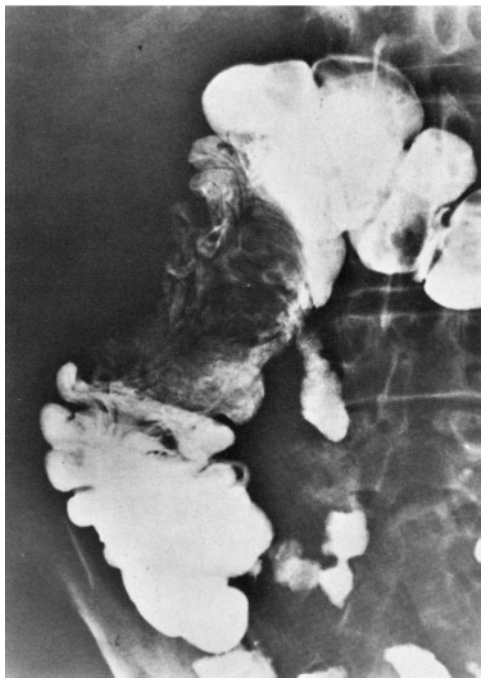


Fig. 9–13. Displacement of the right colon by hydronephrotic right kidney.
The segment between the two hepatic flexures is displaced inferiorly and medially. There is extrinsic flattening of its superior haustral border and marked compression of the lumen by the hugely dilated renal pelvis.
(Reproduced from Meyers.[2])

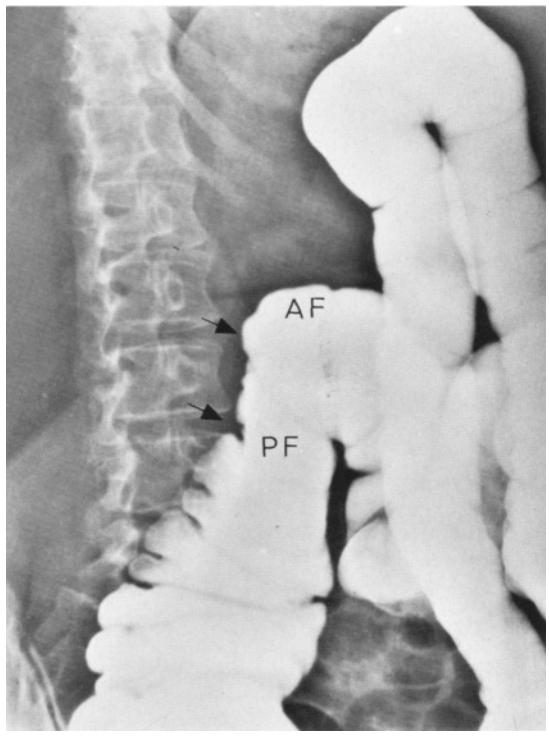


Fig. 9–14. Displacement of right colon by right renal cyst.
Oblique view shows the large intestine between the posterior *(PF)* and anterior *(AF)* hepatic flexures displaced anteriorly and medially, with extrinsic flattening of its posterior haustral row *(arrows).*
(Reproduced from Meyers.[2])

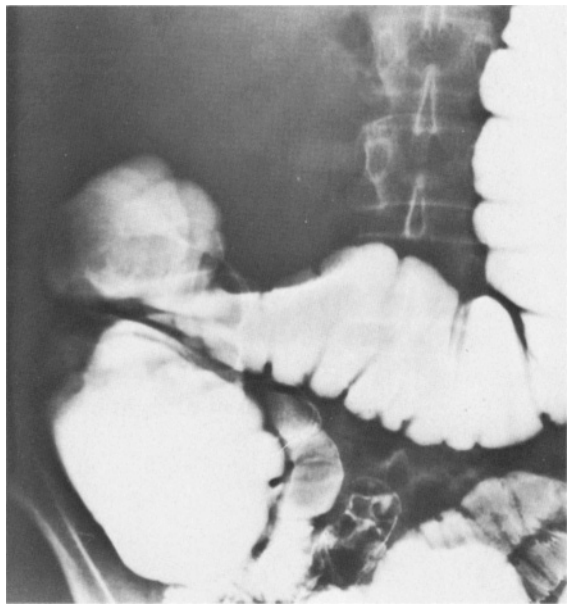


Fig. 9–15. Displacement of right colon by dilated extrarenal pelvis.
Marked pyelectasis from obstruction of the upper ureter results in mass pressure extending to the anterior hepatic flexure.



Fig. 9–16. Displacement of right colon by liver mass.
The segment between the two hepatic flexures is displaced inferiorly and medially by a large mass extending from the inferior surface of the liver anterior to the right kidney.



Fig. 9–17. Displacement of right colon by right multicystic kidney.
Medial displacement and mass effect on the distal ascending colon.

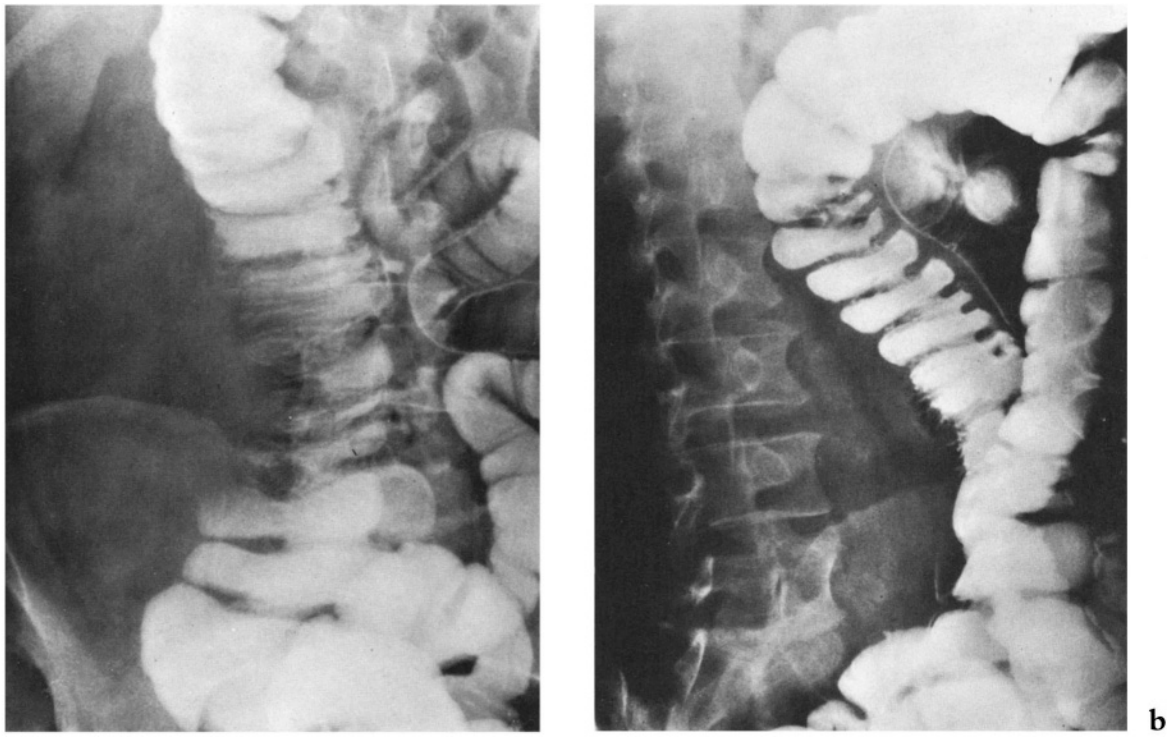


Fig. 9–18. Displacement of right colon by right renal cell carcinoma.
(a and **b)** The mass extends deeply in the flank and markedly displaces the ascending colon medially and anteriorly. The oblique view shows that the posterior haustral contours are flattened by the mass. (Reproduced from Meyers.[2])

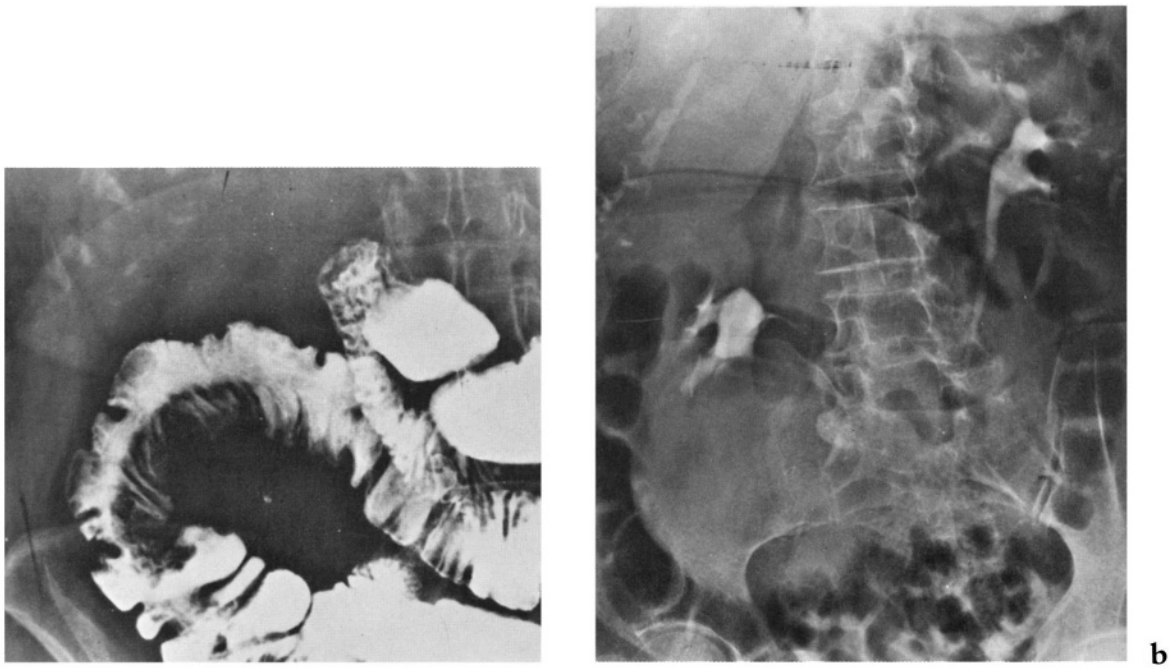


Fig. 9–19. Displacement of right colon by right renal cyst.
(a) Superior displacement of segment between the two hepatic flexures, with extrinsic compression of its inferior haustral row. The mass also affects the ascending colon. The descending duodenum is uninvolved. **(b)** Excretory urogram documents a large mass in the lower renal pole with inframesocolic extension. (Reproduced from Meyers.[2])

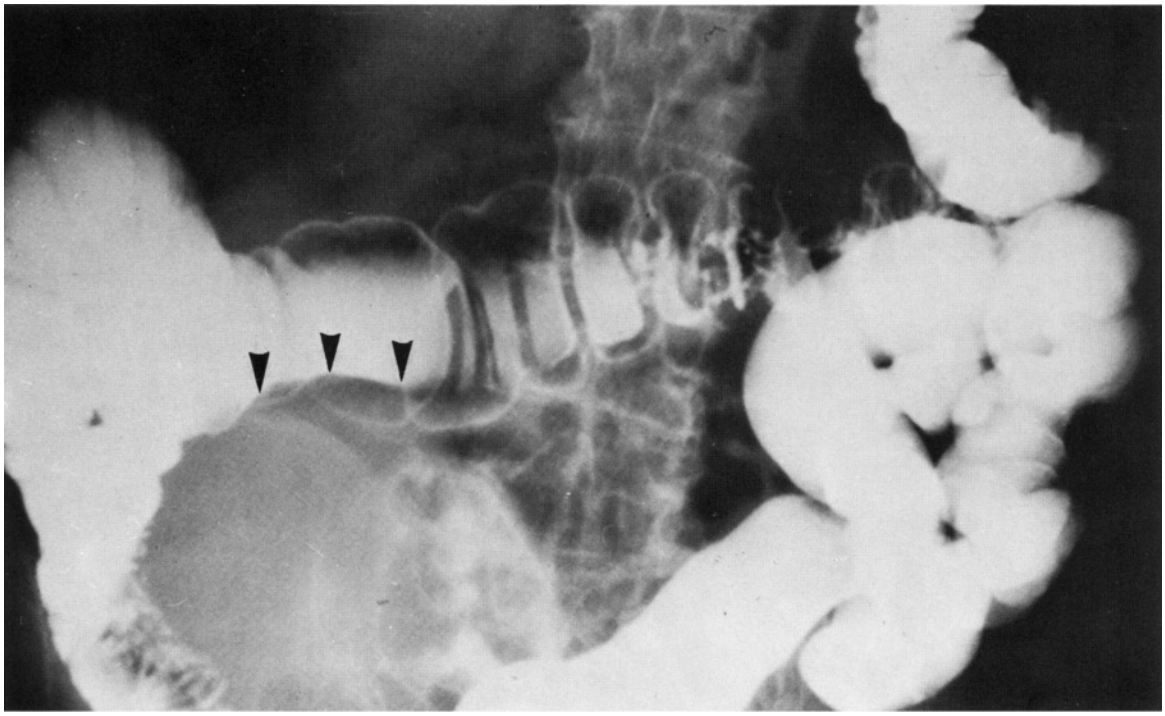


Fig. 9–20. Displacement of right colon by right renal sarcoma.
There is mild extrinsic pressure on the inferior border of the segment between the two hepatic flexures by the inframesocolic mass projecting from the lower renal pole. Note that the pressure effects can be localized particularly to the posterior haustral rows *(arrowheads).*
(Reproduced from Meyers.[2])

and the process may affect adjacent segments of the transverse and ascending colon. Oblique projections document that the affected colon also is usually displaced anteriorly and medially. At times, very discrete pressure changes, selectively on the posterior haustra of this segment, may be recognizable, even on frontal projections (Fig. 9–20), an observation further indicating the extraperitoneal nature of the mass.[4]

The Left Kidney

Colon. Left renal masses come into relationship to the colon usually before they attain a size that displaces the stomach, duodenojejunal junction, or small bowel. Masses arising in the upper half may displace the distal transverse colon inferiorly and anteriorly. Those originating in the lower half are often first revealed by typical effects on specific portions of the left colon. The descending limb of the distal transverse colon appears compressed and displaced laterally and anteriorly (Figs. 9–21 and 9–22). Significantly, the landmark of the anatomic splenic flexure is preserved. Masses projecting from the lower pole displace the descending colon laterally and anteriorly (Fig. 9–23). Again, the anatomic splenic flexure is unaffected.

Stomach and Small Bowel. A left renal mass may bulge through into the peritoneal cavity, as shown in Figures 9–24 through 9–26, to displace the greater curvature of the stomach and jejunal loops.

Ptosis and Rotation

Ptotic descent of the kidney is frequently accompanied by rotation about its vertical axis. The condition is more common on the right where its effects on the bowel

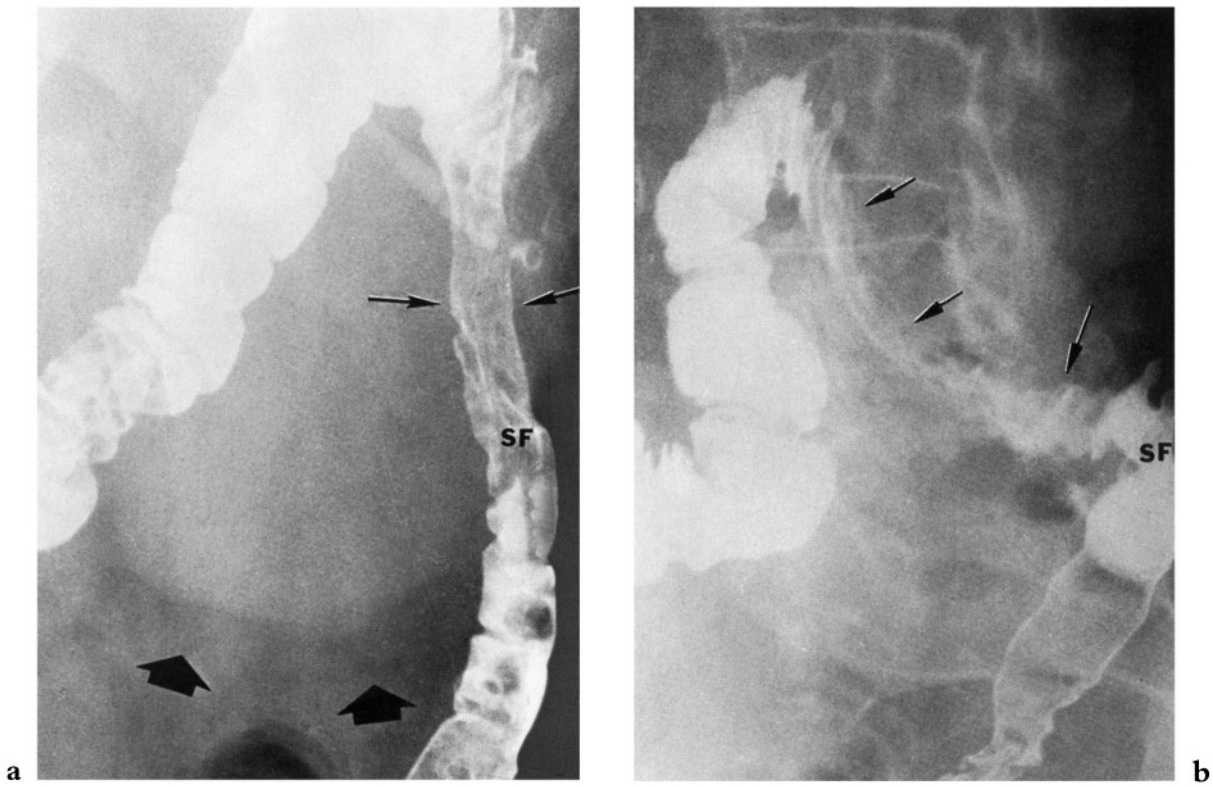


Fig. 9–21. Displacement of the left colon by left renal cyst.
(a and **b)** The anatomic splenic flexure *(SF)* is maintained, but there is lateral and anterior displacement of the descending limb of the distal transverse colon *(arrows).* The mass enlargement of the lower pole of the kidney is identifiable *(large arrows).*
(Reproduced from Meyers.[2])

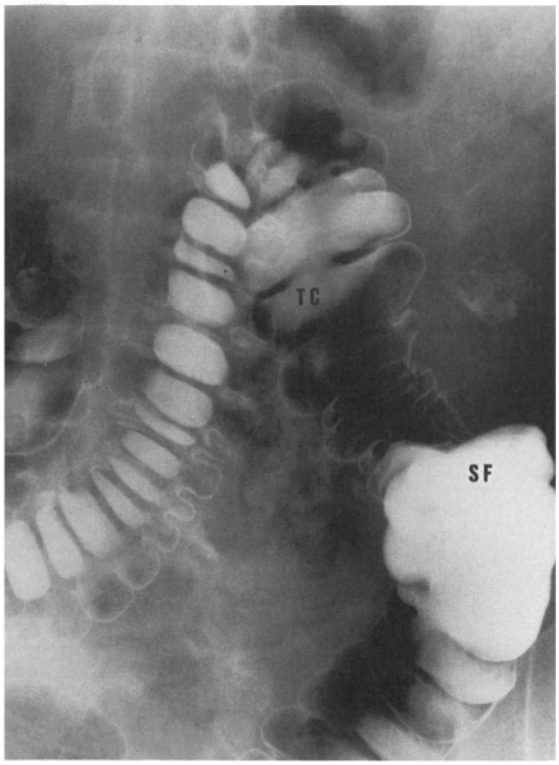
may be misleading unless the anatomic relationships are recognized.[2] The distal descending duodenum may be displaced medially and anteriorly in a manner indistinguishable from a true renal mass (Fig. 9–27). The ptotic kidney may further descend fully to the inframesocolic right lower quadrant so that with rotation it displaces primarily small bowel loops (Fig. 9–28).

Invasive Renal Cell Carcinoma

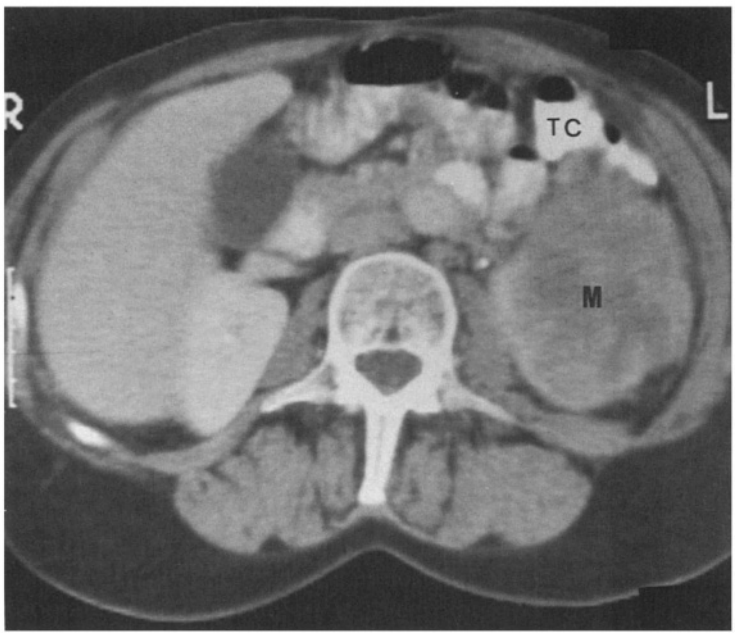
Renal neoplasms may directly invade adjacent segments of bowel, sometimes as recurrences many years after the primary tumor has been resected. On the right, the descending duodenum, and on the left, the distal transverse and proximal descending colon are typically involved. They tend to produce bulky intraluminal masses without significant obstruction, since they generally elicit no desmoplastic response (Fig. 9–29).[5]

Perinephritis and Renointestinal Fistulas

Advanced perirenal infection may break through fascial boundaries to involve overlying bowel.[6] The anatomic relationships of the kidneys, the enveloping fascial planes, and the colon are basic to an understanding of

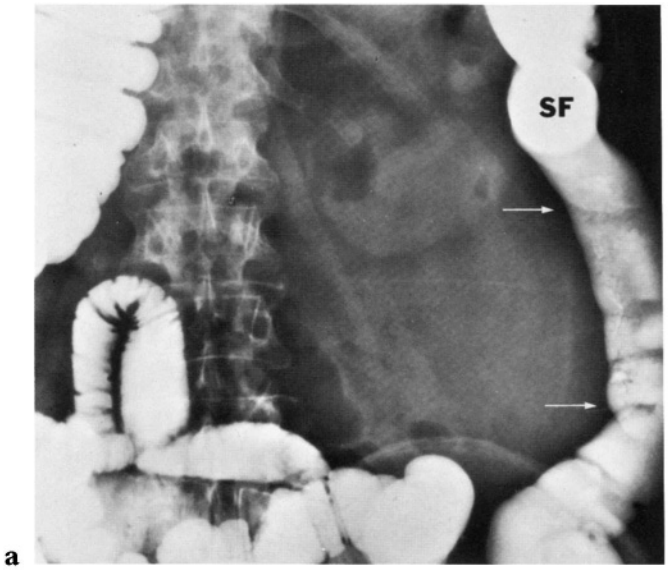


a

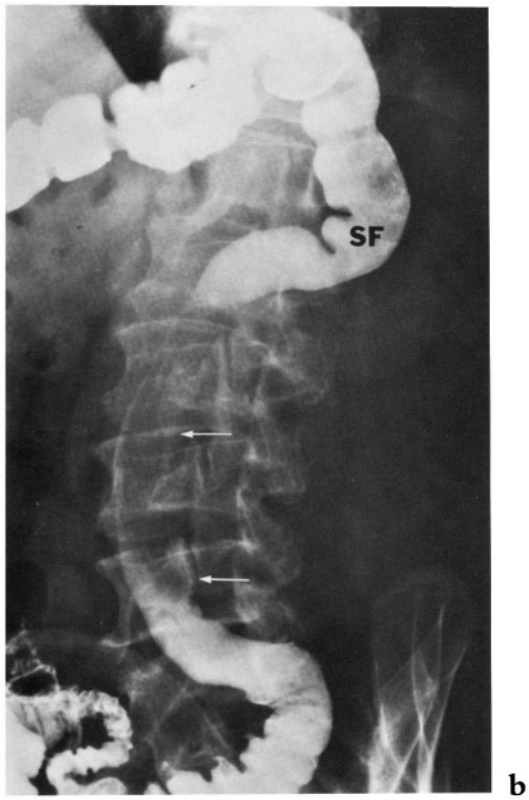


b

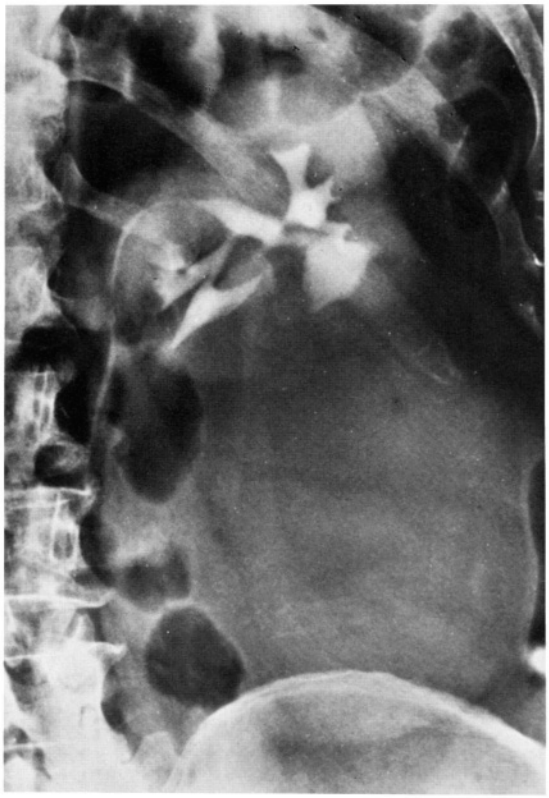
Fig. 9–22. Displacement of the left colon by left renal carcinoma.
(a and **b)** Barium enema and CT show calcified left renal mass *(M)* producing anterior displacement of distal mesenteric transverse colon *(TC).* The anatomic splenic flexure *(SF)* is maintained.



a



b



c

Fig. 9–23. Displacement of left colon by left renal cyst.
(a and **b)** The descending colon is displaced laterally and anteriorly *(arrows)* by a large cyst originating from the lower renal pole. The anatomic splenic flexure *(SF)* is unaffected.
(c) Intravenous urography confirms a huge cyst arising from the lower pole.
(Reproduced from Meyers.[2])

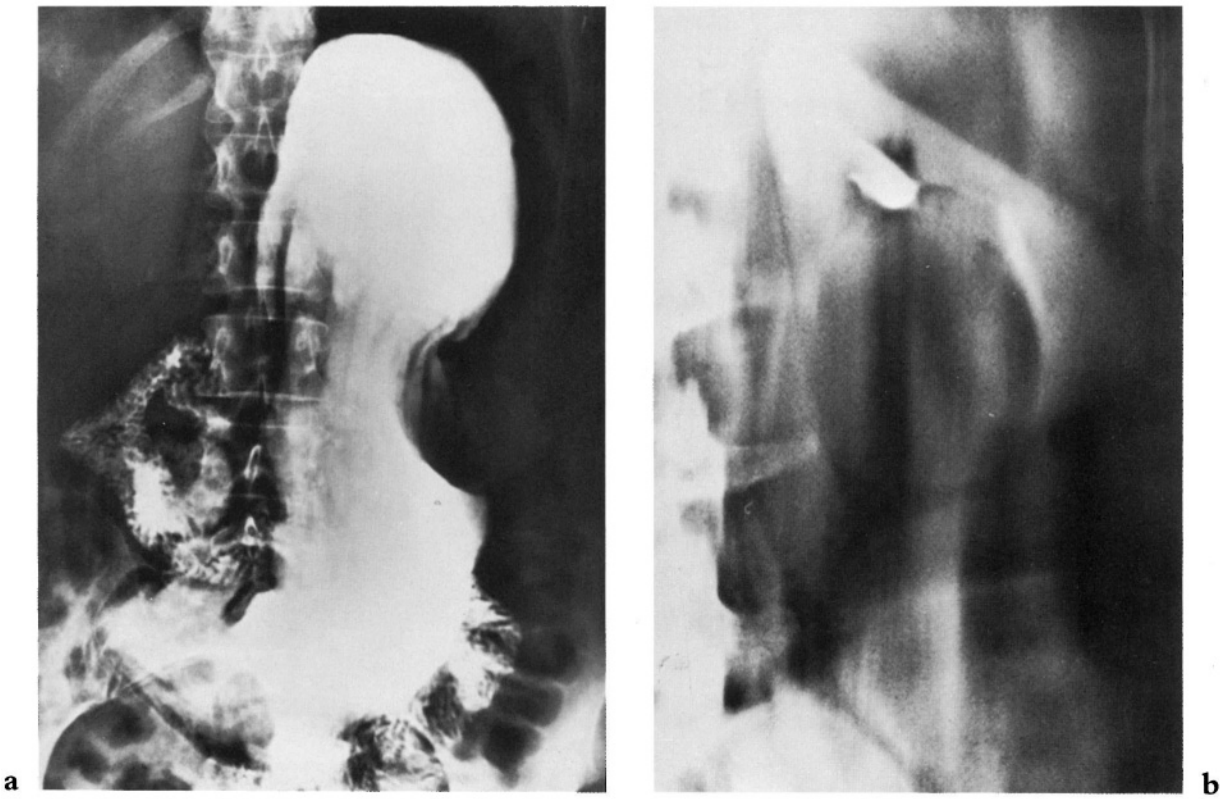


Fig. 9–24. Displacement of stomach by left renal cyst.
(a) Smooth extrinsic pressure upon the greater curvature of the stomach.
(b) Nephrotomogram documents a large cyst arising from the left kidney. It can be presumed to be spherical, with as great an AP dimension to bring it into relationship to the stomach as its coronal dimension.

the spread of inflammation (Figs. 9–30 and 9–31). The distal transverse colon courses anterior to the lower half of the left kidney. The splenic flexure demarcates the transition between the mesenteric transverse colon and the extraperitoneal descending colon. It lies on a plane posterior to the hepatic flexure and is attached to the diaphragm, opposite the 10th and 11th ribs, by the phrenicocolic ligament, which helps support the lower end of the spleen. The descending colon passes downward along the lateral border of the left kidney, turning somewhat medially toward the lateral border of the psoas muscle at the lower pole. At this level, the descending colon lies within areolar tissue in the anterior pararenal space behind the posterior parietal peritoneum. Normally, it is separated posteriorly from the kidney and perirenal fat by the anterior renal fascia; however, its medial and posterior walls face the left kidney and the richest deposit of perirenal fat, which resides behind and lateral to the lower renal pole.

The pathogenesis involves a site of renal infection that breaks through the capsule of the kidney to contaminate the perirenal space. The infection may spread through the perirenal fat as diffuse perinephritis, but coalescence into an abscess has a definite tendency to localize in the rich fat dorsolateral to the lower renal pole.[7,8] The inflammatory process is usually confined to the perirenal

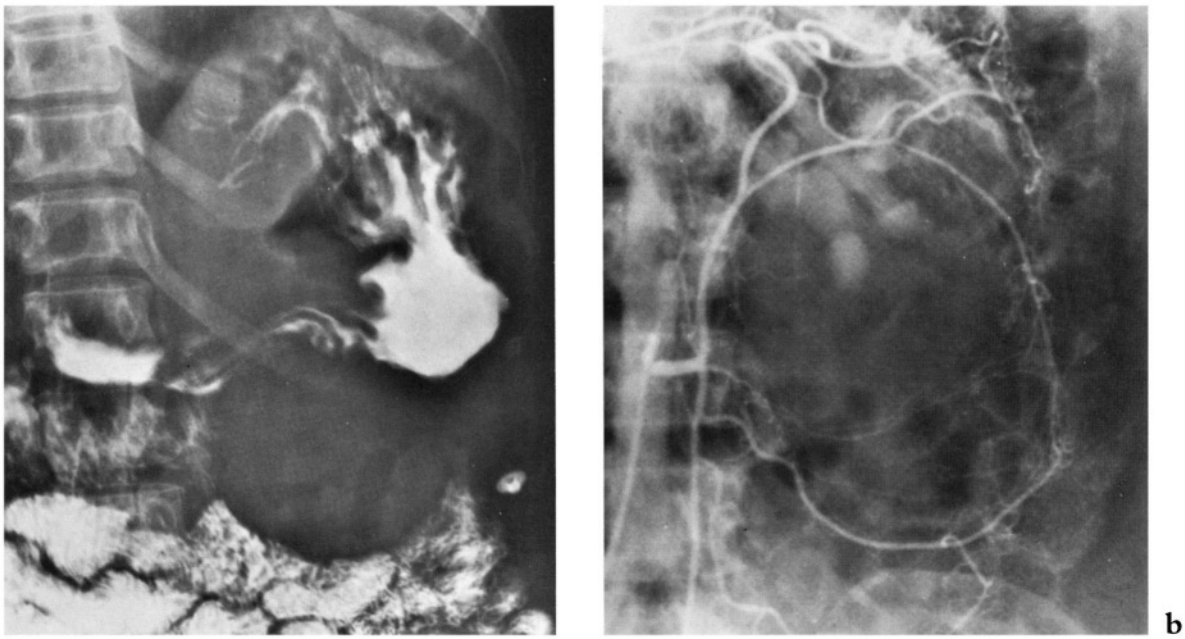


Fig. 9–25. Displacement of stomach and small bowel by left renal cyst.
(a) The round mass elevates the greater curvature of the stomach and displaces the duodenojejunal junction medially and small bowel loops inferiorly.
(b) Selective inferior mesenteric arteriogram shows arcuate displacement of the ascending left colic artery and its branches by the renal mass as it bulges through into the peritoneal cavity.
(Reproduced from Meyers.[2])



Fig. 9–26. Displacement of small bowel by left renal cyst.
CT demonstrates jejunal loops displaced anteriorly by cysts arising from the lower pole of the left kidney.

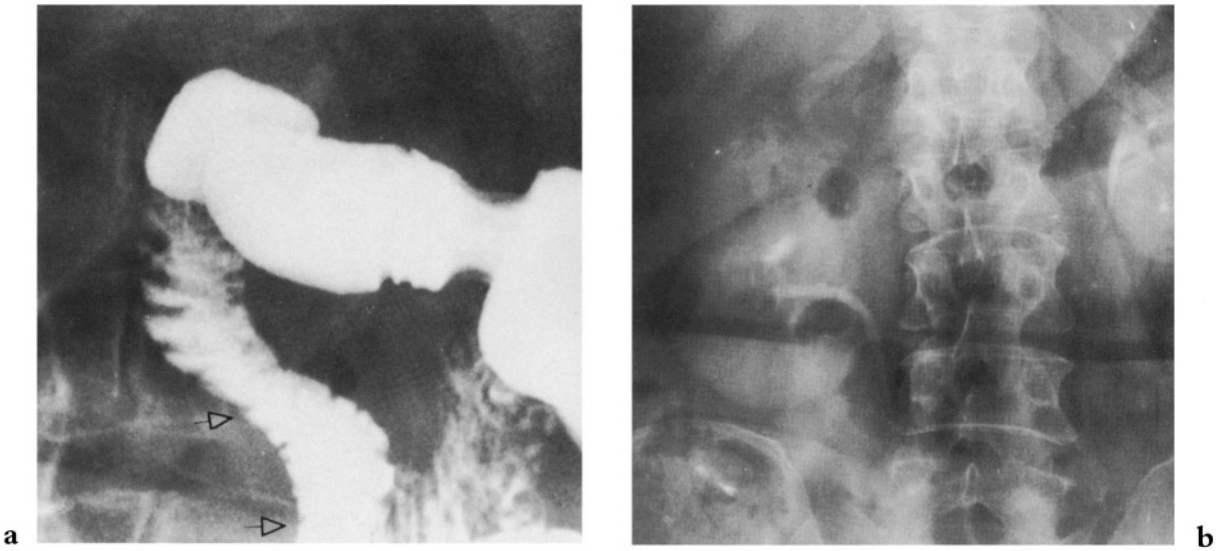


Fig. 9–27. Displacement of the descending duodenum by a ptotic right kidney.
(a) The distal segment of the descending duodenum is displaced anteriorly and medially *(arrows).*
(b) Intravenous urogram shows a ptotic right kidney with rotation about its vertical axis.
(Reproduced from Meyers.[2])

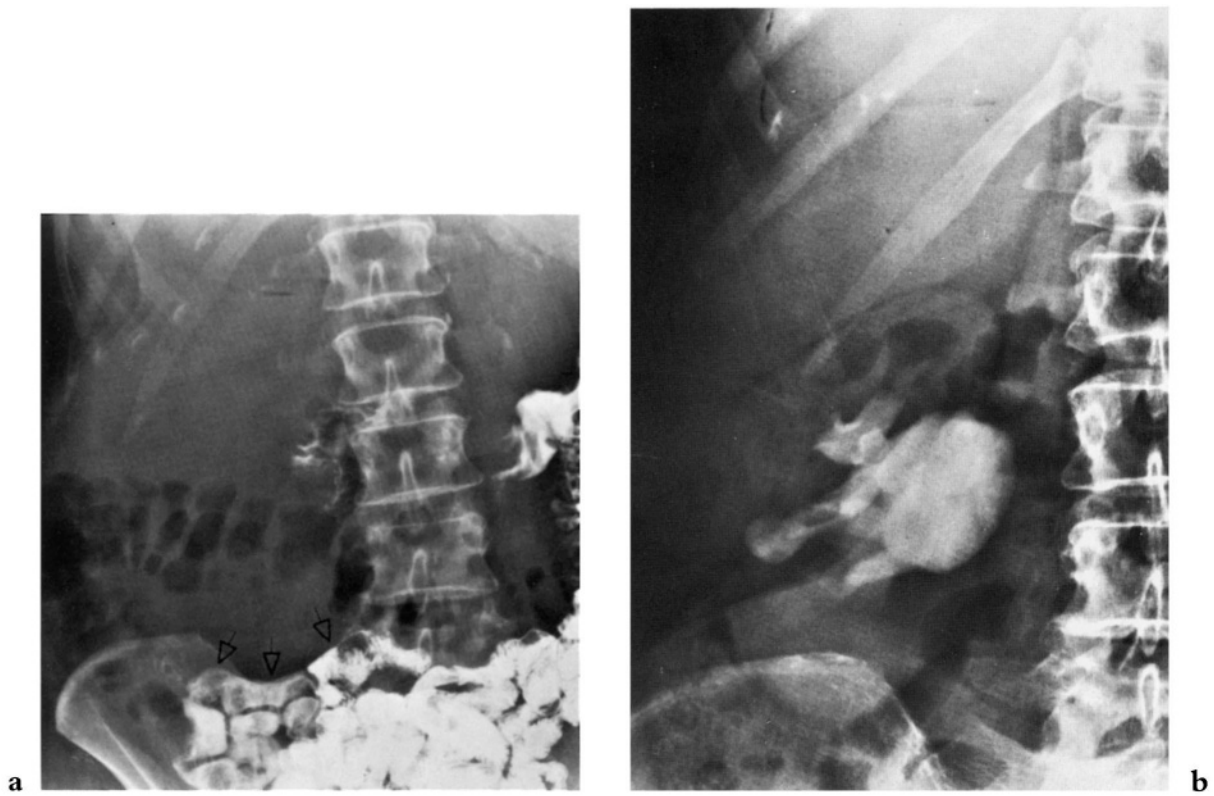


Fig. 9–28. Displacement of small bowel by a ptotic right kidney.
(a) There is gentle arcuate displacement of ileal loops *(arrows)* by a soft-tissue right lower quadrant mass.
(b) Intravenous urogram shows a hydronephrotic, ptotic right kidney.
(Reproduced from Meyers.[2])-

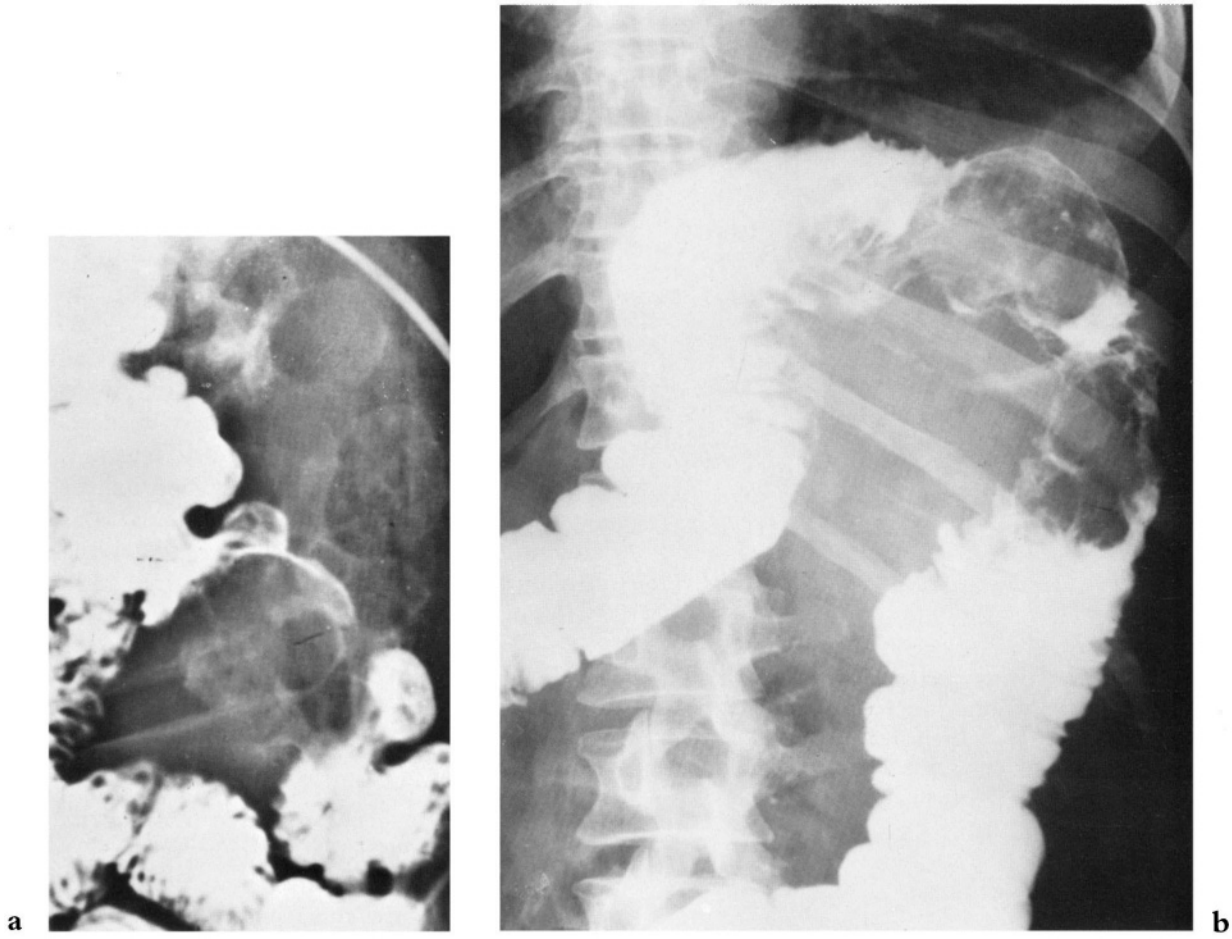


Fig. 9–29. Direct invasion of the colon by left renal carcinoma.
(a and **b)** Two different cases showing extrinsic and intramural masses of the distal transverse and proximal descending colon with bulky polypoid intraluminal extensions. **(b,** reproduced from Meyers.[2])

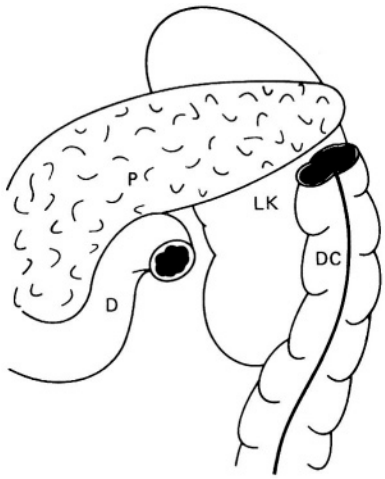


Fig. 9–30. Frontal drawing illustrating the relationship of the descending colon *(DC)* to the left kidney *(LK)* distal to the splenic flexure.
P = pancreas; *D* = duodenum.
(Reproduced from Meyers.[6])

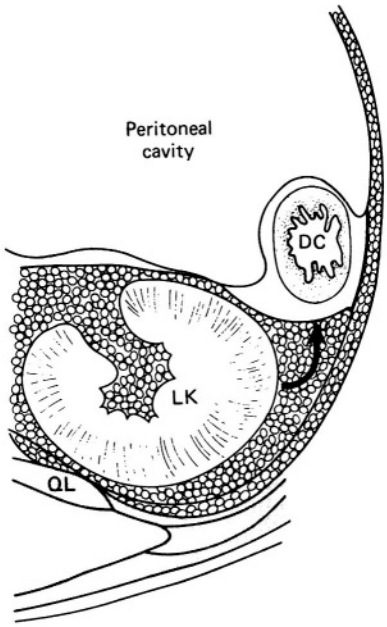


Fig. 9–31. Horizontal cross-section through the left flank demonstrating the anatomic relationships.
The anterior renal fascia *(arrow)* demarcates the extraperitoneal descending colon *(DC)* from the left kidney *(LK),* and perirenal fat. *QL* = quadratus lumborum. (Reproduced from Meyers.[6])

compartment by the renal fascia. More fulminating infections break through the fascial boundaries and spread to the overlying structures. On the left, the distal transverse colon and, particularly, the proximal or mid-descending colon and, on the right, the ascending colon are involved.

Changes reflecting at least inflammatory adherence may affect principally the medial or posterior contour of the colon or be circumferential. They are manifested primarily by spastic narrowing, scalloped induration, and inflammatory mucosal thickening[6] (Figs. 9–32 through 9–35). In the descending colon, localization to the area distal to the splenic flexure overlaps the site involved in the extension of pancreatitis to the colon,[9] but lack of associated changes involving the flexure itself is a helpful differential point. Extravasated pancreatic enzymes passing along the transverse mesocolon into the phrenicocolic ligament result in inflammatory changes affecting, most characteristically, the splenic flexure. The defects do not closely simulate either the ulcerations and pseudosacculations of granulomatous colitis or the mucosal edema and thumb-printing of ischemic colitis.

A gross extraperitoneal sinus communication represents advanced transmural erosion (Figs. 9–36 through 9–39). Most renointestinal fistulas are secondary to an underlying chronic kidney infection that establishes communication usually with the descending duodenum or left colon.[10–14] Traumatic fistulas are not common but their relative incidence appears to be increasing.[14] Although they may be immediately obvious, they may also appear insidiously months later. Rarely is the communication caused by a primary process of the bowel[15] (Fig. 9–40).

Operative intervention is almost always indicated in renointestinal fistulas. In most cases, the affected kidneys have been the seat of parenchymal infection and stone disease for long periods before detection and have little if any remaining function. Most reported successes involve nephrectomy and bowel closure.[11] Conservative methods are indicated for renointestinal fistulas detected before severe renal damage has occurred and in selected cases of fistulas.

Renal Agenesis and Ectopia

Agenesis or ectopia of the kidney is frequently accompanied by characteristic malposition of specific portions of the bowel.[16] Particular segments of the intestine may occupy the area of the renal fossa on the side of agenesis or ectopia, or show characteristic displacement and extrinsic mass effect by an ectopic kidney in as many as 75% of the cases.[16,17]

The clinical value of these observations is twofold:

1. Identification of the characteristic intestinal malposition or displacement on a barium contrast study uncovers the renal anomaly, which may have multiple clinical implications.

These observations not only allow one to suspect congenital renal anomalies during barium enema examinations, but help in assessment of the nature of the renal abnormality when excretory urography reveals an apparently solitary kidney. In the pediatric patient, they may be particularly helpful in the differential diagnosis between renal agenesis and multicystic dysplastic kidney.[18] Although the ureter and trigone are absent in 80% of cases of agenesis,[19,20] one-third of cases of multicystic dysplastic kidney also have no demonstrable ureter or trigone at cystoscopy.[19] Several observers have concluded that nonvisualization of the kidney on excretory urography with normal position of the colon excludes agenesis or ectopia as diagnostic considerations.[18,21]

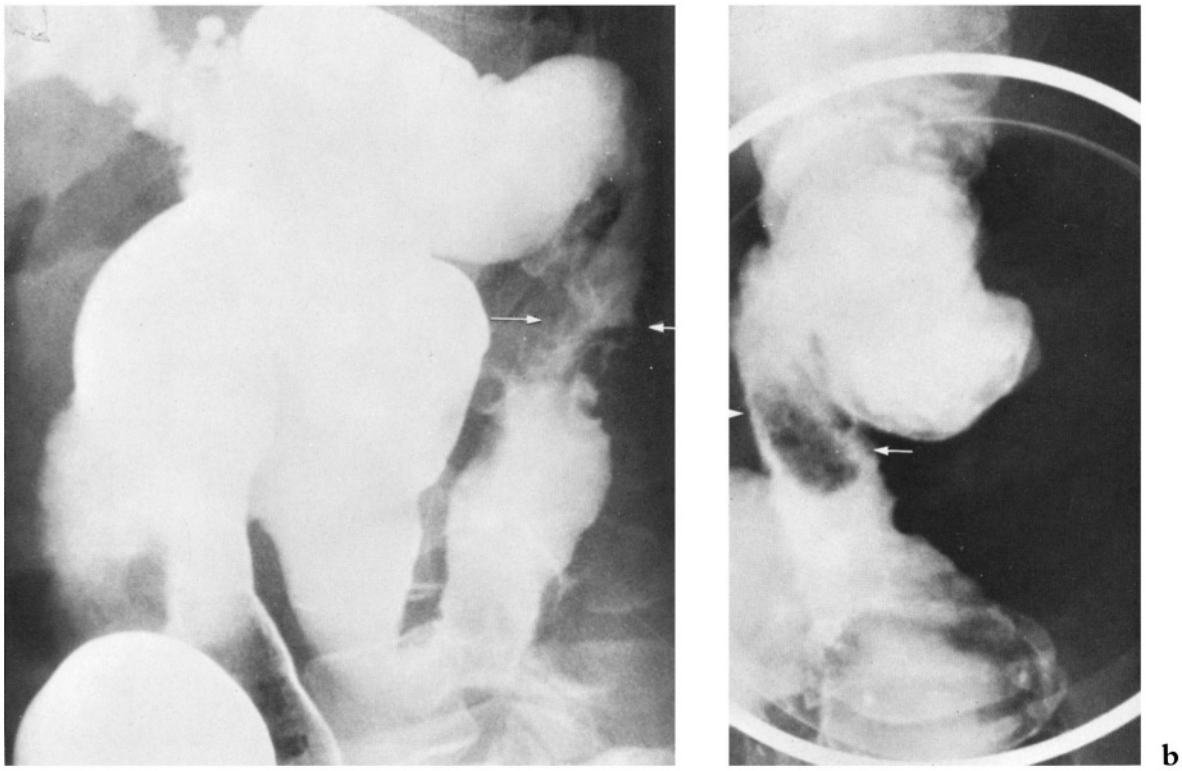


Fig. 9–32. Colonic changes secondary to left perinephritis.
Lateral radiograph **(a)** and frontal spot film **(b)** of a barium enema study demonstrate persistent irregular narrowing 5 cm in length *(arrows)* just distal to the splenic flexure. The mucosal folds are intact, and there is no significant obstruction. Attention was then directed toward the left kidney, and a radiologic workup revealed three 5 × 4 cm perirenal abscesses. At nephrectomy, the lateral surfaces of the masses were adherent to the descending colon.
(Reproduced from Meyers.[6])

2. Such bowel changes should not be mistaken for a form of internal hernia, abnormality of rotation of the intestines, or displacement by a tumor mass or organomegaly.

Embryologic Considerations. Ashley and Mostofi[19] believe that the initiating factor in renal agenesis is in the metanephric blastema. Disturbances of embryologic growth from the fourth to the eighth week of fetal life may result in renal ectopia. Normally, the kidney reaches its mature level opposite the second lumbar vertebra at the end of the second month. During their migration, the kidneys also rotate 90° so that their convex borders, originally directed dorsally, become directed laterally.

The normal developmental ascent of the kidneys is necessary for the formation of the extraperitoneal perirenal fascial planes.[16,20,22] With either agenesis or ectopia of the kidney, extraperitoneal connective tissue in the flanks fails to condense into well-defined fascial layers. In contrast, the perirenal fascia is present in cases of ptotic kidney.

Figure 9–41 is an anatomic cross-section through an ectopic kidney in the pelvis. While the usual perirenal fascial layers immediately enveloping it are clearly demarcated, these could not be identified in the upper extraperitoneal space on the same side; they were present on the opposite side where the kidney was normally positioned. I have documented these associated features

text continues on page 519

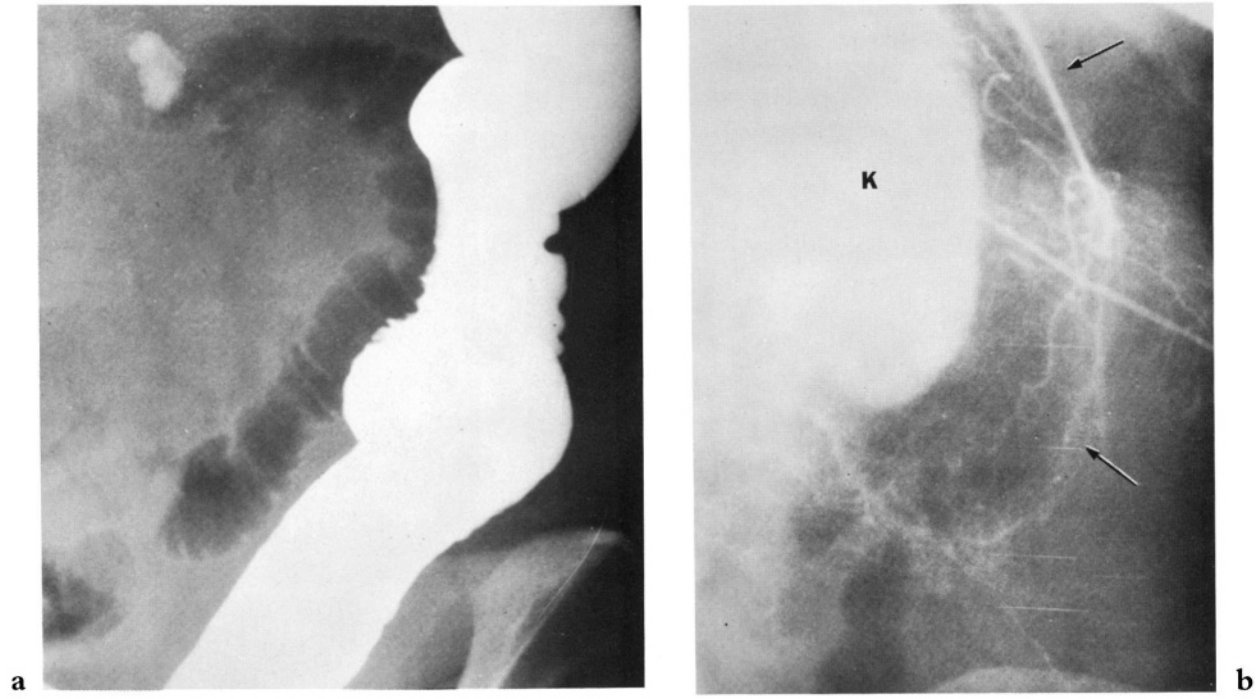


Fig. 9–33. Colonic changes secondary to left perinephritis.
(a) Barium enema study reveals localized rigidity and scalloping along the medial wall of the mid-descending colon. A left renal calculus is evident.
(b) Selective renal arteriography documented changes of xanthogranulomatous pyelonephritis. On nephrogram phase, wide displacement of the capsular artery *(arrows)* indicates a diffuse perirenal abscess. This was confirmed at nephrectomy, which also revealed the inflammatory process adhering to the medial wall of the descending colon. *K* = kidney.
(Reproduced from Meyers.[6])



Fig. 9–34. Colonic changes secondary to left perinephritis.
Barium enema study shows displacement and mucosal fixation *(arrows)* along the medial wall of the descending colon. Staghorn calculi are evident in the left kidney. The colonic changes are secondary to a large peripheral abscess which required drainage.

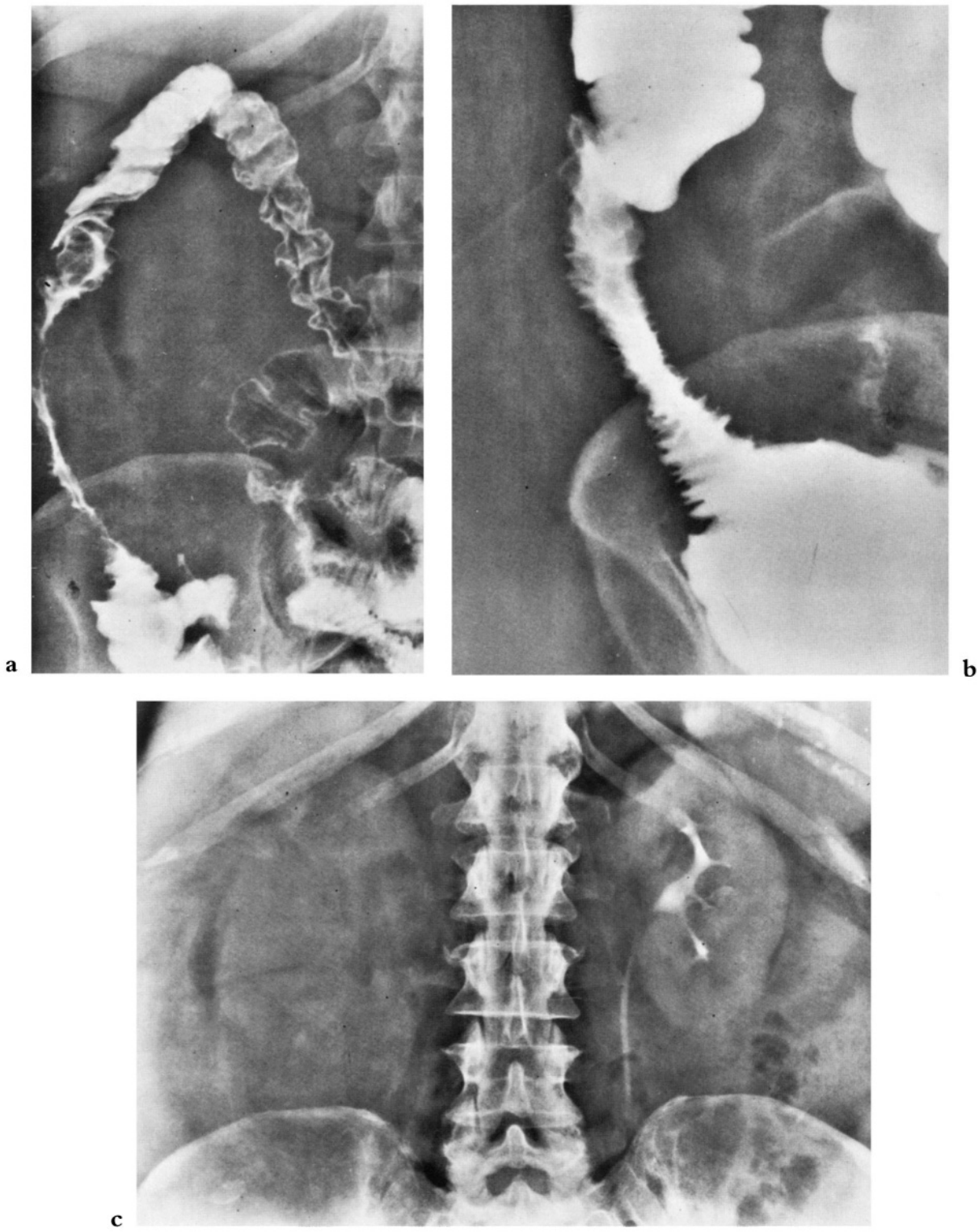


Fig. 9–35. Colonic changes secondary to right perinephritis.
(a and **b)** Barium enema study shows mass displacement and inflammatory mucosal thickening of the ascending colon.
(c) Intravenous urography demonstrates no function in an enlarged right kidney containing an opaque calculus.
Nephrectomy confirmed the presence of xanthogranulomatous pyelonephritis with a perirenal abscess adherent to the ascending colon.

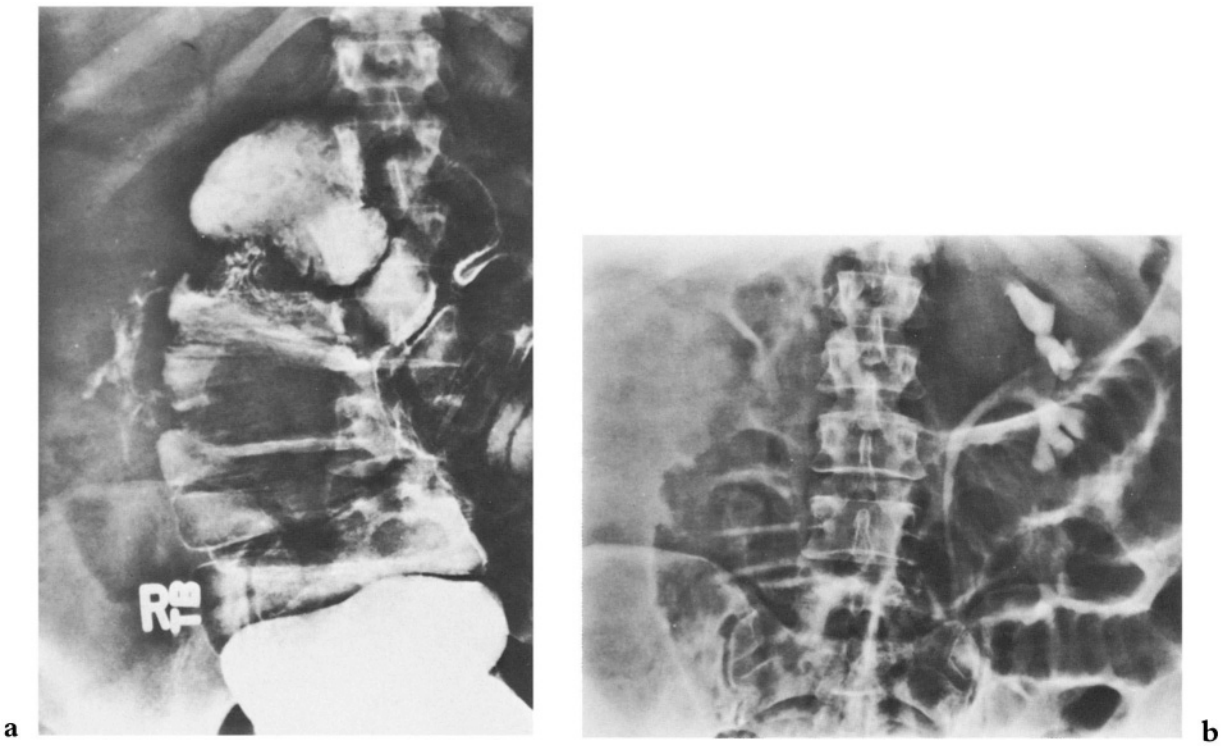


Fig. 9–36. Renointestinal fistula secondary to right perinephritis.
(a) Barium enema study shows loculated extravasation from the distal ascending colon, which also presents a stricture with intact mucosal folds.
(b) Excretory urography demonstrates no function on the right. Distortion of the colonic gas shadow with faint extraluminal gas collections are apparent.
A perirenal abscess secondary to xanthogranulomatous pyelonephritis had established a fistulous communication with the colon.

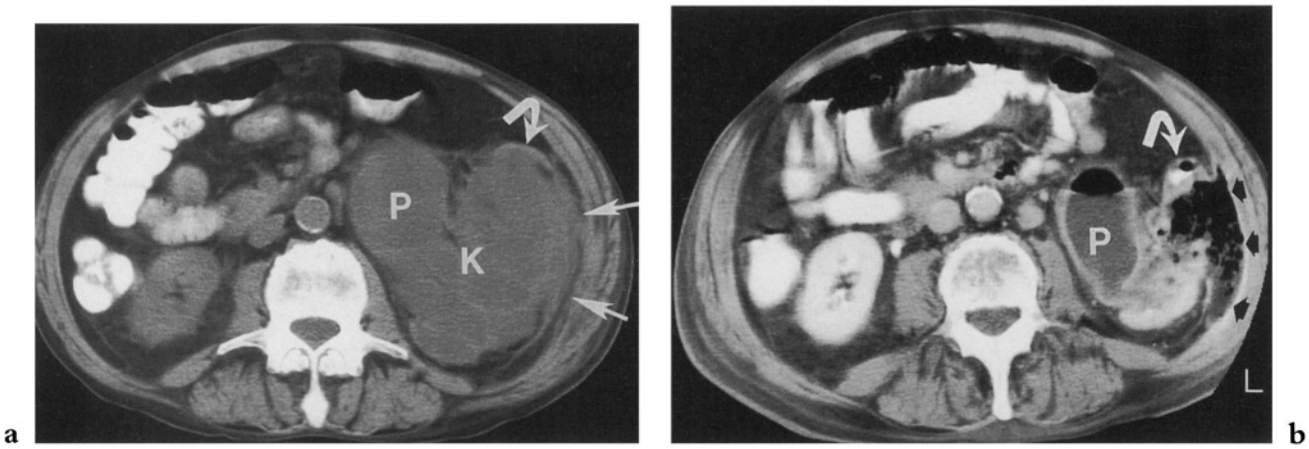
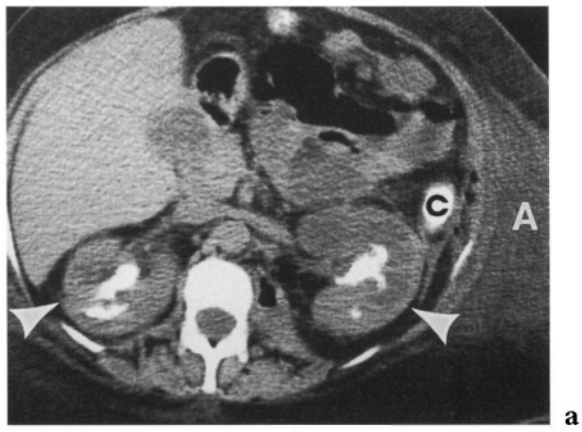
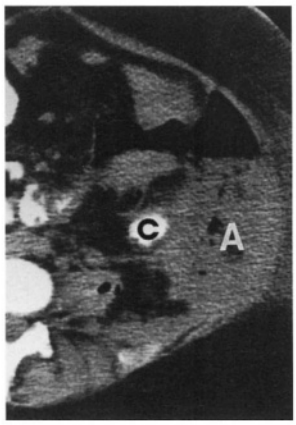


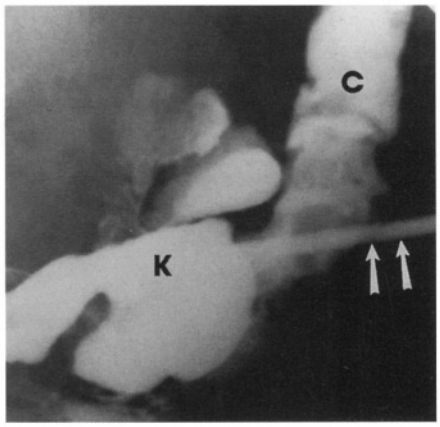
Fig. 9–37. Renocolic fistula secondary to left perinephritis.
(a) Unenhanced CT shows dilatation of the collecting system *(K)* and the pelvis *(P)* of the left kidney. Inflammatory changes *(straight arrows)* abut the collapsed descending colon *(curved arrow).*
(b) CT with intravenous contrast 1 week later demonstrates a fluid-gas level in an obstructed and thick-walled renal pelvis *(P).* Perirenal abscess *(black arrows)* is adherent to the posterior wall of the descending colon *(curved arrow),* proved to be the site of two renocolic fistulas.
(Reproduced from Parvey et al.[10])



a

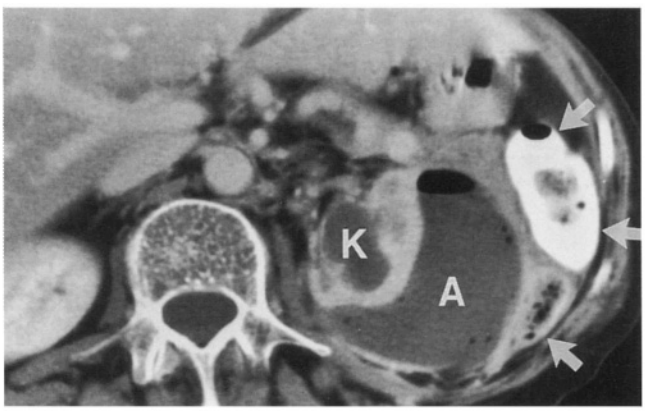


b

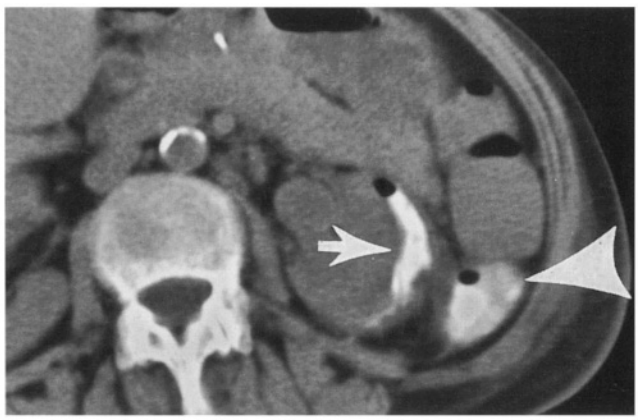


c

Fig. 9–38. Renocolic fistula secondary to xanthogranulomatous pyelonephritis with perirenal abscess.
(a and **b)** CT without intravenous contrast shows bilateral staghorn calculi *(arrowheads)* and hypodense areas within the left kidney representing xanthogranulomatous pyelonephritis. Inflammatory changes and a large perirenal abscess *(A)* extend into the lateral abdominal wall near the descending colon *(C).*
(c) Antegrade contrast study via nephrostomy tube *(arrows)* demonstrates fistulous communication from the collecting system of the left kidney *(K)* into the descending colon *(C).* Intravenous urography showed a nonfunctioning left kidney.
(Reproduced from Parvey et al.[10])



a



b

Fig. 9–39. Renocolic fistula secondary to pyelonephritis and perirenal abscess.
(a) CT with intravenous contrast shows a large perirenal abscess *(A)* that abuts the descending colon *(arrows). K* = kidney.
(b) CT after contrast injection into the perirenal drainage catheter discloses contrast extending from the left perirenal space *(arrow)* into the descending and sigmoid colon *(arrowhead).*
(Reproduced from Parvey et al.[10])

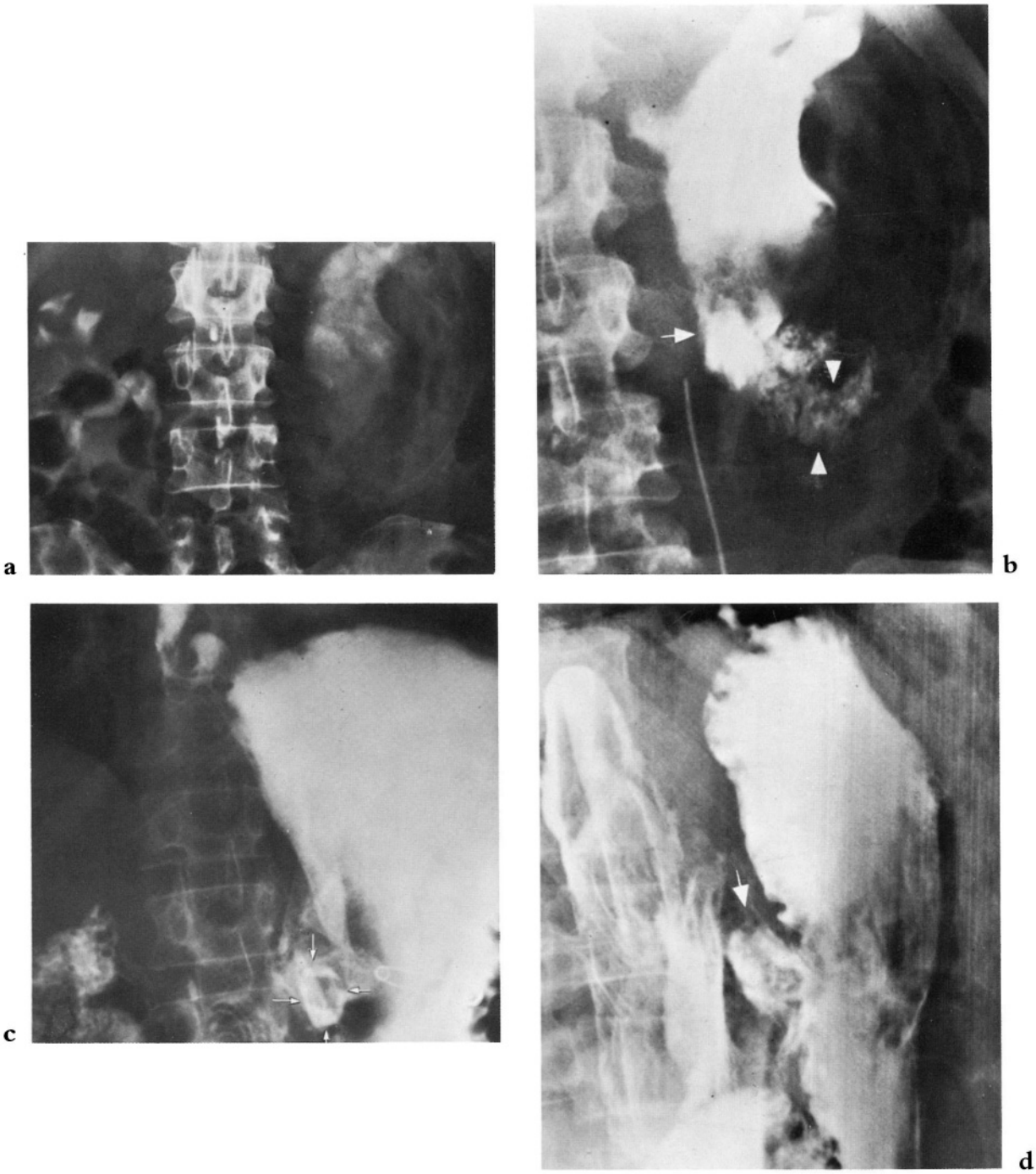


Fig. 9–40. Renogastric fistula secondary to gastric ulcer.
(a) Excretory urogram. Gross chronic inflammatory changes with distorted collecting system on the left.
(b) Retrograde pyelogram. Loculated extravasation *(arrow)* with opacification of gastric mucosa *(arrowheads).*
(c and **d)** Upper gastrointestinal series documents large ulcer on posterior wall of stomach *(arrows)* penetrating to the left kidney.
(Reproduced from Meyers.[2])

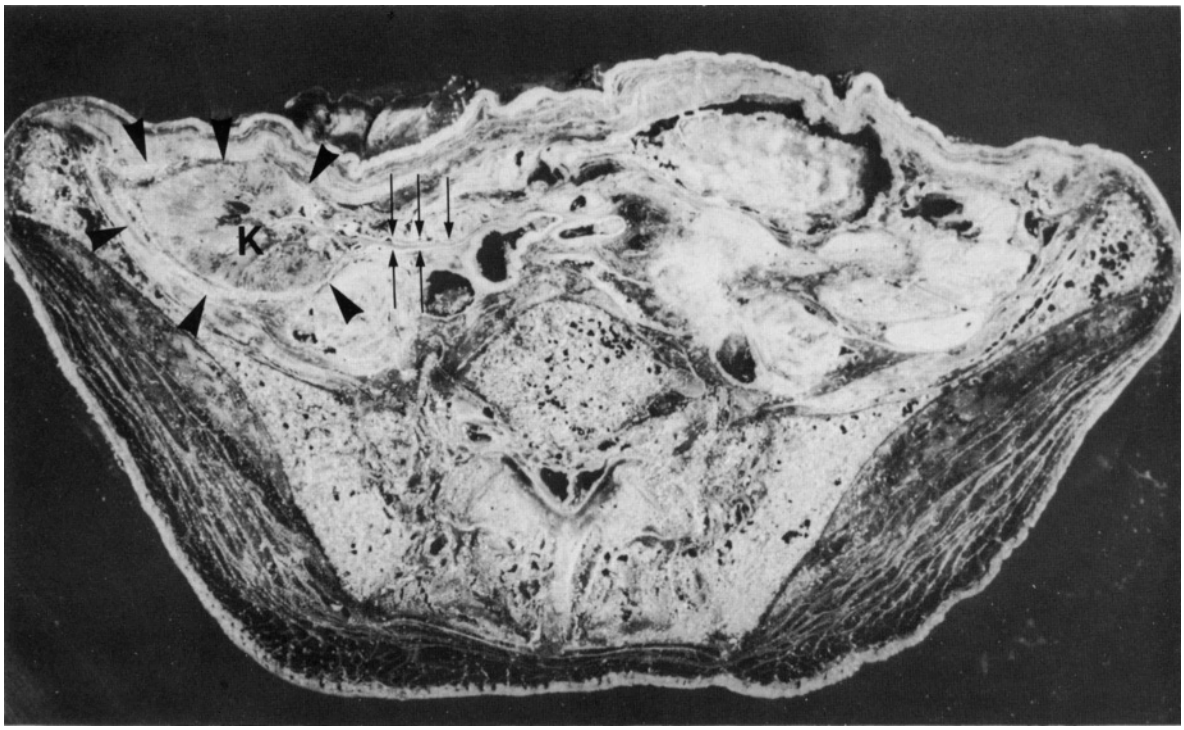


Fig. 9–41. Anatomic cross-section through pelvis at the level of the iliac crest.
An ectopic right kidney *(K),* deriving its blood supply *(arrows)* from the lower abdominal aorta, maintains its investment by well-defined extraperitoneal fascial planes *(arrowheads).* These layers of perirenal fascia are not developed cephalad to the ectopic kidney, where only pliable fat constitutes the extraperitoneal tissues. (Reproduced from Meyers et al.[16])

in vivo by computed tomography. Similarly, cases of renal agenesis and crossed fused ectopia studied by retroperitoneal pneumography document failure of the perirenal fascia to form on the side of the absent kidney (Figs. 9–42 and 9–43).

The lack of restraining fascia appears to contribute to the ease with which bowel malpositions itself into the pliable extraperitoneal fat in the "empty" renal fossa. The associated findings strongly suggest that development of not only the extraperitoneal perirenal fascia, but also portions of the intestinal mesenteric fixation, are embryologically dependent on normal ascent of the kidney.[16]

Incidence. These anomalies are not rare. Unilateral renal agenesis and renal ectopia have been found more frequently on radiographic examination (1 in 500) than in autopsy series (1 in 700 to 1500).[19,23,24] The incidence of crossed fused ectopia is only 1 in 7500. An overrepresentation may be assumed in urologic cases because pathologic conditions, such as stone formation or hydronephrosis, are more common. There is a male-to-female preponderance in a ratio of 3:2, and the anomalies are more common on the left side.[19,20,25]

Complications and Associated Anomalies. While such renal anomalies may be compatible with a long life, the incidence of renal disease in a congenitally solitary kidney as a cause of death is high.[19] In unilateral agenesis, the opposite kidney has been found to be diseased in one-third[25] to almost two-thirds[26] of the cases, usually secondary to chronic pyelonephritis. Compensatory hypertrophy of the solitary kidney results in a palpable mass in the flank about 25% of the time.[26] Furthermore, because it projects below the rib cage, it is more susceptible to injury.

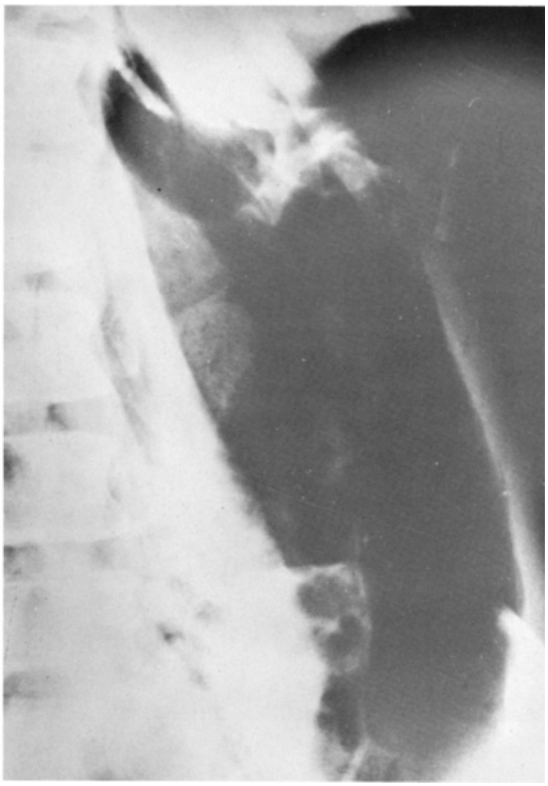


Fig. 9–42. Unilateral left renal agenesis.
Presacral retroperitoneal pneumography demonstrates that none of the perirenal fascial layers has developed on the affected side.
(Reproduced from Meyers et al.[16])

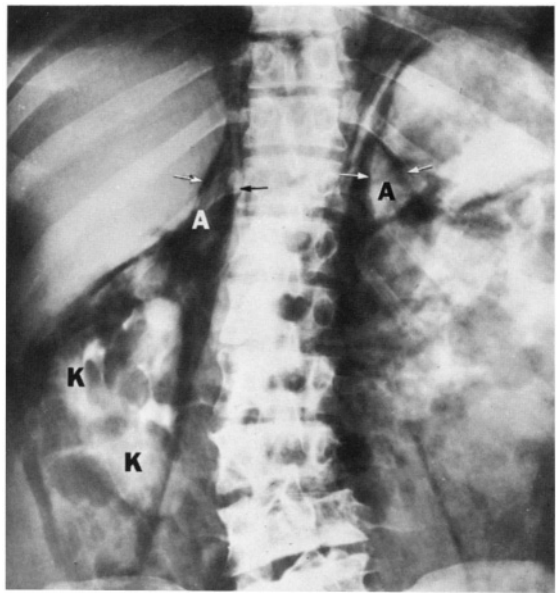


Fig. 9–43. Crossed renal ectopia with fusion.
Presacral retroperitoneal pneumogram with excretory urography. While the adrenal glands *(A)* have developed normally, the extraperitoneal fat has failed to condense into well-defined connective tissue fascial layers on the left, opposite the fused kidneys *(K)*.
(Reproduced from Meyers et al.[16])

In an ectopic kidney or crossed renal ectopia with fusion, the incidence of complications such as lithiasis, infection, and hydronephrosis also approaches 50%.[27] Pain in the lower abdomen may lead to such erroneous diagnoses as appendicitis, diverticulitis, neoplasm of the colon, mesenteric cyst, and ovarian disease.

Pelvic and horseshoe kidneys are prone to injury from any mechanism that compresses the kidney against the spine or sacrum, as in seatbelt injuries.[28]

Pelvic ectopy is important in obstetrics because it may complicate delivery. In a review of the subject, Anderson and associates concluded that most women with pelvic kidney may be delivered vaginally, but if all of the renal tissue lies in the pelvis, as in bilateral ectopy or solitary fused pelvic kidney, cesarean section is the best method of delivery.[29]

Anomalies of structures arising from the urogenital ridge are associated with these renal conditions in as many as 18.5% of cases.[19,25,27,30–32] These include vaginal atresia; hypoplastic, unicornuate, or didelphys uterus (Fig. 9–44); and the absence of an ovary. Less often, monoorchidism and abnormality of the vas deferens are seen in males. The Müllerian duct system develops at a later stage in embryogenesis than the Wolffian duct and is therefore more likely to undergo malformation, which has been postulated to account for the higher incidence of associated genital anomalies in females than males.

The ipsilateral adrenal gland is often identified on CT as a disk-shaped organ with a parasagittal orientation that appears linear on cross-section.[17,33] (Figs. 9–44c and 9–45). Presumably, this results from the absence of a normally located kidney, which exerts a mass effect on the large, globular fetal adrenal before it shrinks.

Extragenitourinary tract anomalies are frequently associated with unilateral renal agenesis in children[25,34] (Fig. 9–46).

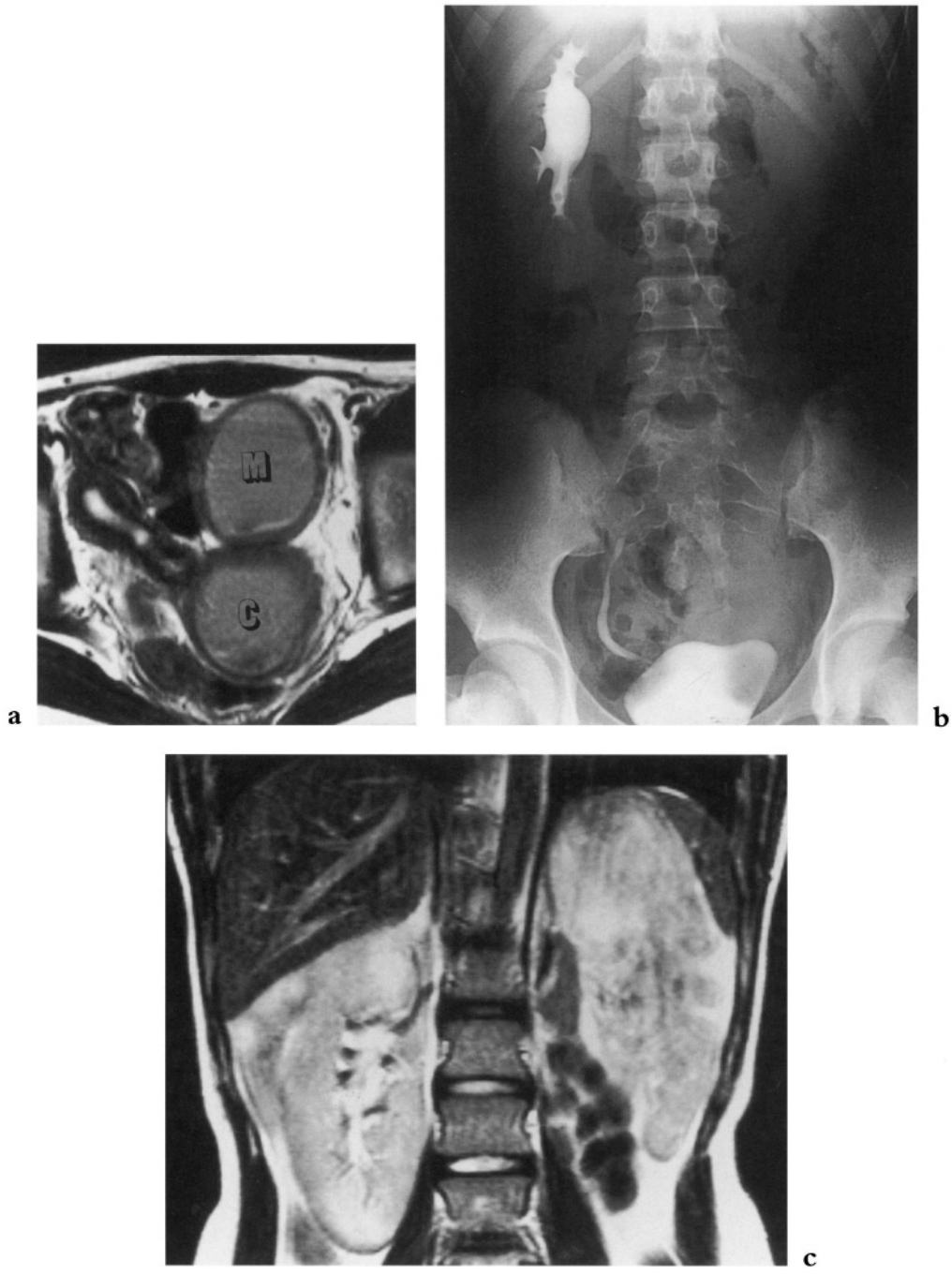


Fig. 9–44. Renal agenesis associated with uterus didelphys.
(a) Axial T2-weighted MR image in a 12-year-old girl demonstrates uterus didelphys and duplicated upper vagina with left sided hematometra *(M)* and hematocolpos *(C),*
(b) Intravenous urography and **(c)** coronal T2-weighted image of the upper abdomen demonstrate a kidney only on the right. It is hypertrophied, and the renal axis shows slight clockwise rotation. In **c,** note malposition of bowel in the "empty" renal fossa and a linear configuration of the left adrenal gland.
(Reproduced from Tanaka et al.[32])

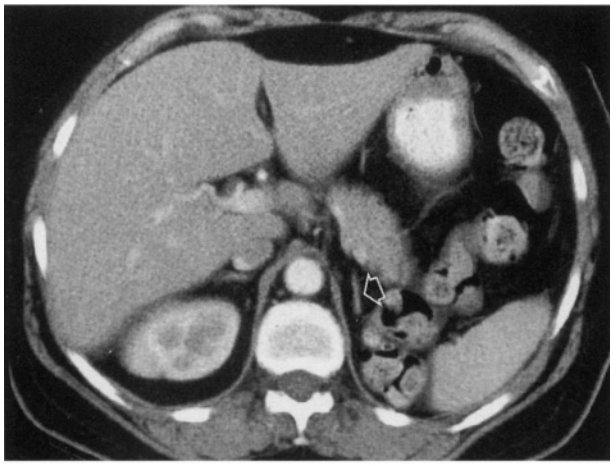


Fig. 9–45. Colonic malposition in left renal agenesis. CT demonstrates deflection of the colon deeply within the "empty" renal fossa medial to the spleen. Note the elongated linear configuration of the left adrenal gland *(arrow).*

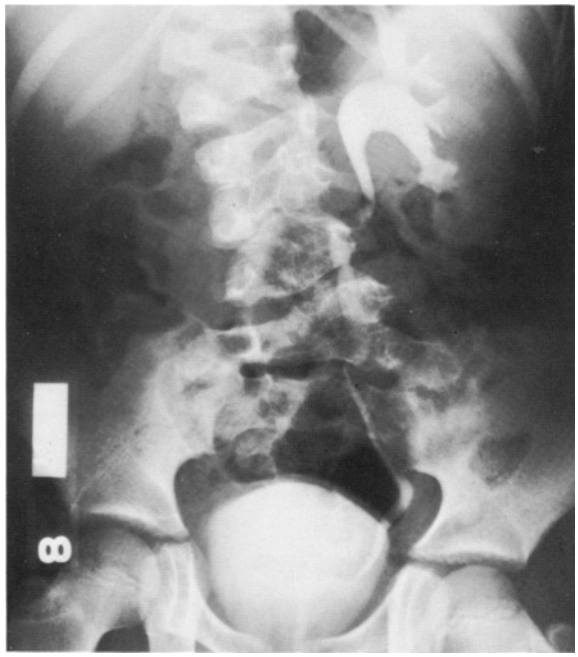


Fig. 9–46. Renal agenesis in association with congenital scoliosis.
This child presented with congenital scoliosis of the lumbar spine with anomalies, including butterfly vertebrae. Intravenous urography demonstrates absence of the right kidney and compensatory hypertrophy on the left.

The Right Side

On the right side, the descending duodenum may be abnormally positioned posteriorly. Normally, the second portion of the duodenum descends immediately anterior to the medial half of the right kidney. In the right lateral projection during an upper gastrointestinal series, the descending duodenum projects anterior to the lumbar spine. With congenital absence or failure of ascent of the right kidney, the descending duodenum may occupy the area of the renal bed and project well over the lumbar spine (Figs. 9–47 and 9–48). Its course on a frontal radiograph appears normal.

Proximal jejunal loops may also occupy a similar position, filling in the renal fossa and coursing abnormally posteriorly (Figs. 9–47 and 9–48).

In right renal agenesis or ectopia, the posterior position of jejunal loops within the renal bed might be most readily confused with a right paraduodenal hernia.[35] The loops, however, do not possess the characteristic circular grouping, stasis, and dilatation; the identifiable afferent and efferent limbs; or the fixation and nondisplacement within an encapsulated hernial sac, despite multiple positions. Distinction is further made by arteriography. In agenesis of the right kidney, jejunal loops and their mesentery and vessels are deflected anterior to the superior mesenteric artery into the right flank. In a right paraduodenal hernia, jejunal loops and their mesentery and vessels pass through the fossa of Waldeyer posterior to the superior mesenteric artery into a hernial sac of the ascending mesocolon. Frontal projections alone thus show similar findings, with the jejunal arteries arising normally from the left side of the superior mesenteric artery and then coursing abruptly to the right to supply a group of small bowel loops in the right abdomen. Lateral projections during aortography or, more clearly, during selective superior mesenteric arteriography readily differentiate between the two.

The posterior hepatic flexure of the colon may show characteristic posteromedial angulation, occupying the area of the right renal fossa[21] (Figs. 9–49 and 9–50).

The Left Side

On the left side, there may be striking posteromedial malposition of the distal transverse colon. Normally, the highest portion of the large intestine in the left upper quadrant ("roentgenographic" splenic flexure) retains the mesenteric attachment of the transverse colon. Distal to this, it courses inferiorly between the medial surface of the spleen and the anterolateral aspect of the left kidney to the anatomic splenic flexure in relation to the splenic angle. The anatomic splenic flexure is normally not only the most posterior but also the most fixed portion of the large intestine, being restrained by the phrenicocolic ligament.[36] Distal to this point, the colon continues as the extraperitoneal descending colon.

With agenesis or ectopia of the left kidney, the mesenteric distal transverse colon may be deflected posteriorly and medially into the "empty" renal fossa area. Similarly, the anatomic splenic flexure of the colon may be deflected toward the same site (Figs. 9–45, 9–51 through 9–53). The colonic malposition may be evident as a finding on plain films (Fig. 9–54).

Figure 9–55 illustrates colonic herniation through a large foramen of Bochdalek. Associated left renal agenesis is indicated by the medial malposition of the subdiaphragmatic distal transverse colon and anatomic splenic flexure at the level of the phrenicocolic ligament.

The most common condition from which these characteristic changes must be distinguished is a congenital anomaly of fixation of the left colon.[37] Here, the splenic flexure may be medially situated, but it is in association with a freely mobile and medially located descending colon.

In left renal agenesis or ectopia, the posteromedial deflection of the distal transverse colon and anatomic splenic flexure into the renal bed should also not be confused for displacement by an enlarged spleen. Splenomegaly may depress the anatomic splenic flexure of the colon but does not displace it medially. In the entity known as wandering spleen,[38–40] laxity or absence of its supporting structures, including the phrenicocolic ligament, allows the organ to migrate from the left upper quadrant. The anatomic splenic flexure may then be sharply angulated medially (Figs. 9–56 and 9–57), a consequence of traction by the splenic pedicle.

These changes in intestinal position have not been seen with renal dysplasia, after flank nephrectomies, or with acquired atrophy of the kidney. In the latter, adipose replacement between the intact perirenal fascial layers contributes to this. However, colonic malposition may be noted after anterior nephrectomies (Figs. 9–58 through 9–62), because of the operative mobilization of the colon and violation of the anterior renal fascia. Occasionally, after left nephrectomy, the tail of the pancreas falls posteriorly and occupies the medial aspect of the renal bed, adjacent to the aorta and the left psoas muscle (Figs. 9–60 and 9–61).[42,43]

text continues on page 532

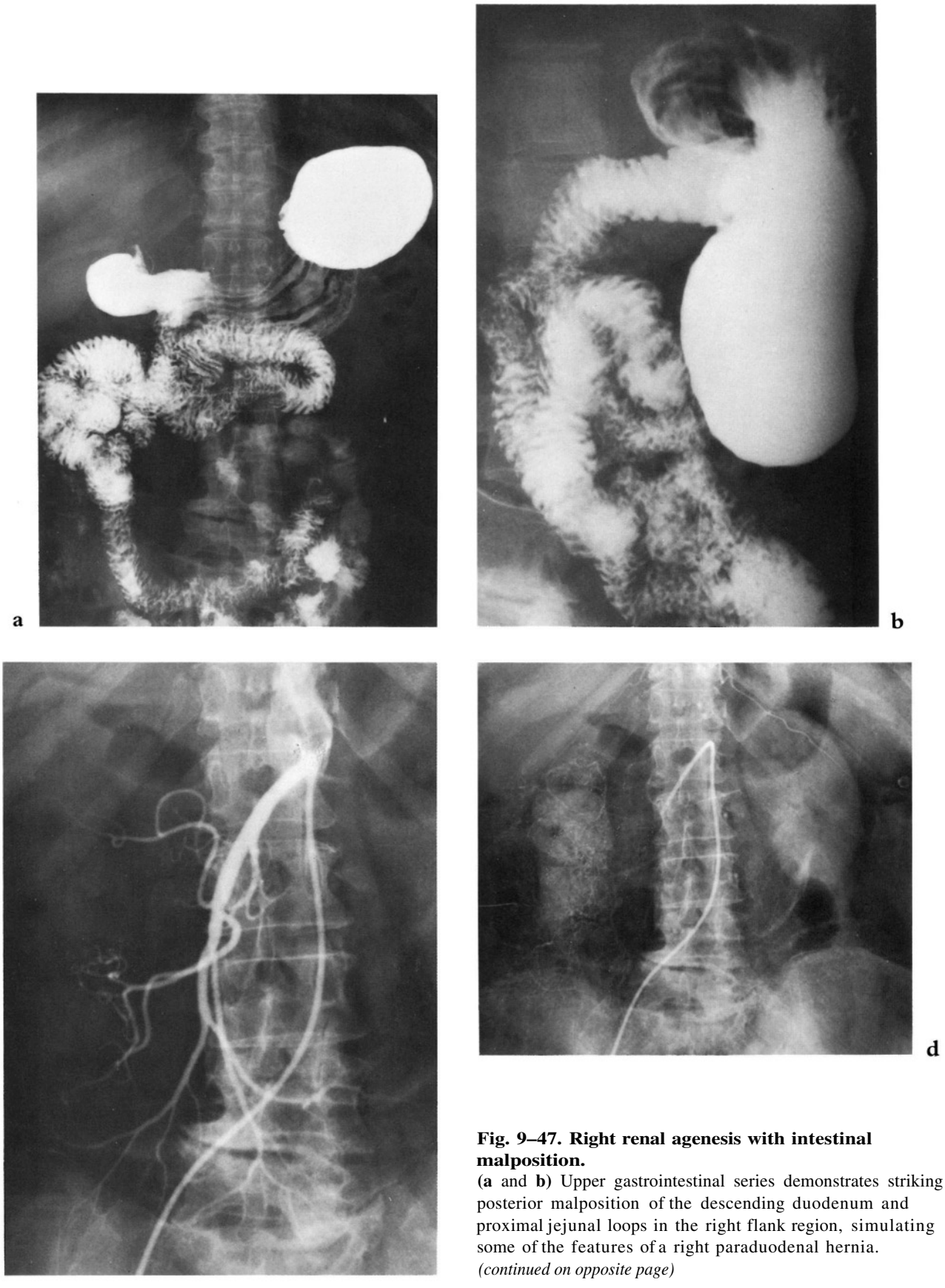


Fig. 9–47. Right renal agenesis with intestinal malposition.
(a and **b)** Upper gastrointestinal series demonstrates striking posterior malposition of the descending duodenum and proximal jejunal loops in the right flank region, simulating some of the features of a right paraduodenal hernia.
(continued on opposite page)

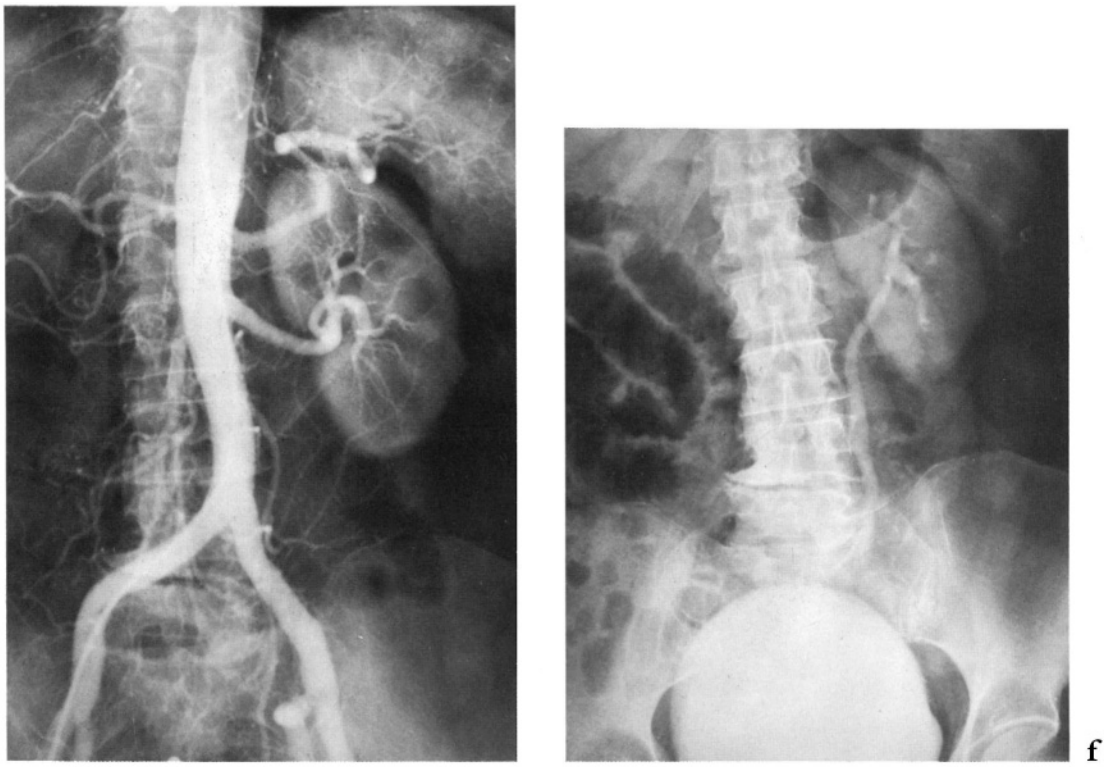
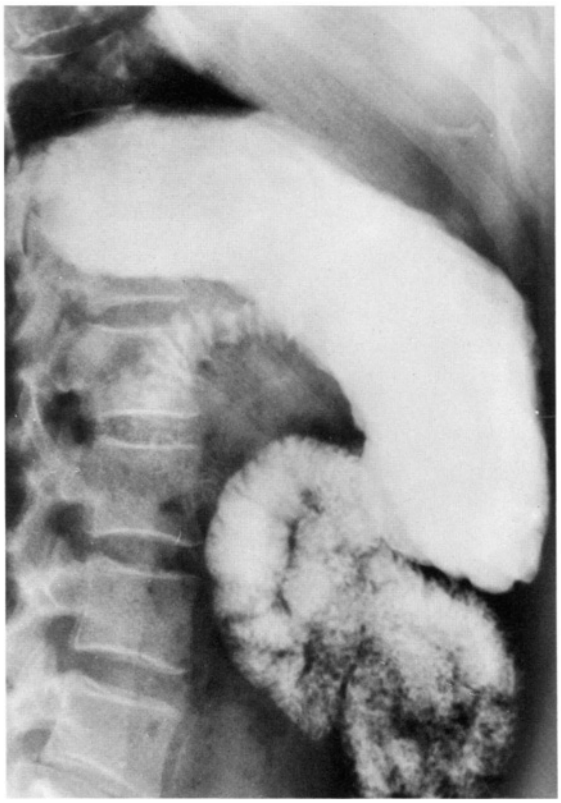


Fig. 9–47. Right renal agenesis with intestinal malposition. (Continued)
(c and **d)** Selective superior mesenteric arteriogram. The arterial phase demonstrates the jejunal arteries arising normally on the left, but then curving to the right midabdomen. The capillary blush of the jejunal loops assumes a general reniform contour.
(e and **f)** Flush aortogram and delayed film reveal absence of the right kidney and renal artery, with compensatory hypertrophy on the left.
(Reproduced from Meyers et al.[16])



a



b



c

Fig. 9–48. Crossed renal ectopia with intestinal malposition.
(a and **b)** Upper GI series demonstrates posterior malposition of descending duodenum and abnormal location of jejunal loops in area of right renal bed. There is also a suggestion of separation of small bowel loops in the left lower quadrant.
(c) Intravenous urogram reveals crossed renal ectopia to the left side.
(Reproduced from Meyers et al.[16])

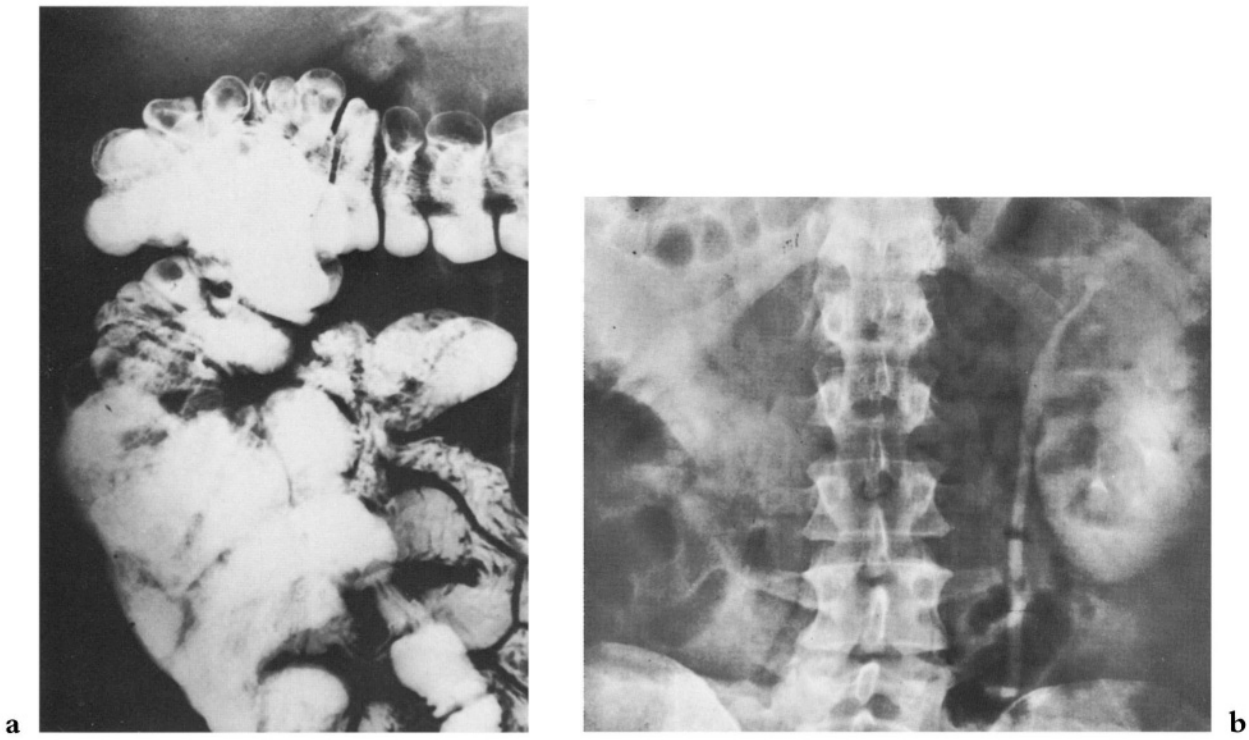


Fig. 9–49. Colonic malposition in right renal agenesis.
(a) Upper GI series, delayed film, demonstrates distal ascending colon and posterior hepatic flexure occupy area of right renal fossa.
(Reproduced from Curtis et al.)[21]
(b) Excretory urography reveals absence of the right kidney and compensatory hypertrophy on the left.

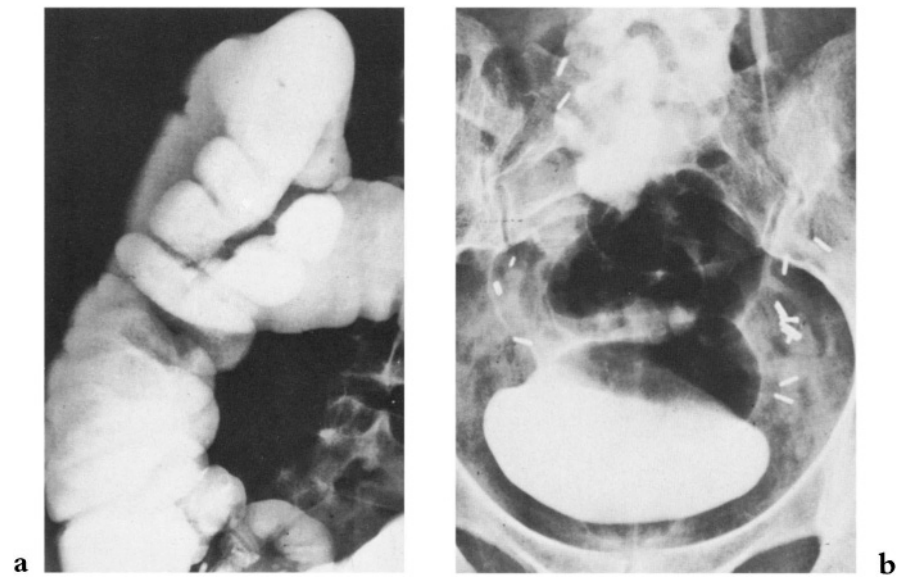


Fig. 9–50. Colonic malposition in right renal ectopia.
(a) Barium enema demonstrates angulated posteromedial deflection of posterior hepatic flexure.
(b) Intravenous urogram reveals right ectopic kidney overlying the lumbosacral junction. (Surgical clips are from a previous hysterectomy.)

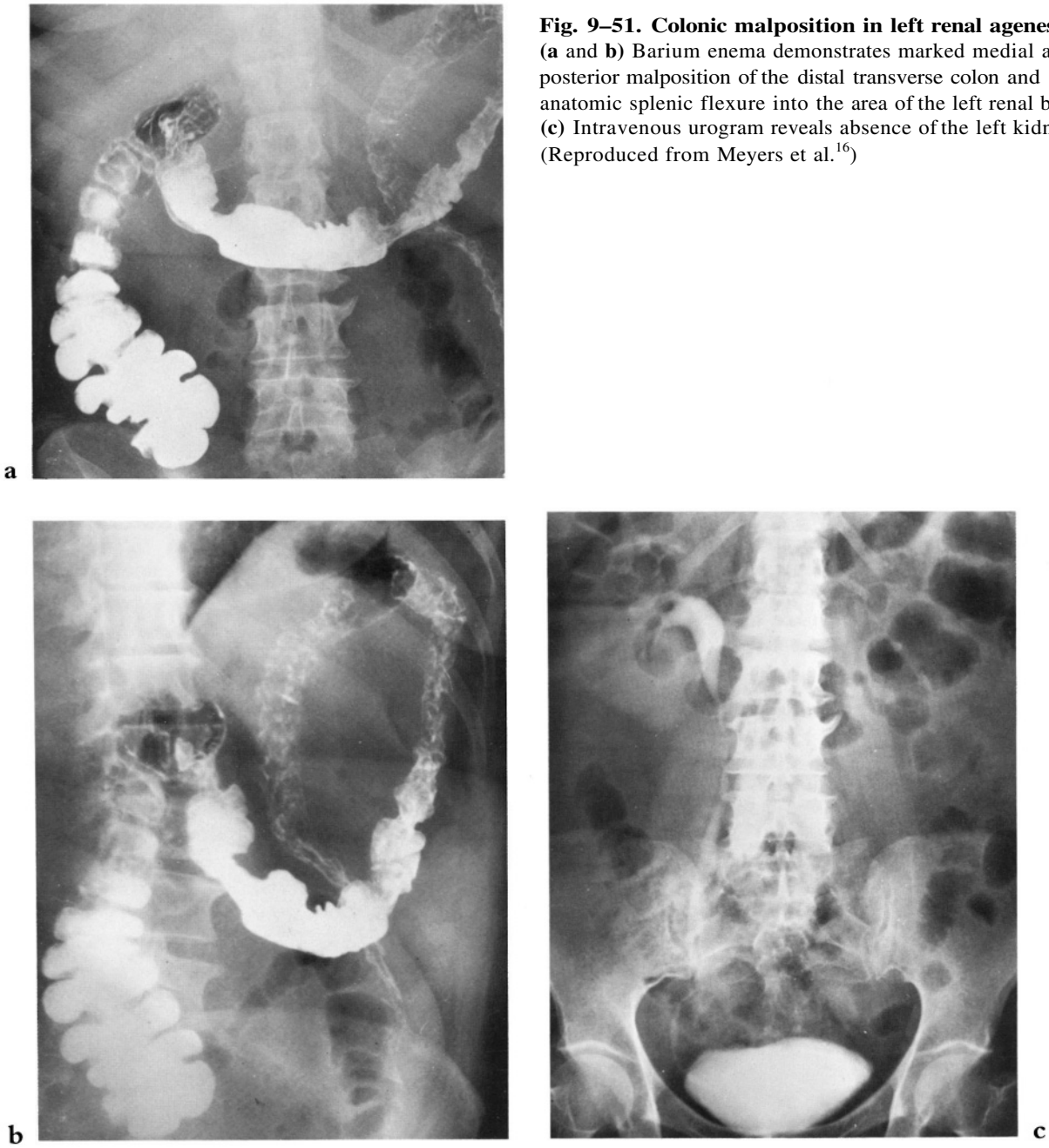


Fig. 9–51. Colonic malposition in left renal agenesis. **(a** and **b)** Barium enema demonstrates marked medial and posterior malposition of the distal transverse colon and anatomic splenic flexure into the area of the left renal bed. **(c)** Intravenous urogram reveals absence of the left kidney. (Reproduced from Meyers et al.[16])

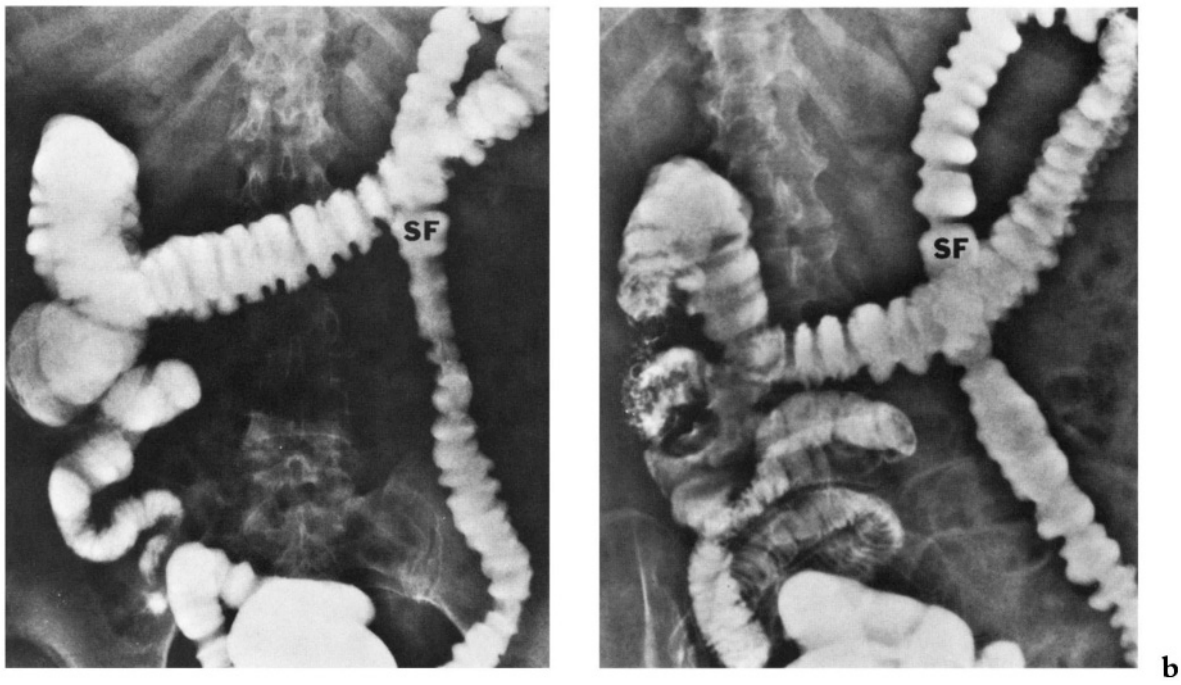


Fig. 9–52. Colonic malposition in left renal agenesis.
(a and **b)** The anatomic splenic flexure *(SF)* is deflected medially and posteriorly, occupying the position of the "empty" renal fossa.
(Reproduced from Meyers.[2])



Fig. 9–53. Crossed renal ectopia with intestinal malposition.
CT demonstrates crossed fused renal ectopia on the right with colon and small bowel loops occupying the "empty" renal fossa on the left. Renal fascia is identifiable on the right *(arrowheads)* but not on the left.

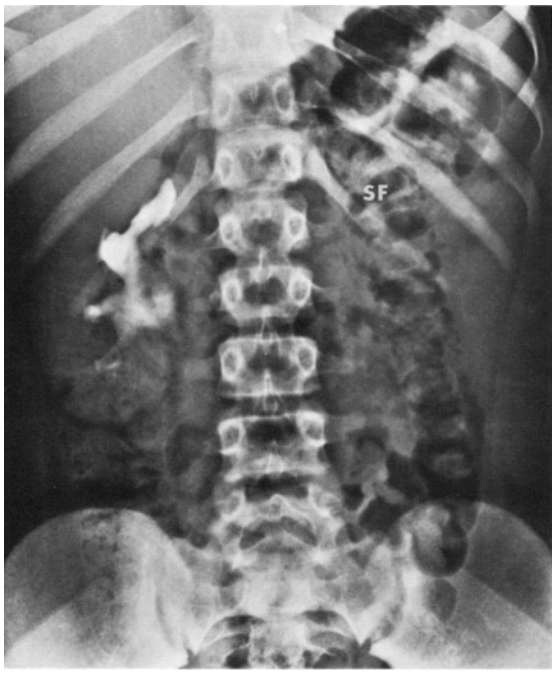


Fig. 9–54. Colonic malposition in left renal agenesis. Excretory urogram. In this child, the anatomic splenic flexure *(SF)* occupies the "empty" renal fossa. There is compensatory hypertrophy of the right kidney. (Reproduced from Meyers.[2])

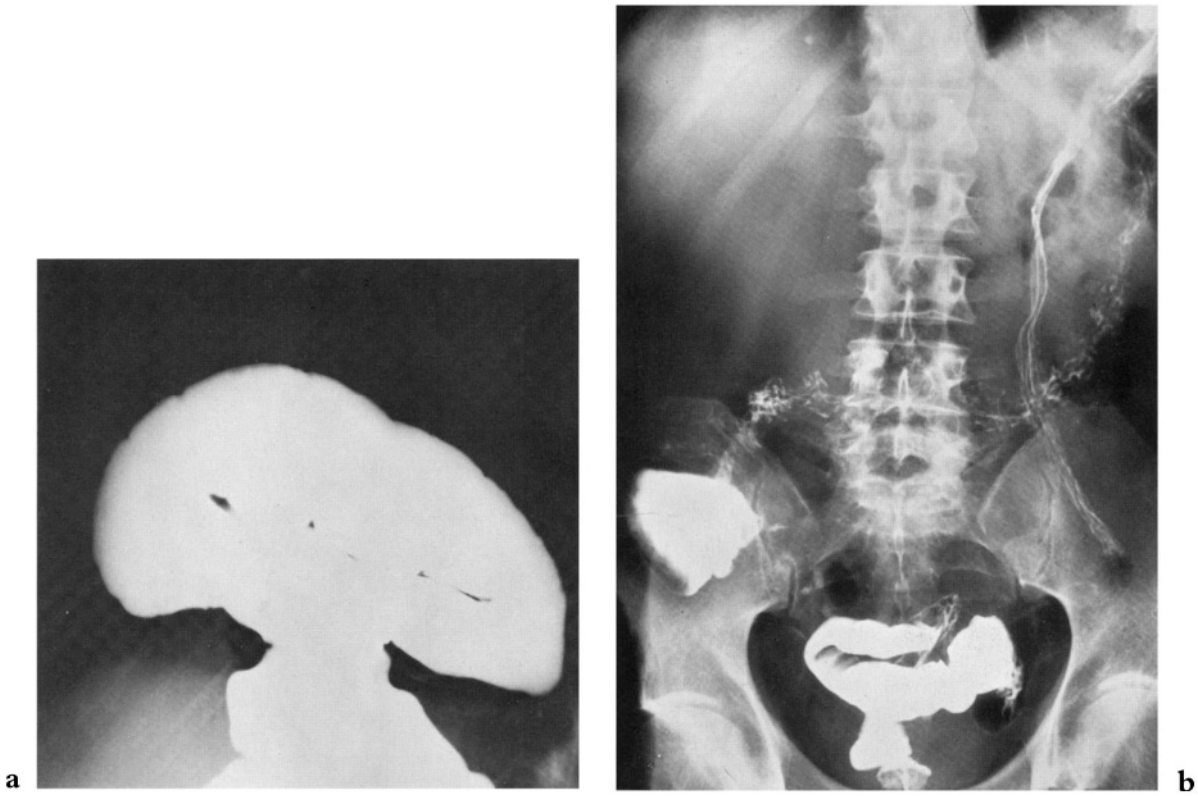


Fig. 9–55. Intrathoracic colonic herniation.
(a) Lateral view of barium enema study shows large intrathoracic herniation of the transverse colon through the foramen of Bochdalek.
(b) There is also marked medial malposition of the distal transverse colon and anatomic splenic flexure into the area of the left renal bed. These changes are secondary to associated agenesis of the left kidney. (Reproduced from Meyers et al.[16])

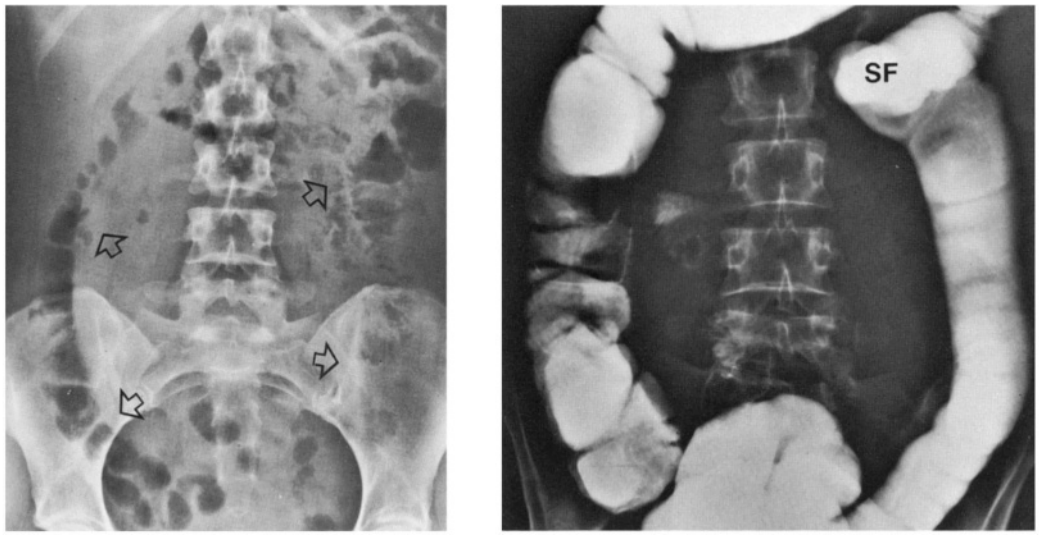


Fig. 9–56. Torsion of wandering spleen.
(a) Plain film shows a large central soft-tissue mass displacing bowel loops *(arrows).*
(b) Barium enema study demonstrates marked medial angulation and malposition of the anatomic splenic flexure *(SF).* This is produced by traction from the twisted splenic pedicle.

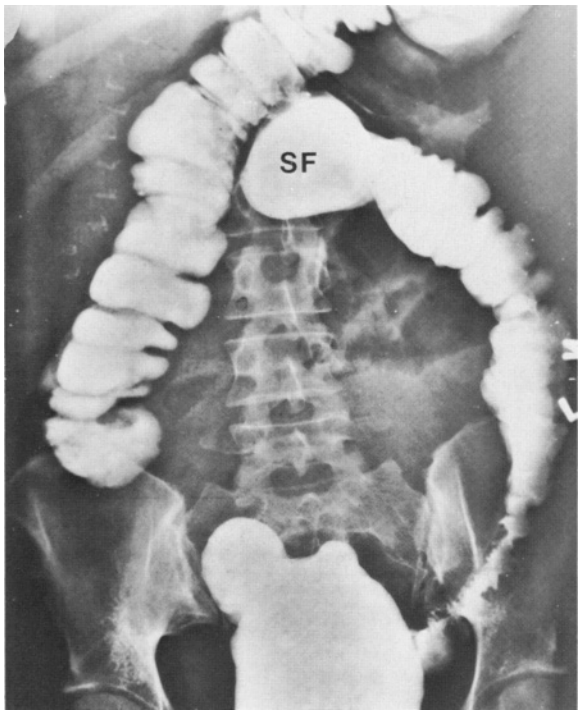


Fig. 9–57. Torsion of wandering spleen.
Barium enema study demonstrates sharply angulated medial malposition of the anatomic splenic flexure *(SF),* produced by traction from an elongated and twisted splenic pedicle. The enlarged congested spleen is indicated by the soft-tissue mass in the lower abdomen displacing the descending and sigmoid colon.

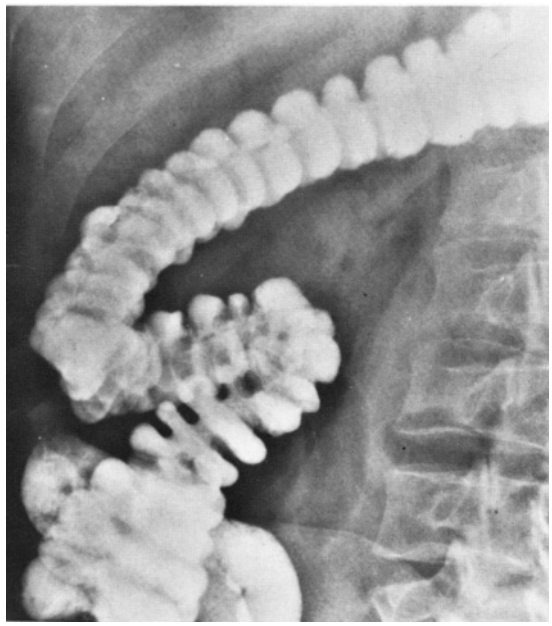


Fig. 9–58. Malposition of the colon following right nephrectomy.
The hepatic flexure is deviated into the "empty" renal fossa.

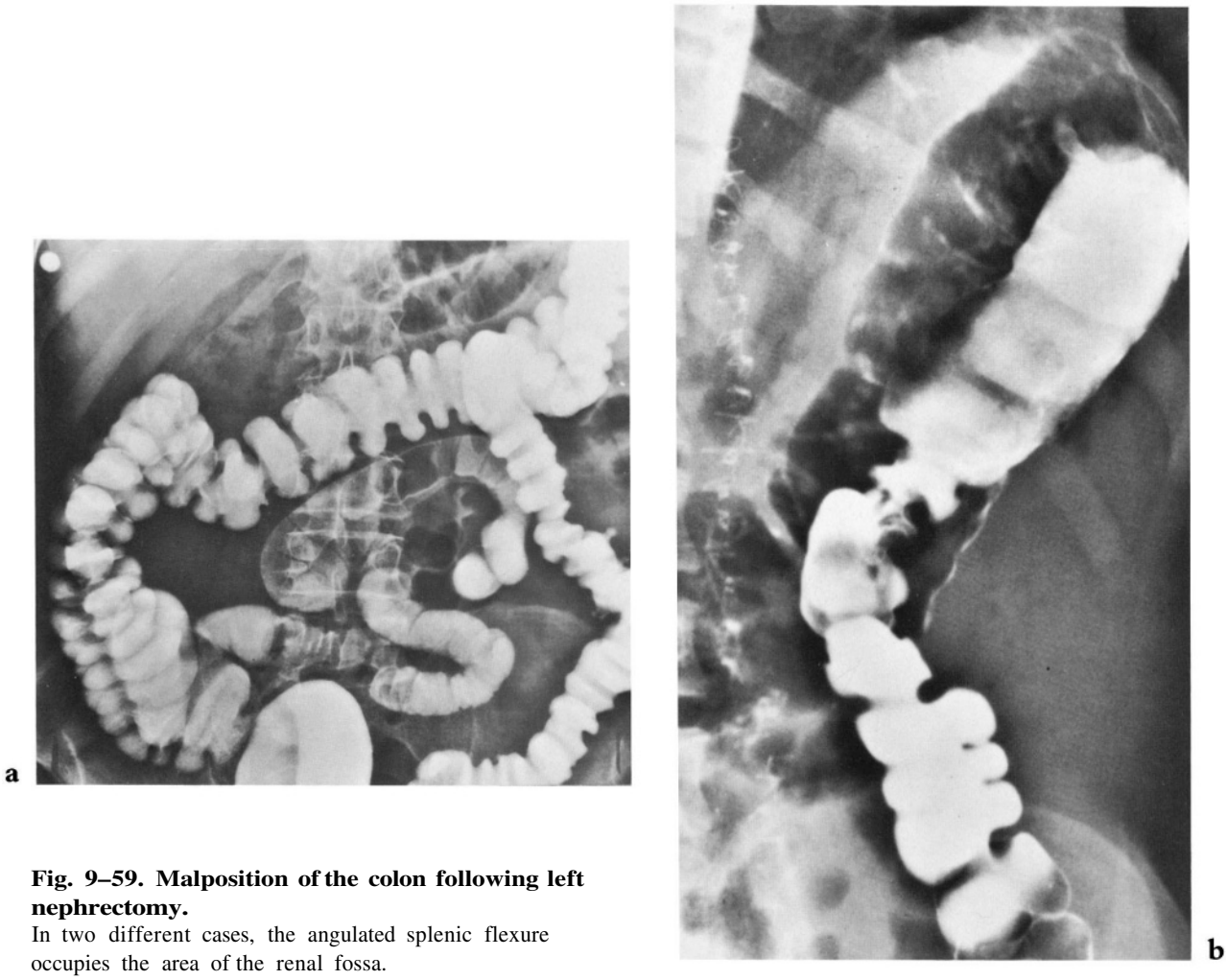


Fig. 9–59. Malposition of the colon following left nephrectomy.
In two different cases, the angulated splenic flexure occupies the area of the renal fossa.

Bowel may be a conspicuous component of lumbar hernias secondary to postoperative flank incisions.[41] (Fig. 9–63).

Direct Intestinal Effects Unique to Renal Ectopia

Ectopic kidneys may be located in the true pelvis (63%), in the iliac fossa or opposite the crest of the ilium (8%), or in the abdomen below the level of the second or third lumbar vertebra and above the crest of the ilium (29%).[24] In cases of ectopic kidney in the true pelvis, there is usually no definite pressure effect upon the sigmoid colon, presumably because the kidney within the sacral hollow does not come into relationship with the anteriorly directed sigmoid loops.[16]

However, renal ectopia in the iliac fossa or lower abdomen may result in a characteristic mass effect on or displacement of the ascending or descending colon.[16]

On plain films or barium contrast studies, the contour of the density that may be seen in ectopic kidneys usu-

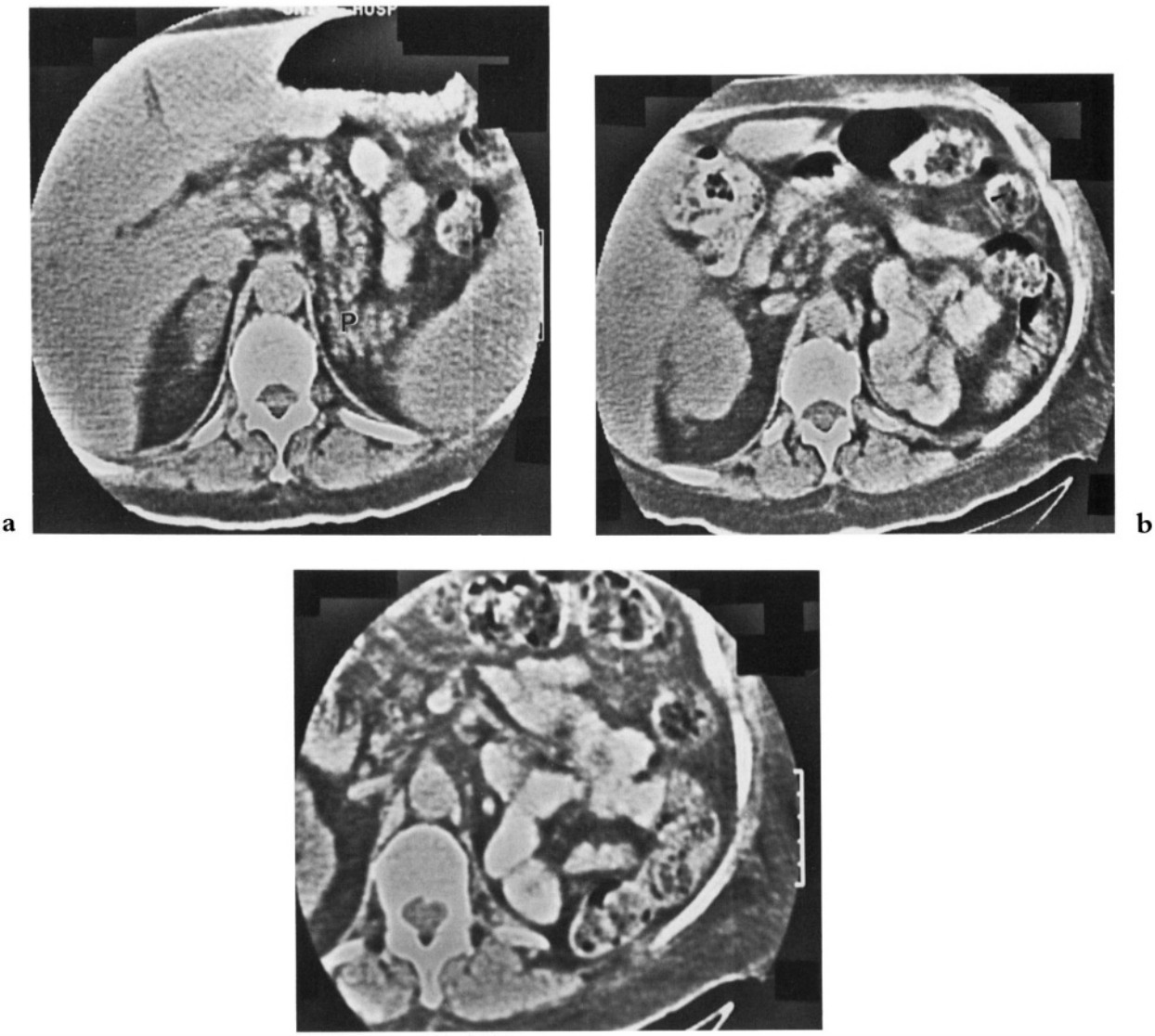


Fig. 9–60. Malposition of the bowel and pancreas following left nephrectomy.
(a) CT scan at level of the spleen shows the tail of the pancreas *(P)* sharply deviated into the renal bed. (Incidentally noted is a right adrenal cyst.)
(b and **c)** At lower levels opacified jejunal loops and feces-containing colon occupy the "empty" renal fossa.

ally is not clearly outlined. Two factors appear to account for this: (a) the relative lack of contrasting extraperitoneal fat in the lower abdomen and upper pelvis, and (b) the common marked anterior malrotation of the ectopic kidney. The latter feature also brings the ectopic kidney in the iliac or lower abdominal area into close relationship with the medial borders of the ascending and descending colon and small bowel loops (Fig. 9–64). Failure to recognize the characteristic mass effects and displacements as secondary to renal ectopia may lead to unnecessary surgery.

If displacement of small bowel loops toward the midline can also be demonstrated, the reniform contour of the "mass" may be shown more clearly (Fig. 9–65).

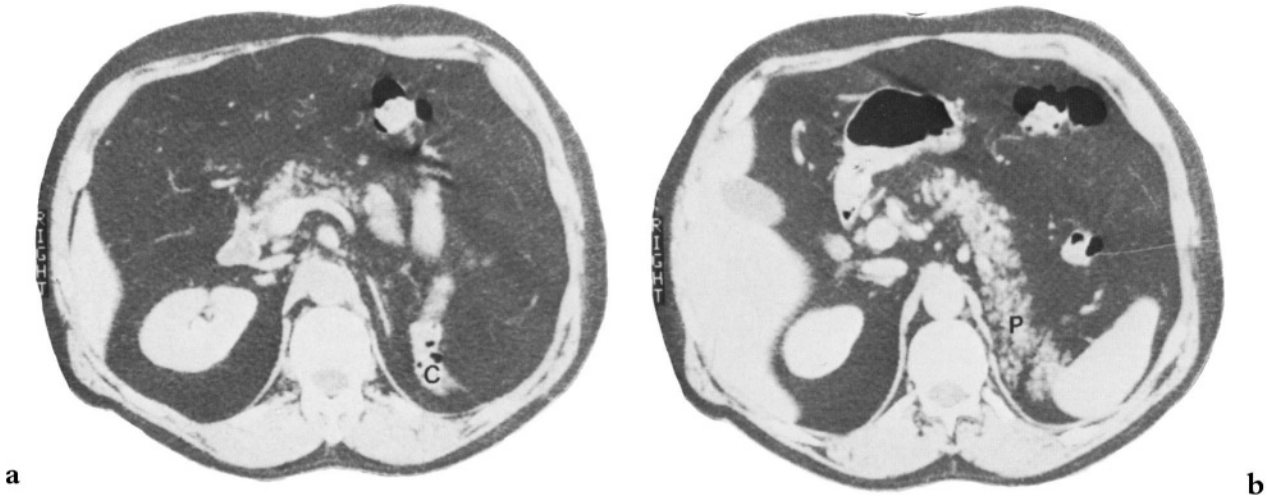


Fig. 9–61. Malposition of the bowel and pancreas following left nephrectomy, demonstrated by computed tomography.
(a and **b)** The splenic flexure of the colon *(C),* opacified by contrast medium, and the tail of the pancreas *(P)* are deviated into the renal bed.

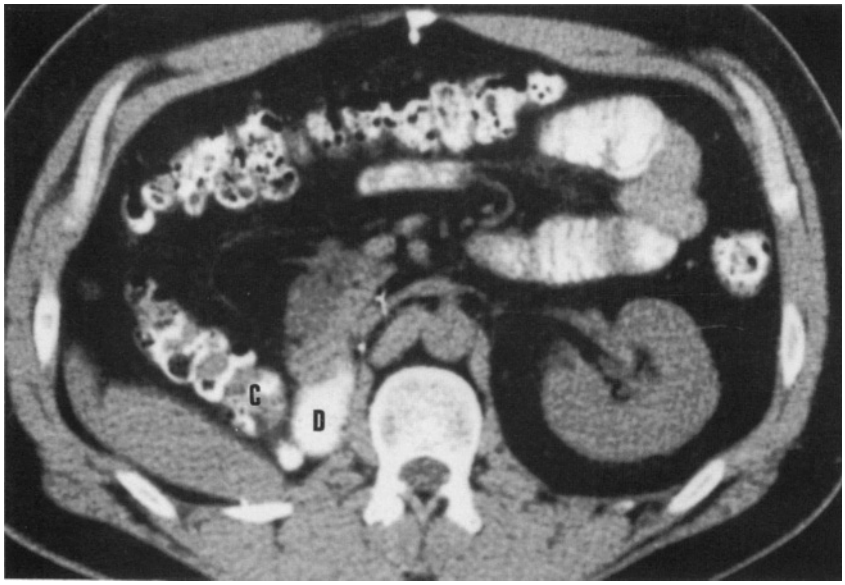


Fig. 9–62. Malposition of the bowel following right nephrectomy.
The hepatic flexure of the colon *(C)* and the descending duodenum *(D),* accompanied by the head of the pancreas, occupy the "empty" renal fossa on the right.

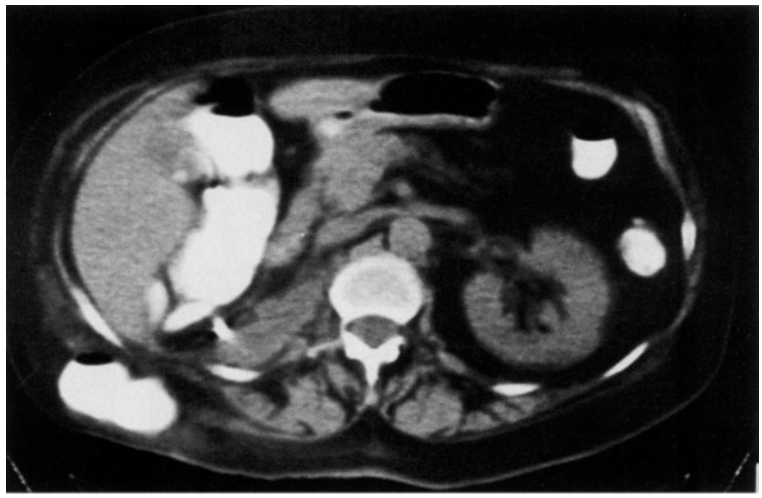


Fig. 9–63. Herniation of the colon following right nephrectomy.
CT demonstrates incisional herniation of the posterior hepatic flexure into the flank.

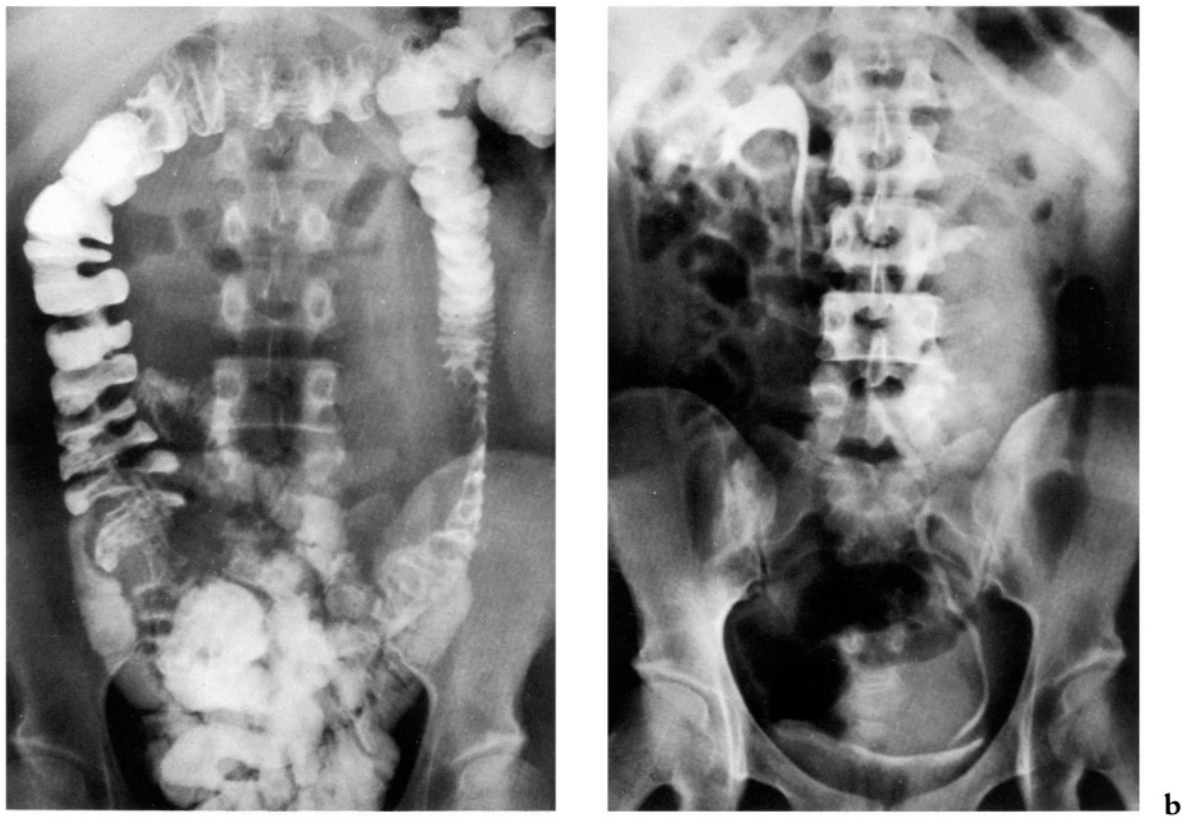


Fig. 9–64. Ectopic kidney in a 24-year-old female with left lower quadrant mass.
(a) Barium enema examination demonstrates extrinsic mass impression on medial aspect of lower descending colon. In addition, the splenic flexure is sharply angulated posteromedially, indicating an empty renal fossa.
(b) Intravenous urogram documents a left ectopic kidney with marked anterior malrotation in relationship laterally to the descending colon.
(Reproduced from Meyers et al.[16])

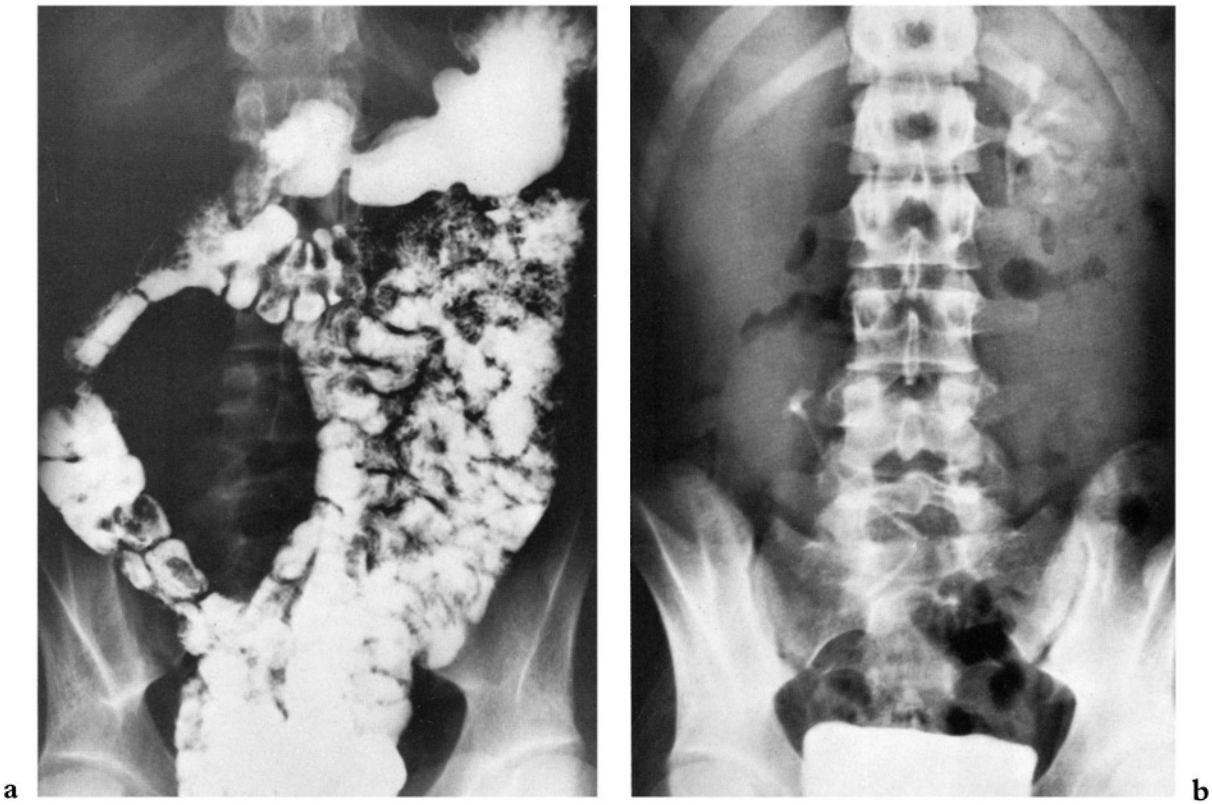


Fig. 9–65. Ectopic kidney.
(a) Small bowel series. Inframesocolic mass displacement of the small bowel and colon in the right lower quadrant. Note reniform contour of mass displacement.
(b) Intravenous urogram reveals an ectopic right kidney with characteristic anterior malrotation.
(Reproduced from Meyers et al.[16])

References

1. Katz AB: Gastrointestinal manifestations of urinary tract disease. J Urol 1953; 69:726–733.
2. Meyers MA: The reno-alimentary relationships: Anatomic-roentgen study of their clinical significance. AJR Rad Ther Nucl Med 1975; 123:386–400.
3. Meyers MA, Volberg F, Katzen B, et al: Haustral anatomy and pathology: A new look. I. Roentgen identification of normal pattern and relationships. Radiology 1973; 108:497–504.
4. Meyers MA, Volberg F, Katzen B, et al: Haustral anatomy and pathology: A new look. II. Roentgen interpretation of pathologic alterations. Radiology 1973; 108:505–512.
5. Meyers MA, McSweeney J: Secondary neoplasms of bowel. Radiology 1972; 105:1–11.
6. Meyers MA: Colonic changes secondary to left perinephritis: New observations. Radiology 1974; 111:525–528.
7. Meyers MA: Acute extraperitoneal infection. Semin Roentgenol 1973; 8:445–464.
8. Meyers MA, Whalen JP, Peelle K, et al: Radiologic features of extraperitoneal effusions: An anatomic approach. Radiology 1972; 104:249–257.
9. Meyers MA, Evans JA: Effects of pancreatitis on the small bowel and colon: Spread along mesenteric planes. AJR 1973; 119:151–165.
10. Parvey HR, Cochran ST, Payan J, et al: Renocolic fistulas: Complementary roles of computed tomography and direct pyelography. Abdom Imaging, 1997; 22: 96–99.

11. Bissada NK, Cole AT, Fried FA: Renoalimentary fistula: Unusual urological problem. J Urol 1973; 110:273–276.
12. Sussman SK, Gallman WH, Cohan RH, et al: CT findings in xanthogranulomatous pyelonephritis with coexistent renocolic fistula. J Comput Assist Tomogr 1987; 11:1088–1090.
13. Bahn DK, Brown RKJ, Reidinger AA, et al: Renal stone ileus. AJR 1988; 150:145–146.
14. Culkin DJ, Wheelers JS, Canning JR: Nephroduodenal fistula. J Urol 1985; 134:528–530.
15. Dunn M, Kirk D: Renogastric fistula: Case report and review of the literature. J Urol 1973; 109:785–787.
16. Meyers MA, Whalen JP, Evans JA, et al: Malposition and displacement of bowel in renal agenesis and ectopia: New observations. AJR Rad Ther Nucl Med 1973; 117:323–333.
17. Hadar H, Gadoth N, Gillon G: Computed tomography of renal agenesis and ectopy. J Comput Assist Tomogr 1984; 8:137–143.
18. Mascatello V, Lebowitz RL: Malposition of the colon in left renal agenesis and ectopia. Radiology 1976; 120:371–376.
19. Ashley DJ, Mostofi FK: Renal agenesis and dysgenesis. J Urol 1960; 83:211–230.
20. Benjamin JA, Tobin CE: Abnormalities of kidneys, ureters, and perinephric fascia: Anatomic and clinical study. J Urol 1951; 65:715–731.
21. Curtis JA, Sadhu V, Steiner RM: Malposition of the colon in right renal agenesis, ectopia, and anterior nephrectomy. AJR 1977; 129:845–850.
22. Meyers MA: Diseases of the Adrenal Glands. Radiologic Diagnosis with Emphasis on the Use of Presacral Retroperitoneal Pneumography. Charles C Thomas, Springfield, IL, 1963.
23. Thompson GJ: Incidence of congenital solitary kidney. J Urol 1948; 59:119–128.
24. Thompson GJ, Pace JM: Ectopic kidney: Review of 97 cases. Surg Gynecol Obstet 1937; 64:935–943.
25. Doroshow L, Abeshouse BS: Congenital unilateral solitary kidney: Report of 37 cases and review of the literature. Urol Surv 1961; 11:219–229.
26. Braasch WF, Merricks JW: Clinical and radiological data associated with congenital and acquired single kidney. Surg Gynecol Obstet 1938; 67:281–286.
27. Farman F: Anomalies of the kidneys. Handbuch der Urologie, vol 7. Malformations. Springer-Verlag, Berlin, 1968.
28. Brennan FJ, Goff WB II: Seatbelt injury to a pelvic kidney as demonstrated by CT. J Comput Assist Tomogr 1993; 17:664–665.
29. Anderson GW, Rice GG, Harris BA: Pregnancy and labor complicated by pelvic ectopic kidney. J Urol 1951; 65:760–776.
30. Fried AM, Oliff M, Wilson EA, et al: Uterine anomalies associated with renal agenesis: Role of gray scale ultrasonography. AJR 1978; 131:973–975.
31. Wiersma AF, Peterson LF, Justema EJ: Uterine anomalies associated with unilateral renal agenesis. Obstet Gynecol 1976; 47:654–657.
32. Tanaka YO, Kurosaki Y, Kobayashi T, et al: Uterus didelphys associated with obstructed hemivagina and ipsilateral renal agenesis: MR findings in seven cases. Abdom Imaging 1998; 23: 437–441.
33. Kenney PJ, Robbins GL, Ellis DA, et al: Adrenal glands in patients with congenital renal anomalies: CT appearance. Radiology 1985; 155:181–182.
34. Macewen GD, Winter RB, Hardy JH: Evaluation of kidney anomalies in congenital scoliosis. J Bone Joint Surg 1972; 54A:1451–1454.
35. Meyers MA: Paraduodenal hernias: Radiologic and arteriographic diagnosis. Radiology 1970; 95:29–37.
36. Meyers MA: Roentgen significance of the phrenicocolic ligament. Radiology 1970; 95:547–554.
37. Balthazar EJ: Congenital positional anomalies of the colon: Radiographic diagnosis and clinical implications. II. Abnormalities of fixation. Gastrointest Radiol 1977; 2:49–56.
38. Gordon DH, Burrell MI, Levin DC, et al: Wandering spleen—The radiological and clinical spectrum. Radiology 1977; 125:39–46.
39. Smulewicz JJ, Clemett AR: Torsion of the wandering spleen. Am J Dig Dis 1975; 20:274–279.
40. Parker LA, Mittelstaedt CA, Mauro MA, et al: Torsion of a wandering spleen: CT appearance. J Comput Assist Tomogr 1984; 8(6):1201–1204.
41. Baker ME, Weinerth JL, Andrian RT, et al: Lumbar hernia: Diagnosis by CT. AJR 1987; 148:565–567.
42. Alter AJ, Uehling DT, Zwiebel WJ: Computed tomography of the retroperitoneum following nephrectomy. Radiology 1979; 133:663–668.
43. Neumann CH, Hessel SJ: CT of the pancreatic tail. AJR 1980; 135:741–745.

The Duodenocolic Relationships: Normal and Pathologic Anatomy

10

The precise anatomic relationships between the duodenal loop and the transverse colon are often of critical importance in the radiologic interpretation of upper abdominal pathology. Their points of most intimate relationship represent anatomic crossroads between intraperitoneal and extraperitoneal structures and thus permit specific localization and diagnosis of a disease process.[1] Because of this relationship, a lesion originating in one may exert its major effects on the other. Particularly if radiologic investigation is initiated by a study that manifests the striking secondary effects, the presentation of findings may then be very misleading until the nature of the relationship and the primary site are appreciated.

Detailed knowledge of the intimate anatomic relationships is essential in the radiologic interpretation of a variety of diseases. These include defects of the mesocolon with internal herniation into the lesser sac, masses developing within the mesocolic leaves, extension of neoplasms, duodenocolic fistulas, gallbladder disease, renal masses, pancreatitis, and abdominal aneurysm.

Anatomic and Normal Radiologic Features

The key to understanding the significance of the duodenocolic relationships is the insertion of the root of the transverse mesocolon and its planes of reflection (Fig. 10–1).

The hepatic flexure of the colon is characteristically composed of two curvatures.[2] The proximal, more posterior one continues from the fixed extraperitoneal ascending colon and is related to the inferior and lateral edge of the right kidney and the posterolateral tip of the liver. The colon then passes immediately anteromedially over the descending duodenum to the second curve of the hepatic flexure, which is more anterior and is related above to the gallbladder.

At a point between the two curvatures of the hepatic flexure, as the colon is in intimate relationship to the descending duodenum (Fig. 10–2), it begins to pick up the peritoneal sling of the transverse mesocolon. The colon in this area is then in virtual contiguity with the second portion of the duodenum, with the very short edge of the beginning reflection of the transverse mesocolon providing a mesenteric plane (Figs. 10–3 and 10–4).

The root of the transverse mesocolon broadly intersects the infraampullary portion of the descending duodenum and then continues along the anterior surface of the pancreas. Here it is attached to the midportion of the head and the inferior surface of the body and tail. The nonperitonealized bare area, wide on the right and progressively thinner toward the left, thus provides a shared anatomic plane, between the pancreas and descending duodenum behind and the transverse colon in front, along the leaves of the transverse mesocolon.

The transverse mesocolon itself is a fan-shaped structure in the horizontal plane of the body. Short at its beginning, it is longest in the midsagittal plane, becom-

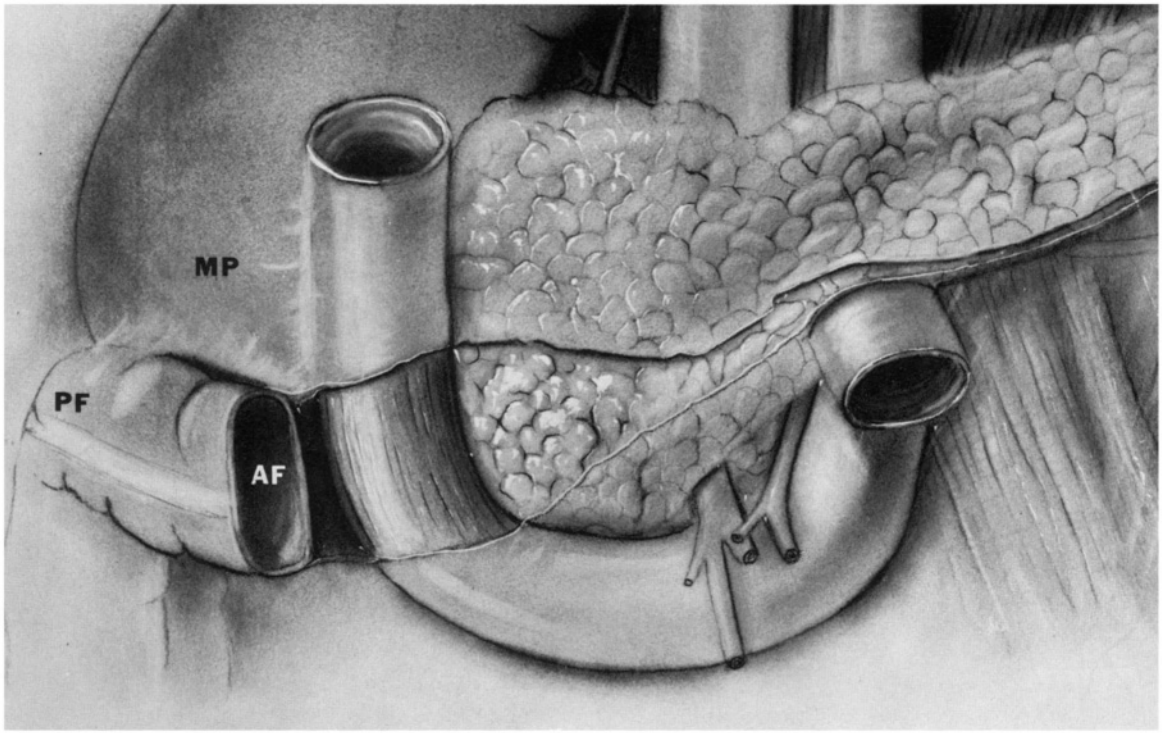


Fig. 10–1. The root of the transverse mesocolon.
It extends across the infraampullary portion of the duodenum and lower border of the pancreas. Note the relationships of the anterior hepatic flexure of the colon *(AF)* and of the duodenojejunal junction. *PF* = posterior hepatic flexure. *MP* marks the location of Morison's pouch, the intraperitoneal posterior extension of the right subhepatic space anterior to the right kidney.
(Reproduced from Meyers and Whalen.[1])



Fig. 10–2. A normal upper GI series frequently shows lateral pressure on the descending duodenum from a feces-distended anterior hepatic flexure of the colon. This reflects their contiguous anatomic relationship.

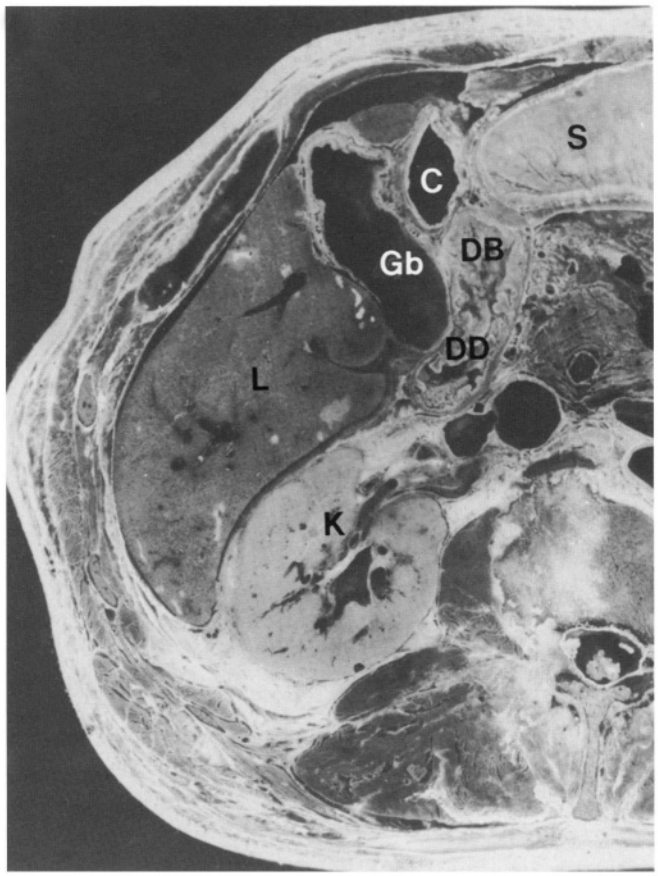


Fig. 10–3. Transverse section through the right abdomen at the level of the duodenal bulb *(DB)* and the proximal descending duodenum *(DD).*
Note the intimate relationship of the hepatic flexure of the colon *(C)* at the beginning reflection of the transverse mesocolon. *S* = stomach; *Gb* = gallbladder; *L* = liver; *K* = kidney.
(Reproduced from Meyers and Whalen.[1])

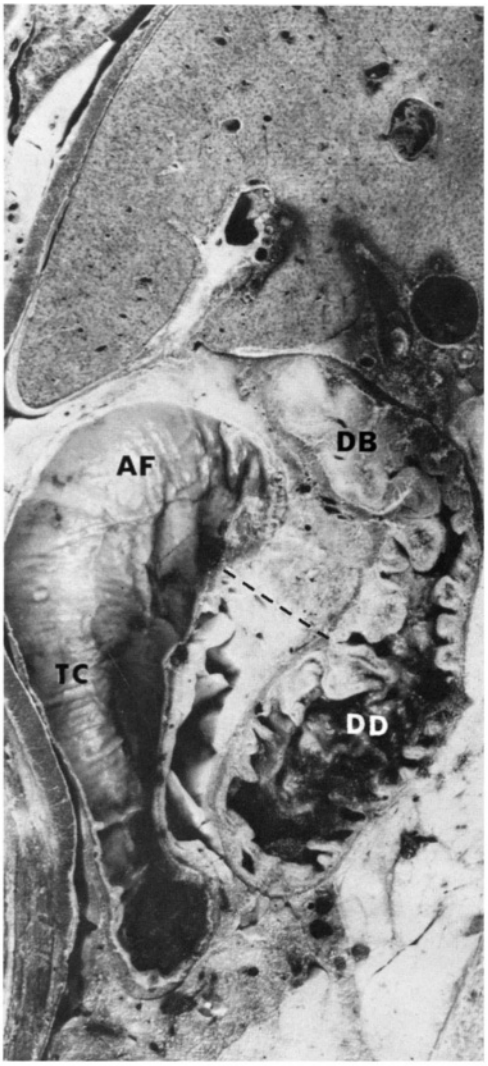


Fig. 10–4. Right parasagittal section at the level of the duodenal bulb *(DB)* and the decending duodenum *(DD),* showing their relationship to the anterior hepatic flexure *(AF)* of the colon before it continues ventrally as the transverse colon *(TC).* The *dashed line* indicates the transverse mesocolon.
(Reproduced from Meyers and Whalen.[1])

ing abbreviated laterally once again as the colon comes into relationship to the left kidney and the spleen. The length of the transverse mesocolon varies. It tends to be short in stocky individuals and long in tall, thin individuals.

The retroperitoneal duodenum bends forward after its ascending portion at the level of the ligament of Treitz to penetrate the posterior parietal peritoneum and continue as the intraperitoneal jejunum.

Although usage of the term *ligament of Treitz* for the duodenojejunal function is widely employed, it is not only inaccurate but may be misleading.[3] The duodenojejunal flexure is generally about 2.5 cm left of the midline at the level of the inferior border of the first lumbar vertebra.[4] In 1853, Treitz[5] (Fig. 10–5) described the suspensory muscle of the duodenum as a thin triangular band ascending behind the pancreas to blend with the dense connective tissue around the stems of the superior mesenteric artery and celiac axis.[6] It is a curious fact that anatomists refer to the structure as the suspensory muscle of the duodenum, whereas clinicians refer to it as the ligament of Treitz. It is generally conceived of and illustrated in anatomic atlases as a thin fibromuscular band limited to the duodenojejunal junction. Yet, exclusive attachment to the flexure is rare. Rather, the muscle is usually attached to the third and fourth portions of the duodenum and frequently to the duodenojejunal flexure as well (Fig. 10–6). At its base, the smooth muscle fibers of the suspensory muscle are continuous with the longitudinal and circular muscle fibers of the duodenum. Superiorly, the muscle is gradually replaced by collagenous and elastic fibers. Its overall length varies from 1.25–6.4 cm. The fibromuscular structure plays an important role in the embryologic rotation of the bowel and in facilitating normal progression of contents from the extraperitoneal duodenum to the mesenteric small bowel and contributes to the effects of the superior mesenteric artery syndrome.[3,8]

The duodenojejunal junction is in intimate relationship to the inferior reflection of the transverse mesocolon (Figs. 10–1 and 10–7). It also serves as a useful landmark for dividing the body and tail of the pancreas.

The duodenojejunal junction, fixed by the ligament of Treitz, generally maintains its position throughout life. The duodenal bulb and proximal portion of the second duodenum, however, tend to descend with age, with progressive laxity of support, a change most marked in the fifth and sixth decades.[9] Nevertheless, the position of the root of the transverse mesocolon, which separates the peritoneal cavity from the lesser sac, can be constantly indicated on an upper GI series by a line drawn from the infraampullary segment of the descending duodenum to a point immediately above the duodenojejunal junction. This delimits the most superior ascent of

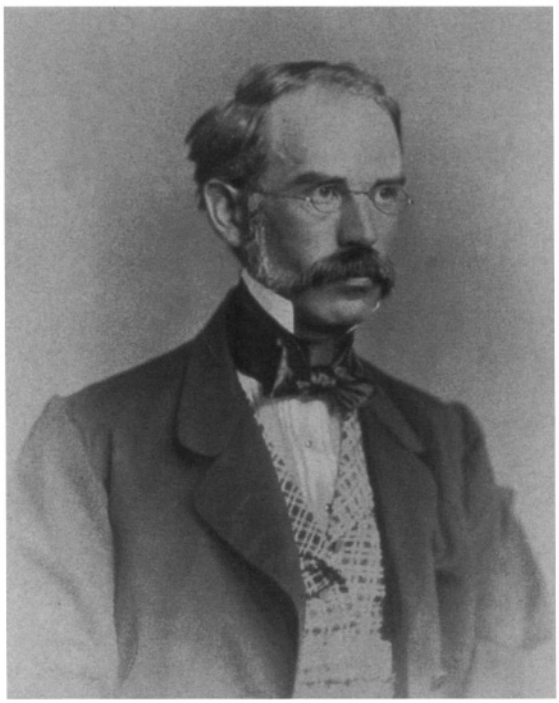


Fig. 10–5. Václav (Wenzel) Treitz (1819–1872), age 41.
Treitz was a Bohemian-born pathoanatoinist who held faculty positions in Vienna, Kraków, and Prague. In 1853, he described "A new muscle in the human duodenum, over elastic sinews and some other anatomical relations," now generally referred to as the *ligament of Treitz.* In 1857 in an article entitled "Hernia Retroperitonealis: A Contribution to the History of the Internal Hernias," he discussed the anatomic relationships at the site of the passage of the duodenum into the jejunum bordered by the inferior mesenteric vein and left colic artery, also called the *vascular arch of Treitz.*
(Courtesy of the Institut für Geschichte der Medizin der Universität Wien, Museum Josephinum, Vienna.)

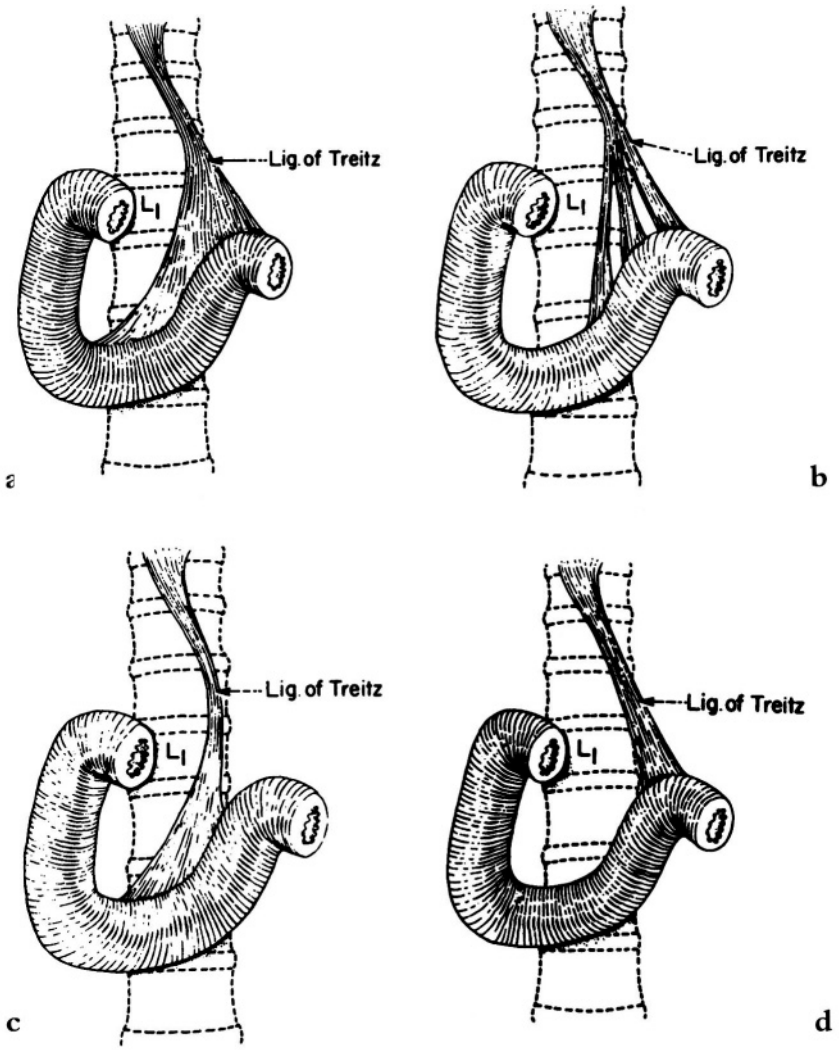


Fig. 10–6. Variations of the attachment of the suspensory muscle of the duodenum (ligament of Treitz).
(a) Attachment to the third and fourth portions of the duodenum and the duodenojejunal flexure. This occurs in 40–61% of cases.
(b) Multiple, separate divisions are not unusual.
(c) Attachment to the third and fourth positions of the duodenum only. This occurs in 31–53% of cases.
(d) Attachment to the duodenojejunal flexure only. This occurs in 0–8% of cases.
(Reproduced from Akin et al.[7])



Fig. 10–7. Left parasagittal section at a level lateral to the duodenojejunal junction.
Shown are the relationships of the proximal jejunal loops *(JL)* to the transverse colon *(TC)* and its mesocolon *(arrowheads),* coursing along the inferior aspect of the tail of the pancreas *(P).* The section is also through the spleen *(Sp)* and the left kidney *(LK).*
(Reproduced from Meyers and Whalen.[1])

small bowel loops posterior to the transverse colon normally possible (Fig. 10–8).

On the right, the colon inferiorly and the descending duodenum medially provide two of the boundaries of the posterior extension of the subhepatic space (Morison's pouch) anterior to the kidney (Fig. 10-1).

Abnormal Radiologic Features

Defect of Mesocolon with Internal Herniation into Lesser Sac

Occasionally, jejunal loops may normally present within the upper abdomen anterior to the transverse colon and, perhaps, the stomach. Cephalad extension of small bowel loops posterior to the transverse colon above the line of the root of the transverse mesocolon in relationship to the descending duodenum and duodenojejunal junction indicates a defect of that mesentery with internal herniation into the lesser sac[1] (Fig. 10–9).

Masses Within the Mesocolic Leaves

Pathologic alteration in the contour of the duodenum by a localized abnormality arising in the origin of the reflections of the transverse mesocolon is shown in Figure 10–10. The bare area is widest at this site so that symmetric growths developing within the leaves may impress upon the duodenum over a considerable length. The typical points of pressure then are at the immediate infraampullary and the genu locations.

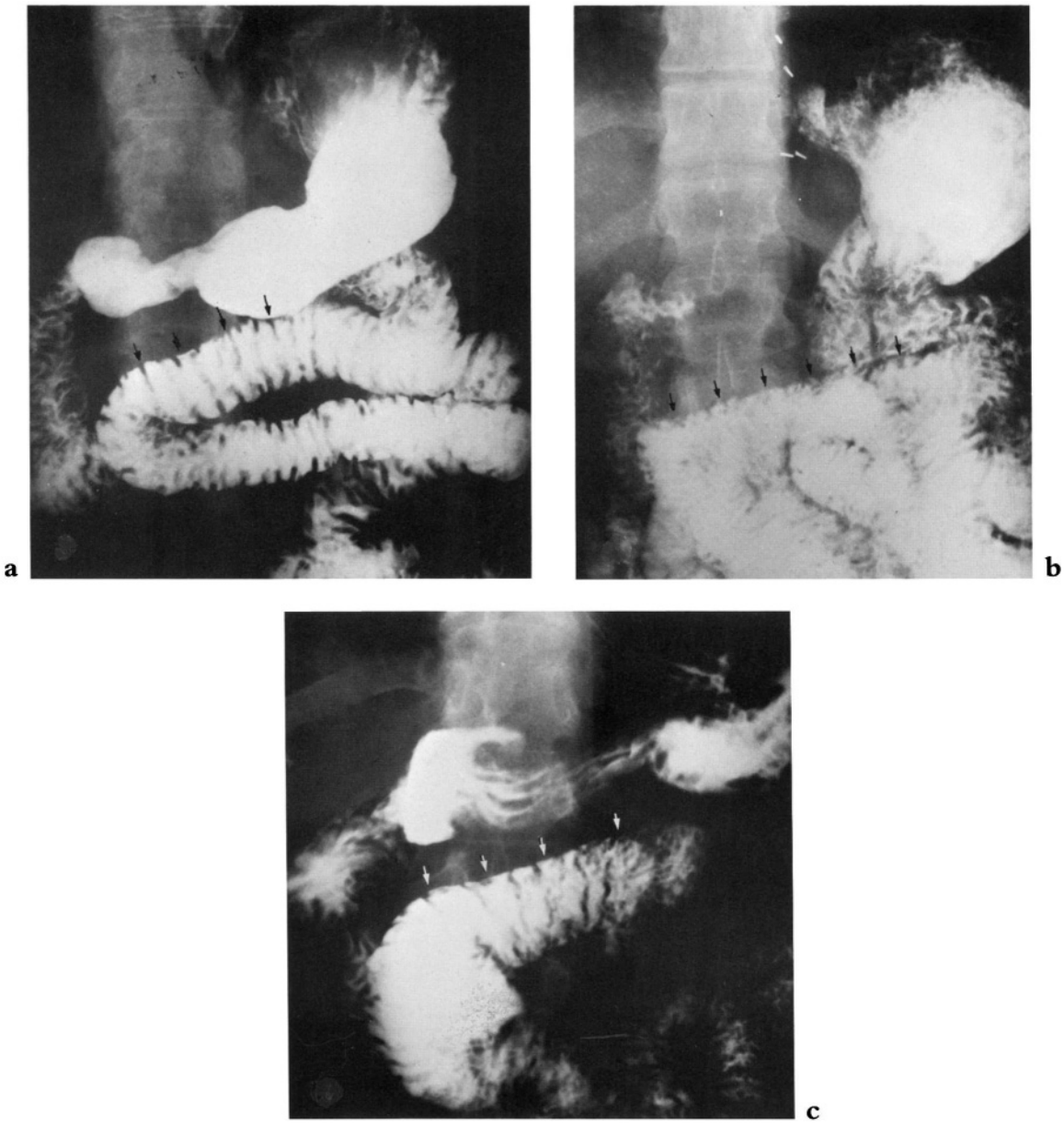


Fig. 10–8. The transverse mesocolon *(arrows)* is outlined by the limitation of cephalad extension of jejunal loops posterior to the transverse colon, resulting in flattening of their superior contour. It corresponds to a line drawn from the mid-descending duodenum to the duodenojejunal junction.
(a) Normal gastrointestinal series.
(b) Post-Billroth II antecolic gastrojejunostomy.
(c) Postduodenojejunostomy.
(Reproduced from Meyers and Whalen.[1])

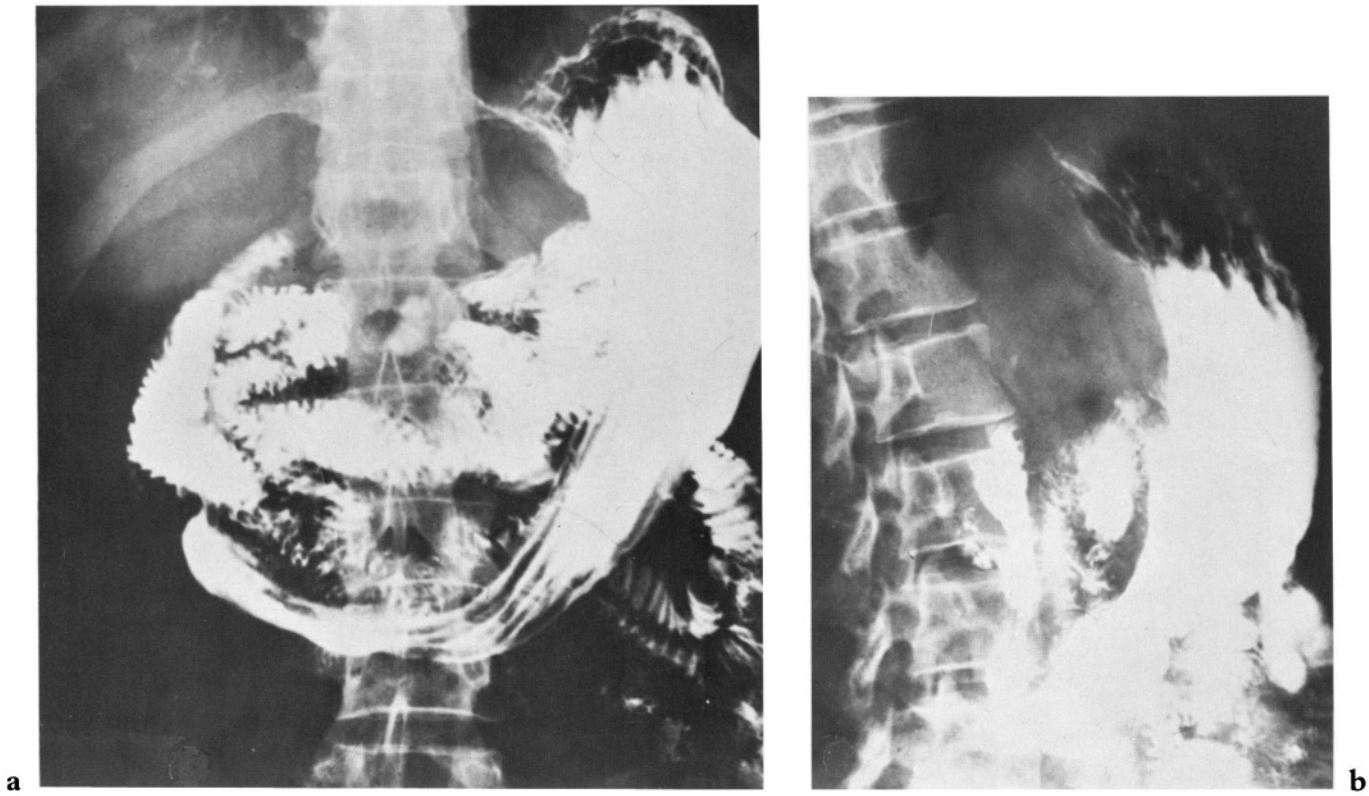


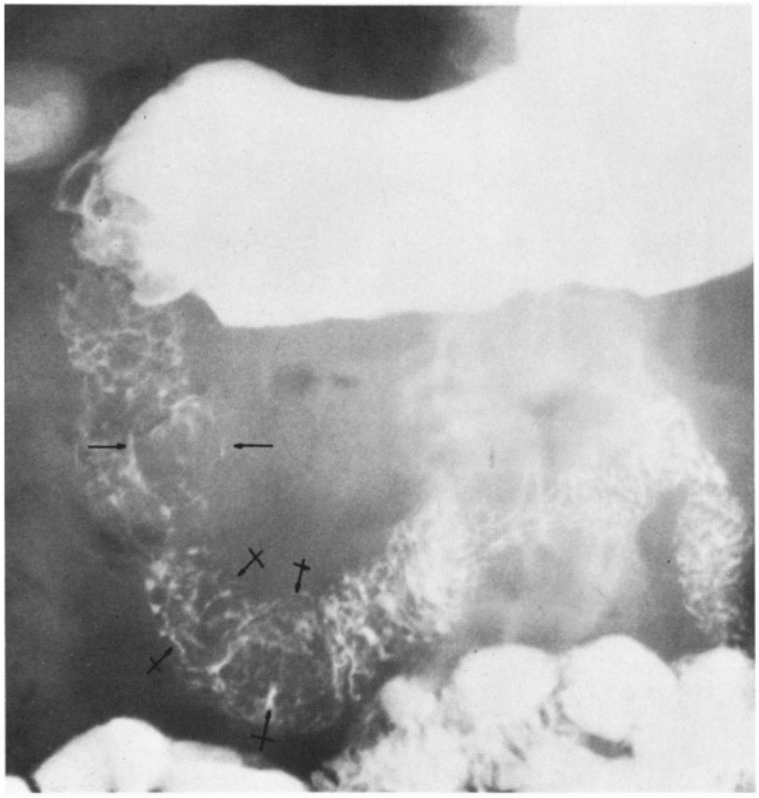
Fig. 10–9. Internal hernia into the lesser sac through a large defect in the transverse mesocolon.
This is indicated by the high position of the loops of small bowel above the normal insertion of the transverse mesocolon, which no longer determines their contour.
(a) Frontal.
(b) Prone oblique. Note that the herniated loops present posterior to the transverse colon and stomach.
(Reproduced from Meyers and Whalen.[1])

Effect upon the Descending Duodenum by Carcinoma of the Hepatic Flexure

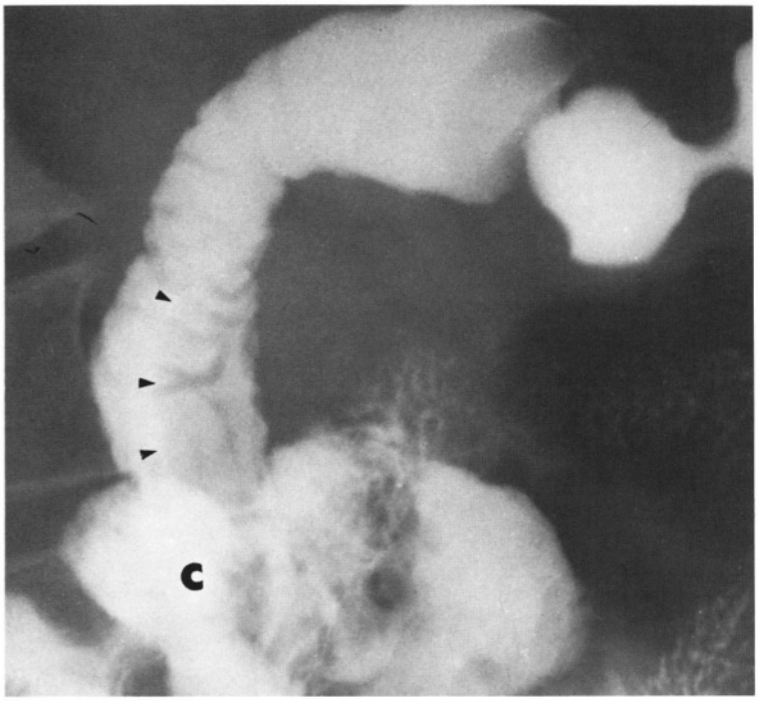
The virtual contiguity of the hepatic flexure to the descending duodenum allows ready spread of a neoplasm.[1,10] Figures 10–11 and 10–12 illustrate early stages of this process. The occult nature of carcinoma of the right colon is well known, and the presence of fever, abdominal distress, and a palpable epigastric mass may lead to radiologic investigation being initiated with an upper gastrointestinal series. In such cases, striking changes involving the descending duodenum may include extrinsic pressure defects and, occasionally, gas-containing cavities (Fig. 10–13a). These may be very misleading unless a barium enema study is done and the primary site in the hepatic flexure of the colon is revealed (Fig. 10–13b).

Duodenocolic Fistulas

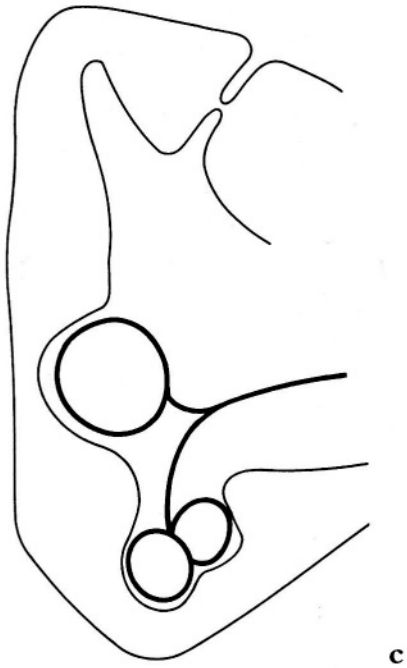
Although most duodenocolic fistulas result from an infiltrating adenocarcinoma of the hepatic flexure,[11] the communication may be established by ulcerative or inflammatory disease.[12–14] Granulomatous colitis is being increasingly recognized as an underlying cause.[13,14] With the right-sided colonic involvement of this transmural inflammatory and ulcerating condition, fistulization may develop between the hepatic flexure particularly or the transverse colon and the duodenum (Figs. 10–14 through 10–16). Malabsorption may result if the small bowel is bypassed significantly, but the fistula need not be a serious complication of Crohn's disease and should not serve as an indication for surgical correction for its own sake.[13–15] Intestinal tuberculosis is another chronic granulomatous disease that may result in fistulization[16,17]



a



b



c

Fig. 10–10. Lymphangitic cysts within the leaves of the transverse mesocolon producing extrinsic nodular indentations on the descending duodenum.
(a) Prone. Three discrete mass impressions are shown *(arrows).*
(b) Right lateral projection. The larger, more proximal indentation presents on the anterior aspect of the descending duodenum *(arrowheads).* Note its relationship to the hepatic flexure of the colon *(C).*
(c) Cysts within the mesocolon leaves bridging the bare area of the descending duodenum. (Reproduced from Meyers and Whalen.[1])



Fig. 10–11. Carcinoma of the hepatic flexure adherent to the descending duodenum.
Upper GI series shows pressure effects on the duodenum by a nodular malignancy within the hepatic flexure outlined by gas. At surgery, this required careful dissection.

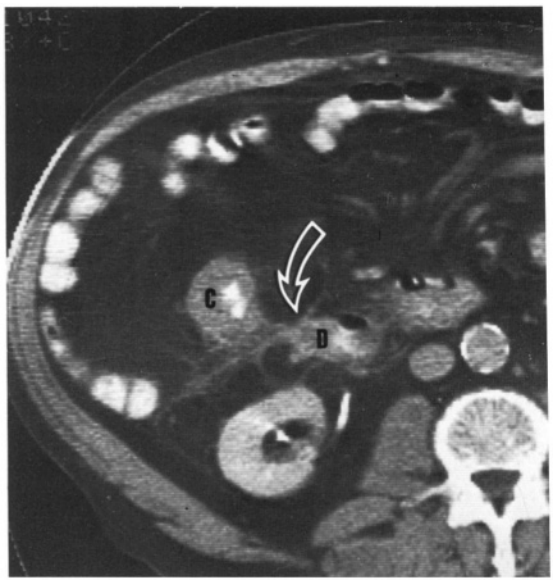


Fig. 10–12. Adherence of colonic carcinoma to duodenum.
Computed tomography shows early adhesive contiguity *(arrow)* to the inferior genu of the duodenum *(D)* of a carcinoma that thickens the wall of the hepatic flexure of the colon *(C).* Thickening of the anterior renal fascia and increased reticulation through the perirenal fat are noted.

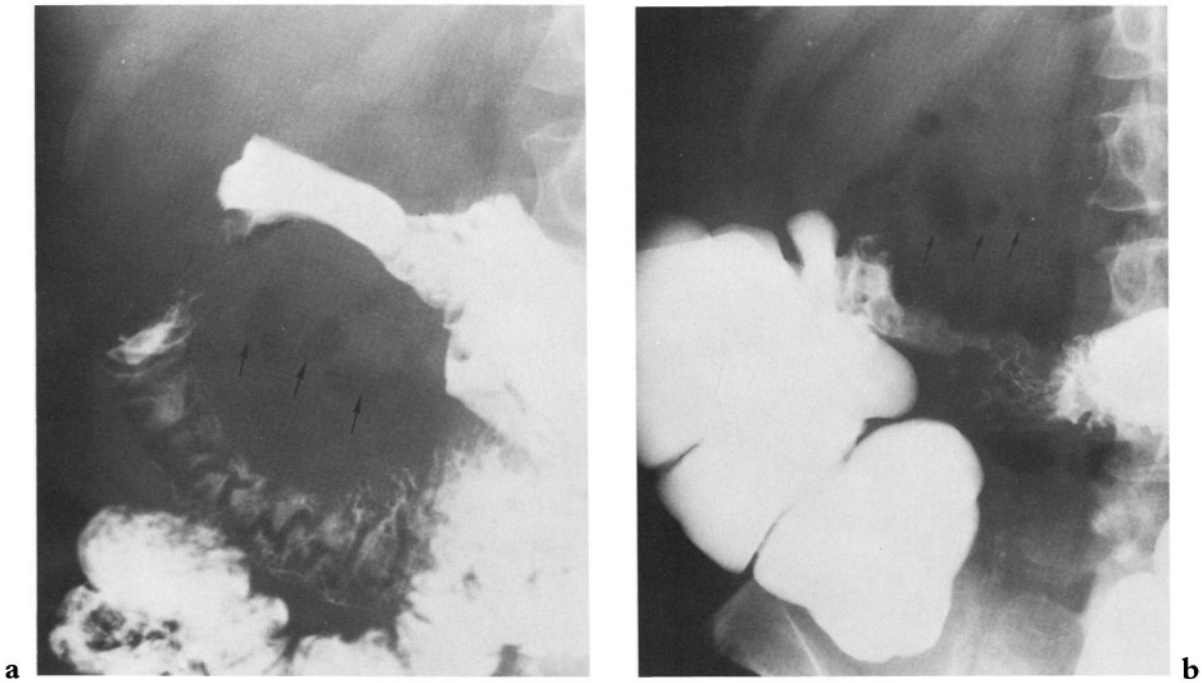


Fig. 10–13. Extension of colonic carcinoma across the mesocolon to the paraduodenal area.
(a) Upper gastrointestinal series reveals numerous gas-containing abscess cavities *(arrows)* within a mass in the area of the head of the pancreas. There are edema and distortion of the mucosal folds of the descending duodenum.
(b) A subsequent barium enema shows a primary infiltrating carcinoma of the anterior hepatic flexure with a pericolonic–paraduodenal abscess.

(Fig. 10–17). A similar duodenocolic fistula may be seen as a postoperative complication (Fig. 10–18).

Examples have been described of fistulous communication between the third part of the duodenum and the transverse colon, which contained a well-marked muscular layer and an intact epithelium. This rare variety is presumably on an embryologic basis.[18]

Effect of Gallbladder Disease on the Duodenocolic Relationships

The nonspecificity of signs and symptoms of diseases of the gallbladder often makes a clinical diagnosis difficult. At times, it is the striking manifestation of the secondary effects on the neighboring bowel that first brings the patient to medical attention.

Inflammatory adhesions may develop between the gallbladder and the postapical duodenum, permitting the development of fistulous communication (Fig. 10–19).

The gallbladder is closely applied to the superior aspect of the anterior hepatic flexure in most individuals[19] (Fig. 10–20). The distance between the inner walls of the gallbladder and the adjacent colon is normally less than 1.5 cm.

When the gallbladder enlarges, as in acute cholecystitis, hydrops, empyema, or Courvoisier's sign of pancreaticoduodenal malignancy, plain films or barium enema study may reveal smooth extrinsic compression of the hepatic flexure (Figs. 10–21 and 10–22). Accompanying pericholecystitis or marked fibrous adhesions may result in mucosal edema or fixation (Fig. 10–23). The postapical duodenum is characteristically displaced

text continues on page 556

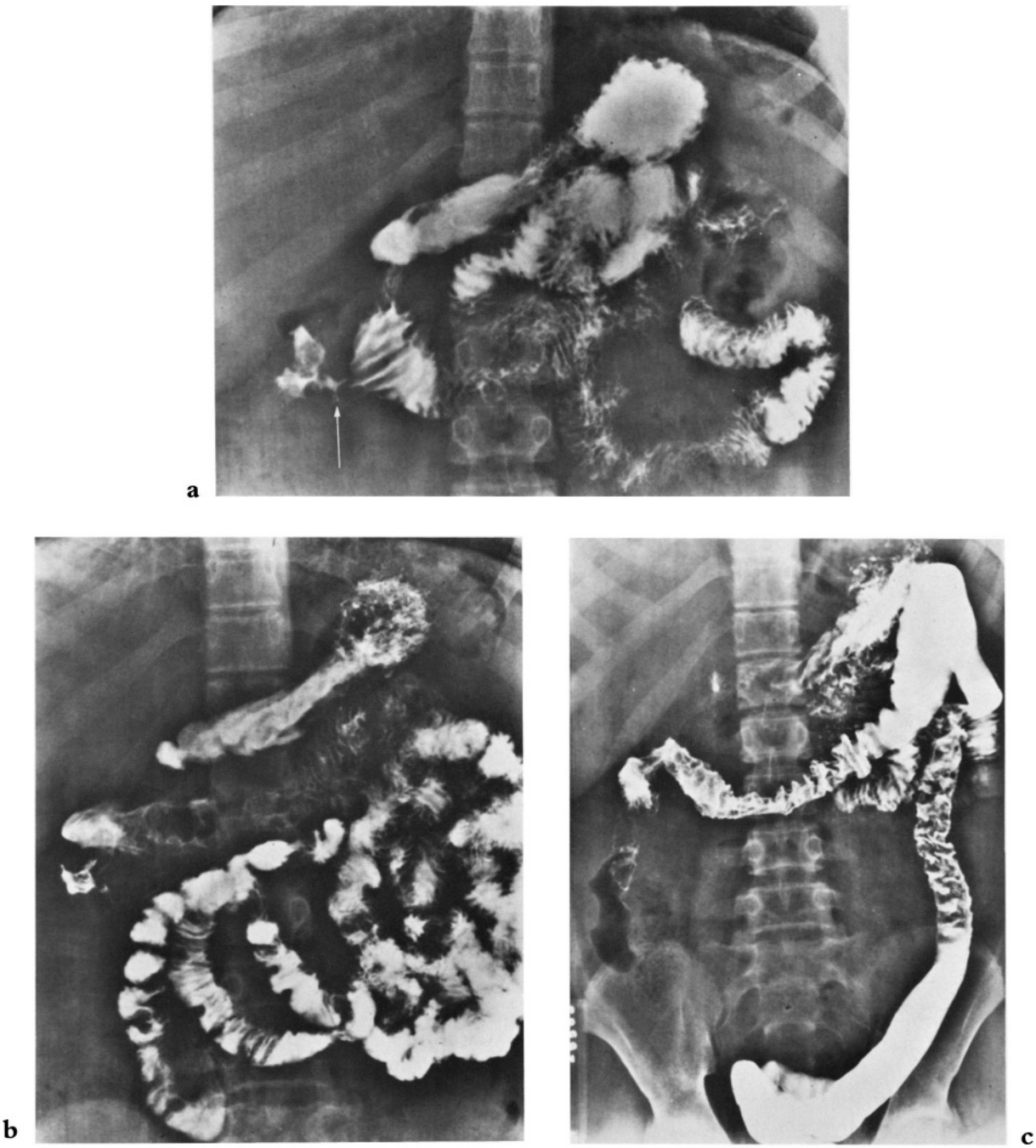


Fig. 10–14. Duodenocolic fistula secondary to granulomatous colitis.
Upper GI series demonstrates fistulous communication *(arrow)* from the infraampullary portion of the descending duodenum to the hepatic flexure, with premature opacification of the transverse colon. Crohn's disease of the large intestine is apparent.

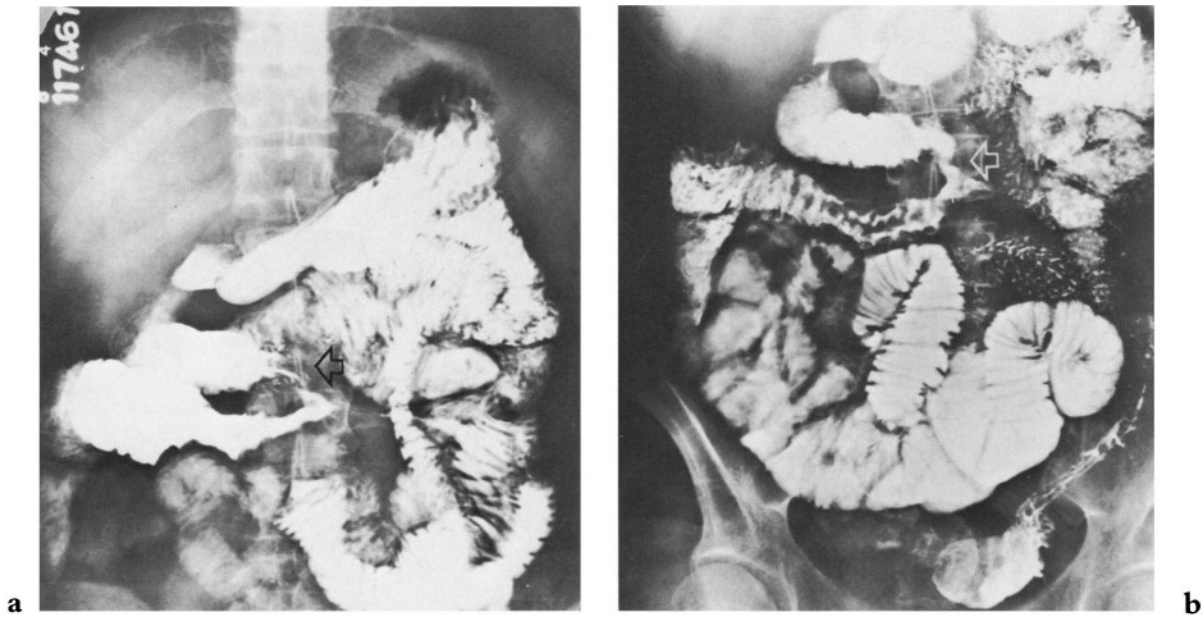


Fig. 10–15. Duodenocolic fistula secondary to granulomatous colitis.
(a and **b)** Upper GI series demonstrates wide communication *(arrows)* between the third portion of the duodenum and the transverse colon, which is involved by Crohn's disease. The partially bypassed small intestinal loops show changes of malabsorption.

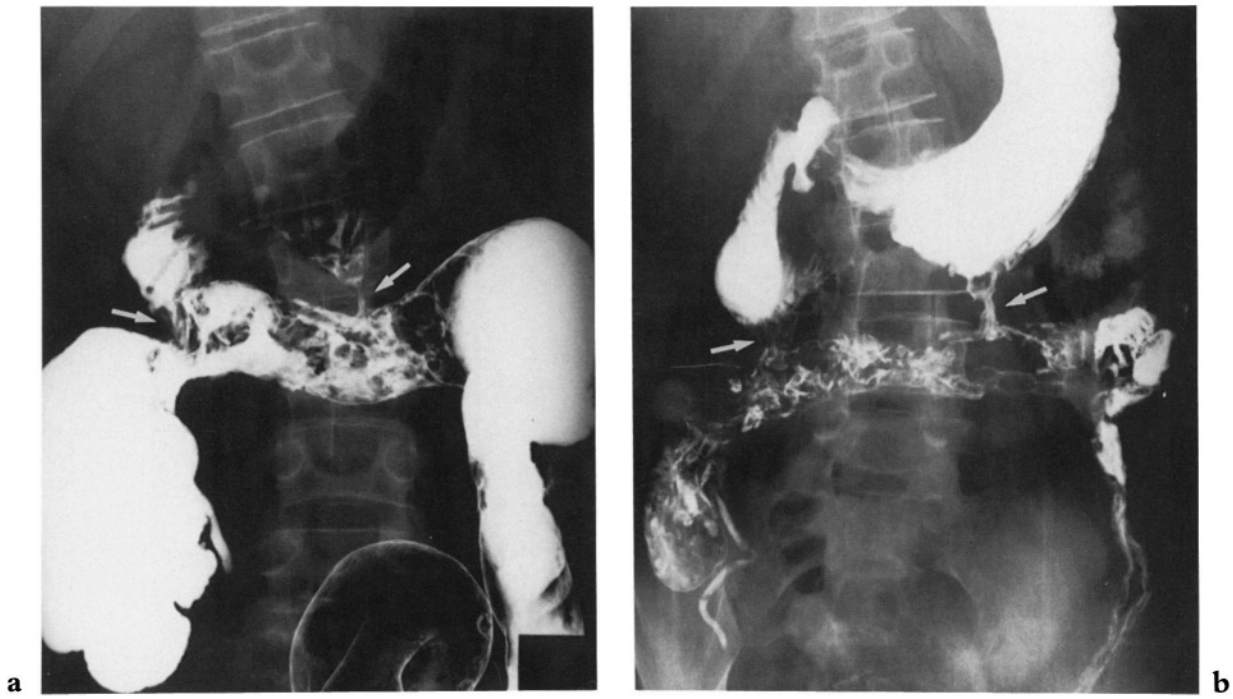


Fig. 10–16. Duodenocolic fistula secondary to granulomatous colitis.
Barium enema **(a)** and upper GI series **(b)** demonstrate fistulas between the hepatic flexure of the colon and the duodenum and between the transverse colon and the greater curvature of the stomach *(arrows).* Extensive Crohn's disease of the large intestine is evident.

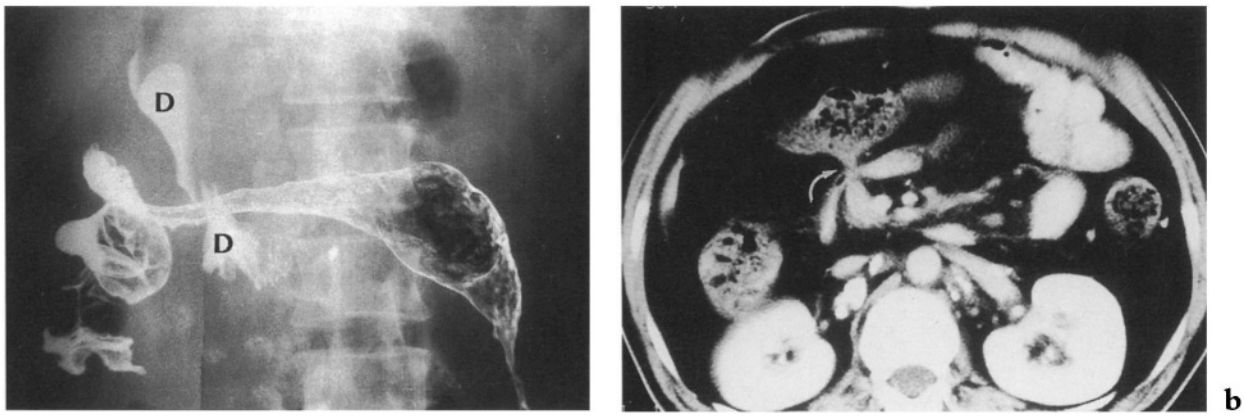
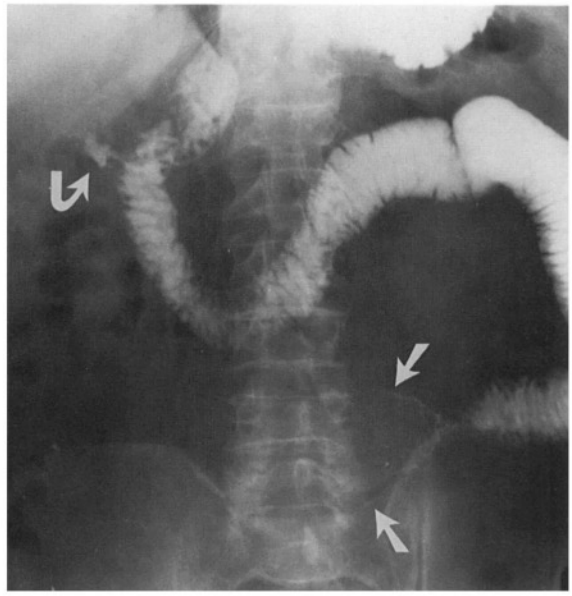


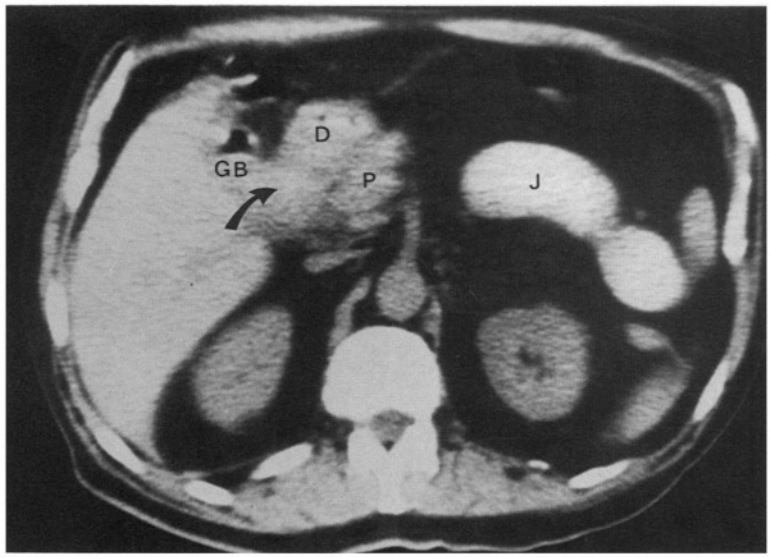
Fig. 10–17. Duodenocolic fistula secondary to intestinal tuberculosis.
(a) Barium enema demonstrates fistulization to the duodenum *(D)* from the colon, which has multiple areas of stricture with severe adhesions. The colonic wall is fibrotic and thin.
(b) CT clearly documents the duodenocolic fistula *(arrow)*.
(Reproduced from Ha et al.[17])



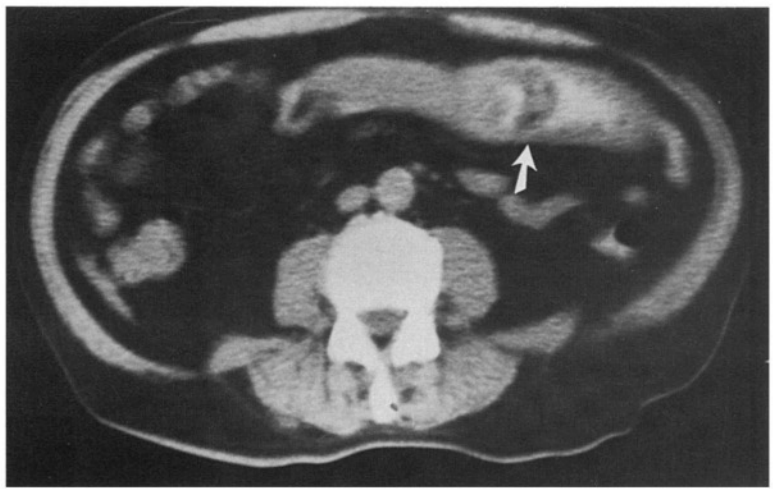
Fig. 10–18. Duodenocolic fistula from chronic "blow-out" of duodenal bulb.
Following a Billroth II gastrojejunostomy, a fistulous communication *(arrow)* has developed between the sewn-over duodenal bulb and the hepatic flexure of the colon.

Fig. 10–19. Cholecystoduodenal fistula with gallstone ileus.
(a) Upper GI series demonstrates tract *(curved arrow)* between the duodenum and gallbladder. A large gallstone is impacted in a proximal jejunal loop *(arrows).*
(b) CT shows inflammatory changes *(arrow)* between the duodenum *(D)* and the shrunken gallbladder *(GB),* which contains air. A dilated loop ofjejunum *(J)* is evident. *P* = pancreas.
(c) At a lower level, the partially calcified cholesterol gallstone within the obstructed loop is documented *(arrow).*


a



b


c

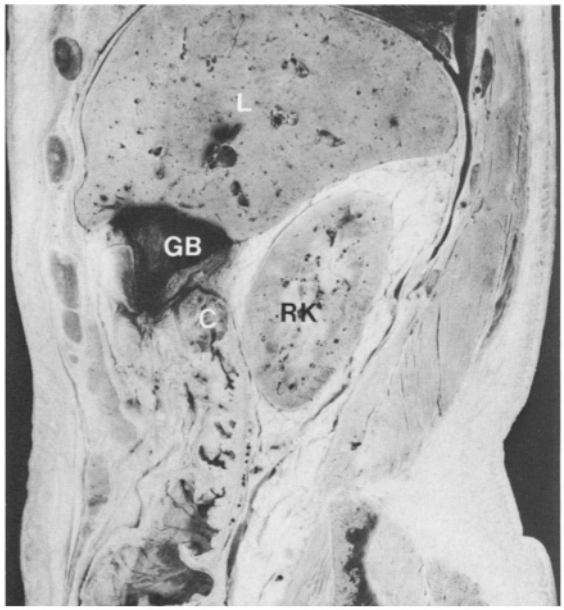


Fig. 10–20. Right parasagittal section, showing the close relationship of the gallbladder *(GB)* to the anterior hepatic flexure of the colon *(C). L* = liver; *RK* = right kidney.

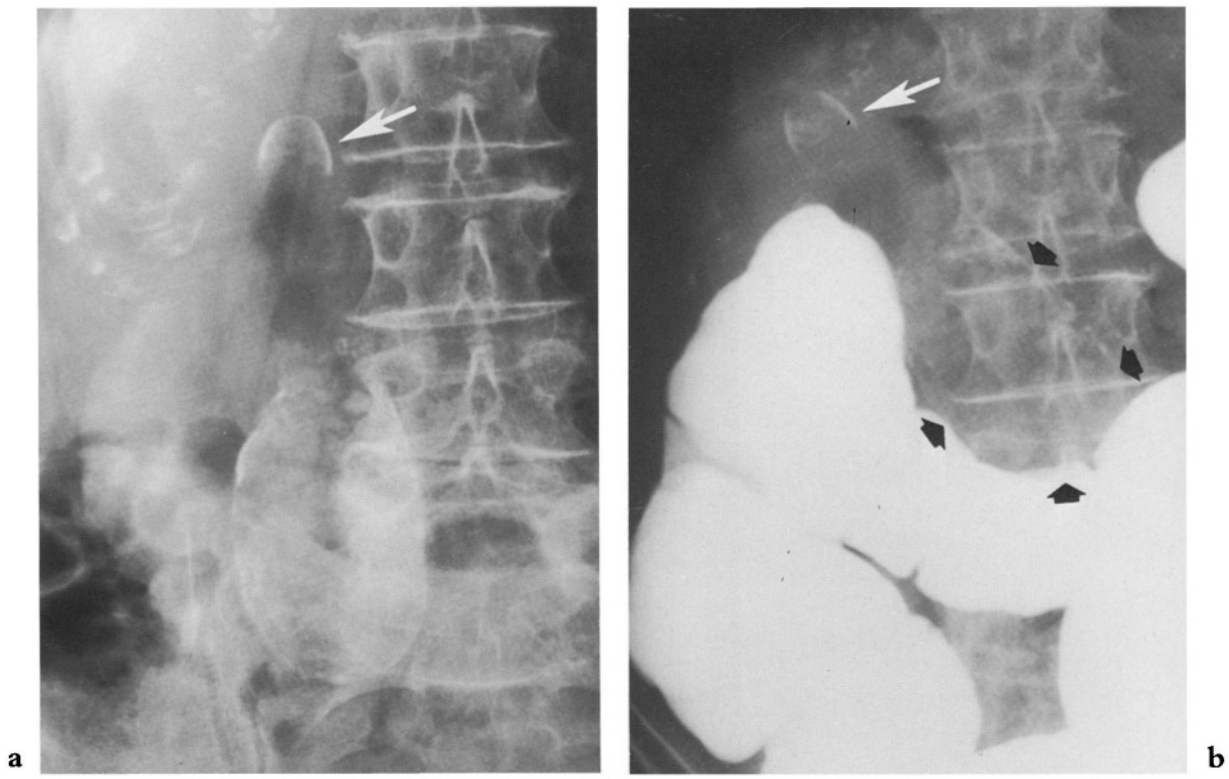


Fig. 10–21. Impression of adherent "porcelain" gallbladder.
(a) Plain film shows large calcified gallbladder with impacted stone in its neck *(arrow).*
(b) Barium enema study demonstrates displacement of gallbladder *(black arrows)* and impression upon anterior hepatic flexure to which it is adherent. *White arrow* shows impacted stone.
(Reproduced from Ghahremani and Meyers.[19])

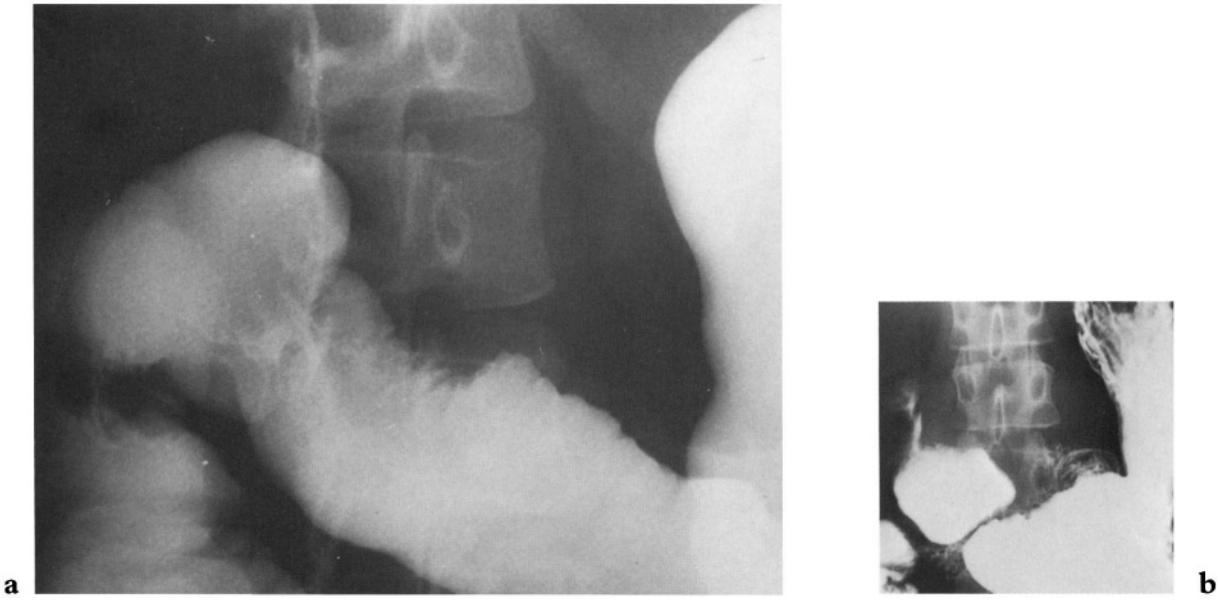


Fig. 10–22. Acute cholecystitis.
(a) Mass impression on superior aspect of anterior hepatic flexure, with mucosal irregularities.
(b) Medial displacement and spasm of proximal descending duodenum.
(Reproduced from Ghahremani and Meyers.[19])

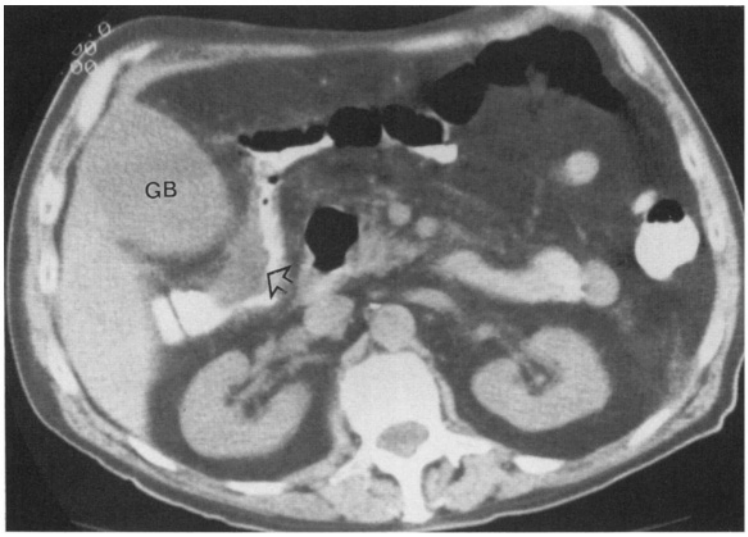


Fig. 10–23. Acute acalculous cholecystitis.
The inflammatory process of the gallbladder *(GB)* produces intramural edema within the superior aspect of the anterior hepatic flexure of the colon *(arrow)*.

medially and may show features of spasm, luminal narrowing, and mucosal irregularities. Carcinoma of the gallbladder commonly infiltrates all layers of its wall and rapidly extends into the surrounding structures. As many as 15% show evidence of colonic invasion on barium enema studies (Fig. 10–24). CT readily illustrates invasion of the colon (Fig. 10–25a) or duodenum (Fig. 10–25b). Fistulous communication between the duodenum and colon may occur from acute cholecystitis or carcinoma of the gallbladder[22,23] (Figs. 10–26 through 10–32).

text continues on page 560

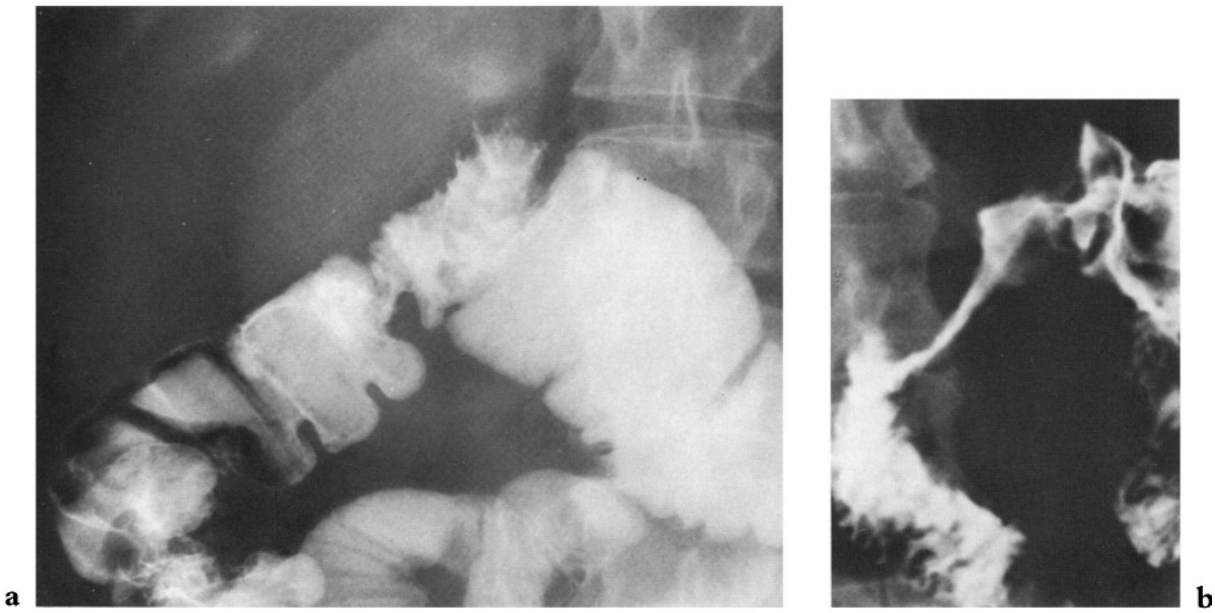


Fig. 10–24. Carcinoma of the gallbladder.
(a) Fixation of mucosal folds of anterior hepatic flexure.
(b) Marked compression, narrowing, and medial displacement of the proximal descending duodenum. (Reproduced from Ghahremani and Meyers.[19])

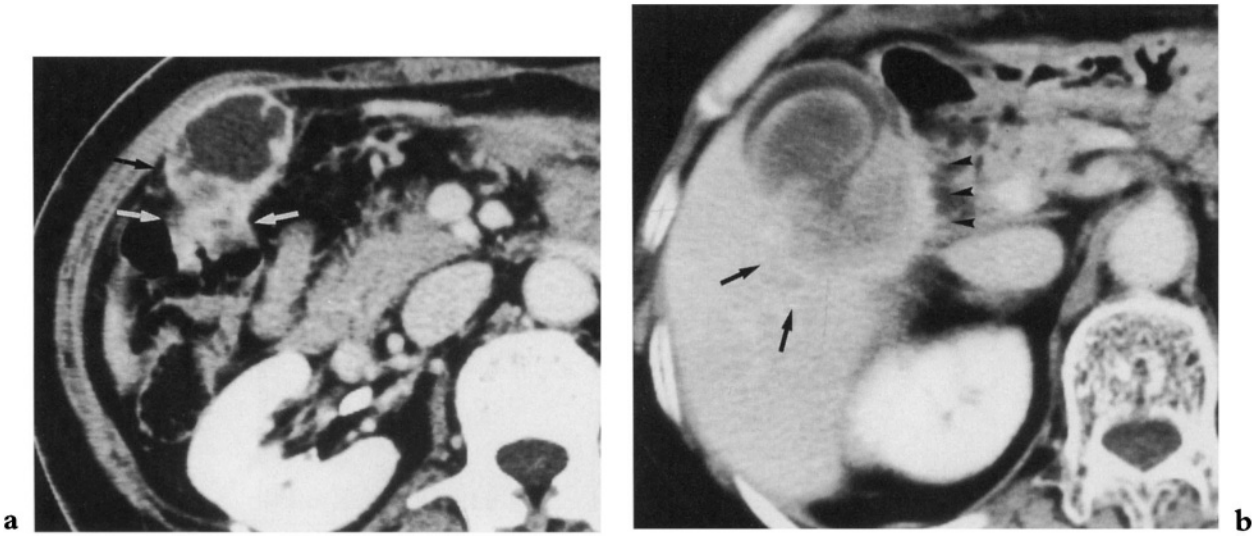


Fig. 10–25. Gallbladder carcinoma invading the colon (a) and duodenum (b) in two different cases.
(a) CT demonstrates irregular thickening of the gallbladder wall *(black arrow)* and direct extension to the hepatic flexure of the colon *(white arrows).* (Reproduced from Ohtani et al.[20])
(b) CT shows an intraluminal mass of the gallbladder extending into the hepatic parenchyma *(arrows).* Contrast enhancement of the lateral wall of the descending duodenum *(arrowheads)* indicates direct invasion. (Reproduced from Ohtani et al.[21])

Fig. 10–26. Cholecystoduodenal fistula secondary to chronic cholecystitis.
Enhanced CT demonstrates a narrow fistula *(small arrow)* between the contracted gallbladder *(black arrow)* and the duodenum *(white arrow).*
(Reproduced from Shimono et al.[23])

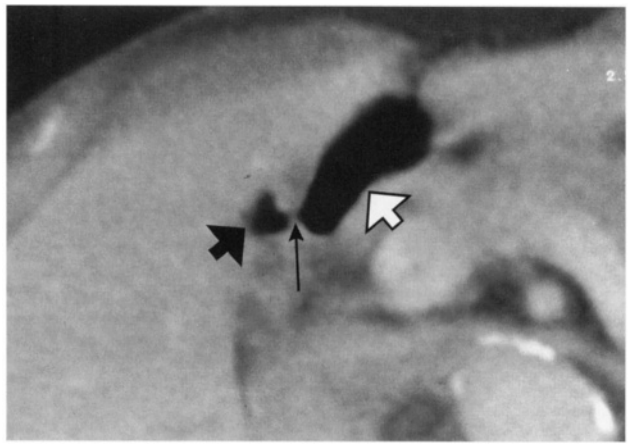




Fig. 10–27. Cholecystoduodenal fistula.
Enhanced CT shows air–fluid levels in the contracted gallbladder *(black arrow),* the result of a fistula from the duodenum *(white arrow).*
(Reproduced from Shomono et al.[23])

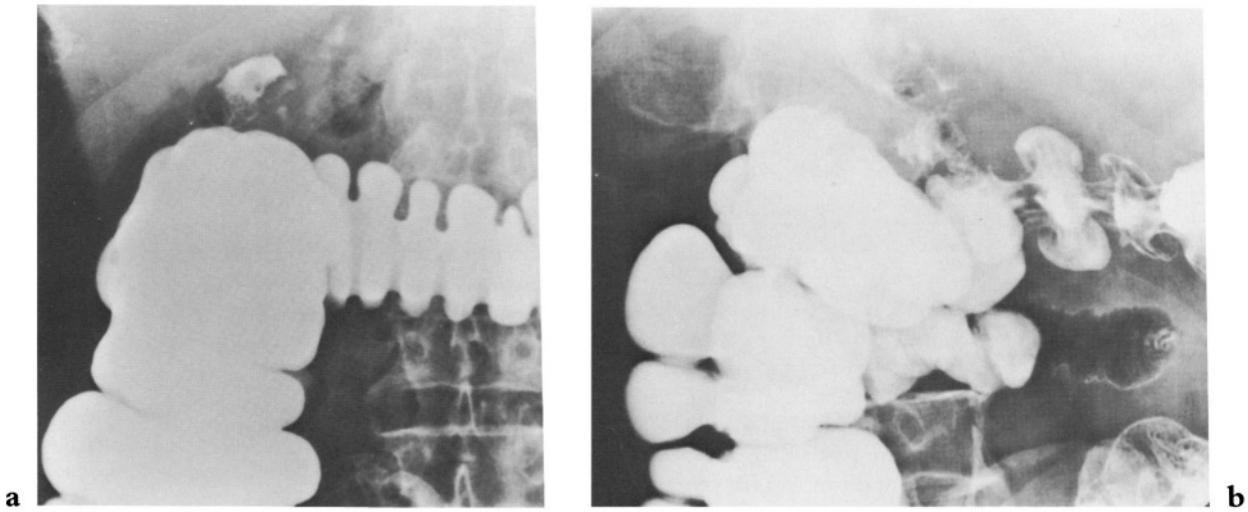


Fig. 10–28. Cholecystocolic fistula secondary to chronic cholecystitis.
(a) Frontal and **(b)** oblique views during a barium enema study demonstrate communication between the anterior hepatic flexure and a small deformed gallbladder.

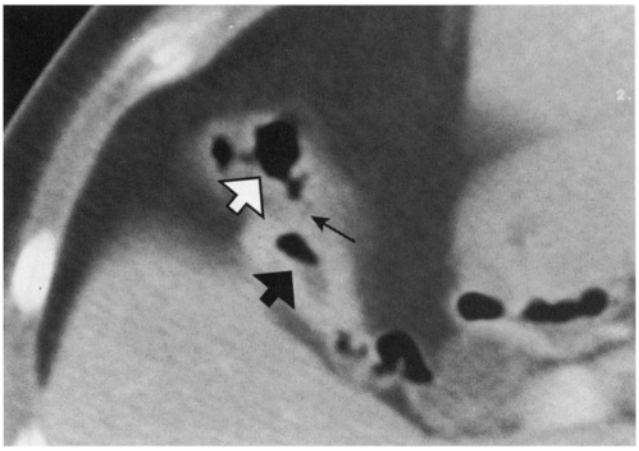


Fig. 10–29. Cholecystocolic fistula.
Enhanced CT demonstrates a narrow fistula *(small arrow)* between the gallbladder *(black arrow)* and the colon *(white arrow).*
(Reproduced from Shimono et al.[23])

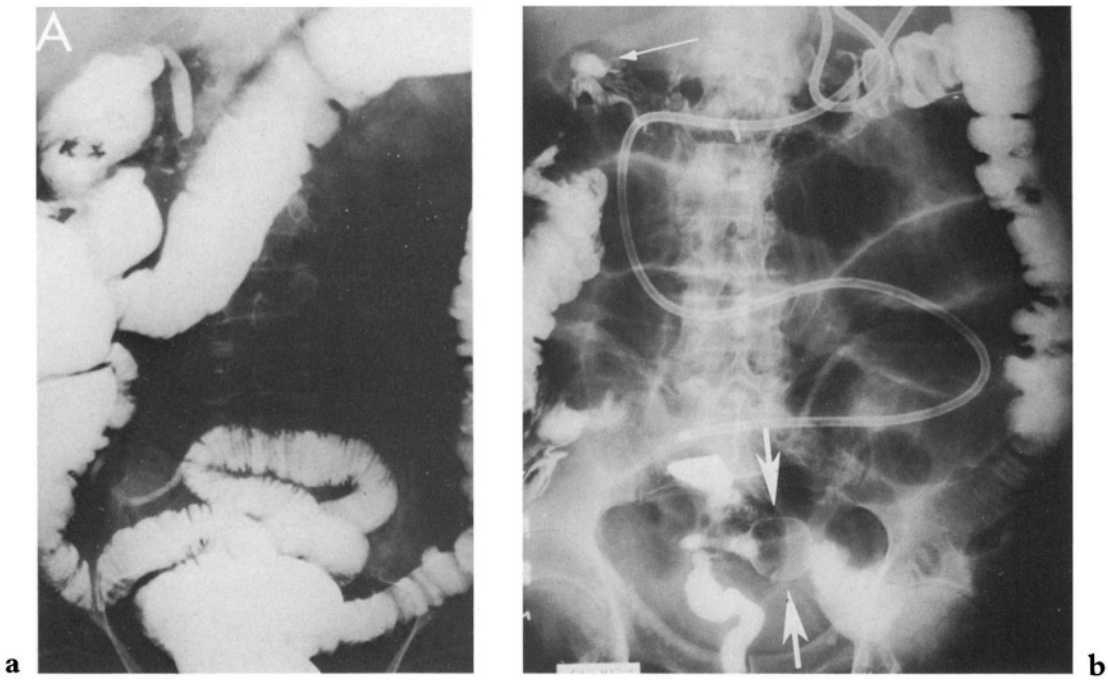


Fig. 10–30. Cholecystocolic fistula complicating chronic cholecystitis in two patients.
(a) Barium enema study demonstrates a wide communication between the fundus of the gallbladder containing stones and the adherent hepatic flexure.
(b) Gallstone ileus due to impaction of large nonopaque gallstones *(large arrows)* in the sigmoid colon with distended intestinal loops proximally. The Cholecystocolic fistula and the shrunken gallbladder *(small arrow)* are partially opacified with barium.
(Reproduced from Ghahremani and Meyers.[19])

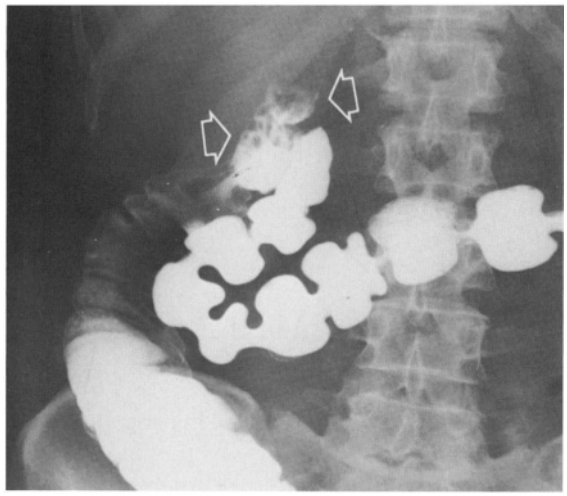


Fig. 10–31. Cholecystocolic fistula secondary to carcinoma of the gallbladder.
Barium enema study demonstrates the malignancy infiltrating the anterior hepatic flexure and projecting within the partially opacified gallbladder lumen *(arrows).*

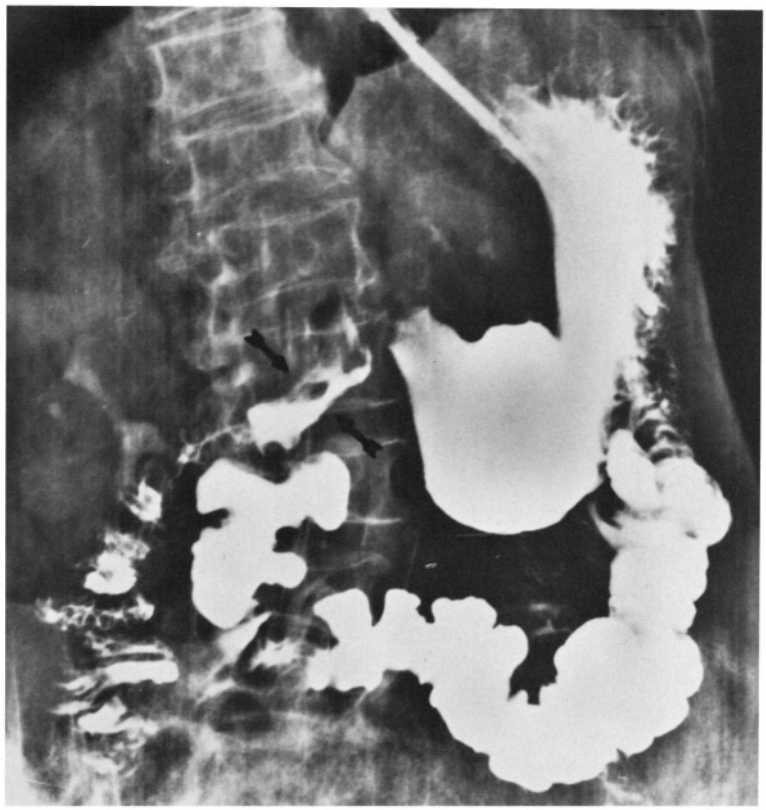


Fig. 10–32. Carcinoma of the gallbladder with duodenocolic fistula.
Upper GI series demonstrates the communication to the hepatic flexure of the colon across the malignant bed of the gallbladder *(arrows).*
(Reproduced from Ghahremani and Meyers.[19])

Duodenocolic Displacements from Right Renal Masses

The right kidney bears intimate relationships to both the descending duodenum and the region of the hepatic flexures of the colon. Renal masses may thus be revealed by their characteristic effects on the bowel. This is discussed in Chapter 9.

Effect on Colon of Mass Arising in Descending Duodenum

It has been shown that the distal hepatic flexure is in intimate relationship posteriorly to the descending duodenum. Localized anterior displacement of this portion of the colon then indicates a mass arising not in the nearby right kidney or gallbladder but specifically in the second portion of the duodenum.[19] Following identification of the displacement on an initial barium enema study, radiologic investigation can then be immediately directed to the primary site.

Inframesocolic Extension of Neoplasm of Third Duodenum

The third portion of the duodenum lies retroperitoneally below the root of the transverse mesocolon. Extension of a mass arising in this structure is then revealed on barium enema examination by a characteristic elevation of the proximal transverse colon (Fig. 10–33a). While this type of displacement may occur secondary to such conditions as mesenteric cysts or primary ret-

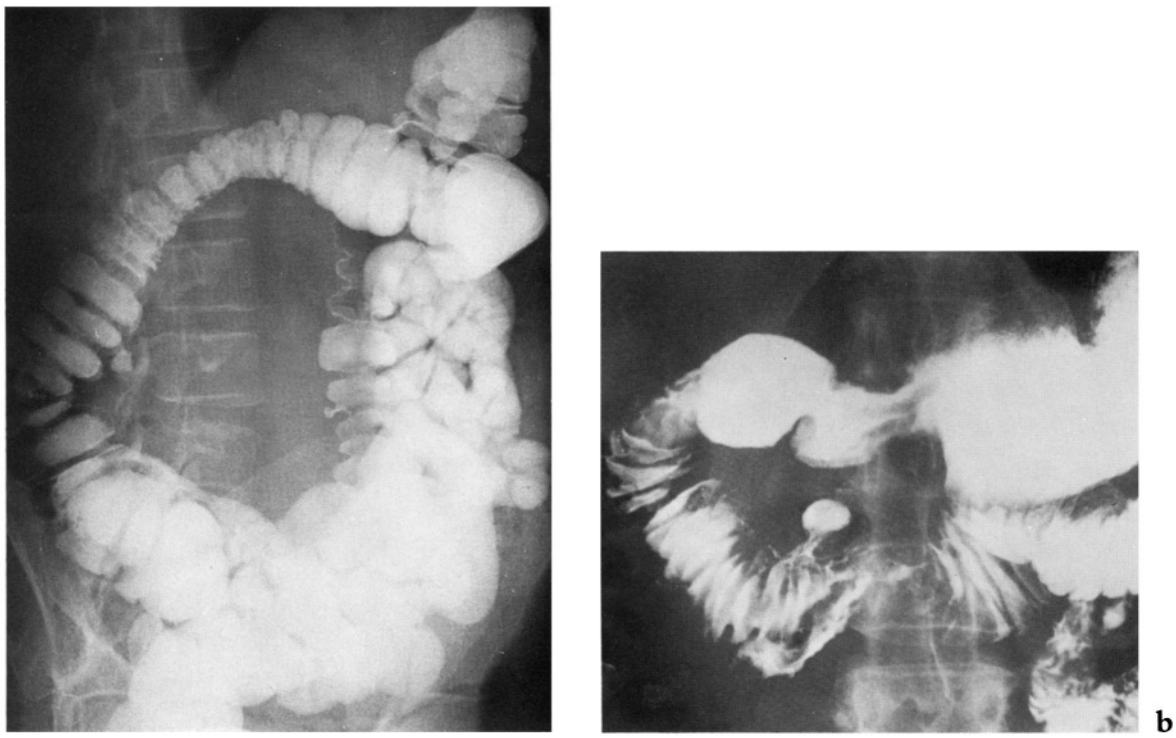


Fig. 10–33. Leiomyosarcoma of third portion of the duodenum with large extramural component.
(a) There is gross elevation and displacement of the proximal transverse colon by a huge mass.
(b) Upper GI series documents the changes of leiomyosarcoma arising in the transverse duodenum, characterized by irregular ulcerations and sinus tracts within a lobulated and serpiginous submucosal tumor. (Reproduced from Meyers.[24])

roperitoneal tumors, initial identification of this inframesocolic component should lead to careful investigation of the transverse duodenum (Fig. 10–33b).

Acute Pancreatitis

Several of the plain film changes associated with acute pancreatitis, while strongly suggestive of the diagnosis, are by no means pathognomonic. Ileus of the transverse colon in a pattern approaching the "colon cut-off" sign may be seen in a variety of conditions.[1] "Sentinel-loop" dilatation of the descending duodenum may occur secondary to acute cholecystitis or acute right perinephritis. However, simultaneous paralytic dilatation of both, secondary to the effects of the extravasated enzymes along the shared anatomic planes, is diagnostic of acute pancreatitis (Fig. 10–34).

Duodenojejunal Junction: Relation to Colon

The intimate relationship of the duodenojejunal junction superiorly to the root of the transverse mesocolon as it extends across the pancreas is of importance in the identification of both locally arising processes and remote colonic pathology.

At this level, the mesocolon is generally long enough so that the transverse colon is considerably anterior. It is then apparent that minor effects on the distal transverse colon on an initial barium enema study may be shown to reflect a process that predominantly involves the ascending duodenum or duodenojejunal junction (Figs. 10–35 and 10–36).



Fig. 10–34. Acute pancreatitis.
The radiologic finding of associated ileus of the transverse colon and of the descending duodenum (shown by stasis of barium within the dilated loop, here superimposed upon the gas-distended transverse colon) is diagnostic of this condition.

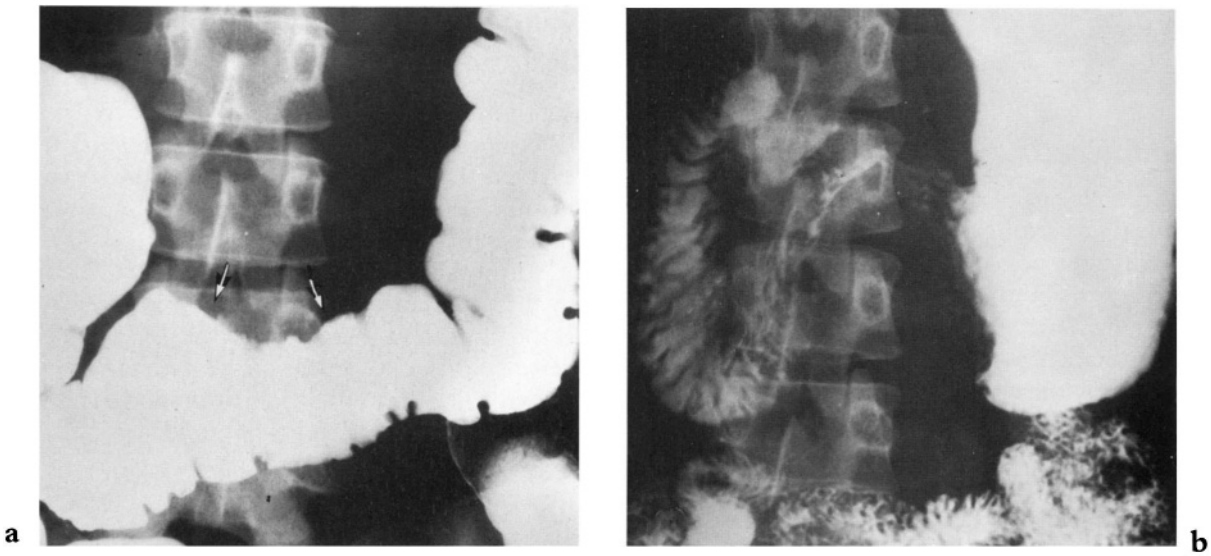


Fig. 10–35. Cyst of the posterior parietal peritoneum below the root of the mesocolon.
(a) Mild extrinsic pressure effect on the superior contour of the transverse colon *(arrows).*
(b) Gross medial displacement of the fourth portion of the duodenum and duodenojejunal junction, with pressure on the greater curvature of the gastric antrum.
(Reproduced from Meyers and Whalen.[1])

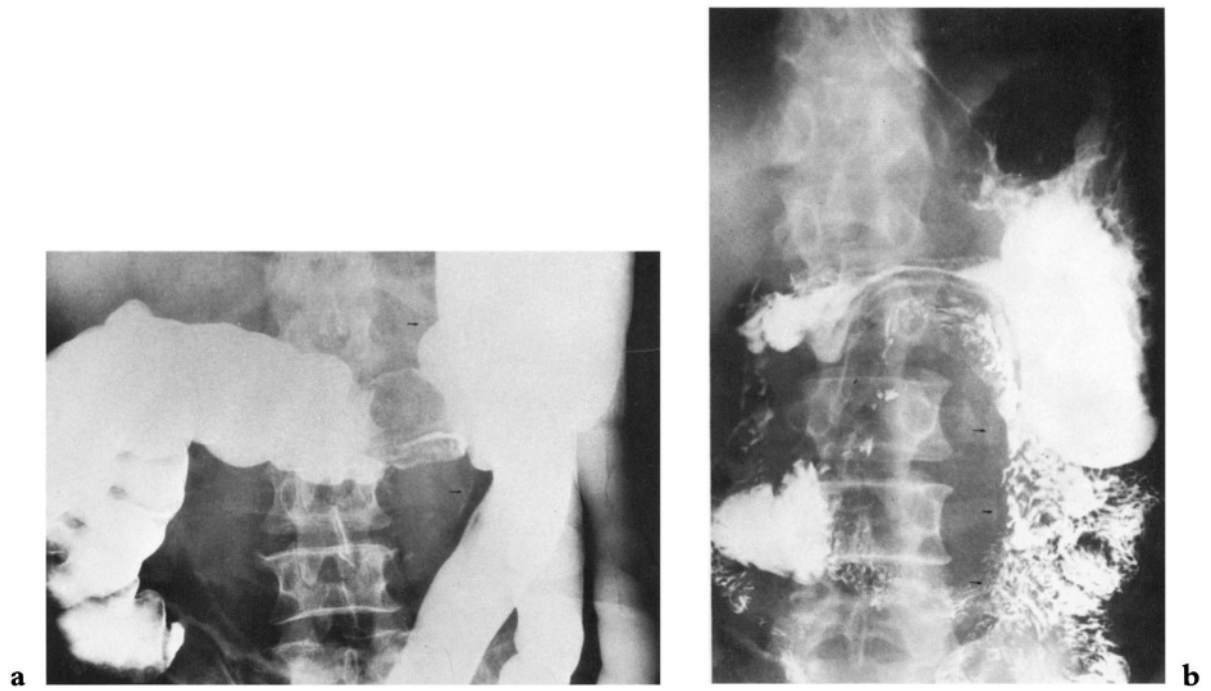


Fig. 10–36. Large calcified aneurysm of the abdominal aorta *(arrows).*
(a) There is mild pressure on the transverse colon, but **(b)** marked medial displacement of the ascending duodenum and superior displacement of the duodenojejunal junction.
(Reproduced from Meyers and Whalen.[1])

References

1. Meyers MA, Whalen JP: Roentgen significance of the duodenocolic relationships: An anatomic approach. AJR 1973; 117:263–274.
2. Whalen JP, Riemenschneider PA: Analysis of normal anatomic relationships of colon as applied to roentgenographic observations. AJR Rad Ther Nucl Med 1967; 99:55–61.
3. Meyers MA: Treitz redux: The ligament of Treitz revisited. Abdom Imaging 1995; 29:421–424.
4. Chou CK, Chang JM, Tsai TC, et al: CT of the duodenojejunal junction. Abdom Imaging 1995; 20:425–430.
5. Fox RS, Fox CG, Graham W III: Václav Treitz (1819–1872): Czechoslovakian pathoanatomist and patriot. World J Surg 1985; 9:361–366.
6. Treitz W: Uber Einen Neven Muskel Am Duodenum. Vjschr prakt Heilk (Prague) 1853; 37:113–144.
7. Akin JT Jr, Gray SW, Skandalakis JE: Vascular compression of the duodenum: Presentation of ten cases and review of the literature. Surgery 1976; 79:515–522.
8. van der Zypen E, Révész E: Investigation of development, structure and function of the phrenicocolic and duodenal suspensory ligaments. Acta Anat 1984; 119:142–148.
9. Friedman SM: Position and mobility of duodenum in living subject. Am J Anat 1946; 79:147–165.
10. Treitel H, Meyers MA, Maza V: Changes in the duodenal loop secondary to carcinoma of the hepatic flexure of the colon. Br J Radiol 1970; 43: 209–213.
11. Vieta JO, Blanco R, Valentini GR: Malignant duodenocolic fistula: Report of two cases, each with one or more other synchronous gastrointestinal cancers. Dis Colon Rectum 1976; 19:542–552.
12. Perri F, Annese V, Federici T, et al: Benign duodenocolic fistula: An unusual cause of gastrointestinal bleeding. Gastrointest Endosc 1993; 39:827–830.
13. Korelitz BI: Colonic-duodenal fistula in Crohn's disease. Dig Dis 1977; 22:1040–1048.
14. Jacobson IM, Schapiro RH, Warshaw AL: Gastric and duodenal fistulas in Crohn's disease. Gastroenterology 1985; 89:1347–1352.
15. Herlinger H, O'Riordan D, Saul S, et al: Nonspecific involvement of bowel adjoining Crohn disease. Radiology 1986; 159:47–51.
16. Tandon HD, Prakash A: Pathology of intestinal tuberculosis and its distinction from Crohn's disease. Gut 1972; 13:260–269.
17. Ha HK, Ko GY, Yu ES, et al: Intestinal tuberculosis with abdominal complications: Radiologic and pathologic features. Abdom Imaging 1999; 24:32–38.
18. Torrance B, Jones C: Three cases of spontaneous duodenocolic fistula. Gut 1972; 13:627–630.
19. Ghahremani GG, Meyers MA: The cholecystocolic relationships: A roentgen-anatomic study of the colonic manifestations of gallbladder disorders. AJR 1975; 125:21–34.
20. Ohtani T, Shirai Y, Hatakeyama K: Diagnosis and staging of gallbladder carcinoma by computed tomography. *In* Neoplasms of the Digestive Tract: Imaging, Staging and Management. Edited by MA Meyers. Lippincott-Raven, Philadelphia, 1998, pp 485–492.
21. Ohtani T, Shirai Y, Tsukada K et al: Spread of gallbladder carcinoma: CT evaluation with pathologic correlation. Abdom Imaging 1996; 21:195–201.
22. Wolloch Y, Glanz I, Dintsman M: Spontaneous biliary-enteric fistulas: Some considerations on the management of gallstones. Am J Surg 1976; 131: 680–683.
23. Shimono T, Nishimura K, Hayakawa K: CT imaging of biliary enteric fistula. Abdom Imaging 1998; 23:172–176.
24. Meyers MA: Leiomyosarcoma of the duodenum: Radiographic and arteriographic features. Clin Radiol 1971; 22:257–260.

Intestinal Effects of Pancreatitis: Spread Along Mesenteric Planes

11

Acute inflammation of the pancreas may be classified into four groups:

1. *Acute edematous pancreatitis* is the most common form; there is localized or diffuse swelling of the organ.
2. *Acute hemorrhagic pancreatitis* is caused by the digestive effects of liberated trypsin and elastase on pancreatic vessels. The first changes caused by this vascular necrosis are found in the outer layer, but the damage usually progresses rapidly to involve the entire thickness of the vessel wall, with disruption of the intima.[1]
3. *Acute gangrenous pancreatitis* is rare because of the rich vascularization of the pancreas.
4. *Acute suppurative pancreatitis* secondary to superimposed infection may range from a localized pancreatic abscess to diffuse involvement, perhaps as a gas-producing process.

Localized changes on characteristic portions of the small intestine and colon are produced by the extravasated enzymes of pancreatitis, which follow definite anatomic planes.[2] The lesions range from transient spasm to ischemic atrophy and the development of obstructive strictures as well as remote exudative abscesses. Extension of the effects of pancreatitis may occur through the loose retroperitoneal tissue planes of the anterior pararenal spaces. Notably, however, the mesenteric pathways most often involved and that direct the spread of pancreatic enzymes to remote sites in the intestinal tract are the transverse mesocolon and the small bowel mesentery. These observations have been confirmed by computed tomography.[3–5] Fat necrosis is most common in these two sites and in the omentum.[6]

Anatomic Considerations

Virtually all of the pancreas is an extraperitoneal organ. However, a nonperitonealized bare area results from the reflections of the posterior parietal peritoneum to form the two leaves of the transverse mesocolon.[7] This extends across the lower border of the organ anteriorly (Fig. 11–1). On the right, the transverse mesocolon begins at the point where the anterior hepatic flexure of the colon immediately crosses ventral to the second portion of the duodenum. The bare area then extends as a broad strip across the infraampullary portion of the descending duodenum and continues across the head, body, and tail of the pancreas. The ascending colon and the proximal, more posterior hepatic flexure are completely extraperitoneal.

Significantly, the tail of the pancreas, after extending across the left kidney, is actually intraperitoneal in that it is incorporated or ensheathed within the leaves of the splenorenal ligament. By definition, any structure within a mesenteric attachment is intraperitoneal. Anatomic continuity is established by the peritoneal reflections constituting the supporting ligaments of the left upper quadrant. Figures 11–2 and 11–3 show the relationships of the tail of the pancreas within the splenorenal ligament to the transverse mesocolon, phrenico-

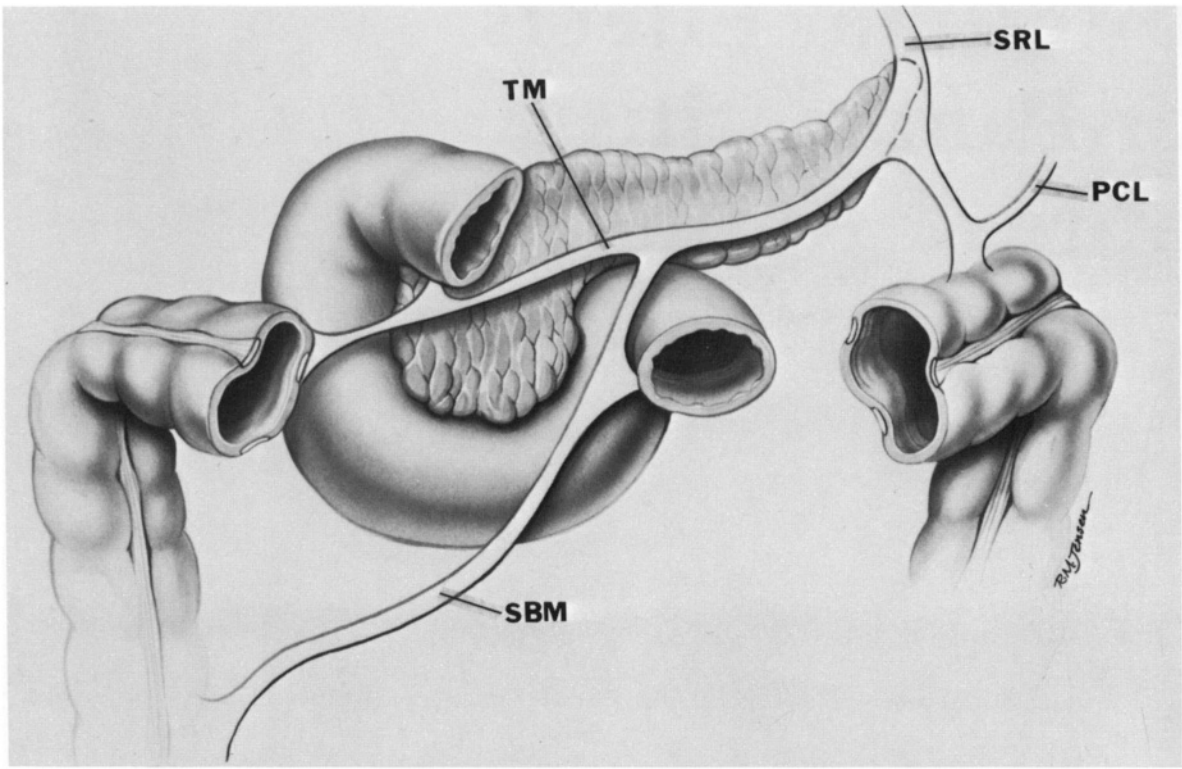


Fig. 11–1. Mesenteric relationships of the pancreas.
Frontal drawing shows the relationships of the transverse mesocolon *(TM)* and its continuity with the small bowel mesentery *(SBM),* splenorenal ligament *(SRL),* and phrenicocolic ligament *(PCL).*
(Reproduced from Meyers and Evans.[2])

colic ligament, and the peritoneal reflections of the descending colon. The phrenicocolic ligament[8] is attached to the anatomic splenic flexure of the colon at the omental and mesocolic taeniae.[9] It represents the most lateral continuity of the transverse mesocolon and splenorenal ligament and thereby marks the site of transition from the intraperitoneal transverse colon to the extraperitoneal descending colon.

Of further clinical significance is the fact that the root of the small bowel mesentery, at its origin near the inferior portion of the pancreas, is anatomically continuous with that of the transverse mesocolon (Fig. 11–1). At this point, it is in relationship to the midportion of the transverse duodenum. It then extends obliquely toward the right lower quadrant to insert, most often, at the cecocolic junction. Thus, anatomic continuity is established along the root of the mesentery from the pancreas to the third portion of the duodenum, jejunal loops, ileal loops, and cecum.

In this way, mesenteric planes are provided for the direct spread of extravasated pancreatic enzymes (Figs. 11–4 and 11–5):

1. Along the mesocolon to the transverse colon. Extension along its planes to its lateral limits proceeds (a) on the right, to the hepatic flexure and perhaps the distal ascending colon, and (b) on the left, to the anatomic splenic flexure just below the tip of the spleen.
2. Along the small bowel mesentery to jejunal loops and the ileocecal region.

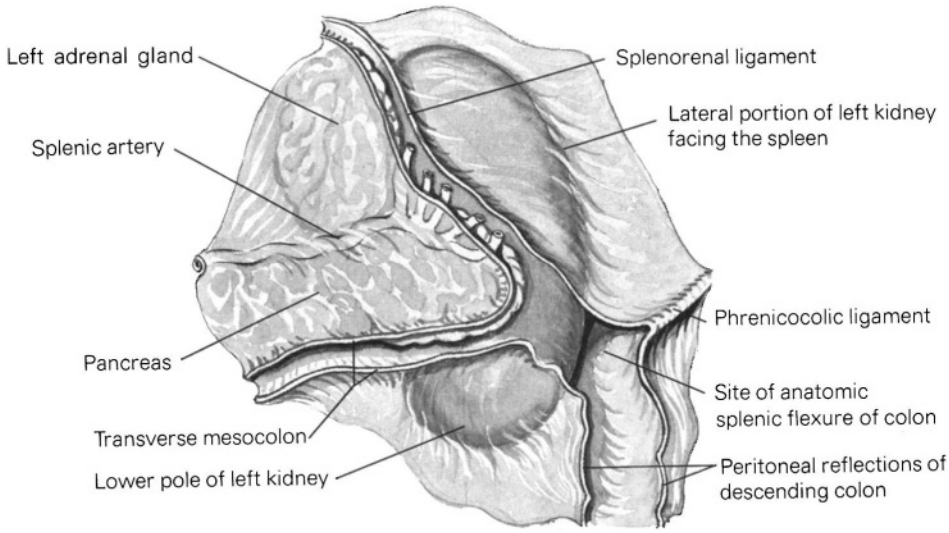


Fig. 11–2. Posterior peritoneal reflections of the left upper quadrant, demonstrating continuity of the transverse mesocolon and splenorenal ligament with the phrenicocolic ligament and the peritoneal reflections of the descending colon. The tail of the pancreas resides within the splenorenal ligament.

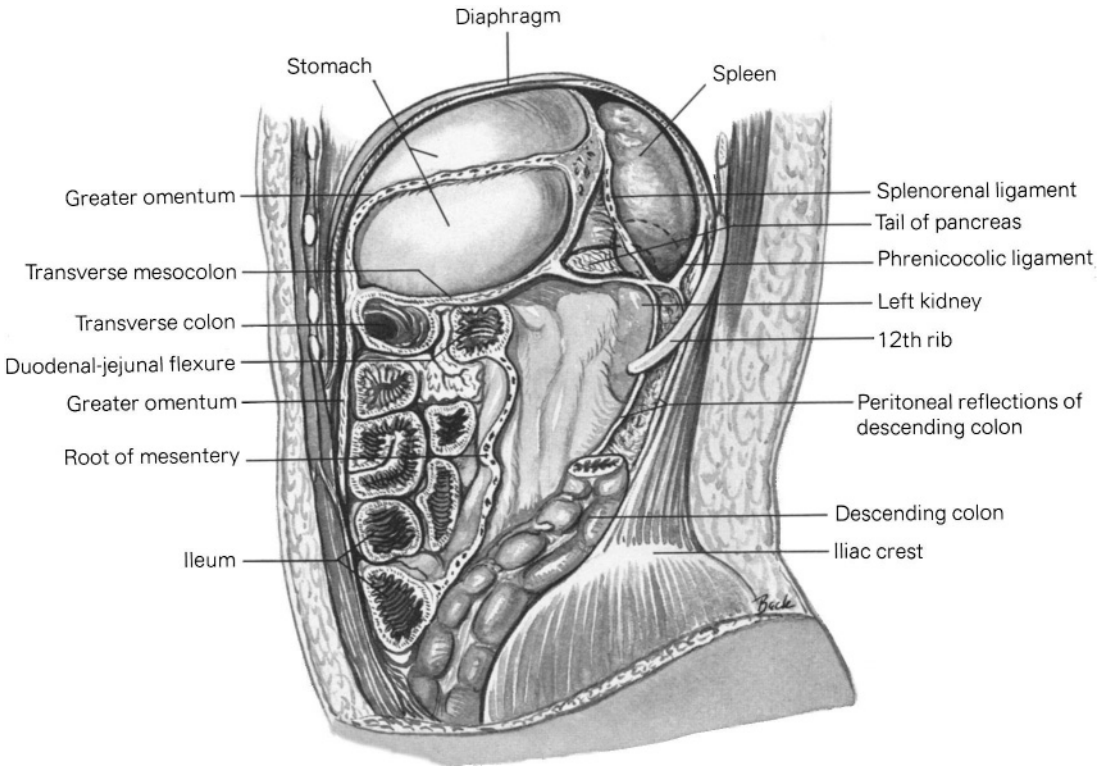


Fig. 11–3. Left parasagittal drawing, emphasizing peritoneal reflections. Note the tail of the pancreas within the splenorenal ligament and its continuity with the transverse mesocolon and phrenicocolic ligament.

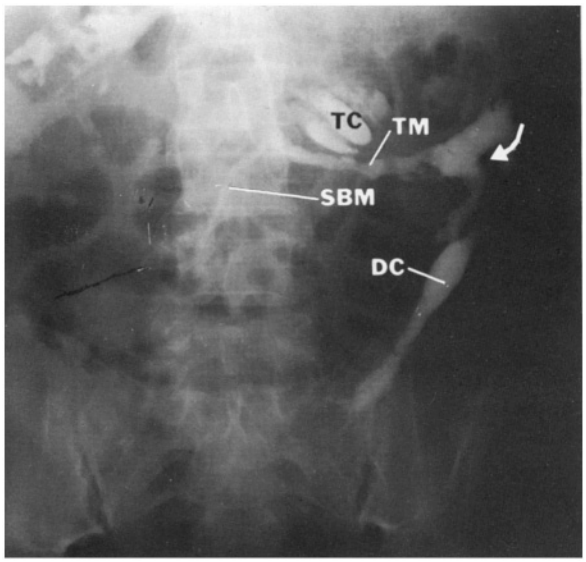


Fig. 11–4. Opacification *in vivo* of continuity of mesenteric roots and bare areas in relationship to the pancreas.
In this patient who has had a right hemicolectomy and ileotransverse colostomy, fistulography strikingly illustrates communication between the root of the transverse mesocolon *(TM),* root of the small bowel mesentery *(SBM),* and the bare area of the descending colon *(DC).* At the site of the phrenicocolic ligament *(arrow),* there is communication with the transverse colon *(TC)* and a left cutaneous fistula.

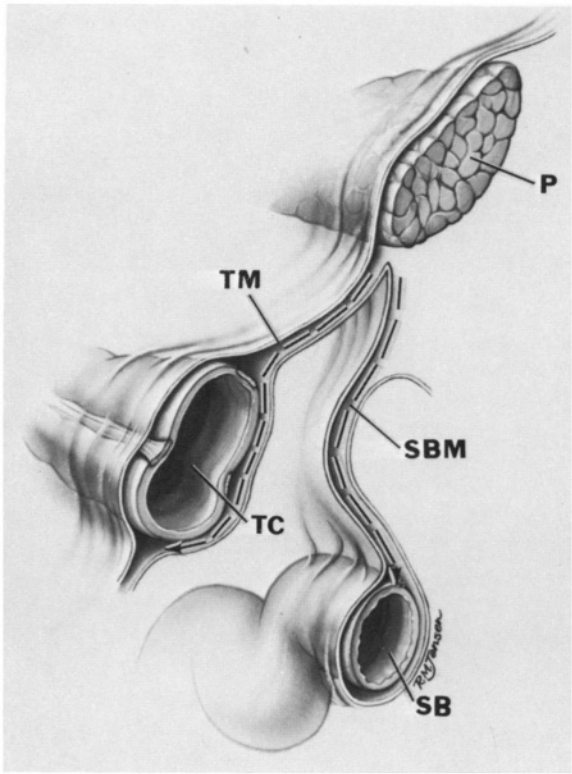


Fig. 11–5. Anatomic pathways of spread from the pancreas.
Lateral drawing. The *arrowed-dashed lines* show the planes of spread from the pancreas *(P)* to the transverse colon *(TC),* characteristically toward its lower border, and to the small bowel *(SB). TM* = transverse mesocolon; *SMB* = small bowel mesentery.
(Redrawn from Meyers and Evans.[2])

Effects of Pancreatitis on the Colon: Spread Along the Transverse Mesocolon

The segment of large intestine involved by pancreatitis reflects the pathophysiology of the disease and the anatomic relationships of the pancreas to the mesenteric planes of the transverse mesocolon. Inflammation localized to the head of the organ may extend to the hepatic flexure and perhaps the distal ascending colon. Diffuse pancreatitis may spread to involve the entire transverse colon, with a definite tendency to exert its major effects on the splenic flexure.

Hepatic Flexure

With spread of liberated enzymes from the head of the pancreas into the right anterior pararenal space across the beginning of the transverse mesocolon, the hepatic flexure may show localized or diffuse inflammatory changes (Fig. 11–6). Occasionally, the "cut-off" process of a stricture resulting from pericolic fat necrosis may closely simulate an annular carcinoma[2,10] (Fig. 11–7).

In 1956, Price[11] coined the term "colon cut-off" sign in acute pancreatitis for isolated gaseous distention of the ascending colon and hepatic flexure with sharp delimitation of the gas shadow just to the left of the flexure. In two patients, he noted a similar cellulitis-like process spreading from the edematous head of the pancreas between the two layers of the transverse mesocolon to the mesocolic border of the colon just to the left of the hepatic flexure.

Transverse Colon and Splenic Flexure

Since Price's report, however, the term "colon cut-off" sign has lost its original definition and has been applied to multiple sites of spasm and narrowing of the colon secondary to pancreatitis. Stuart[12] employed it to designate collapse with absence of gas in the midportion of the transverse colon, which appeared to be cut off from the gas-containing hepatic and splenic flexures. This was a constant finding in both supine and erect plain films of the abdomen in six patients with acute pancreatitis. Brascho and co-authors[13] found the gaseous dilatation to involve the ascending and entire transverse colon, with the cut-off point at the splenic flexure. In my experience,[2] as well as that of others,[14–17] this is by far the most common single site involved.



Fig. 11–6. Acute pancreatitis with extension to hepatic flexure.
Barium enema shows diffuse mild spasm and edematous mucosal changes of the hepatic flexure and distal ascending colon from extension of extravasated pancreatic enzymes via the right anterior pararenal compartment.

On plain films, the most common abnormality in the large intestine in cases of acute pancreatitis is gaseous distention of the transverse colon. This often represents a paralytic ileus secondary to the extravasated enzymes within the transverse mesocolon (Figs. 11–8 through 11–11). More directly irritative effects may be manifested by spasm and edema[18] (Figs. 11–12 through 11–14).

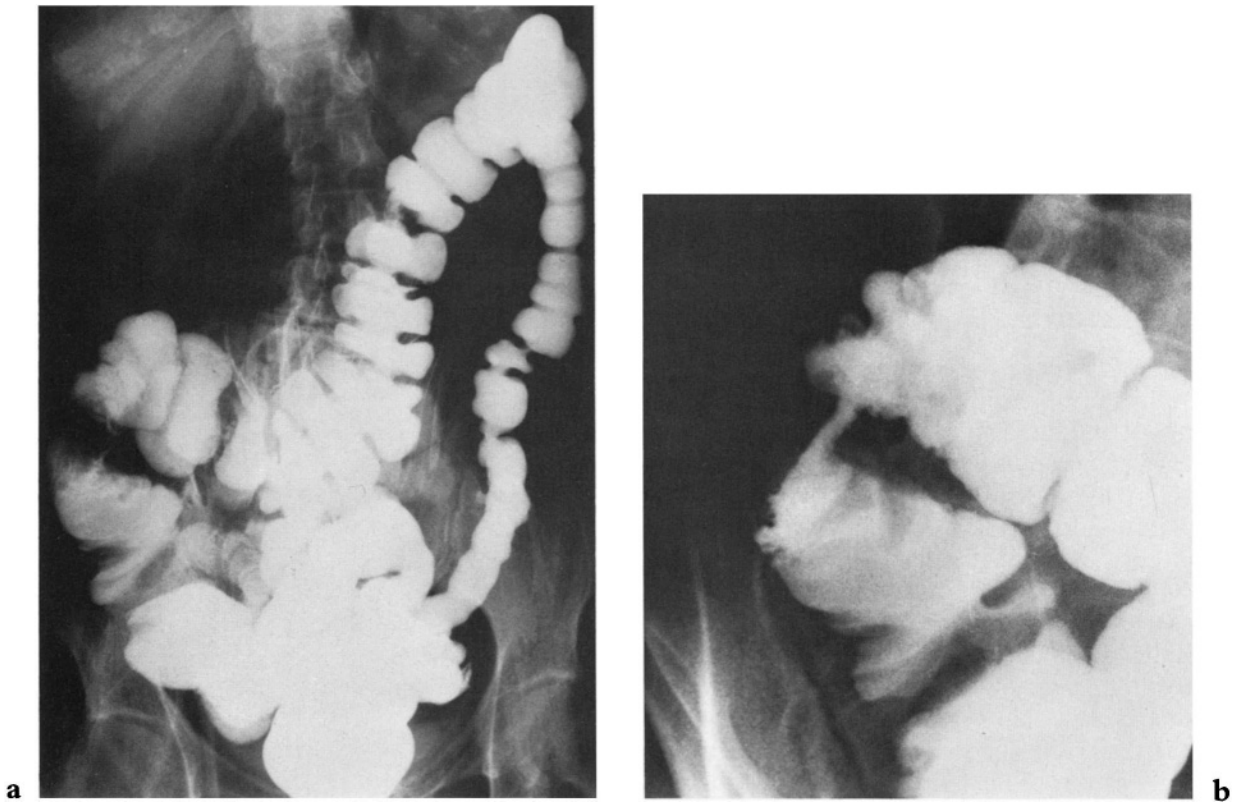


Fig. 11–7. Acute suppurative pancreatitis with extension to hepatic flexure.
(a and **b)** Barium enema and spot film demonstrate an annular constricting lesion of the distal ascending colon. The constant narrowing and overhanging shelflike margin mimic an "apple-core" carcinoma. Exploratory laparotomy disclosed a large peripancreatic abscess with retroperitoneal extension down to and involving the hepatic flexure and distal ascending colon, where an extramural inflammatory stricture was encountered. Areas of fat necrosis were present in the transverse mesocolon, pericolonic tissue, and greater omentum.
(Reproduced from Meyers and Evans.[2])

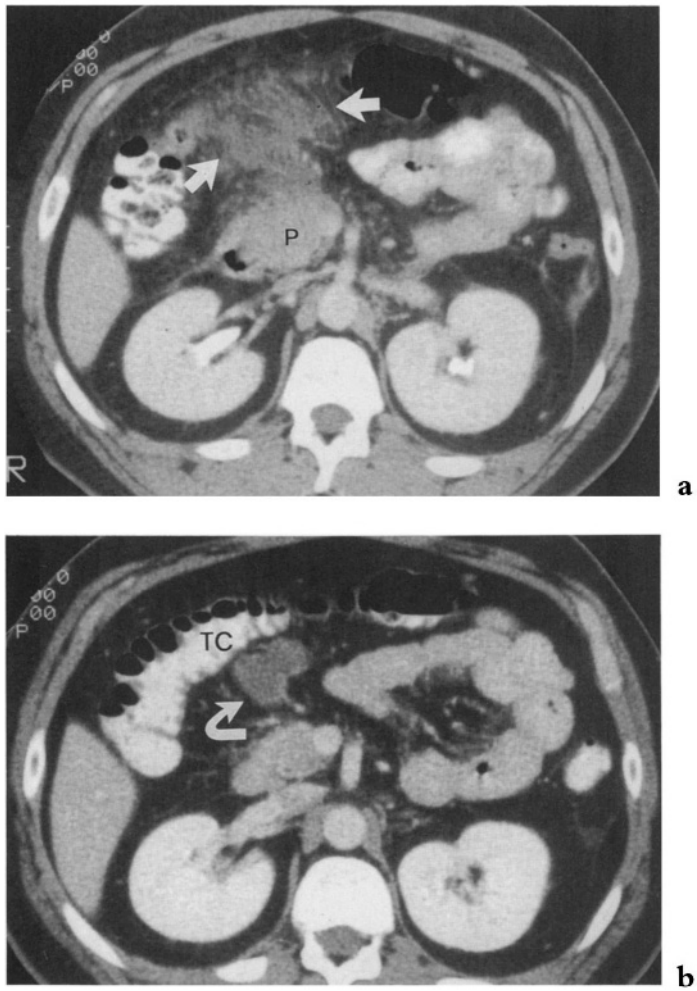


Fig. 11–8. Acute pancreatitis with extension in mesocolon approaching the transverse colon.
(a) During an episode of acute pancreatitis, CT shows enlargement of the pancreatic head *(P)* and phlegmonous extension into the transverse mesocolon *(arrows).*
(b) Three months later, the process has condensed and become encapsulated as a small pseudocyst within the transverse mesocolon *(arrow).* Note that the process stops just short of affecting the transverse colon *(TC).*
(Courtesy of Emil Balthazar, M.D., Bellevue Hospital, New York University School of Medicine, New York, NY.)

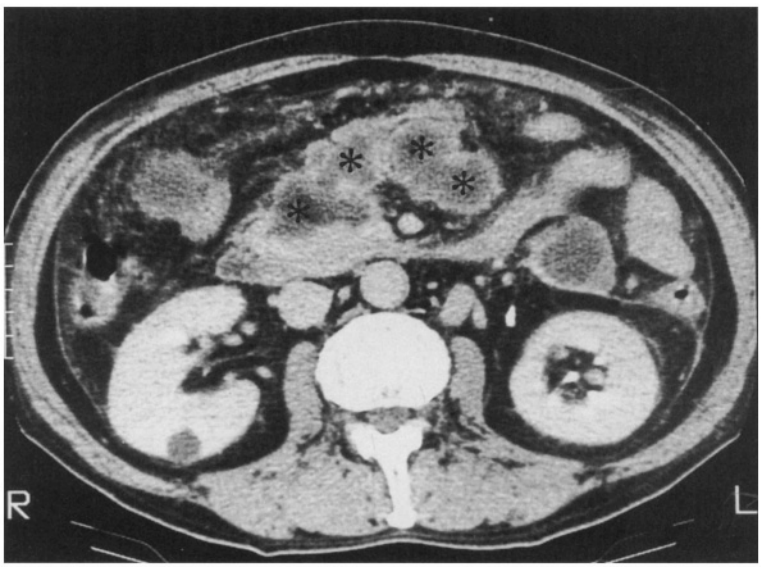


Fig. 11–9. Mesocolic involvement by pancreatitis.
CT demonstrates multiple pseudocysts of the pancreas *(asterisks)* have extended into the transverse mesocolon, whose fatty tissue is infiltrated by the inflammatory process.

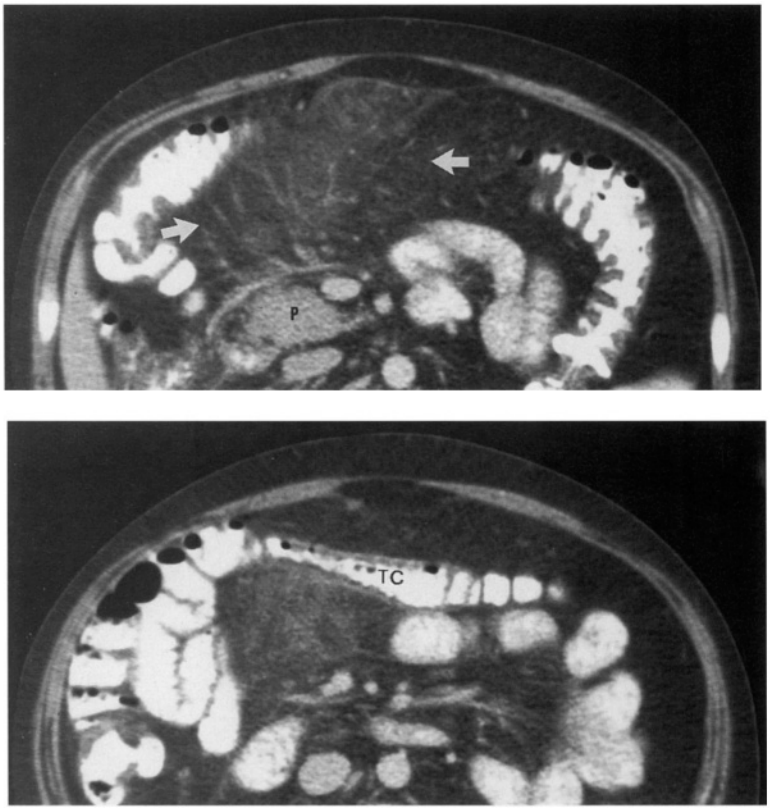


Fig. 11–10. Extension of acute pancreatitis to transverse colon.
(a) At the level of the uncinate process of the pancreas *(P),* inflammatory changes progress through the transverse mesocolon *(arrows)* toward the right, with associated conspicuous branches of the middle colic vessels.
(b) The infiltrate compresses and distorts the transverse colon *(TC).*

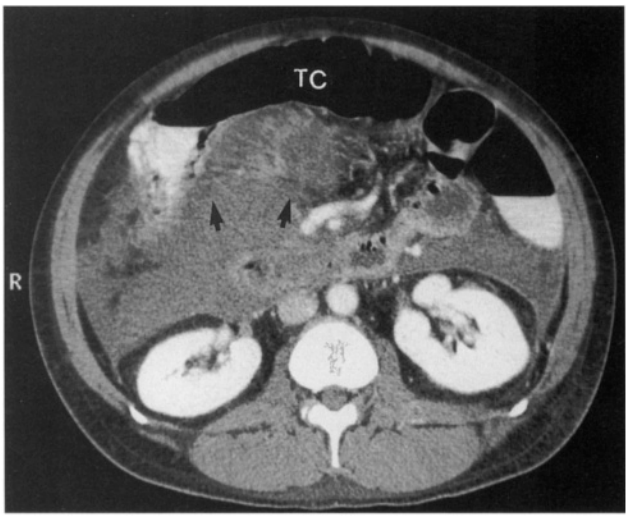


Fig. 11–11. Fulminant acute pancreatitis extending through the transverse mesocolon.
Phlegmonous changes involve the anterior pararenal spaces bilaterally and extend across the mesocolon *(arrows)* toward the transverse colon *(TC),* which exhibits ileus.



Fig. 11–12. Acute pancreatitis.
Plain film shows diffuse spasm and edema of the transverse colon due to extensive inflammatory exudate that also displaces the stomach superiorly and the transverse colon inferiorly.

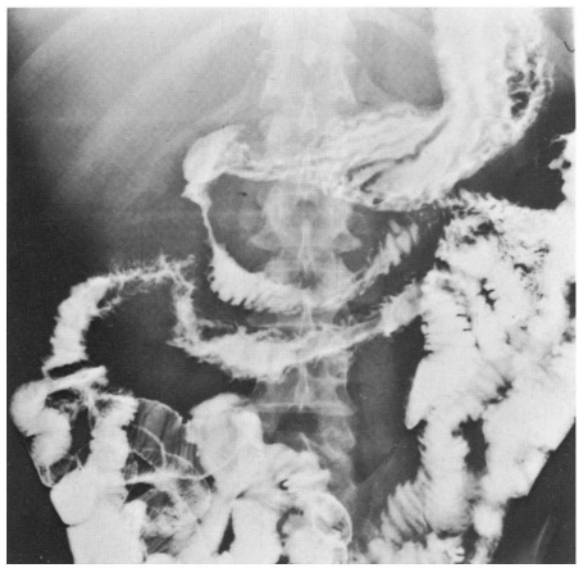


Fig. 11–13. Acute pancreatitis.
Diffuse inflammation of transverse colon, shown by spastic narrowing and gross mucosal irregularities on delayed film of upper GI series.

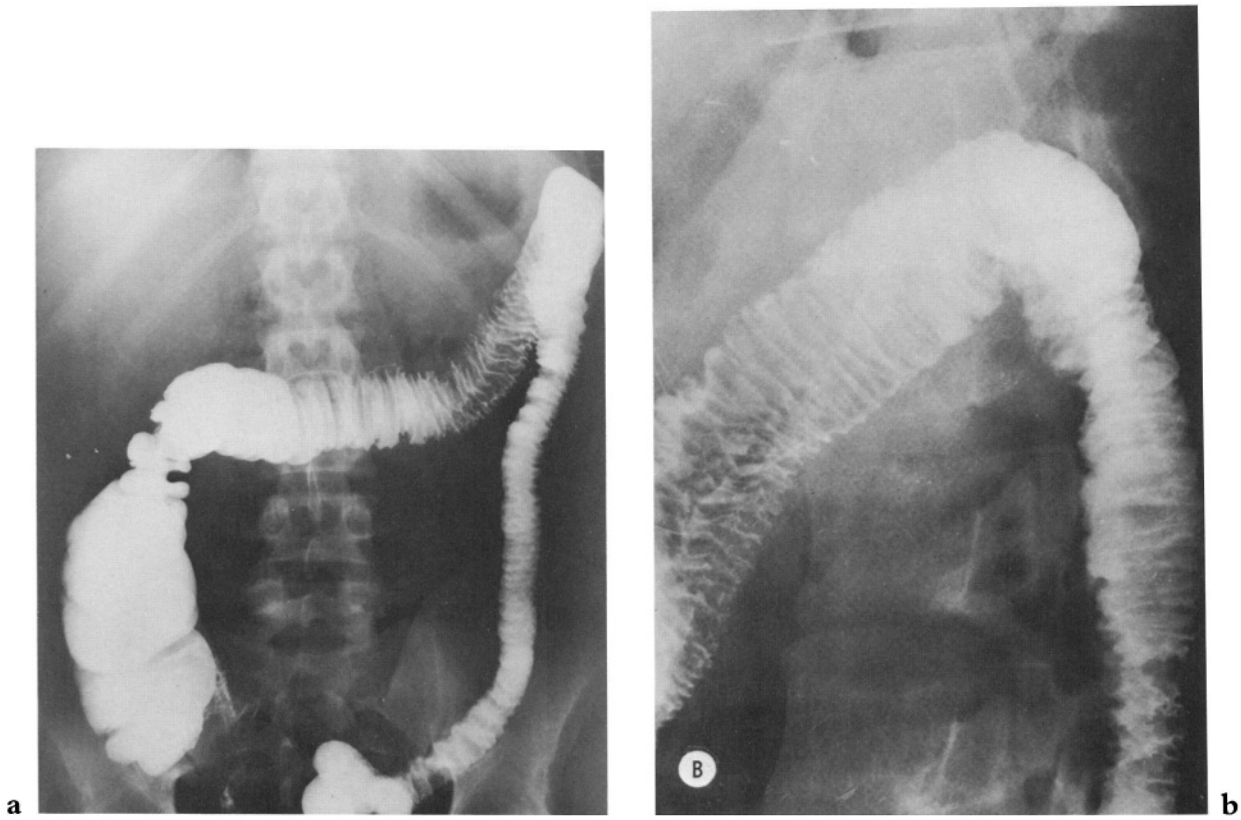


Fig. 11–14. Acute pancreatitis.
Diffuse inflammation of transverse colon. Frontal **(a)** and oblique **(b)** views of barium enema study demonstrate mucosal edema.
(Reproduced from Thompson et al.[18])

The natural extension of the inflammatory process into the phrenicocolic ligament may result in severe spasm or an incomplete mechanical obstruction at the level of the anatomic splenic flexure immediately inferior to the tip of the spleen[8] (Fig. 11–15). The obstruction need not be permanent and may resolve as pancreatitis subsides (Figs. 11–16 through 11–18). However, if the inflammation is more severe and particularly if it is accompanied by fat necrosis, barium enema study shows narrowing of the splenic flexure with irregular nodular or serrated margins and distorted mucosal folds secondary to the extramural inflammatory infiltrate. Occasionally, a significant degree of retrograde obstruction may be met, and the changes may simulate carcinoma.[19] A granulomatous and fibrotic reaction may then result in a stricture of the splenic flexure. It is for these reasons that most colon strictures secondary to pancreatitis occur in the splenic flexure.[15–17,20]

This is illustrated in Figure 11–19 in a case of traumatic pancreatitis. Barium enema examination discloses irregular flattening of the lower border of the transverse colon along its length, ending abruptly at the level of the anatomic splenic flexure (Fig. 11–19a) Distal to this site, the extraperitoneal descending colon resumes a normal haustral pattern. This pattern of asymmetric involvement of the lower contour of the mesenteric transverse colon is characteristic of extension of disease from the pancreas along the transverse mesocolon and phrenicocolic ligament.[21] The narrowing with irregular nodular defects demonstrated in the splenic flexure (Fig. 11–19b, c) is obviously organic and not functional in nature and thus indicates direct passage of considerable pancre-



Fig. 11–15. Acute pancreatitis extending into the phrenicocolic ligament.
Phlegmonous changes spread extensively through the mesocolon, and fluid extends into the phrenicocolic ligament *(arrows)* immediately lateral to the anatomic splenic flexure of the colon *(C).* Gallstones are present.
(Courtesy of René Le Gall, M.D., Papeete, Tahiti.)

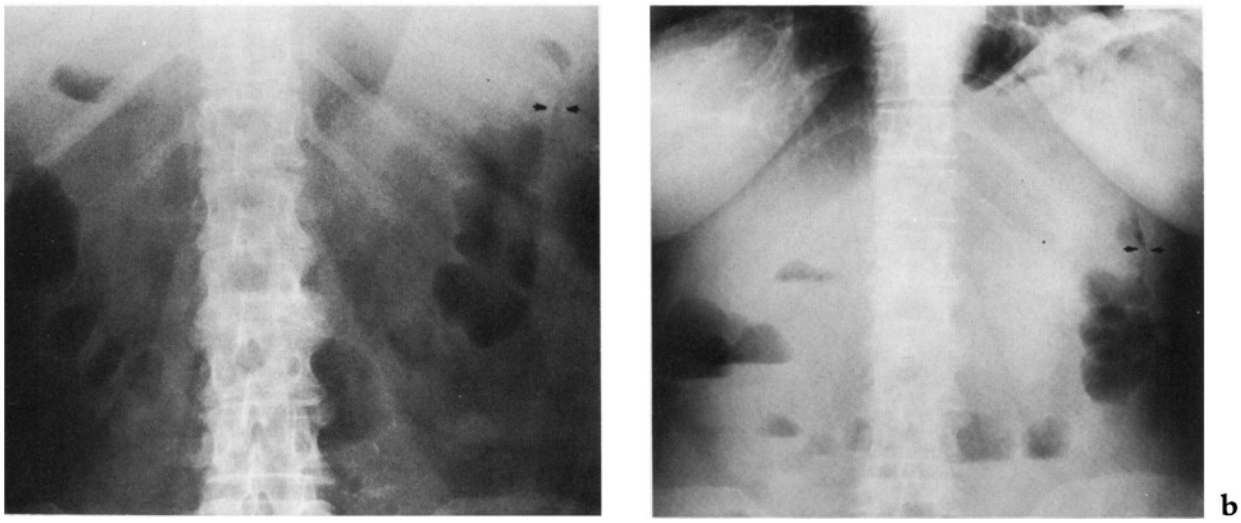


Fig. 11–16. Acute pancreatitis.
(a) Supine and **(b)** erect. Dilatation and air-fluid levels of the transverse colon extend to a narrowed segment of the splenic flexure *(arrows).*
Barium enema study 1 week after conservative therapy showed no abnormalities, indicating that these changes were due to spasm secondary to the irritating effects of enzymes within the phrenicocolic ligament.
(Reproduced from Meyers and Evans.[2])

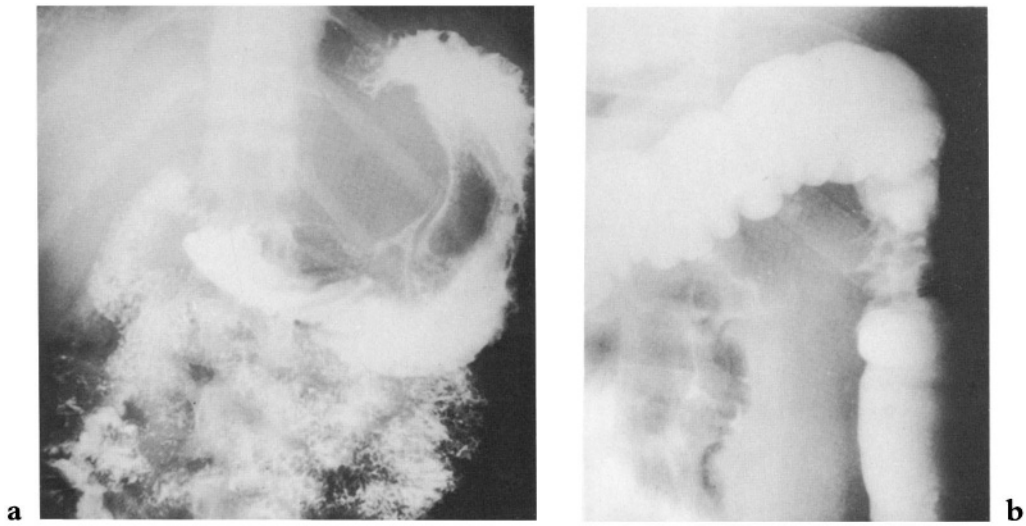


Fig. 11–17. Pancreatic pseudocyst with pericolitis.
While the upper gastrointestinal series **(a)** demonstrates the pressure effect on the stomach produced by a large organizing pancreatic pseudocyst, the barium enema study **(b)** shows localized narrowing and spiculation of the mucosal pattern of the anatomic splenic flexure from extravasated pancreatic enzymes.

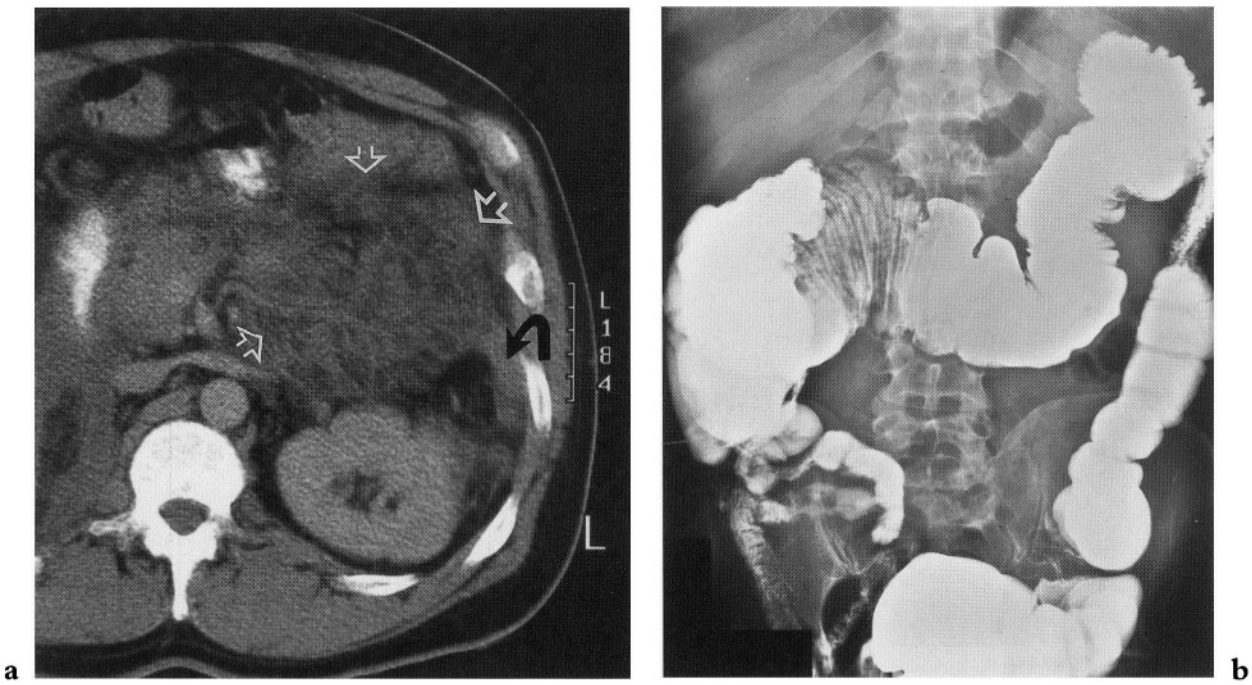


Fig. 11–18. Acute pancreatitis extending across the transverse mesocolon to the anatomic splenic flexure of the colon.
(a) CT shows gross extension of pancreatic inflammatory changes through the mesocolon *(arrows)* to the region of the phrenicocolic ligament *(curved arrow).*
(b) Barium enema reveals spasm of the splenic flexure with proximal colonic dilatation.

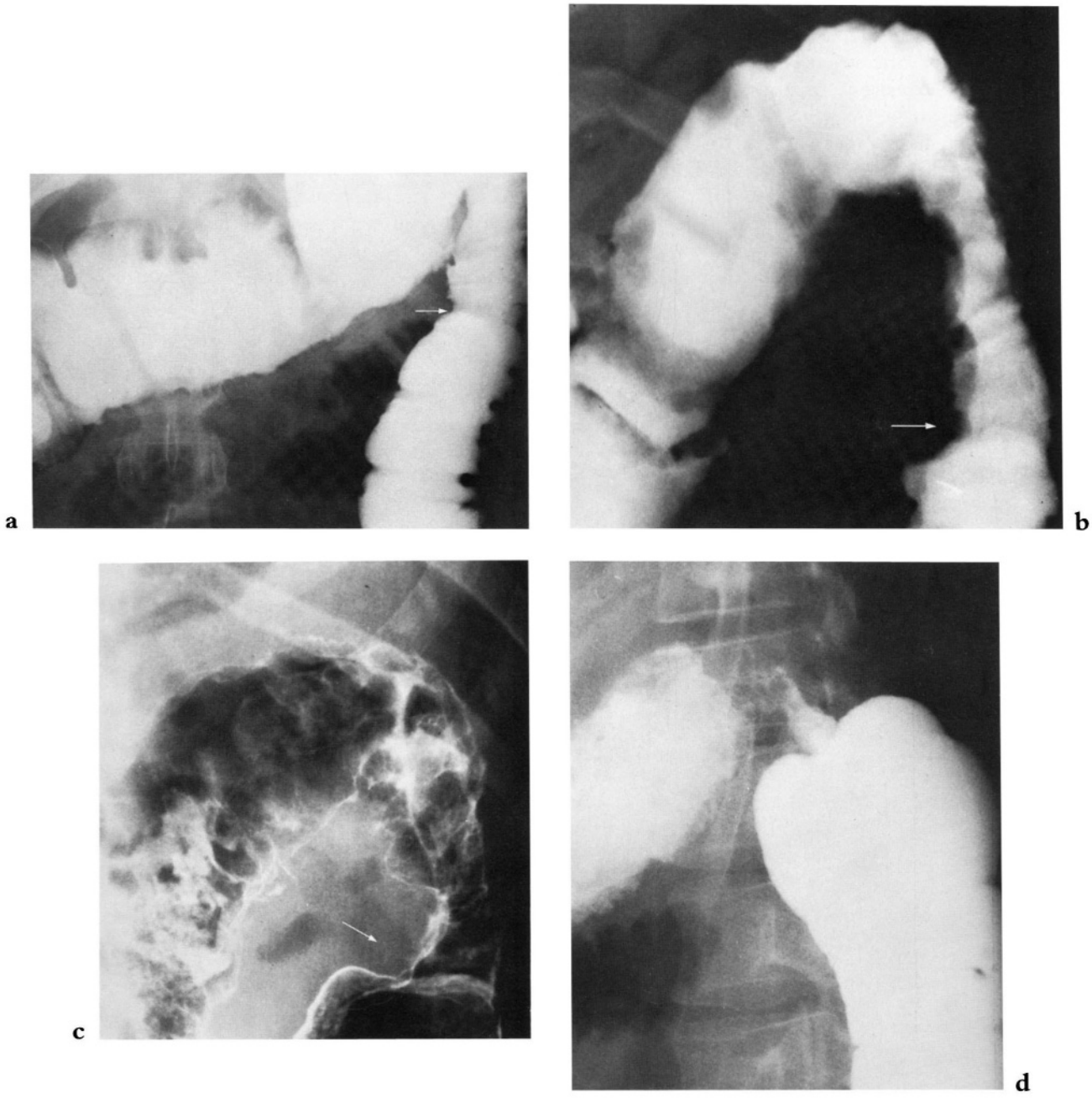


Fig. 11–19. Traumatic pancreatitis, with development of stricture of splenic flexure.
(**a**) Flattening of the inferior haustral contour of the transverse colon. Pseudosacculations result on the uninvolved superior border. The process ends at the level of the phrenicocolic ligament at the anatomic splenic flexure of the colon *(arrow).*
(**b** and **c**) Scalloped narrowing of the splenic flexure on filled and air studies. The intramural lesions end precisely at the level of the phrenicocolic ligament *(arrows).*
(**d**) Three months later, there is a marked fibrotic stenosis of the splenic flexure, reducing its lumen to a diameter of less than 3 mm. Surgical resection of the stricture, induced by fat necrosis, was required.
(Reproduced from Meyers and Evans.[2])

atic enzymes into the phrenicocolic ligament. From the severe changes in the splenic flexure, the probable development of a fibrotic stricture (Fig. 11–19d) should be anticipated and serial evaluations by barium enema studies obtained.

If the inflammatory process erodes through the wall of the colon at this site, extraperitoneal sinus tracts or fistulas to adherent small bowel loops may be demonstrated (Figs. 11–20 through 11–22).

Pancreatic pseudocysts may spontaneously rupture into an adjacent hollow viscus, the colon and particularly the splenic flexure being the most common site[22–24] (Figs. 11–23 through 11–25). Fistulization does not occur in the initial acute phase of pancreatitis, but rather as a consequence of pancreatic suppuration or pseudocyst. Pancreatic gas may be the consequence of fistulization, rather than secondary to pancreatic abscess alone.[25] The mechanism involves enzymatic digestion of the cyst wall or vascular insult that produces progressive necrosis and rupture. While temporary or even permanent remission may result from this spontaneous decompression,[24] major gastrointestinal bleeding is seen in about 30% because of erosion of large arteries,[22,24] and sepsis with conversion of the pseudocyst into an abscess

text continues on page 582

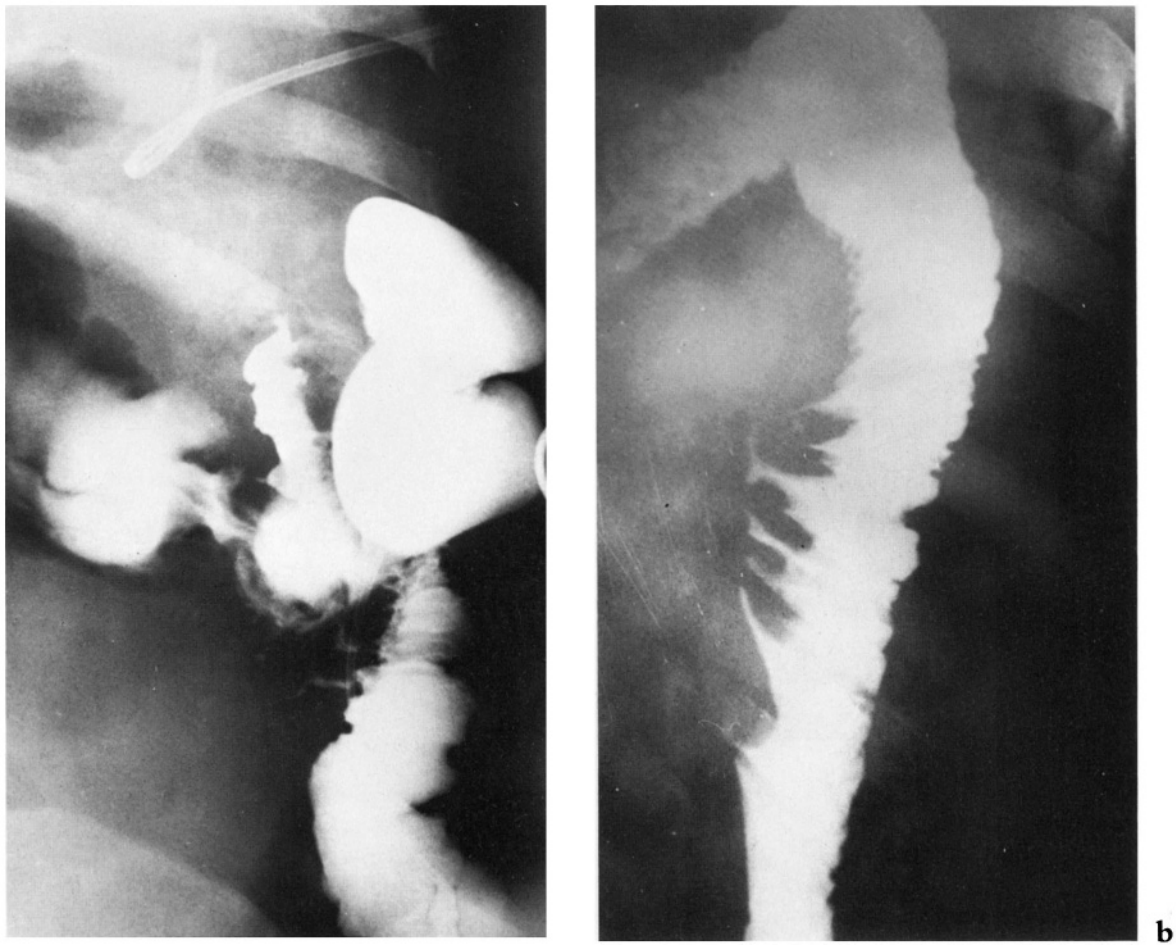


Fig. 11–20. Gas-producing abscess of pancreas.
(a) Multiple gaseous lucencies of tail of pancreas at site of draining catheter. Barium enema demonstrates extension via the phrenicocolic ligament to anatomic splenic flexure with multiple sinus tracts of varying size.
(b) Four months later, multiple residual sinus tracts are present.
(Reproduced from Meyers and Evans.[2])



Fig. 11–21. Acute pancreatitis with transmural erosion.
(**a** and **b**) Severe spread of enzymes into the phrenicocolic ligament produces a fixed and irregular narrowing of the anatomic splenic flexure of the colon. Transmural erosion is shown by faint barium extravasation laterally.

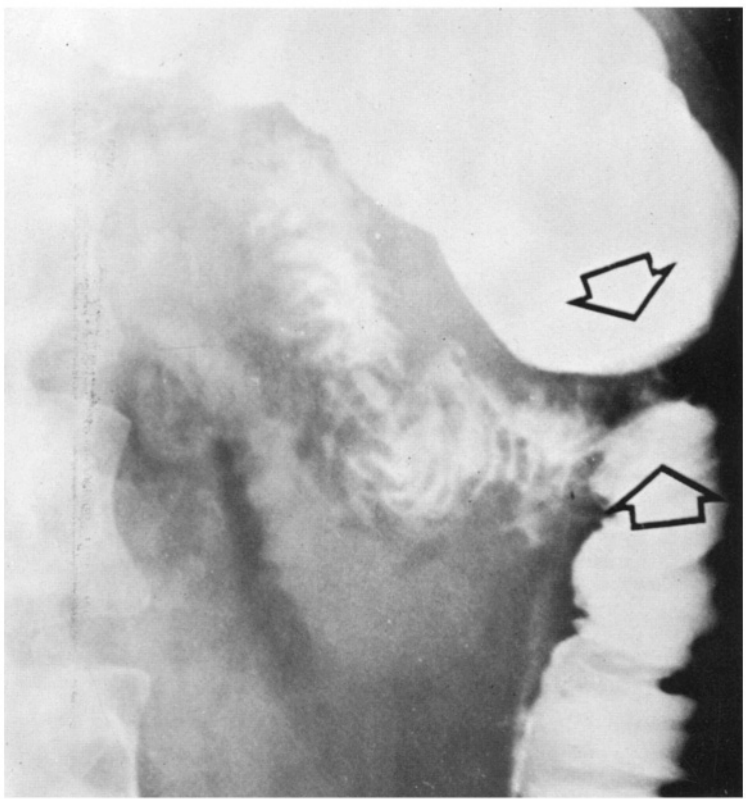


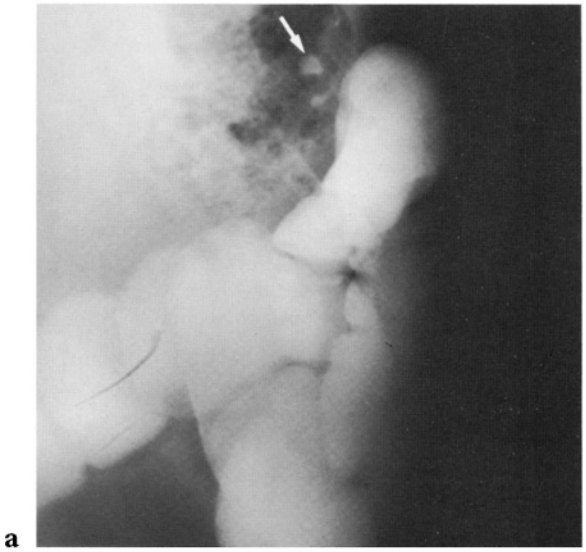
Fig. 11–22. Acute suppurative pancreatitis with transmural erosion.
Extravasated enzymes within the phrenicocolic ligament have resulted in incomplete obstruction of the splenic flexure *(arrows)* and transmural digestion with fistulization to a small bowel loop and a long extraperitoneal sinus tract from the narrowed splenic flexure.
(Reproduced from Meyers and Evans.[2])



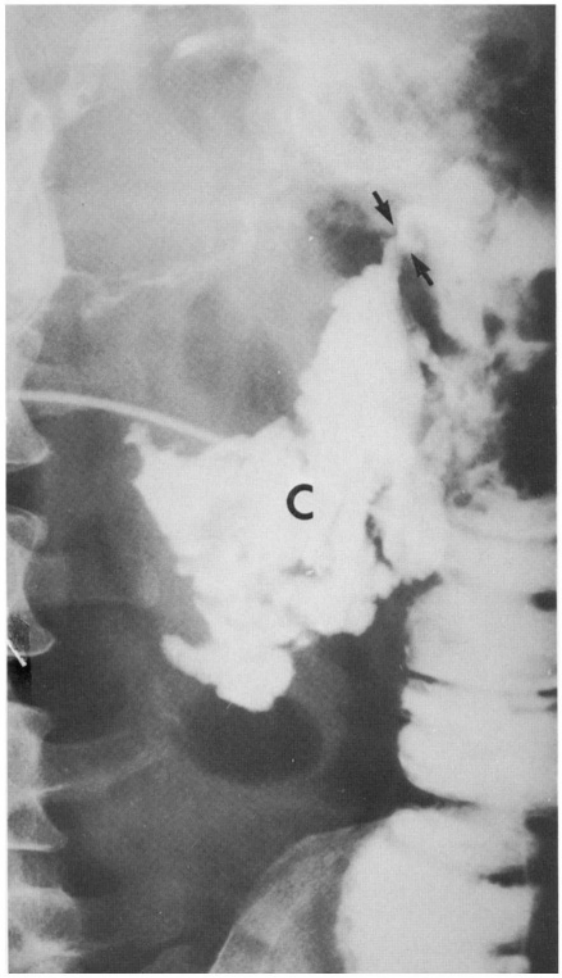
Fig. 11–23. Spontaneous rupture of pancreatic pseudocyst into colon.
Barium enema study demonstrates communication at anatomic splenic flexure into pseudocyst cavity of tail of pancreas.



Fig. 11–24. Spontaneous drainage of pancreatic pseudocyst into colon.
Barium enema study reveals that a fistulous communication has been established between the region of the anatomic splenic flexure and an irregular pseudocyst extending retroperitoneally from the tail of the pancreas.



a



b

Fig. 11–25. Spontaneous fistula formation from infected pancreatic pseudocyst to colon.
(a) Pancreatic abscess with extraluminal gas loculation displaces splenic flexure of colon. A small amount of contrast material has extravasated into the abscess *(arrow)*.
(b) Fistulogram performed after drainage of abscess demonstrates the irregular cavity *(C)* with the tract *(arrows)* extending to the colon.
(Courtesy of J.L. Clements, Jr., M.D., Emory University School of Medicine, Atlanta, GA.)

is frequent. The recommended operative procedure is proximal diverting colostomy and debridement with external drainage of the peripancreatic collection.[22]

Extraperitoneal dissection inferiorly may result in pseudocyst formation within the anterior pararenal space (Figs. 11–26 through 11–29), with effects on the long limbs of the colon, sigmoid colon, and rectum, and rarely may progress as far as the groin.[26–30] Fat necrosis at this site may mimic many other disease processes. The patient illustrated in Figure 11–30 presented with an acute abdomen and an inflamed scrotum that drained "beef-broth" material with a high amylase content secondary to fat necrosis. The barium enema study indicates the pathway of the pancreatic enzymes into the phrenicocolic ligament and inferiorly beyond the sigmoid colon to the inguinal region.

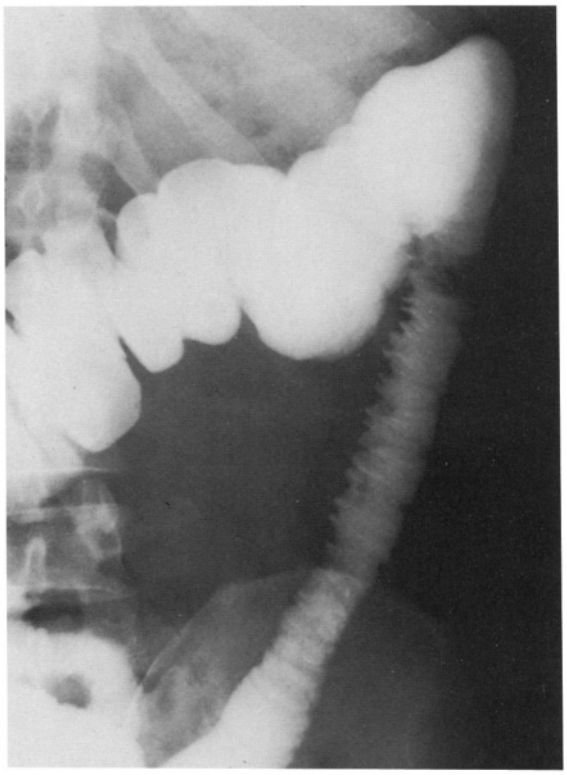


Fig. 11–26. Acute pancreatitis extending to descending colon.
Beginning at the level of the anatomic splenic flexure and extending downward, the descending colon shows spasm, limited distensibility, and edematous changes that are more marked on the medial wall. These changes reflect the inferior extension of the pancreatic inflammatory process through the anterior pararenal space. Extraluminal gas stippling is due to early abscess formation.

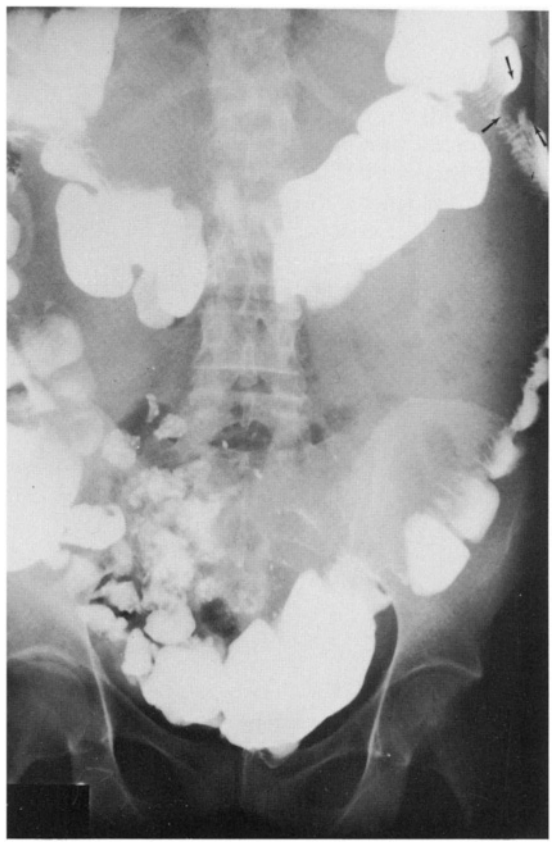


Fig. 11–27. Extension of pancreatitis into the pelvis.
Effects on the anatomic splenic flexure *(arrows)* from extravasated enzymes are shown. A large pseudocystic soft-tissue mass extends inferiorly through the left anterior pararenal space to the pelvis, resulting in displacement and mucosal inflammatory changes of the descending colon.

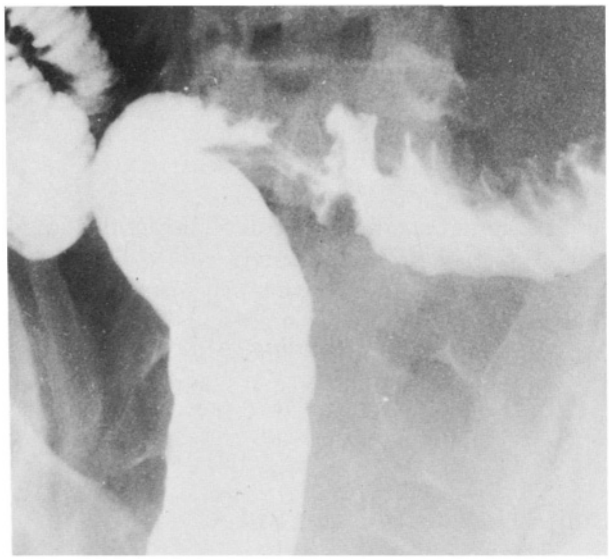


Fig. 11–28. Extension of pancreatitis into the pelvis.
Massive pancreatitic exudate dissecting along the left retroperitoneum into the pelvis results in extensive edema of the sigmoid colon with mass effect and displacement of the rectum to the right.
(Reproduced from Farman et al.[26])

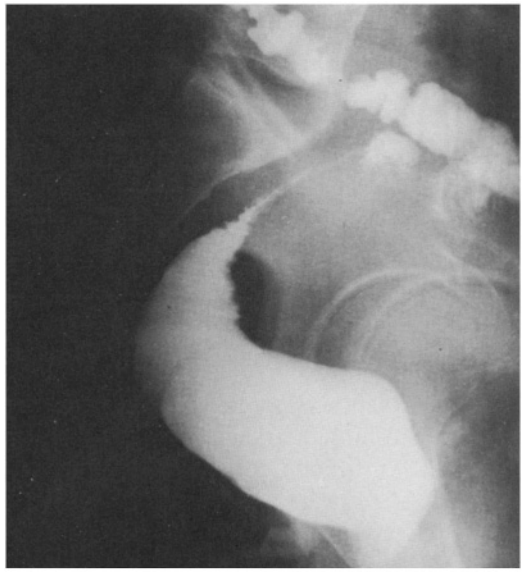


Fig. 11–29. Extension of pancreatitis into the pelvis.
A pseudocyst of the pancreas extends retroperitoneally to the pelvis with extrinsic compression and partial obstruction of the distal sigmoid colon.



Fig. 11–30. Extension of acute pancreatitis into scrotum.
Pseudocyst formation in the tail of the pancreas depresses the distal transverse colon. In addition, extravasated enzymes within the phrenicocolic ligament result in localized narrowing of the anatomic splenic flexure *(top arrow).* Inferior extension extraperitoneally on the left is revealed by compression of the sigmoid colon *(bottom arrow).*
(Courtesy of Jack Farman, M.D., Columbia-Presbyterian Medical Center, New York, NY.)

Effects of Pancreatitis on the Duodenum, Small Bowel, and Cecum: Spread Along Small Bowel Mesentery

The inflammatory process associated with extravasated pancreatic enzymes may disseminate along the root of the small bowel mesentery, either for a portion or for its entire length. Figure 11–31 demonstrates these anatomic relationships near the beginning of the mesentery. Spread through the leaves brings the process to intestinal vessels and to an individual or multiple loops (Fig. 11–32). Figure 11–33 documents communication of the pancreas with the length of the mesenteric root. This pathway provides a plane of spread to the right lower quadrant (Fig. 11–34).

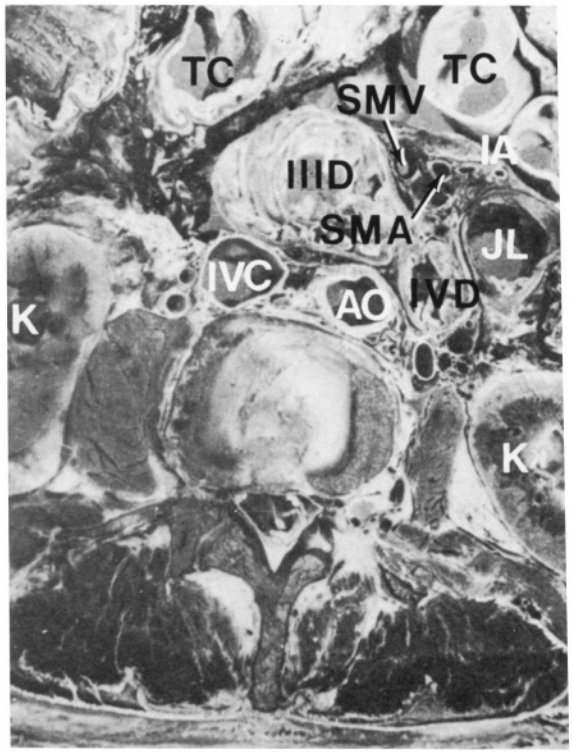


Fig. 11–31. Anatomic cross-section immediately below the pancreas shows the relationships of the superior mesenteric artery *(SMA)* and vein *(SMV),* in the root of the mesentery, to the third portion of the duodenum *(III D)* as it continues into the fourth duodenum *(IV D).* Intestinal arteries *(IA)* course in the mesentery to loops of jejunum *(JL). AO* = aorta; *K* = kidney; *IVC* = inferior vena cava; *TC* = transverse colon.

Duodenum

Compression of the third portion of the duodenum may result from an indurated mesenteric root.[32] This typically occurs in its midportion, which may appear sharply cut off (Fig. 11–35), with dilatation and stasis proximally. Such a mechanical process undoubtedly accounts for many instances of the duodenal "ileus" seen in acute pancreatitis.

Small Bowel and Cecum

As the enzymes progress further down the root of the mesentery, jejunitis may be evident (Fig. 11–36). It has long been recognized that "sentinel loops" from localized paralytic ileus of small bowel may accompany pancreatitis.[33] Jejunal and occasionally ileal changes characterized by marked persistent spasm of some segments and dilatation of others, with coarsening of the mucosal folds, may be seen (Figs. 11–37 and 11–38).

Ischemic changes in the intestine as well may be produced by the digestive effects of the liberated enzymes or by thrombosis from areas of fat necrosis. Microaneurysms, pseudoaneurysms, stenoses, and occlusions are being increasingly recognized in mesenteric vessels following pancreatitis.[34,35] The vascular consequences may range from fibrotic strictures[20,26] (Fig. 11–39) to gangrene of the bowel[14,37–40] (Fig. 11–40).

Figure 11–41 illustrates the findings in a case of malabsorption and jejunal mucosal atrophy secondary to chronic relapsing pancreatitis. Protracted ischemia of the intestine from the vascular effects of pancreatic enzymes in the mesentery underlay the chronic malabsorption in this case. It thus appears that some of the features of pancreatic malabsorption may be on a vascular basis. Localized anatomic changes of mesenteric vessels from the digestive effects of pancreatic enzymes may result in vascular shunts and ischemic malabsorption.

Acute pancreatitis may clinically mimic an acute appendicitis with peritoneal signs localized predominantly in the right lower quadrant. This is a reflection of the process spreading along the length of the root of the small bowel mesentery to result in inflammatory changes of distal ileal loops or the cecum.[2] Plain film findings

text continues on page 590

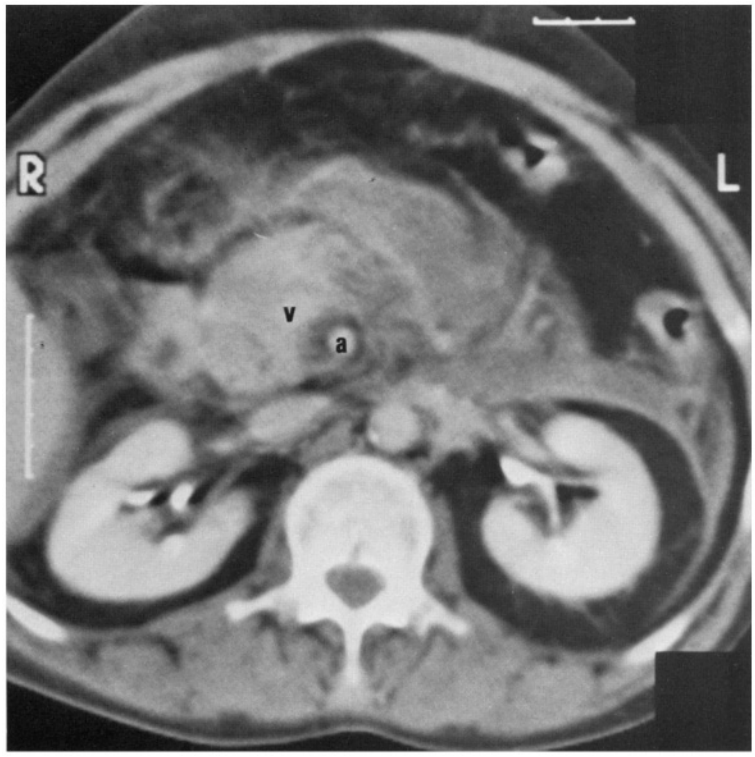


Fig. 11–32. Spread of pancreatitis through the small bowel mesentery.
In a case of acute pancreatitis, CT shows the inflammatory reaction extending through the small bowel mesentery, displacing the superior mesenteric artery *(a)* and vein *(v)* and intestinal branches. The fat encircling the superior mesenteric artery is maintained. The process also extends within the extraperitoneal anterior pararenal space on the left.
(Reproduced from Meyers et al.[5])

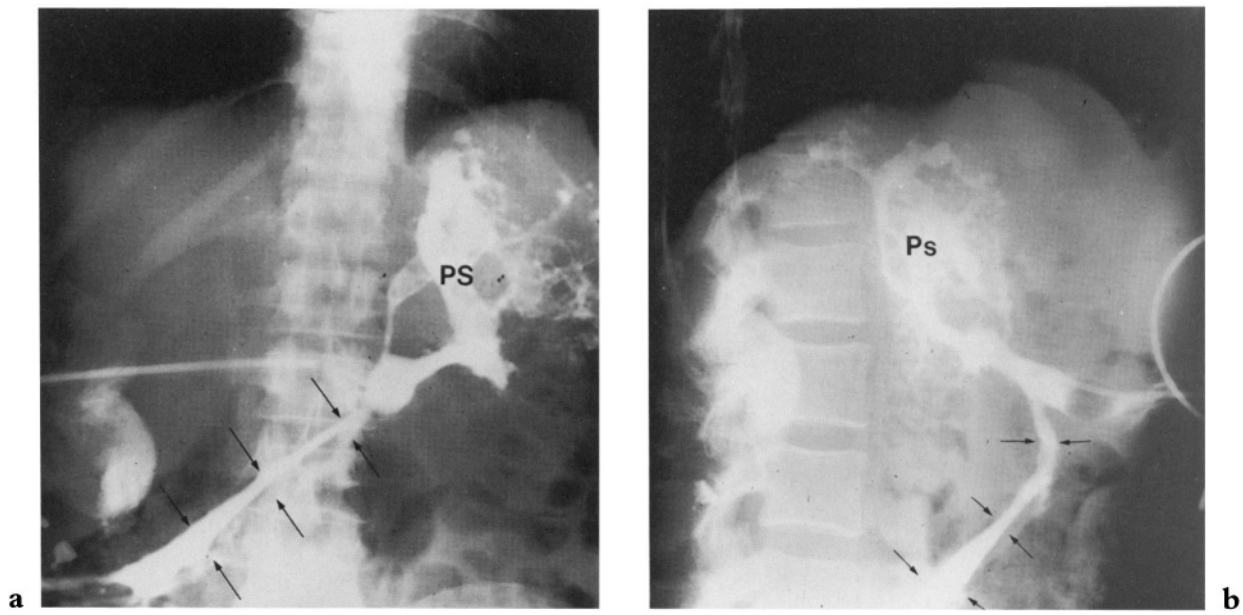


Fig. 11–33. Opacification of mesenteric root *in vivo*.
(a and **b)** Injection of contrast material through tube draining a loculated pseudocyst *(Ps)* of the tail of the pancreas demonstrates communication dissecting along the root of the small bowel mesentery *(arrows)*. Note its typically oblique course toward the right lower quadrant in relation to duodenum, jejunum, ileum, and cecum.
(Courtesy of Jack Farman, M.D., Columbia-Presbyterian Medical Center, New York, NY.)

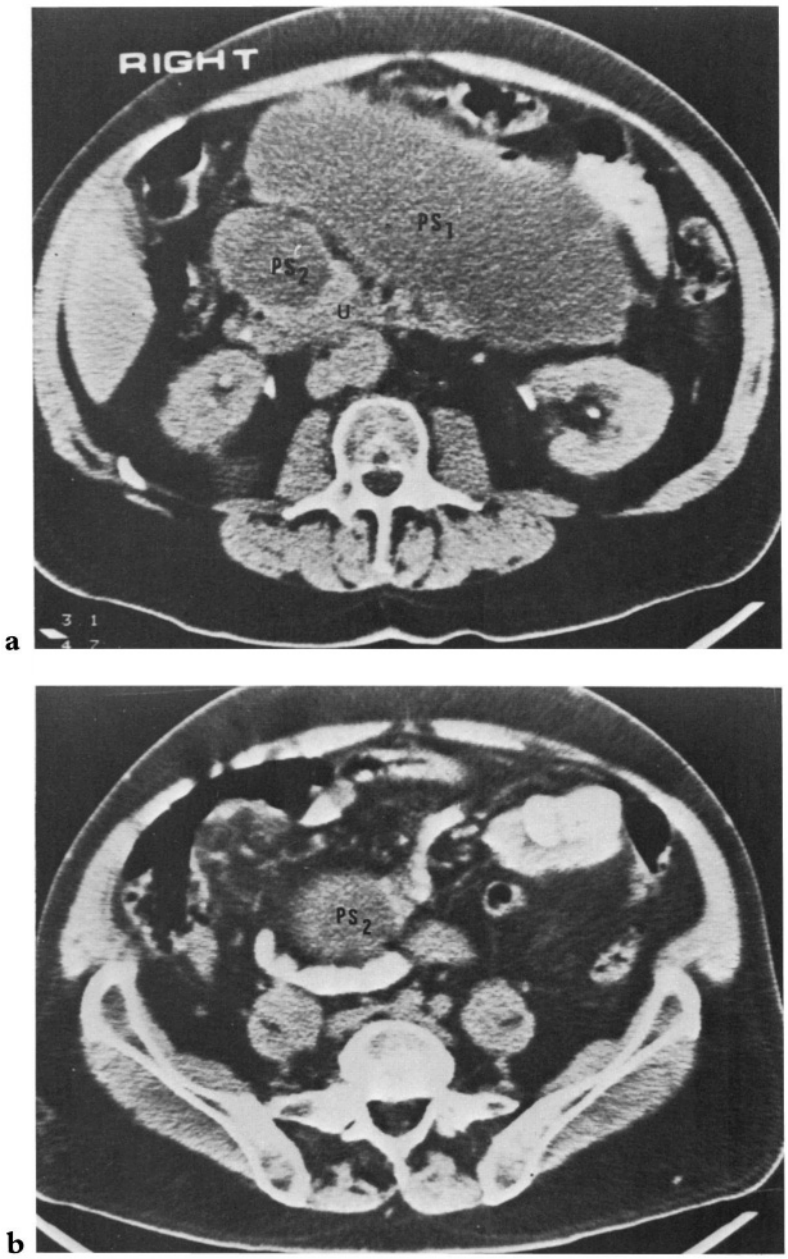


Fig. 11–34. Spread of pancreatic pseudocyst down the mesenteric root.
(a) While a large pancreatic pseudocyst *(PS_1)* occupies the lesser sac, a smaller one *(PS_2)* has developed in the region of the uncinate process *(U)*.
(b) The smaller pseudocyst has dissected down the root of the small bowel mesentery to reside in the right lower quadrant in relation to a distal ileal loop. (From Oliphant M, Berne AS.[31])

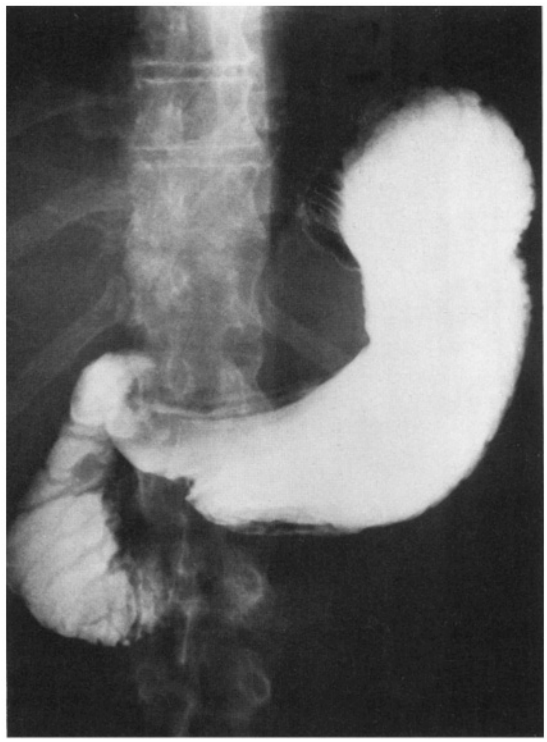


Fig. 11–35. Obstruction of the midportion of the transverse duodenum by pancreatitis extending down the mesenteric root. An associated finding is enlargement of the ampulla of Vater.
(Reproduced from Meyers and Evans.[2])

Fig. 11–36. Acute pancreatitis with jejunitis.
Besides displacement and mucosal changes in the duodenal loop, evidence of extension of pancreatic enzymes into the small bowel mesentery is shown by their effects on proximal jejunal loops. These demonstrate mucosal edema and sites of spastic narrowing with proximal dilatation.

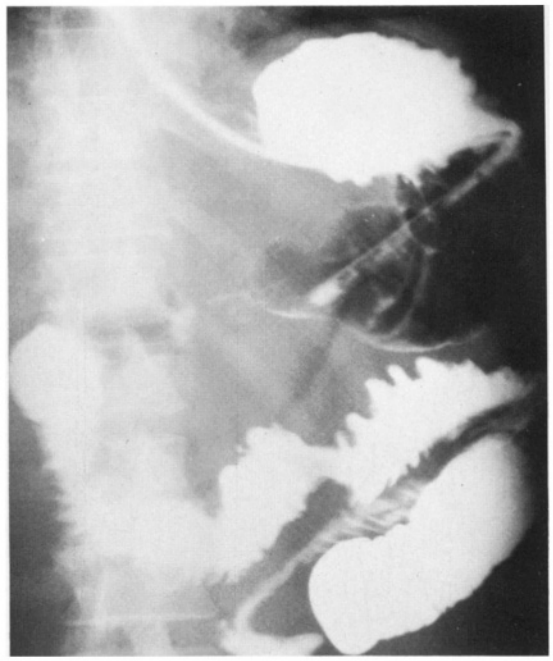




Fig. 11–37. Acute pancreatitis.
Jejunitis and ileitis are a consequence of extensive spread of pancreatic enzymes throughout the small bowel mesentery. This is shown by mucosal edema and sites of spastic narrowing with intervening dilatation.

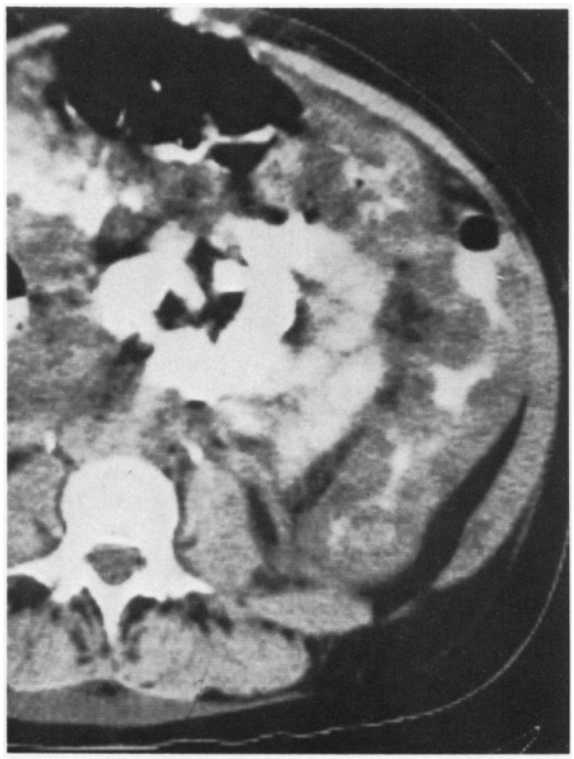


Fig. 11–38. Acute pancreatitis.
CT shows infiltration of the mesentery with severe inflammatory changes of the small bowel and colon.

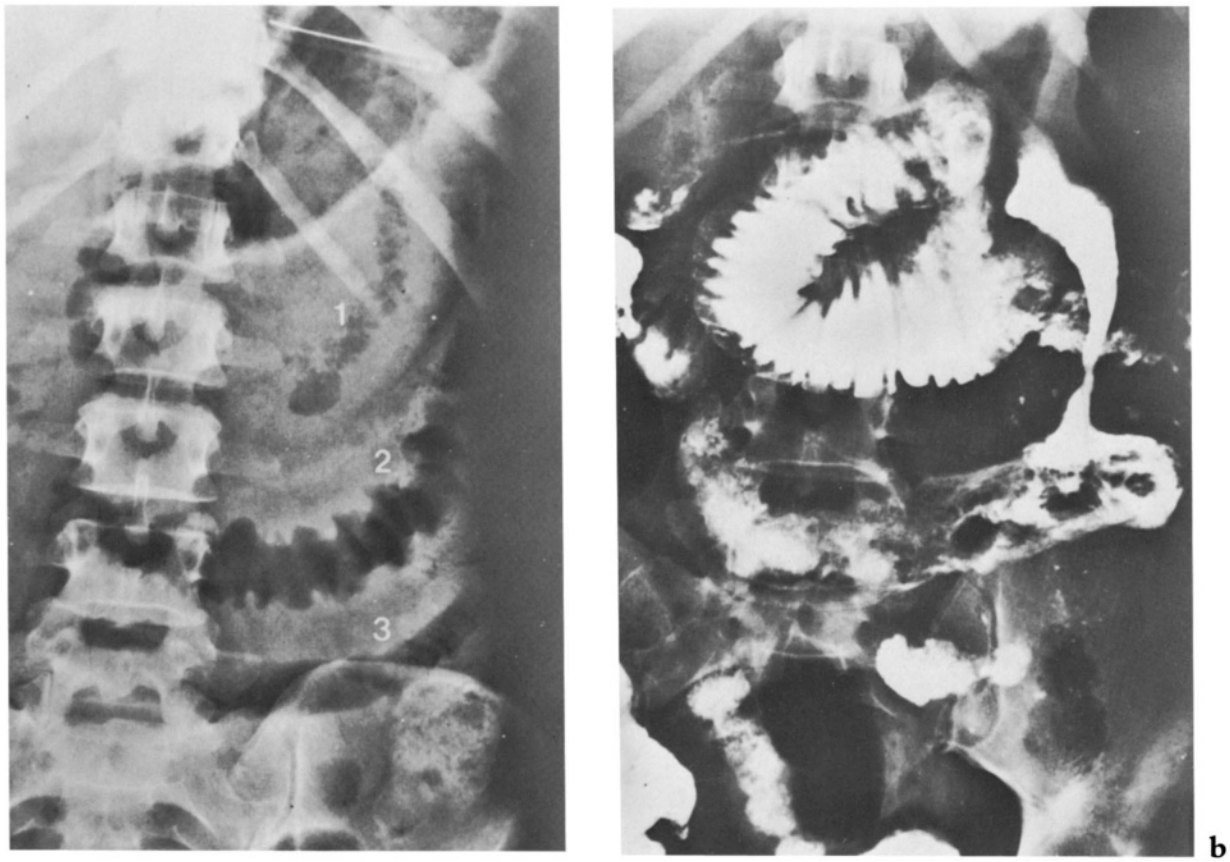


Fig. 11–39. Pneumatosis intestinalis and ischemic changes secondary to pancreatitis.
(a) Plain film shows three grossly abnormal fixed small bowel loops characterized by *(1)* bubbly gas collections, *(2)* thumbprinting and edematous mucosa, and *(3)* markedly effaced or ulcerated mucosa.
(b) Small bowel series. The involved loops show narrowing, ulceration, and pneumatosis.
These features indicate ischemic bowel changes with superimposed pneumatosis. Follow-up 1 month later, following conservative treatment, showed stricture formation in the jejunal segment.
(Reproduced from Meyers et al.[36])

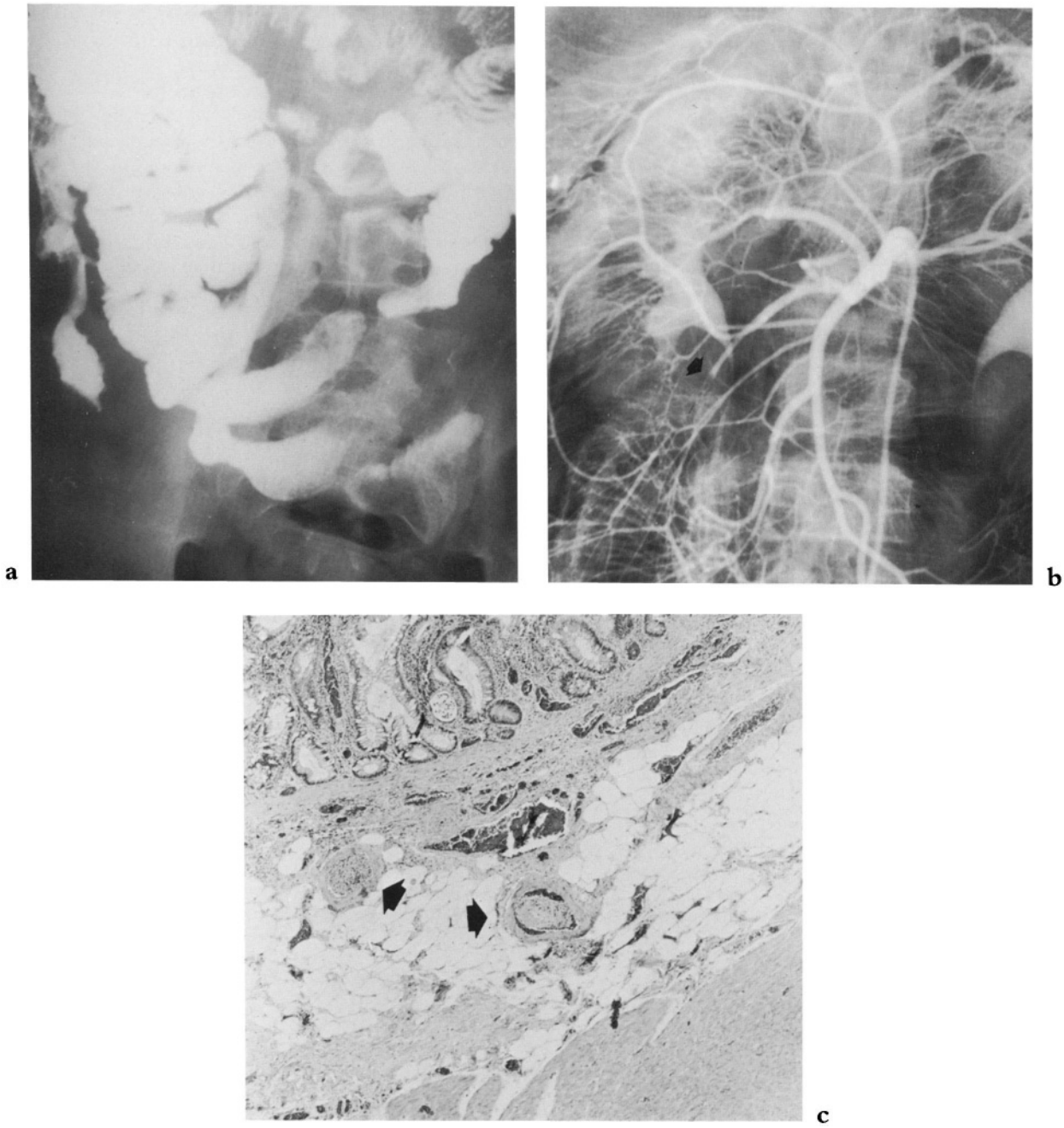


Fig. 11–40. Colonic necrosis complicating traumatic pancreatitis in a 14-year-old male.
(a) Upper GI and small bowel series reveal ischemic changes in the distal small bowel, cecum, and ascending colon. There is a tubular appearance of distal small bowel with loss of mucosal markings, fixation, and separation of loops. The cecum is conical, and there is marked spasm of the ascending colon.
(b) Selective superior mesenteric arteriography demonstrates occlusion of ileocolic branches with intraluminal thrombi *(arrow).*
Laparotomy showed pancreatitis with widespread fat necrosis and necrosis with perforation of the cecum and ascending colon. Thrombi were identified in the ileocolic artery and mesenteric branches to the ascending colon.
(c) Histologic examination of the hemicolectomy specimen shows two organizing thrombi *(arrows)* in the submucosal arterial branches and severe venous congestion. Mesenteric veins also showed organized and fresh thrombus formation (hematoxylin–eosin, × 25).
(Reproduced from Dallemand et al.[38])



Fig. 11–41. Chronic relapsing pancreatitis with ischemic atrophy of the intestinal mucosa.
The most pronounced changes in this case involve the duodenum and proximal jejunum, which are strikingly abnormal in appearance. The duodenal loop has a dilated moulagelike appearance. The duodenum and loops of jejunum have a tubular toothpaste-like aspect because of the absence of a mucosal relief pattern. Despite the castlike appearance, the involved loops are flaccid and distensible and lack evidence of fixation, rigidity, or thickening. (Reproduced from Meyers and Evans.[2])

may then include localized ileus of small bowel loops in the right lower quadrant (Fig. 11–42). This may be a transient, irritative phenomenon. At times, it may portend the development of a pseudocystic collection that can be demonstrated by its displacement of or mass effects upon ileal loops and the cecum (Figs. 11–43 through 11–45). Since this occurs only with severe pancreatitis, concomitant effects upon other portions of the bowel are usually present. This pathway may be graphically illustrated by CT (Fig. 11–34) or MRI (Fig. 11–46).



Fig. 11–42. Acute hemorrhagic pancreatitis.
Extravasated enzymes passing down the length of the root of the small bowel mesentery produce localized distention of distal ileal loops *(arrows)* in the right lower quadrant. (Reproduced from Meyers.[2])

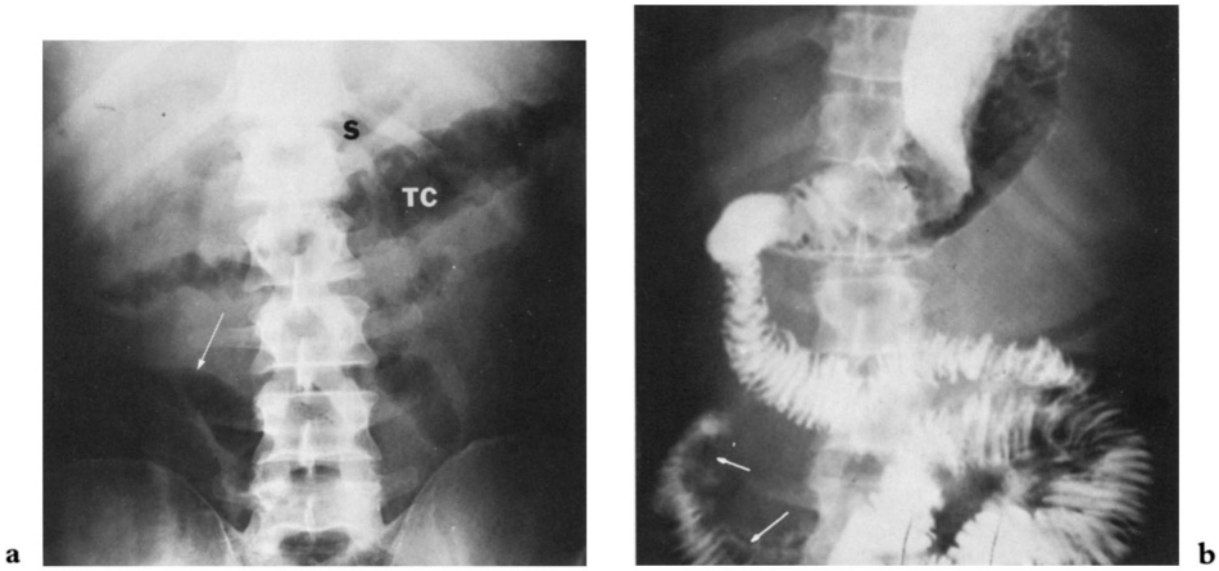


Fig. 11–43. Acute suppurative pancreatitis.
(a) Admission plain film shows small bowel ileus predominantly in the right lower quadrant *(arrow).* Note the normal relationship of the stomach *(S)* and transverse colon *(TC).*
(b) Barium study 8 days later documents jejunitis and the presence of an exudative abscess displacing distal ileal loops *(arrows)* at the end of the small bowel mesentery, associated with the development of a large pseudocyst in the tail of the pancreas.
(Reproduced from Meyers and Evans.[2])



Fig. 11–44. Acute pancreatitis extending the length of the small bowel mesentery has resulted in a right lower quadrant pseudocystic collection displacing the terminal ileum and cecum *(arrows).* Changes are also seen in the midtransverse colon near the confluence of the roots of the transverse mesocolon and small bowel mesentery.
(Reproduced from Meyers and Evans.[2])

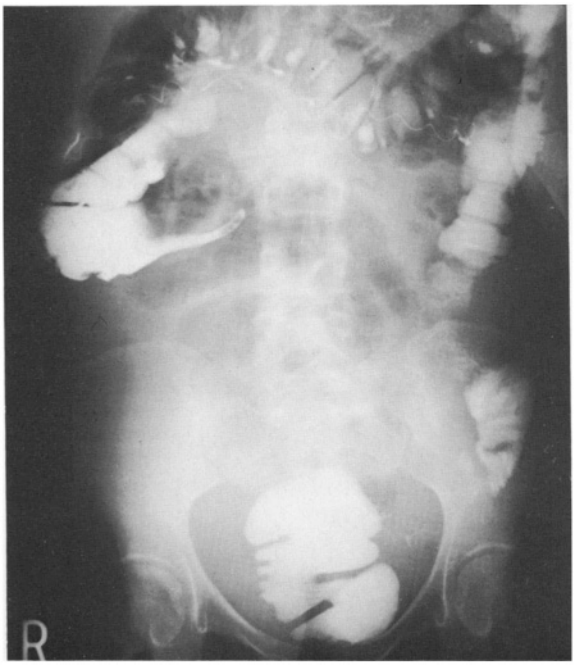


Fig. 11–45. Massive right lower quadrant pancreatic pseudocyst causes elevation of cecum and appendix.

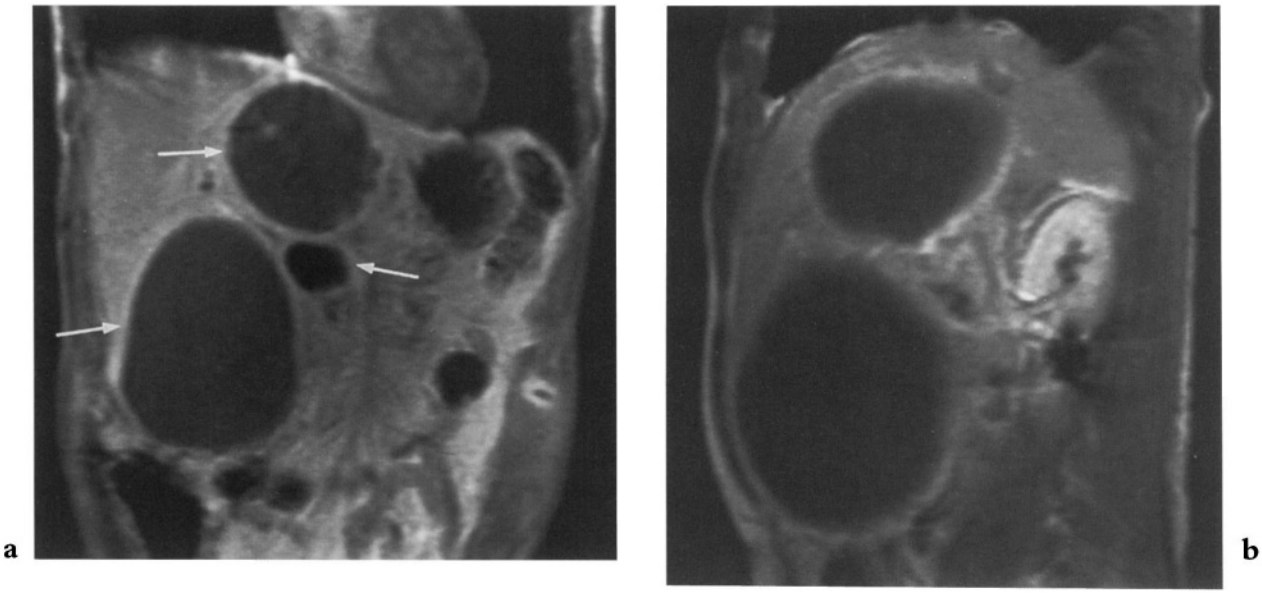


Fig. 11–46. Right lower quadrant extension of pancreatic pseudocysts.
(a) Coronal and **(b)** sagittal T1-weighted gadolinium-enhanced MR images demonstrate the relationships of three pancreatic pseudocysts *(arrows),* one of which has localized in the right lower quadrant of the abdomen. (Reproduced from Semelka RC, Ascher SM, Reinhold C: MRI of the Abdomen and Pelvis: A Text-Atlas. Wiley-Liss, New York, 1997, with permission.)

References

1. Rich AR, Duff GI: Experimental and pathologic studies on pathogenesis of acute hemorrhagic pancreatitis. Bull Johns Hopkins Hosp 1936; 58:212–259.
2. Meyers MA, Evans JA: Effects of pancreatitis on the small bowel and colon: Spread along mesenteric planes. AJR 1973; 119:151–165.
3. Mendez G, Isikoff MB, Hill MC: CT of acute pancreatitis: Interim assessment. AJR 1980; 135:463–469.
4. Jeffrey RB, Federle MP, Laing FC: Computed tomography of mesenteric involvement in fulminant pancreatitis. Radiology 1983; 147:185–188.
5. Meyers MA, Oliphant M, Berne AS, et al: The peritoneal ligaments and mesenteries: Pathways of intra-abdominal spread of disease. Annual oration. Radiology 1987; 163:593–604.
6. Waring HJ, Griffiths HE: Acute pancreatitis. Br J Surg 1924; 11:476–490.
7. Meyers MA, Whalen JP: Roentgen significance of duodenocolic relationships: Anatomic approach. AJR Rad Ther Nucl Med 1973; 117:263–274.
8. Meyers MA: Roentgen significance of the phrenicocolic ligament. Radiology 1970; 95:539–545.
9. van der Zypen E, Révész E: Investigation of development, structure and function of the phrenocolic and duodenal suspensory ligaments. Acta Anat 1984; 119:142–148.
10. Aronson AR, Davis DA: Obstruction near hepatic flexure in pancreatitis: Rarely reported sign. JAMA 1961; 176:133–134.
11. Price CWR: "Colon cut-off sign" in acute pancreatitis. Med J Aust 1956; 1:313–314.
12. Stuart C: Acute pancreatitis: Preliminary investigation of new radiodiagnostic sign. J Fac Radiologists 1956; 8:50–58.
13. Brascho DJ, Reynolds TN, Zanca P: Radiographic "colon cut-off sign" in acute pancreatitis. Radiology 1962; 79:763–768.
14. Forlini E: Stenosi del colon da pancreatitis. Gior Clin Med 1927; 8:609–620.
15. L'Hermine C, Pringot J, Monnier JP, et al: Le retentissement colique des pancréatites: A propos de 39 observations 1980; J Radiol 61:27–34.
16. Mohuiddin S, Sakiyalak P, Gullick HD, et al: Stenosing lesions of the colon secondary to pancreatitis. Arch Surg 1971; 102:229–231.
17. Remington JH, Mayo CW, Docketty MB: Stenosis of colon secondary to chronic pancreatitis. Proc Staff Meet Mayo Clin 1947; 22:260-264.
18. Thompson WM, Kelvin FM, Rice RP: Inflammation and necrosis of the transverse colon secondary to pancreatitis. AJR 1977; 128:943–948.
19. Schwartz S, Nadelhaft J: Simulation of colonic obstruction at splenic flexure by pancreatitis: Roentgen features. AJR Ther Nucl Med 1957; 78:607–616.
20. Hunt DR, Mildenhall P: Etiology of strictures of the colon associated with pancreatitis. Am J Dig Dis 1975; 20:941–946.
21. Meyers MA, Volberg F, Katzen B, et al: Haustral anatomy and pathology: A new look. II. Roentgen interpretation of pathologic alterations. Radiology 1973; 108:505–512.
22. Berne TV, Edmondson HA: Colonic fistulization due to pancreatitis. Am J Surg 1966; 111:359-363.
23. Bohlman TW, Katon RM, Lee TG, et al: Use of endoscopic retrograde cholangiopancreatography in the diagnosis of pancreatic fistula: A case report and review of the literature. Gastroenterology 1976; 70:582–584.
24. Clements JL Jr, Bradley EL III, Eaton SB Jr: Spontaneous internal drainage of pancreatic pseudocysts. AJR 1976; 126:985–991.
25. Alexander ES, Clark RA, Federle MP: Pancreatic gas: Indication of pancreatic fistula. AJR 1982; 139:1089–1093.
26. Farman J, Kotcher R, Dallemand S, et al: Unusual pelvic complications of a pancreatic pseudocyst. Gastrointest Radiol 1978; 3:43–45.
27. Salvo AF, Nematolahi H: Distant dissection of a pancreatic pseudocyst into the right groin. Am J Surg 1973; 126:430–432.
28. Strax R, Tooms BD, Rauschkolb EN: Correlation of barium enema and CT in acute pancreatitis. AJR 1981; 136:1219–1220.
29. Warshaw AL: Inflammatory masses following acute pancreatitis. Phlegmon, pseudocyst, and abscess. Surg Clin North Am 1974; 54:621–636.
30. Gumaste VV, Gupta R, Wasserman D, et al: Co-Ionic involvement in acute pancreatitis. Am J Gastroenterol 1995; 90:640–641.
31. Oliphant M, Berne AS: Computed tomography of the subperitoneal space: Demonstration of direct spread of intraabdominal disease. J Comput Assist Tomogr 1982; 6:1127–1137.
32. Simon M, Lerner MA: Duodenal compression by mesenteric root in acute pancreatitis and inflammatory conditions of bowel. Radiology 1962; 79: 75–80.
33. Safrit HD, Rice RP: Gastrointestinal complications of pancreatitis. Radiol Clin North Am 1989; 27(1): 73–79.
34. Boijsen E, Tylen U: Vascular changes in chronic pancreatitis. Acta Radiol Diagn 1972; 12:34–38.

35. Walter JF, Chuang VP, Bookstein JJ, et al: Angiography of massive hemorrhage secondary to pancreatic disease. Radiology 1977; 124:337–342.
36. Meyers MA, Ghahremani GG, Clements JL Jr, et al: Pneumatosis intestinalis. Gastrointest Radiol 1977; 2:91–105.
37. Collins JJ Jr, Peterson LM, Wilson RE: Small intestinal infarction as a complication of pancreatitis. Ann Surg 1968; 167:433–436.
38. Dallemand S, Farman J, Stein D, et al: Colonic necrosis complicating pancreatitis. Gastrointest Radiol 1977; 2:27–30.
39. Griffiths RW, Brown PW Jr: Jejunal infarction as a complication of pancreatitis. Gastroenterology 1970; 58:709–712.
40. Katz P, Dorman MJ, Aufses AH Jr: Colonic necrosis complicating postoperative pancreatitis. Ann Surg 1974; 179:403–405.

Pathways of Regional Spread in Pancreatic Cancer

12

Chusilp Charnsangavej, M.D.

Regional spread of pancreatic ductal adenocarcinoma is common at the time of diagnosis, and it is often associated with poor prognosis.[1–4] This is because the pancreas is an organ that is located in the retroperitoneum adjacent to many structures and organs, and there is no fibrous capsule or fascial plane to confine the organ. The pathways of regional spread include local organ or structure invasion, perineural spread, vascular invasion, and lymph node metastasis. Diagnosis of regional spread of pancreatic ductal adenocarcinoma is important for surgical planning because the prognosis of patients undergoing pancreatic resection with a positive margin and lymph node metastases is very poor. Conventional imaging modalities such as CT, MR imaging, and ultrasonography often understage locally advanced disease at pretreatment staging. However, new imaging techniques, such as helical CT with thin-section collimation and fast MR imaging with intravenous dynamic contrast enhancement, have improved the ability to define locally advanced disease.

This chapter defines the pathways of regional spread of pancreatic ductal adenocarcinoma on imaging studies based on the anatomic relationship between the pancreas and its surrounding structures, organs and adjacent blood vessels, lymphatic vessels and nodes, and nerves.

Anatomy of the Pancreas

The pancreas lies transversely along its long axis in the anterior pararenal space of the retroperitoneum.[5,6] The head of the pancreas lies within the C-loop of the second portion of the duodenum. The lateral surface of the head is against the serosa of the duodenum. The posterior surface of the head is separated from the inferior vena cava by only retroperitoneal fat and on occasion small posterior peripancreatic nodes. Medially, the head of the pancreas is closely related to the superior mesenteric artery (SMA) and superior mesenteric vein (SMV). At the caudal portion of the head, a small portion of the pancreas extends behind the SMA and SMV, forming an uncinate process. It is connected to the SMA and SMV by small twigs of vessels that are branches of the jejunal artery and vein or that arise directly from the posterior wall of the SMA and SMV and a plexus of nerves between the head of the pancreas and the SMA. The cranial portion of the head of the pancreas is located on the right side of the SMA and SMV. As the SMV joins the splenic vein to form the portal vein, it courses behind the head of the pancreas, and from that point, extending to the left retroperitoneum, the head of the pancreas becomes the body.

The body and tail of the pancreas course transversely to the left side of the retroperitoneum toward the splenic hilum. After passing in front of the abdominal aorta and celiac axis, it curves posteriorly and in the cranial direction. In most cases, it follows the course of the splenic artery and vein, staying anterior and slightly caudal to those vessels.

Anteriorly, the pancreas is covered by posterior peritoneal layers that form the posterior wall of the lesser sac and the inframesocolic compartment of the peritoneal cavity. Just at the caudal margin along the body and tail of the pancreas, the root of the transverse mesocolon, which is formed by those two posterior peritoneal layers, merges anteriorly to suspend the transverse colon into the peritoneal cavity. The root of the transverse

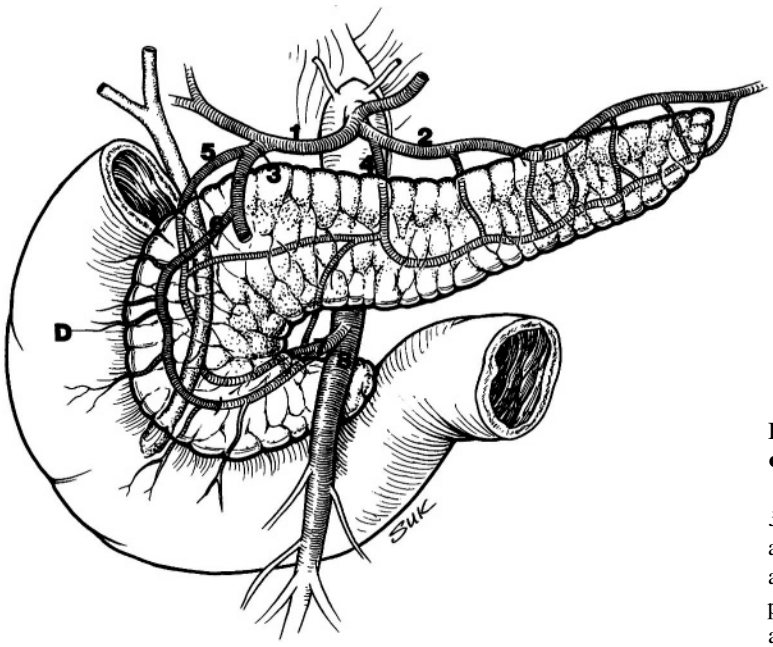


Fig. 12–1. Illustration of the arterial anatomy of the pancreas.
1 = common hepatic artery; *2* = splenic artery; *3* = gastroduodenal artery; *4* = dorsal pancreatic artery; *5* = posterior superior pancreaticoduodenal artery (SPDA); *6* = anterior SPDA; *7* = inferior pancreaticoduodenal artery; *8* = superior mesenteric artery; *D* = duodenum.

mesocolon extends to the right, traversing across the head of the pancreas and second portion of the duodenum. The transverse mesocolon forms the inferior boundary of the lesser sac.

Vascular Anatomy

The pancreas receives blood supply from multiple branches of the celiac axis and the SMA.[5–8] The head of the pancreas is supplied by a network of arteries that originates from three major arteries (Fig. 12–1). The gastroduodenal artery (GDA) descends from the common hepatic artery (CHA) in the retropyloric space between the pylorus and the cranial portion of the head of the pancreas. Proximally, it gives off a branch posteriorly that runs along the posterior lateral surface of the pancreatic head along the common bile duct, the posterior superior pancreaticoduodenal artery (SPDA). The GDA continues its course in the craniocaudal direction anterior to the head of the pancreas and then bifurcates to form a branch coursing anteriorly in the gastrocolic ligament to become the right gastroepiploic artery, which runs along the greater curvature of the pylorus. The other branch continues in the craniocaudal direction close to the anterior surface of the pancreas as the anterior SPDA. The posterior and anterior SPDAs then form an anastomotic network around the head of the pancreas with the inferior pancreaticoduodenal artery (IPDA) and a branch of the dorsal pancreatic artery.

The IPDA arises from the proximal jejunal artery or directly from the SMA. These arteries usually originate from the posterior wall of the SMA. The IPDA gives off a few small branches to the uncinate process and gives off a branch posteriorly to join the posterior SPDA and another branch anteriorly to join the anterior SPDA.

The dorsal pancreatic artery originates from the posterior or caudal surface of the celiac axis or the proximal 1–2 cm of the common hepatic or splenic artery. It can be identified behind the proximal portion of the body of the pancreas. It usually gives off a branch to the right, medial to the cranial portion of the head of the pancreas and the portal vein. This branch runs medially along the head of the pancreas and anastomoses with the peripancreatic arcade around the head of the pancreas.

The body and tail of the pancreas receive their blood supply from the dorsal pancreatic artery and multiple branches along the course of the splenic artery. The dorsal pancreatic artery courses along the body and tail and anastomoses with small branches from the splenic artery.

The venous drainage of the head of the pancreas forms a network around the head and follows a branching pattern similar to the artery (Fig. 12–2). The anatomy of these veins is relatively constant, but the course of the veins and their drainage patterns differ from the artery. The confluence of the SMV and the splenic vein forms the portal vein. The relationship of these three veins with the pancreas is most important in pancreatic surgery. The segment of the SMV at the caudal portion of the head of the pancreas receives two important

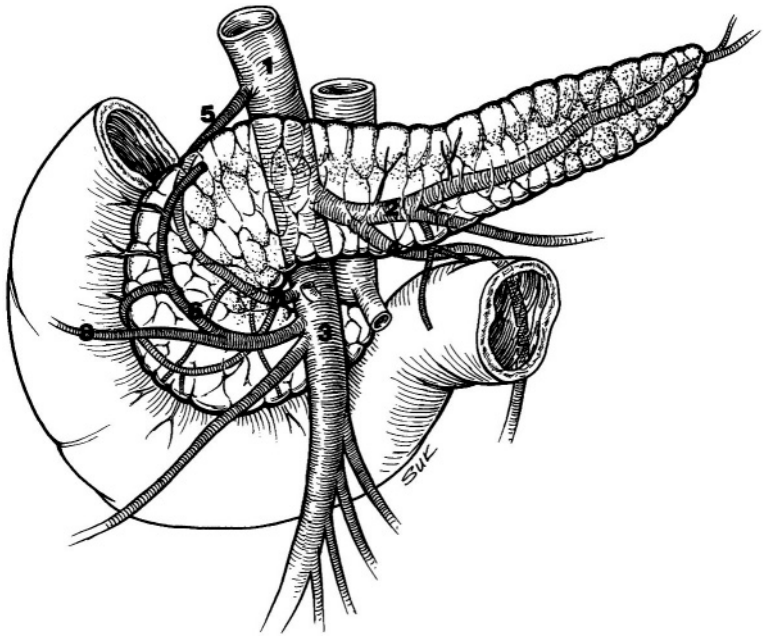


Fig. 12–2. Illustration of the venous anatomy of the pancreas.
1 = portal vein; *2* = splenic vein; *3* = superior mesenteric vein; *4* = inferior mesenteric vein; *5* = posterior superior pancreaticoduodenal vein (SPDV); *6* = anterior SPDV; *7* = inferior pancreaticoduodenal vein; *8* = right colic vein.

branches that are closely associated with the uncinate process and the head, the proximal jejunal vein, and the gastrocolic trunk. The proximal jejunal vein that drains the proximal segment of the jejunum frequently drains into the SMV posteriorly. Before it enters into the SMV, it picks up the drainage from the inferior pancreaticoduodenal vein (IPDV). The gastrocolic trunk, which is formed by the right gastroepiploic vein, the middle colic vein, and the right colic vein, runs in the gastrocolic ligament and drains into the SMV anteriorly. The posterior superior pancreaticoduodenal vein (SPDV) follows the bile duct and drains into the caudal surface of the main portal vein within 2 cm of the confluence of the SMV and splenic vein, in most cases. The anterior SPDV is a smaller vein that runs horizontally along the anterior surface of the head of the pancreas before joining the gastrocolic trunk and draining into the SMV.

At the confluence of the SMV and the splenic vein that forms the portal vein, the inferior mesenteric vein may join the portal vein in this region; 60–70% join the splenic vein and 30–40% join the SMV. The portal vein then ascends behind the head of the pancreas to enter into the hepatoduodenal ligament. This segment of the SMV and portal vein is in close contact with the pancreas.

Venous drainage of the body and tail of the pancreas is more variable, but it consists of multiple small branches draining into the splenic vein that courses along the tail and body of the pancreas.

Lymphatic Anatomy

Lymphatic vessels of the pancreas originate from the interlobular network in the pancreatic parenchyma.[5,6] They form collecting trunks that follow the pancreatic and peripancreatic blood vessels and drain into the regional lymph nodes according to the pancreatic regions.[9] Lymphatic drainage of the body and the tail of the pancreas drains into the nodes at the splenic hilum and follows the splenic artery to the celiac node, which is the principal nodal group.

The lymphatic drainage of the anterior cephalad portion of the head of the pancreas follows lymphatic vessels along the anterior SPDA to the pyloric (or "subpyloric") nodal group, which consist of several lymph nodes along the GDA where it originates from the CHA. This nodal group is located behind the pylorus and anteriosuperior to the head of the pancreas. Posteriorly, the lymphatic drainage of the cephalad portion follows the bile duct to drain into the nodes along the bile duct posterior to the portal vein in the hepatoduodenal ligament and can continue to the hepatic hilar node. The alternate route is to follow the posterior SPDA to the pyloric node. These pathways can also be defined as the superior or ascending pathways, and they drain into the celiac node as their principal node.[9]

The lymphatic drainage of the caudal portion of the head of the pancreas and the uncinate process follows the inferior pancreaticoduodenal vessels to the superior mesenteric artery lymph node and drains into the ret-

roperitoneal paraaortic lymph node. This pathway can be defined as the inferior or descending pathway.[9]

Several classification systems, including those from the Japanese Pancreatic Society[4] and our institution,[10] have been adopted to define the precise location of nodal stations based on surgical pathologic specimens. The systems usually describe nodal station in relationship to the pancreas and the peripancreatic vessels. The anterior and posterior pancreaticoduodenal nodes are those nodes near the pancreaticoduodenal groove anterior and posterior to the pancreas. The superior nodes are those nodes cephalad to the plane of the main pancreatic duct from the neck of the pancreas to the ampulla, and caudal to that plane are the inferior nodes. These systems are not practical to apply on cross-sectional imaging studies such as CT because the plane of the pancreatic duct is oriented obliquely. However, nodal groups along the GDA, pancreaticoduodenal arcades, and IPDA can be defined with a proper helical scanning technique.

Pancreatic Nerve Plexus

The pancreas is innervated by the networks of the sympathetic and parasympathetic chain that pass through the celiac ganglia and superior mesenteric ganglia. The nerves from the celiac and superior mesenteric plexus generally follow the arteries supplying the pancreas.

Imaging Studies

Advances in thin-section helical CT have improved the ability to demonstrate precise pancreatic anatomy. With proper intravenous contrast enhancement techniques, small vessels around the pancreas can readily be shown in most patients.[11–16] The relationships between the pancreas and surrounding structure and organs are easily defined. However, nerve plexi, lymphatic vessels, and normal lymph nodes are still not regularly defined with current imaging technology. In this section, I define the anatomy of the pancreas and peripancreatic vessels based on the vascular anatomy as seen on thin-section helical CT.

CT Anatomy of the Pancreatic Head

The vessels around the head of the pancreas can be identified on CT by following the course of the SMV, the gastrocolic trunk, the gastroduodenal artery, the posterior SPDA and SPDV, the anterior SPDA and SPDV, the proximal jejunal vessels, and the IPDA and IPDV (Fig. 12–3). These vessels form excellent anatomic landmarks around the head of the pancreas. At the level of the cranial portion of the head of the pancreas, the gastroduodenal artery is located in the retropyloric space at the anterolateral surface and can be seen in almost every case. The posterior SPDA and SPDV can be identified along the posterior lateral surface accompanying the bile duct in 72–88% of CT scans.[11–13] The posterior SPDV can be followed cranially, and it drains into the caudal surface of the suprapancreatic segment of the portal vein. Medial to the pancreatic head and behind the pancreatic neck, the SMV is routinely seen here, and on occasion, the branch of the dorsal pancreatic artery to the head of the pancreas may be seen. The 1MV can be seen draining into the left side of the SMV in this location in 50–70%.

At the midlevel of the head of the pancreas, the anatomic landmark is the gastrocolic trunk where it enters into the SMV.[15] Although the branching patterns that form the gastrocolic trunk may vary, the site where it enters into the SMV and the position of the SMV in relationship to the head of the pancreas are constant. The gastrocolic trunk enters into the SMV anteriorly, and the SMV is usually anterior and medial to the head. The position of the posterior SPDV and the bile duct remains the same at the posterolateral surface of the head of the pancreas. The anterior SPDA continues the same course of the gastroduodenal artery at the anterolateral surface of the head, but the anterior SPDV can be seen draining into the gastrocolic trunk. The anterior SPDV is a small vein that is closely approximated to the head. Its course can be similar to a larger right colic vein that is located at the root of the transverse mesocolon and also drains into the gastrocolic trunk. This may explain the difference in the ability to identify this vein, as reported by Crabo et al. and Ibukuro et al. (98% vs. 50%, respectively).[11,12] At this same level of the head of the pancreas, the branches of the IPDV may be identified at the posterior surface of the head as it forms a network with the posterior SPDV.

At the level of the caudal portion of the head and the uncinate process, the IPDV can be identified medial to the head as it connects with the proximal jejunal vein before entering into the posterior wall of the SMV. This type of anatomy can be seen in 66–90% of cases. The branching pattern of the IPDA and proximal jejunal artery is similar to that of the veins.

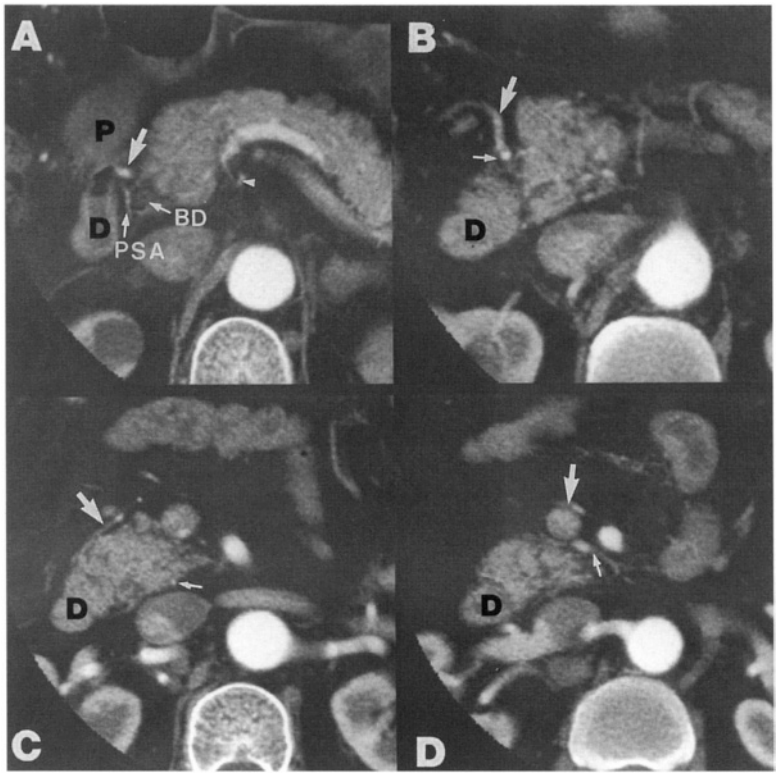
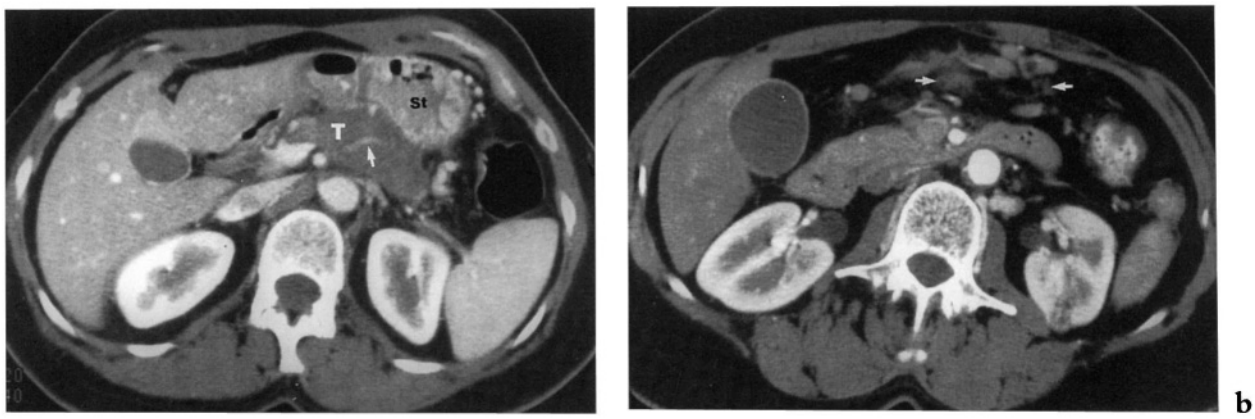


Fig. 12–3. Arterial anatomy of the pancreas (see text).
(a) The gastroduodenal artery *(arrow)* is behind the pylorus *(P).* The posterior superior pancreaticoduodenal artery *(PSA)* accompanies the bile duct *(BD).* The dorsal pancreatic artery *(arrowhead)* gives off a branch medial to the pancreatic head. *D* = duodenum.
(b) The gastroepiploic artery *(large white arrow)* is branching out from the gastroduodenal artery *(small white arrow),*
(c) The anterior superior pancreaticoduodenal artery *(large white arrow)* and posterior inferior pancreaticoduodenal artery *(small white arrow)* form an arcade around the head of the pancreas.
(d) Anterior to the uncinate process is the jejunal vein *(small white arrow)* draining into the SMW *(large white arrow).*

Pathways of Regional Spread in Pancreatic Cancer

Local Organ Invasion

Pancreatic ductal adenocarcinoma has a propensity to invade adjacent organs and structures surrounding the pancreas, depending on the site of the primary tumor. The tumors in the tail and body of the pancreas often present at an advanced stage because of the lack of symptoms (Fig. 12–4). The tumors may involve the spleen, stomach, and the splenic flexure of the colon, and not infrequently, they invade the surrounding retroperitoneal organs such as the left adrenal gland, the upper pole of the left kidney, and the left renal vein and spread along the transverse mesocolon (Fig. 12–4). This locally advanced disease is usually associated with vascular involvement along the celiac axis (Figs. 12–4 and 12–5) and the superior mesenteric artery and with distant metastasis to the liver and peritoneum, which makes it unlikely that patients will be operable candidates.



a b

Fig. 12–4. Locally advanced pancreatic carcinoma with invasion of the splenic artery and the stomach and metastases in the transverse mesocolon.
(**a**) Large tumor *(T)* from body of pancreas with invasion of the posterior wall of stomach *(St)* and encasement of the splenic artery *(arrow),*
(**b**) CT 4 cm caudal to **a** shows multiple tumor deposits *(arrows)* in the transverse mesocolon.



Fig. 12–5. Locally advanced pancreatic carcinoma *(T) of* body of pancreas with perivascular and perineural involvement of celiac plexus *(arrow).*

The primary tumors in the head of the pancreas, on the other hand, present earlier because of the high potential of obstructive jaundice. Yet, most of the tumors, even though they are small, extend beyond the contour of the pancreas at presentation. Local organ involvement such as the duodenum by carcinoma of the head of the pancreas is common (Fig. 12–6), but it does not have impact on resectability because both the pancreas and duodenum are removed together at pancreaticoduodenectomy. Involvement of the inferior vena cava and the transverse mesocolon is rare (Fig. 12–6), but their involvement are not absolute criteria of unresectability and will be considered on an individual basis. At our institution, pancreatic surgeons use the following criteria as guidelines for resectability of pancreatic carcinoma at the head of the pancreas: (a) lack of distant metastasis such as hepatic and peritoneal metastasis; (b) no involvement of the superior mesenteric artery or

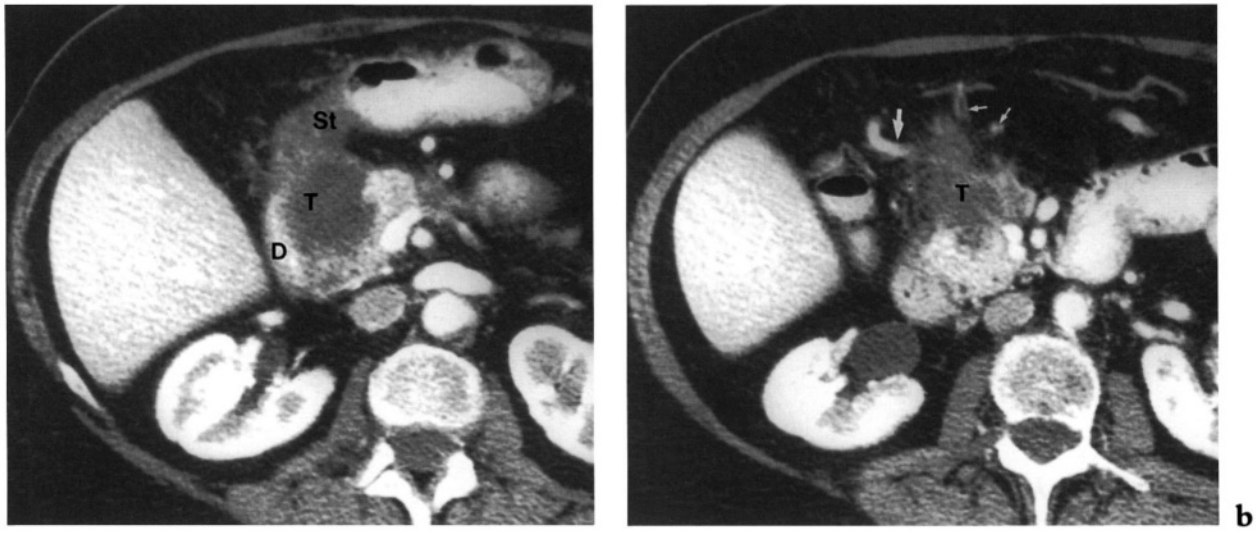


Fig. 12–6. Ductal adenocarcinoma of head of pancreas with local invasion to duodenum, stomach and transverse mesocolon.
(a) CT shows hypodense tumor *(T)* involving the duodenum *(D)* and posterior wall of antrum of stomach *(St).*
(b) CT 2 cm caudal to **a** shows tumor *(T)* extending into the transverse mesocolon along the gastroepiploic *(large white arrow)* and middle colic veins *(small white arrows).*

celiac axis; and (c) the superior mesenteric and portal venous confluence must be patent.[17] Vascular involvement is described in the next section.

Vascular Involvement

Identification of pathways of tumor spread is important for surgical planning in order to achieve a margin-negative resection, particularly when the tumor spreads beyond the usual extent of pancreaticoduodenectomy or when the tumor is located in the retroperitoneum behind the SMA where direct intraoperative assessment is not possible until the final stage of resection (Figs. 12–7 and 12–8). However, tumors arising from the pancreas adjacent to the duodenum tend to infiltrate along the anterior SPDA toward the gastroduodenal artery behind the pylorus (Fig. 12–9) and the proper hepatic artery in the hepatoduodenal ligament or along the posterior SPDV toward the inferior surface of the portal vein. Tumors arising in the cranial portion of the pancreatic head near the neck may infiltrate superiorly toward the CHA (Fig. 12–10) or infiltrate inferiorly into the mesentery and transverse mesocolon and along the SMV. Tumors arising from the uncinate process may infiltrate along the IPDA or IPDV toward the posterior surface of the SMA (Fig. 12–8) or into the jejunal mesentery where the IPDA originates from. Tumors arising from the head of the pancreas near the confluence of the gastrocolic trunk where it drains into the SMV may infiltrate into the base of the transverse mesocolon along the middle colic artery or vein (Fig. 12–6). Knowledge of this anatomy and of the potential pathways of local tumor invasion is important for surgical planning when an aggressive surgical approach is planned.

We defined CT criteria of vascular involvement and used these criteria to assess vascular involvement in 56 patients with pancreatic ductal adenocarcinoma who underwent surgical exploration.[18,19] When there was a fat plane (type A) or normal pancreatic parenchyma (type B) separating the tumor from adjacent vessels, the tumor was resected without venous resection in 21 of 22 patients (95%). When the tumor was inseparable from the vessels but the points of contact formed a convexity against the vessel (type C), it was not reliable to predict whether the tumor was fixed against the vessel (Fig. 12–11). When the tumor was partially encircling (type D), the tumor was fixed against the vessels in most cases (Figs. 12–8 and 12–12). The resectable rate was 47%, but resection also required venous resection. When the tumor was completely encircling (type E) or



Fig. 12–7. Tumor *(T)* involving the head of the pancreas.
Note tumor infiltrate *(t)* along the superior mesenteric artery *(arrow).* It is not possible to distinguish perivascular or perineural invasion in this case because the nerve plexus also accompanies the artery. The lesion is not resectable.



Fig. 12–8. Tumor *(T)* involving the uncinate process.
Note hypodense tumor infiltrate along the inferior pancreaticoduodenal artery *(small arrow)* behind the superior mesenteric artery *(large arrow).* This lesion is not resectable.



Fig. 12–9. Tumor in cephalad portion of head of pancreas.
Tumor *(T)* involves the gastroduodenal artery *(large arrow)* and the replaced right hepatic artery *(small arrows)* from the SMA.

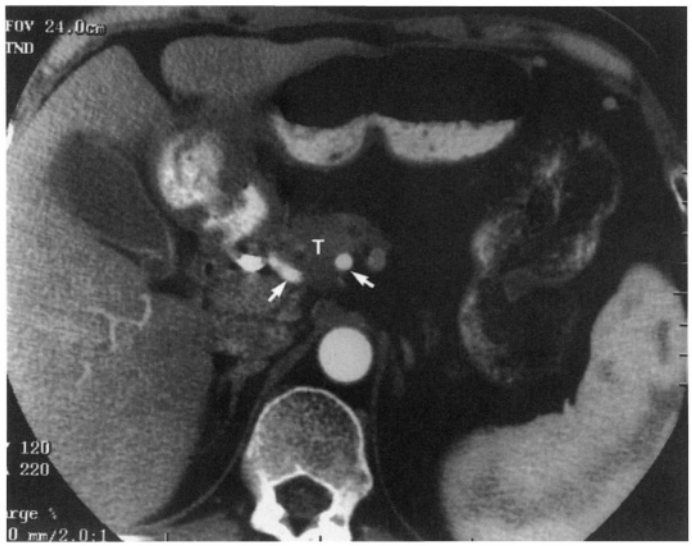


Fig. 12–10. Tumor *(T)* at neck of pancreas with direct involvement of the common hepatic artery *(arrow).*



Fig. 12–11. Ductal adenocarcinoma of head of pancreas. Medial extension of tumor *(small arrow)* just abuts the SMA *(large arrow),* a type C vascular involvement. Patient did not undergo resection because metastatic disease in liver was found on follow-up study.

occluding (type F) the vessel, all tumors were not resectable with a negative margin. We believe that these improved results are largely due to scanning with thin sections during the bolus phase of intravenous contrast enhancement, when the lesion and its extent along the vessels are easier to identify.

With our scanning technique described earlier, we have shown that CT accurately defines the extent of vascular involvement and correctly predicts resectability in 88% of patients.

Nodal Metastasis

Lymph node metastases are common in pancreatic tumors because of rich lymphatic networks around the pancreas. They are found in 40–75% of patients with tumors larger than 2 cm on pathologic examinations.[4] The majority of lymph node metastases are found at the peripancreatic nodal group, including the anterior and posterior peripancreatic nodes, pancreaticoduodenal lymph nodes, pyloric nodes (Fig. 12–13), and inferior

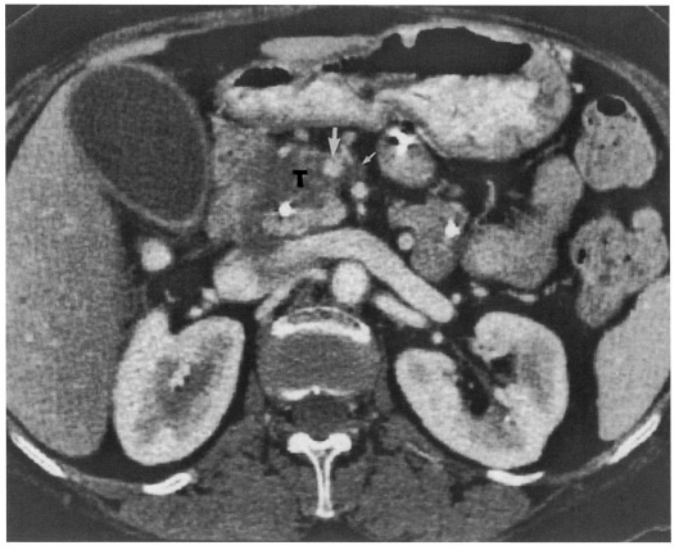


Fig. 12–12. Ductal adenocarcinoma of head of pancreas. Tumor *(T)* involves the superior mesenteric vein *(large arrow),* a type D involvement. Tumor was resected with venous resection. The small hypodense nodule *(small arrow)* between the SMV and SMA was confirmed to be a metastatic node.



Fig. 12–13. Pancreatic ductal adenocarcinoma involving body and cephalad portion of head of pancreas. Note node *(n)* anterior to the gastroduodenal artery *(arrow)* and behind the gastric antrum *(St).* A metastatic node was confirmed at surgery. *T* = tumor in body of pancreas.

nodes along the IPDA (Fig. 12–14). Metastases to the nodes in the hepatoduodenal ligament, common hepatic nodes, and celiac node are rare (less than 10%).[4] Currently, preoperative assessment of nodal metastasis by CT or MR is not accurate enough to make an impact on surgical planning because no better criteria of nodal metastasis can be applied other than the size.[20–22] MR may provide a better potential because metastatic nodes may be hyperintense on T2-weighted images, but this potential has yet to be proved. The Radiology Diagnostic Oncology Group study has shown that the sensitivity to predict nodal metastasis was only 37% by CT and 34% by MR, and the specificity was 60% by CT and 76% by MR, with the positive and negative predictive values ranging between 47% and 57%.[21] The results from our unpublished data using the thin-section CT scanning technique are similar to this study. We believe that these poor results are due to several factors, including (a) the inability to diagnose microscopic metastasis in small nodes (3–5 mm); (b) the large inflammatory nodes mistaken as metastasis; (c) poor understanding of the pathways of nodal metastasis in pancreatic tumors in cross-sectional imaging; and (d) possibly misinterpreting tumor infiltration as a nonnodal disease. It should be emphasized that nodal metastasis around the pancreas would not impact surgical planning because metastatic nodes are mostly removed in the specimen of pancreaticoduodenectomy; however, its presence would influ-



Fig. 12–14. Large tumor *(T)* involving head of pancreas. Multiple hypodense nodes are shown along the SMA and jejunal mesentery *(short arrows)* and the upper paraaortic region *(long arrow).* This is the descending or inferior pathway of nodal metastasis.

ence the outcome of surgery. It is more important to recognize nodal metastasis in the nodal groups, such as the mesenteric nodes, the common hepatic artery node, and the celiac node, that may not be included in the resected specimen because metastasis to these nodes would preclude patients from surgery.

Recently, we developed new criteria to try to improve the sensitivity and specificity in predicting nodal metastasis in patients with pancreatic carcinoma.[23] We have observed that (a) low-density nodes with irregular margins are highly specific for metastatic disease but they are not sensitive enough to detect the majority of metastatic nodes (Figs. 12–12 and 12–14); (b) using the size of lymph node larger than 5 mm in the inferior pancreatic nodal group increases the sensitivity to detect nodal metastasis; and (c) enlarged nodes in the periportal and common hepatic nodal groups are nonspecific and can be seen in patients with chronic pancreatitis or node-negative pancreatic cancer.

Perineural Invasion

Perineural invasion is common in pancreatic ductal adenocarcinoma. However, the diagnosis is made on histologic examination and rarely by imaging studies because of the inability to define nerves around the pancreas. There are no objective criteria to define perineural invasion by imaging studies. It is also possible that perivascular invasion along the arteries around the pancreas is, in fact, perineural invasion because most of the peripancreatic nerves accompany the peripancreatic vessels (Figs. 12–5 and 12–7).

Conclusion

Identification of pathways of tumor spread is important for surgical planning in order to achieve a margin-negative resection, particularly when the tumor spreads beyond the usual extent of pancreaticoduodenectomy. The anatomic relationship between the pancreas and peripancreatic vessels and the knowledge of the pathways of lymphatic drainage of the pancreas are important to define the extent of the disease before definitive surgery, which carries a high risk and a marginal long-term result.

References

1. Warshaw AL, Fernandez-del Castillo C: Pancreatic carcinoma. N Engl J Med 1992; 326:455–465.
2. Evans DB, Abbruzzese JL, Rich TA: Cancer of the pancreas. *In* Cancer Principles and Practice of Oncology. Edited by VT DeVita Jr, S Hellman, SA Rosenberg. Lippincott-Raven, Philadelphia, 1997, pp 1054–1087.
3. Yeo CJ, Cameron JL, Lillemoe KD, et al: Pancreaticoduodenectomy for cancer of the head of the pancreas. Ann Surg 1995; 221:721–733.
4. Kobari M, Matsuno S, Ohashi O, et al: Staging systems for pancreatic cancer and distribution of metastases. *In* Pancreatic Cancer: Problems in General

Surgery. Edited by LW Traverso. Lippincott-Raven, Philadelphia, 1997, pp. 43–50.
5. Netter FH: Normal anatomy of the liver, biliary tract and pancreas. *In* The Ciba Collection of Medical Illustrations, vol. 3: Digestive System: Liver, Biliary Tract and Pancreas. Ciba, Summit, NJ, 1979, pp 2–31.
6. Bannister LH: Alimentary system: Pancreas, liver and gallbladder. *In* Gray's Anatomy, 38th ed. Edited by PL Williams, LH Bannister, MM Berry, et al. Churchill Livingstone, London, 1995, pp 1790–1812.
7. Falconer CW, Griffiths E: The anatomy of the blood vessels in the region of the pancreas. Br J Surg 1950; 37:334–344.
8. Reichardt W, Cameron R: Anatomy of the pancreatic vein: A postmortem and clinical phlebographic investigation. Acta Radiol Diagn 1980; 21:33–41.
9. Rouvier H, Tobias MJ (trans): Lymphatic system of the abdomen and pelvis. *In* Anatomy of the Human Lymphatic System. Edwards Brothers, Ann Arbor, MI, 1938, pp 203–205.
10. Staley CA, Cleary KR, Abbruzzese JL, et al: The need for standardized pathologic staging of pancreaticoduodenectomy specimens. Pancreas 1996; 12:373–380.
11. Crabo LG, Conley DM, Graney DO, et al: Venous anatomy of the pancreatic head: Normal CT appearance in cadavers and patients. AJR 1993; 160:1039–1045.
12. Ibukuro K, Tsukiyama T, Mori K, et al: Peripancreatic veins on thin-section (3 mm) helical CT. AJR 1996; 167:1003–1008.
13. Chong M, Freeny PC, Schmiedl UP: Pancreatic arterial anatomy: Depiction with dual-phase helical CT. Radiology 1998; 208:537–542.
14. Hommeyer SC, Freeny PC, Crabo LG: Carcinoma of the head of the pancreas: Evaluation of the pancreaticoduodenal veins with dynamic CT—potential for improved accuracy in staging. Radiology 1995; 196:233–238.
15. Mori H, McGrath FP, Malone DE, et al: The gastrocolic trunk and its tributaries: CT evaluation. Radiology 1992; 182:871–877.
16. Mori H, Miyake H, Aikawa H, et al: Dilated posterior superior pancreaticoduodenal vein: Recognition with CT and clinical significance in patients with pancreaticobiliary carcinomas. Radiology 1991; 181:793–800.
17. Fuhrman GM, Charnsangavej C, Abbruzzese JL, et al: Thin-section contrast enhanced computed tomography accurately predicts the resectability of malignant pancreatic neoplasms. Am J Surg 1994; 167:104–113.
18. Loyer E, David C, Dubrow RA, et al: Vascular involvement in pancreatic adenocarcinoma: Reassessment by thin-section CT. Abdom Imaging 1996; 21:202–206.
19. Fuhrman GM, Leach SD, Staley CA, et al: Rationale for en-bloc vein resection in the treatment of pancreatic adenocarcinoma adherent to the superior mesenteric-portal vein confluence. Ann Surg 1996; 223:154–162.
20. Freeny PC, Marks WM, Ryan JA, et al: Pancreatic ductal adenocarcinoma: Diagnosis and staging with dynamic CT. Radiology 1988; 166:125–133.
21. Megibow AJ, Zhou XH, Rotterdam H, et al: Pancreatic adenocarcinoma: CT versus MR imaging in the evaluation of resectability—Report of the Radiology Diagnostic Oncology Group. Radiology 1995; 195:327–332.
22. Zeman RK, Cooper C, Zeiberg AS, et al: TNM staging of pancreatic carcinoma using helical CT. AJR 1997; 169:459–464.
23. Takahashi N, Thomas JW, Charnsangavej C: Significance of periportal and peripancreatic lymph nodes in patients with pancreatic carcinoma and chronic pancreatitis: Helical CT evaluation. Radiology 1998; 209 (P):329.

The Subperitoneal Space: Normal and Pathologic Anatomy

13

Michael Oliphant, M.D.
Alfred S. Berne, M.D.
Morton A. Meyers, M.D.

Conventional distinction between intraperitoneal and extraperitoneal sites is often helpful in differential diagnostic considerations.[1,2] Yet it should be understood that the abdomen and pelvis constitute an anatomic continuum that is punctuated by the mesenteries, ligaments, and fasciae, which may either confine pathology or actually provide an avenue for disease spread. It is essential to recognize the anatomic continuity of subserous connective tissue with its vessels and lymphatics—structures deep to the posterior parietal peritoneum with extensions into the peritoneal cavity of the abdomen and pelvis as it is invested between the layers of the mesenteries and ligaments—that underlies the holistic concept of the subperitoneal space. A scaffold with precise anatomic planes is provided for spread of disease not only between intraperitoneal structures, but also between extraperitoneal and intraperitoneal sites.[1–7] This unifying schema is the basis for understanding the dissemination of intraabdominal disease, including malignancies and inflammatory and traumatic processes, both focally and at areas distant from the site of origin.

The subperitoneal space's continuity with the thorax above and the lower limbs below also provides access for the bidirectional spread of disease involving these sites. It is the fundamental continuity that provides the rationale for understanding the paradoxical clinical appearance of disease at a distance from its site of origin. The graphic display of the anatomy with modern imaging modalities coupled with the current knowledge of the morphology of the subperitoneal space provides a comprehensive clinical delineation of disease processes and an improved understanding of the pathogenesis of direct spread of disease.

Embryologic Considerations

Knowledge of the development of the subperitoneal space is a prerequisite to recognizing pathologic conditions and understanding the pathogenesis of direct spread.[8–11] The conceptualization of the abdomen and pelvis as one space, the subperitoneal space, and its continuity with the thorax requires the reexamination of standard embryology from a holistic perspective.[1,4,5,7,12] The primitive coelom is formed at the end of the 3rd week as the intraembryonic mesoderm and either side of the midline differentiates into a paraxial and intermediate portion and a lateral plate. The appearance at this time of intracellular clefts laterally divides the lateral plate into the somatic mesodermal layer and splanchnic mesodermal layer (Fig. 13–1). A serous membrane also forms and lines these layers and the coelomic cavity. Subsequent development divides the single embryonic coelom into the thorax and abdomen. The thorax contains the pleural and pericardial spaces and the abdomen the peritoneal space. It is important to remember that throughout development continuity is preserved between the pleural and peritoneal spaces; the pericardial space becomes isolated by the 5th to 6th week (Fig. 13–2a,b).

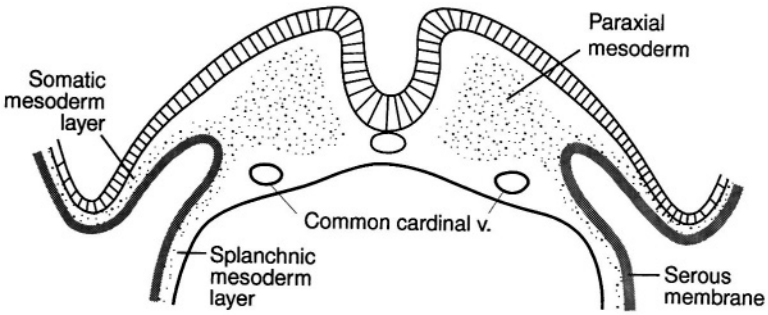


Fig. 13–1. Schematic drawing of a transverse section through an embryo at the end of the third week of gestation.
The somatic mesoderm and the splanchnic mesoderm result from the division of the lateral plate. The serous membrane is formed from the tissue lining the intraembryonic cavity. (Reproduced from Oliphant et al.[12])

The somatic mesoderm forms the parietal layer of the serous membrane and eventually lines the pleural and peritoneal cavities. The splanchnic mesoderm forms the visceral layer of the serous membrane and covers the abdominal and thoracic viscera. The space subjacent to the serous membrane defines the single subserous space, which in the adult is the subperitoneal space of the abdomen/pelvis and the subpleural space of the thorax.

The respiratory diaphragm forms by the 8th week and divides the embryonic coelomic cavity into the thorax and abdomen (Fig. 13–3). During this division, the integrity of the subserous space is maintained by that portion of the subserous space traversing the diaphragmatic hiatuses and apertures—the thoracoabdominal continuum.[12] The esophageal hiatus lies ventral and cranial to the aortic hiatus with the esophagus, vagus nerves, and esophageal vessels coursing within the subserous space. The aortic hiatus is an osseoaponeurotic opening between the diaphragm and vertebral column containing the aorta, hemizygous and azygous veins,

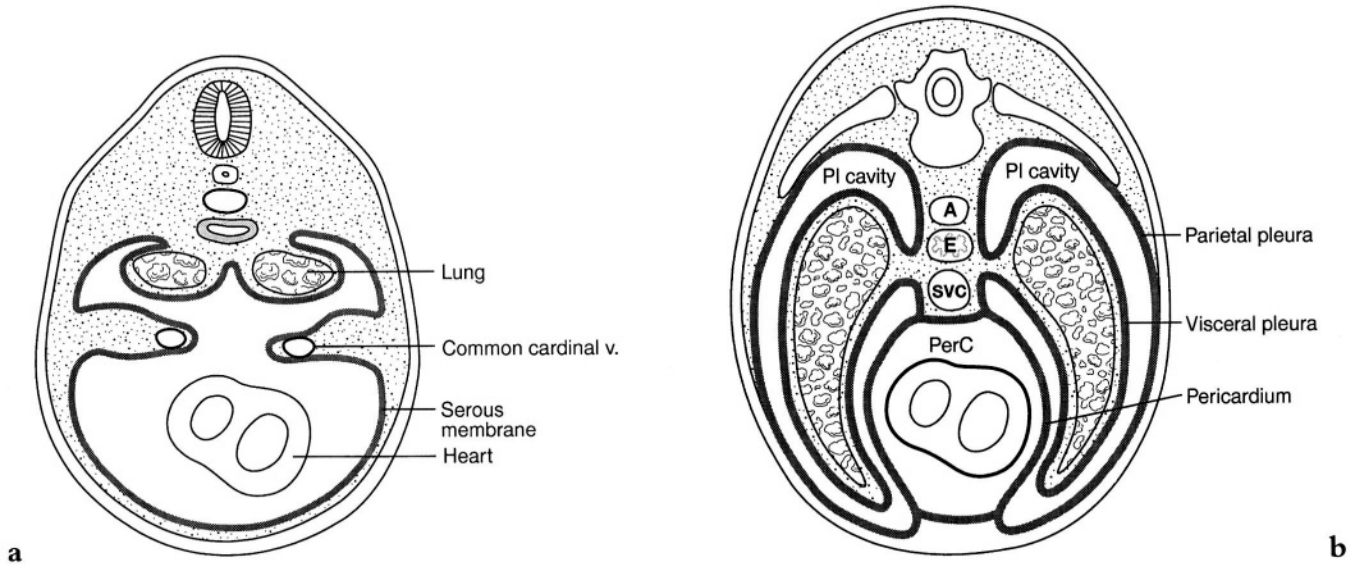


Fig. 13–2. (a) Schematic drawing of a transverse section through an embryo at 4–5 weeks' gestation.
The lung buds are growing into the pericardioperitoneal canals, forming the pleuropericardial folds. The serous membrane lines the coelomic cavity. The subserous space is the stippled area subjacent to the serous membrane.
(b) Schematic drawing of a transverse section through an embryo at 5–6 weeks' gestation.
Complexity of the serous membrane results as it fuses ventrally forming the pericardium (*PerC* = pericardial cavity) and as the pleuropericardial folds fuse bilaterally at the root of the lungs. The serous membrane lines the pleural cavities as the visceral pleura and parietal pleura. The subpleural space is the *stippled area* subjacent to the pleura. The common cardinal veins form the superior vena cava *(SVC). A* = aorta; *E* = esophagus; *Pl cavity* = pleural cavity.
(Reproduced from Oliphant et al.[12])

and the thoracic duct within the subserous space. The vena caval foramen is the most ventral of the three hiatuses and transmits only the inferior vena cava. The wall of this vessel is adherent to the margins of the foramen and interrupts continuity of the subserous space.[13] Ventrally, there are small apertures between the sternum and costal cartilage, allowing continuity of the subserosal space as the superior epigastric branch of the internal mammary artery and lymphatics course from the thorax to the abdomen.

The abdominal cavity, formed by the 8th week, provides the space within which the viscera grow, shift position, and move without hindrance. To achieve this goal, the developing abdominal organs are suspended by two opposing splanchnic mesodermal layers that form a double-layered mesentery at 3½ weeks—the primitive mesentery.

The gut arises by the infolding of ectoderm at 3 weeks to form a tube. The splanchnic mesoderm contains the gut and extends as a double layer from the dorsal to the ventral walls of the coelomic cavity. Thus, the primitive mesentery divides the coelomic cavity in halves and contains the gut within its component layers. The gut at this time is a straight tube and divides the primitive mesentery into the dorsal mesentery and the ventral mesentery (Fig. 13–4a.) At this time, the liver appears, partially enclosed within the ventral mesentery.

The primitive mesentery contains a layer of connective tissue beneath its epithelium. The development of the vascular system is heralded by the appearance of numerous islands that form plexiform networks throughout this mesenchyme. These plexuses fuse and give rise to the abdominal vessels. At the end of 4 weeks, the aorta has formed and has developed three prominent ventral branches: the celiac artery in the stomach–pancreas region, the superior mesenteric artery in the small intestine region, and the inferior mesenteric artery in the large intestine region. These three vessels course through the mesenteries to the gastrointestinal system.

Over the next several weeks, the small intestine mesentery grows along with the intestine as it loops outside the coelomic cavity. It reenters the cavity at 12 weeks. During this time, the ventral and dorsal mesenteries undergo specialization.

The ventral mesentery is intimately related to the liver, the lower esophagus, stomach, and upper duodenum. The rapid growth of the liver splits the ventral mesentery (Fig. 13–4b) into anterior and posterior portions, the *falciform ligament* and the *lesser omentum,* respectively. The free edge of the falciform ligament contains the left paraumbilical vein, which obliterates at birth, forming the round ligament. The lesser omentum is also termed the *gastrohepatic ligament,* and its free edge,

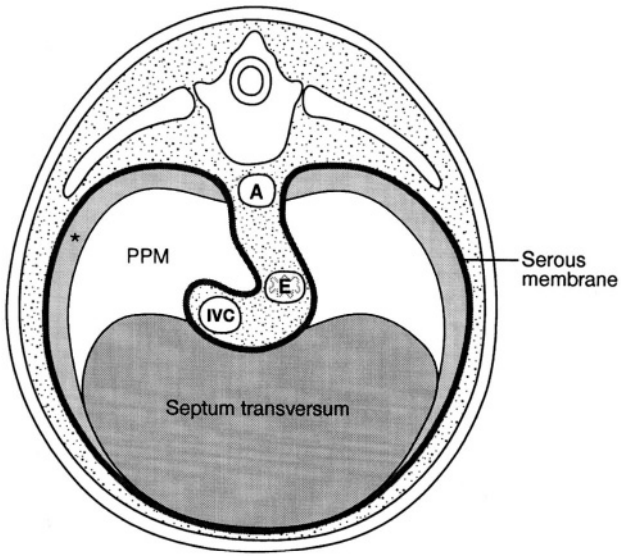


Fig. 13–3. Schematic drawing of transverse section illustrating the hiatuses of the respiratory diaphragm at the fourth month of life.

The pleuroperitoneal membrane *(PPM)* fuses with the septum transversum and the esophageal mesentery, forming the respiratory diaphragm. Esophageal mesentery encloses that portion of the subserous space that contains the esophagus *(E)* and the inferior vena cava *(IVC). Stippled area* = subserous space.

The serous membrane lines the diaphragm and invaginates dorsomedially, encasing the subserous space. *A* = aorta; *asterisk* = muscular rim from body wall, forming periphery of diaphragm.

(Reproduced from Oliphant et al.[12])

the *hepatoduodenal ligament,* which contains the common bile duct, the portal vein, and the hepatic artery. The lesser omentum rotates from the sagittal to the frontal position as a result of the growth of the liver and rotation of the stomach.

The liver is surrounded by the ventral mesentery except for its upper surface, where it is in contact with the diaphragm (bare area of the liver). Where the peritoneal covering of the liver is continuous with the coelomic peritoneum, the reflections are named the coronary ligaments.

The dorsal mesentery extends from the lower end of the esophagus to the rectum. Throughout its length it serves as a pathway for blood vessels, lymphatics, and nerves to the gut. It is a continuous mesentery suspending the gut, and its subsegments take their names from the regions served, i.e., region of the stomach, the dorsal mesogastrium; region of the duodenum, the dorsal mesoduodenum; region of the colon, the dorsal mesoco-

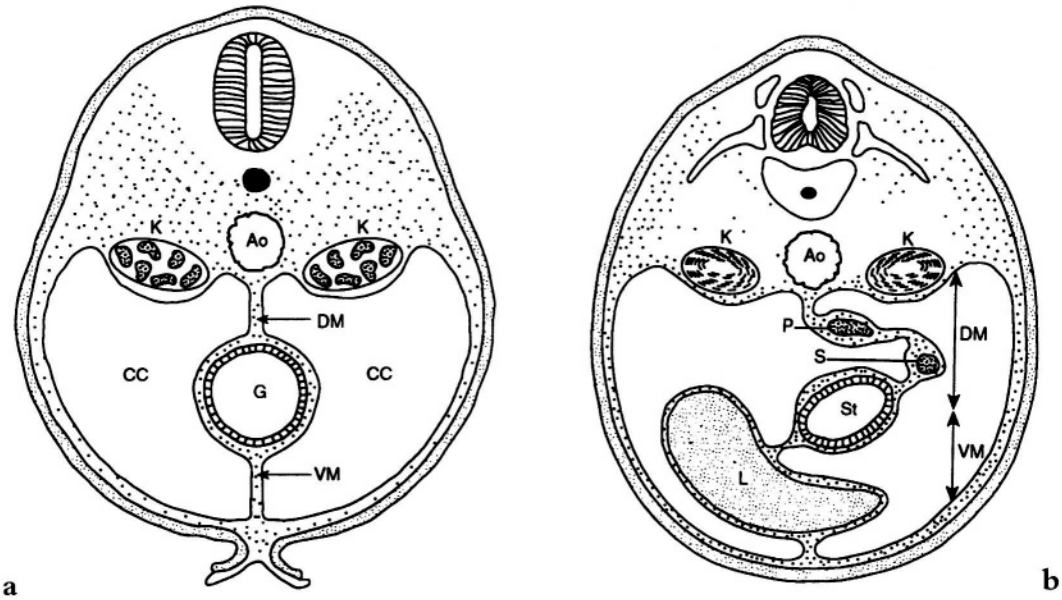


Fig. 13–4. (a) Diagrammatic transverse section through an embryo at the end of 4 weeks.
The splanchnic mesoderm, the *heavy black line* outlining the coelomic cavity *(CC),* has fused in the midline and formed a double-layered membrane, the primitive mesentery. The gut *(G)* is contained within and divides the primitive mesentery into the dorsal mesentery *(DM)* and ventral mesentery *(VM). Ao* = aorta; *K* = mesonephros.
(b) Diagrammatic transverse section through the liver *(L),* stomach *(St),* spleen *(S),* and pancreas *(P).*
With subsequent development, the ventral mesentery *(VM)* will form the falciform ligament and gastrohepatic ligament, and the dorsal mesentery *(DM)* will form the gastrosplenic ligament and the splenorenal ligament as the pancreas becomes retroperitoneal. *K* = kidney; *Ao* = aorta.
(Modified from Langman.[8])

lon; and the region of the jejunum and ileum, the mesentery proper. The dorsal mesogastrium continues to grow after the stomach completes its rotation. This ongoing growth forms a duplication of the mesogastrium upon itself anterior to the transverse colon and small intestine. Later, the four leaves fuse and are suspended from the greater curvature of the stomach as the greater omentum.

The spleen appears between the folds of the mesogastrium at the 5th week and, with growth, bulges into the left upper portion of the coelomic cavity. The dorsal mesogastrium connecting the spleen and stomach is the gastrosplenic ligament. The dorsal mesogastrium between the spleen and dorsal midline fuses with the posterior abdominal wall, whereas the remaining part connects the spleen and left kidney and is designated the splenorenal ligament.

The head and body of the pancreas grow within the dorsal mesoduodenum and extend into the mesogastrium. As the pancreas grows, the stomach rotates and the duodenum moves from the midline to the right. The duodenum and pancreas lie against the dorsal abdominal wall, and the right dorsal mesoduodenum fuses at that site, except at the pylorus and duodenal bulb. The tail of the pancreas lies within the mesogastrium, which usually fuses with the adjacent dorsal body wall. It is important to recognize that the pancreas, while positioned beneath the coelomic peritoneum, is connected by the subperitoneal space within the mesenteries to the other abdominal organs.

The dorsal mesocolon undergoes extensive loss of its mesentery. After the ascending and descending portions of the colon come to lie in their lateral positions, their mesocolons fuse with the dorsal wall of the coelom. However, the appendix and caput of the cecum retain their mesenteries. The transverse mesocolon persists. It fuses and covers the duodenum at the colon's crossing, forming the duodenocolic ligament. At the splenic flexure, the left lateral extension of the transverse mesocolon to the diaphragm forms the phrenicocolic ligament. The formed mesenteric connection between the stomach and transverse colon is designated the gastrocolic ligament. The sigmoid mesocolon persists. The primitive mesorectum obliterates.

The mesentery of the small intestinal loop undergoes dramatic changes as the small intestine elongates faster

than the coelomic cavity grows. The mesenteric attachment grows correspondingly as it is carried out into the umbilical cord with the bowel loops. The completed rotation and reentry of the small bowel and its mesentery occur by the 12th week. In this process, the cecum comes to lie on the right, the transverse colon crosses ventral to the duodenum, and the small intestine lies caudad and to the left of the ascending colon. The rotation of this mesentery occurs about the axis of the superior mesenteric artery. The focal point of the rotation is the root of the superior mesenteric artery as it originates from the aorta. From its narrow origin, the mesentery of the intestine spreads out like a fan. The intestine is freely movable on the mesentery until the 14th week, when the secondary fusions affix portions of gut, forming new lines of attachment. The root of the small bowel mesentery finally affixes itself posteriorly and extends dorsally from the left upper to the right lower abdomen. The root of the small intestine mesentery is in continuity with the attachment of the transverse mesocolon in the left upper abdomen and the peritoneum overlying the ascending colon on the right side. In this manner, the root of the small bowel mesentery interconnects the upper and lower portions of the abdomen.

The broad ligament is formed by the mesenchymal shelf that bridges the lateral walls of the pelvis. In the center is the uterus, and the lateral sheets extending to the lateral pelvic walls form the broad ligament. The broad ligament is covered by peritoneal folds continuous from the pelvic walls to cover the uterus. Within the broad ligament, the blood vessels and nerves course from the pelvic wall to the uterus. The mesovarium and mesosalpinx accompanied by their blood, lymphatic, and nerve supply are intimately related with the broad ligament. The subperitoneal space within the broad ligament interconnects the female pelvic organs with the remainder of the abdomen.

With the completion of development of the mesenteries and ligaments and the planes of attachments and fixations, the interconnections between contiguous and remote sites within the abdomen formed by the subperitoneal space are complete.

The subperitoneal space can be defined as the anatomic continuum deep to the peritoneum that both covers the coelomic cavity and the abdominal and pelvic viscera and extends within the folds that are the mesenteries and ligaments.

Anatomic Considerations

Embryologic development explains the continuity of the subpleural and subperitoneal spaces (Fig. 13–5) and the pervasive presence of the subperitoneal space deep to the peritoneum that develops in the abdomen and pelvis (Figs. 13–6 and 13–7). The subperitoneal space includes the areolar and adipose tissue and to a large extent the vascular, lymphatic, and neural scaffolds that form the pathways that serve to facilitate the direct spread of many diseases in the abdomen and pelvis.[13,15,16] These scaffolds with accompanying connective tissue course within the ligaments and mesenteries that relate to the intraperitoneal organs but also the extraperitoneal structures and organs such as the kidneys, adrenal glands, and the interstices of the solid peritoneal organs, e.g., the liver and spleen. All of the classical extraperitoneal compartments are similarly interconnected by this single huge potential space that lies beneath the peritoneum and courses through the abdomen and pelvis from the thoracoabdominal diaphragm to the pelvic diagram, containing branches of the scaffold. Once abdominal

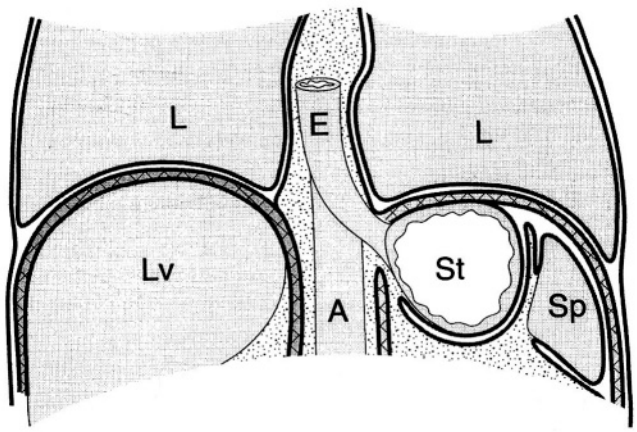


Fig. 13–5. Schematic drawing of a coronal section through the thoracoabdominal continuum.
The esophagus *(E)* and aorta *(A)* are shown traversing that portion of the subserous space *(stippled area)* interconnecting the thorax and abdomen. *Dark line* is the subserous membrane. *Cross-hatched area* is the diaphragm. L = lung; *Lv* = liver; *St* = stomach; *Sp* = spleen.
(Reproduced from Oliphant et al.[12])

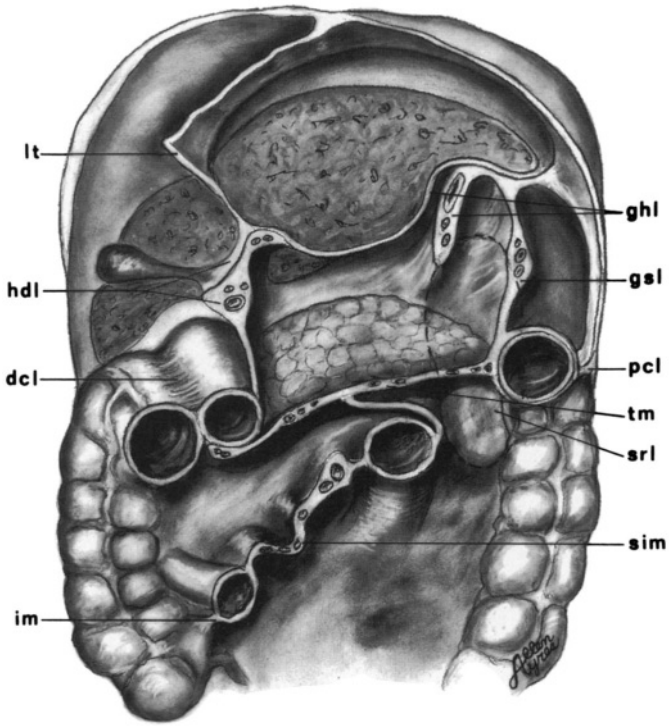


Fig. 13–6. Anatomic drawing of the upper folds containing the subperitoneal space. *lt* = ligamentum teres; *hdl* = hepatoduodenal ligament; *dcl* = duodenocolic ligament; *im* = terminus of sim (ileal mesentery); *ghl* = gastrohepatic ligament; *gsl* = gastrosplenic ligament; *pcl* = phrenicocolic ligament; *tm* = transverse mesocolon; *srl* = splenorenal ligament; *sim* = small intestine mesentery.
(Reproduced from Oliphant et al.[5])

disease enters the subperitoneal space, tracking by the directly spreading process can follow the well-known anatomic specifics of these vascular, neural, and lymphatic channels.

The central cephalocaudad spread is directed largely by the dominant paths provided by the aorta and its three major anterior branches (celiac, superior mesenteric, and inferior mesenteric arteries) and its two main lateral branches (the renal arteries) (Fig. 13–8). The anterior arteries and their branches and the lateral arteries course within the subperitoneal space connecting the suspended abdominal organs, the pancreas, kidneys, and adrenal glands.

Ventral Mesentery Derivatives

The ventral mesentery derivatives are the gastrohepatic, hepatoduodenal, and falciform ligaments.

The free edge of the gastrohepatic ligament is the hepatoduodenal ligament, which contains the portal triad. In the liver hilum, Glisson's capsule is the extension of the tissue of the subperitoneal space that accompanies the portal vein, hepatic artery, bile ducts, and lymphatics into the periportal spaces.

As the gastrohepatic ligament extends superiorly, the planes of reflection continue to form the falciform ligament. This extends from the liver to the anterior abdominal wall, carrying the ligamentum teres in its free edge.

These ligaments provide pathways interconnecting the liver, gallbladder, duodenum, stomach, pancreas, and distal esophagus.[1,3,5,6]

Dorsal Mesentery Derivatives

The dorsal mesogastrium gives rise to a series of ligaments interconnecting the organs in the left upper abdomen: the gastrosplenic, splenorenal, and gastrocolic ligaments and the greater omentum.

This network of ligaments in the left upper quadrant establishes local continuity between the stomach, spleen, pancreas, left kidney, and transverse colon and global continuity with the entire abdomen as extensions of the subperitoneal space.[1,3,5,6,18–20]

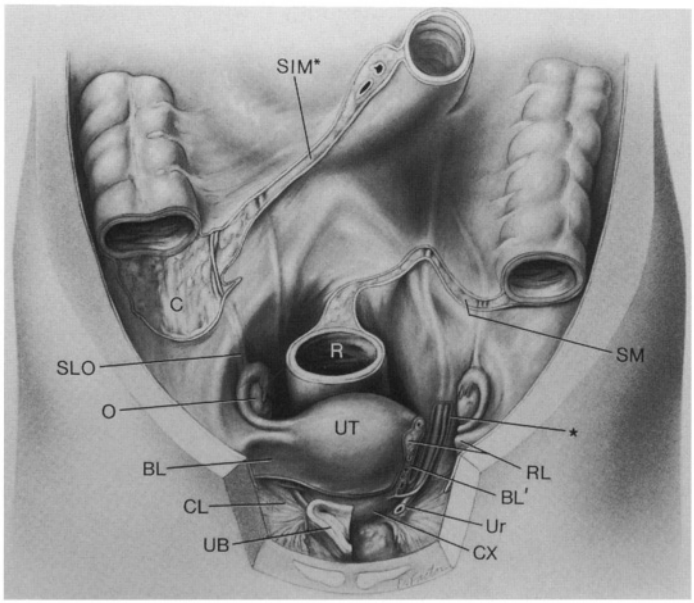


Fig. 13–7. Anatomic drawing of the subperitoneal space in the lower abdomen and pelvis. Note the continuity of the space beneath the posterior parietal peritoneum and the abdominal and pelvic walls with the roots of the small intestine and sigmoid mesenteries and the pelvic ligaments. *SIM** = root of small intestine mesentery; *SM* = root of sigmoid mesocolon; *BL* = broad ligament; *BL* = cut section through broad ligament showing contained vascular structures; *CL* = cardinal ligament; *SLO* = suspensory ligament of ovary; *RL* = round ligament. Attention is also focused on the continuity of the lower abdominal and pelvic organs created by the subperitoneal space. *C* = cecum and posterior parietal peritoneum cut away; note relationship of SIM* to C; *O* = ovary; *UT* = uterus; *CX* = cervix; *UB* = urinary bladder; *R* = rectum; *Ur* = ureter as it traverses the broad ligament with uterine artery crossing anteriorly; *star* = posterior parietal peritoneum cutaway and showing the subperitoneal space with ureter and artery. Note continuity with broad ligament. (Reproduced from Oliphant et al.[14])

The dorsal mesocolon gives rise to the transverse mesocolon. Near the uncinate process of the pancreas, the root of the transverse mesocolon is confluent with the root of the small intestine mesentery. The right lateral extension of the transverse mesocolon over the duodenum and colon is designated the duodenocolic ligament and the left lateral extension is the phrenicocolic ligament.

Thus, the subperitoneal space subtended by the transverse mesocolon is in continuity with the subperitoneal space interconnecting the organs of the left upper quadrant, the small intestine mesentery, and the right lower abdomen via the root of the small intestine mesentery. [1,3,5,6.21–25]

The superior mesenteric artery extends from the aorta anteriorly and with its branches courses along within the subperitoneal space in the derivative of the mesentery proper.

The root of the mesentery extends obliquely from the distal duodenum at the lower border of the pancreas on the left side of L2 to the cecum in the right lower quadrant. The line of attachment passes from the duodenojejunal junction, where it is in continuity with the root of the transverse mesocolon over the third portion of the duodenum, obliquely across the aorta and inferior vena cava, the right ureter, and psoas muscle, to the right iliac region.[26] The peritoneal reflections from the root of the mesentery in the region of the terminal ileum reflect to continue as the posterior peritoneum overlying the posterior and right lateral wall of the abdomen. The connective tissue within this portion blends and connects with the subperitoneal tissue in the retoperitoneum of the right posterior lower abdomen wall. From the base of the small bowel mesentery the peritoneum of the posterior abdominal wall envelops the ventral surface of the ascending colon. The vasculature supplying these structures lies within the subperitoneal space between the base of the mesentery and the medial border of the ascending colon. The subperitoneal tissue in the right lower abdomen continues cephalad to the

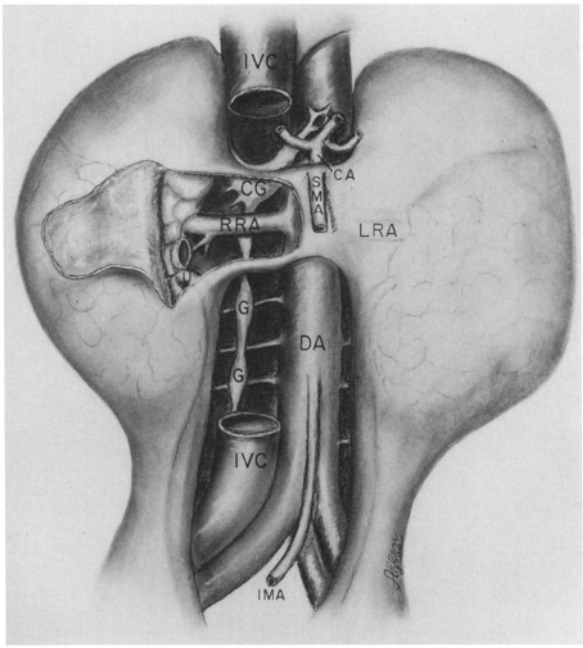


Fig. 13–8. Anatomic drawing of the subperitoneal space showing the central vascular scaffold and its interconnection with the renal arteries and the three ventral branches of the aorta.
A portion of the right anterior renal fascia has been incised and the flap turned laterally. The right renal artery *(RRA)* and proximal right ureter *(U)* are seen within the right renal hilum. A portion of the inferior vena cava *(IVC)* has been removed, allowing visualization of the right celiac ganglion *(CG)* and lumbar ganglia *(G).* The ventral branches of the aorta *(DA)* are the celiac axis *(CA),* the superior mesenteric artery *(SMA),* and the inferior mesenteric artery *(IMA).* *LRA* = left renal artery.
(Reproduced from Oliphant and Berne.[17])

diaphragm and caudad over the pelvic musculature along the right lateral pelvic wall. Thus, the root of the small bowel mesentery interconnects the upper abdomen and the right lower abdomen,[20,26] which in turn is in continuity with the pelvis.

Lateral Continuity

The lateral pathways of communication of the subperitoneal space between the abdomen and pelvis are formed by the convergence of the pararenal spaces caudal to the perirenal space and their descent into the pelvis. The lateral extent of the distal anterior renal fascia lies dorsal to the ascending and descending colon. This portion of the colon is covered ventrally by the posterior parietal peritoneum. The transversalis fascia covers the inner surface of the abdominal musculature, attaches to the crest of the ilium, and continues into the pelvis to become the endopelvic fascia covering the pelvic musculature. These fasciae and the peritoneal lining define the lateral continuation of the subperitoneal space from the abdomen into the pelvis.

On the *right side,* the junction of the root of the small intestine mesentery in the right lower quadrant with the subperitoneal space at the proximal ascending colon provides continuity with all the above-described connections of the root of the mesentery in addition to the continuity with the right lateral abdomen and right lateral pelvis.[14]

On the *left side,* there are two main avenues of communication within the subperitoneal space between the left lower abdomen and the pelvis: the *central pathway* and the *lateral pathway.*[27]

The *central pathway* contains the lower abdominal aorta and inferior mesenteric artery, forming a major communication between the left abdomen and the pelvis. The inferior mesenteric artery arises at the level of the third lumbar vertebra and passes caudally within the subperitoneal space ventral and to the left of the aorta and in relationship to the root of the sigmoid mesocolon as it descends into the pelvis. At its plane of reflection from the lateral pelvic wall, the root of the sigmoid mesocolon is in intimate relationship to the left ureter. The sigmoid mesocolon extends to and envelops the sigmoid colon.

The aorta also interconnects laterally with the pelvis as it bifurcates, forming the common iliac arteries that course to the lateral pelvis. Thus, the central and lateral pathways of the subperitoneal space interconnect also along the major arterial pathways.

These central and lateral pathways, along with the root of the sigmoid mesocolon provide continuity for spread of disease between the abdomen and the pelvis on the left.

Continuity with the Female Organs

The subperitoneal connective tissue enveloped within the peritoneal layers of the broad ligament provides the pathway for the uterine vessels branching from the internal iliac arteries as well as their accompanying lymphatics and nerves. The distal ureters course through the base of the broad ligament along with vessels and nerves. Its lower portion is called the cardinal ligament or the transverse cervical ligament of Mackenrodt. The cardinal ligament provides the main support of the cervix and upper vagina. The subperitoneal space within the cardinal ligaments blends laterally beneath the parietal peritoneum overlying the pelvic muscles and continues to follow the course of the major pelvic vessels anteri-

orly. The round ligaments proceed to enter the inguinal rings, and posteriorly the uterosacral ligaments extend to and surround the rectum to insert onto the distal sacrum. All are part of the subperitoneal space. As in the male, the peritoneum also reflects over the urinary bladder and rectum.

The broad ligament encloses the subperitoneal space that surrounds the suspended female pelvic organs and interconnects them with the lateral pelvic walls. In doing so, it forms a continuum between the female pelvis and the abdomen.[14]

Abnormal Imaging Features

The continuity of the subperitoneal space and its interconnections is vividly demonstrated by CT in Figures 13–9 and 13–10. Subperitoneal gas is seen diffusing

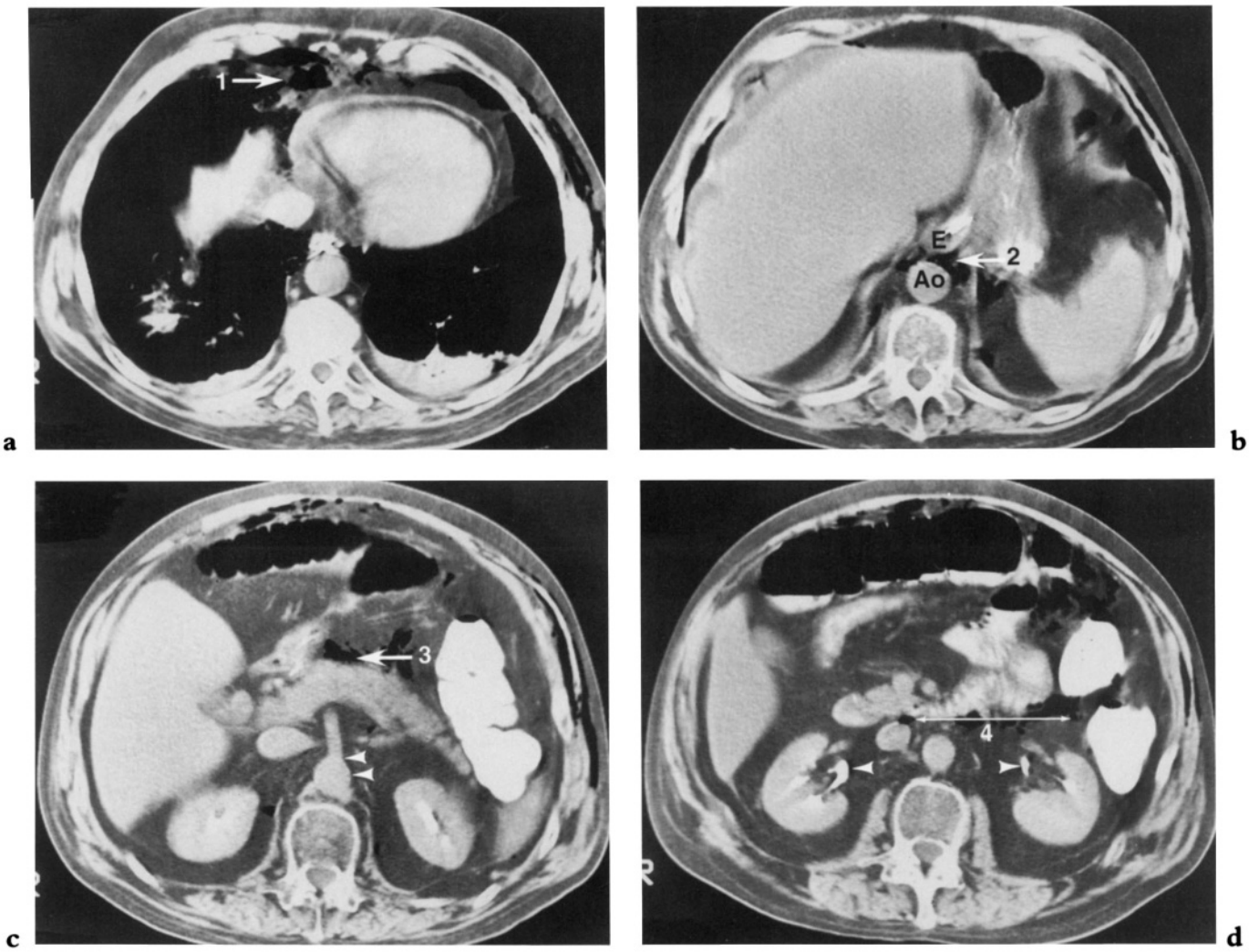


Fig. 13–9. Gas originating in the mediastinum diffusing inferiorly via the subperitoneal space through the abdomen and pelvis.

(a) CT scan at lower thorax. Pneumomediastinum is seen anteriorly *(arrow 1)*

(b) Scan through upper abdomen at esophagogastric junction. *E* = esophagus; *Ao* = aorta. Note gas *(arrow 2)* as it courses through the diaphragmatic hiatus and on both sides of the diaphragmatic crura.

(c) Scan at level of origin of superior mesenteric artery *(arrowheads).* Gas has dissected along the celiac axis and is demonstrated in the peripancreatic region *(arrow 3).* Note air coursing into the transverse mesocolon *(anterior to arrow).*

(d) Scan at level of renal hila. Gas traversing in the subperitoneal space from right to left *(double-headed arrow 4).* Air is seen at the renal hila in the region of the ureteropelvic junctions *(arrowheads).* *Continued on following page*

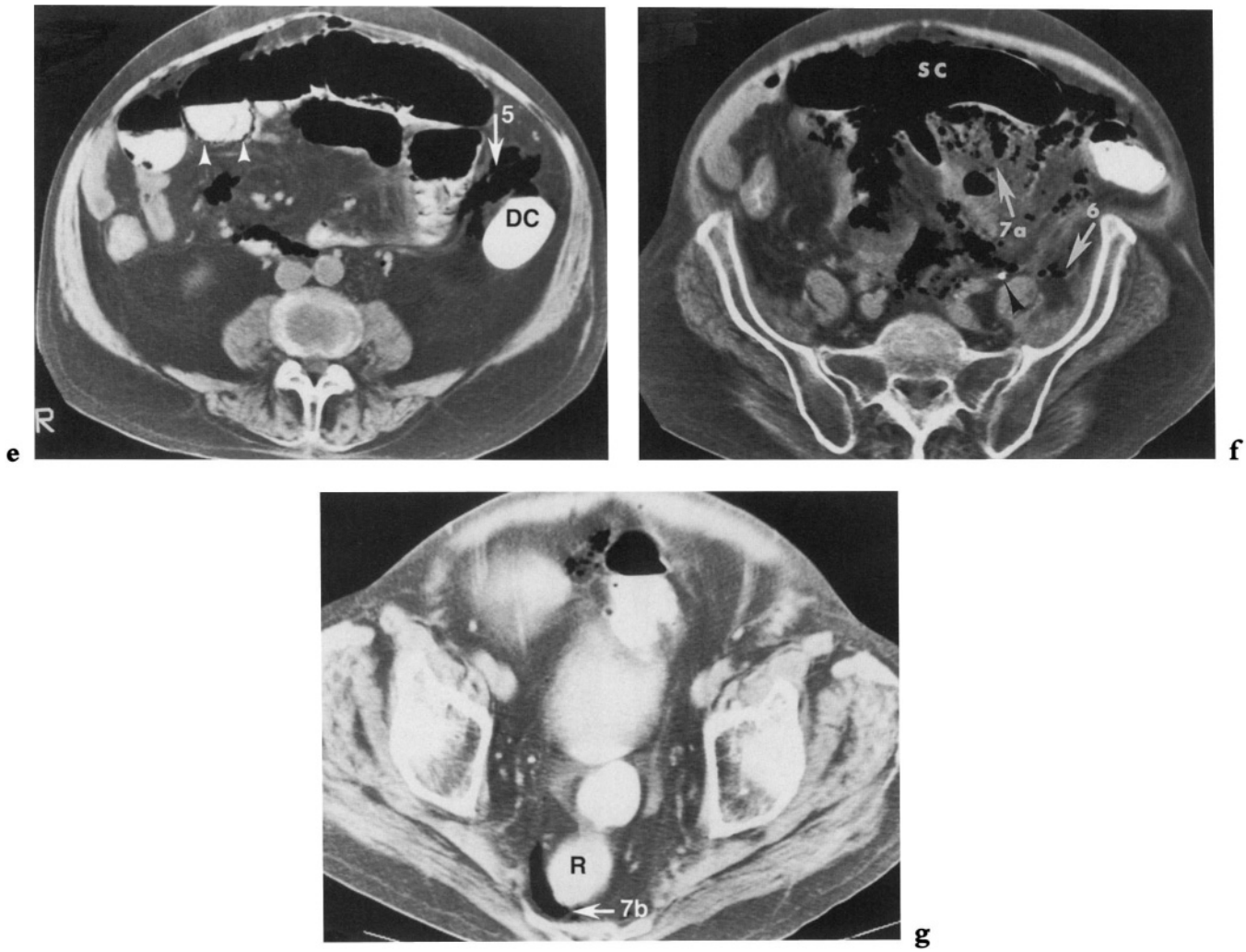


Fig. 13–9. Gas originating in the mediastinum diffusing inferiorly via the subperitoneal space through the abdomen and pelvis. (Continued)
(e) Scan through lower abdomen below kidneys. Gas has diffused caudally in the left lateral abdomen in the subperitoneal space *(arrow 5). DC* = descending colon. Intramural air in transverse colon *(arrowheads).* Note air also coursing anterior to aorta and inferior vena cava.
(f) Scan at level of upper pelvis. Gas courses in left lateral pelvis *(arrow 6)* and diffuses into the sigmoid mesocokm *(arrow 7a)*. Note intramural air within the sigmoid colon *(SC).*
(g) Section through upper rectum. Perirectal gas is present *(arrow 7b). R* = rectum.
(Reproduced from Oliphant et al.[27])

throughout a major portion of the space. The gas originates from the mediastinum in the first case and from the rectum in the second instance. These cases demonstrate the mediastinum's continuity with the subperitoneal space. The gas accompanies the celiac artery and its branches into the interconnecting peritoneal folds of the upper abdomen. Gas extends to and partially surrounds the stomach and spleen since the peritoneal folds envelop these organs (Figs. 13–9c and 13–10f). The gas dissects along the renal vasculature to the right and left kidneys and outlines an anterior communication across the midline (Figs. 13–9d and 13–10e). Central diffusion of gas can be traced along the lower abdominal aorta to its bifurcation. There is central-to-lateral continuity in the subperitoneal space at the level of the iliac vessels bilaterally and also along the inferior mesenteric artery on the left side. Gas on the left is seen in continuity with the left lateral pelvis as well as in the subperitoneal space

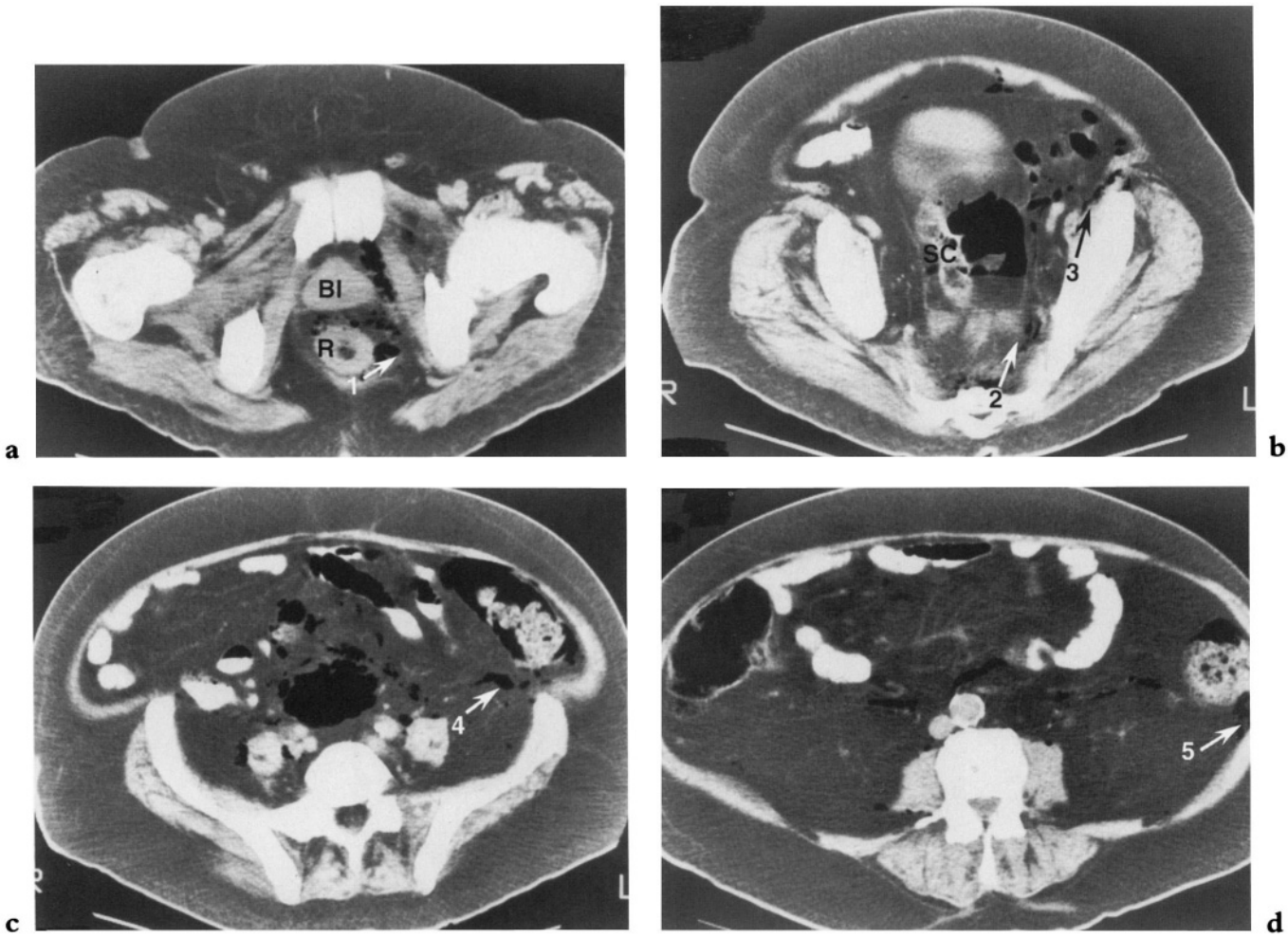


Fig. 13–10. Gas originating from a rectal perforation diffusing within the subperitoneal space superiorly to the mediastinum.
(a) CT scan at level of rectum. Perirectal gas *(arrow 1)* and perivesical air are demonstrated. *R* = rectum; *Bl* = bladder.
(b) Scan at level of greater sciatic notch. Gas courses cephalad and anterior *(arrow 2)* to left lateral pelvis *(arrow 3).* Air-fluid level caused by the rectal perforation is seen intimately related to the sigmoid colon (SC).
(c) Scan at level of upper pelvis junction with lower abdomen shows gas coursing along left lateral pathway *(arrow 4).*
(d) Scan of lower abdomen below kidneys demonstrates gas diffuses cephalad in the left lateral subperitoneal space *(arrow 5).* *Continued on following page*

extending within the sigmoid mesocolon (Fig. 13–9f). Intramural gas in the transverse colon (Fig. 13–9e) and sigmoid colon (Fig. 13–9f) has resulted from the dissection along their mesocolons. A third case of gas diffusion (Fig. 13–11) graphically displays the subperitoneal continuum. Subperitoneal gas originating from a perforated sigmoid diverticulum diffused from the pelvis through the abdomen, predominately along the central pathway. Further cephalad spread of the gas occurred through the thoracoabdominal continuum to the mediastinum.

These three striking cases clearly indicate potential for bidirectional spread of disease processes throughout the abdomen and pelvis and the continuity of the abdomen with the mediastinum.

Abdominal neuroblastoma notoriously presents beyond the confines of its site of origin in 60–70% of patients.[17] This is due to its propensity to infiltrate the adjacent areolar tissue and thus gain access to the subperitoneal space. The permeative nature of this malignancy allows it to grow along the vascular scaffold and

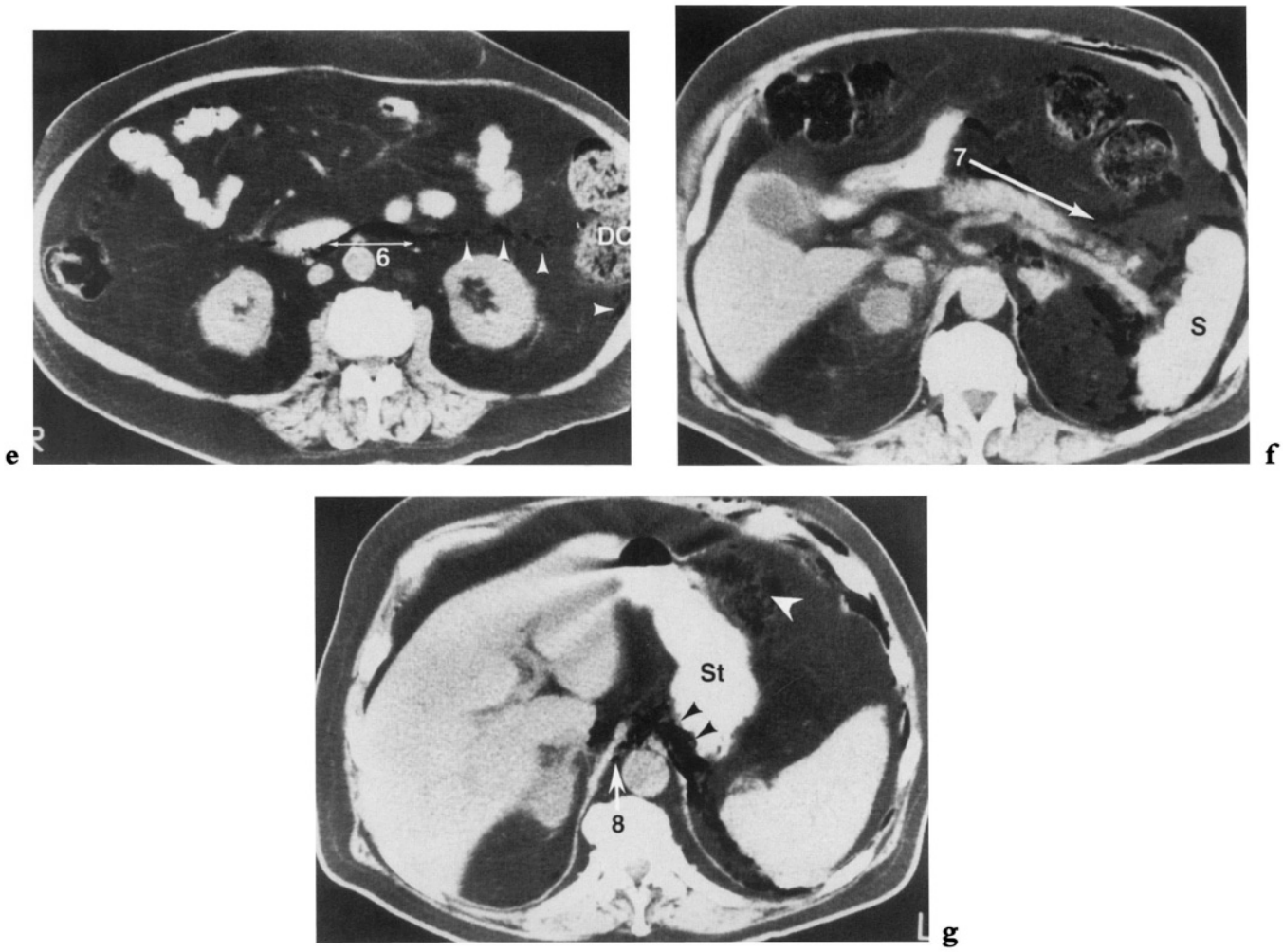


Fig. 13–10. Gas originating from a rectal perforation diffusing within the subperitoneal space superiorly to the mediastinum. (Continued)

(e) Scan at level of lower pole of kidneys. Gas is coursing along midline anterior to aorta and inferior vena cava *(double-headed arrow 6).* Also note gas extending from pericolic area on left toward midline *(arrowheads). DC* = descending colon.

(f) Scan at level of pancreatic body. Gas has diffused along celiac axis and is seen in the peripancreatic area *(arrow 7)* and in the splenic hilum and perisplenic area. *S* = spleen.

(g) Scan at upper abdomen shows gas in right retrocrural region courses through aortic hiatus to mediastinum *(arrow 8)* and anterior *(white arrowhead)* and posterior *(black arrowheads)* to stomach *(St).*

(Reproduced from Oliphant et al.[27])

thereby invade the various subperitoneal space pathways for its direct spread. The observation that adrenal neuroblastoma that originates in the perirenal space readily and commonly crosses the midline to invade the contralateral perirenal space (Figs. 13–12 and 13–13) is explained by direct extension along the vascular scaffold. The perirenal spaces are naturally separated by the aorta and inferior vena cava. Whereas this subdivision may prevent fluids (blood, exudate, extravasated urine) from crossing the midline, a permeative tumor such as neuroblastoma may spread between the perirenal spaces by growing aggressively along the renal vascular structures.[17]

Neuroblastoma initially spreads medially to the paracaval and paraaortic areas, where it encases these vessels. The tumor can then grow along the renal vessels to dis-

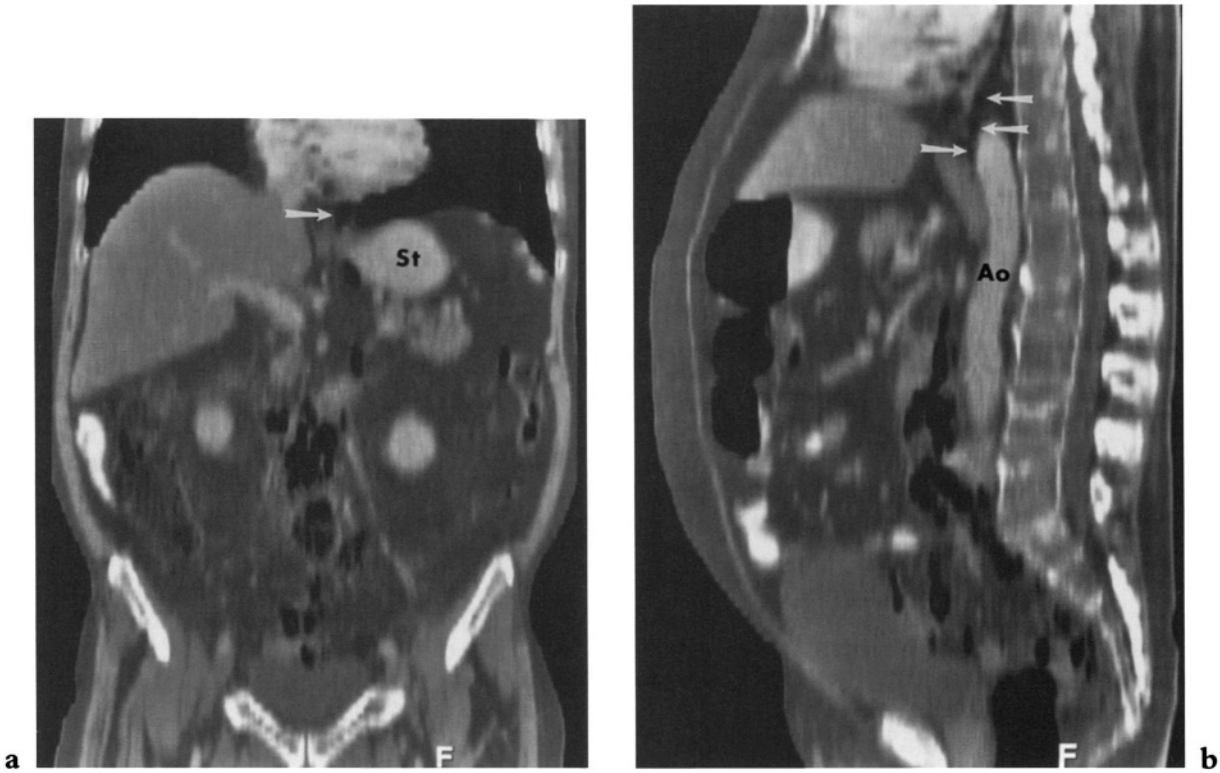


Fig. 13–11. Gas originating from a perforated sigmoid diverticulum diffusing through the pelvis and abdomen via the subperitoneal space and into the mediastinum.
(a) CT scan coronal reconstruction. The gas within the pelvis diffuses through the abdomen to the esophageal hiatus. *Arrow* = gas within the esophageal hiatus; *St* = stomach.
(b) CT scan midline sagittal reconstruction. Gas within the subperitoneal continuum diffuses along the central pathway. Small amount of gas is traversing the aortic hiatus *(arrows). Ao* = aorta.
(Courtesy of Michiel Feldberg, M.D., University Hospital, Utrecht, the Netherlands.)

place and invade the kidneys (Figs. 13–12a and 13–13b) and obstruct the collecting system. This presentation can mimic primary intrarenal masses.[28]

Once a permeative tumor has advanced to the aorta and vena cava it can spread cephalad and/or caudad, with direct access then via the celiac axis and its branches to the gastrohepatic ligament, where pressure on the esophagogastric junction may cause dysphagia,[17] and to the hepatoduodenal ligament with invasion of the liver across Glisson's capsule (Fig. 13–12b).

Neuroblastoma can also permeate the root of the small bowel mesentery to grow within its fanlike extensions following the superior mesenteric artery and its branches, occupying a major portion of the abdominal cavity (Fig. 13–13b).

In the upper abdomen, the avenues of spread provided by the major peritoneal ligaments and mesenteries and their characteristic clinical features have been clearly established.[1,6] Their critical role in the dissemination of inflammatory and neoplastic processes is detailed in Chapters 3, 4, 10, and 11. Extension through the subperitoneal stratum within ligaments in the left upper quadrant is further illustrated in Figures 13–14 and 13–15.

The mesenteric root of the small bowel interconnects the left upper abdomen to the right lateral abdomen[1,6,20] (Fig. 13–16). Opacification of the mesenteric root throughout its length provides a striking *in vivo* model of this portion of the subperitoneal continuum (Fig. 13–16). In acute pancreatitis, extravasated enzymes may encapsulate to form a pancreatic pseudocyst. This may progress down the mesenteric root and often down its entire length to the right lower quadrant (Fig. 13–17).

As in neuroblastoma, the development of lymphomatous masses within the mesenteric root is often based on the anatomic continuity of the subperitoneal space

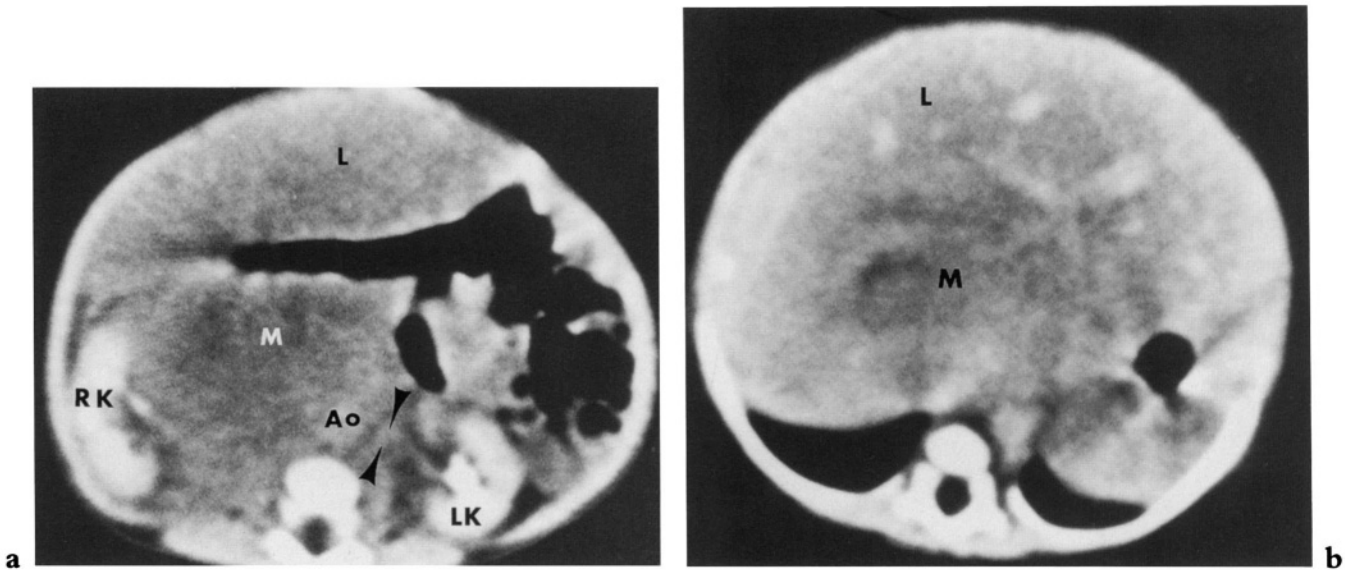


Fig. 13–12. Neuroblastoma in a neonate with subperitoneal spread along the vascular scaffold from the right adrenal area to the kidneys, the hepatoduodenal ligament, and into the liver.
(a) Right adrenal mass *(M)* that infiltrates the right perirenal space extends to the right renal hilum, where it displaces and obstructs the right kidney *(RK),* encases the aorta *(Ao),* and extends along the left renal vasculature *(arrowheads)* toward the left kidney *(LK). L* = liver.
(b) Scan 2 cm cephalad. Direct spread of mass *(M)* along the celiac axis to the hepatoduodenal ligament and extending into the liver *(L).*
(Reproduced from Oliphant and Berne.[17])

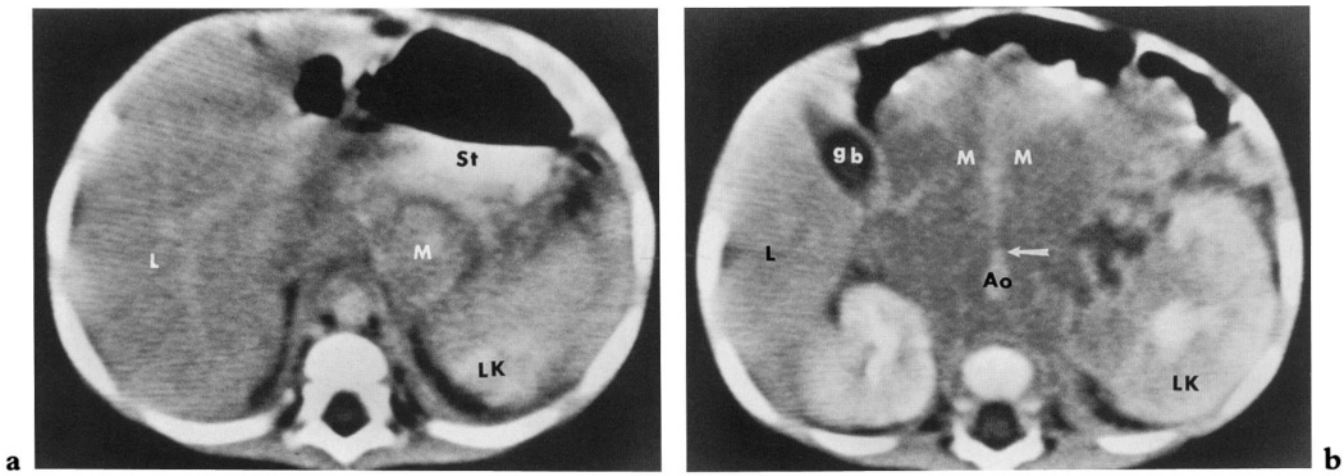


Fig. 13–13. Neuroblastoma extending along the vascular scaffold to the left kidney and into the small bowel mesentery.
(a) Scan of the upper abdomen shows distinct left adrenal mass *(M). LK* = left kidney; *(S)* = stomach; *L* = liver.
(b) Scan at the origin of the superior mesenteric artery *(arrow).* The mass infiltrates the left perirenal space and displaces, invades, and obstructs the left kidney *(LK).* Tumor also encases and elevates the aorta *(Ao).* It crosses to encase the inferior vena cava and invade the right perirenal space. The mass spreads along the aorta to the superior mesenteric artery and infiltrates the small intestine mesentery *(M). gb* = gallbladder; *L* = liver.
(Reproduced from Oliphant and Berne.[17])

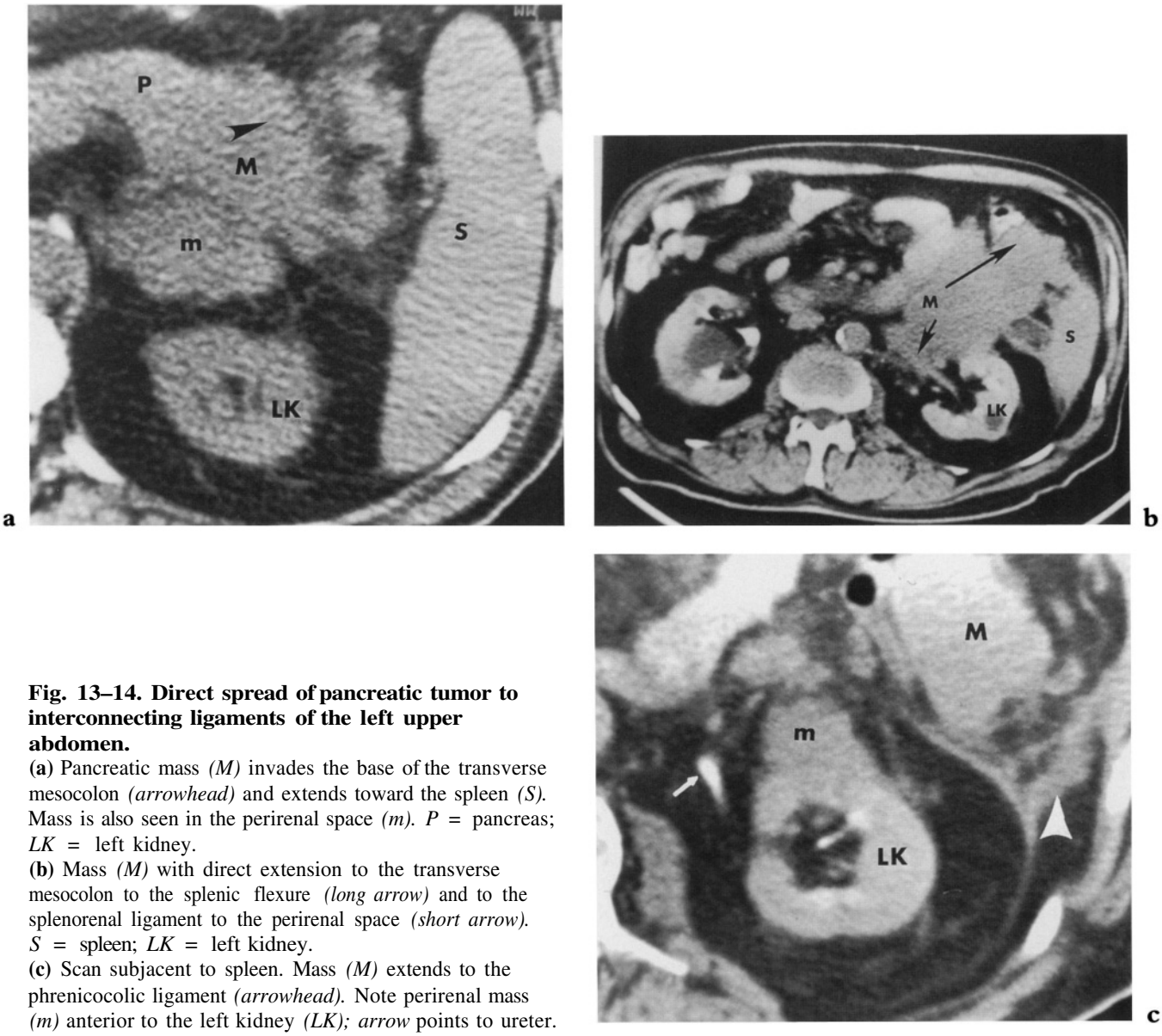


Fig. 13–14. Direct spread of pancreatic tumor to interconnecting ligaments of the left upper abdomen.
(a) Pancreatic mass *(M)* invades the base of the transverse mesocolon *(arrowhead)* and extends toward the spleen *(S).* Mass is also seen in the perirenal space *(m). P* = pancreas; *LK* = left kidney.
(b) Mass *(M)* with direct extension to the transverse mesocolon to the splenic flexure *(long arrow)* and to the splenorenal ligament to the perirenal space *(short arrow). S* = spleen; *LK* = left kidney.
(c) Scan subjacent to spleen. Mass *(M)* extends to the phrenicocolic ligament *(arrowhead).* Note perirenal mass *(m)* anterior to the left kidney *(LK); arrow* points to ureter.

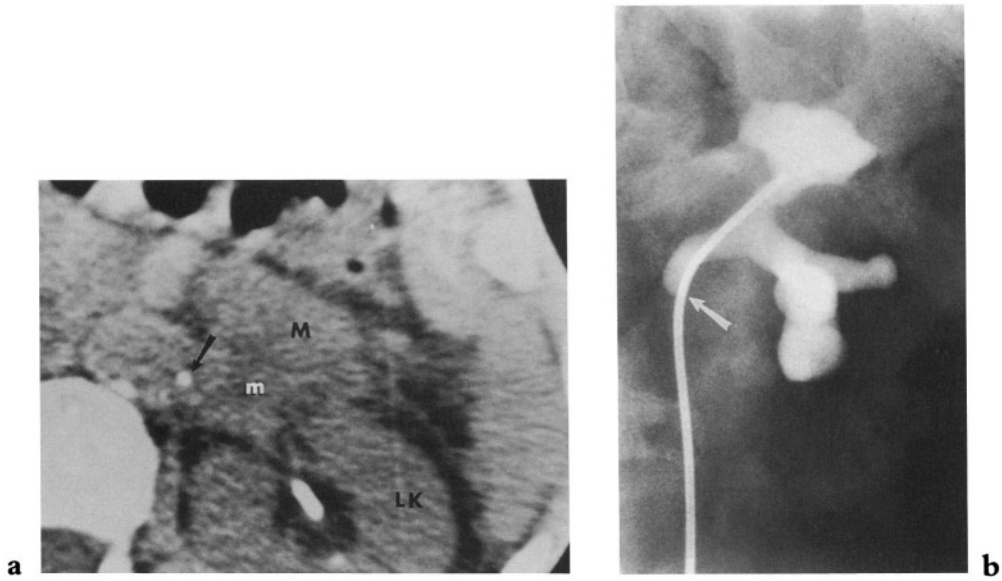


Fig. 13–15. Direct spread of pancreatic tumor to obstruct the left ureter at the ureteropelvic junction.
(a) Mass *(M)* arising in the tail of the pancreas invades the perirenal space via the splenorenal ligament and spreads to the ureteropelvic junction *(m)* to obstruct the left ureter. *Arrow* points to opaque catheter at site of obstruction.
(b) Injection of contrast material through catheter that traverses the site of obstruction *(arrow)*.

(Figs. 13–18 and 13–19). Indeed, we have observed that many of the characteristic growth patterns of mesenteric lymphoma are secondary to spread in the small bowel mesentery. Lymphoma may present or originate in the mesenteric root, and extension may be as multiple or conglomerate densities or stellate infiltration of the mesentery.[20] Spread through the subserous connective tissue of the subperitoneal space accompanying the superior mesenteric artery and its branches brings the process into relationship with the small bowel and colon. Lymphoma can involve the wall of the small bowel, specifically its mesenteric border.[26] When mesenteric lymphoma coexists with paraaortic and/or paracaval adenopathy, a differential imaging feature is the plane of demarcation detectable between the lymphomatous mass infiltrating the mesenteric leaves and the extraperitoneal adenopathy (Fig. 13–18b).

The caudal termination of disease in the mesenteric root is in the right lower quadrant. Tumor involving the ileal portion of the small bowel mesentery may infiltrate the right lateral abdominal wall.[14] It is evident that the mesentery is the conduit through which disease can spread from the upper abdomen to the right lower quadrant and/or encroach upon the coelomic cavity.

In a similar manner, the continuity of the subperitoneal space provides an avenue of spread that may result in a mesenteric hematoma from blood of renal origin that may track medially along the renal artery to the aorta and subsequently along the superior mesenteric artery and its branches (Fig. 13–20). Fulminating pelvic bleeding may track laterally and then spread cephalad within the subperitoneal space to dissect into the mesenteric root to produce significant mesenteric hematoma (Fig. 13–21).

Dissection by means of the central pathway is illustrated in Figure 13–22. In this instance, hemorrhage from a lower abdominal aortic aneurysm spreads along the plane of the inferior mesenteric artery into the sigmoid mesocolon to present a hematoma at this site. Pancreatitis, with direct spread laterally and caudally to the pelvis and sigmoid colon (Fig. 13–23), and diverticulitis, with direct spread from the sigmoid mesocolon to the left lateral pelvis and abdomen (Fig. 13–24), illustrate

text continues on page 630

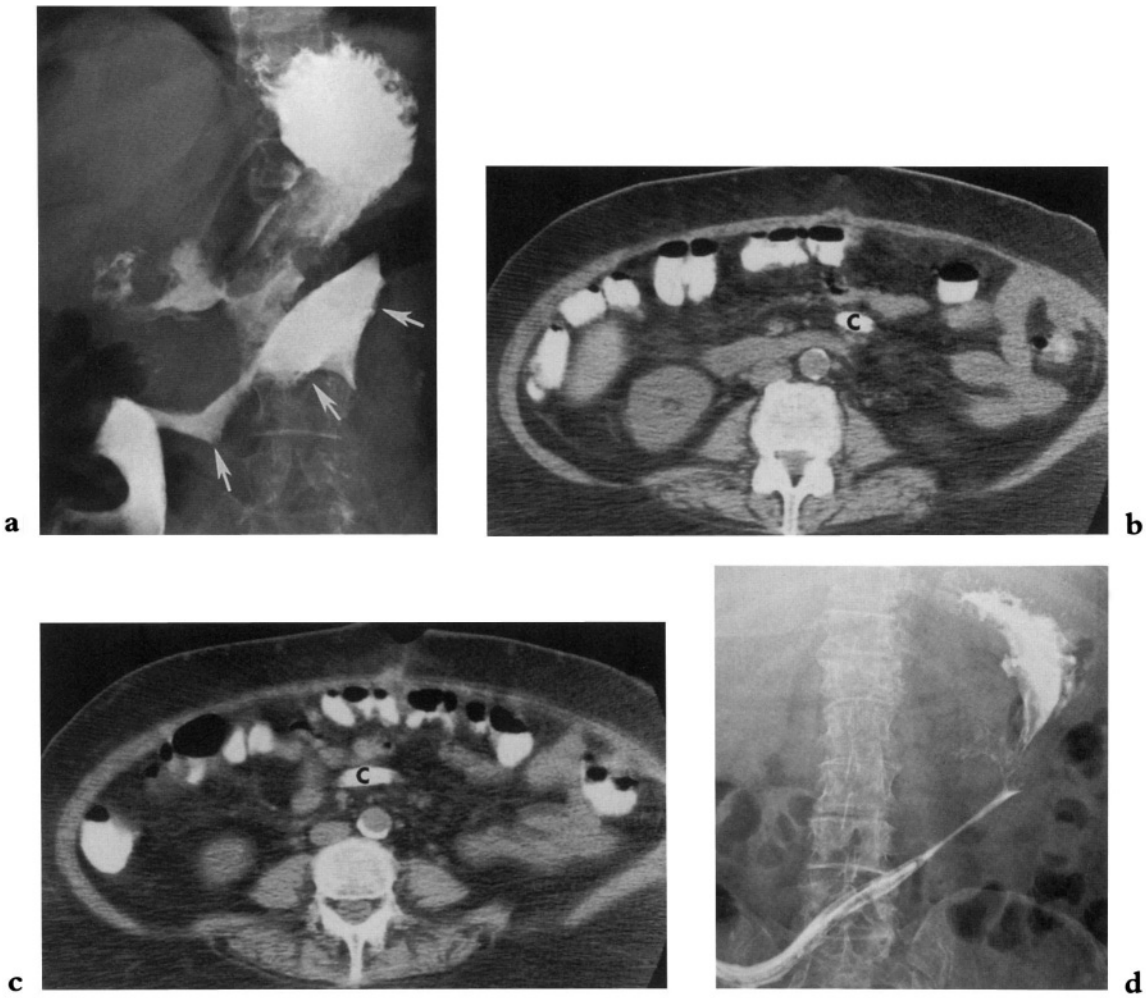


Fig. 13–16. Opacification of mesenteric root *in vivo* secondary to communication from a gastric ulcer.
(a) Upper GI series demonstrates striking continuity across the subperitoneal space from a penetrating posterior ulcer of the greater curvature of the stomach through the length of the root of the small bowel mesentery *(arrows)* to the bare area of the ascending colon. Note its typically oblique course toward the right lower quadrant relating to duodenum, jejunum, ileum, and cecum.
(b and **c)** Following intraoperative drainage, CT demonstrates the catheter *(c)* precisely placed within the mesenteric root.
(d) Sinography via the catheter confirms continued communication between the root of the small intestine mesentery and the stomach
(Reproduced from Oliphant et al.[20])

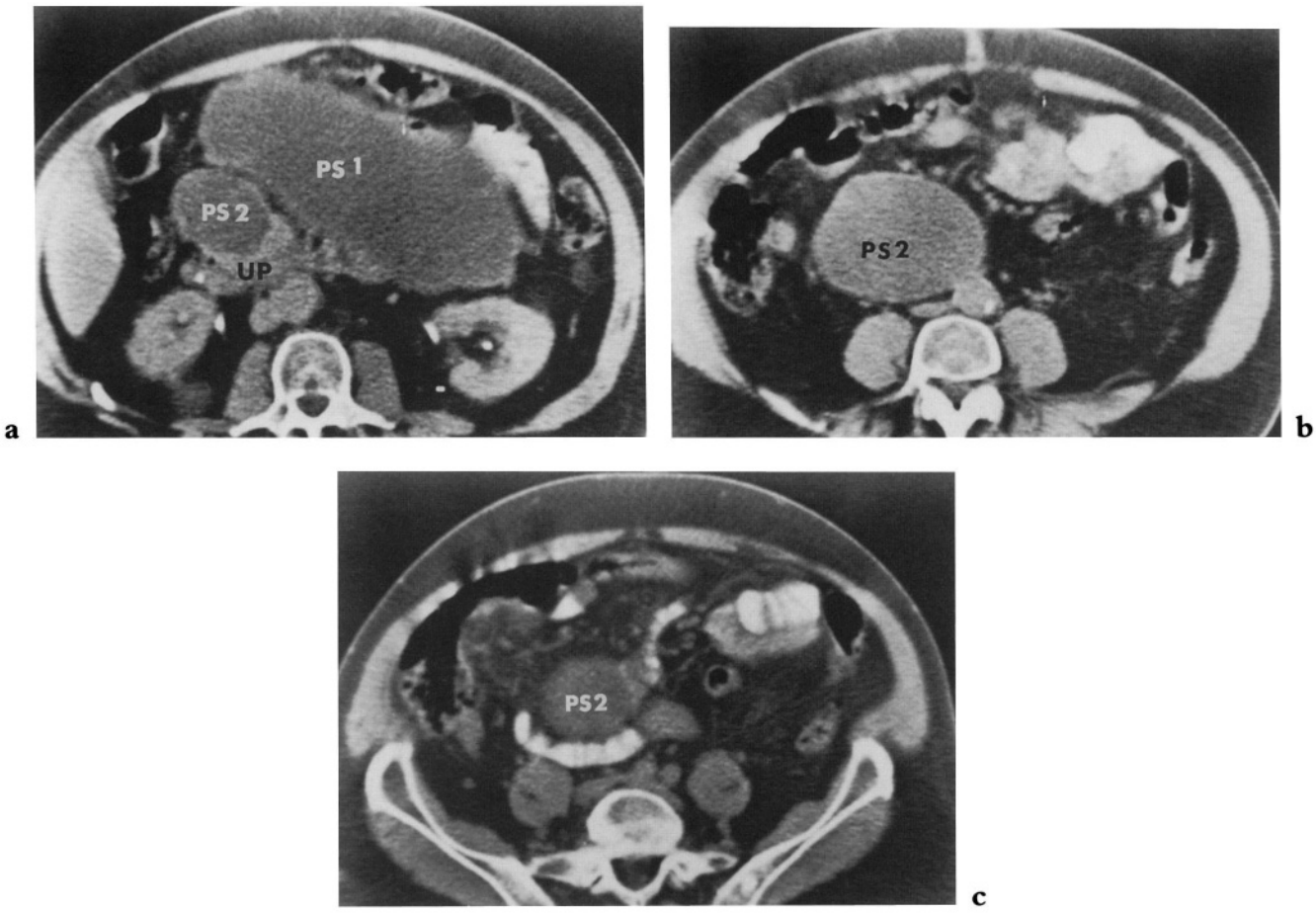
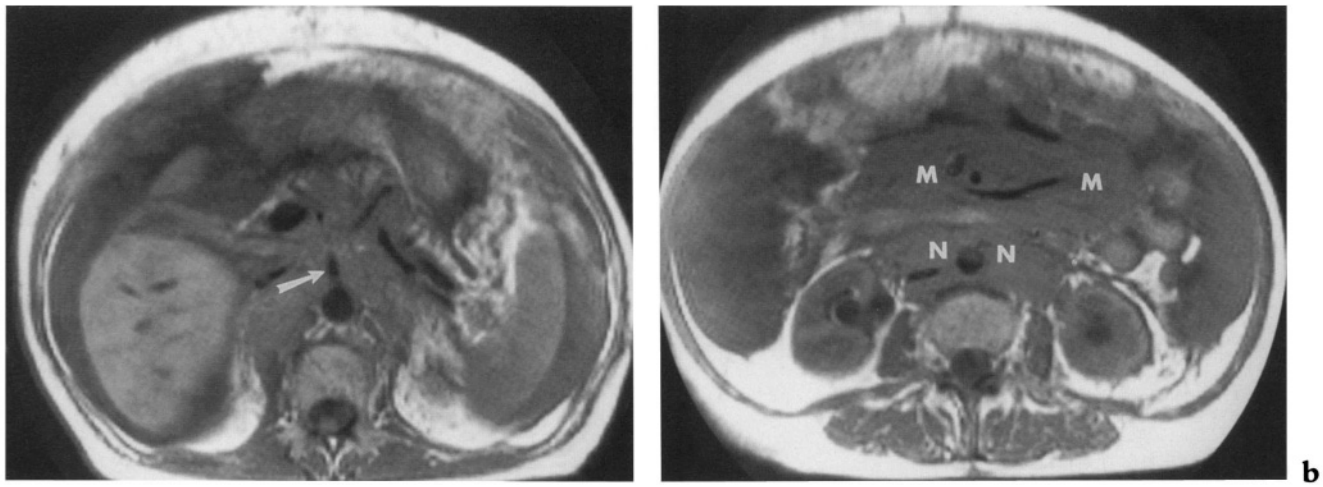


Fig. 13–17. Continuity of the subperitoneal space from the upper abdomen to the right lower abdomen: spread of pancreatic pseudocyst within the root of the small intestine mesentery.
(a) A large pancreatic pseudocyst *(PS1)* occupies the lesser sac. Another pseudocyst *(PS2)* occupies the root of the small intestine mesentery, originating in the region of the uncinate process of pancreas *(UP).*
(b) This pseudocyst *(PS2)* dissects inferiorly within the root of the small intestine mesentery.
(c) Its course can be followed down the length of the mesenteric root into the right lower quadrant, where it lies in relation to a distal ileal loop.
(Reproduced from Oliphant and Berne.[3])



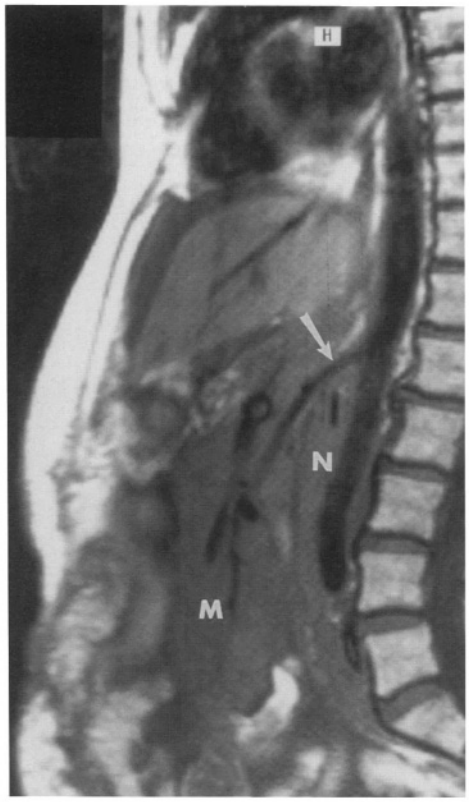


Fig. 13–18. Continuity of lymphoma with paraaortic and paracaval adenopathy and small intestine mesenteric tumor via the subperitoneal space.
(a) MRI, T1-weighted axial image, demonstrates mass surrounding the aorta and extending along the superior mesenteric artery *(arrow)* into the mesentery.
(b) Axial T1-weighted image at level of the kidneys shows conglomerate mesenteric lymphoma *(M)* and nodal masses *(N)* encasing the aorta and inferior vena cava. Note cleft between *M* and *N*.
(c) T1-weighted sagittal image shows aorta with superior mesenteric artery *(arrow)*. The aorta is encased in tumor *(N)* that extends along the superior mesenteric artery and into the small bowel mesentery *(M)*.
(Reproduced from Oliphant et al.[20])

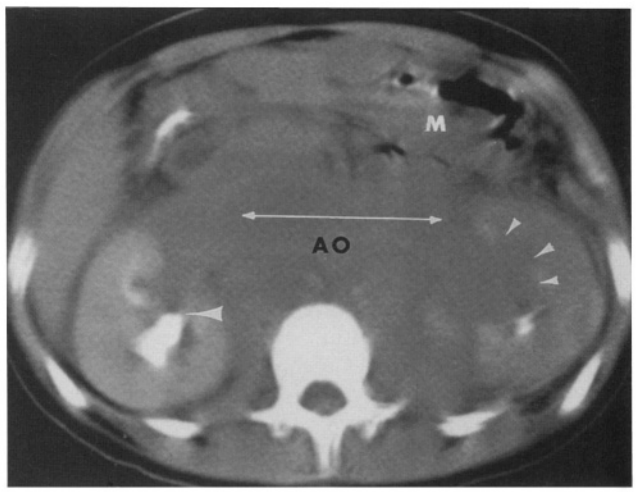


Fig. 13–19. Widespread subperitoneal continuity of Burkitt's lymphoma.
CT scan at level of the renal hila shows large mass encasing and displacing the aorta *(AO)* anteriorly and spreading bidirectionally along the faintly visualized renal arteries *(double-headed arrow)*. The tumor invades and obstructs the right kidney at the ureteropelvic junction *(large arrowhead)* and invades the left kidney at the hilum *(arrowheads)*. *M* = mass in small intestine mesentery.
(Reproduced from Oliphant et al.[20])

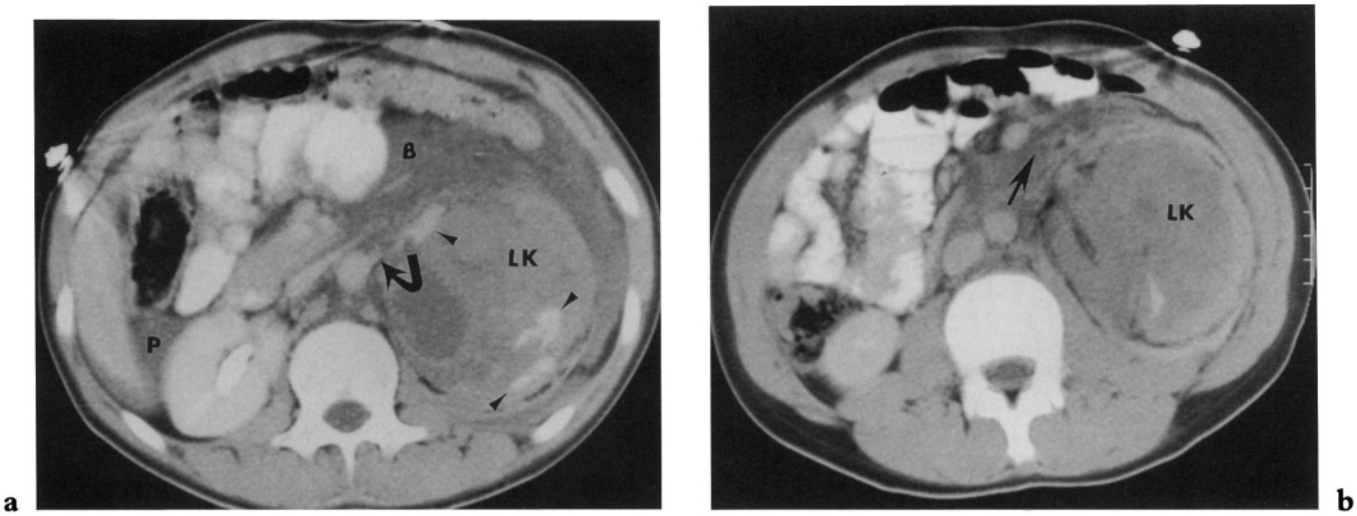


Fig. 13–20. Spread to small bowel mesentery of hemorrhage from trauma to left kidney.
(a) CT at level of left renal artery. This 26-year-old male was in a motor vehicle accident and suffered a fractured left kidney *(LK).* The left renal artery was severed *(curved arrow)* and was subsequently documented by angiography. Hyperdensities represent extravasated contrast medium *(arrowheads).* Blood is present in the small bowel mesentery *(B).* Free peritoneal blood *(P)* from fractured spleen.
(b) CT caudad to renal artery. Blood in mesenteric root extends through the small bowel mesentery *(arrow). LK* = fractured left kidney.
(Reproduced from Oliphant et al.[20])

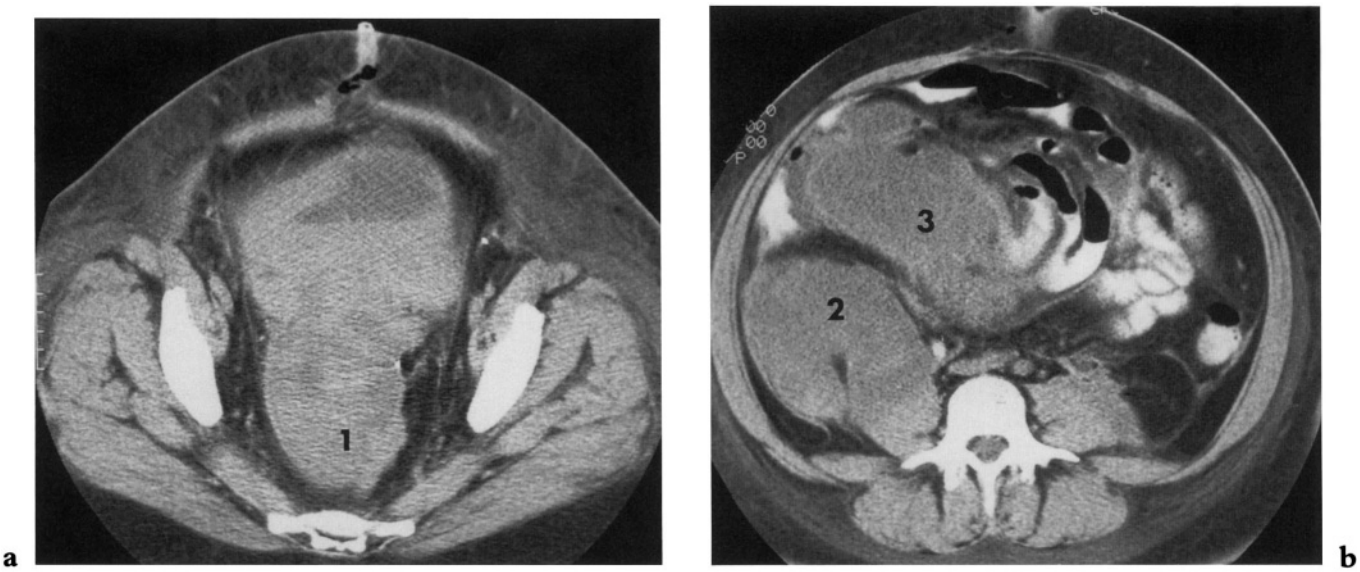


Fig. 13–21. Direct spread of hemorrhage from the pelvis cephalad to the right lateral abdomen and into the small intestine mesentery via the subperitoneal space.
This 31-year-old female, receiving anticoagulants for disorders of multiple heart valves, underwent a total hysterectomy and bilateral salpingo-oophorectomy for a bleeding ovarian cyst. Postoperatively, she developed **(a)** massive pelvic bleeding *(1)* that extended to the right lateral pelvic wall and **(b)** to the right posterior abdominal wall *(2)* and dissected through the abdominal subperitoneal space on the right to the ileal portion of the small intestine mesentery *(3).*
(Reproduced from Oliphant et al.[20])

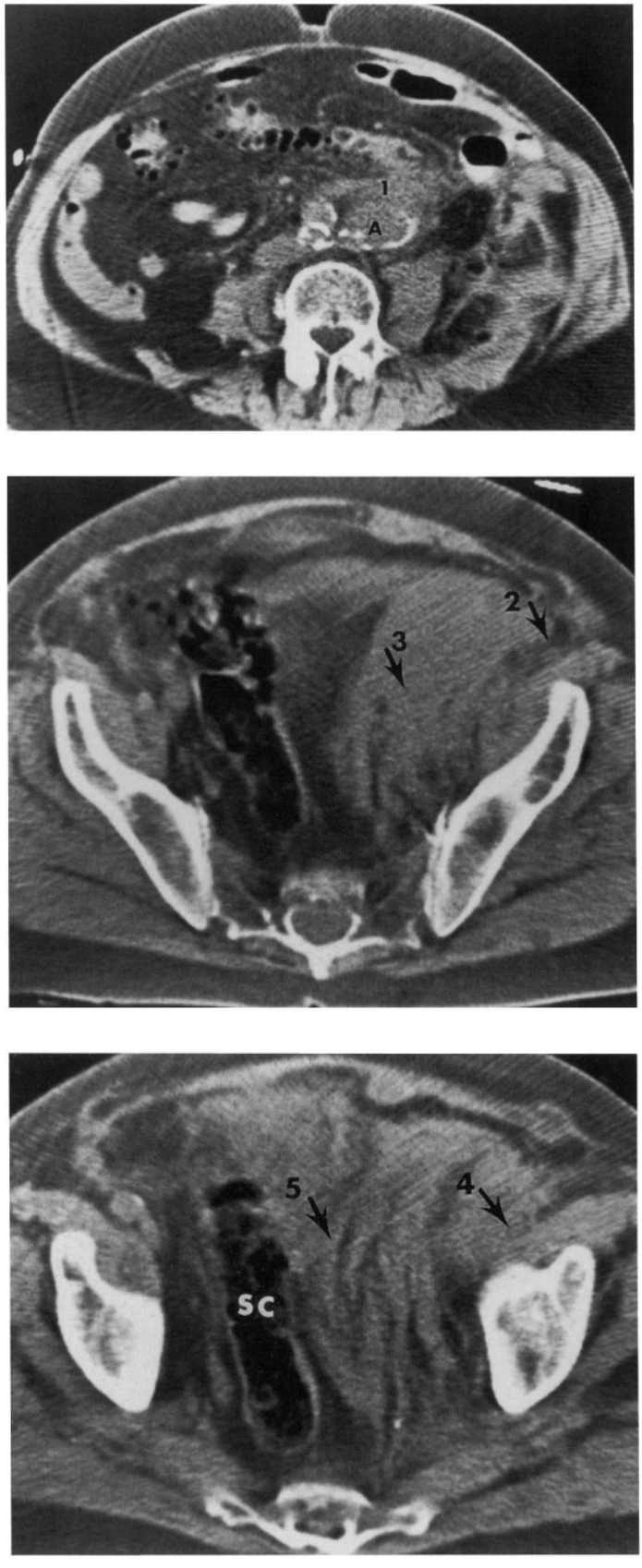


Fig. 13–22. Continuity of subperitoneal space from the lower central abdomen to the left pelvis: direct spread of hemorrhage from a ruptured aortic aneurysm along the inferior mesenteric artery distribution to the sigmoid mesocolon.

(a) CT at level of bifurcation of abdominal aorta shows blood *(1)* dissecting within the subperitoneal space in the region of the inferior mesenteric artery. *A* = aneurysm.

(b) In the upper pelvis, hematoma is present within the lateral wall of the pelvis *(arrow 2)* and the sigmoid mesocolon *(arrow 3).*

(c) Inferiorly, blood is clearly identifiable within the sigmoid mesocolon *(arrow 5),* displacing the sigmoid colon *(SC)* to the right. Blood in the lateral wall of the left pelvis remains evident *(arrow 4).*

(Reproduced from Oliphant et al.[21])

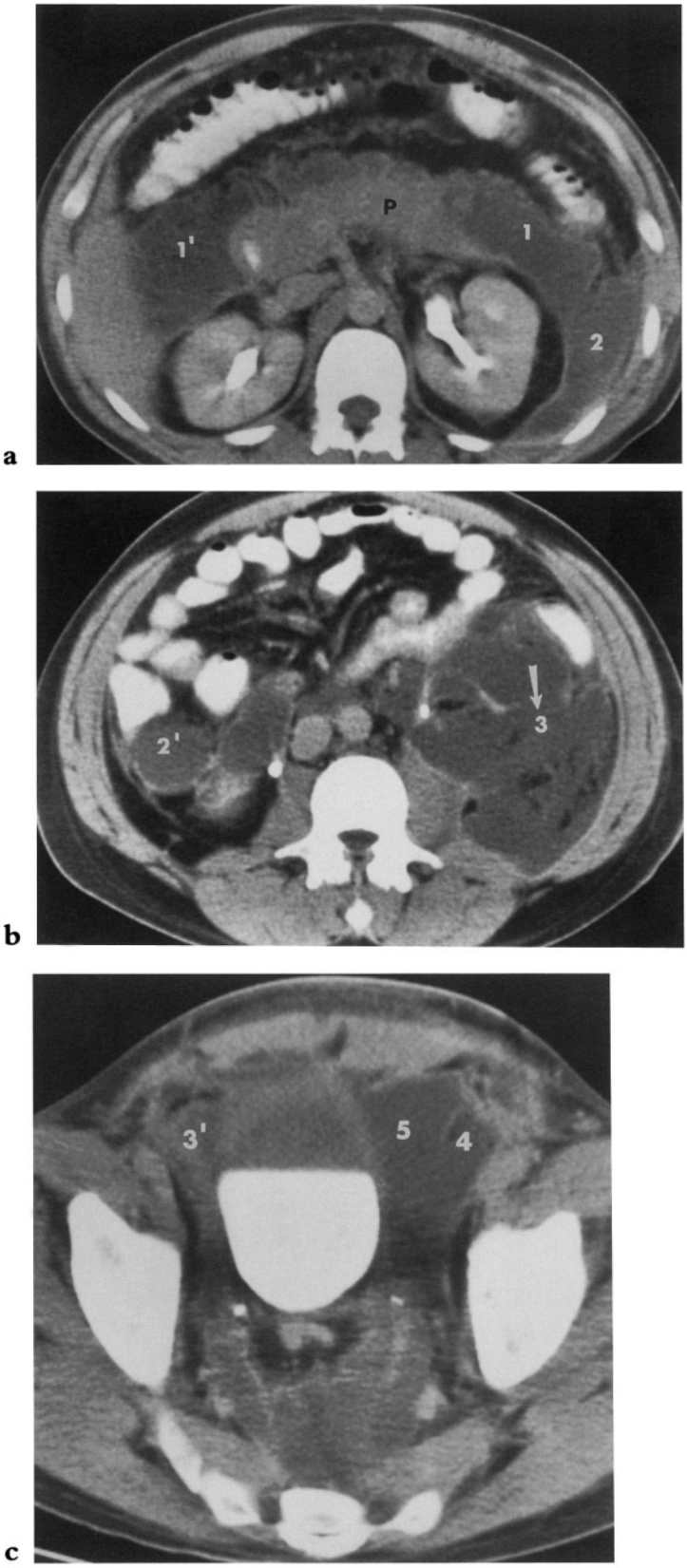


Fig. 13–23. Continuity of the subperitoneal space along the left lateral abdomen into the pelvis: direct spread of inflammation from pancreatitis to the pelvis and sigmoid mesocolon.
(a) Inflammation in the anterior pararenal spaces extends laterally to the left *(1)* and to the right *(1)*. There is extension to the left posterior abdominal wall *(2)*. *P* = pancreas.
(b) Below the level of the kidneys, the process extends down the left *(arrow 3)* and the right *(2)* posterior abdomen.
(c) Inferiorly, the inflammation on the left extends to the lateral pelvis *(4)* and the sigmoid mesocolon *(5),* and on the right to the lateral pelvis *(3')*. The process also extends into the posterior pelvic subperitoneal space
(Reproduced from Oliphant et al.[27])

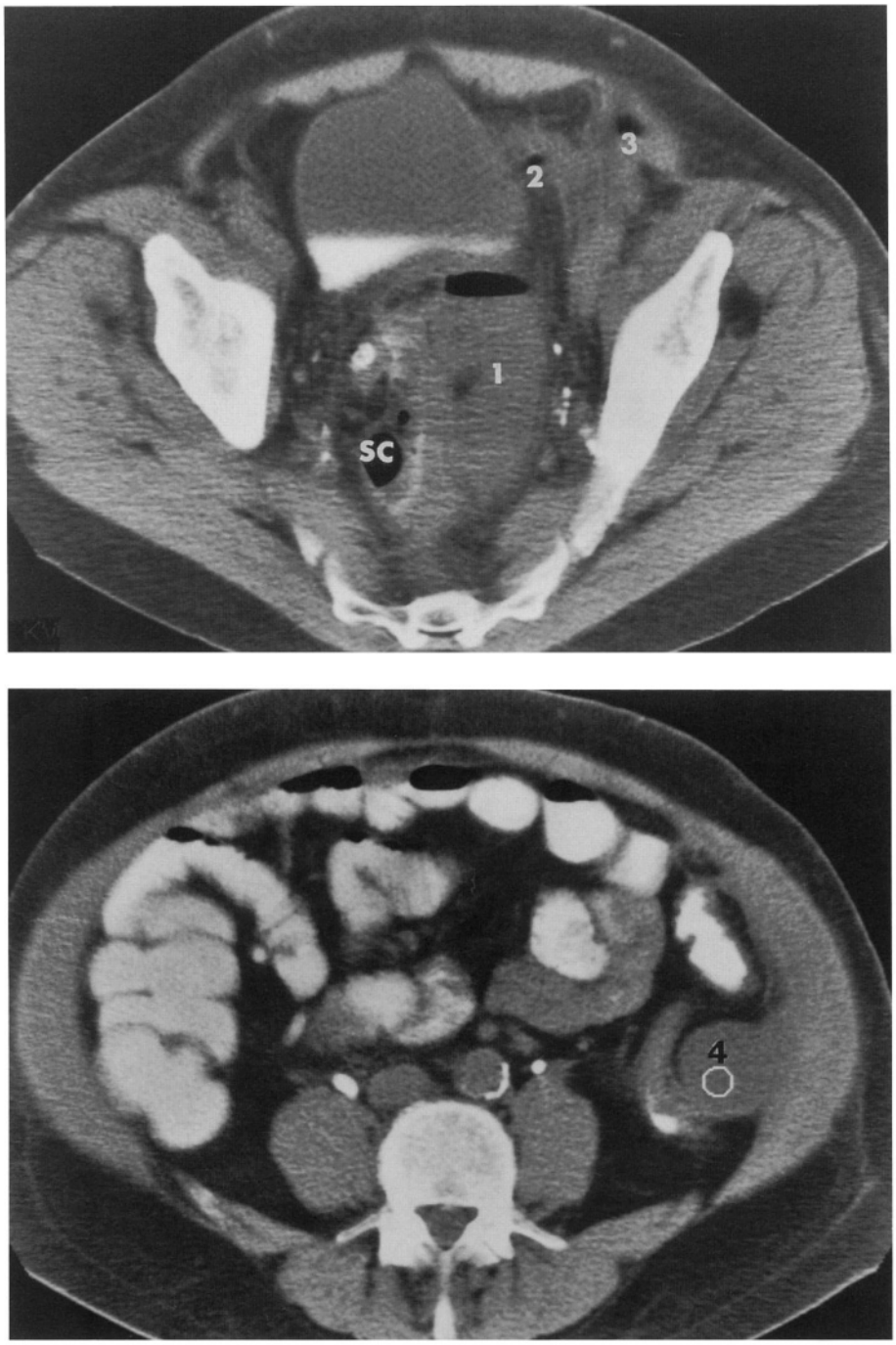


Fig. 13–24. Continuity of the subperitoneal space from the left pelvis to the abdomen: direct spread of pelvic inflammation from a sigmoid diverticular abscess to the left lateral abdomen.
(a) An abscess with an air-fluid level has developed in the sigmoid mesocolon *(1)*. The inflammation spreads to other segments of the mesocolon *(2)* and the left lateral wall *(3)* at the junction of the abdomen and pelvis.
(b) In the lower abdomen, the abscess has localized in the subperitoneal space laterally *(4)*.
(Reproduced from Oliphant et al.[27])

bidirectional spread of inflammatory disease along these pathways.

The lateral continuity of the subperitoneal space is unique in that no major blood vessels course in this portion; yet, this anatomic continuity is the basis for understanding the direct spread of disease between the abdomen and female pelvis.[14] Figures 13–25 and 13–26 document bidirectional spread of tumor between the abdomen and the female pelvis. These cases illustrate massive disease extending along the right lateral pelvic wall and the broad ligament simultaneously. Distinction between these two areas of involvement can be appreciated by noting a "cleft" of normal tissue lying between the areas of tumefaction (Fig. 13–25c–e). This is analogous to the plane of demarcation between the adenopathy and small bowel mesenteric tumefaction described previously (Fig. 13–18). In a similar manner, inflammatory processes can spread through this same pathway of the subperitoneal space, at times over a considerable distance (Fig. 13–27).

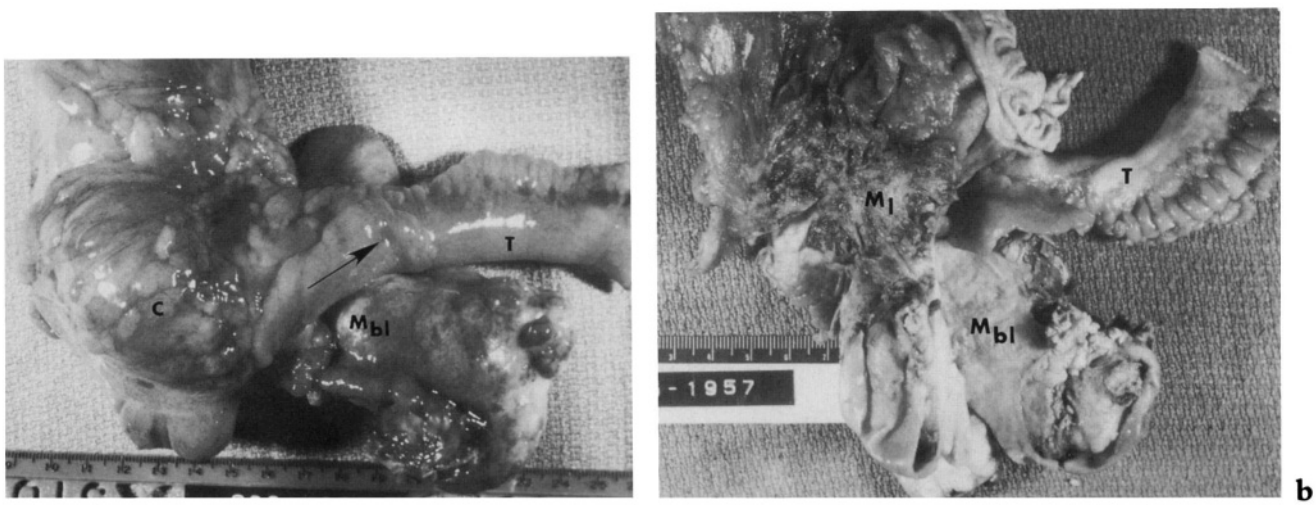


Fig. 13–25. Continuity of subperitoneal spread from the right adnexa to the mesentery of the small bowel.
A 72-year-old female with ovarian carcinoma demonstrates direct spread to the broad ligament, right lateral pelvic wall, right posterior abdomen, cecum, and mesentery of the terminal ileum.
(a) Gross pathology specimen. Large mass is present in the broad ligament *(M_{bl})*. The cecum *(C)* is bulged forward by tumor lying posteriorly. Tumor extends along the serosa *(arrow)* of the terminal ileum *(T)*.
(b) Anterolateral portion of the cecum and terminal ileum *(T)* have been removed, exposing mass *(M_l)*. This mass is in direct continuity with the broad ligament *(M_{bl})*. *Continued on opposite page*

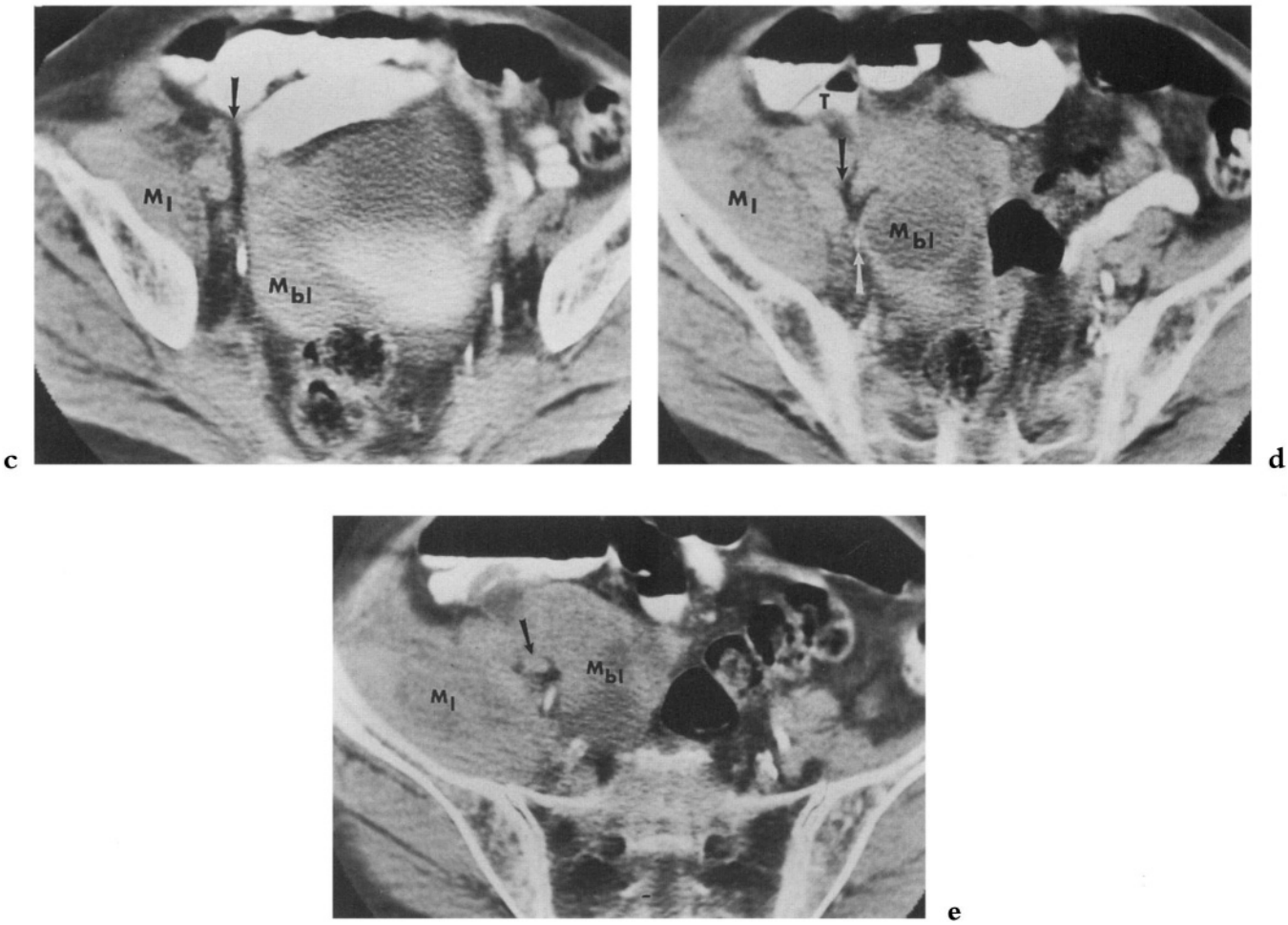


Fig. 13–25. Continuity of subperitoneal spread from the right adnexa to the mesentery of the small bowel. (Continued)

(c) CT at level of greater sciatic notch shows mass in broad ligament *(M_{bl})* and mass in lateral pelvic wall *(M_l)*. *Arrow* points to cleft between the two sites.

(d) Inferiorly, tumor is seen in the broad ligament *(M_{bl})* and the lateral pelvic wall *(M_l)*. The tumor extends to the posterior abdominal wall and then to the root of the small intestine mesentery, shown subjacent to the terminal ileum *(T)*. *Arrows* indicate the cleft between tumor in the broad ligament and the lateral pelvic wall.

(e) Scan at junction of right lower abdomen and pelvis reveals confluence of tumor in the broad ligament *(M_{bl})* and the lateral pelvic wall *(M_l)*. *Arrow* lies within this confluence and also points to cleft, which represents the iliac vessels within the adipose tissue of the lateral pelvic wall, displaced medially.

(Reproduced from Oliphant et al.[14])

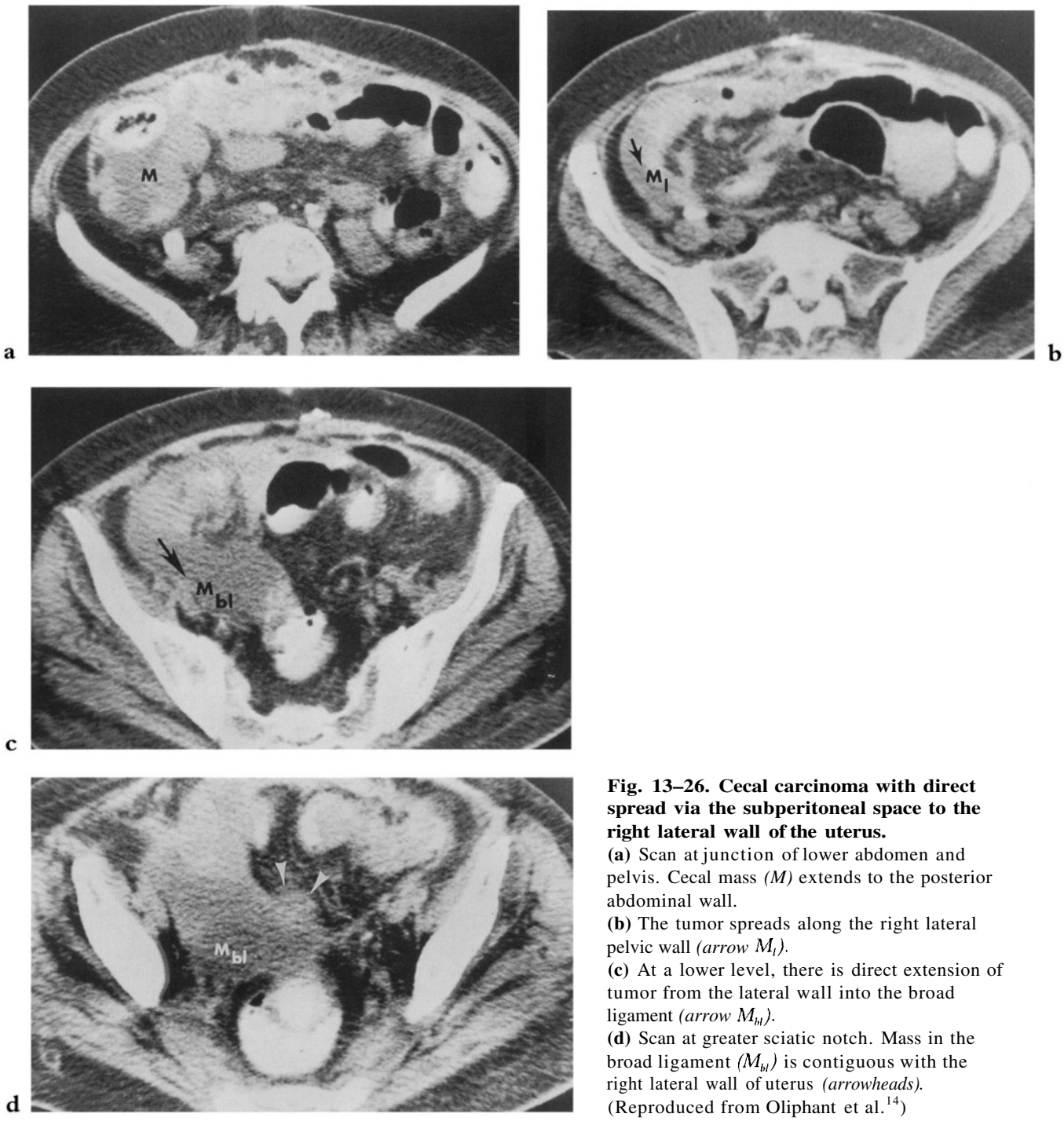
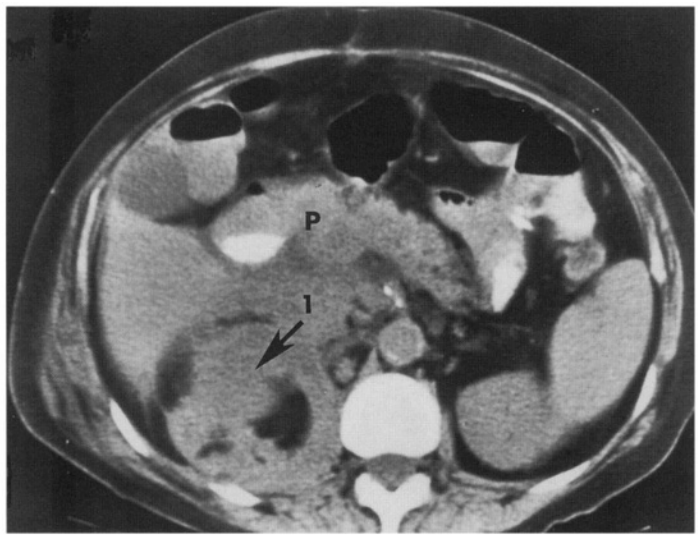
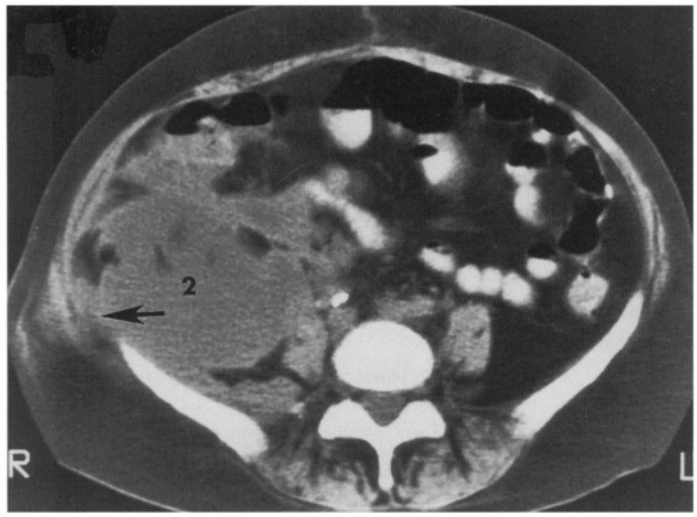


Fig. 13–26. Cecal carcinoma with direct spread via the subperitoneal space to the right lateral wall of the uterus.
(a) Scan at junction of lower abdomen and pelvis. Cecal mass *(M)* extends to the posterior abdominal wall.
(b) The tumor spreads along the right lateral pelvic wall *(arrow M_l)*.
(c) At a lower level, there is direct extension of tumor from the lateral wall into the broad ligament *(arrow M_{bl})*.
(d) Scan at greater sciatic notch. Mass in the broad ligament *(M_{bl})* is contiguous with the right lateral wall of uterus *(arrowheads)*.
(Reproduced from Oliphant et al.[14])

Fig. 13–27. Subperitoneal spread of inflammation from pancreatitis to the broad ligament and into the lateral flank.
(a) CT at level of pancreas *(P).* Inflammation courses from the anterior pararenal space to the right posterior abdomen *(arrow 1).*
(b) The inflammation extends down the right posterior abdomen *(2)* and through Petit's triangle to the right flank *(arrow).*
(c) In the upper pelvis, the inflammatory process extends to the right lateral pelvis *(3)* and into the broad ligament *(4).* Note "cleft" *(arrow)* between *3* and *4.*
(d) Inferiorly, inflammation within the broad ligament *(5)* extends to the uterus *(Ut).*



a



b



c



d

References

1. Meyers MA: Dynamic Radiology of the Abdomen: Normal and Pathological Anatomy, 4th ed. Springer-Verlag, New York, 1993.
2. Feldberg MAM: Computed Tomography of the Retroperitoneum: An Anatomical and Pathological Atlas with Emphasis on the Fascial Planes. Martinus Nijhoff, Boston, 1983.
3. Oliphant M, Berne AS: Computed tomography of the subperitoneal space: Demonstration of direct spread of intraabdominal disease. J Comput Assist Tomogr 1982; 6(6):1127–1137.
4. Oliphant M, Berne AS: Holistic concept of the anatomy of the abdomen: A basis for understanding direct spread of disease. Contemp Diagn Radiol 1985; 8(10):1–6.
5. Oliphant M, Berne AS, Meyers MA: Subperitoneal spread of intraabdominal disease. *In* Computed Tomography of the Gastrointestinal Tract: Including the Peritoneal Cavity and Mesenteries. Edited by MA Meyers. Springer-Verlag, New York, 1986, pp 95–136.
6. Meyers MA, Oliphant M, Berne AS, et al: The peritoneal ligaments and mesenteries: Pathways of intraabdominal spread of disease. Annual oration. Radiology 1987; 163:593–604.
7. Oliphant M, Berne AS, Meyers MA: The subperitoneal space of the abdomen and pelvis: Planes of continuity. AJR 1996; 167:1433–1439.
8. Langman J: Medical Embryology, 2nd ed. Williams & Wilkins, Baltimore, 1969.
9. Arey LB: Developmental Anatomy: A Textbook and Laboratory Manual of Embryology, 5th ed. WB Saunders, Philadelphia, 1946, pp 187–234, 244–263, 265–306.
10. Patten BM. Human Embryology, 3rd ed. New York, McGraw-Hill, 1968, pp 406–426.
11. Moore KI: The Developing Human: Clinically Oriented Embryology, 4th ed. Philadelphia, WB Saunders, 1988, pp 59–169.
12. Oliphant M, Berne AS, Meyers MA: The subserous thoracoabdominal continuum: Embryologic basis and diagnostic imaging of disease spread. Abdom Imaging 1999; 24:211–219.
13. Gray H: The Digestive System. *In* Anatomy of the Human Body. Edited by CM Gross. Lea & Febiger, Philadelphia, 1965, pp 1207–1311.
14. Oliphant M, Berne AS, Meyers MA: Imaging the direct bidirectional spread of disease between the abdomen and female pelvis via the subperitoneal space. Gastrointest Radiol 1988; 13:285–298.
15. Pernkopf E: Abdominal Viscera. *In* Atlas of Topographical and Applied Human Anatomy. WB Saunders, Philadelphia, 1976, vol 2, pp 268–281, 304–322.
16. Anson BJ, Curtis AH: Anatomy of the female pelvis. *In* Obstetrics and Gynecology. Edited by AH Curtis. WB Saunders, Philadelphia, 1933, pp 1–79.
17. Oliphant M, Berne AS: Mechanism of direct spread of neuroblastoma: CT demonstration and clinical implications. Gastrointest Radiol 1987; 12:59–66.
18. Meyers MA, McSweeney J: Secondary neoplasms of the bowel. Radiology 1972; 105:1–11.
19. Meyers MA: Intraperitoneal spread of malignancies and its effect on the bowel. Second Annual Leeds Lecture. Clin Radiol 1981; 32:129–146.
20. Oliphant M, Berne AS, Meyers MA: Spread of disease via the subperitoneal space: The small bowel mesentery. Abdom Imaging 1993; 18:109–116.
21. Meyers MA: Roentgen significance of the phrenicocolic ligament. Radiology 1970; 95:539–545.
22. Meyers MA, Whalen JP: Roentgen significance of the duodenocolic relationships: An anatomic approach. AJR 1973; 117:263–274.
23. Meyers MA, Evans JA: Effects of pancreatitis on the small bowel and colon: Spread along mesenteric planes. AJR 1973; 119:151–165.
24. Meyers MA, Volberg F, Katzen B, et al: Haustral anatomy and pathology: A new look. I. Roentgen identification of normal pattern and relationships. Radiology 1973; 108:497–504.
25. Meyers MA, Volberg F, Katzen B, et al: Haustral anatomy and pathology: A new look. II. Roentgen interpretation of pathologic alterations. Radiology 1973; 108:505–512.
26. Meyers MA: Clinical involvement of mesenteric and antimesenteric borders of small bowel loops. II. Radiologic interpretation of pathological alterations. Gastrointest Radiol 1976; 1:48–58.
27. Oliphant M, Berne AS, Meyers MA: Bidirectional spread of disease via the subperitoneal space: The lower abdomen and left pelvis. Abdom Imaging 1993; 18:117–125.
28. Oliphant M, Berne AS, Meyers MA. Direct spread of subperitoneal disease into solid organs: Radiologic diagnosis. Abdom Imaging 1995; 20:141–147.

The Small Bowel: Normal and Pathologic Anatomy

14

The distinctive course, coiled nature, and position of the small bowel are provided by the mesentery. The most characteristic gross anatomic feature of the jejunum and ileum is their organization into a series of bowel loops, compactly arranged in the midabdomen. In the routine interpretation of small intestinal series, little attention is directed to this unique organization of the bowel. Indeed, the confluence or overlapping of small bowel loops often presents a misleading appearance. Their serpentine, undulating course ordinarily poses a diagnostic challenge in identifying the presence of a localized abnormality.

However, the anatomic relationships inherent in this characteristic arrangement of the small intestine into loops of bowel may provide significant diagnostic information.[1,2] Pathologically, many disease processes selectively involve the mesenteric or antimesenteric borders of the small intestine. An understanding of their anatomic definition and relationships permits radiologic identification of the specific borders.[1]

Anatomic Considerations

The *mesentery* (Fig. 14–1) suspends the jejunum and ileum from the posterior abdominal wall. It is composed of fatty extraperitoneal connective tissue, blood vessels, nerves, lymphatics, and an investment of peritoneum that reflects from the posterior parietal peritoneum. Features associated with the fan-shaped dimensions of the mesentery make it a unique suspensory ligament and contribute to the characteristic nature of small bowel loops.

The attached border, *the root of the mesentery,* extends obliquely from the point of termination of the duodenum, at the lower border of the pancreas on the left side of the second lumbar vertebra, to the cecum in the right iliac fossa near the right sacroiliac articulation. In that course, the line of attachment passes from the duodenojejunal flexure down over the front of the third part of the duodenum, then obliquely across the aorta, the inferior vena cava, the right ureter, and the psoas major

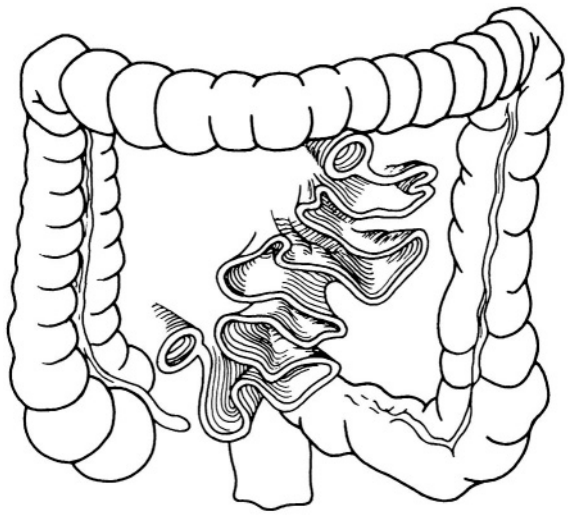


Fig. 14–1. The small bowel mesentery.
It extends from its line of attachment, or root, in a series of fanlike ruffles to suspend the jejunum and ileum. The undulating course of its intestinal edge constitutes a series of convexities and concavities. Peritoneal recesses extend between the mesenteric reflections.
(Reproduced from Meyers.[1])

muscle, to the right iliac region. From the root, the mesentery extends in a series of fanlike ruffles to suspend the jejunum and ileum. There are usually six main folds, from the margins of which secondary folds project in all directions, and from those again even a third series may be formed. A series of peritoneal recesses are formed between the ruffles of the small bowel mesentery. The root of the mesentery is only about 15 cm (6 in.) long and is fixed in position. It is much thicker than the part near the gut, since it contains between its layers a considerable amount of fatty fibroareolar extraperitoneal tissue and the large vascular trunks that supply the intestine (Fig. 14–2).

The *base,* or unattached border, *of the mesentery* is frilled out to an enormous degree so that, while the root measures only 6–7 in., the free border is extended to 20–22 ft (Fig. 14–3). The great length of the intestinal border is produced by plication of the mesentery along its edge for a depth of from 6–8 cm (2½–3½ in.).

The *length of the mesentery* (Fig. 14–3), measured from its root to the attached edge of the intestine directly opposite, is usually 20–22 cm (8–9 in.). It is greater at that part that suspends the coils of the intestine lying between 2 and 3 m (6 and 11 ft) from the duodenum, where it may reach a length of 25 cm (10 in.). It tends to increase in length as age advances.

Normal Radiologic Observations

From these basic considerations, several principles may be derived that have practical diagnostic application to radiology of the abdomen.[2]

Axis of the Root of the Small Bowel Mesentery

The plane of attachment of the small bowel mesentery may be drawn by an imaginary line extending from the midtransverse duodenum or duodenojejunal junction to the ileocecal junction. The root of the mesentery most often inserts at the termination of the ileum with the colon and only rarely on the ascending colon or the distal ileum. On plain films, the line may be drawn from the left of L2 to the right sacroiliac articulation.

The axis of the root may be defined more clearly by barium contrast studies, which then relates more directly to small bowel loops. Figure 14–4 illustrates two different cases of nonrotation of the jejunum, a common developmental variant. The root of the small bowel mesentery is shown by the oblique plane providing the medial demarcation of these jejunal loops. The root may also be identified in cases of normal development and fixation of the mesentery. In the small bowel series shown in Figure 14–5, the attached border of the mesentery can be appreciated as the oblique plane from which the loops are suspended. The axis can be readily appreciated by sectional imaging (Fig. 14–6).

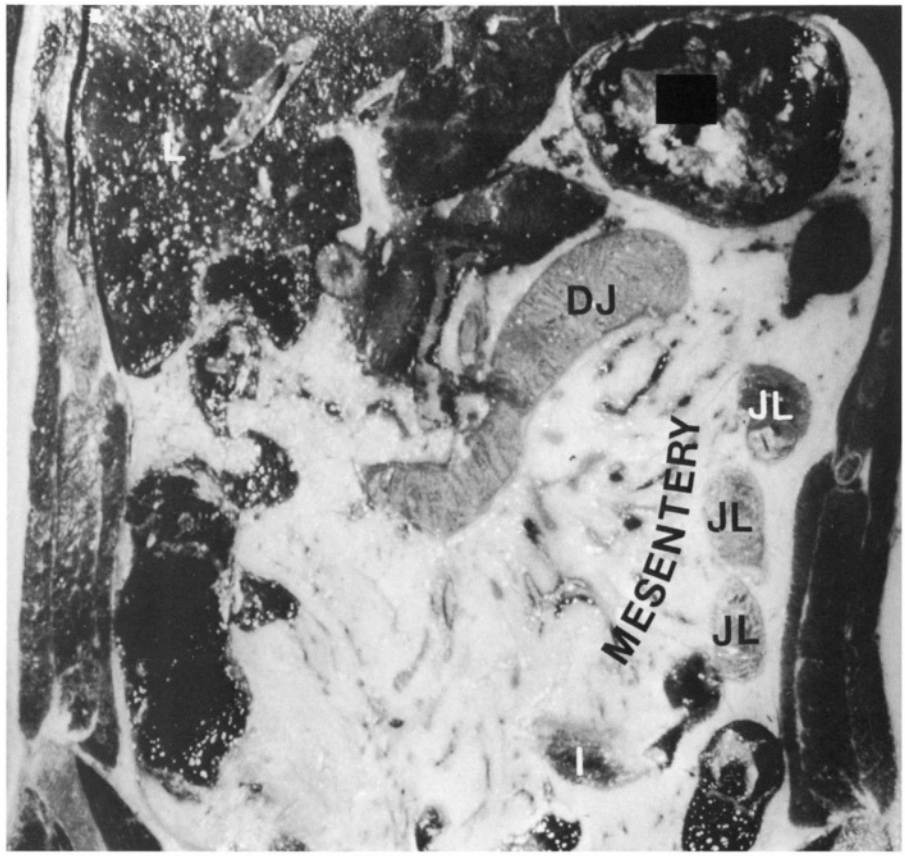
It is these normal relationships of small bowel loops to the supporting mesentery that basically determine the radiologic findings in cases of mechanical obstruction. The dilated loops are then each tensely suspended from the mesenteric root as peristalsis persists; the hydrodynamic consequences lead to the classic "stepladder" configuration (Fig. 14–7).

Undulating Changeable Nature of Coils of Bowel Loops

A fan-shaped supporting ligament such as the mesentery, with an attachment of only 6 in. and an average length of 8–9 in., must suspend 20–22 ft of small bowel. This remarkable feat is accomplished by the unique plication or frilling of its intestinal border. The mesentery extends from its root in a series of fanlike ruffles. This geometric arrangement provides an unusually long border to suspend the jejunum and ileum. It is precisely this feature that contributes to the characteristic undulating nature of the coils of small intestine. The mesentery is of such a length that the loops are able to move freely in the abdominal cavity, and consequently the position occupied by any portion of the small bowel, with the usual exception of the beginning of the jejunum and the ending of the ileum, cannot be stated with certainty. Nevertheless, in general, the jejunum occupies the superior and left portions of the peritoneal cavity below the stomach, and the ileum the inferior and right divisions.

The changeable position of jejunal and ileal loops *in vivo* is most easily documented by comparing portions of the intubated small bowel on sequential films, as in Figure 14–8. These show the loops are movable on the root of the mesentery, but they maintain the convexities of the ruffles. Specific intestinal segments (nos. *1* through *4)* can be matched and demonstrate varying positions within the peritoneal cavity. The changeable

text continues on page 640



a



b

Fig. 14–2. Anatomy of the small bowel mesentery.

(a) Coronal anatomic section taken at the level of the third and fourth portions of the duodenum and the duodenojejunal junction *(DJ).* It demonstrates the fatty elastic nature of the mesentery, which contains the intestinal vessels as it radiates from its root to suspend loops of jejunum *(JL)* and ileum *(I). L* = liver. (Courtesy of Manuel Viamonte, M.D., Mount Sinai Hospital, Miami Beach, FL.; reproduced from Meyers.[1])

(b) Transverse section shows fat-laden mesenteric leaves. Each sheath contains numerous vessels *(arrowheads)* radiating toward small bowel loops. These vessels can be traced back to the superior mesenteric vessel.

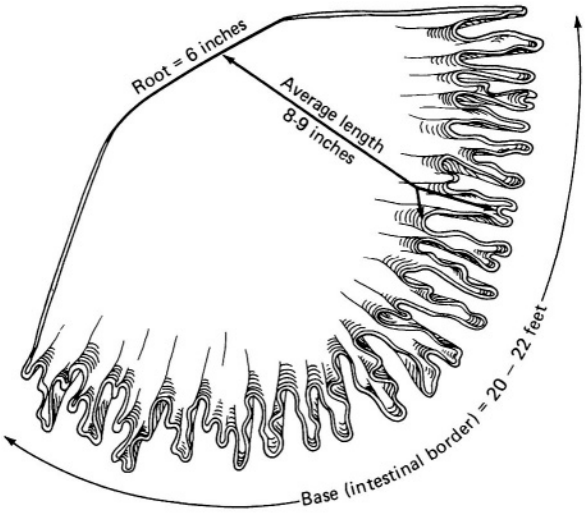


Fig. 14–3. Dimensions of the small bowel mesentery. The length of the intestinal border to an extent approximately 40 times that of its root is brought about by its unique frilled nature. This determines the characteristic formation of the small bowel into loops.
(Reproduced from Meyers.[1])

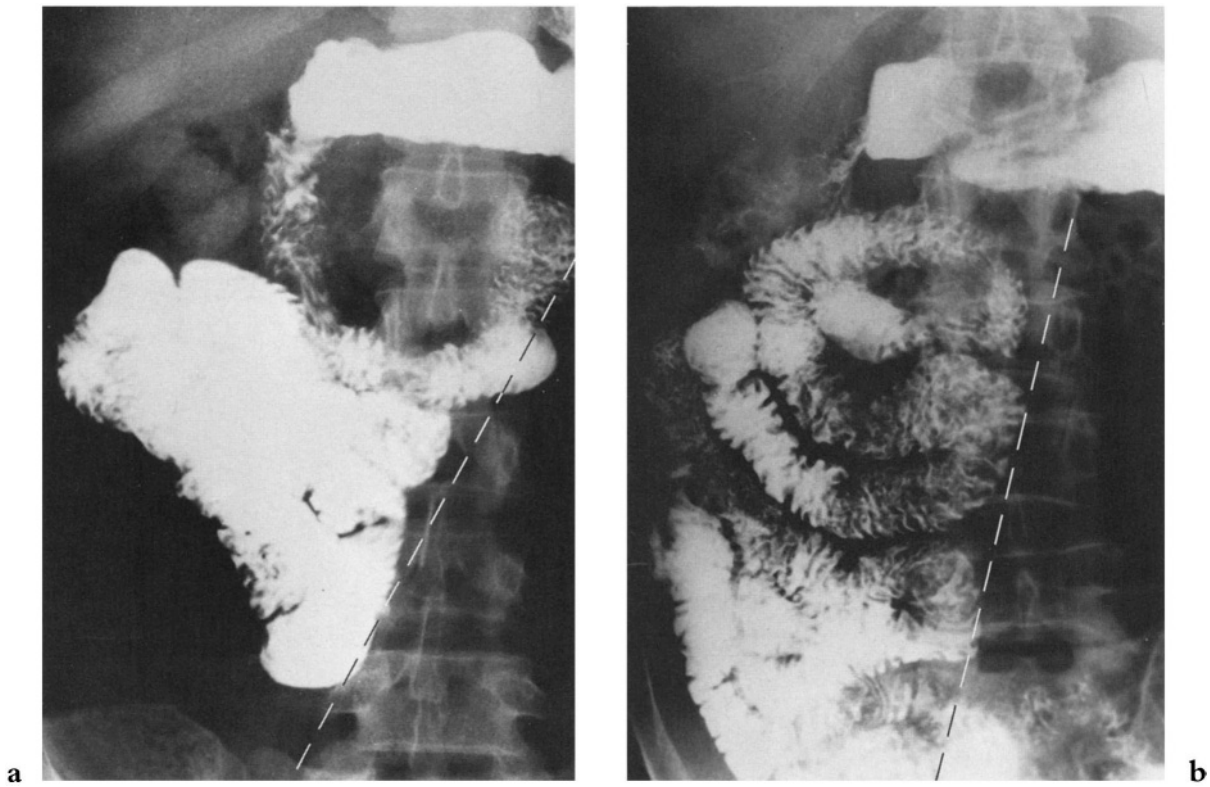
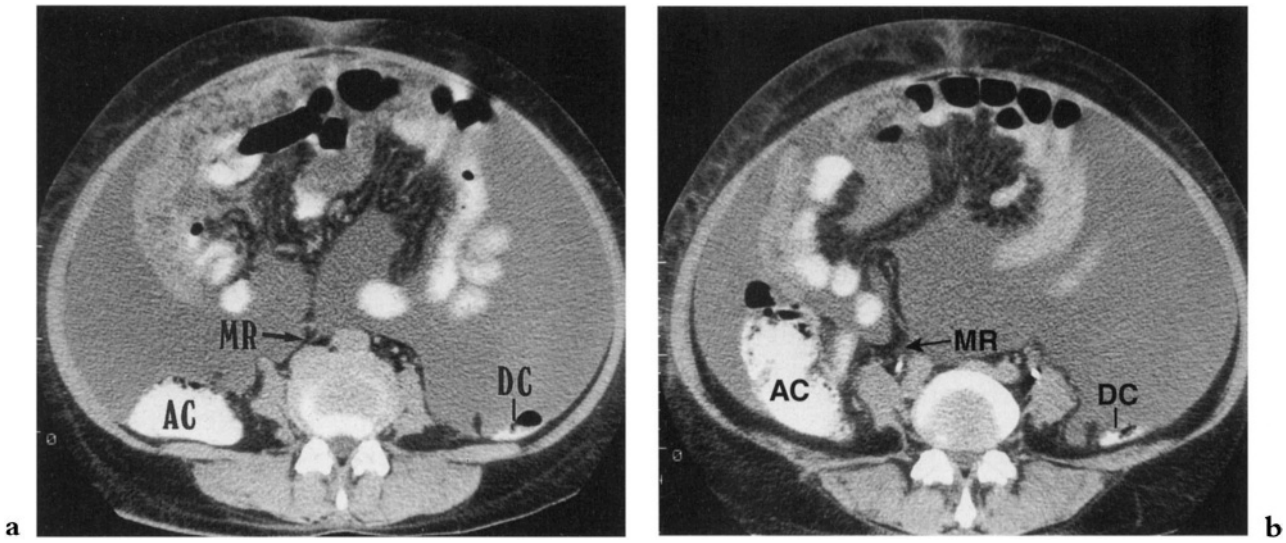


Fig. 14–4. Two different cases of nonrotation of the jejunum in the right abdomen. The oblique plane that provides the medial demarcation of the loops of bowel identifies the axis of the root of the small bowel mesentery *(dashed line).*
(Reproduced from Meyers.[1])



Fig. 14–5. The root of the small bowel mesentery.
This is revealed as the oblique plane *(arrows)* from which the intestinal coils are suspended. In this instance, it provides a line of transition between jejunal loops (shown by their prominent valvulae conniventes), which project to the patient's left, and ileal loops (with less conspicuous valvulae), which extend to the right.
(Reproduced from Meyers.[1])



a b

Fig. 14–6. Axis of the root of the small bowel mesentery.
Two different levels of CT, **a** 5 cm cephalad to **b**, in a patient with massive ascites, show rightward movement of the mesenteric root *(MR)* inferiorly. Consequently, the right infracolic space becomes smaller inferiorly. This favors the dynamics of metastatic seeding in the right lower quadrant in relation to distal ileal loops. *AC* = ascending colon; *DC* = descending colon.
(Courtesy of Yong Ho Auh, M.D., Asan Medical Center, Seoul, Korea.)

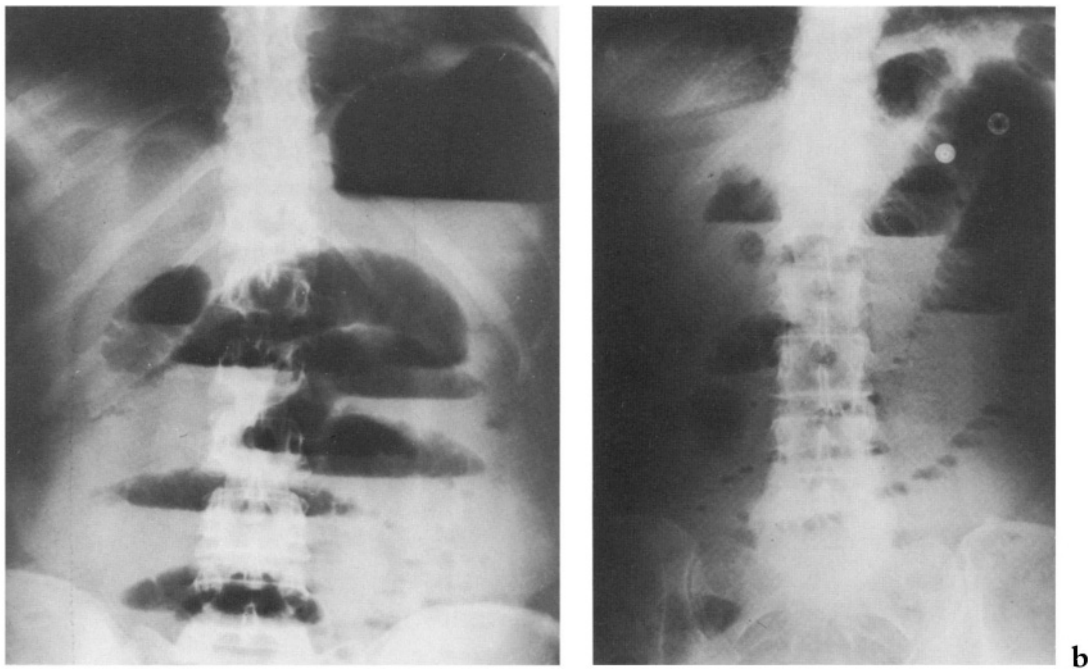


Fig. 14–7. Mechanical small bowel obstruction.
(**a** and **b**) Erect films in two different cases illustrate the "stepladder" arrangement of dilated obstructed loops. This pattern is related to tension anchored on the root of the mesentery.

location is difficult to evaluate during routine contrast studies of the small intestine, chiefly because of the common inaccuracy in tracing the continuity of opacified, superimposed bowel loops.

Identification of Mesenteric and Antimesenteric Borders of Small Bowel Loops

It is necessary to recognize the axis of the root of the mesentery and the undulating, changeable nature of the small bowel loops to understand the basis for the radiologic identification of their mesenteric and antimesenteric borders.[1] Figure 14–9 illustrates certain constant geometric properties of the mesentery. The base of the mesentery, from which the jejunum and ileum are suspended, is essentially a series of alternating convexities and concavities connected by intervening limbs. Any single limb is thus shared by a convexity and a concavity on either side. A limb or straight segment of small bowel, therefore, connects one convex loop with the next concave loop. Any curved line presents basically two surfaces—one convex, the other concave—determined by the point of reference. In the small bowel, the point of reference used is the root of the mesentery. By definition, therefore, the concept of convexity or concavity of bowel loops is determined by the axis of the root of the small bowel mesentery. Figure 14–9, *top* illustrates that limbs *1* and *2* constitute the convex loop *A,* limbs *2* and *3* form the concave loop *B,* and limbs *3* and *4* produce the convex loop *C.*

Another phenomenon of the ruffled nature of the mesentery and small bowel loops results, depending on positional relationships to the mesenteric root. If rotation occurs toward the left (Fig. 14–9, *right*), there is no essential change in the convex–concave relationships of bowel loops. However, if rotation on the mesenteric root occurs toward the right (Fig. 14–9, *left*), there may be a complete reversal of these relationships. Figure 14–9, *left* shows that now loop *A* is concave, *B,* convex; *C,* concave; etc. It must also be recognized that *in vivo* the small bowel loops do not act synchronously in rotating in position on the mesenteric root. One coil may be

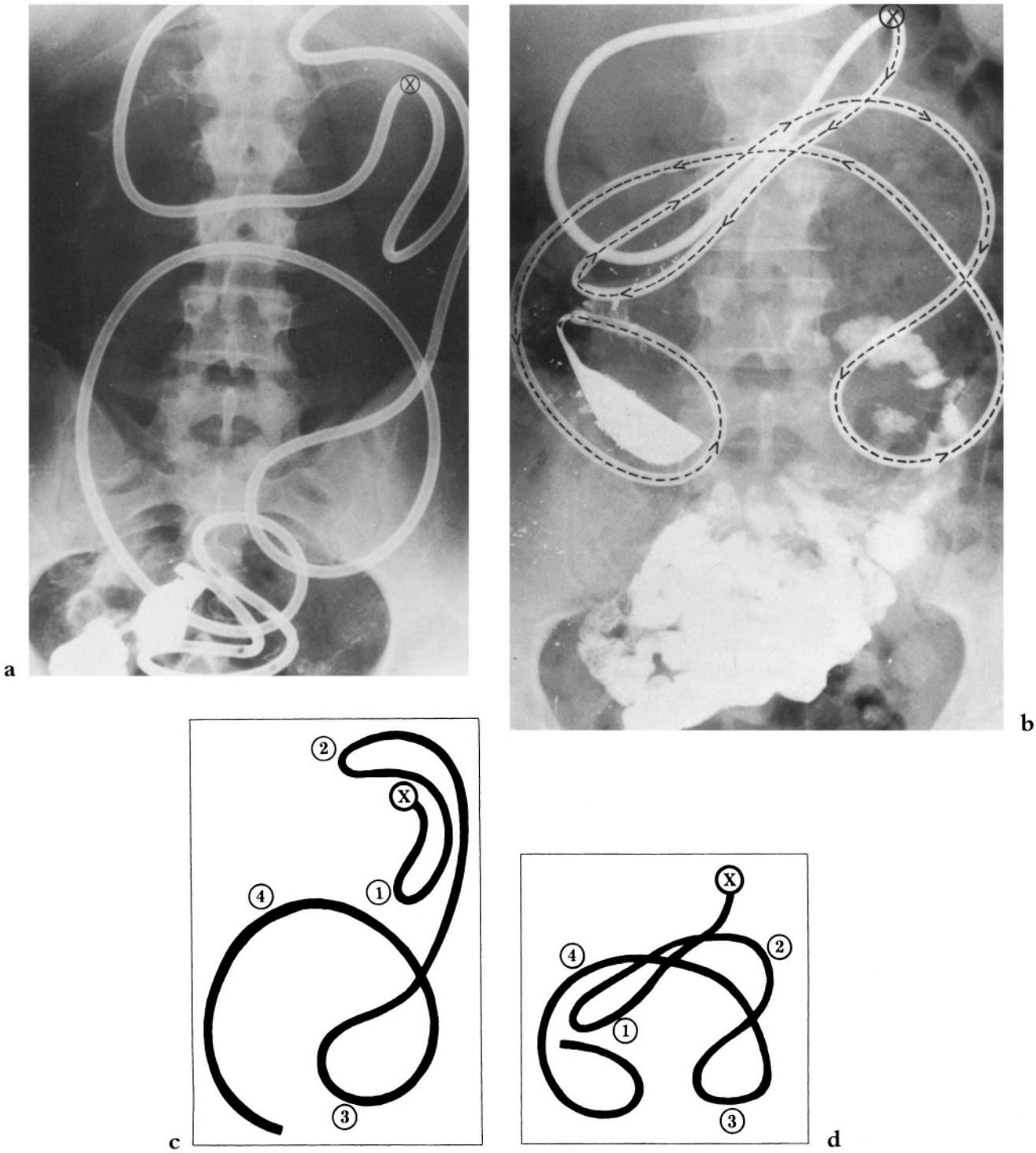


Fig. 14–8. Changeable position of small bowel loops.
(a and **b)** Radiographs of the intubated small intestine 1 day apart, demonstrating striking variations in the positions of the bowel loops. (*X* marks the duodenojejunal junction).
(c and **d)** Tracings illustrate that changes in position and arcing convexities of some bowel segments are more marked than in others.
(Reproduced from Meyers.[1])

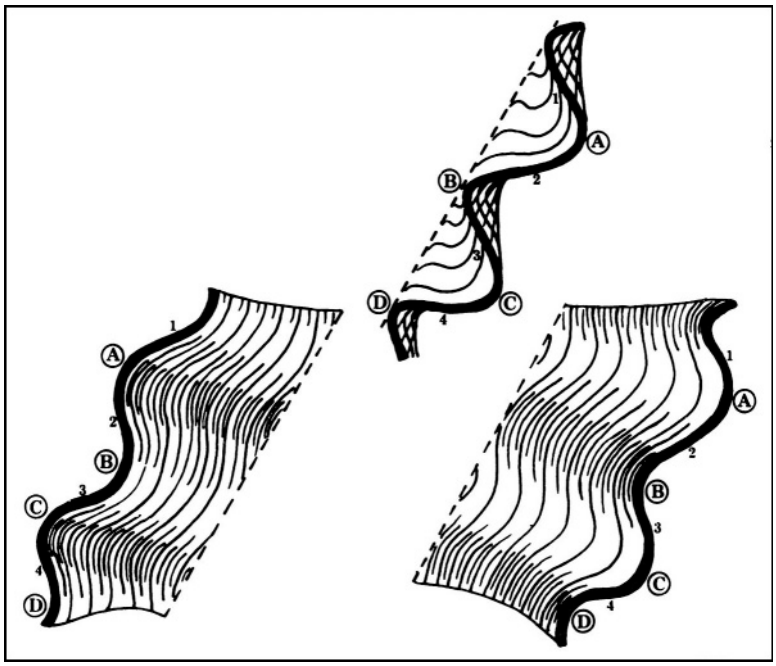


Fig. 14–9. Diagram of the ruffled edge of the mesentery.
This immediately suspends the small bowel loops. *(Top)* Vertical (sagittal). *(Left)* Rotation to the right. *(Right)* Rotation to the left. The *dashed line* indicates the root of the small bowel mesentery.
(Reproduced from Meyers.[1])

horizontal (transverse), the next vertical (sagittal), the next in the coronal plane, and the next obliquely oriented between any of these three planes. The variability is further increased by the fact that these mesenteric projections may extend toward the left or toward the right and may alternate. Position of the patient, peristaltic dynamics, and factors of intraabdominal pressure are likely determinants.

Thus, several conclusions can be derived from these observations that can be accurately applied in the radiologic–anatomic identification of small bowel loops.[1] Figure 14–10 illustrates these:

1. *The concave margin of a small bowel loop, facing toward the axis of the root of the mesentery is the mesenteric border.* This is true whether the loop is positioned to the left or to the right of the mesenteric root. This is shown in segments 1, 2, 5, and 6 in Figure 14–10.

2. *The convex margin of a small bowel loop, facing away from the axis of the root of the mesentery, constitutes the antimesenteric border.* This is also true, of course, whether the loop projects to the left or to the right of the mesenteric root.*

3. *Even if loops are suspended in the midline, their mesenteric and antimesenteric borders can be identified similarly if they project in the coronal plane. This is shown in segment 3* in Figure 14–10.

4. The precise distinction between mesenteric and antimesenteric borders can be routinely applied in a detailed small bowel series (Fig. 14–11). When viewed in a frontal x-ray, a loop projecting in the sagittal or horizontal plane may not present its mesenteric and antimesenteric borders for definition. This occurs most often near the midline overlying the mesenteric root, as shown in segment *4* of Figure 14–10. Pressure films or radiographs with the patient positioned obliquely may render such a loop convex and allow delineation of its mesenteric and antimesenteric borders. Viewed in the axial or sagittal plane, these intestinal borders are easily appreciable on computed tomography or magnetic resonance imaging (Figs. 14–12 and 14–13).

* It can further be appreciated that consequent to the fixation of the mesenteric ruffles, the convex margin of a bowel loop facing toward the axis of the root of the mesentery may at times also constitute the mesenteric border of that particular loop (Fig. 14–1 and loops *A* and *C* in Fig. 14–9b). However, while this may be anatomically true, its radiologic application would be untrustworthy.

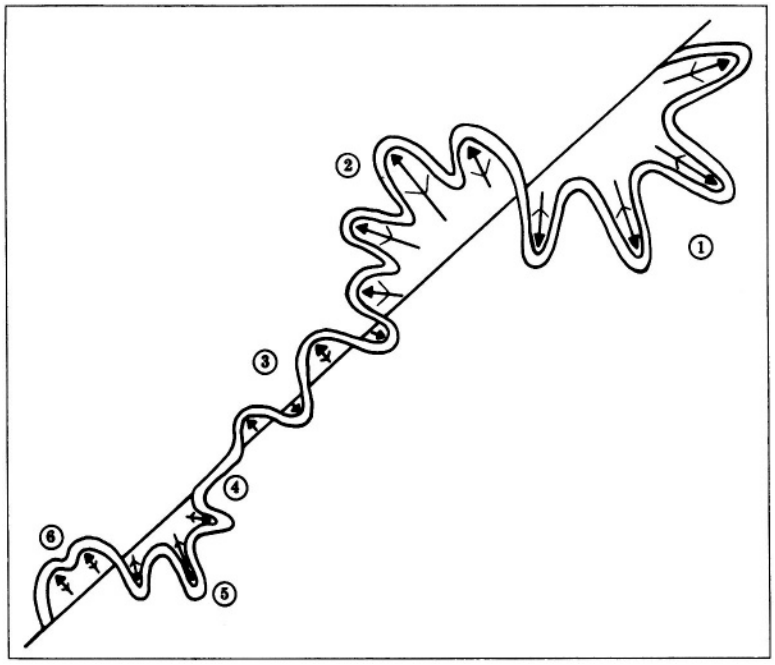


Fig. 14–10. Variable orientations of small bowel loops to mesenteric root.
The mesenteric border *(arrows)* constitutes the concave margin of a loop facing the root. The antimesenteric border is the convex margin of a loop facing away from the root. (Reproduced from Meyers.[1])

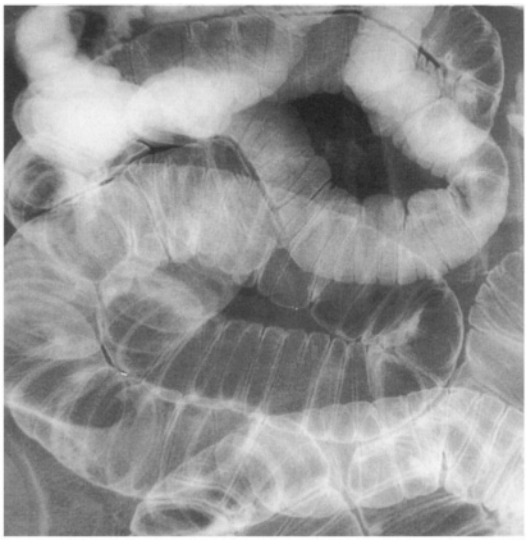


Fig. 14–11. Biphasic enteroclysis study of the small intestine.
Suspended by the fanlike ruffles of the mesentery, the 20–22 ft of small bowel course in an undulating pattern, resulting in the variously termed *coils of bowel* or *intestinal loops.* Each coil or loop presents a concave mesenteric and convex antimesenteric contour. The normal folds are symmetric.

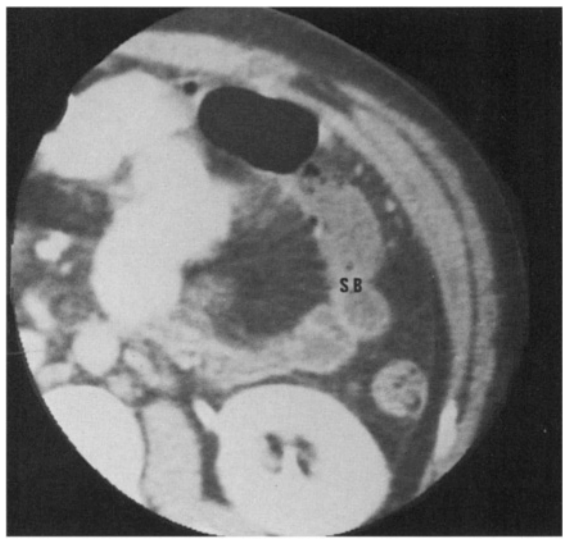
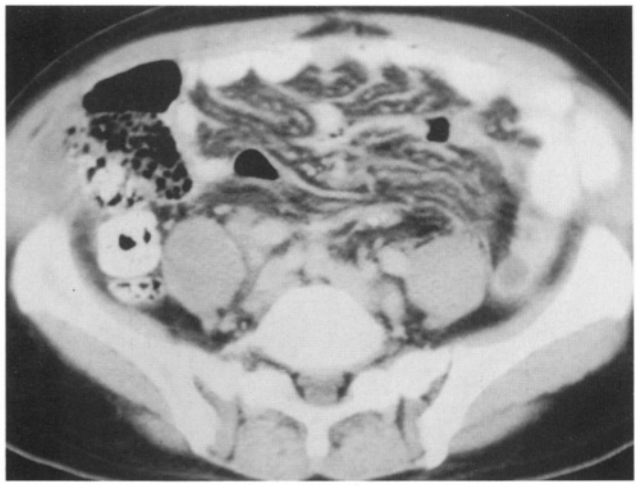
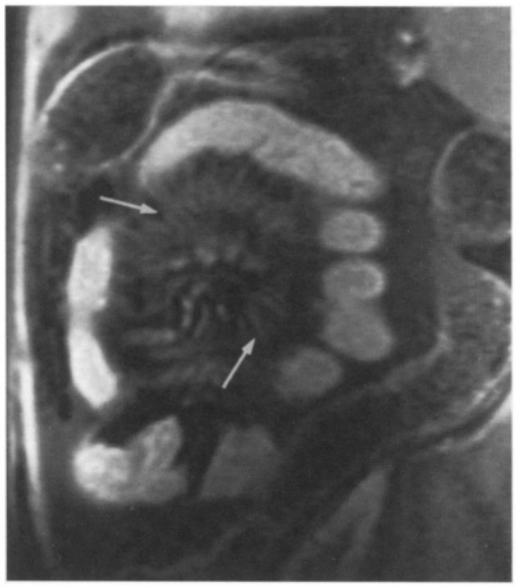


Fig. 14–12. Intestinal borders.
Computed tomography identifies fat-containing leaf of mesentery with vascular branches extending to the concave mesenteric border of small bowel loop *(SB).*



a



b

Fig. 14–13. Intestinal borders.
Two different examples of tuberculous peritonitis illustrate the radiation of thickened vessels coursing through the mesentery to the mesenteric borders of multiple small bowel loops.
(a) Axial CT.
(Courtesy of Emil Balthazar, M.D., Bellevue Hospital, New York University School of Medicine, New York, NY.)
(b) Sagittal T1-weighted fat suppressed MR image. The terminal intestinal branches *(arrows)* fan out to the bowel loops. Ascites is present.
(Reproduced from Semelka RC, Ascher SM, Reinhold C: MRI of the Abdomen and Pelvis. Wiley-Liss, New York, 1997.)

Abnormal Radiologic Features

Many small bowel abnormalities selectively involve either the mesenteric or antimesenteric borders of small intestinal loops solely or predominantly. Precise radiologic distinction between these margins can localize and diagnose a variety of intraabdominal disease states, which otherwise share many common features. Table 14–1 summarizes the characteristic localization of involvement in a variety of conditions. Application of these principles is particularly helpful at any early stage of the lesion or when there may otherwise be an extensive differential diagnosis.

Diverticulosis of the Small Intestine

Acquired diverticula of the small bowel are usually multiple and are practically limited to the upper part of the jejunum.[3] Examination of a specimen (Fig. 14–14a) documents that the diverticula do not arise randomly from the circumference of the small intestine but are strikingly situated at or immediately alongside the mes-

Table 14–1 Pathologic localization

	Sole or predominant border of small bowel involved	
Diseases	Mesenteric	Antimesenteric
Diverticulosis	■	
Meckel's diverticulum		■
Scleroderma		■
Intestinal duplication	■	
Seeded metastases	■	
Hematogenous metastases		■
Carcinoid tumors		
Desmoplastic mesenteric mass	■	
Multiple carcinoids		■
Regional enteritis		
Rigidity, ulcerations, sinus tracts	■	
Pseudosacculations		■
CT comb sign	■	
Lymphoma	■	
Bleeding		
Intramural thumbprints	■	
Postfibrotic pseudodiverticula		■

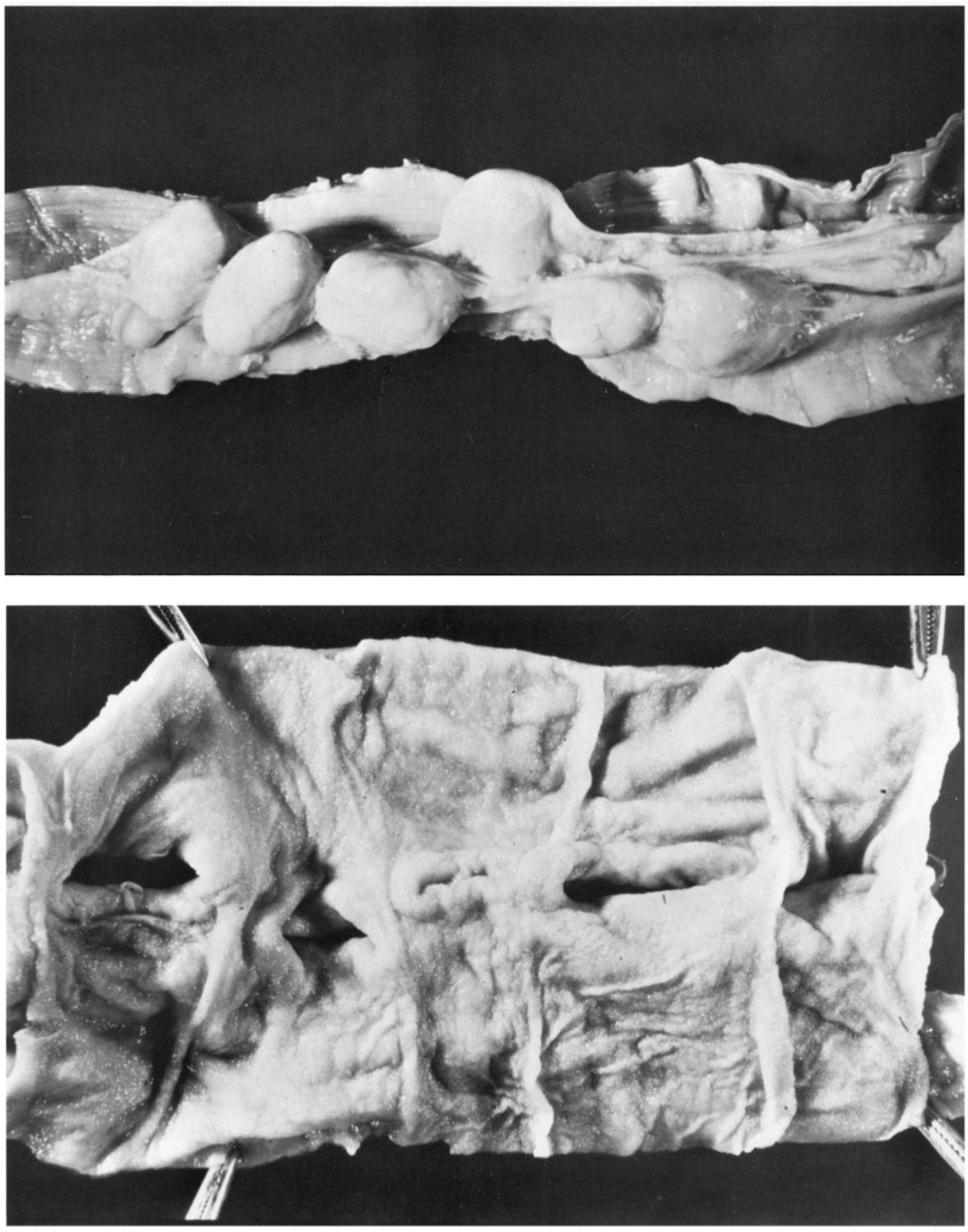


Fig. 14–14. Gross specimen of diverticulosis of the jejunum.
(a) The loop is opened by cutting along the antimesenteric border. The multiple diverticula arise in a row distinctly from the mesenteric borders, invaginating between the leaves of the mesentery.
(b) Viewed from the mucosal aspect, the elliptical orifices extend along the line of attachment of the mesentery.
(Reproduced from Meyers.[2])

enteric border, pushing their way between the leaves of the mesentery. The long axis of their domes, as well as of their elliptical orifices (Fig. 14–14b), tends to parallel the longitudinal axis of the bowel. Such diverticula of the small intestine are of the "pulsion" mucous membrane type. They arise in relation to the sites of penetration of the bowel wall by the vasa recta, which enter on the mesenteric border.[4]

This precise localization of small bowel diverticula to the mesenteric border can be identified radiologically in 75% of cases.[2] The saccules usually are amorphous, without a mucosal pattern, and characteristically extend from the concave (mesenteric) margins of jejunal loops curved away from the axis of the root of the mesentery (Figs. 14–15 and 14–16). Diverticula of the terminal ileum also follow this pattern (Fig. 14–17).

Meckel's Diverticulum

A Meckel's diverticulum represents a remnant of the omphalomesenteric (vitelline) duct.[5,6] This pouchlike persistence had the same anatomic structure as the remainder of the intestine, and thus contains all four histologic layers. Meckel's diverticulum is supplied by the remnants of a nonbranching primitive vitelline artery that arises from an ileal artery[7,8] (Fig. 14–18). It generally follows the "rule of twos": it is present in 2% of people, averages 2 in. in length, and is found in the distal ileum about 2 ft proximal to the ileocecal valve.

The radiologic hallmark of a Meckel's diverticulum[2,9] is thus based on its identification as a saccule extending precisely from the antimesenteric, convex border of a terminal ileal loop (Figs. 14–19 through 14–22), usually in the right lower quadrant. This can be seen in almost two-thirds of instances.[2] Because of the variability in position of small bowel loops, the segment from which a Meckel's diverticulum arises may, at times, project within other areas of the abdomen,[10] but its localization nevertheless to the antimesenteric border can be of great diagnostic value (Fig. 14–23).

Scleroderma

In involvement of the small bowel by scleroderma, muscle atrophy results in atonicity and dilatation. Replacement of the atrophied muscle by collagen occurs in a patchy fashion, with perivascular accumulation in the submucosa. Accordion-pleating of the mucosal folds occurs in the face of luminal dilatation, resulting in a typical "hidebound" appearance.[11] The individual folds are not thickened. At sites without sclerosis, areas of more normal or atrophic bowel may bulge out between the

text continues on page 650

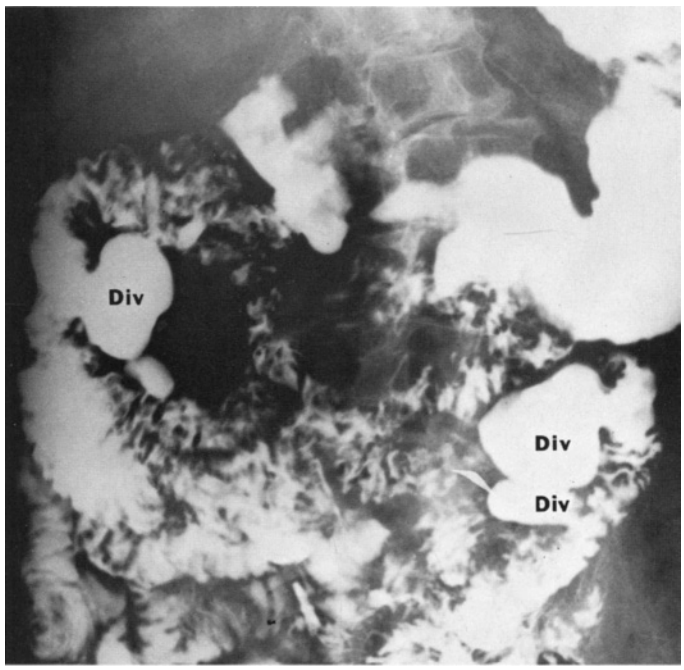


Fig. 14–15. Acquired diverticula of the small intestine. Multiple diverticula *(Div)* project from the mesenteric borders of jejunal loops. (Reproduced from Meyers.[2])

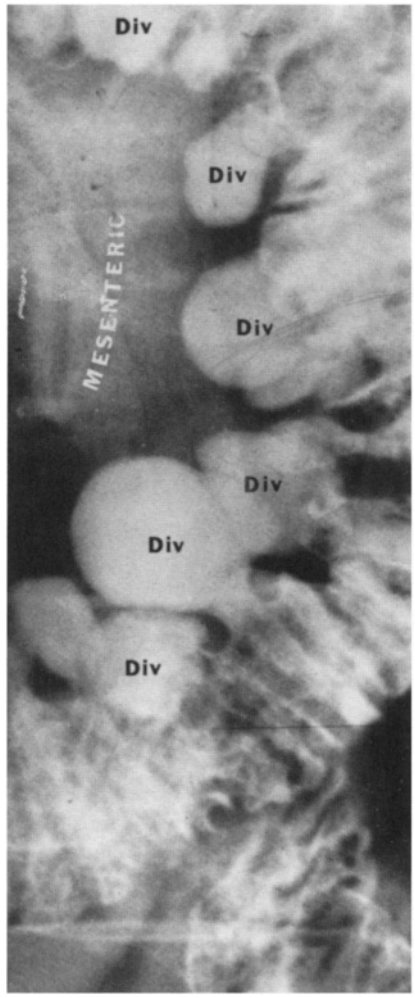


Fig. 14–16. Diverticulosis of the small bowel. Pressure spot film localizes the diverticula *(Div)* as specifically arising from the concave, mesenteric border of a jejunal loop. (Reproduced from Meyers.[2])

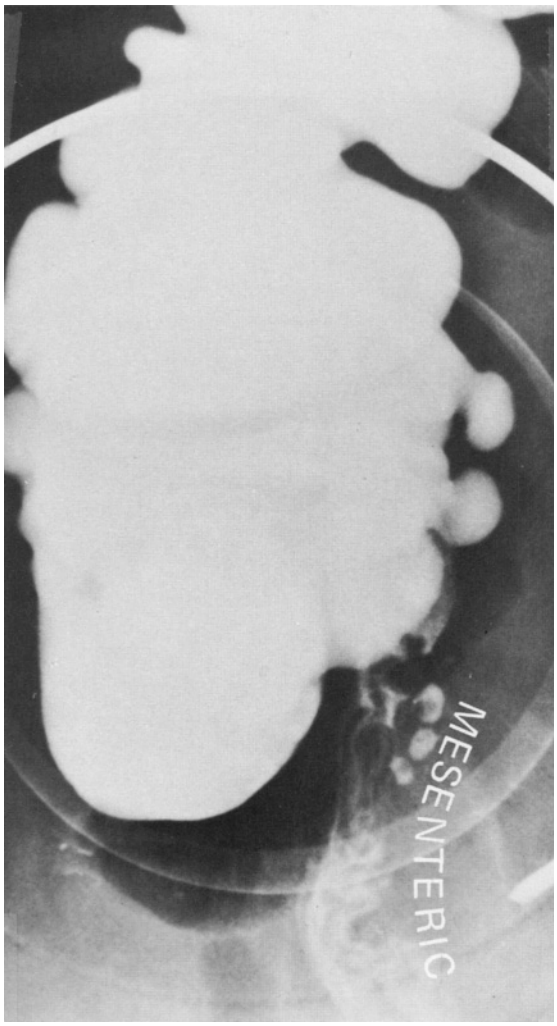


Fig. 14–17. Diverticulosis of the terminal ileum. Pressure spot film shows the diverticula arising from the mesenteric border. A few cecal diverticula are also present.



Fig. 14–18. Vitelline artery supply to Meckel's diverticulum.
Intraoperative selective injection of methylene blue into the vitelline artery stains the artery *(arrows)* and Meckel's diverticulum *(MD)* arising from the antimesenteric border of the ileum. There is no staining of the ileum and mesentery.
(Reproduced from Okazaki et al.[7])

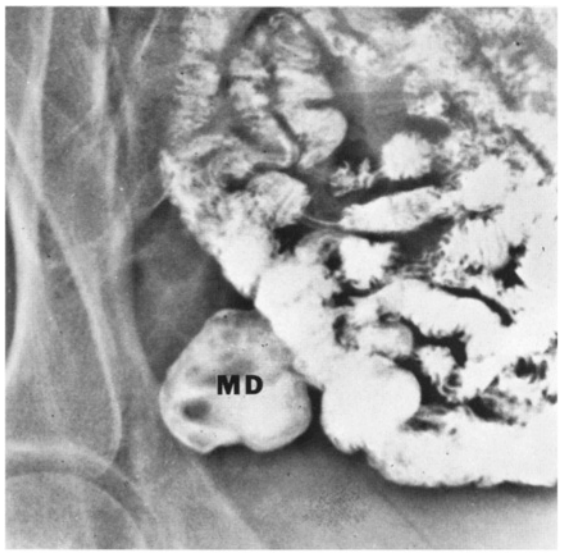


Fig. 14–19. Meckel's diverticulum.
The saccule *(MD)* extends from the antimesenteric convex border of a terminal ileal loop. (The filling defects within it in this instance are secondary to calculus formation.)
(Reproduced from Meyers.[2])

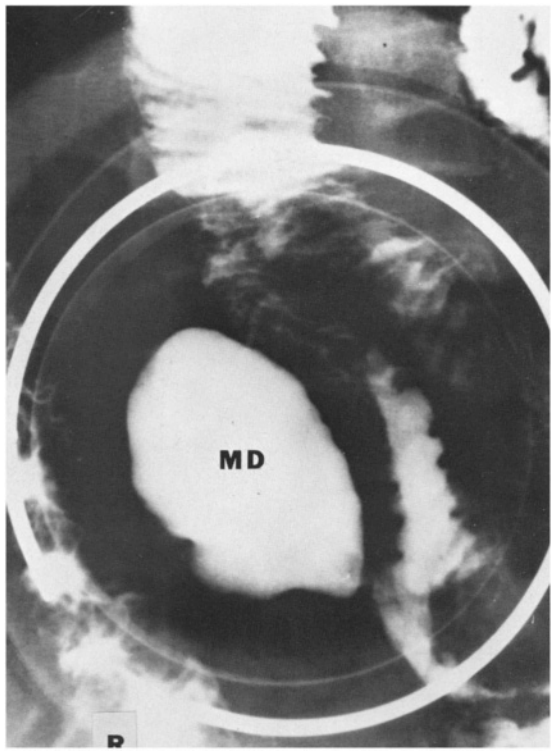


Fig. 14–20. Meckel's diverticulum.
The large saccule *(MD)* extends from the antimesenteric border of a terminal ileal loop, which it indents in the right lower quadrant of the abdomen.
(Reproduced from Meyers.[2])

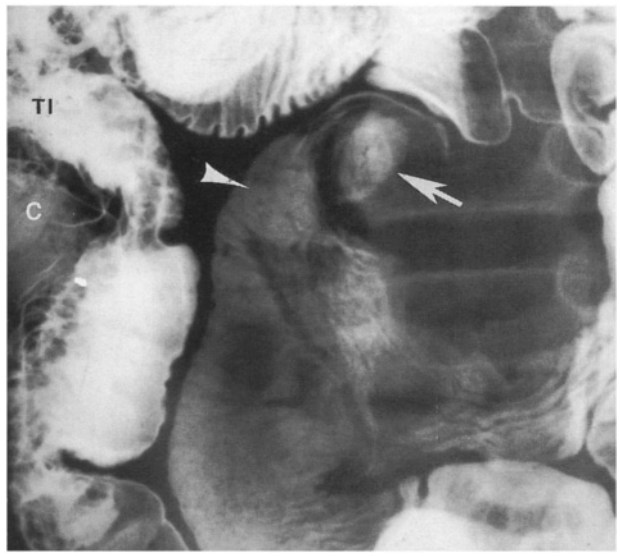


Fig. 14–21. Meckel's diverticulum in an 8-year-old boy with cramping pain and melena.
Enteroclysis demonstrates a large Meckel's diverticulum arising from the antimesenteric border of distal ileum showing typical junctional fold pattern *(arrowhead),* with large ulceration in an area of ectopic gastric mucosa *(arrow).* *TI* = terminal ileum; *C* = cecum.
(Reproduced from Maglinte et al.[9])

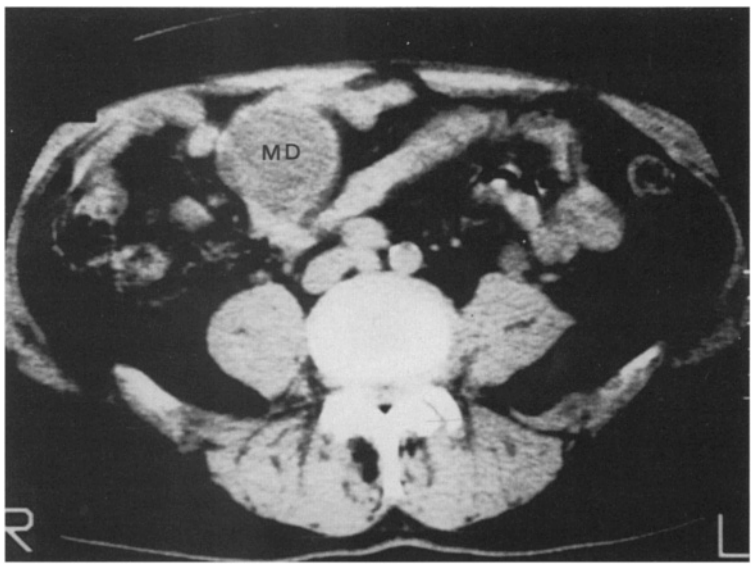


Fig. 14–22. Meckel's diverticulum.
CT demonstrates a 5-cm Meckel's diverticulum *(MD)* attached to the antimesenteric side of the ileum. The fibrous remnant of the vitelline duct extends between the diverticulum and the umbilical region.
(Courtesy of Gary Ghahremani, M.D., Evanston, IL.)

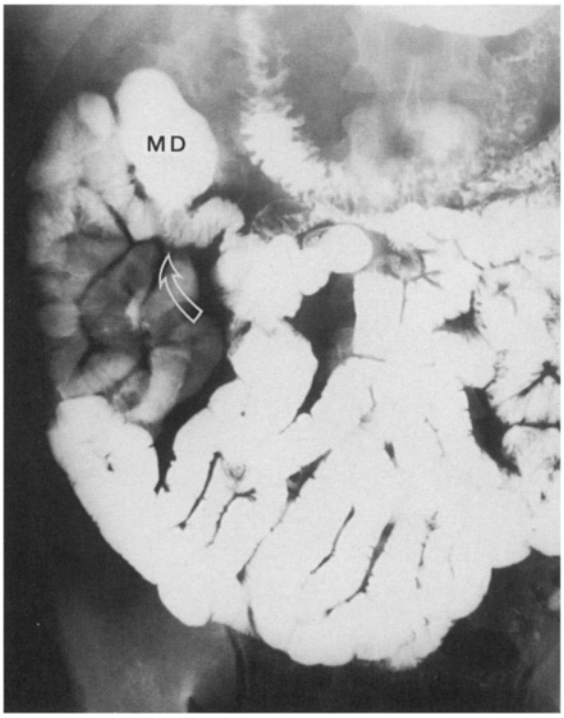


Fig. 14–23. Meckel's diverticulum.
The opacified saccule *(MD)* attached to the antimesenteric border of a midileal loop *(curved arrow)* occupies the subhepatic region in the right upper quadrant.
(Courtesy of Gary Ghahremani, M.D., Evanston, IL.)

tethered sections, producing sacculations or pseudodiverticula[13] (Fig. 14–24). In distinction to true diverticula, these are wide-mouthed and occur on the antimesenteric border. Sacculations are typical of scleroderma, though more commonly seen in the colon than in the small bowel.

Intestinal Duplication

The cystic structure of an intestinal duplication (also called "enteric cyst" or "enterogenous cyst") may, but usually does not, communicate with the adjacent intestinal lumen. The muscular coats of the duplication are intimately adherent to and, at times, are microscopically an integral part of the muscularis of the alimentary tract. Ladd and Gross[14] noted that it arises most often in relationship to the ileum and typically from its mesenteric border. Symptomatology in children includes obstruction, pain, and hemorrhage because of interference with the intestinal blood supply, leading to sloughing of the ileal mucosa. Complete extirpation of the mass along with resection of the adjacent portion of the intestine is thus necessary.

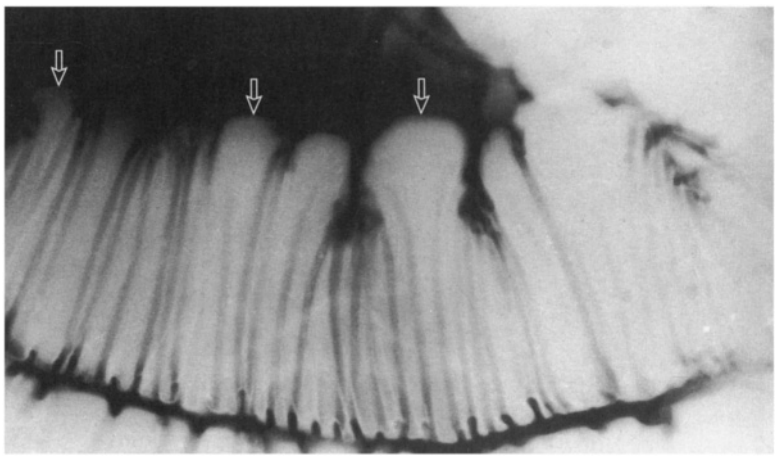


Fig. 14–24. Scleroderma with multiple sacculations.
Small bowel series demonstrates jejunal dilatation, compact apposition of normal-sized folds, and multiple wide-mouthed sacculations arising from the antimesenteric border *(arrows).*
(Reproduced from Herlinger and Maglinte.[12])

With an understanding of the radiologic identification of the mesenteric and antimesenteric borders of small bowel loops, barium contrast studies may be of considerable help in the diagnosis. A noncommunicating intestinal duplication may be revealed as an extrinsic soft-tissue mass displacing an ileal loop upon its mesenteric margin. This precise localization may be seen in 60% of cases.[2] The lumen of a communicating duplication may be opacified to clearly demonstrate it as a tubular or spherical structure, specifically arising in relationship to the mesenteric border (Fig. 14–25).

Seeded Metastases

The distribution of seeded metastases within the abdomen, as discussed in Chapter 4, has been shown to follow the dynamic pathways of the circulation of ascitic fluid.[15–17] The malignant cells are shed by the primary neoplasm and then transported by the ascites. They are then deposited and subsequently grow as seeded metastases at the sites of stasis or pooling of the ascitic fluid. In the midabdomen, pooling occurs within the peritoneal recesses of the mesenteric ruffles.[18] Flow occurs in a series of rivulets or cascades from one mesenteric recess to the next lower, with the largest and most consistent pool formed at the termination of the small bowel mesentery at the ileocolic junction. The seeded metastases lodge and grow, therefore, on the mesenteric borders and involve distal ileal loops in over 40% of all cases.[16]

The distinctive radiologic feature lies in the localization of changes to the mesenteric border of distal ileal loops, evident in over 75% of seeded metastases in the right lower quadrant of the abdomen.[2] Mass changes and associated desmoplastic tethering of mucosal folds constitute the basic characteristics. Figure 14–26 illustrates multiple masses indenting the mesenteric borders of individual distal ileal loops in a case of seeded metastases from carcinoma of the ovary. They are strikingly oriented in relation to the axis of the small bowel mesentery. The associated desmoplastic response, another sign highly distinctive of seeded lesions,[18] results in angulated tethering of the mucosal folds on the mesenteric borders only. Angulation of the loops themselves at the sites of the serosal masses on the mesenteric borders (Fig. 14–27) further indicates the desmoplastic process.

Hematogenous Metastases

The vasa recta of the bowel penetrate the wall on the mesenteric border. They then extend intramurally for variable distances before ramifying toward the antimesenteric border to arborize into the rich submucosal plexus.

The most common hematogenous metastasis to the small bowel clinically encountered is metastatic melanoma.[17] Its dissemination can be observed radiologically to follow, at times, the field of a specific arterial distribution.[17] The embolic metastases typically present as

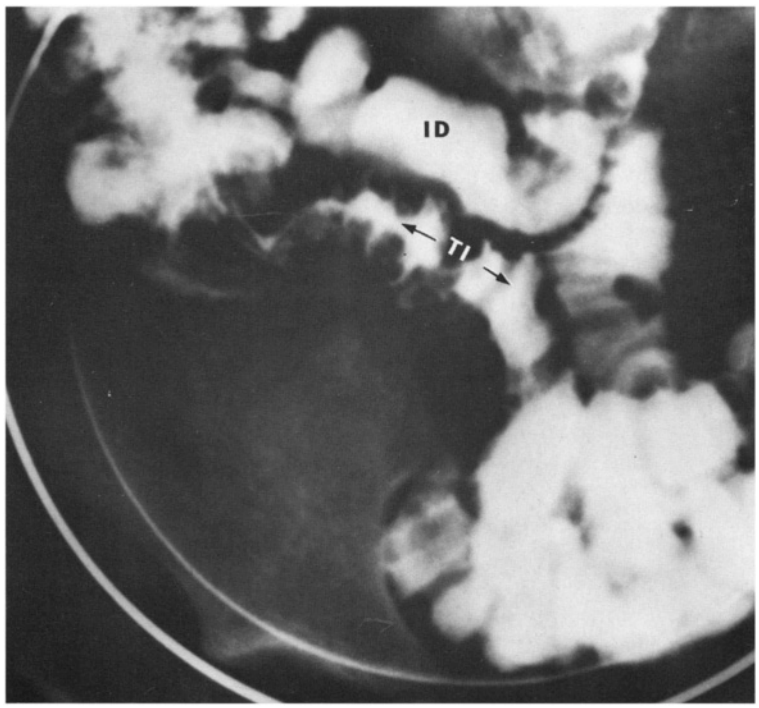


Fig. 14–25. Duplication of terminal ileum.
The intestinal duplication *(ID)* is identified as a tubular structure without a recognizable mucosal pattern, lying along the mesenteric border of the terminal ileum *(TI)* with which it communicates.
(Reproduced from Meyers.[2])

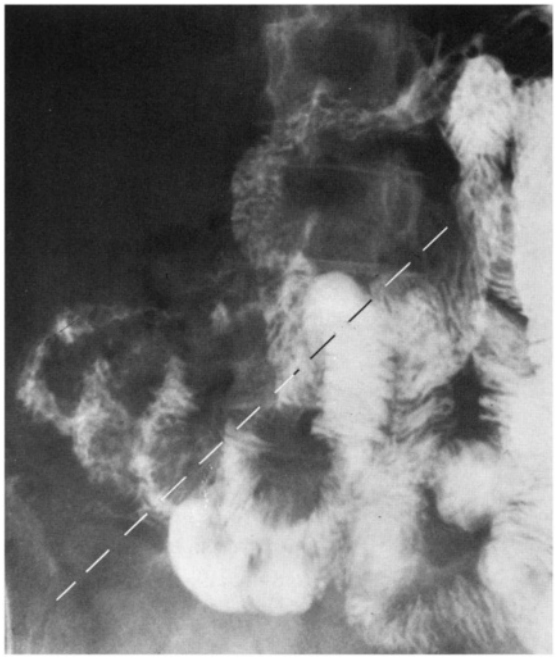


Fig. 14–26. Seeded metastases from ovarian carcinoma.
Multiple masses cause scalloped displacement on the mesenteric borders of ileal loops in the right lower quadrant. Mucosal tethering is also localized to the mesenteric margins.
Note the relationship of these changes to the axis of the small bowel mesentery, indicated by the *line of dashes.*
(Reproduced from Meyers.[2])



Fig. 14–27. Seeded metastases from carcinoma of the ovary.
Multiple serosal masses indent the mesenteric margins of angulated ileal loops in the right lower quadrant. Luminal narrowing and some desmoplastic angulation result in proximal obstruction.
(Reproduced from Meyers.[2])

submucosal filling defects, often with central ulceration ("bull's-eye" lesions), within a single or multiple intestinal loops. However, when visualized on one wall of a bowel loop, they are localized precisely to its antimesenteric border (Fig. 14–28) in 80% of cases.[2] This correlates with experimental studies indicating that strictly mechanical and circulatory factors can account for the distribution of some secondary tumors.[19] The radiologic–anatomic observation presumably reflects lodgment and subsequent growth of embolic malignant cells within the smaller arterial arborizations on the antimesenteric border.

Carcinoid Tumors

Almost 90% of intestinal carcinoids occur in the distal ileum.[20,21] Invasion through the intestinal wall may stimulate an intense desmoplastic reaction in the surrounding submucosa and mesentery. A characteristic manifestation is a mesenteric mass with radiating linear strands[22] (Figs. 14–29 and 14–30).

Ileal carcinoids are multiple in approximately one-third of cases.[20,21,25] Most comprise more than three lesions, while in a small percentage dozens of lesions of variable sizes may stud a discrete segment of the bowel.[20,21] Although they may be separated by several centimeters, skip areas are uncommon. These multiple lesions are considered by Warner et al. to be secondary mucosal deposits rather than independent primaries.[26] Previously viewed as multicentric neoplastic foci, meticulous analysis suggests that the phenomenon reflects mucosal metastases from a dominant parent carcinoid tumor, occurring as a process of retrograde submucosal lymphatic spread. Multiple carcinoid tumors thus show a strong predilection for the antimesenteric border of the small intestine.[26]



Fig. 14–28. Hematogenous metastatic melanoma.
A large submucosal mass with a prominent central ulceration is localized to the convex, antimesenteric margin of a distal jejunal loop.
(Reproduced from Meyers.[2])



Fig. 14–29. Carcinoid of the ileum.
CT demonstrates a round 2-cm mesenteric mass with stellate radiation of fibers toward the adjacent mesentery and borders of loops. The wall of the involved loop is thickened and angulated. The mass shows a discrete central calcification, and a small lymph node is present in the adjacent tissue.
(Reproduced from Maccionni et al.[23])

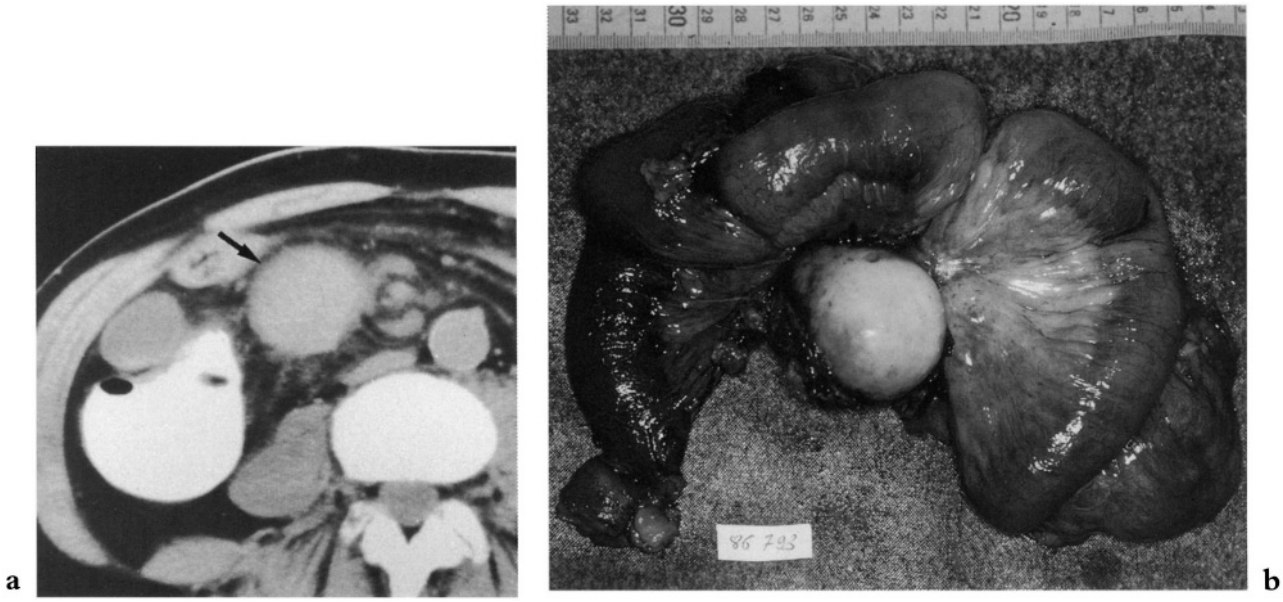


Fig. 14–30. Carcinoid of the ileum.
(a) CT shows a mesenteric mass *(arrow)* with emanating strands corresponding to thickened neurovascular bundles.
(b) Corresponding gross specimen after surgical resection confirms the mesenteric location of the tumor.
(Reproduced from Pelage et al.[24])

Regional Enteritis

The general radiologic findings of regional enteritis correlate closely with the gross pathologic features. The involved bowel, often affected by "skip lesions," is sharply delimited from contiguous gut and has a narrowed lumen, which is sometimes strictured. The bowel wall is rigid and thick, the mesentery is often markedly thickened and edematous, and the mesenteric lymph nodes are enlarged. The swollen, inflamed mucosa develops a cobblestone appearance as longitudinal and transverse ulcers intersect. As these extend deeply through the wall, sinus tracts and fistulas may be present.

Other specific, more localized changes of regional enteritis have been observed surgically and pathologically. In their pioneering report in 1932, Crohn, Ginzburg, and Oppenheimer noted on opening the intestine that a series of small linear ulcerations lying in a groove on the mesenteric side of the intestine is almost always present.[27] It has also been observed that there is a close relationship between the destructive changes in the mucosa and the extent of increased mesenteric fat.[28] The development of pseudodiverticula, furthermore, is probably related to eccentric skip areas.[28]

I have directly applied these discrete pathologic observations in regional enteritis to the radiologic alterations for a more definite diagnosis.[1,2,29] The process may be identified, particularly in its early stages, as localized predominantly to the mesenteric borders of involved loops. Mesenteric border ulcers are a virtually pathognomonic finding in approximately 30% of patients with Crohn's disease.[29] The findings of mucosal irregularities, ulcerations, fixation and rigidity, sinus tracts, and extrinsic mass tumefaction may be confined or most evident on the concave margins (Figs. 14–31 through 14–35). The linear ulcer along the concave border may extend over a few or many centimeters and can be continuous or interrupted. It may be accentuated by a thin line of radiolucency, which reflects inflammatory reaction and fibrosis underneath the ulcer.[29] The fact that the antimesenteric wall may not be symmetrically involved at the same time but, rather, retains some degree of pliability may be revealed by the development of pseudosacculations from the convex border.

In severely involved loops, the segmental, skip nature of the lesions may result in pseudosaccular outpouchings from both the mesenteric and antimesenteric borders.

It follows that pseudosacculations or the appearance

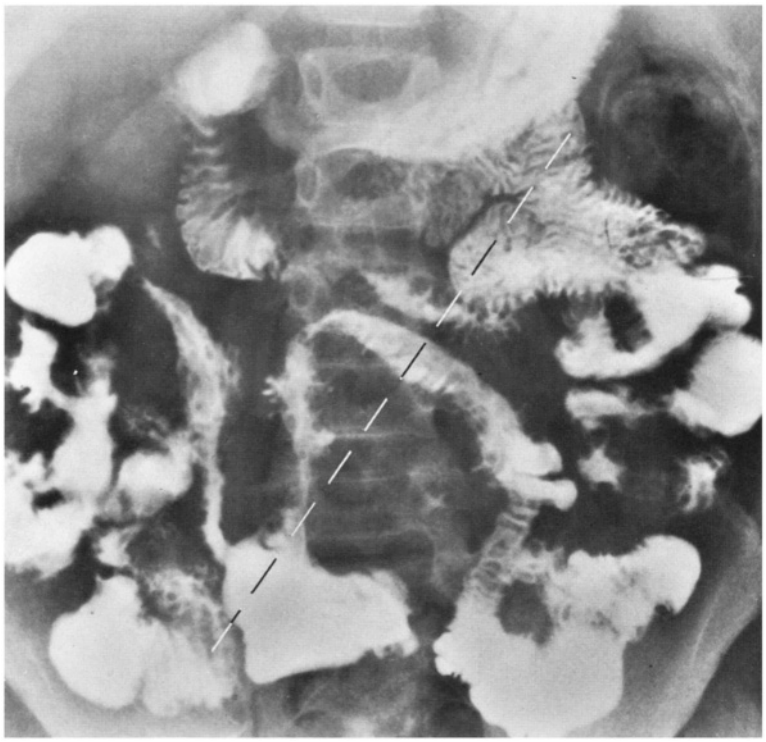


Fig. 14–31. Regional enteritis.
Diffuse involvement of ileum. One loop demonstrates ulcerations and small sinus tracts along the concave, mesenteric border at the site of mesenteric tumefaction.
Pseudosacculations on the convex margin of the loop indicate that the antimesenteric border retains some pliability.
The *dashed line* indicates the axis of the root of the mesentery.
(Reproduced from Meyers.[2])

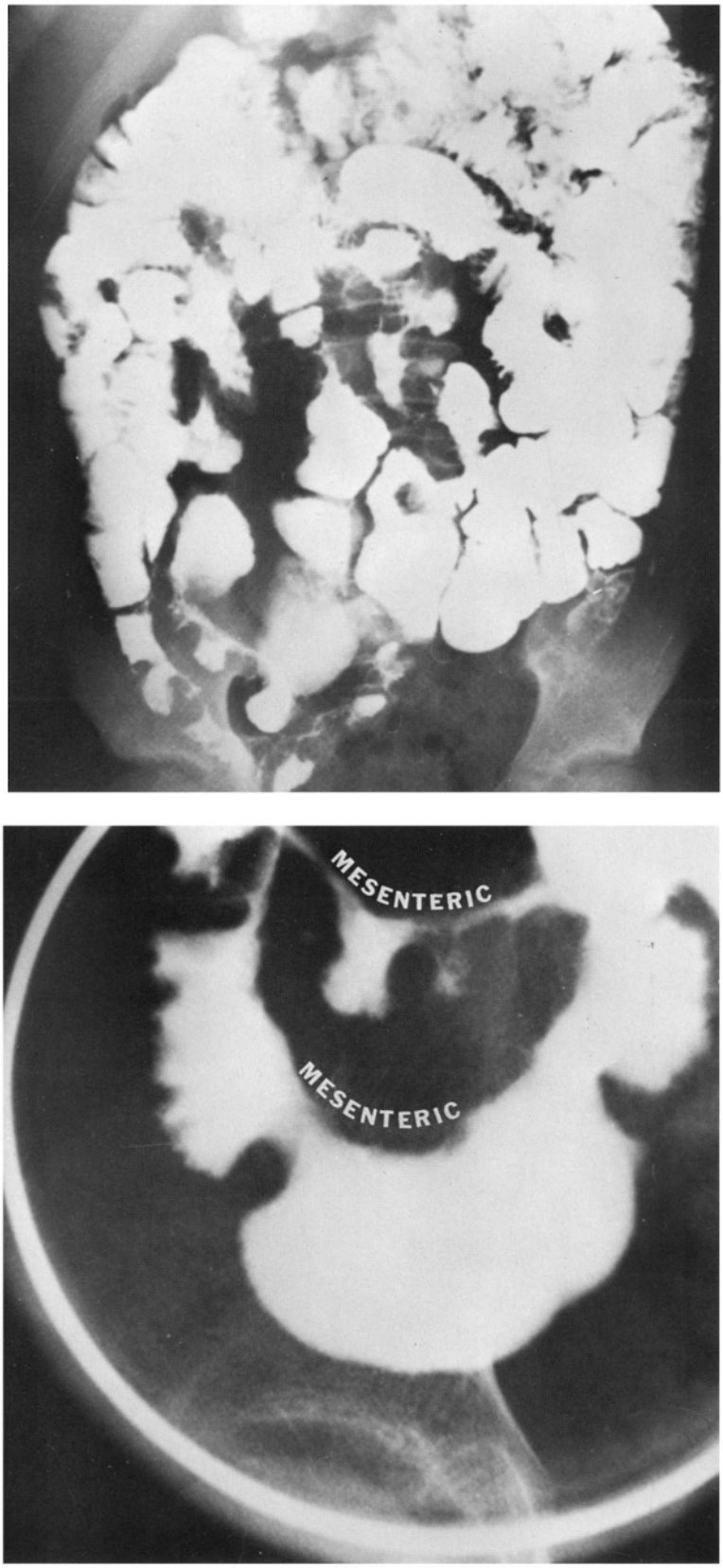


Fig. 14–32. Regional enteritis in an 11-year-old male.
Small bowel series **(a)** with pressure spot film of distal ileum **(b)** show rigidity from the ulcerative process clearly limited to the mesenteric borders and pseudosaccular outpouchings from the more pliable antimesenteric margins.
(Reproduced from Meyers.[2])

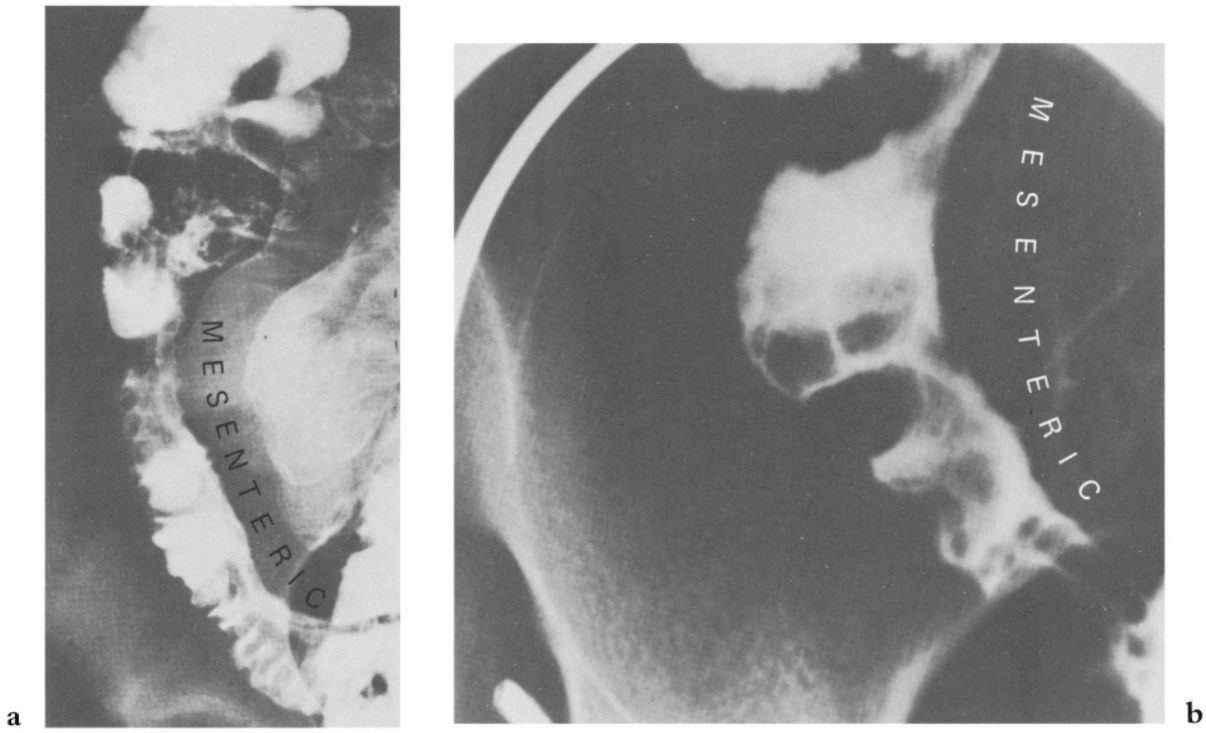


Fig. 14–33. Regional enteritis in two different cases.
(a and **b)** Flattening and rigidity are conspicuously localized to the mesenteric border of the terminal ileum. The antimesenteric border retains some pliability as shown by pseudosaccular outpouchings.

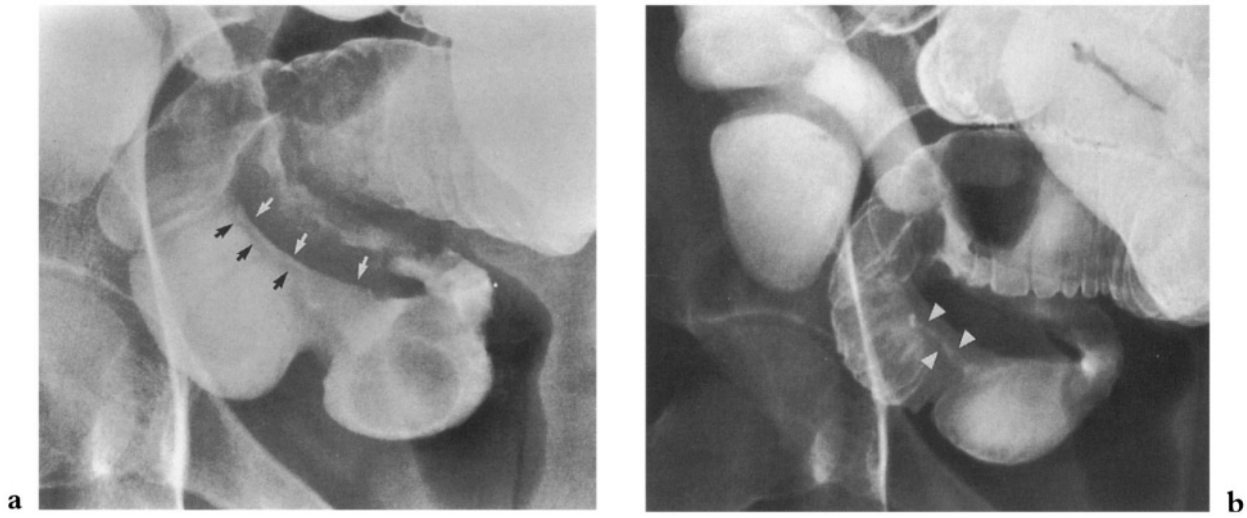


Fig. 14–34. Regional enteritis.
(a) A linear ulcer *(white arrows)* can be clearly identified on the rigid mesenteric border of a diseased ileal loop. It is accentuated by a thin radiolucent line *(black arrows)* that reflects underlying inflammatory reaction and fibrosis. Pseudosacculations bulge from the antimesenteric border. The distal ileum is narrowed with the diffuse ulceronodular form of Crohn's disease.
(b) On another view, the linear ulcer *(arrowheads)* is seen *en face.*
(Courtesy of Dean Maglinte, M.D., Indianapolis, IN.)

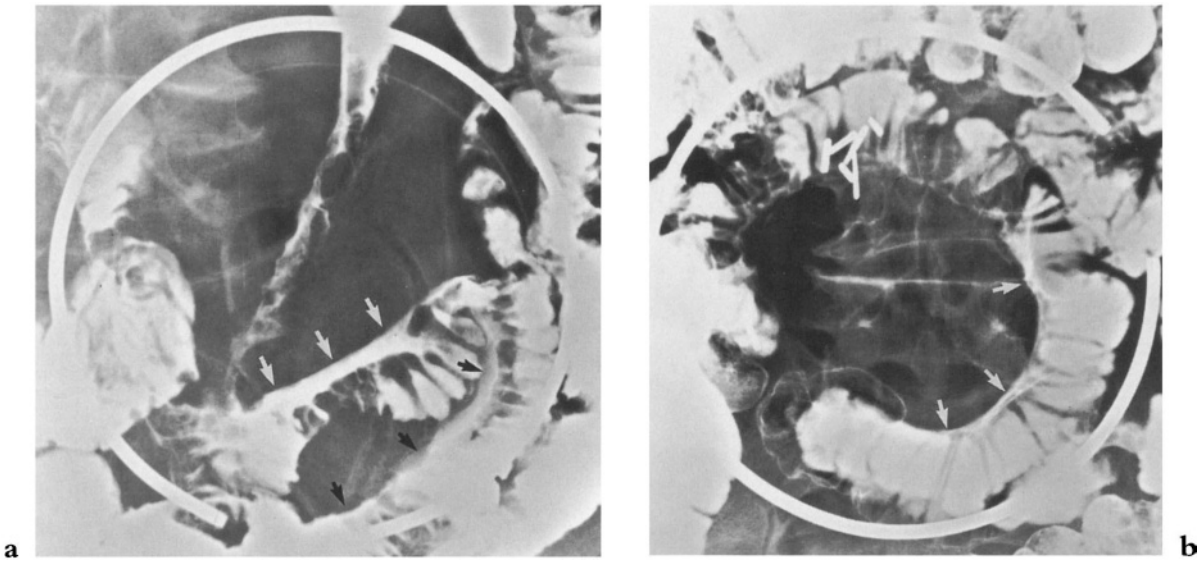


Fig. 14–35. Regional enteritis, with postsurgical recurrence.
(a) Striking linear ulcers on mesenteric borders *(white arrows* and *black arrows)* with pleated pseudosacculations on antimesenteric border.
(b) Nine years later, after surgical resection, there is evident recurrence. Hallmarks again include mesenteric linear ulceration *(arrows)* and antimesenteric outpouchings.

of diverticula limited solely to the mesenteric borders are not a feature of regional enteritis.

Another sign highly characteristic of Crohn's disease is also based on discrete radiologic–pathologic correlation. Contrast-enhanced spiral CT scans often show vascular changes in the mesentery, manifested as dilatation, tortuosity, and wide spacing of the vasa recta as they approach the mesenteric border of involved ileum. I have termed these distinctive changes the *comb sign* or *vascular jejunization of the ileum*[30] (Fig. 14–36). Normally, the distal arterial arcades in the mesentery of the ileum are multitiered, so that the vasa recta that arise from the furthest arcade are numerous, short, and closely spaced. This arterial architecture is in contrast to the jejunum, where the vasa recta are longer and more widely spaced from each other. Increased mesenteric fat, termed fibrofatty proliferation of the mesentery, accompanies transmural involvement of the bowel by Crohn's disease. The markedly dilated vessels pass through the hypertrophied mesenteric and subserosal fat in which perivascular fibrosis develops[31] (Fig. 14–37). The prominent vasa recta are seen by CT as elongated, widely spaced vessels. Identification of such hypervascularity indicates active disease and is useful in differentiating regional enteritis from lymphoma or metastases, which tend to be hypovascular lesions.[30]

Lymphoma

Within the small bowel, malignant lymphoma involves the distal ileum most often (Fig. 14–38). Growth may be predominantly away from the intestinal lumen, in an exoenteric fashion. Mass extension into the mesentery may produce extrinsic compression of the bowel lumen. This form of the disease and primary mesenteric lymphoma are characterized radiologically by the presence of mesenteric masses extrinsically compressing and distorting the concave borders of small bowel loops (Fig. 14–39).

Intramural and Mesenteric Bleeding

Bleeding into the wall of the small intestine and into the mesentery may be a consequence of many different disorders. It is seen in mesenteric thromboses and emboli, segmental ischemic disease, abdominal trauma, anticoagulation medication, underlying diseases associated with

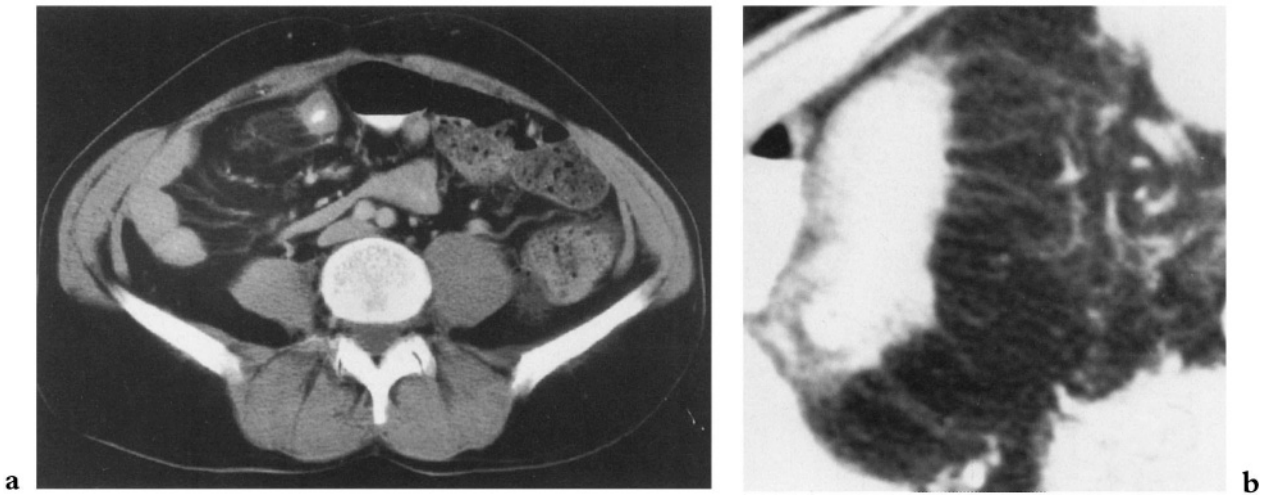


Fig. 14–36. CT comb sign of Crohn's disease in two cases.
(a) Spiral CT demonstrates a distal ileal loop with mural thickening, including a curvilinear zone of fluid. Increased mesenteric fat is present in the right lower quadrant, within which enhanced vessels show dilatation and tortuosity. The vasa recta approaching the mesenteric side of the diseased loop are pushed apart by the fatty proliferation, resulting in the *comb sign.*
(b) In another patient, an enlarged view demonstrates the conspicuous features of the *comb sign.*

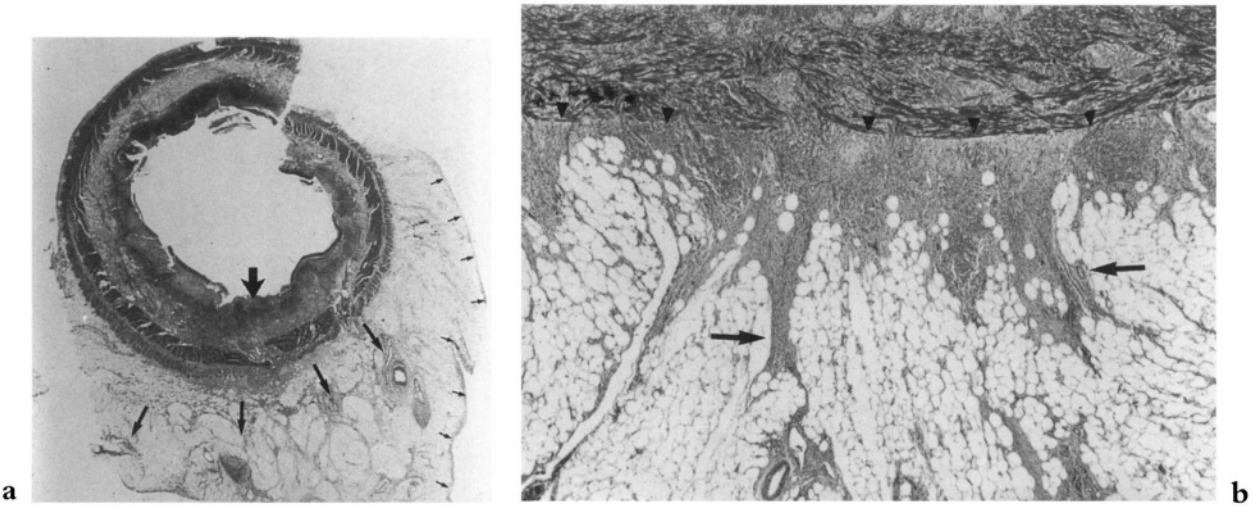


Fig. 14–37. Crohn's disease with fibrofatty proliferation and hypervascularity of the mesentery.
(a) Low magnification of cross-sectioned ileum with transmural Crohn's disease and mesenteric border ulceration *(thick arrow).* The serosa *(small arrows)* is displaced from the muscularis propria by an increased accumulation of fat. Transmural fibroinflammatory changes involve vessels and extend into the fat *(medium arrows).*
(b) Chronic inflammation with subsequent fibrosis extends in a fanlike perivascular pattern *(arrows)* into the mesenteric fat from the edge of the muscularis propria *(arrowheads).* (Trichrome stain, × 12.)
(Reproduced from Herlinger et al.[31])

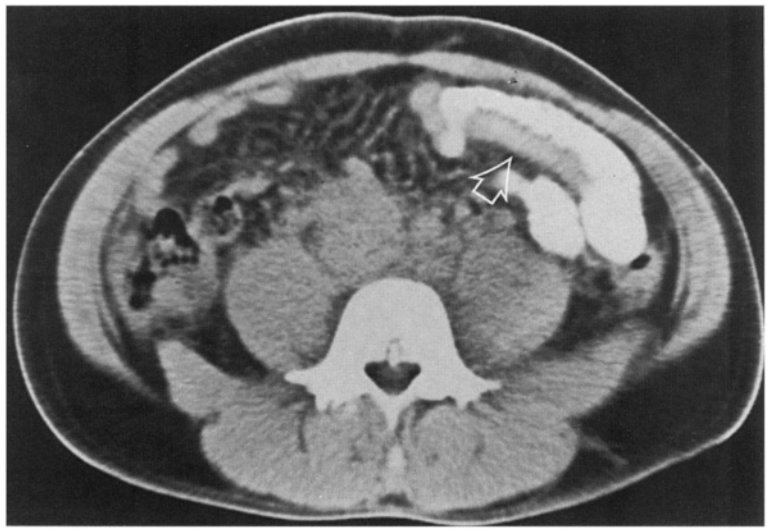


Fig. 14–38. Hodgkin's lymphoma.
CT demonstrates mural thickening of an opacified ileal loop in the left lower quadrant strikingly limited to its mesenteric border *(arrow).* This is accompanied by retroperitoneal adenopathy and stellate infiltration of the mesentery.



Fig. 14–39. Lymphosarcoma.
The process is revealed as masses discretely separating and pressing on the concave mesenteric borders of distal ileal loops in the right lower quadrant.
(Reproduced from Meyers.[2])

coagulation defects (hemophilia, leukemia, multiple myeloma, lymphoma, and metastatic carcinoma), and the vasculitis of collagen diseases (polyarteritis nodosa, systemic lupus erythematosus), thromboangiitis obliterans (Buerger's disease), and the Henoch-Schönlein syndrome.

While diffuse intramural fluid results in a compact appearance of prominent mucosal folds, sometimes described as the "stacked-coin" or "picket-fence" arrangement, coalescence of the submucosal edema and hemorrhage produces the characteristic scalloped or nodular filling defects along the contours of the bowel referred to as "thumbprinting."

These distinctive thumbprint defects in intramural intestinal bleeding are by far most consistently localized to the mesenteric borders of the loops (Figs. 14–40 through 14–42). In advanced cases, the defects may

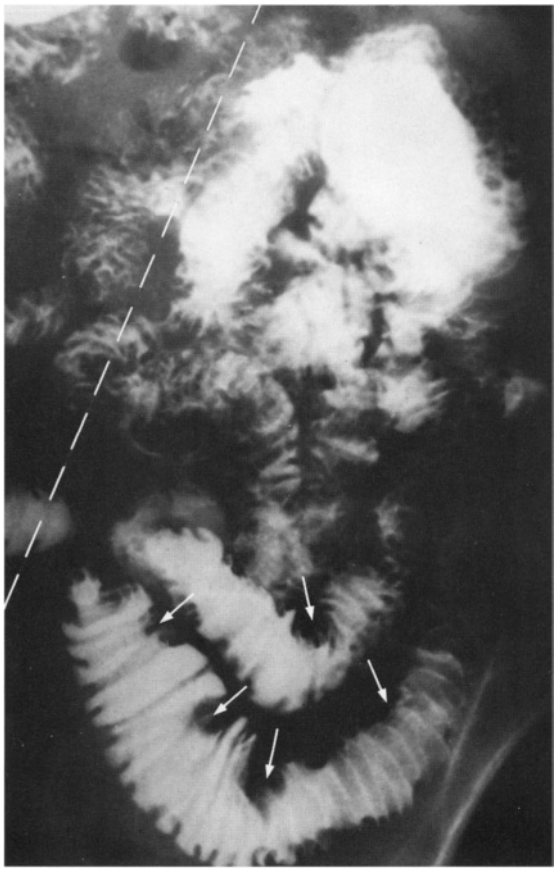


Fig. 14–40. Intramural bleeding, secondary to overanticoagulation.
Rectal bleeding in a 56-year-old male on anticoagulants while recovering from a myocardial infarction prompted this small intestinal series. Note that the thumbprint defects *(arrows)* of coalescent intramural blood are localized specifically to the concave, mesenteric borders. (The *dashed line* indicates the mesenteric root.) Diffuse submucosal fluid is also present.
(Reproduced from Meyers.[2])

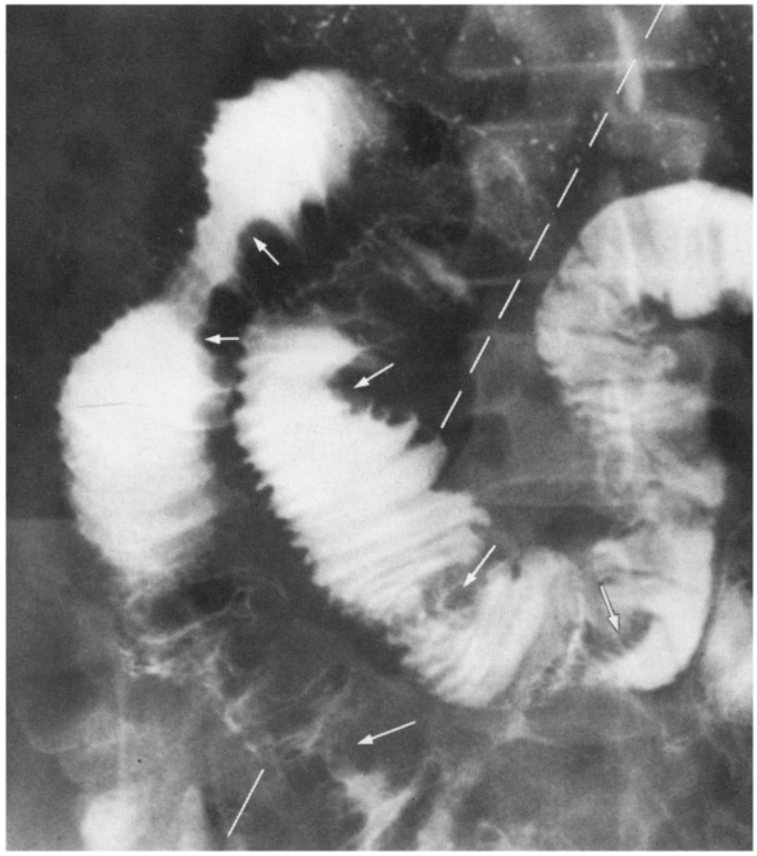


Fig. 14–41. Intramural bleeding in a heroin addict.
The thumbprint filling defects *(arrows)* of intramural bleeding are confined to the concave mesenteric borders. The *dashed line* indicates the axis of the root of the mesentery. Intramural fluid is also evident.
(Reproduced from Meyers.[2])

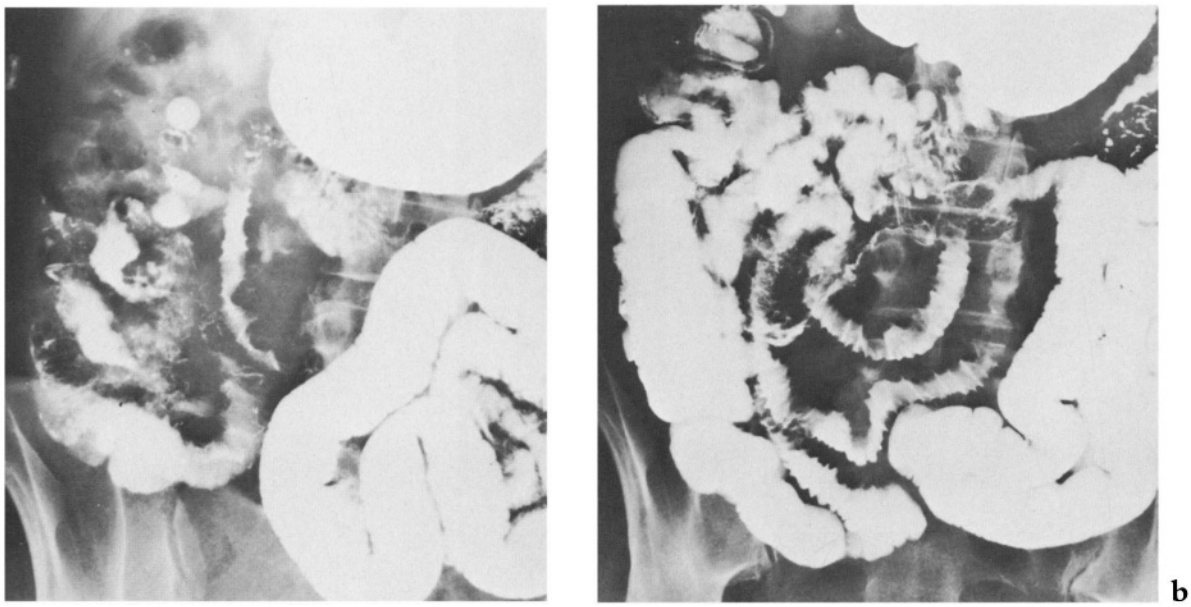


Fig. 14–42. Ischemic enteritis.
(a and **b)** Small bowel series (45 min and 2 hr, respectively) in a female taking oral contraceptive pills show the features of ischemic enteritis involving several ileal loops, with the changes most prominent on their mesenteric borders.

randomly involve both margins of the involved loops, but in early or limited stages, the nodular masses are clearly localized to the concave borders in 75% of patients.[2] These defects are typically superimposed on a pattern indicating diffuse intramural fluid. If fibrosis progresses, the antimesenteric border then forms multiple sacculations or pseudodiverticula. Severe involvement may result in a concentric stricture.

Mesenteric bleeding exaggerates and tends to fix the coiled nature of the small intestine. It is further revealed by mass separation and extrinsic compression on the mesenteric borders of the loops (Fig. 14–43).

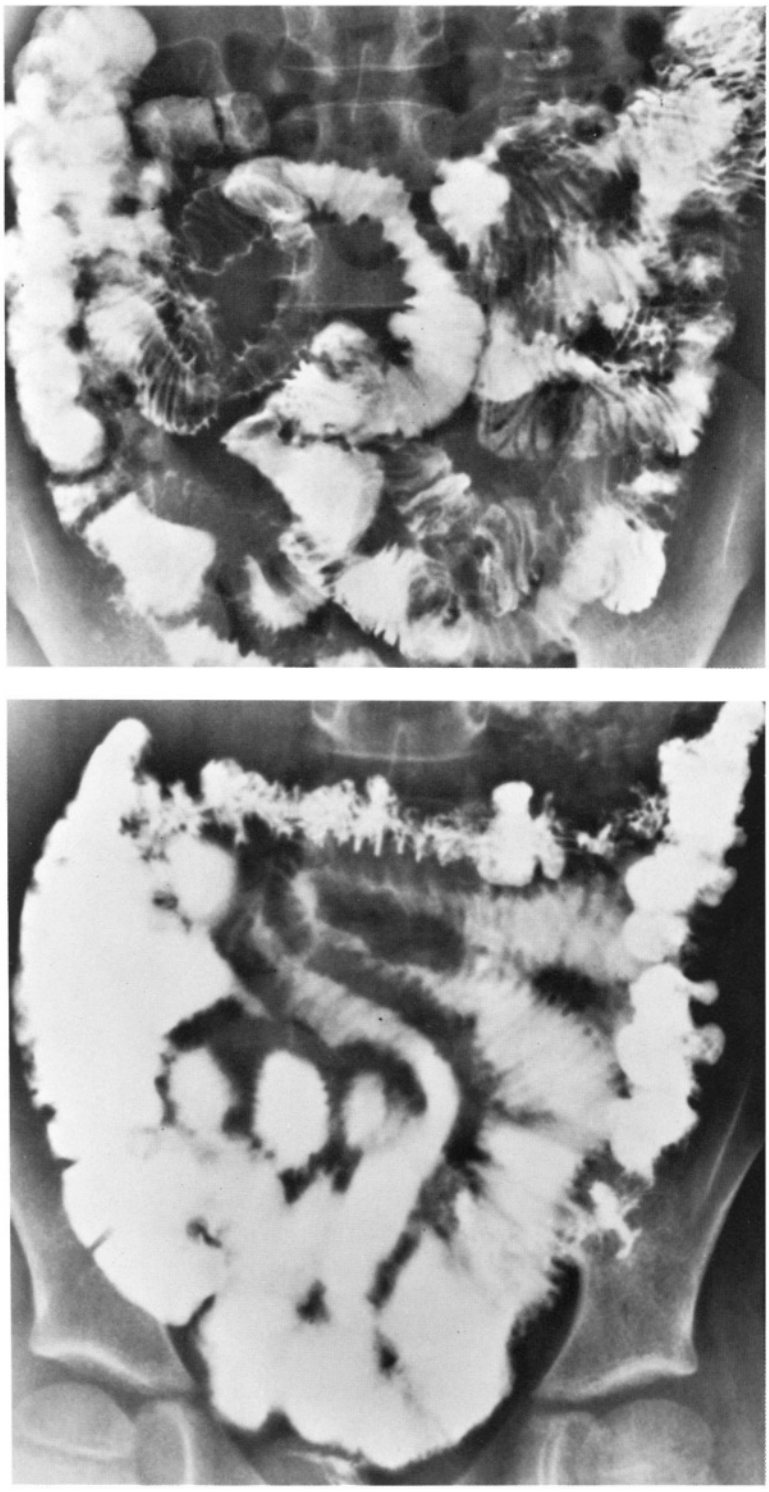


Fig. 14–43. (a and b) Two different cases of mesenteric bleeding secondary to Henoch-Schönlein purpura.
Bleeding into the mesentery has resulted in mass separation and displacement upon the concave, mesenteric borders of small bowel loops.
Accompanying intramural fluid is also evident.
(Reproduced from Meyers.[2])

References

1. Meyers MA: Clinical involvement of mesenteric and antimesenteric borders of small bowel loops. I. Normal pattern and relationships. Gastrointest Radiol 1976; 1:41–48.
2. Meyers MA: Clinical involvement of mesenteric and antimesenteric borders of small bowel loops. II. Radiologic interpretation of pathological alterations. Gastrointest Radiol 1976; 1:49–58.
3. Maglinte DDT, Chernish SM, DeWeese R, et al: Acquired jejunoileal diverticular disease: Subject review. Radiology 1986; 158:577–580.
4. Edwards HC: Diverticulosis of the small intestine. Ann Surg 1936; 103:230–254.
5. Meckel JF: Ueber die divertikel am darmkanal. Arch die Physiol 1809; 9:421–453.
6. Rossi P, Gourtsoyiannis N, Bezzi M, et al: Meckel's diverticulum: Imaging diagnosis. AJR 1996; 166: 567–573.
7. Okazaki M, Higashihara H, Saida Y, et al: Angiographic findings of Meckel's diverticulum: The characteristic angiographic appearance of the vitelline artery. Abdom Imaging 1993; 18:15–19.
8. Mitchell AWM, Spencer J, Allison DJ: Meckel's diverticulum: Angiographic findings in 16 patients. AJR 1998; 170:1329–1333.
9. Maglinte DDT, Elmore MF, Isenberg M, et al: Meckel diverticulum: Radiologic demonstration by enteroclysis. AJR 1980; 134:925–932.
10. Ghahremani GG: Radiology of Meckel's diverticulum. Crit Rev Diagn Imaging 1986; 26(1):1–43.
11. Horowitz A, Meyers M: The "hide bound" small bowel of scleroderma: Characteristic mucosal fold pattern. AJR 1973; 119:332–334.
12. Herlinger H, Maglinte D: Clinical Radiology of the Small Intestine. WB Saunders, Philadelphia, 1989, p 591.
13. Queloz JM, Woloshin HJ: Sacculation of the small intestine in scleroderma. Radiology 1972; 105:513–515.
14. Ladd WE, Gross RE: Surgical treatment of duplications of the alimentary tract: Enterogenous cysts, enteric cysts, or ileum duplex. Surg Gynecol Obstet 1940; 70:295–307.
15. Meyers MA: The spread and localization of acute intraperitoneal effusions. Radiology 1970; 95:547–554.
16. Meyers MA: Distribution of intra-abdominal malignant seeding: Dependency on dynamics of flow of ascitic fluid. AJR Rad Ther Nucl Med 1973; 119:198–206.
17. Meyers MA, McSweeney J: Secondary neoplasms of the bowel. Radiology 1972; 105:1–11.
18. Meyers MA: Malignant seeding along small bowel mesentery: Roentgen features. AJR Rad Ther Nucl Med 1975; 123:67–73.
19. Coman DR, deLong RP, McCutcheon M: Studies on the mechanisms of metastasis. The distribution of tumors in various organs in relation to the distribution of arterial emboli. Cancer Res 1951; 11:648–651.
20. Moertel CG, Sauer WG, Dockerty MB, et al: Life history of the carcinoid tumor of the small intestine. Cancer 1961; 14:901–912.
21. Moertel CG: An odyssey in the land of small intestine tumors. J Clin Oncol 1987; 5:1503–1522.
22. Woodard PK, Feldman JM, Paine SS, et al: Midgut carcinoid tumors: CT findings and biochemical profiles. J Comput Assist Tomogr 1995; 19:400–405.
23. Maccioni F, Rossi P, Gourtsoyiannis N, et al: US and CT findings of small bowel neoplasms: Pictorial review. Eur Radiol. In press.
24. Pelage J-P, Soyer P, Boudiaf M, et al: Carcinoid tumors of the abdomen: CT features. Abdom Imaging 1999; 24:240–245.
25. Strodel WE, Talpos G, Eckhauser F, et al: Surgical therapy for small-bowel carcinoids. Arch Surg 1983; 118:391–397.
26. Warner TF, O'Reilly GO, Power LH: Carcinoid diathesis of the ileum. Cancer 1979; 43:1900–1905.
27. Crohn BB, Ginzburg L, Oppenheimer GD: Regional ileitis. JAMA 1932; 99:1323–1329.
28. Marshak RH, Wolf BS: Chronic ulcerative granulomatous jejunitis and ileojejunitis. AJR 1953; 70: 93–112.
29. Herlinger H, Rubesin SE, Furth EE: Mesenteric border linear ulcer in Crohn disease: Historical, radiologic, and pathologic perspectives. Abdom Imaging 1998; 23:122–126.
30. Meyers MA, McGuire PV: Spiral CT demonstration of hypervascularity in Crohn disease: "Vascular jejunization of the ileum" or the "comb sign." Abdom Imaging 1995; 20:327–332.
31. Herlinger H, Furth EE, Rubesin SE: Fibrofatty proliferation of the mesentery in Crohn disease. Abdom Imaging 1998; 23:446–448.

The Colon: Normal and Pathologic Anatomy

15

The distinctive haustral contour of the large intestine is provided by three bands of longitudinal muscle—the taeniae coli. Since the taeniae are shorter than the length of the colon itself, their tethering action in relation to the circular muscle results in the characteristic haustral sacculations. The colonic haustra are thus organized into three distinct rows, each of which has characteristic anatomic relationships.[1]

The development and action of the taeniae have been carefully studied by Lineback.[2] In the embryo, the outer layer of muscle originates in the caudal end of the bowel and extends upward until it eventually encases the colon. The three taenial bands are well marked by the 100-mm stage. Haustra are not generally seen in infancy, however (Fig. 15–1). It is not until the third year of life that the disproportionate increase in length between the colon and its longitudinal muscle bands results in the colon's being consistently bunched up, forming its characteristic saccular haustrations (Fig. 15–2).

Internally, the colon presents a relatively smooth surface, except for the semicircular folds of the haustral pouches. Section of a longitudinal muscle band at the level of a haustration obliterates the haustration and causes the bowel segment to lengthen. The taeniae function not only as shortening bands for the colon but as strong, fixed longitudinal cables on which the circular fibers are fixed (Fig. 15–3). The waves of contraction in the circular muscle occur independently and asynchronously in each of the three intertaenial regions,[2,3] and it is this contraction that further produces the haustral clefts. The contribution of both the longitudinal muscle bands and the contraction of the circular muscle to the formation of the haustral folds accounts to some degree for their variable appearance on barium enema examination.[1,4]

In the routine interpretation of barium enema studies, little attention is ordinarily directed to the organization of the large intestine into three constituent rows of haustra. Indeed, the overlapping of the contours of the sacculations is generally considered a bothersome feature in contrast to the more readily apparent outlines of the stomach or small bowel loops. Careful evaluation

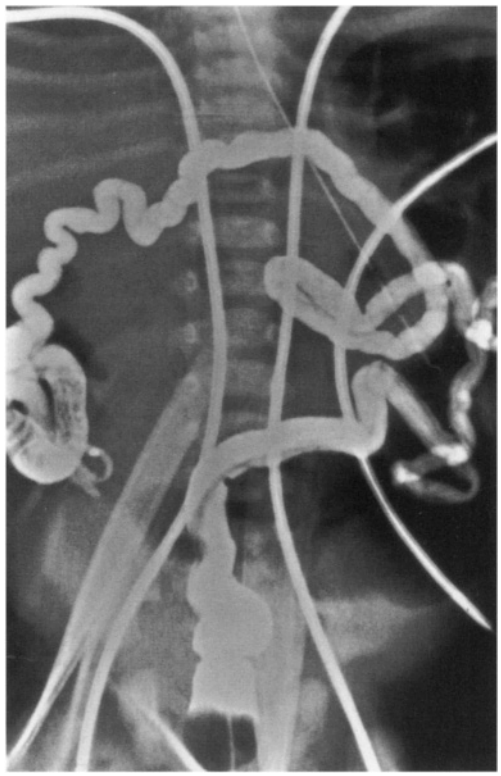


Fig. 15–1. Long, redundant ahaustral colon in an infant.
Since the colon grows in length faster than the development of the taeniae, the latter come to act as tethering cables to accordion the contour of the large intestine.



Fig. 15–2. The "wrinkled" skin of the shar-pei dog can be likened to the haustral configuration of the colon. Foreshortening of redundancy results in multiple folds or sacculations.

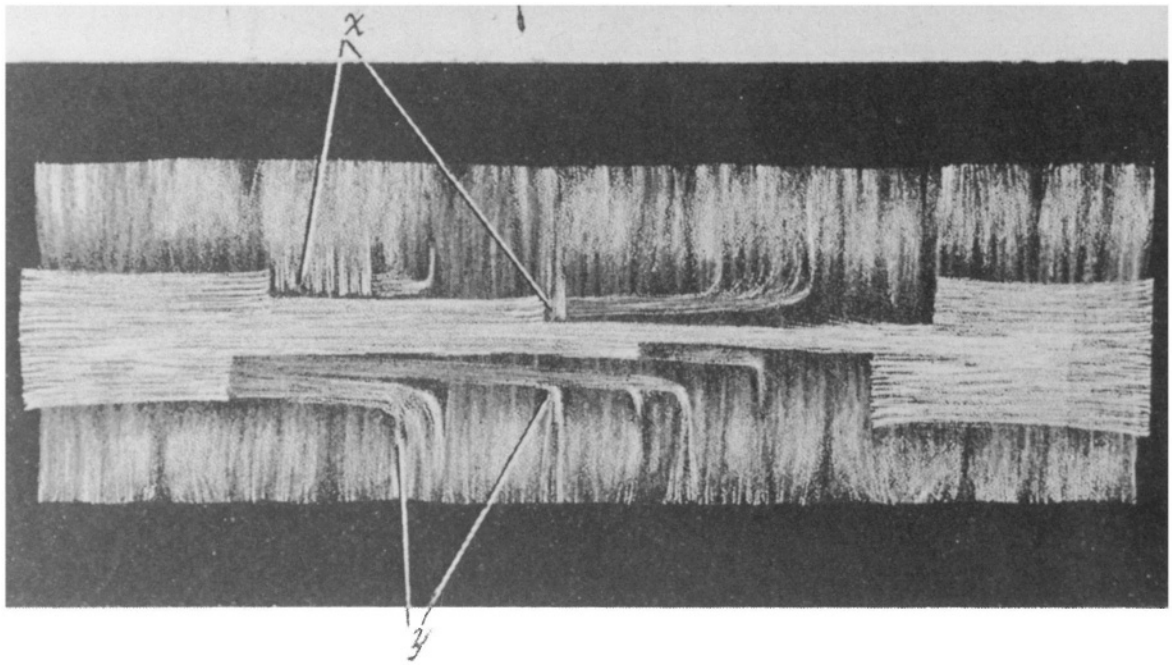


Fig. 15–3. Interconnections of colonic muscle between the layers.
Longitudinal muscle fibers *(y)* of the taenia turn at right angles and fuse with the circular muscle layer *(x).* This linkage provides a point for contraction, limiting the formation of interhaustral clefts to the zones between adjacent taeniae.
(Reproduced from Lineback.[2])

of the anatomic profiles of the haustra, however, provides a precise basis for the radiologic analysis of a variety of abdominal diseases. In cases of extrinsic mass impressions on the colon or extension of an adjacent process to the large intestine, detailed analysis of the specific group of haustral sacculations first or principally involved leads to more precise localization and thereby identification of the primary process.[5] Basic to an appreciation of pathologic alterations, however, is an understanding of the normal haustral anatomy and relationships.

Anatomic Considerations

The colon has a complete outer longitudinal muscle coat, less than half the thickness of the inner circular muscle.[2,6] The outer longitudinal layer is thickened by three bands of muscle, the taeniae coli, each of 0.5–1.0 cm in width. They are most distinct in the ascending and transverse colon. In the lower descending and sigmoid colon, they increase at the expense of the rest of the outer longitudinal muscle coat and at the level of the rectum become merged into broad diffuse bands (Fig. 15–4).

Figure 15–5a shows that each of the taeniae is named according to its topographic situation relative to the transverse colon:

1. The *taenia mesocolica* (TM) is situated on the posterosuperior surface of the transverse colon at the line of attachment of the transverse mesocolon.
2. The *taenia omentalis* (TO) runs along the anterosuperior surface of the transverse colon and is in relation to the line of attachment of the greater omentum extending inferiorly and of the gastrocolic ligament above.
3. The *taenia libera* (TL), so called because it is free and not related to any mesenteric or omental attach-

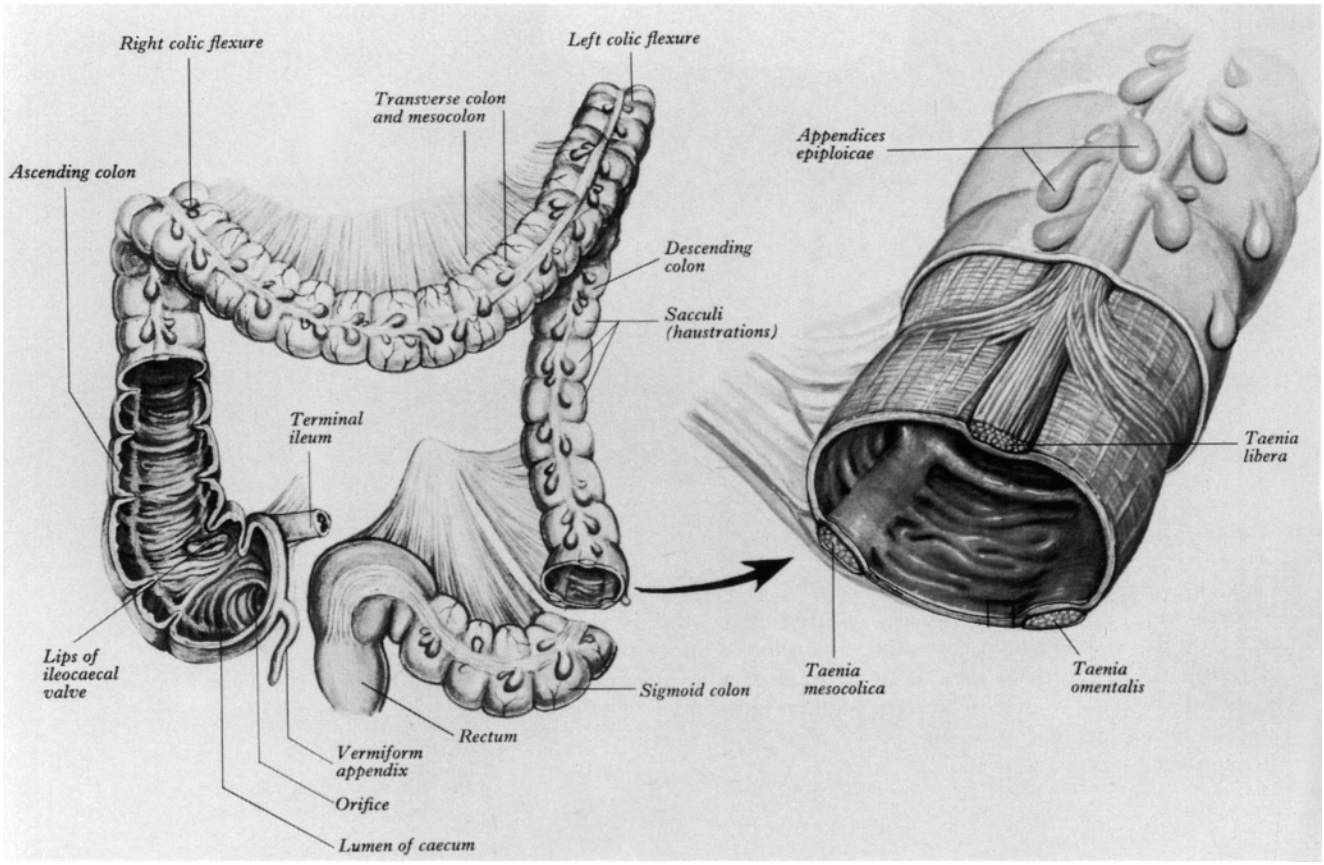


Fig. 15–4. General anatomy of the colon.
(From William and Bannister,[7])

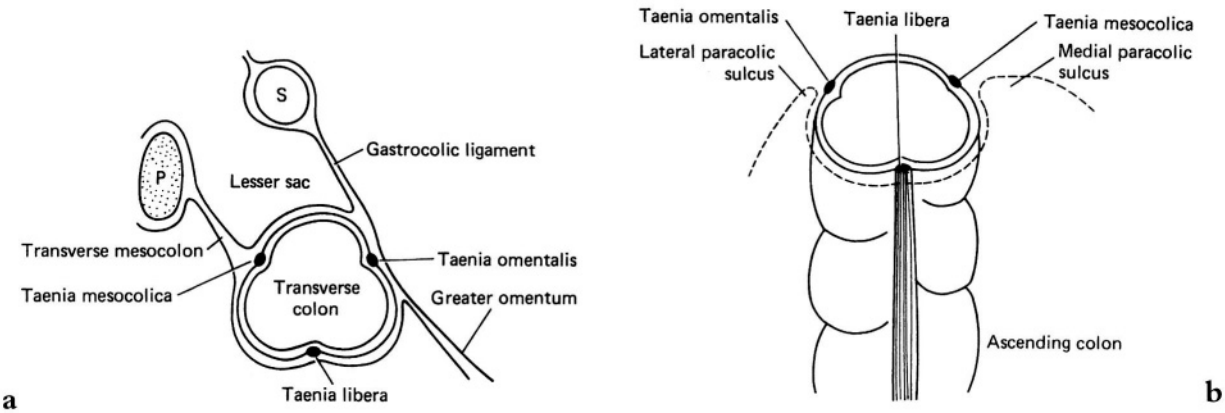


Fig. 15–5. Position and relationships of the taeniae and haustra of the colon.
(a) Sagittal diagram of transverse colon. *P* = pancreas; *S* = stomach.
(b) Horizontal diagram of ascending colon. The peritoneal reflections *(dashed line)* are shown in relation to the haustra. In the descending colon, the relationships are mirrorlike.
(Reproduced from Meyers et al.[1])

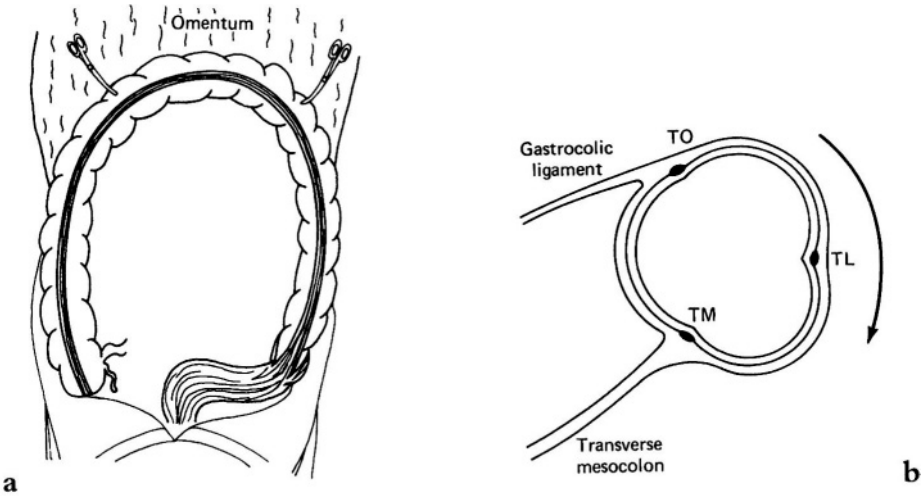


Fig. 15–6. (a) Colon in situ, colon uplifted, demonstrating continuity of the taenia libera from the ventral surface of the ascending and descending colon to the undersurface of the transverse colon.
(b) Position of the three taeniae in the uplifted transverse colon and the anterior rotation (indicated by *arrow*) that occurs when it assumes its normal position in the body. The taeniae and haustral rows then have the relationships shown in Fig. 10–5a.
(Reproduced from Meyers et al.[1])

ment, is found on the posteroinferior aspect of the transverse colon.

These relationships of the taeniae are not maintained on the ascending and descending portions of the colon (Fig. 15–5b). Here the TM lies posteromedial, the TO posterolateral, and the TL anterior. The changing relationships of the taeniae are most simply understood if it is recalled that there is some anterior rotation of the transverse colon on its mesocolon relative to the flexures (Figs. 15–6 and 15–7). Nevertheless, continuity of the taeniae and thereby of the haustral rows can be easily traced.

Classification of Organization of Haustral Rows

Three distinct rows of haustral sacculations are thus produced (Fig. 15–5), which can be referred to by the taeniae that give their form:

1. TM-TO. In the transverse colon, this row provides the superior (mesenteric) contour. Here the haustra bear two important relationships: (a) they face the inferior recess of the lesser sac, providing its lower boundary, and

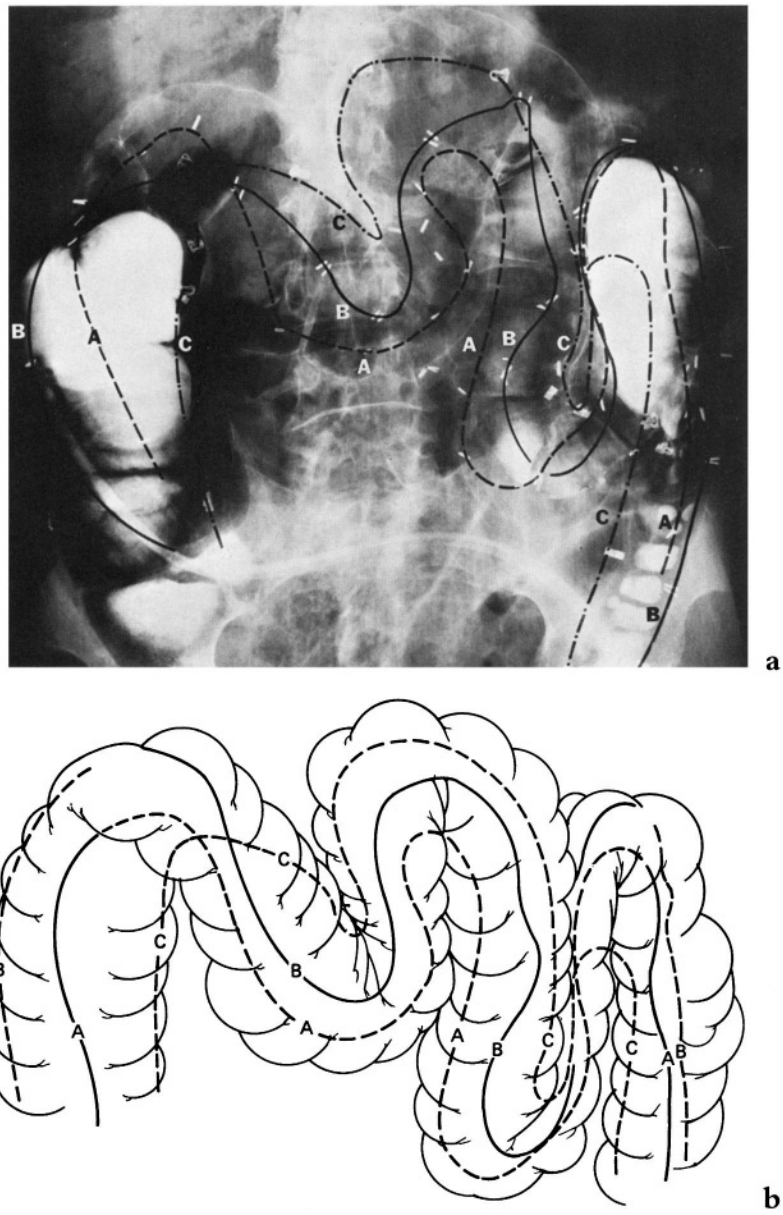


Fig. 15–7. Postmortem double-contrast radiograph marked *in situ* with metallic clips.
The change in both course and relative position between the ascending, transverse, and descending colon is shown. *A* = taenia libera; *B* = taenia omentalis; *C* = taenia mesocolica.
(Reproduced from Meyers et al.[1])

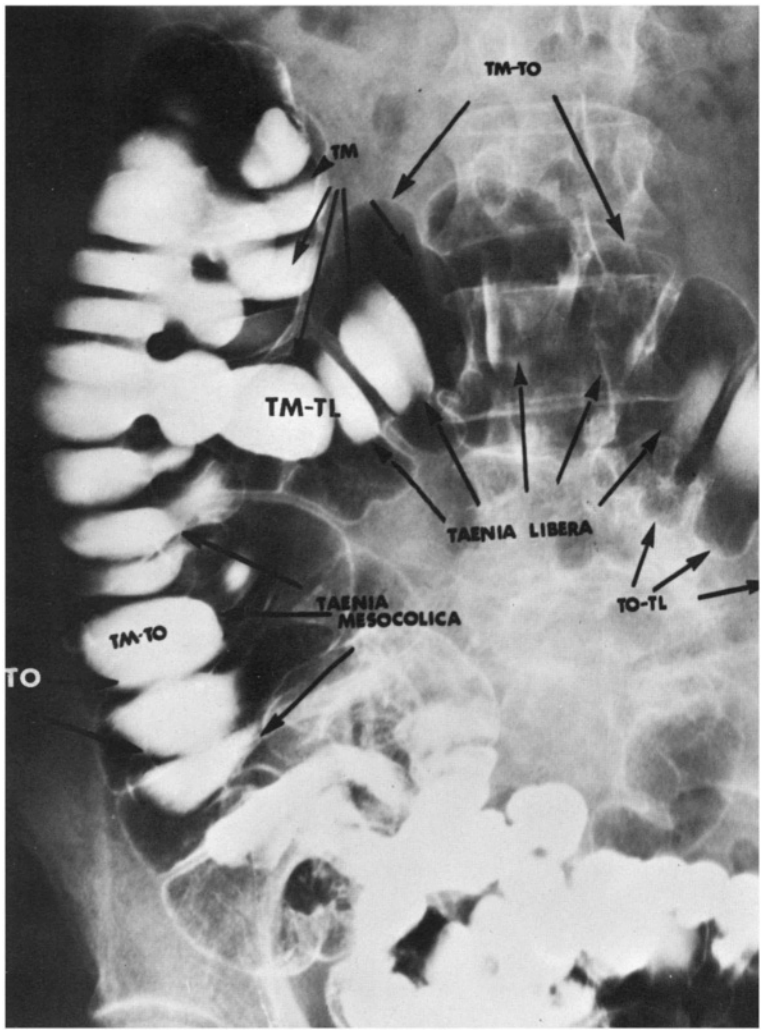


Fig. 15–8. Double contrast barium enema examination.
Supine projection. The three taeniae and the organization of the haustra into three identifiable rows are clearly shown.
TL = taenia libera; *TO* = taenia omentalis; *TM* = taenia mesocolica.
(Reproduced from Meyers et al.[1])

(b) they are in most direct continuity with the gastrocolic ligament extending downward from the stomach.

In the ascending and descending colon, these sacculations occupy the posterior third. This row of haustra is unique in that their contour completely faces extraperitoneal structures only.

2. TM-TL. In the transverse colon, this haustral row faces posteriorly and is in most direct continuity with the transverse mesocolon.

In the ascending and descending colon, these haustra constitute the medial third of the colonic contour (mesenteric border) and are in relation to the shallow intraperitoneal recess of the medial paracolic gutter.

3. TO-TL. In the transverse colon, this group of sacculations provides the inferior (antimesenteric) contour and is the most anterior row. It is thus in relation to the greater omentum and anterior abdominal wall.

In the ascending and descending colon, these haustra constitute the lateral (antimesenteric) contour and are in most intimate relationship to the deep intraperitoneal lateral paracolic gutter.

Normal Radiologic Observations

The haustral recesses, bordered by the course of the taeniae, can be identified easily by routine barium enema examination, particularly with double contrast studies.[1] Their distinctive organization into rows and the position and anatomic limits as well as the relationships of each row are clearly delineated.

In the supine position, barium gravitates to the dependent posterior row of sacculations in the middle third. This outlines the TM-TO row in the ascending colon (Fig. 15–8) and the TM-TL row in the transverse colon (Figs. 15–8 and 15–9). At the same time, air tends to outline the border-forming haustral rows.

In the prone position, the more ventral haustral groups are visualized more clearly. These include the TO-TL and TM-TL haustra of the ascending colon (Fig. 15–10) and the TO-TL and TM-TO haustra of the transverse colon (Fig. 15–11). Demarcation is provided by their shared taenia.

Precise correlation of the relative position of the haustral rows is further provided in lateral projections (Fig. 15–12).

The haustra are almost invariably demarcated clearly in the ascending and transverse colon and less often in the descending colon. The size of the haustra in each row is roughly equal, except in the lower descending colon. Here the TO and TL broaden and quickly approximate each other, reducing their intervening lateral haustral row. Sigmoid loops only rarely demonstrate haustral delineation. Because of their shape and the effects of gravity, the entire contour of a haustrum is not visualized in a single view. Yet, with the multiple views conventionally employed in a barium-contrast study, the complete contours of all of the haustral rows are usually seen. Decubitus and optimally obliqued or lateral projections adequately complement frontal views.

The appearance of the altered relations of the rows of haustra as they continue around the hepatic flexure from the ascending colon to the transverse colon is best ap-

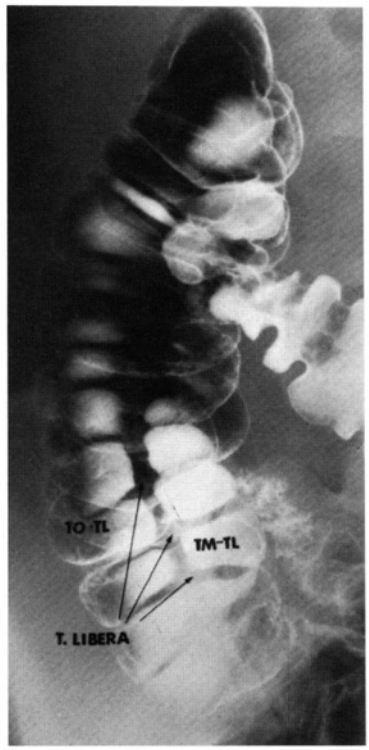


Fig. 15–10. Prone projection.
The TO-TL and TM-TL rows in the ascending colon are delineated by the indentation of the taenia libera.
(Reproduced from Meyers et al.[1])

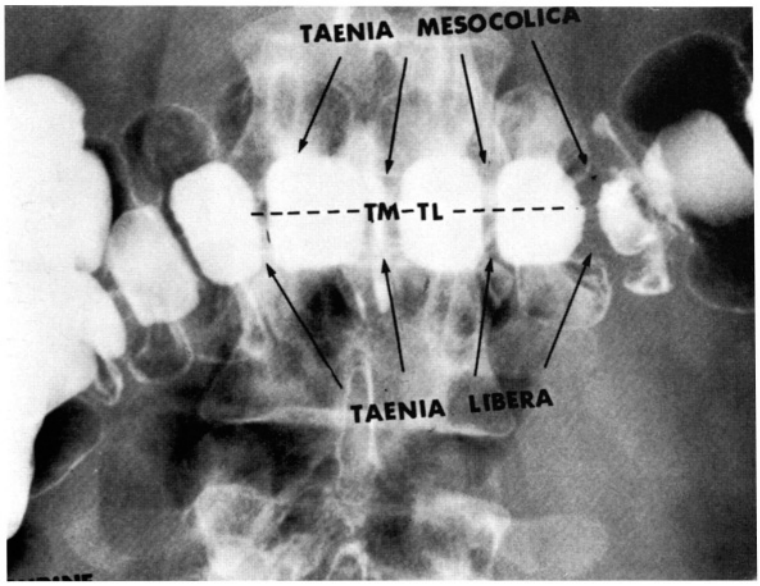


Fig. 15–9. Double contrast barium enema.
In the supine position, barium fills the posterior TM-TL row of haustra in the internal third of the transverse colon, while air outlines the border-forming TM-TO row superiorly and the TO-TL row inferiorly.
(Reproduced from Meyers et al.[1])

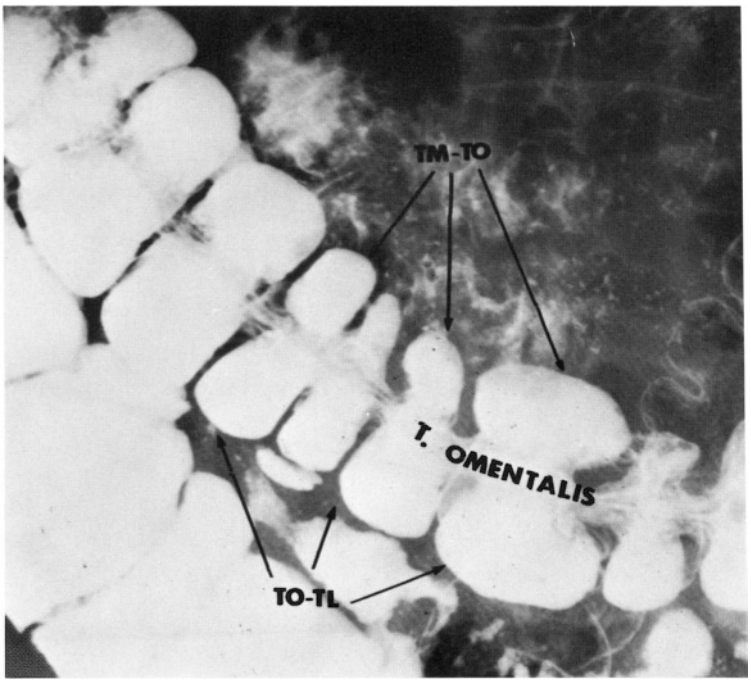


Fig. 15–11. Prone projection.
The TM-TO and TO-TL rows in the transverse colon are delineated by the taenia omentalis. (Reproduced from Meyers et al.[1])

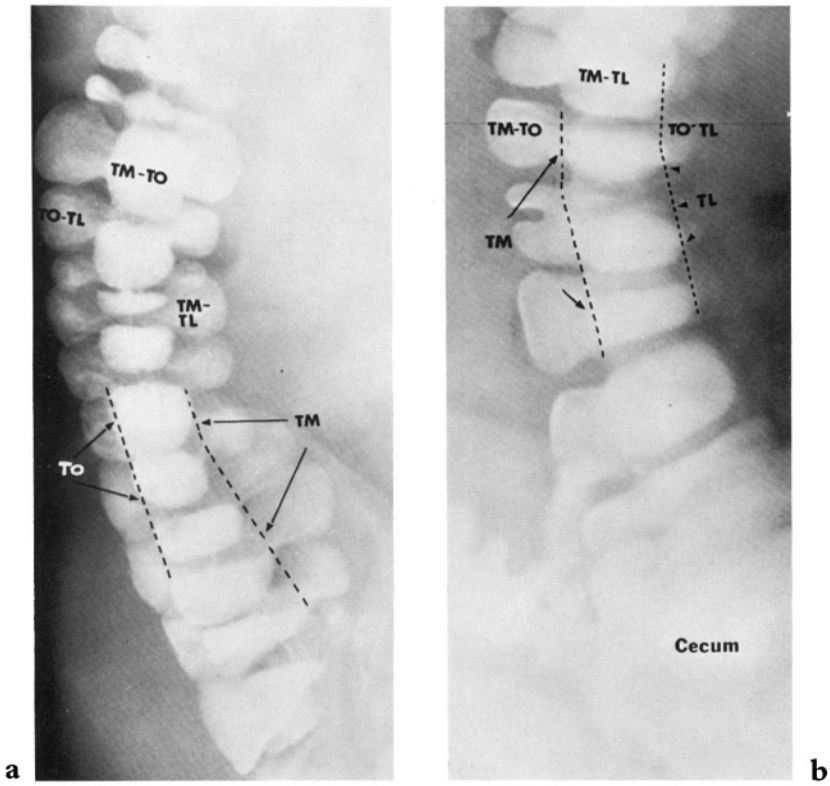


Fig. 15–12. Ascending colon.
(a) Supine.
(b) Left lateral. Note that the three rows of haustra can be identified clearly in the lateral view. Multiple projections afford clearer visualization of their complete contour. (Reproduced from Meyers et al.[1])

preciated on oblique projections (Fig. 15–13). It can then be noted that the TM, for example, curves around the flexure from a posteromedial position on the ascending colon to assume a posterosuperior course on the transverse colon. Similarly, because of the rotation at the flexure, the other taeniae alter their course. In this way, continuity of the rows of haustra themselves can be traced.

Even with contractions of portions of the colon, the haustral rows may still be identified (Fig. 15–14). In a mass peristaltic movement, the wave of contraction may involve only one haustral row (Fig. 15–15). This may simulate a filling defect unless the haustral relationships are recognized.

Classically, interdigitation of haustral folds has been considered a plain film landmark for the identification of the large intestine and particularly in the differentiation from gas-distended small bowel loops. However, reliance on this feature, without an understanding of the haustral anatomy, may be misleading. While it is true that the folds between two adjacent rows of haustra often interdigitate, it must be recognized that each row of sacculations may contract independently of the other two. In this way, the third row of haustra may not be appreciated on a single projection, either because it is in a state of contraction or obscured by superimposed shadows or densities (Figs. 15–16 and 15–17). The haustral folds visualized at the contours of the colon may then project in the same plane, rather than in an interdigitating manner, and be mistaken for the semicircular folds of a distended small bowel loop.

Appendices epiploicae, which appear as lobulated masses of subserosal fat, usually 2–5 cm long and 1–2 cm thick, are arranged in two separate longitudinal rows along the taenia libera and adjacent to the taenia omentalis. They extend from the cecum to the rectosigmoid junction and are most prominent in size and number in the descending colon and sigmoid colon[8–10] (Fig. 15–18).

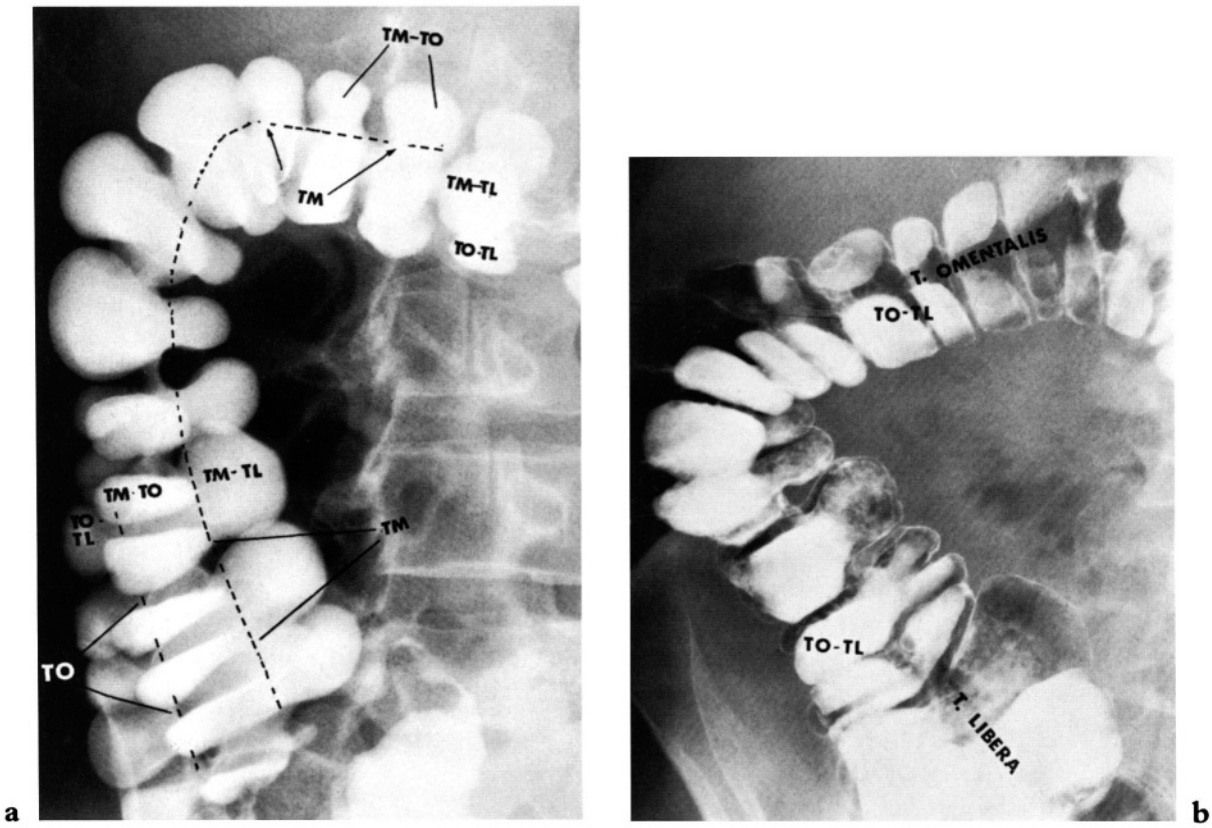


Fig. 15–13. The altered relationships of the taeniae and the haustral rows around the hepatic flexure are demonstrated.
(a) Prone.
(b) Left posterior oblique projection.
(Reproduced from Meyers et al.[1])

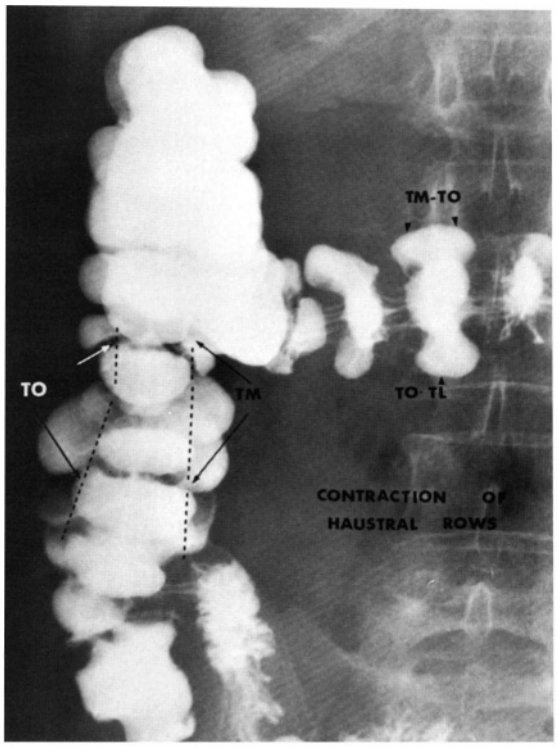


Fig. 15–14. Contraction of haustra.
Each row remains identifiable. Note that in the transverse colon the rows are aligned transiently.
(Reproduced from Meyers et al.[1])



Fig. 15–15. Mass contraction limited to the TM-TO haustral row of the ascending colon mimics a filling defect due to a lesion.

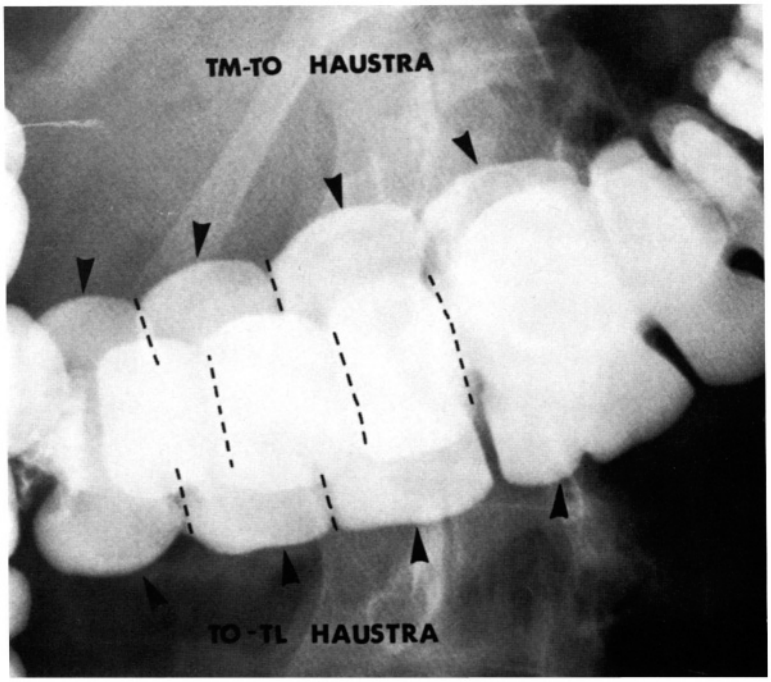


Fig. 15–16. In this instance, the interhaustral clefts of the border-forming TM-TO and TO-TL groups do not interdigitate.
Note, however, that the folds of each do interdigitate with those of the centrally projecting TM-TL group.
(Reproduced from Meyers et al.[1])



Fig. 15–17. This example of pneumatosis coli with gas within the interhaustral septa illustrates clearly that the clefts on the two opposing walls do not interdigitate.

Abnormal Radiologic Features

Specific haustral rows of the colon may be involved by a variety of intraabdominal lesions. Characteristic groups of sacculations are affected by mesenteric pathways of extension of disease to the colon, extrinsic compression by organomegaly and masses, a spectrum of intra- and extraperitoneal processes, and intrinsic colonic diseases. Radiologic identification of pathologic alterations involving predominantly one haustral row allows precise localization and diagnosis.[5]

Lesions Within the Gastrocolic Ligament

Figure 15–19 shows that processes extending along or arising within the gastrocolic ligament may be clearly identified by their specific effect on the transverse colon. Anatomic dissections have shown that the point of attachment of the gastrocolic ligament is actually within a couple of centimeters cephalad to the taenia omentalis. Injection experiments consistently demonstrate that the mesenteric plane of extension is preferentially upward along the TM-TO haustral row.[5] This constitutes the superior border of the transverse colon.

Selective involvement of this row of sacculations may thus reveal extension of a carcinoma of the stomach along the gastrocolic ligament (Figs. 15–20 and 15–21). With even greater mural invasion and consequent fixation, the haustral pattern of the uninvolved TO-TL row on the inferior contour of the transverse colon is often thrown into a pseudosaccular appearance (Fig. 15–20).

The pseudosacculations of the haustral row opposite to that primarily involved by fixation are basically a functional phenomenon. They are largely a consequence of disordered peristaltic contractions and thus change in size, shape, and axis. In contrast, the pseudosacculations of scleroderma of the colon are constant structures brought about by atrophy of the muscle and collagenous replacement. Characteristically, they have wide mouths, contain fecaliths, and fail to contract on postevacuation studies. They are most consistently seen arising from the TO-TL haustra of the transverse colon (Fig. 15–22).

Lesions originating within the gastrocolic ligament may produce similar changes of the TM-TO haustra, but characteristically, they are either more localized or lack the tethering of mucosal folds. Fig. 15–23 illustrates localized changes involving only three haustra of the TM-TO row secondary to an actinomycotic abscess within the gastrocolic ligament. If a mass within the ligament bulges anteriorly, it may characteristically extend to depress the TO-TL haustral row as well (Fig. 15–24).

Not all instances of extrinsic involvement of the TM-TO row reflect a lesion within the gastrocolic ligament.

text continues on page 681

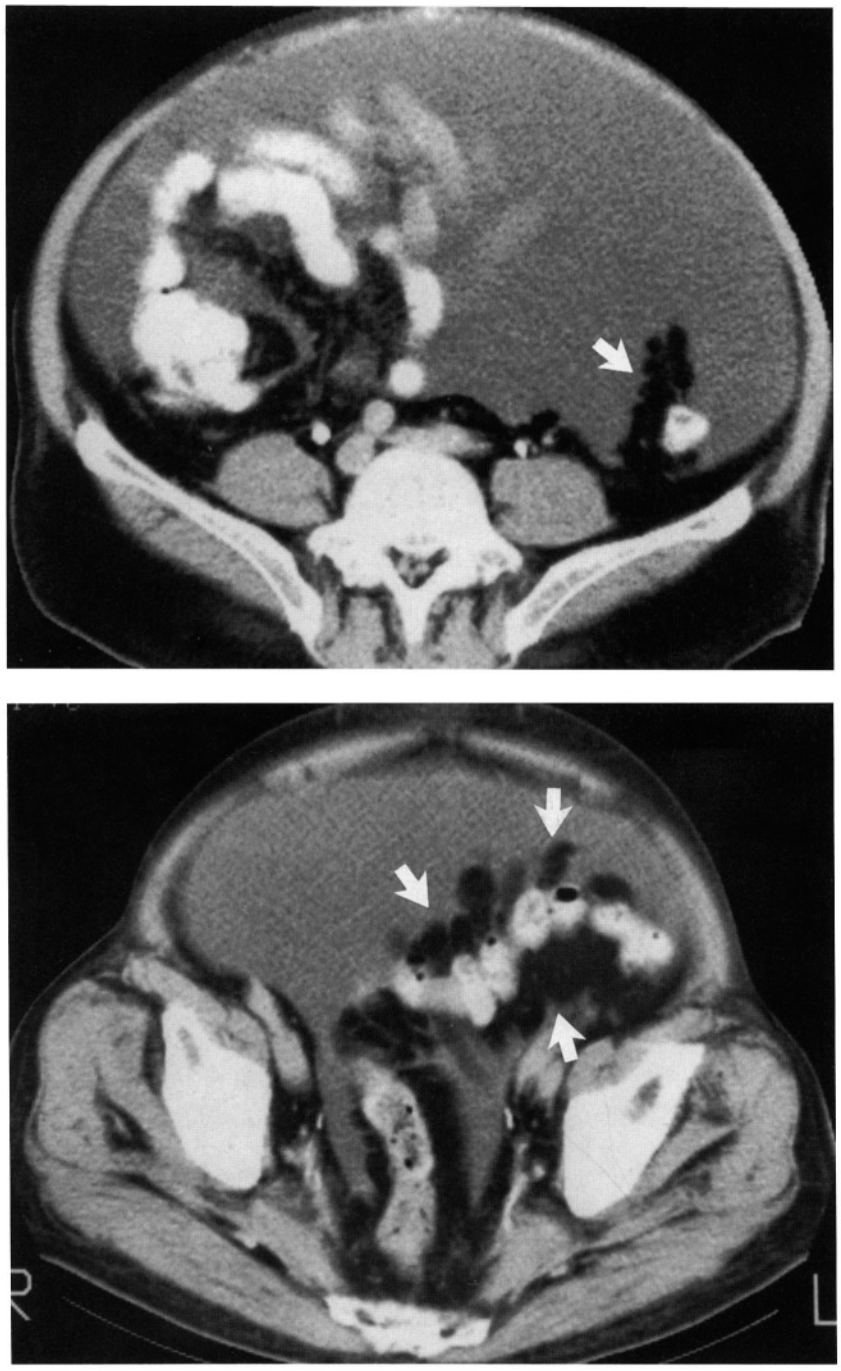


Fig. 15–18. Appendices epiploicae of the colon.
(a and **b)** In an instance of massive ascites, appendices epiploicae are visible as tabulated and fingerlike projections from the descending and sigmoid colon *(arrows).* These appendages are contiguous with subserosal pericolic fat.

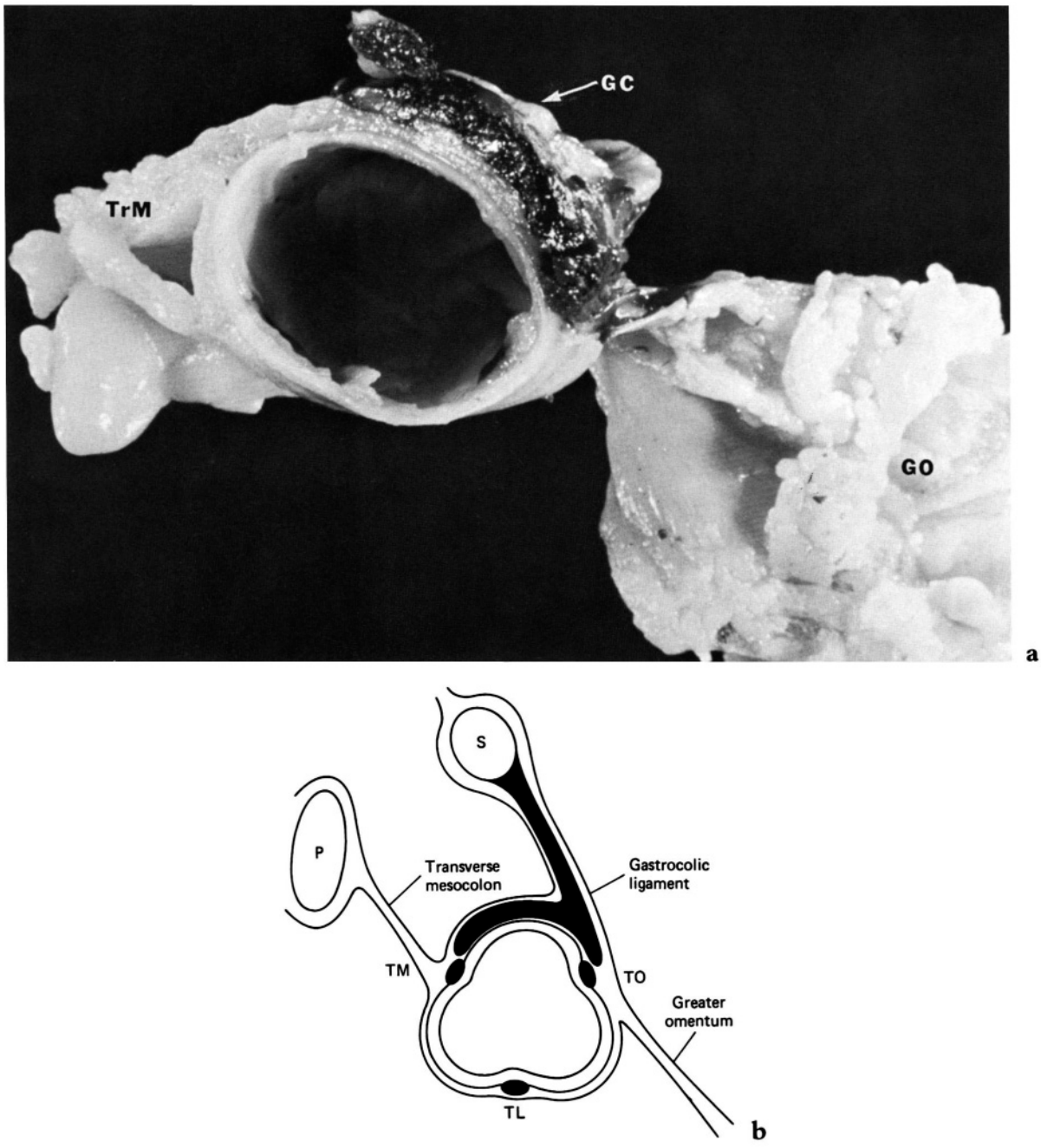


Fig. 15–19. Sagittal section through the transverse colon.
Specimen shows that injection of contrast material into the gastrocolic ligament spreads preferentially to the superior TM-TO haustral row. *GC* = gastrocolic ligament; *GO* = greater omentum; *TM* = transverse mesocolon; *S* = stomach; *P* = pancreas.
(Reproduced from Meyers et al.[5])

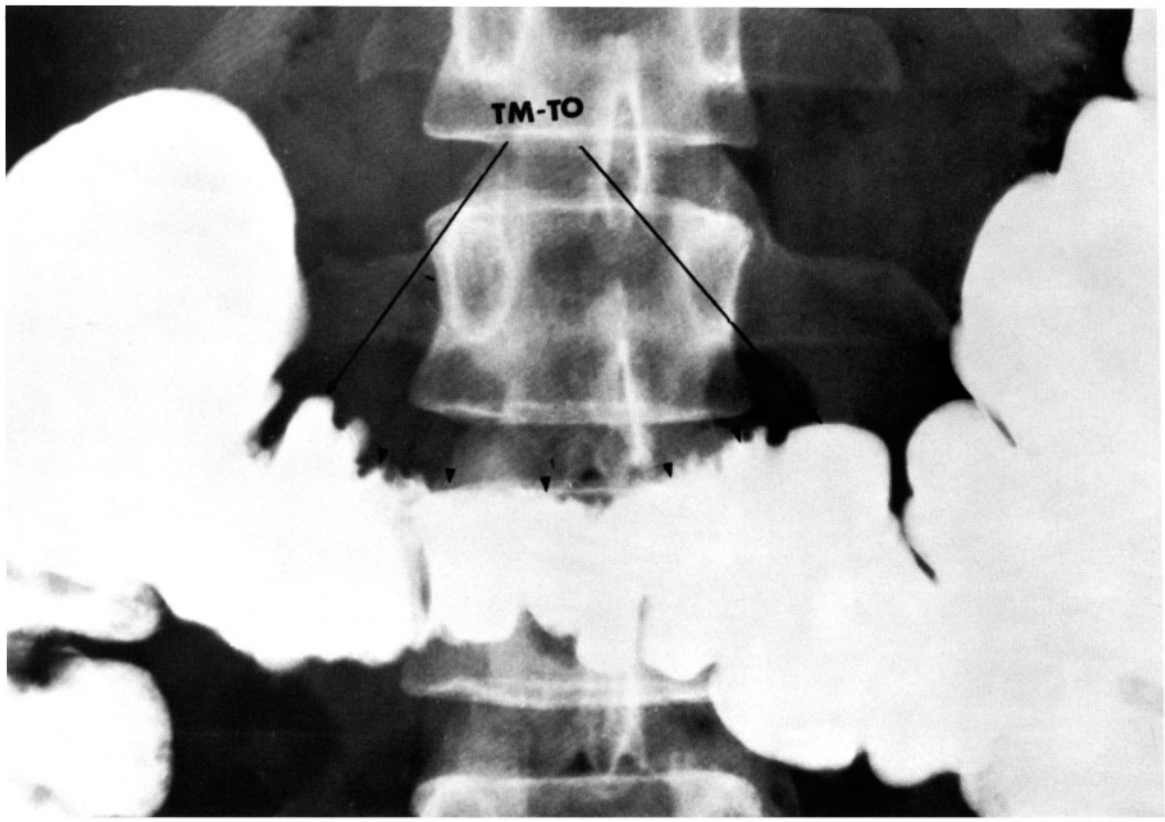


Fig. 15–20. Extensive invasion of the TM-TO row *(arrowheads)* by gastric carcinoma spreading down the gastrocolic ligament.
The fixation results in pseudosaccular haustral outpouchings from the uninvolved TO-TL row on the inferior border.
(Reproduced from Meyers et al.[5])

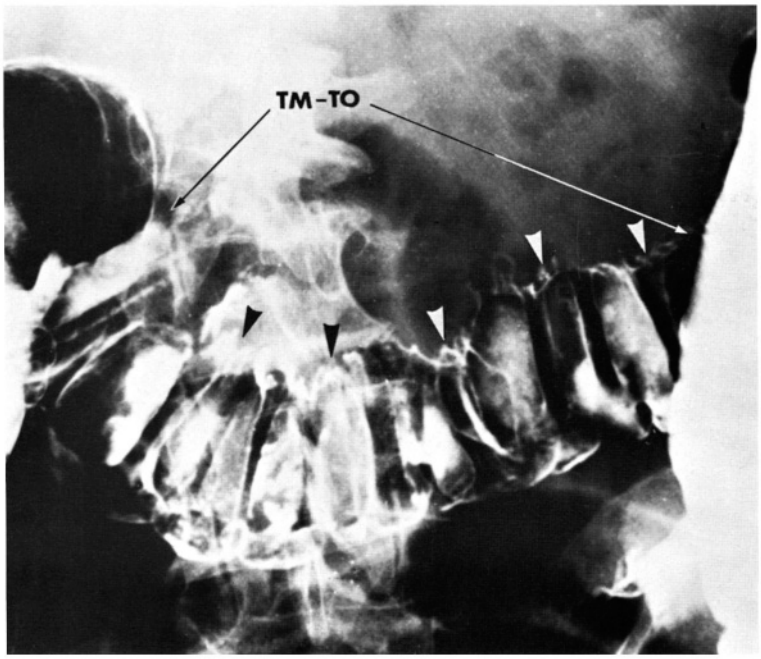


Fig. 15–21. Carcinoma of the stomach extending down the gastrocolic ligament involves the TM-TO haustral row on the superior contour of the transverse colon *(arrowheads).* The TM-TL and TO-TL rows are not affected.
(Reproduced from Meyers et al.[5])

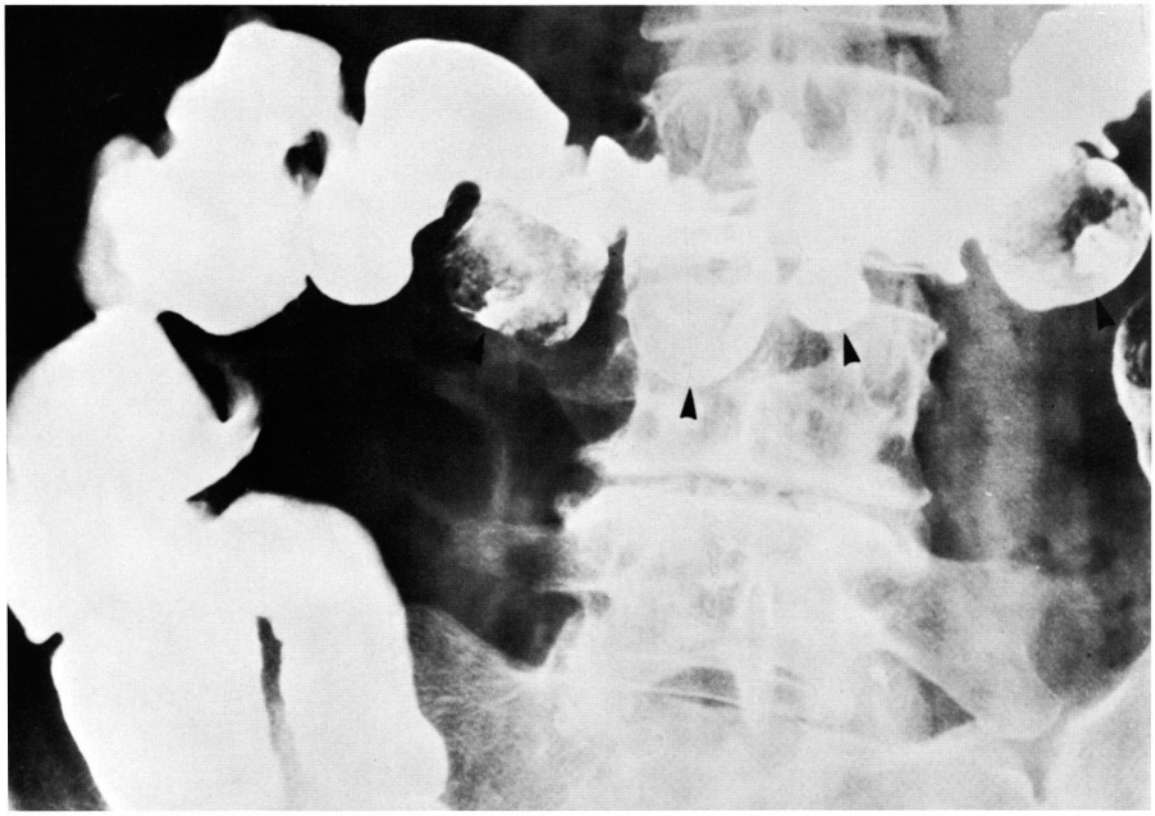


Fig. 15–22. Scleroderma of the colon.
Fecalith-containing pseudosacculations *(arrowheads)* arise characteristically from the TO-TL haustral row. (Reproduced from Meyers et al.[5])

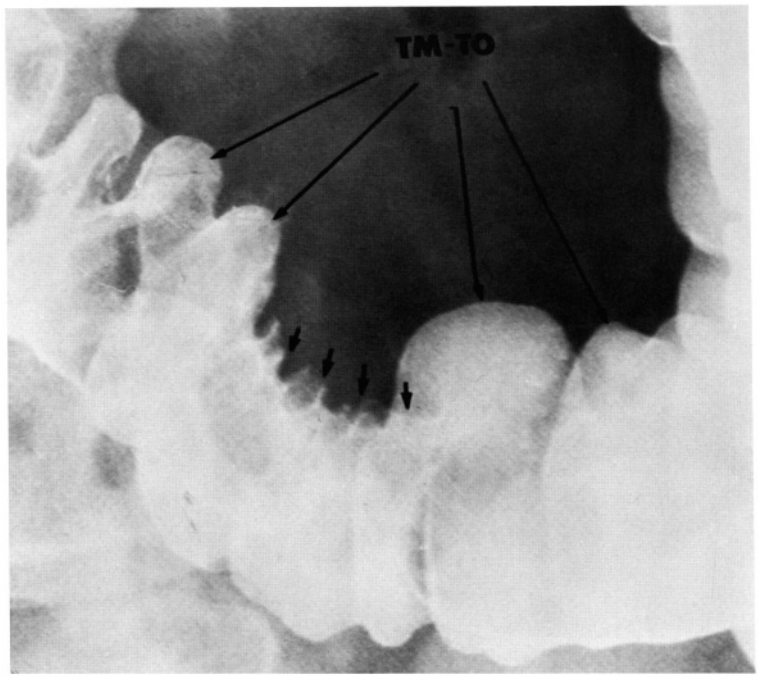
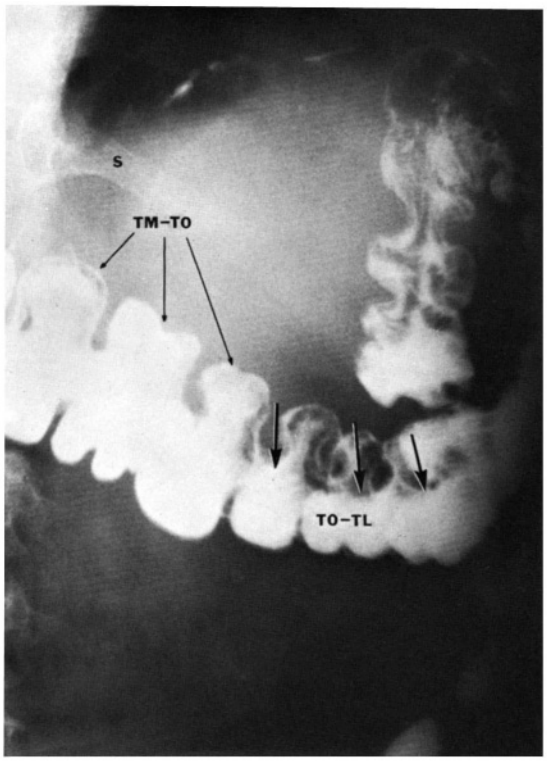
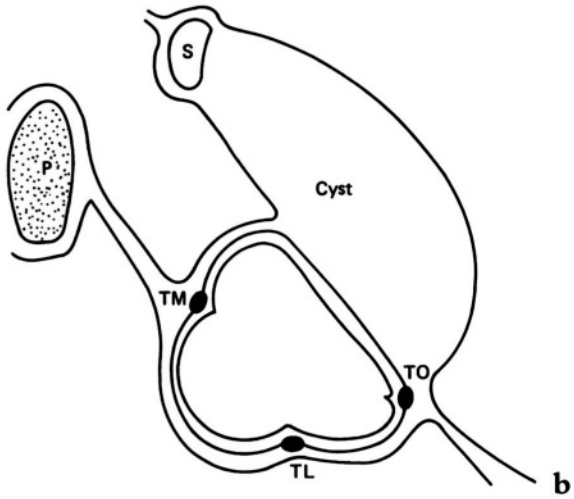


Fig. 15–23. Localized abscess in the gastrocolic ligament results in effacement, depression, and mucosal irregularities of TM-TO haustra *(arrows)* in the transverse colon.
(Reproduced from Meyers et al.[5])



a



b

Fig. 15–24. Hemorrhagic cyst of the gastrocolic ligament.
(a) Mass in the region of the gastrocolic ligament bulges anteriorly into the greater peritoneal cavity. It elevates the stomach *(S),* compresses the TM-TO row from in front, and depresses the superior contour of the TO-TL row *(arrows).*
(b) Haustral changes. *S* = stomach; *P* = pancreas.



Fig. 15–25. Courvoisier gallbladder secondary to pancreatic carcinoma.
Double-contrast barium enema. Prone film demonstrates extrinsic mass compression on the superior borders of the TM-TO haustral row of the hepatic flexure.

The normal gallbladder may locally indent the superior border of this row in the hepatic flexure. Conspicuous depression, however, indicates enlargement of the gallbladder, as may be seen in hydrops, empyema, or a Courvoisier condition (Fig. 15–25). Figure 15–26 illustrates the value of haustral analysis in the diagnosis of choledochal cyst.

Lesions Within the Transverse Mesocolon

Anatomic dissections and injection experiments have documented that the mesenteric plane of the transverse mesocolon extends preferentially downward along the TM-TL haustra toward the TO-TL row[5] (Fig. 15–27). This constitutes the inferior border of the transverse colon.

Pancreatic lesions, by extending along the leaves of the transverse mesocolon, may then be revealed by their characteristic effects on the inferior haustral row. In severe pancreatitis, extravasated enzymes typically flatten the lower contours of the TO-TL row (Fig. 15–28). The enzymes may spread along the limits of the transverse mesocolon toward the left, so that the effects on the colon may end specifically at the level of the phrenicocolic ligament. The haustral pattern of the uninvolved

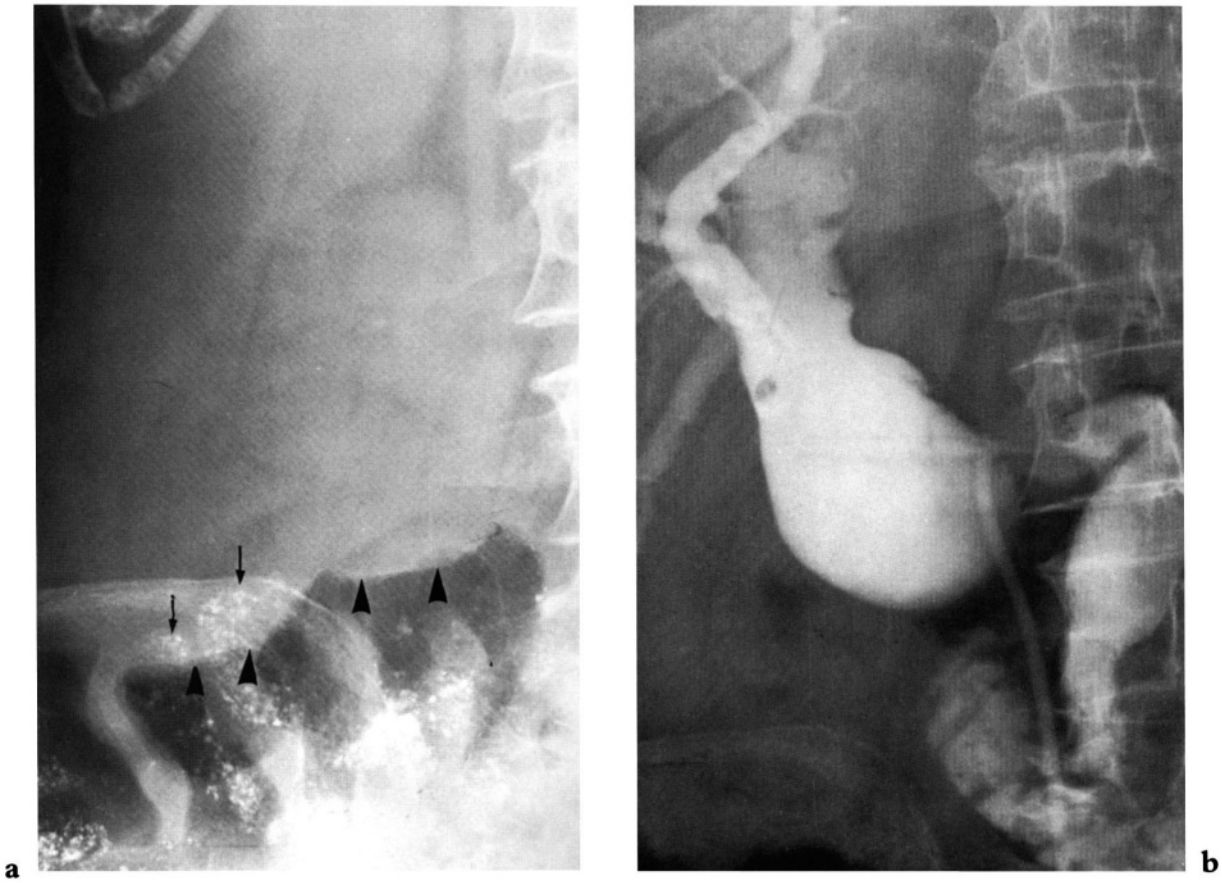
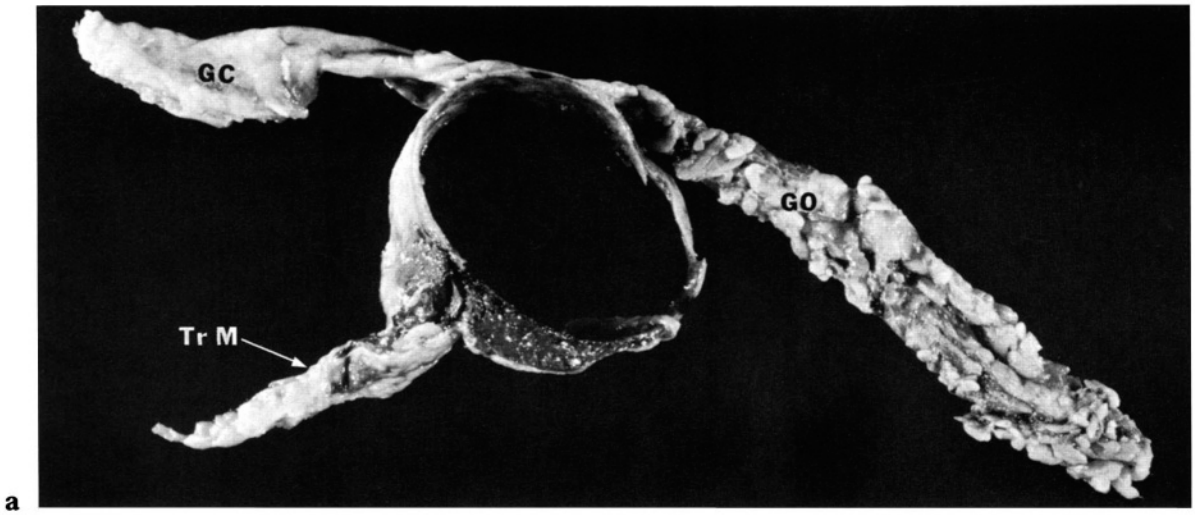
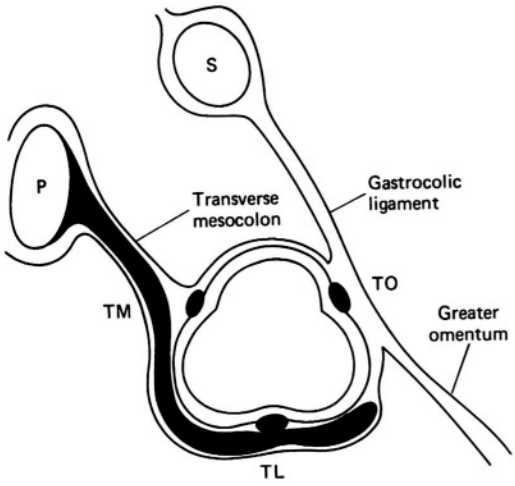


Fig. 15–26. Choledochal cyst.
(a) Supine radiograph, oral cholecystogram. There is nonopacification of the gallbladder. Residual Telepaque outlines unaffected TM-TL haustra *(arrows).* However, the TM-TO row shows a double convex depression *(arrowheads).*
(From Meyers et al.[5])
(b) At surgery, an enlarged gallbladder containing stones accounted for the lateral depression. This T-tube study shows that a choledochal cyst accounts for the medial depression of the TM-TO row.



a



b

Fig. 15–27. Sagittal section through transverse colon. Specimen shows that contrast material injected into the transverse mesocolon spreads preferentially downward along the TM-TL haustra toward the TO-TL row. *TrM* = transverse mesocolon; *GC* = gastrocolic ligament; *G*O = greater omentum; *S* = stomach; *P* = pancreas. (Reproduced from Meyers et al.[5])

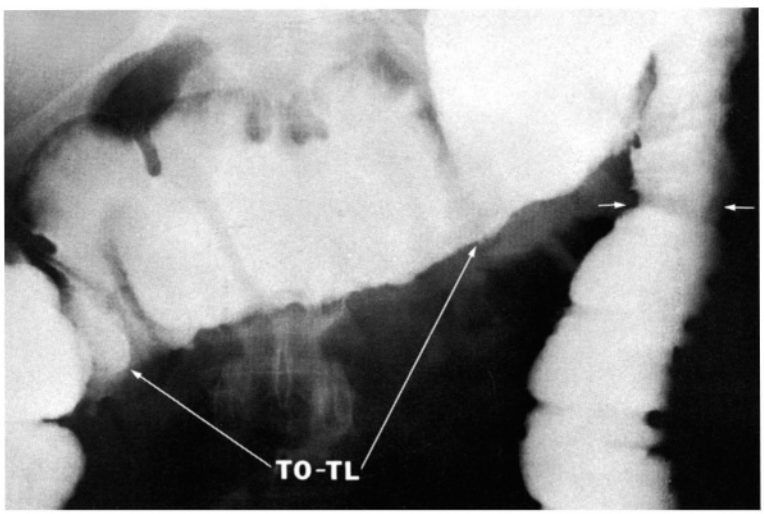


Fig. 15–28. Traumatic pancreatitis. The extravasated enzymes have spread along the transverse mesocolon to involve the TO-TL row on the inferior contour with irregular flattening and rigidity. The process ends laterally at the level of the phrenicocolic ligament *(arrows).* The fixation results in pseudosaccular haustral outpouchings from the uninvolved TM-TO row on the superior border.
This constellation of findings is pathognomonic of a process originating in the pancreas and extending along the transverse mesocolon. (Reproduced from Meyers et al.[5])

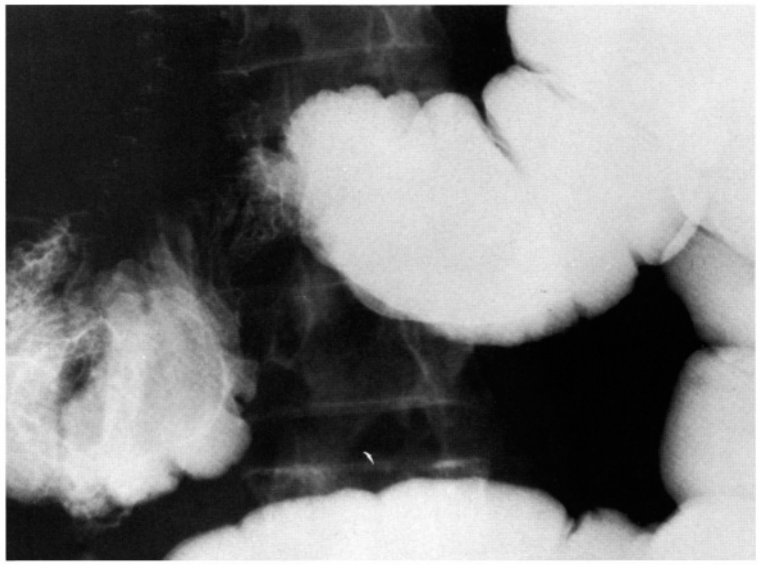


Fig. 15–29. Carcinoma of the pancreas extending along the transverse mesocolon results in fixation and mass along the inferior border of the transverse colon.

TM-TO row on the superior contour of the transverse colon is often thrown into a pseudosaccular appearance.

In a similar manner, direct extension of carcinoma of the pancreas to the transverse colon along the mesocolon characteristically involves the TO-TL row first or predominantly (Fig. 15–29).

Distinction Between Intraperitoneal and Extraperitoneal Processes

Figure 15–30 illustrates that in the ascending or descending colon, two of the haustral rows face intraperitoneal structures. The TO-TL sacculations are in relation to the lateral paracolic gutter and the TM-TL row to the medial paracolic sulcus and the small bowel loops. Intraperitoneal processes in these areas, then, produce predominant changes on these haustra. In contrast, the posterior TM-TO row is unique in bearing relationship only to extraperitoneal processes, which are often clinically occult and radiologically confusing. Changes limited to this haustral row thus clearly indicate the site of the abnormality as extraperitoneal in nature.

Ascending Retrocecal Appendicitis

These observations have been most useful in the diagnosis of ascending retrocecal appendicitis.[11] An ascending retrocecal position of the appendix is surprisingly common; its incidence ranges from 26% in surgical cases[12] to 65% in an autopsy series[13] (Fig. 15–31). In this position, the appendix may be intraperitoneal or extraperitoneal (Fig. 15–32). It may be identified on plain films, contrast studies, and sectional imaging studies (Fig. 15–33).

Many complications of appendicitis are related to anatomic variations in the position of the appendix, re-

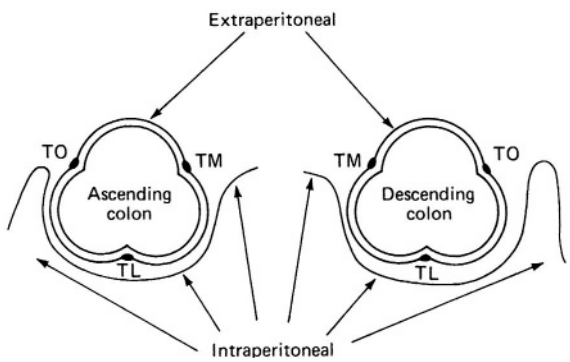


Fig. 15–30. Intraperitoneal and extraperitoneal relationships.
In the ascending and descending colon, the TO-TL and TM-TL rows bear intraperitoneal relationships and the TM-TO haustra face extraperitoneal structures. (Reproduced from Meyers et al.[5])

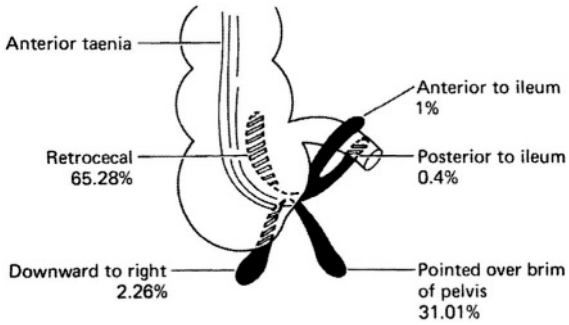


Fig. 15–31. Incidence of variations in position of the appendix, as determined by Wakely.[13]

flected clinically in the problem of differential diagnosis of acute appendiceal disease and lesions of the gallbladder, liver, right kidney, and base of the right lung or pleura. The radiologic features, however, constitute a characteristic pattern that permits precise localization and diagnosis. Inflammation associated with an intraperitoneal ascending retrocecal appendix occurs in the right paracolic gutter and involves the lateral (TO-TL) haustral row of the ascending colon (Fig. 15–34). In contrast, inflammation associated with an extraperitoneal ascending retrocecal appendix affects primarily the posterior (TM-TO) haustral row (Figs. 15–35 through 15–38). Computed tomography may readily demonstrate the extraperitoneal inflammatory collection and its effect upon the colon[14,15] (Fig. 15–39) and perhaps associated consequences[17] (Fig. 15–40). A subhepatic appendix and its inflammatory complications may be readily evident (Figs. 15–41 through 15–43). The appendix itself may show definite abnormalities, including mass displacement (Fig. 15–34), sinus tracts (Fig. 15–37), and opacification of the abscess cavity. Fulminating infection may infiltrate the flank wall and subcutaneous tissues (Fig. 15–44).

If the appendix is not visible, I have observed that its location can still be confidently inferred by the position of the ileocecal valve, owing to the embryologic development of rotation and fixation.[11] If the appendix is intraperitoneal and points inferiorly toward the pelvis, the ileum enters the cecum from the medial aspect so that the customary position of the ileocecal valve is on the medial wall. However, with an ascending retrocecal appendix, the ileum enters from behind so that the ileocecal valve may be seen on the posterior wall.

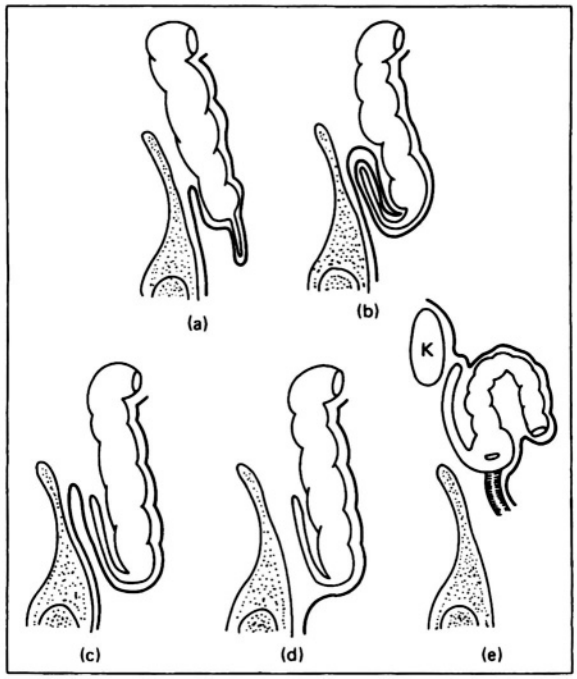


Fig. 15–32. Normal variations in the position and peritoneal fixation of the appendix.
(a) Intraperitoneal, pointing over the brim of the pelvis.
(b) Intraperitoneal, ascending retrocecal.
(c) Extraperitoneal, ascending retrocecal. A paracecal fossa is present.
(d) Extraperitoneal, ascending retrocecal.
(e) Extraperitoneal, ascending retrocecal, lying anterior to the right kidney *(K)* deep to the liver, associated with an undescended subhepatic cecum. The terminal ileum, also extraperitoneal, enters the cecum from behind.
(Reproduced from Meyers and Oliphant.[11])

Abdominal Trauma

In cases of abdominal trauma with medial displacement of the ascending or descending colon, identification of the haustral row primarily affected may be the key in the differential diagnosis between intraperitoneal and extraperitoneal bleeding. Intraperitoneal fluid in the lateral paracolic gutter tends to compress the TO-TL row. In contrast, extraperitoneal blood in relationship to the colon flattens particularly the TM-TO haustral row (Fig. 15–45).

text continues on page 692



Fig. 15–33. Ascending retrocecal appendix with an appendicolith.
(a) Plain film. A gas-containing appendix *(arrows)* can be visualized through the feces-laden ascending colon.
(b) Tortuous portions of the retrocecal appendix *(arrows)* are shown on CT. Incidentally noted is the opacified ureter anterior to the psoas muscle.
(c) An appendicolith is evident within its cephalad tip *(arrow).*

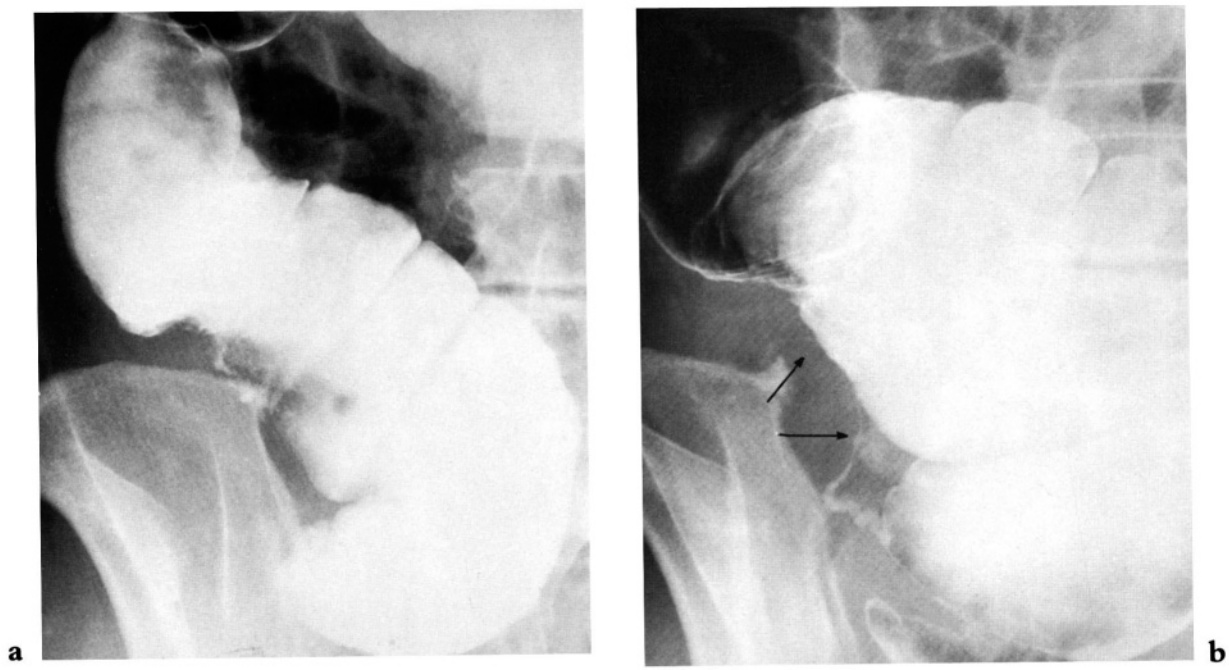


Fig. 15–34. Intraperitoneal ascending retrocecal appendicitis.
(a) Frontal view shows mass displacement and nodular deformity of the lateral contour of the proximal ascending colon.
(b) Oblique view reveals gentle arcuate mass displacement of an ascending retrocecal appendix *(arrows).* The posterior wall of the proximal ascending colon is grossly intact.
(Reproduced from Meyers and Oliphant.[11])

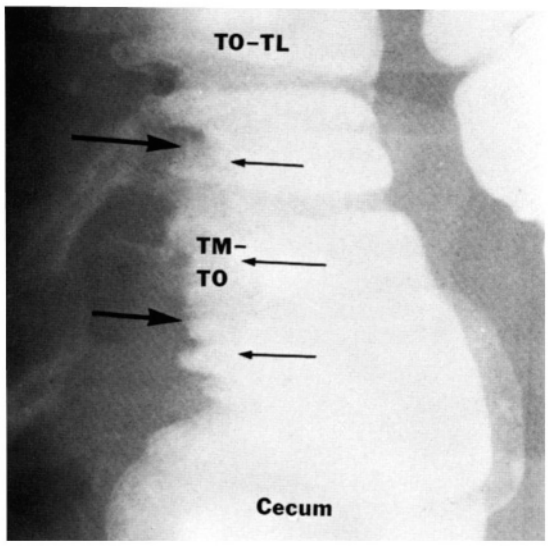


Fig. 15–35. Extraperitoneal appendicitis.
Lateral view. The extraperitoneal nature of the inflammatory process associated with an ascending retrocecal appendix is revealed by the predominant involvement of the TM-TO row *(large arrows).* The posterior border of the TO-TL row is relatively unaffected *(small arrows).*
(Reproduced from Meyers et al.[5])

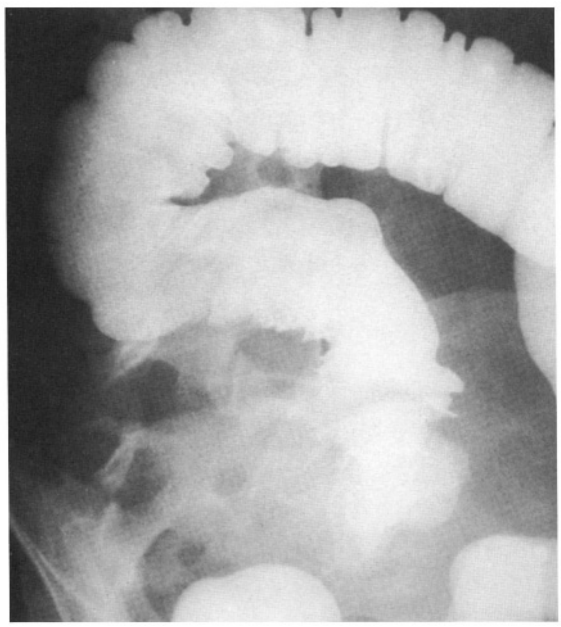
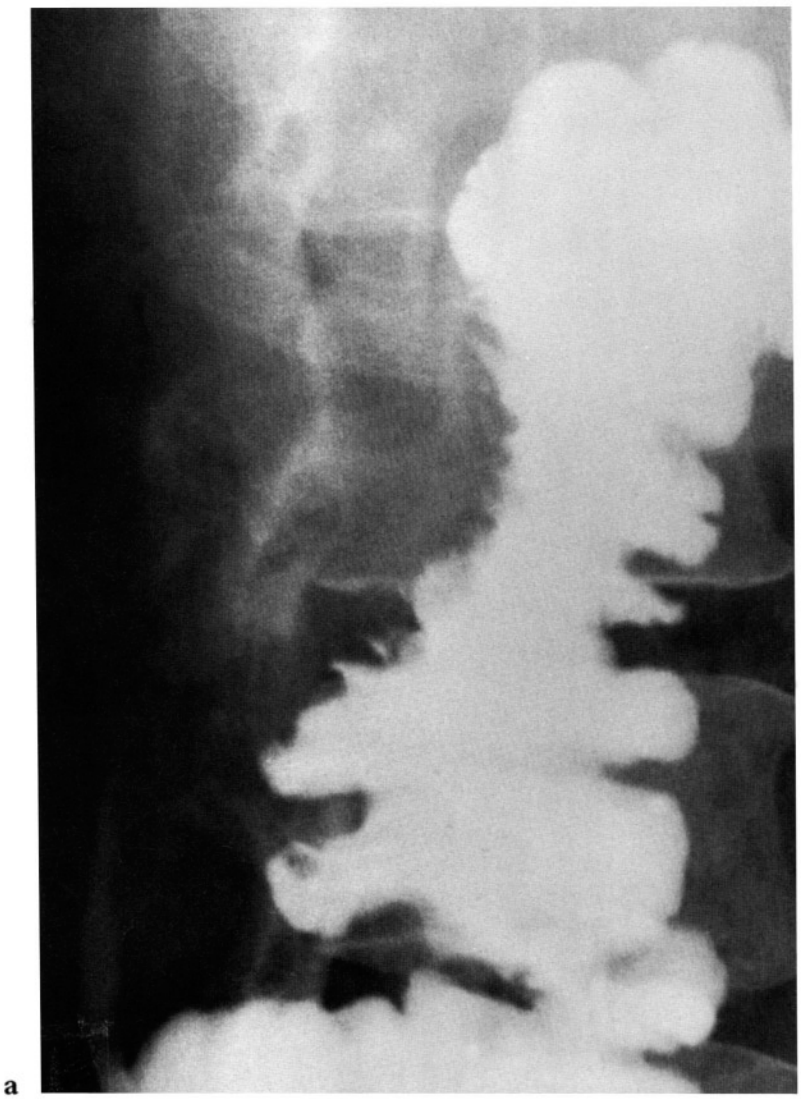


Fig. 15–36. Extraperitoneal appendicitis.
Oblique view of barium enema study demonstrates anterior and medial displacement of the cecum and proximal ascending colon by a large abscess secondary to a perforated retrocecal appendix. The appendix is not opacified, but note the posterior position of the ileocecal valve.

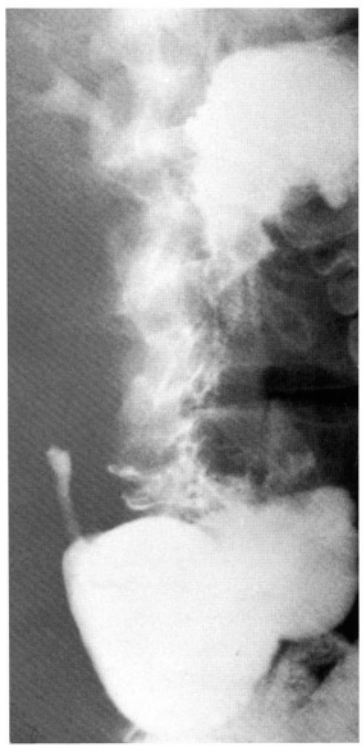
Fig. 15–37. Extraperitoneal appendicitis.
(a) A prominent fixed irregular mass involves the posterolateral contour of the ascending colon, accompanied by some deformity of the opposing haustra.
(b and **c)** Associated inflammatory findings are suggested by the frequent spastic changes, producing further narrowing of the lumen over varying lengths. Minute sinus tracts extend from the tip of an ascending retrocecal appendix.
(Reproduced from Meyers and Oliphant.[11])



a



b



c

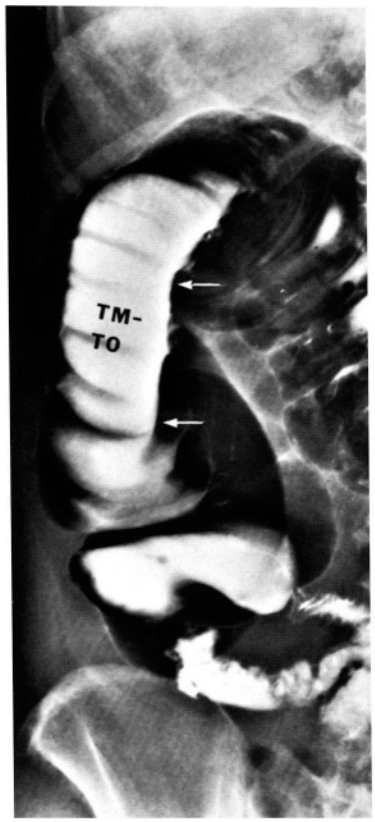


Fig. 15–38. Extraperitoneal appendicitis.
Supine study demonstrates extrinsic flattening of the medial border of the TM-TO haustral row of the ascending colon *(arrows).* This change localizes the primary process to the extraperitoneal space. There is reflux into the terminal ileum but no opacification of the appendix.

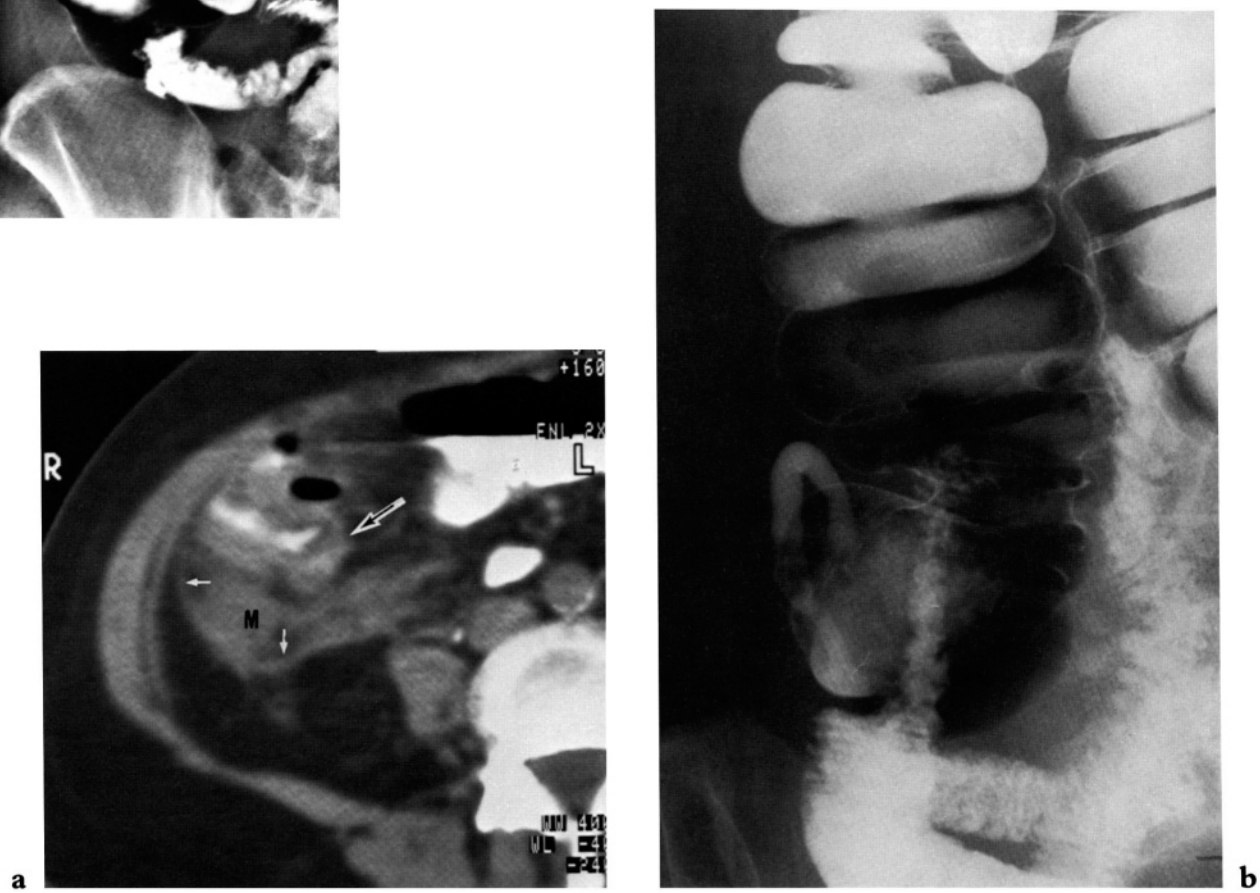


Fig. 15–39. Extraperitoneal appendicitis.
(a) CT demonstrates an inflammatory mass *(M)* in the right anterior pararenal space below the level of the kidney. The ascending colon, filled with oral contrast medium, shows irregular bowel-wall thickening posteriorly due to inflammatory edema *(large arrow).* There is associated thickening of the lateroconal and anterior renal fasciae *(small arrows).*
(b) A barium enema study performed 2 years earlier demonstrates a retrocecal position of the appendix. (Reproduced from Feldberg et al.[16])

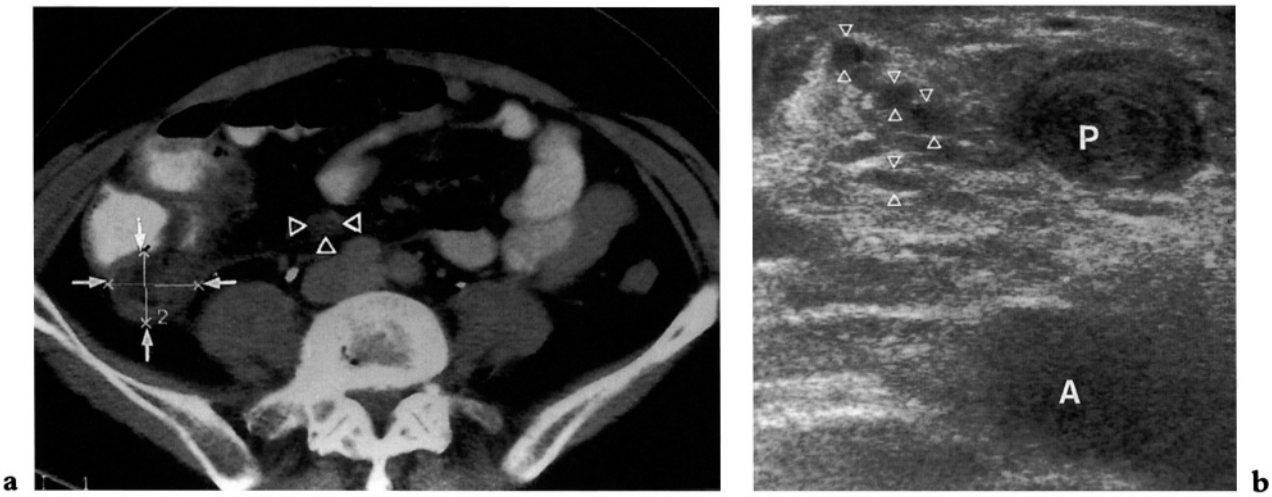


Fig. 15–40. Retrocecal appendiceal abscess and pylephlebitis.
(a) CT reveals an abscess *(arrows)* secondary to a perforated retrocecal appendix and suspicion of thrombosis of the superior mesenteric vein *(arrowheads).*
(b) Transverse intraoperative ultrasound scan shows a thrombosed and thickened extrahepatic portal vein *(P).* Numerous venous collaterals *(paired arrowheads)* are present around the vein in the hepatoduodenal ligament. *A* = abdominal aorta.
(Reproduced from Farin et al.[17])

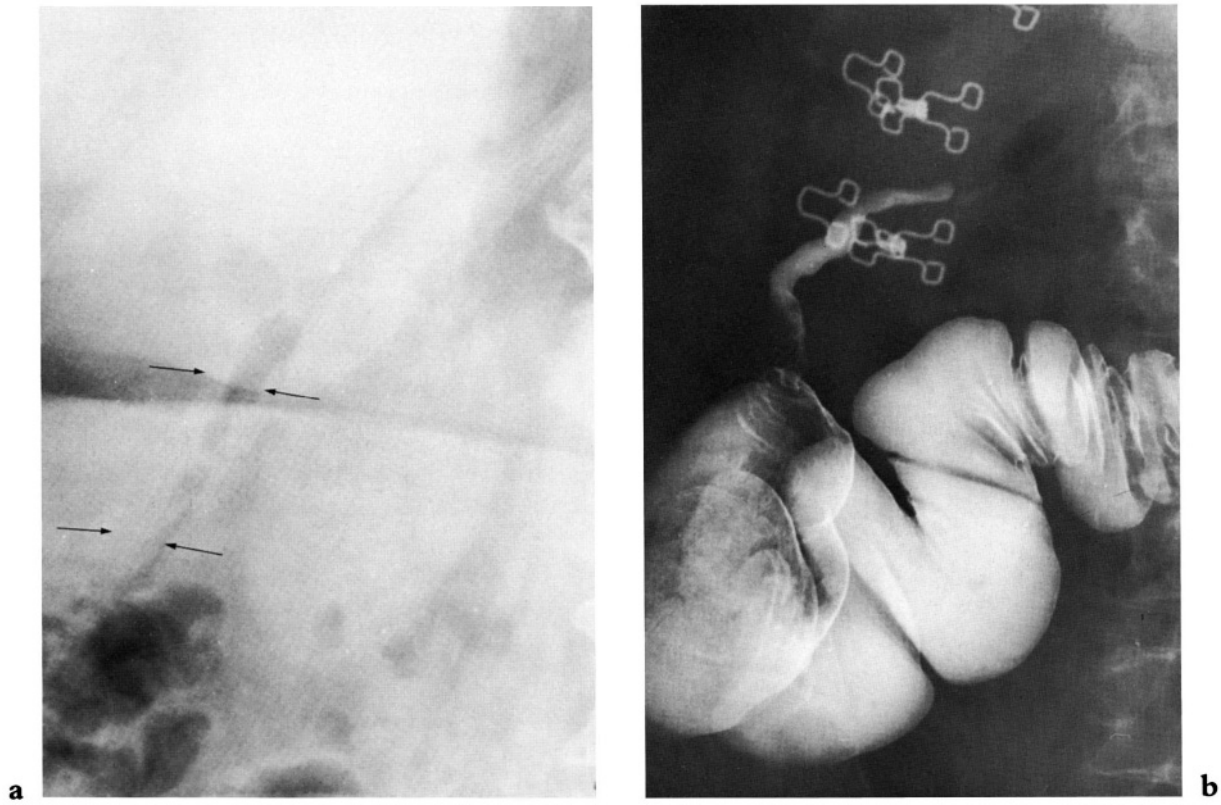


Fig. 15–41. Ascending subhepatic appendix.
(a) Plain film. Tubular radiolucency *(arrows)* is directed superiorly and medially beneath the edge of the liver, anterior to the right kidney.
(b) Barium enema study verifies the position of the appendix and its association with a mobile undescended cecum.
(Reproduced from Meyers and Oliphant.[11])

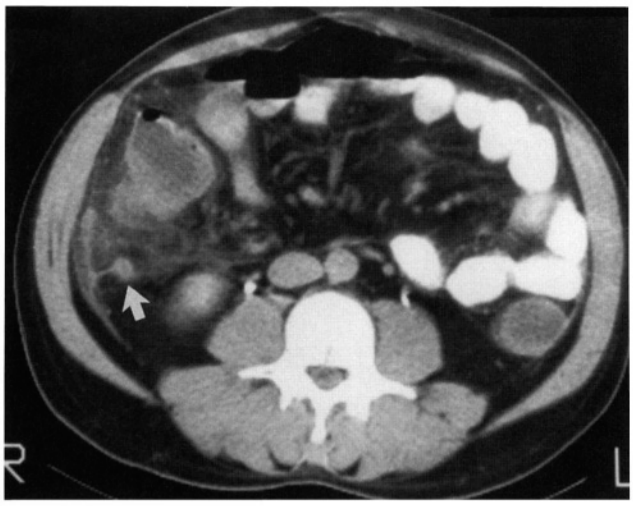


a

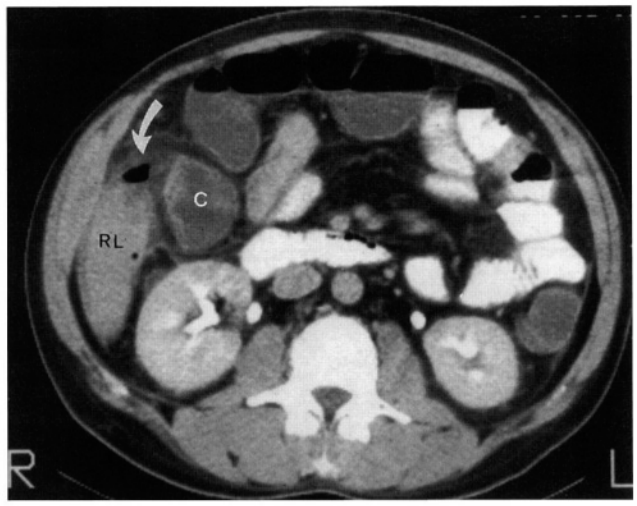


b

Fig. 15–42. Subhepatic ascending appendix.
(a) Barium enema shows a nondescended subhepatic cecum and ascending appendix.
(b) CT displays the position of the retroperitoneal, ascending retrocecal appendix *(arrows)* anterior to the right kidney.
(Reproduced from Feldberg et al.[16])



a



b

Fig. 15–43. Retrocolic appendicitis with subhepatic abscess.
(a) A retrocolic appendix, collapsed and with a thickened wall, is present *(arrow)* along with periappendicular inflammatory changes.
(b) Secondary to perforation of the subhepatic appendix, a collection of air *(arrow)* with associated inflammatory changes has developed beneath the right lobe of the liver *(RL)* lateral to the hepatic flexure of the colon *(C)*.
(Courtesy of Emil Balthazar, M.D., Bellevue Hospital, New York University School of Medicine, New York, NY).

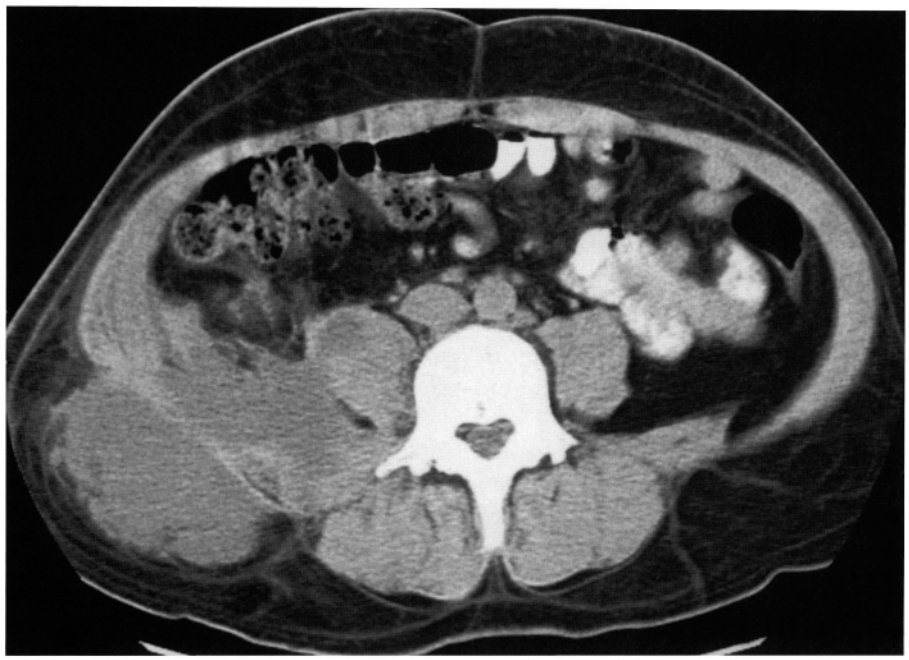


Fig. 15–44. Extraperitoneal appendicitis with abscess formation across Petit's triangle. Fulminant inflammatory changes secondary to perforation of an ascending retrocecal extraperitoneal appendix have led to abscess formation in the right psoas muscle, deep in the flank, and striking extension via Petit's triangle to the subcutaneous tissues.

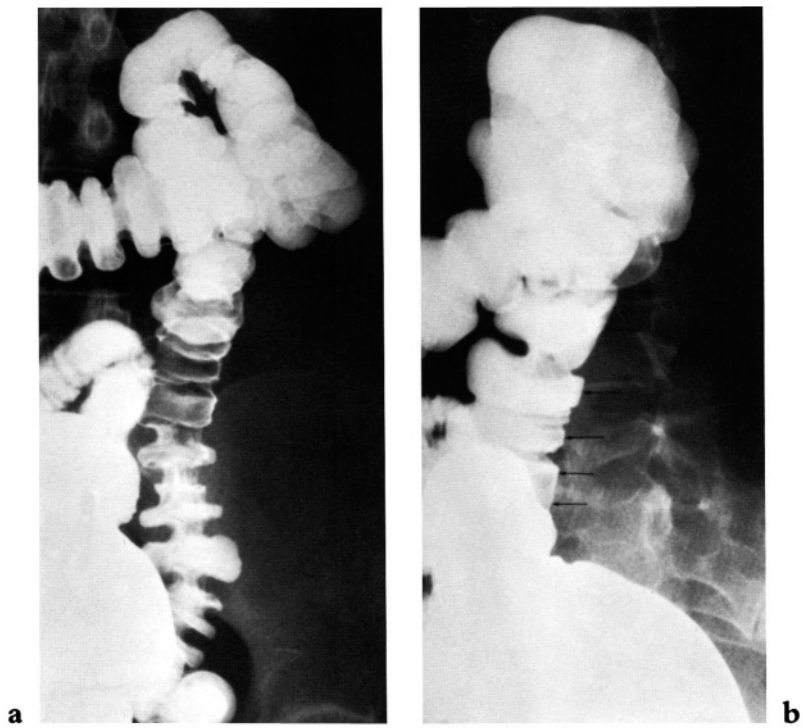


Fig. 15–45. Extraperitoneal hematoma.
(a) The descending colon is medially displaced, but significantly, there is no pressure effect on its lateral TO-TL row.
(b) Oblique view shows some anterior displacement but with definite straightening of the contours of the posterior TM-TO row *(arrows)* by the mass. This finding localizes the mass to the extraperitoneal space and distinguishes it from an intraperitoneal fluid mass occupying the lateral paracolic gutter.
(Reproduced from Meyers et al.[5])

Malignant Seeding

Malignant intraperitoneal seeding, following the pathways of flow of ascitic fluid as described in Chapter 4, tends to localize to the TO-TL row of the ascending colon. Embolic metastases, in accord with the intramural arterial distribution, also tend to develop in the antimesenteric row of haustra.

Duplication of the Colon

Duplications of the colon have a well-developed smooth muscle layer, are lined by colonic mucosa, and are adherent to and often communicate with the large intestine.[18] They typically displace the colon along the mesenteric border and thus lie in relationship to the TM-TL haustral row of the ascending or descending colon and the TM-TO row of the transverse colon (Figs. 15–46 and 15–47). Because the two colons share a common blood supply and in most cases there is only a single mesentery, resection of the supernumerary colon or microcolon is usually impossible.[19,20]

Diverticulosis and Diverticulitis

Colonic diverticula do not arise randomly from the circumference of the large intestine but tend to originate in four distinct rows (Fig. 15–48): (a) on either side of the TM and (b) near the mesenteric borders of the TO and TL.[5,21] These are related to the points of intramural penetration through connective tissue septa of the colonic wall.[21] Their sites of origin from the TM-TL and TM-TO haustra can be identified clearly on routine radiographic studies (Fig. 15–49).

Bona fide diverticula do not arise from the TO-TL antimesenteric row of sacculations. At surgery or autopsy, only pinhead protrusions may be noted occasionally in association with this row, but they are not identifiable on contrast studies, and no clinical significance has been attributed to them. On frontal and even oblique views, diverticula may project laterally from the lower descending and sigmoid colon. This appearance is related to the fact that the TO and TL anatomically approach each other in this region, reducing the dimensions of their intervening haustra. Lateral views, however, consistently show that these diverticula actually arise from the posterior wall (TM-TO).

Colonic Diverticular Angioarchitecture and Hemorrhage

Colonic diverticulosis increases in incidence with each decade of adult life and occurs in as many as 35–50% of individuals over 60 years of age.[22] Diverticula of the large intestine constitute a common source of lower gastrointestinal bleeding, both occult and massive, and are a particularly common cause of right-sided colonic hemorrhage.[21,23,24] Colonic diverticulosis is the most frequent

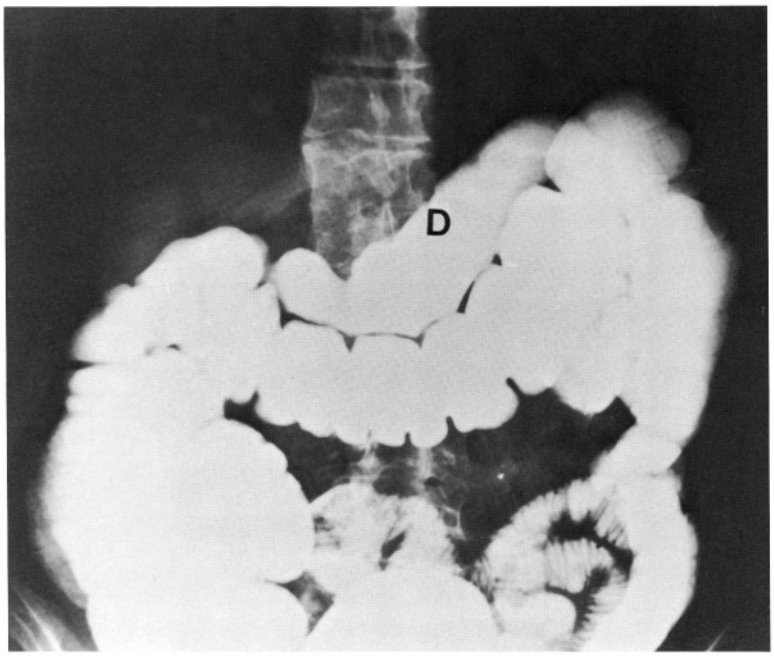


Fig. 15–46. Duplication of colon.
Barium enema study demonstrates a tubular communicating duplication *(D)* within the mesentery of the transverse colon. Its lower border conforms to the superior haustral row of the transverse colon.

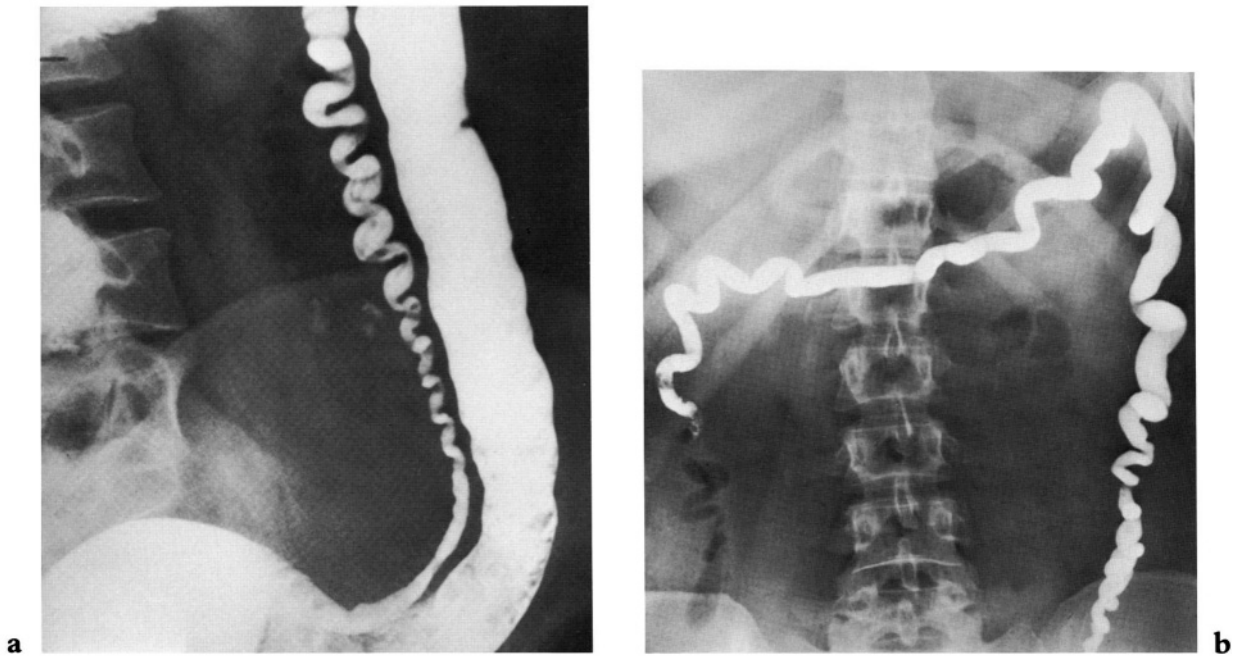


Fig. 15–47. Duplication of colon.
(a) Barium enema study demonstrates a narrow, tortuous duplication in the mesentery of the descending colon.
(b) Following selective opacification of the duplication, the "microcolon" is outlined throughout the mesenteric border of the large intestine, ending blindly at the level of the cecum.
(Reproduced from Beyer et al.[19])

cause of severe rectal bleeding.[25] The hemorrhage is typically acute, massive, and life threatening, in contrast to the mild and often intermittent bleeding secondary to diverticulitis, which apparently originates from highly vascularized granulation tissue lining inflamed diverticula.[26]

Angioarchitecture and Pathogenesis of Bleeding. Meyers et al. have defined the characteristic angioarchitecture of colonic diverticula[21] and shown their structural predisposition to massive bleeding.[27,28] The four distinct longitudinal rows from which diverticula arise (Fig. 15–50) correspond closely with the four sites of penetration of

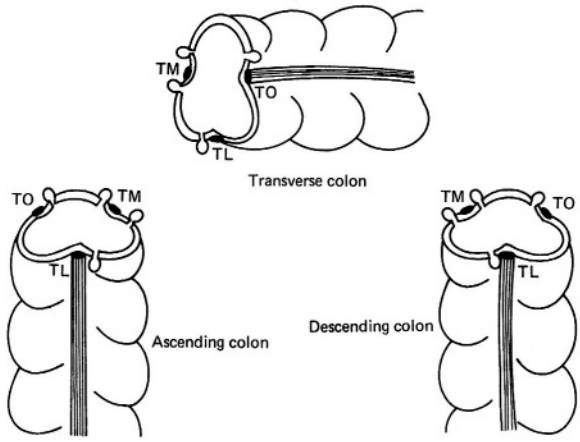


Fig. 15–48. Sites of origin of colonic diverticula.
Note that the antimesenteric TO-TL haustral row does not give rise to diverticula.
(Reproduced from Meyers et al.[5])

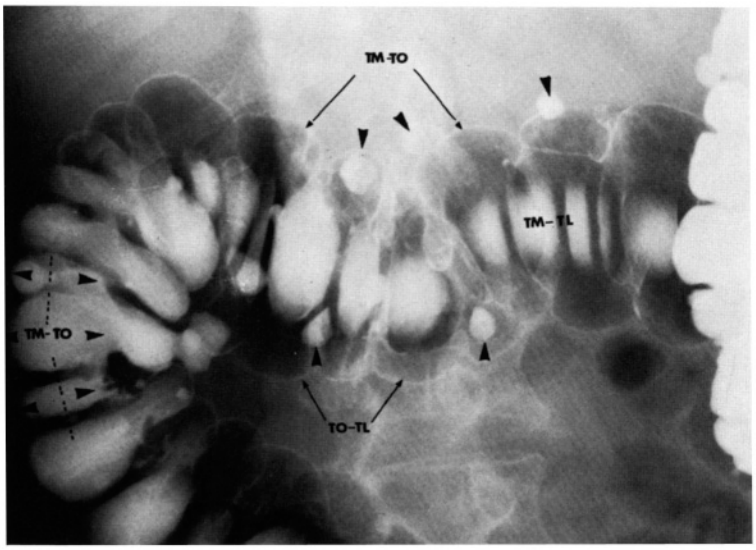


Fig. 15–49. Diverticula *(arrowheads)* arise from the TM-TO and TM–TL rows, but none originates from the antimesenteric TO-TL haustra. (Reproduced from Meyers et al.[5])



Fig. 15–50. Photograph of descending colon showing multiple diverticula *(D)* arising in a row adjacent to a taenia *(T).*
(Reproduced from Meyers et al.[21])

the major branches of the vasa recta, the colonic branches of the marginal artery (Fig. 15–51).

Injection studies have shown that a prominent long vasa recta courses in an intimate subserosal position over the dome of every colonic diverticulum (Figs. 15–52 and 15–53a) to reappear as either a single or multiple submucosal branches along the antimesenteric side of its orifice (Fig. 15–53b). Rather than the point of vascular penetration directly leading to a weakness (locus minoris resistentiae) in the bowel wall predisposing to the formation of diverticula,[29] we have shown that it is the obliquely oriented connective-tissue septa separating the circular smooth muscle bundles of the colonic walls that constitute the common plane of least resistance. It is clearly through these septa that both the vasa recta consistently penetrate the colonic wall from the serosa to the submucosa (Fig. 15–54) and the diverticula form from mucosal protrusions.[21] Segmentation of the colon produced by muscular contraction leads to localized increased intraluminal pressure that results in herniation

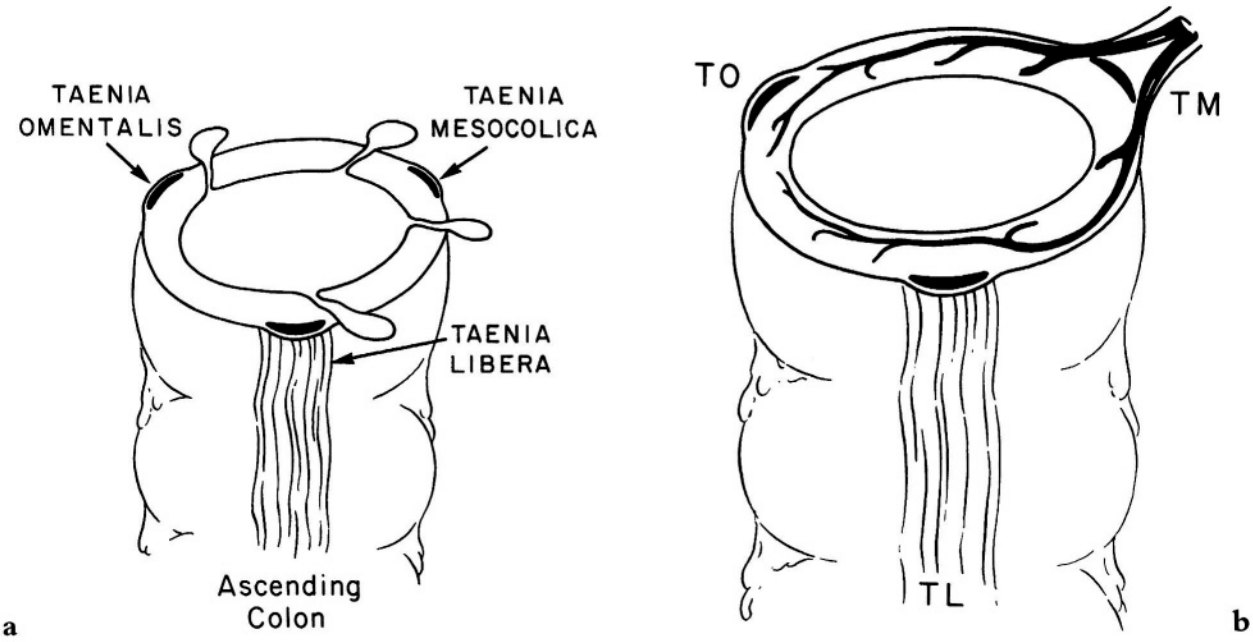


Fig. 15–51. (a) Sites of origin of colonic diverticula in relation to taenia.
Diverticula point toward mesenteric border.
(b) Intramural blood supply of colon.
Vasa recta reach bowel wall and divide into long subserosal branches that then penetrate obliquely through bowel wall. Short branches penetrate near the taenia mesocolica *(TM).* They continue in submucosa, finally ramifying into rich plexus.
(Reproduced from Meyers et al.[27])

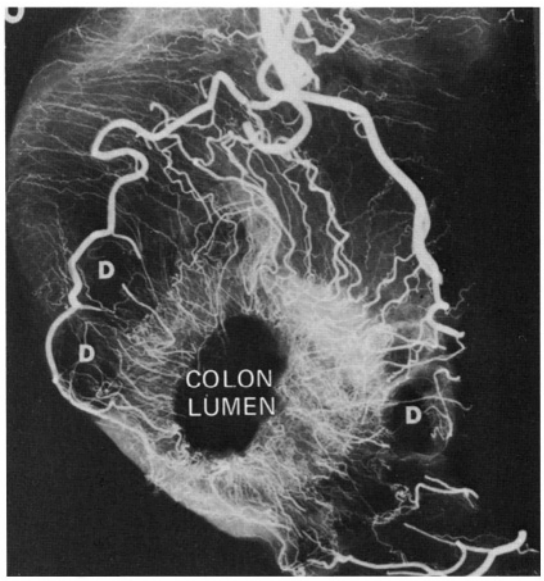


Fig. 15–52. Radiograph of sigmoid colon with injected arterial supply.
The circumferential branches of the vasa recta are deflected immediately over the domes of diverticula *(D),* and short branches of these are displaced around their necks.
(Reproduced from Meyers et al.[21])

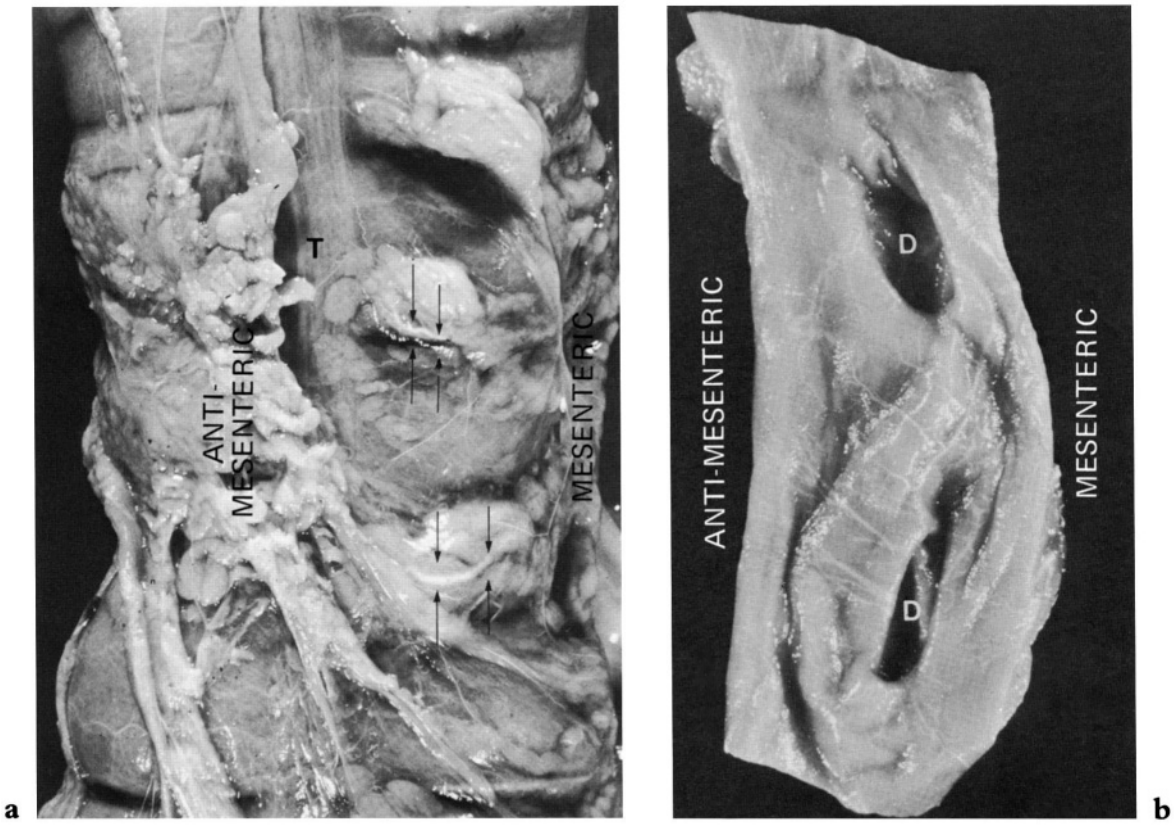


Fig. 15–53. Gross vascular relationships of colonic diverticula.
(a) Photograph of serosal surface of ascending colon. Prominent injected vasa recta *(arrows)* course from the mesenteric side on the right over the domes of two diverticula. In penetrating the colonic wall, they disappear from view on the antimesenteric borders of the diverticula, near a taenia *(T)*.
(b) Enlarged photograph of the mucosal surface of two diverticula. The branches of the injected vasa recta reappear in the submucosa on the antimesenteric side of the orifices of the diverticula *(D)*.
(Reproduced from Meyers et al.[21])

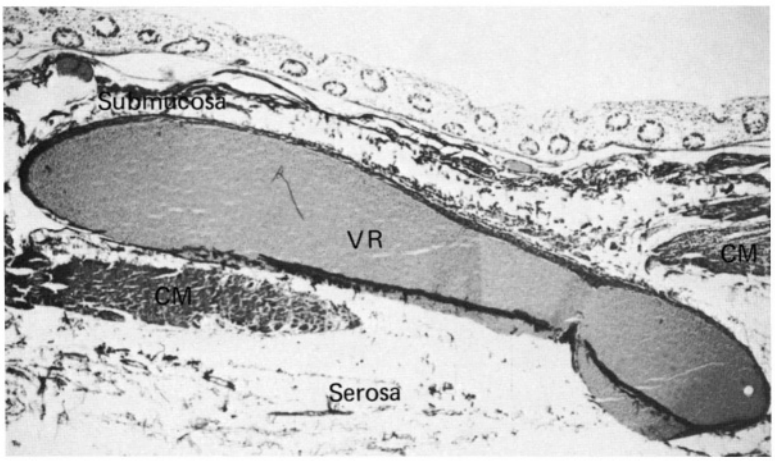


Fig. 15–54. Penetration of vasa recta *(VR)* from serosa to submucosa.
Transverse histologic section shows that it occurs through a widened, obliquely oriented connective-tissue cleft between fascicles of circular muscle *(CM)*.
(Reproduced from Meyers et al.[21])

of mucosa and submucosa through these natural weaknesses in the colonic wall.[30,31]

These anatomic relationships result in a remarkably constant angioarchitecture of colonic diverticula (Figs. 15–55 and 15–56). An artery of considerable relative size, the vas rectum, intimately courses in the serosa over the dome of the diverticulum; at this point, it is separated from the lumen of the diverticulum by only mucosa and a few strands of attenuated muscle fibers. The vas rectum then penetrates the colonic wall along the antimesenteric margin of the diverticulum, lying close to its neck and orifice.

The pathogenesis of massively bleeding diverticulosis is primarily determined by their distinctive angioarchitecture.[27,28] Histologic changes at the precise site of bleeding show asymmetric rupture of the vas rectum

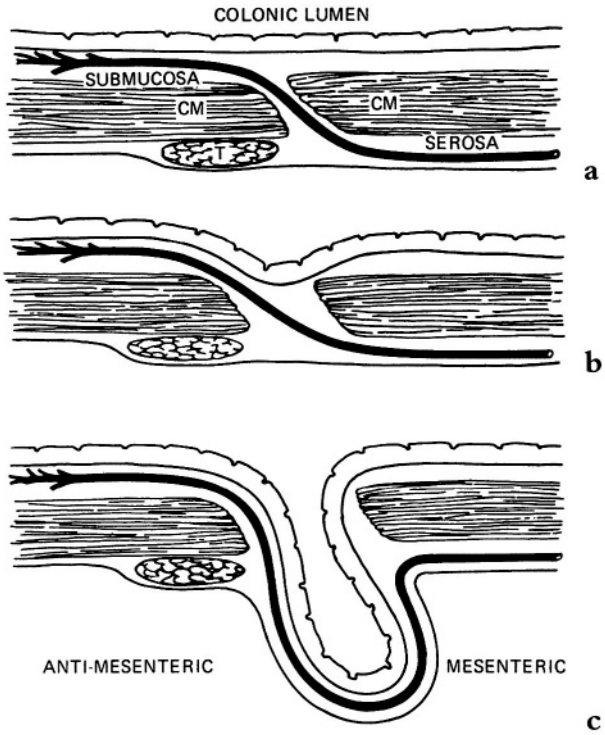


Fig. 15–55. Structural dynamics of diverticular formation and vascular relationships.
(a) The vas rectum normally penetrates the colonic wall from the serosa to the submucosa through an obliquely oriented connective-tissue septum in the circular muscle *(CM).* This occurs near the mesenteric side of a taenia *(T).*
(b) The mucosal protrusion marking the development of a diverticulum occurs through, and consequently widens, the connective-tissue cleft. In doing this, it begins to lift up the artery.
(c) With transmural extension of the diverticulum, the vas rectum is displaced over its dome and therefore penetrates to the submucosa on the antimesenteric border of its neck and orifice.
(Modified from Meyers et al.[21])

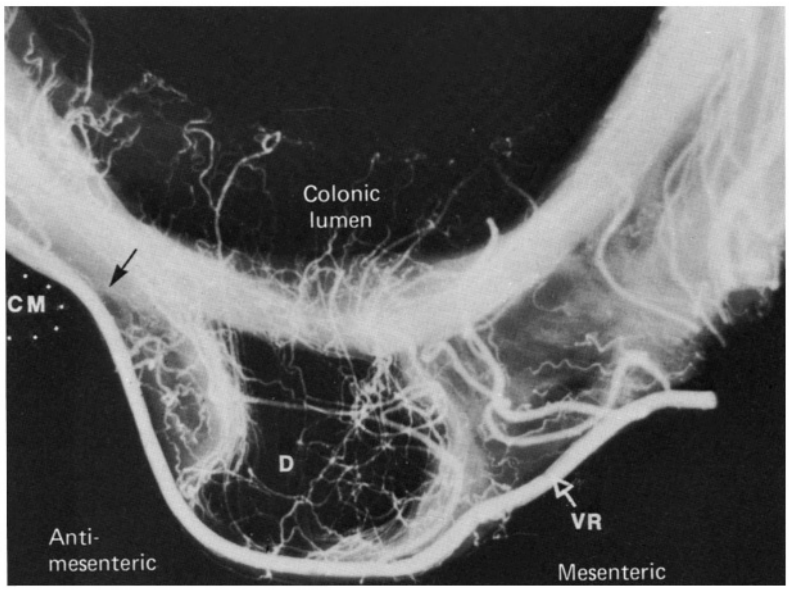


Fig. 15–56. Characteristic angioarchitecture of colonic diverticula.
Radiograph of colonic diverticulum with injected vas rectum. The vas rectum *(VR)* approaches the diverticulum *(D)* from its mesenteric border, arches in the serosa immediately over its dome, and penetrates the colonic wall on its antimesenteric margin *(arrow). CM* designates the approximate location of circular muscle. (Original magnification, ×8.)
(Modified from Meyers et al.[21])

toward the lumen of the diverticulum precisely at its dome or antimesenteric margin. The changes are associated with conspicuous eccentric intimal thickening of the vas rectum, often with medial thinning and duplication of the internal elastic lamina (Figs. 15–57 through 15–59). The mechanism involves injurious factors arising within the diverticular or colonic lumen that induce eccentric intimal proliferation and weakening of the associated vasa recta, predisposing to rupture and massive bleeding (Fig. 15–60). It is important to recognize that

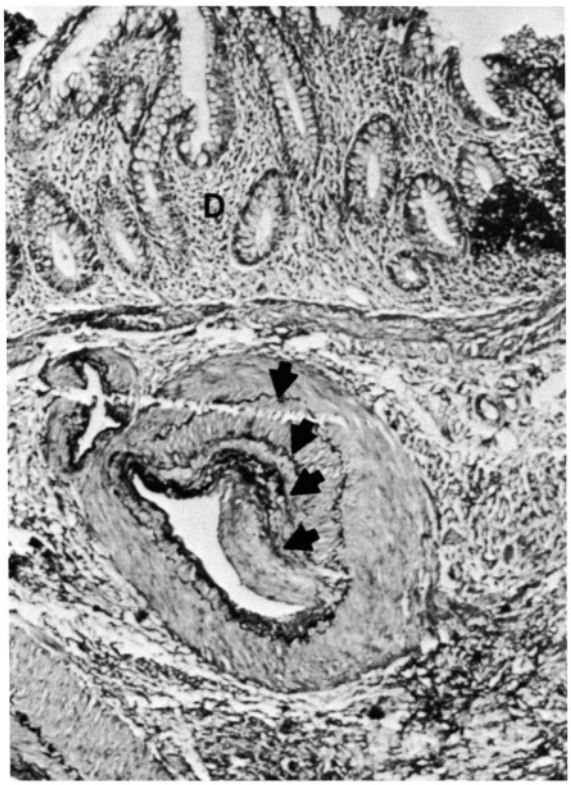


Fig. 15–57. Eccentric mural changes in vas rectum in case of bleeding diverticulum.
Vas rectum in area of hemorrhage demonstrates duplication of internal elastic lamina *(arrows)* with lamellar arrangement and marked eccentric thickening of intima. *D* = mucosa of diverticulum. (Elastic van Gieson; original magnification, ×65.)
(Reproduced from Meyers et al.[28])

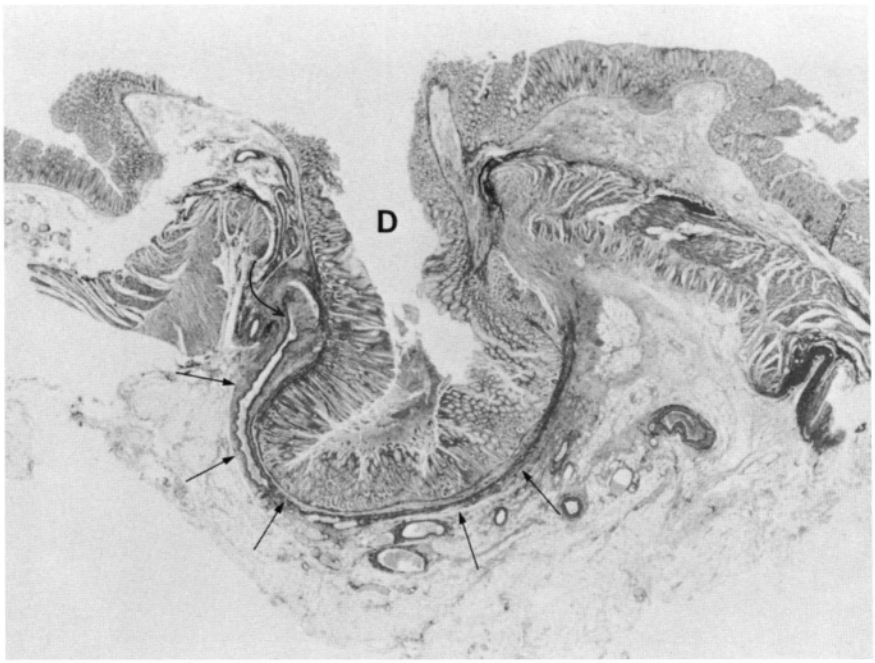


Fig. 15–58. Histologic section through the bleeding point in a case of colonic diverticular hemorrhage.
The vas rectum *(arrows)* courses over the dome of the diverticulum from the right, extends along its antimesenteric margin, and has ruptured *(curved arrow)* near the neck of the diverticulum. (Elastic van Gieson; original magnification, ×65.)
(Reproduced from Meyers et al.[28])

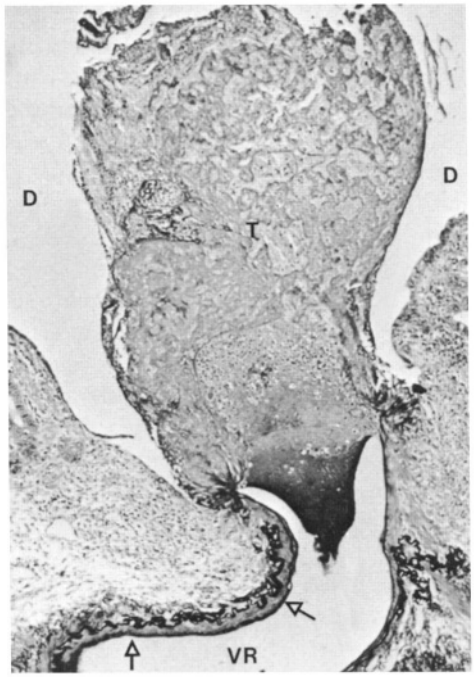


Fig. 15–59. Histologic section through the bleeding point in a case of colonic diverticular hemorrhage.
A thrombus *(T)* projects from the lumen of the ruptured vas rectum *(VR)* through a small mucosal erosion into the lumen of the diverticulum *(D).* The vas rectum shows marked intimal thickening *(arrows)* that is visible deep to the darkly stained internal elastic lamina. The thickening is strikingly eccentric toward the lumen of the diverticulum, and the media of the artery is absent in this area. (Elastic van Gieson; original magnification, ×65.)
(Reproduced from Meyers et al.[28])

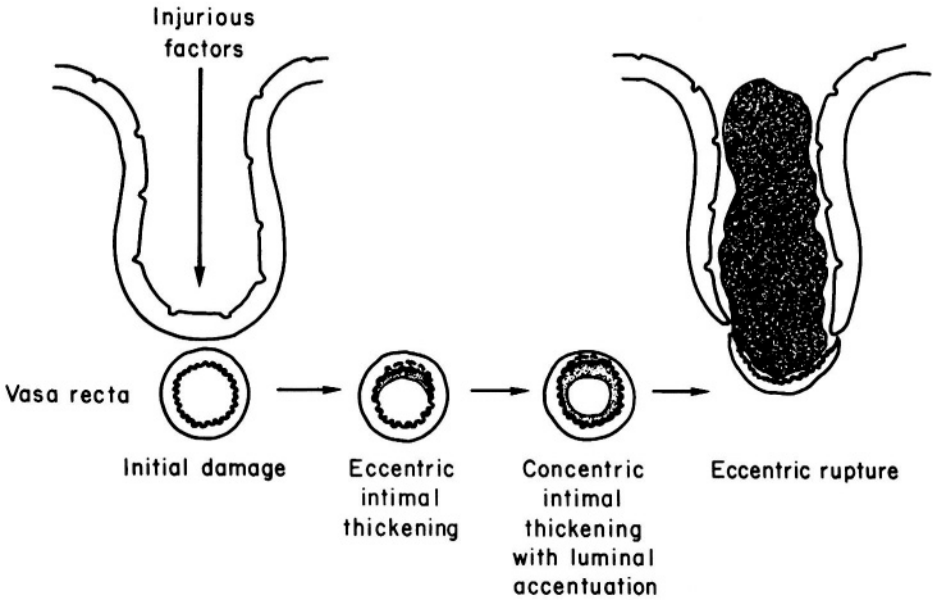


Fig. 15–60. Pathogenesis of colonic diverticular hemorrhage.
Progressive eccentric changes weaken the wall of the vas rectum, which finally ruptures into the lumen of the diverticulum.
(Reproduced from Meyers et al.[28])

smooth muscle cells of the media develop the intimal layer, so that intimal proliferation results in attenuation and weakening of the muscular component of the vas rectum. This explains why rectal hemorrhage, rather than intraperitoneal or extraperitoneal bleeding, is a consequence of this condition.

The predominance of hemorrhage from right-sided diverticula is noteworthy since the majority of diverticula are located in the descending and sigmoid colon, and only about one-third of patients with diverticulosis have diffuse involvement of the large intestine. One anatomic feature distinguishes right-sided from left-sided diverticula, which may explain their increased frequency of bleeding. Because the diverticula arising in the right colon have wider necks and domes, their vasa recta are exposed over a greater length to injurious factors arising from the colon.[27,28]

Arteriographic Diagnosis and Management. In the diagnosis and management of massive diverticular hemorrhage, the primary problem is accurate localization of the bleeding point. Selective arteriography may readily accomplish this, allowing a trial of nonoperative control of hemorrhage by infusion of vasopressin, permitting more specific and limited colonic resection when bleeding is uncontrolled or recurrent.[24,32,33] Extravasation is shown in virtually all cases of acutely bleeding diverticula[23,24] as a circular accumulation of the contrast medium within the confines of the diverticulum (Fig. 15–61) that, in the presence of extremely brisk bleeding, may overflow to opacify the lumen of one or several haustral sacculations. The feeding vas rectum itself can be identified and, at times, its precise point of rupture[21] (Fig. 15–61).

Vasoconstrictive therapy immediately following arteriographic diagnosis and localization provides an effective method that may make operation avoidable.[23,32,33]

Bleeding may recur within hours or days of the initial control,[23,33] but the temporary cessation of bleeding provides time for stabilization of the patient's clinical condition before segmental colectomy. Occasionally, rebleeding has been encountered within several months,[23] which may be a consequence of dislodgment of the thrombus that characteristically extends into the lumen of the diverticulum.[21,27,28] Recurrent bleeding from a second distant diverticulum has been documented only rarely.[34]

If vasopressin fails to control diverticular bleeding in a patient who is a poor surgical risk, embolization of the bleeding artery may be carried out,[34] but this incurs the risk of potential ischemic injury to the colon[35,36] because of the relative lack of collateral blood supply.

Colonoscopic treatment by bipolar electrocoagulation of the identified bleeding vessel in the neck of the diverticulum[37] or by peridiverticular epinephrine injection[38] has been recently reported.

Diverticulitis

The majority of diverticula are related to extraperitoneal tissues (Fig. 15–48). Diverticulitis may thus result in a localized inflammatory process involving only the TM-TL or TM-TO haustra (Fig. 15–62). Mesenteric abscesses and extraperitoneal gas or abscesses are well-

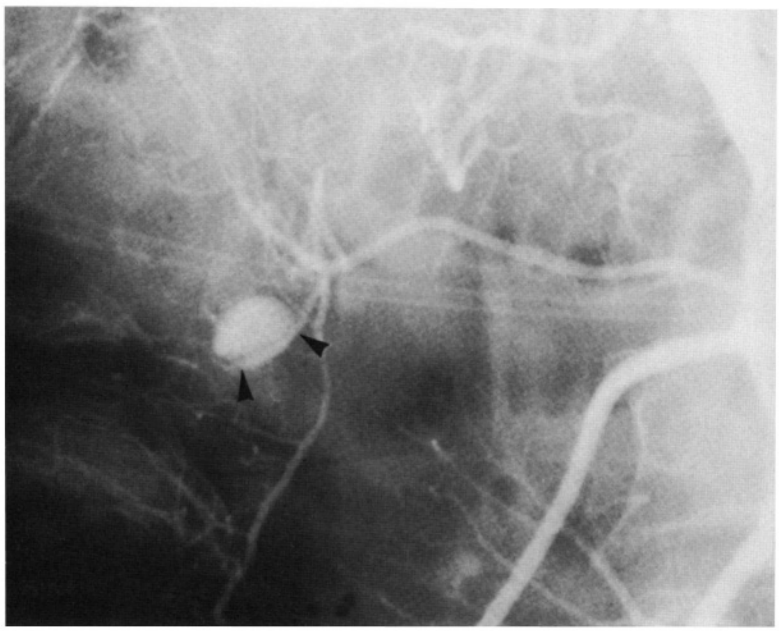


Fig. 15–61. Extravasation into an acutely bleeding right colon diverticulum shown by selective superior mesenteric arteriography.
A vas rectum *(arrowheads)* courses typically over the dome of the diverticulum and appears intact in this segment, indicating its point of arterial rupture to be on the antimesenteric margin of the diverticulum.
(Reproduced from Meyers et al.[21])

recognized complications of diverticulitis[39] (Fig. 15–63). Many cases of intestinovesical fistulas are secondary to extraperitoneal extension of an inflammatory or suppurative process from the diverticulum and then perforation through the base of the urinary bladder (Fig. 15–64). Rarely, communication from a perforated diverticulum may be established to the inferior mesenteric venous drainage, leading to intrahepatic portal venous gas[40] (Figs. 15–65 and 15–66). Furthermore, the absence of diverticular origin from the lateral haustral rows facing

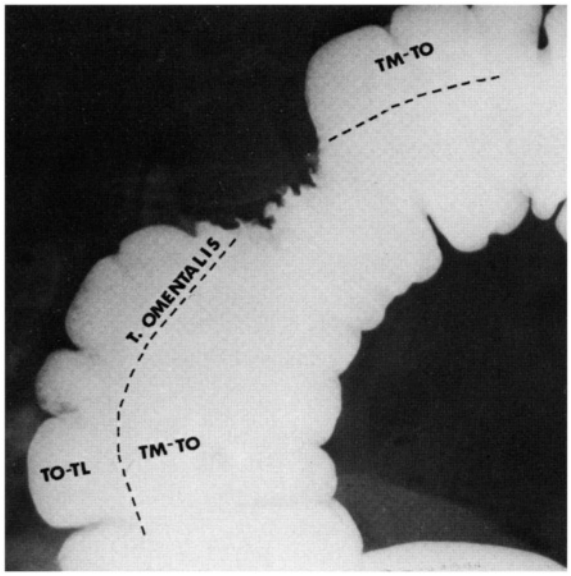


Fig. 15–62. Diverticulitis of the hepatic flexure.
Left posterior oblique projection. Localized inflammatory changes involve the TM-TO haustra.
(Reproduced from Meyers et al.[5])

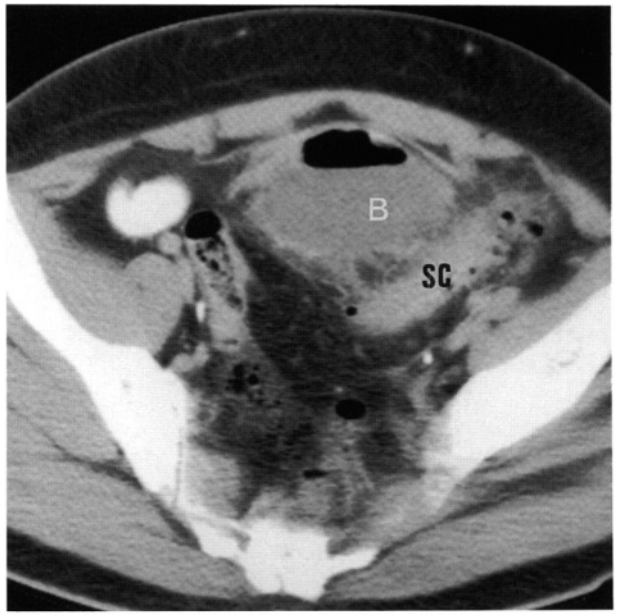


Fig. 15–64. Sigmoid diverticulitis with fistulization to urinary bladder.
CT documents inflammatory adherence of the sigmoid colon *(SC),* demonstrating mural thickening and several gas containing diverticula to the urinary bladder *(B),* which has air in its lumen.



a



b

Fig. 15–63. Extraperitoneal diverticular abscess.
(a) Gas-containing diverticular abscess *(A)* is characteristically localized to the extraperitoneal fatty tissue within the pelvis, having arisen from **(b)** underlying diverticula-bearing sigmoid colon involved with circular muscle hypertrophy.

the intraperitoneal lateral paracolic gutters provides an explanation for the low incidence of subhepatic and subphrenic abscesses secondary to diverticulitis. Thus, localized involvement of the TO-TL haustra alone cannot be secondary to diverticulitis. Inflammatory reaction of these haustra consequent to diverticulitis affecting one or both of the mesenteric rows indicates an extensive paracolic abscess.

Diverticulitis Complicating Granulomatous Colitis

Granulomatous colitis (Crohn's disease of the colon) is not unusual in patients over the age of 50 years and may affect any segment of the colon. The sigmoid colon is involved in 72% of primary Crohn's colitis and in 35% of granulomatous ileocolitis.[42] Diverticulosis is also

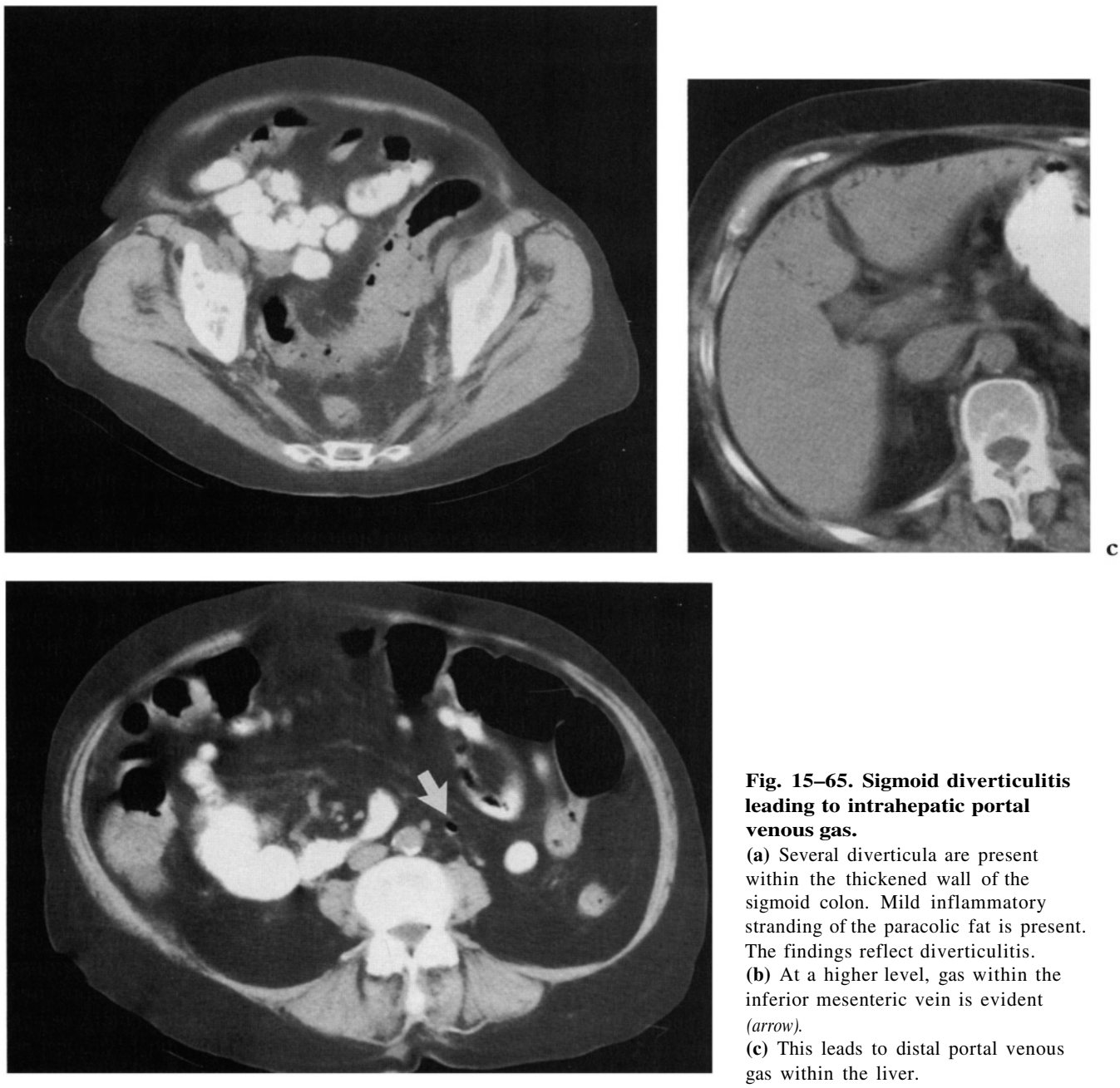


Fig. 15–65. Sigmoid diverticulitis leading to intrahepatic portal venous gas.
(a) Several diverticula are present within the thickened wall of the sigmoid colon. Mild inflammatory stranding of the paracolic fat is present. The findings reflect diverticulitis.
(b) At a higher level, gas within the inferior mesenteric vein is evident *(arrow).*
(c) This leads to distal portal venous gas within the liver.

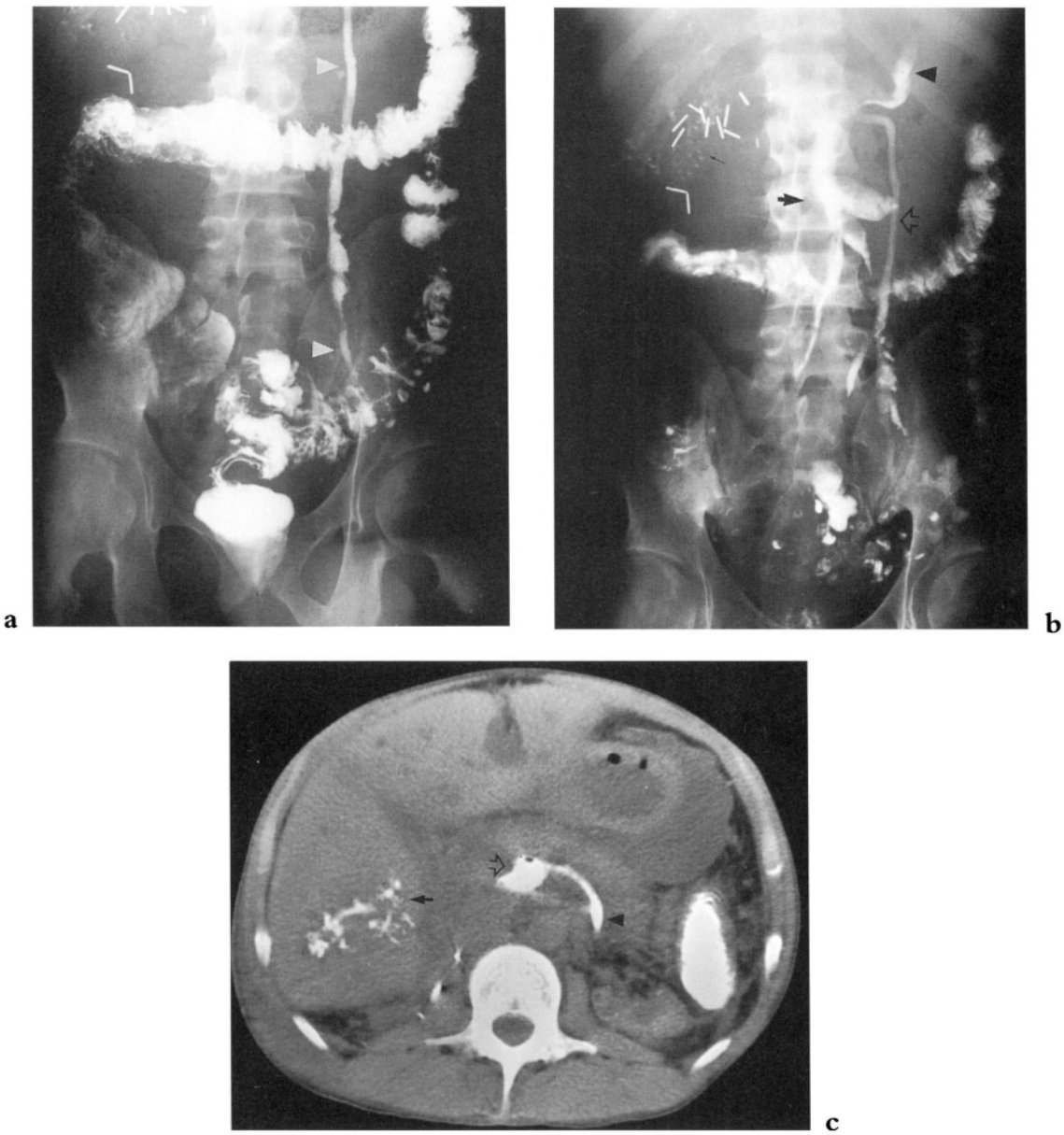


Fig. 15–66. Colovenous fistula complicating sigmoid diverticulitis.
(a) Abdominal radiograph following an attempted barium enema study demonstrates opacification of a long linear structure in the left abdomen, representing the inferior mesenteric vein *(arrowheads).* Multiple sigmoid diverticula are present.
(b) A delayed film reveals barium within the inferior mesenteric vein *(open arrow),* splenic vein *(arrowhead),* the superior mesenteric vein *(large arrow),* and portal venous radicles *(small arrow).*
(c) Noncontrast CT shows barium entering the splenic vein from the inferior mesenteric vein *(arrowhead),* passing into the portal venous confluence *(open arrow),* and within portal venous radicles in the right hepatic lobe *(closed arrow).*
(Reproduced from Rossman and Burr.[41])

common in this age group, particularly involving the sigmoid colon. The clinical and radiologic difficulty in distinguishing between segmental granulomatous colitis and diverticulitis has been described.[43,44] Clinically, either may present with pain, partial obstruction, a lower abdominal mass, rectal bleeding, fever, and leukocytosis. Often, however, "the diagnostic problem is not primarily the distinguishing of Crohn's colitis from diverticular disease, but recognizing when the diseases coexist."[45] I have shown, however, that the relationship is not one of chance coexistence, but rather that the involvement of diverticula by granulomatous colitis causes a 2- to 10-fold increased incidence of diverticulitis.[46]

Granulomatous colitis is characterized by transmural inflammation, mucosal ulceration, and fissuring of the bowel wall, typically accompanied by the presence of a granulomatous tissue response.[47] In contrast, diverticulitis results from a microperforation or macroperforation of a diverticulum with sequelae such as deep sigmoiditis, perisigmoiditis (peridiverticulitis), or frank peritonitis.[48]

Because diverticula represent protrusions of mucosa and submucosa into and through the bowel wall, their involvement by Crohn's disease facilitates the transmural extension and paracolic complications of this disease process. The mucosal lining of diverticula may be the site of giant cell granulomas (Fig. 15–67) and aphthous ulcerations overlying lymphoid follicles, which may extend as dissecting intramural tracts (Fig. 15–68) and lead to the formation of pericolic abscesses.

The radiologic signs of peridiverticulitis complicating granulomatous colitis usually show clear evidence of the underlying pathologic changes. These include (a) the presence of aphthous ulcers, superficial ulcerations overlying areas of lymphoid hyperplasia, within diverticula that may indicate a predisposition to their rupture (Fig. 15–69); (b) localized diverticular perforation, perhaps with multiple communications (Figs. 15–70 and 15–71); and (c) mass pressure on the sigmoid colon from the paracolic abscess. Any extraluminal longitudinal sinus tract is thus almost invariably on the mesenteric border of the colon (Fig. 15–72).

Based on these histologic and radiologic observations, the pathogenic mechanisms of diverticulitis complicating granulomatous colitis are established (Fig. 15–73):

1. The earliest lesion of Crohn's disease is lymphoid hyperplasia followed by superficial ulceration.[49,50] When this type of aphthous ulcer involves the mucosa of a diverticulum, it may undergo infection to result in peridiverticulitis.
2. The deep fissuring characteristic of Crohn's disease may establish communication with one or several diverticula that may then be followed by peridiverticulitis and/or abscess formation.
3. A paracolic abscess secondary to transmural fissuring ulcerations of severe Crohn's disease may penetrate through the domes of adjacent diverticula with further dissecting peridiverticulitis.

Summary

Table 15–1 summarizes the basic features that enable identification of the specific haustral rows and the most

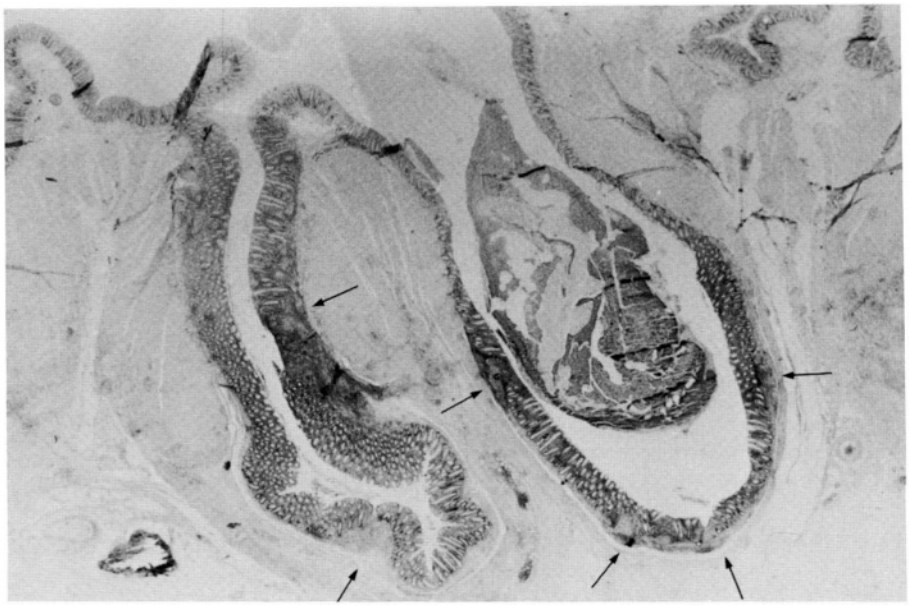


Fig. 15–67. Diverticular involvement by Crohn's disease.
Noncaseating granulomas *(arrows)* involve the mucosa of two sigmoid diverticula. (Original magnification, × 8.) (Reproduced from Meyers et al.[46])



Fig. 15–68. Diverticular involvement by Crohn's disease.
Dissecting intramural tract *(arrows)* extends from ulcerated diverticulum *(D).* (Original magnification, ×18.) (Reproduced from Meyers et al.[46])



Fig. 15–69. Granulomatous colitis with ulcerated diverticulosis.
Aphthous ulcerations are present within two diverticula *(arrows)* adjacent to a localized area of colonic mural induration containing minute mucosal ulcerations. (Reproduced from Meyer et al.[46])

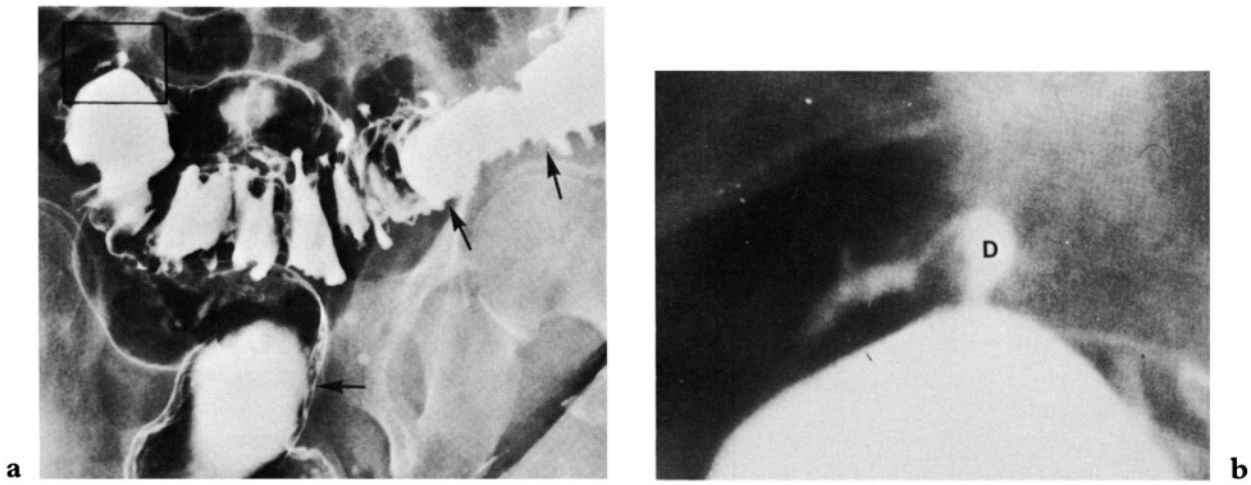


Fig. 15–70. Diverticulitis complicating granulomatous colitis.
(a) Crohn's disease is evident by the indentation and ulceration on the left side of the rectum and the gross changes in the proximal sigmoid colon *(arrows).* Multiple diverticula are present.
(b) Enlargement of boxed area shows 8 × 1 mm sinus tract penetrating from a sigmoid diverticulum *(D).* (Reproduced from Meyers et al.[46])

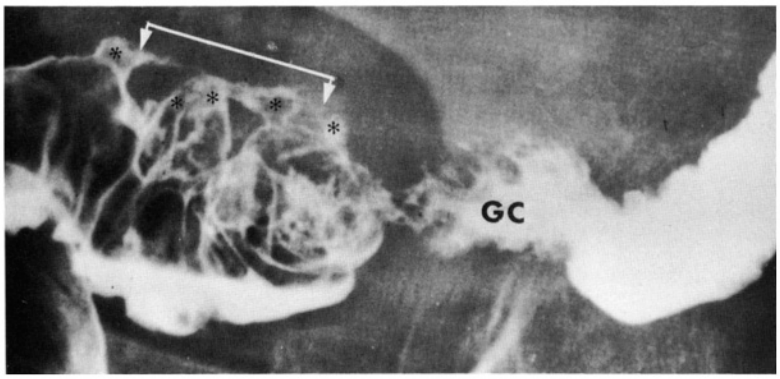


Fig. 15–71. Diverticulitis complicating granulomatous colitis.
A 4.5-cm sinus tract *(bracket)* in the paracolic tissues communicates with five sigmoid diverticula *(asterisks).* The surrounding abscess produces a mild mass impression on the colon. Proximally, granulomatous colitis is shown by a narrowed lumen and a grossly distorted mucosa with multiple ulcerations *(GC).*
(Reproduced from Meyers et al.[46])

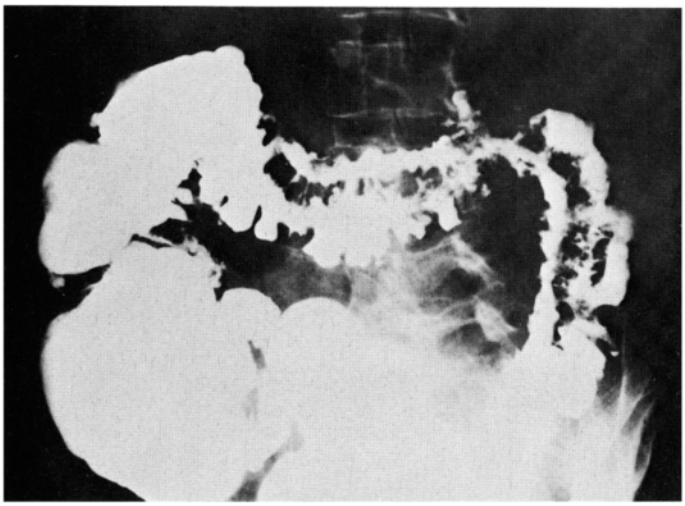


Fig. 15–72. Granulomatous colitis with extraluminal longitudinal sinus tract.
An extremely long continuous tract follows the mesenteric border of the sigmoid, descending, and transverse colon. It can be presumed that this striking paracolic localization is due to the communicating form of peridiverticulitis as a consequence of involvement by Crohn's disease.
(Reproduced from Marshak et al.[43])

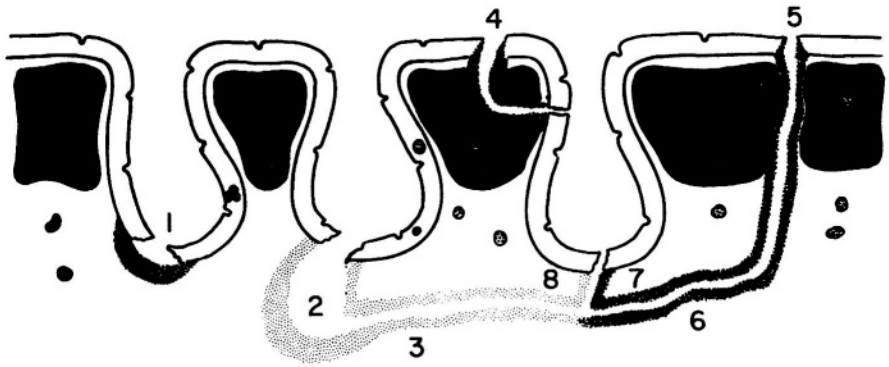


Fig. 15–73. Pathogenesis of diverticulitis complicating granulomatous colitis.
An aphthous ulcer involving the mucosal lining of a diverticulum *(1)* may lead to perforation, with the formation of a peridiverticular abscess *(2).* This may then extend as a longitudinal paracolic sinus tract *(3).* A fissuring ulcer of granulomatous colitis may directly perforate into a diverticulum *(4).* Complete transmural fissuring *(5)* may result in an abscess, deep to the muscularis propria, which may take the form of a longitudinal sinus tract *(6).* Perforation of the domes of diverticula with peridiverticulitis may occur secondary to extension from either granulomatous colitis *(7)* or dissecting diverticulitis *(8).*
(Reproduced from Meyers et al.[46])

Table 15–1 Haustra Anatomy and Pathology

	Ascending and descending colon			Transverse colon		
	TM-TO	TO-TL	TM-TL	TM-TO	TO-TL	TM-TL
Position	Posterior	Lateral	Medial	Superior	Inferior	Posterior
Major relationship	Extraperitoneal structures	Lateral paracolic sulcus	Medial paracolic sulcus	Gastrocolic ligament (stomach, lesser sac)	Greater omentum, anterior abdominal wall	Transverse mesocolon (pancreas)
Outlining on double-contrast studies						
Supine	Barium	Air	Air	Air	Air	Barium
Prone	Air	Barium	Barium	Barium	Barium	Air
Gross designation		Antimesenteric border	Mesenteric border	Mesenteric border	Antimesenteric border	
Localized or predominant involvement	Primary extraperitoneal lesions Diverticulitis	Exudate, malignant seeding in lateral intraperitoneal gutter Embolic metastases Never localized diverticulitis; in association with involvement of other haustral rows, indicates an extensive paracolic abscess	Extension from primary small bowel process Diverticulitis	Extension of gastric carcinoma Primary masses of gastrocolic ligament Enlarged gallbladder Choledochal cyst Diverticulitis	Extension of pancreatic carcinoma and pancreatitis Primary masses of transverse mesocolon Scleroderma Never localized diverticulitis; in association with involvement of other haustral rows, indicates an extensive paracolic abscess	Extension of pancreatic carcinoma and pancreatitis Primary masses of transverse mesocolon Diverticulitis

common conditions resulting in localized involvement. Application of these principles is particularly helpful in the diagnosis of a variety of disease processes at a stage before gross displacement and distortion of the colon result. These concepts allow the precise localization and often the specific diagnosis of an extracolonic lesion at its earliest stage of extension to the large intestine and permit the radiologist to further refine the diagnosis of intraabdominal disease.

References

1. Meyers MA, Volberg F, Katzen B, et al: Haustral anatomy and pathology: A new look. I. Roentgen identification of normal patterns and relationships. Radiology 1973; 108:497–504.
2. Lineback PE: Studies on the musculature of the human colon with special reference to the taeniae. Am J Anat 1925–1926; 36–37:357–383.
3. Ritchie JA: Movement of segmental constrictions in the human colon Gut 1971; 12:335–355.
4. Hawkins CF, Hardy TL: On the nature of haustration of the colon. J Fac Radiol 1950; 2:95–98.
5. Meyers MA, Volberg F, Katzen B, et al: Haustral anatomy and pathology: A new look. II. Roentgen interpretation of pathologic alterations. Radiology 1973; 108:505–512.
6. Pace JL, Williams I: Organization of the muscular wall of the human colon. Gut 1969; 10:352–359.
7. Williams PL, Bannister LH: Gray's Anatomy. 38th ed. New York: Churchill Livingstone, 1995.
8. Ghahremani GG, White EM, Hoff FL, et al: Appendices epiploicae of the colon: Radiologic and pathologic features. RadioGraphics 1992; 12:59–77.
9. Derchi LE, Reggiani L, Rebaudi F, et al: Appendices epiploicae of the large bowel: Sonographic appearance and differentiation from peritoneal seeding. J Ultrasound Med 1988; 7:11–14.
10. Rioux M, Langis P: Primary epiploic appendagitis: Clinical, US, and CT findings in 14 cases. Radiology 1994; 191:523–526.
11. Meyers MA, Oliphant M: Ascending retrocecal appendicitis. Radiology 1974; 110:295–299.
12. Collins DC: 71,000 human appendix specimens. A final report summarizing forty years' study. Am J Proctol 1963; 14:365–381.
13. Wakely CPG: The position of the vermiform appendix as ascertained by an analysis of 10,000 cases. J Anat 1933; 67:277–283.
14. Feldberg MAM, Hendriks MJ, van Waes P: Computed tomography in complicated acute appendicitis. Gastrointest Radiol 1985; 10:289–295.
15. Balthazar EG, Megibow AJ, Hulnick D et al: CT of appendicitis. AJR 1986; 147:705–710.
16. Feldberg MAM, Hendriks MJ, van Waes PFGM: Acute appendicitis. *In* Computed Tomography of the Gastrointestinal Tract: Including the Peritoneal Cavity and Mesentery. Edited by MA Meyers. Springer-Verlag, New York, 1986.
17. Farin P, Paajanen H, Miettinen P: Intraoperative US diagnosis of pylephlebitis (portal vein thrombosis) as a complication of appendicitis: A case report. Abdom Imaging 1997; 22:401–403.
18. Kottra JJ, Dodds WJ: Duplication of the large bowel. AJR 1971; 113:310–315.
19. Beyer D, Friedmann G, Müller J: Duplication of the colon: Report of two cases and review of the literature. Gastrointest Radiol 1981; 6:151–156.
20. Ravitch MM: Hind gut duplication: Doubling of colon and genital urinary tracts. Ann Surg 1953; 137:588–601.
21. Meyers MA, Volberg F, Katzen B, et al: Angioarchitecture of colonic diverticula: Significance in bleeding diverticulosis. Radiology 1973; 108:249–261.
22. Hughes LE: Postmortem survey of diverticular disease of the colon. I. Diverticulosis and diverticulitis. Gut 1969; 10:336–344.
23. Athanasoulis CA, Baum S, Rosch J, et al: Mesenteric arterial infusions of vasopressin for hemorrhage from colonic diverticulosis. Am J Surg 1975; 129: 212–216.
24. Casarella WJ, Kanter IE, Seaman WB: Right-sided colonic diverticula as a cause of acute rectal hemorrhage. N Engl J Med 1972; 286:450–453.
25. Noer RJ, Hamilton JE, Williams DJ, et al: Rectal hemorrhage: Moderate and severe. Ann Surg 1962; 155:794–805.
26. Mobley JE, Dockerty MB, Waugh JM: Bleeding in colonic diverticulitis. Am J Surg 1957; 94:44–51.
27. Meyers MA, Alonso DR, Baer JW: Pathogenesis of massively bleeding colonic diverticulosis: New observations. AJR 1976; 127:901–908.
28. Meyers MA, Alonso DR, Gray GF, et al: Pathogenesis of bleeding colonic diverticulosis. Gastroenterology 1976; 71:577–583.
29. Drummond H: Sacculi of the large intestine, with special reference to their relations to the blood vessels of the bowel wall. Br J Surg 1916; 4:407–413.
30. Arfwidsson S, Dock NG: Pathogenesis of multiple diverticula of the sigmoid colon in diverticular disease. Acta Chir Scand (Suppl) 1964; 342:5–68.

31. Painter NS, Truelove SC, Ardran GM, et al: Segmentation and the localization of intraluminal pressures in the human colon, with special reference to the pathogenesis of colonic diverticula. Gastroenterology 1965; 49:169–177.
32. Baum S, Rosch J, Dotter CT, et al: Selective mesenteric arterial infusions in the management of massive diverticular hemorrhage. N Engl J Med 1973; 288:1269–1272.
33. Eisenberg H, Laufer I, Skillman JJ: Arteriographic diagnosis and management of suspected colonic diverticular hemorrhage. Gastroenterology 1973; 64: 1091–1100.
34. Goldberger LE, Bookstein JJ: Transcatheter embolization for treatment of diverticular hemorrhage. Radiology 1977, 122:613–617.
35. Mitty HA, Efremidis S, Keller RJ: Colonic stricture after transcatheter embolization for diverticular bleeding. AJR 1979; 133:519–521.
36. Rosenkrantz H, Bookstein JJ, Rosen RJ, et al: Postembolic colonic infarction. Radiology 1982; 142: 47–51.
37. Savides TJ, Jensen DM: Colonoscopic hemostasis for recurrent diverticular hemorrhage associated with a visible vessel: A report of three cases. Gastrointest Endosc 1994; 40:70–72.
38. Ramirez FC, Johnson DA, Zierer ST, et al: Successful endoscopic hemostasis of bleeding colonic diverticula with epinephrine injection. Gastrointest Endosc 1996; 43:167–170.
39. Feldberg MAM, Hendricks MJ, van Waes PFGM: Role of CT in diagnosis and management of complications of diverticular disease. Gastrointest Radiol 1985; 10:370–377.
40. White TB, Allen HA III, Ives CE: Portal and mesenteric vein gas in diverticulitis: CT findings. AJR 1998; 171:525–526.
41. Rossman MD, Burr LG: Colovenous fistula complicating diverticulitis. Abdom Imaging 1997; 22: 513–515.
42. Sleisenger MH, Fordtran JS: Gastrointestinal Disease, 5th ed. WB Saunders, Philadelphia, 1993, p 1273.
43. Marshak RH, Lindner AE, Pochaczevsky R, et al: Longitudinal sinus tracts in granulomatous colitis and diverticulitis. Semin Roentgenol 1976; 11: 101–110.
44. Schmidt GI, Lennard-Jones JE, Morson BC, et al: Crohn's disease of the colon and its distinction from diverticulitis. Gut 1968; 9:7–16.
45. Johnson WD, Roth JLA: Diagnosis and differential diagnosis of chronic ulcerative colitis and Crohn's colitis. *In* Inflammatory Bowel Disease. Edited by JB Kirsner, RG Shorter. Lea & Febiger, Philadelphia, 1975.
46. Meyers MA, Alonso DR, Morson BC, et al: Pathogenesis of diverticulitis complicating granulomatous colitis. Gastroenterology 1978; 74:24–31.
47. Lockhart-Mummery HE, Morson BC: Crohn's disease of the large intestine. Gut 1964; 5:493–509.
48. Fleischner FG: Diverticular disease of the colon. New observations and revised concepts. Gastroenterology 1971; 60:316–324.
49. McGovern VJ, Goulston SJM: Crohn's disease of the colon. Gut 1968; 9:164–176.
50. Morson BC: The muscle abnormality in diverticular disease of the sigmoid colon. Br J Radiol 1963; 36:385–392.

Internal Abdominal Hernias

16

An internal abdominal hernia is defined as the protrusion of a viscus through a normal or abnormal aperture within the confines of the peritoneal cavity. The hernial orifice may be a preexisting anatomic structure, such as the foramen of Winslow, or a pathologic defect of congenital or acquired origin.

The literature on the subject has been composed principally of case reports, often based on observations made at surgery or autopsy. The role of preoperative radiologic diagnosis of internal hernias has generally not been appreciated. Indeed, in the differential diagnosis of radiographic findings of intestinal obstruction or unusual-appearing grouping of bowel loops,[1–5] "some type of internal hernia" is often loosely entertained without a precise appreciation of types and distinctive findings. However, with an awareness of the underlying anatomic features and of the dynamics of intestinal entrapment, the correct diagnosis of an internal hernia can be made in most instances.

The nomenclature of a specific hernia is determined by the location of the hernial ring and not by the eventual position of the sac or the involved intestinal loops. Internal hernias within the lesser sac, for example, may occur from various directions, namely, through the foramen of Winslow or through defects in the transverse mesocolon or lesser omentum. Based on their anatomic location of origin, internal hernias may be conveniently classified into the following groups:

1. Paraduodenal
2. Foramen of Winslow
3. Pericecal
4. Intersigmoid
5. Transmesenteric and transmesocolic
6. Retroanastomotic

The majority of internal hernias result from congenital anomalies of intestinal rotation and peritoneal attachment.[6–9] Acquired defects of the mesentery or peritoneum secondary to abdominal surgery or trauma may also serve as the hernial ring.[10–13] The retroperitoneal group of internal hernias is more frequently encountered in adults, whereas the transmesenteric types are more commonly present in the pediatric age group.[6,8,14]

The autopsy incidence of internal hernia has been reported to be between 0.2 and 0.9%.[6,15] Many are small and easily reducible, so that they may remain relatively asymptomatic during life.[16,17] In other cases, the patients present with a history of intermittent attacks of vague epigastric discomfort, colicky periumbilical pain, nausea, vomiting—especially after intake of a large meal—and recurrent intestinal obstruction. The discomfort may be altered or relieved by change in position. Internal hernias account for 0.5–3% of all cases of intestinal obstruction,[6,18] with a very high rate of mortality, exceeding 50% in most series.[6,12,19] Delayed diagnosis leads to extensive and often irreparable intestinal damage. Adhesions between the intestinal loops or between the bowel and hernial sac develop, further resulting in obstruction or circulatory compromise.[20]

Figure 16–1 summarizes the relative incidence of internal hernias at the various susceptible sites. In general, the small bowel examination provides the most useful diagnostic hallmarks, which include (a) abnormal location and disturbed arrangement of the small intestine; (b) sacculation and crowding of several small bowel loops owing to encapsulation within the hernial sac (serial radiographs and fluoroscopy with palpation and change in the patient's position may disclose that the loops cannot be separated but rather move *in toto*); and (c) segmental

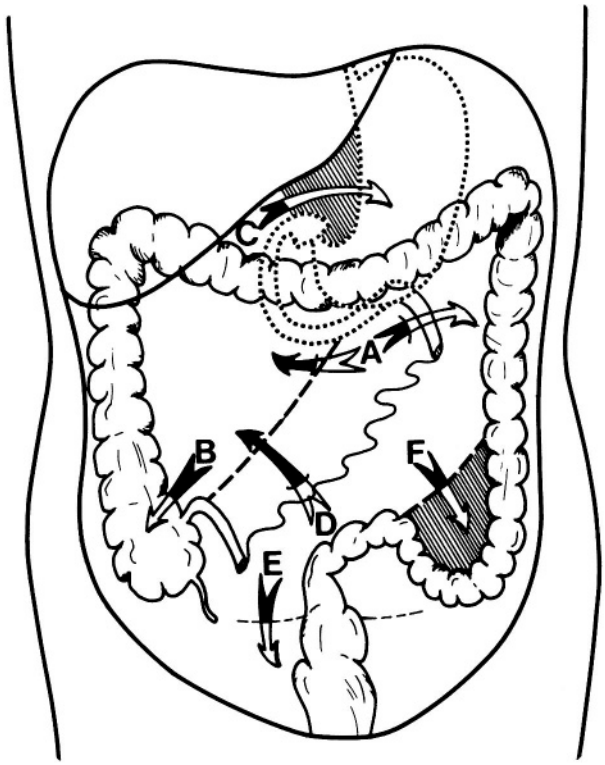


Fig. 16-1. Location and relative incidence of internal hernias according to the collective review by Hansmann and Morton[21]: *(A)* paraduodenal hernias, 53%; *(B)* pericecal hernias, 13%; *(C)* foramen of Winslow hernias, 8%; *(D)* transmesenteric hernias, 8%; *(E)* hernias into pelvic structures, *7%;(F)* transmesosigmoid hernias, 6%. (Reproduced from Ghahremani and Meyers.[16])

dilatation and prolonged stasis within the herniated loops.

Without a specific radiologic diagnosis, a small internal hernia may not be evident at laparotomy for a variety of reasons: the hernia may reduce spontaneously or following inadvertent traction on small bowel loops at the time of surgery; the usual exploratory laparotomy is often inadequate for evaluation of all significant peritoneal fossae and possible mesenteric defects that represent the potential sites of herniation; and the potential space of a peritoneal fossa is generally not evident from the relatively small size of its orifice.[17,20,22]

Paraduodenal Hernias

Paraduodenal hernias are the most common type of internal abdominal hernias, accounting for over half of reported cases. They are basically congenital in origin, representing entrapment of the small intestine beneath the mesentery of the colon related to embryologic rotation of the midgut and variations in peritoneal fixation and vascular folds.[9,23,24] Nevertheless, repeated encapsulations of intestinal loops can increase the size of the peritoneal defect and result in total or subtotal herniation of the small bowel.[20,22] Seventy-five percent occur on the left side and 25% on the right.[6,17]

Anatomic Considerations

Left Paraduodenal Hernias

Although nine normal and aberrant paraduodenal folds and fossae have been classically described,[25] there is only one fossa to the left of the duodenum capable of developing into the sac of a hernia, termed the paraduodenal fossa (fossa of Landzert)[26] (Fig. 16–2). This fossa, present in about 2% of autopsy cases,[20] is situated at some distance to the left of the ascending or fourth portion of the duodenum and is caused by the raising up of a peritoneal fold by the inferior mesenteric vein as it runs along the lateral side of the fossa and then above it. Small intestine may herniate through the orifice posteriorly and downward toward the left, lateral to the ascending limb of the duodenum, extending into the descending mesocolon and left portion of the transverse mesocolon. The free edge of the hernia thus contains the inferior mesenteric vein and the ascending left colic artery. Confusion can be minimized if it is understood that the hernial orifice is in a paraduodenal location but the herniated loops present at a distance—more clearly, as a hernia into the descending mesocolon[23] (Fig. 16–3).

The hernia may contain only a few loops and be spontaneously reducible. Evaluation during symptom-free intervals is likely to be misleadingly negative. Since the afferent loop enters the sac from behind where the duodenum emerges from its fixed retroperitoneal position, only the efferent loop of the intestine truly passes through the hernial orifice.

Right Paraduodenal Hernias

The mesentericoparietal fossa (fossa of Waldeyer)[28] is in the first part of the mesentery of the jejunum, immediately behind the superior mesenteric artery and inferior to the transverse duodenum (Figs. 16–2 and 16–4). The fossa's orifice looks to the left, its blind extremity to the right and downward, directly in front of the posterior parietal peritoneum. This fossa is present in 1% of cases.[20] Right paraduodenal hernias most commonly

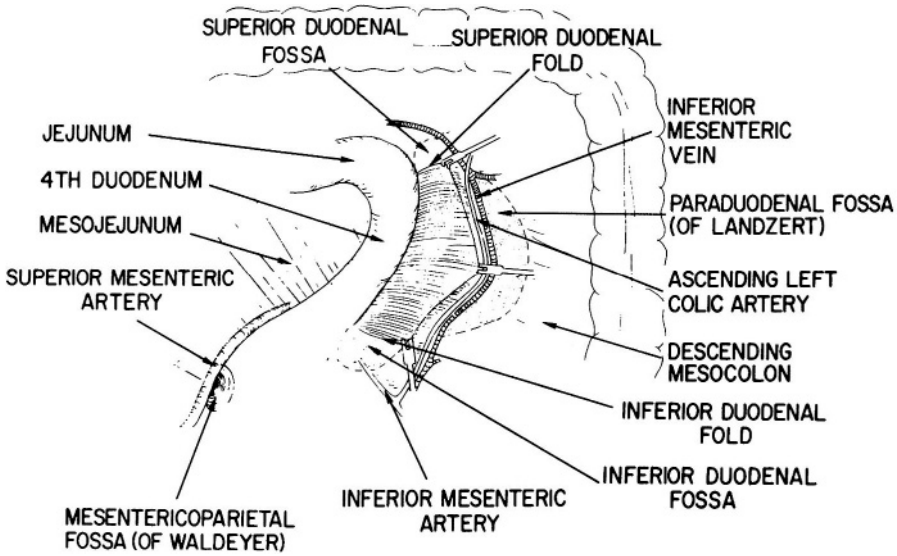


Fig. 16–2. The paraduodenal fossa of Landzert and the mesentericoparietal fossa of Waldeyer.
The transverse colon and mesocolon have been elevated and the proximal jejunal loop deflected medially in order to identify the fossae clearly. Behind the fossae lie the parietal peritoneum and retroperitoneal organs.
(Reproduced from Meyers.[27])

involve the mesentericoparietal fossa (Fig. 16–5), representing an entrapment of the small bowel behind the ascending mesocolon and the right half of the transverse mesocolon, more accurately conceived therefore as hernias into the ascending mesocolon. The superior mesenteric and ileocolic arteries are then in the free edge of the sac.[9,23] Because both afferent and efferent loops pass through the hernial orifice, right paraduodenal hernias are usually more massive and fixed than those occurring on the left side.[16,17]

Clinical Features

The clinical manifestations of paraduodenal hernias may range from chronic or intermittent mild digestive complaints to acute intestinal obstruction with perhaps gangrene and peritonitis.[17,29,30] A history of indigestion or periodic cramps, vomiting, and distention frequently dating back to childhood may be elicited. Postprandial pain is a characteristic symptom and may be relieved by postural changes. Distention is typically of a mild degree because the obstruction is usually high in the intestinal tract. Compression of the inferior mesenteric vein in the neck of the left hernial sac may result in vascular obstruction with the development of hemorrhoids, dilated anterior abdominal veins, and venous congestion and infarction of the bowel.[31]

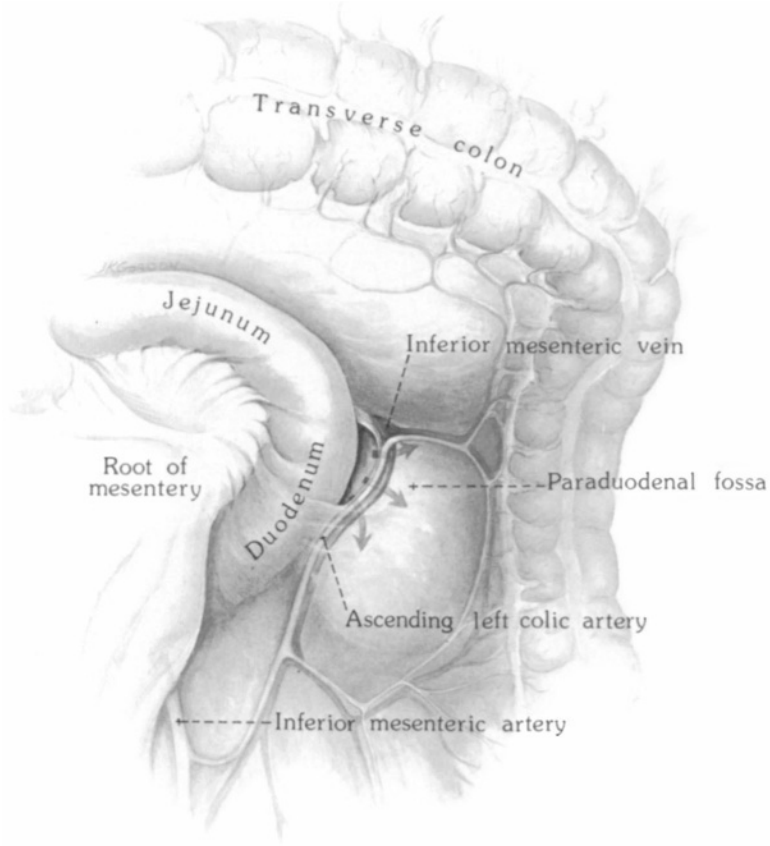
Radiologic and Arteriographic Features

The preoperative diagnosis of paraduodenal hernia can be established only by radiologic evaluation. Studies are best performed during a symptomatic period. Examination in intervals between recurrent internal herniation may be negative or may demonstrate mild degrees of dilatation, stasis, and perhaps edematous mucosal folds that may be falsely attributed solely to adhesions. Diligent serial filming is essential to diagnosis.

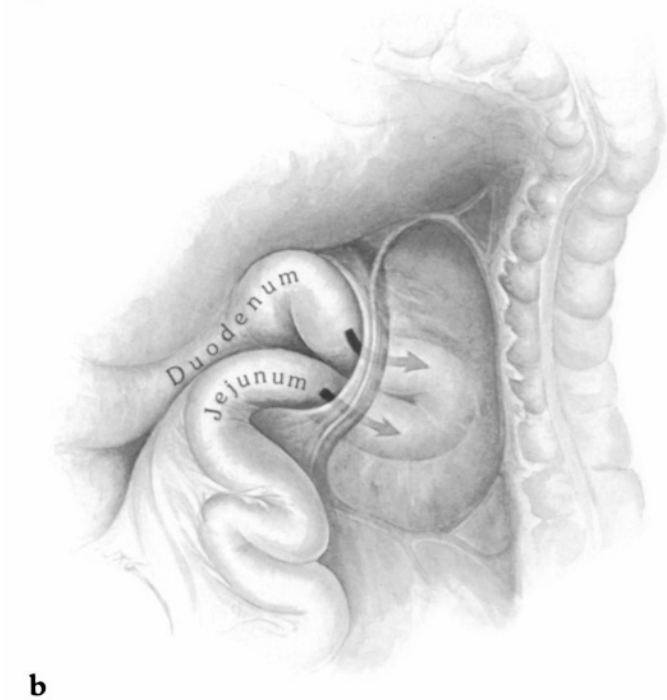
In patients with a small left paraduodenal hernia (Figs. 16–6 through 16–9) a circumscribed mass of a few loops—most typically, jejunal—may be seen in the left upper quadrant immediately lateral to the ascending duodenum. The herniated loops may depress the distal transverse colon and indent the posterior wall of the stomach. Stasis of barium within the hernial contents and mild dilatation of the duodenum may be associated findings. Small right paraduodenal hernias present a similar ovoid grouping of small bowel loops lateral and inferior to the descending duodenum (Figs. 16–10 and 16–11).

Large paraduodenal hernias can contain several or most of the small bowel loops. These form a circumscribed ovoid mass having its main axis lateral to the midline and its inferior border convex downward (Figs. 16–12 through 16–15). The encapsulation within the hernial sac prevents separation or displacement of the

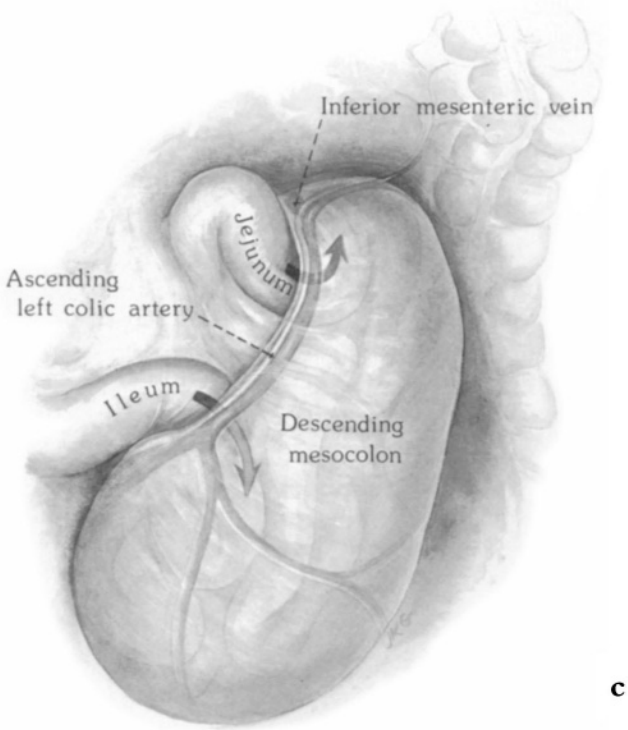
text continues on page 724



a



b



c

Fig. 16–3. Development of a left paraduodenal hernia.
(a–c) The small bowel loops herniate via the fossa of Landzert into the descending mesocolon. Note the position of the inferior mesenteric vein and ascending left colic artery in the anterior margin of the neck of the sac.

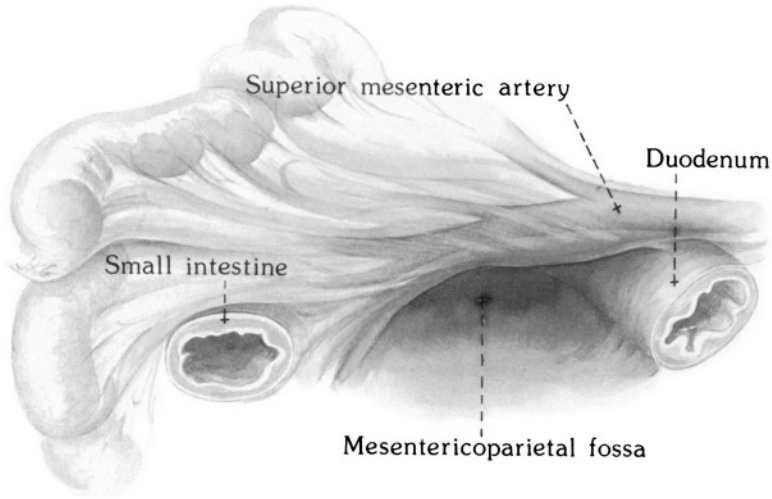


Fig. 16–4. Lateral drawing of the mesentericoparietal fossa of Waldeyer showing its position behind the superior mesenteric artery and small bowel mesentery. Note also its infraduodenal position.

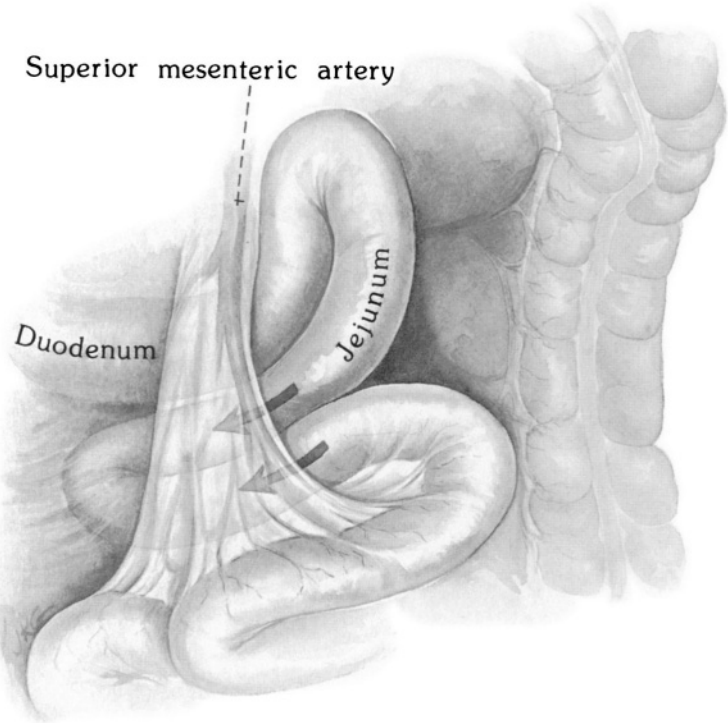


Fig. 16–5. Development of a right paraduodenal hernia via the fossa of Waldeyer toward the ascending mesocolon. Note the position of the superior mesenteric artery anterior to the hernia and in the leading edge of the sac.

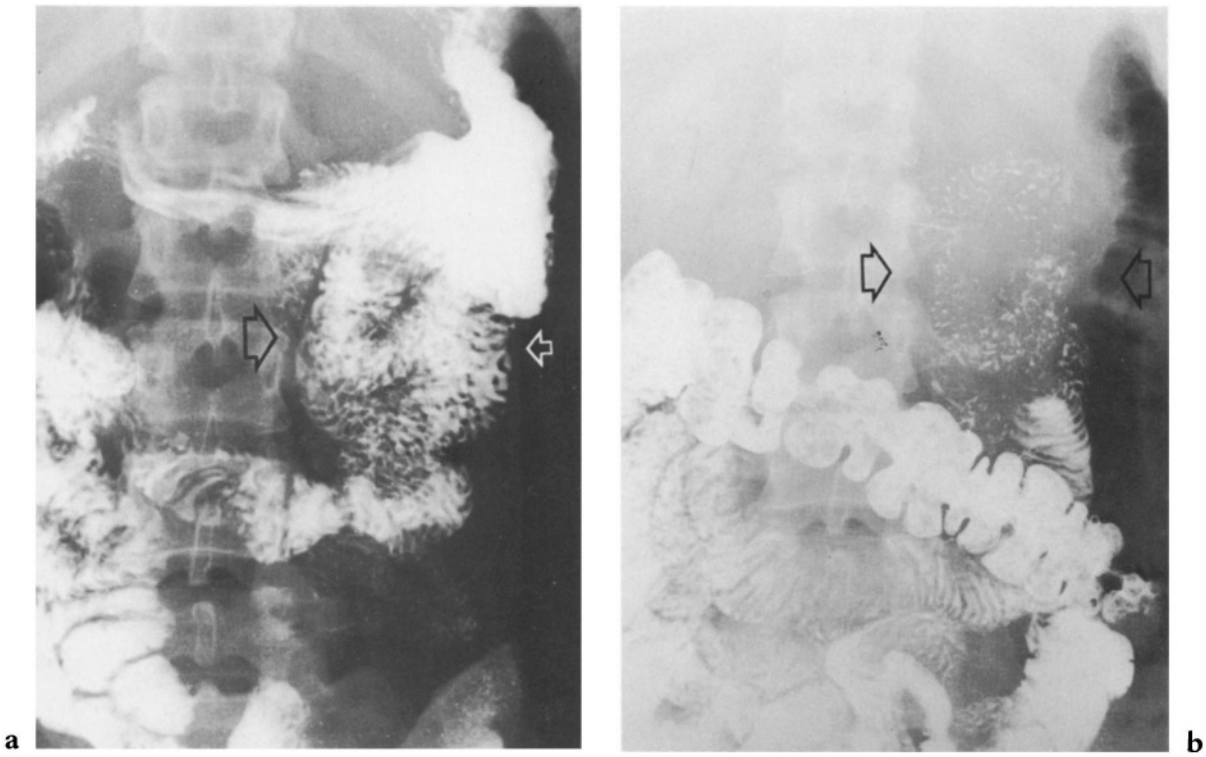


Fig. 16–6. Small left paraduodenal hernia.
(a) Small bowel series shows a circumscribed ovoid mass of herniated jejunal loops immediately lateral to the ascending duodenum *(arrows).*
(b) Two-hour film demonstrates stasis of barium within these loops *(arrows)* and depression of the distal transverse colon. At surgery, the hernial sac contained only a couple feet of jejunum. This was readily reduced, and the peritoneal defect was repaired.
(Reproduced from Meyers.[17])

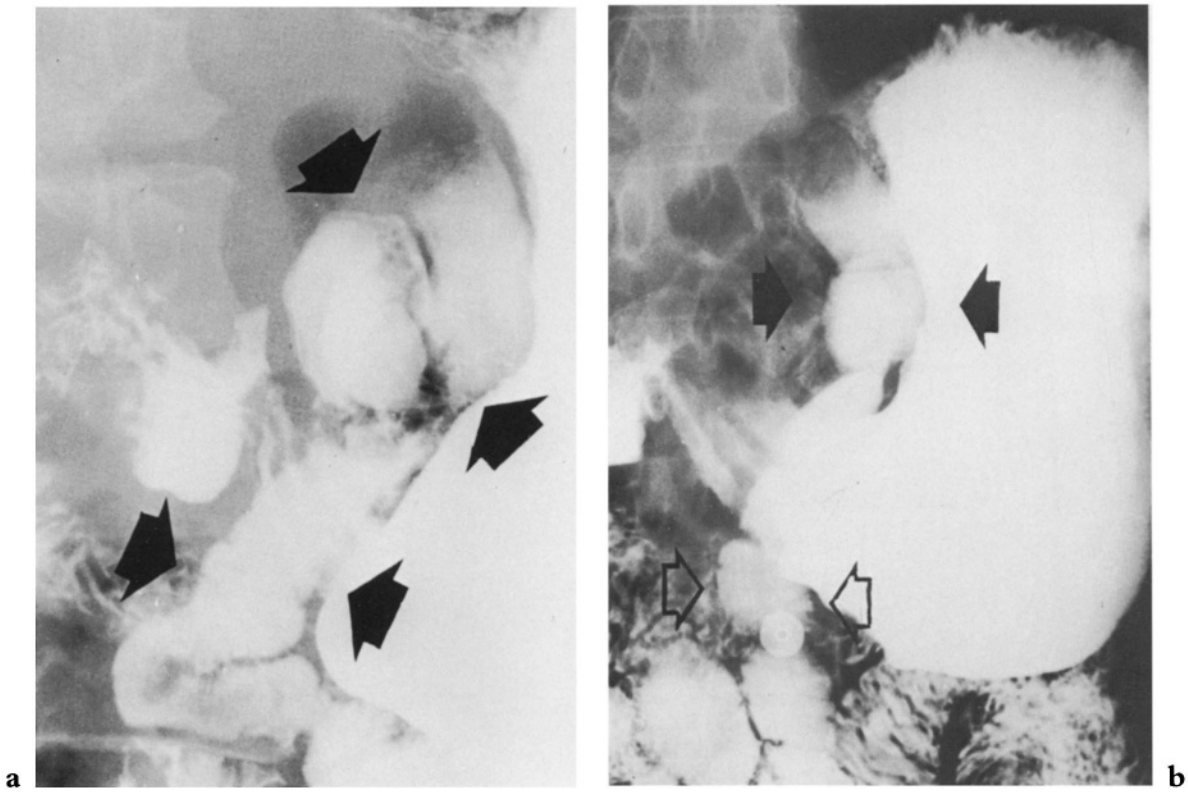


Fig. 16–7. Small left paraduodenal hernia.
(a) Prone oblique and **(b)** frontal projections demonstrate a proximal jejunal loop within the hernial sac *(arrows)* behind the stomach, rising above the duodenojejunal junction into the descending mesocolon and especially into the left half of the transverse mesocolon. Note the pressure of the loop on the posterior wall of the stomach. A chronically deformed duodenal bulb is also present.
(Reproduced from Meyers.[17])



Fig. 16–8. Small left paraduodenal hernia.
A dilated jejunal loop resides abnormally high lateral to the fourth portion of the duodenum and mildly displaces the duodenojejunal junction medially. Its degree of dilatation and encapsulation is sufficient to produce pressure deformity on the posterior wall of the adjacent stomach. Although no hernia was present at the time of autopsy, a paraduodenal fossa admitting three to four fingers was found. This would readily allow intermittent herniation of jejunum as illustrated.
(Reproduced from Meyers.[17])

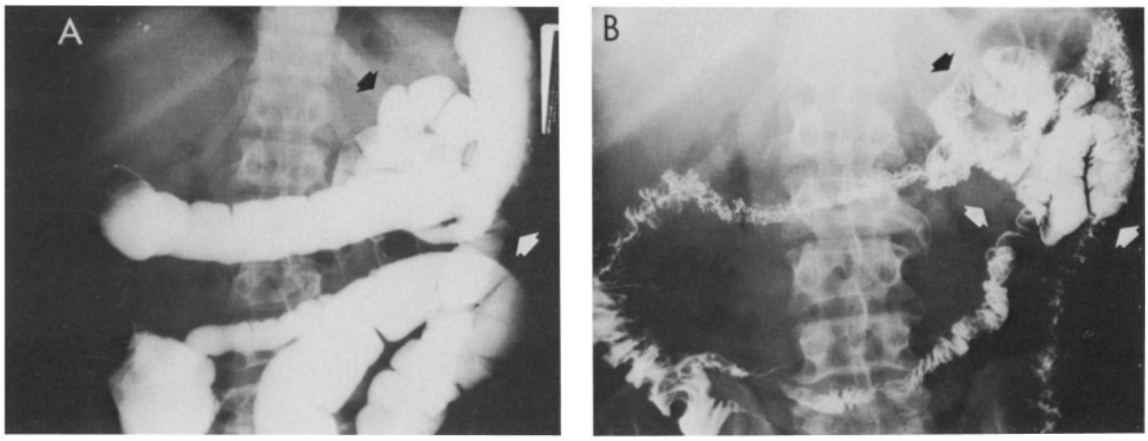


Fig. 16–9. Left paraduodenal hernia.
(a and **b)** Filled and postevacuation barium enema study demonstrates refluxed proximal ileal loops forming a circumscribed ovoid mass *(arrows)* with stasis within the left paraduodenal fossa.

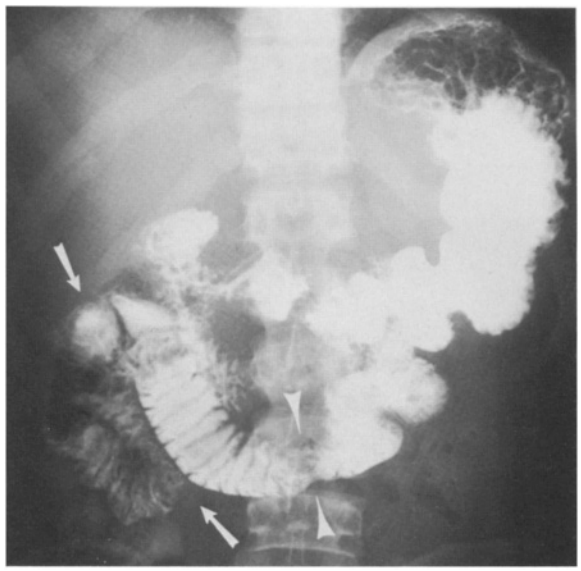


Fig. 16–10. Small right paraduodenal hernia.
A circumscribed grouping ofjejunal loops *(arrows)* has herniated into the ascending mesocolon and the right portion of the transverse mesocolon. The dilated afferent jejunal limb shows a localized constriction *(arrowheads)* at the hernial orifice behind the superior mesenteric artery. (Reproduced from Ghahremani and Meyers.[32])

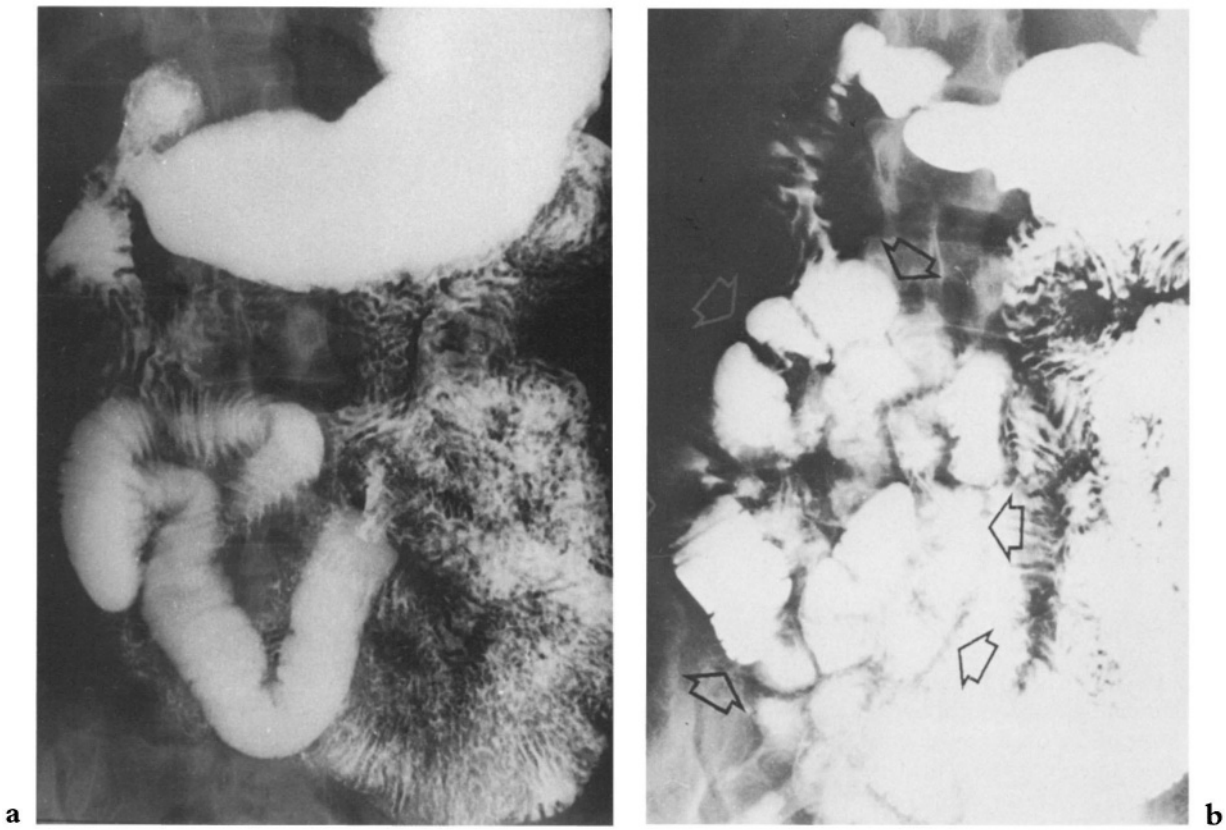
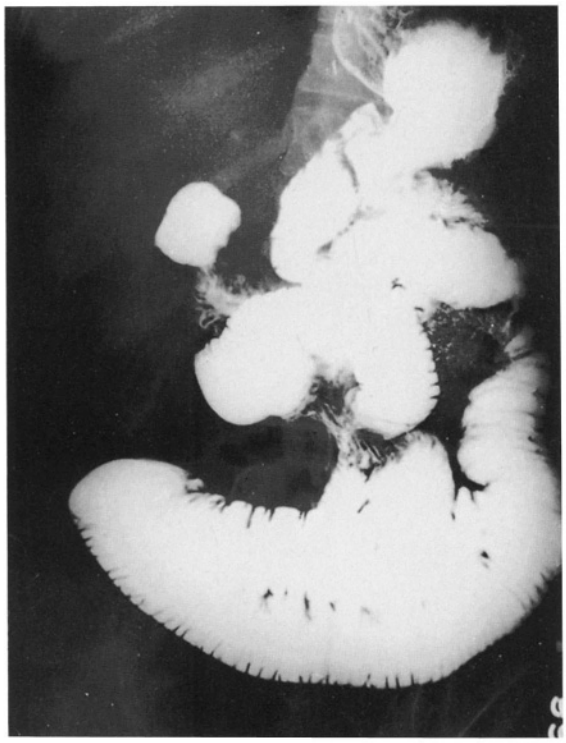


Fig. 16–11. Right paraduodenal hernia.
(a) The afferent and efferent limbs, which lie close together, both appear obstructed.
(b) Later the small intestinal loops within the circumscribed ovoid hernial sac *(arrows)* into the ascending mesocolon are still dilated but with a smaller degree of obstruction. The alternating sites of narrowing represent adhesions between loops.
(Reproduced from Meyers.[17])



Fig. 16–12. Large left paraduodenal hernia.
Upper GI series (LAO position) shows an encapsulated cluster of multiple small bowel loops in the fossa of Landzert, with a mild impression upon the posterior wall of the stomach *(black arrows).* A typically tapered efferent limb is demonstrated *(white arrows).*
(Reproduced from Schlaffer et al.[33])

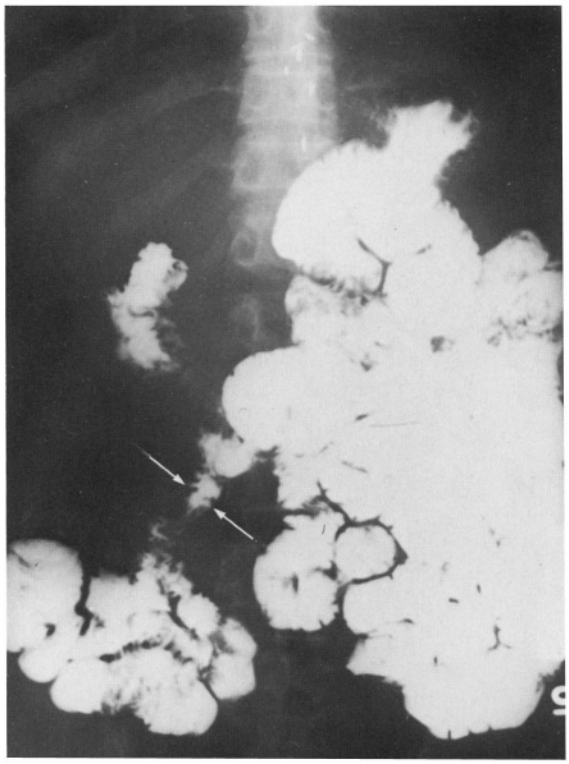
Fig. 16–13. (Right) Large left paraduodenal hernia in a 42-year-old female with persistent postprandial pains despite multiple abdominal operations.
(a) Most of the small bowel loops are gathered in the left side of the abdomen, forming a circumscribed mass with a convex inferior margin. Internal adhesions within the sac narrow bowel loops at multiple sites.
(b) Lateral projection shows retroperitoneal displacement of the herniated intestine.
(c) A serial film demonstrates that the efferent loop *(arrows)* leads from the hernial sac to the normally situated distal ileum. Despite multiple postural changes, the grouped position of the small bowel loops remained unchanged. *(continued on pages 721 and 722)*



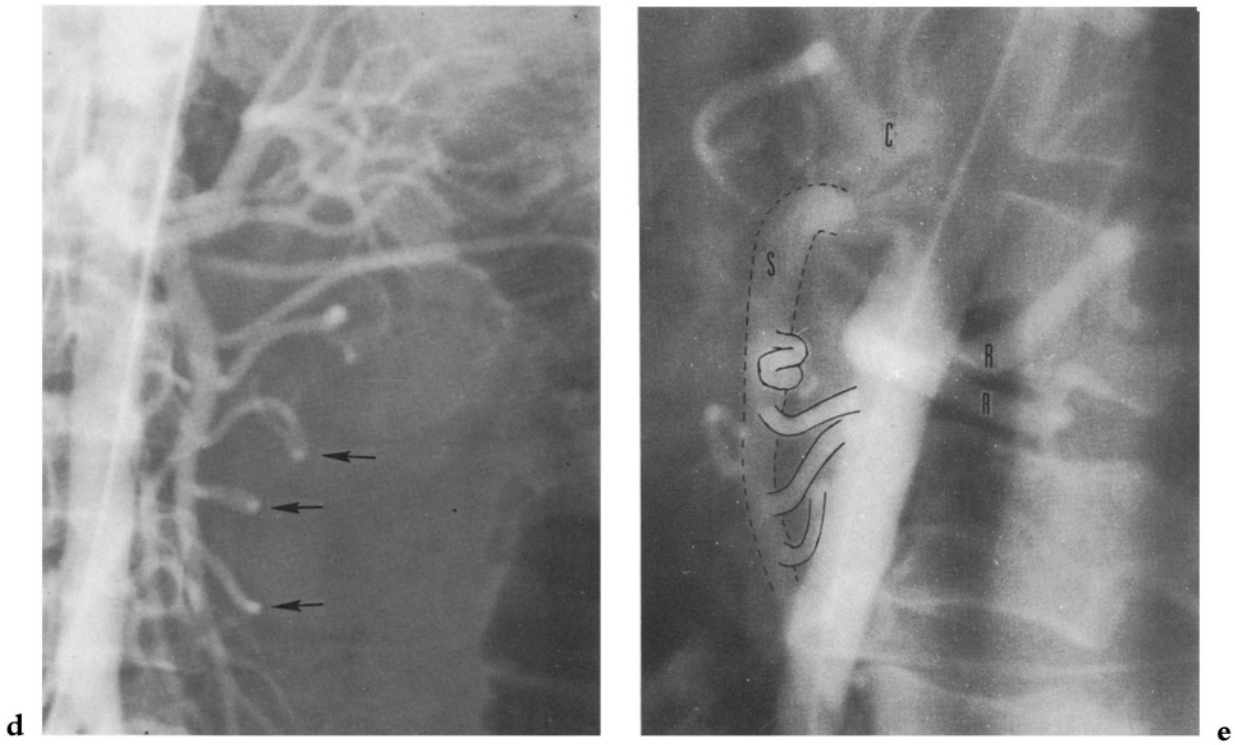
a



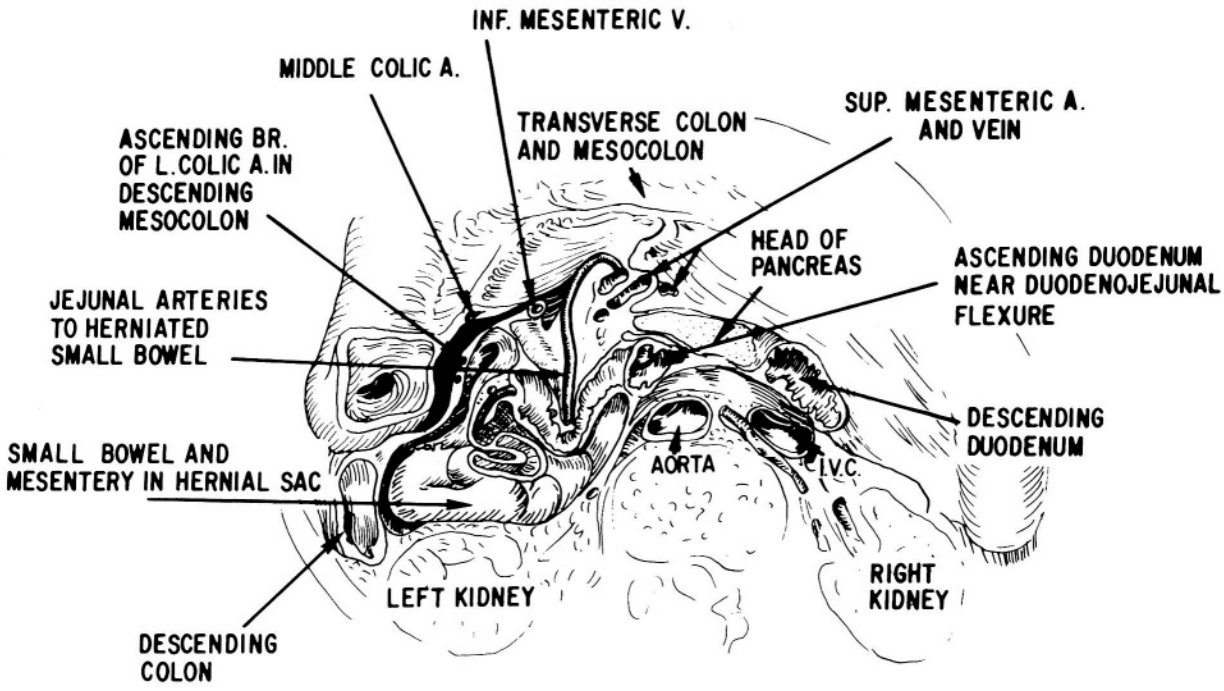
b



c



d e



f

Fig. 16–13. Continued. **(d** and **e)** Aortogram shows that the upper jejunal arteries are redirected medially and posteriorly just beyond their origins from the superior mesenteric artery *(arrows).* This characteristic reversal of their course indicates the posteromedial border of the hernial orifice, beyond which the intestinal loops herniate. **(f)** Horizontal diagram of anatomic relationships of jejunal arteries redirected medially and posteriorly to left paraduodenal hernia into the descending mesocolon.
(Reproduced from Meyers.[27])

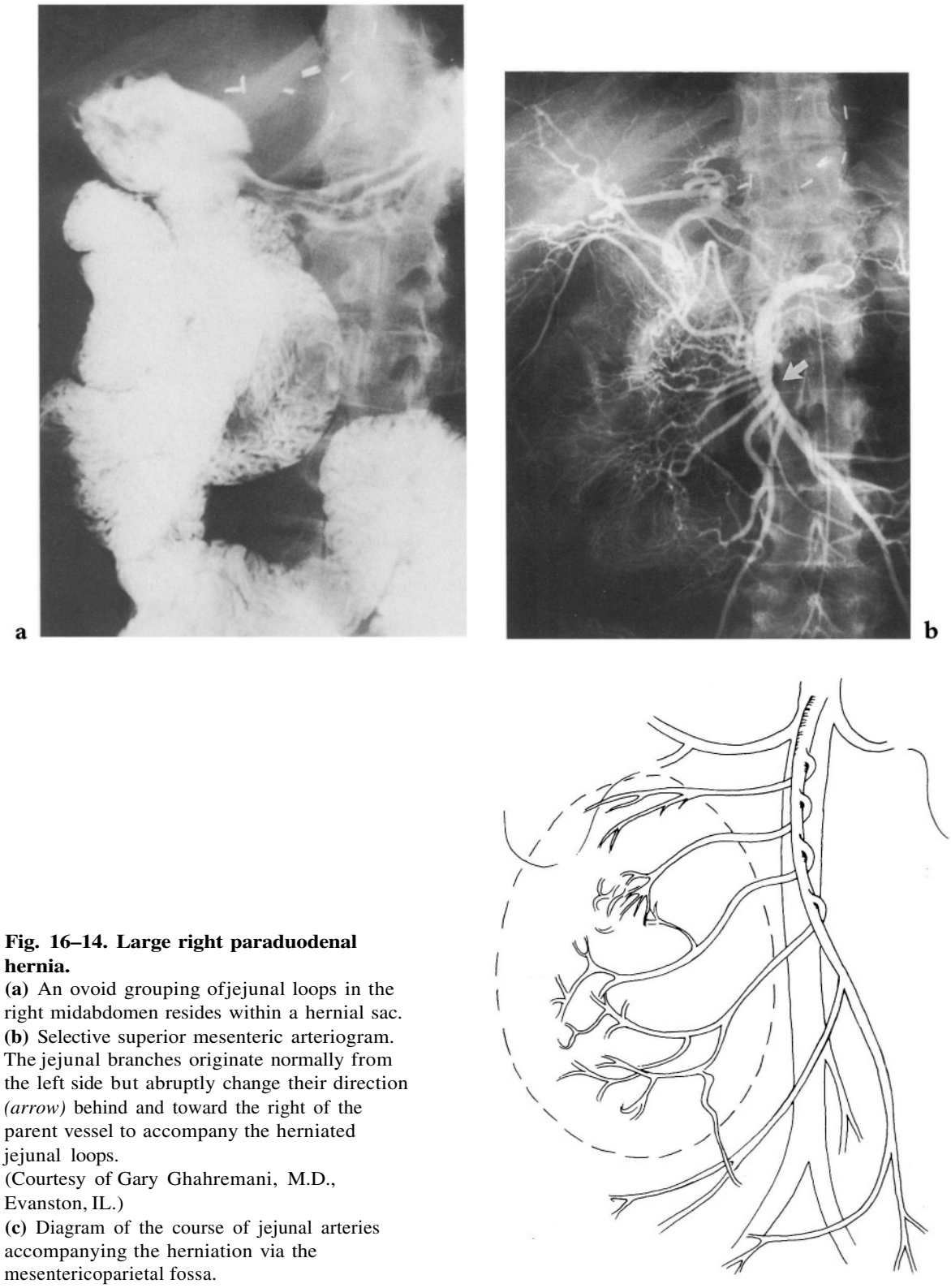


Fig. 16–14. Large right paraduodenal hernia.
(a) An ovoid grouping ofjejunal loops in the right midabdomen resides within a hernial sac.
(b) Selective superior mesenteric arteriogram. The jejunal branches originate normally from the left side but abruptly change their direction *(arrow)* behind and toward the right of the parent vessel to accompany the herniated jejunal loops.
(Courtesy of Gary Ghahremani, M.D., Evanston, IL.)
(c) Diagram of the course of jejunal arteries accompanying the herniation via the mesentericoparietal fossa.

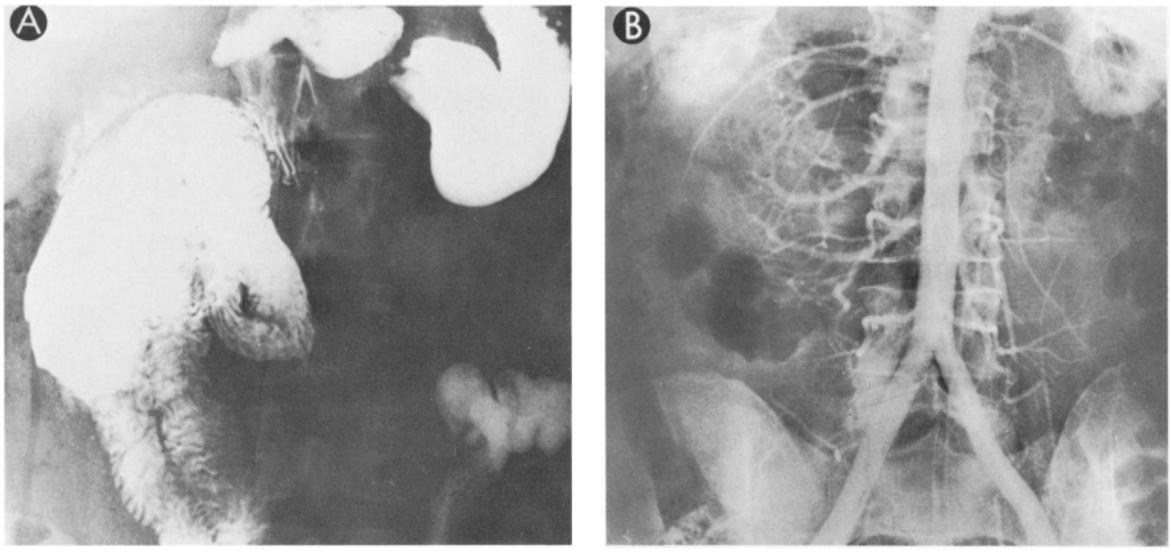


Fig. 16–15. Large right paraduodenal hernia.
(a) The right midabdomen is occupied by a circumscribed grouping of virtually all of the intestinal loops, representing a total herniation into the ascending mesocolon and right portion of the transverse mesocolon. The cecum was normally positioned.
(b) On aortography, the jejunal arteries are demonstrated to course to the right, accompanying the circumscribed herniated loops and their mesentery.
(Reproduced from Lechner and Gebhardt.[34])

individual loops from the rest of the hernial contents during fluoroscopic manipulation. Stasis of the contrast material and dilatation of the herniated loops may also be evident. At the hernial orifice, the efferent loop of the left paraduodenal hernia shows an abrupt change of caliber (Figs. 16–12 and 16–13c). In a right paraduodenal hernia, however, both the afferent and the efferent loops appear closely apposed and narrowed. Lateral films are particularly useful for detection of retroperitoneal displacement of the hernial content, showing the loops projecting well over the spine.[17,20] On barium enema examination, the descending colon may be seen to be anterior, to the left, or posterior to a left paraduodenal hernia. The ascending colon always lies lateral to a right paraduodenal hernia, however, and the cecum is found in its normal position.[17]

The position of the major mesenteric vessels in the anterior margin of the neck of the paraduodenal hernial sac is important embryologically, surgically, and radiologically. Not only the intestinal loops, but their mesentery and vessels are incorporated into the hernia. Arteriographic visualization of these vessels, particularly of the position of their branches supplying the small bowel loops, can assist in the radiologic diagnosis of paraduodenal hernias.[17,27] In a right paraduodenal hernia, the jejunal arteries that normally arise from the left side of the superior mesenteric artery reverse their direction and course behind the parent vessel to supply the herniated jejunal loops within the fossa of Waldeyer (Figs. 16–14b,c and 16–15b). In a left paraduodenal hernia, I have noted that the proximal jejunal arteries show an abrupt change of course along the medial border of the hernial orifice, where they are redirected posteriorly behind the inferior mesenteric vessels to accompany the herniated loops (Fig. 16–13d–f). A line connecting the points at which these arteries suddenly change their course indicates the medial border of the hernial orifice beyond which the small intestinal loops herniate.[17,27]

The computed tomography findings in left paraduodenal hernia involve (a) encapsulation of bowel loops at the level of the duodenojejunal junction or interposed between the stomach and pancreas, or behind the descending colon; (b) dilatation and air-fluid levels in the trapped loop; and (c) narrowing of the efferent limb[35–38] (Figs. 16–16 through 16–19). Normal vascular relationships, although perhaps with mild displacement by the herniated loops, are useful landmarks.

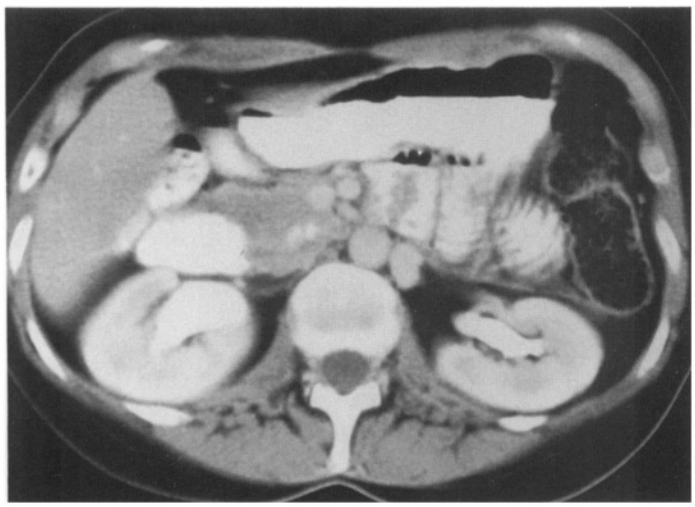
In right paraduodenal hernia, the major CT findings are (a) looping of jejunal branches of the superior mesenteric artery and vein to the right and posterior in a



Fig. 16–16. CT findings in small left paraduodenal hernias, in three separate cases.
(a) CT at the level of the superior mesenteric artery shows a rounded, encapsulated cluster of small bowel loops behind the transverse colon, caudal to the tail of the pancreas and immediately anterior to the left adrenal gland. (Reproduced from Olazabal et al.[39])
(b) CT reveals a horseshoe appearance of an encapsulated bowel loop within a well-defined hernial sac. Some stasis is evident. The jejunal vessels are sharply deviated to the left to accompany the herniated loops and radiate inside the hernial sac to accompany them.
(c) CT demonstrates several mildly dilated jejunal loops encapsulated behind the stomach with pressure effect upon its posterior wall. Sites of angulation and narrowing involving the small bowel loops reflect adhesions within the hernial sac.



a



b

Fig. 16–17. Left paraduodenal hernia.
(a) Small bowel series demonstrates ovoid encapsulation of jejunal loops adjacent and to the left of the fourth portion of the duodenum.
(b) CT shows a cluster of mildly dilated small bowel loops with air-fluid levels behind the stomach on the left adjacent to the duodenojejunal junction. The superior mesenteric vessels are normally positioned.
(Reproduced from Warshauer and Mauro.[37])

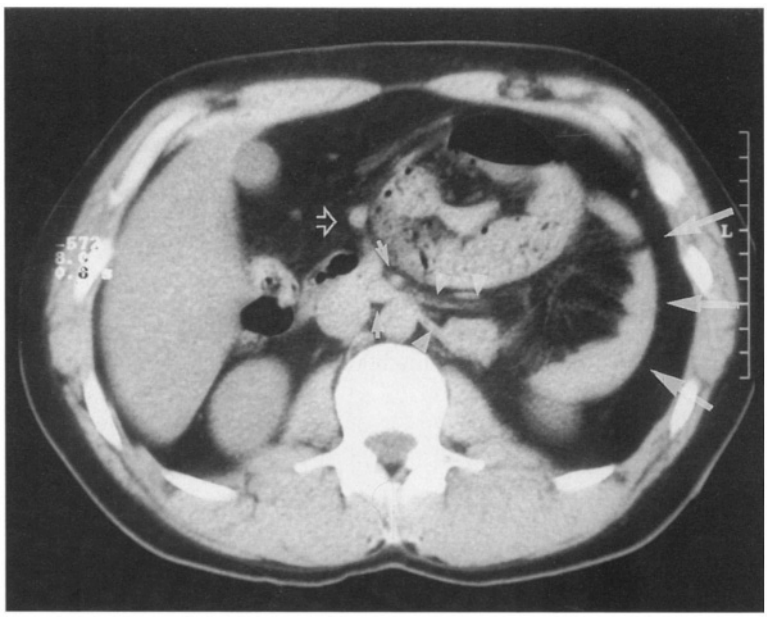


Fig. 16–18. Left paraduodenal hernia: CT findings.
CT shows encapsulated bowel loops with typical smooth convex lateral border of the hernial sac within the fossa of Landzert *(large arrows).* Normal relationships of the superior mesenteric artery and vein *(small white arrows)* with lateral and posterior displacement of their branches caused by the herniated bowel loops. There is anterior and superior displacement of the inferior mesenteric vein *(open white arrow).*
(Reproduced from Schaffler et al.[33])

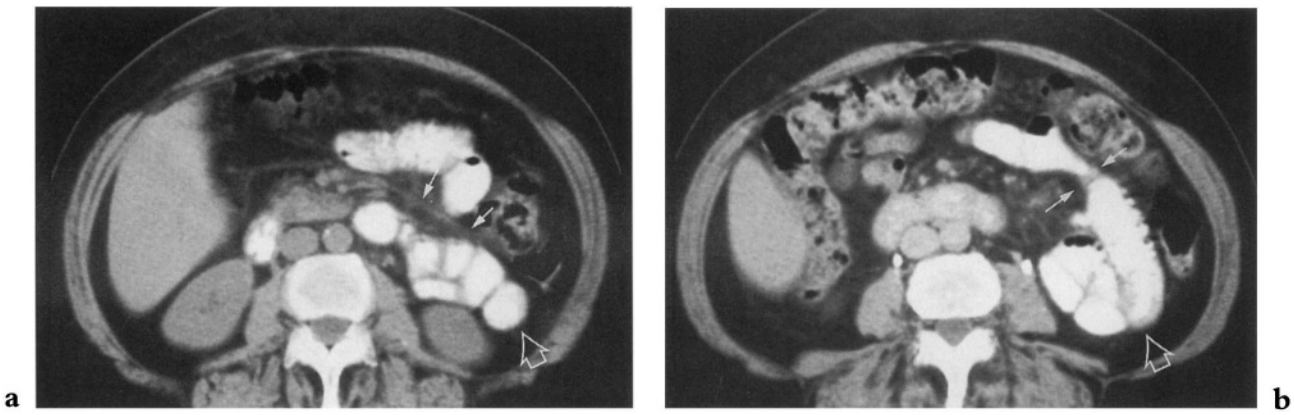


Fig. 16–19. Left paraduodenal hernia: CT findings.
(a and **b)** Two sections of the upper abdomen demonstrate a jejunal loop *(open arrows)* extending deep between the descending colon and left kidney. Focal narrowing of the loop occurs at its exit from the hernial sac, as delineated by the left colic branch of the inferior mesenteric artery *(solid arrows).*
(Reproduced from Ghahremani.[38])

fashion analogous to the arteriographic findings, and (b) clustering or encapsulation of small bowel loops in the right midabdomen[37] (Fig. 16–20). If the hernia is associated with small bowel malrotation, two CT findings of malrotation will also be present: (a) rotation by which the superior mesenteric vein is located more left and ventral in relation to the superior mesenteric artery than normal,[41–44] and (b) absence of the normal horizontal duodenum[37] (Fig. 16–21). These vascular changes can be distinguished from volvulus superimposed upon malrotation. A characteristic CT sign of small bowel volvulus is the whirl sign, in which the bowel and mesenteric folds encircle the superior mesenteric artery and vein[45–49] (Fig. 16–22). Typical vascular alterations may be readily illustrated by ultrasonography[50,51] (Fig. 16–23), and arteriography documents a twirled pattern of the superior mesenteric artery, producing the appearance of a barber pole[48,52,53] (Fig. 16–24).

In the rare developmental anomaly known as peritoneal encapsulation, characterized by a delicate membrane enveloping a fixed cluster of nondilated intestinal loops, vascular relationships are maintained.[54,55]

A unique case of bilateral paraduodenal hernias has been recently reported[56] (Fig. 16–25).

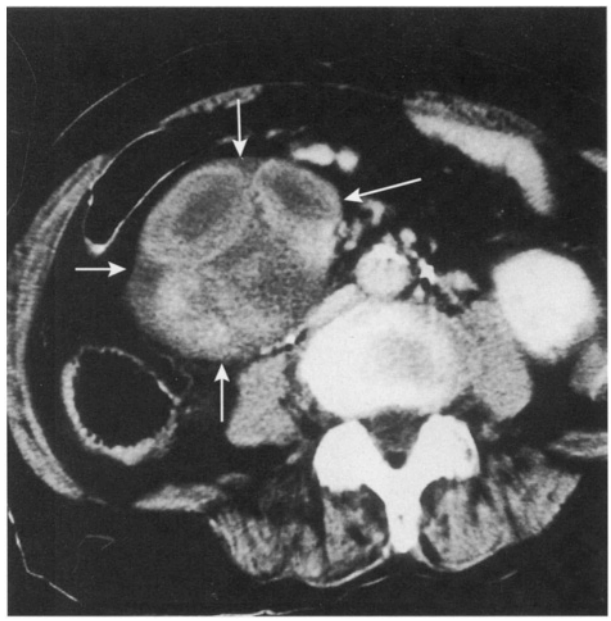


Fig. 16–20. Right paraduodenal hernia: CT findings.
CT demonstrates a saclike collection of dilated intestinal loops with thickened walls, entrapped within the right paraduodenal fossa.
(Courtesy of Sakae Nagaoka, MD, Takeshi Arita MD, and Naofumi Matsunaga MD, Japan.)

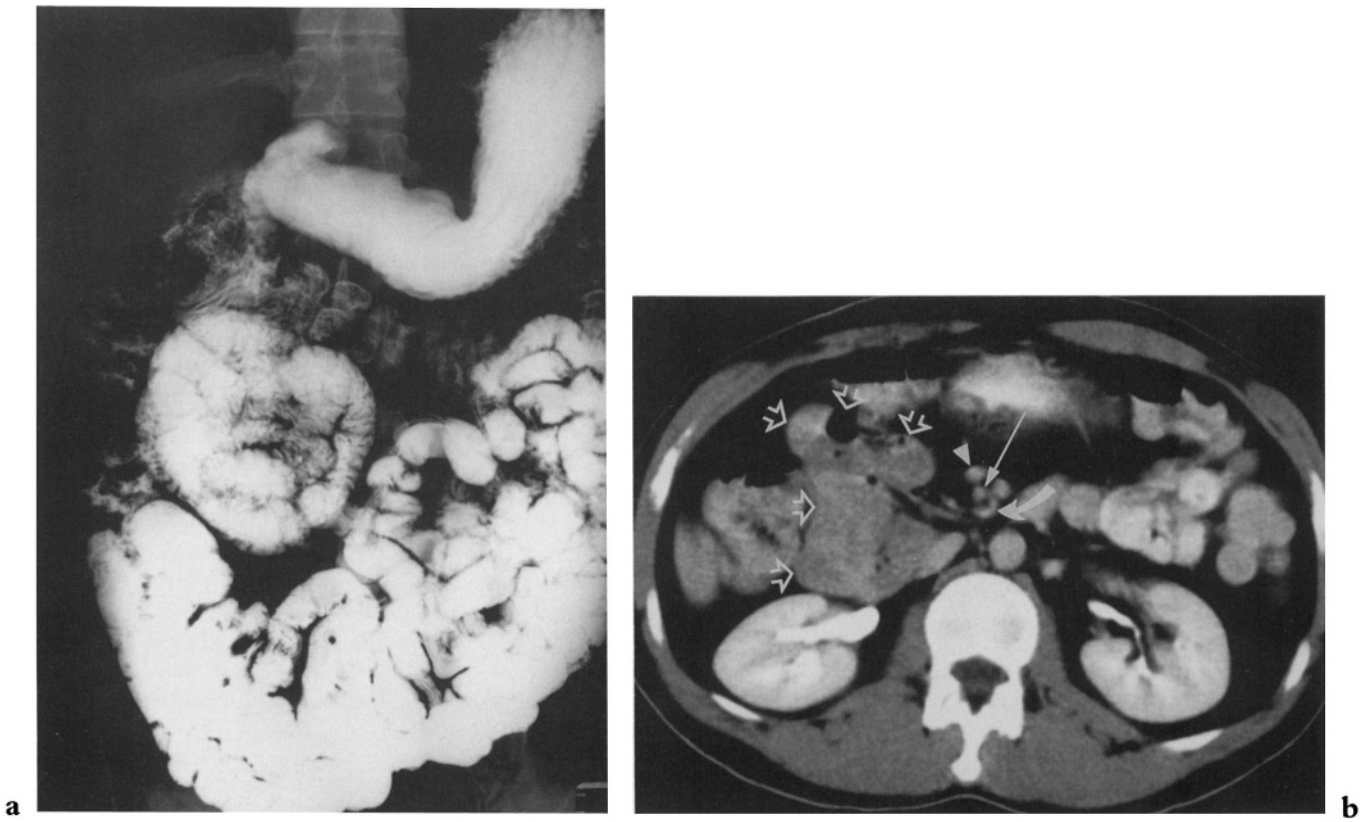


Fig. 16–21. Right paraduodenal hernia.
(a) Small bowel series shows spherical encapsulation of jejunal loops in the right midabdomen.
(b) CT demonstrates absence of the normal horizontal duodenum consistent with nonrotation of the small bowel, multiple loops of which are encapsulated in the right midabdomen *(open arrows).* The normally rotated ascending colon lies lateral to these small bowel loops. The superior mesenteric vein *(arrowhead)* is rotated anterior and to the left of its normal position, and there is looping of arterial and venous jejunal branches *(curved arrow)* behind the superior mesenteric artery *(long arrow)* and into the hernial sac.
(Reproduced from Warshauer and Mauro.[37])

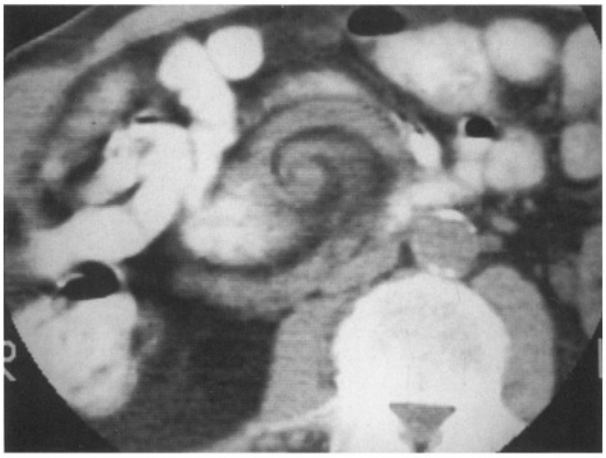


Fig. 16–22. The whirl sign of small bowel volvulus.
CT demonstrates a whirling appearance in which small bowel loops, mesenteric folds, and intestinal branches encircle the superior mesenteric artery and vein. Surgery revealed a 360-degree volvulus of the ileum.
(Reproduced from Izes et al.[48])

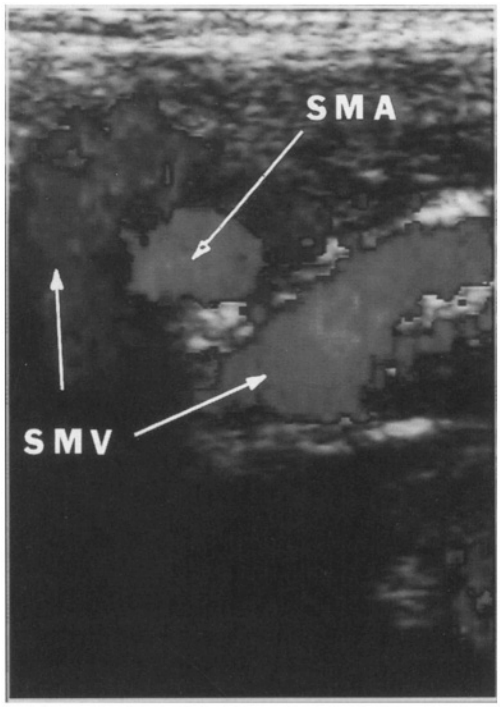


Fig. 16–23. Midgut volvulus in an infant.
Gray scale reproduction of color flow Doppler ultrasonogram in the transverse plane demonstrates the superior mesenteric vein *(SMV)* wrapping around the superior mesenteric artery *(SMA).*
(Reproduced from Hayden.[51])



Fig. 16–24. Midgut volvulus.
Selective superior mesenteric arteriogram demonstrates a twirled appearance of the superior mesenteric artery.
(Reproduced from Izes et al.[48])

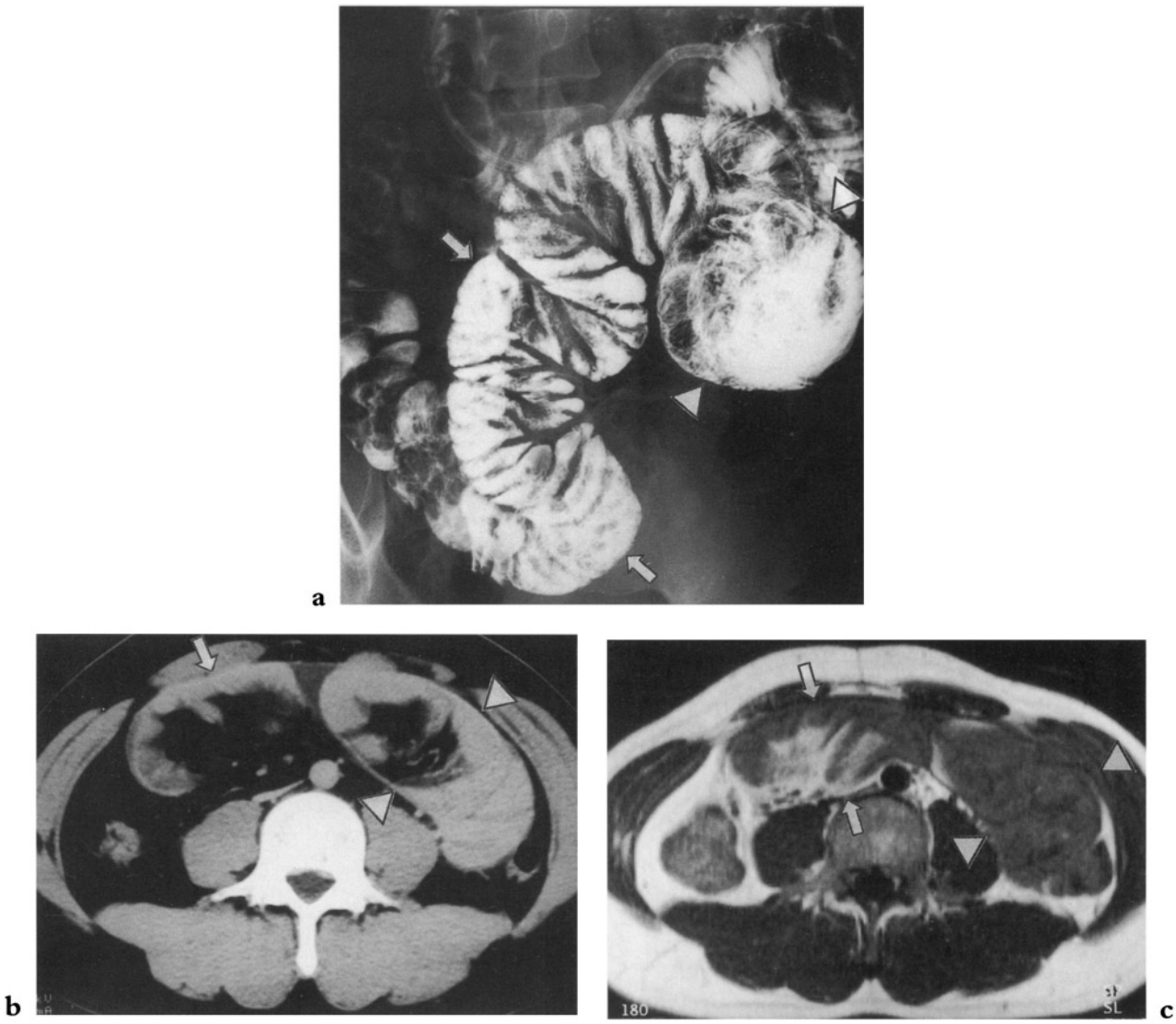


Fig. 16–25. Bilateral paraduodenal hernias.

(a) Oblique projection from a small bowel series demonstrates a large right *(arrows)* and small left *(arrowheads)* circumscribed, ovoid cluster of small intestine. The individual loops could not be separated from this mass with compression.

(b) CT after the administration of intravenous contrast and **(c)** axial T1-weighted MR image demonstrate right *(arrows)* and left *(arrowheads)* circumscribed groups of dilated small bowel loops. On CT, the hernial sacs clearly enhance. On MRI, motion artifacts are limited since these hernias are fixed to the retropentoneum and are often adhered to the hernia sac.

(Reproduced form Oruchi et al.[56])

Internal Hernias Through the Foramen of Winslow

The greater peritoneal cavity communicates with the omental bursa (lesser peritoneal sac) through the epiploic foramen of Winslow. This potential opening is situated beneath the free edge of the lesser omentum, cephalad to the duodenal bulb and deep to the liver, and usually admits one and occasionally two fingers. In life, its anterior and posterior boundaries are usually in contact. The foramen may open to some extent when the trunk is flexed, as in the sitting position.[57] The omental bursa is limited in front by the stomach, lesser omentum, and the gastrocolic ligament, and behind by the posterior abdominal wall. Herniation of bowel through the foramen of Winslow accounts for 8% of all internal hernias.[6,21] The small intestine alone is involved in the herniation in 60–70% of cases and the terminal small bowel, cecum, and ascending colon in 25–30%. Other viscera such as the transverse colon, omentum, or gallbladder are found occasionally.[6,58,59]

Predisposing causes include a common or abnormally long mesentery or persistence of the ascending mesocolon, permitting excessive mobility of the bowel and enlargement of the foramen.[60] Alterations in intraabdominal pressure, including parturition, straining, and large meals, may tend to provoke the onset of the herniation,[57] which may also be facilitated by an elongated right lobe of the liver directing the mobile intestinal loops toward the foramen of Winslow.[61] The onset is usually acute, with severe progressive pain and signs of bowel obstruction. Some relief of pain may be achieved with forward bending or the knee-chest position.[57] The pressure and stretching of the common bile duct by herniated colon may rarely produce an enlarged gallbladder[62] or jaundice.[57]

The characteristic plain film findings are demonstration of a circumscribed collection of gas-containing intestinal loops high in the abdomen medial and posterior to the stomach, associated with mechanical small bowel obstruction (Figs. 16–26 and 16–27). Distinction from other conditions that can present with gas in the lesser sac (e.g., perforated peptic ulcer or abscess) is possible by identification of the presence of a mucosal pattern and fluid levels within the herniated bowel. The fluid levels do not conform precisely to the anatomic recesses of the lesser omental cavity. If the colon is involved in the hernia, there may be a single air–fluid level, but several fluid levels may be present if a segment of small intestine is involved. The stomach is displaced to the left and anteriorly. Dilated small bowel loops generally develop throughout the abdomen. When the cecum and ascending colon are involved in the hernia, the right iliac fossa appears empty,[63–65] and interhaustral septa rather than valvulae conniventes may be identified within the herniated loop (Fig. 16–28). When the small intestine is the segment involved in the hernia, it can sometimes be identified progressing anterior to the hepatic flexure of the colon as it passes up to the foramen. Compression at this site then leads to distention of the ascending colon and cecum as well.

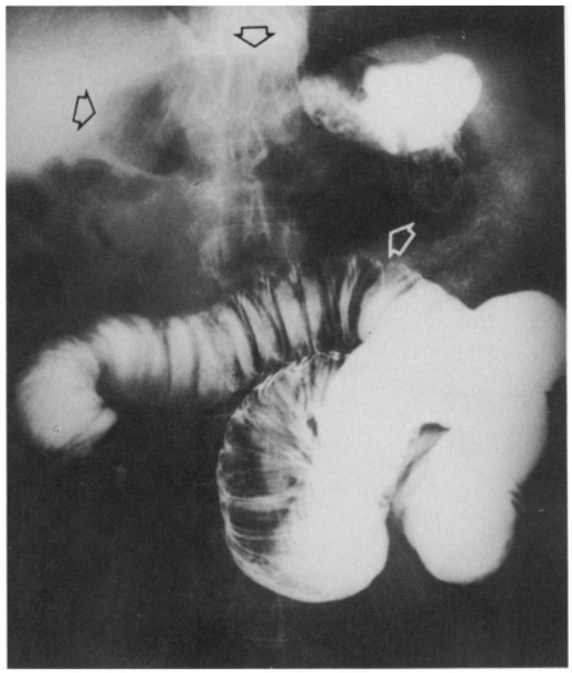


Fig. 16–26. Foramen of Winslow hernia.
Small bowel examination demonstrates marked dilatation of jejunum proximal to an obstruction in the right upper abdomen. The gas-containing herniated small bowel loops are visible within the lesser sac *(arrows)* medial to the stomach.
(Reproduced from Ghahremani and Meyers.[16])

Barium studies readily confirm the diagnosis.[57,61,64,66] The stomach is characteristically displaced anteriorly and to the left, and the first and second portions of the duodenum may also be displaced to the left[63] (Figs. 16–27b, 16–29, 16–30). A small bowel series document the site of obstruction corresponding to the anatomic location of the foramen of Winslow between the duodenal bulb and the hilus of the liver. A barium enema study reveals obstruction with a tapered point near the hepatic flexure if the herniation contains the cecum and ascending colon[57,61,65,68] (Figs. 16–30 and 16–31). If the

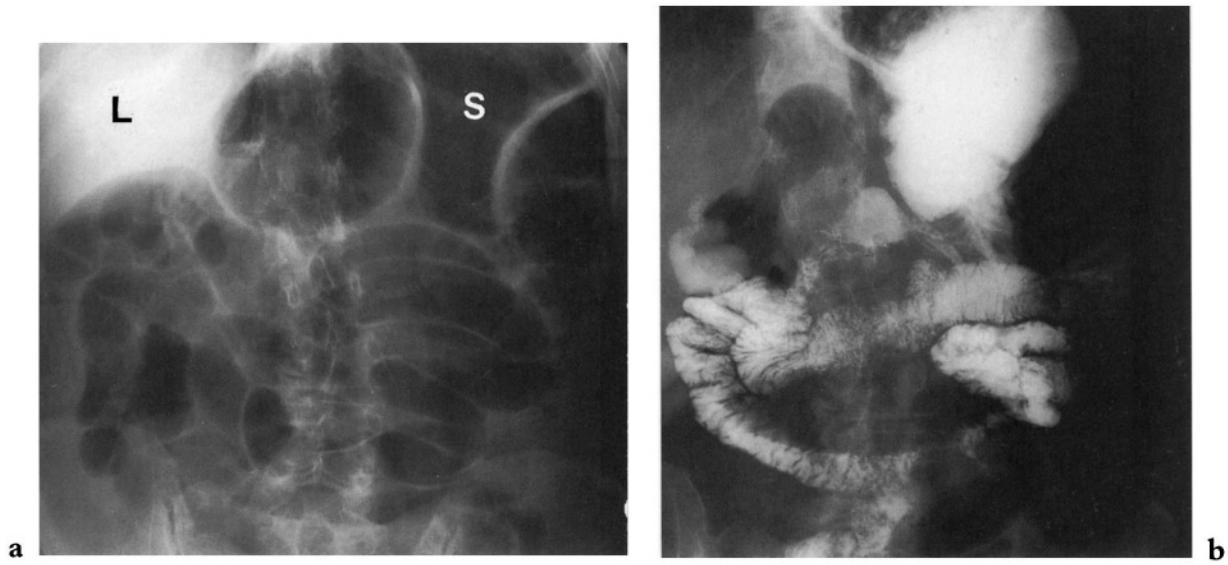


Fig. 16–27. Cecal herniation through the foramen of Winslow.
(a) Supine abdominal film shows marked dilatation of the small bowel. An abnormal collection of gas is seen in the lesser peritoneal sac between the liver *(L)* and the stomach *(S)*.
(b) Upper GI series reveals displacement of the stomach and the first and second parts of the duodenum to the left. There is less gas in the small intestine and within the lesser sac owing to partial spontaneous reduction of the hernia.
(Reproduced from Henisz et al.[63])

small bowel alone is herniated, retrograde flow may be arrested in the transverse colon because of traction on the mesentery by the herniating small bowel.[57,66]

Computed tomography establishes the anatomic landmarks clearly (Figs. 16–32 through 16–34) and may document bowel and mesenteric changes precisely at the foramen of Winslow. The findings are readily distinguishable from the rare anatomic variant in adults of a retrogastric course of the transverse colon demonstrated by CT.[70]

The radiographic presentation may be complicated at times if there are associated defects in the gastrocolic or

text continues on page 737

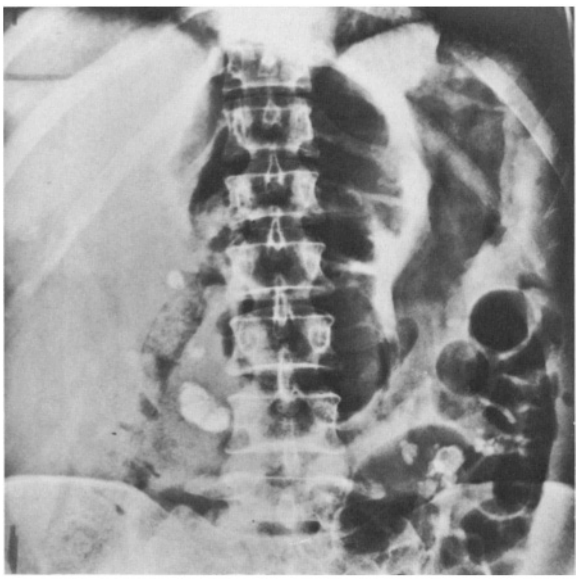


Fig. 16–28. Cecal herniation through the foramen of Winslow.
Plain film demonstrates gas-containing cecum with identifiable interhaustral septa within the lesser sac, displacing the stomach toward the left.

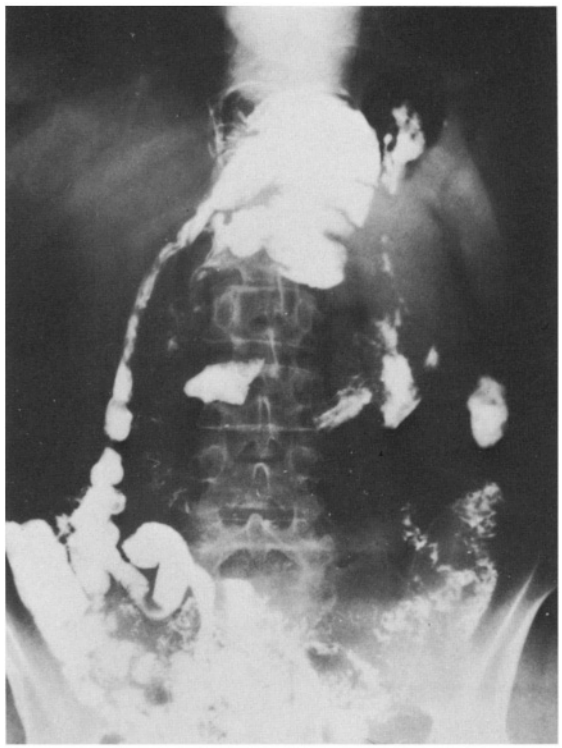


Fig. 16–29. Foramen of Winslow hernia.
Delayed film from upper GI series demonstrates stretched terminal ileum ascending through the foramen of Winslow with the cecum and ascending colon within the lesser sac medial to the stomach.
(Reproduced from Schwartz and Feuchtwanger.[67])

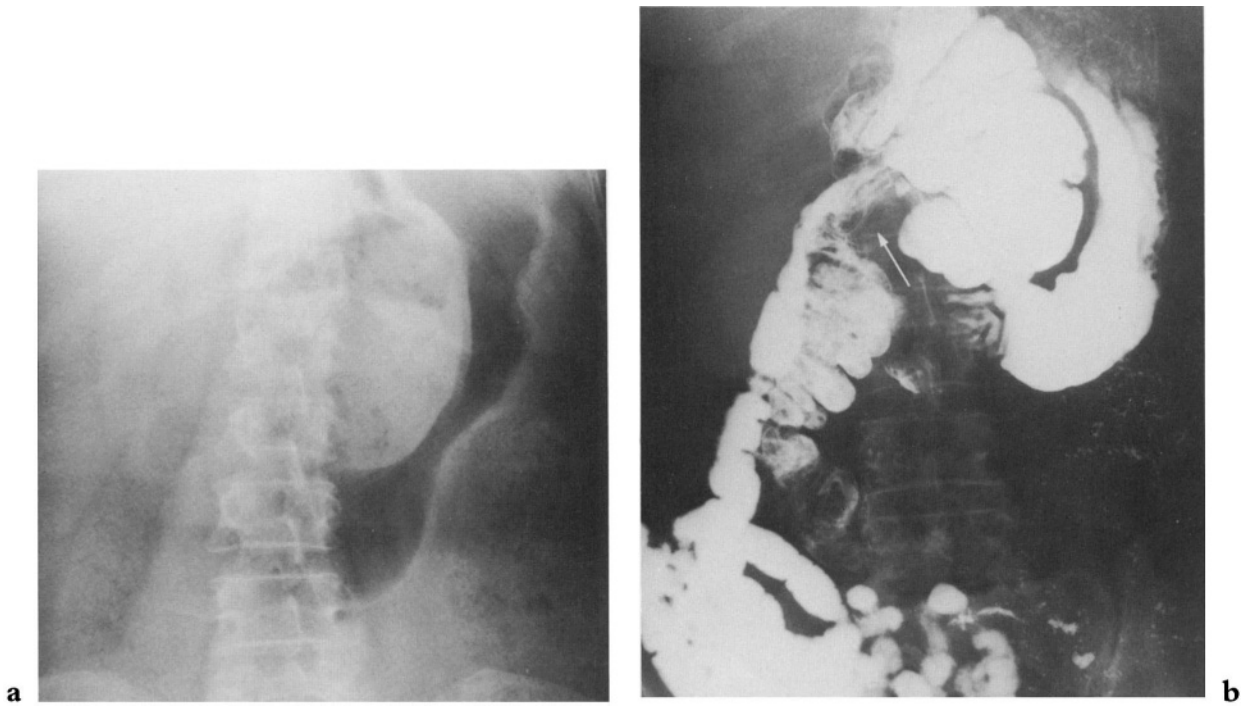


Fig. 16–30. Foramen of Winslow hernia.
(a) Plain film shows mottled gas density consistent with large bowel impressing upon the lesser curvature of the stomach.
(b) Small bowel follow-through confirms herniation of the cecum and ascending colon into the lesser sac. Note the compression of the ascending colon at the foramen of Winslow *(arrow).*
(Reproduced from Goldberger and Berk.[68])

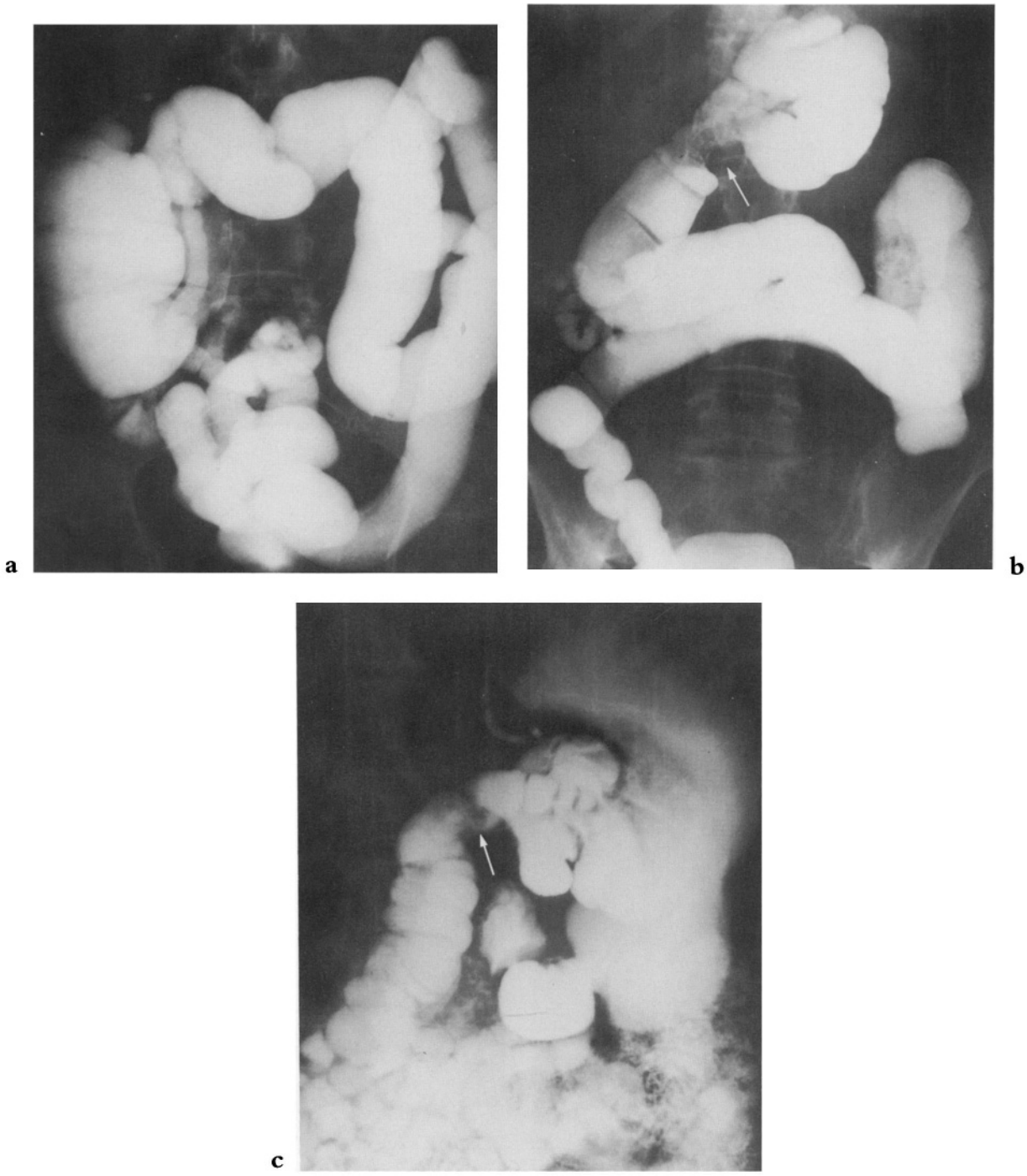


Fig. 16–31. Foramen of Winslow hernia.
(a) Barium enema shows failure of fixation of the right colon. The cecum and appendix arise into the right upper quadrant of the abdomen.
(b and **c)** Barium enema study and small bowel follow-through 4 years later. The cecum and ascending colon have herniated into the lesser sac, indenting the stomach. Compression of the ascending colon as it passes through the foramen of Winslow can be identified *(arrows).*
A large ovarian cyst that has developed since the preliminary study causes elevation and stretching of the sigmoid colon. This may have contributed to increased intraabdominal pressure and the formation of the internal herniation.
(Reproduced from Goldberger and Berk.[68])

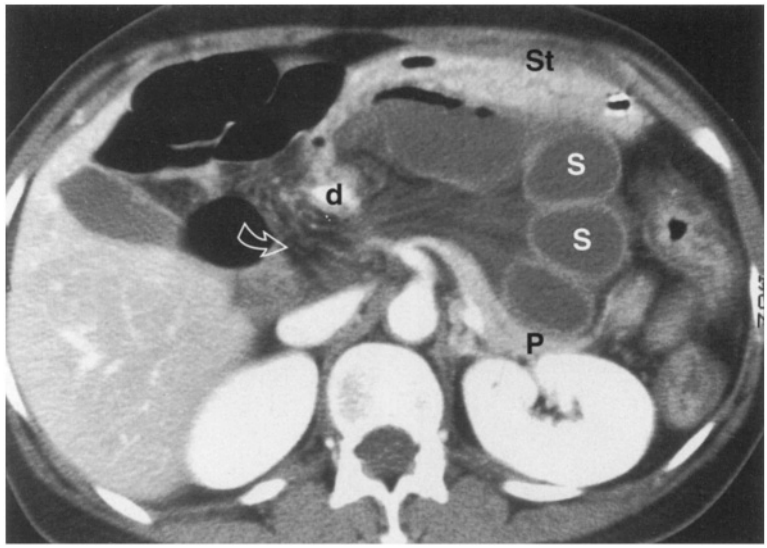


Fig. 16–32. Strangulated lesser sac hernia.
Dynamic contrast-enhanced CT demonstrates multiple dilated, fluid-filled loops of small intestine *(S)* in the lesser sac, between the stomach *(St)* and pancreas *(P).* The entrance of the mesenteric vascular pedicle with mesenteric fat is seen at the widened foramen of Winslow *(arrow)* behind the duodenum *(d).* Mesenteric edema and a small amount of lesser sac ascites are present.
(Courtesy of Jay Heiken, MD, Mallinckrodt Institute of Radiology, St. Louis, MO.)

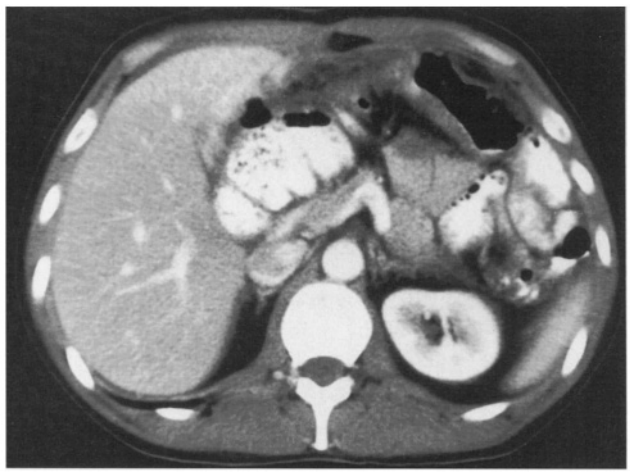


Fig. 16–33. Cecal herniation through the foramen of Winslow.
CT shows the opacified cecum in the lesser sac, between the liver, stomach, and pancreas.

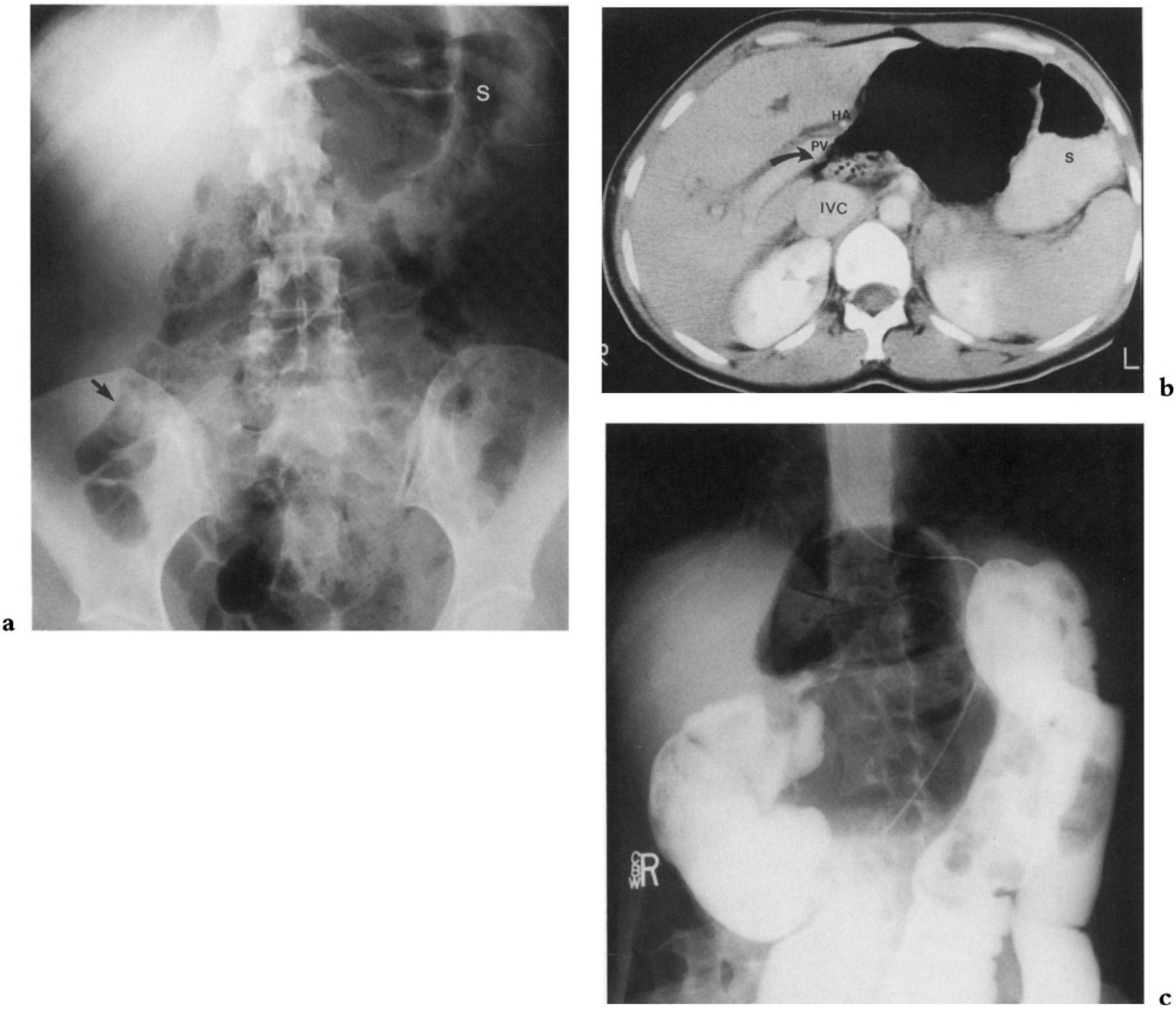


Fig. 16–34. Cecal herniation through the foramen of Winslow.
(a) Supine abdominal film demonstrates dilated loop of colon in the epigastrium with displacement of the stomach *(S)* to the left. Stool-filled bowel in the right lower quadrant *(arrow)* was originally thought to represent cecum.
(b) CT at the level of the celiac axis shows a collection of air in the lesser sac displacing the stomach *(S)* anteriorly and laterally. The collection has a beaklike projection *(arrow)* extending anterior to the inferior vena cava *(IVC)* and posterior to the portal vein *(PV)* and hepatic artery *(HA).* This tapered bowel loop is precisely at the foramen of Winslow.
(c) Water-soluble contrast enema confirms the location of the air-filled cecum in the lesser sac posteromedial to the nasogastric tube.
(Reproduced from Wojtasek et al.[69])

gastrohepatic omentum allowing reentry of the herniated loops into the greater peritoneal cavity.[57]

Unusual sites of entry into the lesser sac include the transverse mesocolon (see Fig. 16–47), gastrocolic ligament,[71] and gastrohepatic ligament.[72]

Pericecal Hernias

Four peritoneal fossae in the ileocecal region as well as congenital and acquired defects in the mesentery of the cecum or appendix may lead to development of a pericecal hernia.[7,9,19,73] The variety of other terms (ileocolic, retrocecal, ileocecal, paracecal) used to classify these hernias appear to have limited practical value in the radiologic differential diagnosis and surgical management.[16]

In the collective review of 467 internal hernias by Hansmann and Morton,[21] 13% involved the ileocecal region. The clinical manifestations are usually intermittent episodes of right lower abdominal pain, tenderness small bowel distention, nausea, and vomiting. Chronic incarceration may produce symptoms compatible with a periappendiceal abscess, Crohn's disease, or intestinal obstruction owing to adhesions.[9,19]

In most cases, a portion of ileum passes through defects in the mesentery of the cecum to occupy the right paracolic gutter. The correct diagnosis may be suggested on plain radiographs of the abdomen (Fig. 16–35). More useful are the delayed films of the small bowel series or a barium enema examination in which reflux into the terminal ileum has been achieved. Careful fluoroscopic evaluation and radiographs in lateral and oblique projections are particularly valuable for the demonstration of the fixed position of herniated loops posterolateral to the cecum.[16] This is also true for the diagnosis of internal hernias that rarely develop through defects in a persistent ascending mesocolon[18] (Fig. 16–36). In this condition, the radiologic differentiation from a transitory transmigration of the small intestine anteriorly over the ascending colon into the right paracolic gutter has clinical and prognostic significance.

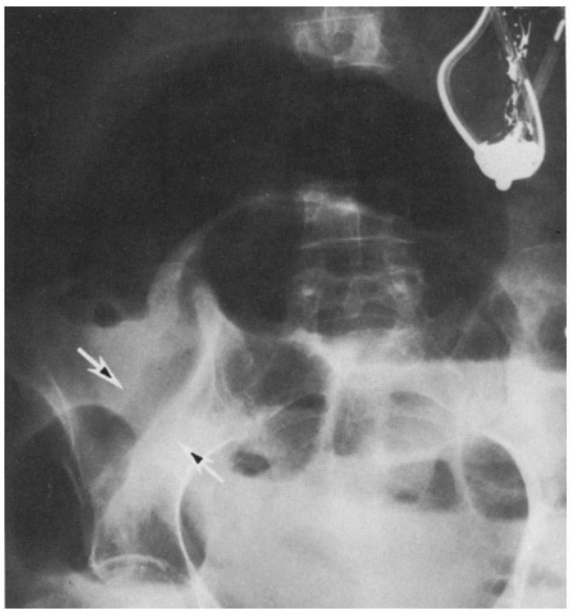


Fig. 16–35. Pericecal hernia.
The distal ileum protruding through a defect in the mesentery of the cecum is seen in the right lower abdomen, and there is gaseous distention of the proximal small intestine. The narrowed afferent segment of the herniated ileal loop *(arrow)* is identified.
(Reproduced from Ghahremani and Meyers.[16])

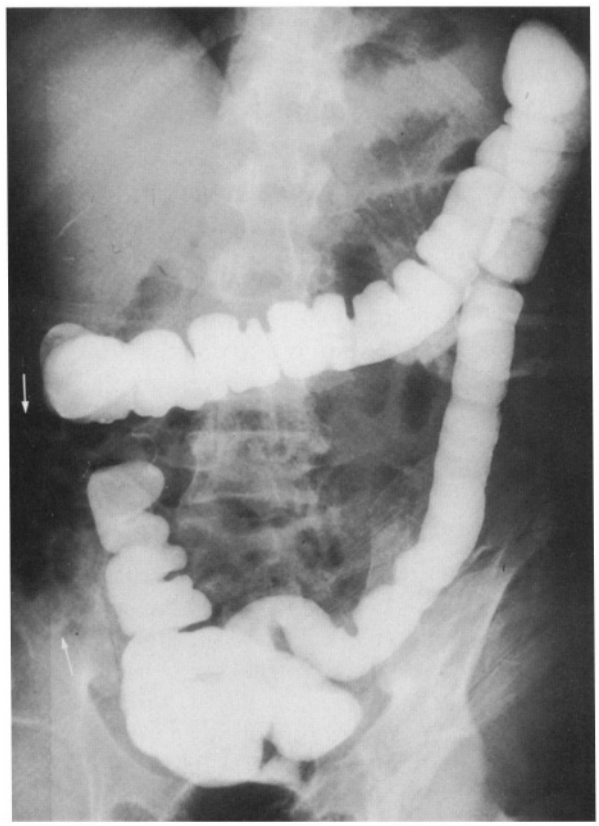


Fig. 16–36. Herniation of the ileal loops through a defect in a persistent ascending mesocolon.
There is moderate dilatation of the proximal small bowel, and there are gas-containing loops in the right paracolic gutter *(arrows)* displacing the ascending colon medially.
(Reproduced from Ghahremani and Meyers.[16])

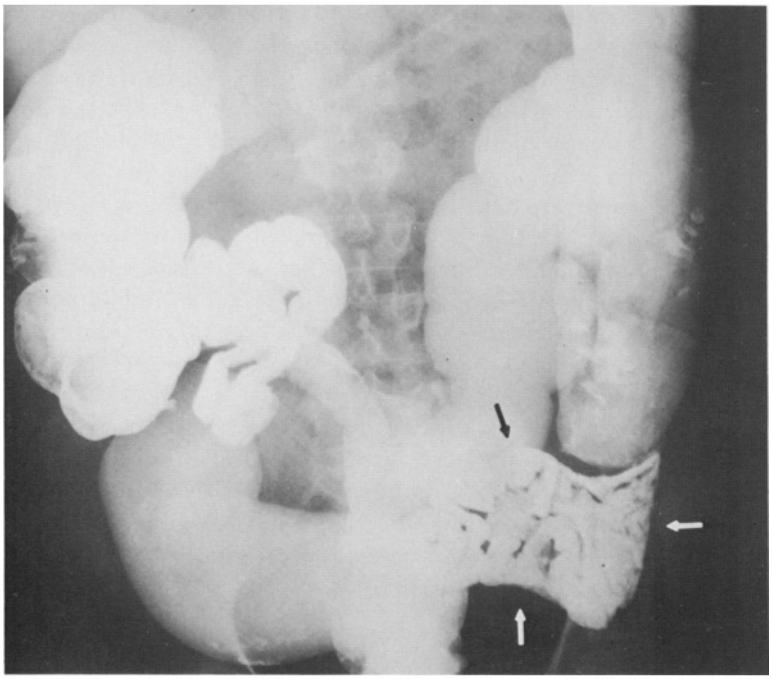


Fig. 16–37. Intersigmoid hernia.
Barium enema examination, with retrograde filling of the small bowel, shows encapsulation of several ileal loops *(arrows)* within the intersigmoid fossa.
(Reproduced from Ghahremani and Meyers.[32])

Intersigmoid Hernias

The intersigmoid fossa is a peritoneal pouch formed between the two loops of the sigmoid colon and its mesentery. This pocket is found in 65% of cadavers and serves as a potential site for an intersigmoid hernia.[9,16,18] This is usually a reducible hernia containing a few small bowel loops. Incarceration is uncommon.

The radiologic diagnosis of intersigmoid hernia is best made by retrograde filling of the small intestine during barium enema examination. Figure 16–37 shows the encapsulated ileal loops in a characteristic relationship to the sigmoid colon.

Two other similar, but rare, entities are (a) the intramesosigmoid hernia, which involves a defect of only one of the constituent mesenteric leaves, the separation of which forms the hernial sac;[18] and (b) the transmesosigmoid hernia, in which a usually large defect in both layers of the sigmoid mesentery allows herniation of the small bowel loops toward the left lower abdomen posterolateral to the sigmoid colon[18,19] (Fig. 16–38).

Radiologic differentiation of the three types of hernia involving the mesosigmoid is often difficult and irrelevant in terms of their ultimate surgical management. Observation of an intimate relationship between the sigmoid colon and intestinal loops clumped or fixed posterior and lateral to it can serve as a useful criterion to indicate the probability of an internal hernia involving the mesosigmoid.[16]

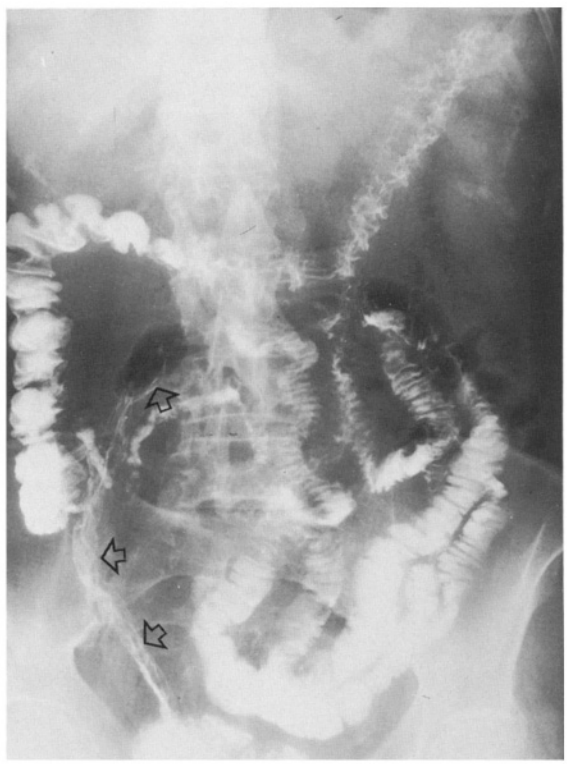


Fig. 16–38. Transmesosigmoid hernia.
The postevacuation film of a barium enema study demonstrates herniated small bowel loops occupying the left lower abdomen. The sigmoid colon *(arrows)* is elevated and displaced to the right.
(Reproduced from Ghahremani and Meyers.[16])

The findings are to be distinguished from a persistent descending mesocolon[7,18,60] that may occasionally contain defects involving both layers; small bowel loops may then pass behind the descending colon and fill the left paracolic gutter (Fig. 16–39).

Transmesenteric and Transmesocolic Hernias

About 5–10% of all internal hernias occur through defects in the mesentery of the small intestine.[12,13,21] An etiologic relationship to prenatal intestinal ischemic accidents seems probable, because in infants with atretic intestinal segments such defects and herniation are frequently associated.[14] In fact, nearly 35% of these hernias occur in the pediatric age group, in which they constitute the most common type of internal hernias.[8,14] In adults, however, most mesenteric defects serving as the hernial ring are probably the result of previous surgery, abdominal trauma, or intraperitoneal inflammation.[12,13]

The mesenteric defects are often located close to the ligament of Treitz or the ileocecal valve. The rather small size of the defect (usually 2–5 cm) and the absence of a limiting hernial sac account for a relatively high incidence of strangulation and intestinal gangrene, with a mortality rate of about 50% for surgically treated patients and 100% for those without surgical treatment.[12]

Radiographs of the abdomen usually demonstrate mechanical small bowel obstruction and, occasionally, a single distended "closed loop," with perhaps apposition of the afferent and efferent limbs (Fig. 16–40). The small bowel series or barium enema study with reflux may further assist in the diagnosis by showing a constriction around the closely approximated afferent and efferent loops of the herniated intestine[73,74] (Fig. 16–41). These findings invariably signal a surgical emergency, although clinical and radiologic differentiation of the hernia from small bowel volvulus or entrapment beneath peritoneal

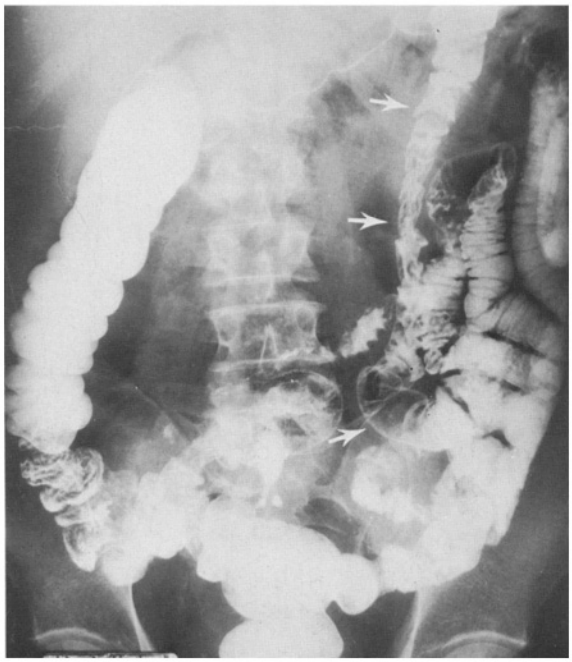


Fig. 16–39. Persistent descending mesocolon.
The ileal loops opacified by reflux during barium enema examination occupy the left paracolic gutter. The descending colon *(arrows)* is displaced toward the midline. The presence of a probable defect in the mesocolon is not yet verified surgically in this patient.
(Reproduced from Ghahremani and Meyers.[16])

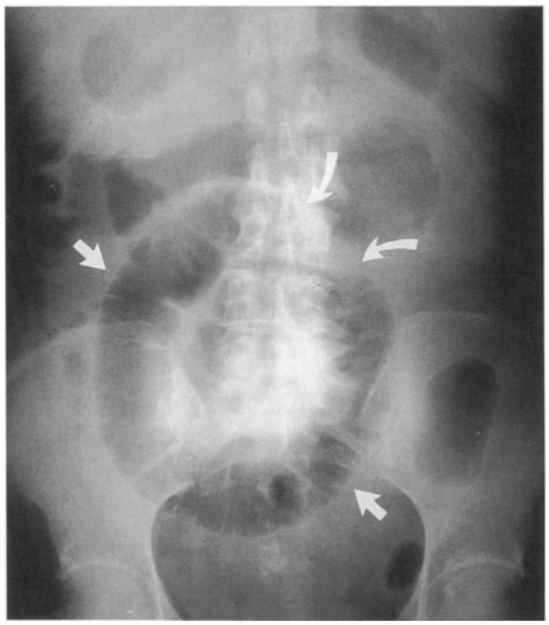


Fig. 16–40. Transmesenteric hernia.
Herniation of a jejunal loop through a defect in the small bowel mesentery. Note the typical presentation of a distended closed loop *(straight arrows)* with approximation of its ends at the hernial orifice *(curved arrows).*
(Reproduced from Ghahremani and Meyers.[16])

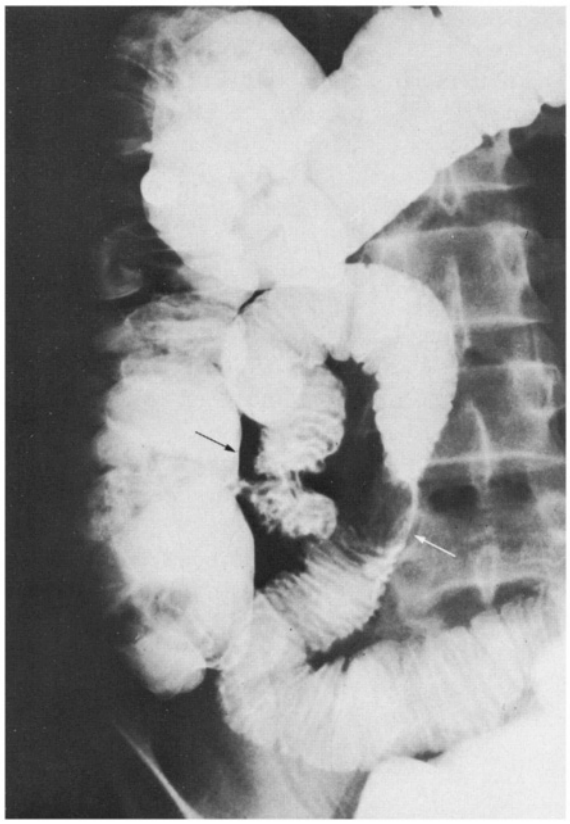


Fig. 16–41. Transmesenteric hernia.
Herniation of the distal ileum through a congenital defect in the mesentery of a Meckel's diverticulum. Barium enema study with reflux shows constriction around the closely approximated afferent and efferent loops *(arrows)* of the ileum.
(Reproduced from Dalinka et al.[74])

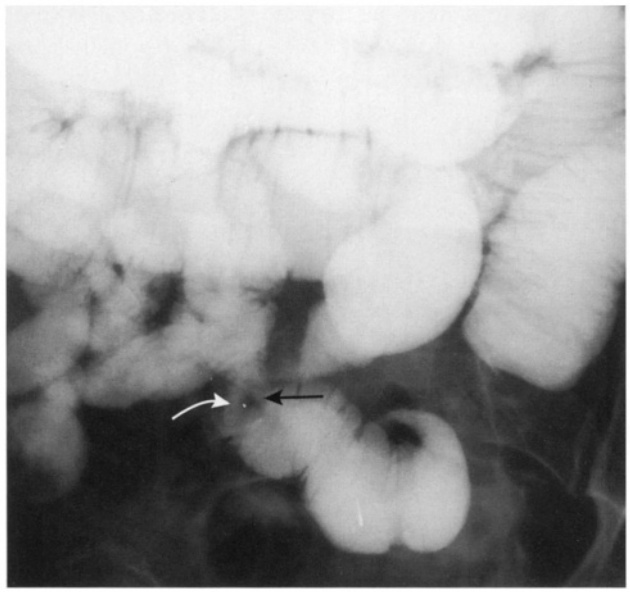


Fig. 16–42. Partial volvulus through mesenteric defect.
A postsurgical defect in the mesentery provides the site for an internal hernia. Volvulus is indicated by the crossing of the afferent and efferent limbs at the point of obstruction *(arrows).*
(Reproduced from Maglinte et al.[75])

adhesions may be impossible.[16] Volvulus of the herniated loops may be shown by crossing of the involved limbs at the point of obstruction[75] (Fig. 16–42). Computed tomography displays the relationships of the herniated loops (Fig. 16–43) and may reveal complications (Fig. 16–44). Even if the mesenteric defect itself is not recognized, disclosure of the mesenteric vascular pedicle may be diagnostic for internal hernia (H. Mori, personal communication). Arteriography may reveal an abrupt change in the course of the superior mesenteric artery and displacement of the visceral branches, indicating an internal hernia with the site of the herniation suggested by the change in the course of the vessels[77,78] (Fig. 16–45).

Defects in the transverse mesocolon may rarely provide access for internal herniation of small bowel loops posterior to the transverse colon into the lesser sac[7,79,80] (Figs. 16–46 and 16–47). Although these defects may result from trauma, inflammation, or operative procedures, most are probably congenital in origin. Since the orifice is usually very large with an avascular space in the base of the mesocolon, many loops may herniate without strangulation, gangrene, or even significant obstruction. Reentry into the greater peritoneal cavity is frequent, via the routes of the foramen of Winslow, the gastrohepatic ligament, and the gastrocolic ligament[81] (Fig. 16–48).

text continues on page 744

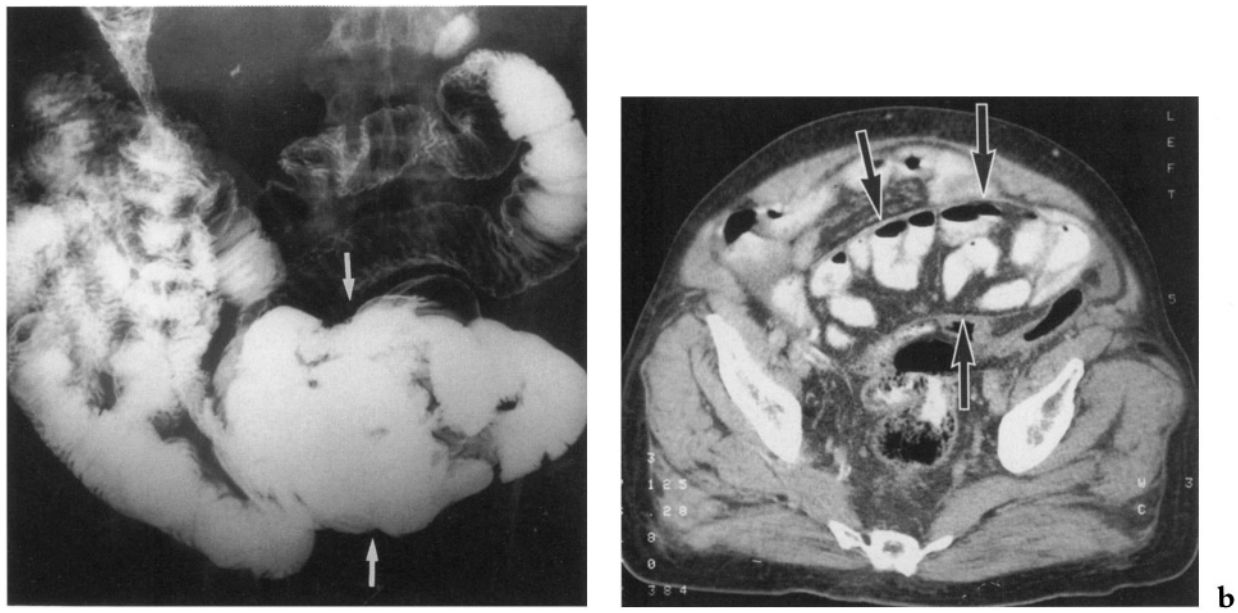


Fig. 16–43. Transmesenteric hernia.
(a) Small bowel series shows a peculiar grouping of small bowel loops in the lower abdomen *(arrows).*
(b) CT demonstrates these multiple loops are circumscribed within a transmesenteric hernial sac *(arrows).*
(Reproduced from Miller et al.[76])

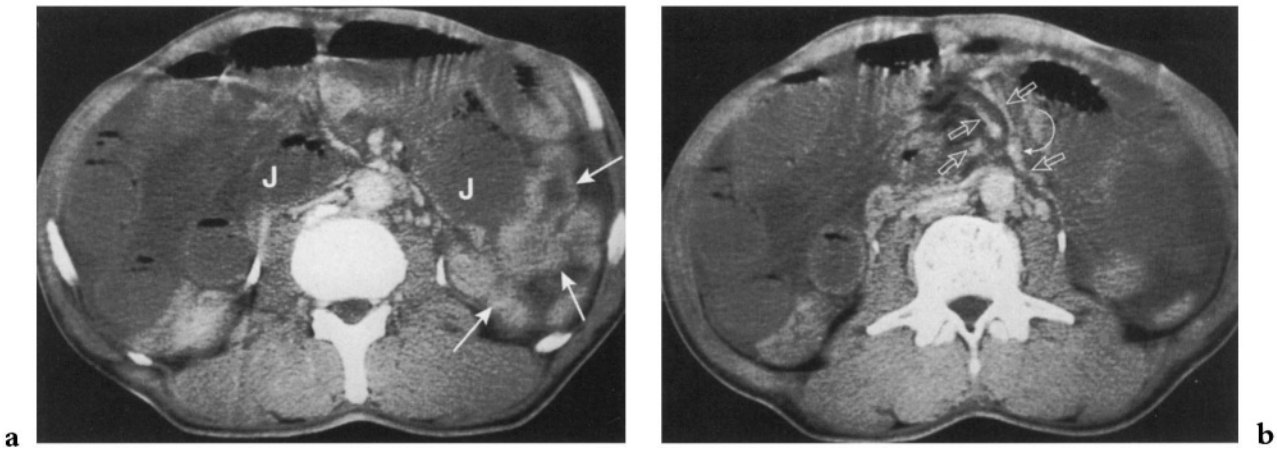


Fig. 16–44. Strangulated transmesenteric hernia.
Almost all the jejunal loops have herniated through a large defect of the small bowel mesentery and twisted, with resultant necrosis.
CT after administration of intravenous contrast demonstrates **(a)** normal proximal jejunal loops *(arrows),* a markedly distended fluid-filled loop of twisted jejunum *(J),* and **(b)** superior mesenteric artery and vein with abrupt angulation at the twisted site *(open arrows)* with dilated collateral veins *(curved arrow).*
(Courtesy of Hiromu Mori, MD, Oita Medical University, Oita, Japan.)

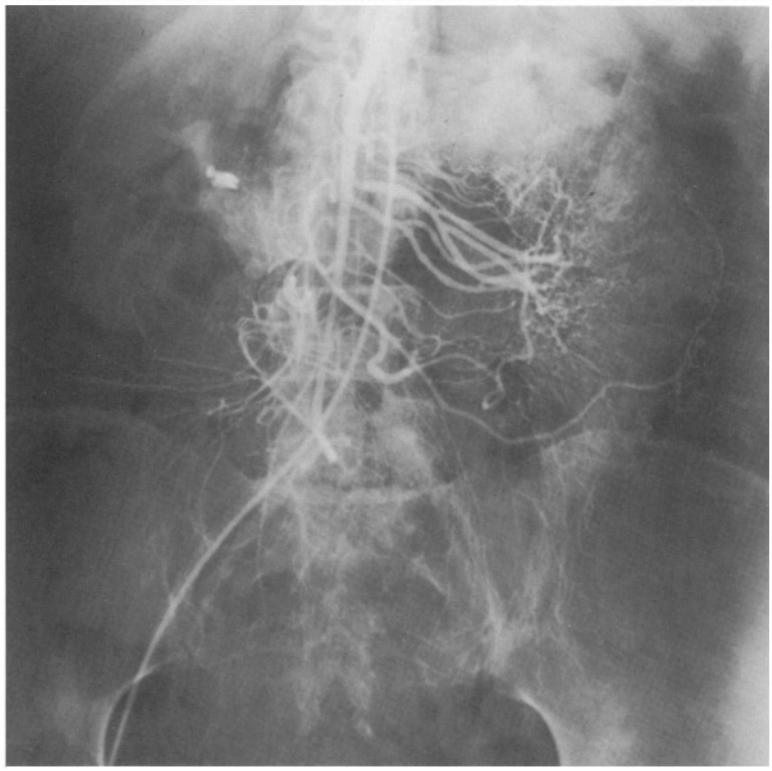
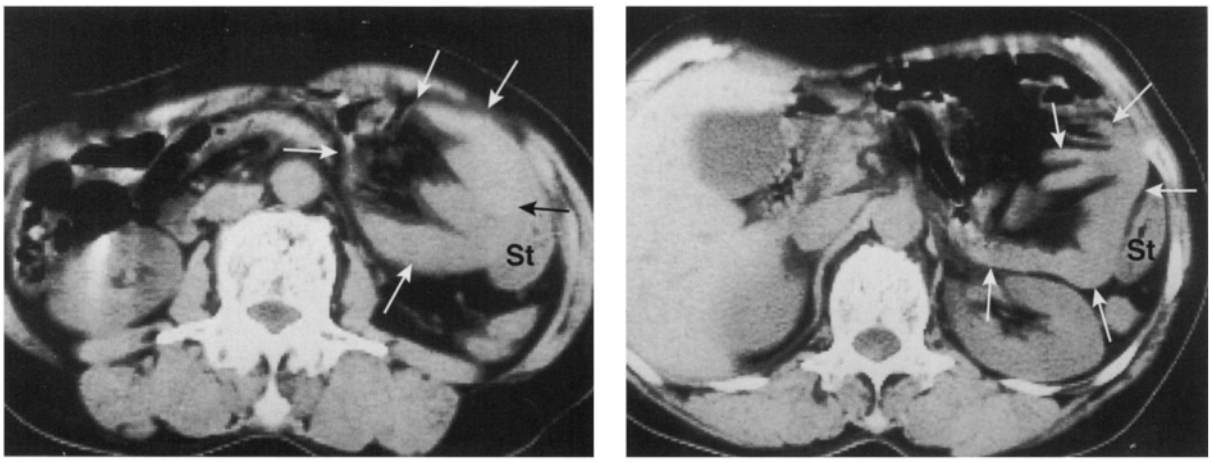


Fig. 16–45.Transmesenteric hernia.
Arteriogram in a 48-year-old female with acute abdominal symptoms shows an abrupt change in the course of the superior mesenteric artery, which is seen to fold back on itself. The terminal ileal and ileocolic branches course in a twisting fashion toward the left upper quadrant and fan toward the right flank instead of distributing in the normal lower abdominal course from the left to the right.
At surgery, herniation of the entire right colon and half of the small bowel with a twist through a 10-cm congenital defect in the small bowel mesentery was found. This was reduced manually and the defect closed.
(Reproduced from Cohen and Patel.[77])



a b

Fig. 16–46. Transmesocolic hernia into the lesser sac.
(a and **b)** CT demonstrates that jejunal loops along with their mesenteric fat and vessels *(arrows)* have herniated into the lesser sac through a defect of the transverse mesocolon. *St* = stomach.
(Courtesy of Hiromu Mori, MD, Oita Medical University, Oita, Japan.)

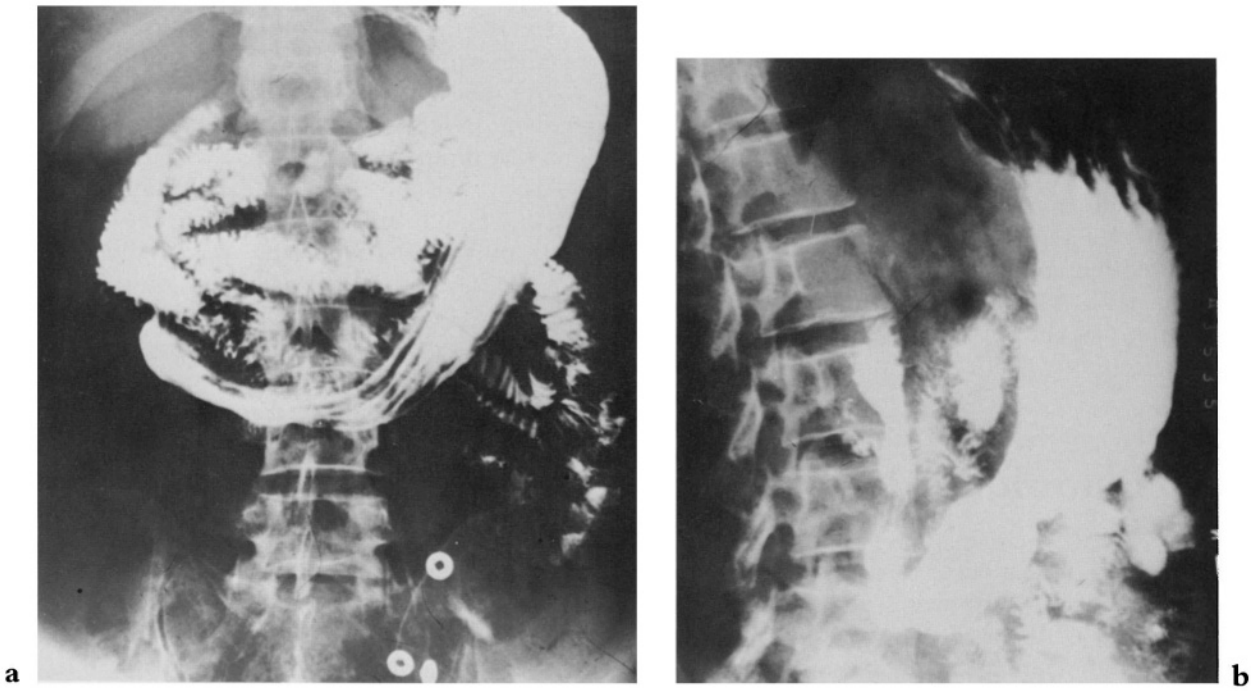


Fig. 16–47. Transmesocolic hernia into the lesser sac.
(a) Prone and **(b)** oblique radiographs demonstrate multiple small bowel loops above and posterior to the displaced stomach. They have entered the lesser sac through a large defect in the transverse mesocolon. (Reproduced from Meyers and Whalen.[80])

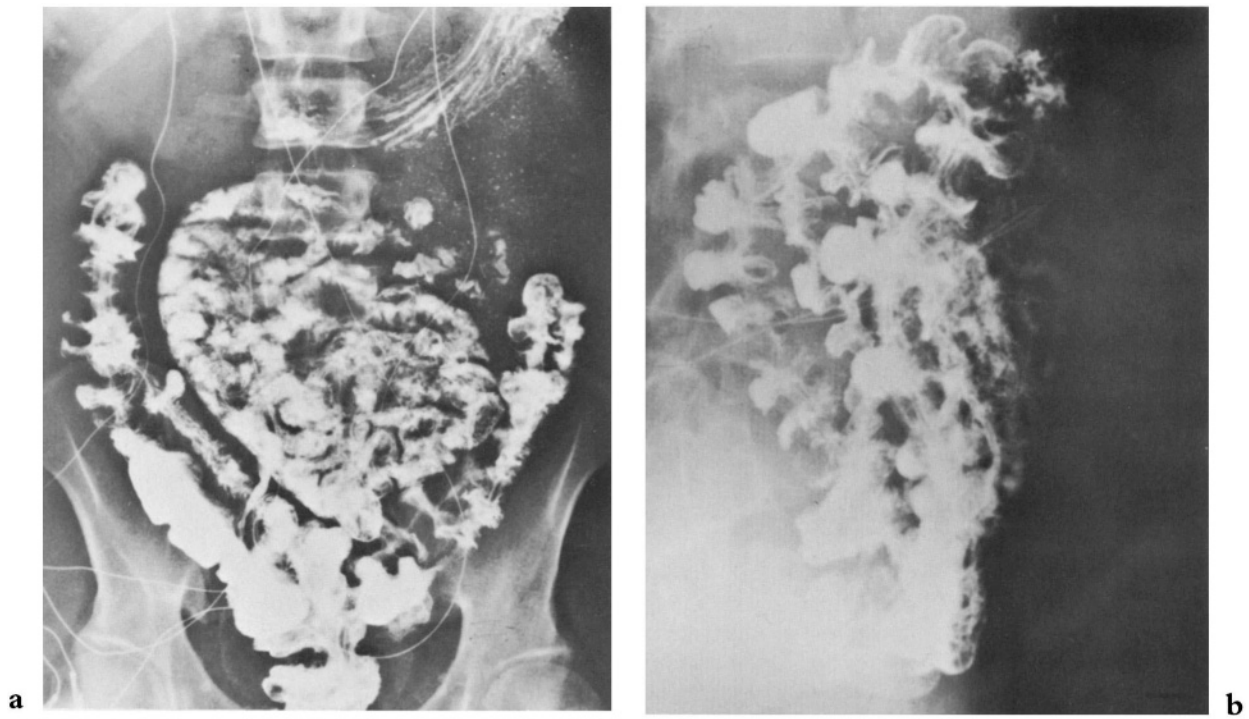


Fig. 16–48. Transmesocolic hernia.
(a) Supine and **(b)** lateral radiographs demonstrate virtually the entire small bowel loops have herniated through a large defect in the transverse mesocolon into the lesser sac. They have then bulged anteriorly into or through the gastrocolic ligament to displace the transverse colon inferiorly and posteriorly. (Courtesy of Alan Herschman, M.D., New Brunswick, NJ.)

Hernias Through the Falciform Ligament

Internal hernias through the falciform ligament are rare. About 80% occur in adults,[82] and most lead to bowel incarceration.[82,83] Figure 16–49 documents the CT findings of a closed–loop obstruction with vascular compromise. Intrahepatic anastomoses between the biliary tree and bowel for hilar cholangiocarcinoma[84,85] may mimic this appearance (Fig. 16–50).

Retroanastomotic Hernias

Retroanastomotic hernias occur usually in patients who have undergone partial gastrectomy and gastrojejunostomy, particularly of the antecolic variety.[11,86] The superior border of the hernial ring is formed by the transverse mesocolon, the inferior border by the ligament of Treitz, and the anterior aspect by the gastrojejunostomy together with the afferent limb of the jejunum[11] (Fig. 16–51). The herniated loop is usually the efferentjejunal segment or, less commonly, an excessively long afferent limb that protrudes into the retroanastomotic space.

About half of these hernias manifest themselves within 1 month and another 25% within 1 year after the operation,[87] with symptoms of cramping abdominal pain and signs of a high small bowel obstruction. These nonspecific findings may be mistaken for stomal edema, dumping, or pancreatitis, and the correct diagnosis may be delayed until strangulation has developed.[10,11,87] This contributes to the reported mortality rate of 32% for surgically treated cases and almost 100% for untreated patients.[11]

Careful fluoroscopic evaluation discloses that the obstruction is situated not at the gastric stoma but more distally in either of the anastomotic limbs. Gradual opacification of the partially obstructed efferent loop shows its abnormal position just lateral and posterior to the gastrojejunostomy (Fig. 16–52). Some degree of dilatation and stasis is usually associated.

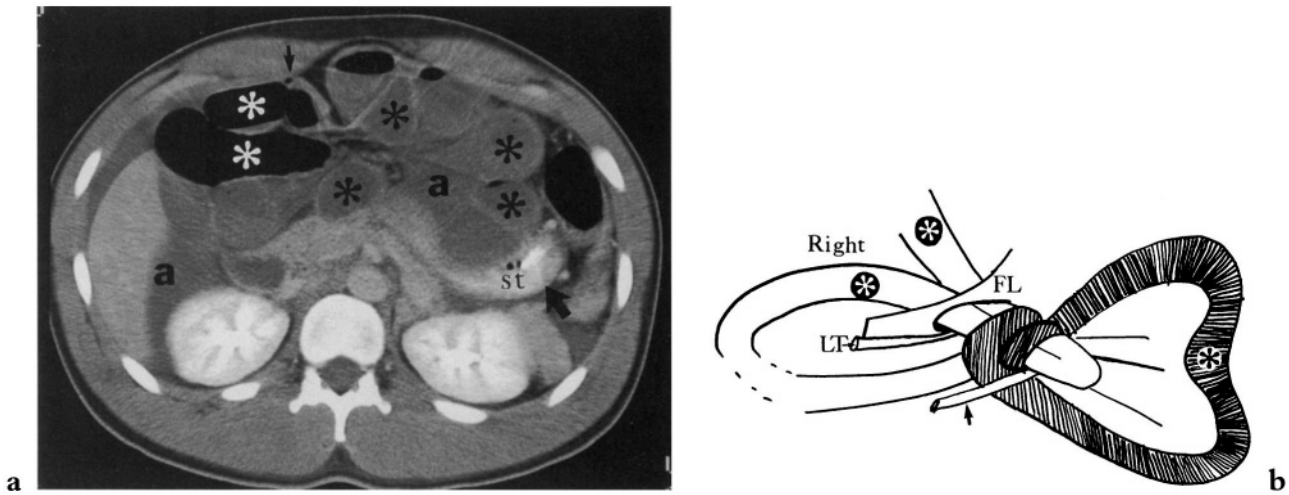


Fig. 16–49. Small bowel herniation through the falciform ligament.
(**a**) Postcontrast CT demonstrates multiple dilated fluid–filled small bowel loops *(black asterisks)* anterior to the stomach *(st).* They show inhomogenous enhancement of a thickened bowel wall. These loops are tethered toward the site of volvulus to the left of the level of the falciform ligament; to the right, the thin-walled loops proximal to the obstructing hernia are air-filled and dilated *(white asterisks).* Collapsed distal small bowel with gas bubble can be identified *(small arrow).* Fluid *(a)* is seen around the liver and in the small bowel mesentery.
(b) Diagram of surgical findings, showing jejunal herniation from right to left through a rent in the falciform ligament *(FL)* between the ligamentum teres *(LT)* and the anterior abdominal wall. Volvulus with infarction involves the herniated segment on the left side.
(Reproduced from Walker and Baer.[83])



Fig. 16–50. Hepatojejunostomy simulating a hernia through the falciform ligament.
In this patient with a cholangiocarcinoma of the common bile duct, surgical anastomosis of a jejunal loop to the left hepatic duct mimics the appearance of herniation through the falciform ligament.

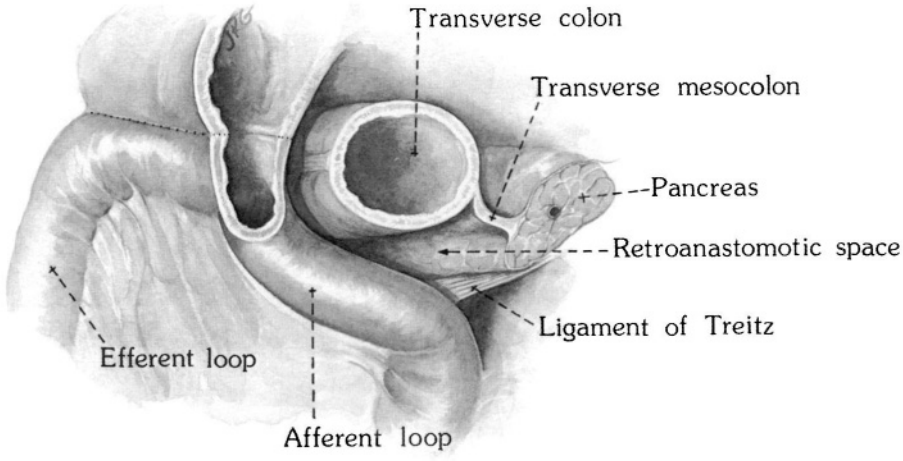


Fig. 16–51. Lateral drawing of the retroanastomotic hernial ring in the antecolic gastrojejunostomy.

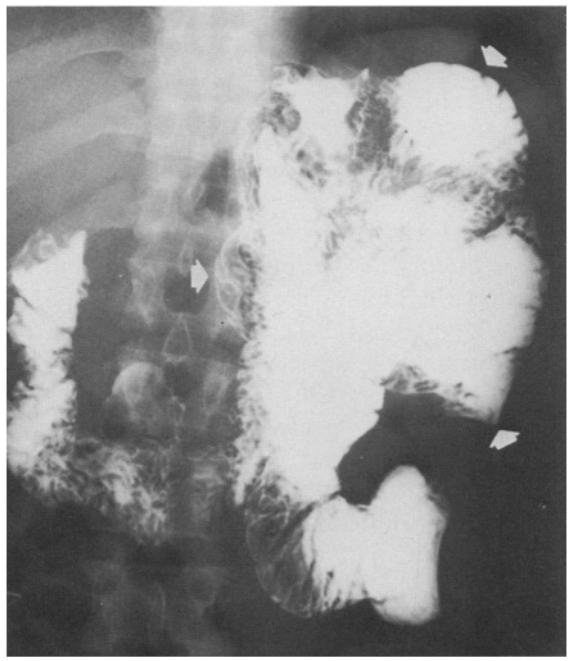


Fig. 16–52. Retroanastomotic hernia.
Upper GI series post-Billroth II shows the herniated efferent loop encapsulated in the left upper quadrant *(arrows).* The afferent loop with a duodenal diverticulur also opacified with barium.
(Courtesy of Gary G. Ghahremani, M.D., Evanston Hospital, Evanston, IL.)

References

1. Balthazar EJ: intestinal malrotation in adults: Roentgenographic assessment with emphasis on isolated complete and partial nonrotations. AJR 1976; 126:358–367.
2. Wang CA, Welch CE: Anomalies of intestinal rotation in adolescents and adults. Surgery 1963; 54:839–855.
3. Gale ME, Gerzof SG, Kiser LC, et al: CT appearance of afferent loop obstruction. AJR 1982; 138: 1085–1088.
4. Jaramillo D, Raval B: CT diagnosis of primary small-bowel volvulus. AJR 1986; 147:941–942.
5. Lieberman JM, Haaga JR: Case report: Duodenal malrotation. J Comput Assist Tomogr 1982; 6(5): 1019–1020.
6. Jones TW: Paraduodenal hernia and hernias of the foramen of Winslow. *In* Hernia. Edited by IM Nyhus, HN Harkins. JB Lippincott, Philadelphia, 1964, pp 577–601.
7. Mueller EC: Congenital internal hernia. Am J Surg 1959; 97:201–204.
8. Pennell TC, Shaffner LS: Congenital internal hernia. Surg Clin North Am 1971; 51:1355–1359.
9. Zimmerman LM, Laufman H: Intra-abdominal hernias due to developmental and rotational anomalies. Ann Surg 1953; 138:82–91.
10. Hardy JD: Problems associated with gastric surgery: Review of 604 consecutive patients with annotation. Am J Surg 1964; 108:699–716.
11. Vitello JM, Rutledge RH: Retroanastomotic hernia. *In* Hernia, 4th ed. Edited by LM Nyhus, RE Condon. JB Lippincott, Philadelphia, 1995, pp 475–484.
12. Mock CJ, Mock HE Jr: Strangulated internal hernia associated with trauma. Arch Surg 1958; 77:881–886.
13. Stone AM, Janin Y, Wise L: Mesenteric hernia. *In* Hernia, 4th ed. Edited by LM Nyhus, RE Condon. JB Lippincott, Philadelphia, 1995, pp 467–474.
14. Murphy DA: Internal hernias in infancy and childhood. Surgery 1964; 55:311–315.
15. Williams AJ: Roentgen diagnosis of intra-abdominal hernia. An evaluation of the roentgen findings. Radiology 1952; 59:817–825.
16. Ghahremani GG, Meyers MA: Internal abdominal hernias. Curr Probl Radiol 1975; 5:1–30.
17. Meyers MA: Paraduodenal hernias. Radiologic and arteriographic diagnosis. Radiology 1970; 95:29–37.
18. Bertelsen S, Christiansen J: Internal hernia through mesenteric and mesocolic defects. A review of the literature and a report of two cases. Acta Chir Scand 1967; 133:426–428.
19. Nathan H: Internal hernia. J Int Coll Surg 1960; 34:563–571.
20. Parsons PB: Paraduodenal hernia. AJR 1953; 69: 563–589.
21. Hansmann GH, Morton SA: Intra-abdominal hernia. Report of a case and review of the literature. Arch Surg 1939; 39:973–986.
22. Berens JJ: Small internal hernias in the paraduodenal area. Arch Surg 1963; 86:726–732.
23. Callander CL, Rusk GY, Nemir A: Mechanism, symptoms, and treatment of hernia into descending mesocolon (left duodenal hernia); plea for change in nomenclature. Surg Gynecol Obstet 1935; 60:1052–1071.
24. Roberts WH, Dalgleish AE: Internal hernia of embryological origin. Anat Rec 1966; 155:279–285.
25. Moynihan BGA: On Retroperitoneal Hernia. Duodenal folds and fossae. Bailliere, Tindall and Cox, London, 1889, pp 19–70.
26. Landzert: Über die hernie Retroperitonealis (Treitz) und ihre Beziehungen zur Fossa duodenojejunalis. St Petersb Med Ztschr, MF 1871; 2:306–350.
27. Meyers MA: Arteriographic diagnosis of internal (left paraduodenal) hernia. Radiology 1969; 92: 1035–1037.
28. Waldeyer W: Hernia retroperitonealis, nebst Bermerkungen zur Anatomie des Peritoneums. Arch Pathol Anat 1874; 60:66–92.
29. Filtzer H, Sedgewick CE: Strangulated paraduodenal hernia. Report of a case. Surg Clin North Am 1973; 53:371–374.
30. Freund H, Berlatzky Y: Small paraduodenal hernias. Arch Surg 1977; 112:1180–1183.
31. Mayo CW, Stalker LK, Miller JM: Intra-abdominal hernia. Review of 39 cases in which treatment was surgical. Ann Surg 1941; 114:875–885.
32. Ghahremani GG, Meyers MA: Hernias. *In* Surgical Radiology. Edited by JG Teplick, ME Haskin. WB Saunders, Philadelphia, 1981.
33. Schlaffer GJ, Groell R, Kammerhuber F, et al: Anterior and upward displacement of the inferior mesenteric vein: A new diagnostic clue to left paraduodenal hernias? Abdom Imaging. 1999; 24:29–31.
34. Lechner G, Gebhardt HD: Rechtseitäge paraduodenale Hernie. Fortschr Roentgenstr 1966; 105: 904–907.
35. Day DL, Drake DG, Leonard AS, et al: CT findings in left paraduodenal herniae. Gastrointest Radiol 1988; 13(1):27–29.

36. Passas V, Karavias D, Grilias D, et al: Computed tomography of left paraduodenal hernia. J Comput Assist Tomogr 1986; 10(3):542–543.
37. Warshauer DM, Mauro MA: CT diagnosis of paraduodenal hernia. Gastrointest Radiol 1992; 17: 13–15.
38. Ghahremani GG: Abdominal and Pelvic Hernias. *In* Textbook of Gastrointestinal Radiology. Edited by Gore RM, Levine MS, Laufer I. WB Saunders, Philadelphia, 1994.
39. Olazabal O, Guasch I, Casas D: Case report: CT diagnosis of nonobstructive left paraduodenal hernia. Clin Radiol 1992; 46:288–289.
40. Vohra R, Gothi R, Doda SS et al: CT features of left paraduodenal hernia: A case report. Asian Oceanian J Radiol 1996; 1:45–47.
41. Nichols DM, Li DK: Superior mesenteric vein rotation: A CT sign of midgut malrotation. AJR 1983; 141:707–708.
42. Schatzkes D, Gordon DH, Haller JO, et al: Malrotation of the bowel: Malalignment of the superior mesenteric artery-vein complex by CT and MR. J Comput Assist Tomogr 1990; 14:93–95.
43. Zerin JM, DiPietro MA: Mesenteric vascular anatomy at CT: Normal and abnormal appearances. Radiology 1991; 179:739–742.
44. Chou CK, Chang JM, Tzeng WS: CT of the mesenteric vascular anatomy. Abdom Imaging 1997; 22:477–482.
45. Fischer JK: Computed tomographic diagnosis of volvulus in intestinal malrotation. Radiology 1981; 140:145–146.
46. Fujimoto K, Nakamura K, Nishio H, et al: Whirl sign as CT finding in small-bowel volvulus. Eur Radiol 1995; 5:555–557.
47. Chou CK, Tsai TC: Small bowel volvulus. Abdom Imaging 1995; 20:431–435.
48. Izes BA, Scholz FJ, Munson JL: Midgut volvulus in an elderly patient. Gastrointest Radiol 1992; 17: 102–104.
49. Bernstein SM, Russ PD: Midgut volvulus: A rare cause of acute abdomen in an adult patient. AJR 1998; 171:639–641.
50. Pracros JP, Sann L, Genin G, et al: Ultrasound diagnosis of midgut volvulus: The "whirlpool" sign. Pediatr Radiol 1992; 22:18–20.
51. Hayden CK Jr: Ultrasonography of the gastrointestinal tract in infants and children. Abdom Imaging 1996; 21:9–20.
52. Buranasiri S, Baum S, Nusbaum M, et al: The angiographic diagnosis of midgut malrotation with volvulus in adults. Radiology 1973; 109:555–556.
53. Griska LB, Popky GL: Angiography in midgut malrotation in intestinal malrotation. Radiology 1981; 140:145–146.
54. Sieck JO, Cowgill R, Larkworthy W: Peritoneal encapsulation and abdominal cocoon: Case reports and a review of the literature. Gastroenterology 1983; 84:1597–1601.
55. Casas JD, Mariscal A, Martinez N: Peritoneal encapsulation: AJR 1998; 171:1017–1019.
56. Oriuchi T, Kinouchi Y, Hiwatashi N, et al: Bilateral paraduodenal hernias: Computed tomography and magnetic resonance imaging appearance. Abdom Imaging 1998; 23:278–280.
57. Erskine JM: Hernia through the foramen of Winslow. Surg Gynecol Obstet 1967; 125:1093–1109.
58. Dardik H, Cowen R: Herniation of the gallbladder through the epiploic foramen into the lesser sac. Ann Surg 1967; 165:644–646.
59. Vint WA: Herniation of the gallbladder through the epiploic foramen into the lesser sac: Radiologic diagnosis. Radiology 1966; 86:1035–1040.
60. Popky GL, Lapayowker MS: Persistent descending mesocolon. Radiology 1966; 86:327–331.
61. Hollenberg MS: Radiographic diagnosis of hernia into the lesser peritoneal sac through the foramen of Winslow. Report of a case. Surgery 1945; 18: 498–502.
62. Khilnani MT, Lautkin A, Wolf BS: Internal hernia through the foramen of Winslow. J Mount Sinai Hosp 1959; 26:188–193.
63. Henisz A, Matesanz J, Westcott JL: Cecal herniation through the foramen of Winslow. Radiology 1974; 112:575–578.
64. Cimmino CV: Lesser sac hernia via the foramen of Winslow. A case report. Radiology 1953; 60: 57–59.
65. Stankey RM: Intestinal herniation through the foramen of Winslow. Radiology 1967; 89:929–930.
66. Lefort H, Dax H, Vallet G: Herniation through the foramen of Winslow (roentgenologic and clinical considerations based on an analysis of 25 cases). J Radiol 1967; 48:157–166.
67. Schwartz A, Feuchtwanger MM: Hernia through the foramen of Winslow. Isr J Med Sci 1968; 4: 117–121.
68. Goldberger LE, Berk RN: Cecal hernia into lesser sac. Gastrointest Radiol 1980; 5:169–172.
69. Wojtasek DA, Codner MA, Nowak EJ: CT diagnosis of cecal herniation through the foramen of Winslow. Gastrointest Radiol 1991; 16:77–79.
70. Oldfield AL, Wilbur AC: Retrogastric colon: CT demonstration of anatomic variations. Radiology 1993; 186:557–561.

71. Inoue Y, Nakamura H, Mizumoto S, et al: Lesser sac hernia through the gastrocolic ligament: CT diagnosis. Abdom Imaging 1996; 21:145–147.
72. Tran TL, Regan F, Al-Kutobi MAO: Computed tomography of lesser sac hernia through the gastrohepatic omentum. Br J Radiol 1991; 64:372–374.
73. Rooney JA, Carroll JP, Keeley JL: Internal hernias due to defects in the meso-appendix and mesentery of small bowel, and probable Ivemark syndrome. Report of two cases. Ann Surg 1963; 157:254–258.
74. Dalinka MK, Wunder JF, Wolfe RD: Internal hernia through the mesentery of a Meckel's diverticulum. Radiology 1970; 95:39–40.
75. Maglinte DDT, Herlinger H, Nolan DJ: Radiologic features of closed loop obstruction: Analysis of 25 confirmed cases. Radiology 1991; 179:383–387.
76. Miller PA, Mezwa DG, Feczko P, et al: Imaging of abdominal hernias. RadioGraphics 1995; 15:333–347.
77. Cohen AM, Patel S: Arteriographic findings in congenital transmesenteric internal hernia. AJR 1979; 133:541–543.
78. Kondi ES, Gallitano AL, Katz SJ: A new variant of intra-abdominal hernia. Ann Surg 1975; 181:442–446.
79. Gallagher HW: Spontaneous herniation through the transverse mesocolon: A review of the literature and the report of a case. Br J Surg 1949; 36:300–305.
80. Meyers MA, Whalen JP: Roentgen significance of the duodenocolic relationships. An anatomic approach. AJR 1973; 117:263–274.
81. Carlisle BB, Killen DA: Spontaneous transverse mesocolic hernia with re-entry into the greater peritoneal cavity: Report of a case with review of the literature. Surgery 1967; 62:268–273.
82. Estrada RL: Hernias Involving the Falciform Ligament. *In* Internal Abdominal Hernias. RG Landes, Austin, TX, 1994, pp 195–204.
83. Walker S, Baer JW: Herniation of small bowel through the falciform ligament: CT demonstration. Abdom Imaging 1995; 20:161–163.
84. Chevrel JP, Duchene P, Salama G: Anatomical bases of intrahepatic bilio-digestive anastomoses. Acta Clin 1980; 2:159–167.
85. Mizumoto R, Kawarada Y, Suzuki H: Surgical treatment of hilar carcinoma of the bile duct. Surg Gynecol Obstet 1986; 162:153–158.
86. Morton CB, Alrich EM, Hill LD: Internal hernia after gastrectomy. Ann Surg 1955; 141:759–764.
87. Sabesta DG, Robson MC: Petersen's retroanastomotic hernia. Am J Surg 1968; 116:450–453.

Pathways of Extrapelvic Spread of Disease

17

Diseases arising from the pelvic contents may first manifest themselves by signs and symptoms remote from their source of origin. Gastrointestinal tract perforations, in particular, may dissect along anatomic planes of the pelvis to first present in the buttock, hip, thigh, and even the lower leg and the retroperitoneal space of the abdomen. Pain, mass, or crepitation at these sites may be very misleading since the origin of the underlying inflammatory condition or the neoplastic, traumatic, or foreign body perforation of the bowel within the pelvis often remains clinically occult. Radiologic evaluation may be crucial in redirecting the diagnostic and therapeutic approach as well as in documenting the extent of disease.

The most common extraabdominal extension of gastrointestinal tract perforations, beyond the development of ischiorectal abscesses, is to the buttocks, hips, and lower extremities. Spread of necrotizing fasciitis to the male genitalia (Fournier gangrene) is rare.[1] Of the cases in the literature reported as subcutaneous emphysema of the leg arising from intestinal perforations,[2–5] diverticulitis and appendicitis account for most of those resulting from infection. Carcinoma of the colon with perforation, uterine carcinoma, foreign body, and trauma to the rectum have been other causes.

Most cases of extraperitoneal spread reported have created serious diagnostic problems with admitting diagnoses of thrombophlebitis, sciatica, gas gangrene, inguinal abscess, Spigelian hernia, and even fractured hip, until surgery or autopsy uncovered a definitive diagnosis. The clinical presentation is often pain in the hip or buttock.[2,6–10] With the development of crepitation, particularly in the thigh, incision may then display severe necrotizing fasciitis. It is often not until blunt dissection is then carried out along the femoral canal, beneath the inguinal ligament, that an extraperitoneal abscess is revealed as evidence of a more severe process extending from the pelvis.

The pathogenesis of subacute cellulitis and emphysema of gastrointestinal origin depends on four basic factors[11]: (a) perforation of the bowel, (b) an adequate pressure gradient between the lumen of the bowel and ultimately the subcutaneous space, (c) the anatomic site of perforation, and (d) infection.

The major mechanism of gas formation is not the gas-forming organisms in feces, but the pressure gradient between the lumen of the gut and surrounding tissue. Large pressure gradients are associated with vigorous peristaltic contractions.[12] Gas pressures in the intestinal lumen may rise to more than 60 cm H_2O during peristalsis, while soft-tissue tension is usually about 5 cm H_2O. The intraabdominal pressure may be greatly increased by the contraction of the diaphragmatic and abdominal muscles. This increased pressure is transmitted to the contents of the intestinal tract and promotes their evacuation, especially at sites of perforation when the sphincters are intact.[12,13] This mechanism, enhanced by bacterial gas formation, accounts for the rapidity of its accumulation.

The anatomic site of perforation largely determines the pathway of spread of the sinus tract to the subcutaneous position. The usual route of extravasation from the bowel is directly through a pathologic defect in the parietal peritoneum or fascia contiguous with this defect into the intermuscular planes and subcutaneous spaces. Solid parenchymatous organs and serous membranes have a relatively great resistance to the diffusion of gases, whereas loose areolar and fascial structures readily allow the passage of gas.

Cases of perforated diverticulitis or carcinoma of the sigmoid or descending colon usually present in the left

leg or buttock, and appendicitis or perforation of the cecum in the right leg and buttock. Because of variations in position and length of the appendix and in redundancy of the sigmoid, perforations from these sites may extend to the side opposite to that ordinarily expected. Traumatic or neoplastic perforation of the rectum may present in either or both buttocks and legs. Spread from the pelvis may occur also into the abdominal wall and upward as an extraperitoneal abscess.[3,14–16]

The most common offending organism is *Escherichia coli.* Occasionally, cultures isolate *Clostridium welchii, Aerobacter aerogenes,* and *Proteus.*[6,8,9,14,16]

Surgical findings have not often localized the particular pathway of spread in the presence of a pelvic abscess with frequent necrotizing dissection toward the inguinal region, perineum, thigh and hip joint, buttock, and paravertebral gutter.[8,14]

I have established the correlation between the anatomic pathways and the radiologic documentation of the extrapelvic spread of disease.[2] The insertions of the iliopsoas, piriformis, and obturator internus muscles, within their fascial investments, and the ensheathed penetrations of the superior gluteal arteries provide avenues of dissection to the buttocks, hips, and thighs.



Fig. 17–1. Midcoronal anatomic section through the pelvis at the level of the urinary bladder *(B),* prostate gland *(PG),* and loops of sigmoid colon *(SiC).*

The course and relationships of the psoas major *(1),* iliacus *(2),* obturator internus *(3),* levator ani *(4),* and gluteal muscles *(5)* are shown. These are invested by fascia. The superior gluteal vessels *(arrows)* pass out of the pelvis at the level of the greater sciatic foramina.

(Courtesy of Manuel Viamonte, Jr., M.D., Mt. Sinai Hospital, Miami Beach, FL. Reproduced from Meyers and Goodman.[2])

Anatomic Considerations

Figure 17–1 is an anatomic section showing the relationships of the major muscles of the pelvis. The levator ani and coccygeus muscles form the floor of the pelvis (pelvic diaphragm). This is the most inferior portion of the body wall and closes the abdominopelvic cavity. The obturator internus and the piriformis muscles originate within the pelvis and thus form part of the pelvic wall, but they are really muscles of the lower limbs.

The endopelvic fascia is the internal investing fascia of the pelvis. Its parietal layer (Fig. 17–2) covers the levator ani, coccygeus, and the intrapelvic portions of the obturator internus and piriformis muscles. It is directly continuous above with the transversalis (endoabdominal) fascia lining the abdominal cavity. The visceral layer of the endopelvic fascia covers the urinary bladder, lower third of the ureters, uterus, vagina, and the rectum.

Four of the pelvic muscles have important extrapelvic insertions. These are illustrated in Figure 17–3:

1. The psoas major originates from the transverse processes and bodies of the lumbar vertebrae and inserts on the lesser trochanter of the femur.
2. The iliacus originates primarily from the upper two-thirds of the iliac fossa and the ala of the sacrum and inserts with the tendon of the psoas major on the lesser trochanter of the femur. In its common insertion, it comprises the iliopsoas muscle group.
3. The piriformis originates from the sacrum and the margin of the greater sciatic foramen and inserts on the greater trochanter of the femur.
4. The obturator internus originates from the margins of the obturator foramen and inserts on the greater trochanter of the femur.

It is also important to recognize that the pelvic blood vessels lie in front of the pelvic fascia, i.e., superficial to the parietal layer of the endopelvic fascia. The superior and inferior gluteal branches of the internal iliac arteries passing out of the pelvis (Fig. 17–1) must perforate the fascia and carry extensions of the fascia with them to the gluteal region. For example, the fascia of the piriformis is prolonged outward through the greater sciatic foramen and joins the gluteal fascia. The internal iliac vessels and their branches lie in the subperitoneal tissue in front of the fascia, and the branches to the gluteal region, particularly the superior gluteal artery (the largest branch of the hypogastric artery), emerge in special sheaths of this tissue, paralleling the border of the piriformis, to reach and supply the gluteus muscles.

In this way, the fascial investments of the iliopsoas, piriformis, and obturator internus muscles and the fascial sheaths of the superior gluteal arteries provide anatomic pathways to the buttocks, hips, and thighs. Superiorly, the pelvic tissues above the levator ani and coccygeus muscles are continuous with the extraperitoneal portion of the abdomen.

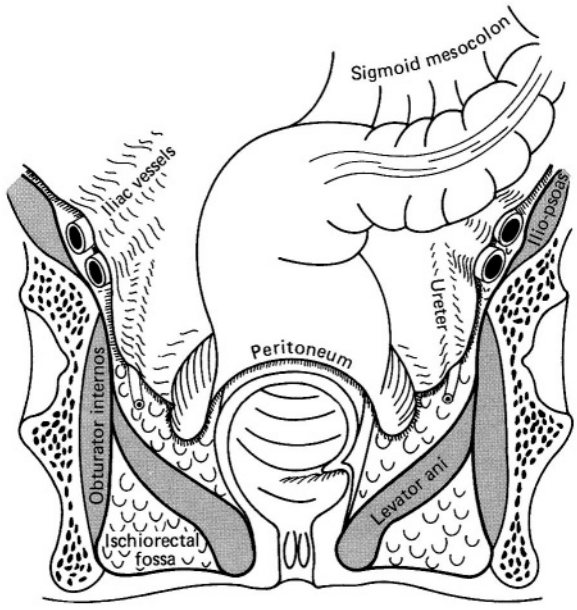


Fig. 17–2. Posterior coronal section at level of the rectum showing planes of pelvic fascia ***(bold lines).*** The endopelvic fascia covers the major muscles of the pelvis. The internal iliac arteries lie superficial to the fascia and then continue within tunneled extensions as they pass to the gluteal region.
(Reproduced from Meyers and Goodman.[2])

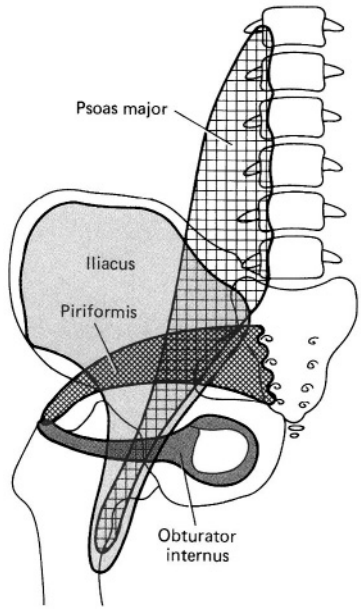


Fig. 17–3. Extrapelvic insertions of abdominal and pelvic muscles.
The iliopsoas muscle group inserts medially on the lesser trochanter of the femur, and the piriformis and obturator internus insert laterally on the greater trochanter. (Reproduced from Meyers and Goodman.[2])

Radiologic Findings

Radiologic findings may first identify the presence, extent, and location of the primary process. Subcutaneous emphysema presents as gas in the fascial planes between the muscles and interstitial tissues, in contrast to gas gangrene where the gas lies within the muscles. In the hip, it may first appear about the greater or lesser trochanter.[2,7,10,16] The first site of appearance or area of maximum development of cellulitis or subcutaneous emphysema should indicate the appropriate anatomic level and likely nature of perforation of the bowel. Radiologic studies may then confirm the cause and anatomic pathway of spread. Computed tomography may be particularly useful in this regard.[17]

Figure 17–4 illustrates gluteal spread from a traumatic perforation of the rectum occasioned by a barium enema study. Dissection from the pelvis toward the gluteal area is strikingly illustrated in this case by the extravasated contrast agent tracking within the fascial extension of the superior gluteal artery through the greater sciatic foramen. Indeed, the vessel is shown as a tubular filling defect within its opacified endopelvic sheath. Tenderness in the buttock was a consequence of this anatomic extension.

Figure 17–5 illustrates a similar pathway in an instance of sigmoid diverticulitis perforating to the buttock, in a patient presenting with fever and vague pain in the right buttock. Perforation of the sigmoid colon in this case is directed along the extension of the superior gluteal artery through the greater sciatic foramen to the right buttock. The initial symptom of pain in this site heralded the progression to a prominent gluteal abscess.

Figure 17–6 illustrates extension within the fascial investment of the piriformis muscle from perforating sigmoid diverticulitis in a patient presenting with fever and pain in the left hip. Loculated extravasation from this area along the plane of the piriformis muscle extended to the left buttock and hip.

Figure 17–7 shows a tract of gas bubbles along the piriform muscle first revealed by CT, with the fistulous communication from perforation of an occult adenocarcinoma of the sigmoid colon confirmed by barium enema study.

Figure 17–8 illustrates an instance of the clinical and radiographic presentation of septic arthritis of the hip complicating an underlying sigmoid diverticulitis. This may be initially very misleading in the absence of soft-tissue gas.[19]

Figure 17–9 demonstrates clinically occult extrapelvic spread in a case of appendicitis in a patient presenting with fever and right hip pain and tenderness. Necrotic cellulitis and interstitial emphysema of the right thigh in this patient progressed via the iliopsoas muscle group from a perforated appendicitis that was not diagnosed antemortem.

Figure 17–10 reveals extension of intrapelvic malignancy into the thigh along the course of the obturator internus muscle. The outlets provided by the muscles and lymphatics in their fascial investments through the

text continues on page 760

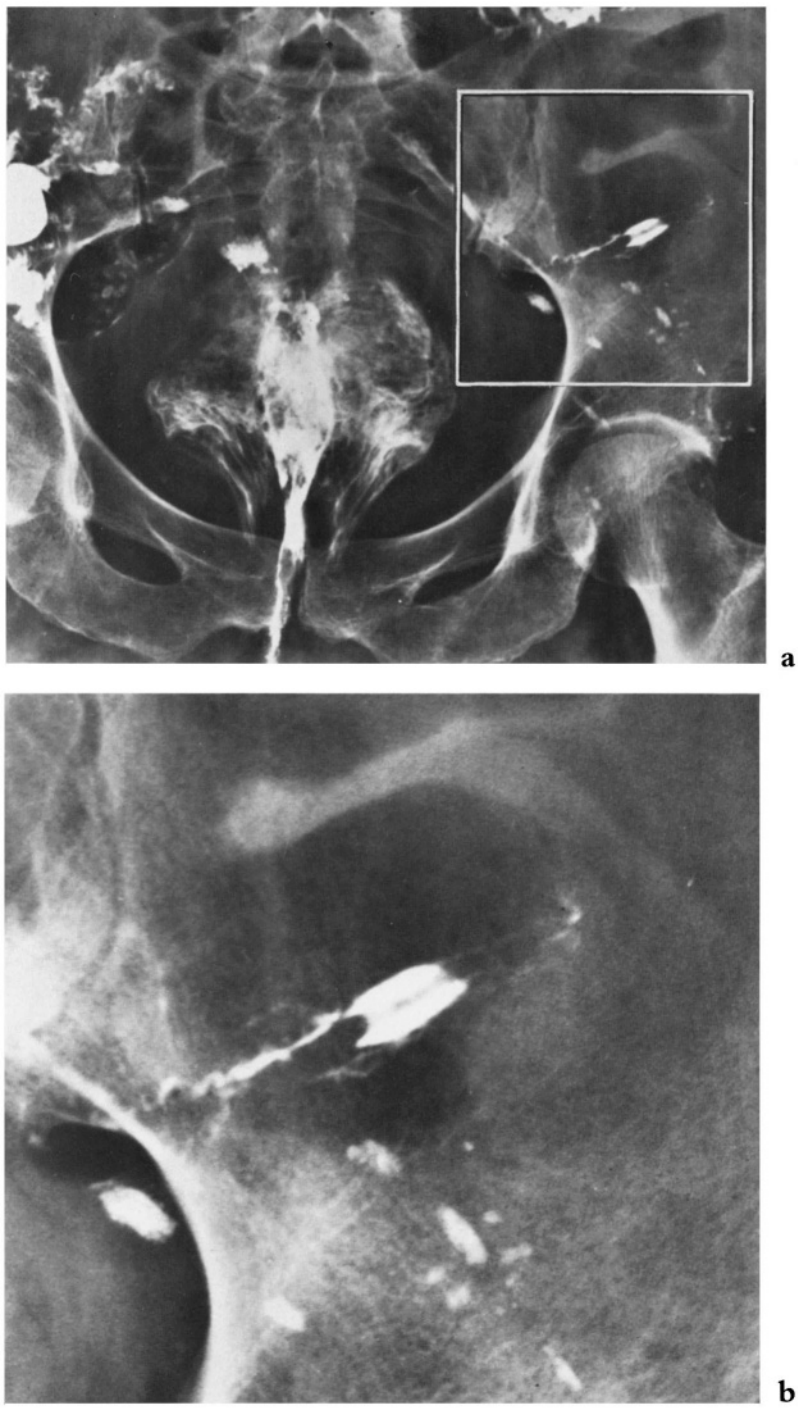


Fig. 17–4. Rectal extravasation complicating a barium enema study, with gluteal spread.
(a) Postevacuation film. Contrast agent has infiltrated the intramural and extrarectal pelvic tissues.
(b) Magnification of area outlined in **a** demonstrates extravasation within the tunneled fascial sheath of the superior gluteal artery progressing through the greater sciatic foramen toward the buttock.
(Reproduced from Meyers and Goodman.[2])

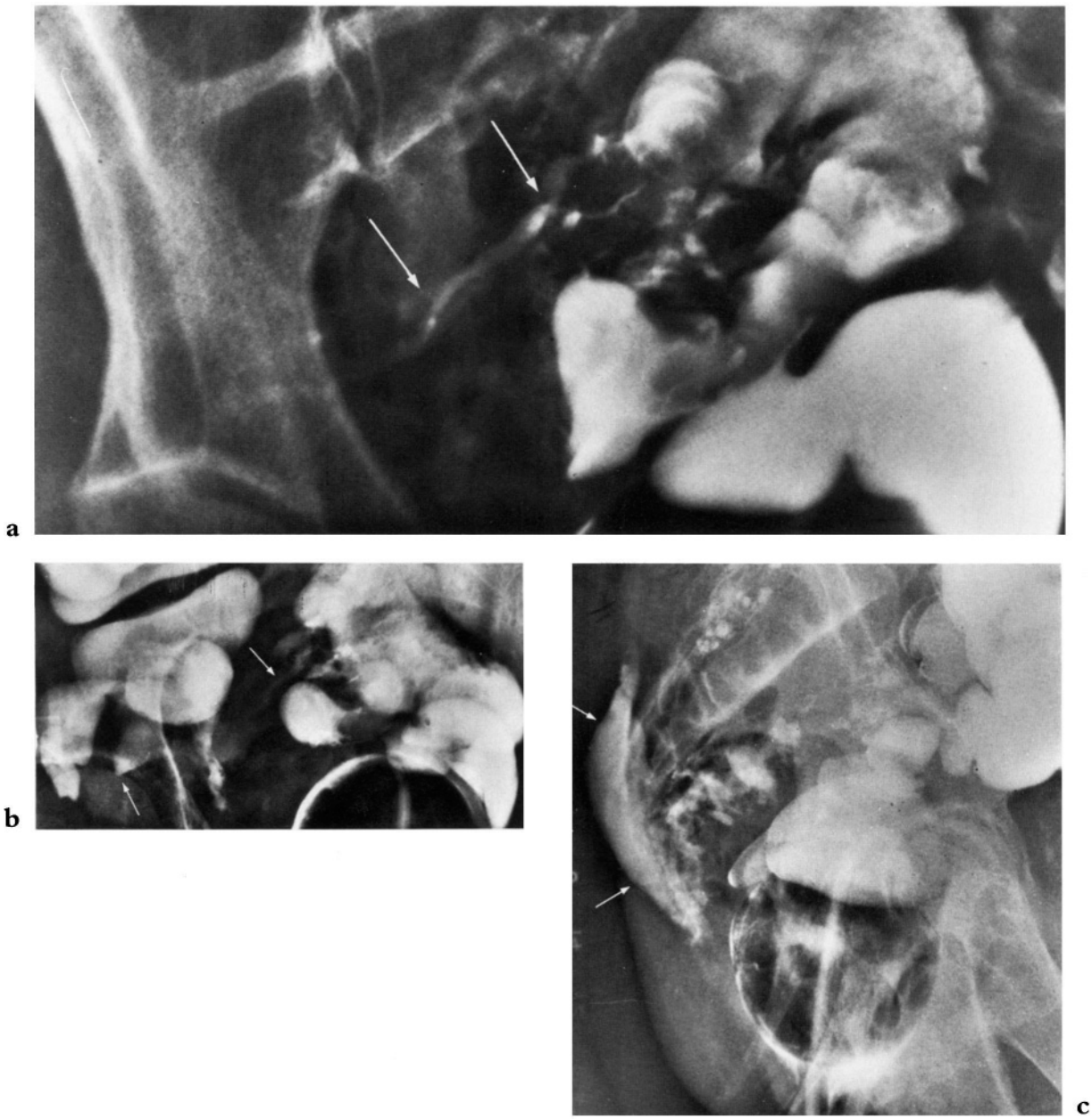


Fig. 17–5. Sigmoid diverticulitis perforating to the right buttock.
(a) Sinus tract *(arrows)* leads from a site of inflammatory narrowing in the sigmoid colon along the course of the superior gluteal artery to the right buttock.
(**b** and **c**) Ten days later, a follow-up study shows that the sinus tract remains evident, and there is now a large abscess cavity *(arrows)* deep in the gluteal muscle.
(Reproduced from Meyers and Goodman.[2])

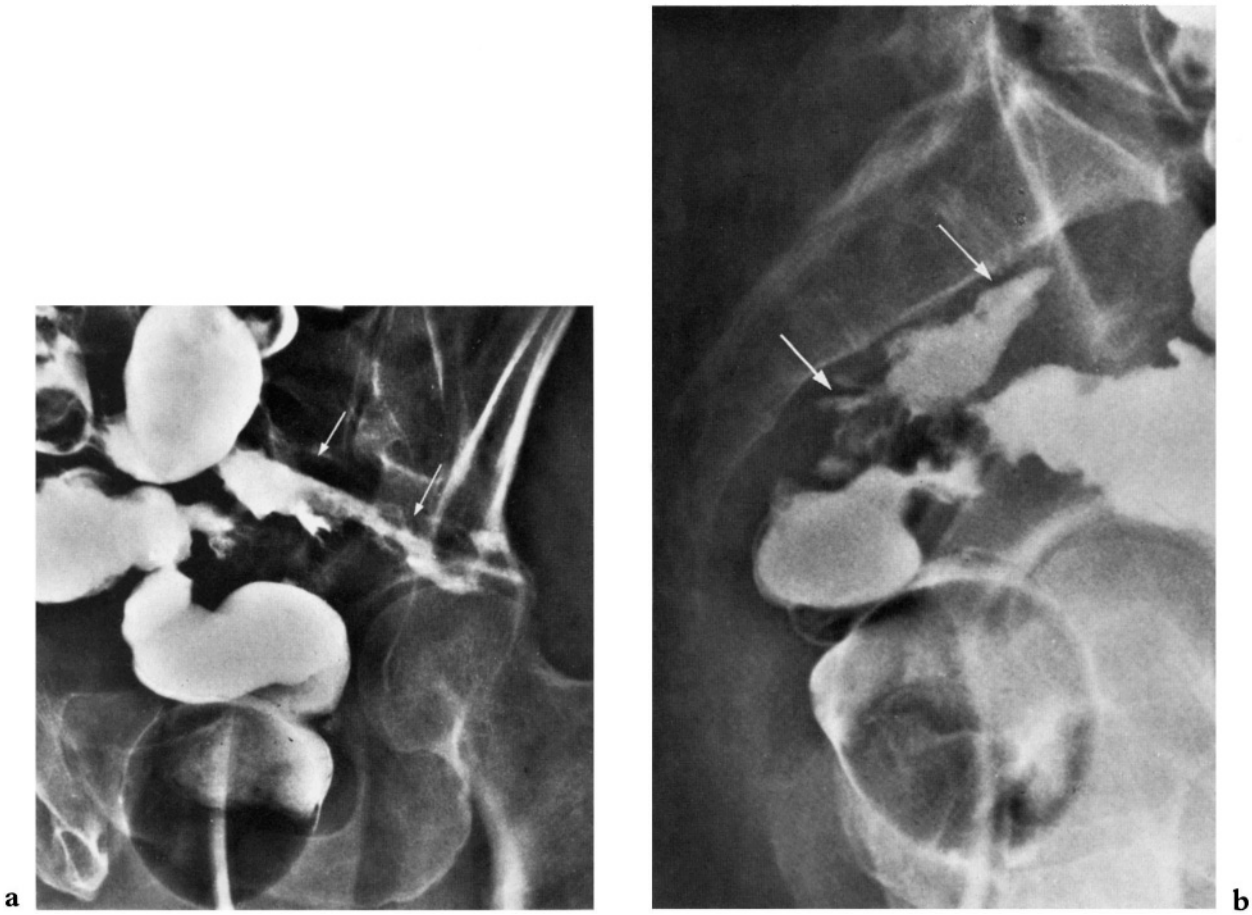


Fig. 17–6. Sigmoid diverticulitis perforating to the left buttock and hip.
Oblique **(a)** and lateral **(b)** projections of barium enema study demonstrate extension from inflammatory narrowing of the distal sigmoid colon along the course of the piriformis muscle *(arrows).*
(Reproduced from Meyers and Goodman.[2])



Fig. 17–7. Perforated sigmoid carcinoma extending to the hip.
(a) CT demonstrates fistulous tract *(arrows)* following the plane of the piriform muscle to the greater trochanter.
(b) Barium enema confirms communication form a perforated sigmoid colon to a large abscess cavity around the greater trochanter. (Reproduced from Jager et al.[4])

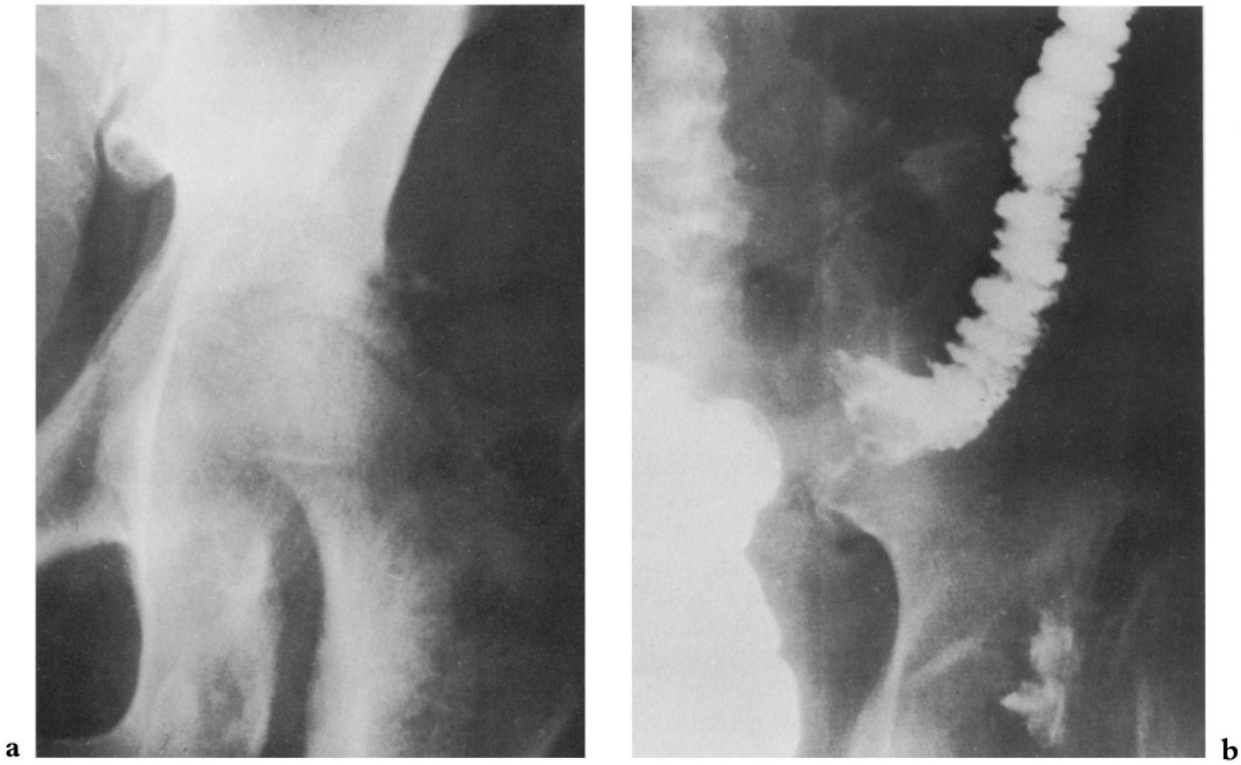


Fig. 17–8. Septic arthritis of the left hip secondary to sigmoid diverticulitis.
(a) Destruction of the hip joint due to septic arthritis.
(b) Barium enema study shows segmental narrowing of the sigmoid colon due to acute diverticulitis. Barium has entered the hip joint through a fistulous communication.
(Reproduced from Smith et al.[18])

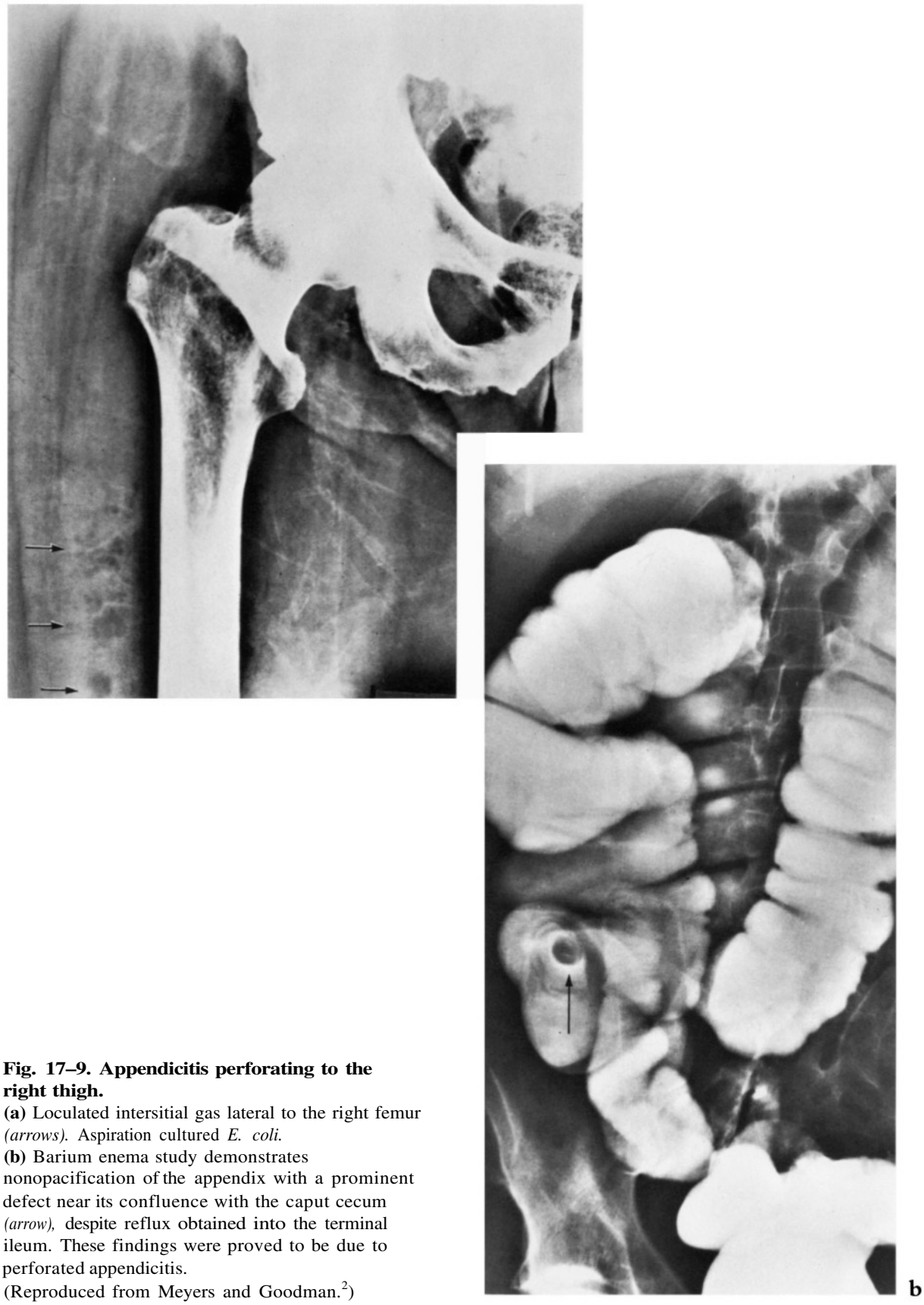


Fig. 17–9. Appendicitis perforating to the right thigh.
(a) Loculated intersitial gas lateral to the right femur *(arrows).* Aspiration cultured *E. coli.*
(b) Barium enema study demonstrates nonopacification of the appendix with a prominent defect near its confluence with the caput cecum *(arrow),* despite reflux obtained into the terminal ileum. These findings were proved to be due to perforated appendicitis.
(Reproduced from Meyers and Goodman.[2])

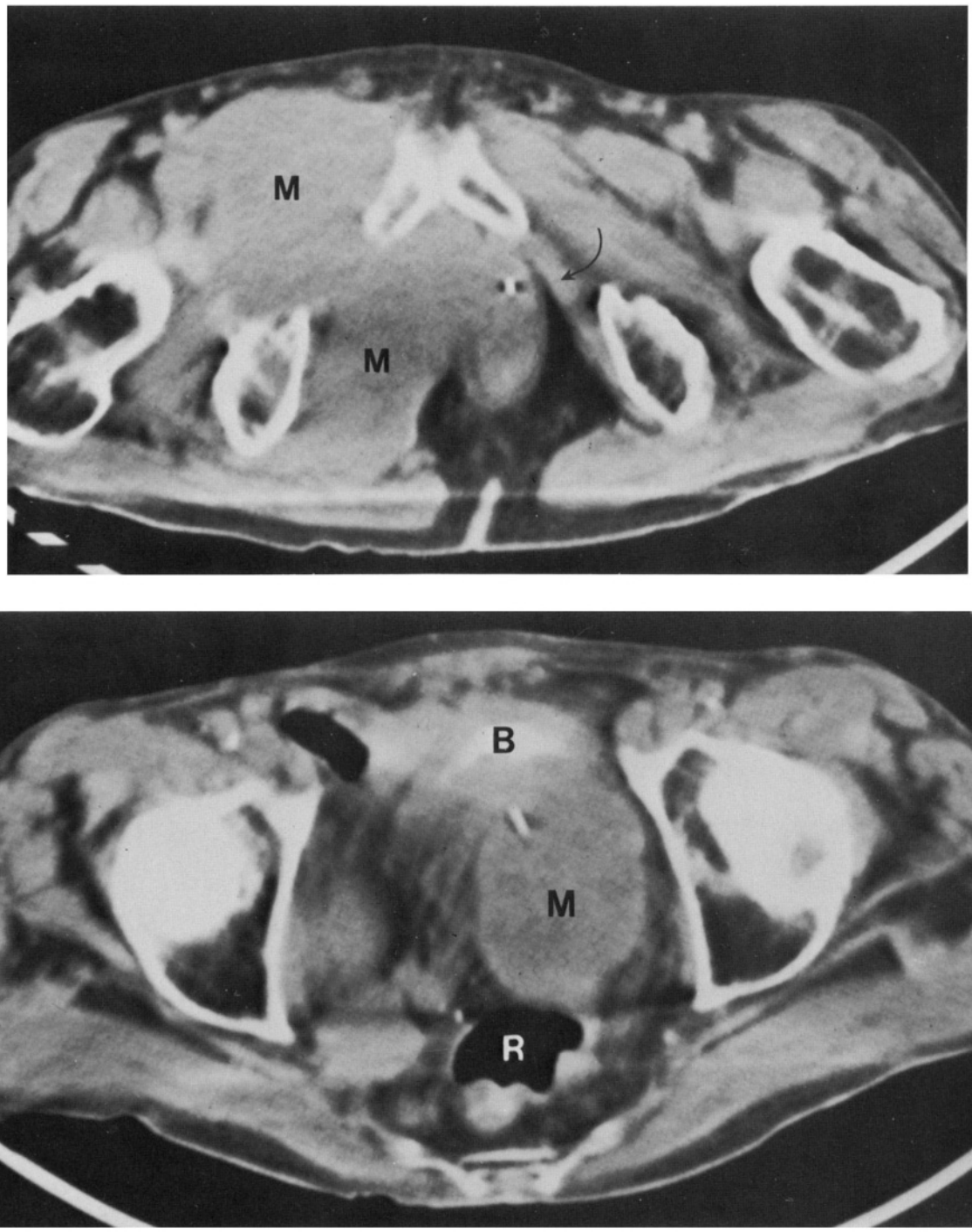


Fig. 17–10. Recurrence of carcinoma of the colon extending through the obturator foramen to the thigh.

(a) CT scan at the level of the symphysis pubis demonstrates the recurrent mass *(M)* extending from the pelvis through the obturator foramen on the right to the thigh. The normal obturator internus muscle is seen on the left *(curved arrow).*

(b) At a higher level, the mass continues to the ischiorectal fossa, displacing the rectum *(R)* to the left and lying between the rectum and the urinary bladder *(B).*

foramina may constitute anatomic pathways for the extrapelvic spread of carcinomas and lymphomas.[17,19–22]

Figure 17–11 demonstrates a patient initially thought to have urolithiasis with scrotal referred pain shown by CT to have a perforated retrocecal appendix with extension to the inguinal canal.

Figure 17–12 illustrates that, superiorly, extension from the subperitoneal pelvic tissues preferentially seeks out the posterior pararenal compartment of the extraperitoneal region of the abdomen.[2,23–27] The characteristic features allow precise radiologic localization, as detailed in Chapter 8.

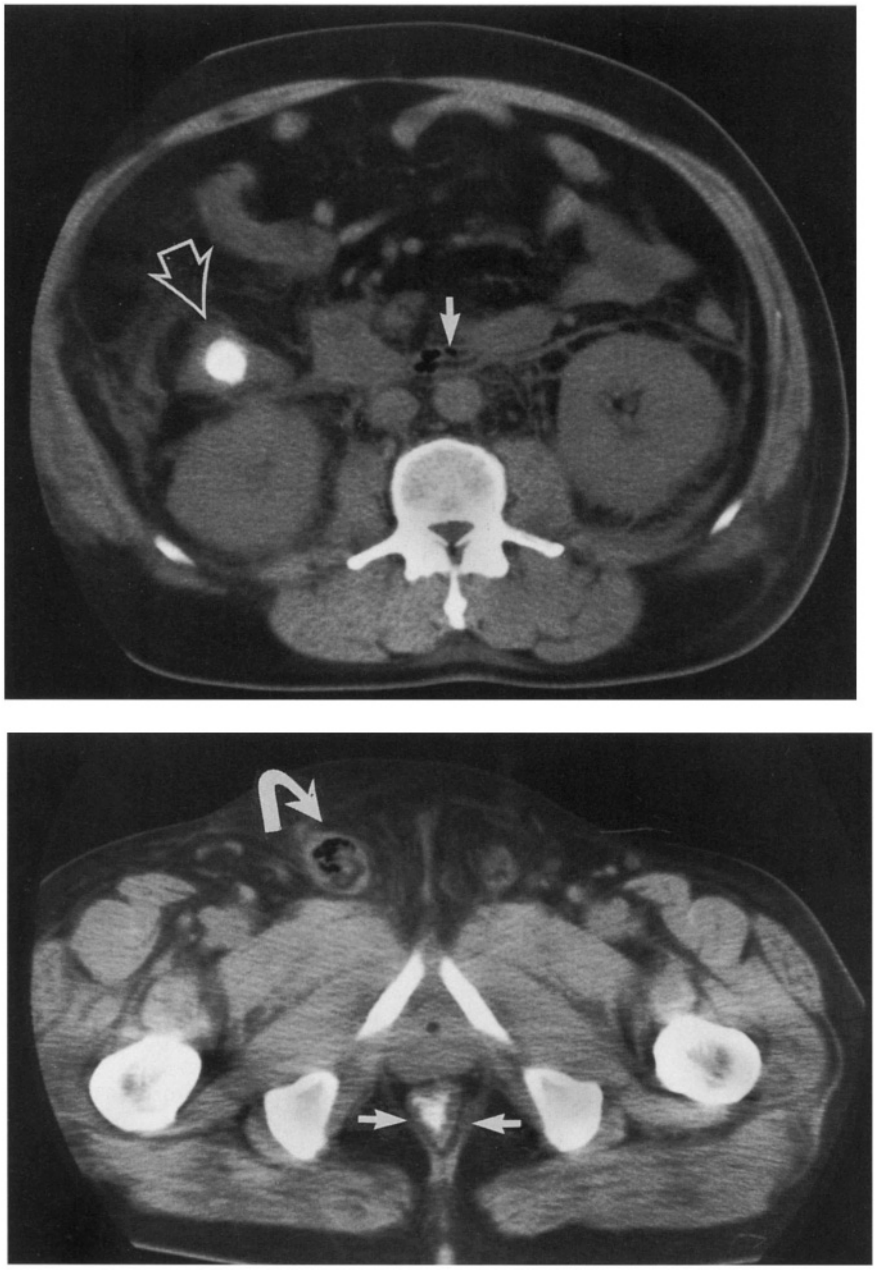


Fig. 17–11. Perforated retrocecal appendix extending to the inguinal canal.
(a) CT shows retrocecal appendix with a coprolith surrounded by an abscess *(open arrow)* in the anterior pararenal space. Extraperitoneal gas is present in the midline anterior to the great vessels *(arrow).*
(b) Perirectal gas *(arrows)* is associated with gas in the inguinal canal *(curved arrow).*
(Courtesy of Michiel Feldberg, M.D., University of Utrecht, The Netherlands.)



Fig. 17–12. Extraperitoneal hemorrhage from iliac artery.
Difficulty in passing the catheter through the iliac artery during attempted cardiac catheterization was encountered. Contrast agent was introduced to evaluate the cause of the difficulty, and this demonstrated local extravasation. Right lower quadrant guarding and tenderness developed. Delayed film demonstrates persistent localized extravasation *(arrow)* from the right external iliac artery.
A soft-tissue mass representing a large amount of blood now occupies the right abdomen. This displaces the lower pole of the kidney laterally, obstructs the ureter, and obliterates the lateral edge of the psoas muscle and the flank stripe. These features localize the hematoma to the extraperitoneal posterior pararenal compartment.
(Reproduced from Meyers and Goodman.[2])

References

1. Gaeta M, Volta S, Minutoli A, et al: Fournier gangrene caused by a perforated retroperitoneal appendix: CT demonstration. AJR 1991; 156:341–342.
2. Meyers MA, Goodman KJ: Pathways of extrapelvic spread of disease: Anatomic-radiologic correlation. AJR 1975; 125:900–909.
3. Edwards JD, Eckhauser FE: Retroperitoneal perforation of the appendix presenting as subcutaneous emphysema of the thigh. Dis Colon Rectum 1986; 29(7):456–458.
4. Jager GJ, Rijssen HV, Lamers JJH: Subcutaneous emphysema of the lower extremity of abdominal origin. Gastrointest Radiol 1990; 15:253–258.
5. Jager GJ, Joosten F, vo Berkmortel FW, et al: Subcutaneous emphysema of the lower extremity secondary to a perforated esophageal carcinoma. Abdom Imaging 1995; 20:23–25.
6. Fiss TW Jr, Cigtay OS, Miele AJ, et al: Perforated viscus presenting with gas in the soft tissues (subcutaneous emphysema). AJR 1975; 125:226–233.

7. Korsten J, Mattey WE, Bastidas J, et al: Subcutaneous emphysema of the thigh secondary to ruptured diverticulum of the ascending colon. Radiology 1973; 106:555–556.
8. Linscheid RJ, Kelly PJ, Symmonds RE: Emphysematous cellulitis of the hip and thigh resulting from enteric fistula. J Bone Joint Surg 1963; 45:1691–1697.
9. Mzabi R, Himal HS, MacLean LD: Gas gangrene of the extremity: The presenting clinical picture in perforating carcinoma of the caecum. Br J Surg 1975; 62:373–374.
10. Pickels RF, Karmody AM, Tspogas MJ, et al: Subcutaneous emphysema of the lower extremity of gastrointestinal origin: Report of a case. Dis Colon Rectum 1974; 17:82–86.
11. Oetting HK, Kramer NE, Branch WE: Subcutaneous emphysema of gastrointestinal origin. Am J Med 1955; 19:872–886.
12. Quigley JP, Brody DA: A physiologic and clinical consideration of pressures developed in the digestive tract. Am J Med 1952; 13:73–81.
13. Burt CV: Pneumatic rupture of intestinal canal with experimental data showing mechanism of perforation and pressure required. Arch Surg 1931; 22:875–902.
14. Ainsworth J: Emphysema of the leg following perforation of the pelvic colon or rectum. Br J Radiol 1959; 32:54–55.
15. Altemeier WA, Alexander JW: Retroperitoneal abscess. Arch Surg 1961; 83:512–524.
16. Shaffer RD: Subcutaneous emphysema of the leg secondary to toothpick ingestion. Arch Surg 1969; 99:542–545.
17. Meshkov SL, Seltzer SE, Finberg HJ: CT detection of intraabdominal disease in patients with lower extremity signs and symptoms. J Comput Assist Tomogr 1982; 6(3):497–501.
18. Smith HJ, Berk RN, Janes JO, et al: Unusual fistulae due to colonic diverticulitis. Gastrointest Radiol 1978; 2:387–392.
19. Smith WS, Ward RM: Septic arthritis of the hip complicating perforation of abdominal organs. JAMA 1966; 195:170–172.
20. Abratt RP, Pontin AR, Roman TE, et al: Tumour spread through the obturator foramen. Br J Radiol 1985; 58:673–674.
21. Rao BK, Lange TA, Hafez GR, et al: Extension of recurrent rectal carcinoma through sciatic foramen: Diagnosis by computed tomography. Comp Radiol 1982; 6:193–197.
22. Raval B, Lakmi N: CT demonstration of preferential routes of the spread of pelvic disease. CRC Diagn Imaging 1987; 27:17–48.
23. Meyers MA: Acute extraperitoneal infection. Semin Roentgenol 1973; 8:445–464.
24. Meyers MA: Radiologic features of the spread and localization of extraperitoneal gas and their relationship to its source: An anatomical approach. Radiology 1974; 111:17–26.
25. Meyers MA, Whalen JP, Peelle K, et al: Radiologic features of extraperitoneal effusions: An anatomic approach. Radiology 1972; 104:249–257.
26. Illescas FF, Baker ME, McCann R, et al: CT evaluation of retroperitoneal hemorrhage associated with femoral arteriography. AJR 1986; 146:1289–1292.
27. Trerotola SO, Kuhlman JE, Fishman EK: Bleeding complications of femoral catheterization: CT evaluation. Radiology 1990; 174:37–40.

Index

A
abdominal aorta, 562, 627
abdominal cavity
  formation, 609
  posterior wall, 2
abdominal wall abscess, 126
abscesses. *See also* infections
  abdominal wall, 126
  anterior pararenal space, 359, 362–363
  drainage of, 124
  epidemiology, 57
  extraperitoneal diverticular, 701
  falciform ligament, 123, 125–126
  gas-producing, 413, 578
  gastrocolic ligament, 679
  gastrohepatic ligament, 123, 127
  hepatoduodenal ligament, 123
  intraperitoneal spread, 79–118
  lesser sac, 93, 95–97, 99, 101
  ligamentum teres, 123, 126
  liver, 127
  lumbar triangle pathway, 382
  management, 124–127
  Morison's pouch, 83, 84, 86, 88, 92
  paracolic gutter, 86
  pararenal space, 452–463, 453, 458–460
  pelvic, 79–83, 85
  perihepatic space, 102
  perirenal, 409, 412–413, 416, 418–420, 431, 434–435, 571
  perirenal roentgen signs, 418, 420
  perirenal subcapsular, 437
  postappendectomy, 85
  posterior pararenal, 356
  postoperative neocompartments, 103, 112–115, 117, 119
  pouch of Douglas, 83, 85
  psoas, 474–476, 480–482
  retrocecal appendiceal, 689
  secondary to perforated gallbladder, 100
  sigmoid diverticular, 629
  subhepatic, 83–84, 89–93, 90, 690
  subphrenic, 83, 89–93, 102–107, 109
  surgical foreign bodies, 104, 106, 116
accessory spleen, 43
acquired diverticula, 646
adenocarcinoma, esophagogastric junction with nodal metastases, 295
adenopathies. *See also* lymphatic drainage
  metastatic, 306
  paraaortic, 625
  paracaval, 625
adrenal glands, 51, 346, 499
adventitia, 270
Aerobacter aerogenes, 412, 750
air-dome sign, 324
alantois, 48
alimentary tract, peritoneal investment, 59
American Joint Committee on Cancer, 269
anastomoses, 87, 93, 179
aneurysms, 562, 627
annular invasion
  by prostatic carcinoma, 185
  transverse colon, 144, 148, 150, 151
anterior pararenal space, 356–408
  abscess, 359, 362–363
  bleeding, 388–389, 392–397
  blood collection, 361
  collections, 356–361, 402
  compartmentalization, 396–399, 402
  components of, 403
  description, 334, 336
  emphysematous pancreatitis, 376
  extension of pelvic hemorrhage, 397
  extension to bare area of liver, 385
  fluid collection, 377
  granulomatous ileocolitis abscess, 384
  hemorrhage, 338
  inflammatory changes, 362
  opacification, 338
  pancreatic pseudocysts, 375
  pancreatitis, 369–371, 378
  pelvic and mesenteric continuities, 392, 396
  phlegmon, 363
  retroduodenal hemorrhage, 368
  sources of effusions, 357–396, 360
  urine extravasation, 395
anterior superior bubble, 326–328
anterior superior pancreaticoduodenal artery, 596
anterior superior pancreaticoduodenal vein, 597
antibiotics, 124
anticoagulation, 440, 660. *See also* bleeding
aorta, 562, 627
aortoenteric fistulae, 477
aortic aneurysm rupture, 627
aortocaval fistulae, 433
appendectomy, abscess after, 85
appendices epiloicae, 673, 676
appendicitis
  ascending retrocecal, 683–686
  extraperitoneal, 384, 462, 686–688, 691
  perforating to thigh, 758
  retrocecal extraperitoneal, 461
  retrocolic with subhepatic abscess, 690
appendicoliths, 685
appendix
  ascending subhepatic, 689–690
  development of, 15
  elevated by pancreatic pseudocyst, 591
  perforated, 357, 362, 760
  retrocecal appendiceal abscess, 689
  variations in position, 684
arteriography
  diverticular hemorrhage, 700
  perirenal abscesses, 418, 420
arteriovenous malformations, pancreatic, 36, 41
arthritis, septic, 757
ascending colon. *See* colon, ascending
ascending subhepatic appendix, 689–690
ascitic fluid
  falciform ligament and, 385
  flow in the peritoneal cavity, 193
  small bowel mesentery, 200
atresia, 11

B
bacterial peritonitis, 224
bile duct air, 325
Billroth II antecolic gastrojejunostomy, 545
biloma, infected, 121, 122
biphasic enteroclysis, 643
bleeding. *See also* anticoagulation; hemorrhages
  anterior pararenal space, 388–389, 392
  and colonic microarchitecture, 693–694
  Henoch-Schönlein purpura, 662
  intramural, 657, 659, 661
  mesenteric, 657, 659, 661
  mural changes in vas rectum, 698
  right anterior pararenal space, 393
blind-ending bifid ureters, 48
blind-ending ureteral bud, 50
blood. *See also* bleeding; fluid collection; hemorrhages
  collection in lumbar triangles, 382
  extraperitoneal, 333
  pelvic recesses, 84
bowel. *See also* small bowel
  displacement, 418
  duodenal web and duplication of, 10–12
  and the left kidney, 494
  malposition postnephrectomy, 533–534
  spread of secondary neoplasms, 131
breast carcinomas, 243–252
bronchogenic carcinomas, 245, 252, 253
Burkitt's lymphoma, 625
buttocks, 754–755

C
calcified deposits, 208, 214, 228–229, 562
cancers. See specific cancers; specific organs/tissues
carcinomatosis, mimicry of, 233
cardinal ligament, 614
caudate process, 137
cecal carcinomas, 180, 632
cecum
  carcinoma, 180, 632
  effects of pancreatitis, 584, 590
  elevated by pancreatic pseudocyst, 591
  herniation through the foramen of Winslow, 732–736
  metastatic lymph nodes, 302
  pathway of nodal metastases, 300
  radiologic features, 195–196
  vessels, 298–299
  volvulus, 16, 18, 19
cellulitis, subacute, 749
central inferior mesenteric lymph nodes, 163
cholangitis, 28
cholecystitis
  acute, 555
  chronic, 557, 558, 559
cholecystoduodenal fistulas, 553, 557, 558
choledochal cysts, 23–25, 27, 681
choledochocele, 28
circumferential invasion, 144, 186
classification systems
  of acute pancreatitis, 565
  American Joint Committee on Cancer, 269
  colorectal carcinoma TNM staging, 269
  esophageal cancer TNM staging, 265–266
  gastric cancer TNM staging, 266–269
  internal hernias, 711
  intraperitoneal abscesses, 79
  Japanese Research Society for Gastric Cancer, 269
  renal cell carcinoma, 444, 446
  secondary neoplasm spread to the bowel, 131
  Union Internationale Contra le Cancer, 269
Clostridium, 412, 750
"cobblestones," small bowel, 166, 181
colectomy, splenic flexure, 118
colic veins, 597
colon
  abnormal radiographic observations, 675–704
  ahaustral, 665
  anatomy and pathology of haustra, 707
  ascending
    carcinoma, 303
    metastatic melanoma, 244
    normal, 672
    pathway of nodal metastases, 300
  barium enema examination, 670, 671
  breast carcinoma metastases, 249–251
  carcinoma adherent to the duodenum, 548
  changes secondary to perinephritis, 513–516
  contractions, 673, 674
  descending
    extension of acute pancreatitis, 582
    extraperitoneal hematomas, 691
    multiple diverticula, 694
    pathway of nodal metastases, 301, 306
    peritonealization, 349
    vessels, 298–299
  direct renal cell carcinoma invasion, 188
  displacement
    by abdominal trauma, 684
    by descending duodenum mass, 560
    by renal agenesis, 522
    by renal cysts, 505–507
    by the right kidney, 500
  double-contrast radiograph, 670
  duplication, 14, 692, 693
  embryology, 665
  extraperitoneal perforation, 357, 362
  fistula formation from pancreatic pseudocyst, 581
  fusion fascia, 399
  general anatomy, 666
  granulomatous colitis, 702, 704
  haustra, 665–675
  herniation postnephrectomy, 535
  interconnections of muscle, 666
  intraperitoneal and extraperitoneal relationships, 683–684
  intrathorac herniation, 530
  invasion by gallbladder carcinoma, 556
  invasion by renal carcinoma, 511
  and the left kidney, 495
  lymph nodes, 300
  lymphatic drainage, 300–301, 301, 306
  malposition
    following nephrectomy, 531–532
    and renal agenesis, 527–530
    and renal ectopia, 527, 529
  metastatic bronchogenic carcinoma, 253
  metastatic seeding to, 692
  necrosis, 589
  normal and pathologic anatomy, 665–710
  normal layers, 270
  normal radiographic observations, 670–675
  origin of diverticula, 693, 695
  pancreatic pseudocyst drainage, 580
  and pancreatitis, 587
  pathogenesis of diverticular hemorrhage, 699
  prone projections, 671, 672
  rectosigmoid, 185
  recurrence of carcinoma to thigh, 759
  relation to the duodenum, 539–563
  relation to the left kidney, 504, 511
  retrorenal, 352
  and the right kidney, 493, 499–504
  scleroderma, 679
  sigmoid
    abscess, 483
    appendices epiloicae, 676
    arterial supply, 695
    carcinoma extending to hip, 756
    direct invasion, 182, 183, 190, 192
    diverticulitis, 701, 702, 754–755
    left colic node metastases, 306
    and mesocolon, 299–300
    midcoronal pelvis section, 750
    pathway of nodal metastases, 301, 306
    perforation, 466–467, 469–470
    radiologic features, 199, 205
    renal cell carcinoma metastases, 254
    septic arthritis secondary to diverticulitis, 757
  spread of pancreatitis, 569, 574, 578, 582
  "thumbprinting," 166, 181
  transverse colon
    annular invasion, 144
    carcinoma, 304
    circumferential invasion, 144
    direct invasion, 142–144
    extension of acute pancreatitis, 571–575
    mesenteric reflections, 142
    and mesocolon, 299
    pathway of nodal metastases, 300–301
    sagittal section, 155, 677
    spread of pancreatitis, 569, 574
colon carcinomas
  extending to hip, 756
  extension to paraduodenal area, 549
  extrapelvic presentation, 749–750
  metastatic to the liver and lymph nodes, 292

paraduodenal area spread, 162
recurrence to thigh, 759
seeded sigmoid mesocolon, 207
transverse colon, 304
colorectal carcinomas, 269
colovenous fistulas, 703
comb sign, 644, 658
common hepatic artery, 596, 597
computed tomography
diagnosis and localization of abscesses, 118
peritoneal carcinomatosis, 233, 235
congenital scoliosis, 522
contrast, in radiographs, 6
contrast material
double-contrast radiograph, 670
extravasated, 108, 110, 444
gastrocolic ligament, 677
psoas muscle, 475
transverse mesocolon, 682
coronary ligaments, 59, 60, 62, 113
Courvoisier gallbladder, 680
Crohn's disease. *See* granulomatous colitis
crossed-fused renal ectopia, 48, 49
cul-de-sac. *See* pouch of Douglas
Cullen's sign, 377, 389
cupola sign, 319–320
cystadenocardinoma, 217–218
cystohepatic duct of Luschka, 23, 24
cysts
below root of mesocolon, 562
choledochal, 23–25, 27, 681
colon displacement, 505–507
gastric duplication, 13
hemorrhagic, 680
infected renal, 435
lymphangitic, 547
ovarian, 213, 732
pancreatic, 36, 42
posterior parietal peritoneum, 562
renal, 353, 496–498, 501, 503, 505, 508–509
cystostomy tube, misplaced, 87

D

diaphragm, 609
early embryology, 9–10
muscle slip sign, 320–321
diaphragmatic defects, gastric volvulus, 16
diaphragmatic node metastases, 293
direct invasion, 132–181, 150, 182–191
diverticula
acquired, 646
angioarchitecture, 697
histology of bleeding point, 698–699
mural changes in vas rectum, 698
origin of, 693, 694, 695
pathogenesis of hemorrhage, 699
structural dynamics of formation, 697
vascular supply, 695, 697
diverticulitis, 700–702
complicating granulomatous colitis, 704–706
and diverticulosis, 692–704
extrapelvic presentation, 749–750
perforating to buttock, 754–755
septic arthritis secondary to, 757
diverticulosis
and diverticulitis, 692–704
hemorrhages, 692–695, 697–698, 700
jejunum, 645
small bowel, 644, 646, 647
small bowel localization, 644
terminal ileum, 647
doges's cap sign. *See* Morison's pouch, air
dorsal mesentery, 609–610, 612–614
dorsal pancreatic artery, 596
ductus venosus, 29, 31, 32
duodenal bulb
chronic "blow-out," 552
metastatic melanoma, 240
parasagittal section, 541
transverse section, 541
duodenal ulcers, 90, 91, 373
duodenal web, 10–12
duodenocolic fistulas, 546, 549, 559
chronic "blow-out" of duodenal bulb, 552
secondary to granulomatous colitis, 550–551
secondary to intestinal tuberculosis, 552
duodenocolic ligament, 122, 152–156, 161
duodenoduodenal fistulas, 165
duodenojejunal junction, 651
duodenojejunostomy, 545
duodenum, 596
anatomic relationships, 160
colonic carcinoma adherence to the, 548
displacement by an adrenal mass, 499
displacement by metastases, 499
displacement by ptotic kidney, 510
effects of pancreatitis, 584
extraperitoneal perforation, 365–367
fusion fascia, 399
"hammock," 12
hepatic flexure carcinoma, 546
inframesocolic extension, 560–561
invasion by gallbladder carcinoma, 556
invasion by pancreatic carcinoma, 601
invasion by renal cell carcinoma, 186–187
leiomyosarcoma, 560
malposition and renal agenesis, 524–525
malposition and renal ectopia, 526
parasagittal section, 541
perforation during ERCP, 408
relation to the colon, 539–563
and the right kidney, 493, 496–497
rupture, retroperitoneal hemorrhages, 407
suspensory muscle attachment, 543
transverse, obstruction by pancreatitis, 586
transverse section, 541

E

ectoderm, 9, 10
embolic metastases, 238–254
embryology
abdominal anatomy, 9–55
colon, 665
diaphragm, 9–10
eight-week embryo, 51
five-week embryo, 11, 48
four-month fetus, 609
fourth to fifth week embryo, 608
four-week embryo, 10, 29, 610
gastric volvulus, 16–19
gastrointestinal tract, 9, 10–20
genital system, 50–51
gut, 13–16
hepatobiliary system, 21–25
kidneys, 45–50, 513
liver, 609
nervous system, 9
pancreas, 32–42
portal venous system, 25–32
seven-week embryo, 50
six-week embryo, 15, 51
spleen, 43–44
subperitoneal space, 607–611
ten-week fetus, 16
three-month fetus, 29
three-week embryo, 608
urinary bladder, 48, 50
urogenital system, 45–51
emphysema, 749
endoderm, 9, 10
enteric cysts, 13
enteroliths, Meckel's diverticulum with, 21
epiploic foramen, 68, 69, 77, 731–737
Escherichia coli, 412, 750
esophageal cancers
T1, 273
T1sm, 273
T3, 276–277
T4, 279, 281–282
T staging, 272, 275
TNM staging, 265–266
esophageal mesentery, 12
esophagogastric junction, 295
esophagus, wall, 271
extramedullary hematopoiesis, 448, 450
extraperitoneal appendicitis, 686–688
extraperitoneal compartments, 334–346, 353
extraperitoneal paravesical pelvic spaces
anatomic considerations, 477–480
diagram, 478
fluid collection, 480–483
extraperitoneal spaces, 333–491, 469
eye fixation, 6

F

falciform ligament, 62, 102
abscess, 123, 125, 126
and ascites, 385
formation of, 609
hernias through, 744
metastasis, 220–221
pancreatic fluid in, 388
spread of pancreatitis, 389
supine film signs of pneumoperitoneum, 310, 311–313
vascular landmarks, 289
vascular relationships, 384
fascia d'accolement, 396

figure-ground reversal, 5, 6
fistulas
  aortoenteric, 477
  aortocaval, 433
  cholecystoduodenal, 553, 557, 558, 559
  colovenous, 703
  duodenocolic, 546, 549, 550–551, 552, 559
  duodenoduodenal, 165
  formation from pancreatic pseudocyst, 581
  renocolic, 517
  renogastric, 518
flank stripes, 337, 361
flow patterns
  ascitic fluid, 193
  intraperitoneal exudates, 112
  lymph in carcinoma, 166
  peritoneal fluid, 92–93
fluid collections
  coalescence of perirenal effusions, 416
  pancreaticoduodenal compartment, 402
  perirenal and subcapsular, 430–433, 438–439, 444
  posterior pararenal space, 451, 452
  retromesenteric plane, 402
  retrorenal plane, 402
football sign, 324
foramen of Bochdalek, 11
foramen of Winslow, 68, 77, 731–737
foregut-midgut junction, 15
foreign bodies, 104, 106, 116
foreign body retention, 103, 106, 116
fossa of Landzert. *See* paraduodenal fossa
fossa of Waldeyer. See mesentericoparietal fossa
fusion fascia, 399, 400–401, 407

G
gallbladder
  adherent "porcelain," 554
  choledochal cysts, 681
  diseases, 549, 556
  duplication, 26, 27
  ectopic and accessory, 23
  intrahepatic, 25
  perforated, 100
  right parasagittal section, 554
  wandering, 23, 24
gallbladder carcinomas, 204, 556, 559
gallium–67, abscess diagnosis, 124
gallstones, 28, 553
gas. *See also* intraperitoneal air
  diffusion via the subperitoneal space, 615–619
  extraperitoneal, 333–334, 463–464, 466–468, 471, 473
  intrahepatic portal, 702
  left upper quadrant, 324, 325
  pancreatic abscess production of, 578
  perforated retrocecal extraperitoneal appendicitis, 461
  pneumatosis coli, 675
  pressures in intestinal lumen, 749
  subdiaphragmatic, 471–473
  supradiaphragmatic, 467, 471
gastrectomy, steps in, 114
gastric arteries, 100
gastric carcinomas
  antrum, 277
  extension along gastrocolic ligament, 142–151
  extension to liver, 139
  lymph node stations, 133
  mural penetration, 268
  seeded paracolic gutter, 211
  seeded sigmoid mesocolon, 208–209
  seeded small bowel mesentery, 201, 204, 206
  spread across gastrosplenic ligaments, 168–173
  spread down gastrocolic ligament, 678
  staging, 266–269
  staging by MR imaging, 271
  T2, 275
  T3, 277–278
  T4, 282
gastric duplication cyst, 13
gastric rotation, 14
gastric ulcers, 107, 234, 623
gastric volvulus, 16–19
gastrocolic fistulas, 153
gastrocolic ligament
  abscesses, 679
  anatomy, 140, 142–152, 289
  carcinoma, 678
  hemorrhagic cyst, 680
  injected contrast material, 677
  lesions, 675, 681
  metastatic spread, 142–143, 145–152
  nodal metastases, 295
  pancreatic carcinoma extension, 153
  relation to transverse mesocolon, 682
  vascular landmarks, 289
gastroduodenal artery, 596, 597
gastrohepatic ligament
  abscess, 122, 123, 127
  anatomy, 134, 136, 138, 288–289
  formation of, 609
  lymph node metastases, 138
  malignant hepatic invasion, 139
  nodal metastases, 293, 295
  relation to lesser sac, 69, 70
  transection of, 114–115
  vascular landmarks, 289
gastrointestinal cancers
  lymph node metastases, 287–307
  staging of, 265–286
gastrointestinal series, normal, 545
gastrointestinal tract
  early embryology, 9
  embryological development, 10–20
  relation to kidneys, 493–537
  upper diagnostic series, 540
gastropancreatic fold, 75
gastropancreatic plica, 73
gastrosplenic ligament
  anatomy, 156, 158, 166, 167, 289
  gastric carcinoma, 168
  lymphoma, 168
  nodal metastases, 297
  vascular landmarks, 289
genital system embryology, 50–51
Gerota, Dimitrie, 336
gonadal ridge, 51
granulomatous colitis
  comb sign, 658
  diverticulitis complicating, 702, 704–706
  duodenocolic fistula, 550–551
  similarity to metastatic carcinoma, 249
granulomatous ileocolitis, 384
greater omentum, 15. *See also* gastrohepatic ligament
  ascites between leaves, 71
  caking, 230, 232–233
  cysts, 13
  and the gastrocolic ligament, 289
  inflammation, 234
  metastatic ovarian cancer, 156
  "milky spots," 230
  nodular metastases, 232
  seeded metastases on, 230–232
  varices, 234
  vascular landmarks, 289
Grey Turner's sign, 377, 383, 384, 402
gut, embryology, 13–16

H
"hammock" duodenum, 12
haustra
  anatomy and pathology, 665–696, 707
  diverticulitis, 700–702
hematogenous metastases, 644, 651–652, 653
hematomas
  extraperitoneal, 691
  extrarenal, 431
  flank, 337
  paravesical spaces, 480
  perirenal, 416–417
  perirenal subcapsular, 438–443
  posterior pararenal space, 455
  prevesical spaces, 481–482
  psoas, 477, 480–482
  renorenal septum, 445
  retroduodenal and intramural, 367
  transverse mesocolon, 157
hemorrhages. *See also* anticoagulation; bleeding
  anterior pararenal space, 338
  colonic diverticular, 692–695, 697–698, 698–699, 700
  continuity of subperitoneal space, 626–627
  from iliac artery, 761
  perirenal spaces, 436
  posterior pararenal space, 451, 453, 454–457
  retroperitoneal, 407
  splenic artery, 394
hemorrhagic cysts, 680
hemothorax, 216

Henoch-Schönlein purpura, 662
hepatic angle, 355, 357
hepatic arteries, 136, 388
hepatic duct diverticula, 25
hepatic edge, 317
hepatic flexure
  carcinoma, 181, 303–304, 546, 548
  diverticulitis of, 701
  perforation, 361
  and the right kidney, 494
  spread of pancreatitis, 569, 570, 574, 578, 582
hepatic lobar agenesis, 21, 23
hepatic lobectomy, steps, 113
hepatic notch, 317–319
hepatic sinusoids, 27
hepatobiliary carcinomas, 287–307
hepatobiliary system, 21–25
hepatocellular carcinomas, 34, 292, 293
hepatoduodenal ligament
  abscess, 121, 122, 123
  anatomy, 288–289
  formation of, 609
  inflammatory thickening, 140
  intrahepatic extension, 386
  nodal metastases, 140
  pancreatic pseudocysts, 387
  vascular landmarks, 289
hepatoduodenal ligaments, 134–136, 138
hepatojejunostomy, 745
hepatorenal fossa, 60. *See also* Morison's pouch
hernias
  foramen of Bochdalek, 11
  internal, 44–45
  internal abdominal, 711–748
  into lesser sac, 546
  location and incidence, 711–712
  simulation by hepatojejunostomy, 745
herniation
  colonic, postnephrectomy, 535
  intrathorac colonic, 530
  mesocolon, 544, 546
  physiologic, 16
heroin addiction, 660
hindgut mesentery, 51
Hodgkin's lymphoma, 659
horseshoe kidneys, 48, 49
hydronephrotic kidney, 423, 501
hydrostatic pressure, 92–93
hyperechoic layers, 270
hypoechoic tumor, 273

I
ileocecal junction, 249
ileocecal valve, 15
ileocolic mesentery, 298–299
ileum
  carcinoid, 303, 653
  duplication of, 651
  herniation of loops, 737
  radiologic features, 195–196
  regional enteritis, 654—657
iliac artery, 761
iliacus muscles, 751
iliopsoas abscess, 476
image analysis, dynamics of, 1–7
infections. *See also* abscesses
  extraperitoneal, 333
  gas-producing, 374, 412–415
  intraperitoneal spread, 57–130
  posterior pararenal space, 452–463
  pseudocysts, 375
inferior mesenteric vein, 597
inferior pancreaticoduodenal vein, 597
inferior vena cava, 69
infracolic spaces, 57, 192
inframesocolic compartment, 297–306
In^{111}-labeled leukocyte scanning, 124
internal abdominal hernias, 711–748
internal hernias, 44–45
intersigmoid hernias, 738–739
intestinal duplication, 644, 650–651
intestinal mucosa, 590
intestinal tract embryology, 15
intraembryonic coelom, 10
intraluminal diverticulum, 13
intramural thumbprints, 644
intraperitoneal abscesses, 79
intraperitoneal air. *See also* gas
  detection, 309
  manifestations of, 309–31
  supine film signs, 309–329
intraperitoneal exudates, 112
intraperitoneal fluid drainage, 194
intrauterine ischemia, 11
inverted V sign, 310, 315, 316
ischemic atrophy, 590
ischemic enteritis, 661
isotopic scans, abscess diagnosis, 124

J
Japanese Research Society for Gastric Cancer, 269
jejunal arteries, 722
jejunitis, 587
jejunum, 189, 638, 645

K
kidneys. *See also* renal carcinomas; renal cell carcinomas; renal cysts; renal fascia; renal septa
  agenesis, 48–49, 512–513, 519–523, 532
  agenesis and colonic malposition, 527–530
  agenesis and intestinal malposition, 524–525
  bridging renal septa, 438–439, 442, 444–445
  capsular anatomy, 430
  colon displacement, renal sarcomas, 504
  crossed ectopia, 520
  crossed-fused renal ectopia, 48, 49
  direct invasion, 184–185
  displacement of the descending duodenum, 560
  ectopia and colonic malposition, 527
  ectopia and intestinal malposition, 526, 529
  ectopic, 512–513, 519–520, 523, 532–533, 535, 536
  embryologic considerations, 513
  embryology, 45–50
  fixation, 418
  horseshoe kidneys, 48, 49
  hydronephrotic, 423, 501
  infected renal cysts, 435
  left, 494–495
  multicystic, 502, 512
  pancreatic pseudocyst, 391
  perirenal and subcapsular collections, 430–433, 438–439, 444
  ptosis, 504–505
  radiologic observations, 496–535
  relation to the colon, 511
  renal capsule anatomy, 430
  right, 493–494
  roentgen signs of abscesses, 418, 420
  rotation, 504–505
  seventh week embryonic, 50
Krukenberg tumors, 192, 232–233, 236

L
lamina propria, 272
laparotomy pads, 120
lateroconal fascia, 352
leaping dolphins sign, 320–323
left upper quadrant gas, signs of, 324, 325
leiomyomatosis peritonealis disseminata, 233
leiomyosarcoma, of duodenum, 560
lesser omentum. *See* gastrohepatic ligament
lesser sac
  abscesses, 93, 95–97, 99, 101
  air, 324
  anatomy of, 2, 63–64, 68–79
  boundaries, 69
  fluid in, 78, 80, 81
  during gastric rotation, 14
  herniated, 78
  mesocolon internal herniation into, 544, 546
  opacification, 71
  pancreatic fluid, 97
  pancreatic pseudocyst, 98
  peritoneal fluid, 94
  pseudocysts, 101
  relationships, 68
  strangulated hernia, 735
ligament of Treitz, 542, 543
ligaments. See also specific ligaments
  colectomy of the splenic flexure, 118
  peritoneal, 132
  spread of infection via, 116, 118
  surgical transection, 113–116, 118
  vascular landmarks, 289
ligamentum teres
  abscess, 123, 126
  fissure sign, 322–324
  supine film signs of pneumoperitoneum, 310, 311–313, 315

umbilical vein within, 29
vascular relationships, 384
ligamentum venosum, 385
linitis plastica, 247
liver
abscesses, 127
anterior surface, 314
caudate lobe and the lesser sac, 72
"claw" sign, 230
colon displacement, 502
communication with right perirenal space, 342
cystic disease, 23
ectopic tissue with malignancy, 23
embryology, 609
extension of pancreatitis, 387
extracapsular lesions, 231
fifth week embryo, 12
fluid lateral to, 89
free air superimposed on, 326–327
hepatic abscess, 123
lucent, 326–327
lymphatic drainage, 289–291
pancreatic pseudocysts, 127
papillary process, 137
peritoneal ligaments, 288
relationship to stomach, 139
right hepatic lobectomy, 113
seeded metastases, 217–218, 229–230
stab wound, 108
visceral surface, 62
liver bud, 29
lumbar triangles, 380–382
luminance, and eye fixation, 6
lung carcinomas, 253–254
lymph. *See also* lymphatic drainage
altered flow in carcinoma, 166
extravasation, 453
posterior pararenal extravasation, 464
lymph nodes
central inferior mesenteric, 163
colon segments, 300
common hepatic node, 292
diaphragmatic node metastases, 293
draining right colon, 160
gastrohepatic ligament metastases, 138
hepatic hilar node HCC metastases, 292
metastases, 162–164, 283
pancreatic cancer metastases, 603–605
paraduodenal, 163
pathways of metastases, 287–307
portacaval, 136–137
posterior periportal nodes, 292
spread of colonic carcinoma, 162
stations in gastric cancer, 133
lymphadenopathy, pericardiac, 216
lymphangitic cysts, 547
lymphatic drainage. *See also* lymph; lymph nodes
colon, 300–301, 306
of the liver, 289–291
pancreatic, 597–598
stomach, 292–293, 294
lymphatic penetration, 166, 179–182
lymphatic stranding, 355
lymphocyst, 463
lymphomas
cecum, 302
gastrosplenic ligaments, 168
Hodgkin's, 659
liver, 293
within mesentery, 178
perirenal, 448
small bowel localization, 644, 657
splenic, 297
subpcritoneal continuity, 625
lymphomatosis, peritoneal, 237
lymphosaroma, 659

M

magnetic resonance imaging
diagnosis and localization of abscesses, 118, 124
peritoneal carcinomatosis, 235, 238
malignancies. See also specific cancers
intraperitoneal spread, 131–263
pathways of spread, 131
small bowel localization, 644
staging gastrointestinal cancers, 265–286
Meckel's diverticulum, 19–22, 644, 646, 648–650
mediastinum, gas diffusion, 615–616
melanomas, metastases, 239–245
mesenteric lymphoma, 179
mesenteric reflections
direct invasion of malignancies, 132–165
major upper abdominal, 132, 133
to the transverse colon, 142
mesenteric root
opacification, 568, 585, 623
pancreatic pseudocyst spread, 586
mesentericoparietal fossa, 712–713, 715
mesenteries. See specific mesentery
mesocolon
ascending, vessels, 298
cyst below root of, 562
descending, persistent, 20
dorsal, 613
extension of acute pancreatitis, 571–572
formation of, 610
herniation into lesser sac, 544, 546
masses within leaves, 544
sigmoid, calcified metastases, 208
and sigmoid colon, 299–300, 470
transverse, 545
anatomy, 152–156, 157
embryology, 15
extension of acute pancreatitis, 576
extravasated pancreatic enzymes, 682
hematoma, 157
injected contrast material, 682
insertion, 539–540
lesions within, 681–683
location, 192
pancreatic carcinoma, 156, 158, 160, 600–601, 683
spread of infection, 57
and transverse colon, 299
mesoderm, 9, 10
mesoenteric cysts, 13
mesogastrium, 43
mesonephric duct, 51
mesotheliomas, 233, 236
metastatic seeding. *See also* malignancies; *specific cancers*
"caking," 218
to the colon, 692
colon lymph nodes, 300–301, 306
greater omentum, 230–232
lymphatic drainage of the liver, 289–290
lymphatic drainage of the stomach, 292
Morison's pouch, 212
pcrihepatic, 212, 216–218, 229–230
pcrihepatic nodules, 219, 225
peritoneal sites, 193–233
pouch of Douglas, 195–198
small bowel localization, 644, 651
small bowel mesentery, 195–196, 198
subdiaphragmatic, 212, 216–218, 229–230
by surgical techniques, 233
midgut, 10, 29, 729
midgut nonrotation, 29
midgut volvulus, 29, 729
midgut–hindgut junction, 15
"milky spots," greater omentum, 230
Morison, Rutherford, 59
Morison's pouch, 59. *See also* hepatorenal fossa
abscesses, 83–84, 86, 88, 92
air, 314, 323
anatomic relationships, 61
fluid–filled, 62
metastatic seeding, 212, 214–215
radiologic features, 205
triangular dependent recess, 88
mucosa, esophageal wall, 271
multistable images, 6
muscularis mucosae, 271, 273
muscularis propria, 270, 271

N

needle track seeding, 233, 237
neocompartments, postoperative, 103, 112–115, 117, 119
neoplasms. *See* malignancies; *specific cancers*
nephrectomy, 533–535
nervous system, embryology, 9
neurenteric cysts, 13
neuroblastoma, 620

O

obturator internus muscle, 751
Ochsner's extrapleural approach, 124–125
omentum. *See* gastrohepatic ligament; greater omentum
omphalomesenteric duct, 15
ovarian carcinomas
calcified perihepatic implants, 228–229
direct invasion by, 182, 190, 191, 192

invasion of sigmoid colon, 182, 183–184
liver metastases, 230
metastatic, 156
perihepatic dissemination, 216, 218
seeded metastases, 652
seeded paracolic gutter, 210–211
seeded small bowel mesentery, 201–203, 205
subdiaphragmatic seeding, 217
subperitoneal spread of, 630–631
ovarian cysts, 213, 732
ovaries, 51

P

Page kidney, 438–439
pancreas
agenesis of, 34–36, 40
anatomic pathways of spread, 568
anatomy, 565–567, 595–598
annular, 33, 36, 37, 38
distinction between anlagen, 35
divisum, 33–34, 38, 39
embryology, 32–42
extravasation, 390
fatty infiltration, 35
formation of, 35, 610
gas-producing abscess, 578
gas-producing infection, 374
head, 36, 598
imaging studies, 598
infected pseudocysts, 374
lymphatic anatomy, 597–598
malposition postnephrectomy, 533–534
mesenteric relationships, 566
nerve plexus, 598
vascular anatomy, 596–597
pancreatic carcinomas
advanced, 600
along transverse mesocolon, 683
Courvoisier gallbladder secondary to, 680
direct invasion, 621–622
invasion of the transverse colon, 156
invasion of the transverse mesocolon, 156
nodal metastases, 140
pancreatic head, 602, 603, 604
pancreatic neck, 603
pathways of spread, 595–606
seeded sigmoid mesocolon, 207, 209
seeded small bowel mesentery, 202–204, 206
spread across phrenicocolic ligament, 175–176
spread to the gastrocolic ligament, 153
spread to transverse mesocolon, 158, 160
pancreatic cysts, 36, 42
pancreatic ductal adenocarcinomas, 595, 599–605, 604
pancreatic enzyme extravasation, 566
pancreatic fluid, 97
pancreatic pseudocysts, 13
along hepatoduodenal ligament, 387
colonic fistula formation, 581
intrahepatic, 127
and left gastric artery, 100
within lesser sac, 98
lower right quadrant, 591
pericolitis and, 576
perirenal, 390–391
within root of mesentery, 624
rupture of, 578, 580
spread down mesenteric root, 586
pancreaticoduodenal compartment, 402
pancreaticoduodenal space, 405
pancreatitis
abscess drainage, 372
acute, 101, 561, 565–594, 587, 591
acute edematous, 565
acute gangrenous, 565
acute hemorrhagic, 565, 590
acute suppurative, 565, 570, 579, 591
anterior pararenal spaces, 378
chronic relapsing, 590
components of anterior pararenal space, 403
emphysematous, 376
extension to liver, 387
fascial reactions, 367–372, 377, 385, 388
fulminating acute, 371
Grey Turner's sign, 377, 383, 384, 402
left-right communication, 408
lumbar triangles, 382
pelvic extension, 582–583
perirenal fat, 390
posterior pararenal spaces, 379, 381
resolving, 404
spasm and edema, 573
spread along falciform ligament, 389
spread along fusion fascia, 407
subperitoneal spread, 628, 633
traumatic, 577, 589, 682
of ventral anlage, 39
papillary process, 137
para-aortic adenopathy, 625
paracaval adenopathy, 625
paracentesis, 237
paracolic gutter, 59
abscess, 86, 110–111
ascitic flow, 193
contrast material extravasation, 110
location, 192
postappendectomy abscess, 87
radiologic features, 205
seeded by gastric carcinoma, 211
seeded by ovarian carcinoma, 210–211
paraduodenal area, 161
paraduodenal fossa, 712–713
paraduodenal hernias
anatomic considerations, 712–713
bilateral, 730
features, 713
left, 714–718, 720–723, 725–727
location and incidence, 712
right, 715, 718–719, 723–724, 727–728
paraduodenal lymph nodes, 163–164
paramesonephric duct, 51
pararenal spaces. *See* anterior pararenal space; posterior pararenal space
parasagittal diagram, 60
paravesical recesses, 192–193
paravesical spaces, 479–480, 483
pelvis
abscesses, 79–83, 85
blood gravitating to recesses, 84
contents, 4
coronal section, 751
cross–section, 519
extension of pancreatitis, 398, 582–583
extrapelvic insertion of muscles, 751, 752
extraperitoneal diverticular abscesses, 701
fluid accumulation, 82, 83
location, 192
midcoronal section, 750
planes of fascia, 751
subperitoneal spread of inflammation, 628–629
volume of, 57, 59
pericolitis, 576
periduodenal lucency, 327
perihepatic ligaments, 116, 118
perihepatic space, 102, 225
perinephritis
colonic changes secondary to, 513–516
renocolic fistulae, 517
and renointestinal fistulas, 505, 508, 512
peripheral vision, reading radiographs, 4
perirectal spaces, 479–480
perirenal abscesses, 517
perirenal bridging septa, 354
perirenal fat, 390
perirenal lymphomas, 448
perirenal spaces
abscesses, 418–421
and bare area of the liver, 342
continuity, 336
definition, 334, 336
extravasation into, 418
fluid collections, 409
fluid distention, 411–412
gas-producing infections, 412–415
hemorrhage, 436
medial fascial closure, 339
metastases, 450–451
midline communication, 341
opacification, 411–412
pseudocysts, 420, 422–430
retroperitoneal fibrosis, 450
roentgen anatomy, 409
roentgen signs of perirenal abscesses, 418, 420
sources of effusions, 409, 412
subcapsular abscess, 437
peritoneal cavity
anatomic features, 192
ascitic flow, 193
intraabdominal spaces, 193
metastatic seeding, 192–238
posterior reflections, 193
seeded sites, 193–233
peritoneal fluid
distribution, 92–93
extension into the lesser sac, 94

peritoneal leiomyosarcomatosis, 233
peritoneal ligaments, vascular landmarks, 289
peritoneal lymphomatosis, 233, 237
peritoneal mesentery, 132
peritoneal mesothelioma, 236
peritoneal reflections, 613
peritoneal serous papillary carcinoma, 233
peritoneal-pleural communication, 216
peritoneum
  "caking," 218
  carcinomatosis, 223
  diaphragmatic, 218
  metastasis, 220
  posterior attachments, 57–59
  posterior reflections and recesses, 58
  pseudomyxoma peritonei, 226–227
  seeded metastases, 222
peritonitis
  bacterial, 224
  tuberculous, 223–224
perivesical spaces, 479–480
Petit's triangle, 691
phlegmon, 110, 363
photopic vision, in visual search, 4
phrenicocolic ligament, 59
  anatomy, 156, 158, 174
  extension of acute pancreatitis, 575
  location, 192
  relation to transverse mesocolon, 154
  spread of pancreatic carcinoma, 175–176
piriformis muscles, 751
pleuroperitoneal membranes, 12
pneumatosis coli, 675
pneumatosis intestinalis, 588
pneumoperitoneum
  less than 1 mL, 329
  metastatic seeding after, 238
  supine film signs, 309–329
pneumoscrotum, 324, 326
polysplenia syndrome, 44, 47
portacaval lymph nodes, 136–137
portal veins, 597
  agenesis, 32, 34
  aneurysmal dilatation, 31–32, 33
  preduodenal, 31
portal venous system, 25–32
portohepatic venous shunt, 27, 29, 30
posterior pararenal space
  abscess, 462
  collections, 451, 452–463
  communication to extraperitoneal spaces, 343
  definition, 336
  demarcation, 341
  fat, 465
  infection post nephrectomy, 452–463
  pancreatitis, 379, 383
  roentgen anatomy, 451
  sources of effusions, 451, 453
posterior parietal peritoneum, cyst, 562
posterior peritoneal reflections
  left upper quadrant, 567
  parasagittal view, 567
posterior superior pancreaticoduodenal artery, 596
posterior superior pancreaticoduodenal vein, 597, 598
postfibrotic pseudodiverticula, 644
postoperative neocompartments, 103, 112–115, 117, 119
posture, peritoneal fluid distribution, 92–93
Pott's disease, 476
pouch of Douglas, 79–82
  abscesses, 83, 84
  metastatic seeding, 195–198
  radiologic features, 194–196
  relationships, 194
prececal hernias, 737
preduodenal portal veins, 27, 31
prevesical spaces, 479–480, 481–482
prostate gland, 750
prostatic carcinomas
  annular rectal invasion, 185
  circumferential rectal invasion, 186
  direct invasion from, 182, 184
Proteus, 750
pseudo Rigler's sign, 317
pseudocysts. *See also* pancreatic pseudocysts
  lesser sac, 101
pseudomyxoma peritonei, 226–227
pseudosacculations, 644
psoas
  abscess and hematoma, 473, 477, 480–482
  abscess extension to lumbar triangle pathway, 382
  loss of margin, 418
  tuberculous abscess, 476
psoas major muscles, 751
psoas muscle, anatomy, 353, 355
ptosis, renal, 504–505
pyonephrosis, calculous, 421

R

radiographs, perception, 4–7
radioimmunoscintigraphy, 238
rectal carcinomas
  T1N1, 274
  T2, 275, 276
  T3, 279
rectal tubulovillous adenoma, T1, 274
rectosigmoid colon, 185
rectosigmoid junction. *See* pouch of Douglas
rectum
  breast carcinoma metastases, 252
  direct invasion by ovarian carcinoma, 191
  extravasation with gluteal spread, 753
  gas diffusion from perforation, 617–618
  normal wall, 271
  perforation, 466, 469
regional enteritis, 644, 654–657
renal carcinomas
  abdominal metastases, 245
  colon invasion, 511
  displacement of the colon, 506
renal cell carcinomas. *See also* kidneys
  colon displacement, 503
  invasion of colon, 188
  invasion of the descending duodenum, 186–187
  invasion of the jejunum, 189
  invasive, 505
  sigmoid colon metastases, 254
  staging, 444, 446, 448
  stage I, 446
  stage II, 446
  stage IIIa, 447
  stage IVa, 447–448
renal cysts, 353. *See also* kidneys
  colon displacement, 501, 503, 505
  displacement of the colon, 507
  displacement of the duodenum, 496–498
  displacement of the stomach, 508–509
  infected, 435
  small bowel displacement, 509
renal fascia. *See also* kidneys
  attachment of adrenal gland, 346
  cone, 410, 423
  layers of, 350–352
  medial insertion, 347
  midline continuity, 340
  midline termination, 339
  pancreatitis, 378
  thickened, 369
  thickening, 348
renal septa. *See also* kidneys
  bridging, 438–439, 442, 444–445
  posterior, 353
renocolic fistulae, 517
renogastric fistulae, 518
renointestinal fistulas, 505, 508, 512
renointestinal relationships, 493–537
renorenal septum retraction, 353
reticulum cell sarcoma, 465
retroanastomotic hernias, 744, 745
retrocecal appendiceal abscess, 689
retrocolic appendicitis, 690
retrocolic fascia of Toldt, 396
retroduodenopancreatic fascia of Treitz, 396
retromesenteric colonic space, 405, 406
retropancreatic fascia of Treitz, 396
retroperitoneal fibrosis, 448, 450
retroperitoneal lymphoma, 179
retroperitoneum, adult female, 3
retrorenal spaces, 406
right inferior coronary ligaments, 60
right superior coronary ligaments, 60. *See also* coronary ligaments
right upper quadrant, 59–79
Rigler's sign, 316–317
Robson system, 444, 446
root of the small bowel mesentery, 57, 613, 624

S

saccadic movements, viewing time, 6
scleroderma
  colon, 679
  small bowel localization, 644, 646, 650
sclerosing mesenteritis, 233
scoliosis, 458
scrotum, 583

sectional imaging modalities, abscesses, 118–124
septum transversum, 12
serosa, 270
sigmoid colon. *See* colon, sigmoid
sigmoid diverticulitis, 85
sigmoid diverticulum, 619
sigmoid mesocolon, 207–209, 628
sinus tracts
  granulomatous colitis with, 706
  small bowel localization, 644
  spread of disease, 749
Sister Mary Joseph's nodule, 232, 234, 235
size, and eye fixation, 6
slip sign, 320–323
small bowel. *See also* bowel
  abnormal radiologic observations, 644, 646, 650–652, 654, 659, 661
  biphasic enteroclysis, 643
  breast carcinoma metastases, 248
  "cobblestones," 166, 181
  displacement by ptotic kidney, 510
  displacement by renal cysts, 509
  displacement by the right kidney, 500
  effects of pancreatitis, 584, 590
  herniation, 744
  identification of borders, 640, 642–644
  localization of pathologies, 644
  metastatic bronchogenic carcinoma, 252
  metastatic melanoma, 239, 241–245
  normal and pathologic anatomy, 635–663
  normal radiologic observations, 636, 640, 642
  obstruction, 640
  and pancreatitis, 587
  and the right kidney, 497
  undulating coils of loops, 636, 640–641, 643
  volvulus, 728
small bowel mesentery, 635–636
  anatomic relationships, 177
  anatomy, 158–159, 199, 635–636
  ascitic fluid, 200
  axis of the root, 636
  coronal section, 637
  dimensions, 638
  extension of acute pancreatitis, 591
  extension of pelvic hemorrhage, 397
  lymphoma continuity via subperitoneal space, 625
  metastatic seeding, 198
  radiologic features, 196, 199
  relation to transverse mesocolon, 154
  root, 639
  seeded gallbladder carcinoma, 204
  seeded gastric carcinoma, 201, 204, 206
  seeded ovarian carcinoma, 201–203, 205
  seeded pancreatic carcinoma, 202–204, 206
  spread of pancreatitis, 585
  subperitoneal spread of ovarian carcinoma, 630–631
  transverse section, 637
  tuberculosis peritonitis, 224
small intestine. *See* small bowel
somatopleure, 10
splanchnopleure, 10
spleen
  accessory, 43
  bleeding from, 388, 392
  fluid lateral to, 89
  formation, 610
  lymphoma, 297
  peritoneal attachments, 391
  polysplenia syndrome, 44
  spread of gastric carcinoma, 169–171
  wandering, 16–17, 43–45, 46, 531
splenic angles, 355
splenic artery, 388, 394, 596, 600
splenic buds, 43
splenic flexure, 569, 574, 578, 582
splenic veins, 597
splenorenal ligaments
  anatomy, 156, 158, 166
  bridge for splenic area bleeding, 388, 392
  gastric volvulus, 16
  relation to transverse mesocolon, 154
  spread of gastric carcinoma, 172–173
  vascular landmarks, 289
sponges, retained, 120
squamous cell carcinomas, T4, 280
staghorn calculus, 417
staging
  definition, 265
  gastrointestinal cancers, 265–286
stenosis, embryonic, 11
stomach. *See also* gastric carcinomas; gastric ulcers
  breast carcinoma metastases, 246–248
  carcinoma, 296
  displacement by renal cyst, 508–509
  invasion by pancreatic carcinoma, 600, 601
  lung carcinoma metastases, 253–254
  lymphatic drainage, 292–293, 294
  metastatic melanoma, 239, 240
  peritoneal ligaments, 288
  relationship to liver, 139
  staging gastric carcinoma, 266–269
subcapsular abscess, 437
subcapsular hematomas, 438–443
subhepatic abscesses, 87
subhepatic space, 59, 60–62
submucosa, 270, 271
subperitoneal space, 613
  abnormal imaging features, 615–619, 622, 630
  anatomy, 607–634
  central vascular scaffold, 614
  continuity with female organs, 614–615
  embryology, 607–611
  gas diffusion via, 615–619
  lateral continuity, 614
  lower abdomen and pelvis, 613
  upper folds, 612
subperitoneal spread, neuroblastoma, 620
subphrenic space, 59
  abscesses, 93, 102–107, 109, 111
  anatomy of, 62, 63
  seeded metastases, 214–215
subserosa, 270
superior mesenteric artery, 15, 16, 595, 596, 613
superior mesenteric vein, 595, 597, 598
supramesocolic compartment, 287–288
surgical foreign bodies, 104, 106, 116

T

taenia libera, 142, 667–675, 692–697
taenia mesocolica, 142, 667–675, 691–697
taenia omentalis, 142, 667–675, 693–697
thoracoabdominal continuum, 611
"thumbprinting"
  bleeding, 659, 660
  colon, 166, 181
TNM staging systems, 265–269, 444, 446
Toldt, Carl, 398
topographic changes, in radiographs, 6
towels, retained, 120
transmesenteric hernias, 739–742
transmesocolic hernias, 739, 742–743
transmesosigmoid hernias, 738–739
transmural erosion, 579
transmural invasion, 152
transperitoneal approach, 125
transverse cervical ligament of Mackenrodt. *See* cardinal ligament
transverse colon. *See* colon, transverse
transverse duodenum. *See* duodenum, transverse
transverse mesocolon. *See* mesocolon, transverse
trauma
  abdominal, 684
  colon displacement, 684
  liver stab wound, 108
  pancreatitis, 577, 589, 682
Treitz, Václav, 542
Trendelenburg's transpleural approach, 125
triangle sign, 317, 318
tuberculous peritonitis, 223–224, 233
tubulovillous adenoma, rectal, 274

U

ultrasonography
  diagnosis and localization of abscesses, 118
  peritoneal carcinomatosis, 235, 238
umbilical ligament, urachus, 316
umbilical veins, 29
Union Internationale Contra le Cancer, 269
urachus, 316
ureteral bud, blind-ending, 50
ureters
  blind-ending bifid, 48
  obstruction by pancreatic tumor, 622
urinary bladder
  disruption, 483
  eight-week embryo, 51

embryology, 48, 50
hemitrigone, 49
midcoronal pelvis section, 750
urinary tract, embryology, 45–50
urine, extravasation, 395, 422
uriniferous perirenal pseudocysts
after hysterectomy, 427
after pelvilithotomy, 424–425
clinical signs and symptoms, 423
early development, 422
etiology and pathogenesis, 422–423
radiologic findings, 423–430
treatment, 425
urinoma. *See* uriniferous perirenal pseudocysts
urogenital system, embryology, 45–51
uterus didelphys, 521

V
vasa recta, 694, 696, 698, 700
vascular systems
pancreatic, 596–599
ventral mesentery, derivatives, 612
viewing time, and saccadic movements, 6
viscera, abdominal, 2
visual search, of radiographs, 4
vitelline arteries, 648
vitelline veins, 29
volvulus
cecal, 16, 18, 19
gastric, 16–19
midgut, 29, 729
small bowel, 728
splenic flexure, 20
von Hippel-Lindau disease, 42

W
wandering gallbladder, 23, 24
wandering spleen, 16, 17, 43–46, 531

Y
yolk sac, 10
yolk stalk, 10

Z
Zuckerandl, Emil, 336